NANO-BIOSORBENTS FOR DECONTAMINATION OF WATER, AIR, AND SOIL POLLUTION

Edited by
Adil Denizli
Nisar Ali
Muhammad Bilal
Adnan Khan
Tuan Anh Nguyen

ELSEVIER

Micro & Nano Technologies Series

NANO-BIOSORBENTS FOR DECONTAMINATION OF WATER, AIR, AND SOIL POLLUTION

This page intentionally left blank

NANO-BIOSORBENTS FOR DECONTAMINATION OF WATER, AIR, AND SOIL POLLUTION

Edited by

ADIL DENIZLI
Professor, Hacettepe University, Department of Chemistry, Ankara, Turkey

NISAR ALI
Professor, School of Chemistry Chemical Engineering, at Huaiyin Institute of Technology, Huaian, China

MUHAMMAD BILAL
School of Life Science and Food Engineering, Huaiyin Institute of Technology, Huaian, China

ADNAN KHAN
Professor, Institute of Chemical Sciences, at the University of Peshawar, Peshawar, Pakistan

TUAN ANH NGUYEN
Principal Research Scientist, Vietnam Academy of Science and Technology, Hanoi, Viet Nam

ELSEVIER

Elsevier
Radarweg 29, PO Box 211, 1000 AE Amsterdam, Netherlands
The Boulevard, Langford Lane, Kidlington, Oxford OX5 1GB, United Kingdom
50 Hampshire Street, 5th Floor, Cambridge, MA 02139, United States

Notices
Knowledge and best practice in this field are constantly changing. As new research and experience broaden our understanding, changes in research methods, professional practices, or medical treatment may become necessary.

Practitioners and researchers must always rely on their own experience and knowledge in evaluating and using any information, methods, compounds, or experiments described herein. In using such information or methods they should be mindful of their own safety and the safety of others, including parties for whom they have a professional responsibility.

To the fullest extent of the law, neither the Publisher nor the authors, contributors, or editors, assume any liability for any injury and/or damage to persons or property as a matter of products liability, negligence or otherwise, or from any use or operation of any methods, products, instructions, or ideas contained in the material herein.

Library of Congress Cataloging-in-Publication Data
A catalog record for this book is available from the Library of Congress

British Library Cataloguing-in-Publication Data
A catalogue record for this book is available from the British Library

ISBN: 978-0-323-90912-9

Publisher: Matthew Deans
Acquisitions Editor: Edward Payne
Editorial Project Manager: Rafael G. Trombaco
Production Project Manager: Prem Kumar Kaliamoorthi
Cover Designer: Matthew Limbert

Typeset by STRAIVE, India

Dedication

This book has been prepared during the second year of the Covid-19 pandemic with many efforts and contributions from authors across the globe.

During the writing stage, many authors/editors were in lockdown or infected by SARS-CoV-2.

The book is dedicated to those authors we have lost to coronavirus.

This page intentionally left blank

Contents

12. Cellulose-based nanobiosorbents: An insight

Ilgım Göktürk, Duygu Çimen, Merve Asena Özbek, Fatma Yılmaz, and Adil Denizli

13. Synthesis and properties of cellulose-based nanobiosorbents

Anindita De, Mridula Guin, and N.B. Singh

14. Introduction to cellulose-based nanobiosorbents

Cassamo Ussemane Mussagy and Agnes Magri

15. Cellulose composites as nanobiosorbents for ecological remediation

Zari Fallah, Ehsan Nazarzadeh Zare, Mahmood Tajbakhsh, and Vinod V.T. Padil

16. Modification and derivatization of cellulose-based nanobiosorbents and their utilization in environmental remediation

Sajjad Ullah, Elias Paiva Ferreira-Neto, Saima Sohni, Akbar Ali, and Rashida Parveen

17. Cellulose-based nano-biosorbents in water purification

Oluwaseun J. Ajala, A. Khadir, Joshua O. Ighalo, and Great C. Umenweke

III

Chitosan-based nanobiosorbents for deterioration of environmental matrices

IV

Multifarious biopolymers as nanobiosorbents for decontamination of environmental matrices

This page intentionally left blank

Contributors

Katya M. Aguilar-Pérez Tecnologico de Monterrey, School of Engineering and Sciences, Atizapan de Zaragoza, Mexico

Oluwaseun J. Ajala Department of Industrial Chemistry, University of Ilorin, Ilorin; Department of Pure and Applied Chemistry, Ladoke Akintola University of Technology Ogbomoso, Ogbomoso, Nigeria

Mohammed Salim Akhter Department of Chemistry, College of Science, University of Bahrain, Zallaq, Bahrain

F.J. Alguacil National Center for Metallurgical Research (CSIC), Madrid, Spain

Akbar Ali Government College University Faisalabad, Faisalabad, Pakistan

Nisar Ali Key Laboratory of Regional Resource Exploitation and Medicinal Research, Faculty of Chemical Engineering, Huaiyin Institute of Technology, Huaian, Jiangsu Province, China

Charles Pizan Aquino Laboratory of Physical Chemistry Research, Faculty of Sciences, National University of Engineering, Lima, Peru

Ahmad Reza Bagheri Department of Chemistry, Yasouj University, Yasouj, Iran

Ranjan K. Bhuyan P.G. Department of Physics, Government (Autonomous) College, Angul, Odisha, India

Muhammad Bilal School of Life Science and Food Engineering, Huaiyin Institute of Technology, Huaian, China

Luis Fernando Tavares Borges Institute of Chemistry, UNESP-São Paulo State University; National Institute for Alternative Technologies of Detection, Toxicological Evaluation & Removal of Micropollutants and Radioactives (INCT-DATREM), Araraquara, SP, Brazil

Merve Çalışır Department of Chemistry, Hacettepe University, Ankara, Turkey

Fredy Lucho Rondinel Carhuas Laboratory of Physical Chemistry Research, Faculty of Sciences, National University of Engineering, Lima, Peru

Swati Chatur Department of Chemistry, G.M.D Arts, B.W Commerce and Science College, Savitribai Phule Pune University, Nashik, Maharashtra, India

Duygu Çimen Department of Chemistry, Hacettepe University, Ankara, Turkey

Andrija Ćirić Faculty of Science, Chemistry Department, University of Kragujevac, Kragujevac, Serbia

Eduardo Jara Cornejo Laboratory of Physical Chemistry Research, Faculty of Sciences, National University of Engineering, Lima, Peru

Harshal Dabhane Department of Chemistry, G. M.D Arts, B.W Commerce and Science College; Department of Chemistry, K.R.T. Arts, B.H. Commerce and A.M. Science College, Savitribai Phule Pune University, Nashik, Maharashtra, India

Anindita De Department of Chemistry and Biochemistry, Sharda University, Greater Noida, India

Adil Denizli Department of Chemistry, Hacettepe University, Ankara, Turkey

Guilherme L. Dotto Department of Chemical Engineering, Federal University of Santa Maria (UFSM), Santa Maria, RS, Brazil

Hossein Esmaeili Department of Chemical Engineering, Bushehr Branch, Islamic Azad University, Bushehr, Iran

Zari Fallah Faculty of Chemistry, University of Mazandaran, Babolsar, Iran

Elias Paiva Ferreira-Neto Institute of Chemistry-Sa˜o Paulo State University (UNESP), Araraquara, Brazil

Alipasha Geramifard Department of Mechanical Engineering, Shiraz Branch, Islamic Azad University, Shiraz, Iran

Suresh Ghotekar Department of Chemistry, Smt. Devkiba Mohansinhji Chauhan College of Commerce and Science, University of Mumbai, Silvassa, Dadra and Nagar Haveli (UT), India

Ilgım Göktürk Department of Chemistry, Hacettepe University, Ankara, Turkey

Mridula Guin Department of Chemistry and Biochemistry, Sharda University, Greater Noida, India

Fatma Gurbuz Department of Environmental Engineering, University of Aksaray, Aksaray, Turkey

Christian Ronald Jacinto Hernández Laboratory of Physical Chemistry Research, Faculty of Sciences, National University of Engineering, Lima, Peru

Joshua O. Ighalo Department of Chemical Engineering, University of Ilorin, Ilorin; Department of Chemical Engineering, Nnamdi Azikiwe University, Awka, Nigeria

Hafiz M.N. Iqbal Tecnologico de Monterrey, School of Engineering and Sciences, Monterrey, Mexico

Ghanshyam Jadhav Department of Chemistry, K.R.T. Arts, B.H. Commerce and A.M. Science College, Savitribai Phule Pune University, Nashik, Maharashtra, India

Efthimia Kaprara Department of Chemical Engineering, Aristotle University of Thessaloniki, Thessaloniki, Greece

Fahmeeda Kausar School of Chemistry and Chemical Engineering, Shanghai Jiao Tong University, Shanghai, China

A. Khadir Young Researcher and Elite Club, Yadegar-e-Imam Khomeini (RAH) Shahre Rey Branch, Islamic Azad University, Tehran, Iran

Adnan Khan Institute of Chemical Sciences, University of Peshawar, Peshawar, Khyber Pakhtunkhwa, Pakistan

Sabir Khan Laboratory of Physical Chemistry Research, Faculty of Sciences, National University of Engineering, Lima, Peru; Institute of Chemistry, UNESP-São Paulo State University, Araraquara, SP, Brazil

Bhagaban Kisan Post Graduate Department of Physics, Utkal University, Bhubaneswar, Odisha, India

Evgenios Kokkinos Department of Chemistry, Aristotle University of Thessaloniki, Thessaloniki, Greece

Vesna Krstić Mining and Metallurgy Institute Bor; University of Belgrade, Technical Faculty Bor, Bor, Serbia

Minashree Kumari Department of Civil Engineering, Indian Institute of Technology Delhi, Hauz Khas, Delhi, India

Eder C. Lima Institute of Chemistry, Federal University of Rio Grande do Sul (UFRGS), Porto Alegre, RS, Brazil

Rosario López Laboratory of Physical Chemistry Research, Faculty of Sciences, National University of Engineering, Lima, Peru

Agnes Magri Fundaçao Oswaldo Cruz, Fiocruz-Ceara, Eusébio, Brazil

Sumeet Malik Institute of Chemical Sciences, University of Peshawar, Peshawar, Khyber Pakhtunkhwa, Pakistan

Sandra Quispe Martínez Laboratory of Physical Chemistry Research, Faculty of Sciences, National University of Engineering, Lima, Peru

Vijay Medhane Department of Chemistry, K.R. T. Arts, B.H. Commerce and A.M. Science College, Savitribai Phule Pune University, Nashik, Maharashtra, India

Dora I. Medina Tecnologico de Monterrey, School of Engineering and Sciences, Atizapan de Zaragoza, Mexico

Ily Marilú Maza Mejía Laboratory of Physical Chemistry Research, Faculty of Sciences, National University of Engineering, Lima, Peru

Snežana Milić University of Belgrade, Technical Faculty Bor, Bor, Serbia

Bahareh Kamyab Moghadas Department of Chemical Engineering, Shiraz Branch, Islamic Azad University, Shiraz, Iran

Ranjan K. Mohapatra Department of Chemistry, Government College of Engineering, Keonjhar, Odisha, India

Bianca Mortari Institute of Chemistry, UNESP-São Paulo State University; National Institute for Alternative Technologies of Detection, Toxicological Evaluation & Removal of Micropollutants and Radioactives (INCT-DATREM), Araraquara, SP, Brazil

H.C. Ananda Murthy Department of Applied Chemistry, School of Applied Natural Sciences, Adama Science and Technology University, Adama, Ethiopia

Cassamo Ussemane Mussagy Department of Engineering of Bioprocesses and Biotechnology, School of Pharmaceutical Sciences, São Paulo State University (UNESP), Araraquara, São Paulo, Brazil

Nadia Nazish Department of Zoology, University of Sialkot, Sialkot, Pakistan

Tuan Anh Nguyen Institute for Tropical Technology, Vietnam Academy of Science and Technology, Hanoi, Vietnam

Mehmet Odabaşı Department of Chemistry, Faculty of Science, Aksaray University, Aksaray, Turkey

Rajeshwari Oza Department of Chemistry, S.N. Arts, D.J.M. Commerce and B.N.S. Science College, Savitribai Phule Pune University, Sangamner, Maharashtra, India

Merve Asena Özbek Department of Chemistry, Hacettepe University, Ankara, Turkey

Vinod V.T. Padil Institute for Nanomaterials, Advanced Technologies and Innovation (CXI), Technical University of Liberec (TUL), Liberec, Czech Republic

Roberto Parra-Saldivar Tecnologico de Monterrey, School of Engineering and Sciences, Monterrey, Mexico

Rashida Parveen Government Girls Degree College Dabgari, Peshawar, Pakistan

Gino Picasso Laboratory of Physical Chemistry Research, Faculty of Sciences, National University of Engineering, Lima, Peru

Tahir Rasheed Interdisciplinary Research Center for Advanced Materials, King Fahd University of Petroleum and Minerals (KFUPM), Dhahran, Saudi Arabia

Komal Rizwan Department of Chemistry, University of Sahiwal, Sahiwal, Pakistan

J.I. Robla National Center for Metallurgical Research (CSIC), Madrid, Spain

Arpita Roy Department of Biotechnology, School of Engineering & Technology, Sharda University, Greater Noida, India

Gerson A. Ruiz-Córdova Laboratory of Physical Chemistry Research, Faculty of Sciences, National University of Engineering, Lima, Peru

Gustavo Ruiz-Pulido Tecnologico de Monterrey, School of Engineering and Sciences, Atizapan de Zaragoza, Mexico

Dnyaneshwar Sanap Department of Chemistry, G.M.D Arts, B.W Commerce and Science College, Savitribai Phule Pune University, Nashik, Maharashtra, India

Sameera Shafi Institute of Chemistry, The Islamia University of Bahawalpur, Bahawalpur, Pakistan

Konstantinos Simeonidis Department of Chemical Engineering, Aristotle University of Thessaloniki, Thessaloniki, Greece

N.B. Singh Department of Chemistry and Biochemistry; Research Development Cell, Sharda University, Greater Noida, India

V.M. Sivakumar Department of Chemical Engineering, Coimbatore Institute of Technology, Coimbatore, India

Saima Sohni Institute of Chemical Sciences, University of Peshawar, Peshawar, Pakistan

Maria Del Pilar Taboada Sotomayor Institute of Chemistry, UNESP-São Paulo State University; National Institute for Alternative Technologies of Detection, Toxicological Evaluation & Removal of Micropollutants and Radioactives (INCT-DATREM), Araraquara, SP, Brazil

Mahmood Tajbakhsh Faculty of Chemistry, University of Mazandaran, Babolsar, Iran

Sajad Tamjidi Department of Chemical Engineering, Shiraz Branch, Islamic Azad University, Shiraz, Iran

M. Thirumarimurugan Department of Chemical Engineering, Coimbatore Institute of Technology, Coimbatore, India

Sergio Espinoza Torres Laboratory of Physical Chemistry Research, Faculty of Sciences, National University of Engineering, Lima, Peru

Marina Uđilanović Faculty of Science, Chemistry Department, University of Kragujevac, Kragujevac, Serbia

Sajjad Ullah Institute of Chemical Sciences, University of Peshawar, Peshawar, Pakistan

B. Uma Maheswari Department of Chemical Engineering, Coimbatore Institute of Technology, Coimbatore, India

Great C. Umenweke Department of Chemistry, University of Kentucky, Lexington, KY, United States

Tamara Urošević Mining and Metallurgy Institute Bor, Bor, Serbia

Jaime Vega-Chacón Laboratory of Physical Chemistry Research, Faculty of Sciences, National University of Engineering, Lima, Peru

Yasmin Vieira Graduate Program of Chemistry, Federal University of Santa Maria (UFSM), Santa Maria, RS, Brazil

Javier Lobaton Vila Institute of Chemistry, UNESP-São Paulo State University; National Institute for Alternative Technologies of Detection, Toxicological Evaluation & Removal of Micropollutants and Radioactives (INCT-DATREM), Araraquara, SP, Brazil

Ye Wenjie Key Laboratory of Regional Resource Exploitation and Medicinal Research, Faculty of Chemical Engineering, Huaiyin Institute of Technology, Huaian, Jiangsu Province, China

Yong Yang Key Laboratory of Regional Resource Exploitation and Medicinal Research, Faculty of Chemical Engineering, Huaiyin Institute of Technology, Huaian, Jiangsu Province, China

Fatma Yılmaz Vocational School of Gerede, Department of Chemistry Technology, Bolu Abant Izzet Baysal University, Bolu, Turkey

Ehsan Nazarzadeh Zare School of Chemistry, Damghan University, Damghan, Iran

Shakeel Zeb Institute of Chemistry, UNESP-São Paulo State University; National Institute for Alternative Technologies of Detection, Toxicological Evaluation & Removal of Micropollutants and Radioactives (INCT-DATREM), Araraquara, SP, Brazil

Cao Zhou Key Laboratory of Regional Resource Exploitation and Medicinal Research, Faculty of Chemical Engineering, Huaiyin Institute of Technology, Huaian, Jiangsu Province, China

Anastasios Zouboulis Department of Chemistry, Aristotle University of Thessaloniki, Thessaloniki, Greece

PART I

Basics principles

This page intentionally left blank

CHAPTER

1

Nano-biosorbents for contaminant removal: An introduction

Duygu Çimen[a], *Ilgım Göktürk*[a], *Merve Çalışır*[a], *Fatma Yılmaz*[b], *and Adil Denizli*[a]

[a]Department of Chemistry, Hacettepe University, Ankara, Turkey [b]Vocational School of Gerede, Department of Chemistry Technology, Bolu Abant Izzet Baysal University, Bolu, Turkey

1.1 Introduction

Nanotechnology focuses on the production of nanoscale materials for commercial use to obtain new structural and functional materials (Whitesides, 2005). One of the nanoscale materials used in many fields is nanobiopolymers. Nanobiopolymers, one of the nanoscale materials used in many fields, have attracted great attention in recent years due to their biodegradability, sustainability and biocompatibility (Yang et al., 2019). Nanobiopolymers such as nanochitin, nanostarch, nanocellulose, and nanosilk are produced from renewable sources and living organisms. In addition, they are sustainable natural nanoscale materials with their structural features, biocompatibility, non-toxicity, abundant availability, and easy of modification (Hassan et al., 2019; Sahana and Rekha, 2018).

The most abundant, biodegradable and renewable natural polymer in the world is cellulose. Recently, cellulose in a nanoscale form (i.e., nanobiocellulose) has been recognized as a reliable green substrate for use in a wide variety of applications. Because nanobiocellulose contains many hydroxyl groups, it is an important nanobiopolymer of choice for surface modifications. Moreover, besides being a renewable and good mechanical property and being a low-cost material, nanobiocellulose has very low toxicity, biodegradability, biocompatibility, and antimicrobial effects (Nascimento et al., 2016; Prasad Reddy and Rhim, 2014).

Nanochitin, one of the bio-based nanomaterials, has recently been of great interest due to its similar properties to the structure of nanocellulose (Facchine et al., 2021; Shen et al., 2016). Nanochitins are preferred to reduce adverse environmental impacts such as dependence on fossil fuels and the use of reagents/hard solvents to increase the use of bio-based components.

https://doi.org/10.1016/B978-0-323-90912-9.00001-0

In addition, these materials have advantages due to tunable surface chemistry and morphology that they can be used in many different applications. Therefore, it is frequently used in medical uses, water treatment, emulsion stabilization, and many other fields (Bai et al., 2018; Salaberria et al., 2014; Zeng et al., 2011).

In many recent studies, it is becoming widespread to investigate the biomedical properties of silk at the nanoscale (Keten and Buehler, 2010; Melke et al., 2016). Nanosilk is a natural glycoprotein polymer produced from spider and silkworm and is suitable for use in many areas with its high biocompatibility, non-toxicity, and easy degradation. Silk-based nanomaterials (nanoparticles, nanofibers, nanocomposites) are used in a variety of applications (Kundu et al., 2013; Vepari and Kaplan, 2007). In addition to all these, microbial nanobiopolymers have begun to attract the attention of scientists as an interesting alternative. Among biocompatible nanobiopolymers, starch is used as suitable biological supports for the development of green and heterogeneous catalysts with its low cost, efficient selectivity, structure diversity, high reactivity, non-toxicity, and environmentally friendly nature (Shaabani et al., 2008; Zarnegar et al., 2019).

In addition, as a natural and renewable polymer, starch is used for catalytic processes in chemical synthesis. These natural nanobiopolymers are often used for the biomedical fields, food industry, water treatment agent, composite filler, and catalytic nano-systems (Chen et al., 2015; Safari and Sadeghi, 2017). Nanobiopolymers are generally produced from forestry and agricultural products such as silk, coconut, wood, cotton, and crab/shrimp shell (Moon et al., 2011). Nanobiopolymers are biodegradable compared to petroleum-based polymers and are produced by various mechanical, chemical, and synthetic biological techniques (Omenetto and Kaplan, 2010). High energy consumption is required in the production techniques of nanobiopolymers, chemical modification, and mechanical isolation methods. Balancing the efficiency and sustainability of the isolation methods (enzymatic, chemical, and/or mechanical isolation approaches) is very important in nanobiopolymer isolation. Enzyme isolations are one of the most environmentally friendly isolation approaches. Generally, chemical and mechanical methods are used together (Yang et al., 2019).

In this chapter, after giving information about nanobiopolymer types and production technologies, information from recent studies of nanobiopolymers for decontamination of environmental pollutants in recent years is shared in detail.

1.2 Nanobiopolymers

Nanobiopolymers are organic molecules that can be obtained from renewable natural resources. They are established by chain reactions of biological monomers and found abundantly in nature. Biopolymers have remarkable physical properties (Crini, 2005). They are used in environmentally sensitive applications and also one of the most popular focuses of researchers as cheap and easily produced substances and their nano-sized (1–100 nm) versions are promising for many fields. These nanobiopolymers are a set of chemicals synthesized by living organisms throughout their lives and can have different monomer types and structures (Jancar et al., 2010; Kumar et al., 2010). The most common biopolymers in natural systems are generally polysaccharides, accompanied by some protein structures. Sugar

monomers linked together by glycosidic bonds form the structure of polysaccharides (Klemm et al., 2011). They have many important roles in living beings such as structure support, energy source, and enabling selective transition between cells. Cellulose, starch, chitin, and silk can be counted among these nanobiopolymers that can be synthesized in metabolism (Torres et al., 2019).

1.2.1 Nanocellulose

One of the most common polysaccharides encountered in nature is cellulose. The first use of cellulose goes back to ancient times. Cellulose, which is mostly used in the paper industry today, was similarly preferred as the raw material of papyrus in Ancient Egypt. In addition to writing, it has been utilized in different ways in daily-use gadgets such as baskets and ropes. The elucidation of the structure of cellulose, which is utilized in most of human life, has only been found in the nineteenth century. Cellulose is the primary material of the plant wall and also forms half of the biomass of photosynthetic organisms (Heinze, 2015). Cellulose is a renewable resource, therefore it is an exceptional option for the production of biopolymer-based materials. The fibrillated structure of cellulose draws attention when it comes down to the nano-level. Cellulose synthesis is based on the interaction between Van der Waals and hydrogen bonds and reaches its final structure by stacking the fibrils. These fibrils can have a size of 3 to 5 nm and have a square cross-section (Moon et al., 2011). The polymeric structure of cellulose can be suitable for different fields. Many forms such as fibril, whisker, crystalline have already begun to be investigated in different research areas. It is possible to obtain cellulose not only from plants but also from bacteria and fungi as well.

Wood pulp can also be a source for nanocellulose and different types of nanocellulose have been produced. Micro-fibrillated cellulose (MFC) is produced using sugar-beet, potato tubers, hemp, flax as a source and is about 5–60 nm in diameter. Nano-crystalline cellulose (NCC) is produced from woods, cotton, hemp, linseed, cereal plants, cellulose from algae sources and is obtained by acid hydrolysis method. The size range is between 5 and 70 nm in diameter. Sources of bacterial nano-cellulose (BNC) include alcohols, low molecular and weight sugars and are obtained by bacterial synthesis. Their diameter is between 20 and 100 nm (Lindström et al., 2014). Types of nanocellulose and their promising examples for future studies will be mentioned in the scope of the chapter.

1.2.2 Nanochitin

Chitin is another natural polymer found quite abundantly in nature just like cellulose. Chitin is a polysaccharide that forms the exoskeleton of many terrestrial arthropod animals such as insects and spiders (Olatunji, 2015). Crab and shrimp shells from seafood consumption are the source of the chitin trade. Chitin molecule ($C_8H_{13}O_5N$) shows a long chain structure formed by repeating two *N*-acetylglucosamine units linked by β-1,4 bonds and is a long-chain polymer of *N*-acetylglucosamine, a glucose derivative. The structure of chitin is also composed of nanofibers like cellulose. These nanofibers are protein embedded and their sizes are 2–5 nm in diameter and 300 nm in length, and also the most common forms are α-chitin

and β-chitin (Faria et al., 2016; Raabe et al., 2006). Chitin, a hydrophobic material, is insoluble in most organic solvents, which limits its use. At this point, chitosan, the acetylated derivative of chitin, meets the demands. Unlike chitin, chitosan dissolves in weakly acidic solutions. Chitin and chitosan are widely used in areas such as environmental sanitation applications, natural packaging materials, food preservatives, and beauty products (Morin-Crini et al., 2019). The reduced degree of acetylation of chitosan makes it a great candidate for use in biomedical fields and increases the range of use. It can also be integrated into drug delivery systems, thanks to its solubility in acidic environments (Prabaharan, 2012). There are also nanocomposite materials in which chitin and chitosan are used together. Chitosan fortified with chitin whiskers is a good example of these ingredients. Providing the combination of their unique advantages, this material has improved tensile strength and water absorption resistance (Sriupayo et al., 2005). Chitosan, can be combined with other natural polymers and integrated into different systems as well.

1.2.3 Nanosilk

Silk fibroin (SF) is a natural glycoprotein polymer that contains H-chain and L-chain. It is produced from silkworms and spiders. SF forms can be quite versatile such as films, scaffolds, hydrogels, microspheres, and nanofibers. This protein-based nanomaterial is very suitable for use in medical research due to its high biocompatibility, non-toxicity, easily degradable and non-inflammatory characteristics (Fei et al., 2013). In addition, silk fibroins have properties such as reducing metal ions in aqueous solutions and being antibacterial (Duan et al., 2018; Sakabe et al., 1989). Pure silk fibroins have the disadvantage that they dissolve easily in water and this limits the study range of the material. However, this obstacle can be overcome by combining nano-silk with other materials. Silk fibroin contains a glue-like protein called sericin, and the removal of this component is important for the use of silk fibroins because it has been reported that this protein is responsible for allergic reactions to silk (Zaoming et al., 1996). Later, this information lost its validity after the sericin protein could be used as a biocompatible material. It was soon proven that the main allergic reaction was caused by the combination of sericin and fibroin (Chirila et al., 2013). Fibroin and sericin protein are separated from each other in a thermochemical way and this process is called degumming. Silk nanofibroins contain high amounts of glycine and their tight binding gives silk fibroin highly stable β-sheet nanocrystals (Hayashi et al., 1999). The main molecular interactions in these crystalline β-layers are hydrogen bonds. Although hydrogen bonds are known as weak bonds, it is these bonds that underlie the rigidity and tensile strength of silk. Weak hydrogen bonds give silk nanofibroins amazing advantages such as self-assembly and self-heal (Keten et al., 2010).

1.2.4 Nanostarch

Starch, a biopolymer of plant origin, is most often derived from wheat, corn, potatoes, and rice. Its granular structure can be quite large (up to 100 μm) and its size can vary depending on the amorphous and crystallinity containing form (Zobel, 1988). Its shape-related properties

also vary according to the obtained plant, for example, the crystallinity can be changed between 15% and 45% (Tan et al., 2007). Starch is a polysaccharide just like cellulose and chitin. Starch, which has two macromolecules called amylose and amylopectin, consists of D-glucose units. Amylose is a sparsely branched chain and has an average weight of 370,350 Da, making it one of the largest natural polymers on earth (Suortti et al., 1998). Amylopectin, on the other hand, has α (1–4) binding and makes a branch at every 22–77 glucose unit, and these branches determine the crystal structure of starch. The crystal structure of starch forms the basis of its biological and physical properties (Vamadevan et al., 2018). According to the botanical source from which it was obtained, starch may also contain lipids and phosphorus and these components can change the characteristics of starch by Maillard reaction (Rizzi, 2004). Down to the nanoscale we first encounter starch nanoparticles with sizes in the range of 50–200 nm. The abundance of starch in nature is directly related to being able to produce starch nanoparticles economically. In addition, nano-sized starch has many uses with its biocompatible and degradable properties that do not leave toxic waste (Dufresne, 2006). Starch nanoparticles have a high specific surface area and strength. The starch surface is rich in hydroxyl groups; therefore it is open to a variety of chemical reactions associated with the positive surface (Angellier et al., 2005a,b). This feature provides the advantage of being able to use starch nanoparticles in various composites. Nano-sized starch is classified as starch nanoparticles and different methods are used to prepare starch nanocrystals, its subclass. Starch nanocrystals are a popular research subject in recent years with their easy degradation and regenerative properties. Its dimensions are 5–7 nm thick and 20–40 nm long and 15–30 nm wide (Putaux et al., 2003). Both starch nanoparticles and starch nanocrystals have attracted great attention in a wide variety of applications and due to their potential making the combination with different materials.

1.2.5 Microbial nanobiopolymers

Microbial nanopolymers are a great discovery for the "green" based polymers that today's world acutely needs. These polymers have a biotechnology-based nano-production process and have begun to take their place in studies as promising alternatives. Microbial strains of bacteria, yeast, or molds can be used for microbial nanopolymer synthesis (Fang et al., 2017; Khan et al., 2018; Li et al., 2011). It is possible to synthesize these nanostructures not only using these organisms but also with other microorganisms as well (Gatenholm et al., 2016). Microbial nanobiopolymers have favorable properties. One of them is that their chemical composition can be determined and the size and shape can be adjusted as desired. Besides, the environment in which these syntheses take place does not require heavy physicochemical conditions. Another advantage is that microbial cells are relatively easy to grow and can be formed in desired quantities (Prasad et al., 2016). In order to surpass traditional methods, there are obstacles to be overcome in microbial nanobiopolymer synthesis. The successful applications of microbial nanobiopolymers will increase when the deficiencies in nanomaterial purification, some problems related to the functions of biocoating agents and economic imbalances in production are eliminated.

1.3 Nanobiopolymer fabrication techniques

Synthetic polymer-based materials, which have become the most widely used materials in the last decade, have caused serious problems affecting the environment and human health. These problems arise from both material applications and their production processes. In addition, since most synthetic polymer-based products do not naturally degrade, they create environmental, social, and financial burdens, causing additional problems (Zhu et al., 2016). Biopolymers such as cellulose, chitin, silk, starch, and bacterial polysaccharides have found widespread use area in recent years due to their extensive availability, sustainability, biocompatibility, and biodegradability (Balakrishnan et al., 2017; Bamba et al., 2017; Kargarzadeh et al., 2017; Yang et al., 2019). These natural nanobiopolymers as starting materials are used when creating new structural and functional materials. While structural advantages are retained in these approaches (e.g., complex hierarchical structure (Naleway et al., 2015) and nano-environment (Jancar et al., 2010; Klemm et al., 2011; Kumar et al., 2010), additional functions resulting from unique nanosized effects (e.g., optical transparency, structural color, and extracellular matrix-like porous networks) (Giesa et al., 2014) are earned.

In recent years, while nanobiopolymers are obtained from biological materials such as wood and cotton, various mechanical, chemical, and bacterial-derived methods have been created. The resulting nanobiopolymers have been used in various high-tech fields such as transparent display panels, ultrafiltration membranes, energy storage devices, and catalytic supports (Ling et al., 2017, 2018). Herein, we focused on the green industrial production of nanobiopolymers that can have lower environmental impact and have less toxicity to human health. High energy and toxic reagent consumption is required in nanobiopolymer production techniques using mechanical isolation and chemical modification methods (Dufresne, 2017).

1.3.1 Nanocellulose isolation

Nanocellulose consists of two groups classified as cellulose nanofibrils (CNFs) and cellulose nanocrystal (CNC or cellulose nanofibers), depending on their morphological structure. Cellulose-based materials in nature, which have a complex hierarchical structure, are in scale ranging from angstrom level to macroscopic levels. According to their sources, nanocellulose is divided into three classes as wood nanocellulose, cotton nanocellulose, and bacterial cellulose. Chirayil et al. performed extraction of cellulose nanofibrils from isora fiber using the steam blast method as shown in Fig. 1.1 (Chirayil et al., 2014a,b).

The most common sources of cellulose are wood and plant fibers, but the isolation of cotton celluloses is relatively difficult due to the strong hydrogen bonds between CNFs. The nanocellulose isolation can be done by the degradation of cellulose fibers in colloidal suspensions of cellulose catalyzed by sulfuric acid (H_2SO_4). Cellulose nanocrystals (CNCs) have so far been obtained by isolating them from a variety of natural cellulose sources. CNCs are a good alternative for producing advanced materials from biopolymer as they have outstanding chemical, mechanical, thermal, and optical properties. The processes used in the extraction of CNCs from various sources (non-edible biomass and agro-industrial wastes) were tabulated by Owoyokun et al. (Trache et al., 2020). Some critical aspects of the classical

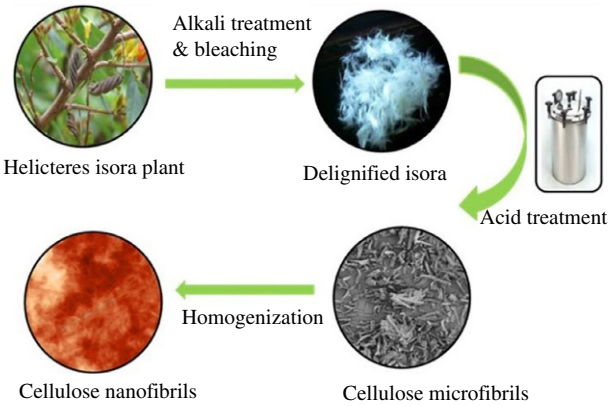

FIG. 1.1 Extraction procedure from isora nanofibrils (Chirayil et al., 2014a,b).

approach (acid hydrolysis) and innovative methodologies for obtaining CNC are discussed in this review.

Acid hydrolysis is the classical production methodology for obtaining CNCs, using sulfuric acid by heating to 80°C for 40–60 min and widely exploited for the production of CNC from diverse sources of cellulose. Parameters such as acid concentration, reaction time, and reaction temperature are effective in controlling acid hydrolysis of wood pulp. Time and temperature not only affect the properties of nanocellulose, but also change the acid–pulp ratio by affecting the acid concentration. Although H_2SO_4 is the most commonly used acid in nanocellulose preparation, it is also possible to use other acids such as hydrochloric acid (HCl), hydrobromic acid (HBr), and phosphoric acid (H_3PO_4) to prepare CNC. But, hydrochloric acid, and hydrobromic acid will not have any surface charges and a stable colloidal dispersion is, therefore, harder to form when compared to sulfuric acids (Börjesson and Westman, 2015).

Nanocellulose source agricultural residues are the most used materials. Acid hydrolysis of soy hulls for 30 min resulted in needle-like KKK formation with high crystallinity (Flauzino Neto et al., 2013). Nanocellulose was extracted by Rashid and Dutta from the husks of short, medium and long rice grains. A schematic representation of the process used to extract cellulose and nanocellulose from rice husk is shown in Fig. 1.2 (Rashid and Dutta, 2020).

The extraction of CNCs from pinewood through sulfuric acid hydrolysis yielded about 70%. Acid concentration and temperature are reported to be the strongest determinants for CNC yield. Crystallinity index, surface charge, particle size, and relatively uniform dispersity are consistent with the quality of CNCs obtained via acid hydrolysis (Kandhola et al., 2020). CNCs have been extracted from rice husks through by three-step process: alkaline hydrolysis, subsequent bleaching, and final grinding process (Fathi et al., 2018). Fabrication of CNCs from the walnut shell through alkali/acidic hydrolysis has been achieved with a high yield (92%) and medium crystallinity degree (49%) (Hemmati et al., 2018). Enzymatic hydrolysis does not require the use of highly corrosive reagents and an enormous quantity of water to obtain CNCs. However, the yield obtained is generally lower than that obtained from physical–chemical processes. Enzymatic hydrolysis and high pressure have been used to

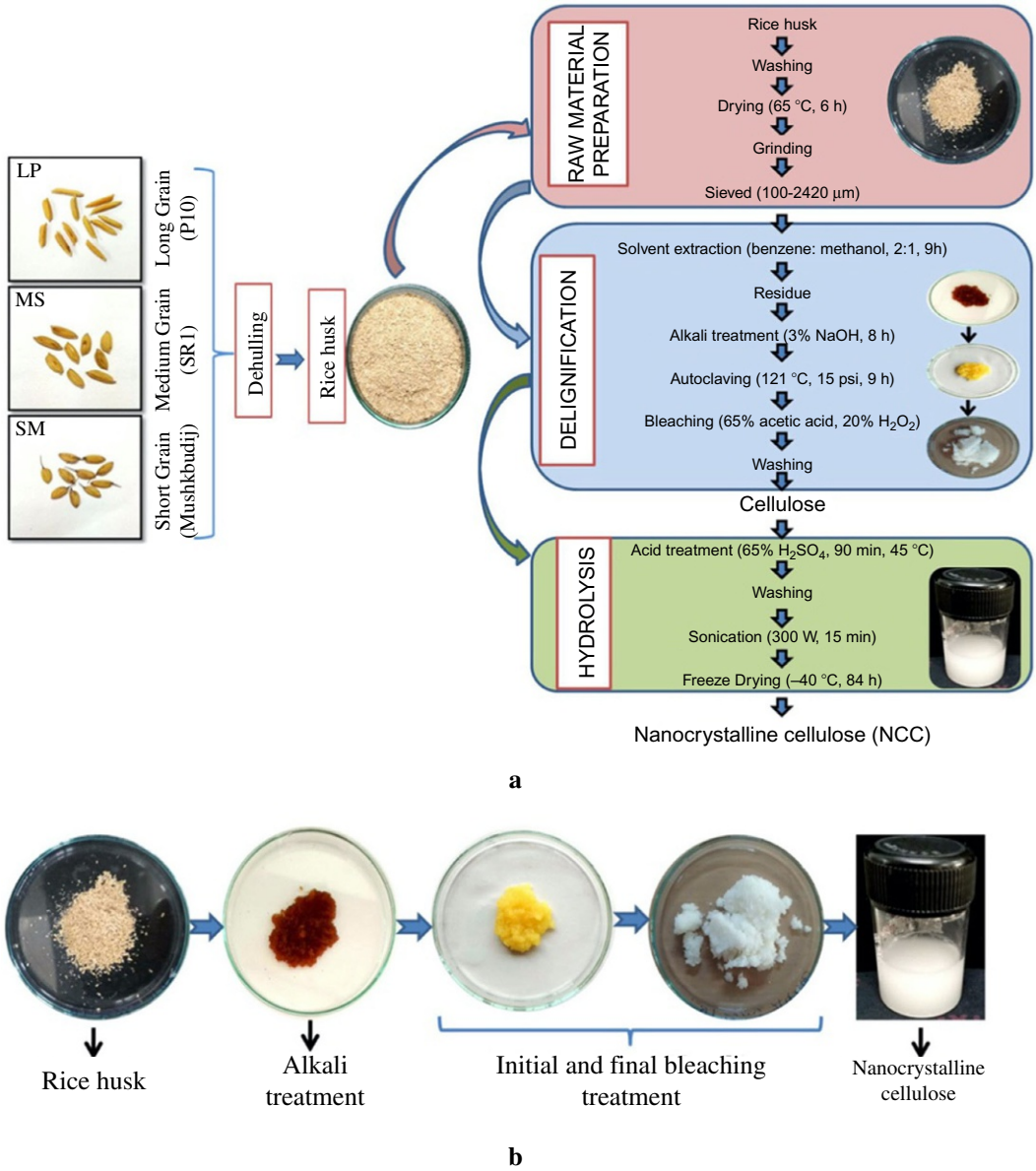

FIG. 1.2 (A) Extraction process of cellulose and nanocellulose from rice husk. (B) Visual states of the material for the different extraction process stages (Rashid and Dutta, 2020).

produce CNCs from rice and oat husk-based cellulose. Rice and oat husks-based CNCs and the respective aerogels were reported to have a uniform structure, a high-water absorption capacity, and a large pore size (de Oliveira et al., 2019).

CNFs are about 10–100 nm in width and 0.5–10 mm in length and composed of several to dozens of elementary fibrils. CNFs can be produced using higher plants, tunics, algae, and

other organisms (Moon et al., 2011). In general, CNF isolation is provided by the mechanical processing that enables high shear-induced longitudinal splitting of cellulose fibers (W. Chen et al., 2018). Another mechanical process commonly used in cellulose isolation is ultrasonication. In order to reduce the particle size of cellulose pulps, mechanical treatments are often applied in combination (Li et al., 2011). However, a major problem with these mechanical methods is their limited size reduction capabilities. Accordingly, various mechanical, chemical, and enzymatic pre-treatments have been used to produce smaller CNFs. Berto et al. combined the enzymatic pre-treatment of cellulose fibers with mechanical defibrillation to obtain cellulose nanofibrils (CNF). Fig. 1.3 shows the morphology of nanofibrils isolated from bleached eucalyptus kraft pulp (BEKP) (Berto et al., 2021).

The steam explosion causes the pulp to be steamed under pressure for a certain period of time, followed by a rapid pressure relief, causing the fiber cell wall to rupture. Steam explosion is a widely used pre-treatment method for CNF isolation. The steam explosion causes the hemicelluloses hydrolysis resulting in cleavage of hemicellulose–lignin bands (Berto et al., 2021).

Lignin and hemicellulose were removed from wood powder with acidified sodium chloride (NaCl) and potassium hydroxide (KOH) solution, and CNFs of 15–20, 12–35, and 12–55 nm in width were successfully isolated (Taer et al., 2020). Kentaro weakened the

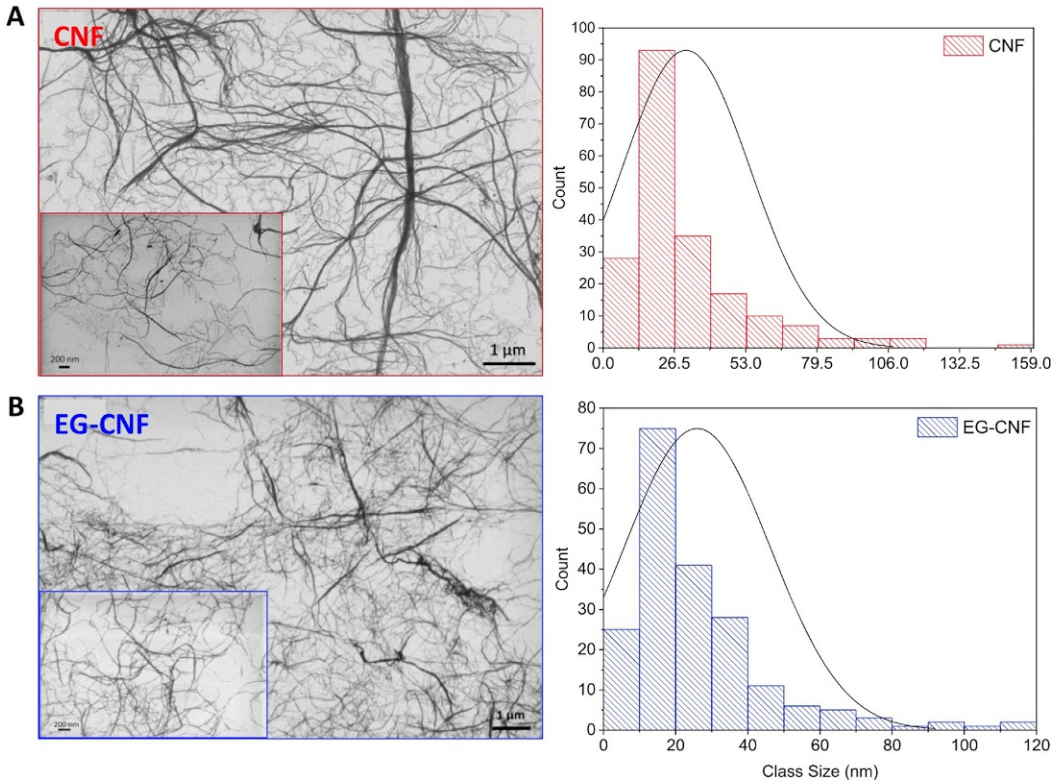

FIG. 1.3 Morphology of nanofibrils isolated from BEKP via defibrillation (A) without and (B) with EG pre-treatment (Berto et al., 2021).

hydrogen bonds of cellulose pulps using NaOH and fabricated 12–20 nm in width CNFs from dried cellulose pulps (Abe, 2016).

Enzyme pretreatment technique is used as another strategy to improve the degree of isolation. Recently the endoglucanases have been used to separate wood cellulose pulps. Hideno et al. investigated the effects of celluloses for nanofibrillation of cotton ball and dried cotton fibers (Hideno et al., 2016). Thus, after the mechanical isolation of pre-treated cotton fibers, 10–50 nm wide CNFs were produced.

Mechanical, chemical, and enzymatic pre-treatments are used to significantly improve the isolation degree of cellulose sources, but these approaches still cannot exfoliate cellulose fibers into elemental fibrils with a width of 3–4 nm. Oxidation of cellulose pulp mediated by 2,2,6,6-tetramethylpiperidine-1-oxyl radical (TEMPO) was carried out to improve the degree of isolation. TEMPO-oxidized cellulose nanofibril film preparation using nanostructured bacterial cellulose was performed by Chitbanyong et al. (2020). Typical TEMPO-mediated oxidation route used for chemical modification of cellulose pulps is summarized by Chirayil et al. (2014a).

1.3.2 Nanochitin isolation

Chitin is isolated primarily from the crustacean exoskeleton and is the most versatile and promising biomaterial after cellulose. Chitin has recently gained attention due to the progress of chitin nanofiber (ChNF) isolation, although it is difficult to process because it is not soluble in water. Nanokitins are often exfoliated from crab, shrimp (α-chitin), or squid pens (β-chitin). Sources of this chitin consist of chitin (20–30%) as well as a mixture of non-chitin, proteins, inorganic salts, and lipids (0–14%). Therefore, before the chitin is isolated, it must undergo a series of pre-treatments to remove impurities (Ilyas et al., 2021; Liu et al., 2021).

The isolation of nanochitin is carried out in all four critical steps which are: (i) removal of residual proteins by alkaline or enzymatic hydrolysis application (ii) removal of inorganic salts by HCl aqueous solution application (iii) extraction of astaxanthin pigments and lipids by organic solvents application (iv) white chitin products obtaining through residues treatment. In this section, information about the four typical methods used in the isolation of nanochitin, acid hydrolysis, TEMPO mediated oxidation, partial deacetylation, and mechanical isolation will be summarized.

Selective isolation methods for the preparation of chitin nanocrystals (ChNCs) were reviewed by Yang et al. (2019). A series of acid hydrolysis approaches developed to prepare a suspension of chitin crystallite particles were evaluated. At present, for the isolation of chitin nanocrystals, mineral acids (H_2SO_4, HCl, HBr) are usually used primarily. Estimation of the strength of single chitin nanofibrils via sonication-induced fragmentation by HCI acid hydrolysis was performed by Bamba et al. (2017). Using HCl solution, Narkevicius et al. prepared the ChNCs pre-treated with NaOH solution leading to the yield of ChNCs of around 79 wt% (Narkevicius et al., 2019). In Fig. 1.4, five different acidic deep eutectic solvents (DESs) composed of choline chloride and organic acids (oxalic acid dihydrate, lactic acid, malonic acid, citric acid monohydrate or DL-malic acid) were applied to fabricate chitin nanocrystals (ChNCs) by Narkevicius et al. (2019).

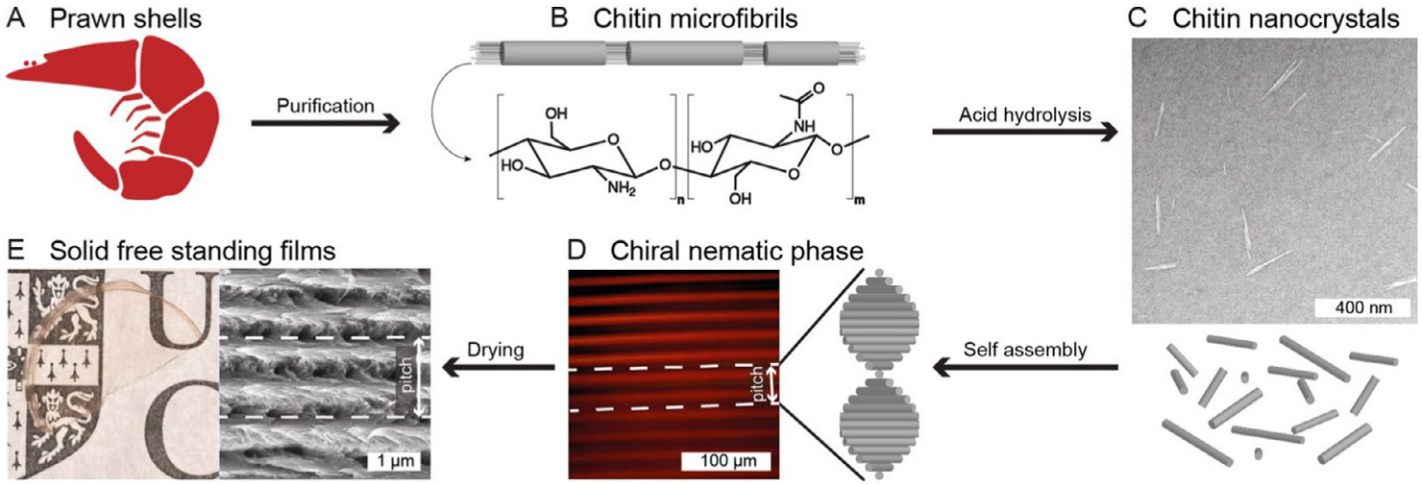

FIG. 1.4 Overview of chitin nanocrystal preparation. (A) prawn shell chitin powder (B) purification to yield chitin microfibrils (C) acid hydrolysis to form chitin nanocrystals (D) self-assembly of the colloidal chitin nanocrystal suspension to form chiral nematic phase (E), transparent film that retains helicoidal nanoarchitecture (Narkevicius et al., 2019).

Chitin microfibers separation was performed by mechanical action application to form slender filaments by disrupting the bonds connecting fibrils via hydrogen bonds. Under acidic or neutral conditions, mechanical processes such as ultrasonication, grinding, high-pressure waterjet system application, and high-pressure homogenization are often used separately or simultaneously (Yang et al., 2020b). Ultrasound produces high energy, which destroys the hydrogen bond between polymer chains. Ultrasound both converts chitin powders into chitin fibers and converts chitin gels to nanofiber dimension (Gopi et al., 2018; Huang et al., 2015; Jung et al., 2019; Lu et al., 2013; Wang et al., 2017). By applying simple mechanical grinding, the nanofibers of the purified chitin can be separated. The produced shear force can refine the fibers at a nanometer scale (Missoum et al., 2013). Ifuku et al. purified five kinds of mushrooms by applying chemical method. Separation of chitin nanofibers from the cell wall of mushrooms was performed by putting dried chitin and acetic acid into a grinding machine for grinding (Ifuku et al., 2011). High-pressure system is also a commonly used for the fine treatment of fibers, and the diameter of treated fibers can reach nanometer level (Wu et al., 2014). Peng et al. successfully formed chitin nanowhiskers with a diameter of 10–50 nm and a length of about 800 nm using a high-pressure homogenization system (Peng et al., 2019). Salaberria et al. reported a friendly environmental method for processing chitin nanofibers using dynamic high-pressure homogenization (Salaberria et al., 2015).

TEMPO (2,2,6,6-tetramethylpiperidine-1-oxide)-mediated oxidation and partial deacetylation system enables ultrahigh length–diameter ratio features. The actual oxidant used in TEMPO/Co-oxidation system is nitrosonium ion and can be synthesized from TEMPO. Fan et al. extracted β-chitin from tubeworm by oxidation with TEMPO/NaClO/NaBr system and chitin nanofibers having a width of about 20–50 nm were obtained (Fan et al., 2009). TEMPO/NaClO/NaBr system oxidizes the chitin only under alkaline conditions. Pang et al. produced for the first time 5–10 nm sized chitin nanofibers using the TEMPO/$NaClO_2$/NaClO system under weakly acidic conditions (Pang et al., 2017). Chitin nanocrystals with a width of 6–15 nm by using the same system at pH 6.8 were prepared by Jiang et al. (2018). The yield of ChNCs can be as high as 90% by TEMPO-mediated oxidation, while the traditional acid hydrolysis method can only reach 60%.

The partial deacetylation method can be used as another method for αChNFs isolation. NaOH used as an agent for partial deacetylation influences the degree of N-acetylation. Partial deacetylation of chitin to obtain uniform anisotropic zwitterionic ChNCs by alkaline periodate oxidation was reported by Liu et al. (2021). Isolation of chitin from Omani shrimp shells by deacetylation with 50% NaOH was evaluated by Hoqani et al. (Said Al Hoqani et al., 2020). Optimization of chitin extraction procedure from shrimp waste using deacetylation method was examined by Pădureţu et al. (2019). Vázquez et al. optimized acetylation conditions by combining the enzymatic and chemical processes for high purity chitin and chitosan production from Illexargentinus pens (Vázquez et al., 2017).

1.3.3 Nanosilk isolation

The methods of producing nanosilk are still in their infancy compared to the isolation of nanocellulose and nanoscide. Silk nanofibrils (SNFs) were formed from the *B. mori* silk fibers with the developed formic acid/$CaCl_2$ solvent system by Zhang et al. (2014). Fabrication of

fibrils by shear-induced self-assembly of native silk proteins was examined by Greving et al. (2012). An effective, low-cost and eco-friendly method for preparing UV resistant silk fabric was developed by Cai et al. (2021). Mehdi et al. produced submicron silk particles by milling process. Nanosilk particles was produced from the silkfibers by applying bead milling. The effect of various processing parameters such as milling speed, milling time, bead load, and pH on particle size was investigated in a bead mill (Kazemimostaghim et al., 2013). Ling et al. reported ultrathin filtration membrane preparation from SNFs exfoliated from natural *B. mori* silk fibers. The appearance and characterization of the SNF dispersion and membranes were shown in Fig. 1.5 (Ling et al., 2016).

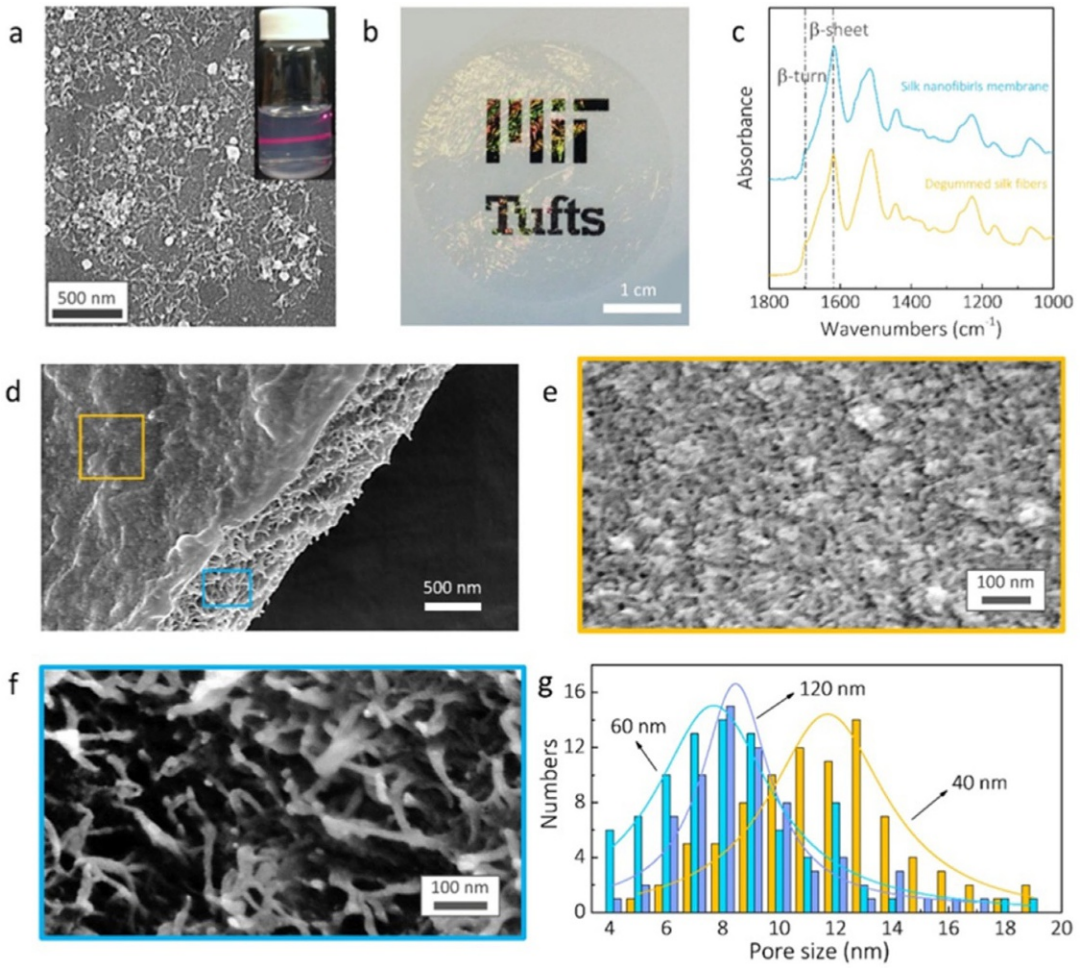

FIG. 1.5 Visual appearance and structural characterization of the SNF dispersion and membranes. (A) SEM image of SNFs (B) Image of SNF membrane (C) FTIR spectra of SNF membrane and degummed silk fibers. (D–F) SEM images of SNF membranes. (E) Top view and (F) cross-sectional SEM images of membranes, respectively. (G) Pore size distribution of the SNF membranes (thicknesses: 40, 60, and 120 nm) (Ling et al., 2016).

1.3.4 Nanostarch isolation

The interest in the production of nanomaterials from renewable sources increases with the increase of environmental awareness in the society. The past years have witnessed the isolation of so-called nanopolysaccharides from renewable materials such as cellulose, chitin, and starch. Lavoine et al. introduced a chapter emphasizing the different routes used to prepare nanopolysaccharides from cellulose, chitin, and starch (Lavoine et al., 2019). Nanostarch consists of two categories called starch nanocrystal (SNC) and starch nanoparticle (SNP), which show different crystallinity properties. Acid hydrolysis, where acids enter the amorphous region and break the glycosidic bonds, is the most useful method used to isolate nanostarch. In this method, crystal regions are preserved due to their compact structure. Until now, acids such as H_2SO_4, HNO_3, HCl, and H_3PO_4 have been used in the extraction process of nanostarch. Among these acids, HCl and HNO_3 have stronger hydrolysis ability than H_2SO_4 and H_3PO_4. Starch nanocrystals were obtained by aqueous suspension of waxy maize starch granules followed by hydrolysis with sulfuric acid (Angellier et al., 2005a). Xiao et al. produced broken rice starch nanoparticles in the 100, 200, 400, and 800 nm mean particle diameters by applying the H_2SO_4 hydrolysis method (Xiao et al., 2020). SNCs were produced from different sources (waxy maize starch, NWS; regular maize starch, NCS) by H_2SO_4 treatment (Wang et al., 2020).

Efficiency increases when acid hydrolysis is used in combination with physical/mechanical approaches. Kim et al. combined the acid hydrolysis with ultrasonication and reported the yield of starch nanoparticles (SNP's) as 15% for acid hydrolysis alone and 78% for the combined process. Fig. 1.6 shows FE-SEM images of starch nanoparticles produced by acid hydrolysis treatment at 4°C or 4/40°C for 6 days and then followed by ultrasonication application (Kim et al., 2013). Pineda and coworkers combined ultrasound application with acid hydrolysis treatment to obtain potato SNP's (Rodrigez Pineda, 2018).

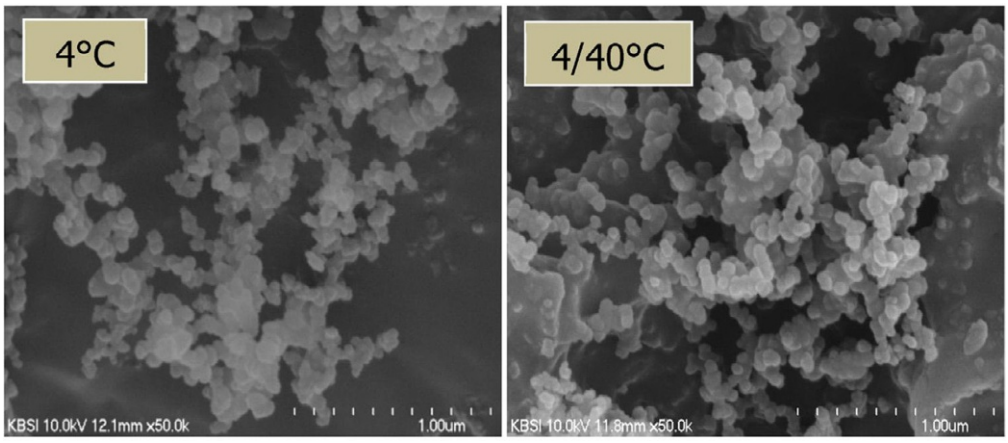

FIG. 1.6 FE-SEM images of starch nanoparticles (SNP's) (Kim et al., 2013).

After enzymatic pretreatment, acid hydrolysis of natural starch granules increases the rate of hydrolysis. Natural starch was used for the production of SNP's by recrystallizing linear glucans after debranching by hydrolysis with enzymatic way (David Chena et al., 2018).

SNP's are prepared by subjecting starch granules to mechanical and thermal processes such as high-pressure homogenization and reactive extrusion. In the extrusion technique, starch granules undergo significant structural changes under the influence of relatively high temperature, pressure, and shear forces. SNP's were prepared from corn starch, either by adding crosslinkers or by reactive extrusion without the addition (Song et al., 2011).

High-pressure homogenization causes partial or complete disruption of the crystal structure as in the case of ultrasonication. Ding and Kan used high-pressure homogenization as an effective method for SNP's production with an average size of 300 nm (Ding and Kan, 2017). Ahmad et al. reported a new fabrication method for "green" starch nanoparticles (SNP's) from local sago (*Metroxylon sagu*) starch granules by employing a high-pressure homogenization procedure (Ahmad et al., 2020).

Gamma irradiation is one of the methods used to reduce the size of starch. Ling and coworkers discussed the mechanism of enhancing dehydration performance based on particle size analysis (Ling et al., 2017, 2018).

Nano-sized starch particles were produced by the addition of organic solvents causing the starch dispersions to precipitate. Anti-solvent nanoprecipitation can be used for controlling nanoparticle properties such as size and morphology (Qin et al., 2016). Nanoprecipitation can be used in combination with other techniques to improve efficiency. Sana et al. investigated SNP's (corn starch) production by a solvent–antisolvent precipitation method using a spinning disc reactor (SDR) (Sana et al., 2019).

Nanoparticles from different biopolymers (starch, alginate, gelatine, chitosan, agar, etc.) can be produced by the electrospraying method. SNP's have been prepared from maize, amylose, and amylopectin with a size of 97 nm, 98 nm, and 113 nm, respectively. Nanoparticles produced by maize starch were developed by Ghaeb et al. (2015). Synthesis and modification approaches for starch nanoparticles were reviewed by Kumari and coworkers (Kumari et al., 2020).

1.3.5 Microbial nanobiopolymers

Microbial nanobiopolymers with excellent biocompatibility and biodegradability are interesting alternatives to petroleum-based polymers. Nanobiopolymers can be isolated from natural materials and can be synthesized directly from microorganisms. Biopolymers are produced by living organisms by means of enzymes.

Bacteria are used in the production of a diverse variety of biopolymers such as polyamides (amino acids linked by peptide bonds), polysaccharides (sugars or sugar acids linked by glycosidic bonds), polyphosphates (inorganic phosphates connected by anhydride bonds), and polyesters (hydroxyl fatty acids connected by ester bonds) (Ghosh et al., 2021). Microbial approaches, which have a short production cycle, are not restricted by climatic and geographic environments compared to chemical synthesis methods.

Microbial polysaccharides are a class of biopolymers and produced during metabolic processes by microorganisms such as bacteria, fungi, and blue-green algae. Microbial

polysaccharides are classified according to their biological functions as (a) intracellular storage polysaccharides (glycogen) (b) capsular polysaccharides closely linked to the cell surface (e.g., K30 O-Antigen) and (c) extracellular bacterial polysaccharides important for biofilm formation and pathogenicity (for example, xanthan, sphingan, alginate, cellulose, etc.). After secretion into the surrounding medium, they can be harvested from the cell-free culture supernatant in a continuous production process. There are 76 types of microorganisms that produce extracellular polysaccharides. Some of these polysaccharides are xanthan gum, gellan gum, welan gum, chitosan, trehalose, hyaluron, curdlan, dextran, pullulan, and bacterial cellulose, etc. (Schmid et al., 2015). An agitated or static fermentation process can be applied under suitable conditions to produce bacterial cellulose (BC). Microorganisms groups such as fungi, bacteria, and algae are used to synthesize BC. Bacterial cellulose produced by different *Komagataeibacter xylinus* strains was evaluated by Singhsa et al. (2018). Microbial polyhydroxyalkanoates (PHAs) are biopolyesters produced by microorganisms as intracellular granules under nutrient stress. Microbial synthesis occurs by converting carbon sources directly into PHA during fermentation (Muneer et al., 2020). Green synthesis of polyhydroxyalkanoatepolymer by *Bacillus iocasae* was performed by Ammar et al. (2021).

1.4 Environmental applications of nanobiopolymers

In recent years, nanobiopolymers have become an important subject for various research fields due to their features such as renewability, usability, and biocompatibility. Due to the high availability and renewable character of lignocellulosic biomass, research on nanocellulose is increasing day by day with the use of different cellulosic residues and wastes produced from agricultural and industrial activities (García et al., 2016).

Nanocellulose, which has a wide application potential, emerges as a new-generation bio-based adsorbent. The availability of various surface modifications in terms of functionality, surface charge density, processability, and reactivity increases the use of bio-based adsorbents for a broad family of pollutants. Nano-sized cellulose adsorbents offer many advantages over inorganic nanoparticles in terms of cost-effectiveness, sustainability, high aspect ratio, proper surface functionalization, and high adsorbent capacity. Because nanocellulose can be classified as a non-toxic material and 100% biodegradable, it makes them environmentally friendly adsorbent for bioremediation (Mahfoudhi and Boufi, 2017).

As an enzymatic synthesis of cellulose, bacterial cellulose (BC) was also used as an adsorbent for metal ions after surface modifications. Because the functionalization of the uncharged surface of nanofibres is often required to increase the adsorption capacity (Mahfoudhi and Boufi, 2017). Tamahkar et al. prepared Cibacron Blue F3GA-attached bacterial cellulose nanofibers for selective removal of Hg^{2+} with an adsorption capacity of 928 mg/g, while the Hg^{2+} adsorption capacity of unmodified bacterial cellulose nanofibers was 0.62 mg/g (Tamahkar et al., 2018). Derazshamshir et al. prepared molecularly imprinted bacterial cellulose nanofibers for selective and efficient removal of phenol from wastewaters, because phenols are toxic in the aquatic environment and lead to the death of aquatic organisms, and also carcinogenic to humans (Derazshamshir et al., 2020).

Nanocellulose, which is also used as an adsorbent for organic oils, was reported by Gu et al. (2020). They functionalized CNF with oleic acid (hydrophobic agent) and nano magnetite (Fe_3O_4). The adsorption capacities of the functionalized CNF towards ethyl acetate,

cyclohexane, and vacuum pump oil were 56.32, 68.06, and 33.24 g/g, accordingly. Luo et al. prepared a hybrid film. Firstly, celery cellulose nanofibrils (CCNF) were separated after oxalic acid hydrolysis followed by microfluidization. Then, lignin/hemicellulose solution containing CCNF was cast into film structures which showed a high methylene blue removal efficiency ranged from 192.1–429.9 mg/g (Luo et al., 2020).

Chitin is an important structural polysaccharide after cellulose and is the most abundant polymer in nature. Chitin and its derivatives used for environmental applications include the bioremediation of inorganic and organic pollutants from water and soil, as well as the bioconversion of chitinous waste into unicellular proteins, bioethanol, and biofertilizers (Singh et al., 2020).

Rajak et al. prepared a novel and eco-friendly chitin functionalized iron-enriched hydroxyapatite nanocomposite (HAP-Fe^0-Ct) which can be used for Cr (VI) removal from chromite ore processing residues (COPR) contaminated complex groundwater matrices (Rajak et al., 2021). COPR are real environmental threats leading to leaching of Cr (VI) into ground-water. Cr (VI) has proven to be carcinogenic.

Naeimi et al. modified nanochitosan, which is extracted from shrimp wastes, via Schiff base ligand. Then, graphene oxide was added to obtain a nanohybrid material to be a potential bioadsorbent for Pb(II) and Cu(II) biosorption from aqueous solutions (Naeimi et al., 2021). A reduction precipitation method was used to synthesize magnetic chitosan graphene oxide nanocomposites (EDTA-MCS/GO) for the removal of heavy metals, such as Pb^{2+}, Cu^{2+}, and As^{3+}, from aqueous solutions by Shahzad et al. (2017). Functionalized nanocellulose, chitosan, and other modified chitosan adsorbents are not only limited to heavy metal removal but also extended to a wide application in textile industries such as removal of dye (Faiz Norrrahim et al., 2021; Pal et al., 2021).

Carneiro et al. investigated the use of biopolymeric membranes prepared with chitosan (CS), alginate (AG), and a chitosan/alginate combination (CS/AG) for the adsorption of glyphosate, which is a non-selective herbicide, present in water samples. The alginate membrane was unable to adsorb the herbicide, while CS and CS/AG membranes presented an adsorption capacity of 10.88 mg/g, and 8.70 mg/g, respectively (Carneiro et al., 2015).

In another study, polypyrrole (PPy) nanosilk, nanowire array and nanorod array films were synthesized on carbon cloth substrate through electrochemical polymerization by Ki et al. The synthesized films were further applied in an efficient dual rotating disk photo fuel cell to treat real textile wastewater, which was also employed as fuel to be purified to generate electricity simultaneously with nanostructured PPy disks (Li et al., 2019). Several biopolymer adsorbents for various types of inorganic and organic pollutants were listed in Table 1.1 (Faiz Norrrahim et al., 2021; Pal et al., 2021).

1.5 Conclusion

Demand for renewable energy, renewable energy sources, and environmentally friendly materials is increasing day by day. In recent years, with the development of nanotechnology, the production and use of nanobiopolymers in different fields have become more important. Nanobiopolymers such as nanocellulose, nanochitin, nanosilk, and nanostarch are natural, non-toxic, low-cost, sustainable materials that can be produced from living organisms, with ease of modification and biocompatibility. How to create manufacturing techniques to

TABLE 1.1 Biopolymer adsorbents for various types of inorganic and organic pollutants.

Biopolymer adsorbent	Pollutants	Adsorption capacity (mg/g)	Ref.
BC–CB nanofibers	Hg^{2+}	928	Tamahkar et al. (2018)
BC-MIP nanofibers	Phenol	146	Derazshamshir et al. (2020)
Oleic acid and Fe_3O_4 functionalized CNF	Cyclohexane Ethyl acetate Vacuum pump oil	68 56 33	Gu et al. (2020)
CCNF	Methylene blue	192–430	Luo et al. (2020)
HAP-Fe^0-Ct	Cr(IV)	13.9 ± 0.46	Rajak et al. (2021)
Chit–Schiff–GO nanopolymer	Pb(II) Cu(II)	466 698.8	Naeimi et al. (2021)
EDTA-MCS/GO	Pb^{2+} Cu^{2+} As^{3+}	206.52 207.26 42.75	Shahzad et al. (2017)
Chitosan Chitosan/alginate membranes	Glyphosate	10.88 8.70	Carneiro et al. (2015)
Surfactant modified chitosan (SMCS) beads	Cd(II)	115	Pal and Pal (2017)
Chi-APTES	As(V)	2.576	Lalhmunsiama et al. (2016)

optimize these nanobiopolymers and how and where to use these nanobiopolymers to produce better materials are thought to be important in the future. Therefore, it is necessary to ensure the usability and feasibility of the final materials obtained by transitioning from laboratory studies to commercial or industrial production. Even though nanocellulose is a promising material for environmental remediation, until now, most research on its production has only been done on a laboratory scale. The challenges in nanocellulose production are scalability, environmental impact, and cost of treatment pathways. The biggest obstacle to environmental remediation that will affect the application and marketability of nanocellulose material may be economic problems arising from its toxicology. Generally, chemical, mechanical, and synthetic biological methods such as chemical and enzymatic treatment, acid hydrolysis, and different isolation are used in the production of nanobiopolymers. In this chapter, after giving information about nanobiopolymer types and production techniques, some studies on decontamination of environmental pollutants in the literature are summarized for nanobiopolymers.

1.6 Future outlook

In recent years, nanobiopolymers have become an important subject for various research fields due to their features such as renewability, usability, and biocompatibility.

Nanobiopolymers have demonstrated many advantages suited for environmental remediation in terms of heavy metal, dye, pesticide, herbicide, and organic oils removal. The main challenges are the energy consumption and yield in preparation, as well as the toxicity of the final product (Shak et al., 2018). As a result, it is thought that the use of natural, biocompatible, sustainable, low-cost, and non-toxic nanobiopolymers in different areas will expand and their applicability in wider areas will increase in the upcoming years. The discovery of cellulose nanomaterial is a milestone in materials science and engineering. Due to the high availability and renewable character of lignocellulosic biomass, research on nanocellulose will increase day by day with the use of different cellulosic residues and wastes produced from agricultural and industrial activities. Because renewable nanocellulose shows low toxicity and has a large surface area, and also it can be easily functionalized, these features make it a potential candidate for various applications, including optoelectronics, tissue regeneration, bio-based food packaging, and especially environmental applications such as wastewater and water treatment.

References

Abe, K., 2016. Nanofibrillation of dried pulp in NaOH solutions using bead milling. Cellulose 23 (2), 1257–1261. https://doi.org/10.1007/s10570-016-0891-4.

Ahmad, A.N., Lim, S.A., Navaranjan, N., Hsu, Y.I., Uyama, H., 2020. Green sago starch nanoparticles as reinforcing material for green composites. Polymer 202. https://doi.org/10.1016/j.polymer.2020.122646.

Ammar, E.M., El-Sheshtawy, H.S., El-Shatoury, E.H., Amer, S.K., 2021. Green synthesis of polyhydroxyalkanoate polymer by Bacillus iocasae. Polym. Int. https://doi.org/10.1002/pi.6219.

Angellier, H., Molina-Boisseau, S., Belgacem, M.N., Dufresne, A., 2005a. Surface chemical modification of waxy maize starch nanocrystals. Langmuir 21 (6), 2425–2433. https://doi.org/10.1021/la047530j.

Angellier, H., Molina-Boisseau, S., Lebrun, L., Dufresne, A., 2005b. Processing and structural properties of waxy maize starch nanocrystals reinforced natural rubber. Macromolecules 38 (9), 3783–3792. https://doi.org/10.1021/ma050054z.

Bai, L., Huan, S., Xiang, W., Rojas, O.J., 2018. Pickering emulsions by combining cellulose nanofibrils and nanocrystals: phase behavior and depletion stabilization. Green Chem. 20 (7), 1571–1582. https://doi.org/10.1039/c8gc00134k.

Balakrishnan, P., Sreekala, M.S., Kunaver, M., Huskić, M., Thomas, S., 2017. Morphology, transport characteristics and viscoelastic polymer chain confinement in nanocomposites based on thermoplastic potato starch and cellulose nanofibers from pineapple leaf. Carbohydr. Polym. 169, 176–188. https://doi.org/10.1016/j.carbpol.2017.04.017.

Bamba, Y., Ogawa, Y., Saito, T., Berglund, L.A., Isogai, A., 2017. Estimating the strength of single chitin nanofibrils via sonication-induced fragmentation. Biomacromolecules 18 (12), 4405–4410. https://doi.org/10.1021/acs.biomac.7b01467.

Berto, G.L., Mattos, B.D., Rojas, O.J., Arantes, V., 2021. Single-step fiber pretreatment with monocomponent endoglucanase: defibrillation energy and cellulose nanofibril quality. ACS Sustain. Chem. Eng. 9 (5), 2260–2270. https://doi.org/10.1021/acssuschemeng.0c08162.

Börjesson, M., Westman, G., 2015. Crystalline nanocellulose—preparation, modification, and properties. In: Cellulose – Fundamental Aspects and Current Trends. IntechOpen.

Cai, H., Gao, L., Chen, L., Chen, X., Liu, Z., Li, Z., Dai, F., 2021. An effective, low-cost and eco-friendly method for preparing UV resistant silk fabric. J. Nat. Fibers, 1–13. https://doi.org/10.1080/15440478.2021.1875362.

Carneiro, R.T.A., Taketa, T.B., Gomes Neto, R.J., Oliveira, J.L., Campos, E.V.R., de Moraes, M.A., da Silva, C.M.G., Beppu, M.M., Fraceto, L.F., 2015. Removal of glyphosate herbicide from water using biopolymer membranes. J. Environ. Manag. 151, 353–360. https://doi.org/10.1016/j.jenvman.2015.01.005.

Chen, Q., Yu, H., Wang, L., Ul Abdin, Z., Chen, Y., Wang, J., Zhou, W., Yang, X., Khan, R.U., Zhang, H., Chen, X., 2015. Recent progress in chemical modification of starch and its applications. RSC Adv. 5 (83), 67459–67474. https://doi.org/10.1039/c5ra10849g.

Chen, W., Yu, H., Lee, S.Y., Wei, T., Li, J., Fan, Z., 2018. Nanocellulose: a promising nanomaterial for advanced electrochemical energy storage. Chem. Soc. Rev. 47 (8), 2837–2872. https://doi.org/10.1039/c7cs00790f.

Chirayil, C.J., Joy, J., Mathew, L., Mozetic, M., Koetz, J., Thomas, S., 2014a. Isolation and characterization of cellulose nanofibrils from Helicteres isora plant. Ind. Crop. Prod. 59, 27–34. https://doi.org/10.1016/j.indcrop.2014.04.020.

Chirayil, C.J., Mathew, L., Thomas, S., 2014b. Review of recent research in nano cellulose preparation from different lignocellulosic fibers. Rev. Adv. Mater. Sci. 37 (1–2), 20–28. http://www.ipme.ru/e-journals/RAMS/no_13714/03_13714_cintil.pdf.

Chirila, T.V., Suzuki, S., Bray, L.J., Barnett, N.L., Harkin, D.G., 2013. Evaluation of silk sericin as a biomaterial: in vitro growth of human corneal limbal epithelial cells on *Bombyx mori* sericin membranes. Prog. Biomater. 14. https://doi.org/10.1186/2194-0517-2-14.

Chitbanyong, K., Pisutpiched, S., Khantayanuwong, S., Theeragool, G., Puangsin, B., 2020. TEMPO-oxidized cellulose nanofibril film from nano-structured bacterial cellulose derived from the recently developed thermotolerant Komagataeibacter xylinus C30 and Komagataeibacter oboediens R37–9 strains. Int. J. Biol. Macromol. 163, 1908–1914. https://doi.org/10.1016/j.ijbiomac.2020.09.124.

Crini, G., 2005. Recent developments in polysaccharide-based materials used as adsorbents in wastewater treatment. Prog. Polym. Sci. 30 (1), 38–70. https://doi.org/10.1016/j.progpolymsci.2004.11.002.

David Chena, A., Evžen, Š., Pavel, U., Eva, M., 2018. Starch nanoparticles – two ways of their preparation. Czech J. Food Sci., 133–138. https://doi.org/10.17221/371/2017-cjfs.

de Oliveira, J.P., Bruni, G.P., el Halal, S.L.M., Bertoldi, F.C., Dias, A.R.G., Zavareze, E.D.R., 2019. Cellulose nanocrystals from rice and oat husks and their application in aerogels for food packaging. Int. J. Biol. Macromol. 124, 175–184. https://doi.org/10.1016/j.ijbiomac.2018.11.205.

Derazshamshir, A., Göktürk, I., Tamahkar, E., Yılmaz, F., Sağlam, N., Denizli, A., 2020. Phenol removal from wastewater by surface imprinted bacterial cellulose nanofibres. Environ. Technol. 41 (24), 3134–3145. https://doi.org/10.1080/09593330.2019.1600043.

Ding, Y., Kan, J., 2017. Optimization and characterization of high pressure homogenization produced chemically modified starch nanoparticles. J. Food Sci. Technol. 54 (13), 4501–4509. https://doi.org/10.1007/s13197-017-2934-8.

Duan, Y., Chen, X., Shao, Z.Z., 2018. The silk textile embedded in silk fibroin composite: preparation and properties. Chin. J. Polym. Sci. 36 (9), 1043–1046. https://doi.org/10.1007/s10118-018-2117-8.

Dufresne, A., 2006. Comparing the mechanical properties of high performances polymer nanocomposites from biological sources. J. Nanosci. Nanotechnol. 6 (2), 322–330. https://doi.org/10.1166/jnn.2006.906.

Dufresne, A., 2017. Nanocellulose: From Nature to High Performance Tailored Materials. De Gruyter.

Facchine, E.G., Bai, L., Rojas, O.J., Khan, S.A., 2021. Associative structures formed from cellulose nanofibrils and nanochitins are pH-responsive and exhibit tunable rheology. J. Colloid Interface Sci. 588, 232–241. https://doi.org/10.1016/j.jcis.2020.12.041.

Faiz Norrrahim, M.N., Mohd Kasim, N.A., Knight, V.F., Mohamad Misenan, M.S., Janudin, N., Ahmad Shah, N.A., Kasim, N., Wan Yusoff, W.Y., Mohd Noor, S.A., Jamal, S.H., Ong, K.K., Zin Wan Yunus, W.M., 2021. Nanocellulose: a bioadsorbent for chemical contaminant remediation. RSC Adv. 11 (13), 7347–7368. https://doi.org/10.1039/d0ra08005e.

Fan, Y., Saito, T., Isogai, A., 2009. TEMPO-mediated oxidation of β-chitin to prepare individual nanofibrils. Carbohydr. Polym. 77 (4), 832–838. https://doi.org/10.1016/j.carbpol.2009.03.008.

Fang, F.Z., Zhang, X.D., Gao, W., Guo, Y.B., Byrne, G., Hansen, H.N., 2017. Nanomanufacturing—perspective and applications. CIRP Ann. 66 (2), 683–705. https://doi.org/10.1016/j.cirp.2017.05.004.

Faria, R.R., Guerra, R.F., De Sousa Neto, L.R., Motta, L.F., Franca, E.D.F., 2016. Computational study of polymorphic structures of α- and β-chitin and chitosan in aqueous solution. J. Mol. Graph. Model. 63, 78–84. https://doi.org/10.1016/j.jmgm.2015.11.001.

Fathi, H.I., El-Shazly, A.H., El-Kady, M.F., Madih, K., 2018. Assessment of new technique for production cellulose nanocrystals from agricultural waste. Mater. Sci. Forum 928, 83–88. https://doi.org/10.4028/www.scientific.net/MSF.928.83.

Fei, X., Jia, M., Du, X., Yang, Y., Zhang, R., Shao, Z., Zhao, X., Chen, X., 2013. Green synthesis of silk fibroin-silver nanoparticle composites with effective antibacterial and biofilm-disrupting properties. Biomacromolecules 14 (12), 4483–4488. https://doi.org/10.1021/bm4014149.

Flauzino Neto, W.P., Silvério, H.A., Dantas, N.O., Pasquini, D., 2013. Extraction and characterization of cellulose nanocrystals from agro-industrial residue – soy hulls. Ind. Crop. Prod. 42 (1), 480–488. https://doi.org/10.1016/j.indcrop.2012.06.041.

García, A., Gandini, A., Labidi, J., Belgacem, N., Bras, J., 2016. Industrial and crop wastes: a new source for nanocellulose biorefinery. Ind. Crop. Prod. 93, 26–38. https://doi.org/10.1016/j.indcrop.2016.06.004.

Gatenholm, P., Berry, J., Rojas, A., Sano, M.B., Davalos, R.V., Johnson, K., O'Rourke, L., 2016. Bacterial nanocellulose biomaterials with controlled architecture for tissue engineering scaffolds and customizable implants. In: Bacterial NanoCellulose: A Sophisticated Multifunctional Material. CRC Press, pp. 197–216. https://www.crcpress.com/Bacterial-NanoCellulose-A-Sophisticated-Multifunctional-Material/Gama-Gatenholm-Klemm/p/book/9781138073166.

Ghaeb, M., Tavanai, H., Kadivar, M., 2015. Electrosprayed maize starch and its constituents (amylose and amylopectin) nanoparticles. Polym. Adv. Technol. 26 (8), 917–923. https://doi.org/10.1002/pat.3501.

Ghosh, S., Lahiri, D., Nag, M., Dey, A., Sarkar, T., Pathak, S.K., Edinur, H.A., Pati, S., Ray, R.R., 2021. Bacterial biopolymer: its role in pathogenesis to effective biomaterials. Polymers 13 (8). https://doi.org/10.3390/polym13081242.

Giesa, T., Pugno, N.M., Wong, J.Y., Kaplan, D.L., Buehler, M.J., 2014. What's inside the box? – length-scales that govern fracture processes of polymer fibers. Adv. Mater. 26 (3), 412–417. https://doi.org/10.1002/adma.201303323.

Gopi, S., Kargl, R., Kleinschek, K.S., Pius, A., Thomas, S., 2018. Chitin nanowhisker – inspired electrospun PVDF membrane for enhanced oil-water separation. J. Environ. Manag. 228, 249–259. https://doi.org/10.1016/j.jenvman.2018.09.039.

Greving, I., Cai, M., Vollrath, F., Schniepp, H.C., 2012. Shear-induced self-assembly of native silk proteins into fibrils studied by atomic force microscopy. Biomacromolecules 13 (3), 676–682. https://doi.org/10.1021/bm201509b.

Gu, H., Zhou, X., Lyu, S., Pan, D., Dong, M., Wu, S., Ding, T., Wei, X., Seok, I., Wei, S., Guo, Z., 2020. Magnetic nanocellulose-magnetite aerogel for easy oil adsorption. J. Colloid Interface Sci. 560, 849–856. https://doi.org/10.1016/j.jcis.2019.10.084.

Hassan, M.E., Bai, J., Dou, D.Q., 2019. Biopolymers; definition, classification and applications. Egypt. J. Chem. 62 (9), 1725–1737. https://doi.org/10.21608/EJCHEM.2019.6967.1580.

Hayashi, C.Y., Shipley, N.H., Lewis, R.V., 1999. Hypotheses that correlate the sequence, structure, and mechanical properties of spider silk proteins. Int. J. Biol. Macromol. 24 (2–3), 271–275. https://doi.org/10.1016/S0141-8130(98)00089-0.

Heinze, T., 2015. Cellulose: structure and properties. Adv. Polym. Sci. 271, 1–52. https://doi.org/10.1007/12_2015_319.

Hemmati, F., Jafari, S.M., Kashaninejad, M., Barani Motlagh, M., 2018. Synthesis and characterization of cellulose nanocrystals derived from walnut shell agricultural residues. Int. J. Biol. Macromol. 120, 1216–1224. https://doi.org/10.1016/j.ijbiomac.2018.09.012.

Hideno, A., Abe, K., Uchimura, H., Yano, H., 2016. Preparation by combined enzymatic and mechanical treatment and characterization of nanofibrillated cotton fibers. Cellulose 23 (6), 3639–3651. https://doi.org/10.1007/s10570-016-1075-y.

Huang, Y., Yao, M., Zheng, X., Liang, X., Su, X., Zhang, Y., Lu, A., Zhang, L., 2015. Effects of chitin whiskers on physical properties and osteoblast culture of alginate based nanocomposite hydrogels. Biomacromolecules 16 (11), 3499–3507. https://doi.org/10.1021/acs.biomac.5b00928.

Ifuku, S., Nomura, R., Morimoto, M., Saimoto, H., 2011. Preparation of chitin nanofibers from mushrooms. Materials 4 (8), 1417–1425. https://doi.org/10.3390/ma4081417.

Ilyas, H.N., Zia, K.M., Rehman, S., Ilyas, R., Sultana, S., 2021. Utilization of shellfish industrial waste for isolation, purification, and characterizations of chitin from Crustacean's sources in Pakistan. J. Polym. Environ. https://doi.org/10.1007/s10924-020-02037-7.

Jancar, J., Douglas, J.F., Starr, F.W., Kumar, S.K., Cassagnau, P., Lesser, A.J., Sternstein, S.S., Buehler, M.J., 2010. Current issues in research on structure-property relationships in polymer nanocomposites. Polymer 51 (15), 3321–3343. https://doi.org/10.1016/j.polymer.2010.04.074.

Jiang, J., Yu, J., Liu, L., Wang, Z., Fan, Y., Satio, T., Isogai, A., 2018. Preparation and hydrogel properties of pH-sensitive amphoteric chitin nanocrystals. J. Agric. Food Chem. 66 (43), 11372–11379. https://doi.org/10.1021/acs.jafc.8b02899.

Jung, H.S., Kim, M.H., Park, W.H., 2019. Preparation and structural investigation of novel β-chitin nanocrystals from cuttlefish bone. ACS Biomater. Sci. Eng. 5 (4), 1744–1752. https://doi.org/10.1021/acsbiomaterials.8b01652.

Kandhola, G., Djioleu, A., Rajan, K., Labbé, N., Sakon, J., Carrier, D.J., Kim, J.W., 2020. Maximizing production of cellulose nanocrystals and nanofibers from pre-extracted loblolly pine Kraft pulp: a response surface approach. Bioresour. Bioprocess. 7 (1). https://doi.org/10.1186/s40643-020-00302-0.

Kargarzadeh, H., Mariano, M., Huang, J., Lin, N., Ahmad, I., Dufresne, A., Thomas, S., 2017. Recent developments on nanocellulose reinforced polymer nanocomposites: a review. Polymer 132, 368–393. https://doi.org/10.1016/j.polymer.2017.09.043.

Kazemimostaghim, M., Rajkhowa, R., Tsuzuki, T., Wang, X., 2013. Production of submicron silk particles by milling. Powder Technol. 241, 230–235. https://doi.org/10.1016/j.powtec.2013.03.004.

Keten, S., Buehler, M.J., 2010. Nanostructure and molecular mechanics of spider dragline silk protein assemblies. J. R. Soc. Interface 7 (53), 1709–1721. https://doi.org/10.1098/rsif.2010.0149.

Keten, S., Xu, Z., Ihle, B., Buehler, M.J., 2010. Nanoconfinement controls stiffness, strength and mechanical toughness of B-sheet crystals in silk. Nat. Mater. 9 (4), 359–367. https://doi.org/10.1038/nmat2704.

Khan, T., Abbas, S., Fariq, A., Yasmin, A., 2018. Microbes: nature's cell factories of nanoparticles synthesis. In: Nanotechnology in the Life Sciences. Springer Science and Business Media B.V, pp. 25–50, https://doi.org/10.1007/978-3-319-99570-0_2.

Kim, H.Y., Park, D.J., Kim, J.Y., Lim, S.T., 2013. Preparation of crystalline starch nanoparticles using cold acid hydrolysis and ultrasonication. Carbohydr. Polym. 98 (1), 295–301. https://doi.org/10.1016/j.carbpol.2013.05.085.

Klemm, D., Kramer, F., Moritz, S., Lindstroem, T., Ankerfors, M., Gray, D., Dorris, A., 2011. ChemInform abstract: nanocelluloses: a new family of nature-based materials. ChemInform 42 (38). https://doi.org/10.1002/chin.201138271.

Kumar, P., Sandeep, K., Alavi, S., Truong, V., 2010. A review of experimental and modeling techniques to determine properties of biopolymer-based nanocomposites. J. Food Sci. 76 (1), E2–E14.

Kumari, S., Yadav, B.S., Yadav, R.B., 2020. Synthesis and modification approaches for starch nanoparticles for their emerging food industrial applications: a review. Food Res. Int. 128. https://doi.org/10.1016/j.foodres.2019.108765.

Kundu, B., Rajkhowa, R., Kundu, S.C., Wang, X., 2013. Silk fibroin biomaterials for tissue regenerations. Adv. Drug Deliv. Rev. 65 (4), 457–470. https://doi.org/10.1016/j.addr.2012.09.043.

Lalhmunsiama, Lee, S.M., Lalchhingpuii, Tiwari, D., 2016. Functionalized hybrid material precursor to chitosan in the efficient remediation of aqueous solutions contaminated with As(V). J. Environ. Chem. Eng. 4 (2), 1537–1544. https://doi.org/10.1016/j.jece.2016.02.015.

Lavoine, N., Durmaz, E., Trovagunta, R., 2019. Preparation and Properties of Nanopolysaccharides. Springer Science and Business Media LLC, pp. 1–54, https://doi.org/10.1007/978-981-15-0913-1_1.

Li, X., Xu, H., Chen, Z.-S., Chen, G., 2011. Biosynthesis of nanoparticles by microorganisms and their applications. J. Nanomater., 1–16. https://doi.org/10.1155/2011/270974.

Li, K., Zhang, H., Ma, Y., Sun, T., Jia, J., 2019. Nanostructured polypyrrole cathode based dual rotating disk photo fuel cell for textile wastewater purification and electricity generation. Electrochim. Acta 303, 329–340. https://doi.org/10.1016/j.electacta.2019.02.102.

Lindström, T., Aulin, C., Naderi, A., Ankerfors, M., 2014. Microfibrillated Cellulose. Wiley, pp. 1–34, https://doi.org/10.1002/0471440264.pst614.

Ling, S., Jin, K., Kaplan, D.L., Buehler, M.J., 2016. Ultrathin free-standing bombyx mori silk nanofibril membranes. Nano Lett. 16 (6), 3795–3800. https://doi.org/10.1021/acs.nanolett.6b01195.

Ling, S., Qin, Z., Huang, W., Cao, S., Kaplan, D.L., Buehler, M.J., 2017. Design and function of biomimetic multilayer water purification membranes. Sci. Adv. 3 (4). https://doi.org/10.1126/sciadv.1601939.

Ling, S., Wang, Q., Zhang, D., Zhang, Y., Mu, X., Kaplan, D.L., Buehler, M.J., 2018. Integration of stiff graphene and tough silk for the design and fabrication of versatile electronic materials. Adv. Funct. Mater. 28 (9). https://doi.org/10.1002/adfm.201705291.

Liu, P., Liu, H., Schäfer, T., Gutmann, T., Gibhardt, H., Qi, H., Tian, L., Zhang, X.C., Buntkowsky, G., Zhang, K., 2021. Unexpected selective alkaline periodate oxidation of chitin for the isolation of chitin nanocrystals. Green Chem. 23 (2), 745–751. https://doi.org/10.1039/d0gc04054a.

Lu, Y., Sun, Q., She, X., Xia, Y., Liu, Y., Li, J., Yang, D., 2013. Fabrication and characterisation of α-chitin nanofibers and highly transparent chitin films by pulsed ultrasonication. Carbohydr. Polym. 98 (2), 1497–1504. https://doi.org/10.1016/j.carbpol.2013.07.038.

Luo, J., Huang, K., Zhou, X., Xu, Y., 2020. Hybrid films based on holistic celery nanocellulose and lignin/hemicellulose with enhanced mechanical properties and dye removal. Int. J. Biol. Macromol. 147, 699–705. https://doi.org/10.1016/j.ijbiomac.2020.01.102.

Mahfoudhi, N., Boufi, S., 2017. Nanocellulose as a novel nanostructured adsorbent for environmental remediation: a review. Cellulose 24 (3), 1171–1197. https://doi.org/10.1007/s10570-017-1194-0.

Melke, J., Midha, S., Ghosh, S., Ito, K., Hofmann, S., 2016. Silk fibroin as biomaterial for bone tissue engineering. Acta Biomater. 31, 1–16. https://doi.org/10.1016/j.actbio.2015.09.005.

Missoum, K., Belgacem, M., Bras, J. (2013). Nanofibrillated cellulose surface modification. A review. Materials 6(5), 1745–1766.

Moon, R.J., Martini, A., Nairn, J., Simonsen, J., Youngblood, J., 2011. Cellulose nanomaterials review: structure, properties and nanocomposites. Chem. Soc. Rev. 3941. https://doi.org/10.1039/c0cs00108b.

Morin-Crini, N., Lichtfouse, E., Torri, G., Crini, G. 2019. Applications of chitosan in food, pharmaceuticals, medicine, cosmetics, agriculture, textiles, pulp and paper, biotechnology, and environmental chemistry. Environ. Chem. Lett. 17, 1667–1692. https://doi.org/10.1007/s10311-019-00904-x.

Muneer, F., Rasul, I., Azeem, F., Siddique, M.H., Zubair, M., Nadeem, H., 2020. Microbial polyhydroxyalkanoates (PHAs): efficient replacement of synthetic polymers. J. Polym. Environ. 28 (9), 2301–2323. https://doi.org/10.1007/s10924-020-01772-1.

Naeimi, A., Amini, M., Okati, N., 2021. Removal of heavy metals from wastewaters using an effective and natural bionanopolymer based on Schiff base chitosan/graphene oxide. Int. J. Environ. Sci. Technol. https://doi.org/10.1007/s13762-021-03247-9.

Naleway, S.E., Porter, M.M., McKittrick, J., Meyers, M.A., 2015. Structural design elements in biological materials: application to bioinspiration. Adv. Mater. 27 (37), 5455–5476. https://doi.org/10.1002/adma.201502403.

Narkevicius, A., Steiner, L.M., Parker, R.M., Ogawa, Y., Frka-Petesic, B., Vignolini, S., 2019. Controlling the self-assembly behavior of aqueous chitin nanocrystal suspensions. Biomacromolecules 20 (7), 2830–2838. https://doi.org/10.1021/acs.biomac.9b00589.

Nascimento, P., Marim, R., Carvalho, G., Mali, S., 2016. Nanocellulose produced from rice hulls and its effect on the properties of biodegradable starch films. Mater. Res. 19 (1), 167–174. https://doi.org/10.1590/1980-5373-MR-2015-0423.

Olatunji, O., 2015. Classification of natural polymers. In: Natural Polymers: Industry Techniques and Applications. Springer International Publishing, pp. 1–17, https://doi.org/10.1007/978-3-319-26414-1_1.

Omenetto, F.G., Kaplan, D.L., 2010. New opportunities for an ancient material. Science 329 (5991), 528–531. https://doi.org/10.1126/science.1188936.

Pădureț u, C.C., Isopescu, R.D., Gîjiu, C.L., Rău, I., Apetroaei, M.R., Schröder, V., 2019. Optimization of chitin extraction procedure from shrimp waste using Taguchi method and chitosan characterization. Mol. Cryst. Liq. Cryst. 695 (1), 19–28. https://doi.org/10.1080/15421406.2020.1723902.

Pal, P., Pal, A., 2017. Surfactant-modified chitosan beads for cadmium ion adsorption. Int. J. Biol. Macromol. 104, 1548–1555. https://doi.org/10.1016/j.ijbiomac.2017.02.042.

Pal, P., Pal, A., Nakashima, K., Yadav, B.K., 2021. Applications of chitosan in environmental remediation: a review. Chemosphere 266, 128934. https://doi.org/10.1016/j.chemosphere.2020.128934.

Pang, K., Ding, B., Liu, X., Wu, H., Duan, Y., Zhang, J., 2017. High-yield preparation of a zwitterionically charged chitin nanofiber and its application in a doubly pH-responsive pickering emulsion. Green Chem. 19 (15), 3665–3670. https://doi.org/10.1039/c7gc01592e.

Peng, C., Xu, J., Chen, G., Tian, J., He, M., 2019. The preparation of α-chitin nanowhiskers-poly (vinyl alcohol) hydrogels for drug release. Int. J. Biol. Macromol. 131, 336–342. https://doi.org/10.1016/j.ijbiomac.2019.03.015.

Prabaharan, M., 2012. Advantages of chitosan as drug delivery sistems. In: Chitosan and Its Derivatives as Promisng Drug Delivery Carriers. ASME Press, pp. 4–8.

Prasad Reddy, J., Rhim, J.W., 2014. Isolation and characterization of cellulose nanocrystals from garlic skin. Mater. Lett. 129, 20–23. https://doi.org/10.1016/j.matlet.2014.05.019.

Prasad, R., Pandey, R., Barman, I., 2016. Engineering tailored nanoparticles with microbes: quo vadis? Wiley Interdiscip. Rev. Nanomed. Nanobiotechnol. 8 (2), 316–330. https://doi.org/10.1002/wnan.1363.

Putaux, J.L., Molina-Boisseau, S., Momaur, T., Dufresne, A., 2003. Platelet nanocrystals resulting from the disruption of waxy maize starch granules by acid hydrolysis. Biomacromolecules 4 (5), 1198–1202. https://doi.org/10.1021/bm0340422.

Qin, Y., Liu, C., Jiang, S., Xiong, L., Sun, Q., 2016. Characterization of starch nanoparticles prepared by nanoprecipitation: influence of amylose content and starch type. Ind. Crop. Prod. 87, 182–190. https://doi.org/10.1016/j.indcrop.2016.04.038.

Raabe, D., Romano, P., Sachs, C., Fabritius, H., Al-Sawalmih, A., Yi, S.B., Servos, G., Hartwig, H.G., 2006. Microstructure and crystallographic texture of the chitin-protein network in the biological composite material of the exoskeleton of the lobster Homarus americanus. Mater. Sci. Eng. A 421 (1–2), 143–153. https://doi.org/10.1016/j.msea.2005.09.115.

Rajak, J.K., Khandelwal, N., Behera, M.P., Tiwari, E., Singh, N., Ganie, Z.A., Darbha, G.K., Abdolahpur Monikh, F., Schäfer, T., 2021. Removal of chromate ions from leachate-contaminated groundwater samples of Khan Chandpur, India, using chitin modified iron-enriched hydroxyapatite nanocomposite. Environ. Sci. Pollut. Res. https://doi.org/10.1007/s11356-021-13549-7.

Rashid, S., Dutta, H., 2020. Characterization of nanocellulose extracted from short, medium and long grain rice husks. Ind. Crop. Prod. 154, 112627. https://doi.org/10.1016/j.indcrop.2020.112627.

Rizzi, G.P., 2004. Role of phosphate and carboxylate ions in maillard browning. J. Agric. Food Chem. 52 (4), 953–957. https://doi.org/10.1021/jf030691t.

Rodrigez Pineda, L., 2018. Preparation and characterization of potato starch nanoparticles with acrylamide by microwave radiation. Cien. Desarrollo 9 (2), 149–159.

Safari, J., Sadeghi, M., 2017. Nanostarch: a novel and green catalyst for synthesis of 2-aminothiazoles. Monatsh. Chem. 148 (4), 745–749. https://doi.org/10.1007/s00706-016-1805-8.

Sahana, T.G., Rekha, P.D., 2018. Biopolymers: applications in wound healing and skin tissue engineering. Mol. Biol. Rep. 45 (6), 2857–2867. https://doi.org/10.1007/s11033-018-4296-3.

Said Al Hoqani, H.A., Al-Shaqsi, N., Hossain, M.A., Al Sibani, M.A., 2020. Isolation and optimization of the method for industrial production of chitin and chitosan from Omani shrimp shell. Carbohydr. Res. 492. https://doi.org/10.1016/j.carres.2020.108001.

Sakabe, H., Ito, H., Miyamoto, T., Noishiki, Y., Ha, W.S., 1989. In vivo blood compatibility of regenerated silk fibroin. Sen'i Gakkaishi 45 (11), 487–490. https://doi.org/10.2115/fiber.45.11_487.

Salaberria, A.M., Labidi, J., Fernandes, S.C.M., 2014. Chitin nanocrystals and nanofibers as nano-sized fillers into thermoplastic starch-based biocomposites processed by melt-mixing. Chem. Eng. J. 256, 356–364. https://doi.org/10.1016/j.cej.2014.07.009.

Salaberria, A.M., Fernandes, S.C.M., Diaz, R.H., Labidi, J., 2015. Processing of α-chitin nanofibers by dynamic high pressure homogenization: characterization and antifungal activity against *A. niger*. Carbohydr. Polym. 116, 286–291. https://doi.org/10.1016/j.carbpol.2014.04.047.

Sana, S., Boodhoo, K., Zivkovic, V., 2019. Production of starch nanoparticles through solvent-antisolvent precipitation in a spinning disc reactor. Green Process. Synth. 8 (1), 507–515. https://doi.org/10.1515/gps-2019-0019.

Schmid, J., Sieber, V., Rehm, B., 2015. Bacterial exopolysaccharides: biosynthesis pathways and engineering strategies. Front. Microbiol. 6 (May). https://doi.org/10.3389/fmicb.2015.00496.

Shaabani, A., Rahmati, A., Badri, Z., 2008. Sulfonated cellulose and starch: new biodegradable and renewable solid acid catalysts for efficient synthesis of quinolines. Catal. Commun. 9 (1), 13–16. https://doi.org/10.1016/j.catcom.2007.05.021.

Shahzad, A., Miran, W., Rasool, K., Nawaz, M., Jang, J., Lim, S.R., Lee, D.S., 2017. Heavy metals removal by EDTA-functionalized chitosan graphene oxide nanocomposites. RSC Adv. 7 (16), 9764–9771. https://doi.org/10.1039/c6ra28406j.

Shak, K.P.Y., Pang, Y.L., Mah, S.K., 2018. Nanocellulose: recent advances and its prospects in environmental remediation. Beilstein J. Nanotechnol. 9 (1), 2479–2498. https://doi.org/10.3762/bjnano.9.232.

Shen, X., Shamshina, J.L., Berton, P., Gurau, G., Rogers, R.D., 2016. Hydrogels based on cellulose and chitin: fabrication, properties, and applications. Green Chem., 53–75. https://doi.org/10.1039/C5GC02396C.

Singh, R., Upadhyay, S.K., Singh, M., Sharma, I., Sharma, P., Kamboj, P., Saini, A., Voraha, R., Sharma, A.K., Upadhyay, T.K., Khan, F., 2020. Chitin, chitinases and chitin derivatives in biopharmaceutical, agricultural and environmental perspective. Biointerface Res. Appl. Chem. 11 (3), 9985–10005. https://doi.org/10.33263/BRIAC113.998510005.

Singhsa, P., Narain, R., Manuspiya, H., 2018. Physical structure variations of bacterial cellulose produced by different Komagataeibacter xylinus strains and carbon sources in static and agitated conditions. Cellulose 25 (3), 1571–1581. https://doi.org/10.1007/s10570-018-1699-1.

Song, D., Thio, Y.S., Deng, Y., 2011. Starch nanoparticle formation via reactive extrusion and related mechanism study. Carbohydr. Polym. 85 (1), 208–214. https://doi.org/10.1016/j.carbpol.2011.02.016.

Sriupayo, J., Supaphol, P., Blackwell, J., Rujiravanit, R., 2005. Preparation and characterization of α-chitin whisker-reinforced chitosan nanocomposite films with or without heat treatment. Carbohydr. Polym. 62 (2), 130–136. https://doi.org/10.1016/j.carbpol.2005.07.013.

Suortti, T., Gorenstein, M.V., Roger, P., 1998. Determination of the molecular mass of amylose. J. Chromatogr. A 828 (1–2), 515–521. https://doi.org/10.1016/S0021-9673(98)00831-0.

Taer, E., Febriyanti, F., Mustika, W.S., Taslim, R., Agustino, A., Apriwandi, A., 2020. Enhancing the performance of supercapacitor electrode from chemical activation of carbon nanofibers derived *Areca catechu* husk via one-stage integrated pyrolysis. Carbon Lett. https://doi.org/10.1007/s42823-020-00191-5.

Tamahkar, E., Türkmen, D., Akgönüllü, S., Qureshi, T., Denizli, A., 2018. Bacterial cellulose nanofibers for efficient removal of Hg 2+ from aqueous solutions. In: Nanotechnology for Sustainable Water Resources. Wiley Blackwell, pp. 501–522, https://doi.org/10.1002/9781119323655.ch16.

Tan, I., Flanagan, B.M., Halley, P.J., Whittaker, A.K., Gidley, M.J., 2007. A method for estimating the nature and relative proportions of amorphous, single, and doubled-helical components in starch granules by 13C CP/MAS NMR. Biomacromolecules 8 (3), 885–891. https://doi.org/10.1021/bm060988a.

Torres, F.G., Troncoso, O.P., Pisani, A., Gatto, F., Bardi, G., 2019. Natural polysaccharide nanomaterials: an overview of their immunological properties. Int. J. Mol. Sci. 20 (20). https://doi.org/10.3390/ijms20205092.

Trache, D., Thakur, V.K., Boukherroub, R., 2020. Cellulose nanocrystals/graphene hybrids—a promising new class of materials for advanced applications. Nano 10, 1523.

Vamadevan, V., Blennow, A., Buléon, A., Goldstein, A., Bertoft, E., 2018. Distinct properties and structures among B-crystalline starch granules. Starch-Stärke 70 (3–4), 1700240. https://doi.org/10.1002/star.201700240.

Vázquez, J.A., Noriega, D., Ramos, P., Valcarcel, J., Novoa-Carballal, R., Pastrana, L., Reis, R.L., Pérez-Martín, R.I., 2017. Optimization of high purity chitin and chitosan production from *Illex argentinus* pens by a combination of enzymatic and chemical processes. Carbohydr. Polym. 174, 262–272. https://doi.org/10.1016/j.carbpol.2017.06.070.

Vepari, C., Kaplan, D.L., 2007. Silk as a biomaterial. Prog. Polym. Sci. 32 (8–9), 991–1007. https://doi.org/10.1016/j.progpolymsci.2007.05.013.

Wang, Q., Chen, S., Chen, D., 2017. Preparation and characterization of chitosan based injectable hydrogels enhanced by chitin nano-whiskers. J. Mech. Behav. Biomed. Mater. 65, 466–477. https://doi.org/10.1016/j.jmbbm.2016.09.009.

Wang, K., Hong, Y., Gu, Z., Cheng, L., Li, Z., Li, C. (2020). Stabilization of Pickering emulsions using starch nanocrystals treated with alkaline solution. Int. J. Biol. Macromol. 155, 273–285.

Whitesides, G.M., 2005. Nanoscience, nanotechnology, and chemistry. Small 1 (2), 172–179. https://doi.org/10.1002/smll.200400130.

Wu, J., Zhang, K., Girouard, N., Meredith, J.C., 2014. Facile route to produce chitin nanofibers as precursors for flexible and transparent gas barrier materials. Biomacromolecules 15 (12), 4614–4620. https://doi.org/10.1021/bm501416q.

Xiao, H., Yang, F., Lin, Q., Zhang, Q., Zhang, L., Sun, S., Han, W., Liu, G.Q., 2020. Preparation and characterization of broken-rice starch nanoparticles with different sizes. Int. J. Biol. Macromol. 160, 437–445. https://doi.org/10.1016/j.ijbiomac.2020.05.182.

Yang, N., Zhang, W., Ye, C., Chen, X., Ling, S., 2019. Nanobiopolymers fabrication and their life cycle assessments. Biotechnol. J. 14 (1). https://doi.org/10.1002/biot.201700754.

Yang, T., Qi, H., Liu, P., Zhang, K., 2020b. Selective isolation methods for cellulose and chitin nanocrystals. ChemPlusChem 85 (5), 1081–1088.

Zaoming, W., Codina, R., Fernandezcaldas, E., Lockey, R., Bukanz, S., 1996. 109 partial characterization of the silk allergens in mulberry silk extract. J. Allergy Clin. Immunol., 210. https://doi.org/10.1016/s0091-6749(96)80327-7.

Zarnegar, Z., Monjezi, H.R., Safari, J., 2019. Arginine-based surface modification of nanostarch, a catalytic carbohydrates in synthesis of heteroaryl sulfides. J. Mol. Struct. 1193, 14–23. https://doi.org/10.1016/j.molstruc.2019.05.017.

Zeng, J.-B., He, Y.-S., Li, S.-L., Wang, Y.-Z., 2011. Chitin whiskers: an overview. Biomacromolecules 13 (1), 1–11. https://doi.org/10.1021/bm201564a.

Zhang, F., Lu, Q., Ming, J., Dou, H., Liu, Z., Zuo, B., Qin, M., Li, F., Kaplan, D.L., Zhang, X., 2014. Silk dissolution and regeneration at the nanofibril scale. J. Mater. Chem. B 2 (24), 3879–3885. https://doi.org/10.1039/c3tb21582b.

Zhu, Y., Romain, C., Williams, C.K., 2016. Sustainable polymers from renewable resources. Nature 540 (7633), 354–362. https://doi.org/10.1038/nature21001.

Zobel, H.F., 1988. Molecules to granules: a comprehensive starch review. Starch-Stärke 40 (2), 44–50. https://doi.org/10.1002/star.19880400203.

CHAPTER

2

Introduction to nano-biosorbents

Adnan Khan[a], *Sumeet Malik*[a], *Nisar Ali*[b], *Yong Yang*[b], *Mohammed Salim Akhter*[c], *and Muhammad Bilal*[d]

[a]Institute of Chemical Sciences, University of Peshawar, Peshawar, Khyber Pakhtunkhwa, Pakistan [b]Key Laboratory of Regional Resource Exploitation and Medicinal Research, Faculty of Chemical Engineering, Huaiyin Institute of Technology, Huaian, Jiangsu Province, China [c]Department of Chemistry, College of Science, University of Bahrain, Zallaq, Bahrain [d]School of Life Science and Food Engineering, Huaiyin Institute of Technology, Huaian, China

2.1 Introduction

The increasing world pollution has also increased the demands of the people for a better living. To cope with the demands of the people, a rush in industrialization has been noticed since last decade. Although modern technology and a rising number of industries have a positive impact on the lives of people (Sahu et al., 2021; M. Khan et al., 2021; S. Khan et al., 2021). At the same time, the rising pollution due to the discharges of these industries has caused hazardous effects. Multiple types of industries have been set up across the world, which is working continually to meet public demands (Karri et al., 2019; Ali et al., 2021). The worth-mentioning ones are the food industries, fiber and textile industries, pharmaceuticals, oil refineries, construction industries, nuclear power plant, canning industries, tanneries, paper, and pulp mills, breweries, etc. (Werkneh and Rene, 2019; Yang et al., 2021) (Fig. 2.1).

The running of these industries also has some demerits like the production of contaminants, byproducts, secondary pollutants, which are discharged out with the wastewater. This highly contaminated wastewater reaches out to the living organisms through multifarious sources and causes precarious damages (Agarwal et al., 2019; Nawaz et al., 2020). The regular contaminants found in the drainages of the industries may be organic or inorganic in nature. Both the categories of contaminants include food additives, synthetic pesticides, insecticides, detergents, solvents, paints, plastics, polycyclic aromatic hydrocarbons, mineral acids, inorganic salts, heavy metals, sulfates, phosphates, nitrates, radioactive pollutants, etc. (Vishnu and Dhandapani, 2021; Ali et al., 2020a) (Fig. 2.2). The mentioned contaminants are

https://doi.org/10.1016/B978-0-323-90912-9.00002-2

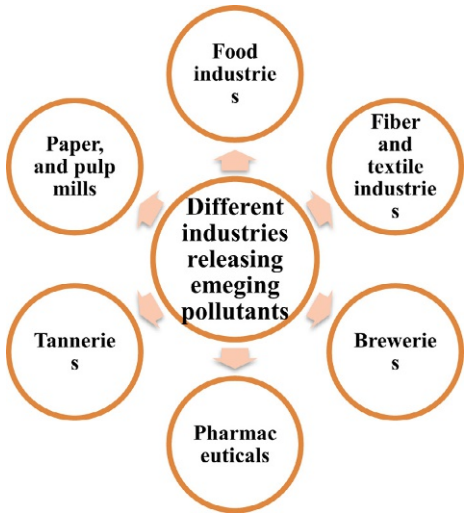

FIG. 2.1 Various industries releasing emerging pollutants.

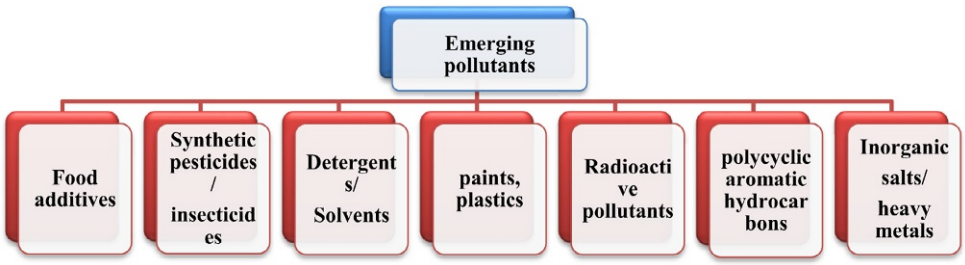

FIG. 2.2 Different organic and inorganic emerging pollutants.

non-biodegradable in nature and have obstructive effects on living organisms including humans, flora, and fauna (Garba et al., 2019; Ali et al., 2020b). Commonly, the contaminated wastewater in plants causes the retarded growth, poor production of products (fruits or vegetables), ultimate death of the plants, etc. In animals also, the contaminated industrial water causes various diseases putting a negative impact on the animal stock (Vidal and Moraes, 2019; Ali et al., 2020c). Similarly, in humans the contaminants obtained from wastewater bodies have mutagenic and carcinogenic effects. The common diseases caused by industrial contaminants include cholera, diarrhea, kidney diseases, skin irritations, asthma, etc. (Prabakar et al., 2018; Khan et al., 2020). Considering the jeopardizing nature of the industrial effluents and the ailments caused by them, researchers are trying to discover efficient methods for the decontamination of the wastewater. Among the most commonly used methods are coagulation/flocculation (Dotto et al., 2019), precipitation (Kartic et al., 2018), membrane filtration (Konvensional, 2017), solvent extraction (Ying et al., 2020), electrolytic processes (Aquino et al., 2017), reverse osmosis (Thaçi and Gashi, 2019), photocatalytic degradation (M. Khan et al., 2021), advanced electrochemical processes (Zazou et al., 2019), etc. Although the stated

methods have greatly been used, there are certain limitations associated with them. The most commonly faced problems while following these methods are the production of secondary pollutants, high-cost consumption, time-taking, inefficiency. To cope with these problems, efforts are being made by scientists to develop more environmentally friendly and green processes for the decontamination of the wastewater (Collivignarelli et al., 2019; Ali et al., 2020d). Recently, nanobiosorption has grabbed the attention of scientists due to its environment-friendly and cost-effective nature.

2.2 Concept of biosorption

The quest for efficient removal of contaminants from the wastewater bodies using a green approach has led the researchers to exploit the biosorption process (Corral-Bobadilla et al., 2021; Ali et al., 2020e). This method can generally be described as the bulk transfer process of substances from liquid to the solid phase via the biological medium. The most commonly employed biological medium may comprise living/nonliving biomass and cellular products (Sheth et al., 2021). The biosorption could be categorized as a metabolically independent and physicochemical process (Kanamarlapudi et al., 2018). The mechanisms generally involved in this process might be adsorption (Li et al., 2020a, b), absorption (Feng et al., 2020), precipitation (Peng et al., 2020), ion exchange (Han et al., 2020), or surface complexation (Li et al., 2020a, b) (Fig. 2.3). While performing the process of biosorption for the removal of contaminants from the wastewater bodies, the contaminant (sorbate), which is in the fluid phase,

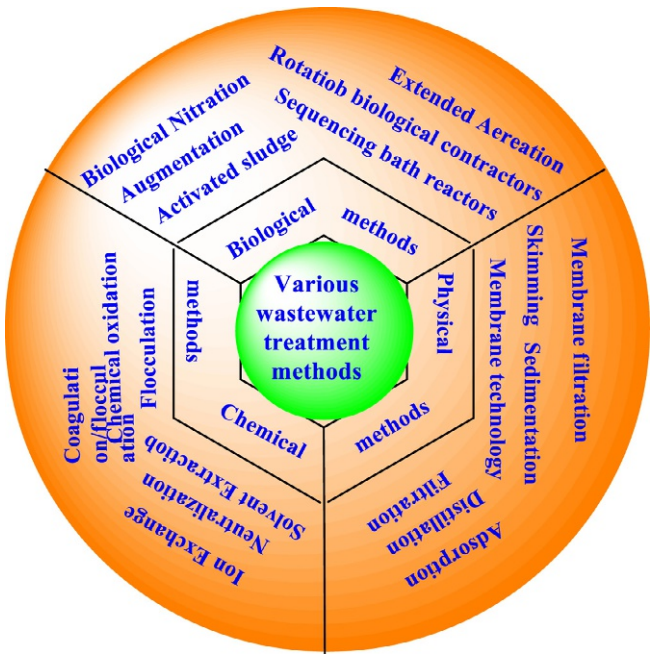

FIG. 2.3 About methods used for treatment of waste water.

interlinks with the solid phase (biosorbent) through mass-transfer (Escudero et al., 2019; Ali et al., 2020f). The process of biosorption can further be subdivided into two categories, batch process or continuous phase system. Batch process consists of stirred systems and is used for little quantities, where equilibrium distribution depends on the contact time (Ubando et al., 2021; Aziz et al., 2020). While in the case of a continuous phase system, fixed-bed columns are required. The process of biosorption is completed in three steps, the first being the transfer of sorbate to the biosorbent surface, commonly known as film diffusion. The second step follows the movement of sorbate into the biosorbent pores, which falls under the intraparticle diffusion. The third and last step refers to sorbate fixing onto biosorbent surface through surface bonding. The first two steps are the rate-determining steps, while the third step is a fast step (Vendruscolo et al., 2017; Sartaj et al., 2020). The process of biosorption has greatly been employed for the removal of contaminants at different levels. The biosorption process is preferred over other classical methods due to its biocompatibility, feasibility, and efficiency. The process of biosorption does not produce any secondary contaminants and the biosorbent can be regenerated for further usage (Eletta and Ighalo, 2019; Ali et al., 2020g). Another prime factor for the biosorption being a favorite decontamination technique is that a number of biological components as biosorbents like industrial wastes, agricultural wastes, bacteria, algae, etc. This ensures the economic efficiency of the process (Castro et al., 2017; Ali et al., 2020h). The biosorbents, being biological in nature, contain plenty of functional groups, which enhances the hydrophobic interactions. The process of biosorption is also affected by the operating environmental factors like pH, time, temperature, the surface area of sorbent, sorbent activation, pressure, etc. (Jobby et al., 2018; Ali et al., 2020i). Although biosorbents have a number of advantages associated with them, the use of pristine biosorbents (without treatment or modification) also has some demerits. The untreated biosorbents have been found to produce high biological oxygen demand (BOD), chemical oxygen demand (COD), and total organic carbon (TOC), which ultimately leads to depletion of water oxygen content (Ibisi and Asoluka, 2018; Ali et al., 2020j). Hence, it is necessary to further treat the biosorbents for improving their ability in the removal of wastewater contaminants. This idea leads the researchers towards applying the principles of nanotechnology upon the biosorbents to produce nano-biosorbents (Bilal et al., 2018; Ali et al. 2020k).

2.3 Incorporation of nanotechnology with biosorption

Recently, nanotechnology has emerged as an advanced discipline of science and technology in the forthcoming years. The nanoparticles are defined to have a nano-size range of 1–100 nm, which lies between the molecular size regime and the macroscopic bulk matter (Mahamadi, 2019; Khan et al., 2019a). The nanoparticles tend to have unique physical, chemical, and electronic properties. Keeping into consideration these properties of nanomaterials, the performance of biosorption can be improved by incorporating with the nanomaterials by trapping the profitable properties of nanomaterials like extremely small size, large surface-to-volume ratio, large surface areas, high reactivity, and better sorption capacity (Yadav et al., 2020; Ali et al., 2019). The production of nano-biosorbents has emerged as promising materials compared to conventional biosorbents for the removal of contaminants. The nano-biosorbents

can be defined as biological components with a structural analysis of having at least one dimension and a size range of less than 100 nm (Taka et al., 2020; Khan et al., 2019b). The properties of the nano-biosorbents include nontoxicity; high sorption capacity, high sensitivity even at lower concentrations (ppb), and feasibility in desorption, which strengthens the reusability of the material (Daneshvar and Hosseini, 2018; Khan et al., 2019c). Other factors that improve the performance of the nano-biosorbents include economic efficiency, selectivity, and capacity of functionalization. Considering the useful aspects of the nano-biosorbents, they have greatly been employed for the removal of different contaminants from the wastewater bodies (Rama, 2019; Ali et al., 2018a). The different methods employed for the synthesis of nano-biosorbents include biosorbent material immobilization onto the inorganic nanoparticles, magnetic modification of natural biosorbents, modification with organic matter, and modification of metal oxides with organic matter, etc. Apart from the unique properties associated with the nano-biosorbents, the properties of the nano-biosorbents can further be improved by applying some advanced technologies (Giese et al., 2020; Sohni et al., 2018). These innovative approaches for treating the nano-biosorbents are discussed as follows.

2.3.1 Magnetic modification of the nano-biosorbents

The magnetic modification of the nano-biosorbents is based on the idea of incorporating magnetic nanoparticles with the biosorbents. This type of nano-biosorbent, once it captures the sorbate particles from the fluid, can be separated by using a magnetic field with lower gradients (Peralta et al., 2021; Ali et al., 2018b) (Fig. 2.4). This separation technique has many

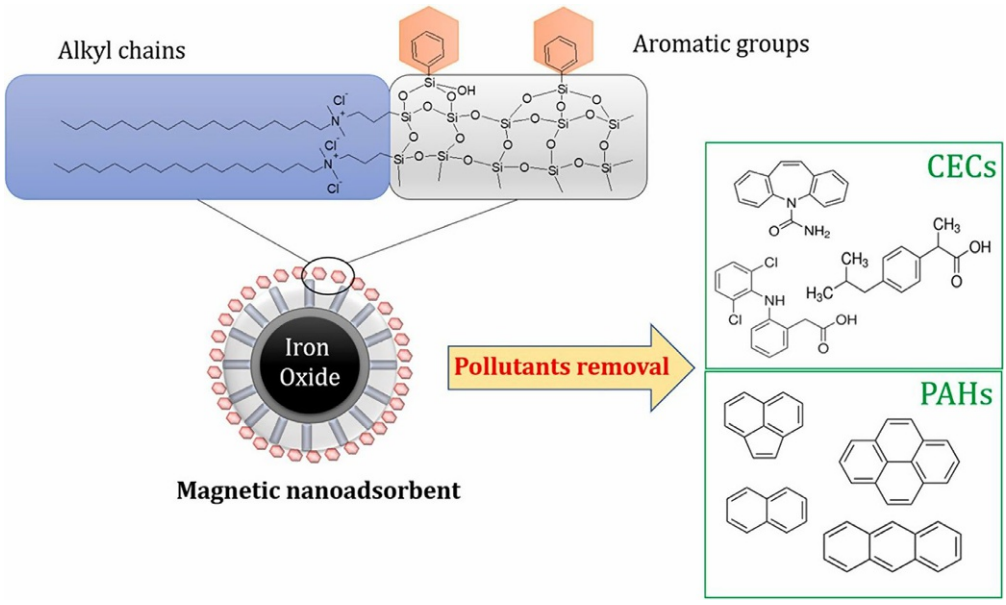

FIG. 2.4 Schematic illustration for the adsorptive removal applications of magnetic mesostructured (MMST) and MMST-Ph nanoadsorbents (Peralta et al., 2021).

advantages over the conventional separation techniques like filtration or centrifugation. Due to this reason, the magnetic modification approach has greatly been employed (Ji et al., 2019; Khan et al., 2017). The most magnetically modified nano-biosorbents include chitosan nanoparticles (Salehi et al., 2020), algal biomass (Boubakri et al., 2017), fruit-waste extracts (Allafchian et al., 2019), stabilization of magnetic nanoparticles with adipic acid-crosslinked pectin (Rakhshaee and Panahandeh, 2011), etc.

2.3.2 Immobilization onto solid surface

Another advanced technique for the treatment of the nano-biosorbents is the immobilization method. The immobilization either follows biosorbent immobilization onto the nanoparticles surface or nanoparticle immobilization on the polymer matrix (e.g., alginate matrix). A number of reports have been presented to date for the immobilization of the nano-biosorbents (Alayli et al., 2021; Khan et al., 2016). The nano-biosorbents obtained from the immobilization of the nanomaterials with the biological component have greatly been utilized in the removal of contaminants from the wastewater bodies (Shakya et al., 2018).

2.3.3 Engineering of nanoscale zero-valent metals

The third type of nano-biosorbents fall under the category of engineered nanoscale zero-valent metals (NZVMs). The NZVMs have greatly been used for the purposes of contaminants removal due to their large surface areas and high reproducibility, which offers a great sorption potential (Phenrat and Lowry, 2019; Khan et al., 2015a). This group of nano-biosorbents shows improved efficiency using less toxic materials and biological components. Also, the magnetic property of these nano-biosorbents enables the removal of contaminants like heavy metals more easily (Li et al., 2020a, b; Khan et al., 2015b).

2.4 Green approach for contaminants removal using nano-biosorbents

The nano-biosorbents have been utilized for the removal of contaminants from wastewater bodies for a long time. Some of the environmental remediation applications of nano-biosrobents have been discussed in detail in this section;

2.4.1 Removal of organic pollutants

A number of contaminants obtained from industries are organic in nature, which includes dyes, pharmaceutical products, pesticides, insecticides, polychlorinated biphenyls, oil-based hydrocarbons, etc. These contaminants are obtained from different types of industries. Shirania et al. (2020) evaluated the performance of a novel nano-biosorbent, Curdled milk, for the ultrasound-assisted removal of eosin blue and aniline blue dyes from the aqueous solution. The nano-biosorbent showed an excellent efficiency for the removal of eosin blue and aniline blue dyes with a maximum sorption capacity of 147.1 and 131.6 mg/g respectively. The obtained results were further analyzed by applying the sorption isotherms and

thermodynamic studies. The system tends to follow Langmuir model and pseudo-second-order kinetics. Tarhan et al., 2019 also studied the sorptive efficiency of magnetic nano-biosorbent for the removal of binary dyes metanil yellow (MY) and reactive black 5 (RB5). The nano-biosorbent was first prepared by cross-linking glutaraldehyde with magnetic chitosan nanoparticles. The biosorption of both MY and RB5 was performed at optimized conditions and a maximum sorption capacity of 620 and 2549 mg/g was obtained for both dyes, respectively (Fig. 2.5). The reaction followed the pseudo-second-order kinetics. Taka et al. (2020) synthesized a polymeric nano-biosorbent by combining the amidation reaction, sol-gel process, and cross-polymerization. The obtained insoluble nanosponge β-cyclodextrin (β-CD) polyurethane modified with phosphorylated multiwalled carbon nanotubes (pMWCNTs) and further decorated with titanium dioxide and silver nanoparticles were then used for the removal of dyes. The obtained nano-biosorbent showed a good efficiency towards the removal of trichloroethylene (TCE) and Congo red (CR) dye with a sorption capacity of 275.05 and 146.96 mg/g, respectively.

Mahmoud et al. (2020a, b, c, d) studied the sorption of negatively charged food dyes, tartrazine, and sunset yellow dye onto the positively charged triethylenetetramine biochar. Firstly, the corncob nanobiochar was prepared through pyrolysis followed by its modification with triethylenetetramine. The modified nanobiochar showed excellent performance for the removal of tartrazine and sunset yellow dye with an efficiency of 93.31% and 92.06% for both respectively. The removal of organic pollutants using different nanobiosorbents has been displayed in Table 2.1.

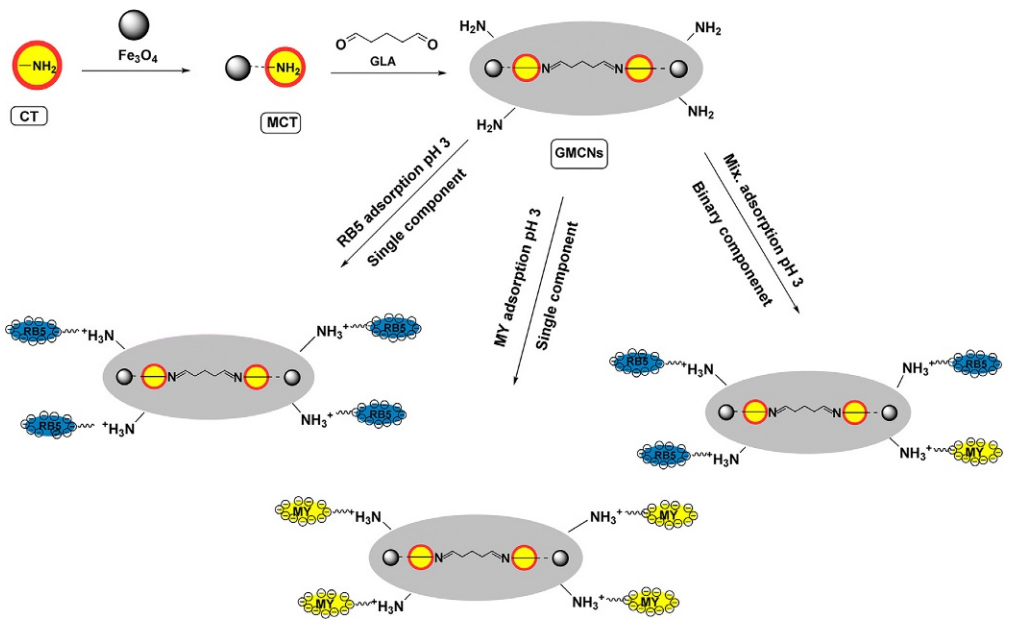

FIG. 2.5 Mechanism for the biosorption of the RB5 and MY onto the GMCNs surface (Tarhan et al., 2019).

TABLE 2.1 Removal of organic contaminants using nano-biosorbents.

Contaminants	Nano-biosorbents	Removal efficiency	Studied conditions			References
			pH	Time	Temp.	
Methylene blue	poly-*m*-phenylenediamine grafted dextrin	76.33 mg/g	8	120	25	Zare et al. (2018)
Methylene blue Malachite green	magnetic polydopamine (PDA) and chitosan (CS) hybrid nanobiosorbent	204 mg/g 61 mg/g	8	120	30	Wang et al. (2016)
Methylene blue	Immobilized *Agrobacterium fabrum* biomass	91 mg/g	11	60	25	Sharma et al. (2018)
Acid red nylon 57	Calcined eggshell modified with titanium oxide nanoparticles	222 mg/g	1–8	40		El-Kemary et al. (2018)
Methylene blue	**cress seed musilage magnetic nanocomposites**	44.6 mg/g		80		Allafchian et al. (2019)
Indigo carmine	**Chitosan (CS)—Cerium oxide (CeO_2) nano-biosorbent**	198 mg/g	3		25	Kekes et al. (2021)
Metformin	**Nanoniochar**	97%		45		Mahmoud et al. (2020a, b, c, d)
Ciprofloxacin	**Magnetic biosorbents**	527.93 mg/g	6		25	Zheng et al. (2020)
Polycyclic aromatic hydrocarbons	**Nanoparticle-supported lipid bilayers**					Wang et al. (2015)
Chlorpyrifos	**Nanoscale *Moringa olivera* seeds waste (nMSW)**	25 mg/g	7	30		Hamadeen et al. (2021)
Nitro toluene derivatives	**Polyamide thin-film composite layered on polysulfone-GO/TiO_2**	90%				Gharehbakhsh et al. (2020)
Rice husk	**2,4-Dichlorophenoxyacetic acid**	96.87%		60	30	Chidambaram (2016)
Methyl orange	**Modified Fe_3O_4 nano-particles with the extracted pectin**	0.446 mmol/g				Rakhshaee et al. (2011)
Methylene blue	**Cellulose-clay nanocomposite hydrogels**	98%				Peng et al. (2016)
Congo red	**Nanobiocomposite**	127.2 mg/g				Azin et al. (2017)

2.4.2 Removal of inorganic pollutants

The nano-biosorbents have also been greatly employed for the removal of inorganic contaminants like heavy metals, phosphates, nitrates, sulfates, cyanides, etc. Salehi et al. (2020)

prepared a novel nano-biosorbent by cross-linking chitosan magnetic beads and modifying them with methionine-glutaraldehyde Schiff's base. The obtained (MG-Chi/Fe_3O_4) was then used for the removal of heavy metals. At the optimized operating conditions the nano-biosorbent showed a removal efficiency of 172.4, 175.4, and 163.9 mg/g for Cu(II), Pb(II), and Cd(II), respectively. Further analysis of the results showed that the system followed the pseudo-second-order kinetics. Daneshvar and Hosseini (2018) also studied the biosorption of Cr (VI) using a magnetic biosorbent. Firstly, the magnetic nanoparticles were synthesized by the chemical co-precipitation method. The obtained magnetic nanoparticles were then incorporated with dead and alkaline activated biomass of *Aspergillus niger*. The finally obtained nano-biosorbent showed a good performance for the removal of Cr (VI) with a removal efficiency of 92%. The analysis of the results showed that the sorption process followed the Temkin model. Mahmoud et al. (2020a, b, c, d) also studied the preparation of a nano-biosorbent through the functionalized graphene quantum dots from rice husk with barium hydroxide. The obtained GQDOs-Ba nano-biosorbent was then used for the removal of Pb(II) and La(III) ions. The nano-biosorbent showed an excellent efficiency for the removal of Pb(II) and La(III) ions with removal percentages of 98.5%–99.8% for lead and 94.6%–96.2% for lanthanum. Esmaeili and Khoshnevisan (2016) also studied the preparation of alginate-coated chitosan nanoparticles (Alg-CS-NPs) and then checked their efficiency for the removal of nickel ions. The obtained nano-biosorbent showed a good removal performance towards nickel removal with a removal efficiency of 94.48%. The obtained results best fitted the Freundlich isotherm model and pseudo-second-order kinetics. The removal inorganic contaminants removal using nano-biosorbing are shown in Table 2.2.

TABLE 2.2 Removal of inorganic contaminants using nano-biosorbents.

Contaminants	Nano-biosorbents	Removal efficiency	Studied conditions			References
			pH	Time (min)	Temp. (°C)	
Cu (II)	Carboxymethylchitosan covalently linked to silica-coated core-shell magnetic nanoparticles	350 mg/g	6	60	25	Plohl et al. (2019)
Cr (VI)	Ethylenediamine-modified amyloid fibrils (nanofibers)	0.68 mg/g	7	60		Leung et al. (2016)
As (III)	Cerium modified chitosan ultrafine nano-biosorbent	57.5 mg/g	8	120	25	Zhang et al. (2016)
Cr (VI)	Amyloid fibrils		7			Leung, 2017
Zn (II)	Zinc imprinted nano-biosorbent	275.48 mg/g				Basak et al. (2014)
Cd (II)	Nanoscale zero-valent iron functionalized *Posidonia oceanica*	320.52 mg/g	7	120		Boubakri et al. (2017)
Pb (II)		411.40 mg/g				
Cu (II)		460.25 mg/g				

Continued

TABLE 2.2 Removal of inorganic contaminants using nano-biosorbents—cont'd

Contaminants	Nano-biosorbents	Removal efficiency	Studied conditions			References
			pH	Time (min)	Temp. (°C)	
U(VI)	Carbon quantum dots loaded on polymer matrix	97.3%	5		70	Mahmoud et al. (2020a, b, c, d)
Cr (VI)	Modified biopolymer chitosan	78.12 mg/g	1.5			Khalil et al. (2021)
Cr (VI)	**Nanoscale *Pisum sativum* pods biochar encapsulated starch hydrogel**	420.13 mg/g				Mohamed and Mahmoud (2020)
Pb (II)	**Amyloid lysozyme fibrils conjugated with polyethyleneimine (PEI)**	493 mg/g			25	Liu et al. (2020)
Phosphate	**Modified magnetite nanoparticles**	4.9 mg/g	7			Abo Markeb et al. (2016)
Phosphate	**Lanthanum molybdate/magnetite**	66%	7	1440	25	Luo et al. (2021)
Cd (II)	**Porous anion-exchanger chelating fibers (PP-*g*-AA-Am)**	125.34 mg/g				Liu et al. (2016)
Nitrate	**Functionalized chitosan-clinoptilolite nanocomposites**	277.7 mg/g				Yazdi et al. (2019)
Nitrate	**Biochar composites with nano zero-valent iron**	148.1 mg/g				Ahmad et al. (2018)
Nitrate	**Polydopamine coated zeolite**		3		10	Gouran-Orimi et al. (2018)

2.5 Conclusion

The ever-rising pollution has triggered researchers and scientists to explore new, cost-effective, and environmentally green opportunities for the removal of contaminants. This has led to the deployment of nano-biosorbents for the removal of various contaminants from wastewater bodies. The presented chapter gives an introduction to the nano-biosorbents and their capabilities towards the removal of contaminants from the wastewater bodies.

References

Abo Markeb, A., Alonso, A., Dorado, A.D., Sánchez, A., Font, X., 2016. Phosphate removal and recovery from water using nanocomposite of immobilized magnetite nanoparticles on cationic polymer. Environ. Technol. 37 (16), 2099–2112.

Agarwal, P., Gupta, R., Agarwal, N., 2019. Advances in synthesis and applications of microalgal nanoparticles for wastewater treatment. J. Nanotechnol. 2019, 1–9.
Ahmad, M., Ahmad, M., Usman, A.R., Al-Faraj, A.S., Abduljabbar, A.S., Al-Wabel, M.I., 2018. Biochar composites with nano zerovalent iron and eggshell powder for nitrate removal from aqueous solution with coexisting chloride ions. Environ. Sci. Pollut. Res. 25 (26), 25757–25771.
Alayli, A., Nadaroglu, H., Turgut, E., 2021. Nanobiocatalyst beds with Fenton process for removal of methylene blue. Appl Water Sci 11 (2), 1–8.
Ali, N., Kamal, T., Ul-Islam, M., Khan, A., Shah, S.J., Zada, A., 2018a. Chitosan-coated cotton cloth supported copper nanoparticles for toxic dye reduction. Int. J. Biol. Macromol. 111, 832–838.
Ali, N., Ismail, M., Khan, A., Khan, H., Haider, S., Kamal, T., 2018b. Spectrophotometric methods for the determination of urea in real samples using silver nanoparticles by standard addition and 2nd order derivative methods. Spectrochim. Acta A Mol. Biomol. Spectrosc. 189, 110–115.
Ali, N., Zada, A., Zahid, M., Ismail, A., Rafiq, M., Riaz, A., Khan, A., 2019. Enhanced photodegradation of methylene blue with alkaline and transition-metal ferrite nanophotocatalysts under direct sun light irradiation. J. Chin. Chem. Soc. 66 (4), 402–408.
Ali, N., Uddin, S., Khan, A., Khan, S., Khan, S., Ali, N., Bilal, M., 2020a. Regenerable chitosan-bismuth cobalt selenide hybrid microspheres for mitigation of organic pollutants in an aqueous environment. Int. J. Biol. Macromol. 161, 1305–1317.
Ali, N., Ahmad, S., Khan, A., Khan, S., Bilal, M., Ud Din, S., Khan, H., 2020b. Selenide-chitosan as high-performance nanophotocatalyst for accelerated degradation of pollutants. Chem. Asian J. 15 (17), 2660–2673.
Ali, N., Bilal, M., Khan, A., Ali, F., Yang, Y., Khan, M., Iqbal, H.M., 2020c. Dynamics of oil-water interface demulsification using multifunctional magnetic hybrid and assembly materials. J. Mol. Liq. 312, 113434.
Ali, N., Khan, A., Malik, S., Badshah, S., Bilal, M., Iqbal, H.M., 2020d. Chitosan-based green sorbent material for cations removal from an aqueous environment. J. Environ. Chem. Eng. 8, 104064.
Ali, N., Khan, A., Bilal, M., Malik, S., Badshah, S., Iqbal, H., 2020e. Chitosan-based bio-composite modified with thiocarbamate moiety for decontamination of cations from the aqueous media. Molecules 25 (1), 226.
Ali, N., Khan, A., Nawaz, S., Bilal, M., Malik, S., Badshah, S., Iqbal, H.M., 2020f. Characterization and deployment of surface-engineered chitosan-triethylenetetramine nanocomposite hybrid nano-adsorbent for divalent cations decontamination. Int. J. Biol. Macromol. 152, 663–671.
Ali, N., Naz, N., Shah, Z., Khan, A., Nawaz, R., 2020g. Selective transportation of molybdenum from model and ore through poly inclusion membrane. Bull. Chem. Soc. Ethiop. 34 (1), 93–104.
Ali, N., Bilal, M., Nazir, M.S., Khan, A., Ali, F., Iqbal, H.M., 2020h. Thermochemical and electrochemical aspects of carbon dioxide methanation: a sustainable approach to generate fuel via waste to energy theme. Sci. Total Environ. 712, 136482.
Ali, N., Azeem, S., Khan, A., Khan, H., Kamal, T., Asiri, A.M., 2020i. Experimental studies on removal of arsenites from industrial effluents using tridodecylamine supported liquid membrane. Environ. Sci. Pollut. Res. 27, 1–12.
Ali, N., Bilal, M., Khan, A., Ali, F., Iqbal, H.M., 2020j. Design, engineering and analytical perspectives of membrane materials with smart surfaces for efficient oil/water separation. TrAC Trends Anal. Chem. 127, 115902.
Ali, N., Bilal, M., Khan, A., Ali, F., Yang, Y., Malik, S., Iqbal, H.M., 2021. Deployment of metal-organic frameworks as robust materials for sustainable catalysis and remediation of pollutants in environmental settings. Chemosphere 272, 129605.
Allafchian, A., Mousavi, Z.S., Hosseini, S.S., 2019. Application of cress seed musilage magnetic nanocomposites for removal of methylene blue dye from water. Int. J. Biol. Macromol. 136, 199–208.
Aquino, J.M., Miwa, D.W., Rodrigo, M.A., Motheo, A.J., 2017. Treatment of actual effluents produced in the manufacturing of atrazine by a photo-electrolytic process. Chemosphere 172, 185–192.
Azin, E., Moghimi, H., Taheri, R.A., 2017. Development of carbon nanotube-mycosorbent for effective Congo red removal: optimization, isotherm and kinetic studies. Desalin. Water Treat. 94, 30–222.
Aziz, A., Ali, N., Khan, A., Bilal, M., Malik, S., Ali, N., Khan, H., 2020. Chitosanzinc sulfide nanoparticles, characterization and their photocatalytic degradation efficiency for azo dyes. Int. J. Biol. Macromol. 153, 502–512.
Basak, G., Das, D., Das, N., 2014. Enhanced Zn (II) uptake using zinc imprinted form of novel nano-biosorbent and its application as an antimicrobial agent. Korean J. Chem. Eng. 31 (5), 812–820.
Bilal, M., Rasheed, T., Sosa-Hernández, J.E., Raza, A., Nabeel, F., Iqbal, H., 2018. Biosorption: an interplay between marine algae and potentially toxic elements—a review. Mar. Drugs 16 (2), 65.

Boubakri, S., Djebbi, M.A., Bouaziz, Z., Namour, P., Amara, A.B.H., Ghorbel-Abid, I., Kalfat, R., 2017. Nanoscale zero-valent iron functionalized Posidonia oceanica marine biomass for heavy metal removal from water. Environ. Sci. Pollut. Res. 24 (36), 27879–27896.
Castro, L., Blázquez, M.L., González, F., Muñoz, J.A., Ballester, A., 2017. Biosorption of Zn (II) from industrial effluents using sugar beet pulp and F. vesiculosus: from laboratory tests to a pilot approach. Sci. Total Environ. 598, 856–866.
Chidambaram, R., 2016. Rice husk as a low cost nanosorbent for 2, 4-dichlorophenoxyacetic acid removal from aqueous solutions. Ecol. Eng. 92, 97–105.
Collivignarelli, M.C., Abbà, A., Miino, M.C., Damiani, S., 2019. Treatments for color removal from wastewater: state of the art. J. Environ. Manag. 236, 727–745.
Corral-Bobadilla, M., Lostado-Lorza, R., Somovilla-Gómez, F., Escribano-García, R., 2021. Effective use of activated carbon from olive stone waste in the biosorption removal of Fe (III) ions from aqueous solutions. J. Clean. Prod. 294, 126332.
Daneshvar, M., Hosseini, M.R., 2018. Kinetics, isotherm, and optimization of the hexavalent chromium removal from aqueous solution by a magnetic nano-biosorbent. Environ. Sci. Pollut. Res. 25 (28), 28654–28666.
Dotto, J., Fagundes-Klen, M.R., Veit, M.T., Palacio, S.M., Bergamasco, R., 2019. Performance of different coagulants in the coagulation/flocculation process of textile wastewater. J. Clean. Prod. 208, 656–665.
Eletta, O.A., Ighalo, J.O., 2019. A review of fish scales as a source of biosorbent for the removal of pollutants from industrial effluents. J. Res. Inf. Civ. Eng. 16 (1), 2479–2510.
El-Kemary, M.A., El-mehasseb, I.M., Shoueir, K.R., El-Shafey, S.E., El-Shafey, O.I., Aljohani, H.A., Fouad, R.R., 2018. Sol-gel TiO2 decorated on eggshell nanocrystal as engineered adsorbents for removal of acid dye. J. Dispers. Sci. Technol. 39 (6), 911–921.
Escudero, L.B., Quintas, P.Y., Wuilloud, R.G., Dotto, G.L., 2019. Recent advances on elemental biosorption. Environ. Chem. Lett. 17 (1), 409–427.
Esmaeili, A., Khoshnevisan, N., 2016. Optimization of process parameters for removal of heavy metals by biomass of cu and co-doped alginate-coated chitosan nanoparticles. Bioresour. Technol. 218, 650–658.
Feng, Y., Liu, P., Wang, Y., Finfrock, Y.Z., Xie, X., Su, C., Xu, Y., 2020. Distribution and speciation of iron in Fe-modified biochars and its application in removal of As (V), As (III), Cr (VI), and Hg (II): an X-ray absorption study. J. Hazard. Mater. 384, 121342.
Garba, Z.N., Zhou, W., Lawan, I., Xiao, W., Zhang, M., Wang, L., Yuan, Z., 2019. An overview of chlorophenols as contaminants and their removal from wastewater by adsorption: a review. J. Environ. Manag. 241, 59–75.
Gharehbakhsh, H., Panahi, H.A., Toosi, M.R., Hassani, A.H., Moniri, E., 2020. Application of polyamide thin-film composite layered on polysulfone-GO/TiO 2 mixed matrix membranes for removal of nitrotoluene derivatives from petrochemical wastewaters. Environ. Sci. Pollut. Res. 27 (34), 42481–42494.
Giese, E.C., Silva, D.D., Costa, A.F., Almeida, S.G., Dussán, K.J., 2020. Immobilized microbial nanoparticles for biosorption. Crit. Rev. Biotechnol. 40 (5), 653–666.
Gouran-Orimi, R., Mirzayi, B., Nematollahzadeh, A., Tardast, A., 2018. Competitive adsorption of nitrate in fixed-bed column packed with bio-inspired polydopamine coated zeolite. J. Environ. Chem. Eng. 6 (2), 2232–2240.
Hamadeen, H.M., Elkhatib, E.A., Badawy, M.E., Abdelgaleil, S.A., 2021. Green low cost nanomaterial produced from *Moringa oleifera* seed waste for enhanced removal of chlorpyrifos from wastewater: Mechanism and sorption studies. J. Environ. Chem. Eng. 9, 105376.
Han, S., Zang, Y., Gao, Y., Yue, Q., Zhang, P., Kong, W., Gao, B., 2020. Co-monomer polymer anion exchange resin for removing Cr (VI) contaminants: adsorption kinetics, mechanism and performance. Sci. Total Environ. 709, 136002.
Ibisi, N.E., Asoluka, C.A., 2018. Use of agro-waste (Musa paradisiaca peels) as a sustainable biosorbent for toxic metal ions removal from contaminated water. Chem. Int. 4 (1), 52.
Ji, J., Chen, G., Zhao, J., 2019. Preparation and characterization of amino/thiol bifunctionalized magnetic nanoadsorbent and its application in rapid removal of Pb (II) from aqueous system. J. Hazard. Mater. 368, 255–263.
Jobby, R., Jha, P., Yadav, A.K., Desai, N., 2018. Biosorption and biotransformation of hexavalent chromium [Cr (VI)]: a comprehensive review. Chemosphere 207, 255–266.
Kanamarlapudi, S.L.R.K., Chintalpudi, V.K., Muddada, S., 2018. Application of biosorption for removal of heavy metals from wastewater. Biosorption 18, 69–116.
Karri, R.R., Shams, S., Sahu, J.N., 2019. Overview of potential applications of nano-biotechnology in wastewater and effluent treatment. In: Ahsan, A., Ismail, A.F. (Eds.), Nanotechnology in Water and Wastewater Treatment. Micro and Nano Technologies. Elsevier, pp. 87–100.

Kartic, D.N., Narayana, B.C.A., Arivazhagan, M., 2018. Removal of high concentration of sulfate from pigment industry effluent by chemical precipitation using barium chloride: RSM and ANN modeling approach. J. Environ. Manag. 206, 69–76.
Kekes, T., Tsakanika, L.A., Kolliopoulos, G., Tzia, C., 2021. Adsorption of indigo carmine onto chitosan-cerium oxide Nano-biosorbent: adsorption isotherms, kinetics, and thermodynamics. IOP Conf. Ser. Earth Environ. Sci. 690 (1), 012048. IOP Publishing.
Khalil, T.E., Elhusseiny, A.F., Ibrahim, N.M., El-Dissouky, A., 2021. Unexpected effect of magnetic nanoparticles on the performance of aqueous removal of toxic Cr (VI) using modified biopolymer chitosan. Int. J. Biol. Macromol. 170, 768–779.
Khan, A., Badshah, S., Airoldi, C., 2015a. Environmentally benign modified biodegradable chitosan for cation removal. Polym. Bull. 72 (2), 353–370.
Khan, A., Wahid, F., Ali, N., Badshah, S., Airoldi, C., 2015b. Single-step modification of chitosan for toxic cations remediation from aqueous solution. Desalin. Water Treat. 56 (4), 1099–1109.
Khan, S.U., Khan, F.U., Khan, I.U., Muhammad, N., Badshah, S., Khan, A., Nasrullah, A., 2016. Biosorption of nickel (II) and copper (II) ions from aqueous solution using novel biomass derived from Nannorrhops ritchiana (Mazri palm). Desalin. Water Treat. 57 (9), 3964–3974.
Khan, A., Begum, S., Ali, N., Khan, S., Hussain, S., Sotomayor, M.D.P.T., 2017. Preparation of crosslinked chitosan magnetic membrane for cations sorption from aqueous solution. Water Sci. Technol. 75 (9), 2034–2046.
Khan, A., Ali, N., Bilal, M., Malik, S., Badshah, S., Iqbal, H., 2019a. Engineering functionalized chitosan-based sorbent material: characterization and sorption of toxic elements. Appl. Sci. 9 (23), 5138.
Khan, A., Shah, S.J., Mehmood, K., Ali, N., Khan, H., 2019b. Synthesis of potent chitosan beads a suitable alternative for textile dye reduction in sunlight. J. Mater. Sci. Mater. Electron. 30 (1), 406–414.
Khan, H., Khalil, A.K., Khan, A., 2019c. Photocatalytic degradation of alizarin yellow in aqueous medium and real samples using chitosan conjugated tin magnetic nanocomposites. J. Mater. Sci. Mater. Electron. 30 (24), 21332–21342.
Khan, H., Gul, K., Ara, B., Khan, A., Ali, N., Ali, N., Bilal, M., 2020. Adsorptive removal of acrylic acid from the aqueous environment using raw and chemically modified alumina: batch adsorption, kinetic, equilibrium and thermodynamic studies. J. Environ. Chem. Eng. 8, 103927.
Khan, M., Khan, A., Khan, H., Ali, N., Sartaj, S., Malik, S., Bilal, M., 2021. Development and characterization of regenerable chitosan-coated nickel selenide nano-photocatalytic system for decontamination of toxic azo dyes. Int. J. Biol. Macromol. 182, 866–878.
Khan, S., Khan, A., Ali, N., Ahmad, S., Ahmad, W., Malik, S., Bilal, M., 2021. Degradation of carcinogenic Congo red dye using ternary metal selenide-chitosan microspheres as robust and reusable catalysts. Environ. Technol. Innov. 22, 101402.
Konvensional, B.T., 2017. A review of oilfield wastewater treatment using membrane filtration over conventional technology. Malays. J. Anal. Sci 21, 643–658.
Leung, W.H., 2017. Development of a Colorimetric Nanosensor and Nano-Biosorbents from Amyloid Fibrils of Hen Lysozyme for Rapid Detection of Chromium (VI) and Removal of Dye and Chromium (VI) Pollutants. Department of Applied Biology and Chemical Technology, Hong Kong Polytechnic University – Dissertations Chromium – Toxicology Water – Purification.
Leung, W.H., So, P.K., Wong, W.T., Lo, W.H., Chan, P.H., 2016. Ethylenediamine-modified amyloid fibrils of hen lysozyme with stronger adsorption capacity as rapid nano-biosorbents for removal of chromium (VI) ions. RSC Adv. 6 (108), 106837–106846.
Li, Z., Liu, Y., Zou, S., Lu, C., Bai, H., Mu, H., Duan, J., 2020a. Removal and adsorption mechanism of tetracycline and cefotaxime contaminants in water by NiFe2O4-COF-chitosan-terephthalaldehyde nanocomposites film. Chem. Eng. J. 382, 123008.
Li, Z., Sun, Y., Yang, Y., Han, Y., Wang, T., Chen, J., Tsang, D.C., 2020b. Biochar-supported nanoscale zero-valent iron as an efficient catalyst for organic degradation in groundwater. J. Hazard. Mater. 383, 121240.
Liu, M., Tao, Z., Wang, H., Zhao, F., Sun, Q., 2016. Preparation and characterization of a series of porous anion-exchanger chelating fibers and their adsorption behavior with respect to removal of cadmium (II). RSC Adv. 6 (116), 115222–115237.
Liu, M., Jia, L., Zhao, Z., Han, Y., Li, Y., Peng, Q., Zhang, Q., 2020. Fast and robust lead (II) removal from water by bioinspired amyloid lysozyme fibrils conjugated with polyethyleneimine (PEI). Chem. Eng. J. 390, 124667.

Luo, F., Feng, X., Jiang, X., Zhou, A., Xie, P., Wang, Z., Wan, J., 2021. Lanthanum molybdate/magnetite for selective phosphate removal from wastewater: characterization, performance, and sorption mechanisms. Environ. Sci. Pollut. Res. 28 (4), 4342–4351.
Mahamadi, C., 2019. Will nano-biosorbents break the Achilles' heel of biosorption technology? Environ. Chem. Lett. 17 (4), 1753–1768.
Mahmoud, M.E., Abdelfattah, A.M., Tharwat, R.M., Nabil, G.M., 2020a. Adsorption of negatively charged food tartrazine and sunset yellow dyes onto positively charged triethylenetetramine biochar: optimization, kinetics and thermodynamic study. J. Mol. Liq. 318, 114297.
Mahmoud, M.E., El-Ghanam, A.M., Saad, S.R., Mohamed, R.H.A., 2020b. Promoted removal of metformin hydrochloride anti-diabetic drug from water by fabricated and modified nanobiochar from artichoke leaves. Sustain. Chem. Pharm. 18, 100336.
Mahmoud, M.E., Fekry, N.A., Abdelfattah, A.M., 2020c. A novel nano-biosorbent of functionalized graphene quantum dots from rice husk with barium hydroxide for microwave enhanced removal of lead (II) and lanthanum (III). Bioresour. Technol. 298, 122514.
Mahmoud, M.E., Fekry, N.A., Abdelfattah, A.M., 2020d. Removal of uranium (VI) from water by the action of microwave-rapid green synthesized carbon quantum dots from starch-water system and supported onto polymeric matrix. J. Hazard. Mater. 397, 122770.
Mohamed, A.K., Mahmoud, M.E., 2020. Nanoscale Pisum sativum pods biochar encapsulated starch hydrogel: a novel nanosorbent for efficient chromium (VI) ions and naproxen drug removal. Bioresour. Technol. 308, 123263.
Nawaz, A., Khan, A., Ali, N., Ali, N., Bilal, M., 2020. Fabrication and characterization of new ternary ferrites-chitosan nanocomposite for solar-light driven photocatalytic degradation of a model textile dye. Environ. Technol. Innov. 20, 101079.
Peng, N., Hu, D., Zeng, J., Li, Y., Liang, L., Chang, C., 2016. Superabsorbent cellulose–clay nanocomposite hydrogels for highly efficient removal of dye in water. ACS Sustain. Chem. Eng. 4 (12), 7217–7224.
Peng, D., Qiao, S., Luo, Y., Ma, H., Zhang, L., Hou, S., Xu, H., 2020. Performance of microbial induced carbonate precipitation for immobilizing cd in water and soil. J. Hazard. Mater. 400, 123116.
Peralta, M.E., Mártire, D.O., Moreno, M.S., Parolo, M.E., Carlos, L., 2021. Versatile nanoadsorbents based on magnetic mesostructured silica nanoparticles with tailored surface properties for organic pollutants removal. J. Environ. Chem. Eng. 9 (1), 104841.
Phenrat, T., Lowry, G.V., 2019. Nanoscale zerovalent iron particles for environmental restoration. In: From Fundamental Science to Field Scale Engineering Applications. Springer Link.
Plohl, O., Ajdnik, U., Gyergyek, S., Ban, I., Vesel, A., Glaser, T.K., Zemljič, L.F., 2019. Superior stability and high biosorbent efficiency of carboxymethylchitosan covalently linked to silica-coated core-shell magnetic nanoparticles for application in copper removal. J. Environ. Chem. Eng. 7 (1), 102913.
Prabakar, D., Manimudi, V.T., Mathimani, T., Kumar, G., Rene, E.R., Pugazhendhi, A., 2018. Pretreatment technologies for industrial effluents: critical review on bioenergy production and environmental concerns. J. Environ. Manag. 218, 165–180.
Rakhshaee, R., Panahandeh, M., 2011. Stabilization of a magnetic nano-adsorbent by extracted pectin to remove methylene blue from aqueous solution: a comparative studying between two kinds of cross-likened pectin. J. Hazard. Mater. 189 (1–2), 158–166.
Rakhshaee, R., Giahi, M., Pourahmad, A., 2011. Removal of methyl orange from aqueous solution by Azolla filicoloides: synthesis of Fe3O4 nano-particles and its surface modification by the extracted pectin of Azolla. Chin. Chem. Lett. 22 (4), 501–504.
Rama, H., 2019. Tracing Heavy Metals in Tomato Plants Watered with Synthetic Wastewater Treated with a Bacterial Coated Calcium Alginate Nanobiosorbent. (Doctoral Dissertation).
Sahu, J.N., Karri, R.R., Zabed, H.M., Shams, S., Qi, X., 2021. Current perspectives and future prospects of nanobiotechnology in wastewater treatment. Sep. Purif. Rev. 50 (2), 139–158.
Salehi, N., Moghimi, A., Shahbazi, H., 2020. Preparation of cross-linked magnetic chitosan with methionine-glutaraldehyde for removal of heavy metals from aqueous solutions. Int. J. Environ. Anal. Chem., 1–17.
Sartaj, S., Ali, N., Khan, A., Malik, S., Bilal, M., Khan, M., Khan, S., 2020. Performance evaluation of photolytic and electrochemical oxidation processes for enhanced degradation of food dyes laden wastewater. Water Sci. Technol. 81 (5), 971–984.
Shakya, M., Rene, E.R., Nancharaiah, Y.V., Lens, P.N., 2018. Fungal-based nanotechnology for heavy metal removal. In: Nanotechnology, Food Security and Water Treatment. Springer Link, pp. 229–253.

Sharma, S., Hasan, A., Kumar, N., Pandey, L.M., 2018. Removal of methylene blue dye from aqueous solution using immobilized Agrobacterium fabrum biomass along with iron oxide nanoparticles as biosorbent. Environ. Sci. Pollut. Res. 25 (22), 21605–21615.
Sheth, Y., Dharaskar, S., Khalid, M., Sonawane, S., 2021. An environment friendly approach for heavy metal removal from industrial wastewater using chitosan based biosorbent: a review. Sustainable Energy Technol. Assess. 43, 100951.
Shirania, M., Akbaria, A., Golib, A., 2020. Application of a novel high-performance nano biosorbent for removal of anionic dyes from aqueous solutions using shuffled frog leaping algorithm: isotherm, kinetic and thermodynamic studies. Desalin. Water Treat. 203, 388–402.
Sohni, S., Gul, K., Ahmad, F., Ahmad, I., Khan, A., Khan, N., Bahadar Khan, S., 2018. Highly efficient removal of acid red-17 and bromophenol blue dyes from industrial wastewater using graphene oxide functionalized magnetic chitosan composite. Polym. Compos. 39 (9), 3317–3328.
Taka, A.L., Fosso-Kankeu, E., Pillay, K., Mbianda, X.Y., 2020. Metal nanoparticles decorated phosphorylated carbon nanotube/cyclodextrin nanosponge for trichloroethylene and Congo red dye adsorption from wastewater. J. Environ. Chem. Eng. 8 (3), 103602.
Tarhan, T., Tural, B., Boga, K., Tural, S., 2019. Adsorptive performance of magnetic nano-biosorbent for binary dyes and investigation of comparative biosorption. SN Appl. Sci. 1 (1), 1–11.
Thaçi, B.S., Gashi, S.T., 2019. Reverse osmosis removal of heavy metals from wastewater effluents using biowaste materials pretreatment. Pol. J. Environ. Stud. 28 (1), 337–341.
Ubando, A.T., Africa, A.D.M., Maniquiz-Redillas, M.C., Culaba, A.B., Chen, W.H., Chang, J.S., 2021. Microalgal biosorption of heavy metals: a comprehensive bibliometric review. J. Hazard. Mater. 402, 123431.
Vendruscolo, F., da Rocha Ferreira, G.L., Antoniosi Filho, N.R., 2017. Biosorption of hexavalent chromium by microorganisms. Int. Biodeterior. Biodegradation 119, 87–95.
Vidal, R.R.L., Moraes, J.S., 2019. Removal of organic pollutants from wastewater using chitosan: a literature review. Int. J. Environ. Sci. Technol. 16 (3), 1741–1754.
Vishnu, D., Dhandapani, B., 2021. A review on the synergetic effect of plant extracts on nanomaterials for the removal of metals in industrial effluents. Curr. Anal. Chem. 17 (2), 260–271.
Wang, H., Kim, B., Wunder, S.L., 2015. Nanoparticle-supported lipid bilayers as an in situ remediation strategy for hydrophobic organic contaminants in soils. Environ. Sci. Technol. 49 (1), 529–536.
Wang, Y., Zhang, Y., Hou, C., Liu, M., 2016. Mussel-inspired synthesis of magnetic polydopamine–chitosan nanoparticles as biosorbent for dyes and metals removal. J. Taiwan Inst. Chem. Eng. 61, 292–298.
Werkneh, A.A., Rene, E.R., 2019. Applications of nanotechnology and biotechnology for sustainable water and wastewater treatment. In: Bui, X.T., Chiemchaisri, C., Fujioka, T., Varjani, S. (Eds.), Water and Wastewater Treatment Technologies. Energy, Environment, and Sustainability. Springer, Singapore, pp. 405–430.
Yadav, V.K., Choudhary, N., Khan, S.H., Malik, P., Inwati, G.K., Suriyaprabha, R., Ravi, R.K., 2020. Synthesis and characterisation of nano-biosorbents and their applications for waste water treatment. In: Duca, G., Vaseashta, A. (Eds.), Handbook of Research on Emerging Developments and Environmental Impacts of Ecological Chemistry. IGI Global, pp. 252–290.
Yang, Y., Ali, N., Khan, A., Khan, S., Khan, S., Khan, H., Bilal, M., 2021. Chitosan-capped ternary metal selenide nanocatalysts for efficient degradation of Congo red dye in sunlight irradiation. Int. J. Biol. Macromol. 167, 169–181.
Yazdi, F., Anbia, M., Salehi, S., 2019. Characterization of functionalized chitosan-clinoptilolite nanocomposites for nitrate removal from aqueous media. Int. J. Biol. Macromol. 130, 545–555.
Ying, Z., Ren, X., Li, J., Wu, G., Wei, Q., 2020. Recovery of chromium (VI) in wastewater using solvent extraction with amide. Hydrometallurgy 196, 105440.
Zare, E.N., Lakouraj, M.M., Kasirian, N., 2018. Development of effective nano-biosorbent based on poly m-phenylenediamine grafted dextrin for removal of Pb (II) and methylene blue from water. Carbohydr. Polym. 201, 539–548.
Zazou, H., Afanga, H., Akhouairi, S., Ouchtak, H., Addi, A.A., Akbour, R.A., Hamdani, M., 2019. Treatment of textile industry wastewater by electrocoagulation coupled with electrochemical advanced oxidation process. J. Water Process. Eng. 28, 214–221.
Zhang, L., Zhu, T., Liu, X., Zhang, W., 2016. Simultaneous oxidation and adsorption of As (III) from water by cerium modified chitosan ultrafine nano-biosorbent. J. Hazard. Mater. 308, 1–10.
Zheng, C., Zheng, H., Hu, C., Wang, Y., Wang, Y., Zhao, C., Sun, Q., 2020. Structural design of magnetic biosorbents for the removal of ciprofloxacin from water. Bioresour. Technol. 296, 122288.

This page intentionally left blank

CHAPTER

3

Nanobiosorbents: Basic principles, synthesis, and application for contaminants removal

Adnan Khan[a], *Sumeet Malik*[a], *Nisar Ali*[b], *Muhammad Bilal*[c], *Yong Yang*[b], *Mohammed Salim Akhter*[d], *Cao Zhou*[b], *Ye Wenjie*[b], *and Hafiz M.N. Iqbal*[e]

[a]Institute of Chemical Sciences, University of Peshawar, Peshawar, Khyber Pakhtunkhwa, Pakistan [b]Key Laboratory of Regional Resource Exploitation and Medicinal Research, Faculty of Chemical Engineering, Huaiyin Institute of Technology, Huaian, Jiangsu Province, China [c]School of Life Science and Food Engineering, Huaiyin Institute of Technology, Huaian, China [d]Department of Chemistry, College of Science, University of Bahrain, Zallaq, Bahrain [e]Tecnologico de Monterrey, School of Engineering and Sciences, Monterrey, Mexico

3.1 Introduction

Clean and fresh water is one of the necessities for living organisms. The rising world pollution has made the supply of freshwater very difficult and challenging (Saxena et al., 2020; Khan et al., 2021b). The contaminants polluting the water sources and the industrial effluents being discharged out in the form of wastewater have stirred a great concern for the supply of pure water. The guarantee to supply clean and pure water for the earth and its occupants has become the topmost task for researchers and scientists (Tshikovhi et al., 2020; Ali et al., 2021). Considering the very limited freshwater assets and their rapid downturn is alarming, which requires proper measures for the treatment. Scientists have taken major steps for the treatment of wastewater bodies to make sure the removal of contaminants (Kennedy et al., 2018; Yang et al., 2021). Some of the conventional methods applied for the removal of the contaminants include coagulation/flocculation (Bruno et al., 2020), reverse osmosis (Jamil et al.,

https://doi.org/10.1016/B978-0-323-90912-9.00003-4

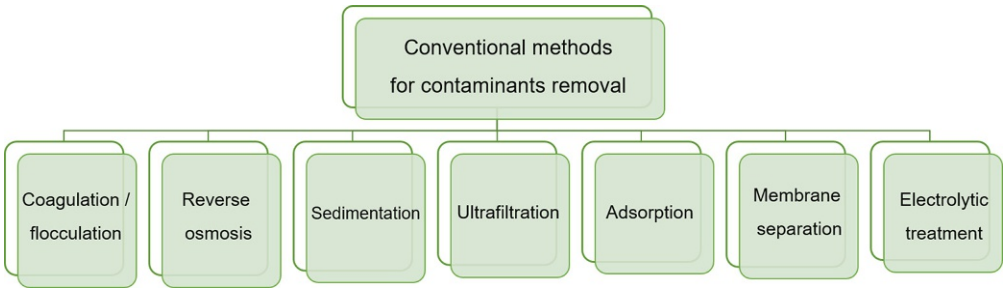

FIG. 3.1 Conventional methods for contaminants removal.

2020), sedimentation (Wang et al., 2020a, b), ultra-filtration (Ran et al., 2020), electrolytic treatment (Yan et al., 2020), electrodialysis (Yang et al., 2020), membrane separation (Naddeo et al., 2020), oxidation (Top et al., 2020), degradation (Khan et al., 2021a), sorption (Khan et al., 2020a), etc. (Fig. 3.1). Each of the mentioned techniques could be applied for the decontamination of the wastewater bodies depending upon the available resources and conditions. Although many applications of these techniques are available for the decontamination of the wastewater, certain limitations are also associated with them (Ijanu et al., 2020; Nawaz et al., 2020).

Some of the mentioned technologies are incompetent and cannot perform the complete removal of the contaminants. In some cases, the production of secondary contaminants has been observed, which requires additional treatment. Another concern while using the mentioned removal techniques is the high costs and requirement of the advanced equipment (Kumar and Deswal, 2021; Ali et al., 2020a). Keeping in view these issues, researchers ought to design such a methodology that is cost-effective, proficient, multifunctional, modular, and flexible in system configuration and size. Among the many used techniques to date, sorption tends to possess a better capability towards contaminants removal (Saidulu et al., 2021; Ali et al., 2020b). The highly selective nature of the sorption process and simple operation have made it a better process compared to others (Bhanot et al., 2020; Ali et al., 2020c). While considering the sorption process for the removal of contaminants, the focus has been given to the use of low-cost sorbents. The best choice is the biosorbents, which are low-cost, renewable, and easily available sources. To further enhance the activity and properties of the biosorbents, they are incorporated with nanotechnology to design nanobiosorbents for efficient removal of contaminants (Dutta and Charingia, 2020; Ali et al., 2020d). The nanobiosorbents have paved the way for the removal of contaminants with a green approach.

3.2 Fundamentals of nanobiosorption

The concept of nanobiosorption commences with designing nanobiosorbents, which can be defined as biomaterials made up of nanometer-scale components. At the nanoscale levels, some significant changes could be observed in the properties of the nanobiosorbents (Yadav et al., 2020; Ali et al., 2020e). The nanobiosorbents possess greater surface-to-volume ratios

compared to the micron-sized ones (Mahamadi, 2019; Ali et al., 2020f). The nanobiosorbents indulge the beneficial aspects of the nanotechnology with the process of biosorption. The nanobiosorbents have a defined ability to attach with the contaminants (heavy metals, dyes, pesticides, inorganic ions, etc.) from the wastewater bodies. The plus point of using biosorption as a method of contaminants removal rather than other methods is that it offers easy availability of low-cost sorbents. Several naturally occurring biomasses of biological nature obtained from industrial byproducts can be used as proficient sorbents (Verma et al., 2021; Aziz et al., 2020). The worth-mentioning biological materials include starch, cellulose, alginate, lignin, chitin, chitosan, glycan, sugarcane bagasse, rice husk, etc. The biosorption process offers tremendous removal of suspended materials from dilute aqueous solutions with high proficiency and rapid kinetics (Kumar et al., 2021; Sartaj et al., 2020). The exceptionally high sensitivity of this process guarantees the removal of contaminants at ppm to ppb levels. The mechanism of biosorption tends to follow a combination of mechanisms like electrostatic interaction, ion exchange, micro-precipitation, complexation, chelation, coordination, absorption, etc. The properties of biosorption can further be enhanced by applying the nanotechnology features (Wang et al., 2019; Ali et al., 2019). The obtained nanobiosorbents thus possess enhanced ability for the removal of multiple contaminants. The nanobiosorbents have extraordinary features like high surface-area-to-volume ratios, renewability, biocompatibility, high natural abundance, better mechanical properties, optical transparency, sustainability, adaptable surface chemistry, inherent environmental inertness, optical transparency, etc. (Bayuo, 2021; Ali et al., 2020g) (Fig. 3.2). Considering these useful features of the nanobiosorbents, they are massively being used for the decontamination of wastewater ensuring the pure supply of water and a green environment.

3.3 General preparation of nanobiosorbents

An important aspect while studying the nanobiosorbents is the methods used for preparing them. The nanobiomaterials are synthesized via different techniques and can be further functionalized to enhance their surface properties (Khan et al., 2020b). The obtained nanobiosorbents thus efficiently remove the contaminants from wastewater bodies. The sorbed inorganic contaminants and ions can be extracted out from the metal surface by washing with acids, while in case of organic contamination, evaporation or submersion in organic solvents is preferred (Channegowda, 2020; Ali et al., 2020h). This section is going to discuss the preparatory techniques of the nanobiosorbents in general. The general idea of synthesizing the bionanocomposites is based on the fact that the material must possess a single-phase having one dimension with less than 100 nm size while the other phase being a biological component (Zare et al., 2018; Ali et al., 2020i). This can also be explained as one of the phases of material consists of the natural polymeric matrix while the other being organic/inorganic filler in the nanoscale range (Fig. 3.3). The most commonly used natural polymeric materials include starches, proteins, pectin, polysaccharides, etc. (Thamer et al., 2021; Ali et al., 2020j).

While the inorganic nanofiller additive part may consist of carbon tubes, polymer nanowhiskers, synthetic polymer nanofibers, solid layered clays, etc. (Nik Abdul Ghani

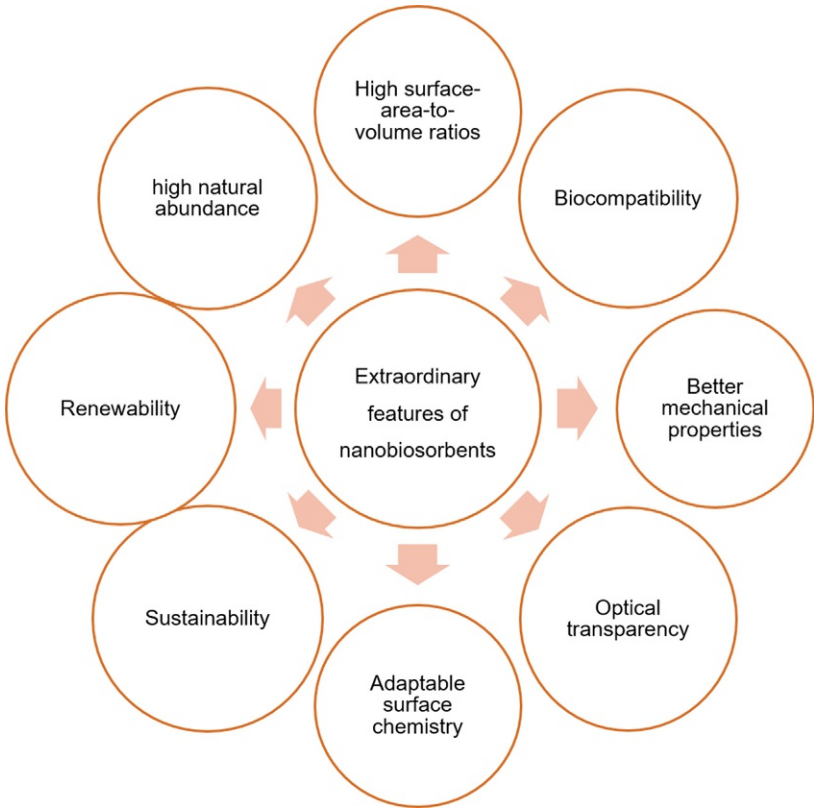

FIG. 3.2 Some of the extraordinary features of nanobiosorbents.

et al., 2021; Ali et al. 2020k). The synthesis of the nanobiocomposites normally follows the general existing strategies considering the requirements and conditions of the operation. The techniques are discussed as follows.

3.3.1 Mechanical mixing of the components

This is the simplest and most commonly used method for the nanobiocomposites synthesis. It operates with the mixing of biopolymer hydrogels and the particles in the solution phase, followed by gelation. The gelation is induced either by changing the temperature (gelatin), or pH (chitosan and collagen) or by the addition of a cross-linking agent (carrageenan or alginate) (Moharrami and Motamedi, 2020; Khan et al., 2019a). This process defines prerequisite surface properties of the inorganic colloids. The conditions for the synthesis process could also be defined so as to obtain products with better properties and well-preserved products (Bao et al., 2017).

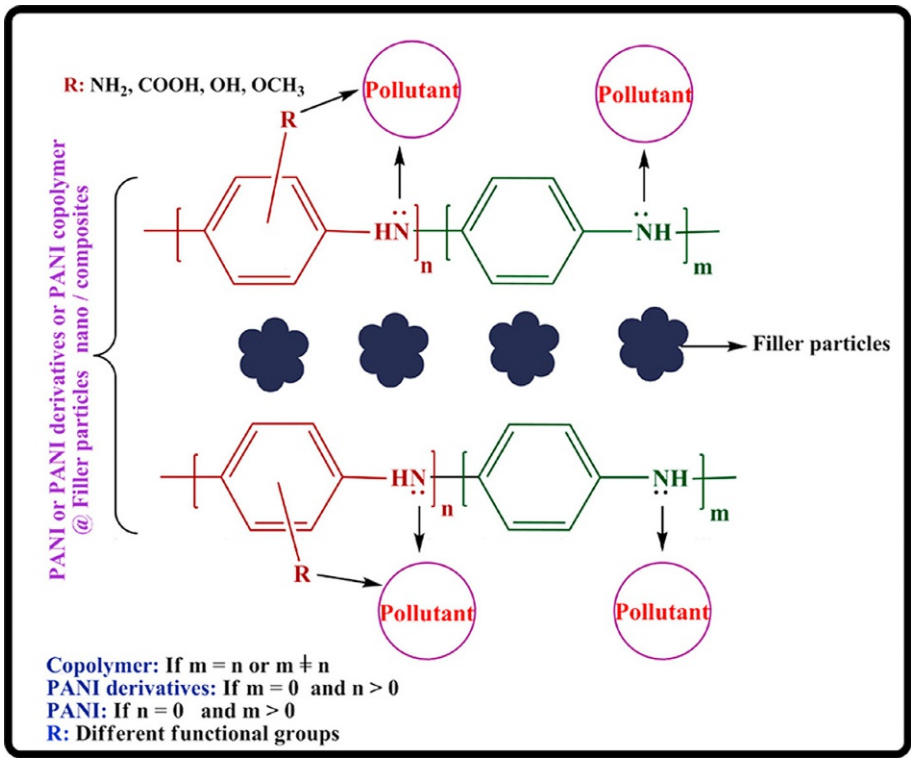

FIG. 3.3 Proposed mechanism of pollutants adsorption by the PANI/PANI derivatives-based nanocomposites. *Reprinted from Zare, E.N., Motahari, A., Sillanpää, M., 2018. Nanoadsorbents based on conducting polymer nanocomposites with main focus on polyaniline and its derivatives for removal of heavy metal ions/dyes: a review. Environ. Res. 162, 173–195, with permission from Elsevier. License Number: 5078040907051.*

3.3.2 In situ particles synthesis

This type of nanocomposite synthesis follows utilizing the biopolymers as the template molecules. The process begins with the inorganic nanoparticle precursor species conversion into solids by a second reaction sequence (Sahoo et al., 2019; Khan et al., 2019b). Firstly, the inorganic precursor is added to the polymer solution followed by gelation. The precursor impregnation can also be performed after the hydrogel is formed. The next step is the mineralization, which is performed by modifying the pH, carbonation, addition of a reducing agent, supplementation, etc. (Pu et al., 2018; Khan et al., 2019c).

3.4 Common natural biopolymers based nanobiosorbents

The horizon of nanobiosorbents is quite broad due to the fact that a number of naturally occurring materials, polymers, biopolymers, etc., can be used in wastewater remediation. The abundance of natural materials and products is one of the reasons for the massive exploitation

of the nanobiomaterials as prospective sorbents for contaminants removal. This section of the chapter is going to discuss some of the most commonly occurring natural biopolymers which have many applications in the field of nanobiosorption for removal of the contaminants (Asere et al., 2019; Shah et al., 2018).

3.4.1 Nanobiosorbents based on cellulosic material

The nanomaterials obtained from cellulosic origin have gained massive attention due to their applications in various fields along with the wastewater remediation area. The cellulosic nanomaterials in the form of cellulose nanocrystals and cellulose nanofibrils have gotten great features attractive to be used as nanobiosorbents for contaminants removal (Hernández-Francisco et al., 2020; Saeed et al., 2018). Although cellulose-based nanobiosorbents have possessed unique applications, which are necessary for the sorption of contaminants, certain environmental factors must also be assessed before using them. The evaluation of costs, biodegradability, non-toxicity, stability, ease of access, life-span, are some of the key points to be considered. The cellulose-based nanobiosorbents have found great applications in the field of sorption of contaminants due to their greater abundance and low costs (Hasan et al., 2021; Neelofar et al., 2017). The pristine cellulose may have some limitations, which can be overcome by chemical modification or through functionalization. The additional treatment of cellulose-based material further enhances its affinity towards the contaminants. The cellulose-based nanobiosorbents thus offer high selectivity, hydrophilicity, biocompatibility, and eco-friendly features towards contaminants removal (Varghese et al., 2019; Khan et al., 2017).

3.4.2 Nanobiosorbents based on chitin/chitosan

Another abundantly found natural biopolymers are chitin and chitosan. Chitosan can be described as a biodegradable and renewable carbohydrate, which can be synthesized by *N*-deacetylation of chitin. Chitosan is commonly found in crustacean's shells and cuticles of insects (Karimi-Maleh et al., 2021a, b; Hussain et al., 2016). The constituents of the chitosan consist of linear amino polysaccharide of glucosamine. The surface of chitosan contains hydrophilic functional groups like amino and hydroxyl groups. The high natural abundance of chitin/chitosan, feasibility of modification, and high sorption capacity makes them excellent materials to be used as nanobiosorbents for the removal of contaminants from the wastewater bodies (Vunain et al., 2016; Khan et al., 2016a, b). The physico-chemical properties of nanobiosorbents include chelating and complexing, hydrophilicity, bio-adhesive nature, crystallinity, solubility in dilute acidic solutions, etc. The low-cost, sustainable, renewable, and eco-friendly nature of the chitosan-based nanobiosorbents has elevated their usage as nanobiosorbents (da Silva Alves et al., 2021; Ali et al., 2018a).

3.4.3 Nanobiosorbents based on starch

Another naturally abundant biopolymer is starch having biodegradable and biocompatible properties. The reserves of starch carbohydrates are commonly found in sundry plants.

The common starch sources include wheat, maize, rice, cassava, etc. (Nasrollahzadeh et al., 2020; Ali et al., 2018b). The structural evaluation of starch shows that it consists of a 3D structure with 15%–45% crystalline range and components of D-glucose units. The hydrolysis of starch produces crystallites, nanocrystals, and microcrystalline starches. The attractive features of the starch-based nanobiosorbents like high abundance, high surface area, biocompatibility, renewability, and low costs (Rigueto et al., 2021; Sohni et al., 2018).

3.4.4 Nanobiosorbents based on gums

Gums are also a class of natural and green biopolymers in the form of polysaccharides and the derivatives of gums have found great applications in the field of wastewater remediation. A common example of gums is guar gum, which is a mucoadhesive polysaccharide (Saya et al., 2021; Wahid et al., 2017). The Guar gum is commonly obtained from the guar beans endosperm and it consists of D-gal-actopyranosyl and D-mannopyranosyl units. Another commonly found example of gums is the gum Arabic or acacia gum. This type of gum consists of D-galactopyranosyl units. The common sources of acacia gum are the branched heteropolysaccharide and a complex exudate of *Acacia seyal* and *Acacia senegal* trees (Ramakrishnan et al., 2021; Khan et al., 2016a, b). The nanobiosorbents obtained from gums have also found applications in the removal of contaminants from the wastewater bodies due to multiple functionalities associated with them.

3.4.5 Nanobiosorbents based on alginate

Alginates can be described as the linear block copolymers, which consist of two uronic acid residues, i.e., α-L-guluronic acid and β-D-mannuronic linked by the β-1,4-glycosidic bonds (Thakur, 2021). The nanobiosorbents based on alginate biopolymers possess unique features like biodegradability, stability, high water permeability, non-toxic nature, etc. These properties make alginate-based nanobiosorbents an excellent choice for the removal of contaminants from the wastewater bodies (Al-Sakkari et al., 2020).

3.4.6 Nanobiosorbents based on pectin

Another worth-mentioning natural polysaccharide is the anionic pectin which can be obtained from the higher plants cell wall. The structure of pectin can be described as a linear polysaccharide present in the intercellular layer of the cell wall of adjacent cells (Mohamed et al., 2020). It mainly consists of D-galacturonic acid units joined together via α-(1–4) glycosidic linkage in the form of chains rich in carboxyl/hydroxyl groups and neutral sugars present. The carboxyl groups present in the chains of pectin are sometimes in the form of methyl esters while in other cases, they can be converted to carboxamide groups by treating with ammonia (Solangi et al., 2021). The nanobiosorbents obtained from the pectin-based materials are biocompatible, non-toxic, flexible, and high molecular weight substances that possess excellent sorption capacity for the removal of different contaminants from the wastewater bodies (Shakibi et al., 2020; Khan et al., 2015a).

3.5 Applications of nanobiosorbents in contaminants removal

The natural abundance of biological entities like biopolymers and the unique characteristics of nanotechnology have been harnessed to obtain nanobiosorbents. These nanobiosorbents have been very helpful towards the removal of multiple contaminants from the wastewater bodies. The employment of nanobiosorbents for the removal of contaminants is a step forward towards a green and clean environment with minimal input and highly efficient results (Khan et al., 2015b). The eco-friendly and greener approach for environmental remediation has grabbed the attention of scientists to utilize natural yet advanced materials, like nanobiosorbents. Table 3.1 summarizes nanobiosorbents efficiency in the removal of various contaminants. Eltaweil et al. (2021) has prepared a zero-valent iron-loaded nanobentonite intercalated carboxymethyl chitosan (nZVI@nBent-CMC) composite. The obtained composite was then used for the successful removal of an anionic dye Congo red and a cationic dye Crystal violet. The results were evaluated and the nanobiosorbent showed an excellent efficiency towards the dye removal with a sorption capacity of 884.95 and 505.05 mg/g for CR and CV, respectively. The sorption process tends to follow the pseudo-second-order kinetics model and the Langmuir sorption isotherm, and the process was thermodynamically spontaneous. Yildirim et al. (2020) synthesized a bio-composite material for the successful removal of heavy metals. The fungal-extract-based nanobiosorbent prepared was then used for the removal of Ni(II) and Cu(II) metals from the aqueous solution. The results showed that removal efficiency of FE-CB was 7.18 and 8.50 mg/g for Cu(II) and Ni(II), respectively. The evaluation of the results showed that the process tends to follow pseudo-second-order kinetics and is spontaneous, endothermic, and favorable. Naeimi et al. (2021) studied the extraction of nano-chitosan from wastes of shrimps followed by its modification with Schiff base ligand and graphene oxide (Fig. 3.4). The obtained nanobiosorbent was used for the removal of Cu(II) and Pb(II) from the aqueous solution. The nano-polymer biomass showed an excellent removal efficiency with the sorption capacity of 698.8 and 466 mg/g for copper and lead ions, respectively. Karimi-Maleh et al. (2021a, b) prepared a novel 1-butyl-3-methylimidazolium bromide (BmImBr) impregnated chitosan beads-based nanobiosorbent for the removal of methylene blue dye. The obtained nanobiosorbent showed excellent efficiency for the removal of the cationic model dye with a percentage of 86%. The environmental conditions of the sorption process were also optimized, and the sorption tends to follow pseudo-first-order kinetics with intrinsic penetration.

3.6 Conclusion

The day-by-day increasing world pollution has forced the scientists and researchers to develop such strategies which are helpful towards a clean and green environment. In light of this fact, naturally abundant biological materials have grabbed the attention because of their unique physico-chemical features. The abundance of presence, non-toxic nature, biocompatibility, renewability, ease of modification, are some of the many useful properties of the bio-based components. Taking advantage of the useful properties of these materials, they are further applied with nanotechnological aspects to obtain nanobiosorbents.

TABLE 3.1 Nanobiosorbents efficiency in the removal of various contaminants.

Nanobiosorbent	Contaminants	Removal efficiency	Studied conditions			Reference
			pH	Time (min)	Temp. (°C)	
Pectin hydrogel from mandarin peel-based metal-organic frameworks composite	Cr(VI)	825.97 mg/g	1	400	25	Mahmoud and Mohamed (2020)
	Pb(II)	913.88 mg/g	5			
Graphene oxide modified persimmon tannin (PT-GO)	Methylene blue	256.58 mg/g			50	Wang et al. (2020a, b)
Ethylenediamine-modified pectins (EPs)	Pb(II)	≥94%	5	60	25	Liang et al. (2020)
β-Cyclodextrin-Chitosan-based cross-linked sorbent	Hg(II)	178.3 mg/g		120		Usman et al. (2021)
	Methylene blue	162.6 mg/g				
	Methyl orange	132.5 mg/g				
Magnetic graphene/chitosan nanocomposite	2-naphthol	99.8%	2			Rebekah et al. (2020)
Chitosan cross linked with SBA-15 nanofibers	Direct yellow 12	40 mg/g	2	30		Masoudnia et al. (2020)
	Direct black ANBN	200 mg/g				
	Acid blue	43.47 mg/g				
Nano-chitin	Cr(VI)	238 mg/g	6	60	25	Sheikhi and Rezaei (2021)
Guar gum/magnetic layered double hydroxide	Methylene blue	85%	9	120		Tabatabaeian et al. (2021)
Cellulosic sisal fiber modified with polypyrrole-polyaniline nanoparticles	Ibuprofen	88%	5	60	30	Khadir et al. (2020)
Gum tragacanth carbohydrate biopolymer	NO_3^-	21 mg/g	7	20	25	Shojaipour et al. (2020)
Magnetic sodium alginate polyelectrolyte nanosphere	Pb(II)	105.8 mg/g		90		Wang et al. (2021)
Agro-industrial waste-based bioadsorbents	Zn(II)	97%		120		Castro et al. (2021)
Nano-magnetite-modified biochar	Cr(VI)	9.92 mg/g				Song et al. (2021)
Polyvinyl alcohol/alginate/zeolite nanohybrid	Ni(II) Co(II)	81.51 mg/g 79.58 mg/g				Tabatabaeefar et al. (2020)

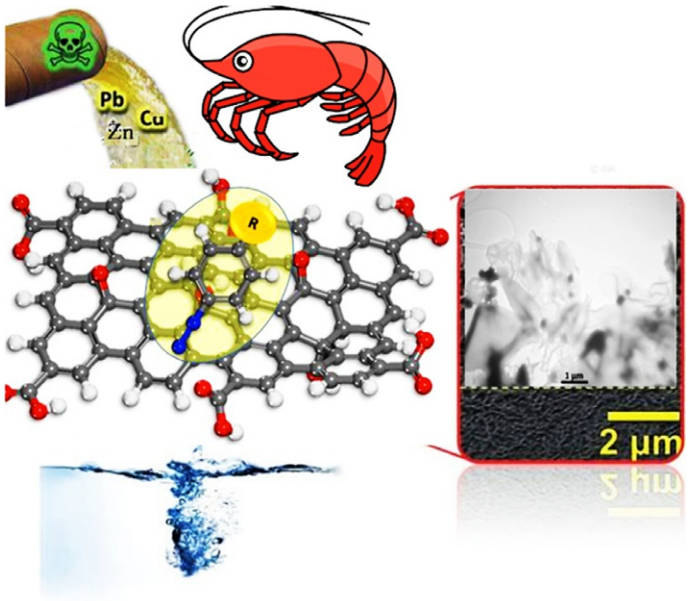

FIG. 3.4 Schematic illustration of chitosan/graphene oxide biosorbent for the removal of heavy metals from wastewaters. *Reprinted from Naeimi, A., Amini, M., Okati, N., 2021. Removal of heavy metals from wastewaters using an effective and natural bionanopolymer based on Schiff base chitosan/graphene oxide. Int. J. Environ. Sci. Technol., 1–12, with permission from Springer Nature. License Number: 5078041222658.*

The nanobiosorbents have been used in the removal of a variety of contaminants to date from the wastewater bodies and have emerged as promising tools towards clean and green environment.

Acknowledgment

Consejo Nacional de Ciencia y Tecnología (MX) is thankfully acknowledged for partially supporting this work under Sistema Nacional de Investigadores (SNI) program awarded to Hafiz M.N. Iqbal (CVU: 735340).

Conflict of interests

The author(s) declare no conflicting interests.

References

Ali, N., Kamal, T., Ul-Islam, M., Khan, A., Shah, S.J., Zada, A., 2018a. Chitosan-coated cotton cloth supported copper nanoparticles for toxic dye reduction. Int. J. Biol. Macromol. 111, 832–838.

Ali, N., Ismail, M., Khan, A., Khan, H., Haider, S., Kamal, T., 2018b. Spectrophotometric methods for the determination of urea in real samples using silver nanoparticles by standard addition and 2nd order derivative methods. Spectrochim. Acta A Mol. Biomol. Spectrosc. 189, 110–115.

Ali, N., Zada, A., Zahid, M., Ismail, A., Rafiq, M., Riaz, A., Khan, A., 2019. Enhanced photodegradation of methylene blue with alkaline and transition-metal ferrite nanophotocatalysts under direct sun light irradiation. J. Chin. Chem. Soc. 66 (4), 402–408.
Ali, N., Uddin, S., Khan, A., Khan, S., Khan, S., Ali, N., Bilal, M., 2020a. Regenerable chitosan-bismuth cobalt selenide hybrid microspheres for mitigation of organic pollutants in an aqueous environment. Int. J. Biol. Macromol. 161, 1305–1317.
Ali, N., Ahmad, S., Khan, A., Khan, S., Bilal, M., Ud Din, S., Khan, H., 2020b. Selenide-chitosan as high-performance nanophotocatalyst for accelerated degradation of pollutants. Chem. Asian J. 15 (17), 2660–2673.
Ali, N., Bilal, M., Khan, A., Ali, F., Yang, Y., Khan, M., Iqbal, H.M., 2020c. Dynamics of oil-water interface demulsification using multifunctional magnetic hybrid and assembly materials. J. Mol. Liq. 312, 113434.
Ali, N., Khan, A., Malik, S., Badshah, S., Bilal, M., Iqbal, H.M., 2020d. Chitosan-based green sorbent material for cations removal from an aqueous environment. J. Environ. Chem. Eng. 8, 104064.
Ali, N., Khan, A., Bilal, M., Malik, S., Badshah, S., Iqbal, H., 2020e. Chitosan-based bio-composite modified with thiocarbamate moiety for decontamination of cations from the aqueous media. Molecules 25 (1), 226.
Ali, N., Khan, A., Nawaz, S., Bilal, M., Malik, S., Badshah, S., Iqbal, H.M., 2020f. Characterization and deployment of surface-engineered chitosan-triethylenetetramine nanocomposite hybrid nano-adsorbent for divalent cations decontamination. Int. J. Biol. Macromol. 152, 663–671.
Ali, N., Naz, N., Shah, Z., Khan, A., Nawaz, R., 2020g. Selective transportation of molybdenum from model and ore through poly inclusion membrane. Bull. Chem. Soc. Ethiop. 34 (1), 93–104.
Ali, N., Bilal, M., Nazir, M.S., Khan, A., Ali, F., Iqbal, H.M., 2020h. Thermochemical and electrochemical aspects of carbon dioxide methanation: a sustainable approach to generate fuel via waste to energy theme. Sci. Total Environ. 712, 136482.
Ali, N., Azeem, S., Khan, A., Khan, H., Kamal, T., Asiri, A.M., 2020i. Experimental studies on removal of arsenites from industrial effluents using tridodecylamine supported liquid membrane. Environ. Sci. Pollut. Res. 27, 1–12.
Ali, N., Bilal, M., Khan, A., Ali, F., Iqbal, H.M., 2020j. Design, engineering and analytical perspectives of membrane materials with smart surfaces for efficient oil/water separation. TrAC Trends Anal. Chem. 127, 115902.
Ali, N., Bilal, M., Khan, A., Ali, F., Yang, Y., Malik, S., Iqbal, H.M., 2021. Deployment of metal-organic frameworks as robust materials for sustainable catalysis and remediation of pollutants in environmental settings. Chemosphere 272, 129605.
Al-Sakkari, E.G., Abdeldayem, O.M., Genina, E.E., Amin, L., Bahgat, N.T., Rene, E.R., El-Sherbiny, I.M., 2020. New alginate-based interpenetrating polymer networks for water treatment: a response surface methodology based optimization study. Int. J. Biol. Macromol. 155, 772–785.
Asere, T.G., Stevens, C.V., Du Laing, G., 2019. Use of (modified) natural adsorbents for arsenic remediation: a review. Sci. Total Environ. 676, 706–720.
Aziz, A., Ali, N., Khan, A., Bilal, M., Malik, S., Ali, N., Khan, H., 2020. Chitosanzinc sulfide nanoparticles, characterization and their photocatalytic degradation efficiency for azo dyes. Int. J. Biol. Macromol. 153, 502–512.
Bao, S., Li, K., Ning, P., Peng, J., Jin, X., Tang, L., 2017. Highly effective removal of mercury and lead ions from wastewater by mercaptoamine-functionalised silica-coated magnetic nano-adsorbents: behaviours and mechanisms. Appl. Surf. Sci. 393, 457–466.
Bayuo, J., 2021. An extensive review on chromium (vi) removal using natural and agricultural wastes materials as alternative biosorbents. J. Environ. Health Sci. Eng. 19, 1–15.
Bhanot, P., Celin, S.M., Sreekrishnan, T.R., Kalsi, A., Sahai, S.K., Sharma, P., 2020. Application of integrated treatment strategies for explosive industry wastewater—a critical review. J. Water Process Eng. 35, 101232.
Bruno, P., Campo, R., Giustra, M.G., De Marchis, M., Di Bella, G., 2020. Bench scale continuous coagulation-flocculation of saline industrial wastewater contaminated by hydrocarbons. J. Water Process Eng. 34, 101156.
Castro, D., Rosas-Laverde, N.M., Aldás, M.B., Almeida-Naranjo, C.E., Guerrero, V.H., Pruna, A.I., 2021. Chemical modification of agro-industrial waste-based bioadsorbents for enhanced removal of Zn (II) ions from aqueous solutions. Materials 14 (9), 2134.
Channegowda, M., 2020. Recent advances in environmentally benign hierarchical inorganic nano-adsorbents for the removal of poisonous metal ions in water: a review with mechanistic insight into toxicity and adsorption. Nanoscale Adv. 2 (12), 5529–5554.
Dutta, M.M., Charingia, A., 2020. Nanotechnology-based nano-biosorbents. In: Handbook of Research on Emerging Developments and Environmental Impacts of Ecological Chemistry. IGI Global, pp. 386–408.

Eltaweil, A.S., El-Tawil, A.M., Abd El-Monaem, E.M., El-Subruiti, G.M., 2021. Zero valent iron nanoparticle-loaded nanobentonite intercalated carboxymethyl chitosan for efficient removal of both anionic and cationic dyes. ACS Omega 6 (9), 6348–6360.

Hasan, M.N., Shenashen, M.A., Hasan, M.M., Znad, H., Awual, M.R., 2021. Assessing of cesium removal from wastewater using functionalized wood cellulosic adsorbent. Chemosphere 270, 128668.

Hernández-Francisco, E., Bonilla-Cruz, J., Márquez-Lamas, U., Suárez-Jacobo, Á., Longoria-Rodríguez, F., Rivera-Haro, J., Lara-Ceniceros, T.E., 2020. Entangled cellulose nanofibrils/nanosheets derived from native mexican agave for lead (II) ion removal. Cellulose 27 (15), 8785–8798.

Hussain, S., Ullah, Z., Gul, S., Khattak, R., Kazmi, N., Rehman, F., Khan, A., 2016. Adsorption characteristics of magnesium-modified bentonite clay with respect to acid blue 129 in aqueous media. Pol. J. Environ. Stud. 25 (5), 1947–1953.

Ijanu, E.M., Kamaruddin, M.A., Norashiddin, F.A., 2020. Coffee processing wastewater treatment: a critical review on current treatment technologies with a proposed alternative. Appl. Water Sci. 10 (1), 1–11.

Jamil, S., Loganathan, P., Kandasamy, J., Listowski, A., McDonald, J.A., Khan, S.J., Vigneswaran, S., 2020. Removal of organic matter from wastewater reverse osmosis concentrate using granular activated carbon and anion exchange resin adsorbent columns in sequence. Chemosphere 261, 127549.

Karimi-Maleh, H., Ayati, A., Davoodi, R., Tanhaei, B., Karimi, F., Malekmohammadi, S., Sillanpää, M., 2021a. Recent advances in using of chitosan-based adsorbents for removal of pharmaceutical contaminants: a review. J. Clean. Prod. 291, 125880.

Karimi-Maleh, H., Ranjbari, S., Tanhaei, B., Ayati, A., Orooji, Y., Alizadeh, M., Sen, F., 2021b. Novel 1-butyl-3-methylimidazolium bromide impregnated chitosan hydrogel beads nanostructure as an efficient nanobio-adsorbent for cationic dye removal: kinetic study. Environ. Res. 195, 110809.

Kennedy, K.K., Maseka, K.J., Mbulo, M., 2018. Selected adsorbents for removal of contaminants from wastewater: towards engineering clay minerals. Open J. Appl. Sci. 8 (8), 355–369.

Khadir, A., Motamedi, M., Negarestani, M., Sillanpää, M., Sasani, M., 2020. Preparation of a nano bio-composite based on cellulosic biomass and conducting polymeric nanoparticles for ibuprofen removal: kinetics, isotherms, and energy site distribution. Int. J. Biol. Macromol. 162, 663–677.

Khan, A., Badshah, S., Airoldi, C., 2015a. Environmentally benign modified biodegradable chitosan for cation removal. Polym. Bull. 72 (2), 353–370.

Khan, A., Wahid, F., Ali, N., Badshah, S., Airoldi, C., 2015b. Single-step modification of chitosan for toxic cations remediation from aqueous solution. Desalin. Water Treat. 56 (4), 1099–1109.

Khan, H., Khalil, A.K., Khan, A., Saeed, K., Ali, N., 2016a. Photocatalytic degradation of bromophenol blue in aqueous medium using chitosan conjugated magnetic nanoparticles. Korean J. Chem. Eng. 33 (10), 2802–2807.

Khan, S.U., Khan, F.U., Khan, I.U., Muhammad, N., Badshah, S., Khan, A., Nasrullah, A., 2016b. Biosorption of nickel (II) and copper (II) ions from aqueous solution using novel biomass derived from Nannorrhops ritchiana (Mazri palm). Desalin. Water Treat. 57 (9), 3964–3974.

Khan, A., Begum, S., Ali, N., Khan, S., Hussain, S., Sotomayor, M.D.P.T., 2017. Preparation of crosslinked chitosan magnetic membrane for cations sorption from aqueous solution. Water Sci. Technol. 75 (9), 2034–2046.

Khan, A., Ali, N., Bilal, M., Malik, S., Badshah, S., Iqbal, H., 2019a. Engineering functionalized chitosan-based sorbent material: characterization and sorption of toxic elements. Appl. Sci. 9 (23), 5138.

Khan, A., Shah, S.J., Mehmood, K., Ali, N., Khan, H., 2019b. Synthesis of potent chitosan beads a suitable alternative for textile dye reduction in sunlight. J. Mater. Sci. Mater. Electron. 30 (1), 406–414.

Khan, H., Khalil, A.K., Khan, A., 2019c. Photocatalytic degradation of alizarin yellow in aqueous medium and real samples using chitosan conjugated tin magnetic nanocomposites. J. Mater. Sci. Mater. Electron. 30 (24), 21332–21342.

Khan, H., Gul, K., Ara, B., Khan, A., Ali, N., Ali, N., Bilal, M., 2020a. Adsorptive removal of acrylic acid from the aqueous environment using raw and chemically modified alumina: batch adsorption, kinetic, equilibrium and thermodynamic studies. J. Environ. Chem. Eng. 8, 103927.

Khan, F.S.A., Mubarak, N.M., Khalid, M., Walvekar, R., Abdullah, E.C., Mazari, S.A., Karri, R.R., 2020b. Magnetic nanoadsorbents' potential route for heavy metals removal—a review. Environ. Sci. Pollut. Res. 27 (19), 24342–24356.

Khan, M., Khan, A., Khan, H., Ali, N., Sartaj, S., Malik, S., Bilal, M., 2021a. Development and characterization of regenerable chitosan-coated nickel selenide nano-photocatalytic system for decontamination of toxic azo dyes. Int. J. Biol. Macromol. 182, 866–878.

Khan, S., Khan, A., Ali, N., Ahmad, S., Ahmad, W., Malik, S., Bilal, M., 2021b. Degradation of carcinogenic Congo red dye using ternary metal selenide-chitosan microspheres as robust and reusable catalysts. Environ. Technol. Innov. 22, 101402.

Kumar, S., Deswal, S., 2021. A review on current techniques used in India for rice mill wastewater treatment and emerging techniques with valuable by-products. Environ. Sci. Pollut. Res. 28, 1–17.

Kumar, A., Singh, R., Upadhyay, S.K., Kumar, S., Charaya, M.U., 2021. Biosorption: the removal of toxic dyes from industrial effluent using phytobiomass—a review. Plant Arch. 21 (1), 1320–1325.

Liang, R.H., Li, Y., Huang, L., Wang, X.D., Hu, X.X., Liu, C.M., Chen, J., 2020. Pb^{2+} adsorption by ethylenediamine-modified pectins and their adsorption mechanisms. Carbohydr. Polym. 234, 115911.

Mahamadi, C., 2019. Will nano-biosorbents break the Achilles' heel of biosorption technology? Environ. Chem. Lett. 17 (4), 1753–1768.

Mahmoud, M.E., Mohamed, A.K., 2020. Novel derived pectin hydrogel from mandarin peel based metal-organic frameworks composite for enhanced Cr (VI) and Pb (II) ions removal. Int. J. Biol. Macromol. 164, 920–931.

Masoudnia, S., Juybari, M.H., Mehrabian, R.Z., Ebadi, M., Kaveh, F., 2020. Efficient dye removal from wastewater by functionalized macromolecule chitosan-SBA-15 nanofibers for biological approaches. Int. J. Biol. Macromol. 165, 118–130.

Mohamed, S.K., Alazhary, A.M., Al-Zaqri, N., Alsalme, A., Alharthi, F.A., Hamdy, M.S., 2020. Cost-effective adsorbent from arabinogalactan and pectin of cactus pear peels: kinetics and thermodynamics studies. Int. J. Biol. Macromol. 150, 941–947.

Moharrami, P., Motamedi, E., 2020. Application of cellulose nanocrystals prepared from agricultural wastes for synthesis of starch-based hydrogel nanocomposites: efficient and selective nanoadsorbent for removal of cationic dyes from water. Bioresour. Technol. 313, 123661.

Naddeo, V., Secondes, M.F.N., Borea, L., Hasan, S.W., Ballesteros Jr., F., Belgiorno, V., 2020. Removal of contaminants of emerging concern from real wastewater by an innovative hybrid membrane process—UltraSound, adsorption, and membrane ultrafiltration (USAMe®). Ultrason. Sonochem. 68, 105237.

Naeimi, A., Amini, M., Okati, N., 2021. Removal of heavy metals from wastewaters using an effective and natural bionanopolymer based on Schiff base chitosan/graphene oxide. Int. J. Environ. Sci. Technol., 1–12.

Nasrollahzadeh, M., Sajjadi, M., Iravani, S., Varma, R.S., 2020. Starch, cellulose, pectin, gum, alginate, chitin and chitosan derived (nano) materials for sustainable water treatment: a review. Carbohydr. Polym. 251, 116986.

Nawaz, A., Khan, A., Ali, N., Ali, N., Bilal, M., 2020. Fabrication and characterization of new ternary ferrites-chitosan nanocomposite for solar-light driven photocatalytic degradation of a model textile dye. Environ. Technol. Innov. 20, 101079.

Neelofar, N., Ali, N., Khan, A., Amir, S., Khan, N.A., Bilal, M., 2017. Synthesis of Schiff bases derived from 2-hydroxy-1-naphth-aldehyde and their tin (II) complexes for antimicribial and antioxidant activities. Bull. Chem. Soc. Ethiop. 31 (3), 445–456.

Nik Abdul Ghani, N.R., Jami, M.S., Alam, M.Z., 2021. The role of nanoadsorbents and nanocomposite adsorbents in the removal of heavy metals from wastewater: a review and prospect. Pollution 7 (1), 153–179.

Pu, S., Hou, Y., Yan, C., Ma, H., Huang, H., Shi, Q., Chu, W., 2018. In situ coprecipitation formed highly water-dispersible magnetic chitosan nanopowder for removal of heavy metals and its adsorption mechanism. ACS Sustain. Chem. Eng. 6 (12), 16754–16765.

Ramakrishnan, R.K., Padil, V.V., Wacławek, S., Černík, M., Varma, R.S., 2021. Eco-friendly and economic, adsorptive removal of cationic and anionic dyes by bio-based Karaya gum—chitosan sponge. Polymers 13 (2), 251.

Ran, Z., Yao, M., He, W., Wang, G., 2020. Efficiency analysis of enhanced Sb (V) removal via dynamic preloaded floc in coordination with ultrafiltration. Sep. Purif. Technol. 249, 117115.

Rebekah, A., Bharath, G., Naushad, M., Viswanathan, C., Ponpandian, N., 2020. Magnetic graphene/chitosan nanocomposite: a promising nano-adsorbent for the removal of 2-naphthol from aqueous solution and their kinetic studies. Int. J. Biol. Macromol. 159, 530–538.

Rigueto, C.V.T., Nazari, M.T., Massuda, L.Á., Ostwald, B.E.P., Piccin, J.S., Dettmer, A., 2021. Production and environmental applications of gelatin-based composite adsorbents for contaminants removal: a review. Environ. Chem. Lett. 19, 1–22.

Saeed, K., Sadiq, M., Khan, I., Ullah, S., Ali, N., Khan, A., 2018. Synthesis, characterization, and photocatalytic application of Pd/ZrO_2 and Pt/ZrO_2. Appl. Water Sci. 8 (2), 60.

Sahoo, S.K., Tripathy, M., Hota, G., 2019. In-situ functionalization of GO sheets with AlOOH-FeOOH composite nanorods: an eco-friendly nanoadsorbent for removal of toxic arsenate ions from water. J. Environ. Chem. Eng. 7 (5), 103357.
Saidulu, D., Gupta, B., Gupta, A.K., Ghosal, P.S., 2021. A review on occurrences, eco-toxic effects, and remediation of emerging contaminants from wastewater: special emphasis on biological treatment based hybrid systems. J. Environ. Chem. Eng. 9, 105282.
Sartaj, S., Ali, N., Khan, A., Malik, S., Bilal, M., Khan, M., Khan, S., 2020. Performance evaluation of photolytic and electrochemical oxidation processes for enhanced degradation of food dyes laden wastewater. Water Sci. Technol. 81 (5), 971–984.
Saxena, R., Saxena, M., Lochab, A., 2020. Recent progress in nanomaterials for adsorptive removal of organic contaminants from wastewater. ChemistrySelect 5 (1), 335–353.
Saya, L., Malik, V., Singh, A., Singh, S., Gambhir, G., Singh, W.R., Hooda, S., 2021. Guar gum based nanocomposites: role in water purification through efficient removal of dyes and metal ions. Carbohydr. Polym. 261, 117851.
Shah, S., ud Din, S., Khan, A., & Shah, S. A., 2018. Green synthesis and antioxidant study of silver nanoparticles of root extract of Sageretia thea and its role in oxidation protection technology. J. Polym. Environ. 26 (6), 2323–2332.
Shakibi, S., Hemmatinejad, N., Bashari, A., 2020. Sorbent textiles for colored wastewater made from orange based pectin nano-hydrogel. Fibers Polym. 21 (6), 1275–1282.
Sheikhi, M., Rezaei, H., 2021. Adsorption of hexavalent chromium ions from aqueous solutions using nano-chitin: kinetic, isotherms and thermodynamic studies. Water Pract. Technol. 16 (2), 436–451.
Shojaipour, M., Ghaemy, M., Amininasab, S.M., 2020. Removal of NO_3^- ions from water using bioadsorbent based on gum tragacanth carbohydrate biopolymer. Carbohydr. Polym. 227, 115367.
da Silva Alves, D.C., Healy, B., Pinto, L.A., Cadaval, T.R., Breslin, C.B., 2021. Recent developments in chitosan-based adsorbents for the removal of pollutants from aqueous environments. Molecules 26 (3), 594.
Sohni, S., Gul, K., Ahmad, F., Ahmad, I., Khan, A., Khan, N., Bahadar Khan, S., 2018. Highly efficient removal of acid red-17 and bromophenol blue dyes from industrial wastewater using graphene oxide functionalized magnetic chitosan composite. Polym. Compos. 39 (9), 3317–3328.
Solangi, N.H., Kumar, J., Mazari, S.A., Ahmed, S., Fatima, N., Mujawar, N.M., 2021. Development of fruit waste derived bio-adsorbents for wastewater treatment: a review. J. Hazard. Mater. 416, 125848.
Song, X., Zhang, Y., Cao, N., Sun, D., Zhang, Z., Wang, Y., Lyu, T., 2021. Sustainable chromium (VI) removal from contaminated groundwater using nano-magnetite-modified biochar via rapid microwave synthesis. Molecules 26 (1), 103.
Tabatabaeefar, A., Keshtkar, A.R., Talebi, M., Abolghasemi, H., 2020. Polyvinyl alcohol/alginate/zeolite nanohybrid for removal of metals. Chem. Eng. Technol. 43 (2), 343–354.
Tabatabaeian, R., Dinari, M., Aliabadi, H.M., 2021. Cross-linked bionanocomposites of hydrolyzed guar gum/magnetic layered double hydroxide as an effective sorbent for methylene blue removal. Carbohydr. Polym. 257, 117628.
Thakur, S., 2021. An overview on alginate based bio-composite materials for wastewater remedial. Mater. Today Proc. 37 (Part 2), 3305–3309.
Thamer, B.M., Aldalbahi, A., Moydeen, A.M., Rahaman, M., El-Newehy, M.H., 2021. Modified electrospun polymeric nanofibers and their nanocomposites as nanoadsorbents for toxic dye removal from contaminated waters: a review. Polymers 13 (1), 20.
Top, S., Akgün, M., Kıpçak, E., Bilgili, M.S., 2020. Treatment of hospital wastewater by supercritical water oxidation process. Water Res. 185, 116279.
Tshikovhi, A., Mishra, S.B., Mishra, A.K., 2020. Nanocellulose-based composites for the removal of contaminants from wastewater. Int. J. Biol. Macromol. 152, 616–632.
Usman, M., Ahmed, A., Yu, B., Wang, S., Shen, Y., Cong, H., 2021. Simultaneous adsorption of heavy metals and organic dyes by β-cyclodextrin-chitosan based cross-linked adsorbent. Carbohydr. Polym. 255, 117486.
Varghese, A.G., Paul, S.A., Latha, M.S., 2019. Remediation of heavy metals and dyes from wastewater using cellulose-based adsorbents. Environ. Chem. Lett. 17 (2), 867–877.
Verma, S., Bhatt, P., Verma, A., Mudila, H., Prasher, P., Rene, E.R., 2021. Microbial technologies for heavy metal remediation: effect of process conditions and current practices. Clean Techn. Environ. Policy, 1–23.
Vunain, E., Mishra, A.K., Mamba, B.B., 2016. Dendrimers, mesoporous silicas and chitosan-based nanosorbents for the removal of heavy-metal ions: a review. Int. J. Biol. Macromol. 86, 570–586.

Wahid, F., Mohammadzai, I.U., Khan, A., Shah, Z., Hassan, W., Ali, N., 2017. Removal of toxic metals with activated carbon prepared from *Salvadora persica*. Arab. J. Chem. 10, S2205–S2212.

Wang, B., Sun, Y.C., Sun, R.C., 2019. Fractionational and structural characterization of lignin and its modification as biosorbents for efficient removal of chromium from wastewater: a review. J. Leather Sci. Eng. 1 (1), 1–25.

Wang, Z., Chen, Y., Chen, L., Xi, S., Liu, Y., Dong, Y., Miao, L., 2020a. Ex-situ treatment of sediment from a black-odor water body using activated sludge. Sci. Total Environ. 713, 136651.

Wang, Z., Gao, M., Li, X., Ning, J., Zhou, Z., Li, G., 2020b. Efficient adsorption of methylene blue from aqueous solution by graphene oxide modified persimmon tannins. Mater. Sci. Eng. C 108, 110196.

Wang, J., Guo, M., Luo, Y., Shao, D., Ge, S., Cai, L., Lam, S.S., 2021. Production of magnetic sodium alginate polyelectrolyte nanospheres for lead ions removal from wastewater. J. Environ. Manag. 289, 112506.

Yadav, V.K., Choudhary, N., Khan, S.H., Malik, P., Inwati, G.K., Suriyaprabha, R., Ravi, R.K., 2020. Synthesis and characterisation of nano-biosorbents and their applications for waste water treatment. In: Handbook of Research on Emerging Developments and Environmental Impacts of Ecological Chemistry. IGI Global, pp. 252–290.

Yan, C., Wang, M., Ma, T., Yang, S., Kong, M., Shen, J., Gao, Y., 2020. Study on the experimental performance by electrolysis-integrated ecological floating bed for nitrogen and phosphorus removal in eutrophic water. Sci. Rep. 10 (1), 1–10.

Yang, B.M., Li, J.M., You, Z.Y., Lai, W.L., Kao, C.M., 2020. Using integrated electrodialysis and RO hybrid system to remediate and reclaim perchlorate-contaminated groundwater. Desalination 480, 114377.

Yang, Y., Ali, N., Khan, A., Khan, S., Khan, S., Khan, H., Bilal, M., 2021. Chitosan-capped ternary metal selenide nanocatalysts for efficient degradation of Congo red dye in sunlight irradiation. Int. J. Biol. Macromol. 167, 169–181.

Yildirim, A., Baran, M.F., Acay, H., 2020. Kinetic and isotherm investigation into the removal of heavy metals using a fungal-extract-based bio-nanosorbent. Environ. Technol. Innov. 20, 101076.

Zare, E.N., Motahari, A., Sillanpää, M., 2018. Nanoadsorbents based on conducting polymer nanocomposites with main focus on polyaniline and its derivatives for removal of heavy metal ions/dyes: a review. Environ. Res. 162, 173–195.

This page intentionally left blank

CHAPTER

4

Methods for the synthesis of nano-biosorbents for the contaminant removal

Harshal Dabhane[a,b], *Swati Chatur*[a], *Suresh Ghotekar*[c], *Dnyaneshwar Sanap*[a], *Ghanshyam Jadhav*[b], *Muhammad Bilal*[d], *and Vijay Medhane*[b]

[a]Department of Chemistry, G.M.D Arts, B.W Commerce and Science College, Savitribai Phule Pune University, Nashik, Maharashtra, India [b]Department of Chemistry, K.R.T. Arts, B.H. Commerce and A.M. Science College, Savitribai Phule Pune University, Nashik, Maharashtra, India [c]Department of Chemistry, Smt. Devkiba Mohansinhji Chauhan College of Commerce and Science, University of Mumbai, Silvassa, Dadra and Nagar Haveli (UT), India [d]School of Life Science and Food Engineering, Huaiyin Institute of Technology, Huaian, China

4.1 Introduction

The essential thing to all living things on earth's surface is water, also called a universal solvent due to its versatility used in every field. Water serves a crucial role in the human body which involve in many metabolism processes which are taking place in our body (Sharma and Bhattacharya, 2016). Though about 70% of the area on earth is covered by water, but drinking water is not enough for living things, another problem is nothing but the contamination of drinking water sources. Human as well as natural activity responsible for the discharge of unlike things called as contaminants, there are several types of contaminant reported by researchers like a pathogenic organism, plant nutrients, oxygen demanding waste, sediments, synthetic organic chemicals, micro-plastics, oil, radioactive substances, inorganic chemicals, and heavy metals. Several methods were used for the purification of water by removing the contaminants present in water mainly classified into chemical and physical approaches, such

https://doi.org/10.1016/B978-0-323-90912-9.00004-6

as chemical oxidation, filtration, precipitation, biological treatments, and coagulations (Tran et al., 2019). The degree of purification of water and operational cost is the main factor of discussion, some methods are cost-effective and can be used at high concentration but always question mark about the accuracy, precipitation method is much effective related to the high concentration in which contaminants allow to settle down at the bottom in the form of precipitate and filter off it. The biological contaminants are biodegradable, by using this principle biological waste can be removed from water sources (Kanamarlapudi et al., 2018). Nowadays, nanotechnology is the best tool to obtain multifunctional nano-material having fantastic applications in biomedicine, pharmaceuticals, industries, electronics, electrical devices, and environment, etc. The nan-omaterial's prepared using Top-Down and Bottom-up concepts, several methods were reported for the synthesis of nan-omaterial such as physical, chemical, and biological methods. Recently, nano-material prepared via biological or green methods is the first choice of the researcher because of their merits over known physical and chemical approaches, as the biological method is cost-effective, eco-friendly, quick, and one pot. Hence, biologically synthesized nano-range material having different morphology like nano-wire, nano-tube, nano-flower, nano-spheres, and nano-clusters, used as nano-biosorbent in the treatment of wastewater (Dabhane et al., 2020).

In present days, nano-biosorbent plays a key role in the purification of contaminated water with high efficiency and at low cost, nano-biosorbent can be synthesized using agriculture waste, biomass, biological waste, bacteria, fungus, algae, metal nanoparticles, and characterization was done with help of spectroscopic and microscopic techniques such as UV-DRS, FT-IR, Photo Luminescence, BET, FE-SEM, HR-TEM, EDX, XRD, DLS, AFM which gives information about bandgap, functional group, porosity, size, morphology, elemental composition, crystal plane, etc. Numbers of methods were reported by several researchers by which nano-biosorbent material was synthesized, Chemical method, Physical method, Microwave-assisted, Ball mill, Precipitation method, Sol-Gel method, Green Synthesis, Hammer mill, biological synthesis and used for the efficient removal of pollutants like synthetic dyes, hazardous chemicals, heavy metals, biological waste from water sources (Dabhane et al., 2021; Crini et al., 2019; El-Sayed and El-Sayed, 2014; Mahamadi, 2019; Huang et al., 2020; Tara et al., 2019; Srivastava et al., 2020; Beni and Esmaeili, 2019; Ali, 2012; Amin et al., 2014).

4.2 Types of nano-biosorbents

The synthesis or preparation of nano-biosorbent design is based on the concept of green chemistry, the classification of nano-biosorbent depends on the precursor from which it obtains. The different types of precursors were used for the synthesis of nano-biosorbent as shown below.

1. Agriculture waste.
2. Forest waste.
3. Extract of different parts of plant.
4. Biological precursor.
5. Chemical precursor.
6. Other

The various agriculture waste such as sawdust, sugarcane, DSP, peels of different fruits was used as reducing, and stabilizing agents for the fabrication of nano-biosorbent, similarly forest waste like Chestnut bur used for the same purpose. In most of the research articles, the synthesis of nano-biosorbent was reported using extract and waste of several parts of plants like flowers, roots, latex, leaves, etc. Along with that, biological precursors such as algae, fungus, bacteria were also reported for the biological synthesis of biosorbent which effectively remove the contaminants from water sources. The effective chemical synthesis of nano-biosorbent using a variety of chemical precursors such as chitosan, dextrin, etc., reported by some researchers, the nano-biosorbent synthesized by another precursor also like oil obtained from different natural sources.

4.3 Methods for the synthesis of nano-biosorbents and their applications

Several attempts were made for the synthesis of nano-biosorbent using different precursors from nature, the activity of nano-biosorbent depends on their morphology as well active sites. Table 4.1 summarized the reported synthesis of nano-biosorbent from a variety of sources.

Agriculture waste is the chief and best precursor which is easily available in nature for the synthesis of nano-biosorbent. It shows excellent adsorption activity towards contaminates present in water sources. Garima Mahajan and Dhiraj Sud reported the synthesis of nano carbonized biomass from *Dalbergia sissoo* pods (DSP) which contain lignocellulosic, nitrogenous agricultural waste biomass by calcination method. Initially, the biomass was collected and wash well to remove organic impurity from it, afterword it was dry at 120°C in the oven for 24 h, dried biomass was crush into the nano-size powder and further calcinated at 800° C in furness to obtained DSPC. The morphology of synthesized DSPC was investigated using spectroscopic and microscopic techniques like FTIR, XRD, and SEM. FTIR spectra confirm the presence of different anionic and cationic functional groups which coming from lignin, XRD techniques show the porous spacing and porous size of synthesized DSPC, and finally, SEM image confirms the nano-size of DSPC with regular morphology.

The author, study the application of DSPC for the remediation of Cd (II), Ni (II), and Pb (II), metal ions from water solutions. The batch experiment was conducted to carry out the removal of the above metal ions in aqua media, due to the presence of anionic sites in DSPC it effectively interacted with metal ions and self-undergo oxidation by doing the reduction of the metal. The interaction and reaction between metal and DSPC in aqueous media were confirmed by FTIR techniques which shows the conversion of anionic sites of DSPC into their oxidized form. The author also studied the effects of several parameters on the extraction of metal ions such as pH, adsorption dose, initial metal ion concentration, contact time, and stirring speed. pH is the main factor that influences the rate of adsorption or removal of metal, the present experiment was carried out at pH 1–7 and it was found that maximum adsorptions of Ni (II), Cd (II), and Pb (II) was 95%, 95%, and 98%, respectively. Another main factor is the adsorbent dose which is directly proportional to the rate of adsorption, the rate of adsorption also relies upon the initial concentration of a metal ion in an aqueous solution, when it is presented in higher concentration, the adsorbent dose must be increased for better result,

TABLE 4.1 Summarized the reported synthesis of nano-biosorbent from a variety of sources.

Sr. No.	Nano-biosorbent	Method	Precursor	Condition	Characterization	Product description	Contaminant removal	References
1	Carbonized waste biomass	Calcination	Delbergia sisso pods (DSP)	Calcination at 800 oC	FT-IR, XRD, SEM	Nano-Flaks	Cd (II), Pb (II) and Ni (II) metal ions	Mahajan and Sud (2014)
2	Chitosan-sunflower (CS), chitosan-sunflower-nanoiron (CSN)	Described procedure by Nadaroğlu et al., and Turgut.	chitosan and sunflower waste, an agro-industrial waste and modified using iron nanoparticles	–	FTIR, SEM-EDAX, TEM, XRD, and	Nano-sheet	Methylene Blue dye	Turgut et al. (2020)
3	Sawdust	–	Sawdust and sodium dodecyl sulfate	Dried at of about 60C for 5 h temperature	SEM	Heterogeneous and porous structure	Removal of methylene blue	Ansari et al. (2012)
4	Nanomodified sugarcane bagasse biosorbent	–	sugarcane bagasse (SB) and ferromagnetic nanoparticles (Fe3O4)	Dried at 50°C for 6 h where it was later milled in a rotor mill and stored	FTIR, XRD, and SEM/EDS	Flaks	Cu(II) removal	Carvalho et al. (2020)
5	FNPSA and FNPSOPR	Precipitation	Fe3O4, sodium alginate matrix and saponified orange peel residue	Ultrasound	FTIR, XRD, SEM-EDS DLS and VSM	Spherical	Fluoride from water	Christina and Viswanathan (2015)
6	Sugar beet pulp	Hammer mill	Sugar beet pulp	Air-dried at 40°C	–	sizes of 0.25–0.50 mm	Removal of Pb2+, Cu2+, Zn2+, Cd2+, and Ni2+ cations	Reddad et al. (2002)
7	GQDOs-Ba nano-biosorbent	A bottom-up method	Rice husk	Treated with N2 atmosphere at 700oC for 2 h	FT-IR, SEM, TEM,TGA, and XRD.	Regular aglomerzation	Removal of lead (II) and lanthanum (III)	Sharma et al. (2018)

8	Algal	–	*Ulva fasciata* and Sargassum dentifolium	Dried at 60 oC for 24H.	FT-IR, TEM, ZETA SIZER	0.220 and 0.309 μm	Cu^{2+}	El-Wakeel et al. (2019)
9	Brown algae and chitosan/ PVA nano-fiber membrane	planetary ball mi;;	Sargassum glaucescens	Planetary ball mill (Fara Pajouhesh Isfahan FP2) at 600 rpm for 1 h	SEM	Nanowire and spherical 30–300 nm	Removal of Nickel	Ozdemir et al. (2020)
10	Amberlite XAD-4 loaded with Anoxybacillus kestanboliensis	Biological Method	Anoxybacillus kestanboliensis, XAD-4.	120 rpm and 55°C for 1 day on a rotary shaker	SEM and FT-IR.	Aglomerization	Preconcentrations of Co(II) and Hg(II) in	Leung et al. (2016)
11	Amyloid fibrils	Biological Method	Hen lysozyme	Stirred for 4 h at 50°C and then centrifuged at 14,000 rpm for 4 min	TEM, PL and ZP	Irregular	Removal of dye pollutants	Arshadi et al. (2015)
12	Ostrich bone waste (OBW)	–	Ostrich bone waste (OBW)	Dried oven for 24 h at 70C,	FTIR, XRD, TEM	Aggregation	Phosphate removal	Jain et al. (2017)
13	Nano-cellulose	Precipitation	Aniline and persulfate	Stirred for 26H.	FT-IR, XRD, SEM	rod-like in shape, ∼60 nm in size	Chromium	Pipíška et al. (2020)
14	Magnetically functionalized moss biomass	Microwave	*Rhytidiadelphus squarrosus*	Dried at 60°C for 24 h	(FTIR), XRD, SEM, and EDX	moss leaves	Co^{2+} Ions and thioflavin T	Zare et al. (2018)

the analysis of adsorption studies done based on Freundlich isotherm and Langmuir isotherm models (Mahajan and Sud, 2014).

Synthetic dye is the major constituent of water pollution, different types of dyes were used for several purposes in industrial sectors. The unused dye was present in wastewater dump into water bodies causes many side effects on living things, such type of problem-solving using the nano-biosorbent. The author Esra Turgut and co-workers reported the synthesis of two nano-biosorbent chitosan-sunflower (CS) and chitosan-sunflower-nanoiron (CSN) from chitosan, sunflower waste and modified using iron nanoparticles. The author used reported methods (Gungor et al., 2015; Karaduman et al., 2017; Nadaroglu et al., 2015) for the green synthesis of iron nanoparticles using plant extract of *ficus carica* and $FeCl_2$-$FeCl_3$, the chitosan-sunflower (CS) and chitosan-sunflower-nanoiron (CSN) was prepared using chitosan, pre-dried powder of sunflower waste and green synthesized iron nanoparticles via the reported procedure of Turgut et al. (2020). The synthesized nano-biosorbents was a characterized using FT-IR, UV–Vis, SEM, and TEM technique which shows the low crystal structure and a highly porous surface. The FT-IR spectra of CS and CSN explain the interaction between chitosan-sunflower waste and chitosan-sunflower-nanoiron, respectively, XRD peaks of chitosan-sunflower (CS) at 19.20°, 27.49°, and 32.43° gives the CS structure peaks while the structure of the NPs connected to the peaks of the CS structure in addition to 32.28°, 32.17°, and 37.82° in the presence of peaks of Fe_3O_4 NPs were determined and confirm. The SEM, and TEM images of CS and CSN explain the nearly equal distribution of Fe NPs over the surface of CS which appears as cluster and aggregation due to the magnetic nature of Fe_3O_4 NPs. The author successively used synthesized CS and CSN for the removal of synthetic dyes; he chose Methylene Blue as a reference dye, and analysis was explored according to Langmuir and Freundlich's adsorption isotherm model. The various parameters which affect the rate of adsorption like biosorbent dosage, treating agent, contact time, initial dye concentration, solution pH, and temperature, the interaction during the reaction of methylene blue dye and biosorbent was also studied by UV–Vis, FT-IR, whereas the change in morphology of biosorbent after the adsorption of methylene blue was tested using SEM, and TEM image. It was found that the following optimum condition (pH 5, 30°C, and 60 min) give 80% of CS and 88% of CSN removed MB from aqueous media (Turgut et al., 2020).

Similarly, the author R. Ansari et al. also reported the synthesis of nano-biosorbent utilizing sawdust assisted with sodium dodecyl sulfate (SDS/SD) for the degradation of methylene blue dye. Sawdust is an agricultural waste that is easily available used as the precursor for the synthesis of SDS/SD biosorbent, initially sawdust was washed well and dried at 60°C for 5 h in the oven, then dried sawdust 35 g treat with 500 mL SDS and stirred at ambient temperature for 12 h then dried at 50°C to obtain biosorbent. The morphology of nanostructured SDS/SD was confirmed by SEM technique, SEM image showed the porous and heterogeneous structure of sawdust. Adsorption studies were carried out via two different methods like batch and fixed-bed column systems, and Thomas and the bed-depth service time model (BDST) were employed for study of sorption data, and determining of sorption ability. The analysis and result of biosorption of methylene blue were obtained using Langmuir and Freundlich isotherm equations, the effect of several factors such as initial dye concentration, pH, flow rate, and bed depth on the sorption of MB dye have been reported. The result of biosorption of methylene blue over surfactant-modified sawdust is much efficient than the untreated SD biosorbent (Ansari et al., 2012).

Sugarcane is the main agricultural product in Maharashtra state which is used for the production of sugar whereas sugarcane bagasse is used for the production of alcohol. The sugarcane bagasse was found to be a good biosorbent for the extraction of the pollutants in water, the author Juliana Tosta Theodoro Carvalho and co-workers synthesized nano-modified sugarcane bagasse biosorbent for the extraction of Cu (II) ions in the aqueous medium. The nano-modified sugarcane bagasse was prepared using sugarcane bagasse and ferromagnetic Fe_3O_4 nanoparticles by coprecipitation technique (Labuto et al., 2018; Mascolo et al., 2013; Panneerselvam et al., 2011) in which synthesized Fe3O4 nanoparticles mixed with SB at 80°C for 30 min. The synthesized SB/ Fe_3O_4 and MSB/ Fe_3O_4 were explored by FT-IR, XRD, SEM/EDS techniques, FT-IR spectra explain the presence of different functional groups like hydroxyl (O-H), hydrocarbons (C-H), carbonyl (C=O), C-O, ether (C-O-C), and Fe-O, the above functional group also enlighten the binding sites present in biosorbent. The structural information about the SB/Fe_3O_4 and MSB/Fe_3O_4 obtained from the XRD spectrum confirms the cubic structure, the SEM image also confirms the unequal morphology of SB/Fe_3O_4 and MSB/Fe_3O_4 biosorbent. To determine the charge on the biosorbent surface, it was treated with anionic and cationic such as amaranth red (AM) and methylene blue (MB) dyes. The cationic dye like methylene blue (MB) shows excellent interaction with the anionic surface of biosorbent and vice versa, then after kinetic study for the removal of Cu (II) was investigated at 25°C, pH 6.2 condition and different concentration of Cu (II) ion (Carvalho et al., 2020).

The synthesis of Fe_3O_4 nanoparticles (NPs) and saponified orange peel residue immobilized in sodium alginate matrix (FNPSOPR) as well as Fe_3O_4 NPs immobilized in sodium alginate matrix (FNPSA) as sorbents for fluoride extraction from polluted water reported by author Evangeline Christina, and Pragasam Viswanathan. Initially, Fe_3O_4 NPs were prepared by co-precipitation technique adapted by Thapa et al., further, the synthesized Fe_3O_4 NPs were ultrasonicated with 1.5% sodium alginate solution to obtained magnetic alginate nanoparticles, and to enhance the activity of the catalyst, the surface modification was done in three steps by cross-linking with glutaraldehyde for 20 h, carboxylation with chloroacetic acid for 20 h, and final step is loading with $FeCl_3$ for 24 h. The synthesized surface-modified nanoparticles were analyzed with help of FTIR, SEM-EDX, XRD, DLS, and VSM techniques, the size of Fe_3O_4 NPs was confirmed by SEM, EDX, and DLS techniques, the SEM image confirmed the agglomeration with a mean size of 21 nm was as the hydrodynamic size of the particles was found to be approximately 140 nm by DLS techniques. The XRD data confirmed the cubic morphology with high purity of Fe_3O_4 nanoparticles, also the VSM study shows that synthesized Fe3O4 nanoparticles are superparamagnetic with a coercivity of 70.541 Oe.

The adsorption capacity of synthesized nan-omaterial was found by batch methods with the help of sorption isotherm and reaction kinetics study, for this purpose the uniform bed of FNPSA and FNPSOPR was prepared and sorption study of chlorine ions was studied. The maximum sorption ability of FNPSA and FNPSOPR were found to be 58.24 and 80.33 $mg{\cdot}g^{-1}$ respectively. Five sorption-desorption cycles exhibited 100%, 97.56%, 94.53%, 83.21%, and 76.53% of regeneration of FNPSOPR (Christina and Viswanathan, 2015). Agriculture waste also has a marvelous capacity to adsorbed heavy metal present in water sources, sugar beet pulp is one of the most popular examples, which is used as bioadsorbent, the author Zacaria Reddad et al. reported the adsorption of several metal ions using cost-effective bioadsorbent. In the present study, the commercially available sugar beet pulp was crushed by hammer mill

and get milled particle having size 0.25–0.50 mm which was used for further process. The obtained particles were washed well with help of distilled water to remove the impurity as well different ions, further, they are dried at 40°C and used for adsorption study of metals. The author tested the kinetic study of beet pulp particles by adsorption test, 2 g of beet pulp was dissolved in 800 mL of distilled water stir on a magnetic stirrer and initial concentration of metal chloride 0.0004 M allow to adsorbed on it, the extent of adsorption was recorded by atomic absorption spectrometer. Similarly, the sorption study of nano-biosorbent was carried out, in the same manner, using Langmuir and Freundlich adsorption isotherm (Reddad et al., 2002).

Methylene blue is an important dye used in different industries for several purposes, they also have some side effects on aquatic and human life, hence the need to remove it from water bodies. Several methods were reported and adapted for the removal of methylene blue dye, but one of the best and effective ways is the adsorption of methylene blue dye on the matter. The author Swati Sharma and co-workers reported the synthesis of nano-bioadsorbent using iron oxide nanoparticles and biomass. In the present paper, the author prepares nano-bioadsorbents by the combination of previously synthesized iron oxide NPs and Agrobacterium fabrum biomass in sodium alginate solution over calcium chloride. The morphological study of synthesized nano-bioadsorbent was done with help of the FESEM technique, the elemental composition was determined by EDX technique, and the involvement of functional group was understood by FTIR technique. The batch-wise adsorption study was carried out by determining the optical density of the resultant solution at various parameters like initial dye concentration, temperature, contact time, and pH. In the present study, 1 g of synthesized nano-bioadsorbent was added to different methylene blue concentrations of 25, 50, 100, and 200 mg/L with constant stirring at 160 rpm and 50°C. The amount of adsorption was studied by calculating the optical density of the resultant solution (Sharma et al., 2018).

The biological microorganism also plays the role of nano-bioadsorbent, the author Shaimaa T. El-Wakeel and et al. reported the algal bioadsorbent for the extraction of heavy metal from water medium. In the present study, the author collected the two macro-algal biomasses *Ulva fasciata* and Sargassum dentifolium, washed well, dried, and ground them in a ball mill to micro-size powder. The micro-size powder was characterized using FTIR, TEM, and DLS techniques, after the morphological analysis of nanobioadsorbent was used for the removal of Cu (II) ion from aqueous medium. The adsorption efficiency of nano-bioadsorbent was determined by batch experiment, where the 1 g adsorbent was added in 1lit solution of Cu (II) ion, the efficiency of adsorption was investigated by considering the vital parameter like pH, initial due concentration, temperature, adsorbent dose, and contact time. Finally, the resultant concentration of a metal ion in solution was investigated by inductively coupled plasma-Optical Emission spectroscopy (ICP-OES), and analysis were done with help of Langmuir, Freundlich, and Dubinin–Radush kevich models (Mahamadi, 2019). Similarly, the author A. Esmaeili and A. Aghababai Beni reported the use of brown algae and chitosan/PVA nano-fiber for the removal of nickel.

The preparation of chitosan/VPA nano-fiber and biomass using brown algae was made by the previous procedure given in Esmaeili and Aghababai Beni (2015a, b), the synthesized nano-bioadsorbent was subjected to the characterization using different spectroscopic, and microscopic techniques, FTIR technique confirms the presence functional groups imparted

by chitosan/PVA nano-fiber and *S. glaucescens*. The morphology and surface area of nano-bioadsorbent was investigated with help of SEM and BET techniques. The continuous system was formed by the combination of two reactors which contain three parts, two membranes, and a reactor. In the reactor, the nano-bioadsorbent containing ligand sides bind with the nickel-metal ions and adsorb on its surface, where the biosorption was nickel ion on the surface of adsorbent explained by the mechanisms of electrostatics, ion exchange, complexation, covalent force adsorption, and micro-sized deposition (El-Wakeel et al., 2019).

A novel nano-bioadsorbent composed of Amberlite XAD-4 and Anoxybacillus kestanboliensis was reported by author Sadin Ozdemir and et al., the Anoxybacillus kestanboliensis was isolated from Turkey, were as the morphological and biological analysis was done. The fabrication of dried dead Anoxybacillus kestanboliensis and loaded biomass were prepared according to Ozademir et al. with some modifications. After the preparation of the nano-biosorbent, characterization was done with help of techniques like FTIR, SEM, and EDX mapping. The author also studied the effect of flow rate, amounts of nano-bioadsorbent and resin, influence of eluent type, concentration and volume, the influence of matrix ions on retention of Co(II) and Hg(II), the effect of sample volume and determination of enrichment factor on the efficiency adsorption. Finally, the author reported the maximum biosorption capacity of novel biosorbent as 24.3 and 27.8 mg g^{-1} respectively (Ozdemir et al., 2020). The author reported the synthesis and use of Amyloid Fibrils as a rapid and efficient nano-biosorbent for the removal of dye. In the present study, the Amyloid fibril of hen lysozyme, which is an excellent source of protein nano-fiber considered as nano-biosorbent, this protein nano-fiber was synthesized in one step using the green route. The zeta-potential analysis confirms the positive/negative charges on nano-biosorbent and the hydrophobic region as well, the presence of active charge sides in nano-biosorbent make them more reactive and can form interaction with organic dye and it explains the process of biosorption of organic dye present in aqueous media. The author reported the maximum sorption capacity of biosorbent is 60% in 15 min (Leung and Lo, 2016).

A new nano-biosorbent was reported for the removal of phosphate in synthetic and real water sample synthesized by the combination of Ostrich bone waste and nanoscale zero-valent iron, the author M. Arshadi et al. collected the Ostrich bone waste from the local store, washed well several times using distilled water to remove the unwanted fat and flash, then after put in the oven for 24 h at 70°C, the selected size of particles 305 μ were collected and reflux with the 0.1 M HNO_3 for 2 h to enhance the sorption efficiency towards phosphate. The nano zero-valent iron was synthesized using $FeSO_4.4H_2O$ dissolved in 4/1 (v/v) ethanol/water, then OBW-HNO3 solution was added dropwise and ultrasonicated for 25 min to result from homogeneous solution. Finally, the resultant black color nano-biosorbent was obtained by adding dropwise NaBH4 solution. The morphology of synthesized nano-biosorbent was investigated using TEM, and EDX techniques, where the surface area was known with help of BET techniques, and chemical composition was understood using chemical analysis and ICP-AES techniques. The adsorption study was carried out using batch experiments, were the 0.5 g of synthesized nano-biosorbent shaken with 50 mL solution having a concentration between 0.75 and 1000 mg/L (Arshadi et al., 2015). The author Priyanka Jain and co-workers reported the synthesis of difunctionalized-polyaniline-modified nanocellulose composite sorbent (PANINCC) has been used for the removal of trivalent and hexavalent chromium from water bodies. The polyaniline was synthesized by adding

15 mL ammonium persulfate solution into aniline-HCl solution, into that 10 g of nanocellulose was mixed at ambient temperature with constant stirring for 10 h result in nano-biosorbent. The morphology of the resultant nano-biosorbent was investigated using SEM, TEM, XRD, and confirm the rod-like structure with size 60 nm, where the elemental analysis was done with the help of EDX techniques. The sorption study of chromium chloride over synthesized nano-sorbent was done through batch experiment, in which known concentration of chromium chloride with the variable dosage of nano-sorbent, at different pH, different volume, and at different temperature stirred at 40 min, was the maximum capacity of sorbent was found to be 96% (Jain et al., 2017).

The author Martin Pipíška and co-workers reported the microwave-assisted synthesis of iron oxide nanoparticles and microparticles and they are used in the preparation of Moss biomass from *Rhytidiadelphus squarrosus* moss. The magnetical moss biomass was prepared according to the procedure of Safarik and Safarikova, in which 1 g of $FeSO_4.7H_2O$ was dissolved in 200 mL distilled water and 1 mol/L of NaOH was slowly added with constant stirring to reach the 12 pH of the solution, the resultant suspension was treated in the domestic microwave for 10 min. Finally, suspension mix with the 1 g of *R. squarrosus* biomass in water to get magnetically moss biomass after 60°C for 24 h. The surface characterization of magnetical biomass was done with the help of SEM-EDX, and XRD before and after sorption of Co^{2+} and thioflavin. The adsorption mechanism involves the active sides of nano-biosorbent, the oxygen functionality present in biomass form electrostatic interaction with Co^{2+} and thioflavin (Pipíška et al., 2020). The author reported the development of an effective nano-biosorbent based on poly-*m*-phenylenediammine grafted dextrin for the removal of Pb(II) and methylene blue dye in aqueous media. The synthesis of the present nano-biosorbent is carried out in three steps, first step involves the chemical synthesis of dextrin-g-poly-*m*-phenylenediamine (DgPmPDA), in which 1.25 g Dex was taken in 50 mL of distilled water in 100 three-naked flasks with constant stirring for 30 min at 50°C, after cooling 3.75 mL of HCl (1 M) was added to the same solution and again stir for 30 min at 0–5°C in an inert atmosphere. Then successive addition was taken place of APS solution in 30 min and mPDA solution in 2 min dropwise in an inert atmosphere, finally the resulting precipitate was with water, ammonia, and acetone to remove unreacted chemicals from solution. In the second step, the synthesis of graphene oxide was carried out according to modified hummer's procedure (Marcano et al., 2010). In this procedure the mixture of concentrated H2SO4/H3PO4 was added to a mixture of graphite flask and $KMnO_4$, the mixture was stirred for 12 h at 50°C. Finally, the reaction mixture was poured into an H_2O_2 solution, and obtained black powder was dried at 90°C for 24 h. Finally, the preparation of Dex-g-PmPDA@GO (DgPmPDA@GO) nano-biosorbent was done using the solution blending technique (Lago et al., 2016). In this procedure, both components dispersed in chloroform separately and then were mixed in an ultrasonic bath for 2 h at 25°C.

The characterization of each part of nano-biosorbent was done with help of FTIR, CHN, XRD, FESEM, AFM, and TGA techniques, which confirm the slight agglomeration present in synthesized nano-biosorbent. The adsorption study was carried out considering the effect of pH of the solution, adsorbent dosage, contact time, initial concentration of Pb(II) and methylene blue dye, and experimental data put forth in terms of Langmuir isotherm which is found to good (Zare et al., 2018).

4.4 Conclusion

The numerous techniques of synthesis of nano-biosorbents are discussed in this chapter, as well as their significant application in environmental remediation. The goal is to classify diverse raw materials and assess their uses in diverse environmental uses. The research presented here reveals minute data about the size, shape, characteristics, and uses of nano-biosorbents. For the preparation of nano-biosorbents, several biocompatible reagents and sources, as well as energy-efficient procedures, have been discussed in detail. This chapter explored many roles of nano-biosorbents as catalysts, adsorbents, and their toxicological effects. Furthermore, the synthesis of nano-biosorbents using a green approach, which is currently being developed, has been highlighted. Furthermore, the several green synthesis pathways were assessed critically in terms of their stability, size distribution, and various other aspects. In conclusion, diverse nanotechnology protocols have been investigated in this chapter, which will be useful in future research as a guide to study and use for further improvements in developing better nano-biosorbents to deal with real-world sewage and polluted solutions with the least risk of toxicological effects on the ecosystem. This chapter may be interesting to readers who want to learn more about the synthesis of nano-biosorbents and their remarkable effectiveness in diverse environmental applications.

References

Ali, I., 2012. New generation adsorbents for water treatment. Chem. Rev. 112 (10), 5073–5091. https://doi.org/10.1021/cr300133d.

Amin, M.T., Alazba, A.A., Manzoor, U., 2014. A review of removal of pollutants from water/wastewater using different types of nanomaterials. Adv. Mater. Sci. Eng. 2014, 1–24. https://doi.org/10.1155/2014/825910.

Ansari, R., Seyghali, B., Mohammad-khah, A., Zanjanchi, M.A., 2012. Application of nano surfactant modified biosorbent as an efficient adsorbent for dye removal. Sep. Sci. Technol. 47 (12), 1802–1812. https://doi.org/10.1080/01496395.2012.658485.

Arshadi, M., Gholtash, J.E., Zandi, H., Foroughifard, S., 2015. Phosphate removal by a nano-biosorbent from the synthetic and real (Persian gulf) water samples. RSC Adv. 5 (54), 43290–43302. https://doi.org/10.1039/c5ra03191e.

Beni, A.A., Esmaeili, A., 2019. Biosorption, an efficient method for removing heavy metals from industrial effluents: a review. Environ. Technol. Innov. https://doi.org/10.1016/j.eti.2019.100503.

Carvalho, J.T.T., Milani, P.A., Consonni, J.L., Labuto, G., Martins Carrilho, E.N.V., 2020. Nanomodified sugarcane bagasse biosorbent: synthesis, characterization, and application for Cu(II) removal from aqueous medium. Environ. Sci. Pollut. Res. https://doi.org/10.1007/s11356-020-11345-3.

Christina, E., Viswanathan, P., 2015. Development of a novel nano-biosorbent for the removal of fluoride from water. Chin. J. Chem. Eng. 23 (6), 924–933. https://doi.org/10.1016/j.cjche.2014.05.024.

Crini, G., Torri, G., Lichtfouse, E., Kyzas, G., Wilson, L., et al., 2019. Dye removal by biosorption using cross-linked chitosan-based hydrogels. Environ. Chem. Lett. 17 (4), 1645–1666. https://doi.org/10.1007/s10311-019-00903-y.

Dabhane, H., Ghotekar, S., Tambade, P., Medhane, V., 2020. Plant mediated green synthesis of lanthanum oxide (La_2O_3) nanoparticles: a review. Asian J. Nanosci. Mater. 3 (4), 291–299. https://doi.org/10.26655/AJNANOMAT.2020.4.3.

Dabhane, H., Ghotekar, S., Tambade, P., Pansambal, S., Ananda Murthy, H.C., Oza, R., Medhane, V., 2021. Cow urine mediated green synthesis of nanomaterial and their applications: a state-of-the-art review. J. Water Environ. Nanotechnol. 6 (1), 81–91. https://doi.org/10.22090/jwent.2021.01.008.

El-Sayed, H.E.M., El-Sayed, M.M.H., 2014. Assessment of food processing and pharmaceutical industrial wastes as potential biosorbents: a review. Biomed. Res. Int. 2014, 1–24. https://doi.org/10.1155/2014/146769.

El-Wakeel, S.T., Moghazy, R.M., Labena, A., Husien, S., 2019. Algal biosorbent as a basic tool for heavy metals removal: the first step for further applications. J. Mater. Environ. Sci. 10 (1), 75–87.

Esmaeili, A., Aghababai Beni, A., 2015a. Biosorption of nickel and cobalt from plant effluent by *Sargassum glaucescens* nanoparticles at new membrane reactor. Int. J. Environ. Sci. Technol. 12, 2055–2064. https://doi.org/10.1007/s13762-014-0744-3.

Esmaeili, A., Aghababai Beni, A., 2015b. Novel membrane reactor design for heavy-metal removal by alginate nanoparticles. J. Ind. Eng. Chem. 26, 122–128. https://doi.org/10.1016/j.jiec.2014.11.023.

Gungor, A.A., Celebi, N., Nadaroglu, H., 2015. Removal of basic red 9 in wastewater using green Fenton reaction. Fresenius Environ. Bull. 24 (5B), 1947–1957.

Huang, D., Li, B., Ou, J., Xue, W., Li, J., Li, Z., Guo, X., 2020. Megamerger of biosorbents and catalytic technologies for the removal of heavy metals from wastewater: preparation, final disposal, mechanism and influencing factors. J. Environ. Manag. 261, 109879. https://doi.org/10.1016/j.jenvman.2019.109879.

Jain, P., Varshney, S., Srivastava, S., 2017. Synthetically modified nano-cellulose for the removal of chromium: a green nanotech perspective. IET Nanobiotechnol. 11 (1), 45–51. https://doi.org/10.1049/iet-nbt.2016.0036.

Kanamarlapudi, S.L.R.K., Chintalpudi, V.K., Muddada, S., 2018. Application of biosorption for removal of heavy metals from wastewater. In: Biosorption. IntechOpen, https://doi.org/10.5772/intechopen.77315.

Karaduman, I., Gungor, A.A., Nadaroglu, H., Altundas, A., Acar, S., 2017. Green synthesis of y-Fe_2O_3 nanoparticles for methane gas sensing. J. Mater. Sci. Mater. Electron. 28 (21), 16094–16105. https://doi.org/10.1007/s10854-017-7510-5.

Labuto, G., Cardona, D.S., Debs, K.B., Imamura, A.R., Bezerra, K.C.H., Carrilho, E.N.V.M., Ferreira, P.S.H., 2018. Low cost agroindustrial biomasses and ferromagnetic bionanocomposites to cleanup textile effluents. Desalin. Water Treat. 12, 80–89. https://doi.org/10.5004/dwt.2018.21914v.

Lago, E., Toth, P.S., Pugliese, G., Pellegrini, V., Bonaccorso, F., 2016. Solution blending preparation of polycarbonate/graphene composite: boosting the mechanical and electrical properties. RSC Adv 6 (100), 97931–97940. https://doi.org/10.1039/C6RA21962D.

Leung, W.-H., Lo, W.-H., Chan, P.H., 2016. Amyloid fibrils as rapid and efficient nano-biosorbents for removal of dye pollutants. RSC Adv. 6, 58363–58364.

Mahajan, G., Sud, D., 2014. Nano sized carbonized waste biomass for heavy metal ion remediation. Pol. J. Chem. Technol. 16 (4), 6–13.

Mahamadi, C., 2019. On the dominance of Pb during competitive biosorption from multi-metal systems: a review. Cogent Environ. Sci. 5, 1635335. https://doi.org/10.1080/23311843.2019.1635335.

Marcano, D.C., Kosynkin, D.V., Berlin, J.M., Sinitskii, A., Sun, Z., Slesarev, A., Tour, J.M., 2010. Improved synthesis of graphene oxide. ACS Nano 4 (8), 4806–4814. https://doi.org/10.1021/nn1006368.

Mascolo, M., Pei, Y., Ring, T., 2013. Room temperature co-precipitation synthesis of magnetite nanoparticles in a large pH window with different bases. Materials 6 (12), 5549–5567. https://doi.org/10.3390/ma6125549.

Nadaroglu, H., Gungor, A.A., Celebi, N., 2015. Removal of basic red 9 (BR9) in aqueous solution by using silica with nano-magnetite by enzymatic with Fenton process. Int. J. Environ. Res. 9 (3), 991–1000. https://doi.org/10.22059/IJER.2015.987.

Ozdemir, S., Kılınç, E., Fatih, S., 2020. A novel biosorbent for preconcentrations of Co(II) and Hg(II) in real samples. Sci. Rep. 10 (1). https://doi.org/10.1038/s41598-019-57401-y.

Panneerselvam, P., Morad, N., Tan, K.A., 2011. Magnetic nanoparticle (Fe_3O_4) impregnated onto tea waste for the removal of nickel (II) from aqueous solution. J. Hazard. Mater. 186 (1), 160–168. https://doi.org/10.1016/j.jhazmat.2010.10.102.

Pipíška, M., Zarodňanská, S., Horník, M., Ďuriška, L., Holub, M., Šafařík, I., 2020. Magnetically functionalized moss biomass as biosorbent for efficient Co^{2+} ions and thioflavin T removal. Materials 13 (16), 3619. https://doi.org/10.3390/ma13163619.

Reddad, Z., Gerente, C., Andres, Y., Le Cloirec, P., 2002. Adsorption of several metal ions onto a low-cost biosorbent: kinetic and equilibrium studies. Environ. Sci. Technol. 36 (9), 2067–2073. https://doi.org/10.1021/es0102989.

Sharma, S., Bhattacharya, A., 2016. Drinking water contamination and treatment techniques. Appl. Water Sci. 7 (3), 1043–1067. https://doi.org/10.1007/s13201-016-0455-7.

Sharma, S., Hasan, A., Kumar, N., Pandey, L.M., 2018. Removal of methylene blue dye from aqueous solution using immobilized Agrobacterium fabrum biomass along with iron oxide nanoparticles as biosorbent. Environ. Sci. Pollut. Res. 25 (22), 21605–21615. https://doi.org/10.1007/s11356-018-2280-z.

Srivastava, V., Zare, E.N., Makvandi, P., Zheng, X., Iftekhar, S., Wu, A., Sillanpaa, M., 2020. Cytotoxic aquatic pollutants and their removal by nanocomposite-based sorbents. Chemosphere 258, 127324. https://doi.org/10.1016/j.chemosphere.2020.127324.

Tara, N., Siddiqui, S.I., Rathi, G., Chaudhry, S.A., Inamuddin, Asiri, A.M., 2019. Nano-engineered adsorbent for removal of dyes from water: a review. Curr. Anal. Chem. 15. https://doi.org/10.2174/1573411015666190117124344.

Tran, H.N., Nguyen, H.C., Woo, S.H., Nguyen, T.V., Vigneswaran, S., Hosseini-Bandegharaei, A., Chao, H.-P., 2019. Removal of various contaminants from water by renewable lignocellulose-derived biosorbents: a comprehensive and critical review. Crit. Rev. Environ. Sci. Technol., 1–65. https://doi.org/10.1080/10643389.2019.1607442.

Turgut, E., Alayli, A., Nadaroglu, H., 2020. Preparation of chitosan, sunflower and nano-iron based core shell and its use in dye removal. Adv. Environ. Res. 9 (2), 135–150. https://doi.org/10.12989/aer.2020.9.2.135.

Zare, E.N., Lakouraj, M.M., Kasirian, N., 2018. Development of effective nano-biosorbent based on poly m-phenylenediamine grafted dextrin for removal of Pb (II) and methylene blue from water. Carbohydr. Polym. https://doi.org/10.1016/j.carbpol.2018.08.091.

This page intentionally left blank

CHAPTER

5

An insight into the potential contaminants, their effects, and removal means

Fatma Gurbuz[a] *and Mehmet Odabaşı*[b]

[a]Department of Environmental Engineering, University of Aksaray, Aksaray, Turkey
[b]Department of Chemistry, Faculty of Science, Aksaray University, Aksaray, Turkey

5.1 Contaminants of concern

A substance that has an adverse effect on the receiving environment at higher than normal concentration as a result of human activity may be a reasonable definition for pollutants. On the other hand, contaminants according to the European legislation, as substances that are toxic, persistent, and liable to bioaccumulate are the presence of elevated concentrations in the environment above the natural background level for the area and for the organism (DIRECTIVES, 2013). Hence, contaminants are not defined as pollutants unless they have some harmful effect on living and change the normal composition of an environment (Schultz, 2014). Contaminants can be chemical, microbiological, physical, or radiological substance that are hazardous to environmental compartments and living organisms, even humans.

Major contaminant groups, their effect and removal processes are given here. Important chemical contaminants, such as metals, chlorinated pesticides, halogenated aliphatic hydrocarbons, polychlorinated biphenyls (PCBs), polycyclic aromatic hydrocarbons (PAHs), are discussed. Other contaminants which are not fully realized, however, linked to environmental and human health risks related issues, and are a growing concern of the scientific community over the last decade, are defined as emerging contaminants (ECs) (Lopez et al., 2015). ECs including pharmaceuticals, personal care products, etc. are also summarized in this chapter.

https://doi.org/10.1016/B978-0-323-90912-9.00005-8

5.2 Understanding the major contaminants and sources

A wide group of chemicals can contaminate and impact the environment we live in greatly, and adversely affecting human health. Contaminants can arise from numerous anthropogenic sources such as land-based industrial activities, oil and chemical spills; non-point sources such as storm drains; runoff from agricultural lands, wastewater treatment plants and sewage systems, atmospheric deposition, mineral exploration and exploitation, and riverine inputs. Environmental contamination such as certain metals, pesticides, pharmaceuticals, polyaromatic hydrocarbons solvents, polyhalogenated biphenyls, etc., can occur and represent one of the main challenges driven by anthropogenic activity (Global Chemicals Outlook, 2013; Stuart et al., 2012).

Since aquatic environments receive contaminants due to industrial wastes, inadequate wastewater treatments and leaks, freshwater resources are increasingly polluted worldwide (Bhat et al., 2017; Hampel et al., 2015). A lack of access to safe water supplies is a major concern for public and community health (WHO, Guidelines for Drinking-Water Quality, 2017). To protect human beings from getting exposed to chemicals, under the Water Pollution Control Act (EPA), toxic and priority pollutants are listed in Table 5.1, and codified at 40 CFR 401.15 (Protection of Environment, 2021, 2021) which has reached the number of 129 pollutants.

These high number of chemicals did not include all emerging contaminants (ECs) such as endocrine disruptors (EDs), pesticides, pharmaceuticals, personal care products, hormones, plasticizers, etc. However, some of the ECs are listed in the Contaminant Candidate List 4 (CCL4) which contains 97 chemicals or chemical groups and 12 microbial contaminants (Federal Register, 2016). These are chemicals used in industries, pesticides, disinfection by products, pharmaceuticals, biological toxins (cyanotoxins), and waterborne pathogens. ECs of high concern are broadly distributed in places such as surface and groundwater and have been reported by numerous researchers over the last decade (Lopez et al., 2015).

TABLE 5.1 Major chemical contaminant list summarized.

Types	Contaminants	Sources
Metals, metalloids, organometals	Cadmium, copper, zinc, and iron; lead, mercury, silver; and arsenic asbestos and cyanide	Household effluents, mining, and associated industries, fertilizers, fuels, and well water
Pesticides (carbamates, organophosphates, pyrethroids, organochlorines)	Alachlor, atrazine, 2,4-D, chlorpyrifos Clopyralid, Dinoseb, Diquat Diuron, 1,2-Dibromo-3-chloropropane (DBCP), Endothall epichlorohydrin Heptachlor, Heptachlor epoxide lindane, malathione, and methoxychlor, Oxamyl (Vydate), Picloram, Simazine, Toxaphene	Runoff from herbicides, insecticides, and fungicides, used on row crops
Fertilizers	Nitrates, ammonium nitrogen and phosphates	Effluents from household, agriculture, and aquaculture, Runoff from fertilizer use; leaching from septic tanks, sewage; erosion of natural deposits

TABLE 5.1 Major chemical contaminant list summarized—cont'd

Types	Contaminants	Sources
Pharmaceuticals and personal care products (PCPP)	Fluoxetine (Prozac), Carbamazepine, Diphenhydramine, Antibiotics (Tetracycline, Erythromycin, Analgesics and anti-inflammatories (Ibuprofen, diclofenac, paracetamol etc.) Nitro, polycyclic and phthalates Detergent metabolites (Nonylphenol) Para-hydroxybenzoate, Antiseptics (Triclosan, chlorophane)	Released due to insufficient wastewater treatment, discharge from households and factories
Endocrine-disrupting Compounds (EDCs)	Di(2-ethylhexyl) phthalate, Polychlorinated biphenyls (PCBs) several organochlorine insecticides, Benzo(*a*) pyrene (PAHs)	Hormones, steroids in water cycle, wastewater, due to insufficient wastewater and water treatments
Hydrocarbons	Benzene ethylbenzene, trimethylbenzenes, hexachlorobenzene, hexachloro-cyclopentadiene toluene, xylenes, naphthalene, polycyclic aromatic hydrocarbons (PAHs) (fluorene, benzo(*a*) pyrene, anthracene, phenanthrene etc.)	Mainly distillation products of petroleum, discharge from factories; leaching from gas storage tanks and landfills
Halogenated compounds	polychlorinated biphenyls, (PCBs), dioxins (e.g., TCDD), polychloro dibenzofurans (PCDFs) and organochlorine insecticides, 1,2-dichloropropane, 1,1,2-trichlorethane, tetrachloroethylene, carbon tetrachloride, chloroform	These hydrocarbons arise mostly from industrial (Emissions from waste incineration and other combustion) and household solvents
Hormones and Steroids	Estrone, estradiol dihydrotestosterone (DHT), progesterone cholesterol, coprostanol	Pharmaceuticals, personal care products, industrial additives etc.
Pathogens	Pathogens, *Escherichia coli, Helicobacter pylori, Legionella pneumophila, Mycobacterium avium, Naegleria fowleri, Salmonella enterica, Shigella sonnei*	Viruses *Adenovirus, Caliciviruses, Campylobacter jejuni, Enterovirus, Hepatitis A virus*
Radionuclides	Radium-226-228, uranium, thorium, gross alpha and gross beta emissions	Sources are natural deposits, mill tailings, from oil and gas deposits during their process, mining activities, military waste, coal-fired power plants

Hundreds of millions of people are dangerously contaminated, or chemically polluted by consuming drinking water, because of inadequate treatments of urban, industrial, and agricultural wastewaters. The vast number of chemical in water system poses a significant challenge to policy regulators, engineers, and scientific community (Benotti et al., 2009; Matthiessen et al., 2018).

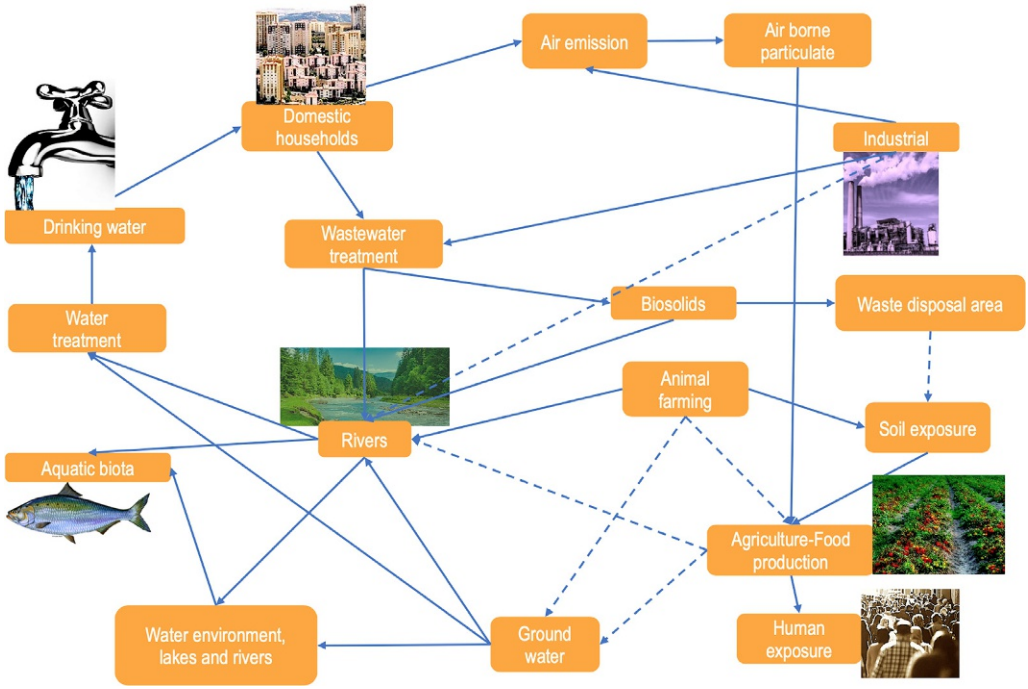

FIG. 5.1 Cycle of contaminants.

The contaminants are implicated in outbreaks of diseases or endocrine effects, and have an impact on fresh water and on nontarget plants and animals in agricultural and urban landscapes and human. Some studies have shown that even extremely low exposure to certain pollutants can have impacts on biological systems (Matthiessen et al., 2018).

The most frequently detected chemicals in the streams were found as caffeine, cholesterol coprostanol, N-Ndiethyltoluamide, triclosan, tri (2-chloroethyl), phosphate, and 4-nonylphenol according to the study by Kolpin et al. (2002). The representative cycle of contaminants in ecological environment is given in Fig. 5.1.

5.3 Metals, metalloids, organometals

Soil, as natural buffer, controls the transport of heavy metals to air, water, and earth (Kabata-Pendias, 2010). Anthropogenic activities build up the concentration of metals particularly in urban soils (Guagliardi et al., 2013). Globally, more people prefer living in urban areas than in rural areas, up until 2018 with 55% of the world's population residing in urban areas and it is projected to increase to 68% by 2050 (2018 Revision of World Urbanization Prospects, 2018).

Metals reach the aqueous environment through effluents of mining and smeltery, leachates from waste dumps, domestic and agricultural use of metals and metal-containing compounds (Nikinmaa, 2014). Metals dissolved in the water environment are more mobile and biologically available compared to the environment in which they are in particulate form. Metals with known toxic effects include lead, mercury, arsenic, cadmium, and chromium. These elements are of great public health significance due to their high degree of toxicity (Kumar et al., 2017; WHO, Guidelines for Drinking-Water Quality, 2017). Radioactive metals due to their ionizing emissions as well as their chemical toxicity, may be potentially hazardous in both cases. Hence the tolerated concentration limits of heavy metals in natural waters have been suggested to be between 0.01 and 0.05 mg/L by the United States Environmental Protection Agency (US-EPA) and the World Health Organization (WHO), (National Primary Drinking Water Regulations, 2009; WHO, Guidelines for Drinking-Water Quality, 2017). Moreover, heavy metals are toxic chemicals, since they are generally harmful for the fauna and flora.

Metal exposure may cause various cardiovascular problems (Myong et al., 2014), reproductive damage (Al-Gubory, 2014), kidney problems (Johri et al., 2010), neurological disorders (Mason et al., 2014), and cancer (Zhang et al., 2014).

5.3.1 Arsenic

Arsenic is a naturally occurring toxic metalloid element that is found ubiquitously in the environment throughout the earth's crust and groundwater; it is also found in the air and food products, especially, crustaceans and seafood. The release of arsenic into the environment proliferates through weathering and mining processes, also by a volcanic activity. Arsenic is a by-product in smelting processes for many ores including cobalt, gold, lead, nickel, and zinc (Olsen and Mørland, 2004). Various arsenic forms with different toxicities appear in three major forms: inorganic (As(0), As(III) and As(V)., organic (monomethyl arsenic), and arsine gas. Inorganic arsenic is particularly arsenite that is considered to be more toxic than organic form, yet arsine is the most toxic form and inhalation of arsine over 10 ppm is lethal (Kuivenhoven and Mason, 2021).

Arsenic pollution in water resources is a major concern due to its presence at high concentration and associated adverse health effects (Gurbuz et al., 2019), as exposure to humans can be lead through consuming of contaminated water and food (Talukder et al., 2012). Notably, in some developing countries, contaminated groundwater appears to be the major source of drinking water (Duker et al., 2005). The World Health Organization (WHO) recommended the maximum acceptable limits for safe drinking water as 10 μg/L (WHO, 2011). Organic arsenic is considered to be insignificant in aquatic environments where crustaceans and other fish are a known source of organic arsenic exposure.

5.3.2 Lead

Lead is poison, a potent neurotoxin, which have deadly effects, have been known for nearly 3000 years. It is possibly first larger scale aquatic environmental issue resulted from lead water pipes that were used by Romans (Retief and Cilliers, 2006). From a drinking-water

perspective, use of lead compounds in older water distribution systems and plumbing is an important issue for human exposure (WHO, Guidelines for Drinking-Water Quality, 2017). Lead in water piping systems is a challenging problem that several countries in the E.U., Australasia, Asia, and USA are still facing; (Harvey et al., 2016; Roy and Edwards, 2019) in addition to this, in most countries where no regulations are in order to restrict the use of lead in paints (Global Report, 2017). Lead from exhaust fumes mainly caused air pollution, so the exposure of lead can occur from inhalation of lead fumes and particles.

Lead is an odorless, colorless, and tasteless chemical unlike other contaminants such carcinogens and killers as pesticides, and even radioactive materials, does not break down over time, not vaporize, and it never disappears. Pb can harm the nervous system, liver, and kidney, resulting in gastrointestinal damage, cause Alzheimer's disease, and even child amentia (Silver et al., 2016). Acute toxicity of lead occurring at high levels and related to occupational exposure is quite uncommon. It has some symptoms, i.e., blindness, brain damage, kidney disease, and convulsions.

5.3.3 Mercury

Mercury (Hg) is highly toxic that is found naturally in the earth's crust however introduced to environment by human activities such as mining, fossil fuel combustion, chlor-alkali industry, paint production, metallurgical processes, and dental residues. It also occurs through natural causes, like weathering, atmospheric volcano emanations, and degasification. It is emitted into air, transported and deposited to terrestrial and aquatic ecosystems. Three forms of mercury are found in nature— elemental mercury (HgO), inorganic mercuric salts (i.e., $HgCl_2$, HgS, Hg_2Cl_2), and organic forms (i.e., ethyl ($C_2H_5Hg^+$), methylmercury (CH_3Hg^+)) (Azevedo et al., 2011; Bjørklund et al., 2017). Mercury poisoning can induce changes in the nervous system of humans, especially in the case of young children (Ralston and Raymond, 2018). Under the vapor form it affects the kidneys, the brain, and the nervous system, and interacts negatively with dopamine. Mercury is toxic to all known living species; especially aquatic organisms are highly exposed to dissolved Methylmercury (Tan et al., 2009). MeHg is quickly absorbed, rapidly distributed to all tissues of fish, and accumulates mainly in their muscle tissue, and slowly metabolized to inorganic form (Arcagni et al., 2018; Ruus et al., 2017).

5.4 Contaminants of emerging concern (CECs)

Contaminants of emerging concern is a phrase used to broadly classify chemicals which do not fall under standard monitoring in the environment and regulatory programs but have the potential to enter the environment and cause known or suspected adverse ecological and/or human health effects (Glassmeyer et al., 2008). Antimicrobials detergent metabolites disinfectants, disinfection by-products, fire retardants, industrial additives, life-style products (Caffeine, Nicotine), PAHs (poly-aromatic hydrocarbons), pharmaceuticals, personal care products, plasticizers, reproductive hormones, solvents, steroids, surfactants are categorized

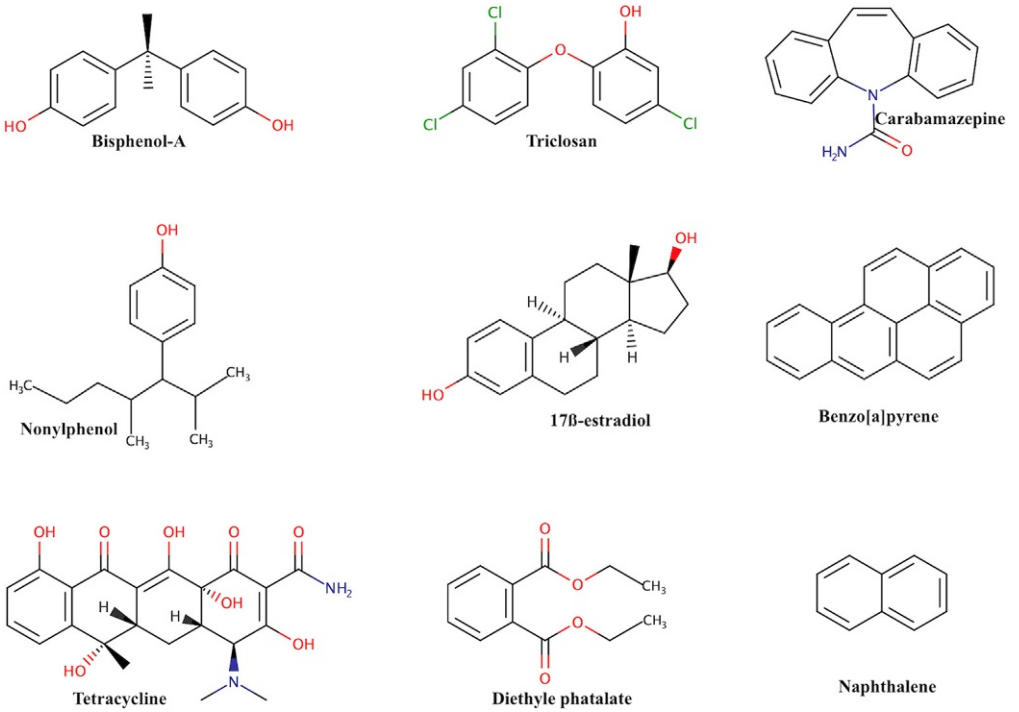

FIG. 5.2 Common contaminants of emerging concern.

as emerging contaminants found mainly in municipal sewage (Raghav et al., 2013; Rodil et al., 2012). Chemical formula of some common contaminants of emerging concern are given in Fig. 5.2.

The removal efficiencies showed that many wastewater treatments plants (WWTPs) are not ideally designed to remove contaminants at trace level such as pharmaceuticals and pesticides due to the failure of conventional wastewater treatment technologies. They have been detected in wastewater, surface water, groundwater, and even treated drinking water at concentrations ranging from a few nanograms per liter (ng/L) to microgram per liter (μg/L) (Grung et al., 2015; Yang et al., 2017). Major groups of EDCs including alkylphenols (APs), bisphenol A (BPA), pharmaceuticals, and personal care products (PPCPs), perfluoroalkyl and polyfluoroalkyl substances (PFASs), phthalates and microplastics (MPs) have been detected in bottled water and have brought potential health risks to humans (Akhbarizadeh et al., 2020). Over 3000 substances were used as pharmaceutical ingredients including antibiotics, antidiabetics, antidepressant drugs, beta-blockers, painkillers, contraceptives, lipids regulators, and X-ray contrast media (Lambert and Skelly, 2016; McGrane, 2016).

The antibiotic ciprofloxacin at the concentration of up to a 6.5 mg/L have been documented alongside over 200 diverse pharmaceuticals in river waters worldwide (aus der Beek et al., 2016; Hughes et al., 2013). Seven antibiotics have been shown to be present in surface waters in the city of Fez, Morocco, in which amoxicillin was present at the highest

concentrations among other antibiotics such as sulfamethoxazole and erythromycin (Oualid et al., 2019). There are many reports about pharmaceuticals and their derivatives in surface water, ground water, and rivers where they can induce acute or chronic toxicity through the food chain with adverse effects on aquatic ecosystems and human health, especially when treated wastewater is reused as reclaimed water (Maniakova et al., 2020; Su et al., 2020). For example, Godoy et al. show that antihypertensive drugs cause growth inhibition in fish, algae, and larval mortality (Godoy et al., 2015). Various (eco)toxicological effects of CECs also have shown by many studies (Saari et al., 2017).

Antibiotics disturb bacterial community structures and change bacterial ecology, and these have led to the development of resistant bacterial strains; this may cause major global public health issue (Grenni et al., 2018). Pharmaceuticals and personal care products (PPCPs) are persistent in water bodies and soil. So these substances lead to multi-drug-resistance microbes, antibiotic-resistant bacteria (ARB), and antibiotic-resistant genes (ARGs) (Chaturvedi et al., 2021). For example, *Klebsiella pneumoniae* resistant to carbapenems and cephalosporin; *E. coli* resistant to fluroquinolones and cephalosporin; *Salmonella* resistant to fluoroquinolones; *Mycobacterium tuberculosis*, resistant to rifampicin (MTB) *Staphylococcus aureus* resistant to methicillin (Tanwar et al., 2014). According to a review, antimicrobial resistance can cause 10 million deaths per year by 2050 (de Kraker et al., 2016). Heavy metals such as arsenic and cadmium has been associated that have influence on antibiotic resistance in paddy soils (Zhao et al., 2020).

There are many CECs that act as so-called endocrine disruptors (EDCs) *(*EPA, Water Quality Criteria, *2008)*. So, these two categories can overlap with one or two differences by means of chemical contaminants. Endocrine-disrupting chemicals**,** EDCs strongly bind to estrogen or androgen receptors and interfere with natural hormones, and bind to activate various hormone receptors such as Androgen Receptor (AR), estrogen receptors (ER), aryl hydrocarbon receptor (AhR), Pregnane X Receptor (PXR), Constitutive Androstane Receptor (CAR), Estrogen-Related Receptor (ERR) and then imitating the natural hormone's action (agonist action). EDCs may also inhibit the pathways of hormones' production (Mnif et al., 2011). EDCs are including pesticides (Combarnous, 2017) mentioned above, antibiotics, disinfectants, fire retardants, industrial additives, lifestyle products (Caffeine, Nicotine), pharmaceuticals, personal care products, plasticizers (BPA), reproductive hormones, solvents, steroids.

In human epidemiologic studies, chemicals such as bisphenols, phthalates, and parabens are associated with endocrine system disorders and linked to them causing a series of changes in menstrual and ovarian function endocrine system (Benjamin et al., 2017). Elevated exposure to phthalates has been associated with female genital tumors, endometriosis, precocious puberty, and ovulation disorders (Smarr et al., 2016). Their presence in PCPs such as, cosmetics, perfumes, deodorants, nail polishes, and skin and hair care products have been reported in literature widely (Gao and Kannan, 2020). Even many species phthalates such as di (2-ethylhexyl) phthalate, di-n-butyl phthalate, butyl-benzyl phthalate, and diethyl phthalate were quantified in drinking water ranging between 0.02 and 0.6 μg/L (Cizmas et al., 2015).

Parabens are also found to be strong estrogen agonists, and their exposure was linked to breast cancer (Jagne et al., 2016) and is designated as endocrine disrupting chemical (Błedzka et al., 2014). They are produced for about 100 years and are considered high production-volume chemicals in Europe, the U.S., and Asia. They are used in cosmetics, as a preservative

in pharmaceuticals due to their chemical stability, low cost, broad-spectrum antimicrobial effect, and as food additives which is authorized in the European Union (*Regulation (EC) No* 1333/2008 of the European Parliament and of the Council of 16 December 2008 on food additives (Text with EEA relevance), 2008), and later approved as food additives in China (Petric et al., 2021), hence distributed and detected in many environments. They have been detected in air, dust, soils, and aqueous environment. For example, propylparaben (3142 ng/L), methylparaben (1062 ng/L) in Chinese river (Błedzka et al., 2014); in European rivers, methylparaben was detected up to 400 ng/L (Kasprzyk-Hordern et al., 2009) and propylparaben was quantified as 69 ng/L (González-Mariño et al., 2009). Even methyl-ethyl-propyl parabens were found in non-processed seafood and fish samples (Wang et al., 2019).

Bisphenol A (BPA) is a chemical which is used to produce polycarbonate plastics and the epoxy resin to add strength and resilience (Rosenfeld and Feng, 2011). It is one of the most widely used EDCs in many consumer products such as in plastic containers, food packaging, and beverage bottles including baby bottles. BPA can slowly leach into the contained materials and then impact reproductive health (Bondesson et al., 2009; Nriagu, 2019). BPA is also utilized in products such as toys, water supply pipes, and medical tubing (Rosenfeld and Feng, 2011). EPA estimates that each year over half million ton of BPA is released into the environment (USEPA, 2010). A specific migration limit of BPA from packaging into food was established as 3 mg/kg by the European Union (EU). The EPA has established a maximum acceptable dose for BPA of 50 μg/kg of body weight per day (Rosenfeld and Feng, 2011). Ingestion of canned food continues being the highest route for human exposure concerning bisphenol and derivatives, however exposure-chlorinated derivatives of bisphenols occur primarily through the consumption of tap water (Caballero-Casero et al., 2016; Guart et al., 2014).

5.4.1 Pesticides

Historically, the awareness on pesticides had emerged and attributed to Rachel Carsons; book "Silent Spring"; she raised a question about widespread use of pesticide Dikloro Difenil Trikloroetan (DDT) and other pests which had led to deterioration of environment and death of many birds (Mnif et al., 2011). The World Health Organization (WHO) has reported annual pesticide poisonings of three million, resulting in 20,000 deaths worldwide (Boedeker et al., 2020). The average annual pesticide use reported for the countries during 2010–2014 for kg per ha; the greatest use was in Japan (18.94), followed by China (10.45), Mexico (7.87), Brazil (6.166), and by the countries, i.e., Germany, France, UK, USA in decreasing orders (W. L. Zhang et al., 2014). Pesticides can cause acute toxic effects in both target and non-target organisms. Many pesticides are persistent to break down in the environment and bioaccumulate in fatty tissues of living organisms and human. The use of pesticides and their detrimental effect on health has drawn attention to their safe level use. *Exposure to pesticides can* be through contact with the skin, ingestion, or inhalation, and cause many *severe* health effects and disorders in the reproductive, nervous, and immune systems. Long-term pesticide exposure can cause cancer (Kim et al., 2017; Ritter et al., 2002). The major chemical classes of pesticides include organochlorine compounds, carbamates, organophosphates, and chlorophenoxy compounds (Ritter et al., 2002).

Most of the disorders are induced by notably organophosphorus, organochlorines, phenoxyacetic acids, and triazine compounds (Mostafalou and Abdollahi, 2017). The most widely used pesticides worldwide are DDT, DDE, lindane, atrazine, simazine, triclosan, and chlorpyriphos (Arlos et al., 2015) which have been associated with the antiandrogenic activity and classified as "endocrine disrupting chemicals" (EDCs) (Rostkowski et al., 2011). Citrus fruits, which are widely consumed in Europe, have been found to contain high amounts of EPDs. Of these, 46%–57% EPDs residues were observed in mandarin, orange, and grapefruit. 17%–40% of vegetables also were found to contain EDPs, most importantly several fruit and vegetables contained not just one pesticide, but an actual mixed up to eight EDPs per sample and cumulative toxic potential effects are not assessed *(*PAN, Pesticide Action Network, *2017)*.

5.4.2 Polycyclic aromatic hydrocarbons

Polycyclic aromatic hydrocarbons (PAHs) are organic pollutants, formed either through various industrial or natural activities (Qiao et al., 2018). Natural sources of PAHs mainly include combustion sources (Forest fires) and volcanic eruptions, as well as biological origin (Itoh et al., 2017). Anthropogenic sources of PAHs are pyrolysis, which include incomplete combustion of coal, petroleum, wood, polymers (Abdel-Shafy and Mansour, 2016), discharge of crude oil, coal tar, asphalt, etc., and mineral oils and petroleum leakage (Goudarzi et al., 2018). Other sources are food cooking processes and municipal waste incineration (Grung et al., 2015; Yang et al., 2017). Incomplete combustion of organic substances gives out about 100 different polycyclic aromatic hydrocarbons (PAHs) which are notably persistent pollutants with various structures and toxicity.

PAHs mostly exist colorless, white or pale-yellow powder comprising of two or more benzene rings. To date, over 400 kinds of PAHs and their health effects have been detected (Pan et al., 2006). Many PAHs, about 16 of them have been categorized as priority contaminants based on their toxicity and frequency of occurrence at hazardous waste sites by the USEPA (Bojes and Pope, 2007). PAHs are a typical class of substances that are carcinogenic, teratogenic, and mutagenic (Yiming et al., 2015).

PAHs have been identified in water sources, sediments, wastewaters, and aquatic organisms, for example, in mussels often occurring in complex chemical mixtures with other contaminants. It was reported that four-ring and five-ring of PAHs such as chrysene and benzo[*a*]pyrene are almost insoluble in water (Adeniji et al., 2018). PAHs are found in different environmental media, in air, water, sediment, bind to the surface of particles, in particle-phase, transport from air to land and to aquatic systems (Vagge et al., 2018). Studies proved that microplastics (MPs) play an important role in the cycling and accumulation of PAHs due to their strong adsorption capacity for lipophilic compounds (Fisner et al., 2017). Hence microplastics (MPs) are listed as emerging threats considering the increasing amount in marine environment (Eriksson et al., 2016). PAH attached MPs easily accumulate aquatic organisms, causing toxic effects stronger than those taken up alone (N. Wang et al., 2019).

PAHs in aquatic environments reported to be detected in various concentrations, for example, from 1.33 ng/L in treated drinking water in Iran to 139,000 ng/L in untreated drinking water in Nigeria. The concentrations of the PAHs were found between 0.5 ng/L and 1,138,000 ng/L in lakes and rivers of various countries. In seawater and groundwater, PAHs

were detected differently—0.02 ng/L in Gulf; 46,600 ng/L in Indonesian Sea; 0.1 ng/L in North China and 739.1 ng/L in Huai River in China (Mojiri et al., 2019). They are also present at levels varying from 1 μg to 300 g/kg soil, depending on the sources of contamination (Rodrigues et al., 2018).

5.5 Removal of emerging contaminants

With the beginning of modern life, daily use as well as many chemicals originated from medical and industrial media (i.e., endocrine disrupting compounds (EDCs), pharmaceuticals, and personal care products (PPCPs), polycyclic aromatic hydrocarbons (PAHs), hormones existing as synthetic and natural, chemicals used for household and industry, some disinfection by-products (DBPs), alternation product of ECs) threaten the health of living things and our environment (Esplugas et al., 2007; Farré et al., 2008). These chemicals, in particular, have serious damage on the ecological balance, which directly or indirectly affects living life such as seas, lakes, rivers, and groundwater. Since it is not possible to purify all emerging contaminants with a single method, different methods are used for different contaminants. Therefore, the method to be chosen to remove emerging contaminants is also related to the environment and amount of contaminants. The cost of treatment should also be kept in mind as well (Kang, 2014). As a consequence, effective removal methods for emerging contaminants of concern are needed as ever (Kümmerer, 2009).

The methods used for the removal of emerging contaminants can be grouped under three main headings as physical, chemical, and biological methods together with subheadings as shown in Fig. 5.3. Although many of these methods can be applicable successfully, some of them have some constraints such as high energy necessity and maintenance costs. Due to these negative effects, important studies have recently been carried out with hybrid methods, which consist of a mixture of the basic methods described above. Important parts of the methods used to remove organic- and inorganic-based emerging contaminants of concerns (ECs) are summarized below as basic information.

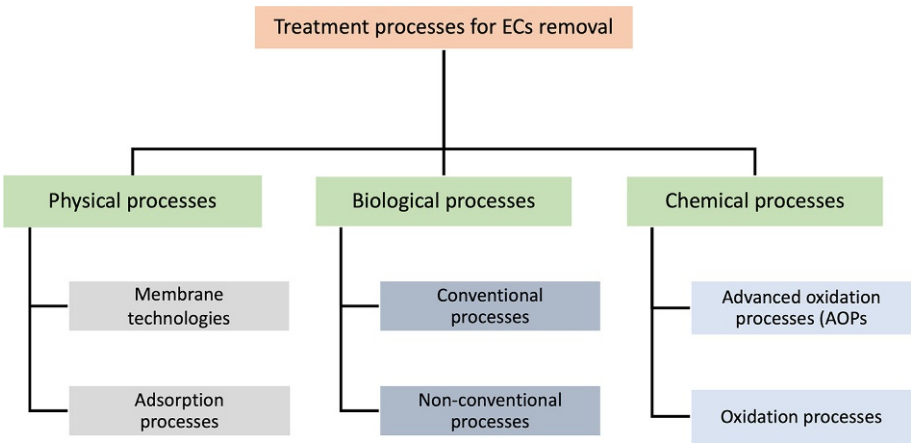

FIG. 5.3 General processes used for treatment of ECs.

5.5.1 ECs removal methods based on physical interaction

Lately, ECs have been indicated as important water pollutants which have adverse impacts on human and wildlife endocrine systems. Due to the chemical structures they contain, ECs are water soluble and can pose a threat to aquatic organisms and humans (Rodriguez-Narvaez et al., 2017). Physical interaction for ECs removal can be classified under two subtitles as adsorption applications and membrane processes.

Adsorption applications

Adsorption is a mass transfer process, and occurs between different phases. These phases can generally be liquid–solid, gas–solid, gas–liquid, or liquid–liquid media. Interactions in adsorption are based on physical or chemical interactions. If some interactions, i.e., weak ionic or van der Waals forces are predominate in the process, this one is defined as physical adsorption, and interactions are reversible. Physical interactions can be single- or multi-layered, and they can be explained by isotherms such as Langmuir or Freundlich, and different mechanisms. Temperature is an important parameter in adsorption. And, low temperature often provides an advantage in physical interactions. Chemisorption process concerns the chemical bonding between adsorbates and solid surfaces. It happens as a monolayer with power interactions. Chemisorption process concerns the chemical bonding between adsorbates and solid surfaces. Both chemisorption and physisorption may be formed simultaneously depending on the conditions (Tareq et al., 2018). Adsorbents are utilized to adsorb any particular contaminant from waste water thanks to intermolecular forces (De Gisi et al., 2016). Adsorption applications utilizing natural, synthetic, and waste substances have been the subject of discussion in recent years for the removal of ECs (Dhangar and Kumar, 2020). The material kind is one of the most significant properties to be considered when opting adsorption as the removal operation. And also, the sustainability of the manufacturing of adsorbent materials is an important matter. The usage of some natural substances can demonstrate to be unsustainable in the long term (Rodriguez-Narvaez et al., 2017).

Activated carbon (AC) is one of the most-used adsorbents due to its high self-exclusive surface area and porosity. It represents encouraging potential for removing the specific ECs. Nevertheless, the raw substances opted for AC importantly impacts the removal performance of ECs (Rodriguez-Narvaez et al., 2017). Carbon nanotubes (CNTs), single-walled or multi-walled nanotubes are another group of adsorbents. It is available in the literature that the opted ECs demonstrate perfect removal performance. Even if CNTs displayed perfect performance in some studies, it has been known that CNTs have weak performance for some other ECs at the same experimental situations (Dhangar and Kumar, 2020).

Biochar is a charcoal-origin substance extensively utilized as a soil amendment. Lately, biochar has been researched for the adsorption of ECs. An important knowledge gap in the usage of biochar is about sustainability of the production process. The scaling of the biochar manufacturing procedure is another important knowledge gap. Biochar manufacturing is overtaken in unproductive small-scale ovens requiring big energy entry. Therefore, correct evaluation of the carbon footprint regarding biochar manufacturing procedure and recognition of cleaner manufacturing operations is mandatory to provide its sustainable usage (Rodriguez-Narvaez et al., 2017).

Other adsorbents for removing of ECs are clay minerals, zeolites, aluminum oxides, graphene oxides, and some polymers (Dhangar and Kumar, 2020). Substances containing different functional groups such as carbohydrate-based structures (i.e., lignin, starch, cellulose, and simple sugars), lipids, proteins, and water are among the basic components of agricultural waste materials. Some previous reports have indicated that agricultural substances including cellulose have a high adsorption performance of different contaminants. Their implementations as adsorbents can be improved via some modifications (De Gisi et al., 2016).

Available adsorbents are limited for selectively removing of ECs. Therefore, various adsorption processes can be integrated with other treatment processes in order to efficiently remove the various ECs (Dhangar and Kumar, 2020). Processes based on low-cost and easily available adsorbents will make them suitable and as alternative for ECs removing. Relying on the adsorbent and adsorbate properties used, a suitable adsorbent option should not be forgotten to ensure the highest level of removal of various types of contaminants.

Membrane process

Membrane process technologies are recently extensively utilized for different applications. Basically, membrane technology is a process based on another physical process in which solutions are filtered by trapping contaminants on the membrane. Membrane process technology has some troubles due to the different physicochemical features of materials and the large range of parameters to be combined for separation enhancement. The convenient separation mechanisms and target contaminants narrow the membrane options.

Membranes for removal of emerging contaminants from water: Which kind of membranes should we use?

The characteristics of membranes such as pore size, hydrophobicity, and surface charge determine the removal of contaminants (Schäfer et al., 2011; Simmons et al., 2011). The important point here is that membrane processes can be classified according to pore sizes and membrane types. In addition, it should not be forgotten that decreasing the pore sizes of the membranes will increase the removal efficiency.

In fact, membrane technology uses biological and non-biological processes together. Non-biological processes are reverse osmosis, ultrafiltration, and nanofiltration, whereas biological processes are membrane bioreactors (MB). MBs are combining membrane-based filtration processes with microfiltration or ultrafiltration systems. Today, MBs are the most reliable and approved systems to obtain clean water from wastewater via the unification of membrane and biological processes (Iorhemen et al., 2016; Nofiana et al., 2019).

Non-biological processes such as reverse osmosis, nanofiltration, microfiltration, ultrafiltration, or pressure-based membrane technologies apply high pressures across membranes used to filter pollutants from the produced water (Abdel-Fatah, 2018). These systems are the most common membrane method in water treatment. And also, membranes should be constantly modified for better performance and use.

Even though membrane-based methods are appropriate for eliminating turbidity and microbiological pollutants, high costs still restrict its fully utilization. Membranes are easily affected by contamination problems by causing unexpected interruptions due to aqueous pollutants (Maddah et al., 2018).

Physical treatment processes containing adsorption and membrane techniques have been shown good performance to eliminate some ECs. There is also a need for methods combining physical and chemical methods for sustainable methods in which ECs will be reduced or deteriorated (Dhangar and Kumar, 2020).

ECs removal by hybrid systems

The combination of some treatment techniques can offer the best solution in point of separation performance and cost. The approaches of conventional techniques for the removal of various ECs are incapable of destroying them fully (Molinari et al., 2020). ECs cause global concerns because of their possible toxicity (Saidulu et al., 2021). The high-quality knowledge required for ECs investigation has requested technological advancements (Pérez-Parada et al., 2012).

Systems, where traditional methods were used alone, were insufficient to remove many ECs types. In this regard, hybrid treatment systems have been the subject of research in the recent years due to their performance in removing different impurities. Various advanced and conventional chemical oxidation processes are extremely demanding and expensive, and their high energy requirement is the drawback and weakness of these methods. Lately, hybrid methods have been developed to cope with the disadvantages of traditional process to eliminate differences of ECs. Hybrid methods, combining chemical, physical and/or biological processes, can be used effectively to remove different types of ECs (Dhangar and Kumar, 2020).

Hybrid systems for removing of ECs consist of biological-physical, biological-chemical, biological-physical-chemical treatment processes. Especially, the unification of the superiorities of three different types of treatment methods, the implementation of these kinds of hybrid methods for ECs removal is very promising. Hybrid treatment methods generally promote as cost effectiveness and sustainability of biological operation for eliminating biodegradable organic substances from wastewater (Saidulu et al., 2021).

In the literature, various hybrid treatment systems have been made about the developments in preventing the spread of ECs to the aquatic environment in wastewater treatment applications (Ahmed et al., 2017). In fact, it is obvious that no single technology can address all troubles. The world of science exists for combinations suitable for needs (Sharma and Bhattacharya, 2017).

Physical removal, chemical oxidation or disinfection and biological transformation are the methods for water or wastewater treatment (Liu et al., 2009). Each of these technologies can be appropriate and cost-effective for a specific purpose. For instance, chlorination is a cost-effective technique for disinfection of drinking water via the distribution system. On the other hand, reverse osmosis is an effective technique for desalination process of seawater. However, one-step method will not be sufficient to achieve the quality required for water management in a wastewater treatment with a matrix containing complex substances (Anastasi et al., 2012). As a result, hybridizing or combining various methods can result in higher quality (Taheran et al., 2018).

The membrane bioreactor is a very useful model for explaining the hybrid treatment method. In this method, hybrid systems in which a membrane is added to a conventional activated sludge system, can increase the quality of the wastewater (Taheran et al., 2016).

Hybrid membrane operation system is a strong key for eliminating ECs from wastewater. By using these processes, a satisfactory operational water quality can be achieved by reducing both environmental and economic impacts while ensuring sustainable reuse in the hydrological circuit (Molinari et al., 2020).

Some hybrid forms were advanced and some of these systems have been controlled at pilot scale in EU countries. However, these methods are costly and prevent them from finding wide application area (Grandclément et al., 2017). Thus, convenient research is required to discover more green and low-cost techniques. Both society and decision-makers must be persuaded to pay for the next generation of wastewater treatment systems based on hybrid technologies.

5.5.2 Chemical operations

Biological wastewater treatment technologies (such as β-blockers, one of the pollutants from pharmaceuticals and personal care products, are subjected to different biological treatments to sweep) can be effective in removing the EC class based on wastewater characteristics and operational parameters. In addition, new advanced treatment techniques in the form of chemical processes are being developed in order to increase the efficiency in cleaning and to further remove ECs. These technologies are called chemical oxidation or aqueous phase oxidation (Comninellis et al., 2008).

Chemical operations aim to convert pollutants in water to inorganic structures such as water, carbon dioxide and nitrogen, or to other minerals by making them less harmful. Chemical operations also aim to convert pollutants into biodegradable compounds (Ahmed et al., 2017). In other words, this technology has been used to reinforce conventional systems and to further the EC removal process (Balcioğlu and Ötker, 2003).

In accordance with this purpose, the combination of some oxidants including metal oxides and metal oxide-based catalysts, as well as chemical agents such as ozone, hydrogen peroxide, chlorine are used for the aqueous phase oxidation of ECs from wastewater (Ikehata et al., 2008). In addition, some energy sources such as electric current, gamma, sun and UV-radiation can be used in this process (Ikehata et al., 2006). These chemical operations are classified as conventional oxidation processes and advanced oxidation processes (AOPs) (Dhangar and Kumar, 2020). Oxidation of ECs in AOPs is based on hydroxyl radicals that facilitate the conversion of pollutants into more biodegradable structures (Ikehata et al., 2006). The rate constants of the reactions of hydroxyl radicals in aqueous solutions are around 106–109 M/s (Malato et al., 2012). All data for chemical-based treatment systems (Ahmed et al., 2017; Klamerth et al., 2012; Prieto-Rodríguez et al., 2013) are listed in Table 5.2.

Chlorination

Most of the chemical oxidation processes have high efficiency in the degradation of less toxic and easily biodegradable ECs in wastewater systems. In the treatment of wastewater, less reactive types such as chlorine (chlorine gas and hypochlorite) and bromine are sometimes used (Noutsopoulos et al., 2014). However, this method is not widely used due to the possibility of formation of high sub-products and less mineralization of ECs in the use of chlorine and chlorine dioxide during treatment (Rivera-Utrilla et al., 2013).

TABLE 5.2 Removal efficiency of ECs with conventional and AOP-based treatment technologies.

Category	ECs	ECs source	Chemical treatment technology	Removal (%)
Beta blockers	Metoprolol, Atenolol, Metoprolol tartrate, Propranolol hydrochloride	Water, Wastewater treatment plants, Hospital wastewater	Gamma radiation Bi electro-Fenton Solar photoelectron-Fenton	90–100 (Metoprolol) 85–88 (Atenolol) 90 (Metoprolol tartrate) 93 (Propranolol hydrochloride)
Analgesics	Carbazepine, Diclofenac, Ibuprofen, Naproxen	Water, Wastewater treatment plants, Distilled water	Gamma radiation, Solar photo-Fenton, Solar photocatalysis, Ultrasonic irradiation/TiO_2	90–100 (Carbazepine) 90–100 (Diclofenac) 90 (Ibuprofen) 98 (Naproxen)
Non-steroidal anti-inflammatory drugs	Ketoprofen, Melenamic acid, Ketoralac	Water, Wastewater treatment plants	Gamma radiation, Solar photo-Fenton, Anodic oxidation	100 (Ketoprofen) 100 (Melenamic acid) 90 (Ketoralac)
Lipit regulators	Clofibric acid, Gemfibrozil	Water, Wastewater treatment plants	Gamma radiation, Solar photocatalysis	100 (Clofibric acid) 85 (Gemfibrozil)
Antibiotics	Amoxicillin, Cefaclor, Chloramphenicol Penicillin G, Penicillin V, Sulfamethoxazole, Cefalexin, Sulfamethazine, Flumequine, Ofloxacin, Ampicillin, Cloxacillin, Ofoxacin, Trimethoprim, Tetracycline	Water, Hospital wastewater, Wastewater treatment plants	Electro-Fenton, Solar photo-Fenton, Photocatalysis/ H_2O_2, Solar photocatalysis, Anodic oxidation, Gamma radiation	95–100 (Amoxicillin) 100 (Cefaclor) 100 (Chloramphenicol) 92 (Penicillin G) 81 (Penicillin V) 53–100 (Sulfamethoxazole) 100 (Cefalexin) 85 (Sulfamethazine) 90 (Flumequine) 90 (Ofloxacin) 100 (Ampicillin) 100 (Cloxacillin) 85 (Ofoxacin) 85 (Trimethoprim) 86 (Tetracycline)
Contrast agent	Iopromide	Water	Gamma radiation	100 (Iopromide)
Pesticides	Atenolol, Metoprolol, Propranolol, Triclosan, Triclocarban, Atrazine, Aldrin, Diazinon, Malathion, 3-Indole butyric acid, Diurin	Water, Hospital wastewater, Wastewater treatment plants	Electro-Fenton, Solar photo-Fenton, Photocatalysis/ H2O2, Solar photocatalysis	95 (Atenolol) 95 (Metoprolol) 95 (Propranolol) 90–100 (Triclosan) 100 (Triclocarban) 60 (Atrazine) 90 (Aldrin) 99 (Diazinon) 99 (Malathion) 90 (3-Indole butyric acid) 85 (Diurin)
Pain relievers	Acetaminophen, Hydroxybiphenyl, Isobroturum	Wastewater treatment plants	Solar photo-Fenton, Electro-Fenton	90–98 (Acetaminophen) 85 (Hydroxybiphenyl) 90 (Isobroturum)

TABLE 5.2 Removal efficiency of ECs with conventional and AOP-based treatment technologies—cont'd

Category	ECs	ECs source	Chemical treatment technology	Removal (%)
Endocrine disrupting compounds	Progesterone, Bisphenol A	Wastewater treatment plants, Aqueous solutions	Solar photo-Fenton, Solar photocatalysis, Ultrasound UV/Fe^{2+}	90 (Progesterone) 80–85 (Bisphenol A)
Anti-inflammatory	4-Aminoantipyrine 4-Asetilaminoantipyrine 4-Formilaminoantipyrine 4-metilaminoantipyrine	Wastewater treatment plants	Solar photo-Fenton, Solar photocatalysis	89 (Antipyrine) 85 (4-Aminoantipyrine) 60 (4-Asetilaminoantipyrine) 85 (4-Formilaminoantipyrine) 85 (4-metilaminoantipyrine)
Stimulants	Caffeine, Paraxanthine	Wastewater treatment plants	Solar photo-Fenton Solar photocatalysis	55–90 (Caffeine) 85 (Paraxanthine)
Diuretics	Hydrochlorothiazide	Wastewater treatment plants	Solar photocatalysis	85 (Hydrochloro-thiazide)

Ozonation

It is the most basic process used in wastewater treatment plants to accelerate biodegradability and increase the efficiency of subsequent treatment processes. (Acero et al., 2010). Because ozone has a high electron density and is a very powerful oxidant that selectively reacts with EC's double bonds and aromatic rings (Acero et al., 2015). Since ozone is a strong oxidant, almost all types of ECs can be effectively removed in this way.

Ozone production is costly because it is an energy-intensive process. In other words, the ozone treatment system can increase the energy demand by 40%–50% compared to the conventional wastewater treatment plants (Ahmed et al., 2017). Another problem with ozonation is the formation of some oxidative by-products and the interference of radical scavengers (Benner et al., 2013; Luo et al., 2014). In summary, high costs, interference and possible by-products should not be ignored in ozonation studies.

Advanced oxidation processes (AOPs)

Advanced oxidation processes (AOPs) have been developed to eliminate the disadvantages experienced in oxidation processes. These processes can be listed as Ferrate process, photocatalysis, solar-Fenton process, electro-Fenton process, and ultrasound irradiation (Salimi et al., 2017). Ferrate (FeO_4^{2-}), an excellent oxidizing agent, has a strong disinfecting effect. It can form $Fe(OH)_3$ gel that can precipitate and remove other ions from the

environment. In addition, it is seen that it is used in the removal of arsenic and some ECs due to its high oxidation property (Ghernaout and Naceur, 2011). The main mechanism used in treatment is oxidation/disinfection with Fe^{6+} and coagulation/flocculation with Fe^{3+} (Jiang, 2007). It is not widely used due to its limited application area, high preparation cost, and poor stability (Roth et al., 2016).

The Electro-Fenton process has been used to eliminate the disadvantages that occur with the traditional Fenton process. In this process, electrochemical production takes place in a controlled manner instead of H_2O_2 (Roth et al., 2016). In the Electro-Fenton process, UVA light is used to allow the rapid degradation of pollutants and to increase the regeneration of Fe^{2+} by producing more OH• radicals (De Luna et al., 2012). Such AOPs provide excellent removal even at concentrations much higher than the optimum limits of pesticides and antibiotics (Adriana et al., 2012). However, high operating and maintenance costs are the biggest factor limiting its widespread use.

In the Solar-Fenton process, another advanced oxidation processes, UV light or natural sunlight is used to generate hydroxyl radical from the H_2O_2 reaction in the presence of Fe. The biggest advantage of this method is that it works under optimum pH conditions (Adriana et al., 2012). Photocatalysis is a process in which chemicals are transformed by activating catalysts with the help of light energy in order to eliminate the disadvantages of slow degradation in photolysis (MacWan et al., 2011; Sornalingam et al., 2016). Semiconductors such as titania and ZnO are frequently used catalysts in the photocatalysis process (Gaya and Abdullah, 2008). It has a wide range of uses in EC decomposition due to its strong oxidation properties, but challenges such as high operating and maintenance costs, energy consumption, and potential toxicity of oxidation byproducts are alarming. In addition, it has been developed in hybrid systems where advanced oxidation processes are used together with biological and physical processes to ensure more effective removal of various ECs.

Fenton process

Fenton process is a suitable option for wastewater treatment, as iron is abundant and does not have toxic effects. Hydroxy radicals are produced by the reaction of hydrogen peroxide in the presence of iron in the Fenton process (Shemer et al., 2006; Wang et al., 2018b).

Chain reaction happens as follows:

$$Fe^{2+} + H_2O_2 \rightarrow Fe^{3+}OH^{\bullet} + OH^{-} \quad (5.1)$$

$$Fe^{3+} + H_2O_2 \rightarrow Fe^{2+} + HO_2^{\bullet} + H^{+} \quad (5.2)$$

The Fe^{2+} ion can be reproduced from Fe(III) by reaction (5.2). However, since reaction (5.2) is much slower than reaction (5.1), Fe (III) will accumulate in solution (De Luna et al., 2012). For this reason, removing of Fe from solution will adversely affect productivity. It will also require a substantial amount of reagent, which will increase process costs. The undesired consumption of the hydroxyl radical formed by iron ions and hydrogen peroxide is another disadvantage of the conventional Fenton process.

$$OH^{\bullet} + Fe^{2+} \rightarrow Fe^{3+} + OH^{-} \quad (5.3)$$

$$OH^{\bullet} + H_2O_2 \rightarrow H_2O + HO_2^{\bullet} \quad (5.4)$$

Because the $HO_2^{\bullet}$ radical formed in reaction (5.4) is a weaker oxidant than the $OH^{\bullet}$ radical, this undesired reaction will reduce the process efficiency. Due to these negativities, catalyst, solar energy or any light source should be used together with the Fenton process to ensure effective removal of ECs from waste water (Ahmed et al., 2017).

Photolysis

Decomposition of ECs by photolysis process is a process that occurs by absorption of light (usually UV) or radiation (Yan et al., 2015). Disinfection of water using UV is the most widely used photolysis technique. Two types of photolysis are used to separate ECs; the first is direct photolysis by direct absorption of photons, and the second is indirect photolysis in the presence of photosensitizers such as hydrogen peroxide (Nguyen et al., 2013). Although both types of photolysis are effective in removing many kinds of ECs such as pesticides, analgesics, beta blockers, EDCs and antibiotics, indirect photolysis is more effective than direct photolysis (Ahmed et al., 2017). In addition, gamma radiations have been effectively applied in the separation of ECs. Gamma radiation-based oxidation process achieved 100% success in removing of ECs such as metoprolol, carbazepine, diclofenac, ketoprofen, mefenamic acid, clofibric acid, cefaclor, and chloramphenicol (Slegers and Tilquin, 2006; Song et al., 2008). With the fact that the gamma radiation method can be used successfully in the removal of ECs, it should be kept in mind that the production of gamma radiation will incur a serious cost for the removal of impurities.

5.5.3 Biological applications

Many researches have represented that the great extent removal of ECs was conducted through both biodegradation and adsorption in the course of biological treatment (secondary treatment) (Ismail and Mokhtar, 2020). Adsorption is an effective and convenient process and has been a large-scale research subject as a good method compared to other waste disposal methods due to its lower cost, compatibility, and easy design (Rasalingam et al., 2014). On the other hand, biological degradation is the method of reduction of large molecular weight ECs into smaller molecules by bacteria, microorganisms (such as algae and fungi) (Garcia-Rodríguez et al., 2014) and even biomineralization into basic inorganic substances such as water and carbon dioxide.

Some parameters such as conducted treatment system, operation conditions, physicochemical features of Ecs, and their biological permanence impact the removal ratio or degradation level of the ECs. The biological treatments are often classed as conventional and non-conventional treatments, whose categorization primarily relies on the wastewater properties (Dhangar and Kumar, 2020). We will explain these two systems with two subheadings.

Conventional processes

Biological transformations and mineralization processes are the leading cleaning processes in conventional wastewater treatment operations (Kanaujiya et al., 2019). For the conventional method of biological degradation, microorganisms take advantage of organic compounds for their growth as major substance. And also, organic compounds excite enzymes for digestion. Many types of ECs that have toxic effects on plants resist microbial growth

and inhibit biodegradation. In response to this process, microbial growth must continue in order for the biodegradation process. And this requires a growth substrate. This process is called as cometabolism (Tran et al., 2013).

Removal and degradation performance of ECs rely on the chemical and biological permanency of ECs, and also physicochemical features, the methods utilized, and treatment conditions of them. The removal of extremely polar substances such as pharmaceuticals is the most significant operation made by microorganisms. The removal ratios mainly depend on connected treatment methods, operation circumstances and target pollutants. The determination of degradation materials in environmental samples is a hard duty. Because they are not only exist at low concentrations but also in complicated matrices that can amalgamate with detection samples (Zhou et al., 2009).

The conventional treatment processes contain activated sludge processes (ASP), trickling filters (TF), moving bed biofilm reactors, nitrification, microalgae/fungi origin treatments, biological activated carbon, and some another aerobic, anaerobic, facultative microbiological treatments.

It has been reported that the treatments of microalgae/fungus origin can effectively remove ECs with the help of phytoremediation and degradation mechanism (de Wilt et al., 2016; Garcia-Rodríguez et al., 2014; Matamoros et al., 2016). These operations displayed effective removal of many ECs. Microbiological processes (such as aerobic, anaerobic, and facultative) are mostly used for excess sludge removal in sewage treatment plants where ECs are adsorbed to suspended particles up to a point. The most intensely applied process all around the world to get rid of many ECs is the activated sludge method. In this process, the mechanism acting for removal process is biodegradation which is conducted by microorganisms in ventilation tank (Braga et al., 2005; Liu et al., 2009). The removal yield of ECs via active sludge processes can be combined with other processes (i.e., biological or advanced oxidation).

Trickling biofilters systems have not been literally investigated for ECs eliminating, but they have been explored by combining with active sludge process for the removal of 55 pharmaceutical and personal care products in South Wales, UK (Kasprzyk-Hordern et al., 2009; Svenson et al., 2003).

Non-conventional processes

Nowadays, even if some biological and physicochemical treatment techniques have been searched to get rid of ECs in wastewater, biologically based methods for wastewater treatment are not suitable for all wastewater components, and the treatment efficiency is affected on a large scale by environmental parameters (Molinari et al., 2020). Some removal operations such as oxidation, adsorption, etc., are used in non-conventional treatment ones (regardless of whether the conventional processes are present). For non-conventional processes used to remove ECs, methods such as biosorption, constructed wetlands and membrane bioreactor can be mentioned.

Biosorption is the biological refinement method in which sorption and bio-oxidation techniques (there is no biodegradation event) are more preponderant because of microorganisms' immobilization onto adsorbent material (Pidlisnyuk et al., 2003). The biosorption method can be used for the removal of different EC types. However, this method needs to be further developed in order to remove more and more different EC types successfully.

Membrane bioreactor is the applied biological treatment method to obtain good quality effluents versus some ECs. In membrane reactor, ECs are eliminated by the system of physical holding and microbial biodegradation at the surface of the membrane which limits the movement of heavy molecules. Membrane bioreactor has the ability to successfully get rid of the ECs that are robust even in activated sludge process and constructed wetlands because of these double mechanism of adsorption and biodegradation (Luo et al., 2014; Radjenović et al., 2009; Westerhoff et al., 2005).

Membrane bioreactor method owns some troubles such as occlusion and becoming of fouling of membrane, operational insufficiency matters, high expense than the constructed wetlands and other set up methods and weak elimination of specific ECs (Buttiglieri and Knepper, 2008; Yang et al., 2006). These troubles may be diminished by utilizing the membrane bioreactor method in combination with some physicochemical techniques.

Analogous of natural wetland operations, constructed wetlands are reproduced under control environmental circumstances, to improve the wastewater utilizing the combining methods such as oxidation, biodegradation, and sorption (Anawar et al., 2019).

Plants, microbes, the porous structure of the soil due to its nature, the chemical structure of the soil are liable for the processes of biological degradation, absorption, and oxidation, respectively. On the other hand, constructed wetlands techniques could be only implemented for lesser wastewater load because it requires large fields to conduct successfully (Matamoros and Bayona, 2008). Additionally, this cost-effective technique with its profits of various specific methods could be utilized to combine with other treatment techniques (i.e., oxidation process, membrane technology method) to obtain higher performance for a widespread range of ECs.

The conventional and non-conventional biological treatment methods have high capacity and are considered operative for the removing of many ECs. However, most of the methods fulfill specifically for the selected groups of ECs. Therefore, to reach higher efficiency for ECs removal, these biological methods could be combined with other physical and chemical treatment methods such as membrane processes (e.g., ultrafiltration, reverse osmosis, nanofiltration regarding), ozonation, and other improved oxidation processes (Dhangar and Kumar, 2020).

5.6 Conclusion

In parallel with the population growth rate and economic development, the improvement in the desired quality of life and the protection of the environment are indispensable components for a good and sustainable future. We understand from the experiences we have gained that, with the transition to modern life the demand for natural resources increases with the increase in population. As a result, with increasing consumption, a successful waste management plan for a green future needs to be made.

Acknowledgments

Prof. Odabaşı acknowledges Dr. Ömür Acet (Tarsus University, Tarsus, Turkey), pH.D. students, Burcu Önal Acet and Emrah Dikici (Aksaray Üniversitesi, Aksaray, Turkey) for their help during the preparation of some parts of this chapter.

References

2018 Revision of World Urbanization Prospects, 2018. https://www.un.org/development/desa/publications/2018-revision-of-world-urbanization-prospects.html.

Abdel-Fatah, M.A., 2018. Nanofiltration systems and applications in wastewater treatment: review article. Ain Shams Eng. J. 9 (4), 3077–3092. https://doi.org/10.1016/j.asej.2018.08.001.

Abdel-Shafy, H.I., Mansour, M.S.M., 2016. A review on polycyclic aromatic hydrocarbons: source, environmental impact, effect on human health and remediation. Egypt. J. Pet. 25 (1), 107–123. https://doi.org/10.1016/j.ejpe.2015.03.011.

Acero, J.L., Benitez, F.J., Teva, F., Leal, A.I., 2010. Retention of emerging micropollutants from UP water and a municipal secondary effluent by ultrafiltration and nanofiltration. Chem. Eng. J. 163 (3), 264–272. https://doi.org/10.1016/j.cej.2010.07.060.

Acero, J.L., Benitez, F.J., Real, F.J., Rodriguez, E., 2015. Elimination of selected emerging contaminants by the combination of membrane filtration and chemical oxidation processes. Water Air Soil Pollut. 226 (5). https://doi.org/10.1007/s11270-015-2404-8.

Adeniji, A.O., Okoh, O.O., Okoh, A.I., 2018. Analytical methods for polycyclic aromatic hydrocarbons and their global trend of distribution in water and sediment. In: Zoveidavianpoor, M. (Ed.), Recent Insights in Petroleum Science and Engineering. Intech, https://doi.org/10.5772/intechopen.71163.

Adriana, L.E., Yu-You, L., Aimin, W., 2012. Biodegradability enhancement of wastewater containing cefalexin by means of the electro-Fenton oxidation process. J. Hazard. Mater., 41–48. https://doi.org/10.1016/j.jhazmat.2012.04.079.

Ahmed, M.B., Zhou, J.L., Ngo, H.H., Guo, W., Thomaidis, N.S., Xu, J., 2017. Progress in the biological and chemical treatment technologies for emerging contaminant removal from wastewater: a critical review. J. Hazard. Mater. 323, 274–298. https://doi.org/10.1016/j.jhazmat.2016.04.045.

Akhbarizadeh, R., Dobaradaran, S., Schmidt, T.C., Nabipour, I., Spitz, J., 2020. Worldwide bottled water occurrence of emerging contaminants: a review of the recent scientific literature. J. Hazard. Mater. 392. https://doi.org/10.1016/j.jhazmat.2020.122271.

Al-Gubory, K.H., 2014. Environmental pollutants and lifestyle factors induce oxidative stress and poor prenatal development. Reprod. BioMed. Online 29 (1), 17–31. https://doi.org/10.1016/j.rbmo.2014.03.002.

Anastasi, A., Spina, F., Romagnolo, A., Tigini, V., Prigione, V., Varese, G.C., 2012. Integrated fungal biomass and activated sludge treatment for textile wastewaters bioremediation. Bioresour. Technol. 123, 106–111. https://doi.org/10.1016/j.biortech.2012.07.026.

Anawar, H.M., Ahmed, G., Strezov, V., 2019. Long-term performance and feasibility of using constructed wetlands for treatment of emerging and nanomaterial contaminants in municipal and industrial wastewater. In: Emerging and Nanomaterial Contaminants in Wastewater: Advanced Treatment Technologies. Elsevier, pp. 63–81, https://doi.org/10.1016/B978-0-12-814673-6.00003-6.

Arcagni, M., Juncos, R., Rizzo, A., Pavlin, M., Fajon, V., Arribére, M.A., Horvat, M., Ribeiro Guevara, S., 2018. Species- and habitat-specific bioaccumulation of total mercury and methylmercury in the food web of a deep oligotrophic lake. Sci. Total Environ. 612, 1311–1319. https://doi.org/10.1016/j.scitotenv.2017.08.260.

Arlos, M.J., Bragg, L.M., Parker, W.J., Servos, M.R., 2015. Distribution of selected antiandrogens and pharmaceuticals in a highly impacted watershed. Water Res. 72, 40–50. https://doi.org/10.1016/j.watres.2014.11.008.

aus der Beek, T., Weber, F.A., Bergmann, A., Hickmann, S., Ebert, I., Hein, A., Küster, A., 2016. Pharmaceuticals in the environment-global occurrences and perspectives. Environ. Toxicol. Chem. 35 (4), 823–835. https://doi.org/10.1002/etc.3339.

Azevedo, J.S., Braga, E.S., Favaro, D.T., Perretti, A.R., Rezende, C.E., Souza, C.M.M., 2011. Total mercury in sediments and in Brazilian Ariidae catfish from two estuaries under different anthropogenic influence. Mar. Pollut. Bull. 62 (12), 2724–2731. https://doi.org/10.1016/j.marpolbul.2011.09.015.

Balcioğlu, I.A., Ötker, M., 2003. Treatment of pharmaceutical wastewater containing antibiotics by O_3 and O_3/H_2O_2 processes. Chemosphere 50 (1), 85–95. https://doi.org/10.1016/S0045-6535(02)00534-9.

Benjamin, S., Masai, E., Kamimura, N., Takahashi, K., Anderson, R.C., Faisal, P.A., 2017. Phthalates impact human health: epidemiological evidences and plausible mechanism of action. J. Hazard. Mater. 340, 360–383. https://doi.org/10.1016/j.jhazmat.2017.06.036.

Benner, J., Helbling, D.E., Kohler, H.P.E., Wittebol, J., Kaiser, E., Prasse, C., Ternes, T.A., Albers, C.N., Aamand, J., Horemans, B., Springael, D., Walravens, E., Boon, N., 2013. Is biological treatment a viable alternative for

micropollutant removal in drinking water treatment processes? Water Res. 47 (16), 5955–5976. https://doi.org/10.1016/j.watres.2013.07.015.
Benotti, M.J., Trenholm, R.A., Vanderford, B.J., Holady, J.C., Stanford, B.D., Snyder, S.A., 2009. Pharmaceuticals and endocrine disrupting compounds in U.S. drinking water. Environ. Sci. Technol. 43 (3), 597–603. https://doi.org/10.1021/es801845a.
Bhat, R.A., Shafiq-ur-Rehman, M.M.A., Dervash, M.A., Mushtaq, N., Bhat, J.I.A., Dar, G.H., 2017. Current status of nutrient load in dal Lake of Kashmir Himalaya. J. Pharmacogn. Phytochem. 6, 165–169.
Bjørklund, G., Dadar, M., Mutter, J., Aaseth, J., 2017. The toxicology of mercury: current research and emerging trends. Environ. Res. 159, 545–554. https://doi.org/10.1016/j.envres.2017.08.051.
Błedzka, D., Gromadzińska, J., Wasowicz, W., 2014. Parabens. From environmental studies to human health. Environ. Int. 67, 27–42. https://doi.org/10.1016/j.envint.2014.02.007.
Boedeker, W., Watts, M., Clausing, P., Marquez, E., 2020. The global distribution of acute unintentional pesticide poisoning: estimations based on a systematic review. BMC Public Health 20 (1). https://doi.org/10.1186/s12889-020-09939-0.
Bojes, H.K., Pope, P.G., 2007. Characterization of EPA's 16 priority pollutant polycyclic aromatic hydrocarbons (PAHs) in tank bottom solids and associated contaminated soils at oil exploration and production sites in Texas. Regul. Toxicol. Pharmacol. 47 (3), 288–295. https://doi.org/10.1016/j.yrtph.2006.11.007.
Bondesson, M., Jönsson, J., Pongratz, I., Olea, N., Cravedi, J.P., Zalko, D., Håkansson, H., Halldin, K., Di Lorenzo, D., Behl, C., Manthey, D., Balaguer, P., Demeneix, B., Fini, J.B., Laudet, V., Gustafsson, J.A., 2009. A CASCADE of effects of bisphenol A. Reprod. Toxicol. 28 (4), 563–567. https://doi.org/10.1016/j.reprotox.2009.06.014.
Braga, O., Smythe, G.A., Schäfer, A.I., Feitz, A.J., 2005. Fate of steroid estrogens in Australian inland and coastal wastewater treatment plants. Environ. Sci. Technol. 39 (9), 3351–3358. https://doi.org/10.1021/es0501767.
Buttiglieri, G., Knepper, T.P., 2008. Removal of emerging contaminants in wastewater treatment: conventional activated sludge treatment. In: Handbook of Environmental Chemistry, volume 5: Water Pollution. 5. Springer, pp. 1–35, https://doi.org/10.1007/698_5_098.
Caballero-Casero, N., Lunar, L., Rubio, S., 2016. Analytical methods for the determination of mixtures of bisphenols and derivatives in human and environmental exposure sources and biological fluids. A review. Anal. Chim. Acta 908, 22–53. https://doi.org/10.1016/j.aca.2015.12.034.
Chaturvedi, P., Singh, A., Chowdhary, P., Pandey, A., Gupta, P., 2021. Occurrence of emerging sulfonamide resistance (sul1 and sul2) associated with mobile integrons-integrase (intI1 and intI2) in riverine systems. Sci. Total Environ. 751. https://doi.org/10.1016/j.scitotenv.2020.142217.
Cizmas, L., Sharma, V.K., Gray, C.M., McDonald, T.J., 2015. Pharmaceuticals and personal care products in waters: occurrence, toxicity, and risk. Environ. Chem. Lett. 13 (4), 381–394. https://doi.org/10.1007/s10311-015-0524-4.
Combarnous, Y., 2017. Endocrine disruptor compounds (EDCs) and agriculture: the case of pesticides. C. R. Biol. 340 (9–10), 406–409. https://doi.org/10.1016/j.crvi.2017.07.009.
Comninellis, C., Kapalka, A., Malato, S., Parsons, S.A., Poulios, I., Mantzavinos, D., 2008. Advanced oxidation processes for water treatment: advances and trends for R&D. J. Chem. Technol. Biotechnol. 83 (6), 769–776. https://doi.org/10.1002/jctb.1873.
De Gisi, S., Lofrano, G., Grassi, M., Notarnicola, M., 2016. Characteristics and adsorption capacities of low-cost sorbents for wastewater treatment: a review. Sustain. Mater. Technol. 9, 10–40. https://doi.org/10.1016/j.susmat.2016.06.002.
de Kraker, M.E.A., Stewardson, A.J., Harbarth, S., 2016. Will 10 million people die a year due to antimicrobial resistance by 2050? PLoS Med. 13 (11). https://doi.org/10.1371/journal.pmed.1002184.
De Luna, M.D.G., Veciana, M.L., Su, C.C., Lu, M.C., 2012. Acetaminophen degradation by electro-Fenton and photoelectro-Fenton using a double cathode electrochemical cell. J. Hazard. Mater. 217–218, 200–207. https://doi.org/10.1016/j.jhazmat.2012.03.018.
de Wilt, A., Butkovskyi, A., Tuantet, K., Leal, L.H., Fernandes, T.V., Langenhoff, A., Zeeman, G., 2016. Micropollutant removal in an algal treatment system fed with source separated wastewater streams. J. Hazard. Mater. 304, 84–92. https://doi.org/10.1016/j.jhazmat.2015.10.033.
Dhangar, K., Kumar, M., 2020. Tricks and tracks in removal of emerging contaminants from the wastewater through hybrid treatment systems: a review. Sci. Total Environ. 738. https://doi.org/10.1016/j.scitotenv.2020.140320.
DIRECTIVES, 2013. https://eur-lex.europa.eu/LexUriServ/LexUriServ.do?uri=OJ:L:2013:226:0001:0017:EN:PDF.
Duker, A.A., Carranza, E.J.M., Hale, M., 2005. Arsenic geochemistry and health. Environ. Int. 31 (5), 631–641. https://doi.org/10.1016/j.envint.2004.10.020.

EPA, Water Quality Criteria, 2008. https://www.epa.gov/wqc/contaminants-emerging-concern-including-pharmaceuticals-and-personal-care-products.

Eriksson, U., Roos, A., Lind, Y., Hope, K., Ekblad, A., Kärrman, A., 2016. Comparison of PFASs contamination in the freshwater and terrestrial environments by analysis of eggs from osprey (*Pandion haliaetus*), tawny owl (*Strix aluco*), and common kestrel (*Falco tinnunculus*). Environ. Res. 149, 40–47. https://doi.org/10.1016/j.envres.2016.04.038.

Esplugas, S., Bila, D.M., Krause, L.G.T., Dezotti, M., 2007. Ozonation and advanced oxidation technologies to remove endocrine disrupting chemicals (EDCs) and pharmaceuticals and personal care products (PPCPs) in water effluents. J. Hazard. Mater. 149 (3), 631–642. https://doi.org/10.1016/j.jhazmat.2007.07.073.

Farré, M.l., Pérez, S., Kantiani, L., Barceló, D., 2008. Fate and toxicity of emerging pollutants, their metabolites and transformation products in the aquatic environment. TrAC Trends Anal. Chem. 27 (11), 991–1007. https://doi.org/10.1016/j.trac.2008.09.010.

Federal Register, 2016. https://www.federalregister.gov/documents/2016/11/17/2016-27667/drinking-water-contaminant-candidate-list-4-final.

Fisner, M., Majer, A., Taniguchi, S., Bícego, M., Turra, A., Gorman, D., 2017. Colour spectrum and resin-type determine the concentration and composition of polycyclic aromatic hydrocarbons (PAHs) in plastic pellets. Mar. Pollut. Bull. 122 (1–2), 323–330. https://doi.org/10.1016/j.marpolbul.2017.06.072.

Gao, C.J., Kannan, K., 2020. Phthalates, bisphenols, parabens, and triclocarban in feminine hygiene products from the United States and their implications for human exposure. Environ. Int. 136. https://doi.org/10.1016/j.envint.2020.105465.

Garcia-Rodríguez, A., Matamoros, V., Fontàs, C., Salvadó, V., 2014. The ability of biologically based wastewater treatment systems to remove emerging organic contaminants—a review. Environ. Sci. Pollut. Res. 21 (20), 11708–11728. https://doi.org/10.1007/s11356-013-2448-5.

Gaya, U.I., Abdullah, A.H., 2008. Heterogeneous photocatalytic degradation of organic contaminants over titanium dioxide: a review of fundamentals, progress and problems. J Photochem Photobiol C: Photochem Rev 9 (1), 1–12. https://doi.org/10.1016/j.jphotochemrev.2007.12.003.

Ghernaout, D., Naceur, M.W., 2011. Ferrate(VI): in situ generation and water treatment – a review. Desalin. Water Treat. 30 (1–3), 319–332. https://doi.org/10.5004/dwt.2011.2217.

Glassmeyer, S.T., Koplin, D.W., Furlong, E.T., Focazio, M., 2008. Environmental presence and persistence of pharmaceuticals: an overview. In: Aga, D.S. (Ed.), Fate of Pharmaceuticals in the Environment and in Water Treatment Systems. CRC Press, p. 3, https://doi.org/10.1201/9781420052336.

Global chemicals outlook, 2013. https://sdgs.un.org/publications/global-chemicals-outlook-towards-sound-management-chemicals-17941.

Global Report, 2017. https://ipen.org/sites/default/files/documents/ipen-global-lead-report-2017-v1_2-en.pdf.

Godoy, A.A., Kummrow, F., Pamplin, P.A.Z., 2015. Occurrence, ecotoxicological effects and risk assessment of antihypertensive pharmaceutical residues in the aquatic environment – a review. Chemosphere 138, 281–291. https://doi.org/10.1016/j.chemosphere.2015.06.024.

González-Mariño, I., Quintana, J.B., Rodríguez, I., Cela, R., 2009. Simultaneous determination of parabens, triclosan and triclocarban in water by liquid chromatography/electrospray ionisation tandem mass spectrometry. Rapid Commun. Mass Spectrom. 23 (12), 1756–1766. https://doi.org/10.1002/rcm.4069.

Goudarzi, G., Geravandi, S., Alavi, N., Idani, E., Salmanzadeh, S., Yari, A.R., Jamshidi, F., Mohammadi, M.J., Ranjbarzadeh, A., Alamdari, F.A., Darabi, F., Rohban, A., 2018. Association between cancer risk and polycyclic aromatic hydrocarbons' exposure in the ambient air of Ahvaz, southwest of Iran. Int. J. Biometeorol. 62 (8), 1461–1470. https://doi.org/10.1007/s00484-018-1543-1.

Grandclément, C., Seyssiecq, I., Piram, A., Wong-Wah-Chung, P., Vanot, G., Tiliacos, N., Roche, N., Doumenq, P., 2017. From the conventional biological wastewater treatment to hybrid processes, the evaluation of organic micropollutant removal: a review. Water Res. 111, 297–317. https://doi.org/10.1016/j.watres.2017.01.005.

Grenni, P., Ancona, V., Barra Caracciolo, A., 2018. Ecological effects of antibiotics on natural ecosystems: a review. Microchem. J. 136, 25–39. https://doi.org/10.1016/j.microc.2017.02.006.

Grung, M., Lin, Y., Zhang, H., Steen, A.O., Huang, J., Zhang, G., Larssen, T., 2015. Pesticide levels and environmental risk in aquatic environments in China – a review. Environ. Int. 81, 87–97. https://doi.org/10.1016/j.envint.2015.04.013.

Guagliardi, I., Buttafuoco, G., Cicchella, D., De Rosa, R., 2013. A multivariate approach for anomaly separation of potentially toxic trace elements in urban and peri-urban soils: an application in a southern Italy area. J. Soils Sediments 13 (1), 117–128. https://doi.org/10.1007/s11368-012-0583-0.

Guart, A., Bono-Blay, F., Borrell, A., Lacorte, S., 2014. Effect of bottling and storage on the migration of plastic constituents in Spanish bottled waters. Food Chem. 156, 73–80. https://doi.org/10.1016/j.foodchem.2014.01.075.
Gurbuz, F., Akpınar, Ş., Ozcan, S., Acet, Ö., Odabaşı, M., 2019. Reducing arsenic and groundwater contaminants down to safe level for drinking purposes via Fe^{3+}–attached hybrid column. Environ. Monit. Assess. 191 (12). https://doi.org/10.1007/s10661-019-7862-9.
Hampel, M., Blasco, J., Segner, H., 2015. Molecular and cellular effects of contamination in aquatic ecosystems. Environ. Sci. Pollut. Res. 22 (22), 17261–17266. https://doi.org/10.1007/s11356-015-5565-5.
Harvey, P.J., Handley, H.K., Taylor, M.P., 2016. Widespread copper and lead contamination of household drinking water, New South Wales, Australia. Environ. Res. 151, 275–285. https://doi.org/10.1016/j.envres.2016.07.041.
Hughes, S.R., Kay, P., Brown, L.E., 2013. Global synthesis and critical evaluation of pharmaceutical data sets collected from river systems. Environ. Sci. Technol. 47 (2), 661–677. https://doi.org/10.1021/es3030148.
Ikehata, K., Jodeiri Naghashkar, N., Gamal El-Din, M., 2006. Degradation of aqueous pharmaceuticals by ozonation and advanced oxidation processes: a review. Ozone Sci. Eng. 28 (6), 353–414. https://doi.org/10.1080/01919510600985937.
Ikehata, K., El-Din, M.G., Snyder, S.A., 2008. Ozonation and advanced oxidation treatment of emerging organic pollutants in water and wastewater. Ozone Sci. Eng. 30 (1), 21–26. https://doi.org/10.1080/01919510701728970.
Iorhemen, O.T., Hamza, R.A., Tay, J.H., 2016. Membrane bioreactor (Mbr) technology for wastewater treatment and reclamation: membrane fouling. Membranes 6 (2). https://doi.org/10.3390/membranes6020033.
Ismail, W.N.W., Mokhtar, S.U., 2020. Various methods for removal, treatment, and detection of emerging water contaminants. In: Nuro, A. (Ed.), Emerging Contaminants. Intech, https://doi.org/10.5772/intechopen.93375.
Itoh, N., Naya, T., Kanai, Y., Kumon, F., Amano, K., 2017. Historical changes in the aquatic environment and input of polycyclic aromatic hydrocarbons over 1000 years in Lake Kitaura, Japan. Limnology 18 (1), 51–62. https://doi.org/10.1007/s10201-016-0488-5.
Jagne, J., White, D., Jefferson, F., 2016. Endocrine-disrupting chemicals: adverse effects of bisphenol A and parabens to Women's health. Water Air Soil Pollut. 227 (6). https://doi.org/10.1007/s11270-016-2785-3.
Jiang, J.Q., 2007. Research progress in the use of ferrate(VI) for the environmental remediation. J. Hazard. Mater. 146 (3), 617–623. https://doi.org/10.1016/j.jhazmat.2007.04.075.
Johri, N., Jacquillet, G., Unwin, R., 2010. Heavy metal poisoning: the effects of cadmium on the kidney. Biometals 23 (5), 783–792. https://doi.org/10.1007/s10534-010-9328-y.
Kabata-Pendias, A., 2010. Trace Elements in Soils and Plants. Springer.
Kanaujiya, D.K., Paul, T., Sinharoy, A., Pakshirajan, K., 2019. Biological treatment processes for the removal of organic micropollutants from wastewater: a review. Curr. Pollut. Rep. 5 (3), 112–128. https://doi.org/10.1007/s40726-019-00110-x.
Kang, J.W., 2014. Removing environmental organic pollutants with bioremediation and phytoremediation. Biotechnol. Lett. 36 (6), 1129–1139. https://doi.org/10.1007/s10529-014-1466-9.
Kasprzyk-Hordern, B., Dinsdale, R.M., Guwy, A.J., 2009. The removal of pharmaceuticals, personal care products, endocrine disruptors and illicit drugs during wastewater treatment and its impact on the quality of receiving waters. Water Res. 43 (2), 363–380. https://doi.org/10.1016/j.watres.2008.10.047.
Kim, K.H., Kabir, E., Jahan, S.A., 2017. Exposure to pesticides and the associated human health effects. Sci. Total Environ. 575, 525–535. https://doi.org/10.1016/j.scitotenv.2016.09.009.
Klamerth, N., Malato, S., Agüera, A., Fernández-Alba, A., Mailhot, G., 2012. Treatment of municipal wastewater treatment plant effluents with modified photo-Fenton as a tertiary treatment for the degradation of micro pollutants and disinfection. Environ. Sci. Technol. 46 (5), 2885–2892. https://doi.org/10.1021/es204112d.
Kolpin, D.W., Furlong, E.T., Meyer, M.T., Thurman, E.M., Zaugg, S.D., Barber, L.B., Buxton, H.T., 2002. Pharmaceuticals, hormones, and other organic wastewater contaminants in U.S. streams, 1999-2000: a national reconnaissance. Environ. Sci. Technol. 36 (6), 1202–1211. https://doi.org/10.1021/es011055j.
Kuivenhoven, Mason, K., 2021. Arsenic toxicity. In: StatPearls. SteatPearls Publishing. http://www.ncbi.nlm.nih.gov/pubmed/31082169.
Kumar, M., Gogoi, A., Kumari, D., Borah, R., Das, P., Mazumder, P., Tyagi, V.K., 2017. Review of perspective, problems, challenges, and future scenario of metal contamination in the urban environment. J. Hazard. Tox. Radioact. Waste 21 (4). https://doi.org/10.1061/(ASCE)HZ.2153-5515.0000351.
Kümmerer, K., 2009. The presence of pharmaceuticals in the environment due to human use – present knowledge and future challenges. J. Environ. Manag. 90 (8), 2354–2366. https://doi.org/10.1016/j.jenvman.2009.01.023.
Lambert, M.R., Skelly, D.K., 2016. Diverse sources for endocrine disruption in the wild. Endocr. Disruptors. https://doi.org/10.1080/23273747.2016.1148803, e1148803.

Liu, Z.h., Kanjo, Y., Mizutani, S., 2009. Removal mechanisms for endocrine disrupting compounds (EDCs) in wastewater treatment – physical means, biodegradation, and chemical advanced oxidation: a review. Sci. Total Environ. 407 (2), 731–748. https://doi.org/10.1016/j.scitotenv.2008.08.039.

Lopez, B., Ollivier, P., Togola, A., Baran, N., Ghestem, J.P., 2015. Screening of French groundwater for regulated and emerging contaminants. Sci. Total Environ. 518–519, 562–573. https://doi.org/10.1016/j.scitotenv.2015.01.110.

Luo, Y., Guo, W., Ngo, H.H., Nghiem, L.D., Hai, F.I., Zhang, J., Liang, S., Wang, X.C., 2014. A review on the occurrence of micropollutants in the aquatic environment and their fate and removal during wastewater treatment. Sci. Total Environ. 473–474, 619–641. https://doi.org/10.1016/j.scitotenv.2013.12.065.

MacWan, D.P., Dave, P.N., Chaturvedi, S., 2011. A review on nano-TiO_2 sol-gel type syntheses and its applications. J. Mater. Sci. 46 (11), 3669–3686. https://doi.org/10.1007/s10853-011-5378-y.

Maddah, H.A., Alzhrani, A.S., Bassyouni, M., Abdel-Aziz, M.H., Zoromba, M., Almalki, A.M., 2018. Evaluation of various membrane filtration modules for the treatment of seawater. Appl Water Sci. https://doi.org/10.1007/s13201-018-0793-8.

Malato, S., Maldonado, M.I., Oller, I., Zapata, A., 2012. Removal of Pesticides from water and wastewater by solar-driven photocatalysis. In: Lofrano, G. (Ed.), Emerging Compounds Removal from Wastewater. Springer, Dordrecht, p. 59, https://doi.org/10.1007/978-94-007-3916-1_4.

Maniakova, G., Kowalska, K., Murgolo, S., Mascolo, G., Libralato, G., Lofrano, G., Sacco, O., Guida, M., Rizzo, L., 2020. Comparison between heterogeneous and homogeneous solar driven advanced oxidation processes for urban wastewater treatment: pharmaceuticals removal and toxicity. Sep. Purif. Technol., 116249. https://doi.org/10.1016/j.seppur.2019.116249.

Mason, L.H., Harp, J.P., Han, D.Y., 2014. Pb neurotoxicity: neuropsychological effects of Lead toxicity. Biomed. Res. Int., 1–8. https://doi.org/10.1155/2014/840547.

Matamoros, V., Bayona, J.M., 2008. Behavior of emerging pollutants in constructed wetlands. In: Barceló, D., Petrovic, M. (Eds.), Emerging Contaminants from Industrial and Municipal Waste. Springer, Berlin, Heidelberg, p. 199, https://doi.org/10.1007/978-3-540-79210-9_6.

Matamoros, V., Uggetti, E., García, J., Bayona, J.M., 2016. Assessment of the mechanisms involved in the removal of emerging contaminants by microalgae from wastewater: a laboratory scale study. J. Hazard. Mater. 301, 197–205. https://doi.org/10.1016/j.jhazmat.2015.08.050.

Matthiessen, P., Wheeler, J.R., Weltje, L., 2018. A review of the evidence for endocrine disrupting effects of current-use chemicals on wildlife populations. Crit. Rev. Toxicol. 48 (3), 195–216. https://doi.org/10.1080/10408444.2017.1397099.

McGrane, S.J., 2016. Impacts of urbanisation on hydrological and water quality dynamics, and urban water management: a review. Hydrol. Sci. J. 61 (13), 2295–2311. https://doi.org/10.1080/02626667.2015.1128084.

Mnif, W., Hassine, A.I.H., Bouaziz, A., Bartegi, A., Thomas, O., Roig, B., 2011. Effect of endocrine disruptor pesticides: a review. Int. J. Environ. Res. Public Health 8 (6), 2265–2303. https://doi.org/10.3390/ijerph8062265.

Mojiri, A., Zhou, J.L., Ohashi, A., Ozaki, N., Kindaichi, T., 2019. Comprehensive review of polycyclic aromatic hydrocarbons in water sources, their effects and treatments. Sci. Total Environ. 696. https://doi.org/10.1016/j.scitotenv.2019.133971.

Molinari, R., Lavorato, C., Argurio, P., 2020. Application of hybrid membrane processes coupling separation and biological or chemical reaction in advanced wastewater treatment. Membranes 10 (10), 1–30. https://doi.org/10.3390/membranes10100281.

Mostafalou, S., Abdollahi, M., 2017. Pesticides: an update of human exposure and toxicity. Arch. Toxicol. 91 (2), 549–599. https://doi.org/10.1007/s00204-016-1849-x.

Myong, J.-P., Kim, H.-R., Jang, T.-W., Lee, H.E., Koo, J.-W., 2014. Association between blood cadmium levels and 10-year coronary heart disease risk in the general Korean population: the Korean National Health and nutrition examination survey 2008–2010. PLoS One 9 (11). https://doi.org/10.1371/journal.pone.0111909, e111909.

National Primary Drinking Water Regulations, 2009. https://www.epa.gov/sites/production/files/2016-06/documents/npwdr_complete_table.pdf.

Nguyen, L.N., Hai, F.I., Kang, J., Price, W.E., Nghiem, L.D., 2013. Removal of emerging trace organic contaminants by MBR-based hybrid treatment processes. Int. Biodeterior. Biodegrad. 85, 474–482. https://doi.org/10.1016/j.ibiod.2013.03.014.

Nikinmaa, M., 2014. What causes aquatic contamination. In: An Introduction to Aquatic Toxicology. Elsevier Inc, pp. 1–240.

Nofiana, Raharjo, S.H., Istirokhatun, T., Susanto, H., 2019. Reuse of domestic wastewater by membrane technologies towards sustainable city development. IOP Conf. Ser. Earth Environ. Sci. 248 (1). https://doi.org/10.1088/1755-1315/248/1/012053.

Noutsopoulos, C., Mamais, D., Mpouras, T., Kokkinidou, D., Samaras, V., Antoniou, K., Gioldasi, M., 2014. The role of activated carbon and disinfection on the removal of endocrine disrupting chemicals and non-steroidal anti-inflammatory drugs from wastewater. Environ. Technol. 35 (6), 698–708. https://doi.org/10.1080/09593330.2013.846923.

Nriagu, J., 2019. Pollution sources and human health. In: Encyclopedia of Environmental Health. Elsevier, pp. 1–508. http://www.sciencedirect.com/science/book/9780444639523.

Olsen, V., Mørland, J., 2004. Forgiftning med arsen. Tidsskr. Nor. Laegeforen. 124 (21), 2750–2753.

Oualid, C., Btissam, A., Sanae, A., Elodie, M.-G., Fabrice, A., Marc, C., Samira, E.F., Ilham, E.A., Bouchra, O., 2019. Occurrence and seasonal variation of antibiotics in Fez-Morocco surface water. Am. J. Environ. Sci., 127–136. https://doi.org/10.3844/ajessp.2019.127.136.

PAN, Pesticide Action Network, 2017. https://www.pan-europe.info/sites/pan-europe.info/files/public/resources/reports/Report_ED%20pesticides%20in%20EU%20food_PAN%20Europe.pdf.

Pan, L.Q., Ren, J., Liu, J., 2006. Responses of antioxidant systems and LPO level to benzo(a)pyrene and benzo(k) fluoranthene in the haemolymph of the scallop Chlamys ferrari. Environ. Pollut. 141 (3), 443–451. https://doi.org/10.1016/j.envpol.2005.08.069.

Pérez-Parada, A., Gómez-Ramos, M.d.M., Bueno, M.J.M., Uclés, S., Uclés, A., Fernández-Alba, A.R., 2012. Analytical improvements of hybrid LC-MS/MS techniques for the efficient evaluation of emerging contaminants in river waters: a case study of the Henares River (Madrid, Spain). Environ. Sci. Pollut. Res. 19 (2), 467–481. https://doi.org/10.1007/s11356-011-0585-2.

Petric, Z., Ruzić, J., Zuntar, I., 2021. The controversies of parabens – an overview nowadays. Acta Pharma. 71 (1), 17–32. https://doi.org/10.2478/acph-2021-0001.

Pidlisnyuk, V.V., Marutovsky, R.M., Radeke, K.-H., Klimenko, N.A., 2003. Biosorption processes for natural and waste water treatment–part II: experimental studies and theoretical model of a biosorption fixed bed. Eng. Life Sci., 439–445. https://doi.org/10.1002/elsc.200301858.

Prieto-Rodríguez, L., Oller, I., Klamerth, N., Agüera, A., Rodríguez, E.M., Malato, S., 2013. Application of solar AOPs and ozonation for elimination of micropollutants in municipal wastewater treatment plant effluents. Water Res. 47 (4), 1521–1528. https://doi.org/10.1016/j.watres.2012.11.002.

Protection of Environment. (2021). https://www.ecfr.gov/cgi-bin/text-idx?SID=15e352a79a295dd3e0f1699119f82c04&mc= true&node=se40.31.401_115&rgn=div8.

Qiao, M., Bai, Y., Cao, W., Huo, Y., Zhao, X., Liu, D., Li, Z., 2018. Impact of secondary effluent from wastewater treatment plants on urban rivers: polycyclic aromatic hydrocarbons and derivatives. Chemosphere 211, 185–191. https://doi.org/10.1016/j.chemosphere.2018.07.167.

Radjenović, J., Petrović, M., Barceló, D., 2009. Fate and distribution of pharmaceuticals in wastewater and sewage sludge of the conventional activated sludge (CAS) and advanced membrane bioreactor (MBR) treatment. Water Res. 43 (3), 831–841. https://doi.org/10.1016/j.watres.2008.11.043.

Raghav, M., Eden, S., Mitchell, K., Witte, B., 2013. Contaminants of Emerging Concern in Water. The Arroyo, Water Resources Research.

Ralston, N.V.C., Raymond, L.J., 2018. Mercury's neurotoxicity is characterized by its disruption of selenium biochemistry. Biochim. Biophys. Acta Gen. Subj. 1862 (11), 2405–2416. https://doi.org/10.1016/j.bbagen.2018.05.009.

Rasalingam, S., Peng, R., Koodali, R.T., 2014. Removal of hazardous pollutants from wastewaters: applications of TiO_2-SiO_2 mixed oxide materials. J. Nanomater. 2014. https://doi.org/10.1155/2014/617405.

Anon., 2008. Regulation (EC) No 1333/2008 of the European Parliament and of the Council of 16 December 2008 on food additives (Text with EEA relevance). https://eur-lex.europa.eu/eli/reg/2008/1333/oj.

Retief, F., Cilliers, L., 2006. Lead poisoning in ancient Rome. Acta Theriol. 26 (2), 147. https://doi.org/10.4314/actat.v26i2.52570.

Ritter, L., Solomon, K., Sibley, P., Hall, K., Keen, P., Mattu, G., Linton, B., 2002. Sources, pathways, and relative risks of contaminants in surface water and groundwater: a perspective prepared for the Walkerton inquiry. J. Toxicol. Environ. Health A 65 (1), 1–142. https://doi.org/10.1080/152873902753338572.

Rivera-Utrilla, J., Sánchez-Polo, M., Ferro-García, M.A., Prados-Joya, G., Ocampo-Pérez, R., 2013. Pharmaceuticals as emerging contaminants and their removal from water. A review. Chemosphere 93 (7), 1268–1287. https://doi.org/10.1016/j.chemosphere.2013.07.059.

Rodil, R., Quintana, J.B., Concha-Graña, E., López-Mahía, P., Muniategui-Lorenzo, S., Prada-Rodríguez, D., 2012. Emerging pollutants in sewage, surface and drinking water in Galicia (NW Spain). Chemosphere 86 (10), 1040–1049. https://doi.org/10.1016/j.chemosphere.2011.11.053.

Rodrigues, M.O., Abrantes, N., Gonçalves, F.J.M., Nogueira, H., Marques, J.C., Gonçalves, A.M.M., 2018. Spatial and temporal distribution of microplastics in water and sediments of a freshwater system (Antuã River, Portugal). Sci. Total Environ. 633, 1549–1559. https://doi.org/10.1016/j.scitotenv.2018.03.233.

Rodriguez-Narvaez, O.M., Peralta-Hernandez, J.M., Goonetilleke, A., Bandala, E.R., 2017. Treatment technologies for emerging contaminants in water: a review. Chem. Eng. J. 323, 361–380. https://doi.org/10.1016/j.cej.2017.04.106.

Rosenfeld, P.E., Feng, L., 2011. The Environmental Protection Agency's regulatory definition. In: Risks of Hazardous Wastes. Elsevier Inc.

Rostkowski, P., Horwood, J., Shears, J.A., Lange, A., Oladapo, F.O., Besselink, H.T., Tyler, C.R., Hill, E.M., 2011. Bioassay-directed identification of novel antiandrogenic compounds in bile of fish exposed to wastewater effluents. Environ. Sci. Technol. 45 (24), 10660–10667. https://doi.org/10.1021/es202966c.

Roth, H., Gendel, Y., Buzatu, P., David, O., Wessling, M., 2016. Tubular carbon nanotube-based gas diffusion electrode removes persistent organic pollutants by a cyclic adsorption - electro-Fenton process. J. Hazard. Mater. 307, 1–6. https://doi.org/10.1016/j.jhazmat.2015.12.066.

Roy, S., Edwards, M.A., 2019. Preventing another lead (Pb) in drinking water crisis: lessons from the Washington D.C. and Flint MI contamination events. Curr. Opin. Environ. Sci. Health 7, 34–44. https://doi.org/10.1016/j.coesh.2018.10.002.

Ruus, A., Hjermann, D., Beylich, B., Schøyen, M., Øxnevad, S., Green, N.W., 2017. Mercury concentration trend as a possible result of changes in cod population demography. Mar. Environ. Res. 130, 85–92. https://doi.org/10.1016/j.marenvres.2017.07.018.

Saari, G.N., Scott, W.C., Brooks, B.W., 2017. Global scanning assessment of calcium channel blockers in the environment: review and analysis of occurrence, ecotoxicology and hazards in aquatic systems. Chemosphere 189, 466–478. https://doi.org/10.1016/j.chemosphere.2017.09.058.

Saidulu, D., Gupta, B., Gupta, A.K., Ghosal, P.S., 2021. A review on occurrences, eco-toxic effects, and remediation of emerging contaminants from wastewater: special emphasis on biological treatment based hybrid systems. J. Environ. Chem. Eng. 9 (4). https://doi.org/10.1016/j.jece.2021.105282.

Salimi, M., Esrafili, A., Gholami, M., Jonidi Jafari, A., Rezaei Kalantary, R., Farzadkia, M., Kermani, M., Sobhi, H.R., 2017. Contaminants of emerging concern: a review of new approach in AOP technologies. Environ. Monit. Assess. 189 (8). https://doi.org/10.1007/s10661-017-6097-x.

Schäfer, A.I., Akanyeti, I., Semião, A.J.C., 2011. Micropollutant sorption to membrane polymers: a review of mechanisms for estrogens. Adv. Colloid Interf. Sci. 164 (1–2), 100–117. https://doi.org/10.1016/j.cis.2010.09.006.

Schultz, M.M., 2014. Chemicals of environmental concern. In: Encyclopedia of Toxicology, third ed. Elsevier, pp. 805–809, https://doi.org/10.1016/B978-0-12-386454-3.01004-6.

Sharma, S., Bhattacharya, A., 2017. Drinking water contamination and treatment techniques. Appl Water Sci, 1043–1067. https://doi.org/10.1007/s13201-016-0455-7.

Shemer, H., Kunukcu, Y.K., Linden, K.G., 2006. Degradation of the pharmaceutical metronidazole via UV, Fenton and photo-Fenton processes. Chemosphere 63 (2), 269–276. https://doi.org/10.1016/j.chemosphere.2005.07.029.

Silver, M.K., Li, X., Liu, Y., Li, M., Mai, X., Kaciroti, N., Kileny, P., Tardif, T., Meeker, J.D., Lozoff, B., 2016. Low-level prenatal lead exposure and infant sensory function. Environ. Health 15 (1). https://doi.org/10.1186/s12940-016-0148-6.

Simmons, F.J., Kuo, D.H.W., Xagoraraki, I., 2011. Removal of human enteric viruses by a full-scale membrane bioreactor during municipal wastewater processing. Water Res. 45 (9), 2739–2750. https://doi.org/10.1016/j.watres.2011.02.001.

Slegers, C., Tilquin, B., 2006. Final product analysis in the e-beam and gamma radiolysis of aqueous solutions of metoprolol tartrate. Radiat. Phys. Chem. 75 (9), 1006–1017. https://doi.org/10.1016/j.radphyschem.2005.12.020.

Smarr, M.M., Kannan, K., Buck Louis, G.M., 2016. Endocrine disrupting chemicals and endometriosis. Fertil. Steril. 106 (4), 959–966. https://doi.org/10.1016/j.fertnstert.2016.06.034.

Song, W., Chen, W., Cooper, W.J., Greaves, J., Miller, G.E., 2008. Free-radical destruction of β-lactam antibiotics in aqueous solution. J. Phys. Chem. A 112 (32), 7411–7417. https://doi.org/10.1021/jp803229a.

Sornalingam, K., McDonagh, A., Zhou, J.L., 2016. Photodegradation of estrogenic endocrine disrupting steroidal hormones in aqueous systems: progress and future challenges. Sci. Total Environ. 550, 209–224. https://doi.org/10.1016/j.scitotenv.2016.01.086.

Stuart, M., Lapworth, D., Crane, E., Hart, A., 2012. Review of risk from potential emerging contaminants in UK groundwater. Sci. Total Environ. 416, 1–21. https://doi.org/10.1016/j.scitotenv.2011.11.072.

Su, D., Ben, W., Strobel, B.W., Qiang, Z., 2020. Occurrence, source estimation and risk assessment of pharmaceuticals in the Chaobai River characterized by adjacent land use. Sci. Total Environ. 712. https://doi.org/10.1016/j.scitotenv.2019.134525.

Svenson, A., Allard, A.S., Ek, M., 2003. Removal of estrogenicity in Swedish municipal sewage treatment plants. Water Res. 37 (18), 4433–4443. https://doi.org/10.1016/S0043-1354(03)00395-6.

Taheran, M., Brar, S.K., Verma, M., Surampalli, R.Y., Zhang, T.C., Valéro, J.R., 2016. Membrane processes for removal of pharmaceutically active compounds (PhACs) from water and wastewaters. Sci. Total Environ. 547, 60–77.

Taheran, M., Naghdi, M., Brar, S.K., Verma, M., Surampalli, R.Y., 2018. Emerging contaminants: here today, there tomorrow! Environ. Nanotechnol. Monit. Manag. 10, 122–126. https://doi.org/10.1016/j.enmm.2018.05.010.

Talukder, A.S.M.H.M., Meisner, C.A., Sarkar, M.A.R., Islam, M.S., Sayre, K.D., Duxbury, J.M., Lauren, J.G., 2012. Effect of water management, arsenic and phosphorus levels on rice in a high-arsenic soil-water system: II. Arsenic uptake. Ecotoxicol. Environ. Saf. 80, 145–151. https://doi.org/10.1016/j.ecoenv.2012.02.020.

Tan, S.W., Meiller, J.C., Mahaffey, K.R., 2009. The endocrine effects of mercury in humans and wildlife. Crit. Rev. Toxicol. 39 (3), 228–269. https://doi.org/10.1080/10408440802233259.

Tanwar, J., Das, S., Fatima, Z., Hameed, S., 2014. Multidrug resistance: an emerging crisis. Interdiscip. Perspect. Infect. Dis. 2014. https://doi.org/10.1155/2014/541340.

Tareq, R., Akter, N., Azam, M.S., 2018. Biochars and biochar composites: low-cost adsorbents for environmental remediation. In: Biochar from Biomass and Waste: Fundamentals and Applications. Elsevier, pp. 169–209, https://doi.org/10.1016/B978-0-12-811729-3.00010-8.

Tran, N.H., Urase, T., Ngo, H.H., Hu, J., Ong, S.L., 2013. Insight into metabolic and cometabolic activities of autotrophic and heterotrophic microorganisms in the biodegradation of emerging trace organic contaminants. Bioresour. Technol. 146, 721–731. https://doi.org/10.1016/j.biortech.2013.07.083.

USEPA, 2010. Bisphenol A Action Plan. https://www.epa.gov/sites/production/files/2015-09/documents/bpa_action_plan.pdf.

Vagge, G., Cutroneo, L., Castellano, M., Canepa, G., Bertolotto, R.M., Capello, M., 2018. The effects of dredging and environmental conditions on concentrations of polycyclic aromatic hydrocarbons in the water column. Mar. Pollut. Bull. 135, 704–713. https://doi.org/10.1016/j.marpolbul.2018.08.006.

Wang, Y., Wang, X., Li, M., Dong, J., Sun, C., Chen, G., 2018b. Removal of pharmaceutical and personal care products (PPCPs) from municipalwaste water with integrated membrane systems, MBR-RO/NF. Int. J. Environ. Res. Public Health 15 (2). https://doi.org/10.3390/ijerph15020269.

Wang, N., Hu, X., Lu, S., Ma, S., Kang, L., Liao, S., Yu, Y., 2019. Interrelationship of anthropogenic activity and parabens in fish from Taihu Lake during 2009–2017. Environ. Pollut. 252, 1002–1009. https://doi.org/10.1016/j.envpol.2019.06.041.

Westerhoff, P., Yoon, Y., Snyder, S., Wert, E., 2005. Fate of endocrine-disruptor, pharmaceutical, and personal care product chemicals during simulated drinking water treatment processes. Environ. Sci. Technol. 39 (17), 6649–6663. https://doi.org/10.1021/es0484799.

WHO, 2011. Arsenic in Drinking-Water. https://www.who.int/water_sanitation_health/publications/arsenic/en.

WHO, Guidelines for Drinking-Water Quality, 2017. https://www.who.int/water_sanitation_health/publications/gdwq4-with-add1-chapters/en/.

Yan, C., Nie, M., Yang, Y., Zhou, J., Liu, M., Baalousha, M., Lead, J.R., 2015. Effect of colloids on the occurrence, distribution and photolysis of emerging organic contaminants in wastewaters. J. Hazard. Mater. 299, 241–248. https://doi.org/10.1016/j.jhazmat.2015.06.022.

Yang, W., Cicek, N., Ilg, J., 2006. State-of-the-art of membrane bioreactors: worldwide research and commercial applications in North America. J. Membr. Sci. 270 (1–2), 201–211. https://doi.org/10.1016/j.memsci.2005.07.010.

Yang, Y., Ok, Y.S., Kim, K.H., Kwon, E.E., Tsang, Y.F., 2017. Occurrences and removal of pharmaceuticals and personal care products (PPCPs) in drinking water and water/sewage treatment plants: a review. Sci. Total Environ. 596–597, 303–320. https://doi.org/10.1016/j.scitotenv.2017.04.102.

Yiming, J., Haiying, H., Mengru, W., Xuan, Y., Yong, C., Pu, L., Xiangkai, L., 2015. Pseudomonas sp. LZ-Q continuously degrades phenanthrene under hypersaline and hyperalkaline condition in a membrane bioreactor system. Biophys. Rep., 156–167. https://doi.org/10.1007/s41048-016-0018-3.

Zhang, W.L., Du, Y., Zhai, M.M., Shang, Q., 2014. Cadmium exposure and its health effects: a 19-year follow-up study of a polluted area in China. Sci. Total Environ. 470–471, 224–228. https://doi.org/10.1016/j.scitotenv.2013.09.070.

Zhao, X., Shen, J.P., Zhang, L.M., Du, S., Hu, H.W., He, J.Z., 2020. Arsenic and cadmium as predominant factors shaping the distribution patterns of antibiotic resistance genes in polluted paddy soils. J. Hazard. Mater., 389. https://doi.org/10.1016/j.jhazmat.2019.121838.

Zhou, J.L., Zhang, Z.L., Banks, E., Grover, D., Jiang, J.Q., 2009. Pharmaceutical residues in wastewater treatment works effluents and their impact on receiving river water. J. Hazard. Mater. 166 (2–3), 655–661. https://doi.org/10.1016/j.jhazmat.2008.11.070.

CHAPTER

6

Advantages of nanoadsorbents, biosorbents, and nanobiosorbents for contaminant removal

Bahareh Kamyab Moghadas[a], *Hossein Esmaeili*[b], *Sajad Tamjidi*[a], *and Alipasha Geramifard*[c]

[a]Department of Chemical Engineering, Shiraz Branch, Islamic Azad University, Shiraz, Iran
[b]Department of Chemical Engineering, Bushehr Branch, Islamic Azad University, Bushehr, Iran
[c]Department of Mechanical Engineering, Shiraz Branch, Islamic Azad University, Shiraz, Iran

6.1 Introduction

Water is one of the most critical natural sources in the world and is necessary for the survival of all creatures. The global population is regularly growing, and releasing pollutants in industrial and surface wastewater is raising. Agricultural wastes, industrial and human residues play crucial factors in sewage pollution. These items produce different contaminants, changed the water cycle, and increased global concerns, which their final impact is on human health and wildlife (Khatri and Tyagi, 2015; Abedpour et al., 2020). Several kinds of contaminants in wastewater, including metals, radionuclides, rare earth elements, dyes, phenolic and aromatic derivatives, pesticides, pharmaceuticals, and drugs, have been examined widely (Crini et al., 2019; Huang et al., 2019). In the past few decades, different techniques have been developed for treating wastewater, including ion exchange, micro, and ultrafiltration, reverse osmosis, evaporation, solvent extraction, coagulation, precipitation, sedimentation, gravity, flotation, oxidation, electrolysis, electrodialysis, distillation, adsorption, etc. From the techniques mentioned above, adsorption is a considerable technique for treating wastewater because of its easy operation, inexpensive, and abundance of adsorbents. Adsorbents can remove soluble and insoluble materials (e.g., organic and inorganic) and biological pollutants (Santhosh et al., 2016; El Hefnawy et al., 2020).

https://doi.org/10.1016/B978-0-323-90912-9.00006-X

In this method, the adsorbed contaminants should be recovered from the adsorbent surface. Among various treatments, biosorption is recognized as an environmentally friendly method to eliminate contaminants from wastewater because of using natural materials and renewable biomass as sorbents (Dev et al., 2020; Tamjidi et al., 2021a). Over the years, the use of bioadsorbents has received much attention. Most bioadsorbents are usually categorized into five groups, including (1) agricultural waste, (2) marine material, (3) microbial biosorbents, (4) industrial by-products, and (5) minerals. The advantages of these biomaterials are high biosorption capacity, availability in large quantities, low cost, simple desorption of the adsorbed contaminant, and high reusability of the biosorbent (Kanamarlapudi et al., 2018; Hussain et al., 2018). Generally, there are many organic and inorganic bioadsorbents with high sorption capacity, including cottonseed shell, fungal biomass, algae biomass, shrimp shell and chitin, bagasse, eggshell waste, agricultural wastes-derived activated carbon (AC) generated from, plant waste, vegetable wastes, chitosan, cellulose, bone ash, Turkish coffee, coal ash, resins, silica gel, zeolite, clay, sawdust, oil-extracted soybean, tea waste, used coffee, brewery seed residue, walnut shell, almond, etc., have been applied as biosorbents in the treatment of wastewater containing different types of contaminants (Dev et al., 2020; Hussain et al., 2018).

The main purpose of this chapter is a comprehensive review of the application of biosorbents, nanosorbents, and nanobiosorbents as low-cost and efficient adsorbents to remove contaminants from water and wastewater. To do so, different types of contaminants, their characteristics, different types of biosorbents, nanosorbents, and nanobiosorbents and their performance, and the impact of effective factors on the sorption process have been thoroughly studied.

6.2 Types of contaminants

There is very little freshwater on the planet, which is polluted due to improper discharge of waste into rivers. The rapid growth of technology and industrialization is the main reason for adding contaminants to water. Drinking contaminated water causes many diseases that kill many people every year. The polluted water is harmful to human beings and has adverse impacts on the entire ecosystem. Marine life is very disturbed because of the dumping of waste in the sea. There are two types of pollutants in the effluent, including inorganic and organic materials. Inorganic pollutants contain toxic metal ions, while organic pollutants contain dyes, pharmaceutical drugs, pesticides, volatile organic compounds, and aromatic hydrocarbons. Both organic and inorganic pollutants affect the environment. Even at low concentrations, the presence of toxic metal ions can lead to many harmful diseases for living organisms. Organic contaminants like dyes used in many industries as coloring material are very toxic and carcinogenic.

Other organic contaminants like pesticides have significant toxic impacts on living organisms. Since contaminants in water have a bad influence on all organisms and the environment, their elimination is critical (Saxena et al., 2020; Akpor et al., 2014). A summary of the most critical contaminants in wastewater is described below.

6.2.1 Dyes

Dyes can be made naturally or synthetically, which is applied for painting, printing, leather, paper, and other materials. The annual generation of dyes in different industries is estimated to be more than seven. Annually, about 100 tons of dye is discharged as residue into wastewater. Dye is a dangerous class of organic contaminants that are directly and indirectly released into water resources. Therefore, removing dyes from wastewater and water is a major concern for the environment. Dyes also have acute impacts on organisms, depending on the contact duration and dye concentration (Bello et al., 2021). Therefore, these cases pose a serious threat to water quality and human health, thereby becoming a vital concern. Due to the need to remove the dye, the relevant industries must treat the colored effluents before discharging them into the water. Therefore, the scientific community has a great responsibility to treat wastewater by developing efficient methods. Dyes can cause skin irritation, allergic dermatitis, mutation, cancer, etc. They are categorized as cationic (basic dyes), anionic (acid and reactive dyes), and non-ionic dyes (dispersive dyes) (Bharathi and Ramesh, 2013).

Cationic dyes

Cationic dyes are extensively used in nylon, wool, acrylic, and silk dyeing. These dyes contain various chemical structures. Also, they are considered toxic colorants and cause harmful impacts like skin irritation, allergic dermatitis, mutations, and cancer. Moreover, these dyes are called basic dyes and have positive charges on their structure.

Furthermore, cationic dyes are water-soluble and produce colored cations in water. Basic dyes are more visible and have high brightness and color intensity. Methylene blue, methyl violet, rhodamine 6G, malachite green, and basic yellow are the most important cationic dyes (Corda and Kini, 2018). All of these dyes are toxic, mutagenic, and carcinogenic. They are harmful to human health and contagious for aquatic life. The high dosage of these dyes in seawater inhibits light penetration and affects aquatic plants' photosynthesis process. The azo dyes are toxic as they contain toxic metal ions and aromatic amines, which are nonbiodegradable in the water for a long time (Saxena et al., 2020).

Anionic dyes

Anionic dyes have negative charges on their structure. They contain different combinations of the most diverse color classes with characteristic differences in structure as a common feature (for example, triphenylmethane, anthraquinone, azoic, and nitro dyes). Also, direct dyes are anionic dyes, and the group of anionic azo dyes consists of a large part of reactive dyes. Most reactive dyes interact with some materials such as wool and cotton to form covalent forms (Bharathi and Ramesh, 2013). Direct red 23, Congo red, Reactive Black 5, and Methyl orange are the most common anionic dyes. The application of each dye depends on its structure and ability to connect (Bello et al., 2021).

Non-ionic dyes

Non-ionic dyes include dispersing dyes, mainly used to generate colored plastics, polyamide, polyester, etc. The dispersed dyes can lead to allergies. Direct Green 97 is a sample of nonionic dyes (Bello et al., 2021).

6.2.2 Heavy metal

Heavy metals are natural substances in the environment. Human works like agricultural, coal mills, mining, coal power plants, casting factories, and metallurgy would change the geochemical cycle of the atmosphere and biochemical equilibrium. These human activities result in the excessive release of heavy metals like lead, mercury, chromium, copper, cadmium, nickel, zinc, and iron (Wuana and Okieimen, 2011).

Heavy metals are a class of materials with an atomic density above 5 g/cm^3. Density is related to the chemical features of heavy metals. Heavy metals are classified into three groups according to the periodic table, including lanthanide series (e.g., La), actinide series (e.g., Ac), and some metallic elements of group P. Generally, these metals are in groups 3–16 in period 4 onwards in the periodic table (Bello et al., 2021). Heavy metals can be found directly or indirectly. With the development of industries and human activities, heavy metal ions are increasingly released into the environment, especially in developing countries. These contaminants are produced in the wastewaters generated by industries such as mining operations, industrial and agricultural chemicals, plating industry, paper production, battery manufacturing, and animal waste. International authorities regularly monitor these metals' impacts on human and animal health like FAO, EPA, and WHO. Should the concentration of heavy metals like nickel, arsenic, zinc, chromium, mercury, lead, selenium, and cadmium exceeds the permissible limits set by WHO, those can lead to acute and chronic intoxication and damage central nerve function, cardiovascular and digestive systems, liver, kidneys, lungs, and endocrines (Tamjidi et al., 2019). Fig. 6.1 illustrates the sources and impacts of heavy metals on the health of humans, animals, and other organisms.

6.2.3 Pharmaceutical drugs

Pharmaceutical drugs are the materials used to save human and animal life. But when these drugs are discharged into the water in large amounts, they are considered a threat to all living organisms' lives. Prolonged exposure to drugs causes many problems for vital human organs. The reason for the toxicity of drugs is their bioaccumulation. Medications used regularly, such as analgesics, antibiotics, chemical products used in chemotherapy, and even some antidepressants, are the main ingredients of pharmaceutical waste. The presence of persistent antibiotics such as sulfonamides and chloramphenicol in wastewater is a serious concern (Saxena et al., 2020).

6.2.4 Pesticides/insecticides

Pesticides are extensively used in agricultural production to protect plants against weeds, fungi, and pests. Residues of pesticides are widely dispersed in groundwaters and soils. There are different ways for environmental pollution by pesticides, including runoff from agricultural land, industrial effluents, and direct entry through spray and dust. Also, residues of pesticides have important environmental effects on aquatic ecosystems (Taghizade Firozjaee et al., 2018).

Pesticides became a serious concern for environmental sustainability. Also, pesticide pollution has long-term impacts on the environment. Pesticides such as atrazine interfere with

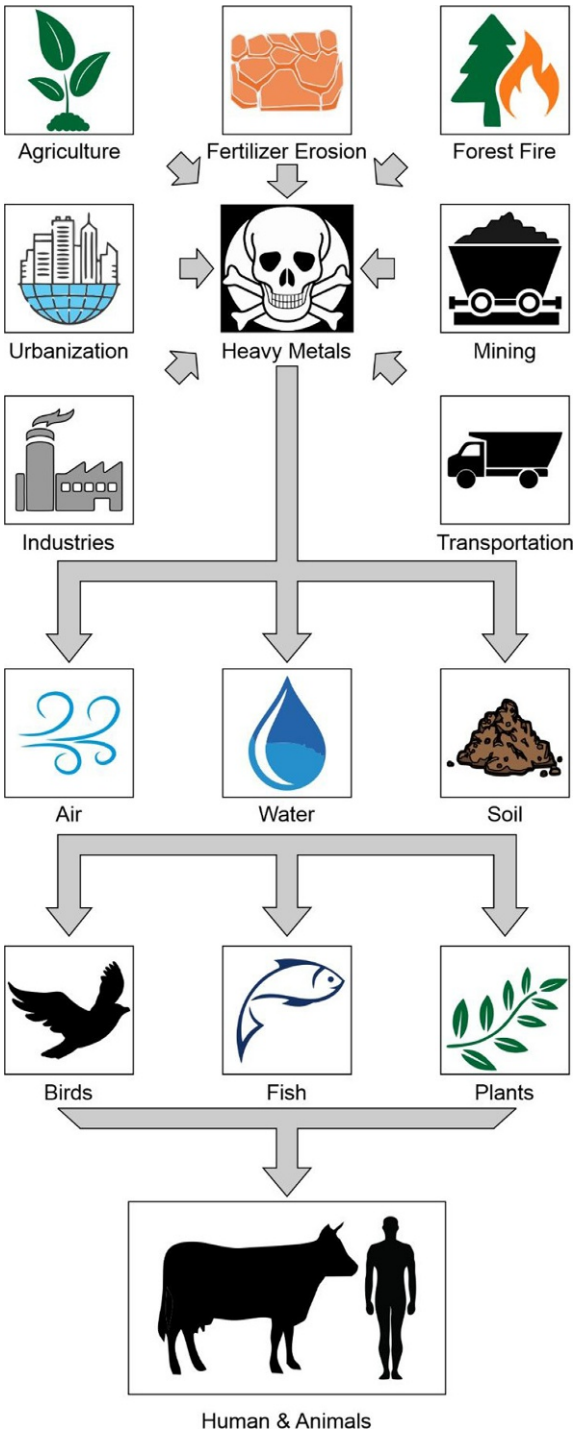

FIG. 6.1 Sources and impacts of heavy metals.

the hormonal activity of humans and animals. Even in trace amounts, some pesticides are very harmful that can lead to death, and that's why removing the pesticide from aqueous media is critical to saving humans and other creatures (Saxena et al., 2020).

6.2.5 Other contaminants

The other organic pollutants include volatile organic compounds, polyaromatic hydrocarbons, toluene, humic acid, phenol, aromatic amines, etc. These organic contaminants have an adverse impact on the environment. Organic compounds like toluene and benzene directly affect the human nervous system. Prolonged exposure can damage the kidneys, liver, and lungs. The aromatic compounds are also utilized in industries for the synthesis of chemicals. These polyaromatic hydrocarbons are toxic as they cause cataracts, nausea, kidney, vomiting, eye irritation, and liver damage. Due to the high toxicity of these contaminants, they should be removed (Saxena et al., 2020).

6.3 Different methods for wastewater treatment

Various physical, chemical, and biological procedures like ion exchange, electrochemical, chemical deposition, flocculation, coagulation, membrane process, and sorption are applied to recover and separate heavy metals from aqueous wastewater solution (Sobhanardakani et al., 2018; Duman and Ayranci, 2010; Chen et al., 2011; Pamukoglu and Kargi, 2006). Fig. 6.2 illustrates different types of conventional methods to eliminate pollutants. Along with the advantages and disadvantages of each, knowing these factors is beneficial for selecting and using these methods to eliminate pollution (Renu et al., 2017; Gunatilake, 2015).

6.3.1 Electrochemical method

The electrochemical method can be an efficient alternative to traditional methods. The most critical procedures in this field are electrocoagulation, electroflotation, and electrodeposition. The mechanism of decomposition of organic material in the electrochemical process is because of the electrons transfer between electrodes and organic materials. This technology relatively needs high-cost equipment and high investments, which has limited this method. Other disadvantages of this technology are sludge disposal and effluent neutralization (Sillanpää and Shestakova, 2017; Fernandes et al., 2015).

6.3.2 Coagulation and flocculation

Flocculation or coagulation followed by filtration and sedimentation are used to eliminate heavy metals from wastewater. Coagulation is destabilizing colloids by neutralizing the forces that keep them apart. Many coagulants are used for wastewater treatment, including aluminum, ferric chloride, and ferrous sulfate, leading to the effective elimination of pollutants from wastewater. Coagulation is one of the most critical wastewater treatment procedures, but only suspended particles and colloids are the main coagulation objects.

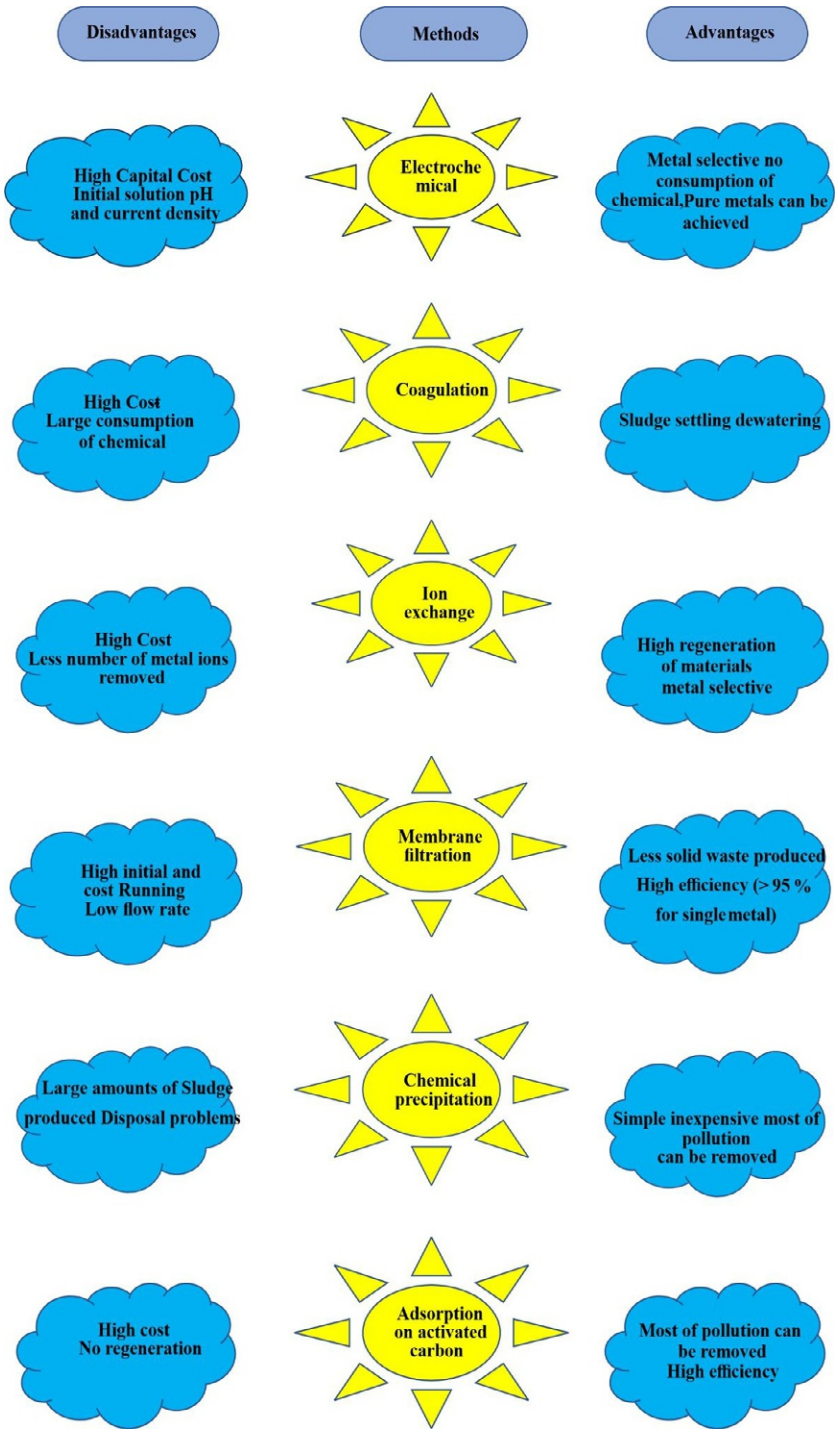

FIG. 6.2 Different procedures and their advantages and disadvantages.

Flocculation is polymers' action to create bridges between the flocs and attach particles to large agglomerates. However, it is almost impossible to eliminate heavy metals from wastewater directly by these clots. Generally, coagulation-flocculation cannot completely treat the heavy metal wastewater. Therefore, coagulation-flocculation should be followed using other treatment methods (Fu and Wang, 2011; Teh et al., 2016).

6.3.3 Ion-exchange process

The ion-exchange process has been extensively used for removing heavy metals from water because of its many advantages like high removal efficiency, high treatment capacity, and fast kinetics. Ion-exchange resins are found in both synthetic and natural forms and have a special ability to exchange metal cations with metals in the effluent. Among the materials applied in the ion-exchange process, synthetic resins are commonly preferred as they effectively separate heavy metals from water (Fu and Wang, 2011).

6.3.4 Membrane filtration

Membrane technology is another promising technology for the high removal of micropollutants from water. In this process, both biological (membrane bioreactors) and non-biological processes (e.g., reverse osmosis, nanofiltration, and ultrafiltration) are used. A membrane bioreactor is a combination of membrane system (e.g., micro- and ultrafiltration) and biological reactor. Membrane bioreactors are the most important and prominent process these days to attain relatively clean water from sewage. Non-biological process or pressurized membrane technology such as nanofiltration, microfiltration, ultrafiltration, and reverse osmosis processes utilize high pressures along the membrane to remove pollutants from the water.

Consequently, membrane processes are very useful for eliminating turbidity and microbial contaminants. However, the high cost of operation still limits its use. Membranes easily suffer from fouling problems, leading to unexpected interruptions during the treatment of pollutants (Ismail and Mokhtar, 2020; Obotey Ezugbe and Rathilal, 2020).

6.3.5 Chemical precipitation

The precipitation method is an effective technique in which pollutants are removed from the solution as sediment. Then, the sediments can be centrifuged or filtered to separate from the liquid solution. Also, this technology is a simple and cheap method. Moreover, it can be used for water softening, removing heavy metals from metal plating waste, removing hydrocarbon compounds from emulsified solutions, and removing phosphate and nitrate from wastewater. The obtained precipitate is separated from the solution by sedimentation or filtration in the technological system, and the treated water is then decanted and respectively discharged or re-used (Pohl, 2020; Mavhungu et al., 2021).

6.3.6 Sorption method

The sorption process is a cost-effective and effective method to treat effluent. The sorption process results in flexibility in the use, design, and treatment of high-quality wastewaters. Also, adsorption is an efficient and reversible process. Suitable adsorbents can be reused several times, and this is one of the most important properties of adsorbents. Sorption is a result of a reaction between the surface of the sorbent and adsorbed pollutants. This method could be applied even at low concentrations (1 mg/L). Selecting a suitable sorbent is one of the most critical factors in the sorption process (Bello et al., 2021; Kumar et al., 2019a). There are two types of sorption process, which include physical and chemical sorption.

Physical sorption occurs when the sorbent and sorbate are subjected to weak van der Waals forces, polarity, hydrogen bonding, and dipole-dipole interaction. In the physical sorption, metal ions adsorb electrostatically on the sorbent surface. Also, chemical sorption between the adsorbate (contaminant) and the sorbent surface occurs by chemical bonding. Unlike physical sorption, the chemical sorption process is irreversible and requires high activation energy. Fig. 6.3 illustrates physical and chemical sorption mechanisms between the sorbent and sorbate (Mavhungu et al., 2021). The sorption process has three stages. In the first stage, the contaminant is transferred from the bulk phase to the outer surface of the adsorbent. In the second stage, the contaminant diffuses from the outer surface of the adsorbent into the adsorbent pores, including macropores, transitional pores, and micropores. In the last stage, the contaminant is adsorbed on the pores of the adsorbent surface. Fig. 6.4 demonstrates these three stages of the sorption process (Sirocki et al., 2013)

6.4 Biosorption

Removal of contaminants and tiny particles from wastewater using biological sorbents is called as biosorption. Fungus biomass, bacteria biomass, industrial wastes, agricultural wastes, algae, and other polysaccharide materials are some important biosorbents, which can be effectively used in the sorption process (Mathew et al., 2016). All biomaterials can be used as bioadsorbent for separating dyes, heavy metals, pharmaceuticals, pesticides,

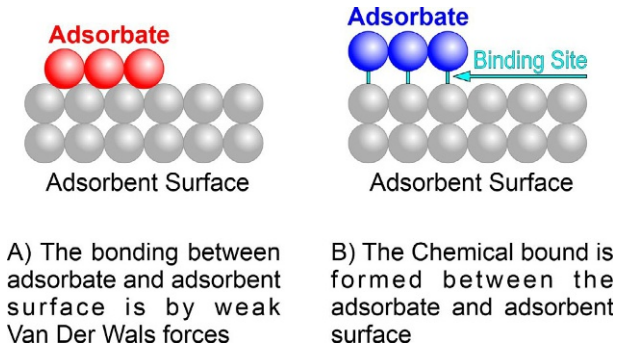

FIG. 6.3 The mechanisms of physical (A) and chemical sorption (B).

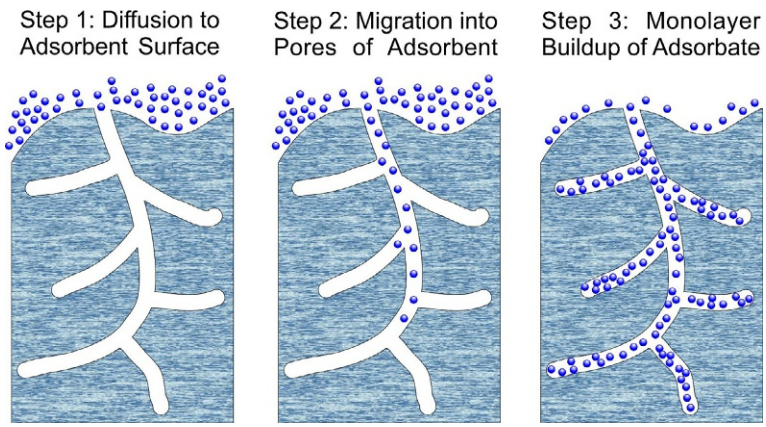

FIG. 6.4 Three steps of the sorption process.

and other pollutants (Khoo et al., 2021). However, selecting a suitable bioadsorbent for a particular contaminant is a challenge and requires an experimental work. Different mechanisms of the biosorption process are demonstrated in Fig. 6.5. As shown, different functional groups of biosorbents and various mechanisms have been indicated (Mathew et al., 2016). The biosorption process over other contaminants removal methods has several advantages, including cheaper producing biomass (fungi or bacteria), large volumes treatment of wastewater, sorption of numerous heavy metal ions at a time, good performance under a wide range of conditions (e.g., pH and temperature), simple and high reusability and reduced amounts of waste production (Khoo et al., 2021).

6.5 Factors affecting the biosorption process

Different factors affect the biosorption process, including pH, temperature, initial concentration of the pollutant, and biosorbent dosage, which are described below:

6.5.1 Effect of pH

The initial pH of the solution has a key role in altering the surface charge of the adsorbent and the degree of ionization of the adsorbed ions during the sorption process. The solution pH is one of the most critical variables in the adsorption process. In general, in strong acidic conditions, the adsorbent's functional groups are surrounded by hydrogen ion (H^+). This phenomenon results in the active sites' occupation by H+ ions, and the number of active sites on the sorbent surface to adsorb metal ions is reduced. Also, an electrostatic repulsion force is created because of the like charge of H^+ and metal ions, which prevents the interaction between the adsorbent's metal ions and active sites. Moreover, the concentration of hydroxide

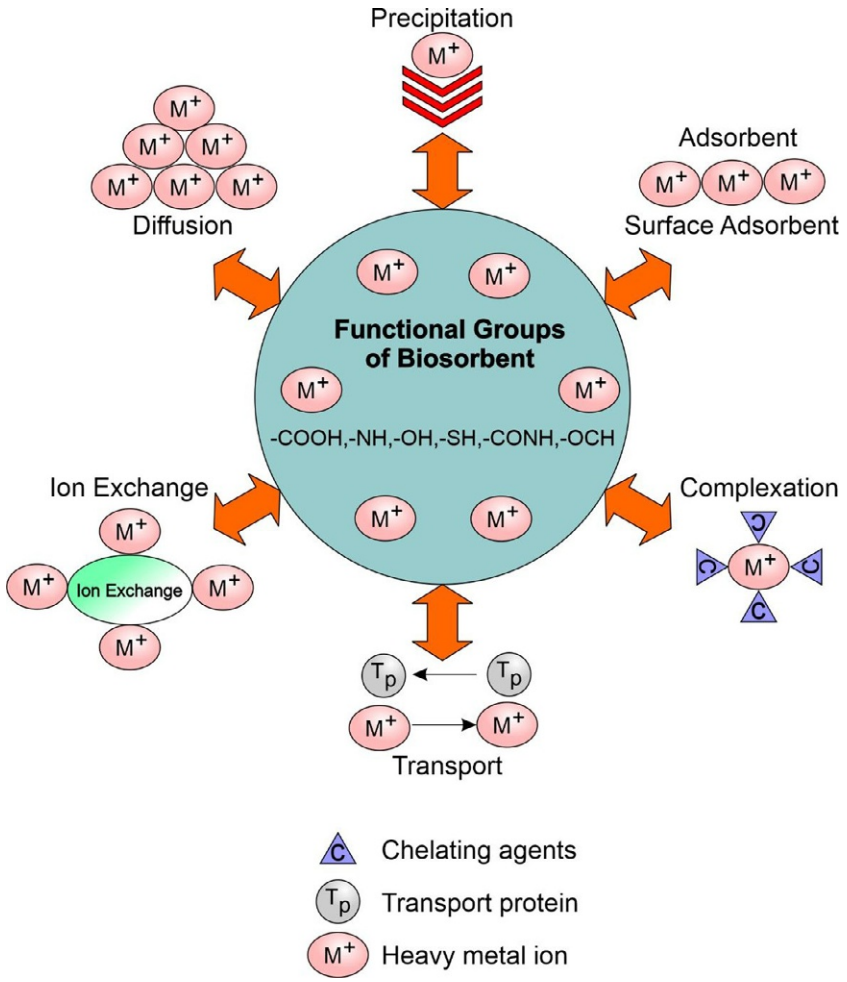

FIG. 6.5 Biosorbent mechanisms.

ions (OH^-) at high pH values is more elevated. Therefore, there is no competition between metal cations and OH- ions, resulting in increased sorption efficiency (Thanki et al., 2021).

6.5.2 Effect of temperature

Temperature is a critical factor in the sorption process because of the sorption process at ambient temperature (25°C). In endothermic reactions, the uptake capacity and uptake efficiency increase with increasing temperature because of the increase in surface activity and the availability of more active sites. Also, the uptake efficiency for exothermic processes increases with decreasing temperature. Both phenomena follow the Arrhenius equation (El-Sayed and El-Sayed, 2014).

6.5.3 Effect of initial pollutions concentration

The initial concentration of the contaminant in aquatic solution plays an important role in the mass transfer between the solute and the sorbent. In initial concentrations, the graph's slope is high, and the uptake efficiency is the highest value. Therefore, the uptake efficiency decreases with increasing ion concentration. The increase in uptake rate at low concentrations is because of the low proportion of ions to active sites on the surface of the adsorbent. Besides, the proportion of ions to active sites increases at a high concentration of ions, leading to a decrease in sorption efficiency (Tamjidi et al., 2021b).

6.5.4 Effect of biosorbent dose

The adsorbent dosage plays an essential role to transfer the contaminant from aqueous media to the adsorbent surface. Also, it determines the capacity of an adsorbent to adsorb the contaminant. The sorption rate of a solute (contaminant) increases the sorbent dosage because the active sites on the sorbent surface increase with increasing the sorbent dosage, resulting in adsorbing more contaminants. Moreover, the highest sorption capacity of the adsorbent can be determined by investigating the impact of this factor (Iftekhar et al., 2018).

6.5.5 Effect of contact time

Contact time is another critical factor in the sorption process. This parameter determines the minimum time required for the adsorption of a specific contaminant concentration using the adsorbent. Also, the equilibrium state can be determined by the investigation of contact time. After reaching a specific time, the adsorption becomes constant or slow, which shows that all adsorbent sites are filled, and no vacant sites are there to adsorb more pollutants (Saxena et al., 2020).

6.5.6 Effect of agitation rate

Agitation rate is another important factor in the sorption process because it determines the energy required to stir the solution and minimize mass transfer resistance. The sorption capacity increases with increasing the agitation rate. While turbulence increases the uptake of contaminants, it may degrade the structure of the bioadsorbent. A moderate rate creates the best homogeneity for an aqueous solution with a high sorption capacity. High agitation rates result in a vortex phenomenon that results in the loss of the suspension's homogenous nature. Also, excessive turbulence reduces the interaction time between the adsorbate and adsorbent, reducing the sorption rate (El-Sayed and El-Sayed, 2014; Zahoor, 2011).

6.6 Types of adsorbents and their properties in wastewater treatment

Identifying the adsorbent for the adsorption process is a major challenge. The production of efficient adsorbents for the sorption of metal ions is one of the most important goals. An extensive range of materials in nature can be utilized as bioadsorbent to remove contaminants

from water. Any plant, microbial biomasses, agriculture wastes, and by-products discharged into the effluent from different industries can be used as biosorbents. Therefore, it is critical to choose a bioadsorbent from a large spectrum of materials (Kanamarlapudi et al., 2018a). Fig. 6.6 shows a wide range of materials used as bioadsorbents.

6.6.1 Agricultural waste materials

Agricultural wastes are abundant, low cost, and environmentally friendly resources, which can be used as very effective adsorbents. Coconut shells, pistachio peel, banana peel, pomegranate peel, orange peel, pomelo peel, garlic peel, tea waste, rice hulls ash, and peat bagasse are the most common types of agricultural wastes, which have been extensively used to remove dyes and heavy metal ions. The main compounds in agricultural wastes are hemicelluloses, cellulose, lipids, lignin, proteins, simple sugars, and starches. These compounds include various kinds of functional groups, which are appropriate for the adsorption of pollutants. Previous studies confirm agricultural waste's effectiveness in removing contaminants from effluents (Kumar et al., 2019a). Table 6.1 illustrates the utmost sorption capacity and the optimal sorption conditions for eliminating contaminants from effluent using agricultural wastes. As shown in Table 6.1, pistachio peels, garlic peels, and pomegranate peels have shown high sorption efficiencies of pollutants. Also, pistachio peels and rice hulls ash have shown excellent sorption capacities.

6.6.2 Industrial by-products

Nowadays, industrial activities produce a huge amount of solid wastes. Some of these solid wastes are reused, and others are sent to landfills. The ability to use these materials in the sorption process is an interesting and attractive issue because these industrial wastes

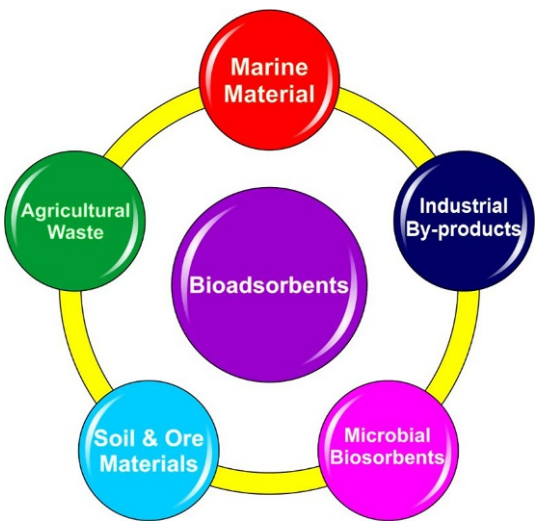

FIG. 6.6 General classification of various types of bioadsorbents.

TABLE 6.1 Capacity and optimal conditions of various agricultural wastes in the removal of pollutants from water and wastewater.

Bio-adsorbent	Pollutant	pH	Ion conc. (mg/L)	Dose (g/L)	Time (h)	Removal efficiency (%)	q_{max} (mg/g)	References
Orange peel	Cd(II)	6	0.001	0.025	3	93.72	–	Li et al. (2008)
Orange peel	Ni (II)	6	0.001	0.025	3	80.11	–	Li et al. (2008)
Orange peel	Zn(II)	6	0.001	0.025	3	87.23	–	Li et al. (2008)
Orange peel	Co(II)	6	0.001	0.025	3	81.06	–	Li et al. (2008)
Pomegranate peel	Ni(II)	6.5	50	10	7	–	50	Bhatnagar and Minocha (2010)
Pomegranate peel	Cu(II)	5.8	20	0.25	2	–	55	El-Ashtoukhy et al. (2008)
Pomegranate peel	Pb(II)	5.6	50	0.25	2	–	64	El-Ashtoukhy et al. (2008)
Banana peel	Cd(II)	8	10	0.1	0.5	97	35.52	Memon et al. (2008)
Tea waste	Cu(II)	5.5	100	1.5	1.5	64	48	Amarasinghe and Williams (2007)
Tea waste	Pb(II)	5.5	200	1.5	1.5	92	65	Amarasinghe and Williams (2007)
Pistachio peels	Methylene blue	8	100	0.15	1	99	602	Vučurović et al. (2014)
Rice hulls ash	Methylene blue	6.8	50	3	2	95	690	Chandrasekhar and Pramada (2006)
Rice hulls ash	Indigo carmine	6.5	50	10	8	96	65.9	Lakshmi et al. (2009)
Coffee powder	Rhodamine B	2	15	0.05	3	–	5.255	Shen and Gondal (2017)
Coffee powder	Rhodamine 6G	2	15	0.05	3	–	17.369	Shen and Gondal (2017)
Pomelo peel	Reactive blue 114	2	100	20	1.5	85	16	Argun et al. (2014)
Garlic peel	Direct red 12B	2	50	0.3	0.4	99	37.96	Asfaram et al. (2014)
Pomegranate peel	Congo red	7	30	20	0.5	98	55	Ghaedi et al. (2012)

are almost available and free of cost and pose a major problem in their disposal. Industrial wastes include fly ash, steel, fertilizer, aluminum, leather, and paper industry wastes. Fly ash is a substance produced by combustion processes. The high content of alumina and silica in fly ash makes it an appropriate option for utilization as a low-cost adsorbent. Also, blast furnace slag, dust, and sludge are examples of steel industry wastes, which can be used in the uptake process.

Moreover, red mud is a waste material produced in the aluminum industry when the bauxite ores are scorched. Red mud contains various minerals, which can be used as a novel source of adsorbent (De Gisi et al., 2016). Table 6.2 illustrates the maximum sorption capacity

TABLE 6.2 Capacity and optimal conditions of various industrial by-products in the removal of pollutants from water and wastewater.

Bio-adsorbent	Pollutant	pH	Ion conc. (mg/L)	Dose (g/L)	Time (h)	Removal efficiency (%)	q_{max} (mg/g)	References
Fly ash	Fe (II)	6	11.78	0.06	2	86.7	–	Hegazi (2013)
Fly ash	Pb (II)	6	1.17	0.06	2	76.06	–	Hegazi (2013)
Fly ash	Cu(II)	6	5.43	0.06	2	98.54	–	Hegazi (2013)
Marble Powder	As (v)	6	1000	–	1	>90	–	Bibi et al. (2015)
Basic oxygen furnace slag	Cu(II)	6	1200	0.5	2	–	380	Xue et al. (2013)
Solid waste from the leather industry	As (v)	1	40–60	–	24	–	26.4	Oliveira et al. (2008)
Solid waste from the leather industry	Cr(VI)	1	700	–	24		133.3	Oliveira et al. (2008)
Blast furnace dust	Basic blue 6	6.5	0.0005	1	2	–	34	Jain et al. (2003)
Blast furnace sludge	Basic blue 6	6.5	0.0005	1	2	–	67	Jain et al. (2003)
Carbonaceous adsorbent prepared from carbon slurry of the fertilizer industry	Basic violet 3	6.5–7.5	0.0005	1	2	–	161	Jain et al. (2003)
Carbonaceous adsorbent prepared from carbon slurry of the fertilizer industry	Basic orange 2	6.5–7.5	0.0005	1	2	–	75	Jain et al. (2003)
Carbonaceous adsorbent prepared from carbon slurry of the fertilizer industry	Basic blue 9	6.5–7.5	0.0005	1	2	–	92	Bhatnagar et al. (2003)

and the optimal adsorption conditions to remove pollutants from water using industrial by-products. As demonstrated, some materials such as fly ash, basic oxygen furnace slag, and carbonaceous materials produced by carbon slurry of the fertilizer industry showed the high capability to remove contaminants from wastewater.

6.6.3 Marine materials

Marine materials are a class of bioadsorbents, which have received many attractions due to their low cost, biocompatibility, availability, and containing chitin and chitosan. Due to the high price of AC, producing chitosan and chitin sorbents has received much attention. Chitin is more attractive as an adsorbent due to its abundance in nature. Chitin can be found in the exoskeleton of crabs. A large quantity of chitin can be generated from the canned crab industry. Chitosan is produced from chitin and found in some fungi' cell walls, such as Mucorales strains, which can be employed as an efficient bioadsorbent. Also, peat moss is available as a cheap bioadsorbent with a high sorption capacity for various pollutants. Lignin and cellulose are the two main compounds of peat. These components contain polar functional groups, which can play a role in chemical bonding. Due to these features, peat moss has a high cationic capacity and can be used as an efficient biosorbent to remove various pollutants (Dev et al., 2020; Ali et al., 2012). Table 6.3 illustrates the maximum adsorption capacity and the optimal adsorption conditions to remove wastewater's pollutants using marine material. As shown, chitosan–alkali lignin composite, *Oreochromis niloticus* fish scales have shown high sorption capacities among other biosorbents for removing contaminants from aqueous solution.

6.6.4 Microbial biosorbents

Microorganisms have a high capability to remove contaminants from water and wastewater. Many studies have been performed from a toxicological point of view. Research has shown that dead microbial biomass can bind contaminants through different chemical mechanisms (Vijayaraghavan and Yun, 2008). Most microorganisms can tolerate undesirable conditions. Fig. 6.7 shows various microorganisms that can be used as biosorbent. These microorganisms include algae, bacteria, and fungi. For using microorganisms to remove pollutants from wastewater, they can be as dead or living microorganisms. However, using dead microbial biomass to eliminate contaminants is preferred to live microbial biomass due to the absence of nutrients in effluents. Therefore, the dead microbial biomass is more economically viable and is considered ideal candidates for treating complex effluents with a low pollutant concentration. Many microbial origin materials have been widely investigated as bioadsorbents for eliminating metal ions. Most microbial biomass comprises many functional groups that indicate their high potential as bioadsorbents (Kanamarlapudi et al., 2018b).

Bacteria as biosorbent

Bacteria are a group of single-celled living organisms that belong to the group of prokaryotes. They are found in soil and water and as other organisms' symbionts. Also, they are found in an extensive variety of forms, including rods (e.g., *Bacillus*), cocci (e.g., *Streptococcus*), spiral (e.g., *Rhodospirillum*), and filamentous (e.g., *Sphaerotilus*). Eubacteria have a simple cell

TABLE 6.3 Capacity and optimal conditions of various marine material in the removal of pollutants from water and wastewater.

Bio-adsorbent	Pollutant	pH	Ion conc. (mg/L)	Dose (g/L)	Time (h)	Removal Efficiency (%)	q_{max} (m/g)	References
Calcined Solamen vaillantisnail shell	Cu(II)	5	2	10	1	96.70	26.04	Esmaeili et al. (2020)
Calcined Solamen vaillantisnail shel	Co (II)	6	2	10	1	96.54	29.41	Esmaeili et al. (2020)
Calcined Solamen vaillantisnail shel	pb (II)	5	2	10	1	94.4	33.5	Esmaeili et al. (2020)
Calcined bicolor oyster shell	As(III)	7	2	10	1.33	96.88	60.98	Teimouri et al. (2018)
Calcined bicolor oyster shell	Hg(II)	6	2	10	1.33	95.72	42.02	Teimouri et al. (2018)
shrimp peel species of Vanam	Pb(II)	6	5	60	2.1	98	24.43	Foroutan et al. (2015)
Garden grass	Cu(II)	6	60	5	7	–	58.34	Hossain et al. (2012)
Ulva onoi alkali-pretreated	Cd(II)	7.8	10	1	12	–	90.7	Suzuki et al. (2005)
Ulva onoi untreated	Cd(II)	7.8	10	1	12	–	61.9	Suzuki et al. (2005)
Peat moss	pb(II)	–	500	1	2	–	40	McLellan and Rock (1988)
Chitosan–alkali lignin composite	Remazol brilliant blue R	2	10	2	1	–	111.11	Nair et al. (2014)
Oreochromis niloticus fish scales	Reactive blue 5G	2	100	0.1	24	–	241.2	Ribeiro et al. (2015)
shells of Rapana gastropod	Brilliant red HE-3B	1.2	50	6	24	96	65.9	Suteu et al. (2012)

structure, which lacks cell nuclei but possesses cell walls. The bacterial cell wall provides structural integrity to the cell but differs from all other organisms because of the presence of peptidoglycan (*N*-acetylmuramic acid and poly-*N*-acetylglucosamine). The cell wall composition of bacteria is one of the most critical factors in detecting bacterial species. Accordingly, there are two kinds of bacteria, including Gram-positive and Gram-negative bacteria. In the structure of these bacteria, some membranes are useful to eliminate pollutants from wastewater (Saravanan et al., 2021). Biosorption of various pollutants by different

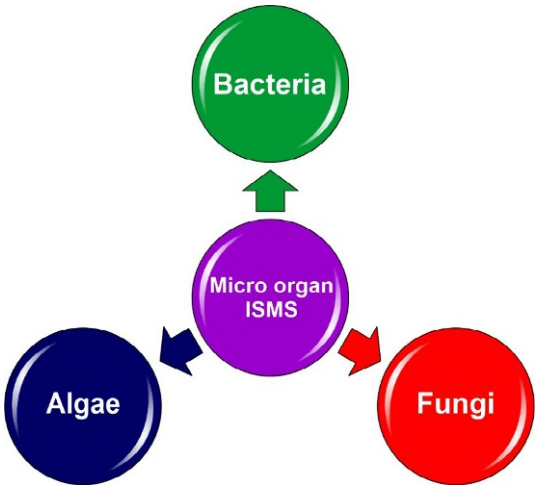

FIG. 6.7 Various microorganisms as biosorbents.

bacteria is given in Table 6.4. As demonstrated, *Desulfovibrio desulfuricans* has shown significant biosorption capacity compared to other bacteria in removing contaminants.

Algae as biosorbent

Algae is one of the earliest plant life species that include about 40,000 different species. Algae can annually produce 52 billion tons of organic carbon, which is 50% of the world's total organic carbon generation. The structure of algae consists of many pores, which have created high active sites. Also, their structure is divided into two groups, including eukaryotes (brown, red, green, and diatoms) and prokaryotes (blue-green algae or cyanobacteria). Algae are also categorized into micro- and macro. Moreover, species of seaweed have porous cell wall structures. Furthermore, the cell wall of algae consists of remarkable amounts of starch, cellulose, hemicellulose, glycogen, and polysaccharides. These compounds contain several active groups like amino, carboxyl, hydroxyl, sulfate, etc., which can form chemical bonds with metal ions, indicating the sorption potential of microalgae. The binding groups in the algae surface, such as NO^{-3}, COO^{-}, OH^{-}, RS^{-}, $PO_3{}^{-4}$, SH^{-}, and RO^{-} have a critical role in the uptake of pollutants. Essentially, the most prominent feature of algae is its diverse colors. Based on this property, the algae can be divided into four classes: brown, green, red, and green-blue algae, as illustrated in Fig. 6.8 (Thanki et al., 2021). Table 6.5 illustrates the utmost sorption capacity and the optimal sorption conditions to remove pollutants from wastewater using different types of algae. According to previous studies, some algae, such as *Sargassum dentifolium* and *Spirulina platensis* with sorption capacities of 250 and 482.2 mg/g, respectively, showed the highest sorption capacity compared to other algae.

Fungi as biosorbent

Fungus is another type of biosorbent, which has significant features. The cell wall in fungi is composed of acid polysaccharides like chitin and chitosan. The presence of several compounds in their structure, such as phosphate, amine, and hydroxyl groups, help them to

TABLE 6.4 Biosorption of various pollutants by different bacteria.

Bio-adsorbent	Pollutant	pH	Ion conc. (mg/L)	dose (g/L)	Time (h)	Removal efficiency (%)	q_{max} (mg/g)	References
Enterobacter cloacae	Cd(II)	5	–	0.1	2	58.9	–	Saravanan et al. (2021)
Desulfovibrio desulfuricans	Pd (II)	2	25	0.15	96	>90	128.2	De Vargas et al. (2004)
Desulfovibrio fructosivorans	Pd (II)	2	25	0.15	96	>90	119.8	De Vargas et al. (2004)
Desulfovibrio vulgaris	Pd (II)	2	25	0.15	96	>90	106.3	De Vargas et al. (2004)
D. desulfuricans	Pt(IV)	2	25	0.15	96	>90	62.5	De Vargas et al. (2004)
D. fructosivorans	Pt(IV)	2	25	0.15	96	>90	32.3	De Vargas et al. (2004)
D. vulgaris	Pt(IV)	2	25	0.15	96	>90	40.1	De Vargas et al. (2004)
Arthrobacter nicotianae IAM 12342	Th	3.5	0.05	0.1	1	–	75.9	Nakajima and Tsuruta (2004)
Bacillus subtilis IAM 1026	Th	3.5	0.05	0.1	1	–	71.9	Nakajima and Tsuruta (2004)
Bacillus licheniformis IAM 111054	U	3.5	0.05	0.1	1	–	45.9	Nakajima and Tsuruta (2004)
B. subtilis IAM 1026	U	3.5	0.05	0.1	1	–	52.4	Nakajima and Tsuruta (2004)
Lactobacillus delbrueckii	Reactive orange 16	6	10	0.1	72	63	–	Zuraida et al. (2013)
L. delbrueckii	Reactive black 5	6	10	0.1	72	55	–	Zuraida et al. (2013)

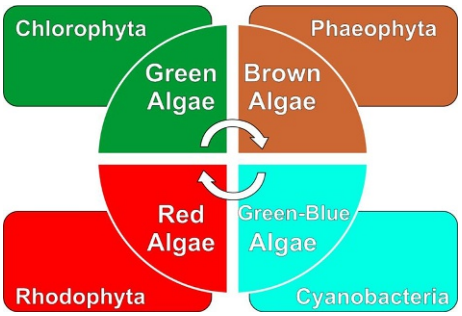

FIG. 6.8 General classifications of algae.

TABLE 6.5 Capacity and optimal conditions of different algae in the removal of contaminants from wastewater.

Bio-adsorbent	Pollutant	pH	Ion Conc. (mg/L)	Dose (g/L)	Time (h)	Removal efficiency (%)	q_{max} (mg/g)	References
Ulva fasciata	Cu(II)	4.5	10	0.5	0.5	88	125	Bahaa et al. (2019)
Sargassum dentifolium	Cu (II)	4.5	10	0.5	1	71	250	Bahaa et al. (2019)
Sargassum oligocystum	NH^{4+}	8	100	5	1.33	96.2	7.46	Yeganeh et al. (2019)
Cladophora	Cu (II)	5.2	10	1	2	70	–	Jaafari and Yaghmaeian (2019)
Cladophora	Cr(III)	5	10	1	2	80	–	Jaafari and Yaghmaeian (2019)
Cladophora	Cd (II)	7	10	1	2	85	–	Jaafari and Yaghmaeian (2019)
Padina sanctaecrucis	Co (II)	6	20	4	1.3	96.68	13.96	Foroutan et al. (2018)
P. sanctaecrucis	Cu (II)	6	20	4	1.3	94.51	13.73	Foroutan et al. (2018)
Ulva lactuca	Methylene blue	8	25	1.25	1.8	91.92	–	Pratiwi et al. (2019)
Sargassum sp.	Acid black 1	4.2	40	6	0.5	96.8	–	Vijayaraghavan and Shanthakumar (2018)
Cyanobacterium	Reactive red 198	2	100	0.15	1	94	–	Axelsson et al. (2006)
Spirulina platensis	Reactive red 120	2	50	1	1	97.1	482.2	Cardoso et al. (2012)

adsorb heavy metals, dyes, and other contaminants. Table 6.6 indicates different types of fungi and their characteristics.

Various types of fungi as biosorbents can be used to eliminate contaminants from the effluent, including mycelium, fungal pellets, and dead fungi. The fungus can survive at a high concentration of metal ions; thus, they can remove metal ions from wastewater. The uptake of metal ions by fungus occurs because of compounds such as chitin, chitosan, phosphate, glucuronic acid, and polysaccharides on the cell walls of fungi. Also, there are different functional groups in the structure of fungi, such as carboxyl, phosphate, hydroxyl, amine, and sulfhydryl, which have an essential role in the uptake of pollutants. Fungi and their enzymes, such as laccase and lignin peroxidase, can bioremediate various wastewaters (Kumar et al., 2019b). Biosorption of various contaminants by different fungi is given in Table 6.7. According to previous research, *Aspergillus* sp. TS-A CGMCC could remove mordant Yellow 1 with a removal efficiency of 98.6%, which showed the highest removal efficiency among various fungi.

TABLE 6.6 Characteristics of major fungal divisions.

Division	Characteristics
Chytridiomycota	The fungi produce zoospores capable of moving on their own through a liquid medium by simple flagella
Zygomycola	The hyphae do not have one nucleus per cell but rather have long multinucleate, haploid hyphae that comprise their mycelia. A sexual reproduction is by spores produced in stalked sporangia
Ascomycota	They contain more than 30,000 species of unicellular (yeasts) to multicellular fungi. Yeasts reproduce asexually by budding and sexually by forming a sac/ascus
Basidiomycota	Mushrooms, toadstools, and puffballs arc commonly encountered basidiomycetes. These conspicuous features of the fungi are their productive structures. Sexual reproduction involves the formation of basidiospores on club-shaped cells known as basidia
Deuteromycota	A group of fungi that either lack the perfect stage (i.e., sexual reproduction) or whose perfect stage is as yet undiscovered. They are produced most frequently by conidia or conidia-like spores. Many forms of deuteromycota are pathogenic, affecting man, animals, or plants

TABLE 6.7 Sorption capacity, removal efficiency, and optimal conditions for the removal of pollutants from water and wastewater using various fungi.

Bio-adsorbent	Pollutant	pH	Ion conc. (mg/L)	Dose (g/L)	Time (h)	Removal efficiency (%)	q_{max} (mg/g)	References
Trichoderma sp. BSCR0	Cr(VI)	5	200	1.6	2	96.5	–	Smily and Sumithra (2017)
Bacillus subtilis	Cr (III)	4	100	0.5	6	90	23.9	Aravindhan et al. (2012)
M. rouxii (IM-80)	Hg (II)	5.5	100	10	24	95.3	–	Martinez-Juarez et al. (2012)
M. rouxii mutant	Hg (II)	5.5	100	10	24	88.7	–	Martinez-Juarez et al. (2012)
Mucor sp1	Hg (II)	5.5	100	10	24	80.4	–	Martinez-Juarez et al. (2012)
Mucor sp1	Hg (II)	5.5	100	10	24	78.3	–	Martinez-Juarez et al. (2012)
Aspergillus niger	F(I)	6	10	1	24	83	–	Acosta-Rodríguez et al. (2018)
A. niger	Co(II)	5	100	1	24	71.4	–	Acosta-Rodríguez et al. (2018)
A. niger	Silver (I)	6	100	1	24	48	–	Acosta-Rodríguez et al. (2018)

Continued

TABLE 6.7 Sorption capacity, removal efficiency, and optimal conditions for the removal of pollutants from water and wastewater using various fungi—Cont'd

Bio-adsorbent	Pollutant	pH	Ion conc. (mg/L)	Dose (g/L)	Time (h)	Removal efficiency (%)	q_{max} (mg/g)	References
A. foetidus	Reactive black 5	2	100	2	24	–	65	Kaushik and Malik, 2009)
Pleurotus ostreatus	Disperse orange 3	5	200	0.1	120	57	–	Kaushik and Malik, 2009)
Trametes versicolor	Grey lanaset G	4.5	210	1.8	144	>80	–	Kaushik and Malik (2009)
T. versicolor	Grey lanaset G	4.5	150	3.2	18	>80	–	Kaushik and Malik (2009)
Ganoderma sp. WR-1	Cibacron brilliant	–	100	0.02	8	96	–	Revankar and Lele (2007)
Aspergillus sp. TS-A CGMCC	Mordant Yellow 1	6	50	1	120	98.6	–	Kang et al. (2018)

6.6.5 Soil and ore materials

Soil, clays, zeolites, and ore fall into this group. The sorption capability of clay is related to the negative charges on the fine grain silicate minerals structure. Negative charges can be neutralized by the sorption of positively charged cations like dyes. Also, clays have shown high specific surface area (about 800 m^2/g), which are effective in the uptake process. There are various kinds of clays, but montmorillonite clay is expected to have the maximum sorption capacity compared to others. Moreover, clays can be modified by various materials to increase its performance in removing pollutants from wastewater. Furthermore, zeolites contain silicate minerals and are applied at commercial scales. Clinoptilolite is probably the most abundant species of natural zeolite. The uptake features of zeolites depend on their ion-exchange capability. Besides, sand, soil, sediment, and ore minerals can be used to eliminate organic contaminants from water. Soils are used to remove environmental contaminants by sorption. Many studies have shown high sorption efficiency of soils in removing pesticides, glyphosate, and phenolic compounds (De Gisi et al., 2016). The sorption capacity, sorption efficiency, and optimal conditions for various adsorbents in removing pollutants from water are reported in Table 6.8. Among the various adsorbents, bentonite showed high sorption capacity (1667 mg/g) of methylene blue, which is a remarkable value.

6.6.6 Nanoadsorbent

Nanoadsorbents are effective materials for removing contaminants from wastewater due to the high surface area, a large number of active sites, high sorption capacity, and tunable

TABLE 6.8 Sorption capacity, sorption efficiency, and optimal conditions of various soil and ore materials in the removal of pollutants from water and wastewater.

Bio-adsorbent	Pollutant	pH	Ion conc. (mg/L)	Dose (g/L)	Time (h)	Removal efficiency (%)	q_{max} (mg/g)	References
Bentonite	Sb(III)	6	0.05	25	24	–	0.5	De Gisi et al. (2016)
Bentonite	Sb(V)	6	0.05	25	24	–	0.5	De Gisi et al. (2016)
Bentonite clay	Cr(III)	6	10	1	1.5	95.21	151.5	Ahmadi et al. (2020)
Bentonite clay	Cr(VI)	3	10	1	1.5	95.74	161.3	Ahmadi et al. (2020)
Bentonite	Methylene blue	7.9	100	1	3	–	1667	De Gisi et al. (2016)
Bentonite	Basic red 2	11	10	1.5	1	–	274	De Gisi et al. (2016)
Calcined alunite	Acid blue 40	2	25	1.25	1.5	–	212.8	De Gisi et al. (2016)
Clay	Basic blue 9	6.3	30	0.25	2	–	300	De Gisi et al. (2016)
Modified sepiolite	Reactive yellow 176	–	25	50	2	–	169.1	De Gisi et al. (2016)
Modified zeolite	Reactive black 5	–	25	50	2	–	45.8	De Gisi et al. (2016)

pore size. Also, the morphology and shape of nanosorbents play a critical role in their properties and performance. Synthesis of nanoadsorbents is performed using bottom-up and top-down processes. The top-down process can synthesize nanobiosorbents via various methods such as ball milling, reactive milling, and mechanical alloying. Also, the bottom-up process is a modern process to produce nanoparticles. Sol-gel, molecular self-assembly, and physical/chemical vapor deposition are the most important bottom-up processes to produce nanoadsorbents. Several novel nanosorbents have been recently synthesized and used to remove contaminants from sewage like silica/Fe3O4 nanoparticles (NPs), nanometals, and nanometal oxides zeolites, magnetic NPs like AC/Fe_3O_4 nanoparticles and bentonite/$CuFe_2O_4$ nanocomposite, carbon nanotubes, etc. Table 6.9 shows sorption capacity, sorption efficiency, and optimal conditions for different nanoadsorbents in removing pollutants from wastewater (El-Sayed, 2020). As reported in Table 6.9, some nanoadsorbents such as CaO/Fe_3O_4/SDS, Fe_3O_4/tetrasulfide nanocomposite, CaO/Fe_3O_4, MgO nanoparticles, and clay/starch/Fe_3O_4 have shown excellent performance for removing pollutants from effluents.

TABLE 6.9 Capacity and optimal conditions of various nanoadsorbents in the removal of pollutants from water and wastewater.

Nano-adsorbent	Pollutant	pH	Ion conc. (mg/L)	Dose (g/L)	Time (h)	Removal efficiency (%)	q_{max} (mg/g)	References
CaO/Fe_3O_4/SDS	Cr(III)	5	5	2	0.83	98.7	5.9	Tamjidi and Esmaeili (2019)
Fe_3O_4/tetrasulfide nanocomposite	Hg(II)	4	50	50	0.33	98.8	303	Vojoudi et al. (2017)
Fe_3O_4/tetrasulfide nanocomposite	Pb(II)	4	50	50	0.33	95.7	270.27	Vojoudi et al. (2017)
Fe_3O_4/tetrasulfide nanocomposite	Pd(II)	4	50	50	0.33	96.4	256.41	Vojoudi et al. (2017)
CaO/Fe_3O_4	Co(II)	6	5	2	0.5	94.32	227.27	Shakerian and Esmaeili (2018)
CaO/Fe_3O_4	Pb(II)	6	5	2	0.5	97.24	217.39	Shakerian and Esmaeili (2018)
Natural clay/Fe_3O_4/ graphene oxide	Cr (VI)	3	10	1	1	98.84	71.41	Esmaeili and Tamjidi (2020)
Bentonite clay@ $MnFe_2O_4$	Cr(III)	6	10	1.5	2	97.37	175.4	Ahmadi et al. (2020)
Bentonite clay@ $MnFe_2O_4$	Cr(VI)	3	10	1.5	2	98.65	178.6	Ahmadi et al. (2020)
Chitosan conjugated magnetite nanoparticle	Pb(II)	6.1	–	1.04	0.99	92.15	**192.308**	Cheraghipour and Pakshir (2020)
Zeolite/Fe_3O_4	Methylene blue	7	2	2.8	3	97.5	2.57	Nyankson et al. (2019)
Nano zerovalent iron	Acidic dye 36	5.5	30	0.5	0.025	94.29	125.8	Delnavaz and Kazemimofrad (2020)
AC/bentonite/ Fe_3O_4	Reactive red 198	8	5	2	0.83	94.87	4.86	Mirzapour et al. (2020)
Clay/starch/Fe_3O_4	Methyl violet	9	10	1.5	2.5	99.73	29.67	Ansari Mojarad et al. (2020)
Zinc (II) oxide nanorods loaded on AC	Crystal violet	–	14	0.025	0.085	98.66	81.6	Dil et al. (2017)
Zinc (II) oxide nanorods loaded on AC	Methylene blue	–	18	0.025	0.085	99.46	83.9	Dil et al. (2017)

TABLE 6.9 Capacity and optimal conditions of various nanoadsorbents in the removal of pollutants from water and wastewater—Cont'd

Nano-adsorbent	Pollutant	pH	Ion conc. (mg/L)	Dose (g/L)	Time (h)	Removal efficiency (%)	q_{max} (mg/g)	References
MgO NPs	Reactive black 5	10	100	0.025	0.833	99.26	500	Jamil et al. (2015)
MgO NPs	Reactive orange 122	2	100	0.03	1.16	99.53	333.34	Jamil et al. (2015)

6.7 Conclusion

The biosorption process has attracted much attention in recent years because they have several environmentally friendly, high-performance, and low-cost benefits. Many studies have been performed during the last decade, which gives useful information about different types of biosorbents and their performance in removing contaminants from wastewater. Also, biosorbents have shown that they have high reusability, which is a critical factor in the process's economics. Another type of material is nanoadsorbents, which have been extensively used in previous studies. Nanoadsorbents have several advantages, which the most important property of them is their high specific surface area. Recently, a combination of bioadsorbent and nanoadsorbent has been used, which have been indicated as high ability and capacity to eliminate contaminants from wastewater. Sawdust, AC produced from leaves of trees, eggshell waste, agricultural wastes, and shrimp peel are examples of effective biosorbents, which have been widely used in previous works. Also, Fe_3O_4/CaO NPs, bentonite/Fe_3O_4 NPs, MgO NPs, bentonite/$CuFe_2O_4$ NPs, and AC/Fe_3O_4 NPs are several examples of efficient nanoadsorbents. In this book chapter, characteristics, advantages, various types of nanoadsorbents and bioadsorbents, capacity and efficiency of nano- and bio-adsorbents, different types of contaminants in wastewater, different methods for the removal of contaminants, and impact of effective factors on the sorption process were thoroughly discussed.

References

Abedpour, M., Kamyab, B., Tamjidi, S., 2020. Equilibrium and kinetic study of simultaneous removal of cd (II) and Ni (II) by acrylamide-based polymer as effective adsorbent: optimization by response surface methodology (RSM). Int. J. Environ. Anal. Chem., 1–8.

Acosta-Rodríguez, I., Cárdenas-González, J.F., Rodríguez Pérez, A.S., Oviedo, J.T., Martínez-Juárez, V.M., 2018. Bioremoval of different heavy metals by the resistant fungal strain Aspergillus niger. Bioinorg. Chem. Appl. 2018, 1–7.

Ahmadi, A., Foroutan, R., Esmaeili, H., Tamjidi, S., 2020. The role of bentonite clay and bentonite clay@ $MnFe_2O_4$ composite and their physico-chemical properties on the removal of Cr (III) and Cr (VI) from aqueous media. Environ. Sci. Pollut. Res. 27, 1–4.

Akpor, O.B., Otohinoyi, D.A., Olaolu, D.T., Aderiye, B.I., 2014. Pollutants in wastewater effluents: impacts and remediation processes. Int. J. Environ. Res. Earth Sci. 3 (3), 050–059.

Hussain, S., Anjali, K.P., Hassan, S.T., Dwivedi, P.B., 2018. Waste tea as a novel adsorbent: a review. Appl. Water Sci. 8 (6), 1–16.

Ali, I., Asim, M., Khan, T.A., 2012. Low cost adsorbents for the removal of organic pollutants from wastewater. J. Environ. Manag. 113, 170–183.
Amarasinghe, B.M., Williams, R.A., 2007. Tea waste as a low cost adsorbent for the removal of Cu and Pb from wastewater. Chem. Eng. J. 132 (1–3), 299–309.
Ansari Mojarad, A., Tamjidi, S., Esmaeili, H., 2020. Clay/starch/Fe_3O_4 nanocomposite as an efficient adsorbent for the removal of methyl violet dye from aqueous media. Int. J. Environ. Anal. Chem., 1–22.
Aravindhan, R., Fathima, A., Selvamurugan, M., Rao, J.R., Balachandran, U.N., 2012. Adsorption, desorption, and kinetic study on Cr (III) removal from aqueous solution using *Bacillus subtilis* biomass. Clean Techn. Environ. Policy 14 (4), 727–735.
Argun, M.E., Güclü, D., Karatas, M., 2014. Adsorption of reactive blue 114 dye by using a new adsorbent: pomelo peel. J. Ind. Eng. Chem. 20 (3), 1079–1084.
Asfaram, A., Fathi, M.R., Khodadoust, S., Naraki, M., 2014. Removal of direct red 12B by garlic peel as a cheap adsorbent: kinetics, thermodynamic and equilibrium isotherms study of removal. Spectrochim. Acta A Mol. Biomol. Spectrosc. 127, 415–421.
Axelsson, J., Nilsson, U., Terrazas, E., Aliaga, T.A., Welander, U., 2006. Decolorization of the textile dyes reactive red 2 and reactive blue 4 using Bjerkandera sp. strain BOL 13 in a continuous rotating biological contactor reactor. Enzym. Microb. Technol. 39 (1), 32–37.
Bahaa, S., Al-Baldawi, I.A., Yaseen, S.R., Abdullah, S.R., 2019. Biosorption of heavy metals from synthetic wastewater by using macro algae collected from Iraqi Marshlands. J. Ecol. Eng. 20 (11), 18–22.
Bello, O.S., Alao, O.C., Alagbada, T.C., Agboola, O.S., Omotoba, O.T., Abikoye, O.R., 2021. A renewable, sustainable and low-cost adsorbent for ibuprofen removal. Water Sci. Technol. 83 (1), 111–122.
Bharathi, K.S., Ramesh, S.T., 2013. Removal of dyes using agricultural waste as low-cost adsorbents: a review. Appl Water Sci 3 (4), 773–790.
Bhatnagar, A., Minocha, A.K., 2010. Biosorption optimization of nickel removal from water using Punica granatum peel waste. Colloids Surf. B: Biointerfaces 76 (2), 544–548.
Bhatnagar, A., Jain, A.K., Gupta, V.K., Jain, S., Suhas, S., 2003. A comparative assessment of adsorbents prepared from industrial wastes for the removal of cationic dye. J. Indian Chem. Soc. 80, 267–270.
Bibi, S., Farooqi, A., Hussain, K., Haider, N., 2015. Evaluation of industrial based adsorbents for simultaneous removal of arsenic and fluoride from drinking water. J. Clean. Prod. 87, 882–896.
Cardoso, N.F., Lima, E.C., Royer, B., Bach, M.V., Dotto, G.L., Pinto, L.A., Calvete, T., 2012. Comparison of Spirulina platensis microalgae and commercial activated carbon as adsorbents for the removal of reactive red 120 dye from aqueous effluents. J. Hazard. Mater. 241, 146–153.
Chandrasekhar, S., Pramada, P.N., 2006. Rice husk ash as an adsorbent for methylene blue—effect of ashing temperature. Adsorption 12 (1), 27–43.
Chen, X., Lam, K.F., Yeung, K.L., 2011. Selective removal of chromium from different aqueous systems using magnetic MCM-41 nanosorbents. Chem. Eng. J. 172 (2–3), 728–734.
Cheraghipour, E., Pakshir, M., 2020. Process optimization and modeling of Pb (II) ions adsorption on chitosan-conjugated magnetite nano-biocomposite using response surface methodology. Chemosphere 260, 127560.
Corda, N.C., Kini, M.S., 2018. A review on adsorption of cationic dyes using activated carbon. In: MATEC Web of Conferences. vol. 144. EDP Sciences, p. 02022.
Crini, G., Lichtfouse, E., Wilson, L.D., Morin-Crini, N., 2019. Conventional and non-conventional adsorbents for wastewater treatment. Environ. Chem. Lett. 17 (1), 195–213.
De Gisi, S., Lofrano, G., Grassi, M., Notarnicola, M., 2016. Characteristics and adsorption capacities of low-cost sorbents for wastewater treatment: a review. Sustain. Mater. Technol. 9, 10–40.
De Vargas, I., Macaskie, L.E., Guibal, E., 2004. Biosorption of palladium and platinum by sulfate-reducing bacteria. J. Chem. Technol. Biotechnol. 79 (1), 49–56.
Delnavaz, M., Kazemimofrad, Z., 2020. Nano zerovalent iron (NZVI) adsorption performance on acidic dye 36 removal: optimization of effective factors, isotherm and kinetic study. Environ. Prog. Sustain. Energy 39 (4), e13349.
Dev, V.V., Baburaj, G., Antony, S., Arun, V., Krishnan, K.A., 2020. Zwitterion-chitosan bed for the simultaneous immobilization of Zn (II), Cd (II), Pb (II) and Cu (II) from multi-metal aqueous systems. J. Clean. Prod. 255, 120309.
Dil, E.A., Ghaedi, M., Asfaram, A., 2017. The performance of nanorods material as adsorbent for removal of azo dyes and heavy metal ions: application of ultrasound wave, optimization, and modeling. Ultrason. Sonochem. 34, 792–802.

Duman, O., Ayranci, E., 2010. Attachment of benzo-crown ethers onto activated carbon cloth to enhance the removal of chromium, cobalt and nickel ions from aqueous solutions by adsorption. J. Hazard. Mater. 176 (1–3), 231–238.
El Hefnawy, M., Shaaban, A.F., ElKhawaga, H.A., 2020. Effective removal of Pb (II), Cd (II) and Zn (II) from aqueous solution by a novel hyper cross-linked nanometer-sized chelating resin. J. Environ. Chem. Eng. 8 (3), 103788.
El-Ashtoukhy, E.S., Amin, N.K., Abdelwahab, O., 2008. Removal of lead (II) and copper (II) from aqueous solution using pomegranate peel as a new adsorbent. Desalination 223 (1–3), 162–173.
El-Sayed, M.E., 2020. Nanoadsorbents for water and wastewater remediation. Sci. Total Environ. 739, 139903.
El-Sayed, H.E., El-Sayed, M.M., 2014. Assessment of food processing and pharmaceutical industrial wastes as potential biosorbents: a review. Biomed. Res. Int. 2014, 146769.
Esmaeili, H., Tamjidi, S., 2020. Ultrasonic-assisted synthesis of natural clay/Fe_3O_4/graphene oxide for enhance removal of Cr (VI) from aqueous media. Environ. Sci. Pollut. Res. 27 (25), 31652–31664.
Esmaeili, H., Tamjidi, S., Abed, M., 2020. Removal of Cu (II), Co (II) and Pb (II) from synthetic and real wastewater using calcified Solamen Vaillanti snail shell. Desalin. Water Treat. 174, 324–335.
Fernandes, A., Pacheco, M.J., Ciríaco, L., Lopes, A., 2015. Review on the electrochemical processes for the treatment of sanitary landfill leachates: present and future. Appl. Catal. B Environ. 176, 183–200.
Foroutan, R., Esmaeili, H., Fard, M.K., 2015. Equilibrium and kinetic studies of Pb (II) biosorption from aqueous solution using shrimp peel. Int. Res. J. Appl. Basic Sci. 9 (11), 1954–1965.
Foroutan, R., Esmaeili, H., Abbasi, M., Rezakazemi, M., Mesbah, M., 2018. Adsorption behavior of Cu (II) and Co (II) using chemically modified marine algae. Environ. Technol. 39 (21), 2792–2800.
Fu, F., Wang, Q., 2011. Removal of heavy metal ions from wastewaters: a review. J. Environ. Manag. 92 (3), 407–418.
Ghaedi, M., Tavallali, H., Sharifi, M., Kokhdan, S.N., Asghari, A., 2012. Preparation of low cost activated carbon from *Myrtus communis* and pomegranate and their efficient application for removal of Congo red from aqueous solution. Spectrochim. Acta A Mol. Biomol. Spectrosc. 86, 107–114.
Gunatilake, S.K., 2015. Methods of removing heavy metals from industrial wastewater. Methods 1 (1), 14.
Hegazi, H.A., 2013. Removal of heavy metals from wastewater using agricultural and industrial wastes as adsorbents. HBRC J. 9 (3), 276–282.
Hossain, M.A., Ngo, H.H., Guo, W.S., Setiadi, T., 2012. Adsorption and desorption of copper (II) ions onto garden grass. Bioresour. Technol. 121, 386–395.
Huang, Q., Song, S., Chen, Z., Hu, B., Chen, J., Wang, X., 2019. Biochar-based materials and their applications in removal of organic contaminants from wastewater: state-of-the-art review. Biochar 1 (1), 45–73.
Iftekhar, S., Ramasamy, D.L., Srivastava, V., Asif, M.B., Sillanpää, M., 2018. Understanding the factors affecting the adsorption of lanthanum using different adsorbents: a critical review. Chemosphere 204, 413–430.
Ismail, W.N., Mokhtar, S.U., 2020. Various methods for removal, treatment, and detection of emerging water contaminants. In: Emerging Contaminants. IntechOpen.
Jaafari, J., Yaghmaeian, K., 2019. Optimization of heavy metal biosorption onto freshwater algae (Chlorella coloniales) using response surface methodology (RSM). Chemosphere 217, 447–455.
Jain, A.K., Gupta, V.K., Bhatnagar, A., Suhas, 2003. A comparative study of adsorbents prepared from industrial wastes for removal of dyes. Sep. Sci. Technol. 38 (2), 463–481.
Jamil, N., Mehmood, M., Lateef, A., Nazir, R., Ahsan, N., 2015. MgO nanoparticles for the removal of reactive dyes from wastewater. Adv. Mater. TechConnect Briefs 1, 353–356.
Kanamarlapudi, S.L., Chintalpudi, V.K., Muddada, S., 2018. Application of biosorption for removal of heavy metals from wastewater. In: Biosorption. 18. IntechOpen, pp. 69–116. Waste tea as a novel adsorbent: a review.
Kang, Y., Xu, X., Pan, H., Tian, J., Tang, W., Liu, S., 2018. Decolorization of mordant yellow 1 using Aspergillus sp. TS-A CGMCC 12964 by biosorption and biodegradation. Bioengineered 9 (1), 222–232.
Kaushik, P., Malik, A., 2009. Fungal dye decolourization: recent advances and future potential. Environ. Int. 35 (1), 127–141.
Khatri, N., Tyagi, S., 2015. Influences of natural and anthropogenic factors on surface and groundwater quality in rural and urban areas. Front. Life Sci. 8 (1), 23–39.
Khoo, K.S., Chia, W.Y., Chew, K.W., Show, P.L., 2021. Microalgal-bacterial consortia as future prospect in wastewater bioremediation, environmental management and bioenergy production. Indian J. Microbiol. 61, 1–8.
Kumar, K.V., Gadipelli, S., Wood, B., Ramisetty, K.A., Stewart, A.A., Howard, C.A., Brett, D.J., Rodriguez-Reinoso, F., 2019a. Characterization of the adsorption site energies and heterogeneous surfaces of porous materials. J. Mater. Chem. A 7 (17), 10104–10137.

Kumar, A., Kumar, V., Singh, J., 2019b. Role of Fungi in the removal of heavy metals and dyes from wastewater by biosorption processes. In: Recent Advancement in White Biotechnology Through Fungi. Springer, pp. 397–418. Champions.
Lakshmi, U.R., Srivastava, V.C., Mall, I.D., Lataye, D.H., 2009. Rice husk ash as an effective adsorbent: evaluation of adsorptive characteristics for indigo carmine dye. J. Environ. Manag. 90 (2), 710–720.
Li, X., Tang, Y., Cao, X., Lu, D., Luo, F., Shao, W., 2008. Preparation and evaluation of orange peel cellulose adsorbents for effective removal of cadmium, zinc, cobalt and nickel. Colloids Surf. A Physicochem. Eng. Asp. 317 (1–3), 512–521.
Martinez-Juarez, V.M., Cárdenas-González, J.F., Torre-Bouscoulet, M.E., Acosta-Rodríguez, I., 2012. Biosorption of mercury (II) from aqueous solutions onto fungal biomass. Bioinorg. Chem. Appl. 2012, 156190.
Mathew, B.B., Jaishankar, M., Biju, V.G., Beeregowda, K.N., 2016. Role of bioadsorbents in reducing toxic metals. J. Toxicol. 2016, 4369604.
Mavhungu, A., Foteinis, S., Mbaya, R., Masindi, V., Kortidis, I., Mpenyana-Monyatsi, L., Chatzisymeon, E., 2021. Environmental sustainability of municipal wastewater treatment through struvite precipitation: influence of operational parameters. J. Clean. Prod. 285, 124856.
McLellan, J.K., Rock, C.A., 1988. Pretreating landfill leachate with peat to remove metals. Water Air Soil Pollut. 37 (1), 203–215.
Memon, J.R., Memon, S.Q., Bhanger, M.I., Memon, G.Z., El-Turki, A., Allen, G.C., 2008. Characterization of banana peel by scanning electron microscopy and FT-IR spectroscopy and its use for cadmium removal. Colloids Surf. B: Biointerfaces 66 (2), 260–265.
Mirzapour, P., Kamyab Moghadas, B., Tamjidi, S., Esmaeili, H., 2020. Activated carbon/bentonite/Fe3O4 nanocomposite for treatment of wastewater containing reactive red 198. Sep. Sci. Technol. 56, 1–5.
Nair, V., Panigrahy, A., Vinu, R., 2014. Development of novel chitosan–lignin composites for adsorption of dyes and metal ions from wastewater. Chem. Eng. J. 254, 491–502.
Nakajima, A., Tsuruta, T., 2004. Competitive biosorption of thorium and uranium by Micrococcus luteus. J. Radioanal. Nucl. Chem. 260 (1), 13–18.
Nyankson, E., Adjasoo, J., Efavi, J.K., Amedalor, R., Yaya, A., Manu, G.P., Asare, K., Amartey, N.A., 2019. Characterization and evaluation of zeolite A/Fe_3O_4 nanocomposite as a potential adsorbent for removal of organic molecules from wastewater. J. Chem. 2019, 8090756.
Obotey Ezugbe, E., Rathilal, S., 2020. Membrane technologies in wastewater treatment: a review. Membranes 10 (5), 89.
Oliveira, D.Q., Gonçalves, M., Oliveira, L.C., Guilherme, L.R., 2008. Removal of As (V) and Cr (VI) from aqueous solutions using solid waste from leather industry. J. Hazard. Mater. 151 (1), 280–284.
Pamukoglu, M.Y., Kargi, F., 2006. Removal of copper (II) ions from aqueous medium by biosorption onto powdered waste sludge. Process Biochem. 41 (5), 1047–1054.
Pohl, A., 2020. Removal of heavy metal ions from water and wastewaters by sulfur-containing precipitation agents. Water Air Soil Pollut. 231 (10), 1–7.
Pratiwi, D., Prasetyo, D.J., Poeloengasih, C.D., 2019. Adsorption of methylene blue dye using marine algae Ulva lactuca. IOP Conf. Ser.: Earth Environ. Sci. 251 (1), 012012. IOP Publishing.
Renu, Agarwal, M., Singh, K., 2017. Methodologies for removal of heavy metal ions from wastewater: an overview. Interdiscip. Environ. Rev. 18 (2), 124–142.
Revankar, M.S., Lele, S.S., 2007. Synthetic dye decolorization by white rot fungus, Ganoderma sp. WR-1. Bioresour. Technol. 98 (4), 775–780.
Ribeiro, C., Scheufele, F.B., Espinoza-Quinones, F.R., Módenes, A.N., da Silva, M.G., Vieira, M.G., Borba, C.E., 2015. Characterization of Oreochromis niloticus fish scales and assessment of their potential on the adsorption of reactive blue 5G dye. Colloids Surf. A Physicochem. Eng. Asp. 482, 693–701.
Santhosh, C., Velmurugan, V., Jacob, G., Jeong, S.K., Grace, A.N., Bhatnagar, A., 2016. Role of nanomaterials in water treatment applications: a review. Chem. Eng. J. 306, 1116–1137.
Saravanan, A., Kumar, P.S., Yaashikaa, P.R., Karishma, S., Jeevanantham, S., Swetha, S., 2021. Mixed biosorbent of agro waste and bacterial biomass for the separation of Pb (II) ions from water system. Chemosphere 277, 130236.
Saxena, R., Saxena, M., Lochab, A., 2020. Recent progress in nanomaterials for adsorptive removal of organic contaminants from wastewater. ChemistrySelect 5 (1), 335–353.
Shakerian, K.F., Esmaeili, H., 2018. Synthesis of CaO/Fe_3O_4 magnetic composite for the removal of Pb (II) and Co (II) from synthetic wastewater. J. Serb. Chem. Soc. 83 (2), 237–249.

Shen, K., Gondal, M.A., 2017. Removal of hazardous rhodamine dye from water by adsorption onto exhausted coffee ground. J. Saudi Chem. Soc. 21, S120–S127.
Sillanpää, M., Shestakova, M., 2017 June 19. Electrochemical Water Treatment Methods: Fundamentals, Methods and Full Scale Applications. Butterworth-Heinemann, pp. 47–130.
Sirocki, A.R., Lanza, R.A., Connors, S.C., 2013. Removal of Ibuprofen from Drinking Water using Adsorption.
Smily, J.R., Sumithra, P.A., 2017. Optimization of chromium biosorption by fungal adsorbent, Trichoderma sp. BSCR02 and its desorption studies. HAYATI J. Biosci. 24 (2), 65–71.
Sobhanardakani, S., Jafari, A., Zandipak, R., Meidanchi, A., 2018. Removal of heavy metal (Hg (II) and Cr (VI)) ions from aqueous solutions using Fe_2O_3@ SiO_2 thin films as a novel adsorbent. Process. Saf. Environ. Prot. 120, 348–357.
Suteu, D., Bilba, D., Aflori, M., Doroftei, F., Lisa, G., Badeanu, M., Malutan, T., 2012. The seashell wastes as biosorbent for reactive dye removal from textile effluents. Clean: Soil, Air, Water 40 (2), 198–205.
Suzuki, Y., Kametani, T., Maruyama, T., 2005. Removal of heavy metals from aqueous solution by nonliving Ulva seaweed as biosorbent. Water Res. 39 (9), 1803–1808.
Taghizade Firozjaee, T., Mehrdadi, N., Baghdadi, M., Nabi Bidhendi, G.R., 2018. Application of nanotechnology in pesticides removal from aqueous solutions-a review. Int. J. Nanosci. Nanotechnol. 14 (1), 43–56.
Tamjidi, S., Esmaeili, H., 2019. Chemically modified CaO/Fe_3O_4 nanocomposite by sodium dodecyl sulfate for Cr (III) removal from water. Chem. Eng. Technol. 42 (3), 607–616.
Tamjidi, S., Esmaeili, H., Moghadas, B.K., 2019. Application of magnetic adsorbents for removal of heavy metals from wastewater: a review study. Mater. Res. Express 6 (10), 102004.
Tamjidi, S., Esmaeili, H., Moghadas, B.K., 2021a. Performance of functionalized magnetic nanocatalysts and feedstocks on biodiesel production: a review study. J. Clean. Prod. 305, 127200.
Tamjidi, S., Moghadas, B.K., Esmaeili, H., Khoo, F.S., Gholami, G., Ghasemi, M., 2021b. Improving the surface properties of adsorbents by surfactants and their role in the removal of toxic metals from wastewater: a review study. Process. Saf. Environ. Prot. 148, 775–795.
Teh, C.Y., Budiman, P.M., Shak, K.P., Wu, T.Y., 2016. Recent advancement of coagulation–flocculation and its application in wastewater treatment. Ind. Eng. Chem. Res. 55 (16), 4363–4389.
Teimouri, A., Esmaeili, H., Foroutan, R., Ramavandi, B., 2018. Adsorptive performance of calcined Cardita bicolor for attenuating Hg (II) and As (III) from synthetic and real wastewaters. Korean J. Chem. Eng. 35 (2), 479–488.
Thanki, A., Thanki, A., Singh, R., Sohal, K.S., 2021. The application of low-cost natural bio-adsorbents for the removal of heavy metals—a review. In: Sustainable Development Through Engineering Innovations: Select Proceedings of SDEI 2020. Springer, Singapore, pp. 355–371.
Vijayaraghavan, G., Shanthakumar, S., 2018. Effective removal of acid black 1 dye in textile effluent using alginate from brown algae as a coagulant. Iran. J. Chem. Chem. Eng. 37 (4), 145–151.
Vijayaraghavan, K., Yun, Y.S., 2008. Bacterial biosorbents and biosorption. Biotechnol. Adv. 26 (3), 266–291.
Vojoudi, H., Badiei, A., Bahar, S., Ziarani, G.M., Faridbod, F., Ganjali, M.R., 2017. A new nano-sorbent for fast and efficient removal of heavy metals from aqueous solutions based on modification of magnetic mesoporous silica nanospheres. J. Magn. Magn. Mater. 441, 193–203.
Vučurović, V.M., Razmovski, R.N., Miljić, U.D., Puškaš, V.S., 2014. Removal of cationic and anionic azo dyes from aqueous solutions by adsorption on maize stem tissue. J. Taiwan Inst. Chem. Eng. 45 (4), 1700–1708.
Wuana, R.A., Okieimen, F.E., 2011. Heavy metals in contaminated soils: a review of sources, chemistry, risks and best available strategies for remediation. Int. Sch. Res. Not. 2011, 402647.
Xue, Y., Wu, S., Zhou, M., 2013. Adsorption characterization of Cu (II) from aqueous solution onto basic oxygen furnace slag. Chem. Eng. J. 231, 355–364.
Yeganeh, G., Ramavandi, B., Esmaeili, H., Tamjidi, S., 2019. Dataset of the aqueous solution and petrochemical wastewater treatment containing ammonia using low cost and efficient bio-adsorbents. Data Brief 26, 104308.
Zahoor, M., 2011. Effect of agitation speed on adsorption of imidacloprid on activated carbon. J. Chem. Soc. Pak. 33 (6), 305.
Zuraida, M.S., Nurhaslina, C.R., Ku Halim, K.H., 2013. Removal of synthetic dyes from wastewater by using bacteria, Lactobacillus delbruckii. Int. Refereed J. Eng. Sci. 2 (5), 1–7.

This page intentionally left blank

CHAPTER

7

Nanomaterials for removal of heavy metals from wastewater

Fahmeeda Kausar[a], *Ahmad Reza Bagheri*[b], *Tahir Rasheed*[c], *Muhammad Bilal*[d], *Komal Rizwan*[e], *Tuan Anh Nguyen*[f], *and Hafiz M.N. Iqbal*[g]

[a]School of Chemistry and Chemical Engineering, Shanghai Jiao Tong University, Shanghai, China [b]Department of Chemistry, Yasouj University, Yasouj, Iran [c]Interdisciplinary Research Center for Advanced Materials, King Fahd University of Petroleum and Minerals (KFUPM), Dhahran, Saudi Arabia [d]School of Life Science and Food Engineering, Huaiyin Institute of Technology, Huaian, China [e]Department of Chemistry, University of Sahiwal, Sahiwal, Pakistan [f]Institute for Tropical Technology, Vietnam Academy of Science and Technology, Hanoi, Vietnam [g]Tecnologico de Monterrey, School of Engineering and Sciences, Monterrey, Mexico

7.1 Introduction

There are three classes of waste and natural water residing pollutants which are named as poisonous inorganic and organic materials, and micro-pathogens. Normally, 30% of sewage-water residing contaminants are polyatomic compounds and heavy metals from inorganic origin that exist in different water resources were reported by Bora and Dutta in 2014 (Bora and Dutta, 2014). Numerous industries act as source of pollution addition to water bodies and surroundings, for example, agriculture, petroleum, steel and pulp construction, and fabric refinery (Inglezakis et al., 2002). Several diseases in human body like skeletal disorders and heart malfunctioning are the consequences of natural abundance of polyatomic-compounds and heavy elements (Kemp et al., 2013; Rasheed et al., 2019a,c; Rasheed and Nabeel, 2019). Fig. 7.1 illustrates major consequences and adverse health effects of potentially toxic elements, e.g., chromium, manganese, and cobalt (Rasheed et al., 2018b).

https://doi.org/10.1016/B978-0-323-90912-9.00007-1

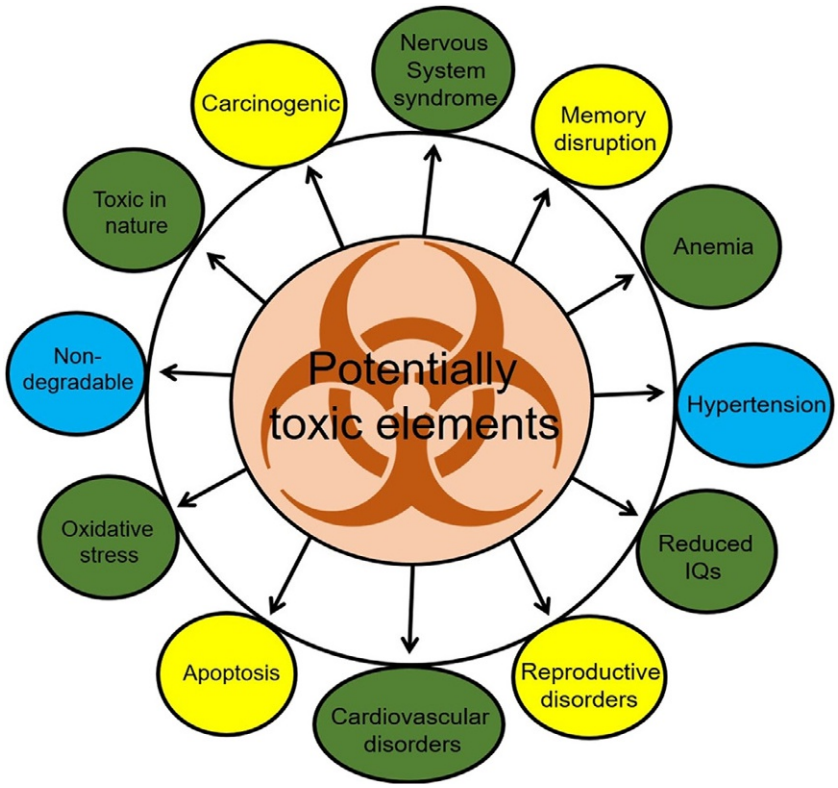

FIG. 7.1 Major consequences and adverse health effects of potentially toxic elements including chromium, manganese, cobalt, nickel, copper, and zinc as target elements. *Reprinted from Rasheed, T., Li, C., Bilal, M., Yu, C., Iqbal, H.M., 2018b. Potentially toxic elements and environmentally-related pollutants recognition using colorimetric and ratiometric fluorescent probes. Sci. Total Environ. 640, 174–193 with permission from Elsevier.*

Environmental hazards are generated from farming, medicinal, dyeing, printing, and fabric industries which are organic origin and are poisonous in nature. Sewage-water residing organic substances comprise 70% of contaminants (Bora and Dutta, 2014; Rasheed et al., 2019d,e,f). Predominantly, industries throw out bio-degradable substances, rather bioaccumulation could occur because of slower degeneration (Rasheed et al., 2018c, 2019g; Vickers, 2017). The removal of organic/inorganic pollutants from drinkable water, specifically medicinal compounds and heavy metals, is important because of their viable impacts owing to long-time vulnerability, however, their small quantity showed no threat to public health (Jelić et al., 2012; Rasheed et al., 2018d,e). Cancer/mutagenicity, genotoxicity, and malfunctioning of endocrine hormones are noticed due to contact with considerable quantity of organic/inorganic pollutants like herbicidal compounds, heavy metals, and dyes (Bilal et al., 2020; Rasheed et al., 2019b, 2020b; Tang et al., 2012). Protozoa, viruses, and bacteria are the most common microscopic water contaminants. Fecal pollution and soil impurification are the frequent factors responsible for addition in water resources

(Ishii et al., 2006; Rasheed et al., 2020a; Zvizdić et al., 2005). Apart from water purity, general human health and surrounding protection are at risk due to presence of microscopic organisms (Hernández et al., 2015).

7.2 Pollution sources and treatment strategies

Water pollution is greatly specified through ornamental problems. Numerous pollutants could be estimated by varying the standard characteristics of water like aroma, color, turbidity, and lucidity. Herein, some of the pollutants are described that distinctively influence appearance and quality of water. Algae and suspended microorganisms impart blue green algae and cyanobacteria while deep green color, zooplankton and dinoflagellates red color, and diatom yellowish brown color to water (Shin et al., 2017). In 2015, Chaussemier et al. reported that red and green color in water is due to Fe and $CaCO_3$ minerals (Chaussemier et al., 2015). Modern industries utilize diverse dyes that produce stain in water like methylene-blue, debuted by Yagub et al. in 2014 (Yagub et al., 2014). In 2012, Goel and Kaur reported cloud/mist formation in water owing to the presence of variant foam-producing detergents. Mostly, different types of pollutants can generate an offensive smell in water due to contagion (Goel and Kaur, 2012). Achudume (2009) and Wing et al. (2014) reported the relation of offensive aroma with oils, petrochemicals, sewage, and degenerating organic matter. By following traditional techniques, diverse health problems are sorted out by purifying wastewater produced on the grounds of industrial, commercial, and household zones (Achudume, 2009; Wing et al., 2014). Lofrano and Brown (2010) introduced the categorization of major kinds of traditional wastewater remediation which includes: (1) physical dissociation (2) biodegradation (3) chemical decaying method. Generally, centrifugal separation or gravity separation are adopted as the easiest techniques as physical separation for wastewater to recuperate unmixed and dispersed contaminants (Lofrano and Brown, 2010). Even though it is a feasible method for wastewater remediation, but still not ultimate because emission parameters are hard to achieve owing to low and variable reaction rate. Biodegradation necessitates microbes which act on organic dispersed/suspended contaminants in sewage and mix or convert them into secure and non-dangerous compounds (Lofrano and Brown, 2010). Operational inefficacy in winter, hard to remove heavy metal ions, operational expensiveness, and apparatus provision are the major issues of treatment through biotechniques, however, emission parameters were smoothly obtained (Oller et al., 2011). On the contrary, chemical decaying method includes water purifiers such as coagulation agents (Sarkar et al., 2006), flocculation agents (Lee et al., 2014) resistors for corrosion (Weiss et al., 2006). These agents are applied for depolluting, standardizing, and softening of water by removing undissolved poisonous and suspended particles, decreasing lather, inhibiting corrosion by reducing water exposure and modulating sludge and scale production (Hayat et al., 2015). Apart from advantages, chlorination has disadvantages too like incompetency in separating pollutants, e.g., inorganic/organic substances and heavy metals from water (Sedlak and von Gunten, 2011). Various sources of potentially toxic elements including lead, cadmium, and mercury are shown in Fig. 7.2 (Rasheed et al., 2018a). Furthermore, detrimental by-products can evolve after reaction of chlorine and water-existing inorganic/organic materials (Gopal et al.,

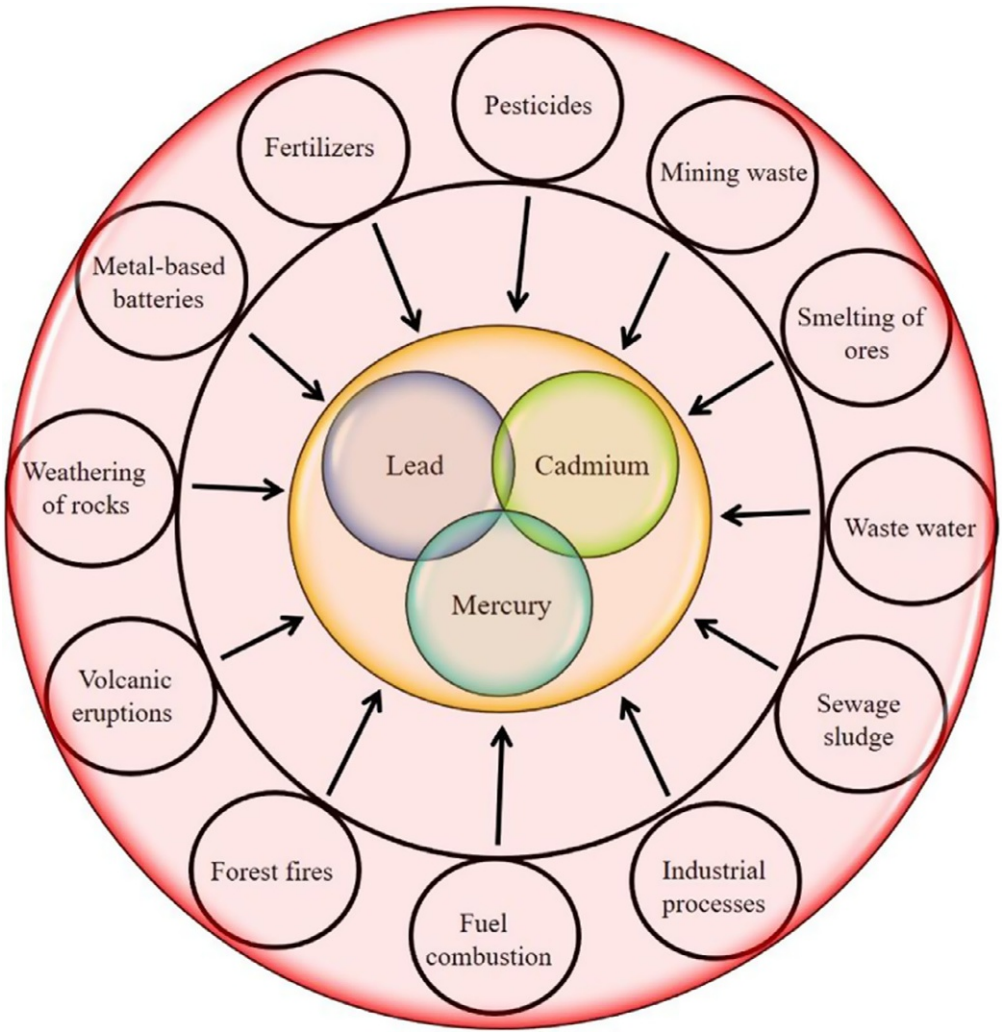

FIG. 7.2 Various sources of potentially toxic elements including lead, cadmium, and mercury. *Reprinted from Rasheed, T., Bilal, M., Nabeel, F., Iqbal, H. M., Li, C., Zhou, Y., 2018a. Fluorescent sensor based models for the detection of environmentally-related toxic heavy metals. Sci. Total Environ. 615, 476–485 with permission from Elsevier.*

2007) causing several kinds of cancer (Richardson et al., 2007). All-inclusive, the intricacy of the wastewater and sewage remediation methodologies and nature of chemicals injected can change the appearance and constitution of water resulting in longer time with greater demand for chemicals which leads to dearness and thus practically unfavorable (Unuabonah et al., 2018). Moreover, many compounds applied chemically can engender secondary contamination, reduce recycling capacity, residual production, unwanted treatment results and complicated synthetic techniques (Yu et al., 2017). Therefore, these constraints proved above-mentioned categories iniquitous for proficient applications.

7.3 Metal based-nanomaterials

During recent decades, the metal-based nanoparticles played significant role in water remediation. For instance, silver-based nanoparticles are reported to have antimicrobial potential so they are employed to disinfect water (Srinivasan et al., 2013). Zinc-based nano-scale materials have potent degradation capability toward the dioxins (Bokare et al., 2013). Nanosized-zero valent iron (nZVI) is comprised of iron (0) and coating of ferric oxide (O'Carroll et al., 2013). It gained attention as an adsorbent to adsorb different heavy metals including mercury (II), chromium (VI), copper (II), nickel (II), cadmium (II) (Liu et al., 2015; Seyedi et al., 2017). Iron (0) offers reducing capability and shell of ferric oxide provides reactive sites and electrostatic linkage with heavy metal particles. Their surface has abundant reactive sites (Cundy et al., 2008). Great reducing potential and huge surface area made nZVI eligible for great performance for remediation of heavy metals from water (Huang et al., 2013). Mechanism of nZVI is variable for different metals and it depends on the standard potential (E0) of different metals (Huang et al., 2013). For instance, Pb (II) has slightly higher E0 in comparison of iron (II) and removal mechanism comprised of reduction and sorption. While in case of chromium (VI) that has greater E0 in comparison of iron (II) an observed mechanism of removal was reduction and precipitation. There are some advantages and disadvantages associated with employment of nZVI for heavy metal removal. According to reports, nZVI oxidized in oxygen environment, and aqueous media which may cause hindrance to reduction phenomena of heavy metals (Tratnyek et al., 2009). Easily aggregation of nZVI may reduce the surface area for reaction and also diminish mobility (O'Carroll et al., 2013). Isolation of nZVI is complex from wastewater. Different modification and alteration methods have been introduced to enhance the nZVI performance through doping nZVI with various metals (copper, nickel, platinum, and lead) and modification of surface chemical (Fu et al., 2014). Unique-modified nZVI material was synthesized through combining of nZVI along with sodium dodecyl sulfate that is kind of an ionic surfactant and contains great capability of migration and dispersion (Huang et al., 2015a). This novel material exhibited great removal potential (253.68 mg/g) toward chromium (VI) elucidating it as potent adsorbent with enhanced adsorption potential and reduced aggregation. Adsorption phenomena obeyed the Freundlich model and also pseudo-second-order kinetics. Various factors as dosage, starting concentration, pH, and contact time were examined and great removal efficiency (approx. 98.919%) obtained. Removal of cadmium (II) and nitrate was carried out by employing nZVI and gold-doped nZVI nanoparticles (Su et al., 2014). By employing gold-doped nZVI, the yield of nitrite decreased from the nitrates in comparison of bare nZVI while removal ratio of cadmium (II) stayed at high level. It is indicated from the results that gold-doped nZVI may be employed for wastewater treatment having cadmium (II) and nitrate. Nanocomposites based on nZVI are also attaining great attention. By utilizing the economical bentonites, the nZVI-based nano-composites were synthesized and then these were utilized to remove lead (II), cobalt (II), nickel (II), zinc (II), cadmium (II), copper (II) from wastewater (Zarime et al., 2018). Aggregation of nZVI could be reduced by incorporation of bentonite in it and this gives nZVI more sites for adsorbing of heavy metals. Composite of bentonite-nZVI showed great removal potential toward heavy metals in comparison of only bentonite. These are also employed to treat ground water (Zhang, 2003). Reports on different metallic

nanoparticles are not sufficiently available for heavy metal removal. Few reports are available regarding interaction between mercury (II) and silver nanoparticles (Fan et al., 2009). Though the reactivity is not great between the mercury (II) and bulk silver. Silver nanoparticles showed great reactivity due to decrease in reduction potential of silver with decrease in size of particles (Pradhan et al., 2002). By coordinating the silver with mercaptosuccinic acid, silver nanoparticle based adsorbent was synthesized (Sumesh et al., 2011). By employing different ratios of silver to mercaptosuccinic acid (MSA), two materials were synthesized and results showed that 1:6 Ag and MSA exhibited greater removal potential toward mercury (II) (approx. 800 mg/g) in comparison of common adsorbents. Further it was demonstrated that cost value was competitive for removal of mercury (II) by utilizing the Ag and MSA. Thereof the Ag-MSA could be a potential source to remove mercury (II). The mercury affinity toward gold was familiar because they may form Au_3Hg AuHg and $AuHg_3$ (Zhang et al., 2016). Lisha and co-workers demonstrated the employment of gold-based nanoparticles which were aluminum supported to remove the mercury (II) (Lisha and Pradeep, 2009). Sodium borohydride was employed for reduction of mercury (II) to mercury (0) and removal efficacy of gold nanoparticles extended to 4.065 g/g which was found greater in comparison of ordinary adsorbents. Employment of gold nanoparticles to remove mercury (II) was found low and these gold nanoparticles can be recovered easily and this exhibited the implementation of gold-based nanoparticles (aluminum-supported) for treatment of wastewater. Citrate-coated gold nanoparticles were synthesized to remove mercury (II) from wastewater (Ojea-Jiménez et al., 2012). The ions of citrate played the role of weak reducing agent which can reduce mercury (II) to mercury (0) thus eliminating the use of sodium borohydride and experiments revealed that mercury concentration reduced from 65 to 1–5 ppb values. The last product obtained was Au_3Hg alloy which on treatment at high temperature and pressure recovers the gold (Sneed et al., 1956).

7.4 Metal oxide-based nanomaterials

Metal oxide-based nanomaterials are considered as a versatile type of materials from both a scientific and technological viewpoint (Sengul and Asmatulu, 2020). Metal oxides are an interesting class of materials intensively investigated nowadays, and displaying unique properties in terms of mechanical stress tolerance, high optical transparency, exceptional carrier mobilities, high surface area, high adsorption capacity, etc. (Medhi et al., 2020). It is worth mentioning that the surface of metal oxides plays critical role for effective interaction with different molecules and ions. The exceptional attributes of metal oxide-based nanomaterials and their recent progresses and development have opened new possibilities and opportunity for applications of these materials in different area and especially for removal of heavy metals as one of the main and hazardous environmental pollutants (Sawan et al., 2020). Metal oxide-based nanomaterials can be synthesized using different synthesis approaches like physical, chemical, and biological methods and also can be in different forms. These amazing features make these materials as applicable and attractive adsorbents for treatment and removal of

harmful heavy metals. In the following, some of the well-known metal oxide-based nanomaterials and their application for removal of heavy metals will be investigated and discussed.

7.4.1 Iron oxide-based nanomaterials

In spite of common advantages of metal oxide-based nanomaterials mentioned above, iron oxide-based nanomaterials also have other distinguished property, in terms of magnetic property, which makes these materials an excellent candidate for removal of heavy metals (Bagheri and Ghaedi, 2020). After adsorption of heavy metals by target adsorbents, it is essential to separate applied sorbents from sample solution or medial. Filtration, precipitation as well as centrifugation are considered as routine methods for separation of sorbents used (Bagheri et al., 2019). Although these methods are useful, they are faced with main limitations. For instance, using these methods, some of the adsorbents may retain in the sample solution which can reduce the performance and applicability of method. Most importantly, these methods are time-consuming (Gholami et al., 2019). To address these drawbacks, application of magnetic adsorbents can be an ideal and an alternative method. Using magnetic adsorbents, applied adsorbents can be separated easily using an external magnet which not only can address the limitations of common separation methods, but also can reduce separation time and also improve performance of the proposed method (Bagheri et al., 2017). To this end, synthesis and application of iron oxide-based nanomaterials as kind of magnetic nanomaterials have been in the hotspot. Up to date, many efforts have been performed for construction of iron oxide-based nanomaterials and their utilization for removal of heavy metals. For example, Mahanty and co-workers synthesized iron oxide nanoparticles based on biological method and used them for removal of Pb (II), Ni (II), Cu (II), and Zn (II) (Mahanty et al., 2020). In this work, manglicolous fungi *Aspergillus tubingensis* (STSP25) obtained from rhizospheric sediment samples of *Avicennia officinalis* were used for preparation of monodispersed, spherical, and crystalline iron oxide nanoparticles. The fabricated nanoparticles had diameter of 73.05 ± 15.47 nm. RSM and ANN methods were used to investigate and optimize the effective parameters. The removal percentage of Pb (II), Ni (II), Cu (II), and Zn (II) were achieved to be 98.0037%, 96.4502%, 92.1984%, and 93.9913%, respectively. Based on the results, the adsorption process was endothermic. The adsorption process was followed by Langmuir isotherm model and pseudo-second-order kinetics. Moreover, the maximum adsorption capacities for Pb (II), Ni (II), Cu (II), and Zn (II) were 206 mg/g, 9.666 mg/g, 8.335 mg/g, and 9.106 mg/g, respectively. Regeneration of applied sorbent as one of the most practical aspect was also investigated and according to results, proposed sorbent was useful for at least five cycles.

To improve the performance of iron oxide nanomaterials, their combination with other materials and production of their composites can be an ideal method. The composites of iron oxide nanomaterials can have more functional groups, surface area, stability, and adsorption capacity compared to iron oxide nanomaterials. To this end, sodium alginate was cross-linked with iron oxide nanoparticles and fabricated composite was sued for removal of lead, copper, and cadmium (Mahmoud et al., 2020). Based on the SEM analysis, prepared sorbent had size

in the range between 150 and 260 nm. The aggregate particles showed good distribution and homogeneity along the examined sample. The other main property of sorbent was its thermal stability which was proved by TGA analysis. BET analysis showed that surface area of iron oxide nanoparticles and fabricated composite were achieved to be 3.7551 and 5.4339 $m^2\ g^{-1}$. Based on the results, the addition of sodium alginate increased the surface area of proposed composite. This fact can be due to the presence of different functional groups in sodium alginate structure which can increase interaction of sorbent and heavy metals. The effect of various parameters on removal process was investigated and they were optimized. Under optimum conditions, applied process was followed by pseudo-second order kinetic model. Also, the maximum adsorption capacities for lead, copper, and cadmium were 564, 158, and 102.2 mg/g, respectively.

7.4.2 Manganese oxide based nanomaterials

Manganese oxide (MnO_x) is one of the popular metal oxides nanomaterials that has attracted a lot of attention (Soejima et al., 2018). MnO_x has unique properties like its magnetic nature, catalytic activity, and high energy density. MnO_2 is one of the metal oxide-based nanoparticles which is cheap and eco-friendly (Yabuuchi and Komaba, 2014). The other main properties of MnO_x-based nanomaterials are their high surface area and also high adsorption capacity. These exceptional features make these materials excellent candidate for application in different areas like catalysts, gas sensor, energy storage, and removal of different contaminates (Kumar et al., 2016; Luo et al., 2008; Subramanian et al., 2014). For instance, Su et al. fabricated hydrous manganese dioxide (HMO) and sued it as effective adsorbent for removal of lead, cadmium, and zinc ions from water (Su et al., 2010). The prepared HMO had amorphous structure with surface area of 100.5 $m^2\ g^{-1}$. In this work, effect of different factors on removal process was investigated and then they were optimized. Tamura et al. (Tamura et al., 1996) suggested that the adsorption of metal ion (M) by HMO can be occurred by below mechanism:

$$-Mn-OH+M^{2+} \Leftrightarrow -Mn-O-M^{+}+H^{+} \tag{7.1}$$

$$-Mn-OH+M^{2+} \Leftrightarrow (-Mn-O)_2-M^{+}+2H^{+} \tag{7.2}$$

Both reactions can be classified as typical ion-exchange processes. Based on the reactions, lower pH is not suitable for adsorption of target ions. FT-IR proved that the adsorption mechanism of Ca(II) by HMO was based on the outer sphere complexation, while adsorption mechanism of lead, cadmium, and zinc ions was according to inner sphere complex formation. Different isotherm models were used to evaluate the adsorption mechanism. Results confirmed that Langmuir model was more suitable than other models which was due to its higher R^2. Langmuir model assumes the monolayer adsorption of target ions on the homogeneous surface of sorbent. In addition, HMO prefers metal sorption in the sequence $Pb^{2+} > Cd^{2+} > Zn^{2+}$, which might rest on the different softness of these metals.

In other study, manganese oxide was supported on a macro-mesoporous biochar and obtained composite was applied for removal of cadmium and lead from water (Wan et al., 2020). In this work, at first, a biochar with enlarged pore channel was fabricated using pyrolysis process. Then, the fabricated biochar was used as support for modification of manganese

oxide on it. SEM analysis showed that manganese oxide nanoparticles were deposited on the surface of biochar. The surface area and pore volume of prepared composite were 561.4 $m^2\ g^{-1}$ and 0.39 $cm^3\ g^{-1}$, respectively. Moreover, TGA analysis proved the high stability of used composite. FTIR and XPS were applied to assess the adsorption mechanism of heavy metals by composite. After adsorption of Pb(II) by composite, the peak intensity of Mn-OH was dramatically decreased which may be related to the exchange of Pb(II) to the protons combined with O atoms in Mn-OH groups. In addition, the peak of Mn-OH was shifted to higher frequency which may be attributed to interaction of Pb and O (Pb-O) based on the inner sphere complexation (two atoms share a pair of electrons, and one atom affords the lone electron pair and the other one provides the empty orbit).

7.4.3 TiO_2-/ZnO-based nanomaterials

One of the other useful metal-based nanoparticles is TiO_2 which have been used in different fields especially industries (Gebru and Das, 2018). TiO_2 nanoparticles have exceptional properties like self-cleaning properties and the ability to remove air pollutants. Moreover, due to catalyst feature of these nanoparticles, they are also applicable as catalyst for degradation of various pollutants (Bian et al., 2018). The other distinguished attributes of TiO_2 nanoparticles are their mechanical and antibacterial properties which make them excellent materials for utilization in different areas (Wang et al., 2019b). In 2018, Lajayer and co-workers used TiO_2 nanoparticles for removal of Cu^{2+} and Cd^{2+} from effluent (Lajayer et al., 2018). The removal process of heavy metals was done using combination of gamma irradiation, methanol, and TiO_2 nanoparticles under different pH values. Applied nanoparticles had surface area and average particle about 50 $m^2\ g^{-1}$ and 21 nm, respectively. SEM and TEM analysis showed that used nanoparticles were homogeneously distributed and had spherical shape. TiO_2 nanoparticles were able to adsorb heavy metals. The radiation process is an emerging treatment method in which the target ions can change to insoluble forms and remove from sample solution or media. Gamma irradiation can generate hydroxyl radical ($OH^{\bullet}$). In the following, these radicals can attack ions and then degrade or reduce them and finally remove them. pH is the most effective factor on removal of heavy metals in this process. In this regard, pH was investigated and optimized. pH can control the generation of $OH^{\bullet}$ and subsequently can improve the removal percentage of heavy metals. This study proved that only 50 kGy irradiation doses with combination of TiO_2 nanoparticles was enough for removing Cu^{2+} and Cd^{2+} more than 90% from the acidic wastewater.

ZnO is another useful nanomaterial for heavy metal treatment. ZnO is an FDA approved food additive and is generally recognized as safe and non-toxic in low concentrations (Sharifan et al., 2020). ZnO nanoparticles have high photo catalytic activity and are believed to be more biocompatible than TiO_2 (Iannone et al., 2017). These nanomaterials have been extensively applied in food industries to preserve colors and prevent spoilage through their antimicrobial activity (Sun et al., 2018). The antimicrobial properties of ZnO nanoparticles are attributed to their ability to damage the cell wall of bacteria and disruption of DNA replication (Khatami et al., 2018). Due to these unique properties, ZnO nanoparticles are considered as one of the versatile materials for removal of heavy metals. For example, Salem and co-workers constructed ZnO nanoparticles for efficient removal of heavy metals (Cr^{3+}, Ni^{2+}, and Co^{2+}) (Salem et al., 2017). XRD analysis proved the crystalline structure of nanoparticles

with average diameter of 28, 25, 73, and 130 nm. SEM analysis confirmed that the shape of ZnO nanoparticles was greatly changed after capturing Cr^{3+} and Co^{2+} ions, while they little changed after adsorption of Ni^{2+}. This fact was due to low ability of ZnO nanoparticles for adsorption of Ni^{2+} ions. The effects of different factors on removal process like ZnO amount, pH, foreign salt ions, activation parameters, and metal ions initial concentration were investigated and optimized. The kinetic of reaction was also evaluated and according to results the adsorption of heavy metals was followed by *pseudo*-second-order kinetic model. Moreover, adsorption of heavy metals was followed by Langmuir isotherm model.

7.4.4 Aluminum oxide-based nanomaterials

Among various metal oxide nanoparticles, aluminum oxide-based nanomaterials have cheap construction cost and high decontamination efficiency (Giles et al., 2011). Most importantly, United Nations Environmental Program (UNEP) agency reported that aluminum oxide nanomaterials are the best available technologies for arsenic removal from water (Sorg, 2000). So, due to these amazing properties, these materials have been broadly applied for removal of heavy metals and particularly arsenic. With respect to this properties, Prabhakar and Samadder fabricated aluminum oxide nanoparticles using low-cost and easy method and used them for removal of arsenite from groundwater (Prabhakar and Samadder, 2018). Proposed nanoparticles are synthesized by solution combustion method. This method is not only easy and cheap, but also is time-saving and also eco-friendly. Based on the DRS analysis, Al_2O_3 nanoparticles had size of 52–85 nm. SEM analysis proved the spherical shape of nanoparticles. At first, the nanoparticles were agglomerated which may be related to the moisture in storing chamber. XRD analysis showed the crystalline structure of particles. In this work, equilibrium time as one of the main factors in application of Al_2O_3 nanoparticles at large and industrial scales was investigated in range of 15–180 min. Results showed that 180 min was efficient for removal of arsenite more than 90%. Other factors like initial concentration, stirring speed, sorbent dosage, temperature, and pH were also investigated and optimized. Evaluation of different isotherm models shoed that Langmuir model was more suitable than other models that shows the monolayer adsorption of arsenite onions onto homogenous surface of sorbent. The maximum adsorption capacities (Q_m) were determined as 500.0, 510.2, 526.3, and 555.5 μg g^{-1} at 298, 308, 318, and 328 K correspondingly. Moreover, kinetic studies showed that adsorption of arsenite onions was followed by pseudo-second-order kinetic model. Thermodynamic studies proved that the adsorption of arsenite onions onto Al_2O_3 nanoparticles was exothermic in nature. The value of ΔH^o lower than 40 kJ mol^{-1} is the indicator of physical adsorption process. The ΔH^o value for this study was obtained to be −26.09 kJ mol^{-1} which confirmed physical adsorption was the prevailing mechanism for removal of arsenite onions by Al_2O_3 nanoparticles. The reusability investigation showed that used nanoparticles were applicable at least for three cycles. The cost of preparation of nano alumina was estimated to be US$ 67/kg. This property makes nano alumina materials as excellent materials for synthesis and application as adsorbent.

In other work, mesoporous bismuth-impregnated aluminum oxide was fabricated and applied as sorbent for removal of arsenic (Zhu et al., 2018b). In this work, adsorption mechanism and application of used sorbent to a lab-scale column were also assessed. The effect of different parameters on removal process was investigated and optimized. Investigation of isotherm

models proved that the maximum adsorption capacity was 26.8 mg/g and the adsorption process was followed by Freundlich model. This model assumes that the adsorption of target analyte/s is multilayer and also it is occurred on the heterogeneous surface of sorbent. The adsorption mechanism is based on the complexation of As (III) onto the surface of sorbent. It is worth mentioning that impregnation of bismuth reduces the specific surface area of aluminum oxide and affected its pore size distribution. However, because of its abundant and well-proportioned mesoporous character, bismuth can complex with As (III) onions and remove them.

7.4.5 MgO based nanomaterials

MgO nanoparticles are non-toxic and used in crucibles, additives in flame-retardant materials, refractory materials, and coating materials (Vesali-Kermani et al., 2020). The size and morphology of oxide particles can be modified using parameters such as pH, ionic strength, and different calcination temperature (Silva et al., 2020). MgO nanoparticles can be fabricated using different synthesis approaches and have been used in different fields (Nguyen et al., 2020). One of the interesting areas for utilizing these materials is pollutants treatment which is due to extensive attributes of MgO nanoparticles such as high surface area and high adsorption capacity. Cai et al. constructed highly active MgO nanoparticles and used them for simultaneous bacterial inactivation and heavy metals (Cd^{2+} and Pb^{2+}) removal from aqueous solution (Cai et al., 2017). The proposed nanoparticles were synthesized using sol–gel and calcination method. The prepared nanoparticles had uniform structure with diameter of 20–30 nm. According to BET analysis, MgO nanoparticles had surface area of 47.85 and 5.26 $m^2\ g^{-1}$. The other interesting property of MgO nanoparticles was their ability for inactivation of *Escherichia coli* (*E. coli*). Results proved that addition of Cd^{2+} improved the inactivation of MgO nanoparticles. After damaging bacterial cells, Cd^{2+} ions can enter to the bacterial cell and thus accelerated bacterial inactivation.

In the other study, MgO and NiO nanoparticles were embedded into silica and obtained composite was applied for removal of Zn^{2+}, Cu^{2+}, and Cr^{3+} (Abuhatab et al., 2020). The effect of different factors was investigated, and they were optimized. The applied sorbent was applicable for removal of ions in short time. The maximum adsorption capacities were achieved to be 37.69, 69.68, 209.51 mg/g for Zn^{2+}, Cu^{2+}, and Cr^{3+}, respectively. These results proved that applied composite is useful for application in large and industrial scales. The thermodynamic studies confirmed that the adsorption of Zn^{2+}, Cu^{2+}, and Cr^{3+} was spontaneous, endothermic, and physical for Cu^{2+} and Cr^{3+}, while exothermic and chemical for Zn^{2+}.

7.4.6 Cerium/zirconium oxide-based nanomaterials

One of the other applicable metal oxides is cerium oxide nanoparticle which have unique properties like antioxidant attributes both in vitro and in vivo (Singh et al., 2020). The antioxidant attributes of cerium oxide nanoparticles is due to redox-cycling between its states (3^+ and 4^+) (Justeau et al., 2018). Cerium oxide nanoparticles are useful in different fields due to its amazing properties like redox activity, free radical scavenging property, biofilm inhibition, etc. (Rossi et al., 2019). Different synthesis methods like physical, chemical, and biological methods have been sued for fabrication of these materials. Due to these features,

Tong and co-workers decorated ultrathin molybdenum disulfide nanosheets with cerium oxide nanoparticles and applied proposed composite (MoS_2/CeO_2) for removal of lead (II) ions (Tong et al., 2018). TEM analysis showed the nanosheets structure of MoS_2. Also, TEM analysis proved that the CeO_2 nanoparticles with size of 3–5 nm and good distribution were uniformly distributed on the MoS_2. TGA analysis showed the good thermal stability of fabricated composite. Effect of different factors like sorbent dosage, contact time, pH, and ionic strength on removal process was investigated and optimized. The adsorption of Pb^{2+} was followed by Langmuir isotherms model. The maximum adsorption capacity of Pb^{2+} was 333 mg/g at pH 2.0. Results showed that the applied composite was also useful for adsorption of other heavy metals. For example, adsorption capacities of Cd^{2+}, Cu^{2+}, Zn^{2+}, Co^{2+}, Ni^{2+}, Mn^{2+} and Cr^{3+} were 3.24, 5.3, 3, 1.8, 1.3, 2.1, and 1.76 mg/g.

Zirconium oxide nanoparticles are another type of metal oxide nanoparticles which have brilliant properties like high surface area that makes them excellent materials for adsorption of heavy metals and removal of them (Ibrahim et al., 2019; Wei et al., 2018). Mahdavi and co-workers synthesized bare and modified nano-zirconium oxide (ZrO_2) and applied them for removal of Cd^{2+}, Cu^{2+}, and Ni^{2+} (Mahdavi et al., 2017). SEM analysis showed that fabricated ZrO_2 nanoparticles had diameter of 137.8 nm with heterogeneous shapes and sizes. According to XRD analysis, nanoparticles had crystalline structure. In this study, effective parameters on removal process were evaluated and optimized. Results proved that the adsorption process of heavy metals was followed by pseudo-second-order rate model ($R^2 > 0.97$) and Freundlich isotherm model. The maximum adsorption capacities of Cd^{2+}, Cu^{2+}, and Ni^{2+} using ZrO_2 nanoparticles and modified ZrO_2 nanoparticles were obtained to be 46.2, 59.7, 39.5, 29.7, 9.2, and 16.7 mg/g, respectively.

7.5 Biochar-supported NMs

Wellbeing of human community and atmosphere are facing threat from heavy metal contamination. Because of ion exchange capability, wide surface area, excellent reactiveness MNPs@BC have developed remarkable interest. Consequently, water is purified from lead, cadmium, chromium, mercury, and arsenic using MNPs@BC (He et al., 2019). Foremost, assessment of MNPs@BC functioning is achieved through its implication in wastewater for heavy metal separation. Furthermore, removing performance of MNPs@BC for heavy metals affected experimental factors, e.g., pH of solution, starting quantity heavy metals, concurrent ions, and dosage. Moreover, oxidation, ion-exchange, coprecipitation, reduction, and adsorption via surface complexation and electrostatic attraction are the mechanistic techniques followed by MNPs@BC action. In order to have a fine apprehension of mechanistic study, elemental mapping, FT-IR, XRD, TEM, SEM, and XPS are the experimental techniques adopted to confirm heavy metals elimination. Herein, the mechanistic approach of MNPs@BC, result of different factors upon heavy-metals elimination and separation capability are described. MNPs@BC is reported enormously for purifying water from heavy metals and its capability for removing is also assessed. The obtained experimental data is examined by employing Sips, Temkin, Langmuir-Freundlich, and Freundlich prototypes. To evaluate the removing tendency of heavy metals second-order kinetics, intraparticle-diffusion

prototype, Elovich and first-order kinetics has been administered. Arsenic, for instance, could be adsorbed in wastewater using biochar infused with iron-manganese-lanthanum (Lin et al., 2019b). By utilizing chemical adsorption, arsenic has been adsorbed from compound through second-order kinetics. A comparatively quick reaction is observed for arsenic adsorption on composite material, i.e., equilibrium achieved in 1 h. Single-layered adsorption is detected for arsenic on composite's surface following Langmuir model. Arsenic demonstrated 14.9 mg/g optimum composite's adsorption capability. Hence, arsenic is efficiently adsorbed via composite. Aqueous solutions were purified by introducing exotic nZVI and n-α-OH-Fe@BC for cadmium elimination (Zhu et al., 2019). Chemisorption controls cadmium-adsorption on composite and greatly elaborated via pseudo-first-order kinetics. Cadmium (II) adsorbed quickly on composite at the rate of 2.54 and 1.17 mg/g per hour. In addition, Langmuir model proved to be the best match for experimental results and 22.37 mg/g and 26.43 mg/g of cadmium (II) are the optimal adsorbing capacities of composite. Cadmium (II) elimination is an excellent predominantly using composites in comparison to other substances. Coexisting bisphenol A (BPA) and cuprous ions are removed from water when treated with biochar-based Fe (0), prepared by Liu et al. in 2018 (Liu et al., 2018). On account of $S_2O_8^{2-}$ and bichar-based Fe (0) implying BPA and cuprous ion, the elimination capacity increased to 98% and 96%, accordingly. Biochar-based ZVI and $S_2O_8^{2-}$ compounds were employed to proficiently clean hydrosphere from organic contaminants and heavy metals (Sun et al., 2019) remove hetero-chloride ions, poisonous materials, instinct cations by introducing Fe-biochar and utilizing afterwards in wastewater from damaged hydromechanical systems. Original wastewater is treated with Fe-biochar to eliminate coexistent dissolved pollutants with extraordinary accomplishment. Simultaneously occurring ions, dosage, quantity of heavy metals, pH of solution in particular, and temperature are diverse operational factors that affect elimination of heavy metals from wastewater. Rate of reaction, substances charge, and dissolution of metal NPs are controlled by essential parameter, i.e., solution pH. nFeS@BC, for example, has been synthesized and applied in water to eliminate chromium (VI) (Lyu et al., 2017). Acidic environment is beneficial for removing chromium since elimination rate improved with decreased pH. In order to reduce chromium (VI), ferrous and sulfide ions are sufficiently provided in acidic environment through dissociation of iron sulfide. Moreover, repulsion between composites and positively charged chromium declined in acidic environment. Aqueous solutions were purified from copper and cadmium by synthesizing and using ferromanganese oxide biochar (Zhou et al., 2018a). pH of solution has direct relation with composite's adsorbing capacity for copper and cadmium. Elevated pH is demanded for adsorption of copper and cadmium because positive charge was noticed at 9.2 pH on composite's surface. In contrast, copper and cadmium fight with H^+ for adsorption sites at lower pH value. In addition, engineering implication has dosage as the major ingredient. Owing to increment in adsorption sites, for instance, separation capability improved accordingly while increased dosage had an opposite impact on adsorbability of copper (II) compounds of biochar/Mn-Al double-layered OH^- (Wang et al., 2019c). Additionally, reactiveness and movement of ions are largely influenced by temperature and suggested as key element for separation of heavy metals. Elevated temperature increased the chance of contact between chromium (VI) and the compound, which is attributable to enhanced collision frequency and hence biochar-supported nZVI effectively removed Cr (VI). Furthermore, chromium (VI) is reduced to chromium (III) at elevated temperature (Zhu et al., 2018a). Lastly, the

functioning of adsorbing agents is disturbed due to concurrence of ions in solutions of heavy metals and water resources. Separation of chromium (VI) is transformed owing to concurrent sulfate, chloride, and bicarbonate anions processed through biochar-supported Fe (0) and was examined by Shang et al. (2017). HCO_3^- can decrease distinctively the elimination proficiency of chromium (VI). In this scenario, adsorption locks have attraction not only for chromium (VI) but also HCO_3^- on compound's exterior covering. Sulfate ions efficiently expanded reactive sites over Fe (0) and initiated its corrosiveness, so its existence also discriminatively enhanced removal of chromium (VI) while chloride ion displayed no remarkable impact. The general mechanism of removal of various contaminants has been illustrated in Fig. 7.3 (Liu et al., 2020).

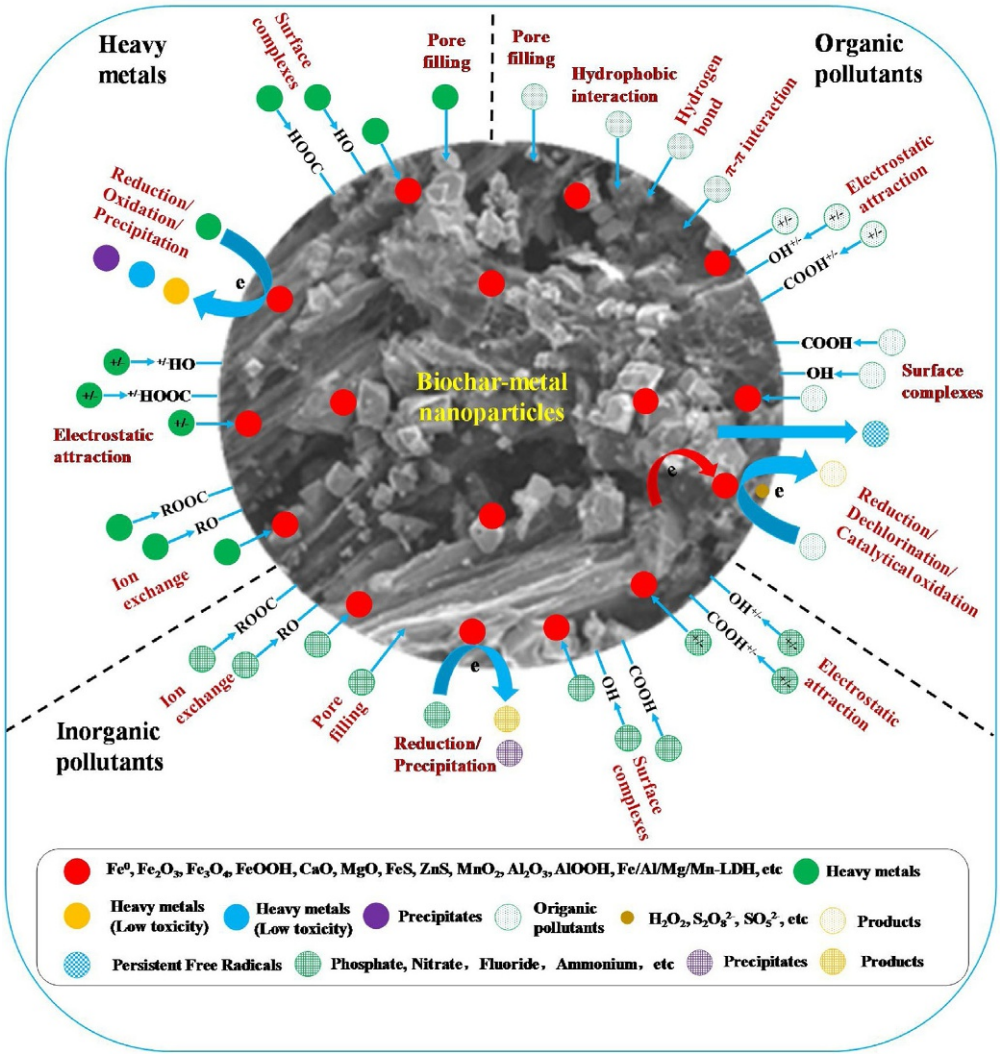

FIG. 7.3 The removal mechanism of the contaminants in water by MNPs@BC (Liu et al., 2020).

7.6 Biochar-supported nanoparticles heavy metals treatment

Adsorption, stabilizing chemicals, frothing, soil corrosion, electro-kinetic treatment, and phyto-treatment are the techniques being utilized for reducing portability of heavy metals in biosphere (Zhai et al., 2018). Out of above given methodologies, toxic effect, biodiversity, and portability of heavy metals have been decreased in soil using harmless MNPs@BC in soil modification to stop heavy metals transference (Lu et al., 2019; Yu et al., 2019). Moreover, soil's physical and chemical characteristics like pH, enzymatic functions, groups microorganisms, redox-potential, and organic texture get transmuted when soil is polluted with heavy metals locally treated with MNPs@BC. Adsorption, ion exchange, precipitating compounds, surface complexation, reducing chemically are the adapted pathways for immobilizing soil residing heavy metals (Beiyuan et al., 2017). MNPs@BC functioning as immobilizer was estimated and also soil remediation for heavy metals pollution was illustrated in many research reports. Recently (Su et al., 2016a) reported that with the addition of 8 g/kg zerovalent iron-biochar for 15 days, for instance, 100% and 92.9% were the estimated immobilizing capacities in soil for chromium (VI) and chromium (0), respectively. Furthermore, cabbage-mustard was subjected to vessel experiment to check developing improvement with the outcome of decreased phyto-toxicity of Cr (II). Transportation of soil occupying cadmium was restricted through encouraging Fe-Mn oxide and organic-matter generation with replaceable cadmium which was achieved by S-Fe-improved biochar treatment of Cd (II) contaminated soil, synthesized by Rajendran et al. (2019), resulting reduced aggregation of Cd (II) in rice. To revivify soil polluted with arsenic, Fe-Mn oxide infused biochar-composites (FMBC) have been prepared and applied on rice to analyze arsenic storage (Lin et al., 2017). By using Fe-Mn oxide, arsenic (III) oxidized to arsenic (V) resulting in bigger ferromanganese panel sheet hindered the mobility of arsenic toward rice from soil, reduced accessibility, and ultimately its aggregation and the remediation was achieved using FMBC. Natural abundance of antimony and cadmium was decreased in plants and ameliorated different soil characteristics such as nutrient components, enzymatic action, pH, and organic texture when cadmium and antimony were inactivated with iron-manganese biochar and was presented by Wang et al. (2019a). In addition, the bioavailability of replaceable antimony and cadmium decreased succeeding improvement through iron-manganese-improved biochar. Organic structure, combination of heavy metals, enzymatic performance in soil, style of microorganism grouping, redox potential, and pH of soil are heavily influenced by implementing MNPs@BC for depolluting heavy metals occupying soil. Plant development, treatment, and upgradation of soil indispensably require such parameters. Plant's development and dissolution of heavy metals necessitate redox-potential and pH of soil. Variation in soil's pH could be acquired after modification with iron-manganese-improved biochar, i.e., pH decreased with alteration and was debuted by Lin et al. (2019a). Therefore, evolution and character of arsenic exist in soil greatly influenced by iron-manganese-improved biochar. Further, performance of soil inhabiting microbes was detected to be disturbed owing to soil's elevated redox potential. With the administration of iron-manganese-improved biochar, organic texture, leftover constituents, and iron-manganese oxides were originated from replaceable arsenic. A betterment in enzymatic performance was noticed with iron-manganese-improved biochar implication. Bioavailability of Proteobacteria and Firmicutes increased and of Bacteroidetes diminished when arsenic

polluted soil was indemnified with iron-manganese-improved biochar. Zhou et al. (2018b) demonstrated aggregated-biomass owing to higher accumulation of amino acids in rice after modification with FMBC. Mobility and transference of cadmium were agitated with elevation of pH value from 0.2 to 1.0 by means of FMBC adaptation. Furthermore, replaceable cadmium could be decreased by implying FMBC alteration and modifying unconsumed scrap afterwards. Rice roots were observed with ferromanganese panel after remediation by means of FMBC. Soil-evolving chromium was remarkably disturbed after indemnification with nZVI@BC and was introduced by Su et al. (2016b). Following alteration, harmless and secure products, e.g., iron-manganese-oxide-tied and organic-matter-tied chromium are generated from replaceable and CO_3^{2-}-bound chromium. Corrosion of Fe (0) and chromium (VI) are reduced with nZVI@BC implication resulting in increment in pH of soil. Besides, bioavailability of cabbage and soil prolificacy has raised after restitution with nZVI@BC. Currently, biochar-based NPs of $FePO_4$ application to crops increase profit and enhanced fertility through soil renovation from cadmium pollution resulting in its diminished toxic effect (Qiao et al., 2017). Moreover, mustard and cabbage encounter less cadmium bio-aggregation after indemnification. Following regular variation in redox properties (Beiyuan et al., 2017) applied dust of pine-wood-biochar to soil for analyzing phyto-availability and transportation of arsenic in order to treat paddy fields. In paddy fields, phyto-availability and transportation of arsenic was influenced by means of alteration in redox-potential (EH). Arsenic portability is promoted at lower EH environment.

7.7 Heavy metals elimination via adsorption

First of all, nano-SiO_2 NCs improved with 2,4-dinitrophenylhydrazine were the compounds utilized for adsorbing heavy metal ions simultaneously (Afkhami et al., 2010). Mn (II), Ni (II), Co (II), Cr (III), Cd (II) and Pb (II) metal ions were analyzed for their adsorbing capacities. Although, just three metal ions were detected to have maximum adsorption abilities, i.e., lead showed 100.0 mg/g, cadmium had 83.3 mg/g and chromium exhibited 100.0 mg/g and were calculated by Afkhami et al. (2010). NPs of MgO displayed optimum adsorbing capability, for example, lead exhibited 2614 mg/g and cadmium showed 2294 mg/g (Xiong et al., 2015). Moreover, improved adsorbing capacity was demonstrated by 2,4-dinitrophenylhydeazine without any modification in the structure (Afkhami et al., 2010; Xiong et al., 2015). However (Afkhami et al., 2010), perceived lower adsorbabilities in contrast to MgO together with nano-SiO_2-improved 2,4-dinitrophenylhydrazine. A combative attraction order for ions of cadmium and lead is: Pb(II) > Cd(II), and was presented by Xiong et al. (2015). In 2014, Wang et al. implied NPs of Fe_3O_4 and presented combative adsorbability of metal ions like chromium (III) and lead (II). Lead (II) elimination was predominantly reduced to 41.4% from 80.6% in chromium (III) environment. In particular, existence of lead (II), chromium (III) experiences minute decrement from 42.4% to 38.5% (Wang et al., 2014). On the whole, cadmium (II) showed less attraction for NPs than lead (II). Reusable NPs of chitosan-$CH_3CH(CH_2)CH(O)CH_2OH$, for instance, were administered for concurrent removal of nickel (II), cadmium (II), and lea (II), and their relevant affinity sequence is: Pb > Cd > Ni (Heidari et al., 2013). Nevertheless,

lower adsobabilities have been observed in comparison to pre-described reports for nickel, cadmium, and lead which are calculated to be 0.87 mg/g, 1.84 mg/g, and 11.30 mg/g, respectively (Heidari et al., 2013). Sepiolite was dispensed for promptly adsorbing cadmium (II) using uranium (V) and radio-nuclide with the collective help of framework and operation research (Huang et al., 2015b). 16.32 mg/g of uranium (V) and 27.78 mg/g of cadmium (II) sorped efficiently through Sepiolite that is relatively high. NMs are also used in aqueous solutions to eliminate bivalent arsenate ions having oxidation states of (III) and (V) (Luo et al., 2013). Although, comparatively little variability was noticed in adsorbing capability values of arsenate (III) and (V). NPs of graphene oxi-dehydrated ZrO_2 were operated in purification of drinking water from arsenic (III) and (V) while their respective adsobabilities were 95.15 mg/g and 84.89 mg/g (Luo et al., 2013). Adsorbing agents as NPs engenders lower adsorbability distinction for simultaneously occurring anions with superior anti-intervention. Besides extraordinary recycling efficiency, 0.002 mg/L thickness was achieved using graphene oxi-dehydrated ZrO_2 NCs which is fairly lesser than 10 mg/L, the desired value of Maximum-Contaminant-Level (MCL), reported by Luo et al. (2013). Drinkable water resources frequently coexist AsO_4^{3-} and $Cr_2O_7^{2-}$ as vital poly-atomic pollutants. $Cu_2(CO_3)(OH)_2$ NPs were employed to inhibit and check AsO_4^{3-} and $Cr_2O_7^{2-}$ simultaneously (Saikia et al., 2011), with 57.1 mg/g and 82.2 mg/g, correspondingly, as optimal adsorbing capability. By way of comparative research study, in contrast to $Cr_2O_7^{2-}$, lower adsorption was noticed on exterior of NP of $Cu_2(CO_3)(OH)_2$ with AsO_4^{3-}. Altogether adsorption-efficiencies (%) for uni-systems are detected higher, i.e., AsO_4^{3-} approximately 66% and $Cr_2O_7^{2-}$ 75% as compared to binary compounds, i.e., AsO_4^{3-} approximately 61% and $Cr_2O_7^{2-}$ 70% on account of hydrophilic $Cu_2(CO_3)(OH)_2$-supported NPs having comparative attachment of AsO_4^{3-} and $Cr_2O_7^{2-}$ anions (Saikia et al., 2011). In 2014, Su et al. scrutinized nanoscale zero-valent iron (nZVI) was for application in groundwater to eliminate Cd and NO_3^- pollutants. NO^{2-} environment denoted for 188 mg/g increment in Cd separation capability of nZVI from 40 mg/g. In addition, nZVI showed increased separation capacity for NO^{2-} to 100% from 30% in cadmium environment. Although, there is inverse concentration relation of Cd^{2+} and NO^{2-}. The yield of NO_2^- is decreased from 20% to just 3% after 1 wt% gold doping of nZVI (Su et al., 2016b).

7.8 Heavy metals removal through photocatalysis

Following photocatalytic mechanism, rate and penetration of contaminant's degradability could be remarkably enhanced (Prihod'ko and Soboleva, 2013). Light-initiated and aided degeneration of contaminants is termed as photocatalysis (Bora and Dutta, 2014). Reactive-radicals production associated with photo-instigated or photo-aided degeneration of pollutants is the backbone of fundamental oxidation-reaction methodology (Sillanpää et al., 2018). In water, the basic-chemistry and procedure involved in contaminants removal by way of photo-decaying or solar-energy is well described and apprehended in various review reports (Bora and Dutta, 2014; Sillanpää et al., 2018). Thus, this discussion does not include duplication. Different photochemical reactions and methodologies are packed in indiscriminate title of advanced oxidation processes (AOPs). Cleaning and remediation of water are being achieved by NPs-supported

AOPs to control water dearth (Bora and Dutta, 2014; Sillanpää et al., 2018). Consequently, many enhanced oxidation processes (EOPs) and advanced oxidation technologies (AOTs) supported on AOP-related NPs were fabricated for elimination of contaminants. Herein, a brief classification of EOPs and AOTs based on NPs has been described, relying on the nature of reactive-radicals production, for remediation of wastewater:

1. Wastewater remediation via ultraviolet and heterogeneous-semiconductors,
2. Catalysis using light,
3. Ozonation through photocatalysis,
4. Photo-Fenton and Fenton reactions,
5. AOP technique in the absence of light; consisting electro-Fenton reaction and SO_4^{2-}-supported AOPs.

Many endeavors are in practice applying NCs and NMs for making degeneration of concurrent contaminants better through photocatalysis, however, a number of reports are already mentioned in literature.

7.9 Photo-Fenton and Fenton reactions

Solar/light radiance along with acidic environment are required to produce OH^--radicals in the presence of catalytic Fe^{2+}-ions and hydrogen peroxide as oxidizing agent constitute photo-Fenton process which is a kind of advanced oxidation processes (AOPs). Fenton-reaction is above reaction in the absence of solar radiance (Sillanpää et al., 2018). Assorted research collections distinctly indicated elimination of independent contaminants, e.g., 2,4-dichlorophenol, enacting NPs being catalyzing agents of miscellaneous photo-Fenton or/and Fenton (Guo et al., 2017), $C_8H_{14}ClN_5$ (Benzaquén et al., 2017), methylene-blue (Chen et al., 2016), methyl orange (Xu et al., 2018), pentachlorophenol (ThanhThuy et al., 2013), rhodamine-B (Chen et al., 2013), and TBBPA (An et al., 2013a). Currently, separation of multiple contaminants by NPs with miscellaneous photo Fenton or/and Fenton was explained tremendously. Nonetheless, there is no perfect apprehension of multiple contaminants remediated "simultaneously" in the given literature. There is ambiguity in execution of single constituent procedure and synchronous elimination for multiple contaminants, however, NPs' degrading proficiency and miscellaneous catalytic ability of photo-Fenton or/and Fenton of NPs have been well elaborated in research reviews(An et al., 2013b), for instance, reported decaying efficacy of 3 mmol per liter at 2.01×10^{-2} per minute, 10 μmol per liter at 5.56×10^{-2} per minute, and 30 μmol per liter at 2.21×10^{-2} per minute by introducing NPs of bismuth ferrite for excellent degeneration. Visible-light and UV radiance exposure were dispensed for phenol and methyl-orange degradation using triple-heterojunctioned NMs of $TiO_2/Fe_2TiO_5/Fe_2O_3$ as photo-Fenton catalyst (Deng et al., 2017). Photocatalytic and adsorptive capabilities twain independently and unified form have gained noticeable interest for purification of wastewater/water (Pi et al., 2018). The execution speed of eliminating/degrading contaminants has been improved by collective implication of photocatalytic and adsorptive effects (Pi et al., 2018). In-depth analysis put constraint of water refinement of

mono-contaminant instead of combined contaminants (Mu et al., 2017). Nevertheless, simultaneous remediation of wastewater/water for not only mono-contaminant administration but also multi-contaminant modulation, photocatalytic and adsorptive properties have been combinedly imposed, e.g., (1) organic contaminants and heavy metals (Benjwal and Kar, 2015), and (2) poly-organic contaminants (Chen et al., 2017). Integrating the adsorptive effect of NCs of titania-activated carbon-carbonized epoxy (TiO_2/AC/CE) in water, methylene-blue as organic-dye, lead (II) and inorganic heavy metals adsorbed or decayed concomitantly (Benjwal and Kar, 2015). Pristine-titanium oxide adsorbed approximately 2% while titanium oxide/AC/CE adsorbed 26% of methylene-blue. Generally, water has been purified from methylene-blue (approx.-90%) and lead (II) (approx.-97%) by implementing NCs of titanium oxide/AC/CE rather using sole titanium oxide which displayed lower efficiency (Benjwal and Kar, 2015). In addition, As (poisonous metal) and ibuprofen (medicinal) were removed utilizing NCs of zinc-iron combined metal oxide while adsorptive and photocatalytic effects were applied for efficient synchronous elimination of organic contaminants and metal ions (Di et al., 2017). Ibuprofen showed degradation efficiency of 95.7% and As exhibited 176.3 mg/g optimal adsorbability when exposed to NCs of zinc-iron combined metal oxide in single constituent approach, while solar-source radiance was used during estimation of elimination capabilities for coexistent multi-contaminants. In comparison to As moieties, ibuprofen degeneration is lower, however, removing efficiency of As was not changed with any obvious effect (Di et al., 2017). However, water occupying poisonous and medicinal coetaneous contaminants were simultaneously eliminated by applying NCs of zinc-iron metal oxide as NMs with N 85% performance (Di et al., 2017). In 2017, NCs of ZnO and oligoaniline were applied by Chen et al. (2017). In synchronous degeneration of congo red, rhodamine B, and methylene-blue for estimating degeneration through photocatalysis affected by adsorption. Following photocatalytic approach succeeding concurrent adsorption, NPs constituting ZnO lacking oligoaniline showed lower catalysis degeneration rate in comparison to NCs comprising ZnO along with oligoaniline in degeneration of dye. A harmony has observed betwixt photocatalytic constituent and adsorbent constituent existing in NCs. In addition, catalyst is noticed with a complementary aid of adsorbent. Nonetheless, in the course of coexistent photocatalytic and adsorptive reaction, owing to decrement in degradability for Congo-red, zinc oxide-oligoaniline NCs specification was not favorable for estimating photocatalytic activity on account of adsorptive activity (Chen et al., 2017).

7.10 Conclusions and future perspectives

Advancement in nanotechnology provides new horizons for development of cost-effective, efficient, and environment friendly nanomaterials. Different nanomaterials have been comprehensively exploited for removal of heavy metals from wastewater. Nanomaterials have excellent features as novel structural and surface characteristics which made them valuable for purification of wastewater. Nanomaterials are excellent sorbents and they have capability to remove ions of heavy metals even at low concentration with high specificity, great selectivity, and high adsorption potential. In this review different

nanomaterials including metal-based nanomaterials, metal oxide-based nanomaterials, biochar-based nanomaterials, and their significant applications in removal of heavy metals from wastewater have been discussed in detail. Still there exist few bottlenecks that direly needed to be overcome to make them excellent in wastewater purification. Most of the nanomaterials tend to aggregate and this decreases their removal potential and their separation from aqueous media is difficult due to nano-size. The nanocomposite seems potent to solve this issue. Still there is a need to pay attention to commercialize the employment of nanomaterials on industrial scale for wastewater purification. Nanomaterials are not available in market so efforts should be paid to develop nanomaterials which can be easily available in market. Attention should be paid to synthesize nanomaterials by employing green chemistry and their cost should be effective. The impact of nanomaterials and toxicities should be taken into consideration by keeping in view the human health and environment. It is also important to synthesize recyclable, cost-effective nanomaterials for their wide applications in daily life. Additionally, different technologies should be developed for water treatment to meet the environmental pollution.

References

Abuhatab, S., El-Qanni, A., Al-Qalaq, H., Hmoudah, M., Al-Zerei, W., 2020. Effective adsorptive removal of Zn2+, Cu2+, and Cr3+ heavy metals from aqueous solutions using silica-based embedded with NiO and MgO nanoparticles. J. Environ. Manag. 268, 110713. https://doi.org/10.1016/j.jenvman.2020.110713.

Achudume, A.C., 2009. The effect of petrochemical effluent on the water quality of Ubeji Creek in Niger Delta of Nigeria. Bull. Environ. Contam. Toxicol. 83 (3), 410–415. https://doi.org/10.1007/s00128-009-9736-2.

Afkhami, A., Saber-Tehrani, M., Bagheri, H., 2010. Simultaneous removal of heavy-metal ions in wastewater samples using nano-alumina modified with 2,4-dinitrophenylhydrazine. J. Hazard. Mater. 181 (1), 836–844. https://doi.org/10.1016/j.jhazmat.2010.05.089.

An, J., Zhu, L., Wang, N., Song, Z., Yang, Z., Du, D., Tang, H., 2013a. Photo-Fenton like degradation of tetrabromobisphenol A with grapheneBiFeO3 composite as a catalyst. Chem. Eng. J. 219, 225–237. https://doi.org/10.1016/j.cej.2013.01.013.

An, J., Zhu, L., Zhang, Y., Tang, H., 2013b. Efficient visible light photo-Fenton-like degradation of organic pollutants using in situ surface-modified BiFeO3 as a catalyst. J. Environ. Sci. 25 (6), 1213–1225. https://doi.org/10.1016/S1001-0742(12)60172-7.

Bagheri, A.R., Ghaedi, M., 2020. Green preparation of dual-template chitosan-based magnetic water-compatible molecularly imprinted biopolymer. Carbohydr. Polym., 116102.

Bagheri, A.R., Ghaedi, M., Asfaram, A., Bazrafshan, A.A., Jannesar, R., 2017. Comparative study on ultrasonic assisted adsorption of dyes from single system onto Fe3O4 magnetite nanoparticles loaded on activated carbon: experimental design methodology. Ultrason. Sonochem. 34, 294–304.

Bagheri, A.R., Arabi, M., Ghaedi, M., Ostovan, A., Wang, X., Li, J., Chen, L., 2019. Dummy molecularly imprinted polymers based on a green synthesis strategy for magnetic solid-phase extraction of acrylamide in food samples. Talanta 195, 390–400.

Beiyuan, J., Awad, Y.M., Beckers, F., Tsang, D.C.W., Ok, Y.S., Rinklebe, J., 2017. Mobility and phytoavailability of As and Pb in a contaminated soil using pine sawdust biochar under systematic change of redox conditions. Chemosphere 178, 110–118. https://doi.org/10.1016/j.chemosphere.2017.03.022.

Benjwal, P., Kar, K.K., 2015. Simultaneous photocatalysis and adsorption based removal of inorganic and organic impurities from water by titania/activated carbon/carbonized epoxy nanocomposite. J. Environ. Chem. Eng. 3 (3), 2076–2083. https://doi.org/10.1016/j.jece.2015.07.009.

Benzaquén, T.B., Cuello, N.I., Alfano, O.M., Eimer, G.A., 2017. Degradation of atrazine over a heterogeneous photo-fenton process with iron modified MCM-41 materials. Catal. Today 296, 51–58. https://doi.org/10.1016/j.cattod.2017.04.021.

Bian, L., Nie, J., Jiang, X., Song, M., Dong, F., Li, W., Xu, B., 2018. Selective removal of uranyl from aqueous solutions containing a mix of toxic metal ions using core–shell MFe2O4–TiO2 nanoparticles of montmorillonite edge sites. ACS Sustain. Chem. Eng. 6 (12), 16267–16278.

Bilal, M., Rasheed, T., Mehmood, S., Tang, H., Ferreira, L.F.R., Bharagava, R.N., Iqbal, H.M.N., 2020. Mitigation of environmentally-related hazardous pollutants from water matrices using nanostructured materials – a review. Chemosphere 253, 126770. https://doi.org/10.1016/j.chemosphere.2020.126770.

Bokare, V., Jung, J.-l., Chang, Y.-Y., Chang, Y.-S., 2013. Reductive dechlorination of octachlorodibenzo-p-dioxin by nanosized zero-valent zinc: modeling of rate kinetics and congener profile. J. Hazard. Mater. 250, 397–402.

Bora, T., Dutta, J., 2014. Applications of nanotechnology in wastewater treatment: a review. J. Nanosci. Nanotechnol. 14 (1), 613–626. https://doi.org/10.1166/jnn.2014.8898.

Cai, Y., Li, C., Wu, D., Wang, W., Tan, F., Wang, X., Qiao, X., 2017. Highly active MgO nanoparticles for simultaneous bacterial inactivation and heavy metal removal from aqueous solution. Chem. Eng. J. 312, 158–166. https://doi.org/10.1016/j.cej.2016.11.134.

Chaussemier, M., Pourmohtasham, E., Gelus, D., Pécoul, N., Perrot, H., Lédion, J., Horner, O., 2015. State of art of natural inhibitors of calcium carbonate scaling. A review article. Desalination 356, 47–55. https://doi.org/10.1016/j.desal.2014.10.014.

Chen, Q., Ji, F., Liu, T., Yan, P., Guan, W., Xu, X., 2013. Synergistic effect of bifunctional Co–TiO2 catalyst on degradation of rhodamine B: Fenton-photo hybrid process. Chem. Eng. J. 229, 57–65. https://doi.org/10.1016/j.cej.2013.04.024.

Chen, W., Yang, X., Huang, J., Zhu, Y., Zhou, Y., Yao, Y., Li, C., 2016. Iron oxide containing graphene/carbon nanotube based carbon aerogel as an efficient E-Fenton cathode for the degradation of methyl blue. Electrochim. Acta 200, 75–83. https://doi.org/10.1016/j.electacta.2016.03.044.

Chen, M., Bao, C., Cun, T., Huang, Q., 2017. One-pot synthesis of ZnO/oligoaniline nanocomposites with improved removal of organic dyes in water: effect of adsorption on photocatalytic degradation. Mater. Res. Bull. 95, 459–467. https://doi.org/10.1016/j.materresbull.2017.08.017.

Cundy, A.B., Hopkinson, L., Whitby, R.L., 2008. Use of iron-based technologies in contaminated land and groundwater remediation: a review. Sci. Total Environ. 400 (1–3), 42–51.

Deng, Y., Xing, M., Zhang, J., 2017. An advanced TiO2/Fe2TiO5/Fe2O3 triple-heterojunction with enhanced and stable visible-light-driven Fenton reaction for the removal of organic pollutants. Appl. Catal. B Environ. 211, 157–166. https://doi.org/10.1016/j.apcatb.2017.04.037.

Di, G., Zhu, Z., Zhang, H., Zhu, J., Lu, H., Zhang, W., Küppers, S., 2017. Simultaneous removal of several pharmaceuticals and arsenic on Zn-Fe mixed metal oxides: combination of photocatalysis and adsorption. Chem. Eng. J. 328, 141–151. https://doi.org/10.1016/j.cej.2017.06.112.

Fan, Y., Liu, Z., Zhan, J., 2009. Synthesis of starch-stabilized Ag nanoparticles and Hg 2+ recognition in aqueous media. Nanoscale Res. Lett. 4 (10), 1230.

Fu, F., Dionysiou, D.D., Liu, H., 2014. The use of zero-valent iron for groundwater remediation and wastewater treatment: a review. J. Hazard. Mater. 267, 194–205.

Gebru, K.A., Das, C., 2018. Removal of chromium (VI) ions from aqueous solutions using amine-impregnated TiO2 nanoparticles modified cellulose acetate membranes. Chemosphere 191, 673–684.

Gholami, H., Arabi, M., Ghaedi, M., Ostovan, A., Bagheri, A.R., 2019. Column packing elimination in matrix solid phase dispersion by using water compatible magnetic molecularly imprinted polymer for recognition of melamine from milk samples. J. Chromatogr. A 1594, 13–22.

Giles, D.E., Mohapatra, M., Issa, T.B., Anand, S., Singh, P., 2011. Iron and aluminium based adsorption strategies for removing arsenic from water. J. Environ. Manag. 92 (12), 3011–3022.

Goel, G., Kaur, S., 2012. A study on chemical contamination of water due to household laundry detergents. J. Hum. Ecol. 38 (1), 65–69. https://doi.org/10.1080/09709274.2012.11906475.

Gopal, K., Tripathy, S.S., Bersillon, J.L., Dubey, S.P., 2007. Chlorination byproducts, their toxicodynamics and removal from drinking water. J. Hazard. Mater. 140 (1), 1–6. https://doi.org/10.1016/j.jhazmat.2006.10.063.

Guo, M., Weng, X., Wang, T., Chen, Z., 2017. Biosynthesized iron-based nanoparticles used as a heterogeneous catalyst for the removal of 2,4-dichlorophenol. Sep. Purif. Technol. 175, 222–228. https://doi.org/10.1016/j.seppur.2016.11.042.

Hayat, H., Mahmood, Q., Pervez, A., Bhatti, Z.A., Baig, S.A., 2015. Comparative decolorization of dyes in textile wastewater using biological and chemical treatment. Sep. Purif. Technol. 154, 149–153. https://doi.org/10.1016/j.seppur.2015.09.025.

He, R., Yuan, X., Huang, Z., Wang, H., Jiang, L., Huang, J., Li, H., 2019. Activated biochar with iron-loading and its application in removing Cr (VI) from aqueous solution. Colloids Surf. A Physicochem. Eng. Asp. 579, 123642. https://doi.org/10.1016/j.colsurfa.2019.123642.

Heidari, A., Younesi, H., Mehraban, Z., Heikkinen, H., 2013. Selective adsorption of Pb(II), Cd(II), and Ni(II) ions from aqueous solution using chitosan–MAA nanoparticles. Int. J. Biol. Macromol. 61, 251–263. https://doi.org/10.1016/j.ijbiomac.2013.06.032.

Hernández, F., Ibáñez, M., Portolés, T., Cervera, M.I., Sancho, J.V., López, F.J., 2015. Advancing towards universal screening for organic pollutants in waters. J. Hazard. Mater. 282, 86–95. https://doi.org/10.1016/j.jhazmat.2014.08.006.

Huang, P., Ye, Z., Xie, W., Chen, Q., Li, J., Xu, Z., Yao, M., 2013. Rapid magnetic removal of aqueous heavy metals and their relevant mechanisms using nanoscale zero valent iron (nZVI) particles. Water Res. 47 (12), 4050–4058.

Huang, D.-L., Chen, G.-M., Zeng, G.-M., Xu, P., Yan, M., Lai, C., He, X.-X., 2015a. Synthesis and application of modified zero-valent iron nanoparticles for removal of hexavalent chromium from wastewater. Water Air Soil Pollut. 226 (11), 375.

Huang, J., Wu, Z., Chen, L., Sun, Y., 2015b. The sorption of Cd(II) and U(VI) on sepiolite: a combined experimental and modeling studies. J. Mol. Liq. 209, 706–712. https://doi.org/10.1016/j.molliq.2015.05.047.

Iannone, F., Casiello, M., Monopoli, A., Cotugno, P., Sportelli, M.C., Picca, R.A., Nacci, A., 2017. Ionic liquids/ZnO nanoparticles as recyclable catalyst for polycarbonate depolymerization. J. Mol. Catal. A Chem. 426, 107–116.

Ibrahim, Y., Abdulkarem, E., Naddeo, V., Banat, F., Hasan, S.W., 2019. Synthesis of super hydrophilic cellulose-alpha zirconium phosphate ion exchange membrane via surface coating for the removal of heavy metals from wastewater. Sci. Total Environ. 690, 167–180.

Inglezakis, V.J., Loizidou, M.D., Grigoropoulou, H.P., 2002. Equilibrium and kinetic ion exchange studies of Pb2+, Cr3+, Fe3+ and Cu2+ on natural clinoptilolite. Water Res. 36 (11), 2784–2792. https://doi.org/10.1016/S0043-1354(01)00504-8.

Ishii, S., Ksoll, W.B., Hicks, R.E., Sadowsky, M.J., 2006. Presence and growth of naturalized *Escherichia coli* in temperate soils from Lake Superior watersheds. Appl. Environ. Microbiol. 72 (1), 612–621. https://doi.org/10.1128/aem.72.1.612-621.2006.

Jelić, A., Petrović, M., Barceló, D., 2012. Pharmaceuticals in drinking water. In: Barceló, D. (Ed.), Emerging Organic Contaminants and Human Health. Springer Berlin Heidelberg, Berlin, Heidelberg, pp. 47–70.

Justeau, C., Vela-Gonzalez, A.V., Jourdan, A., Riess, J.G., Krafft, M.P., 2018. Adsorption of cerium salts and cerium oxide nanoparticles on microbubbles can be induced by a fluorocarbon gas. ACS Sustain. Chem. Eng. 6 (9), 11450–11456.

Kemp, K., Griffiths, J., Campbell, S., Lovell, K., 2013. An exploration of the follow-up up needs of patients with inflammatory bowel disease. J. Crohn's Colitis 7 (9), e386–e395. https://doi.org/10.1016/j.crohns.2013.03.001.

Khatami, M., Varma, R.S., Zafarnia, N., Yaghoobi, H., Sarani, M., Kumar, V.G., 2018. Applications of green synthesized Ag, ZnO and Ag/ZnO nanoparticles for making clinical antimicrobial wound-healing bandages. Sustain. Chem. Pharm. 10, 9–15.

Kumar, R., Kumar, R., Kushwaha, N., Mittal, J., 2016. Ammonia gas sensing using thin film of MnO2 nanofibers. IEEE Sensors J. 16 (12), 4691–4695.

Lajayer, B.A., Najafi, N., Moghiseh, E., Mosaferi, M., Hadian, J., 2018. Removal of heavy metals (Cu 2+ and Cd 2+) from effluent using gamma irradiation, titanium dioxide nanoparticles and methanol. J. Nanostruct. Chem. 8 (4), 483–496.

Lee, C.S., Robinson, J., Chong, M.F., 2014. A review on application of flocculants in wastewater treatment. Process Saf. Environ. Prot. 92 (6), 489–508. https://doi.org/10.1016/j.psep.2014.04.010.

Lin, L., Gao, M., Qiu, W., Wang, D., Huang, Q., Song, Z., 2017. Reduced arsenic accumulation in indica rice (Oryza sativa L.) cultivar with ferromanganese oxide impregnated biochar composites amendments. Environ. Pollut. 231, 479–486. https://doi.org/10.1016/j.envpol.2017.08.001.

Lin, L., Li, Z., Liu, X., Qiu, W., Song, Z., 2019a. Effects of Fe-Mn modified biochar composite treatment on the properties of As-polluted paddy soil. Environ. Pollut. 244, 600–607. https://doi.org/10.1016/j.envpol.2018.10.011.

Lin, L., Song, Z., Khan, Z.H., Liu, X., Qiu, W., 2019b. Enhanced As(III) removal from aqueous solution by Fe-Mn-La-impregnated biochar composites. Sci. Total Environ. 686, 1185–1193. https://doi.org/10.1016/j.scitotenv.2019.05.480.

Lisha, K., Pradeep, T., 2009. Towards a practical solution for removing inorganic mercury from drinking water using gold nanoparticles. Gold Bull. 42 (2), 144–152.

Liu, T., Wang, Z.-L., Sun, Y., 2015. Manipulating the morphology of nanoscale zero-valent iron on pumice for removal of heavy metals from wastewater. Chem. Eng. J. 263, 55–61.
Liu, C.-M., Diao, Z.-H., Huo, W.-Y., Kong, L.-J., Du, J.-J., 2018. Simultaneous removal of Cu2+ and bisphenol A by a novel biochar-supported zero valent iron from aqueous solution: synthesis, reactivity and mechanism. Environ. Pollut. 239, 698–705. https://doi.org/10.1016/j.envpol.2018.04.084.
Liu, J., Jiang, J., Meng, Y., Aihemaiti, A., Xu, Y., Xiang, H., Chen, X., 2020. Preparation, environmental application and prospect of biochar-supported metal nanoparticles: a review. J. Hazard. Mater. 388, 122026.
Lofrano, G., Brown, J., 2010. Wastewater management through the ages: a history of mankind. Sci. Total Environ. 408 (22), 5254–5264. https://doi.org/10.1016/j.scitotenv.2010.07.062.
Lu, L., Shan, R., Shi, Y., Wang, S., Yuan, H., 2019. A novel TiO2/biochar composite catalysts for photocatalytic degradation of methyl orange. Chemosphere 222, 391–398. https://doi.org/10.1016/j.chemosphere.2019.01.132.
Luo, J., Zhang, Q., Garcia-Martinez, J., Suib, S.L., 2008. Adsorptive and acidic properties, reversible lattice oxygen evolution, and catalytic mechanism of cryptomelane-type manganese oxides as oxidation catalysts. J. Am. Chem. Soc. 130 (10), 3198–3207.
Luo, X., Wang, C., Wang, L., Deng, F., Luo, S., Tu, X., Au, C., 2013. Nanocomposites of graphene oxide-hydrated zirconium oxide for simultaneous removal of As(III) and As(V) from water. Chem. Eng. J. 220, 98–106. https://doi.org/10.1016/j.cej.2013.01.017.
Lyu, H., Tang, J., Huang, Y., Gai, L., Zeng, E.Y., Liber, K., Gong, Y., 2017. Removal of hexavalent chromium from aqueous solutions by a novel biochar supported nanoscale iron sulfide composite. Chem. Eng. J. 322, 516–524. https://doi.org/10.1016/j.cej.2017.04.058.
Mahanty, S., Chatterjee, S., Ghosh, S., Tudu, P., Gaine, T., Bakshi, M., Chaudhuri, P., 2020. Synergistic approach towards the sustainable management of heavy metals in wastewater using mycosynthesized iron oxide nanoparticles: biofabrication, adsorptive dynamics and chemometric modeling study. J. Water Process Eng. 37, 101426. https://doi.org/10.1016/j.jwpe.2020.101426.
Mahdavi, S., Amini, N., Merrikhpour, H., Akhzari, D., 2017. Characterization of bare and modified nano-zirconium oxide (ZrO2) and their applications as adsorbents for the removal of bivalent heavy metals. Korean J. Chem. Eng. 34 (1), 234–244. https://doi.org/10.1007/s11814-016-0259-3.
Mahmoud, M.E., Saleh, M.M., Zaki, M.M., Nabil, G.M., 2020. A sustainable nanocomposite for removal of heavy metals from water based on crosslinked sodium alginate with iron oxide waste material from steel industry. J. Environ. Chem. Eng. 8 (4), 104015. https://doi.org/10.1016/j.jece.2020.104015.
Medhi, R., Marquez, M.D., Lee, T.R., 2020. Visible-light-active doped metal oxide nanoparticles: review of their synthesis, properties, and applications. ACS Appl. Nano Mater. 3 (7), 6156–6185. https://doi.org/10.1021/acsanm.0c01035.
Mu, C., Zhang, Y., Cui, W., Liang, Y., Zhu, Y., 2017. Removal of bisphenol A over a separation free 3D Ag3PO4-graphene hydrogel via an adsorption-photocatalysis synergy. Appl. Catal. B Environ. 212, 41–49. https://doi.org/10.1016/j.apcatb.2017.04.018.
Nguyen, D.T.C., Dang, H.H., Vo, D.-V.N., Bach, L.G., Nguyen, T.D., Van Tran, T., 2020. Biogenic synthesis of MgO nanoparticles from different extracts (flower, bark, leaf) of Tecoma stans (L.) and their utilization in selected organic dyes treatment. J. Hazard. Mater. 404, 124146.
O'Carroll, D., Sleep, B., Krol, M., Boparai, H., Kocur, C., 2013. Nanoscale zero valent iron and bimetallic particles for contaminated site remediation. Adv. Water Resour. 51, 104–122.
Ojea-Jiménez, I., López, X., Arbiol, J., Puntes, V., 2012. Citrate-coated gold nanoparticles as smart scavengers for mercury (II) removal from polluted waters. ACS Nano 6 (3), 2253–2260.
Oller, I., Malato, S., Sánchez-Pérez, J.A., 2011. Combination of advanced oxidation processes and biological treatments for wastewater decontamination—a review. Sci. Total Environ. 409 (20), 4141–4166. https://doi.org/10.1016/j.scitotenv.2010.08.061.
Pi, Y., Li, X., Xia, Q., Wu, J., Li, Y., Xiao, J., Li, Z., 2018. Adsorptive and photocatalytic removal of persistent organic pollutants (POPs) in water by metal-organic frameworks (MOFs). Chem. Eng. J. 337, 351–371. https://doi.org/10.1016/j.cej.2017.12.092.
Prabhakar, R., Samadder, S.R., 2018. Low cost and easy synthesis of aluminium oxide nanoparticles for arsenite removal from groundwater: a complete batch study. J. Mol. Liq. 250, 192–201. https://doi.org/10.1016/j.molliq.2017.11.173.
Pradhan, N., Pal, A., Pal, T., 2002. Silver nanoparticle catalyzed reduction of aromatic nitro compounds. Colloids Surf. A Physicochem. Eng. Asp. 196 (2–3), 247–257.

Prihod'ko, R.V., Soboleva, N.M., 2013. Photocatalysis: oxidative processes in water treatment. J. Chem. 2013, 168701. https://doi.org/10.1155/2013/168701.

Qiao, Y., Wu, J., Xu, Y., Fang, Z., Zheng, L., Cheng, W., Zhao, D., 2017. Remediation of cadmium in soil by biochar-supported iron phosphate nanoparticles. Ecol. Eng. 106, 515–522. https://doi.org/10.1016/j.ecoleng.2017.06.023.

Rajendran, M., Shi, L., Wu, C., Li, W., An, W., Liu, Z., Xue, S., 2019. Effect of sulfur and sulfur-iron modified biochar on cadmium availability and transfer in the soil–rice system. Chemosphere 222, 314–322. https://doi.org/10.1016/j.chemosphere.2019.01.149.

Rasheed, T., Nabeel, F., 2019. Luminescent metal-organic frameworks as potential sensory materials for various environmental toxic agents. Coord. Chem. Rev. 401, 213065. https://doi.org/10.1016/j.ccr.2019.213065.

Rasheed, T., Bilal, M., Nabeel, F., Iqbal, H.M., Li, C., Zhou, Y., 2018a. Fluorescent sensor based models for the detection of environmentally-related toxic heavy metals. Sci. Total Environ. 615, 476–485.

Rasheed, T., Li, C., Bilal, M., Yu, C., Iqbal, H.M., 2018b. Potentially toxic elements and environmentally-related pollutants recognition using colorimetric and ratiometric fluorescent probes. Sci. Total Environ. 640, 174–193.

Rasheed, T., Li, C., Fu, L., Nabeel, F., Yu, C., Gong, L., Zhou, Y., 2018c. Development and characterization of newly engineered chemosensor with intracellular monitoring potentialities and lowest detection of toxic elements. J. Mol. Liq. 272, 440–449. https://doi.org/10.1016/j.molliq.2018.09.112.

Rasheed, T., Li, C., Nabeel, F., Qi, M., Zhang, Y., Yu, C., 2018d. Real-time probing of mercury using an efficient "turn-on" strategy with potential as in-field mapping kit and in live cell imaging. New J. Chem. 42 (13), 10940–10946. https://doi.org/10.1039/C8NJ01746H.

Rasheed, T., Li, C., Zhang, Y., Nabeel, F., Peng, J., Qi, J., Yu, C., 2018e. Rhodamine-based multianalyte colorimetric probe with potentialities as on-site assay kit and in biological systems. Sensors Actuators B Chem. 258, 115–124. https://doi.org/10.1016/j.snb.2017.11.100.

Rasheed, T., Li, C., Nabeel, F., Huang, W., Zhou, Y., 2019a. Self-assembly of alternating copolymer vesicles for the highly selective, sensitive and visual detection and quantification of aqueous Hg2+. Chem. Eng. J. 358, 101–109. https://doi.org/10.1016/j.cej.2018.09.216.

Rasheed, T., Nabeel, F., Adeel, M., Bilal, M., Iqbal, H.M.N., 2019b. "Turn-on" fluorescent sensor-based probing of toxic Hg(II) and Cu(II) with potential intracellular monitoring. Biocatal. Agric. Biotechnol. 17, 696–701. https://doi.org/10.1016/j.bcab.2019.01.032.

Rasheed, T., Nabeel, F., Adeel, M., Rizwan, K., Bilal, M., Iqbal, H.M.N., 2019c. Carbon nanotubes-based cues: a pathway to future sensing and detection of hazardous pollutants. J. Mol. Liq. 292, 111425. https://doi.org/10.1016/j.molliq.2019.111425.

Rasheed, T., Nabeel, F., Li, C., Bilal, M., 2019d. Rhodamine-assisted fluorescent strategy for the sensitive and selective in-field mapping of environmental pollutant Hg(II) with potential bioimaging. J. Lumin. 208, 519–526. https://doi.org/10.1016/j.jlumin.2019.01.032.

Rasheed, T., Nabeel, F., Li, C., Zhang, Y., 2019e. Rhodol assisted alternating copolymer based chromogenic vesicles for the aqueous detection and quantification of hydrazine via switch-on strategy. J. Mol. Liq. 274, 461–469. https://doi.org/10.1016/j.molliq.2018.11.014.

Rasheed, T., Nabeel, F., Shafi, S., 2019f. Chromogenic vesicles for aqueous detection and quantification of Hg2+/Cu2+ in real water samples. J. Mol. Liq. 282, 489–498. https://doi.org/10.1016/j.molliq.2019.03.048.

Rasheed, T., Nabeel, F., Shafi, S., Bilal, M., Rizwan, K., 2019g. Block copolymer self-assembly mediated aggregation induced emission for selective recognition of picric acid. J. Mol. Liq. 296, 111966. https://doi.org/10.1016/j.molliq.2019.111966.

Rasheed, T., Hassan, A.A., Bilal, M., Hussain, T., Rizwan, K., 2020a. Metal-organic frameworks based adsorbents: a review from removal perspective of various environmental contaminants from wastewater. Chemosphere 259, 127369. https://doi.org/10.1016/j.chemosphere.2020.127369.

Rasheed, T., Rizwan, K., Bilal, M., Iqbal, H.M.N., 2020b. Metal-organic framework-based engineered materials—fundamentals and applications. Molecules 25 (7). https://doi.org/10.3390/molecules25071598.

Richardson, S.D., Plewa, M.J., Wagner, E.D., Schoeny, R., DeMarini, D.M., 2007. Occurrence, genotoxicity, and carcinogenicity of regulated and emerging disinfection by-products in drinking water: a review and roadmap for research. Mutat. Res. Rev. Mutat. Res. 636 (1), 178–242. https://doi.org/10.1016/j.mrrev.2007.09.001.

Rossi, L., Bagheri, M., Zhang, W., Chen, Z., Burken, J.G., Ma, X., 2019. Using artificial neural network to investigate physiological changes and cerium oxide nanoparticles and cadmium uptake by Brassica napus plants. Environ. Pollut. 246, 381–389.

Saikia, J., Saha, B., Das, G., 2011. Efficient removal of chromate and arsenate from individual and mixed system by malachite nanoparticles. J. Hazard. Mater. 186 (1), 575–582. https://doi.org/10.1016/j.jhazmat.2010.11.036.

Salem, I.A., Salem, M.A., El-Ghobashy, M.A., 2017. The dual role of ZnO nanoparticles for efficient capture of heavy metals and acid blue 92 from water. J. Mol. Liq. 248, 527–538. https://doi.org/10.1016/j.molliq.2017.10.060.

Sarkar, B., Chakrabarti, P.P., Vijaykumar, A., Kale, V., 2006. Wastewater treatment in dairy industries—possibility of reuse. Desalination 195 (1), 141–152. https://doi.org/10.1016/j.desal.2005.11.015.

Sawan, S., Maalouf, R., Errachid, A., Jaffrezic-Renault, N., 2020. Metal and metal oxide nanoparticles in the voltammetric detection of heavy metals: a review. TrAC Trends Anal. Chem. 131, 116014. https://doi.org/10.1016/j.trac.2020.116014.

Sedlak, D.L., von Gunten, U., 2011. The chlorine dilemma. Science 331 (6013), 42. https://doi.org/10.1126/science.1196397.

Sengul, A.B., Asmatulu, E., 2020. Toxicity of metal and metal oxide nanoparticles: a review. Environ. Chem. Lett., 1–25.

Seyedi, S.M., Rabiee, H., Shahabadi, S.M.S., Borghei, S.M., 2017. Synthesis of zero-valent iron nanoparticles via electrical wire explosion for efficient removal of heavy metals. CLEAN–Soil Air Water 45 (3), 1600139.

Shang, J., Zong, M., Yu, Y., Kong, X., Du, Q., Liao, Q., 2017. Removal of chromium (VI) from water using nanoscale zerovalent iron particles supported on herb-residue biochar. J. Environ. Manag. 197, 331–337. https://doi.org/10.1016/j.jenvman.2017.03.085.

Sharifan, H., Moore, J., Ma, X., 2020. Zinc oxide (ZnO) nanoparticles elevated iron and copper contents and mitigated the bioavailability of lead and cadmium in different leafy greens. Ecotoxicol. Environ. Saf. 191, 110177.

Shin, M., Lee, H.-J., Kim, M.S., Park, N.-B., Lee, C., 2017. Control of the red tide dinoflagellate Cochlodinium polykrikoides by ozone in seawater. Water Res. 109, 237–244. https://doi.org/10.1016/j.watres.2016.11.050.

Sillanpää, M., Ncibi, M.C., Matilainen, A., 2018. Advanced oxidation processes for the removal of natural organic matter from drinking water sources: a comprehensive review. J. Environ. Manag. 208, 56–76. https://doi.org/10.1016/j.jenvman.2017.12.009.

Silva, M., Murzin, V., Zhang, L., Baltrus, J., Baltrusaitis, J., 2020. Transition metal-doped MgO nanoparticles for nutrient recycling: an alternate Mg source for struvite synthesis from wastewater. Environ. Sci.: Nano 7 (11), 3482–3496.

Singh, K.R.B., Nayak, V., Sarkar, T., Singh, R.P., 2020. Cerium oxide nanoparticles: properties, biosynthesis and biomedical application. RSC Adv. 10 (45), 27194–27214. https://doi.org/10.1039/D0RA04736H.

Sneed, M.C., Brasted, R.C., King, C., 1956. Comprehensive inorganic chemistry. J. Electrochem. Soc. 103 (3), 83C.

Soejima, T., Nishizawa, K., Isoda, R., 2018. Monodisperse manganese oxide nanoparticles: synthesis, characterization, and chemical reactivity. J. Colloid Interface Sci. 510, 272–279. https://doi.org/10.1016/j.jcis.2017.09.082.

Sorg, T.J., 2000. Regulations on the Disposal of Arsenic Residuals from Drinking Water Treatment Plants. Science Applications International Corporation Reston, Virginia.

Srinivasan, N., Shankar, P., Bandyopadhyaya, R., 2013. Plasma treated activated carbon impregnated with silver nanoparticles for improved antibacterial effect in water disinfection. Carbon 57, 1–10.

Su, Q., Pan, B., Wan, S., Zhang, W., Lv, L., 2010. Use of hydrous manganese dioxide as a potential sorbent for selective removal of lead, cadmium, and zinc ions from water. J. Colloid Interface Sci. 349 (2), 607–612. https://doi.org/10.1016/j.jcis.2010.05.052.

Su, Y., Adeleye, A.S., Huang, Y., Sun, X., Dai, C., Zhou, X., Keller, A.A., 2014. Simultaneous removal of cadmium and nitrate in aqueous media by nanoscale zerovalent iron (nZVI) and Au doped nZVI particles. Water Res. 63, 102–111.

Su, H., Fang, Z., Tsang, P.E., Fang, J., Zhao, D., 2016a. Stabilisation of nanoscale zero-valent iron with biochar for enhanced transport and in-situ remediation of hexavalent chromium in soil. Environ. Pollut. 214, 94–100. https://doi.org/10.1016/j.envpol.2016.03.072.

Su, H., Fang, Z., Tsang, P.E., Zheng, L., Cheng, W., Fang, J., Zhao, D., 2016b. Remediation of hexavalent chromium contaminated soil by biochar-supported zero-valent iron nanoparticles. J. Hazard. Mater. 318, 533–540. https://doi.org/10.1016/j.jhazmat.2016.07.039.

Subramanian, N., Viswanathan, B., Varadarajan, T.K., 2014. A facile, morphology-controlled synthesis of potassium-containing manganese oxide nanostructures for electrochemical supercapacitor application. RSC Adv. 4 (64), 33911–33922.

Sumesh, E., Bootharaju, M., Pradeep, T., 2011. A practical silver nanoparticle-based adsorbent for the removal of Hg2 + from water. J. Hazard. Mater. 189 (1–2), 450–457.

Sun, Q., Li, J., Le, T., 2018. Zinc oxide nanoparticle as a novel class of antifungal agents: current advances and future perspectives. J. Agric. Food Chem. 66 (43), 11209–11220.

Sun, Y., Yu, I.K.M., Tsang, D.C.W., Cao, X., Lin, D., Wang, L., Li, X.-D., 2019. Multifunctional iron-biochar composites for the removal of potentially toxic elements, inherent cations, and hetero-chloride from hydraulic fracturing wastewater. Environ. Int. 124, 521–532. https://doi.org/10.1016/j.envint.2019.01.047.

Tamura, H., Katayama, N., Furuichi, R., 1996. Modeling of ion-exchange reactions on metal oxides with the frumkin isotherm. 1. Acid–base and charge characteristics of MnO2, TiO2, Fe3O4, and Al2O3 surfaces and adsorption affinity of alkali metal ions. Environ. Sci. Technol. 30 (4), 1198–1204.

Tang, W.-W., Zeng, G.-M., Gong, J.-L., Liu, Y., Wang, X.-Y., Liu, Y.-Y., Tu, D.-Z., 2012. Simultaneous adsorption of atrazine and Cu(II) from wastewater by magnetic multi-walled carbon nanotube. Chem. Eng. J. 211-212, 470–478. https://doi.org/10.1016/j.cej.2012.09.102.

ThanhThuy, T.T., Feng, H., Cai, Q., 2013. Photocatalytic degradation of pentachlorophenol on ZnSe/TiO2 supported by photo-Fenton system. Chem. Eng. J. 223, 379–387. https://doi.org/10.1016/j.cej.2013.03.025.

Tong, S., Deng, H., Wang, L., Huang, T., Liu, S., Wang, J., 2018. Multi-functional nanohybrid of ultrathin molybdenum disulfide nanosheets decorated with cerium oxide nanoparticles for preferential uptake of lead (II) ions. Chem. Eng. J. 335, 22–31. https://doi.org/10.1016/j.cej.2017.10.056.

Tratnyek, P.G., Sarathy, V., Nurmi, J.T., 2009. Aging of Iron Nanoparticles in Water: Effects on Structure and Reactivity.

Unuabonah, E.I., Ugwuja, C.G., Omorogie, M.O., Adewuyi, A., Oladoja, N.A., 2018. Clays for efficient disinfection of bacteria in water. Appl. Clay Sci. 151, 211–223. https://doi.org/10.1016/j.clay.2017.10.005.

Vesali-Kermani, E., Habibi-Yangjeh, A., Ghosh, S., 2020. Visible-light-induced nitrogen photofixation ability of g-C3N4 nanosheets decorated with MgO nanoparticles. J. Ind. Eng. Chem. 84, 185–195.

Vickers, N.J., 2017. Animal communication: when I'm calling you, will you answer too? Curr. Biol. 27 (14), R713–R715. https://doi.org/10.1016/j.cub.2017.05.064.

Wan, S., Qiu, L., Tang, G., Chen, W., Li, Y., Gao, B., He, F., 2020. Ultrafast sequestration of cadmium and lead from water by manganese oxide supported on a macro-mesoporous biochar. Chem. Eng. J. 387, 124095. https://doi.org/10.1016/j.cej.2020.124095.

Wang, T., Jin, X., Chen, Z., Megharaj, M., Naidu, R., 2014. Simultaneous removal of Pb(II) and Cr(III) by magnetite nanoparticles using various synthesis conditions. J. Ind. Eng. Chem. 20 (5), 3543–3549. https://doi.org/10.1016/j.jiec.2013.12.047.

Wang, Y.-Y., Ji, H.-Y., Lyu, H.-H., Liu, Y.-X., He, L.-L., You, L.-C., Yang, S.-M., 2019a. Simultaneous alleviation of Sb and cd availability in contaminated soil and accumulation in Lolium multiflorum lam. After amendment with Fe–Mn-Modified biochar. J. Clean. Prod. 231, 556–564. https://doi.org/10.1016/j.jclepro.2019.04.407.

Wang, D., Wang, P., Wang, C., Ao, Y., 2019b. Effects of interactions between humic acid and heavy metal ions on the aggregation of TiO2 nanoparticles in water environment. Environ. Pollut. 248, 834–844.

Wang, S., Zhao, M., Zhou, M., Li, Y.C., Wang, J., Gao, B., Ok, Y.S., 2019c. Biochar-supported nZVI (nZVI/BC) for contaminant removal from soil and water: a critical review. J. Hazard. Mater. 373, 820–834. https://doi.org/10.1016/j.jhazmat.2019.03.080.

Wei, G., Qi, J., Lin, P., Pan, S., Sun, X., Shen, J., Li, J., 2018. Polyethersulfone enwrapped hydrous zirconium oxide nanoparticles for efficient removal of Pb (II) from aqueous solution. Chem. Eng. J. 349, 500–508.

Weiss, S., Jakobs, J., Reemtsma, T., 2006. Discharge of three Benzotriazole corrosion inhibitors with municipal wastewater and improvements by membrane bioreactor treatment and ozonation. Environ. Sci. Technol. 40 (23), 7193–7199. https://doi.org/10.1021/es061434i.

Wing, S., Lowman, A., Keil, A., Marshall, S.W., 2014. Odors from sewage sludge and livestock: associations with self-reported health. Public Health Rep. 129 (6), 505–515. https://doi.org/10.1177/003335491412900609.

Xiong, C., Wang, W., Tan, F., Luo, F., Chen, J., Qiao, X., 2015. Investigation on the efficiency and mechanism of Cd(II) and Pb(II) removal from aqueous solutions using MgO nanoparticles. J. Hazard. Mater. 299, 664–674. https://doi.org/10.1016/j.jhazmat.2015.08.008.

Xu, H.-Y., Li, B., Shi, T.-N., Wang, Y., Komarneni, S., 2018. Nanoparticles of magnetite anchored onto few-layer graphene: a highly efficient Fenton-like nanocomposite catalyst. J. Colloid Interface Sci. 532, 161–170. https://doi.org/10.1016/j.jcis.2018.07.128.

Yabuuchi, N., Komaba, S., 2014. Recent research progress on iron-and manganese-based positive electrode materials for rechargeable sodium batteries. Sci. Technol. Adv. Mater. 15 (4), 043501.

Yagub, M.T., Sen, T.K., Afroze, S., Ang, H.M., 2014. Dye and its removal from aqueous solution by adsorption: a review. Adv. Colloid Interf. Sci. 209, 172–184. https://doi.org/10.1016/j.cis.2014.04.002.

Yu, L., Han, M., He, F., 2017. A review of treating oily wastewater. Arab. J. Chem. 10, S1913–S1922. https://doi.org/10.1016/j.arabjc.2013.07.020.

Yu, H., Zou, W., Chen, J., Chen, H., Yu, Z., Huang, J., Gao, B., 2019. Biochar amendment improves crop production in problem soils: a review. J. Environ. Manag. 232, 8–21. https://doi.org/10.1016/j.jenvman.2018.10.117.

Zarime, N.A., Yaacob, W.Z.W., Jamil, H., 2018. Removal of heavy metals using bentonite supported nano-zero valent iron particles. In: Paper Presented at the AIP Conference Proceedings.

Zhai, X., Li, Z., Huang, B., Luo, N., Huang, M., Zhang, Q., Zeng, G., 2018. Remediation of multiple heavy metal-contaminated soil through the combination of soil washing and in situ immobilization. Sci. Total Environ. 635, 92–99. https://doi.org/10.1016/j.scitotenv.2018.04.119.

Zhang, W.-x., 2003. Nanoscale iron particles for environmental remediation: an overview. J. Nanopart. Res. 5 (3–4), 323–332.

Zhang, Y., Wu, B., Xu, H., Liu, H., Wang, M., He, Y., Pan, B., 2016. Nanomaterials-enabled water and wastewater treatment. NanoImpact 3, 22–39.

Zhou, Q., Liao, B., Lin, L., Qiu, W., Song, Z., 2018a. Adsorption of Cu(II) and Cd(II) from aqueous solutions by ferromanganese binary oxide–biochar composites. Sci. Total Environ. 615, 115–122. https://doi.org/10.1016/j.scitotenv.2017.09.220.

Zhou, Q., Lin, L., Qiu, W., Song, Z., Liao, B., 2018b. Supplementation with ferromanganese oxide–impregnated biochar composite reduces cadmium uptake by indica rice (Oryza sativa L.). J. Clean. Prod. 184, 1052–1059. https://doi.org/10.1016/j.jclepro.2018.02.248.

Zhu, S., Huang, X., Wang, D., Wang, L., Ma, F., 2018a. Enhanced hexavalent chromium removal performance and stabilization by magnetic iron nanoparticles assisted biochar in aqueous solution: mechanisms and application potential. Chemosphere 207, 50–59. https://doi.org/10.1016/j.chemosphere.2018.05.046.

Zhu, N., Qiao, J., Ye, Y., Yan, T., 2018b. Synthesis of mesoporous bismuth-impregnated aluminum oxide for arsenic removal: adsorption mechanism study and application to a lab-scale column. J. Environ. Manag. 211, 73–82. https://doi.org/10.1016/j.jenvman.2018.01.049.

Zhu, L., Tong, L., Zhao, N., Li, J., Lv, Y., 2019. Coupling interaction between porous biochar and nano zero valent iron/nano α-hydroxyl iron oxide improves the remediation efficiency of cadmium in aqueous solution. Chemosphere 219, 493–503. https://doi.org/10.1016/j.chemosphere.2018.12.013.

Zvizdić, S., Rodinis-Pejić, I., Avdić-Kamberović, F., Mujkić, A., Hamzić, S., Puvacić, S., Kudumović, M., 2005. Viruses in water. Med. Arh. 59 (6), 378–381.

This page intentionally left blank

CHAPTER

8

Nanosorbents for heavy metals removal

Tahir Rasheed[a], *Fahmeeda Kausar*[b], *Sameera Shafi*[c], *and Muhammad Bilal*[d]

[a]Interdisciplinary Research Center for Advanced Materials, King Fahd University of Petroleum and Minerals (KFUPM), Dhahran, Saudi Arabia [b]School of Chemistry and Chemical Engineering, Shanghai Jiao Tong University, Shanghai, China [c]Institute of Chemistry, The Islamia University of Bahawalpur, Bahawalpur, Pakistan [d]School of Life Science and Food Engineering, Huaiyin Institute of Technology, Huaian, China

8.1 Introduction

Environmental pollution got great concern encircling not only industrialized countries, but also developing countries through industrial revolution. It is already well apprehended that soil, water, and air are the principal abundant factors for human beings, nevertheless, the fundamental necessity for life on earth for all creatures is water. Although, the health of humans is severely affected by environmental pollution. For developing countries, noteworthy, environmental sanitation of soil, air, and water and strategies for their protection is of keen attention around the globe. Unluckily, the recyclability, efficiency, cost, and environmental benign persist as challenges for remediation of pollution. Organic materials like pesticides, detergents, biomaterials and pharmaceuticals, and inorganic pollutants suchlike arsenic ions and heavy metals (metals with atomic numbers higher than 20) are the major contaminants that exist in water that includes tape, ground and surface water. Usually, arsenic exists as anions mostly in the form of arsenite AsO_3^{3-}, arsenate AsO_4^{3-}, etc., while heavy metals are generally found as cations for example Hg^{2+}, Pb^{2+}, Cd^{2+}, Cr(VI) ions, As(V), As^{3+}, Co^{2+}, Ni^{2+}, Cu^{2+}, Ag^{+}, and Zn^{2+} ions. The human body can develop fatal diseases due to nonbiodegradable heavy metal accumulation, therefore, water pollution owing to heavy metals has become a critical issue for public health.

https://doi.org/10.1016/B978-0-323-90912-9.00008-3

Water is purified from biomaterials, organic contaminants, and toxic elements by following physical, biological, and chemical strategies. The old methodologies (Fu and Wang, 2011) implied for heavy metal remediation relating water mainly include precipitation of chemicals, adsorption (Srivastava et al., 2011), ion-exchange, filtration through membranes, reverse-osmosis, flocculation and coagulation, extraction and flotation, excitation, electrochemical remediation methods, modern oxidation reactions and biosorption technique. For the remediation, two to many strategies operate synergistically in most of the cases. Out of these methods, bacterial pathogens and heavy metals are removed proficiently from water through adsorption, a conventional and basic purpose technique. For instance, activated-carbons minerals from clay, compounds for chelation, and natural zeolite like chitosan are commonly implied in water for heavy metal adsorption. The specialized reagents make precipitates after reactions with heavy metals through chemical precipitation method. Generally, the inorganic precipitants, organic polymers, and organic chelating reagents are the three kinds of reagents that have been utilized.

Conventionally, precipitants of inorganic origin incorporate either hydroxides, e.g., CaO, NaOH, $Ca(OH)_2$, or sulfide. *Ad interim*, diverse freshwater treatment is in practice via organic chelating reagents like *N*,*N*-bis(carboxymethyl)glutamic acid, citric acid, ammonium diethyldithiocarbamate, ethylenediamine-*N*,*N*-disuccinic acid (Race et al., 2016), diethylenetriamine-pentaacetic acid and ethylenediamine-tetraacetic acid, derivatives of thiosemicarbazone (Koduru and Lee, 2014). Heavy metals could also be removed by chelating employing nanomaterials whose surface has been modified proficiently through the above-mentioned organic chelating reagents. Concurrently, biosensors fabricated with organic and bioorganic molecules could be advantageous for the separation of heavy metals from wastewater such as cryptophane (Tassali et al., 2014) and derivatives of oligonucleotide (Li et al., 2016). Besides, multi-functional groups like –OH, $–NH_2$ and –COOH constituting organic polymers such as polyaniline, polystyrene, also work in water for heavy metal extraction. The treatment efficiency greatly enhanced on the ground of advancement in nanotechnology, a proficient alternative for the cause.

NMs having the standard size of 1–100 nm, bear peculiar chemical and physical characteristics namely specific affinity, surface activity, and large surface area. Nevertheless, NMs have fascinated distinctive attentiveness regarding probing and removing organic, inorganic contaminants, and inorganic heavy metals from water. Consequently, the modern development of NMs and nanotechnology present mind-blowing opportunities for environmental sustainability and water treatment. Currently, carbon-based NMs prepared with transfiguration of agricultural junk, for instance, crap shell, sawdust and bark have engrossed a fair deal of attention for the treatment of water. Remarkable endeavors have been made for bench-scale research study and in-field implications, for example, magnetic NMs (Iram et al., 2010), nanotubes of carbon (Upadhyayula et al., 2009), activated-carbon, NMs of transition metals with zero valency. Organic polymers or organic small molecules have been practiced to embellish core/shell structures of nanoparticles (NPs). The NMs have precedence owing to efficiency and elevated adsorption ability. There are some limitations too such as eco-concern, poor recyclability, and expensiveness. Currently, the threat for health is under strict inspection yet.

To date, numerous works have been reported in different published reviews comprising graphene/graphene oxide (G/GO), carbon nanotubes and metal-oxide NMs, etc. (Kyzas and Matis, 2015). This chapter particularly limelight NMs for heavy metal removal from water

covering wastewater, groundwater, and tape water. Herein, the NMs focuses on two classes: (1) Organic NMs and (2) Inorganic NMs. Although, the earlier contains carbon−/silicon-based NMs and transition metal/sulfide/oxide NPs. The composition of the latter is polymer-based organic nanocomposites and polymer organic NMs. Moreover, organic polymers utilized as nanocomposites provide sustenance for cores of inorganic NPs, an overlap between polymer-based organic NMs and inorganic NMs is noticed to some expanse. Moreover, the elaborated procedure for manufacturing and analysis of NMs, including treatments for organic contaminants, together with the implication of biomass as biosorbents are far off of this research topic. Also, the fabrication of NMs acting as nanofiltration-membranes, is not described in this chapter.

8.2 Inorganic NMs

Generally, inorganic NMs are classified as sulfide/oxide/metal NMs, inorganic NMs are divided into transition metal/sulfides/oxides NMs, silica-architectured NMs, carbon-rooted NMs like graphene and other similar nanocomposites. On the ground of distinctive attributes, nanoparticles (NPs) composed of transition metal oxides and metals are widely implied to wastewater for heavy metal ions removal, though, there is grave concern NPs aggregation. In the consequence, these materials vitally advocate NPs regarding recyclability and durability (Astruc et al., 2005). These materials involve inorganic frameworks, organic polymers and small organic molecules. Normally, the nature of organic polymers is synthetic like biopolymers, e.g., chitosan and cellulose, polyaniline, or polystyrene. Therefore, the supports made of organometallic or inorganic polymers have not been implied for such a motive. Magnetic NPs such as Fe_3O_4@-SiO_2, Ni@SiO_2, Fe_3O_4 and Fe_3C have been competently investigated as one of the distant inorganic NMs. Shells and elements with magnetic core are utilized in magnetic NPs are fabrication of NPs. Fig. 8.1 portrays the functionalization of NPs with EDTA

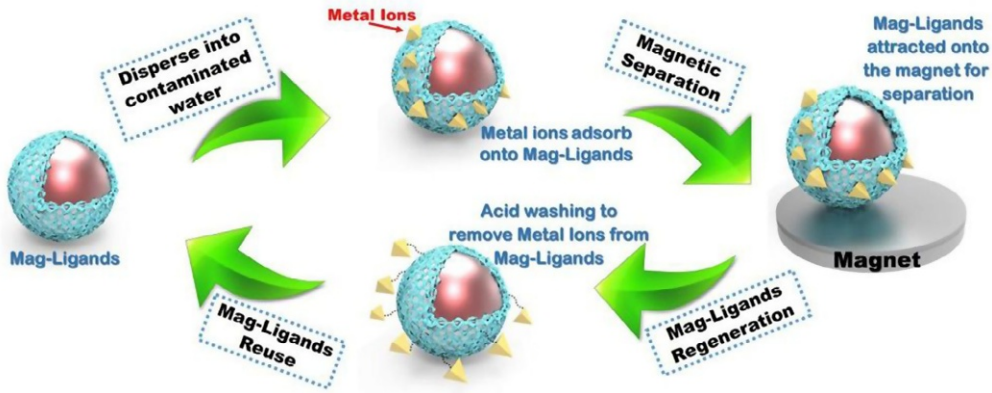

FIG. 8.1 EDTA functionalized magnetic nanoparticle sorbents for cadmium and lead contaminated water treatment. *Reproduced with permission from Huang, Y., & Keller, A.A., EDTA functionalized magnetic nanoparticle sorbents for cadmium and lead contaminated water treatment. Water Res. 80 (2015) 159–168. https://doi.org/10.1016/j.watres.2015.05.011. Copyright 2015, Elsevier.*

(Huang and Keller, 2015), while the magnetic core is likely nickel, iron, cobalt, or relevant alloys and oxides residing superparamagnetic/ferromagnetic characteristics, instead, the constituents of shells are inorganic like SiO_2 (Mashhadizadeh and Amoli-Diva, 2013), surfactants, and organic polymers. The magnetic NPs in inorganic–organic hybrid form, which could be separated comfortably by an external magnetic field, remove toxic elements from water in a selective manner. Water is purified from Cd^{2+}, Cu^{2+} and Pb^{2+} by applying magnetic nanocomposites which furnish feasible proficient, and fast aid.

8.2.1 Transition metal oxide NMs

Iron oxide NMs

Three forms of iron oxide NMs (maghemite (c-Fe_2O_3), magnetite (Fe_3O_4), and hematite (a-Fe_2O_3) NPs act efficiently as photocatalysts and nanosorbents for removing organic and inorganic pollutants along with lethal heavy metal ions from water. Iron-oxide NMs have photolytic properties and implications regarding organic contaminants photodecomposition is not the interest of present topic. In addition, biomass could be capably immobilized by iron-oxide nanomaterials (Šulek et al., 2010).

Magnetic (Fe_3O_4) NMs

Numerous supports of organic and inorganic origin for magnetic Fe_3O_4 NPs stabilization have been broadly scrutinized to remove pollutants out of water. Mostly, NPs are stabilized by organic polymers. Heavy metals such as Cd^{2+}, Zn^{2+}, and Cu^{2+} could efficiently be adsorbed by utilizing, for instance, magnetic Fe_3O_4 implanted with polyethyleneimine (PEI) (Pang et al., 2011). As III and As V could be adsorbed by NPs of polystyrene-based hydrated Fe_2O_3 (Cumbal and SenGupta, 2005). Coating of magnetic Fe_3O_4 NPs was achieved through Poly(glycidylmethacrylate) (PGMA) by way of general radical polymerization, following linking of the surface of NPs with b-cyclodextrin (b-CD). The attained magnetic NPs proved to have satisfactory interaction with a few environmental pollutants, e.g., copper ions and bisphenol A (Wang et al., 2014). Following the carbodiimide method in aqueous solutions, the magnetic surface of Fe_3O_4 NPs modified with carboxymethyl-b-CD grafted with carboxymethyl-b-CD, efficaciously extracted Cu ions (Badruddoza et al., 2011). To modify Fe_3O_4 NPs, copolymers of crotonic acid and acrylic acid, and 3-Aminopropyltriethoxysilane were utilized to remove ions of Cu^{2+}, Pb^{2+}, Zn^{2+} and Cd^{2+} (F. Ge et al., 2012).

NPs stand on amine-functionalized Fe_3O_4, magnetic-chitosan NCs are fabricated through biopolymer, i.e., naturally occurring chitosan. Additionally, NPs are broadly balanced by implying small molecules of organic origin (Zargoosh et al., 2013). Heavy metal ions, for instance, as well as Co^{2+}, Zn^{2+}, Cu^{2+}, Cd^{2+}, and Pb^{2+} ions could be taken out of the industrial waste possibly through improving the surface of Fe_3O_4 NPs with thiosalicylhydrazide by covalent immobilization. NPs of Fe_3O_4 showed increased sensitivity and selectivity for Al^{3+} ion rather than general metal ions in water solutions, when the Schiff base of rhodamine 6G was used for its embellishment (Zhi et al., 2013). For the treatment of heavy metals in aqueous solution, ethylenediaminetetraacetic acid (EDTA) immobilization on the surface of amine-terminated NPs of Fe_3O_4 ceased with amine are topped with immobilized ethylenediaminetetraacetic acid (EDTA) (Zhang et al., 2011).

Zn^{2+} and Cd^{2+} ions can be adsorbed from the aqueous solutions effectively by NPs with magnetic hydroxyapatite ($(Ca10(PO_4)6(OH)_2$, HAP) (Feng et al., 2010). Moreover, the magnetic core is painted with silica oxide and oxides of metals. Pb^{2+} ion, let suppose, was separated through spherical and mono-scattered $Fe_3O_4@SiO_2$-NH_2 nanomaterials with size = 200 nm (Zhang et al., 2013a, 2013b). Notably, an elevated adsorption capability of porous c-AlOOH (boehmite)@SiO_2/Fe_3O_4 magnetic microspheres is perceived for heavy metal ions Hg^{2+}, Cu^{2+}, Pb^{2+}, Cd^{2+}, and Zn^{2+} for consumable water (Wei et al., 2011). Surface of chitosan/SiO_2/Fe_3O_4Magnetic modified with EDTA to act as an adsorbent for Cu^{2+} ions actively in a selective manner, while for buffer solution, water-soluble carbodiimide was utilized being crosslinker (Fig. 8.2) (Ren et al., 2013). Magnetic nano-iron oxide (nano-Fe_3O_4) is infused with nano-silicon oxide (nano-SiO_2) via its surface to act as a sorbent (nano-Fe_3O_4–SiO_2 sorbent), and employed effectively on samples of water to separate heavy metals like Pb^{2+} and Cu^{2+} ions batch equilibrium and micro-column techniques (Kim et al., 2013).

Maghemite (c-Fe_2O_3) nanoparticles

To date, the organic polymer-supported maghemite NPs have been reported abundantly. Single-step polymerization through chemical-oxidation, for instance, was implied for synthesizing maghemite (c-Fe_2O_3) nanoparticles laminated with polyhodanine utilized in aqueous solutions for removing Hg^{2+} ions, given in Fig. 8.3 (Song et al., 2011). Maghemite (c-Fe_2O_3) displayed a sensitive attachment with divalent metal ions when grafted using poly(1-vinylimidazole), while $Cu^{2+} > Ni^{2+} > Co^{2+}$ is their attachment strength order (Takafuji et al., 2004). Poly-I-cysteine laminated NPs of magnetic (c-Fe_2O_3) were used for chelation of Zn^{2+}, Pb^{2+}, Ni^{2+}, Cd^{2+}, Cu^{2+} and As^{2+} ions (White et al., 2009). Also, Cu^{2+} ions are treated in aqueous solution using NPs of magnetic (c-Fe_2O_3) with chitosan coating, a biopolymer, and further adjusted with a-ketoglutaric acid (Zhou et al., 2009b).

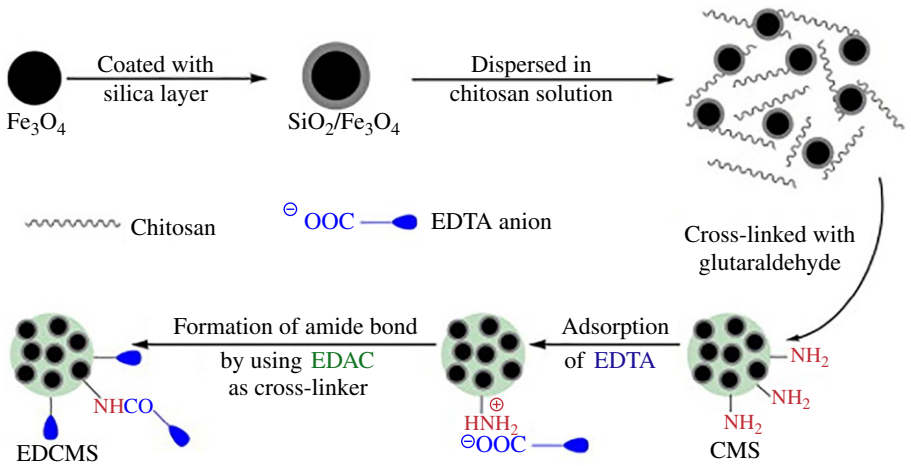

FIG. 8.2 Procedure for the preparation of CMS and EDCMS. *Reproduced with permission from Ren, Y., Abbood, H.A., He, F., Peng, H., Huang, K., Magnetic EDTA-modified chitosan/SiO2/Fe3O4 adsorbent: preparation, characterization, and application in heavy metal adsorption. Chem. Eng. J. 226 (2013) 300–311. https://doi.org/10.1016/j.cej.2013.04.059. Copyright 2013, Elsevier.*

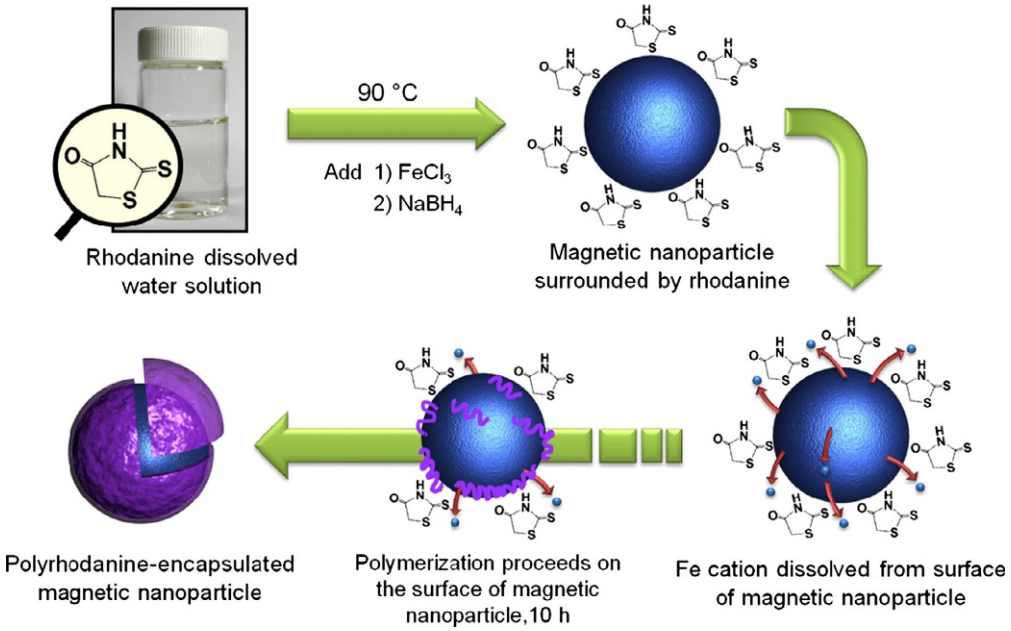

FIG. 8.3 Schematic illustration of the fabrication process of polyrhodanine-encapsulated magnetic nanoparticles. *Reproduced with permission from Song, J., Kong, H., Jang, J., Adsorption of heavy metal ions from aqueous solution by polyrhodanine-encapsulated magnetic nanoparticles. J. Colloid Interface Sci. 359(2) (2011) 505–511. https://doi.org/10.1016/j.jcis.2011.04.034. Copyright 2011, Elsevier.*

Hematite (a-Fe_2O_3) NPs

a-Fe_2O_3 nanostructures doped with manganese and possessing three-dimensional porous structure can excellently remove As III, Cr VI and Pb^{2+} ions, facile through magnetic separation from the fresh water and was introduced by Fu et al. (Cui et al., 2014). A mixture of hematite and magnetite NPs were implied in water to sorbate Cr^{3+}, Cd^{2+} and Pb^{2+} ions (Ahmed et al., 2013). Additionally, a mixture of Al_2O_3 and Fe_2O_3 nanocomposite fiber can also adsorb ions like Hg^{2+}, Ni^{2+}, Cu^{2+} and Pb^{2+} (Mahapatra et al., 2013).

Superparamagnetic nanoparticles

Superparamagnetic particles are generated with magnetic particles residing no permanent magnetic moment and with reduced size. Heavy metals were also removed through sorption by superparamagnetic iron oxide NPs modified with organic ligand (Warner et al., 2010). The surface of dimercapto-succinic acid was functionalized with NPs of supermagnetic iron oxide (Fe_3O_4) exhibited effectively as a sorbent for different ions such as ions of Tl, Cd, Pb, Ag, and Hg (Yantasee et al., 2007). Poisonous elements were separated through NPs fabricated with super-paramagnetic Fe-oxide NP (SPION) and poly(methylmethacrylate) (PMMA) and discriminatively improved surface, while the magnetic-field was employed externally (Wanna et al., 2016).

Titanium oxide NPs and titanate nanostructures

Usually, organic contaminants are photodegraded by employing photocatalytic-TiO_2 NPs (Anandan et al., 2009). Cd^{2+} ions, for instance, could be removed from water by using NPs of titanium dioxide modified through thiolactic acid (Skubal et al., 2002). The sol–gel strategy was applied to synthesize silica gel immobilized TiO_2 NPs which work quantitatively in 4–7 pH range to adhere trace lead in water (Liu and Liang, 2008). Nickel and cadmium ions are rarely preconcentrated by applying TiO_2-nanotubes owing to its notorious extracting capability in solid form (Zhou et al., 2009a). Ions of CrV could be separated with the help of TiO_2, also termed as anatase, NMs after doping with carbon (Mani et al., 2015). For the removing purpose of copper and cadmium ions, different concentrations of NaOH, i.e., 4–15 mol/L, were utilized to prepare titanate-NMs by means of hydrothermal pathway and applied to aqueous-solutions.

Miscellaneous

Provisionally in water, versatile NPs of metal oxide are applied for removing pollutants apart from titanium oxide and ferric oxide NPs. For example, in order to preconcentrate and selectively extract solid-state minute quantities of Pb^{2+} and Cd^{2+} ions, alumina (Al_2O_3) was chemically improved (Ezoddin et al., 2010). Cr VI and AsV ions were remarkably adsorbed by using CeO_2 NPs (Albadarin et al., 2014). Pb^{2+} and As ions were effectually adsorbed in aqueous solutions by applying copper oxide nanostructures (Farghali et al., 2013). For concurrent ultrasound-aided removal of Pb^{2+} from water, activated carbon loaded with CuO NP was efficiently applied (Dil et al., 2017b). Furthermore, they also presented that Co^{2+} and Cd^{2+} ions could be concurrently adsorbed by using ZnO nanorods loaded-activated carbon (Dil et al., 2017a).

Cd^{2+} and Pb^{2+} ions were also removed from aqueous solutions by utilizing the mesoporous stratified ZnO nanorods with pore volume of 0.038 cm^3 and 15.75 $m^2\ g^{-1}$ specific surface area (Kumar et al., 2013). In contrast to undoped-ZnO NPs, Cu^{2+} and Pb^{2+} ions were competently removed from water assets by La-doped ZnO NPs (Wu et al., 2013). Even though both ZnO and MgO are functional for Cu^{2+} extraction from industrial waste up to 98%, however, MgO nano-sorbents demonstrated more capability for its adsorption (Rafiq et al., 2014). For Cr V and Cr III on Mn_3O_4 NMs, the validity of thermodynamics, pH, activation energy and kinetics were also investigated (Cantu et al., 2014). Pb^{2+} and Cd^{2+} were adsorbed by Ni $(OH)_2$ and NiO nanostructures from aqueous solution (Behnoudnia and Dehghani, 2014). Moreover, As III/As V were also removed extraordinarily by ZrO_2 nanostructured and greatly porous spheres. In addition, for purification of freshwater NPs of binary metal-oxides are being synthesized, analyzed, and practiced. In groundwater and soil, for example, As III is immobilized by applying Fe-Mn oxide NPs stabilized with polysaccharide (An and Zhao, 2012).

8.2.2 Transition metal NPs

Gold NPs

For extracting heavy metal ions from water, pH proved to be a key factor for Au-shielded NPs of 4-aminothiophenol in the maintenance of limiting factors (Chauhan et al., 2011). To remove Pb^{2+} and Hg^{2+} from solutions, Au-shielded NPs are fabricated from albumin's serum

(BSA) and agarose-gel-membrane, shortly called Au-NPs@BSA/AGM (Y.-F. Lee et al., 2012). Hg^{2+} ions were detected within the range of 0.1–1000 nM with NPs of magnetic-silica-sphere (MSS)@Au which were functionalized with oligonucleotide. On the other hand, it showed response Ag^{+} less than Hg^{2+}, i.e., within the range of Mn from 10 to 1000 (Liu et al., 2014a,b).

Silver NPs

Instead of eliminating heavy metals, Ag NPs have been famous in treating microbes from biomaterials (Rai et al., 2009). There is limitation regarding heavy metals, e.g., Hg^{2+} relevant to silver-NPs in the reported literature (Sumesh et al., 2011). Currently, Pb^{2+} ions, for instance, are selectively permeated through NCs of polyaniline-tungstophosphate inserted in silver NPs (Khan et al., 2013). For probing low-concentrated (1 ppb) arsenite and arsenate, silver NPs laminated with poly(vinylpyrrolidone) were reported by Yang and coworkers (Mulvihill et al., 2008).

Iron NPs

Notwithstanding the aerobic responsiveness of Fe (0) NPs, they have been extensively implied to water for removing heavy metals. The X-ray photoelectron spectroscopy (XPS) results exposed the usefulness of zero-valent iron NPs participates in either all the situations or its modified oxidized forms which could also be in demand. For eliminating AsIII-ions from groundwater, iron nanoparticles with size 1–120 nm were applied by Choi et al. (Kanel et al., 2005) Architectured core/shell iron NPs sequestrated nickel with 0.13 g nickel per gram iron adsorbing range and was presented by Li et al. (Li and Zhang, 2006). Biodegradable and nontoxic chitosan was applied as a stabilizer to synthesize NPs of chitosan-stabilized-Fe for adsorbing preliminary CrVI-ions (Geng et al., 2009).

In the permeable reactive barriers, heavy metals CrVI and ions Pb^{2+}, Cd^{2+}, Cu^{2+} were discriminatively removed from electroplating wastewater by upgraded chitosan bead-supported Fe NPs, whereas concentration and pH performed an important function (Liu et al., 2013). CrVI was removed successfully from industrial wastewater by Fe NPs having adsorption strength of cellulose (López-Téllez et al., 2011). Cu^{2+} ions were effectively removed by immobilized polyvinyl alcohol/polyacrylic acid hybrid nanofibrous mats of Fe NPs (Xiao et al., 2011). Industrial effluents bearing Cr VI were purified through nanosized bentonite-based Fe-NPs (Shi et al., 2011). Majestically, industrial waste containing uranium pollutants are treated through Fe-NPs (Dickinson and Scott, 2010). Noteworthy, studying branch involving toxicity and implication regarding Fe-NPs necessitates enhanced exploration chiefly the grasping problems regarding zero-valent iron.

8.2.3 Transition metal-sulfide NPs

Currently, Aluru et al. introduced a novel nanopore membrane made of MoS_2, which can work 70% more efficiently than graphene nanopores for desalination of water (Heiranian et al., 2015). For heavy metals removal present in water, this study furnishes a remarkable substitute. In addition, Ghosh et al. also delineated that ZnS quantum dots (Q-dots) stabilized by chitosan could be implemented not only for heavy metal ions (Pb^{2+}, Ag^{+} and Hg^{2+}) in water but also as cation exchanger (Jaiswal et al., 2012). To investigate the biosynthesis of

nanocrystalline ZnS in feigned wastewater, *Shewanella oneidensis* MR-1 was administered which is also a metal reducing agent (Xiao et al., 2015). For purifying industrial wastewater, Ag_2S NPs are employed as ultimate-slush matter (Kim et al., 2010). WS2 layered two-dimensional nano-thickened membranes demonstrated two to five times multiple penetration capability in comparison to membranes fabricated with GO (Sun et al., 2014).

8.2.4 Carbon-based NMs

Carbon-based NMs are extensively used for heavy metal removal on the ground of their upraised sorption extent and non-toxicity (Smith and Rodrigues, 2015). For decades, activated carbon worked for the purification of water and air acting as the foremost famous sorbent. Zhou et al., for example, evaluated the adsorption capacity of cadmium, lead, zinc, and copper ions by carbon black and hydroxyapatite (Chen et al., 2010). Nevertheless, this phenomenon is restricted in tape water for the rare heavy metals at ppb levels. In consequence, fullerenes, graphene materials, and CNTs were fabricated for applications. CNTs demand improvements in their exteriors owing to little metal-adsorbing capability of pristine (Hadavifar et al., 2014). CNTs show enhanced particular surface area and disposability when its surface is loaded with P, N, and O functional groups (Adeleye and Keller, 2014). The anisotropic construction of hydroxide nanocrystal@carbon in double-layer nanosphere, is an excellent example of Cu^{2+} ions removal (Gong et al., 2011). For effective adsorption of heavy metals from water, the surface of nanofibers and nanotubes are grafted with numerous polymers and organic ligands (Kosa et al., 2012).

Carbon-NTs and surface modified NTs

As long as 1991, Iijima brought light to extraordinary properties and implications of carbon nanotubes, CNTs of twain single wall and multiwall are substantially scrutinized involving heavy metals removal from contaminated water (Mubarak et al., 2014). Interestingly, CNTs are synthesized through the chemical vapor deposition (CVD) method. The adsorption capability of CNTs changes owing to surface administration by oxidants such as organic molecules, HNO_3, and $KMnO_4$. Surface modification and oxidation have been largely investigated (Datsyuk et al., 2008). Electrochemical probing and extraction of heavy metals is achieved by CNT-based NMs (Musameh et al., 2011). The metals ions show adsorption aversion order for CNTs at pH = 9, for example, is $Mn^{2+} < Zn^{2+} < Co^{2+} < Pb^{2+} < Cu^{2+}$ using carbon nanotubes (Stafiej and Pyrzynska, 2007).

Multi-wall CTNs were utilized in greater amounts of aqueous-solutions by Wang and coworkers to remove scarce earth-metals like Eu (III) and Sr(II) (Chen et al., 2009). Chitosan incorporated multi-wall CNTs excellently adsorbed metal ions like Ni^{2+}, Zn^{2+}, Cu^{2+},and Cd^{2+} (Salam et al., 2011). Cd^{2+} ions were removed using surface ethylene diamine functionalized multilayered CNTs from aqueous solutions (Vuković et al., 2010). Michael's addition reaction and mussel-influenced chemistry were combined to prepare polydopamine-functionalized CNTs, were employed to remove Cu^{2+} ions. There is a deep inspection of numerous parameters like temperature, pH, adsorbent concentration and initial Cu^{2+} concentration (Zhang et al., 2015). Cd^{2+} and Pb^{2+} ions are efficiently sorbed through GOs NCs and biochar-supported CNTs owing to their amplified surface-area (Liu et al., 2016a). Functionalization

of CNTs through polyethylenimine is reported to investigate adsorbility of Cu^{2+} ions (Xie et al., 2015). Alternative to adsorption, heavy metal-ions removal through architectured-NMs encompassing nanooxides and CNTs removed heavy metal ions that are highly ascribable to foaming hydroxide precipitation, suggestive of lower quality architectured NMs as adsorbing-agents (Yang et al., 2014).

Graphene and GO nanomaterials

Since the recognition of graphene, both graphene (G) and graphene oxide (GO) have attracted remarkable attentiveness. Water contaminants (e.g., organic-compounds and metal ions) are proficiently eliminated through NMs synthesized with graphene and graphene alone (Yusuf et al., 2015). Yuan and coworker, for instance, examined GO absorbability for Zn^{2+} regarding absorbable quantity, contact time, effect of pH, temperature, and foreign ions (Wang et al., 2013). The graphene nanosheets demonstrated remarkable application in preconcentration and removal of gases, in adsorption as adsorbents, removal of metal ions like Pb^{2+} and organic compounds (Yu et al., 2015). Polymer-improved graphene and graphene oxide together with organic compounds are investigated as well (Ma et al., 2012). Heavy metals ions are detected through improved graphene and modified with enhanced sensitivity. Functionalization of magnetic graphene oxide is achieved, for example, with EDTA for removing copper, mercury, and lead ions from water. GO principally imparted to effective adsorption by appealing ample functional groups and metal chelation with EDTA (Cui et al., 2015). The GO N-(trimethoxysilylpropyl)-silanized was assessed as adsorbent for Pb^{2+} and Cu^{2+} ions, different contact time and pH, and antimicrobial implication with varying concentration (Mejias Carpio et al., 2014). Magnetic graphene nanocomposites which are water-soluble and modified using polyacrylic acid GO/Fe_3O_4 exhibited exceptional capability for Pb^{2+}, Cd^{2+}, and Cu^{2+} ions removal (Zhang et al., 2013a, 2013b). GO nanocomposites blended with poly(*N*-vinylcarbazole) were implemented to adsorb Pb^{2+} ion out of aqueous solutions (Musico et al., 2013).

Keeping in view the catechol chemistry, Wang et al. applied controlled self-polymerization for synthesizing GO composites with poly(dopamine) along with functional group coating and further employed for excellent depolluting the waste effluents (Dong et al., 2014). Also, heavy metals are separated effectively by transition metal-oxides functionalization of graphene and graphene oxide like ZnO, TiO_2, MnO_2, and Fe_3O_4 (Zhang et al., 2012) and peculiarly by magnetic-cored graphene and graphene oxide. Aqueous solutions of Hg^{2+} and Pb^{2+}, for instance, were decontaminated using NCs of cobalt-ferrite ($CoFe_2O_4$)-reduced-GO (rGO), collectively as $CoFe_2O_4$-rGO (Zhang et al., 2014).

Aqueous solutions were also treated effectively with magnetic graphene-materials (Fe_3O_4-GS) for eliminating Ni^{2+}, Cd^{2+}, Hg^{2+}, Pb^{2+}, and Cr(VI) ions (Guo et al., 2014). Pb^{2+} ions could also be adsorbed proficiently by implementing magnetic graphene oxide compounds with Fe_3O_4 center and grafted with chitosan (Fan et al., 2013). Cr(VI) ions are effectively cleared magnetic GNCs sandwiched between bilayered iron oxide exterior and Fe central interior. Ferrocene and GO irradiated with microwaves to produce magnetic graphene residing improved adsorption capability towards aqueous Pb^{2+}, CrVI and AsV ions, whereas their removal efficiencies was detected 99% up to 1 ppb level (Gollavelli et al., 2013). Ions like Pb^{2+}, Hg^{2+}, and CrVI were proficiently eliminated using graphene-anchored spongy Fe-Fe_2O_3 matrix (Bhunia et al., 2012).

Cr(VI) ions were removed in extraordinarily quick manner by applying NCs of chitosan-cyclodextrin functionalized with GO (Li et al., 2013). Moreover, Cr(VI) ions were also removed swiftly through nanocomposite prepared with magnetic bicyclodextrin and GO (Fan et al., 2012). Meanwhile, reduced-GO (rGO) and self-assembly strategies were administered to construct aerogels by implementing d-MnO_2 and 3D G succeeding extremely thin d-MnO_2 coating in solution state with nano-thickness and was reported by Zhang et al., while the calculated adsorbing capability for copper ion was 228.46 mg/gram, for cadmium ion 250.31 mg/gram and for lead ion 643.62 mg/gram (Liu et al., 2016a, 2016b). In addition, GO is also applied in aqueous solution located in fixed-bed SiO_2 column for adsorbing copper and lead ions in form of thin sheet (Ding et al., 2014). Although, graphene oxide nano-sorbents entirely eliminate lead(+2) and chromium(VI) ions from pharmaceutical industrial wastes, but small amount of nickel(+2) ion subsidized uniformly with increase in graphene oxide (Gopalakrishnan et al., 2015). GO-based microbots (GOx-microbots) were introduced by San et al. which comprised of platinum, nickel, and nanosized multilayers of GO, and was utilized for removal, transference and capturing of Hg^{2+} as an automotive systems (Vilela et al., 2016). Nonetheless, G/GO are exorbitant so patch a difficulty towards its usage in realistic implications.

8.2.5 SiO_2-supported NMs

SiO_2 deployed nanomaterials have been classified as SiO_2-nanotubes, SiO_2-nanofibers, SiO_2 with nano pore size, silica-laminated magnetic nanoparticles and SiO_2 nanofibers. Biological systems eliminated heavy metals through functionalized nano-porous silica (Yantasee et al., 2010). For developing magnetic SiO_2-NMs and succeeding in collecting heavy metal-ions, -SH containing organic-thiol molecules have been in ample practice as chelating group and support. Following a batch technique, a conjugate NM was produced by immobilizing sulfur-residing organic-ligand named ammonium(4-chloro-2-mercaptophenyl) carbamodithioate (ACMPC) over mesoporous-SiO_2 that probed and removed Hg^{2+} ions instantly (Awual et al., 2016). For the adsorption of cobalt ions in trace concentration from water resources, mesoporous SiO_2-NMs affixed with an organic-ligand named *N*,*N*-di(3-carboxysalicylidene)-3,4-diamino-5-hydroxypyrazole have been debuted (Shahat et al., 2015).

Hg^{2+} ions could also be removed from contaminated water, with an absorptive capability of 57.5 mg per gram, by silica nanofibers after its surface modification with zonal thiol (–SH) groups. The sol–gel polymerization is followed over electrospun polyacrylonitrile (PAN) nanofibers with 3-mercaptopopyl trimethoxysilane to fabricate such NMs, succeeding detachment of PAN and application of dimethylformamide (DMF) afterwards as shown in Fig. 8.4 (Li et al., 2011a). Calcination and electro-spinning methods were applied by Du et al. for fabricating SiO_2-nanotubes (SNTs). Owing to chelation among Pb^{2+} and imino groups, remarkably improves adsorbability after applying symdiphenylcarbazide (SD-SNTs) to surface of SNTs (Wang et al., 2015).

The magnetic-NPs laminated with silica have been classified as silicon-based nanomaterials and magnetic inorganic nanomaterials. In water, for instance, magnetic SiO_2-NPs functionalized with 4,4-difluoro-4-bora-3a, 4a-diaza-s-indacene (BODIP), acting like fluorescence-probe, demonstrated elevated attraction and discriminativeness for lead

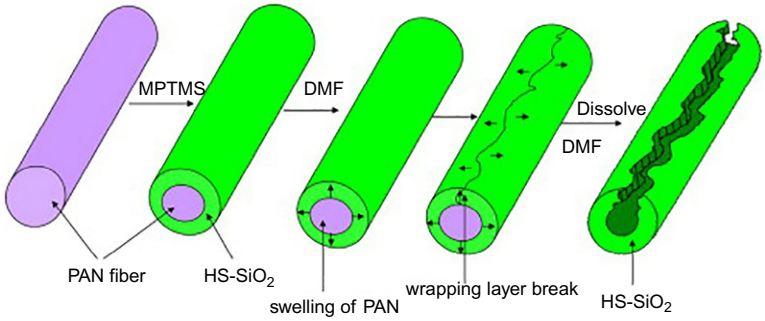

FIG. 8.4 Procedure for the fabrication of zonal mercaptopropyl silica nanofibers obtained by dissolution of the PAN nanofiber templates with DMF. *Reproduced with permission from Li, S., Yue, X., Jing, Y., Bai, S., Dai, Z., Fabrication of zonal thiol-functionalized silica nanofibers for removal of heavy metal ions from wastewater. Colloids Surf. A: Physicochem. Eng. Aspects 380(1) (2011) 229–233. https://doi.org/10.1016/j.colsurfa.2011.02.027. Copyright 2011, Elsevier.*

ions in comparison to contrasting metal-ions involving Hg^{2+}, Cd^{2+}, Ag^{+}, Zn^{2+}, Cu^{2+}, Ca^{2+}, K^{+}, Mg^{2+}, Na^{+} and Li^{+} and also clears human blood from lead ions successfully (Lee et al., 2009). Hg^{2+} ions could also be probed with high sensitivity succeeding adsorption by means of NPs having core of naphthalimide and core of Fe_3O_4@SiO_2 (Zhu et al., 2013). For diagnosis and micro-extraction of minute quantities of ions such as Mn^{2+}, Pb^{2+}, Cd^{2+}, Co^{2+}, Ni^{2+}, Cu^{2+}, cationic-surfactant laminated SiO_2-supported Fe_3O4 NPs were applied to ambient water as adsorbing agent (Karatapanis et al., 2011).

Lead and mercury ions were removed by magnetic SiO_2 nanomaterials with mesoscaled pores and -SH functionalization, collectively termed as SHmSi@Fe_3O_4 (Li et al., 2011b). In water, Hg^{2+} ions were easily located and reprecipitated through –SH-functionalized Fe_3O_4-nanoparticles having mesoscaled pores and laminated with SiO_2 (Hakami et al., 2012). Ions in small quantities such as Pb^{2+}, Hg^{2+}, Cu^{2+}, Cd^{2+}, discriminatively and expeditiously removed using c-s-propyltrimethoxy-silane-improved Fe_3O_4-nanoparticles sheeted with SiO_2 (Huang and Hu, 2008). For adsorbing heavy metals from water, e.g., chitosan and cellulose residing polyfunctional groups like –COOH, –OH, $–NH_2$, etc., dithizone was employed by Hu et al. to improve artificially prepared organic polymer-based NCs and bio-polymers (Kangoa et al., 2013). For chelating heavy metals, the slow adsorption rate and little surface area restrict their implication, however, carbon NMs and transition metal NPs in the absence of functional groups and having broader surface area are widely applied.

The fabrication and implication of polymer-based nanocomposites and NMs furnished a substitute chance for removing water-inhabiting heavy metals. In contrast to organic polymers, activated carbon and metal/oxide NPs, nanosorbents in the form of polymer-supported nanocomposites and polymer NMs have multifunctional groups and larger surface areas. Heavy metal ions like Cr (3, 4), Hg^{2+} and Pb^{2+} have also been adsorbed using ion-exchange and chelation of functional groups (Bhatnagar and Sillanpää, 2009). Polymer-matrix encompasses inorganic nanoparticles following varied classes of polymeric NCs. Polymer-nanorods, polymer-nanocrystals, polymer-nanofibers are different kinds of polymeric nanomaterials. For eliminating poisonous compounds from water, NCs are employed which are prepared using alginate for supporting biopolymer (Ngomsik et al., 2009).

8.3 Polymer-organic NMs

Notwithstanding, the organic polymers are extensively studied/implied for eliminating heavy-metals from contaminated water, while proficient fabrication of polymer NMs is still an issue of debate. For the adsorption of Hg^{2+}, Huang and coworkers, for example, utilized m-sulfophenylenediamine (SP) and aniline (AN) in hydrochloric acid through oxidative precipitation polymerization in the absence of any external stabilizer for synthesizing copolymer sulfophenylenediamine-NPs. The 30:70 ratio of SP/AN demonstrated pivotal character as proficient Hg^{2+} adsorbent and detected with 98.8% absorbability of 497.7 mg/g (Lü et al., 2007). Poly(5-sulfo-1-aminoanthraquinone) NPs can eliminate Hg^{2+} and Pb^{2+} ions with elevated percentages and be revealed by Huang et al. (2011). Specifically, for the purification of water, the fabrication and implications of biopolymer celluloses (Olivera et al., 2016), nanocomposites, and chitosan-founded NMs have captivated curiosity.

Usually, cellulose nanofibers are synthesized by way of steam explosion and electrospinning. H_2SO_4 or HCl hydrolysis of indigenous cellulosic fibers to fabricate cellulose nanowhiskers and nanocrystals (Fung et al., 2011). The adsorption capability of cellulose NMs for the ions of heavy metal alters with chemical tempering of its surface functional groups (Man et al., 2011), for example, carboxylated cellulose nanocrystals (Hokkanen et al., 2014). To separate Ag^{+} ions from polluted water, chitin-nanocrystals, cellulose nanocrystals and cellulose nanofibers were introduced by Liu et al. (2014a, 2014b). Above 90% sorbability of Pb^{2+}, Cd^{2+}, Ni^{2+}, and Cr^{3+} has been increased by treating nanocellulose fibers, grafted on copolymer, with $CH_2 = CHSO_3H$ (Kardam et al., 2012). Nanoscaled cellulose fibers (NCFs) were applied to aqueous solutions for removing Cd^{2+}, Pb^{2+} and Ni^{2+} ions, while the standard diameter was 6 nm (Kardam et al., 2014). The depositing capability of copper and ferric ions is enhanced via functional-groups, developed by phosphorylating nanosized precipitates of cellulose (Liu et al., 2015). Owing to the biophosphonate's complexation strength of V^{5+} ion residing groups, biophosphonated nanocellulose can adsorb efficiently vanadium ions from aqueous solutions (Sirviö et al., 2016).

Carboxylated cellulose nanocrystals were noticed by Tong, et al. for adsorbing heavy metal ions from aqueous solutions (Yu et al., 2013). For adsorbing Co^{2+} ions, nuclear-industrial effluent is treated with multi-carboxylic groups containing nanobentonite or nanocellulose NCs grafted with poly(itaconic acid) or poly(methacrylic acid) (Anirudhan et al., 2016). In comparison to μ-chitosans, nano-chitosans are found to show rapid adsorbing capabilities with efficient performance (Dyal et al., 2003). For adsorbing ions like Zn^{2+}, Co^{2+}, Cd^{2+}, Cu^{2+}, Pb^{2+}, and Hg^{2+}, poly(maleic acid) was grafted onto chitosan followed by glutaraldehyde crosslinking resulting in chitosan-supported poly(maleic acid) nanomaterials with 400–900 nm in size (Ge and Hua, 2016). In particular, chitosan NPs are synthesized through ionic gelation (Du et al., 2008).

The wastewater was also treated by chitosan nanorods, synthesized by using polyanion tripolyphosphate crosslinked with lower Mw chitosan (Sivakami et al., 2013). Pb^{2+} and Cu^{2+} ions were also adsorbed through electrospun-constructed chitosan nanofibers (Haider and Park, 2009). Nickel ions are also removed through nanoparticles of chitosan-poly(acrylic acid) (Wang and Kuo, 2008). For adsorbing heavy metals, nano-fibered

membranes with polyethylene oxide and chitosan architecture were employed with priority: $Ni^{2+} > Cu^{2+} > Cd^{2+} > Pb^{2+}$ (Aliabadi et al., 2013). In water, Cd^{2+}, Cu^{2+}, and CrVI ions were removed by utilizing chitosan and nano-hydroxypatite combination.

To adsorb heavy metals, many strategies are followed by nano-cellulose and nanochitosan, for example, complex-formation, ion pair pore/surface arrangement, chelation with metals, ion-exchange and electrostatic-interactions (Kwok et al., 2014). Nanochitosan-chromium(VI) interactions, for instance, were ascribed to the electrostatic attraction (Kwok et al., 2014). Following an ion-exchange mechanism, Cu^{2+} ions were removed by applying chitosan/chitin nano-hydroxyapatite composite (Kwok et al., 2014). Heavy metals were investigated mechanistically regarding ion exchange and complexation methodologies via sorption by nanocrystals of cellulose improved with succinic acid (Kaleem et al., 2013). Ion exchange and complexation mechanism were exhibited by sulfonated wheat pulp nanocelluloses to remove Pb^{2+} ion (Bhatnagar and Sillanpää, 2009). Concurrently, adsorption of ester functional group incorporating functional groups of OH and Na ions together with heavy metals was achieved via chemisorption using succinic anhydride-modified nano-cellulose after mercerization (Sivakami et al., 2013). By applying nano-cellulosic fibrillated C-painted electrode, concentrations of Cd^{2+} and Pb^{2+} ions were standardized through electrochemical investigations. For adsorption, nano-cellulosic threads encompassed hydroxyl, carboxylate and ionized-aldehyde and was demonstrated in presented strategy (Rajiv Gandhi et al., 2011). Anionic complexation could be responsible for adsorbing nanomagnetic cellulose mercury ions.

8.4 Polymer-supported organic NCs

Since polymer-supported nanocomposites class have been synthesized by applying organic polymers as a support for the preparation of inorganic NPs, for instance, magnetic $Fe/TiO_2/Fe_3O_4$, also termed as inorganic NMs. Normally, organic polymer-based NCs have been categorized as: (1) biopolymer-supported NMs, and (2) synthetic organic polymer-based NMs. Latter category comprises polystyrene, polyaniline (PAN), poly(tetrafluoroethylene), polyhydroxybutyrate (PHB), nafion and polyethylene (PE). The former one covers chitosan, cellulose, and resin or alginate. The latter polymer-supported nanocomposites are utilized in water for the removal of biomaterials, organic contaminants, and heavy metals (Pan et al., 2009). Cu^{2+}, Ag^{+} and Hg^{2+} ions, for specimen, could be removed using tetraethylenepentamine-functionalized magnetic cellulose composite (Klemm et al., 2011).

Ni^{2+}, Cu^{2+}, and Cd^{2+} ions are proficiently adsorbed through nanoframed micro-threaded amino-transformed cellulose (Zhao et al., 2011). Arsenate ions (AsV) are being efficiently adsorbed using amine-modified (1,6-hexanediamine) NCs of cellulose-rooted bacterial Fe_3O_4 (Donia et al., 2012). Cellulose NCs of itaconic acid implanted Fe_3O_4 transformed through 2-mercaptobenzamide are successfully applied on wastewater of factories residing chlor-alkali to efficiently remove Hg^{2+} ions, and was presented by Anirudhan and Shainy (2015). Recently, NPs of magnetic-chitosan have gained a great deal of interest for removing metal-ions like Pt^{2+}, Co^{2+} and Cu^{2+}, as demonstrated in Fig. 8.5 (Anirudhan and Shainy, 2015). For the removal of Cu^{2+} ions from aqueous solutions, microspheres are in practice (Chang et al., 2006). Ren et al. implied Fe_3O_4 and chitosan NPs in combination with metal adsorbed

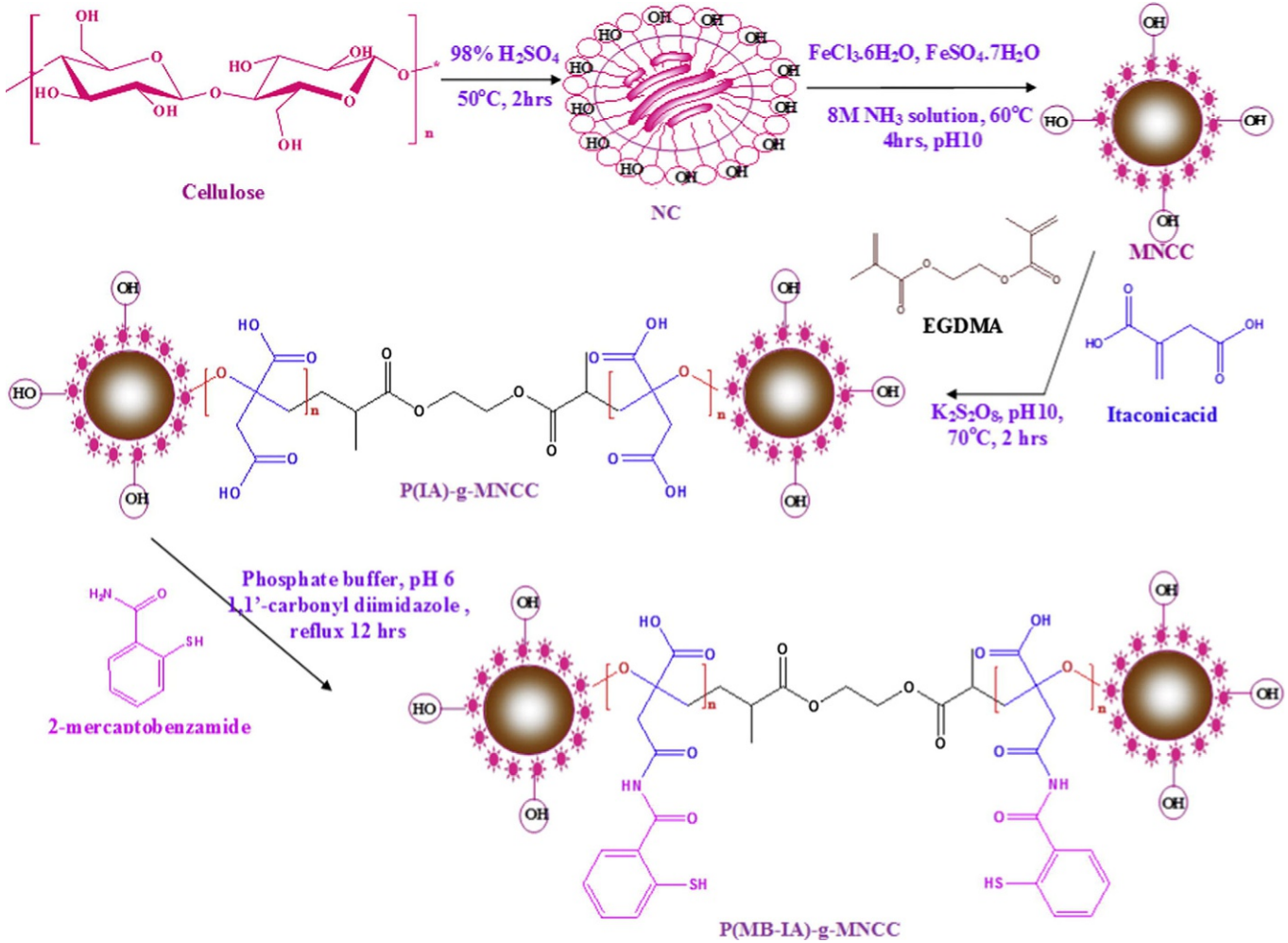

FIG. 8.5 Synthesis of P(MB-IA)-g-MNCC. *Reproduced with permission from Anirudhan, T.S., Shainy, F., Effective removal of mercury(II) ions from chlor-alkali industrial wastewater using 2-mercaptobenzamide modified itaconic acid-grafted-magnetite nanocellulose composite. J. Colloid Interface Sci. 456 (2015) 22–31. https://doi.org/10.1016/j.jcis.2015.05.052. Copyright 2015, Elsevier.*

organic pollutants and heavy metals from aqueous solution, like hydroxypatites, amination, and carboxylation (Ren et al., 2008). Cu^{2+} ions, for instance, are biosorbed by exterior of chitosan-laminated magnetic NPs that are grafted with biomass of *Saccharomyces cerevisiae*. Hg^{2+} and Pb^{2+} ions could also be removed from polluted water through the implementation of nanocrystals (NCs) of ZnSe colloidal surface-decorated polydimethylsiloxane foams, a very active constituent.

8.5 Conclusions and perspectives

Pollution created by human beings is increasing day by day, causing alarming health issues and decreasing availability of clean water for use. The conventional methods and technologies used for wastewater treatment are not efficient enough to remove microbial, organic, inorganic contaminants and this impelled the scientists to follow nanotechnology keeping in view the environmental needs. Nanomaterials take the privilege over bulk materials due to high porosity, great surface area, and excellent reactivity. Because of these exceptional properties, nanomaterials have been extensively used to treat wastewater for removal of heavy metals. This review focused on various nanomaterials including metal oxides, carbon-based nanomaterials, nanocomposites and their potential to remove heavy metals from wastewater. Nanomaterials efficiently adsorb heavy metals but still there are few limitations associated with the use of nanomaterials as they are unstable and have tendency to aggregate which reduces their efficiency. Due to their nanosize, sometimes it becomes difficult to separate them from water. Nanocomposites may be potential candidates to solving these issues. There is need to develop nanomaterials at large scale for market availability and also operating cost should be optimized from economical point of view. Nanomaterials should be synthesized by green chemistry to save environment and eliminate toxicity. The emerging nanomaterials provided potential alternative to conventional adsorbents for removal of heavy metals, but there are few risks and impacts associated with them that cannot be ignored as well. There is still need to put efforts to further elaborate on the capability, synthesis, development, separation, reusability, and cost of nanomaterials.

References

Adeleye, A.S., Keller, A.A., 2014. Long-term colloidal stability and metal leaching of single wall carbon nanotubes: effect of temperature and extracellular polymeric substances. Water Res. 49, 236–250. https://doi.org/10.1016/j.watres.2013.11.032.

Ahmed, M.A., Ali, S.M., El-Dek, S.I., Galal, A., 2013. Magnetite–hematite nanoparticles prepared by green methods for heavy metal ions removal from water. Mater. Sci. Eng. B 178 (10), 744–751. https://doi.org/10.1016/j.mseb.2013.03.011.

Albadarin, A.B., Yang, Z., Mangwandi, C., Glocheux, Y., Walker, G., Ahmad, M.N.M., 2014. Experimental design and batch experiments for optimization of Cr(VI) removal from aqueous solutions by hydrous cerium oxide nanoparticles. Chem. Eng. Res. Des. 92 (7), 1354–1362. https://doi.org/10.1016/j.cherd.2013.10.015.

Aliabadi, M., Irani, M., Ismaeili, J., Piri, H., Parnian, M.J., 2013. Electrospun nanofiber membrane of PEO/Chitosan for the adsorption of nickel, cadmium, lead and copper ions from aqueous solution. Chem. Eng. J. 220, 237–243. https://doi.org/10.1016/j.cej.2013.01.021.

An, B., Zhao, D., 2012. Immobilization of As(III) in soil and groundwater using a new class of polysaccharide stabilized Fe–Mn oxide nanoparticles. J. Hazard. Mater. 211-212, 332–341. https://doi.org/10.1016/j.jhazmat.2011.10.062.

Anandan, S., Kathiravan, K., Murugesan, V., Ikuma, Y., 2009. Anionic (IO3-) non-metal doped TiO2 nanoparticles for the photocatalytic degradation of hazardous pollutant in water. Catal. Commun. 10 (6), 1014–1019. https://doi.org/10.1016/j.catcom.2008.12.054.

Anirudhan, T.S., Shainy, F., 2015. Effective removal of mercury(II) ions from chlor-alkali industrial wastewater using 2-mercaptobenzamide modified itaconic acid-grafted-magnetite nanocellulose composite. J. Colloid Interface Sci. 456, 22–31. https://doi.org/10.1016/j.jcis.2015.05.052.

Anirudhan, T.S., Deepa, J.R., Christa, J., 2016. Nanocellulose/nanobentonite composite anchored with multi-carboxyl functional groups as an adsorbent for the effective removal of cobalt(II) from nuclear industry wastewater samples. J. Colloid Interface Sci. 467, 307–320. https://doi.org/10.1016/j.jcis.2016.01.023.

Astruc, D., Lu, F., Aranzaes, J.R., 2005. Nanoparticles as recyclable catalysts: the frontier between homogeneous and heterogeneous catalysis. Angew. Chem. Int. Ed. 44 (48), 7852–7872. https://doi.org/10.1002/anie.200500766.

Awual, M.R., Hasan, M.M., Eldesoky, G.E., Khaleque, M.A., Rahman, M.M., Naushad, M., 2016. Facile mercury detection and removal from aqueous media involving ligand impregnated conjugate nanomaterials. Chem. Eng. J. 290, 243–251. https://doi.org/10.1016/j.cej.2016.01.038.

Badruddoza, A.Z.M., Tay, A.S.H., Tan, P.Y., Hidajat, K., Uddin, M.S., 2011. Carboxymethyl-β-cyclodextrin conjugated magnetic nanoparticles as nano-adsorbents for removal of copper ions: synthesis and adsorption studies. J. Hazard. Mater. 185 (2), 1177–1186. https://doi.org/10.1016/j.jhazmat.2010.10.029.

Behnoudnia, F., Dehghani, H., 2014. Anion effect on the control of morphology for NiC2O4·2H2O nanostructures as precursors for synthesis of Ni(OH)2 and NiO nanostructures and their application for removing heavy metal ions of cadmium(ii) and lead(ii). Dalton Trans. 43 (9), 3471–3478. https://doi.org/10.1039/C3DT52049H.

Bhatnagar, A., Sillanpää, M., 2009. Applications of chitin- and chitosan-derivatives for the detoxification of water and wastewater — a short review. Adv. Colloid Interf. Sci. 152 (1), 26–38. https://doi.org/10.1016/j.cis.2009.09.003.

Bhunia, P., Kim, G., Baik, C., Lee, H., 2012. A strategically designed porous iron–iron oxide matrix on graphene for heavy metal adsorption. Chem. Commun. 48 (79), 9888–9890. https://doi.org/10.1039/C2CC35120J.

Cantu, Y., Remes, A., Reyna, A., Martinez, D., Villarreal, J., Ramos, H., Parsons, J.G., 2014. Thermodynamics, kinetics, and activation energy studies of the sorption of chromium(III) and chromium(VI) to a Mn3O4 nanomaterial. Chem. Eng. J. 254, 374–383. https://doi.org/10.1016/j.cej.2014.05.110.

Chang, Y.-C., Chang, S.-W., Chen, D.-H., 2006. Magnetic chitosan nanoparticles: studies on chitosan binding and adsorption of Co(II) ions. React. Funct. Polym. 66 (3), 335–341. https://doi.org/10.1016/j.reactfunctpolym.2005.08.006.

Chauhan, N., Gupta, S., Singh, N., Singh, S., Islam, S.S., Sood, K.N., Pasricha, R., 2011. Aligned nanogold assisted one step sensing and removal of heavy metal ions. J. Colloid Interface Sci. 363 (1), 42–50. https://doi.org/10.1016/j.jcis.2011.07.018.

Chen, C.L., Wang, X.K., Nagatsu, M., 2009. Europium adsorption on multiwall carbon nanotube/Iron oxide magnetic composite in the presence of polyacrylic acid. Environ. Sci. Technol. 43 (7), 2362–2367. https://doi.org/10.1021/es803018a.

Chen, J., Li, X.Y., Dong, H., 2010. Formation and characterisations of S phase in plasma carburised high carbon Stellite 21 CoCr alloy. Surf. Eng. 26 (4), 233–241. https://doi.org/10.1179/026708409X12490360426007.

Cui, H.-J., Cai, J.-K., Shi, J.-W., Yuan, B., Ai, C.-L., Fu, M.-L., 2014. Fabrication of 3D porous Mn doped α-Fe2O3 nanostructures for the removal of heavy metals from wastewater. RSC Adv. 4 (20), 10176–10179. https://doi.org/10.1039/C3RA46348F.

Cui, L., Wang, Y., Gao, L., Hu, L., Yan, L., Wei, Q., Du, B., 2015. EDTA functionalized magnetic graphene oxide for removal of Pb(II), Hg(II) and Cu(II) in water treatment: adsorption mechanism and separation property. Chem. Eng. J. 281, 1–10. https://doi.org/10.1016/j.cej.2015.06.043.

Cumbal, L., SenGupta, A.K., 2005. Arsenic removal using polymer-supported hydrated Iron(III) oxide nanoparticles: role of Donnan membrane effect. Environ. Sci. Technol. 39 (17), 6508–6515. https://doi.org/10.1021/es050175e.

Datsyuk, V., Kalyva, M., Papagelis, K., Parthenios, J., Tasis, D., Siokou, A., Galiotis, C., 2008. Chemical oxidation of multiwalled carbon nanotubes. Carbon 46 (6), 833–840. https://doi.org/10.1016/j.carbon.2008.02.012.

Dickinson, M., Scott, T.B., 2010. The application of zero-valent iron nanoparticles for the remediation of a uranium-contaminated waste effluent. J. Hazard. Mater. 178 (1), 171–179. https://doi.org/10.1016/j.jhazmat.2010.01.060.

Dil, E.A., Ghaedi, M., Asfaram, A., 2017a. The performance of nanorods material as adsorbent for removal of azo dyes and heavy metal ions: application of ultrasound wave, optimization and modeling. Ultrason. Sonochem. 34, 792–802. https://doi.org/10.1016/j.ultsonch.2016.07.015.

Dil, E.A., Ghaedi, M., Asfaram, A., Hajati, S., Mehrabi, F., Goudarzi, A., 2017b. Preparation of nanomaterials for the ultrasound-enhanced removal of Pb2+ ions and malachite green dye: Chemometric optimization and modeling. Ultrason. Sonochem. 34, 677–691. https://doi.org/10.1016/j.ultsonch.2016.07.001.

Ding, Z., Hu, X., Morales, V.L., Gao, B., 2014. Filtration and transport of heavy metals in graphene oxide enabled sand columns. Chem. Eng. J. 257, 248–252. https://doi.org/10.1016/j.cej.2014.07.034.

Dong, Z., Wang, D., Liu, X., Pei, X., Chen, L., Jin, J., 2014. Bio-inspired surface-functionalization of graphene oxide for the adsorption of organic dyes and heavy metal ions with a superhigh capacity. J. Mater. Chem. A 2 (14), 5034–5040. https://doi.org/10.1039/c3ta14751g.

Donia, A.M., Atia, A.A., Abouzayed, F.I., 2012. Preparation and characterization of nano-magnetic cellulose with fast kinetic properties towards the adsorption of some metal ions. Chem. Eng. J. 191, 22–30. https://doi.org/10.1016/j.cej.2011.08.034.

Du, W.L., Xu, Z.R., Han, X.Y., Xu, Y.L., Miao, Z.G., 2008. Preparation, characterization and adsorption properties of chitosan nanoparticles for eosin Y as a model anionic dye. J. Hazard. Mater. 153 (1), 152–156. https://doi.org/10.1016/j.jhazmat.2007.08.040.

Dyal, A., Loos, K., Noto, M., Chang, S.W., Spagnoli, C., Shafi, K.V.P.M., Gross, R.A., 2003. Activity of Candida rugosa lipase immobilized on γ-Fe2O3 magnetic nanoparticles. J. Am. Chem. Soc. 125 (7), 1684–1685. https://doi.org/10.1021/ja021223n.

Ezoddin, M., Shemirani, F., Abdi, K., Saghezchi, M.K., Jamali, M.R., 2010. Application of modified nano-alumina as a solid phase extraction sorbent for the preconcentration of cd and Pb in water and herbal samples prior to flame atomic absorption spectrometry determination. J. Hazard. Mater. 178 (1), 900–905. https://doi.org/10.1016/j.jhazmat.2010.02.023.

Fan, L., Luo, C., Sun, M., Qiu, H., 2012. Synthesis of graphene oxide decorated with magnetic cyclodextrin for fast chromium removal. J. Mater. Chem. 22 (47), 24577–24583. https://doi.org/10.1039/C2JM35378D.

Fan, L., Luo, C., Sun, M., Li, X., Qiu, H., 2013. Highly selective adsorption of lead ions by water-dispersible magnetic chitosan/graphene oxide composites. Colloids Surf. B: Biointerfaces 103, 523–529. https://doi.org/10.1016/j.colsurfb.2012.11.006.

Farghali, A.A., Bahgat, M., Enaiet Allah, A., Khedr, M.H., 2013. Adsorption of Pb(II) ions from aqueous solutions using copper oxide nanostructures. Beni-Suef Univ. J. Basic Appl. Sci. 2 (2), 61–71. https://doi.org/10.1016/j.bjbas.2013.01.001.

Feng, Y., Gong, J.-L., Zeng, G.-M., Niu, Q.-Y., Zhang, H.-Y., Niu, C.-G., Yan, M., 2010. Adsorption of cd (II) and Zn (II) from aqueous solutions using magnetic hydroxyapatite nanoparticles as adsorbents. Chem. Eng. J. 162 (2), 487–494. https://doi.org/10.1016/j.cej.2010.05.049.

Fu, F., Wang, Q., 2011. Removal of heavy metal ions from wastewaters: a review. J. Environ. Manag. 92 (3), 407–418. https://doi.org/10.1016/j.jenvman.2010.11.011.

Fung, W.-Y., Yuen, K.-H., Liong, M.-T., 2011. Agrowaste-based nanofibers as a probiotic Encapsulant: fabrication and characterization. J. Agric. Food Chem. 59 (15), 8140–8147. https://doi.org/10.1021/jf2009342.

Ge, H., Hua, T., 2016. Synthesis and characterization of poly(maleic acid)-grafted crosslinked chitosan nanomaterial with high uptake and selectivity for Hg(II) sorption. Carbohydr. Polym. 153, 246–252. https://doi.org/10.1016/j.carbpol.2016.07.110.

Ge, F., Li, M.-M., Ye, H., Zhao, B.-X., 2012. Effective removal of heavy metal ions Cd2+, Zn2+, Pb2+, Cu2+ from aqueous solution by polymer-modified magnetic nanoparticles. J. Hazard. Mater. 211-212, 366–372. https://doi.org/10.1016/j.jhazmat.2011.12.013.

Geng, B., Jin, Z., Li, T., Qi, X., 2009. Kinetics of hexavalent chromium removal from water by chitosan-Fe0 nanoparticles. Chemosphere 75 (6), 825–830. https://doi.org/10.1016/j.chemosphere.2009.01.009.

Gollavelli, G., Chang, C.-C., Ling, Y.-C., 2013. Facile synthesis of smart magnetic graphene for safe drinking water: heavy metal removal and disinfection control. ACS Sustain. Chem. Eng. 1 (5), 462–472. https://doi.org/10.1021/sc300112z.

Gong, J., Liu, T., Wang, X., Hu, X., Zhang, L., 2011. Efficient removal of heavy metal ions from aqueous systems with the assembly of anisotropic layered double hydroxide nanocrystals@carbon Nanosphere. Environ. Sci. Technol. 45 (14), 6181–6187. https://doi.org/10.1021/es200668q.

Gopalakrishnan, A., Krishnan, R., Thangavel, S., Venugopal, G., Kim, S.-J., 2015. Removal of heavy metal ions from pharma-effluents using graphene-oxide nanosorbents and study of their adsorption kinetics. J. Ind. Eng. Chem. 30, 14–19. https://doi.org/10.1016/j.jiec.2015.06.005.

Guo, X., Du, B., Wei, Q., Yang, J., Hu, L., Yan, L., Xu, W., 2014. Synthesis of amino functionalized magnetic graphenes composite material and its application to remove Cr(VI), Pb(II), Hg(II), Cd(II) and Ni(II) from contaminated water. J. Hazard. Mater. 278, 211–220. https://doi.org/10.1016/j.jhazmat.2014.05.075.

Hadavifar, M., Bahramifar, N., Younesi, H., Li, Q., 2014. Adsorption of mercury ions from synthetic and real wastewater aqueous solution by functionalized multi-walled carbon nanotube with both amino and thiolated groups. Chem. Eng. J. 237, 217–228. https://doi.org/10.1016/j.cej.2013.10.014.

Haider, S., Park, S.-Y., 2009. Preparation of the electrospun chitosan nanofibers and their applications to the adsorption of Cu(II) and Pb(II) ions from an aqueous solution. J. Membr. Sci. 328 (1), 90–96. https://doi.org/10.1016/j.memsci.2008.11.046.

Hakami, O., Zhang, Y., Banks, C.J., 2012. Thiol-functionalised mesoporous silica-coated magnetite nanoparticles for high efficiency removal and recovery of hg from water. Water Res. 46 (12), 3913–3922. https://doi.org/10.1016/j.watres.2012.04.032.

Heiranian, M., Farimani, A.B., Aluru, N.R., 2015. Water desalination with a single-layer MoS 2 nanopore. Nat. Commun. 6 (1), 1–6.

Hokkanen, S., Repo, E., Suopajärvi, T., Liimatainen, H., Niinimaa, J., Sillanpää, M., 2014. Adsorption of Ni(II), Cu(II) and Cd(II) from aqueous solutions by amino modified nanostructured microfibrillated cellulose. Cellulose 21 (3), 1471–1487. https://doi.org/10.1007/s10570-014-0240-4.

Huang, C., Hu, B., 2008. Silica-coated magnetic nanoparticles modified with γ-mercaptopropyltrimethoxysilane for fast and selective solid phase extraction of trace amounts of Cd, Cu, Hg, and Pb in environmental and biological samples prior to their determination by inductively coupled plasma mass spectrometry. Spectrochim. Acta B At. Spectrosc. 63 (3), 437–444. https://doi.org/10.1016/j.sab.2007.12.010.

Huang, Y., Keller, A.A., 2015. EDTA functionalized magnetic nanoparticle sorbents for cadmium and lead contaminated water treatment. Water Res. 80, 159–168. https://doi.org/10.1016/j.watres.2015.05.011.

Huang, M.-R., Huang, S.-J., Li, X.-G., 2011. Facile synthesis of polysulfoaminoanthraquinone nanosorbents for rapid removal and ultrasensitive fluorescent detection of heavy metal ions. J. Phys. Chem. C 115 (13), 5301–5315. https://doi.org/10.1021/jp1099706.

Iram, M., Guo, C., Guan, Y., Ishfaq, A., Liu, H., 2010. Adsorption and magnetic removal of neutral red dye from aqueous solution using Fe3O4 hollow nanospheres. J. Hazard. Mater. 181 (1), 1039–1050. https://doi.org/10.1016/j.jhazmat.2010.05.119.

Jaiswal, A., Ghsoh, S.S., Chattopadhyay, A., 2012. Quantum dot impregnated-chitosan film for heavy metal ion sensing and removal. Langmuir 28 (44), 15687–15696. https://doi.org/10.1021/la3027573.

Kaleem, W.A., Muhammad, N., Qayum, M., Khan, H., Khan, A., Aliberti, L., De, F.V., 2013. Antinociceptive activity of cyclopeptide alkaloids isolated from Ziziphus oxyphylla Edgew (Rhamnaceae). Fitoterapia 91, 154–158.

Kanel, S.R., Manning, B., Charlet, L., Choi, H., 2005. Removal of arsenic(III) from groundwater by nanoscale zero-valent Iron. Environ. Sci. Technol. 39 (5), 1291–1298. https://doi.org/10.1021/es048991u.

Kangoa, S., Kaliab, S., Cellib, A., 2013. Prog. Polym. Sci. 38 (8), 1232.

Karatapanis, A.E., Fiamegos, Y., Stalikas, C.D., 2011. Silica-modified magnetic nanoparticles functionalized with cetylpyridinium bromide for the preconcentration of metals after complexation with 8-hydroxyquinoline. Talanta 84 (3), 834–839. https://doi.org/10.1016/j.talanta.2011.02.013.

Kardam, A., Raj, K.R., Arora, J.K., Srivastava, S., 2012. Artificial neural network modeling for biosorption of Pb(II) ions on nanocellulose fibers. BioNanoScience 2 (3), 153–160. https://doi.org/10.1007/s12668-012-0045-6.

Kardam, A., Raj, K.R., Srivastava, S., Srivastava, M.M., 2014. Nanocellulose fibers for biosorption of cadmium, nickel, and lead ions from aqueous solution. Clean Techn. Environ. Policy 16 (2), 385–393. https://doi.org/10.1007/s10098-013-0634-2.

Khan, A., Asiri, A.M., Rub, M.A., Azum, N., Khan, A.A.P., Khan, S.B., Khan, I., 2013. Synthesis, characterization of silver nanoparticle embedded polyaniline tungstophosphate-nanocomposite cation exchanger and its application for heavy metal selective membrane. Compos. Part B 45 (1), 1486–1492. https://doi.org/10.1016/j.compositesb.2012.09.023.

Kim, B., Park, C.-S., Murayama, M., Hochella, M.F., 2010. Discovery and characterization of silver sulfide nanoparticles in final sewage sludge products. Environ. Sci. Technol. 44 (19), 7509–7514. https://doi.org/10.1021/es101565j.

Kim, E.-J., Lee, C.-S., Chang, Y.-Y., Chang, Y.-S., 2013. Hierarchically structured manganese oxide-coated magnetic nanocomposites for the efficient removal of heavy metal ions from aqueous systems. ACS Appl. Mater. Interfaces 5 (19), 9628–9634. https://doi.org/10.1021/am402615m.

Klemm, D., Kramer, F., Moritz, S., Lindström, T., Ankerfors, M., Gray, D., Dorris, A., 2011. Nanocelluloses: a new family of nature-based materials. Angew. Chem. Int. Ed. 50 (24), 5438–5466. https://doi.org/10.1002/anie.201001273.

Koduru, J.R., Lee, K.D., 2014. Evaluation of thiosemicarbazone derivative as chelating agent for the simultaneous removal and trace determination of Cd(II) and Pb(II) in food and water samples. Food Chem. 150, 1–8. https://doi.org/10.1016/j.foodchem.2013.10.104.

Kosa, S.A., Al-Zhrani, G., Abdel Salam, M., 2012. Removal of heavy metals from aqueous solutions by multi-walled carbon nanotubes modified with 8-hydroxyquinoline. Chem. Eng. J. 181-182, 159–168. https://doi.org/10.1016/j.cej.2011.11.044.

Kumar, K.Y., Muralidhara, H.B., Nayaka, Y.A., Balasubramanyam, J., Hanumanthappa, H., 2013. Hierarchically assembled mesoporous ZnO nanorods for the removal of lead and cadmium by using differential pulse anodic stripping voltammetric method. Powder Technol. 239, 208–216. https://doi.org/10.1016/j.powtec.2013.02.009.

Kwok, K.C.M., Koong, L.F., Chen, G., McKay, G., 2014. Mechanism of arsenic removal using chitosan and nanochitosan. J. Colloid Interface Sci. 416, 1–10. https://doi.org/10.1016/j.jcis.2013.10.031.

Kyzas, G.Z., Matis, K.A., 2015. Nanoadsorbents for pollutants removal: a review. J. Mol. Liq. 203, 159–168. https://doi.org/10.1016/j.molliq.2015.01.004.

Lee, H.Y., Bae, D.R., Park, J.C., Song, H., Han, W.S., Jung, J.H., 2009. A selective Fluoroionophore based on BODIPY-functionalized magnetic silica nanoparticles: removal of Pb2+ from human blood. Angew. Chem. Int. Ed. 48 (7), 1239–1243. https://doi.org/10.1002/anie.200804714.

Lee, Y.-F., Nan, F.-H., Chen, M.-J., Wu, H.-Y., Ho, C.-W., Chen, Y.-Y., Huang, C.-C., 2012. Detection and removal of mercury and lead ions by using gold nanoparticle-based gel membrane. Anal. Methods 4 (6), 1709–1717. https://doi.org/10.1039/C2AY05872C.

Li, X.-q., Zhang, W.-x., 2006. Iron nanoparticles: the core – shell structure and unique properties for Ni(II) sequestration. Langmuir 22 (10), 4638–4642. https://doi.org/10.1021/la060057k.

Li, S., Yue, X., Jing, Y., Bai, S., Dai, Z., 2011a. Fabrication of zonal thiol-functionalized silica nanofibers for removal of heavy metal ions from wastewater. Colloids Surf. A Physicochem. Eng. Asp. 380 (1), 229–233. https://doi.org/10.1016/j.colsurfa.2011.02.027.

Li, G., Zhao, Z., Liu, J., Jiang, G., 2011b. Effective heavy metal removal from aqueous systems by thiol functionalized magnetic mesoporous silica. J. Hazard. Mater. 192 (1), 277–283. https://doi.org/10.1016/j.jhazmat.2011.05.015.

Li, L., Fan, L., Sun, M., Qiu, H., Li, X., Duan, H., Luo, C., 2013. Adsorbent for chromium removal based on graphene oxide functionalized with magnetic cyclodextrin–chitosan. Colloids Surf. B: Biointerfaces 107, 76–83. https://doi.org/10.1016/j.colsurfb.2013.01.074.

Li, L., Wen, Y., Xu, L., Xu, Q., Song, S., Zuo, X., Liu, G., 2016. Development of mercury(II) ion biosensors based on mercury-specific oligonucleotide probes. Biosens. Bioelectron. 75, 433–445. https://doi.org/10.1016/j.bios.2015.09.003.

Liu, R., Liang, P., 2008. Determination of trace lead in water samples by graphite furnace atomic absorption spectrometry after preconcentration with nanometer titanium dioxide immobilized on silica gel. J. Hazard. Mater. 152 (1), 166–171. https://doi.org/10.1016/j.jhazmat.2007.06.081.

Liu, T., Yang, X., Wang, Z.-L., Yan, X., 2013. Enhanced chitosan beads-supported Fe0-nanoparticles for removal of heavy metals from electroplating wastewater in permeable reactive barriers. Water Res. 47 (17), 6691–6700. https://doi.org/10.1016/j.watres.2013.09.006.

Liu, P., Sehaqui, H., Tingaut, P., Wichser, A., Oksman, K., Mathew, A.P., 2014a. Cellulose and chitin nanomaterials for capturing silver ions (Ag+) from water via surface adsorption. Cellulose 21 (1), 449–461. https://doi.org/10.1007/s10570-013-0139-5.

Liu, M., Wang, Z., Zong, S., Chen, H., Zhu, D., Wu, L., Cui, Y., 2014b. SERS detection and removal of mercury(II)/silver(I) using oligonucleotide-functionalized Core/Shell magnetic silica sphere@au nanoparticles. ACS Appl. Mater. Interfaces 6 (10), 7371–7379. https://doi.org/10.1021/am5006282.

Liu, P., Borrell, P.F., Božič, M., Kokol, V., Oksman, K., Mathew, A.P., 2015. Nanocelluloses and their phosphorylated derivatives for selective adsorption of Ag+, Cu2+ and Fe3+ from industrial effluents. J. Hazard. Mater. 294, 177–185. https://doi.org/10.1016/j.jhazmat.2015.04.001.

Liu, T., Gao, B., Fang, J., Wang, B., Cao, X., 2016a. Biochar-supported carbon nanotube and graphene oxide nanocomposites for Pb(ii) and Cd(ii) removal. RSC Adv. 6 (29), 24314–24319. https://doi.org/10.1039/C6RA01895E.

Liu, J., Ge, X., Ye, X., Wang, G., Zhang, H., Zhou, H., Zhao, H., 2016b. 3D graphene/δ-MnO2 aerogels for highly efficient and reversible removal of heavy metal ions. J. Mater. Chem. A 4 (5), 1970–1979. https://doi.org/10.1039/C5TA08106H.

López-Téllez, G., Barrera-Díaz, C.E., Balderas-Hernández, P., Roa-Morales, G., Bilyeu, B., 2011. Removal of hexavalent chromium in aquatic solutions by iron nanoparticles embedded in orange peel pith. Chem. Eng. J. 173 (2), 480–485. https://doi.org/10.1016/j.cej.2011.08.018.

Lü, Q.-F., Huang, M.-R., Li, X.-G., 2007. Synthesis and heavy-metal-ion sorption of pure Sulfophenylenediamine copolymer nanoparticles with intrinsic conductivity and stability. Chem. Eur. J. 13 (21), 6009–6018. https://doi.org/10.1002/chem.200700233.

Ma, H.-L., Zhang, Y., Hu, Q.-H., Yan, D., Yu, Z.-Z., Zhai, M., 2012. Chemical reduction and removal of Cr(vi) from acidic aqueous solution by ethylenediamine-reduced graphene oxide. J. Mater. Chem. 22 (13), 5914–5916. https://doi.org/10.1039/C2JM00145D.

Mahapatra, A., Mishra, B.G., Hota, G., 2013. Electrospun Fe2O3–Al2O3 nanocomposite fibers as efficient adsorbent for removal of heavy metal ions from aqueous solution. J. Hazard. Mater. 258-259, 116–123. https://doi.org/10.1016/j.jhazmat.2013.04.045.

Man, Z., Muhammad, N., Sarwono, A., Bustam, M.A., Vignesh Kumar, M., Rafiq, S., 2011. Preparation of cellulose nanocrystals using an ionic liquid. J. Polym. Environ. 19 (3), 726–731. https://doi.org/10.1007/s10924-011-0323-3.

Mani, A.D., Reddy, P.M.K., Srinivaas, M., Ghosal, P., Xanthopoulos, N., Subrahmanyam, C., 2015. Facile synthesis of efficient visible active C-doped TiO2 nanomaterials with high surface area for the simultaneous removal of phenol and Cr(VI). Mater. Res. Bull. 61, 391–399. https://doi.org/10.1016/j.materresbull.2014.10.051.

Mashhadizadeh, M.H., Amoli-Diva, M., 2013. Atomic absorption spectrometric determination of Al3+ and Cr3+ after preconcentration and separation on 3-mercaptopropionic acid modified silica coated-Fe3O4 nanoparticles. J. Anal. At. Spectrom. 28 (2), 251–258. https://doi.org/10.1039/C2JA30286A.

Mejias Carpio, I.E., Mangadlao, J.D., Nguyen, H.N., Advincula, R.C., Rodrigues, D.F., 2014. Graphene oxide functionalized with ethylenediamine triacetic acid for heavy metal adsorption and anti-microbial applications. Carbon 77, 289–301. https://doi.org/10.1016/j.carbon.2014.05.032.

Mubarak, N.M., Sahu, J.N., Abdullah, E.C., Jayakumar, N.S., 2014. Removal of heavy metals from wastewater using carbon nanotubes. Sep. Purif. Rev. 43 (4), 311–338. https://doi.org/10.1080/15422119.2013.821996.

Mulvihill, M., Tao, A., Benjauthrit, K., Arnold, J., Yang, P., 2008. Surface-enhanced Raman spectroscopy for trace arsenic detection in contaminated water. Angew. Chem. Int. Ed. 47 (34), 6456–6460. https://doi.org/10.1002/anie.200800776.

Musameh, M.M., Hickey, M., Kyratzis, I.L., 2011. Carbon nanotube-based extraction and electrochemical detection of heavy metals. Res. Chem. Intermed. 37 (7), 675–689. https://doi.org/10.1007/s11164-011-0307-x.

Musico, Y.L.F., Santos, C.M., Dalida, M.L.P., Rodrigues, D.F., 2013. Improved removal of lead(ii) from water using a polymer-based graphene oxide nanocomposite. J. Mater. Chem. A 1 (11), 3789–3796. https://doi.org/10.1039/C3TA01616A.

Ngomsik, A.-F., Bee, A., Siaugue, J.-M., Talbot, D., Cabuil, V., Cote, G., 2009. Co(II) removal by magnetic alginate beads containing Cyanex 272®. J. Hazard. Mater. 166 (2), 1043–1049. https://doi.org/10.1016/j.jhazmat.2008.11.109.

Olivera, S., Muralidhara, H.B., Venkatesh, K., Guna, V.K., Gopalakrishna, K., Kumar, K., Y., 2016. Potential applications of cellulose and chitosan nanoparticles/composites in wastewater treatment: a review. Carbohydr. Polym. 153, 600–618. https://doi.org/10.1016/j.carbpol.2016.08.017.

Pan, B., Wu, J., Pan, B., Lv, L., Zhang, W., Xiao, L., Zheng, S., 2009. Development of polymer-based nanosized hydrated ferric oxides (HFOs) for enhanced phosphate removal from waste effluents. Water Res. 43 (17), 4421–4429. https://doi.org/10.1016/j.watres.2009.06.055.

Pang, Y., Zeng, G., Tang, L., Zhang, Y., Liu, Y., Lei, X., Xie, G., 2011. PEI-grafted magnetic porous powder for highly effective adsorption of heavy metal ions. Desalination 281, 278–284. https://doi.org/10.1016/j.desal.2011.08.001.

Race, M., Marotta, R., Fabbricino, M., Pirozzi, F., Andreozzi, R., Cortese, L., Giudicianni, P., 2016. Copper and zinc removal from contaminated soils through soil washing process using ethylenediaminedisuccinic acid as a

chelating agent: a modeling investigation. J. Environ. Chem. Eng. 4 (3), 2878–2891. https://doi.org/10.1016/j.jece.2016.05.031.
Rafiq, Z., Nazir, R., Durr-e-Shahwar, Shah, M.R., Ali, S., 2014. Utilization of magnesium and zinc oxide nano-adsorbents as potential materials for treatment of copper electroplating industry wastewater. J. Environ. Chem. Eng. 2 (1), 642–651. https://doi.org/10.1016/j.jece.2013.11.004.
Rai, M., Yadav, A., Gade, A., 2009. Silver nanoparticles as a new generation of antimicrobials. Biotechnol. Adv. 27 (1), 76–83. https://doi.org/10.1016/j.biotechadv.2008.09.002.
Rajiv Gandhi, M., Kousalya, G.N., Meenakshi, S., 2011. Removal of copper(II) using chitin/chitosan nano-hydroxyapatite composite. Int. J. Biol. Macromol. 48 (1), 119–124. https://doi.org/10.1016/j.ijbiomac.2010.10.009.
Ren, Y., Zhang, M., Zhao, D., 2008. Synthesis and properties of magnetic Cu(II) ion imprinted composite adsorbent for selective removal of copper. Desalination 228 (1), 135–149. https://doi.org/10.1016/j.desal.2007.08.013.
Ren, Y., Abbood, H.A., He, F., Peng, H., Huang, K., 2013. Magnetic EDTA-modified chitosan/SiO2/Fe3O4 adsorbent: preparation, characterization, and application in heavy metal adsorption. Chem. Eng. J. 226, 300–311. https://doi.org/10.1016/j.cej.2013.04.059.
Salam, M.A., Makki, M.S.I., Abdelaal, M.Y.A., 2011. Preparation and characterization of multi-walled carbon nanotubes/chitosan nanocomposite and its application for the removal of heavy metals from aqueous solution. J. Alloys Compd. 509 (5), 2582–2587. https://doi.org/10.1016/j.jallcom.2010.11.094.
Shahat, A., Awual, M.R., Naushad, M., 2015. Functional ligand anchored nanomaterial based facial adsorbent for cobalt(II) detection and removal from water samples. Chem. Eng. J. 271, 155–163. https://doi.org/10.1016/j.cej.2015.02.097.
Shi, L.-n., Zhang, X., Chen, Z.-l., 2011. Removal of chromium (VI) from wastewater using bentonite-supported nano-scale zero-valent iron. Water Res. 45 (2), 886–892. https://doi.org/10.1016/j.watres.2010.09.025.
Sirviö, J.A., Hasa, T., Leiviskä, T., Liimatainen, H., Hormi, O., 2016. Bisphosphonate nanocellulose in the removal of vanadium(V) from water. Cellulose 23 (1), 689–697. https://doi.org/10.1007/s10570-015-0819-4.
Sivakami, M.S., Gomathi, T., Venkatesan, J., Jeong, H.-S., Kim, S.-K., Sudha, P.N., 2013. Preparation and characterization of nano chitosan for treatment wastewaters. Int. J. Biol. Macromol. 57, 204–212. https://doi.org/10.1016/j.ijbiomac.2013.03.005.
Skubal, L.R., Meshkov, N.K., Rajh, T., Thurnauer, M., 2002. Cadmium removal from water using thiolactic acid-modified titanium dioxide nanoparticles. J. Photochem. Photobiol. A Chem. 148 (1), 393–397. https://doi.org/10.1016/S1010-6030(02)00069-2.
Smith, S.C., Rodrigues, D.F., 2015. Carbon-based nanomaterials for removal of chemical and biological contaminants from water: a review of mechanisms and applications. Carbon 91, 122–143. https://doi.org/10.1016/j.carbon.2015.04.043.
Song, J., Kong, H., Jang, J., 2011. Adsorption of heavy metal ions from aqueous solution by polyrhodanine-encapsulated magnetic nanoparticles. J. Colloid Interface Sci. 359 (2), 505–511. https://doi.org/10.1016/j.jcis.2011.04.034.
Srivastava, V., Weng, C.H., Singh, V.K., Sharma, Y.C., 2011. Adsorption of nickel ions from aqueous solutions by nano alumina: kinetic, mass transfer, and equilibrium studies. J. Chem. Eng. Data 56 (4), 1414–1422. https://doi.org/10.1021/je101152b.
Stafiej, A., Pyrzynska, K., 2007. Adsorption of heavy metal ions with carbon nanotubes. Sep. Purif. Technol. 58 (1), 49–52. https://doi.org/10.1016/j.seppur.2007.07.008.
Šulek, F., Drofenik, M., Habulin, M., Knez, Ž., 2010. Surface functionalization of silica-coated magnetic nanoparticles for covalent attachment of cholesterol oxidase. J. Magn. Magn. Mater. 322 (2), 179–185. https://doi.org/10.1016/j.jmmm.2009.07.075.
Sumesh, E., Bootharaju, M.S., Anshup, & Pradeep, T., 2011. A practical silver nanoparticle-based adsorbent for the removal of Hg2+ from water. J. Hazard. Mater. 189 (1), 450–457. https://doi.org/10.1016/j.jhazmat.2011.02.061.
Sun, L., Ying, Y., Huang, H., Song, Z., Mao, Y., Xu, Z., Peng, X., 2014. Ultrafast molecule separation through layered WS2 Nanosheet membranes. ACS Nano 8 (6), 6304–6311. https://doi.org/10.1021/nn501786m.
Takafuji, M., Ide, S., Ihara, H., Xu, Z., 2004. Preparation of poly(1-vinylimidazole)-grafted magnetic nanoparticles and their application for removal of metal ions. Chem. Mater. 16 (10), 1977–1983. https://doi.org/10.1021/cm030334y.
Tassali, N., Kotera, N., Boutin, C., Léonce, E., Boulard, Y., Rousseau, B., Berthault, P., 2014. Smart detection of toxic metal ions, Pb2+ and Cd2+, using a 129Xe NMR-based sensor. Anal. Chem. 86 (3), 1783–1788. https://doi.org/10.1021/ac403669p.

Upadhyayula, V.K.K., Deng, S., Mitchell, M.C., Smith, G.B., 2009. Application of carbon nanotube technology for removal of contaminants in drinking water: a review. Sci. Total Environ. 408 (1), 1–13. https://doi.org/10.1016/j.scitotenv.2009.09.027.

Vilela, D., Parmar, J., Zeng, Y., Zhao, Y., Sánchez, S., 2016. Graphene-based microbots for toxic heavy metal removal and recovery from water. Nano Lett. 16 (4), 2860–2866. https://doi.org/10.1021/acs.nanolett.6b00768.

Vuković, G.D., Marinković, A.D., Čolić, M., Ristić, M.Đ., Aleksić, R., Perić-Grujić, A.A., Uskoković, P.S., 2010. Removal of cadmium from aqueous solutions by oxidized and ethylenediamine-functionalized multi-walled carbon nanotubes. Chem. Eng. J. 157 (1), 238–248. https://doi.org/10.1016/j.cej.2009.11.026.

Wang, J.-W., Kuo, Y.-M., 2008. Preparation and adsorption properties of chitosan–poly(acrylic acid) nanoparticles for the removal of nickel ions. J. Appl. Polym. Sci. 107 (4), 2333–2342. https://doi.org/10.1002/app.27247.

Wang, H., Yuan, X., Wu, Y., Huang, H., Zeng, G., Liu, Y., Qi, Y., 2013. Adsorption characteristics and behaviors of graphene oxide for Zn(II) removal from aqueous solution. Appl. Surf. Sci. 279, 432–440. https://doi.org/10.1016/j.apsusc.2013.04.133.

Wang, N., Zhou, L., Guo, J., Ye, Q., Lin, J.-M., Yuan, J., 2014. Adsorption of environmental pollutants using magnetic hybrid nanoparticles modified with β-cyclodextrin. Appl. Surf. Sci. 305, 267–273. https://doi.org/10.1016/j.apsusc.2014.03.054.

Wang, P., Du, M., Zhu, H., Bao, S., Yang, T., Zou, M., 2015. Structure regulation of silica nanotubes and their adsorption behaviors for heavy metal ions: pH effect, kinetics, isotherms and mechanism. J. Hazard. Mater. 286, 533–544. https://doi.org/10.1016/j.jhazmat.2014.12.034.

Wanna, Y., Chindaduang, A., Tumcharern, G., Phromyothin, D., Porntheerapat, S., Nukeaw, J., Pratontep, S., 2016. Efficiency of SPIONs functionalized with polyethylene glycol bis(amine) for heavy metal removal. J. Magn. Magn. Mater. 414, 32–37. https://doi.org/10.1016/j.jmmm.2016.04.064.

Warner, C.L., Addleman, R.S., Cinson, A.D., Droubay, T.C., Engelhard, M.H., Nash, M.A., Warner, M.G., 2010. High-performance, superparamagnetic, nanoparticle-based heavy metal sorbents for removal of contaminants from natural waters. ChemSusChem 3 (6), 749–757. https://doi.org/10.1002/cssc.201000027.

Wei, Y., Yang, R., Zhang, Y.-X., Wang, L., Liu, J.-H., Huang, X.-J., 2011. High adsorptive γ-AlOOH(boehmite)@SiO2/Fe3O4 porous magnetic microspheres for detection of toxic metal ions in drinking water. Chem. Commun. 47 (39), 11062–11064. https://doi.org/10.1039/C1CC14215A.

White, B.R., Stackhouse, B.T., Holcombe, J.A., 2009. Magnetic γ-Fe2O3 nanoparticles coated with poly-l-cysteine for chelation of As(III), Cu(II), Cd(II), Ni(II), Pb(II) and Zn(II). J. Hazard. Mater. 161 (2), 848–853. https://doi.org/10.1016/j.jhazmat.2008.04.105.

Wu, T., Ni, Y., Ma, X., Hong, J., 2013. La-doped ZnO nanoparticles: simple solution-combusting preparation and applications in the wastewater treatment. Mater. Res. Bull. 48 (11), 4754–4758. https://doi.org/10.1016/j.materresbull.2013.08.018.

Xiao, S., Ma, H., Shen, M., Wang, S., Huang, Q., Shi, X., 2011. Excellent copper(II) removal using zero-valent iron nanoparticle-immobilized hybrid electrospun polymer nanofibrous mats. Colloids Surf. A Physicochem. Eng. Asp. 381 (1), 48–54. https://doi.org/10.1016/j.colsurfa.2011.03.005.

Xiao, X., Ma, X.-B., Yuan, H., Liu, P.-C., Lei, Y.-B., Xu, H., Feng, Y.-J., 2015. Photocatalytic properties of zinc sulfide nanocrystals biofabricated by metal-reducing bacterium Shewanella oneidensis MR-1. J. Hazard. Mater. 288, 134–139. https://doi.org/10.1016/j.jhazmat.2015.02.009.

Xie, Y., Huang, Q., Liu, M., Wang, K., Wan, Q., Deng, F., Wei, Y., 2015. Mussel inspired functionalization of carbon nanotubes for heavy metal ion removal. RSC Adv. 5 (84), 68430–68438. https://doi.org/10.1039/C5RA08908E.

Yang, K., Wei, W., Qi, L., Wu, W., Jing, Q., Lin, D., 2014. Are engineered nanomaterials superior adsorbents for removal and pre-concentration of heavy metal cations from water? RSC Adv. 4 (86), 46122–46125. https://doi.org/10.1039/C4RA09375E.

Yantasee, W., Warner, C.L., Sangvanich, T., Addleman, R.S., Carter, T.G., Wiacek, R.J., Warner, M.G., 2007. Removal of heavy metals from aqueous systems with thiol functionalized superparamagnetic nanoparticles. Environ. Sci. Technol. 41 (14), 5114–5119. https://doi.org/10.1021/es0705238.

Yantasee, W., Rutledge, R.D., Chouyyok, W., Sukwarotwat, V., Orr, G., Warner, C.L., Addleman, R.S., 2010. Functionalized Nanoporous silica for the removal of heavy metals from biological systems: adsorption and application. ACS Appl. Mater. Interfaces 2 (10), 2749–2758. https://doi.org/10.1021/am100616b.

Yu, X., Tong, S., Ge, M., Wu, L., Zuo, J., Cao, C., Song, W., 2013. Adsorption of heavy metal ions from aqueous solution by carboxylated cellulose nanocrystals. J. Environ. Sci. 25 (5), 933–943. https://doi.org/10.1016/S1001-0742(12)60145-4.

Yu, J.-G., Yu, L.-Y., Yang, H., Liu, Q., Chen, X.-H., Jiang, X.-Y., Jiao, F.-P., 2015. Graphene nanosheets as novel adsorbents in adsorption, preconcentration and removal of gases, organic compounds and metal ions. Sci. Total Environ. 502, 70–79. https://doi.org/10.1016/j.scitotenv.2014.08.077.

Yusuf, M., Elfghi, F.M., Zaidi, S.A., Abdullah, E.C., Khan, M.A., 2015. Applications of graphene and its derivatives as an adsorbent for heavy metal and dye removal: a systematic and comprehensive overview. RSC Adv. 5 (62), 50392–50420. https://doi.org/10.1039/c5ra07223a.

Zargoosh, K., Abedini, H., Abdolmaleki, A., Molavian, M.R., 2013. Effective removal of heavy metal ions from industrial wastes using Thiosalicylhydrazide-modified magnetic nanoparticles. Ind. Eng. Chem. Res. 52 (42), 14944–14954. https://doi.org/10.1021/ie401971w.

Zhang, F., Zhu, Z., Dong, Z., Cui, Z., Wang, H., Hu, W., Ma, J., 2011. Magnetically recoverable facile nanomaterials: synthesis, characterization and application in remediation of heavy metals. Microchem. J. 98 (2), 328–333. https://doi.org/10.1016/j.microc.2011.03.005.

Zhang, K., Kemp, K.C., Chandra, V., 2012. Homogeneous anchoring of TiO2 nanoparticles on graphene sheets for waste water treatment. Mater. Lett. 81, 127–130. https://doi.org/10.1016/j.matlet.2012.05.002.

Zhang, W., Shi, X., Zhang, Y., Gu, W., Li, B., Xian, Y., 2013a. Synthesis of water-soluble magnetic graphene nanocomposites for recyclable removal of heavy metal ions. J. Mater. Chem. A 1 (5), 1745–1753. https://doi.org/10.1039/c2ta00294a.

Zhang, J., Zhai, S., Li, S., Xiao, Z., Song, Y., An, Q., Tian, G., 2013b. Pb(II) removal of Fe3O4@SiO2–NH2 core–shell nanomaterials prepared via a controllable sol–gel process. Chem. Eng. J. 215-216, 461–471. https://doi.org/10.1016/j.cej.2012.11.043.

Zhang, Y., Yan, L., Xu, W., Guo, X., Cui, L., Gao, L., Du, B., 2014. Adsorption of Pb(II) and Hg(II) from aqueous solution using magnetic CoFe2O4-reduced graphene oxide. J. Mol. Liq. 191, 177–182. https://doi.org/10.1016/j.molliq.2013.12.015.

Zhang, X., Huang, Q., Liu, M., Tian, J., Zeng, G., Li, Z., Wei, Y., 2015. Preparation of amine functionalized carbon nanotubes via a bioinspired strategy and their application in Cu2+ removal. Appl. Surf. Sci. 343, 19–27. https://doi.org/10.1016/j.apsusc.2015.03.081.

Zhao, X., Lv, L., Pan, B., Zhang, W., Zhang, S., Zhang, Q., 2011. Polymer-supported nanocomposites for environmental application: a review. Chem. Eng. J. 170 (2), 381–394. https://doi.org/10.1016/j.cej.2011.02.071.

Zhi, L., Liu, J., Wang, Y., Zhang, W., Wang, B., Xu, Z., Li, G., 2013. Multifunctional Fe3O4 nanoparticles for highly sensitive detection and removal of Al(iii) in aqueous solution. Nanoscale 5 (4), 1552–1556. https://doi.org/10.1039/C2NR33200K.

Zhou, Q.-x., Zhao, X.-n., Xiao, J.-p., 2009a. Preconcentration of nickel and cadmium by TiO2 nanotubes as solid-phase extraction adsorbents coupled with flame atomic absorption spectrometry. Talanta 77 (5), 1774–1777. https://doi.org/10.1016/j.talanta.2008.10.018.

Zhou, Y.-T., Nie, H.-L., Branford-White, C., He, Z.-Y., Zhu, L.-M., 2009b. Removal of Cu2+ from aqueous solution by chitosan-coated magnetic nanoparticles modified with α-ketoglutaric acid. J. Colloid Interface Sci. 330 (1), 29–37. https://doi.org/10.1016/j.jcis.2008.10.026.

Zhu, B., Zhao, J., Yu, H., Yan, L., Wei, Q., Du, B., 2013. Naphthalimide-functionalized Fe3O4@SiO2 core/shell nanoparticles for selective and sensitive adsorption and detection of Hg2+. Chem. Eng. J. 219, 411–418. https://doi.org/10.1016/j.cej.2012.12.068.

CHAPTER

9

Non-toxic nature of nano-biosorbents as a positive approach toward green environment

Sabir Khan[a,b], *Shakeel Zeb*[b,c], *Jaime Vega-Chacón*[a], *Sergio Espinoza Torres*[a], *Sandra Quispe Martínez*[a], *Rosario López*[a], *Ily Marilú Maza Mejía*[a], *Christian Ronald Jacinto Hernández*[a], *Javier Lobaton Vila*[b,c], *Eduardo Jara Cornejo*[a], *Charles Pizan Aquino*[a], *Bianca Mortari*[b,c], *Luis Fernando Tavares Borges*[b,c], *Gerson A. Ruiz-Córdova*[a], *Fredy Lucho Rondinel Carhuas*[a], *Maria Del Pilar Taboada Sotomayor*[b,c], *and Gino Picasso*[a]

[a]Laboratory of Physical Chemistry Research, Faculty of Sciences, National University of Engineering, Lima, Peru [b]Institute of Chemistry, UNESP-São Paulo State University, Araraquara, SP, Brazil [c]National Institute for Alternative Technologies of Detection, Toxicological Evaluation & Removal of Micropollutants and Radioactives (INCT-DATREM), Araraquara, SP, Brazil

9.1 Introduction

The world's freshwater reservoirs become suffering being of developing populations and large-scale agricultural and industrial activities. A massive number of people on the planet are going through the impacts of water and water-borne diseases (Devanathan, 2017). On the large-scale, the color is given to make the products attractive, which causes many colors to go into lakes and rivers, and water becomes dirty (Foguel et al., 2017). A significant number

https://doi.org/10.1016/B978-0-323-90912-9.00009-5

of manufacturing industries directly discharge several major hazardous organic compounds in the water resources, causing water-living organisms to be affected (Zeb, 2018). Some pollution is caused by farming activities, which we call indirect water pollution. For example: spraying chemical fertilizers and pesticides on crops. These chemicals enter through the soil and contaminate water resources (Barbera and McConnell, 1990). The consequences of direct and indirect water pollution are still the same, it can cause disease and possibly the death of any living organism that is in or out of the water. Water pollution is divided into two categories includes direct and indirect contaminations. Direct water pollution can include processing industries such as electronics, electroplating, rubber products, and food and beverage while farming activities, agricultural waste, and untreated sewage can cause indirect water pollution (Singh et al., 2020). In addition to water pollution, different types of pollution were also classified such as Organic (Ekevwe et al., 2018), Inorganic (Rekha Kathal et al., 2016), Radioactive (Bonavigo et al., 2009), Suspended Solid (Dwivedi, 2017), Pathogens (Dwivedi, 2017), Nutrients and Agricultural (Savci, 2012), and Thermal Pollution (Rao, 2017). It has been reported that organic dyes are more toxic and carcinogenic (Villegas-Navarro et al., 2001). The presence of heavy metals such as mercury (Hg), cadmium (Cd), arsenic (As), chromium (Cr), thallium (Tl), and lead (Pb) in organic dyes, being of these heavy metals cause destructive consequences on the life of living creatures. The utilization of colors in different food items causes some destructive infections like tumors and a few different diseases in living creatures (Hameed and El-Khaiary, 2008). Besides, the use of dyes can cause skin and eye sicknesses and yield short breathing problems (Merouani et al., 2010). Therefore it's important to treat the wastewater and make them clean-up for living organisms. Environmental protection agencies and other legislative associations in the world have a distinct fascination with boosting the water worth standard via pollutants elimination and wastewater treatment. Overtime, many technologies have been practiced to harness wastewater namely the physical approach, biological methods, advance oxidation, and electrochemical technologies (Ghoreishi and Haghighi, 2003). Among them, adsorption has gotten broad consideration because of its operational simplicity, high proficiency, cost-adequacy, and its capacity to eliminate a wide scope of impurities (Gupta et al., 2012; Khan et al., 2018; Sophia and Lima, 2018). According to an approximation, the cost of utilizing adsorption innovation to remedy the water contain hazardous materials is about 5.0–200 US dollars/m^3 of water (Gupta et al., 2012). The absorption process has a greater ability to eliminate up to 99.9% of pollution and extensive organic effluents from water have been eliminated via adsorption including pesticides, hydrocarbons, plasticizers, phenols, detergents, biphenyls, and pharmaceutical products (Zeb et al., 2020; Kundu et al., 2018; Klumpp et al., 2003). The term bio-sorption may be defined as the sticking of effluents (heavy metals, dyes, and pharmaceutical products in an aqueous phase) to the solid surface of biological material (bio-sorbent) via different mechanisms. At the moment, being of extensive advantages such as simple, low cost, and harmless to the ecosystem, the researchers consider the bio-sorption method has become the axis of attention (Torres, 2020). Numerous biomaterials have been examined and considered as bio-sorbents to remedy the fluid environment and their names are industrial waste materials (Carvalho Costa et al., 2020), sludge (Kulkarni et al., 2019; Taki et al., 2019), polysaccharides (Hussein et al., 2019), agriculture waste products (Franco et al., 2020; Wang and Huang, 2020), and biopolymers (Zhang et al., 2020). A wide range of wastewater treatment has been reported in the literature but this book chapter only focuses on the basic information and benefits of bio-sorption treatment while also discuss the biological

material which has been considered efficient bio-sorbents and frequently eliminated the contaminations from an aqueous environment.

9.2 Nano-biosorbents surface modification for environmental remediation

Bio-sorbent materials have been considered a keen axis for the removal of pollutants from wastewater because for many aspects including accessible in enormous quantity, affordable, exhibit high adsorption capacity, and simple to control. Bio-sorbent materials are generally classified into four types like plant products, microbes, peat, and bark. Plant products consist of mostly agricultural waste such as bagasse, husk, banana pith, soybean hulls, maize cob, cork biomass, and waste tea, while microbes have been observed as excellent potential bio-sorbents being of their cell composition and stability (Dhankhar and Hooda, 2011). The microbial bio-sorbent is divided into three main categories including bacteria, fungi, and algae. The term peat might be defined as is a collection of partly rotting vegetable matter or natural matter. Peat is another bio-sorbent that has been counted as a promising candidate because of many benefits such as enormous surface area, porosity, low price, and effective accessibility (Robalds, 2015). Out of the different tree parts, tree bark has the most elevated ability to be utilized as a bio-sorbent. The tree bark materials were tested for the removal of pollutants in a fluid environment. Various barks exhibited excellent capability for the removal of heavy metals (Robertson, 1989). The waste from the food industry has occupied a very important place due to its adequate treatment to solve environmental problems, thus we have natural biopolymers that come from living organisms and/or renewable resources. These materials are considered environmentally friendly and sustainable but the most beneficial property of nano-biosorbents is the green nature of the particles and specials physical chemistry properties which allows them to offer a wide variety of applications.

The most abundant biopolymer after cellulose is chitosan and alginate is another important natural biopolymer, all of them are much utilized in wastewater remediation.

9.2.1 Chitosan

Chitosan is a copolymer composed of D-glucosamine (deacetylated unit) and *N*-acetyl-D-glucosamine (acetylated unit) units linked by β-1,4-glycosidic bonds. This linear cationic polysaccharide occurs as a white flake or powdery solid (Nasrollahzadeh et al., 2021). A source like a prawn has been considered most encouraging for the preparation of chitosan. The various sources of a prawn have been investigated in the reported studied such as *Penaeus monodon* commonly known as Giant Tiger prawn and Indian prawn (Biswas and Tarafdar, 2013), and a fenneropenaeus indicus (Paul et al., 2014), while all of these sources are considered as a good extractors for chitosan. The varieties like *Penaeus carinatus* and *Penaeus monodon* are also used to get the chitosan (Puvvada et al., 2012), these specimens have been known from a common name such as shrimps. *Sesarma plicatum* is a species of crab that is considered to be an excellent candidate for the extraction of chitosan (Khaleda Firdous, 2017). Different types of microbial *Aspergillus niger* MTCC, some of which are *Aspergillus niger* MTCC 2208, *Aspergillus niger* Mtcc 1785, and *Aspergillus niger* Mtcc 872, preceded in the preparation of

chitosan (Kumaresapillai et al., 2010). Most of the bacteria and fungus species are used in the production of chitosan because these are promising sources of chitin while these kinds of sources are also used in the industries for the preparation of chitosan. Much information has been based on the chemical synthesis of chitosan, for example Abhrajyoti et al. (Tarafdar and Biswas, 2013) demonstrated the synthesis of chitosan using 10 mg of prawn shell waste and washed with deionized water. After washing the prawn shell waste further used in the demineralization reaction using hydrogen chloride (HCl) at 25°C for 1 h. In the second step, the deproteinization reaction proceeds with 0.5% NaOH at 100°C for a half-hour (30 min). To obtained the chitin slurry and elimination more protein from the sample (shell) repeated the deproteinization process with 3% sodium hydroxide at a temperature of 100°C for a half-hour (30 min). The deacetylation of chitin yielded chitosan washed and dried. Similarly, the same group adopted the second methodology for the preparation of chitosan using 5 g of biomass of shrimp. The deproteinization step achieved using sample biomass of shrimp in aqueous NaOH (4%) at 25 °C for 21 h, for the demineralization the reaction proceeds with 4% hydrochloride acid (HCl) at room temperature for 12 h. The synthesized chitin was dried at normal temperature. The aqueous NaOH (50%) was used to treat chitin at 40 °C for 3 days as result, obtained chitosan and dried the chitosan at room temperature. The use of microbial was reported in the literature for the production of chitosan. Zhang et al. (2012) was used the fermentation process to treat the *Lactobacillus plantarum* ATCC 8014 and *Serratia marcescens* B742. The *L. plantarum* ATCC 8014 bacteria was used with specific conditions such as 2% SSP, 2 days of culture time, 10% incubation level, and 15% glucose. Two steps fermentation treatment of bacteria produced an 18.9% chitin in the presence of a deproteinization rate of 94.5% and a demineralization rate of 93.0%. The advantage of this technique is to use fewer chemicals in the preparation of chitosan.

The uses of prawn shells for the extraction of chitosan (Sumathi et al., 2012). The prawn shell was washed with deionized water to remove the waste particles and dried in an oven at a temperature of 60°C for 24 h. In the next step, the shell is treated with deproteinization and demineralization and as a result, chitin was synthesized. For the extraction of chitosan the reaction is followed by the deacetylation process. Its outcomes demonstrated the antimicrobial.

Action exhibited by the examples on test living organism

The application of chitosan is wide due to the drug-biological, bacteriostatic, antioxidant, antitumor (Pal et al., 2021), But its application extends further, and currently, chitosan is used to purify water, in pollutant removal processes and can act as a flocculant and coagulant, as an adsorbent to remove contaminants such as heavy and highly toxic metals such as arsenic, mercury, and chromium as well also dyes, pesticides, antibiotics, biological pollutants from wastewater. Among other applications, chitosan is required in the administration of drugs, food additives, tissue engineering, and treatment of agricultural soils (Pal et al., 2021).

Overall, chitin and chitosan consist of various functional groups, like hydroxyl (–OH) and amide (R–CO–NH_2) or amine (R–NH_2). Chitin comprises N acetylglucosamine with >40% amide groups, though chitosan is for the most part glucosamine with >60% amine groups (GAF, 1992). The chitosan molecules can form hydrogen and other non-specific interactions because of –NH_2 and –OH groups. Chitosan has more ability to solve in the acidic medium as compare to chitin because a positive charge arranges to form an amine group (–NH_3^+). Thus, the positively charged chitosan particles are isolated via repulsion force power and become

suspended in an acidic medium. The chitosan properties depend on the synthesis process because these processes play an important role to control the level of acetylation, i.e., free amino groups that allow it to bind with negatively charged molecules (Bhardwaj and Kundu, 2010; Hudson and Jenkins, 2001). Chitosan has many attractive properties in the field of wastewater treatment and medical such as biodegradability, low toxicity, good water adsorption efficiency, and anti-fungal effects (Şenel and McClure, 2004; Di Martino et al., 2005).

Chitosan got a greater prevalence in agriculture applications with high accessibility, nonharmful nature, and biodegradability (Di Martino et al., 2005). Chitosan has unique properties being of functional groups and natural chelating which allow it to use in the wastewater treatment for the elimination of different organic compounds and heavy metals (Di Martino et al., 2005) because –OH and $–NH_2$ groups has high flexibility in the structure of chitosan. The chelating properties of chitosan allow them to use in various food applications for example elimination of specific components, particles, and materials such as dyes and fats from food sources (Khor and Lim, 2003; Li et al., 1992). Because of chitosan's capacity to work in numerous structures, it has numerous spaces of interest inside the clinical industry comprising tissue designing (Di Martino et al., 2005; Li et al., 1992; Bhattarai et al., 2005), orthopedic and periodontal applications (Şenel and McClure, 2004; Di Martino et al., 2005), wound healing (Ueno et al., 2001; Ma et al., 2005), and drug delivery (Jayakumar et al., 2005).

Chitosan facing some difficulties in environmental applications like maintaining its stability and removal efficiency. Numerous scientists contemplated the chitosan to treat the wastewater containing Cr(VI) (Elmizadeh et al., 2013), Pb(II), Hg(II) (Nematidil and Sadeghi, 2019), Cr(VI) (Samuel et al., 2019), Zn(II), Cd(II), Pb(II), Cu(II) (Dev et al., 2020), Pb(II) (Li et al., 2019a), and Cu(II) (Liu et al., 2016). The chitosan molecule can form a helical structure around metal ions (Ogawa et al., 1993) because their molecules are appropriately flexible which can interact via coordination bonds with each ion (Wu et al., 2010). Chitosan has been considered an economical sorbent for the treatment of wastewater (Coughlin et al., 1990). Soil and wastewater that contain organic pollutants can be removed with chitosan, although success depends to some extent characteristics of effluents. In addition to removing a heavy metal, it can eliminate organic pollutants such as acid dyes (Wong et al., 2004), reactive dyes (UZUN, 2006), methyl parathion (Yoshizuka et al., 2000), and permethrin pesticide (Moradi Dehaghi et al., 2014). All these pollutants are given in below Table 9.1.

To solve the problems of some chitosan restrictions, there are two types of modifications. The chemical modifications involve modifying amino, hydroxyl, or both groups at the same time and on the other hand, we have the physical modifications that modify the body of the chitosan particles forming sponges, nanoparticles, gel particles through metallic grinding, ionization, or ultrasonic treatment.

Through chemical modification, it is possible to improve the solubility of chitosan, as well as some physical-chemical properties such as thermal stability, rheological properties, resistance to oxidation, and antibacterial properties (Azmy et al., 2019). These chemical modifications consider three active groups that are shown in the order of reactivity: the amino group with the highest reactivity, followed by the primary hydroxyl group, and then the secondary hydroxyl group, from these modifications the applications of chitosan are expanded much more (Dimassi et al., 2018).

On the other hand, water pollution has always been a major concern nationally and globally. In this sense, chitosan and cellulose are low-cost adsorbents and present interesting options in this context (Olivera et al., 2016). On the other hand, the properties of materials at the

TABLE 9.1 Sorption capacity and sorption removal of metals by chitosan nanoparticles.

Ion	Modified chitosan adsorbent	Morphology	Functional groups involved in adsorption	Adsorption capacity	References
Cr (VI)	Citric acid /−/−	NP	NH_3^+, COOH	106.15	Elmizadeh et al. (2013)
Pb(II), Hg(II)	Glu/3-aminopropyl triethoxysilane/−	NP	–OH (Majority)-NH_2 (Few)	38.461	Nematidil and Sadeghi (2019)
Cr(VI)	−/Graphene oxide/−	NP	–OH; –NH	104.16	Samuel et al. (2019)
Zn(II), Cd(II), Pb(II), Cu(II)	GMA/MAA/−	NP	–NH_2	92.27	Dev et al. (2020)
Pb(II)	–/Cucurbit (Bonavigo et al., 2009)/−	NP	C═O, N–C–N, –NH_2	873.6	Li et al. (2019a)
Cu(II)	–/CS_2, GO/Fe_3O_4	NP	–COO–, –NH_2, –CS_2	442.48	Liu et al. (2016)
Acid dyes	Chitosan	–	–	–	Wong et al. (2004)
Reactive dyes	Chitosan	–	–	–	UZUN (2006)
Methyl parathion	Chitosan microparticles/silver-complexes	–	–	–	Yoshizuka et al. (2000)
Permethrin pesticide	Chitosan–ZnO	NP	–	49%–99% for 25 mL	Moradi Dehaghi et al. (2014)

nanoscale are investigated, considering that the larger the materials have constant properties but as the size decreases the percentage of atoms on the surface increases, and this causes a change in the properties of the nanoparticles. In this sense, the present review study focuses on and analyzes the suitability of chitosan as a nano-adsorbent for the removal of heavy metals because chitosan nanoparticles have great properties as an effect of increasing the surface area.

Due to the enormous potential of chitosan nanoparticles, the structural characteristics of chitosan and the different preparation methods are explored, with special emphasis on the application of nanoparticles as metal nano-adsorbents in aqueous solutions.

For more than 10 years, nanochitosan has been tested effectively for the adsorption of metals in an aqueous medium, for example, to evaluate the sorption capacity Cd(II) (Seyedi et al., 2013), arsenate (Kwok et al., 2014). Also, chitosan nanofibers were tested due to their high porosity, large surface area per unit mass, and they are possible adsorbents to remove Pb(II) and Cu(II) (Haider and Park, 2009). Generally, chitosan is used as a modified material, through grafts, obtaining it as a nanoparticle and imparting magnetic properties to apply it as a metal adsorbent through its functional groups that can behave as active sites for the adsorption of contaminants and thus be a bio-adsorbent low cost.

9.2.2 Alginate nano-biosorbents

Sodium alginate is a natural biopolymer extracted from brown algae, it has been used as a bio-sorbents for the purification of wastewater due to its favorable properties that include biocompatibility, low toxicity, and relatively low cost (Lakouraj et al., 2014). The abundant carboxyl and hydroxyl group in the lattice makes alginate an effective candidate for heavy metal removal (Emmerichs et al., 2004). Furthermore, excess hydroxyl and carboxyl functional groups are available throughout the alginate backbone structure, making it an ideal biopolymer to bind with different species in water (Ding et al., 2019).

Alginates were first found in the late nineteenth century to turn into a valuable normal biopolymer (Yadav and Ahmadi, 2019). The brown sea algae are used to synthesized the alginates while brown seaweed has the ability to produced alginates commercially. There are mostly two main sources of alginates: algal sources and bacterial sources (Smidsrod and Skjakbrk, 1990). Recently, researchers used marine macroalgae to extract the alginates. After 80 years, a bacterial source, the mucoid strain of Pseudomonas aeruginosa, was discovered from which bacterial alginates were produced (Linker and Jones, 1966).

The acidic medium allows the polysaccharides to go through hydrolytic cleavage. The mechanism of acid hydrolysis of the glycosidic bond has been reported in the previous literature (Pawar and Edgar, 2012). It includes three stages (1) protonation of the glycosidic oxygen to give the conjugate acid; (2) heterolysis of the conjugate acid forming a non-reducing end group and a carbonium-oxonium ion; and (3) rapid addition of water to the carbonium-oxonium ion, forming a reducing end group. Dry powders such as sodium alginate can be kept in a cool, dry place and away from sunlight for a few months. A cold environment such as a freezer can increase the shelf life while Alginic acid easily degrades than the sodium salt form. Alginate is not only degraded being of acid and base but also at pH 7 value in the existence of decreasing compounds.

Despite these remarkable characteristics of alginate, it presents some limitations that affect the practical application of bio-sorption technology, they tend to be weak in sturdiness and lack mechanical stability, which limits its practical applications; they lack specificity due to the presence of several functional groups, which limits their selectivity; suffer from early saturation due to the occupation of sorption sites, which may require desorption before reuse (Abdi and Kazemi, 2015). Furthermore, for conventional bio-sorbents to have a high surface area, they must be very porous, which has the problem of limiting their adsorption capacity and the speed of the adsorption process due to intraparticle diffusion (Stephen Inbaraj and Chen, 2011).

The nano-biosorbents offer the possibility of developing new materials that overcome these restrictions. Recent publications show these modifications as magnetic modification, immobilization and the development of zero valence metals at the nanoscale level have been considerable interest for the removal of contaminants from a solution (Mahamadi, 2019).

Magnetic modification

The magnetic modification allows the sorbate in the magnetic alginate nano-biosorbent to be separated with a magnet, which is more efficient than filtration or centrifugation. Some of the studies carried out on alginate nano-biosorbents with magnetic modification to remove

metals (Kloster et al., 2017; Verma et al., 2017), dyes (Kazemi and Javanbakht, 2020; Yadav et al., 2020), and organic compounds (Phiri et al., 2019).

Immobilization

The immobilization consists mainly of the immobilization of nanoparticles in the alginate matrix as alginate beads. Some immobilized materials to remove fluoride are Fe_3O_4 nanoparticles immobilized in sodium alginate matrix and Fe_3O_4 nanoparticles and saponified orange peel residue immobilized in sodium alginate matrix (Christina and Viswanathan, 2015).

Nanoscale zero-valent metals

The zero-valent metals prepared at the nanoscale have the advantage of an increase in adsorption capacity, they are relatively less toxic substances and that in certain cases allow rapid magnetic removal (Devatha et al., 2018; Fazlzadeh et al., 2017). The main zero-valent metal used is Fe in a matrix of alginate using to remove heavy metals such as Cr(VI) (Wen et al., 2020), Cu(II) (Kuang et al., 2015), and organic pollutants as PAHs (Abdel-Gawad et al., 2016).

Others works related to the application of alginate-based nano-biosorbent, according to the application and the contaminant, are shown in Table 9.2.

9.2.3 Nanocelullose

Cellulose is a natural biopolymer that can be extracted from wood or cotton and different parts of plants and other sources such as seeds, leaves, stems, pits, and shells (Suhas et al., 2016), also it can be obtained from algae, tunicates, and bacteria (Vazquez et al., 2015). Cellulose shows many characteristics properties such as hydrophilicity, adsorption capacity, non-toxicity, facile chemical modification to improve the low adsorption, crystallinity, good mechanical properties, renewable and biodegradable (Klemm et al., 1998).

Nanocellulose is a natural fiber obtained by defibration of cellulose for different methods and it shows extraordinary properties such as size (1–100 nm), very large surface area, high strength, low thermal expansion, high aspect ratio, and lightweight; additionally, to this properties, nanocellulose has low cost, biocompatibility, functional ability and sustainable source (Carpenter et al., 2015). Nanocellulose has been considered to be one of the most important green materials (Trache et al., 2020).

According to Miyashiro et al. (2020) and Farooq et al. (2020), nanocellulose is usually classified into:

- Cellulose nanofiber (CNF) is a longer and wide nanofibers with 20–100 nm in width and >10,000 nm in length and it is produced by mechanical treatment, is semi-crystalline (Trache et al., 2020).
- Cellulose nanocrystal (CNC) is a crystalline nano-rod with 3–50 nm in width and 50–500 nm in length and it is produced by acid hydrolysis from many sources (Habibi et al., 2010).
- Bacterial nanocellulose (BNC) is a hydrogel (99% water) and is composed of a nanofiber network with 20–200 nm it is synthesized by certain aerobic bacteria and then excreted as exopolysaccharide (Klemm et al., 2011).

TABLE 9.2 Some removal of contaminants using alginate-based nonabsorbent.

Class of nano-biosorbents	Nano-biosorbent	Experimental parameters (optimum)	Maximum adsorption capacity or % removal	Contaminant	References
Magnetic modification	AO-γ-Fe_2O_3-OMWCNTs	Adsorption over pH (4–10) and reusability (87%–82%)	905.5 mg g^{-1}	Methylene blue	Boukhalfa et al. (2019)
	(CA/CMC/$Ni_{0.2}Zn_{0.2}Fe_{2.6}O_4$)	Contact time of 40 min, pH of 5.5, and initial concentration 0.8 g L^{-1}	97.75%, 96.83%, and 97.85% for Nd^{+3}, Tb^{+3}, and Dy^{+3}	Nd (III), Tb (III), and Dy (III)	Javadian et al. (2020)
	POD-PPO-enzymes on alginate-coated magnetic nanocatalysts	Opimum at $T = 20$ °C, pH 8, glutehydrie 1.6%, and enzyme to nanoparticles ratio of 1:200	98.1%	Phenol	Marjani et al. (2021)
Immobilization	Fe_3O_4@n-HAp-Alg	SC raised from pH 3 to 11. The reusability and regeneration upto five successive cycles	29.14 mg g^{-1}	Cr(VI)	Periyasamy et al. (2018)
	Iron oxide nanoparticles embedded in barium alginate beads	Concentration of immobilized 1500 mg L^{-1}, contact time = 240 min, and initial concentration of 10 mg L^{-1}	bRMINP 98.75% and cRMINP 88.88%	Reactive Blue 235	Natarajan and Ponnaiah (2017)
Zero-valent metals	nZVI-SA	20 min of reaction at pH 6.0	96.4%	Cr(VI)	Li et al. (2019b)
	AC/nZVCu/HAp-Alg	Reaction time of 120 min, pH 5.8	39.06 mg g^{-1}	As(III)	Iqbal et al. (2019)

AO, alginate beads; OMWCNTs, oxidized multiwalled carbon nanotubes; CA, calcium alginate; CMC, carboxymethyl chitosan; POD, peroxidases, PPO, polyphenol oxidase; HAp, hydroxyapatite; Alg, alginate; SC, sorption capacity; bRMINP, biologically synthesized iron nanoparticles; cRMINP, chemically synthesized iron nanoparticles; nZVI, nano zero-valent iron; SA, sodium alginate; AC, activated carbon; nZVCu, nano-zerovalent copper.

Nanocellulose composites

Nanocellulose usually is applied in passive nanoremediation, here nanocellulose acts as a support or particle stabilizer for reactive nanoparticles that could be previously modified with polymers. Nasrollahzadeh et al. (2021) and Nata et al. (2011) studied CNF composite with magnetite nanoparticles with a surface functionalized amine group (1,6-hexanediamine) for arsenate removal and this composite adsorbed 90 mg per gram of material. Photocatalytic degradation of mefanamic acid, an emerging pollutant, from aqueous media has been investigated by (Rathod et al., 2018) using nanocellulose/TiO_2 composite, nanocellulose provide a

large surface area to the TiO_2 nanoparticles but also enhance the electron distribution and transfer to the TiO_2 surface, leading to higher photocatalytic activity (Nasrollahzadeh et al., 2021).

Nanocellulose modification

On the other hand, nanocellulose is applied in active nanoremediation, as it acts directly as a pollutant adsorbent material. Nanocellulose contains many reactive hydroxyl groups in its chemical structure (hydrophilic) which allow an easy functionalized since by incorporating chemical molecules into its structure, the efficiency of the binding of many pollutants improve its mechanical properties and allows to offer different applications, among the main surface modifications we have:

- Silylation introduces a substituted silyl group, from alkoxysilane, on the surface of nanocellulose achievement to improve wettability of nanocellulose.
- Sulfonation introduces negative charges (sulfate groups) to the surface of nanocellulose, it improves the dispersion capacity in water.
- Oxidation with 2,2,6,6-Tetramethylpiperidine-1-oxyl (TEMPO) converts alcohol functions of the glucose unit to a carboxylic acid, these negative charges (carboxylate groups) increase electrostatic repulsion and improves dispersion in water.
- Carboxymethylation introduces negative charges (carboxymethyl groups) to the surface of nanocellulose, the electrostatic repulsions facilitate the degradation of biomass into nanosized particles.
- Acetylation uses acetic anhydride and dry acetic acid with a mineral acid as catalyst, this modification increases hydrophobicity.
- Phosphorylation introduces phosphate ester groups into the nanocellulose.
- Grafted nanocellulose (Bagheri and Julkapli, 2018) is a good method to modify the chemical and physical properties of the nanocellulose with another polymer Table 9.3 shows examples of the principals surface modification techniques to nanocellulose (Sharma et al., 2019).

TABLE 9.3 Some examples of surface modification.

Method	Technique	Reactive for modification	Contaminant	Adsorption capacity or % removal	References
Chemical	Silylation	Methyltrimethoxysilane	Oil from water	Up to 102 g g^{-1}	Zhang et al. (2014)
	Acetylation	Acetic anhydride and acetic acid (1.5:1, v/v)	Oil from water	25 g g^{-1}	Zimmermann et al. (2019)
	Phosphorylation	Adenosine-5′-triphosphate (ATP) and $MgCl_2$	Ag^{1+}, Cu^{2+}, and Fe^{3+} from industrial effluents	99%	Liu et al. (2015)

9.3 Magnetic nanoparticles immobilized as nano-biosorbent

Since the surface area to volume ratio increases as the particle size decreases, nanoparticles present higher adsorption capacity than bulk materials owing to the large surface area to volume ratio (Amiri et al., 2019; Sarma et al., 2019). Moreover, magnetic nanoparticles can be manipulated by the application of an external magnetic field gradient allowing the separation of magnetic nanoparticles dispersed in a solution (Avval et al., 2019). This process, usually known as magnetic separation, avoids further steps as filtration or centrifugation, which reduces the cost and the time of effective removal of adsorbates (Horák et al., 2007; Aguilar-Arteaga et al., 2010). Due to these features, magnetic nanoparticles have been employed for the development of efficient nano-adsorbents of pollutants as metals, dyes, drugs, pesticides, among others, which could be easily removed by magnetic separation. Furthermore, after adequate treatment of desorption, the nano-adsorbents could be used newly in several cycles of adsorption-desorption, reducing the unnecessary production of nano-adsorbents (Wang et al., 2021; Ren et al., 2021; Hola et al., 2015). The magnetic separation performance is related to the physicochemical characteristics of the adsorbent such as the proportion of magnetic material, the type of magnetic material, the average particle size, the size distribution, the aggregation degree, the specific surface area, the chemical species present on the surface and the surface charge (Horák et al., 2007; Ko et al., 2017; Arsalani et al., 2021). Magnetic nanoparticles with high saturation magnetization are preferred to achieve a rapid magnetic separation (Shi et al., 2021; Wang et al., 2018). Although the decrease in the size of the nanoparticle could enhance the adsorption capacity, it also produces a depletion in the saturation magnetization (Vega-Chacón et al., 2016). Then it is important to consider these features when a magnetic nano-adsorbent is designed. The adsorption capacity depends on the interactions between adsorbate and the surface of the adsorbent. Some molecules have a low affinity for the surface of magnetic nanoparticles, and it is not useful to employ these nanoparticles without any modification for an efficient adsorption. However, magnetic nanoparticles mixed with a suitable material (as activated carbon, silica, polymers, among others) which have high affinity for the adsorbate produce effective adsorbent which can be magnetically separated (Sarma et al., 2019; Wang et al., 2021). Magnetic nanoparticles are mainly composed of iron, nickel, cobalt, their respective oxides and alloys. However, iron oxide magnetic nanoparticles, such as magnetite (Fe_3O_4) and maghemite (γ-Fe_2O_3), are preferred for most of the technological applications due to their strong magnetic responsiveness, low toxicity (compared with other magnetic nanoparticles), facile surface modification and easy preparation methods with low environmental impact (Kaur et al., 2014).

Yadav and Fulekar (2018) prepared maghemite nanoparticles using the extract of the leaf of the Tridax plant by a sonochemical process. Showing a particle size between 20 and 40 nm and a spherical shape. 1258 emu magnetization. For adsorption studies, by the shake flask method in an incubator of a solution of 20% concentration of heavy metals, shaken at 150 RPM, 30 °C, at a dose of 0.3 mg/100 mL of nanoparticles, sample 85% Pb removal in 2 h and in 24 h reaches 90.85%. The Cd was in a lower proportion, so that after 1 h it reached levels below the detection level, after 1 h it reached 67.8% removal. Maghemite nanoparticles

have limited adsorption sites that, being in a solution with various metals, the components compete with each other to be adsorbed by these sites.

Magnetite nanoparticles were synthesized by Chen et al. (2020) for effective boron removal and isotopic separation in an aqueous solution for the first time. Studies on the thermodynamics of the adsorption process showed that it has a high entropic effect and it was the main driving force leading to negative enthalpy. The adsorption study was developed in the range of pH 2–12, reaching its highest efficiency at pH 7. The studies suggest that an increase in the temperature reduces the boron adsorption capacity of the nanoparticle. Moreover, the nanoparticles could be reused for three adsorption-desorption cycles. The equilibrium and maximum adsorption point was reached after 90 min with an adsorption capacity of 4.57 mmol g at pH 7 at 45 °C. The kinetic of adsorption is described by the quasi-second order model. The nanoparticles show greater separation of the ^{10}B isotope, at pH 6 and 15 °C.

Iconaru et al. (2016) developed magnetite nanoparticles with activity to trace elements for possible environmental applications as adsorbents. The nanoparticles were obtained by the co-precipitation method at room temperature. The nanoparticles exhibited a wide specific surface area (100.52 $m^2\ g^{-1}$) with a pore size of about 24 nm. The equilibrium adsorption experiments were conducted at room temperature and with aqueous solutions containing As(V) and Cu(II) at a concentration range of 0.1–150 mg L^{-1}. The maximum adsorption capacities of the nanoparticles were 66.53 and 9.06 mg g^{-1} for As(V) and for Cu(II), respectively.

Stan et al. (2017) evaluated the effectiveness of three types of green synthesis of magnetite nanoparticles for the removal of antibiotics piperacillin, tazobactam, sulfamethoxazole, tetracycline, trimethoprim, ampicillin, and erythromycin. The particles were synthesized employing extracts of lemon, grape, and cucumber peel. The particles size varies between 8 and 11 nm and areas from 90.5 to 137.4 $m^2\ g^{-1}$. It was found that magnetite synthesized using cucumber peel extract was the most efficient in removing antibiotics from aqueous media. Except for sulfamethoxazole and trimethoprim, a high level of elimination (>90%) of all the other antibiotics was achieved.

Bagbi et al. (2016) evaluates the adsorption of Pb(II) by magnetite nanoparticles synthesized by chemical co-precipitation using ferrous chloride and ferric chloride (molar ratio 1:2, respectively) as precursor iron salts (Nedkov et al., 2006). The magnetite nanoparticles obtained were used to remove Pb(II) ions from aqueous solutions at different initial pH (2.0–7.0), equilibrium time (5–30 min), temperature (5–45 °C), lead concentrations (10–50 mg L) and magnetite dose (0.1 g L^{-1}). After stirring at 200 rpm, adjust the pH with 0.1 M NaOH or HCl and filter the suspensions; Pb (2+) was measured using atomic absorption spectrometry (AAS). The TEM analysis performed on the magnetic material showed monodispersity and uniform size between 8 and 13 nm, spherical shape, without agglomeration. DLS analysis showed hydrodynamic radius values of 45 nm for nanoparticles dispersed in water. On the other hand, SEM analysis showed the particle size of around 50 nm, also spherical and monodisperse. BET surface analysis indicates that magnetite is a mesoporous solid with a BET surface area of 73 $m^2\ g^{-1}$, a pore size of 10.4 nm, and a pore volume of 0.22 $cm^3\ g^{-1}$. FTIR characterizations of lead-adsorbed NPs show two new peaks

due to the Fe–O–Pb bond formed on the surface. TEM micrographs show Pb^{2+} uniformly distributed on the surface of the NPs. It was observed that the adsorption of Pb^{2+} increased with increasing pH. About 100% of Pb^{2+} was removed under the optimal parameter conditions (adsorbent dose: 20 mg L^{-1}, Pb(II) concentration: 50 mg L^{-1}, equilibrium time: 25 min). The magnetite nanoparticles were recovered after being used for adsorption. For this, a HNO_3 diluted solution was used. A 20 mL aliquot of HNO_3 recovers about 80% of the total lead, the rest is recovered by desorption of the nanoparticles.

Rajput et al. (2016) also studied the adsorption capacity of magnetite; in this case, it was for Pb^{2+} and Cr^{6+} in water and wastewater. The NPs were also synthesized by chemical co-precipitation. TEM analysis showed spherical particles of size between 15 and 30 nm in diameter. Meanwhile, VSM analysis exhibited superparamagnetism and magnetic saturation values (Ms) 77.5 emu g^{-1} at 300 K. The BET surface area was 12.7 m^2 g^{-1} and the pore volume was 0.05 cm^3 g^{-1}. The adsorption study was carried out in the range of pH 2.0–10.0, solutions of metal ions between 2 and 100 mg L^{-1} at temperatures between 25 and 45 °C for maximum times of 24 h. The final concentrations of Cr(VI) and Pb(II) were determined by atomic absorption spectroscopy (AAS). As a result, the maximum removal of Cr^{6+} of 58.4% was obtained at pH 2.0, which decreases to values of 10% with increasing pH. On the other hand, the maximum Pb^{2+} adsorption was obtained at pH 5.0. The adsorption capacities according to the Langmuir model were 34.87 mg g^{-1} for Cr(VI) and 53.11 mg g^{-1} for Pb(II) at 45 °C.

Ren et al. (2018) proposes a synthesis of maghemite nanoparticles from glass waste for the adsorption of arsenite. These nanoparticles were prepared from green vitriol and pyrite through a solid-phase redox reaction under N_2 atmosphere.

$$8FeSO_4 + FeS_2 \xrightarrow{N_2} 3Fe_3O_4 + 10SO_2(g)$$

$$4FeSO_4 + O_2 \rightarrow 6Fe_2O_3$$

As(III) adsorption tests were performed by adding maghemite nanoparticles in As(III) solutions of 10 mg L^{-1}. Adsorption isotherms were obtained by varying As(III) concentrations from 5.0 to 70.0 mg L^{-1} at pH 11.0 at different temperatures between 25 and 55 °C. As(III) concentrations were analyzed by inductively coupled plasma-optical emission spectroscopy. The TEM images showed an average particle diameter around 35 nm and the cubic shape of the NPs. The BET surface area found was 14.63 m^2 g^{-1}, pore volume 0.068 cm^3 g^{-1}, and pore size 11.6 nm. The maximum adsorption capacity of the maghemite NPs was 14.4 mg g^{-1} at 55 °C obtained from the Langmuir isotherm. Furthermore, it indicates that the adsorption kinetics follows a pseudo-second-order kinetic model. A thermodynamic analysis carried out confirmed that the adsorption of As(III) in maghemite NPs is a spontaneous and endothermic process, and can have great application in As(III) adsorption processes.

Observing the superparamagnetism properties of magnetite nanoparticles, Germanos et al. (2020) evaluated the impact of said nanoparticles on the adsorption properties of magnetite alginate beds (MABs). For this, a comparative study of alginate beds (ABs) and

magnetic alginate beds (MABs) in the removal of copper (II) from wastewater was carried out. The first changes obtained in the MABs were in their thermal stability due to the presence of magnetic NPs; MABs also retain the superparamagnetism of magnetite NPS. In addition, the intensity of the XRD peaks of MABs is lower than that of magnetite, which confirms that the magnetite has been correctly incorporated into the polymer matrix. Adsorption capacity values of 54.9 and 66.7 mg g^{-1} were obtained for MABs and ABs respectively. However, the MABs have 80% by weight of alginate and 20% of magnetite, so when normalizing the adsorption capacity with respect to the weight of alginate we obtain 68.6 mg g^{-1} for the MABs. The adsorption kinetics follows a pseudo-second-order kinetic model, where the adsorption equilibrium rate constant (k^2) is 3.8×10^{-4} g mg^{-1} min^{-1} for MABs and 1.98×10^{-4} g mg^{-1} min^{-1} for ABs, showing that the adsorption of Cu(II) ions is faster with MABs. This clearly shows the improvement in terms of adsorption when using superparamagnetic nanoparticles.

A comparative study of adsorption between magnetic and superparamagnetic nanoparticles was carried out by Damasceno et al. (2020). In this study, the adsorptions of indigo carmin dye were compared using superparamagnetic magnetite nanoparticles prepared by chemical co-precipitation and commercial magnetite nanoparticles. The adsorption tests were carried out using 0.01 g of NPs and 10 mL of a 20 mg L^{-1} solution of IC dye. After the interaction, the NPs were separated with an external magnetic field and the remaining solution was measured by UV–visible spectrophotometry in the visible region. The BET surface area of NP-synthetized was 127.19 ± 4.94 m^2 g^{-1}, and the average pore diameter was 11.3 nm. Also, NP-SYN showed superparamagnetic behavior, and NP-COM showed ferromagnetic behavior. The maximum removal value of IC dye was between 27% and 38% for synthesized magnetite and between 21% and 29% for commercial magnetite. The removal efficiency and adsorption capacity of NP-SYN were 87% and 17.45 mg g^{-1}, respectively, compared to NP-COM, which presented 33% and 6.12 mg g^{-1}. Therefore, it is recommended to use NP-SYN as they present better adsorption results.

Kulal and Badalamoole (2020) evaluated the effect of magnetite on the hydrogel pectin-*graft*-poly (Nhydroxyethylacrylamide) as an adsorbent for dyes and heavy metals from wastewater. A method for the in situ preparation of magnetite NPs within the gel network was followed for the formation of this magnetic hydrogel (Reddy et al., 2011). The adsorption behavior was evaluated in the R6G dye and in the Cu(II) and Hg(II) ions using solutions with concentrations between 10 and 500 mg L^{-1} and 20 and 1000 mg L^{-1}, respectively, at a temperature of 30 °C. The amount of dye remaining was calculated by UV–visible spectrophotometry, while the concentrations of the remaining metals were measured by atomic absorption spectroscopy. The BET surface analysis showed a higher surface area for the magnetic hydrogel (0.1466 m^2 g^{-1}) and a lower pore volume (0.00379 cm^3 g^{-1}) and pore diameter (103.4 nm). This decrease in porosity is due to the increase in volume due to the presence of the magnetite NPs that cover the empty spaces of the hydrogel network. The kinetic study showed pseudo-first-order adsorption kinetics for R6G and pseudo-second order for Cu (II) and Hg (II) and the absorption capacity obtained by the magnetic hydrogel was higher compared to the non-magnetic hydrogel for the R6G dye, and the Cu(II) and Hg(II) ions. The values obtained with PHEAA/Fe_3O_4 were 57.2, 248.6, and 240.2 mg g^{-1} for R6G, Cu(II), and Hg(II), respectively, as given in Table 9.4.

TABLE 9.4 Determination of different metals were measured by different adsorbent.

Analyte	Detection	Adsorbent		References
Pb^{2+}	AAS	Magnetite (Fe_3O_4)	$Q=$ $S_{BET} = 73\ m^2\ g^{-1}$	Linker and Jones (1966)
Cr^{6+}	AAS	Magnetite (Fe_3O_4)	$Q_{Cr} = 34.9\ mg\ g^{-1}$ $Q_{Pb} = 53.11\ mg\ g^{-1}$	Abdi and Kazemi (2015)
Pb^{2+}			$S_{BET} = 12.7\ m^2\ g^{-1}$	
As^{3+}	ICP-OES	Maghemite	$Q = 14.4\ mg\ g^{-1}$ $S_{BET} = 14.63\ m^2\ g^{-1}$	Stephen Inbaraj and Chen (2011)
Cu^{2+}	AAS	Magnetite alginate beds (MABs)	$Q = 68.6\ mg\ g^{-1}$	Mahamadi (2019)
Indigo carmine dye	UV–vis	Magnetite (Fe_3O_4)	$Q = 17.45\ mg\ g^{-1}$	Kloster et al. (2017)
Rhodamine 6G	UV–vis	Nanocomposite with Fe_3O_4 (Pec-g-PHEAA/Fe_3O_4)	$Q = 57.2\ mg\ g^{-1}$	Verma et al. (2017)
Cu^{2+}	AAS		$Q = 248.6\ mg\ g^{-1}$	
Hg^{2+}				$Q = 240.2\ mg\ g^{-1}$

9.4 Application in heavy metal removal

Numerous literature detailed the name "heavy metals" is used for a group of metals and semi-metals that have been associated with contamination, potential toxicity, and eco-toxicity. According to IUPAC, the term "heavy metals" has received several definitions by different authors, but none of them was considered valid. This is because the term "heavy," which refers to the density of the metal, is not precisely related to the toxicity or eco-toxicity of these elements. Additionally, this classification does not take into account the different physical-chemical and toxicological properties that the metal has according to the compound in which it is found, the amount, or oxidation state. Thanks to this, this term has never been defined by any authorized body like IUPAC and has been used inconsistently. This has led to confusion as to the meaning of the term, leading to the assumption that all so-called "heavy metals" have highly toxic or eco-toxic properties, when in fact, depends on the quantity, the way the metal is found, and the organism to which it refers (Duffus, 2002). With these implications made by IUPAC, it is evident that the definition of the term "heavy metals" is still a controversial subject and is in a stage of evolution, despite being frequently used in several scientific publications. Thus, when it comes to heavy metals, definitions can be based on atomic number, atomic mass, density, toxicity, or other chemical properties. Taking into account that there are different definitions for the group, the elements commonly called "heavy metals" are those most used in industry and are generally toxic to animals, for aerobic and anaerobic processes, but not all are dense or entirely metallic. Includes As, Cd, Cr, Cu, Pb, Hg, Ni, Se, Zn (Duffus, 2002; Sarkar, 2002).

Among these metals, some such as copper and zinc, are necessary for the performance of vital functions of organisms, but in excessive amounts they become toxic. Other metals such as mercury, lead, and cadmium do not have any biological function necessary for the organism and their accumulation can generate serious diseases, being identified as priority hazardous substances. Heavy metals are not biodegradable and are easily bio-accumulated along food chains (Zhang et al., 2019). This class of inorganic contaminants can be released into nature through natural processes such as weathering rocks for example. However, human activities have been increasing the levels of these pollutants in the environment, raising concerns about the disposal of solid waste and effluents without pre-treatment in river systems. Factors such as the increase in urbanization and industrialization, contribute significantly to the increase in the concentration of heavy metals in soil, water, and air. As an example, we can mention agriculture, where fertilizers, pesticides, and fungicides are used, which are potentially toxic to nature. Mining and smelting industries are also important sources of contamination of rivers and lakes since they produce considerable proportions of heavy metal-containing debris such as arsenic, cadmium, lead, and mercury (Sarkar, 2002; Zhang et al., 2019).

Thus, when "heavy metals" are improperly discarded in the environment, these elements can be absorbed by the plants and animals in the vicinity, causing serious poisoning in the organisms that inhabit the region. To achieve environmental protection, the need arises to develop efficient and low-cost methods for the removal of contaminated waste in the water. The conventional techniques currently available, such as evaporation and incineration, have a high cost and their use is not justified when the volume of waste is not large. Therefore, various studies have been carried out looking for innovative solutions that use materials of low cost to treat the toxic aquatic system. Accordingly, bio-sorption appears as an attractive alternative technique for removing toxic metals from contaminated water or at least reducing their effluent level. The technique involves a solid phase of biological origin (bio-sorbent) and a liquid phase (solvent, usually water) containing residues of the species to be adsorbed (sorbate, metal ion; dye). The sorbate is attracted and captured by the solid by different mechanisms and the process continues until reaching equilibrium, allowing its extraction. The advantages of bio-sorption as compare to conventional methods are (i) low cost (associated with the use of naturally abundant renewable biomaterials that can be produced at low cost), (ii) high efficiency (ability to reduce waste metals to less than one part per billion (ppb), (iii) bio-sorbent regeneration, and (iv) the possibility of metal recovery after adsorption (Mahamadi, 2019; Zhang et al., 2019). Bio-sorbents materials are made up of cellulose, lignin, carbohydrates, lipids, starch, hydrocarbons, and proteins (SUD et al., 2008). The bio-sorbent materials which are used to remove the toxic substances from aquatic solution are chitin, chitosan, raw agriculture solids, plant waste, bacterial biomass, and fungi (CRINI, 2006) while numerous agriculture waste materials have been reported in the literature for instance: peel of potato (Aman et al., 2008), the removal of copper (II) utilized sawdust (Ajmal et al., 1998), peel of citrus utilized as an adsorbent for the elimination of heavy metals (Schiewer and Patil, 2008) and mango peel (Iqbal et al., 2009a; Iqbal et al., 2009b). The definition of nano-biosorbent has resembled nanoparticles, the size of biological material at least less than 100 nm (Amin et al., 2014).

The biological nanoparticles have been considered to be predominant over other adsorbents toward the green environment due to their non-toxic nature. The advantage of using

adsorbents on the nanometer scale is that they have a high surface area, which increases chemical activity, adsorption capacity, and reduces resistance to internal diffusion. Classification of nano-biosorbent can be ordered into many categories. According to Mahamadi (2019) the categorization is depending on how they are prepared or synthesized. The removal affinity of biological nanoparticles improved with various modifications, for example, modification with magnetic particles, immobilization of bio-sorbent material on inorganic nanoparticles, a combination of organic materials with nano-biosorbents nanoparticles, and organic materials modified with metal oxides (Mahamadi, 2019).

Biological material like chitosan has stood out enough to be noticed in wastewater treatment because of its low cost, environmentally friendly, and high removal efficiency. Wang et al. (2016) reported the synthesis of magnetic polydopamine-chitosan nanoparticles for the removal of heavy metals. The present study explores the novel hybrid nano-biosorbent that was prepared to employ one-pot synthesis utilizing polydopamine (PDA) and chitosan onto magnetic nanoparticles. The nano-biosorbent material has a greater removal potential of 98.4%, 92%, 95.8% for Hg(II), Pb(II), and Cr(VI), respectively. The nano-biosorbent with superb outcomes could be utilized as a potential applicant for the removal of target pollutant compounds from the fluid medium. The monodisperse magnetic functional chitosan nano-biosorbent has been used for the elimination of Hg(II) from an aqueous environment (Hou et al., 2018). The synthesized chitosan and amine-functionalized magnetite nanoparticle (NH_2-Fe_3O_4) via covalently attached with glutaraldehyde and their adsorption ability enhanced via the functionalized amino-thiourea group. The elimination ability is 98.7% at a preliminary amount of 10 mg L^{-1}. The investigation of novel poly m-phenylenediamine grafted dextrin for the removal of Pb(II) has been reported in the literature (Zare et al., 2018). The blending method was used to synthesize poly m-phenylenediamine grafted dextrinand graphene oxide. The heavy metal Pb(II) adheres to nano-biosorbent material (DgPmPDA@GO) via electrostatic force. Some researchers have utilized polymer-containing graphene oxide nanocomposite for the elimination of two different kinds of heavy metals including cationic and anionic (Perez et al., 2017). The nanocomposite material comprises graphene oxide (GO), polyethyleneimine (PEI), and chitosan (CS) which were employed for the evacuation of chromium (VI) and copper (II). Response surface approach was planned to use for the optimization synthesis of polymer-containing graphene oxide nanocomposite (CS–PEI–GO).

The optimized nanocomposite consists of 2.0% PEI, 1500 ppm GO, and 2.08% GLA, and showed greater elimination efficiency to 91.10% and 78.18% for Cr(VI) and Cu(II), respectively. The multi-cyanoguanidine modified magnetic chitosan nano-absorbent was applied for the evacuation of Hg(II) in the aqueous system (Wang et al., 2013). The removal affinity of modified chitosan has been enhanced via a cross-linking agent with cyanoguanidine group at the same time. The removal percentage has been reached up to 96% at a low amount of model pollutants. The valuable elimination confirmed the tremendous consequences of the nano-biosorbent material (CG-MCS). Pillai et al. (2013) studied the elimination of Cd(II) from the liquid phase on the surface of xanthated nano-banana cellulose. The surface of nano-biosorbent material having sulfur-bearing groups which show more removal affinity toward heavy metal. The bio-sorption competence of the material has been evaluated using different kinds of parameters including time, concentration, pH, and bio-sorbent dosage. The second-order model was used to explain the adsorption kinetics. The nano-biosorbent material has

enough potential and proficient for the elimination of heavy metal contaminate from an aqueous environment. The researchers have been examined the synthesis and application of cerium modified chitosan ultrafine nano-biosorbent for the removal of As(III) (Zhang et al., 2016). The influence of various parameters on the removal capability of nano-biosorbent material (Ce-CNB) was investigated via a batch process. The adsorption phenomena come about through the formation of monodentate and bidentate complexes between hydroxyl groups and arsenite while partial As(III) oxidized to As(V) followed by concurrently adsorbed on the surface of nano-biosorbent (Ce-CNB). The adsorption process was explained using Langmuir isotherm while the pseudo-second-order kinetics was fitted to isotherm. Fig. 9.1 demonstrated the adsorption mechanism on the surface of nano-biosorbent (Ce-CNB) material.

The outcome of the particle with an average size of 3.5 nm proposes that nano-biosorbent (Ce-CNB) has high elimination affinity for the model contamination As(III) from an aqueous phase. Table. 9.5, shows the adsorption of heavy metal on the surface of nano-biosorbent materials while Table. 9.6, summaries of other articles about the adsorption capacity, kinetics, and removal of heavy metals. According to Mahamadi and Almomani (2019), nano-biosorbent provide high adsorption capacity (357 mg g^{-1} for the Pb(II)) while conventional bio-sorbents have less adsorption capacity <200 mg g^{-1} for Pb(II). It has been clear from the mentioned literature that nano-biosorbents have a high potential for the elimination of targeted pollutants from the aqueous phase as compare to conventional bio-sorbents because of their enough mechanical stability, large surface area, selectivity, and easily synthesized. The magnetic microalgae nano-biosorbent was showed a high removal rate and stability toward Cr as compared to a conventional approach (suspended microalgae) (Chen et al., 2019). The green methods which are used for the synthesis of nano-biosorbent are cost-effective and sufficient for the elimination of contaminated substances such as heavy metals from an aquatic phase. Additionally, the removal efficiency of the nano-biosorbent materials is enhanced via immobilization in various kinds of materials including alginate polymeric matrix, chemical and biological modification of the biomass.

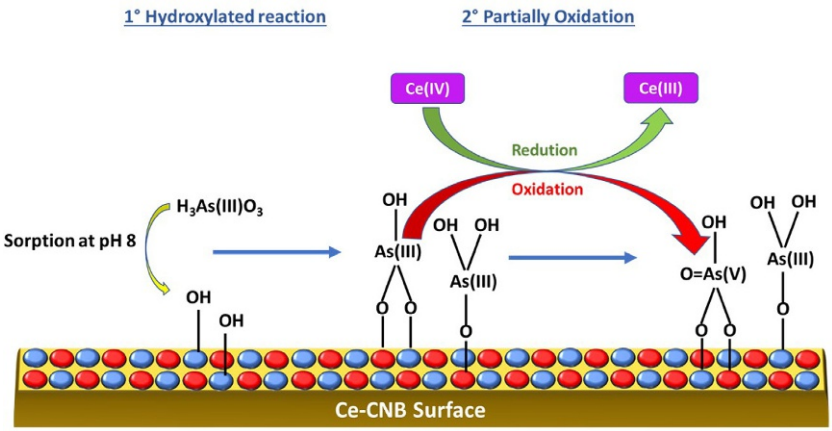

FIG. 9.1 The interaction of As(III) on the surface of nano-biosorbent (Ce-CNB) material adapted from Zhang et al. (2016) with permission from Elsevier.

TABLE 9.5 Description of nano-biosorbents their adsorption capacity and kinetic for heavy metal.

S. no.	Nano-biosorbent	Pollutant	Capacity ($mg\ g^{-1}$)	Kinetics	Source
1	Magnetic polydopamine-chitosan	Hg(II), Pb(II), and Cr(VI)	245.6, 47, 151.6	Pseudo-second-order	Wang et al. (2016)
2	Monodisperse magnetic functional chitosan	Hg(II)	246	Pseudo-second-order	Hou et al. (2018)
3	Poly m-phenylenediamine grafted dextrin	Pb(II)	80	Pseudo-first-order	Zare et al. (2018)
4	Polymer-based graphene oxide nanocomposite	Cr(VI) and Cu(II)	–	–	Perez et al. (2017)
5	Multicyanoguanidine modified magnetic chitosan	Hg(II)	285	Pseudo-second-order	Wang et al. (2013)
6	Xanthatednano banana cellulose	Cd(II)	154.26	Second-order	Pillai et al. (2013)
7	Cerium modified chitosan	As(III)	57.5	Pseudo-second-order	Zhang et al. (2016)

TABLE 9.6 Nano-biosorbents their adsorption capacity and kinetic for heavy metal.

S. no.	Nano-biosorbent	Pollutant	Capacity ($mg\ g^{-1}$)	Kinetics	Source
8	Pleurotusostreatus nanoparticles (PONP)	Mn(II)	130.625	Pseudo-second-order	Ma et al. (2013)
9	Magnetic *Aspergillus niger* composite	Cr(VI)	–	Pseudo-first–pseudo-second order	Daneshvar and Hosseini (2018)
10	Chitosan/magnetite composite beads	Pb(II) and Ni(II)	63.33 and 52.55	–	Tran et al. (2010)
11	Electrospun poly-ethylene oxide (PEO)/chitosan nanofiber membrane	Ni, Cu, Cd, and Pb	175.1, 163.7, 143.8, and 135.4	Pseudo-first–pseudo-second order	Aliabadi et al. (2013)
12	Alginate-coated chitosan nanoparticles	Ni	33.33	Pseudo-second-order	Esmaeili and Khoshnevisan (2016)
13	Nano zero-valent iron (NZVI) on a modified aquatic plant, *Azolla filiculoides*	Pb(II) and Hg(II)	–	Pseudo-first Pseudo-second order	Arshadi et al. (2017)
14	Nanomagnetite-immobilized-baker's yeast composite	Hg(II)	714.3	–	Mahmoud et al. (2015)

9.5 Application emerging contaminant

The approach about emerging contaminants has attracted the attention of researchers in recent years, consisting of various compounds found in water, soil, and air, being of anthropic origin (industrial, domestic, hospital, or agricultural waste) or from natural sources like some species of plants (Lei et al., 2015). These pollutants can have a harmful effect on the ecosystem, but they are not included in control and treatment programs, in other words, they do not have any type of regulation and legislation, that's why they are called emerging contaminants (ECs) (Stuart et al., 2012). Therefore, they will be studied and, depending on the results obtained such as toxicity in the environment, adverse effects on human health, bioaccumulation, amount dispersed in the environment, among others, there will be a future regulation and control of these pollutants (Reichert et al., 2019).

The study of ECs is very important and involves several areas of science, knowing the risk associated with their exposure allows avoiding several problems that would occur in future generations (Bunke et al., 2019). Most of these substances are relatively new and with little known effects (Stuart et al., 2012), but there are also some cases of older and studied contaminants that, even though they were dumped in low concentrations and considered "safe," also had effects that until then were not known (Arguello-Pérez et al., 2019). An example of this happened during the 90s in Florida, where there was a reduction of the alligator's population in the swamps, scientists found that the fertility of these animals was being impaired and the reason was the effect of chlorinated pesticides used in plantations in that region, in which, they affected their endocrine system. American law applied a limit on these pesticides based on their toxicity, but not on the hormonal effects they caused because they were unknown (Guillette et al., 1994).

As previously explained, even though many compounds already have some type of regulation, it is still observed that they may have environmental risks that are still unknown. Due to the low concentration present in the environment, ECs often end up becoming more complex to detect (Relyea, 2009). Currently, with the expansion of industrialization and the growth of consumption, there has been a significant increase in substances classified as ECs (Vélez et al., 2019). And with the increase in this number of substances, there was also greater attention from scientists and researchers and, therefore, resulting in a large increase in published journals, theses, books, and articles, as shown in the following Fig. 9.2, whose data by a specific magazine.

These substances have a variety of classifications, such as pharmaceuticals and personal care products (PPCPs), pesticides, surfactants, plasticizers, flame retardants, among others (Yan et al., 2010).

Pharmaceuticals and personal care products are common and with a wide variety of compounds, with some examples such as synthetic hormones, analgesics, anti-inflammatories, fragrances, cosmetics, among others (Bisognin et al., 2018). They are dumped into the environment through city sewage and animal waste on farms (Derksen et al., 2004) and, even though they are found in low concentrations, it is important to study their capacity to harm the environment and human or animal health, as they have bioaccumulative and endocrine disruptive potential, affecting the growth and reproduction of living beings (Terzić et al., 2008).

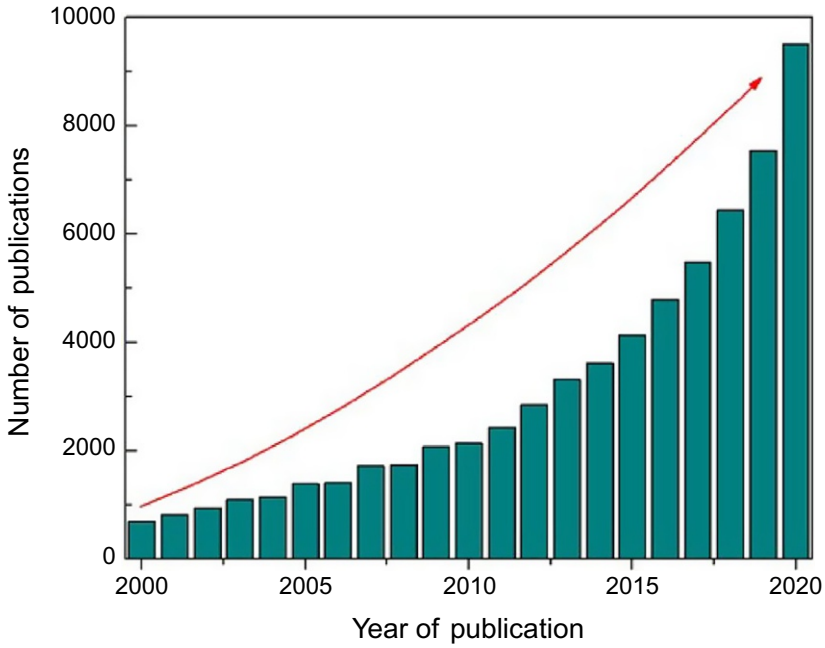

FIG. 9.2 Number of publications referring to ECs in the last 20 years.

Pesticides are compounds very common in agriculture, being used to protect plants against pests and to preserve food. These substances end up contaminating the soil, groundwater, lakes, and rivers, but they can also generate residues in food that will be consumed by the population. Many of these compounds have carcinogenic potential and, even in low amounts, can affect the endocrine system (Gilden et al., 2010).

Surfactants are organic substances that have polar and nonpolar groups in their molecules, which allows a better affinity between water and other liquids, the most common examples being detergents, soaps, and shampoos. They are generally not completely removed by the treatment systems and end up being discharged into the effluents through the sewers, being very toxic to aquatic organisms (Ying, 2006).

Plasticizers are low molecular weight substances used in the production of plastic materials, which consist of several products, whether industrial or in common use. The most well-known compound is bisphenol A (BPA), which is present in several plastic products and packaging and, according to some research, has the capacity to harm the endocrine system of living beings, affecting their fertility, in addition to the immune and nervous systems (Oehlmann et al., 2009).

Flame retardants are brominated compounds that are applied to various objects and electronic products. They are classified as emerging contaminants due to their bioaccumulative capacity, especially in fatty tissue because of their lipophilic characteristics causing several health problems (Smital, 2008).

As mentioned earlier, there is a great diversity of substances considered to be emerging contaminants in addition to those that have been exemplified previously. It is important that health and environmental protection organizations are on the alert about the effects that they can cause, even in very small concentrations, they can present effects that are still unknown that end up affecting the local ecosystem and health of the population.

Within the group of drugs, the detection and quantification of several of these compounds have been studied, for example, Amoxicillin can be found in pharmaceuticals, biological fluids (Hrioua et al., 2021), environmental samples (Lima et al., 2019), and foodstuffs samples (Essousi et al., 2020), this drug has received major interest to analyze and synthesize sensor, biosensors, and nanosorbentes for its detection. An eco-friendly alternative is the use of electrochemical sensors, which can be prepared based on modified electrodes, nanomaterials, and polymers. Essousi et al. have used polymer-based modified electrodes for the detection of amoxicillin. The glassy carbon electrode (GCE) surface was modified with reduced graphene oxide (RGO) and electropolymerized pyrrole in the presence of amoxicillin and the extraction of the template has been carried out by overoxidation of polypyrrole. Results obtained for the %recovery of amoxicillin in milk and serum were 97.6% and 99.7%, respectively (Essousi et al., 2020). Another interesting study is the adsorption of diclofenac in wastewater (Cantarella et al., 2019) is being widely studied due to its high selectivity and its high adsorption affinity toward the polymer (Madikizela and Chimuka, 2016). Cantarella et al. were able to remove 90% of diclofenac from an aqueous solution. In addition, the use of hydrophilic monomer (methacrylic acid) provides excellent material compatibility in water and high selectivity (Cantarella et al., 2019), overcoming limits of the traditional MIP (Bhadra et al., 2016; de Oliveira et al., 2019; Liang et al., 2019). Madikizela et al. investigated the selective removal of naproxen, ibuprofen, and diclofenac from aqueous media using a multitemplate molecular imprinting polymer (MIP) which was synthesized by bulk polymerization consisting of a mixture of toluene and acetonitrile, 2-vinylpyridine, ethylene glycol dimethacrylate, naproxen, ibuprofen, and diclofenac as porogenic solvent, functional monomer, structural monomer and analytes, respectively. The order of selectivity of the reported polymer was Diclofenac > Ibuprofen > Naproxen and the %recovery of analytes in samples of wastewater effluents were 38% naproxen, 69% ibuprofen, and 87% diclofenac. Mohiuddin et al. synthesized a porous molecular imprinting polymer (PMIP) as adsorbents for the solid-phase extraction of diclofenac, using HPLC as a quantification instrument. The synthesis consisted of two stages; The first consisted of preparing polystyrene spheres (PS) from the polymerization reaction of polyvinyl pyrrolidine and styrene in aqueous medium, using potassium persulfate as radical initiator at a temperature of 70 °C. Then, the spheres obtained from PS were wrapped with a layer of silica (SiO_2) through the sol-gel process with a modification that consisted in adding a surfactant such as CTAB, the washes with a solution of ammonium nitrate and THF had the purpose to eliminate the CTAB and the PS, respectively, obtaining the porous silica shells (PSS). The second stage was to support the polymer in the PSS, for this, diclofenac and 4-vinyl pyridine were mixed in acetonitrile. EDGMA and initiator AIBN were then added to initiate polymerization. Finally, the polymers obtained reported high% recovery in aqueous solutions between 95.41% and 124.14%, being an effective method for the quantification of diclofenac (Mohiuddin et al., 2020).

Some of the emerging pollutants classified as alkaloids are caffeine (Teixeira et al., 2020) and nicotine (Cennamo et al., 2014). The advantage of using the packed sorbent microextraction (MEPS) technique for the detection of caffeine is the reduction of the amount of reagent used between 10 and 100 times, that is, from mL to μL (Atarodi and Faghihian, 2019). MEPS uses a microcolumn filled with 1–4 mg of nano-adsorbent material, which provides different extraction mechanisms, such as adsorption or partition, however, the variety of commercially available extractive phases for MEPS is still less than the phase variation of conventional solid-phase extraction (Munyati et al., 2017). While nicotine detection uses a fiber optic sensor taking advantage of the signal provided by surface plasmon resonance. The thin gold film was sputtered by using a sputtering machine. The pre-polymeric mixture for MIP was prepared with l-nicotine as a template, methacrylic acid as functional monomer, DVB as cross-linker, and AIBN as the radical initiator. The polymeric film was prepared by dropping 100 μL of pre-polymeric mixture on the gold layer and spinning at 1000 rpm for 35 s. The polymerization was then carried out at 70°C for about 16 h, achieving a MIP layer with a thickness of about 150 nm (Cennamo et al., 2014).

On the other hand, some researchers analyzed nano-biosorbent of pesticides, Atarodi et al. synthesized a chitosan-based molecular imprinting polymer material impregnated in ZnO photocatalysts for the selective degradation of atrazine in aqueous solutions. The degradation of atrazine was attributed to the action of the polymer obtained and it was evaluated by high-performance liquid chromatography and gas chromatography, showing a selective degradation of atrazine in 80.29% (Atarodi and Faghihian, 2019). Fig. 9.3 shows the polymerization of MICN. Munyati et al. Aldrin-selective alinyl-based molecular imprinting polymers were prepared by reverse emulsion polymerization. The synthesis consisted of the formation of a milky emulsion of surfactant sodium lauryl sulfate, water, benzoyl peroxide, and chloroform. Subsequently, the milky white emulsion was added dropwise to a stirring mixture of aniline monomer and aldrin template in a chloroform solution. The formed product was washed

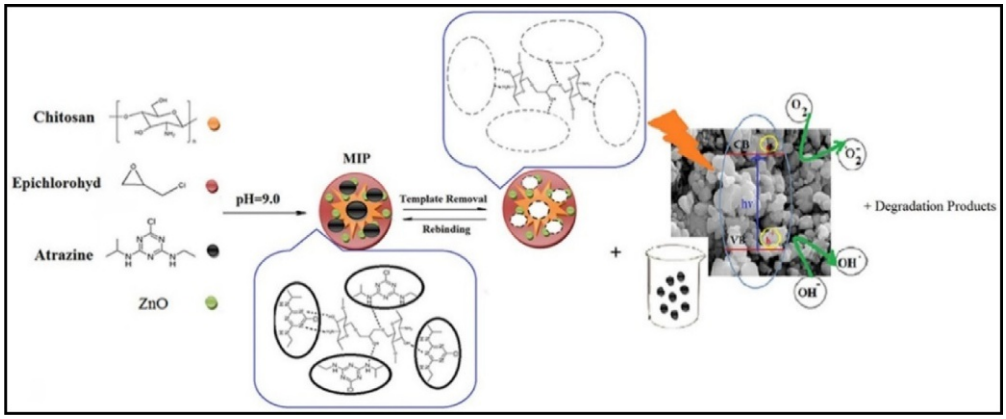

FIG. 9.3 Polymerization of molecularly imprinted chitosan nanocatalysts (MICN) (Atarodi and Faghihian, 2019).

with acetone to break the emulsion and precipitate the molecularly imprinted polyaniline nanoparticles.

Finally, the adsorption characteristics of aldrin and dichlorodiphenyltrichloroethane (DDT) were investigated. The selectivity of the printed nanoparticles was quantitatively analyzed by gas chromatography-time of flight mass spectrometry (GC-TOFMS). Being the distribution coefficients for DDT and aldrin are 0.76 and 1.31 ng μL^{-1}, respectively, indicating that the printed nanoparticles had a stronger affinity for aldrin than for DDT (Munyati et al., 2017). Fig. 9.4 shows the polyaniline polymer synthesis scheme. In the area of personal care products. Lu et al. developed a polymeric material with a core@shell structure with convenient magnetic properties to efficiently remove triclosan (TCS) in aquatic environments. The synthesis consisted of the modification of the magnetic nanoparticles of Fe_3O_4 with sodium citrate to improve the dispersibility in the solution. Then, using the sol-gel method, the Fe_3O_4 nanoparticles were coated with SiO_2, using an isopropanol-water mixture for hydrolysis and condensation, ammonia as a catalyst, and tetraethyl orthosilicate (TEOS) as a precursor to the formation of the SiO_2 layer. Then the Fe_3O_4 nanoparticles coated with SiO_2 (Fe_3O_4@SiO_2) were superficially modified by adding 3-methacryloxypropyltrimethoxysilane (MPS) in a methanol solution in an inert atmosphere for 24 h. Obtaining vinyl groups on the surface of the material (Fe_3O_4@SiO_2-C═C). Then, for the polymerization, Fe_3O_4@SiO_2-C═C, acetonyrtrile, TCS, MAA, EDGMA, and AIBN were mixed as support material, porogenic solvent, analyte or template, functional monomer, cross-linking monomer, and radical initiator respectively obtained (TMIP) was evaluated using HPLC with a UV detector. The recovery results obtained were 96%–106% with a selectivity of 6.321 of TCS with respect to the interferents 2,4,6-trichlorophenol; 2,4-dichlorophenol; 4-chlorophenol and diuron, showing high potential to be convenient absorbents in the application of TCS removal from the aquatic environment (Lu et al., 2020). Fig. 9.5 shows the scheme for obtaining the TMIP synthesis.

A summary Table 9.7 shows some of the nanosorbents currently used for the detection of emerging pollutants, in addition to their method linearity, variety of synthesis processes, and analyte quantification, which is interpreted as a great contribution by these nanosorbent materials in different types of sample matrices.

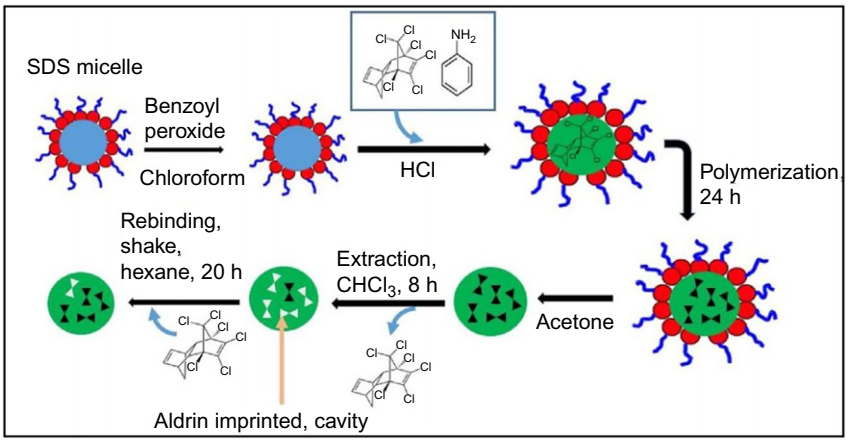

FIG. 9.4 Scheme showing the preparation of molecularly imprinted polyaniline nanoparticles (Munyati et al., 2017).

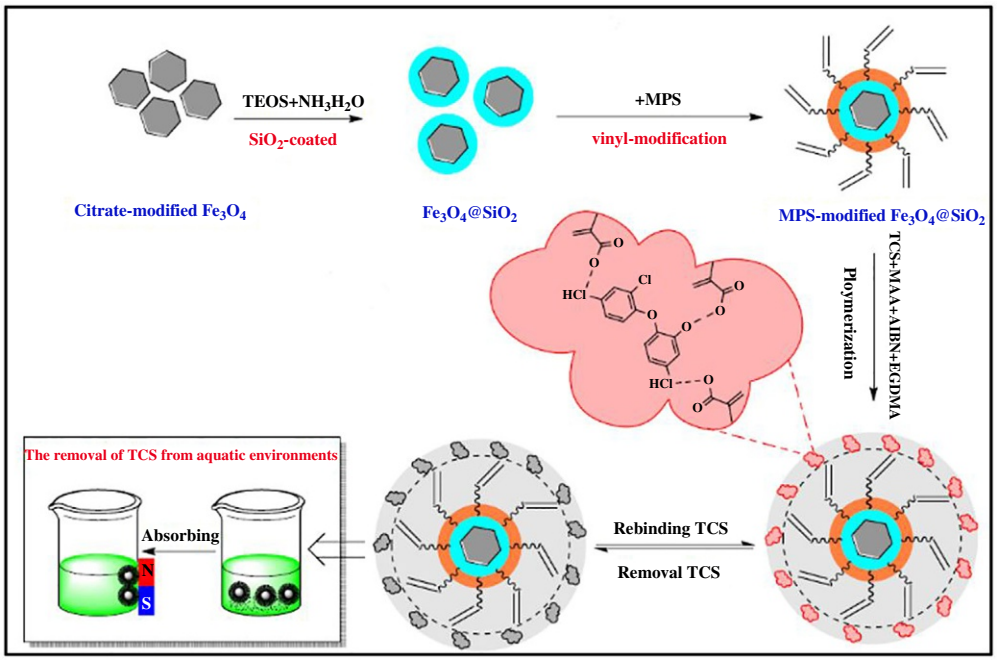

FIG. 9.5 Scheme for the triclosan-MMIP and the application of adsorption, separation, and elimination of triclosan from the aquatic environment.

9.6 Application classic contaminant

There are many researches on the use of nano-biosorbents to remove many harmful composes as the ones described in previous segments of this chapter. There is also some investigation for these materials in order to remove classic contaminants such as fluorides and phosphates.

Fluoride is a very common element in nature, it accounts for about 0.3 g kg^{-1} of the earth's crust and it has been found in many minerals, such as fluorspar, cryolite, fluorite, and fluorapatite. What is more, fluoride is one of the most abundant anions present in drinking water and may be beneficial to human health at low concentrations, for example, the ingestion of 0.8–1.0 mg L^{-1} can protect teeth and promote the development of strong bones. However, ingestion of higher concentrations of fluoride can be harmful to human health. For example, some diseases are dental fluorosis, skeletal fluorosis, brain damage, Alzheimer's syndrome, thyroid disorder, and cancer. Hence, it is necessary for the removal of the excess fluorides from contaminant water to improve the quality of life. For this purpose, many investigations were developed using nano-biosorbents as described in Fig. 9.6 (Christina and Viswanathan, 2015; Cai et al., 2015).

Cai et al. (2015) proposed the use of tea leaf wastes loaded with Al and Fe. Three solutions of ferric chloride, aluminum nitrate, and a mixed solution were prepared in hydrochloric acid. Tea leaf waste and the solutions were added to a beaker and were stirred at 60 °C. The adsorbent dosage, initial fluoride concentration, contact time, and pH were studied in

TABLE 9.7 Some nanosorbents used for the detection of emerging pollutants, with their method of linearity, variety of synthesis, and analyte quantification.

Type CCE	Analyte	Nanosorbent	Method synthesis	Type samples	Linear range (μmol L^{-1})	Method detection	References
Pharmaceuticals	Amoxicillin (Amx)	MIP-rGO/ OPPy/AuNps	Electro polymerization	Serum	1–1000	CV	Essousi et al. (2020)
	Diclofenac	DICLO/MAA/ EGDMA	Bulk polymerization	Waste water	Remove 90%	UV–vis	Cantarella et al. (2019)
Alkaloids	Caffeine	CAF/MAA/	Bulk polymerization	Energy drink	1–50	HPLC–UV detection	Teixeira et al. (2020)
	Nicotine	Nicotine/MAA/ DVB	Bulk polymerization	Wastewater	$0–10^4$	UV-vis	Cennamo et al. (2014)
Pesticides	Tyramine	MIP/CNNS/ rGO-COOH/ GCE	Electro polymerization	Food	0.01–1000	Electrochemiluminescence	Liu et al. (2020a)
	2-Chloro acetamide	MMIP butachlor: MBA: 4-VP: AGG	Bulk polymerization	Agriculture water	1.1×10^{-3}–2.14	MMISPE-HPLC	Ji et al. (2017)
Phenol	2-Chloro phenol	Chloroxylenol/ 4-VBA/EGDMA	UV photo polymerization	River water and sewage	0.04–0.93	MIP-UHPLCPDA	Abu-Alsoud and Bottaro (2021)
Illicit drugs	Cocaine	Cocaine/MAA/ EDMA	Bulk polymerization	Oral fluid	3–10	Ion mobility spectrometry	Sorribes-Soriano et al. (2020)
	Heroin	$Ru(bpy)_3^{2+}$/GCE	Ultrasonic	Urine and saliva	10^{-8}–10^{-4}	Electrochemiluminescence	Shang et al. (2014)

a 50 mL centrifuge tube to which 50 mg bio-sorbent was added to a 25 mL fluoride solution of known concentration. The centrifuge tubes were mixed for 120 min at room temperature in a vapor-bathing constant temperature vibrator. The solution was separated through filtration and the F-conductance was measured.

The study concluded that Tea-Al-Fe and Tea-Al were desirable bio-sorbents for the treatment of drinking water contaminated by fluoride as both showed a strong adsorption ability. What is more, these materials were compared with others in the literature and only orange waste loaded with Sn or Al presented a stronger adsorption ability but it is active at acid pH, which would restrict further application. Furthermore, the contact time of Tea-Al and Tea-Al-Fe is lower than the orange bio-sorbents, which would contribute to a rapid treatment of drinking waters (Table 9.8).

In addition, Christina and Viswanathan (2015) developed an orange-peel-based material. Fe_3O_4 nanoparticles immobilized in sodium alginate matrix (FNPSA) and Fe_3O_4 nanoparticles and saponified orange peel residue immobilized in sodium alginate matrix (FNPSOPR) as sorbents for fluoride removal from contaminated water. The surfaces of the nano-biosorbents were functionalized in order to enable them to adsorb fluoride ions more efficiently from water. In an Erlenmeyer were performed the studies, 50 mL of a solution of known concentration of

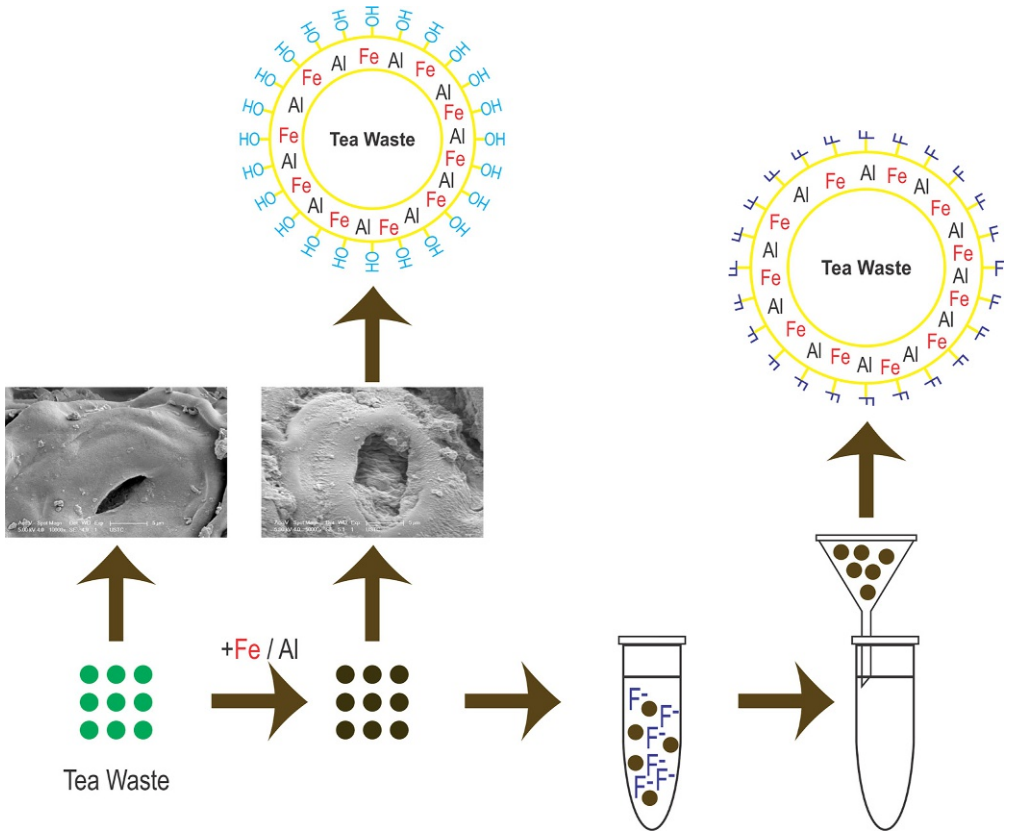

FIG. 9.6 Procedure of the removal of fluoride using the Tea-Al-Fe nano-biosorbent (Cai et al., 2015).

TABLE 9.8 Comparison of fluoride adsorption capacity between loaded tea waste and loaded orange wasted.

Bio-sorbent	q^0 (mg g^{-1})	pH	Contact time (h)	References
Orange-Sn	22.24	3.0	4	Paudyal et al. (2011)
Orange-Al	19.57	6.0	4	
Tea	3.83	2.0–9.0	2	Cai et al. (2015)
Tea-Fe	10.47	2.0	2	
Tea-Al	13.79	4.0–8.0	2	
Tea-Al-Fe	18.52	4.0–8.0	2	

fluoride was added in order to evaluated parameters like contact time, pH, sorbent dosage, initial concentration of fluoride, and temperature. To determinate the fluoride that was not adsorbed, the flasks were stirred at 120 rpm and every 10 min with a fluoride ion-selective electrode, the concentration of fluoride was determined as shown in Fig. 9.7 (Christina and Viswanathan, 2015).

FNPSA and FNPSOPR presented maximum adsorption of 58.24 and 80.33 mg g^{-1}, respectively, both described the Langmuir model of isotherm that suggests monolayer adsorption mechanism of fluoride. FNPSA offered a high fluoride sorption capacity than orange residues materials and calcium alginate matrices. However, FNPSOPR developed a higher sorption capacity, and what is more, it showed good reusability of 76.53% after 5 cycles of alternative adsorption-desorption. Hence, Christina et al. concluded that FNPSOPR could be used as an effective sorbent to remove fluoride from water and improve its quality to obtain permissible limits for its usage (Christina and Viswanathan, 2015).

Phosphorus is an essential element in plant life and its phosphate form, they are necessary for the formation of seeds. Plants absorb phosphates, which is why they are found in plant tissue in a variable concentration, providing a healthy life with greater resistance to disease and damage caused by frost (Navarro Garcia et al., 2013). However, excess phosphorus in the water causes eutrophication, leading to uncontrolled algal blooms that can threaten public safety and environmental safety (Conley et al., 2009). Therefore, it is necessary to develop effective methods to remove excess phosphate before pouring it into the water. Nanobiosorbents are a very promising alternative.

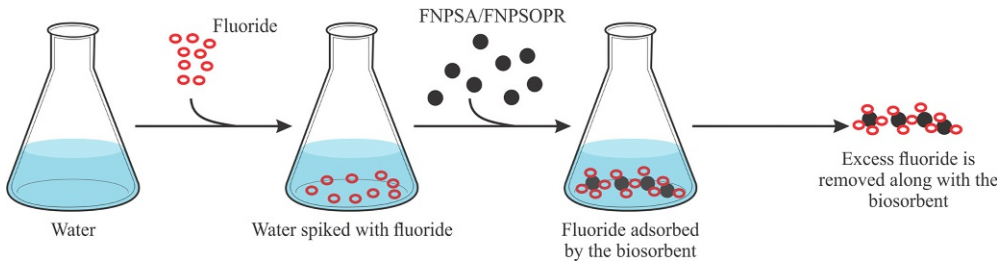

FIG. 9.7 Procedure of fluoride removal using FNPSA or FNPSOPR (Christina and Viswanathan, 2015).

A nano-biosorbents based on ostrich bone waste treated and activated with HNO_3, $FeCl_2$ y HBO_4. In the synthesis, process nanoparticles of Fe^0 were formed and adhere to the surface of the treated ostrich bone waste. The biomaterial serves as a support for the nanoparticles of Fe^0. The treated ostrich bone suppresses the oxidation and aggregation of the nanoparticles of Fe^0 which gives it greater capacity to capture phosphates from the aqueous medium, even in real samples. The contact time to reach 99% equilibrium for the maximum adsorption of phosphate ions was 5 min, after 5 min the adsorption of phosphate ions increased slowly reaching maximum adsorption in 30 min. The adsorption was 326 mg of phosphate ions per gram of the biomaterial, this result was compared with other bio-sorbents was better by presenting a high adsorption capacity. The synthesis of the biomaterial is promising because it is inexpensive, easy to synthesize in large quantities, and chemically and thermally stable (Arshadi et al., 2015). With this information, the material proposed by Arshadi et al. (2015), could be used as a good nano-biosorbents for the removal of phosphate in the Persian Gulf.

Liu et al. (2020a, b) proposed a nano-biosorbent of cerium oxide functionalized lignin. Very briefly, L-NH_2 was mixed with $CeCl_3 \cdot 7H_2O$ for 2 h, in order to absorb Ce^{3+} on the L-NH_2 surface, then a solution of NaOH was slowly added until the pH was 10. Then, the mixture was put in a water bath for 2 h and later reacted at 25 °C for 24 h. Finally, the resulting product was washed with distilled water, filtered by vacuum, and dried at 60 °C for 24 h (Fig. 9.8). The aminated lignin supported on cerium oxide nanoparticles (L-NH_2@Ce) obtained presented an average size of 15 nm, it has a BET surface area of 89.8 $m^2\ g^{-1}$ of L-NH_2@Ce, which is three times greater than that of lignin, and pore volume is 0.23 $cm^3\ g^{-1}$ of L-NH_2@Ce. The nano-biosorbent efficiently captures phosphates in an aqueous medium in the pH range of 5–8. By the Langmuir model, it was determined that the adsorption of phosphate ions is 27.86 mg g^{-1} of the bio-sorbent. Using the in situ precipitation method, phosphate was removed efficiently. The synthesis of the nano-biosorbent is promising because it is inexpensive, the preparation process is simple, the synthesized compound is stable, and the nano-biosorbent can be reused (Liu et al., 2020b).

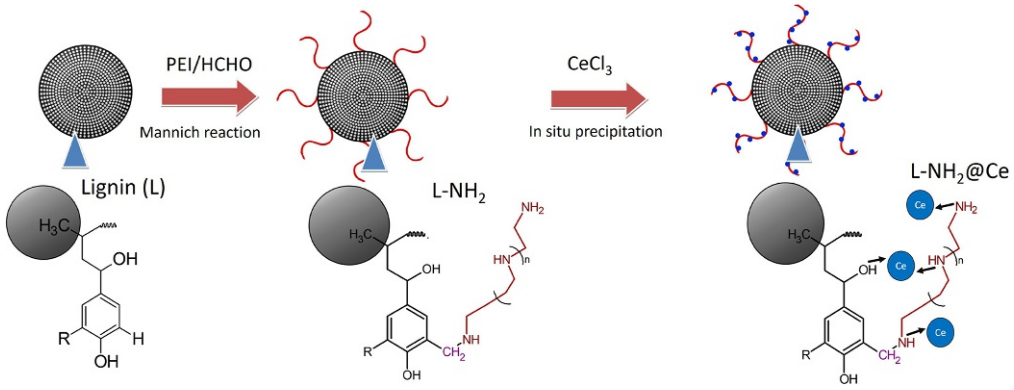

FIG. 9.8 Schematic diagram for the preparation of biosorbent L-NH_2@Ce nanohybrid by In situ precipitation method.

9.7 Advantages of nano-engineered adsorbent and future prospects

Nanocomposites have several properties related to the size of the compositional units that give them a particular characteristic. The high surface:volume ratio gives to nanocomposites special physical and chemical properties and for this reason gained particular attention from engineering researchers, trying to combine the physicochemical advantages with the treatment of waste materials and the possibility of regenerating technological properties with the least possible environmental risk.

Chitosan is one the most abundant biopolymer after cellulose with a wide functionality in its structure, which has a direct relation to biomedical applications and related sciences. Chitosan exhibits a large list of biological activities leading to antitumor activity, immunoadjuvant activity, hypodermic activity, hemostatic activity, antimicrobial activity, biodegradability, among others (Mutreja et al., 2020). Chitosan and its derivatives have attracted attention as nano-adsorbent thanks to their particular physicochemical properties. One of the advantages of chitosan-based materials is the presence of hydroxyl and amino groups in the polymer structure allows the formation of inter-/intramolecular hydrogen bonds between linear structures of chitin, extending their interactions with other materials or polymeric groups to be removed (Nasrollahzadeh et al., 2021). Owing to these properties, chitosan-based materials display outstanding adsorbent performance in the adsorption of heavy metal ions dyes, pesticides, pollutants from wastewater, as aforementioned in this review. Another advantage chitosan-based materials is the ease of modification that involves cross-linking agents (Parastar et al., 2021), grafting (Wang et al., 2020; Banisheykholeslami et al., 2021), mixed with other adsorbents (Safie and Zahrim, 2021; Zhao et al., 2021) among others. Moreover, treatments oriented to improve surface properties and porosity via texture modification of chitosan into new material form as hydrogels (Mittal et al., 2021; Jamali and Akbari, 2021), nanofibers (Bayat et al., 2021; Tan et al., 2020), carbon nanotube (Kavousi and Chavoshi, 2020; Hsan et al., 2020), as well as carbon quantum nanodots (Hammi et al., 2021; Siddique et al., 2020). The combination of surface physical-chemical properties of chitosan as nano-adsorbent with intrinsically inner properties of biopolymer as biocompatibility, biodegradation, non-toxic activation, and a high degree of reuse has shown the versatile and the wide extended innovation of chitosan-based material in science engineering, massive production of ecological products and food packing separation hydrogels.

Alginates are another interesting nanostructured biopolymer with a lot of applications as nano-adsorbent related to the presence of hydroxyl and carboxylate groups in their inner structure. The easy formation of anionic groups allows cationic groups or positive polar organic species from wastewater to be removed with high efficiency via electrostatic interactions (Asadi et al., 2018). The main advantages of this biopolymer are associated with some properties and characteristics as stability, permeability, biodegradability, non-toxic nature (Gao et al., 2020). In addition, the alginates form biohydrogels platforms over which an active component could be supported, improving the surface contact and network structure as well as the functionality of the framework structure (Jiang et al., 2020; Godiya et al., 2019).

Cellulose is another interesting biopolymer material based on specific properties of the structure in the form of nanotubes, nanofibrils (Yu et al., 2020), nanocrystals (Park et al., 2020), with outstanding sorption and catalytic properties usually demanding for water

treatment processes. The applications of cellulose have grown dramatically in recent years due to its versatile properties as environmentally friendly material, low cost, biodegradability, the feasibility of access, stability, and a high degree of reuse as well as the wide ability of integration with other materials particularly as nano and microfibers to synthesize membranes leading to water clean management (Ao et al., 2020). The modified cellulosic-based membranes have shown good performance for the removal of heavy (Ao et al., 2020).

The applications of chitosan, alginates, and celluloses as nano-adsorbents on material engineering, biomedicine, pharmaceutical delivery platforms, biological systems related to biodegradability, and their antioxidant properties have played a substantial role in green chemistry. These applications are associated with the outstanding performance of low-cost nano-adsorbents, accessible, renewable, with very few discharges, therefore, fully in agreement with the needs of society and its inhabitants and the future generations.

References

Abdel-Gawad, S.A., Baraka, A.M., El-Shafei, M.M., Mahmoud, A.S., 2016. Effects of nano zero valent iron and entrapped nano zero valent iron in alginate polymer on poly aromatic hydrocarbons removal ABSTRACT. J. Environ. Biotechnol. Res. 5 (1), 18–28.

Abdi, O., Kazemi, M., 2015. A review study of biosorption of heavy metals and comparison between different biosorbents. J. Mater. Environ. Sci. 6 (5), 1386–1399.

Abu-Alsoud, G.F., Bottaro, C.S., 2021. Porous thin-film molecularly imprinted polymer device for simultaneous determination of phenol, alkylphenol and chlorophenol compounds in water. Talanta 223, 121727.

Aguilar-Arteaga, K., Rodriguez, J.A., Barrado, E., 2010. Magnetic solids in analytical chemistry: a review. Anal. Chim. Acta 674 (2), 157–165.

Ajmal, M., Hussain Khan, A., Ahmad, S., Ahmad, A., 1998. Role of sawdust in the removal of copper(II) from industrial wastes. Water Res. 32 (10), 3085–3091.

Aliabadi, M., Irani, M., Ismaeili, J., Piri, H., Parnian, M.J., 2013. Electrospun nanofiber membrane of PEO/chitosan for the adsorption of nickel, cadmium, lead and copper ions from aqueous solution. Chem. Eng. J. 220, 237–243.

Aman, T., Kazi, A.A., Sabri, M.U., Bano, Q., 2008. Potato peels as solid waste for the removal of heavy metal copper(II) from waste water/industrial effluent. Colloids Surf. B Biointerfaces 63 (1), 116–121.

Amin, M.T., Alazba, A.A., Manzoor, U., 2014. A review of removal of pollutants from water/wastewater using different types of nanomaterials. Adv. Mater. Sci. Eng. 2014, 1–24.

Amiri, M., Salavati-Niasari, M., Akbari, A., 2019. Magnetic nanocarriers: evolution of spinel ferrites for medical applications. Adv. Colloid Interface Sci. 265, 29–44.

Ao, C., et al., 2020. Biodegradable all-cellulose composite membranes for simultaneous oil/water separation and dye removal from water. Carbohydr. Polym. 250, 116872.

Arguello-Pérez, M.Á., Mendoza-Pérez, J.A., Tintos-Gómez, A., Ramírez-Ayala, E., Godínez-Domínguez, E., de Asis Silva-Bátiz, F., 2019. Ecotoxicological analysis of emerging contaminants from wastewater discharges in the coastal zone of Cihuatlán (Jalisco, Mexico). Water 11 (7), 1386.

Arsalani, S., Löwa, N., Kosch, O., Radon, P., Baffa, O., Wiekhorst, F., 2021. Magnetic separation of iron oxide nanoparticles to improve their application for magnetic particle imaging magnetic separation of iron oxide nanoparticles to improve their application for magnetic particle imaging. Phys. Med. Biol. 66, 015002.

Arshadi, M., Gholtash, J.E., Zandi, H., Foroughifard, S., 2015. Phosphate removal by a nano-biosorbent from the synthetic and real (Persian Gulf) water samples. RSC Adv. 5 (54), 43290–43302.

Arshadi, M., Abdolmaleki, M.K., Mousavinia, F., Foroughifard, S., Karimzadeh, A., 2017. Nano modification of NZVI with an aquatic plant Azolla filiculoides to remove Pb(II) and Hg(II) from water: aging time and mechanism study. J. Colloid Interface Sci. 486, 296–308.

Asadi, S., Eris, S., Azizian, S., 2018. Alginate-based hydrogel beads as a biocompatible and efficient adsorbent for dye removal from aqueous solutions. ACS Omega 3 (11), 15140–15148.

Atarodi, H., Faghihian, H., 2019. Selective photodegradation of atrazine by a novel molecularly imprinted nanophotocatalyst prepared on the basis of chitosan. J. Photochem. Photobiol. A Chem. 382, 111892.
Avval, Z.M., et al., 2019. Introduction of magnetic and supermagnetic nanoparticles in new approach of targeting drug delivery and cancer therapy application. Drug Metab. Rev., 1–28.
Azmy, E.A.M., Hashem, H.E., Mohamed, E.A., Negm, N.A., 2019. Synthesis, characterization, swelling and antimicrobial efficacies of chemically modified chitosan biopolymer. J. Mol. Liq. 284, 748–754.
Bagbi, Y., Sarswat, A., Mohan, D., Pandey, A., Solanki, P.R., 2016. Lead (Pb2+) adsorption by monodispersed magnetite nanoparticles: surface analysis and effects of solution chemistry. J. Environ. Chem. Eng. 4 (4), 4237–4247.
Bagheri, S., Julkapli, N.M., 2018. Grafted Nanocellulose as an Advanced Smart Biopolymer. Elsevier Inc.
Banisheykholeslami, F., Hosseini, M., Najafpour Darzi, G., 2021. Design of PAMAM grafted chitosan dendrimers biosorbent for removal of anionic dyes: adsorption isotherms, kinetics and thermodynamics studies. Int. J. Biol. Macromol. 177, 306–316.
Barbera, A.J., McConnell, V.D., 1990. The impact of environmental regulations on industry productivity: direct and indirect effects. J. Environ. Econ. Manag. 18 (1), 50–65.
Bayat, A., Tati, A., Ahmadipouya, S., Haddadi, S.A., Arjmand, M., 2021. Electrospun chitosan/polyvinyl alcohol nanocomposite holding polyaniline/silica hybrid nanostructures: an efficient adsorbent of dye from aqueous solutions. J. Mol. Liq. 331, 115734.
Bhadra, B.N., Seo, P.W., Jhung, S.H., 2016. Adsorption of diclofenac sodium from water using oxidized activated carbon. Chem. Eng. J. 301, 27–34.
Bhardwaj, N., Kundu, S.C., 2010. Electrospinning: a fascinating fiber fabrication technique. Biotechnol. Adv. 28 (3), 325–347.
Bhattarai, N., Edmondson, D., Veiseh, O., Matsen, F.A., Zhang, M., 2005. Electrospun chitosan-based nanofibers and their cellular compatibility. Biomaterials 26 (31), 6176–6184.
Bisognin, R.P., Wolff, D.B., Carissimi, E., 2018. Revisão sobre fármacos no ambiente. Rev. DAE 66 (210), 78–95.
Biswas, G., Tarafdar, A., 2013. Extraction of chitosan from prawn shell wastes and examination of its viable commercial applications. Int. J. Theor. Appl. Res. Mech. Eng. 2, 17–24.
Bonavigo, H., Zucchetti, L., Mankolli, M., 2009. Water radioactive pollution and related environmental aspects. J. Int. Environ. Appl. Sci. 4, 357–363.
Boukhalfa, N., Boutahala, M., Djebri, N., Idris, A., 2019. Kinetics, thermodynamics, equilibrium isotherms, and reusability studies of cationic dye adsorption by magnetic alginate/oxidized multiwalled carbon nanotubes composites. Int. J. Biol. Macromol. 123, 539–548.
Bunke, D., Moritz, S., Brack, W., Herráez, D.L., Posthuma, L., Nuss, M., 2019. Developments in society and implications for emerging pollutants in the aquatic environment. Environ. Sci. Eur. 31 (1), 32.
Cai, H., et al., 2015. Removal of fluoride from drinking water using tea waste loaded with Al/Fe oxides: a novel, safe and efficient biosorbent. Appl. Surf. Sci. 328, 34–44.
Cantarella, M., et al., 2019. Molecularly imprinted polymer for selective adsorption of diclofenac from contaminated water. Chem. Eng. J. 367, 180–188.
Carpenter, A.W., De Lannoy, C.F., Wiesner, M.R., 2015. Cellulose nanomaterials in water treatment technologies. Environ. Sci. Tech. 49 (9), 5277–5287.
Carvalho Costa, A.W.M., et al., 2020. Biosorption of Cr(VI) using coconut fibers from agro-industrial waste magnetized using magnetite nanoparticles. Environ. Technol., 1–12.
Cennamo, N., D'Agostino, G., Pesavento, M., Zeni, L., 2014. High selectivity and sensitivity sensor based on MIP and SPR in tapered plastic optical fibers for the detection of l-nicotine. Sens. Actuators B 191, 529–536.
Chen L, Feng G, Huiqiao H, Jiawei K, Yezi H, Magnetic microalgae biosorption flocculating agent and method for adsorbing chromium in waste water. Patent No. CN109174025, 2019.
Chen, T., Wang, Q., Lyu, J., Bai, P., Guo, X., 2020. Boron removal and reclamation by magnetic magnetite (Fe3O4) nanoparticle: an adsorption and isotopic separation study. Sep. Purif. Technol. 231 (August 2019), 115930.
Christina, E., Viswanathan, P., 2015. Development of a novel nano-biosorbent for the removal of fluoride from water. Chin. J. Chem. Eng. 23 (6), 924–933.
Conley, D.J., et al., 2009. Ecology: controlling eutrophication: nitrogen and phosphorus. Science 323 (5917), 1014–1015.
Coughlin, R.W., Deshaies, M.R., Davis, E.M., 1990. Chitosan in crab shell wastes purifies electroplating wastewater. Environ. Prog. 9 (1), 35–39.
CRINI, G., 2006. Non-conventional low-cost adsorbents for dye removal: a review. Bioresour. Technol. 97 (9), 1061–1085.

Damasceno, B.S., Da Silva, A.F.V., De Araújo, A.C.V., 2020. Dye adsorption onto magnetic and superparamagnetic Fe3O4 nanoparticles: a detailed comparative study. J. Environ. Chem. Eng. 8 (5), 103994.
Daneshvar, M., Hosseini, M.R., 2018. Kinetics, isotherm, and optimization of the hexavalent chromium removal from aqueous solution by a magnetic nanobiosorbent. Environ. Sci. Pollut. Res. 25 (28), 28654–28666.
de Oliveira, H.L., Teixeira, L.S., Dinali, L.A.F., Pires, B.C., Simões, N.S., Borges, K.B., 2019. Microextraction by packed sorbent using a new restricted molecularly imprinted polymer for the determination of estrogens from human urine samples. Microchem. J. 150, 104162.
Derksen, J.G.M., Rijs, G.B.J., Jongbloed, R.H., 2004. Diffuse pollution of surface water by pharmaceutical products. Water Sci. Technol. 49 (3), 213–221.
Dev, V.V., Baburaj, G., Antony, S., Arun, V., Krishnan, K.A., 2020. Zwitterion-chitosan bed for the simultaneous immobilization of Zn(II), Cd(II), Pb(II) and Cu(II) from multi-metal aqueous systems. J. Clean. Prod. 255, 120309.
Devanathan, R., 2017. Energy penalty for excess baggage. Nat. Nanotechnol. 12, 500–501. https://doi.org/10.1038/nnano.2017.53.
Devatha, C.P., Jagadeesh, K., Patil, M., 2018. Effect of green synthesized iron nanoparticles by Azardirachta indica in different proportions on antibacterial activity. Environ. Nanotechnol. Monit. Manag. 9, 85–94.
Dhankhar, R., Hooda, A., 2011. Fungal biosorption—an alternative to meet the challenges of heavy metal pollution in aqueous solutions. Environ. Technol. 32 (5), 467–491.
Di Martino, A., Sittinger, M., Risbud, M.V., 2005. Chitosan: a versatile biopolymer for orthopaedic tissue-engineering. Biomaterials 26 (30), 5983–5990.
Dimassi, S., Tabary, N., Chai, F., Blanchemain, N., Martel, B., 2018. Sulfonated and sulfated chitosan derivatives for biomedical applications: a review. Carbohydr. Polym. 202, 382–396. Elsevier Ltd.
Ding, J., Huang, D., Wang, W., Wang, Q., Wang, A., 2019. Effect of removing coloring metal ions from the natural brick-red palygorskite on properties of alginate/palygorskite nanocomposite film. Int. J. Biol. Macromol. 122, 684–694.
Duffus, J.H., 2002. 'Heavy metals' a meaningless term? (IUPAC Technical Report). Pure Appl. Chem. 74 (5), 793–807.
Dwivedi, A.K., 2017. Researches in water pollution: a review. J. Nat. Appl. Sci. 4, 118–142.
Ekevwe, A.E., Isaac, G.B.A., Aroh, A.O., 2018. Review of organic pollutants in wastewater along the Course of River Gwagwarwa and River Rafin Malam in Kano State-Nigeria. J. Biotechnol. Bioeng. 2, 36–39.
Elmizadeh, H., Khanmohammadi, M., Ghasemi, K., Hassanzadeh, G., Nassiri-Asl, M., Garmarudi, A.B., 2013. Preparation and optimization of chitosan nanoparticles and magnetic chitosan nanoparticles as delivery systems using Box–Behnken statistical design. J. Pharm. Biomed. Anal. 80, 141–146.
Emmerichs, N., Wingender, J., Flemming, H.-C., Mayer, C., 2004. Interaction between alginates and manganese cations: identification of preferred cation binding sites. Int. J. Biol. Macromol. 34, 73–79.
Esmaeili, A., Khoshnevisan, N., 2016. Optimization of process parameters for removal of heavy metals by biomass of Cu and Co-doped alginate-coated chitosan nanoparticles. Bioresour. Technol. 218, 650–658.
Essousi, H., Barhoumi, H., Karastogianni, S., Girousi, S.T., 2020. An electrochemical sensor based on reduced graphene oxide, gold nanoparticles and molecular imprinted over-oxidized polypyrrole for amoxicillin determination. Electroanalysis 32 (7), 1546–1558.
Farooq, A., et al., 2020. Cellulose from sources to nanocellulose and an overview of synthesis and properties of nanocellulose/zinc oxide nanocomposite materials. Int. J. Biol. Macromol. 154, 1050–1073.
Fazlzadeh, M., Rahmani, K., Zarei, A., Abdoallahzadeh, H., Nasiri, F., Khosravi, R., 2017. A novel green synthesis of zero valent iron nanoparticles (NZVI) using three plant extracts and their efficient application for removal of Cr(VI) from aqueous solutions. Adv. Powder Technol. 28 (1), 122–130.
Foguel, M.V., Pedro, N.T.B., Wong, A., Khan, S., Zanoni, M.V.B., del Pilar Taboada Sotomayor, M., 2017. Synthesis and evaluation of a molecularly imprinted polymer for selective adsorption and quantification of Acid Green 16 textile dye in water samples. Talanta 170, 244–251.
Franco, D.S.P., et al., 2020. Araticum (Annona crassiflora) seed powder (ASP) for the treatment of colored effluents by biosorption. Environ. Sci. Pollut. Res. 27 (10), 11184–11194.
GAF, R., 1992. Chitin Chemistry. Macmillan.
Gao, X., Guo, C., Hao, J., Zhao, Z., Long, H., Li, M., 2020. Adsorption of heavy metal ions by sodium alginate based adsorbent—a review and new perspectives. Int. J. Biol. Macromol. 164, 4423–4434.
Germanos, G., Youssef, S., Farah, W., Lescop, B., Rioual, S., Abboud, M., 2020. The impact of magnetite nanoparticles on the physicochemical and adsorption properties of magnetic. J. Environ. Chem. Eng. 8 (5), 104223.

Ghoreishi, S.M., Haghighi, R., 2003. Chemical catalytic reaction and biological oxidation for treatment of non-biodegradable textile effluent. Chem. Eng. J. 95 (1–3), 163–169.
Gilden, R.C., Huffling, K., Sattler, B., 2010. Pesticides and health risks. J Obstet Gynecol Neonatal Nurs 39 (1), 103–110.
Godiya, C.B., Liang, M., Sayed, S.M., Li, D., Lu, X., 2019. Novel alginate/polyethyleneimine hydrogel adsorbent for cascaded removal and utilization of Cu2+ and Pb2+ ions. J. Environ. Manage. 232, 829–841.
Guillette, L.J., Gross, T.S., Masson, G.R., Matter, J.M., Percival, H.F., Woodward, A.R., 1994. Developmental abnormalities of the gonad and abnormal sex hormone concentrations in juvenile alligators from contaminated and control lakes in Florida. Environ. Health Perspect. 102 (8), 680–688.
Gupta, V.K., Ali, I., Saleh, T.A., Nayak, A., Agarwal, S., 2012. Chemical treatment technologies for waste-water recycling—an overview. RSC Adv. 2 (16), 6380.
Habibi, Y., Lucia, L.A., Rojas, O.J., 2010. Cellulose nanocrystals: chemistry, self-assembly, and applications. Chem. Rev. 110 (6), 3479–3500.
Haider, S., Park, S.Y., 2009. Preparation of the electrospun chitosan nanofibers and their applications to the adsorption of Cu(II) and Pb(II) ions from an aqueous solution. J. Membr. Sci. 328 (1–2), 90–96.
Hameed, B.H., El-Khaiary, M.I., 2008. Kinetics and equilibrium studies of malachite green adsorption on rice straw-derived char. J. Hazard. Mater. 153 (1–2), 701–708.
Hammi, N., Marcotte, N., Marinova, M., Draoui, K., Royer, S., El Kadib, A., 2021. Nanostructured metal oxide@carbon dots through sequential chitosan templating and carbonisation route. Carbohydr. Polym. Technol. Appl. 2, 100043.
Hola, K., Markova, Z., Zoppellaro, G., Tucek, J., Zboril, R., 2015. Tailored functionalization of iron oxide nanoparticles for MRI, drug delivery, magnetic separation and immobilization of biosubstances. Biotechnol. Adv. 33 (6), 1162–1176.
Horák, D., Babic, M., Macková, H., Benes, M.J., 2007. Preparation and properties of magnetic nano- and microsized particles for biological and environmental separations. J. Sep. Sci. 30 (11), 1751–1772.
Hou, C., Zhao, D., Zhang, S., Wang, Y., 2018. Highly selective adsorption of Hg(II) by the monodisperse magnetic functional chitosan nano-biosorbent. Colloid Polym. Sci. 296 (3), 547–555.
Hrioua, A., et al., 2021. Recent advances in electrochemical sensors for amoxicillin detection in biological and environmental samples. Bioelectrochemistry 137, 107687.
Hsan, N., Dutta, P.K., Kumar, S., Das, N., Koh, J., 2020. Capture and chemical fixation of carbon dioxide by chitosan grafted multi-walled carbon nanotubes. J. CO_2 Util. 41, 101237.
Hudson, S.M., Jenkins, D.W., 2001. Chitin and Chitosan, Encyclopedia of Polymer Science and Technology. Wiley Interscience, NJ.
Hussein, M.H., Hamouda, R.A., Elhadary, A.M.A., Abuelmagd, M.A., Ali, S., Rizwan, M., 2019. Characterization and chromium biosorption potential of extruded polymeric substances from Synechococcus mundulus induced by acute dose of gamma irradiation. Environ. Sci. Pollut. Res. 26 (31), 31998–32012.
Iconaru, S.L., Guégan, R., Popa, C.L., Motelica-Heino, M., Ciobanu, C.S., Predoi, D., 2016. Magnetite (Fe3O4) nanoparticles as adsorbents for As and Cu removal. Appl. Clay Sci. 134, 128–135.
Iqbal, M., Saeed, A., Zafar, S.I., 2009a. FTIR spectrophotometry, kinetics and adsorption isotherms modeling, ion exchange, and EDX analysis for understanding the mechanism of Cd2+ and Pb2+ removal by mango peel waste. J. Hazard. Mater. 164 (1), 161–171.
Iqbal, M., Saeed, A., Kalim, I., 2009b. Characterization of adsorptive capacity and investigation of mechanism of Cu 2+, Ni 2+ and Zn 2+ adsorption on mango peel waste from constituted metal solution and genuine electroplating effluent. Sep. Sci. Technol. 44 (15), 3770–3791.
Iqbal, J., et al., 2019. Synergistic effects of activated carbon and nano-zerovalent copper on the performance of hydroxyapatite-alginate beads for the removal of As3+ from aqueous solution. J. Clean. Prod. 235, 875–886.
Jamali, M., Akbari, A., 2021. Facile fabrication of magnetic chitosan hydrogel beads and modified by interfacial polymerization method and study of adsorption of cationic/anionic dyes from aqueous solution. J. Environ. Chem. Eng. 9 (3), 105175.
Javadian, H., Ruiz, M., Saleh, T.A., Sastre, A.M., 2020. Ca-alginate/carboxymethyl chitosan/Ni0.2Zn0.2Fe2.6O4 magnetic bionanocomposite: synthesis, characterization and application for single adsorption of Nd+3, Tb+3, and Dy+3 rare earth elements from aqueous media. J. Mol. Liq. 306, 112760.
Jayakumar, R., Prabaharan, M., Reis, R.L., Mano, J.F., 2005. Graft copolymerized chitosan—present status and applications. Carbohydr. Polym. 62 (2), 142–158.

Ji, W., et al., 2017. Selective solid phase extraction of chloroacetamide herbicides from environmental water samples by amphiphilic magnetic molecularly imprinted polymers. Talanta 170, 111–118.
Jiang, H., et al., 2020. Preparation of a novel bio-adsorbent of sodium alginate grafted polyacrylamide/graphene oxide hydrogel for the adsorption of heavy metal ion. Sci. Total Environ. 744, 140653.
Kaur, R., Hasan, A., Iqbal, N., Alam, S., Saini, M.K., Raza, S.K., 2014. Synthesis and surface engineering of magnetic nanoparticles for environmental cleanup and pesticide residue analysis: a review. J. Sep. Sci. 37 (14), 1805–1825.
Kavousi, M., Chavoshi, M.S., 2020. Effect of coated carbon nanotubes with chitosan and cover of flaxseed in the induction of MDA-MB-231 apoptosis by analyzing the expression of Bax and Bcl-2. Meta Gene 26, 100807.
Kazemi, J., Javanbakht, V., 2020. Alginate beads impregnated with magnetic Chitosan@Zeolite nanocomposite for cationic methylene blue dye removal from aqueous solution. Int. J. Biol. Macromol. 154, 1426–1437.
Khaleda Firdous, S.C., 2017. A review: naturally available sources of chitosan and analysis of chitosan derivatives for its antimicrobial activity. Int. J. Recent Sci. Res. 8 (3), 15773–15776.
Khan, S., et al., 2018. Synthesis and characterization of magnetic-molecularly imprinted polymers for the HPLC-UV analysis of ametryn. React. Funct. Polym. 122, 175–182.
Khor, E., Lim, L.Y., 2003. Implantable applications of chitin and chitosan. Biomaterials 24 (13), 2339–2349.
Klemm, D., Philipp, B., Heinze, T., Heinze, U., Wagenknecht, W., 1998. Comprehensive cellulose chemistry: volume I. In: Fundamentals and Analytical Methods. vol. l.
Klemm, D., et al., 2011. Nanocelluloses: a new family of nature-based materials. Angew. Chem. Int. Ed. 50 (24), 5438–5466.
Kloster, G.A., Muraca, D., Mosiewicki, M.A., Marcovich, N.E., 2017. Magnetic composite films based on alginate and nano-iron oxide particles obtained by synthesis 'in situ'. Eur. Polym. J. 94, 43–55.
Klumpp, E., et al., 2003. Sorption of 2,4-dichlorophenol on modified hydrotalcites. Colloids Surf. A Physicochem. Eng. Asp. 230 (1–3), 111–116.
Ko, S., Kim, E.S., Park, S., Daigle, H., Milner, T.E., Huh, C., 2017. Amine functionalized magnetic nanoparticles for removal of oil droplets from produced water and accelerated magnetic separation. J. Nanopart. Res. 19, 132.
Kuang, Y., Du, J., Zhou, R., Chen, Z., Megharaj, M., Naidu, R., 2015. Calcium alginate encapsulated Ni/Fe nanoparticles beads for simultaneous removal of Cu (II) and monochlorobenzene. J. Colloid Interface Sci. 447, 85–91.
Kulal, P., Badalamoole, V., 2020. Magnetite nanoparticle embedded Pectin-graft-poly(N-hydroxyethylacrylamide) hydrogel: evaluation as adsorbent for dyes and heavy metal ions from waste water. Int. J. Biol. Macromol. 156, 1408–1417.
Kulkarni, R.M., Vidya Shetty, K., Srinikethan, G., 2019. Kinetic and equilibrium modeling of biosorption of nickel (II) and cadmium (II) on brewery sludge. Water Sci. Technol. 79 (5), 888–894.
Kumaresapillai, N., Bashab, R.A., Sathish, R., 2010. Production and evaluation of chitosan from Aspergillus niger MTCC strains. Iran. J. Pharm. Res. 10 (3), 553–558.
Kundu, S., Chowdhury, I.H., Naskar, M.K., 2018. Nitrogen-doped nanoporous carbon nanospheroids for selective dye adsorption and Pb(II) Ion removal from waste water. ACS Omega 3 (8), 9888–9898.
Kwok, K.C.M., Koong, L.F., Chen, G., McKay, G., 2014. Mechanism of arsenic removal using chitosan and nanochitosan. J. Colloid Interface Sci. 416, 1–10.
Lakouraj, M.M., Mojerlou, F., Zare, E.N., 2014. Nanogel and superparamagnetic nanocomposite based on sodium alginate for sorption of heavy metal ions. Carbohydr. Polym. 106 (1), 34–41.
Lei, M., et al., 2015. Overview of emerging contaminants and associated human health effects. Biomed. Res. Int. 2015, 1–12.
Li, Q., Dunn, E.T., Grandmaison, E.W., Goosen, M.F.A., 1992. Applications and properties of chitosan. J. Bioact. Compat. Polym. 7 (4), 370–397.
Li, Z., et al., 2019a. Efficient removal of heavy metal ions and organic dyes with cucurbit [8] uril-functionalized chitosan. J. Colloid Interface Sci. 539, 400–413.
Li, Z., Xu, S., Xiao, G., Qian, L., Song, Y., 2019b. Removal of hexavalent chromium from groundwater using sodium alginate dispersed nano zero-valent iron. J. Environ. Manage. 244, 33–39.
Liang, X.X., Omer, A.M., Hu, Z., Wang, Y., Yu, D., Ouyang, X., 2019. Efficient adsorption of diclofenac sodium from aqueous solutions using magnetic amine-functionalized chitosan. Chemosphere 217, 270–278.
Lima, D.R., et al., 2019. Removal of amoxicillin from simulated hospital effluents by adsorption using activated carbons prepared from capsules of cashew of Para. Environ. Sci. Pollut. Res. 26 (16), 16396–16408.
Linker, A., Jones, R.S., 1966. A new polysaccharide resembling alginic acid isolated from pseudomonads. J. Biol. Chem. 241 (16), 3845–3851.

Liu, P., Borrell, P.F., Božič, M., Kokol, V., Oksman, K., Mathew, A.P., 2015. Nanocelluloses and their phosphorylated derivatives for selective adsorption of Ag(+), Cu(2+) and Fe(3+) from industrial effluents. J. Hazard. Mater. 294, 177–185.
Liu, J., Liu, W., Wang, Y., Xu, M., Wang, B., 2016. A novel reusable nanocomposite adsorbent, xanthated Fe3O4-chitosan grafted onto graphene oxide, for removing Cu(II) from aqueous solutions. Appl. Surf. Sci. 367, 327–334.
Liu, M., et al., 2020a. A dual-recognition molecularly imprinted electrochemiluminescence sensor based on g-C3N4 nanosheets sensitized by electrodeposited rGO-COOH for sensitive and selective detection of tyramine. Sens. Actuators B 311, 127901.
Liu, X., et al., 2020b. Cerium oxide nanoparticle functionalized lignin as a nano-biosorbent for efficient phosphate removal. RSC Adv. 10 (3), 1249–1260.
Lu, Y.C., et al., 2020. A novel strategy for selective removal and rapid collection of triclosan from aquatic environment using magnetic molecularly imprinted nano-polymers. Chemosphere 238, 124640.
Ma, Z., Kotaki, M., Inai, R., Ramakrishna, S., 2005. Potential of nanofiber matrix as tissue-engineering scaffolds. Tissue Eng. 11 (1–2), 101–109.
Ma, L., Peng, Y., Wu, B., Lei, D., Xu, H., 2013. Pleurotus ostreatus nanoparticles as a new nano-biosorbent for removal of Mn(II) from aqueous solution. Chem. Eng. J. 225, 59–67.
Madikizela, L.M., Chimuka, L., 2016. Synthesis, adsorption and selectivity studies of a polymer imprinted with naproxen, ibuprofen and diclofenac. J. Environ. Chem. Eng. 4 (4), 4029–4037.
Mahamadi, C., 2019. Will nano-biosorbents break the Achilles' heel of biosorption technology? Environ. Chem. Lett. 17 (4), 1753–1768.
Mahamadi, C., Almomani, F., 2019. On the dominance of Pb during competitive biosorption from multi-metal systems: a review. Cogent Environ. Sci. 5 (1), 1635335.
Mahmoud, M.E., Ahmed, S.B., Osman, M.M., Abdel-Fattah, T.M., 2015. A novel composite of nanomagnetite-immobilized-baker's yeast on the surface of activated carbon for magnetic solid phase extraction of Hg(II). Fuel 139, 614–621.
Marjani, A., Zare, M.H., Sadeghi, M.H., Shirazian, S., Ghadiri, M., 2021. Synthesis of alginate-coated magnetic nanocatalyst containing high-performance integrated enzyme for phenol removal. J. Environ. Chem. Eng. 9 (1), 104884.
Merouani, S., Hamdaoui, O., Saoudi, F., Chiha, M., Pétrier, C., 2010. Influence of bicarbonate and carbonate ions on sonochemical degradation of Rhodamine B in aqueous phase. J. Hazard. Mater. 175 (1–3), 593–599.
Mittal, H., Al Alili, A., Morajkar, P.P., Alhassan, S.M., 2021. GO crosslinked hydrogel nanocomposites of chitosan/carboxymethyl cellulose—a versatile adsorbent for the treatment of dyes contaminated wastewater. Int. J. Biol. Macromol. 167, 1248–1261.
Miyashiro, D., Hamano, R., Umemura, K., 2020. A review of applications using mixed materials of cellulose, nanocellulose and carbon nanotubes. Nanomaterials 10 (2), 1–23.
Mohiuddin, I., Grover, A., Aulakh, J.S., Lee, S.-S., Malik, A.K., Kim, K.-H., 2020. Porous molecularly-imprinted polymer for detecting diclofenac in aqueous pharmaceutical compounds. Chem. Eng. J. 382, 123002.
Moradi Dehaghi, S., Rahmanifar, B., Moradi, A.M., Azar, P.A., 2014. Removal of permethrin pesticide from water by chitosan–zinc oxide nanoparticles composite as an adsorbent. J. Saudi Chem. Soc. 18 (4), 348–355.
Munyati, M.O., Mbozi, A., Siamwiza, M.N., Diale, M.M., 2017. Polyaniline nanoparticles for the selective recognition of aldrin: synthesis, characterization, and adsorption properties. Synth. Met. 233, 79–85.
Mutreja, R., Thakur, A., Goyal, A., 2020. Chitin and chitosan: current status and future opportunities. In: Handbook of Chitin and Chitosan. Elsevier, pp. 401–417.
Nasrollahzadeh, M., Sajjadi, M., Iravani, S., Varma, R.S., 2021. Starch, cellulose, pectin, gum, alginate, chitin and chitosan derived (nano)materials for sustainable water treatment: a review. Carbohydr. Polym. 251, 116986.
Nata, I.F., Sureshkumar, M., Lee, C.K., 2011. One-pot preparation of amine-rich magnetite/bacterial cellulose nanocomposite and its application for arsenate removal. RSC Adv. 1 (4), 625–631.
Natarajan, E., Ponnaiah, G.P., 2017. Optimization of process parameters for the decolorization of Reactive Blue 235 dye by barium alginate immobilized iron nanoparticles synthesized from aluminum industry waste. Environ. Nanotechnol. Monit. Manag. 7, 73–88.
Navarro Garcia, S., Gines, Garcia, N., 2013. Agricultural Chemistry: Chemistry of the Soil and Essential Nutrients for Plants, third ed. Mundi-Press Printing Company, Madrid, Spain, p. 492.
Nedkov, I., Merodiiska, T., Slavov, L., Vandenberghe, R.E., Kusano, Y., Takada, J., 2006. Surface oxidation, size and shape of nano-sized magnetite obtained by co-precipitation. J. Magn. Magn. Mater. 300 (2), 358–367.

Nematidil, N., Sadeghi, M., 2019. Fabrication and characterization of a novel biosorbent and its evaluation as adsorbent for heavy metal ions. Polym. Bull. 76 (10), 5103–5127.
Oehlmann, J., et al., 2009. A critical analysis of the biological impacts of plasticizers on wildlife. Philos. Trans. R. Soc. B 364 (1526), 2047–2062.
Ogawa, K., Oka, K., Yui, T., 1993. X-ray study of chitosan-transition metal complexes. Chem. Mater. 5 (5), 726–728.
Olivera, S., Muralidhara, H.B., Venkatesh, K., Guna, V.K., Gopalakrishna, K., Kumar K, Y., 2016. Potential applications of cellulose and chitosan nanoparticles/composites in wastewater treatment: a review. Carbohydr. Polym. 153, 600–618. Elsevier Ltd.
Pal, P., Pal, A., Nakashima, K., Yadav, B.K., 2021. Applications of chitosan in environmental remediation: a review. Chemosphere 266, 128934. Elsevier Ltd.
Parastar, M., Sheshmani, S., Shokrollahzadeh, S., 2021. Cross-linked chitosan into graphene oxide-iron(III) oxide hydroxide as nano-biosorbent for Pd(II) and Cd(II) removal. Int. J. Biol. Macromol. 166, 229–237.
Park, S.-H., et al., 2020. Poly(acryloyl hydrazide)-grafted cellulose nanocrystal adsorbents with an excellent Cr(VI) adsorption capacity. J. Hazard. Mater. 394, 122512.
Paudyal, H., et al., 2011. Adsorptive removal of fluoride from aqueous solution using orange waste loaded with multivalent metal ions. J. Hazard. Mater. 192 (2), 676–682.
Paul, S., Jayan, A., Sasikumar, C.S., 2014. Extraction and purification of chitosan from chitin isolated from sea prawn (Fenneropenaeus indicus). Asian J. Pharm. Clin. Res. 7, 201–204.
Pawar, S.N., Edgar, K.J., 2012. Alginate derivatization: a review of chemistry, properties and applications. Biomaterials 33 (11), 3279–3305.
Perez, J.V.D., Nadres, E.T., Nguyen, H.N., Dalida, M.L.P., Rodrigues, D.F., 2017. Response surface methodology as a powerful tool to optimize the synthesis of polymer-based graphene oxide nanocomposites for simultaneous removal of cationic and anionic heavy metal contaminants. RSC Adv. 7 (30), 18480–18490.
Periyasamy, S., Gopalakannan, V., Viswanathan, N., 2018. Hydrothermal assisted magnetic nano-hydroxyapatite encapsulated alginate beads for efficient Cr(VI) uptake from water. J. Environ. Chem. Eng. 6 (1), 1443–1454.
Phiri, I., et al., 2019. Simultaneous removal of cationic, anionic and organic pollutants in highly acidic water using magnetic nanocomposite alginate beads. J. Water Process Eng. 31, 100884.
Pillai, S.S., et al., 2013. Biosorption of Cd(II) from aqueous solution using xanthated nano banana cellulose: equilibrium and kinetic studies. Ecotoxicol. Environ. Saf. 98, 352–360.
Puvvada, Y.S., Vankayalapati, S., Sukhavasi, S., 2012. Extraction of chitin from chitosan from exoskeleton of shrimp for application in the pharmaceutical industry. Int. Curr. Pharm. J. 1 (9), 258–263.
Rajput, S., Pittman, C.U., Mohan, D., 2016. Magnetic magnetite (Fe3O4) nanoparticle synthesis and applications for lead (Pb2+) and chromium (Cr6+) removal from water. J. Colloid Interface Sci. 468, 334–346.
Rao, D.S., 2017. Thermal pollution—impact on living organisms. Int. Res. J. Nat. Appl. Sci. 4, 1. ISSN: 2349-4077.
Rathod, M., Moradeeya, P.G., Haldar, S., Basha, S., 2018. Nanocellulose/TiO2 composites: preparation{,} characterization and application in the photocatalytic degradation of a potential endocrine disruptor{,} mefenamic acid{,} in aqueous media. Photochem. Photobiol. Sci. 17 (10), 1301–1309.
Reddy, N.N., Mohan, Y.M., Varaprasad, K., Ravindra, S., Joy, P.A., Raju, K.M., 2011. Magnetic and electric responsive hydrogel-magnetic nanocomposites for drug-delivery application. J. Appl. Polym. Sci. 122 (2), 1364–1375.
Reichert, G., Hilgert, S., Fuchs, S., Azevedo, J.C.R., 2019. Emerging contaminants and antibiotic resistance in the different environmental matrices of Latin America. Environ. Pollut. 255, 113140.
Rekha Kathal, P.L., Kumar, V.C., Puri, L., Baishya, A., Uniyal, R., 2016. Pollution Status of Yamuna River, India—a national concern. Int. Res. J. Environ. Sci. 5, 1–6.
Relyea, R.A., 2009. A cocktail of contaminants: how mixtures of pesticides at low concentrations affect aquatic communities. Oecologia 159 (2), 363–376.
Ren, G., et al., 2018. Facile synthesis of maghemite nanoparticle from waste green vitriol as adsorbent for adsorption of arsenite. J. Mol. Liq. 259 (2017), 32–39.
Ren, J., Zhu, Z., Qiu, Y., Yu, F., Ma, J., Zhao, J., 2021. Magnetic field assisted adsorption of pollutants from an aqueous solution: a review. J. Hazard. Mater. 408 (December 2020), 124846.
Robalds, A., 2015. The Use of Bio Sorbents in the Treatment of Polluted Waters. Department of Environmental Science.
Robertson, F.N., 1989. Arsenic in ground water under oxidizing conditions, southwest United States. Environ. Geochem. Health 11, 171–176.

Safie, N.N., Zahrim, A., 2021. Recovery of nutrients from sewage using zeolite-chitosan-biochar adsorbent: current practices and perspectives. J. Water Process Eng. 40, 101845.
Samuel, M.S., Bhattacharya, J., Raj, S., Santhanam, N., Singh, H., Pradeep Singh, N.D., 2019. Efficient removal of Chromium(VI) from aqueous solution using chitosan grafted graphene oxide (CS-GO) nanocomposite. Int. J. Biol. Macromol. 121, 285–292.
Sarkar, B., 2002. Heavy Metals in the Environment. CRC Press. ISBN: 0-8247-0630-7.
Sarma, G.K., Sen Gupta, S., Bhattacharyya, K.G., 2019. Nanomaterials as versatile adsorbents for heavy metal ions in water: a review. Environ. Sci. Pollut. Res. 26, 6245–6278.
Savci, S., 2012. An agricultural pollutant: chemical fertilizer. Int. J. Environ. Sci. Dev. 3, 73.
Schiewer, S., Patil, S.B., 2008. Modeling the effect of pH on biosorption of heavy metals by citrus peels. J. Hazard. Mater. 157 (1), 8–17.
Şenel, S., McClure, S.J., 2004. Potential applications of chitosan in veterinary medicine. Adv. Drug Deliv. Rev. 56 (10), 1467–1480.
Seyedi, S.M., Anvaripour, B., Motavassel, M., Jadidi, N., 2013. Comparative cadmium adsorption from water by nanochitosan and chitosan. Int. J. Eng. Innov. Technol. 2 (9), 145–148.
Shang, Z.-Y., Han, C.-F., Song, Q.-J., 2014. An electrochemiluminescence sensor with molecularly imprinted polymer for heroin detection. Chin. J. Anal. Chem. 42 (6), 904–908.
Sharma, A., Thakur, M., Bhattacharya, M., Mandal, T., Goswami, S., 2019. Commercial application of cellulose nano-composites—a review. Biotechnol. Rep. 21 (2018), e00316.
Shi, S., et al., 2021. High saturation magnetization MnO2/PDA/Fe3O4 fibers for efficient Pb(II) adsorption and rapid magnetic separation. Appl. Surf. Sci. 541 (August 2020), 148379.
Siddique, A.B., Singh, V.P., Pramanick, A.K., Ray, M., 2020. Amorphous carbon dot and chitosan based composites as fluorescent inks and luminescent films. Mater. Chem. Phys. 249, 122984.
Singh, J., Yadav, P., Pal, A.K., Mishra, V., 2020. Water pollutants: origin and status. In: Pooja, D., Kumar, P., Singh, P., Patil, S. (Eds.), Sensors in Water Pollutants Monitoring: Role of Material. Advanced Functional Materials and Sensors. Springer, Singapore, https://doi.org/10.1007/978-981-15-0671-0_2.
Smidsrod, O., Skjakbrk, G., 1990. Alginate as immobilization matrix for cells. Trends Biotechnol. 8, 71–78.
Smital, T., 2008. Acute and chronic effects of emerging contaminants. In: Emerging Contaminants From Industrial and Municipal Waste. Springer Berlin Heidelberg, Berlin, Heidelberg, pp. 105–142, https://doi.org/10.1007/698_5_105.
Sophia, C.A., Lima, E.C., 2018. Removal of emerging contaminants from the environment by adsorption. Ecotoxicol. Environ. Saf. 150, 1–17.
Sorribes-Soriano, A., Herrero-Martínez, J.M., Esteve-Turrillas, F.A., Armenta, S., 2020. Molecularly imprinted polymer-based device for field collection of oral fluid samples for cocaine identification. J. Chromatogr. A 1633, 461629.
Stan, M., et al., 2017. Removal of antibiotics from aqueous solutions by green synthesized magnetite nanoparticles with selected agro-waste extracts. Process. Saf. Environ. Prot. 107, 357–372.
Stephen Inbaraj, B., Chen, B.H., 2011. Dye adsorption characteristics of magnetite nanoparticles coated with a biopolymer poly(γ-glutamic acid). Bioresour. Technol. 102 (19), 8868–8876.
Stuart, M., Lapworth, D., Crane, E., Hart, A., 2012. Review of risk from potential emerging contaminants in UK groundwater. Sci. Total Environ. 416, 1–21.
SUD, D., MAHAJAN, G., KAUR, M., 2008. Agricultural waste material as potential adsorbent for sequestering heavy metal ions from aqueous solutions—a review. Bioresour. Technol. 99 (14), 6017–6027.
Suhas, V., Gupta, K., Carrott, P.J.M., Singh, R., Chaudhary, M., Kushwaha, S., 2016. Cellulose: a review as natural, modified and activated carbon adsorbent. Bioresour. Technol. 216, 1066–1076.
Sumathi, S., Hamsa, D., Dharani, B., Sivaprabha, J., Malathy, N., Radha, P., Padma, P.R., 2012. Isolation and characterization of chitin from prawn shell waste and incorporation into medical textiles. Int. J. Recent Sci. Res. 3 (8), 676–680.
Taki, K., Gogoi, A., Mazumder, P., Bhattacharya, S.S., Kumar, M., 2019. Efficacy of vermitechnology integration with Upflow Anaerobic Sludge Blanket (UASB) and activated sludge for metal stabilization: a compliance study on fractionation and biosorption. J. Environ. Manage. 236, 603–612.
Tan, P., Zheng, Y., Hu, Y., 2020. Efficient removal of arsenate from water by lanthanum immobilized electrospun chitosan nanofiber. Colloids Surf. A Physicochem. Eng. Asp. 589, 124417.

Tarafdar, A., Biswas, G., 2013. Extraction of chitosan from prawn shell wastes and examination of its viable commercial applications. Int. J. Theor. Appl. Res. Mech. Eng. 2, 3. ISSN: 2319-3182.
Teixeira, L.S., Silva, C.F., de Oliveira, H.L., Dinali, L.A.F., Nascimento, C.S., Borges, K.B., 2020. Microextraction by packed molecularly imprinted polymer to selectively determine caffeine in soft and energy drinks. Microchem. J. 158, 105252.
Terzić, S., et al., 2008. Occurrence and fate of emerging wastewater contaminants in Western Balkan Region. Sci. Total Environ. 399 (1–3), 66–77.
Torres, E., 2020. Biosorption: a review of the latest advances. Processes 8 (12), 1584.
Trache, D., et al., 2020. Nanocellulose: from fundamentals to advanced applications. Front. Chem. 8 (May). https://doi.org/10.3389/fchem.2020.00392.
Tran, H.V., Tran, L.D., Nguyen, T.N., 2010. Preparation of chitosan/magnetite composite beads and their application for removal of Pb(II) and Ni(II) from aqueous solution. Mater. Sci. Eng. C 30 (2), 304–310.
Ueno, H., Mori, T., Fujinaga, T., 2001. Topical formulations and wound healing applications of chitosan. Adv. Drug Deliv. Rev. 52 (2), 105–115.
UZUN, I., 2006. Kinetics of the adsorption of reactive dyes by chitosan. Dyes Pigments 70 (2), 76–83.
Vazquez, A., Foresti, M.L., Moran, J.I., Cyras, V.P., 2015. Extraction and production of cellulose nanofibers BT—handbook of polymer nanocomposites. In: Pandey, J.K., Takagi, H., Nakagaito, A.N., Kim, H.-J. (Eds.), Processing, Performance and Application: Volume C: Polymer Nanocomposites of Cellulose Nanoparticles. Springer Berlin Heidelberg, Berlin, Heidelberg, pp. 81–118.
Vega-Chacón, J., Picasso, G., Avilés-Félix, L., Jafelicci, M., 2016. Influence of synthesis experimental parameters on the formation of magnetite nanoparticles prepared by polyol method. Adv. Nat. Sci. Nanosci. Nanotechnol. 7 (1).
Vélez, V.P.P., et al., 2019. Emerging contaminants in trans-american waters. Ambiente e Agua 14 (6), 1.
Verma, R., Asthana, A., Singh, A.K., Prasad, S., Susan, M.A.B.H., 2017. Novel glycine-functionalized magnetic nanoparticles entrapped calcium alginate beads for effective removal of lead. Microchem. J. 130, 168–178.
Villegas-Navarro, A., Ramirez-M, Y., Salvador-S. B., M.S., Gallardo, J.M., 2001. Determination of wastewater LC50 of the different process stages of the textile industry. Ecotoxicol. Environ. Saf. 48 (1), 56–61.
Wang, Y., Huang, K., 2020. Biosorption of tungstate onto garlic peel loaded with Fe(III), Ce(III), and Ti(IV). Environ. Sci. Pollut. Res. 27 (27), 33692–33702.
Wang, Y., et al., 2013. Preparation and characterization of a novel nano-absorbent based on multi-cyanoguanidine modified magnetic chitosan and its highly effective recovery for Hg(II) in aqueous phase. J. Hazard. Mater. 260, 9–15.
Wang, Y., Zhang, Y., Hou, C., Liu, M., 2016. Mussel-inspired synthesis of magnetic polydopamine–chitosan nanoparticles as biosorbent for dyes and metals removal. J. Taiwan Inst. Chem. Eng. 61, 292–298.
Wang, K., et al., 2018. Polydopamine-coated magnetic nanochains as efficient dye adsorbent with good recyclability and magnetic separability. J. Colloid Interface Sci. 516, 263–273.
Wang, J., Yang, L., Gu, P., 2020. Synthesis and characterization of chitosan grafted molybdenum disulfide composites as an adsorbent for graphene oxide removal. J. Phys. Chem. Solid 143, 109471.
Wang, Y., et al., 2021. Application of magnetic fields to wastewater treatment and its mechanisms: a review. Sci. Total Environ. 773, 145476.
Wen, R., Tu, B., Guo, X., Hao, X., Wu, X., Tao, H., 2020. An ion release controlled Cr(VI) treatment agent: Nano zero-valent iron/carbon/alginate composite gel. Int. J. Biol. Macromol. 146, 692–704.
Wong, Y.C., Szeto, Y.S., Cheung, W.H., McKay, G., 2004. Adsorption of acid dyes on chitosan—equilibrium isotherm analyses. Process Biochem. 39 (6), 695–704.
Wu, F.-C., Tseng, R.-L., Juang, R.-S., 2010. A review and experimental verification of using chitosan and its derivatives as adsorbents for selected heavy metals. J. Environ. Manage. 91 (4), 798–806.
Yadav, M., Ahmadi, Y., 2019. Alginates: source, chemistry, and properties. In: Hasnain, M.S., Nayak, A.K. (Eds.), Alginate: Versatile Polymer in Biomedical Applications and Therapeutics Palm Bay. Apple Academic Press, FL, pp. 1–24.
Yadav, V.K., Fulekar, M.H., 2018. Biogenic synthesis of maghemite nanoparticles (γ-Fe2O3) using Tridax leaf extract and its application for removal of fly ash heavy metals (Pb, Cd). Mater. Today: Proc. 5 (9), 20704–20710.
Yadav, S., et al., 2020. Cationic dye removal using novel magnetic/activated charcoal/β-cyclodextrin/alginate polymer nanocomposite. Nanomaterials 10 (1), 170.
Yan, S., Subramanian, S.B., Tyagi, R.D., Surampalli, R.Y., Zhang, T.C., 2010. Emerging contaminants of environmental concern: source, transport, fate, and treatment. Pract. Period. Hazard. Toxic Radioact. Waste Manage. 14 (1), 2–20.

Ying, G.-G., 2006. Fate, behavior and effects of surfactants and their degradation products in the environment. Environ. Int. 32 (3), 417–431.
Yoshizuka, K., Lou, Z., Inoue, K., 2000. Silver-complexed chitosan microparticles for pesticide removal. React. Funct. Polym. 44 (1), 47–54.
Yu, H., Hong, H.-J., Kim, S.M., Ko, H.C., Jeong, H.S., 2020. Mechanically enhanced graphene oxide/carboxymethyl cellulose nanofibril composite fiber as a scalable adsorbent for heavy metal removal. Carbohydr. Polym. 240, 116348.
Zare, E.N., Lakouraj, M.M., Kasirian, N., 2018. Development of effective nano-biosorbent based on poly m-phenylenediamine grafted dextrin for removal of Pb(II) and methylene blue from water. Carbohydr. Polym. 201, 539–548.
Zeb, S., 2018. Electrochemical oxidation of acid brown 98 using Ti/Ru0.3Ti0.7O2 composite anode. Int. J. Electrochem. Sci., 9428–9440.
Zeb, S., et al., 2020. Silica-based nanomaterials as designer adsorbents to mitigate emerging organic contaminants from water matrices. J. Water Process Eng. 38, 101675.
Zhang, H., Jin, Y., Deng, Y., Wang, D., Zhao, Y., 2012. Production of chitin from shrimp shell powders using Serratia marcescens B742 and Lactobacillus plantarum ATCC 8014 successive two-step fermentation. Carbohydr. Res. 362, 13–20.
Zhang, Z., Sèbe, G., Rentsch, D., Zimmermann, T., Tingaut, P., 2014. Ultralightweight and flexible silylated nanocellulose sponges for the selective removal of oil from water. Chem. Mater. 26, 2659–2668.
Zhang, L., Zhu, T., Liu, X., Zhang, W., 2016. Simultaneous oxidation and adsorption of As(III) from water by cerium modified chitosan ultrafine nanobiosorbent. J. Hazard. Mater. 308, 1–10.
Zhang, F., Tang, X., Huang, Y., Keller, A.A., Lan, J., 2019. Competitive removal of Pb2+ and malachite green from water by magnetic phosphate nanocomposites. Water Res. 150, 442–451.
Zhang, J., Wang, P., Zhang, Z., Xiang, P., Xia, S., 2020. Biosorption characteristics of Hg(II) from aqueous solution by the biopolymer from waste activated sludge. Int. J. Environ. Res. Public Health 17 (5), 1488.
Zhao, M., Li, X., Huang, Z., Wang, S., Zhang, L., 2021. Facile cross-link method to synthesize chitosan-based adsorbent with superior selectivity toward gold ions: batch and column studies. Int. J. Biol. Macromol. 172, 210–222.
Zimmermann, M.V.G., Zattera, A.J., Santana, R.M.C., 2019. Sorbent system based on acetylated microfibrillated cellulose for remediation of oil aquatic environments. Rev. Mater. 24 (2).

CHAPTER

10

Nanoadsorbents for environmental remediation of polluting agents

Katya M. Aguilar-Pérez[a], *Gustavo Ruiz-Pulido*[a], *Dora I. Medina*[a], *Roberto Parra-Saldivar*[b], *Nadia Nazish*[c], *Muhammad Bilal*[d], *and Hafiz M.N. Iqbal*[b]

[a]Tecnologico de Monterrey, School of Engineering and Sciences, Atizapan de Zaragoza, Mexico [b]Tecnologico de Monterrey, School of Engineering and Sciences, Monterrey, Mexico [c]Department of Zoology, University of Sialkot, Sialkot, Pakistan [d]School of Life Science and Food Engineering, Huaiyin Institute of Technology, Huaian, China

10.1 Introduction

Over the last few years, the increasing number of pollutants and ecological risk substances in water has gained considerable attention. Several research groups have focused on the development of new technologies and methods to control water pollution associated to the unmanageable discharge of these materials (Hu et al., 2021). The current demand of clean and freshwater needs to be fulfill worldwide. However, as a result of urbanization, accessibility to enough and high-quality drinking water has become a global challenge (Ahmadi et al., 2020). The unproper assessment and lack of regulation related to discharge of pollutants such as dyes, antibiotics, cosmetic, and some other PPCPs from domestic and industrial sources not only affects human health but also aquatic ecosystems, biodiversity, and entail a high economic impact, especially in not developed countries (Hu et al., 2021). The increasing detection of such contaminants on water has potentiated their classification as "Emerging Contaminants" (Asif et al., 2021). Influencing factors such as strong polarity, refractory volatilization, and bacteriostasis lead to the accumulation of PPCPs in aquatic environment (Yin et al., 2020). Therefore, cost-effective technologies to remove PPCPs in aquatic environment are broadly needed. Advances in nanotechnology have enabled the fabrication of novel nanoadsorbent materials. Nanomaterials are defined as structures with size within 1 and

https://doi.org/10.1016/B978-0-323-90912-9.00010-1

100 nm at least in one dimension (Kreyling et al., 2010) with characteristic physical, chemical, and biological properties due to their small size and high surface area-to-volume ratio (Srivastava et al., 2021). Nanomaterials are suitable for water treatment, given their unique features, specifically large surface area and tunable morphologies, they display great adsorption capacity and efficient degradation of wastewater effluents (Aguilar-Pérez et al., 2021). Among the most widely used nano-adsorbents for water treatment include magnetic nanoparticles, clay-based nanomaterials, zeolites and silica-based nanomaterials, zero-valent metal nanoparticles, metal oxides nanoparticles, carbon-based nanomaterials, and nanocomposites (Aguilar-Pérez et al., 2020a, b).

This chapter presents a compilation of nanoadsorbent materials with special focus on carbon-based and nanoparticle-based materials for wastewater treatment. This was also aimed at providing recent advances in the development of carbon nanotubes, graphene, metallic and biogenic nanoparticles, and to give an overview regarding novel literature reports related to nanoadsorbents for water remediation. Additionally, physiochemical features of nanoadsorbents and their mechanism of action for pollutant's removal in aqueous media are discussed with brief examples.

10.2 Nanoadsorbents and their useful aspects

Nanotechnology offers new alternatives for wastewater remediation through the study and design of novel methods, and materials. Since adsorption is considered as one of the best strategies for pollutants removal in water because of its simple design and highly efficient percentage of removal, the use of nanoadsorbents has displayed a considerable attention (Dhiman and Kondal, 2021). Nanoadsorbents and their mechanism of action provide numerous advantages for their utilization in wastewater treatment (Santhosh et al., 2016). These structures have unique physicochemical features, including nanosize, large surface area and strong solution mobility, high reactivity and enhanced redox and photocatalytic properties (Mohmood et al., 2013; Santhosh et al., 2016; Yaqoob et al., 2020). Moreover, these features allow nanoadsorbents to remove pollutants according to their molecular size, hydrophobicity, and speciation behavior (Nik Abdul Ghani et al., 2021) (Fig. 10.1).

10.3 Carbon-based nanoadsorbents

Nowadays, research in carbon-based nanoadsorbents, comprised by graphene, carbon nanotubes, and activated carbon, and their byproducts has been conducted and employed in wastewater treatment (Gul et al., 2021). Carbon-based nanomaterials (CBNs) are composed entirely or mainly by carbon atoms (Keller et al., 2017; Nasrollahzadeh et al., 2021) and they are characterized by their useful properties for water treatment, including superior chemical stability, high water flux with minimum energy, ease operation, and low energy consumption (Ali et al., 2019). The majority of investigations in CBNs has focused on carbon nanotubes, carbon nanofibers, graphene, fullerenes, and carbon-based composites (Piaskowski and Zarzycki, 2020). Despite their acceptable reputation to remove water

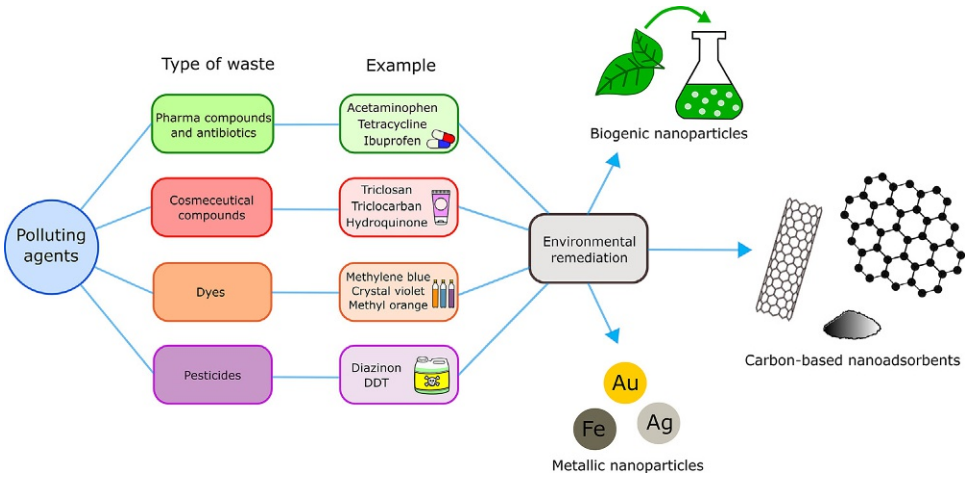

FIG. 10.1 Environmental remediation of various types of polluting wastes using carbon-based nanoadsorbents.

contaminants, CBNs production and functionalization at large scale is still very expensive. Moreover, the use of strategies such as surface modification has been proposed to address this problem (Gul et al., 2021). Development of carbon-based nanocomposites has demonstrated powerful absorption capacity and potential selectivity (Huang et al., 2021; Lee et al., 2018). Several other carbon-based nanomaterials for wastewater treatment are summarized in Table 10.1.

10.3.1 Carbon nanotubes-based nanoadsorbent materials

Carbon nanotubes (CNTs) have gradually become emerging materials for organic pollutant removal. They can be used as adsorbents to remove contaminants in wastewater (Peng et al., 2021). CNTs are carbon's allotropes formed in a cylinder-shaped structure. These

TABLE 10.1 Carbon-based nanomaterials for wastewater treatment.

Nanomaterial	Synthesis process	Contaminant	Characterization techniques	Percentage removal	Reference
Activated carbon	Chemical activation/ calcination	Methylene blue Crystal violet Astrazon blue Indigo carmine	FT-IR TGA SEM TEM XRD	~ 99.9%	Herrera-González et al. (2019)
Activated carbon	Chemical activation/ calcination	Triclosan	FESEM FT-IR	~ 80.77%	Mohd Khori et al. (2018)

Continued

TABLE 10.1 Carbon-based nanomaterials for wastewater treatment—cont'd

Nanomaterial	Synthesis process	Contaminant	Characterization techniques	Percentage removal	Reference
Single-walled carbon nanotubes	Chemical vapor deposition technique	Acid Blue 92	SEM TE FT-IR	~ 99.1%	Balarak et al. (2021)
Multi-walled carbon nanotubes	Chemical vapor deposition technique	Acetamoniphen Naproxen Ibuprofen, Ketoprofen, Aniline Cephalexin Tetracycline	SEM TEM TGA EDS XRD FT-IR	~ 100% ~ 70% ~ 70% ~ 40% ~ 98.9% ~ 96.83% ~ 99.8%	Balarak et al. (2017), Dahane et al. (2013), Jafari and Aghamiri (2011), Zhang et al. (2011)
Multi-walled carbon nanotubes	Chemical vapor deposition technique	Diazinon (pesticide)	SEM TEM BET FT-IR	~ 100%	Dehghani et al. (2019)
Magnetic multi-walled carbon nanotubes	Co-precipitation method	Naproxen	XRD TGA SEM FT-IR	~ 62.2%	İlbay et al. (2015)
Polyvinyl amine functionalized GO—(MWCNTs)—Fe_3O_4 nanocomposite	Modified Hummers' method/ chemical co-precipitation method	Hydroquinone	FT-IR XRD TGA BET AFM SEM EDS	~ 85.3%	Zhou et al. (2020b)
Graphene/ titanium dioxide nanotubes	Hydrothermal method	Acetaminophen	FT-IR UV–Vis XRD TGA	~ 96%	Tao et al. (2015)
Graphene oxide membranes	Layer-by-layer assembly procedure	Methylene blue Rhodamine WT Triclosan Triclocarban	SEM QCM-D	~ 97% ~100% ~ 37% ~100%	Oh et al. (2017)
Graphene oxide	Modified Hummers method	Metformin	SEM TEM FT-IR XPS XRD	~ 80%	Zhu et al. (2017)
Graphene oxide	Modified Hummers method	Malathion Chlorpyrifos	FT-IR XRD FE-SEM TEM	~ 89.03% ~ 88.17%	Yadav et al. (2019)

materials are composed by a hexagonal lattice of carbon atoms in sp^2 hybridization (Lee et al., 2018; Mohmood et al., 2013). CNTs can present either a single-walled (SWCNTs) or a multi-walled shape (MWCNTs) (Ali et al., 2019; Cincinelli et al., 2015). SWCNTs diameter size oscillates around 0 and 3 nm, while MWCNTs can exhibit up to 100 nm size (Thines et al., 2017). Some of the most representative advantages of CTNs include high and rapid absorption, thermal stability, flexibility, and significant storage capacity.(Lee et al., 2018; Santhosh et al., 2016). Moreover, morphology of CNTs is important to determine their properties as nanoadsorbents, for instance, it has been reported that rough surfaces have larger surface area compared to the smooth ones, thus, greater absorption capacity (Jain et al., 2021). Additionally, the study and enhancement of this parameters during fabrication of CNTs are useful in achieving prompt equilibrium time, better adsorption capacity and high selectivity.

Unfortunately, CNTs potentialities may be diminished due to their high hydrophobicity, low dispersion in aqueous medium, and reduced interfacial interaction. Therefore, agglomeration and reduction of their adsorption efficiency (Ali et al., 2019; Lee et al., 2018) may lead potential toxicity to aquatic organisms even at low concentrations (Freixa et al., 2018). Some papers report that CNTs are used for water remediation and can reduce the toxicity of pollutants in one side, but in the other side, CNTs may act as a collectors and carriers of potential pollutants and hazardous materials leading to increased persistence in aquatic environments (Zhang et al., 2020). Overall, since their discovery, CNTs have been extensively used as effective adsorbents, but its application is limited due to its high synthesis and purification cost, compared with absorbents such as activated carbon (Santhosh et al., 2016). CNTs performance can be enhanced through surface modification, for instance, functionalization of CNTs allow them to interact with organic contaminants through hydrophobic interaction, π–π binding and formation of chemical bonds with surface functionalities (Sargin et al., 2020). Finally, it is also important to test novel nanocomposites based on CNTs for wastewater treatment and remediation technologies, to understand the interaction between pollutant and nanomaterial, as well as toxicity and fate of such compounds.

10.3.2 Graphene-based nanoadsorbent materials

Due to the remarkable properties of graphene-based nanomaterials such as porous structure, extraordinary specific surface area, great mechanical and thermal stability, suitable active sites and manageable surface properties, have gained substantial research interests recently (Huang et al., 2021).

Graphene has been utilized as nanoadsorbent for pollution remediation in water bodies (Yaqoob et al., 2020). Its structure basically consist of one-atom-thick planar sheets of sp^2-hybridized carbon atoms packed compactly in six-membered rings (Kim et al., 2018). Graphene and its oxidized derivative (graphene oxide (GO)) can be functionalized with diverse materials, resulting in nanocomposites with significant advantages (e.g., high extraction recovery and improved selectivity) (Huang et al., 2021). Nevertheless, graphene oxide presents some limitations, for example, its absorption capacity may be affected when it interacts with the treated solution due to changes in pH and temperature, ionic strength, or surfactant concentrations (Rienzie et al., 2019). Furthermore, graphene structures have several drawbacks, firstly because bulk graphene tends to agglomerate and restack to procedure graphite

during liquid processing, and secondly, inadequate collection and separation of graphene and its derivatives from treated water, can lead significant recontamination (Choi et al., 2018). Moreover, fabrication of graphene nanocomposites and hybrids has been attracted research interest to use as effective absorbents for the removal of harmful dyes such as methylene blue (Calimli et al., 2020) given their easy dispersion and high availability of absorption sites, thus displaying a better absorption capacity. It is apparent from the vast literature reports related to water remediation that graphene-based materials are suitable nanoadsorbents to remove various water contaminants. However, the research conducted outside laboratory scale is still at a very early stage. More emphasis in investigation with real industrial effluents and in vivo toxicity studies must be performed.

10.4 Nanoparticles-based nanoadsorbent materials

Among nanoadsorbent materials diverse types of nanoparticles have gained attention as convenient strategies for water remediation purposes. Nanoparticles are zero-dimension nanosized materials with size in the range of 1 and 100 nm (Wang et al., 2019). Easy and sustainable synthesis processes, enhanced bioavailability, stability, high surface area, associated sorption sites and high removal percentage are some of the advantages of this nanoadsorbents (Gutierrez et al., 2019; Hu and Cao, 2019; Zhou et al., 2020a). In this chapter, nanoparticle-based materials for wastewater treatment are discussed. On one hand, implementation of conventional metallic nanoparticles (MNPs) and, on the other side, MNPs fabricated through green approaches (biogenic nanoparticles) as nanoadsorbents for contaminants removal in water.

10.4.1 Metallic nanoparticles-based nanoadsorbent materials

MNPs have been explored for diverse applications in electronics, biomedical engineering, optics, among others. Currently, a different option in the environmental sector has opened the possibility to use MNPs for heavy metals and dye removal in water (Vinosha et al., 2019). Silver, copper, and iron figure as some of the most common metals used for fabrication of MNPs. Regarding the mechanism of action, for instance, antimicrobial activities of MNPs to their high size-to-surface ratio. The nanoparticles hamper cellular processes once entering the microbes. Therefore, the nanoparticles surface adhesion with the microbial cell surface leads to its immobilization. For the case of zero-valent iron nanoparticles-based reduction process of contaminants is a redox process, here the metal acts as an electron donor for the reduction of oxidized species. Another mechanism when using silver nanoparticles is amalgamation on the surface of MNPs for sequestration of mercury (Mishra, 2014).

Moreover, influencing factors in the performance of MNPs such as size, stability, and surface modification must be considered prior their application in water treatment. Also, fate and risk models are relevant for a proper management. A study performed in a pilot wastewater treatment plant (WWTP) investigated the behavior of metallic silver nanoparticles (Ag-NPs), the study suggested (Kaegi et al., 2011) that fate and risk models for Ag-NP, colloidal and chemical transformation reactions must be consider on the basis of experiments

conducted at realistic and pertinent NPs concentration levels. Functionalization it is a useful tool to confer better physicochemical properties, however, nature of the surface coating may affect colloidal and chemical behavior of Ag-NPs in aquatic environment. Furthermore, it is vital to approach functionalization toward enhancement of stability of Ag-NPs and other NPs to avoid flocculation and undesirable chemical transformation in water domains. Under (Faraji et al., 2010). Under these circumstances, a significant fragment of NPs may pass the WWTPs and be delivered to the aquatic environment in their original form.

Another study investigated how morphology of FeCu bimetallic nanoparticles (FeCu BMNPs) affected adsorption capacity, rate, and intensity in the removal of As(V) (Sepúlveda et al., 2018). The study was performed at different mass ratios and it was found that at low proportion of Cu in the BMNPs (Fe0.9 Cu0.1) favors the core shell structure (discontinuous shell) and enhances the removal of arsenate (As(V)) relative to the Fe0.5 Cu0.5 material (segregated structure), while the adsorption studies demonstrated that As could be removed by sorption on the FeCu BMNPs, and the best results were observed for an Fe:Cu mass ratio of 0.9:0.1 (Fe0.9 Cu0.1), which exhibited a nonhomogeneous core shell morphology.

10.4.2 Biogenic nanoparticles-based nanoadsorbent materials

In recent years, products based on natural compounds have attracted great attention due to the worldwide development of maintaining good health and minimizing potential risk to the environment. Therefore, biological methods to produce green, reusable, and efficient metallic nanoparticles have made possible to involve the use of biological mass from either plant or microbial as reductant agent via extracellularly or intracellularly (Sebeia et al., 2020). For instance, the use of peptides, enzymes, vitamins, alkaloids and phenolics originally present in plant extracts, bacteria fungi, etc., have enabled the development of cheaper, eco-friendly, and efficient nanoadsorbents such as biogenic nanoparticles. Fabrication of biogenic nanoparticles is possible due to the presence of bioactive molecules. These compounds are mixed with a metal salt solution under specific conditions based on the nature of precursor materials and the final purpose of nanoparticles. (Aguilar-Pérez et al., 2020a, b). Thus, nanoadsorbents-based biogenic nanoparticles have been applied successfully for dye removal from water, reaching adsorption capacity around 704.7 mg/g (Sharbaf Moghadas et al., 2020). In the same way, biologic fabrication of Fe^0 NPs coated with β-Cyclodextrin (βCD) was reported by Nasiri et al. (2019) and successfully utilized for crystal-violet dye removal, reaching adsorption capacity up to 454.5 mg/g. Moreover, green synthesis of (Jain et al., 2021) Fe_2O_3 NPs was performed and compared with calcined Fe_2O_3 NPs to inquire the effect of plant extract on the adsorption performance, both Fe_2O_3 NPs and c-Fe_2O_3 NPs were examined for their use in the removal of methylene blue dye from aqueous solution. The biogenic Fe_2O_3 NPs showed better removal percentage (92%) as compared to c-Fe2O3 (88%) toward methylene blue. In summary, nanoadsorbents-based biogenic nanoparticles may present a sustainable and efficient strategy for wastewater treatment, however, further studies need to be performed to improve their yield and cost-effectiveness. Additionally, stability tests must be addressed to evaluate the performance of biogenic NPs under different conditions throughout the time. Table 10.2 summarizes literature related to MNPs for wastewater treatment.

TABLE 10.2 Literature related to MNPs for wastewater treatment.

Nanomaterial	Synthesis process	Contaminant	Characterization techniques	Percentage removal	Reference
Zero-Valent Cu NPs	Chemical reduction	Ceftriaxone Cefadroxil	TEM EDS HPLC UV–Vis	~ 97% ~ 85%	Oliveira et al. (2018)
Pd-doped ZnO nanostars	Microwave-hydrothermal method	Methyl parathion Pendimethalin Trifluralin	XRD FT-IR TGA FE-SEM FE-TEM EDS XPS UV–Vis	> 92%	Veerakumar et al. (2021)
CuO NPs with *Psidium guajava* leaf extract	Green synthesis method	Nile blue Reactive yellow 160	FE-SEM TEM UV–Vis EDX BET	~ 93% ~ 81%	Singh et al. (2019a)
ZnO NPs CuO NPs NiO NPs Mn_3O_4 NPs CeO_2 NPs SnO_2 NPs	Precipitation method	Methyl orange Methylene blue	FE-SEM TEM XRD EDS UV–ViS BET	~ 93%/~ 98% ~ 12%/~ 15% ~ 49%/~ 55% ~ 20%/~ 26% ~ 78%/~ 83% ~ 93%/~ 98%	Gnanasekaran et al. (2017)
ZnO NPs	Precipitation method	Ibuprofen Ephedrine Propranolol	XRD SEM TEM DLS EDAX	~ 99.8% ~ 99% ~ 99.8%	Hassan et al. (2019)
Bimetallic Ni/Fe NPs	Chemical reduction	DDT	TEM	~ 90%	Tian et al. (2009)
ZrO_2 NPs with *Pseudomonas aeruginosa* bacteria	Extracellular microbial synthesis	Tetracycline	DLS FE-TEM EDX XRD FT-IR	~ 98.73%	Debnath et al. (2020)
Pt and Pd NPs with *Desulfovibrio vulgaris*	Extracellular microbial synthesis	Sulfamethoxazole Ciprofloxacin 17-estradiol	TEM UV–Vis	~ 85% ~ 70% ~ 94%	Martins et al. (2017)
SnO_2 NPs with *Piper betle* leaves	Hydrothermal route	Reactive yellow 186	FT-IR XRD SEM EDX TEM	~ 92.17%	Singh et al. (2018)

TABLE 10.2 Literature related to MNPs for wastewater treatment—cont'd

Nanomaterial	Synthesis process	Contaminant	Characterization techniques	Percentage removal	Reference
Ag NPs with *Trigonella foenum-graecum* leaf extract	Chemical reduction	Reactive blue 19 Reactive yellow 186	XRD EDX FT-IR FE-SEM TEM	~ 88% ~ 86%	Singh et al. (2019b)
ZnO colloidal NPs of Cyanometra ramiflora	Chemical reduction	Rhodamine B	UV–Vis SEM EDS XRD BET FT-IR	~ 98%	Varadavenkatesan et al. (2019)
Se NPs with *S. griseobrunneus*	Extracellular microbial synthesis	Diclofenac sodium	HPLC GC–MS	~ 97.43%	Ameri et al. (2020)

10.5 Concluding remarks and outlook

Advances in nanotechnology have made possible the development of new materials for wastewater treatment. Nanoadsorbents possess unique physiochemical properties that are useful to counteract the increased amounts of hazardous pollutants in water. The irrational use of antibiotics, dyes, and PPCPs represents one of the most relevant sources of water pollution. The current strategies for remediation of water bodies involve numerous drawbacks such as generation of toxic byproducts, use of hazardous solvents, and poor absorption efficiency. To overcome these issues, nanoadsorbent materials have been developed and tested to remove organic, inorganic, and biological pollutants in water. The use of carbon-based nanoadsorbents for this purpose has displayed excellent results. However, their use has been limited due to their processing still is not cost-effective, also possible toxicity to the environment and lack of regulations for their risk assessment. On the other hand, research groups have put efforts to develop more eco-friendly materials. For instance, the use of green chemistry to fabricate MNPs (biogenic nanoparticles), allows the use of precursors recovered from waste bio sources. Nevertheless, the use of controlled environments to test their efficiency and performance is required and may be time-consuming. Despite the significant advances in material science for environmental purposes and knowledge about nanomaterials' capability to remove and degrade hazardous compounds and contaminants, there is still the challenge of recycling these nanomaterials and to be aware of their fate after utilization. Additionally, suitable evaluation of interaction of nanoadsorbents with living organisms must be performed, specially before the transfer from laboratory scale to industrial application.

Acknowledgments

This work was partially supported by Consejo Nacional de Ciencia y Tecnología (CONACYT) Mexico, under Sistema Nacional de Investigadores (SNI) program awarded to H.M.N.I (CVU: 735340) and R.P.-S. (CVU: 35753). The listed author(s) are much obliged to their representative institutes and universities for providing the literature services.

Conflicts of interest

The listed author(s) declare that no competing, conflicting, and financial interests exist in this work.

References

Aguilar-Pérez, K.M., Avilés-Castrillo, J.I., Ruiz-Pulido, G., 2020a. Nano-sorbent materials for pharmaceutical-based wastewater effluents—an overview. Case Stud. Chem. Environ. Eng., 100028. https://doi.org/10.1016/j.cscee.2020.100028.

Aguilar-Pérez, K.M., Avilés-Castrillo, J.I., Ruiz-Pulido, G., Medina, D.I., Parra-Saldivar, R., Iqbal, H.M., 2021. Nanoadsorbents in focus for the remediation of environmentally-related contaminants with rising toxicity concerns. Sci. Total Environ. 779, 146465. https://doi.org/10.1016/j.scitotenv.2021.146465.

Aguilar-Pérez, K.M., Heya, M.S., Parra-Saldívar, R., Iqbal, H.M.N., 2020b. Nano-biomaterials in-focus as sensing/detection cues for environmental pollutants. Case Stud. Chem. Environ. Eng. 2 (September). https://doi.org/10.1016/j.cscee.2020.100055, 100055.

Ahmadi, M.S., Sušnik, J., Veerbeek, W., Zevenbergen, C., 2020. Towards a global day zero? Assessment of current and future water supply and demand in 12 rapidly developing megacities. Sustain. Cities Soc. 61 (June). https://doi.org/10.1016/j.scs.2020.102295.

Ali, S., Rehman, S.A.U., Luan, H.-Y., Farid, M.U., Huang, H., 2019. Challenges and opportunities in functional carbon nanotubes for membrane-based water treatment and desalination. Sci. Total Environ. 646, 1126–1139. https://doi.org/10.1016/j.scitotenv.2018.07.348.

Ameri, A., Shakibaie, M., Pournamdari, M., Ameri, A., Foroutanfar, A., Doostmohammadi, M., Forootanfar, H., 2020. Degradation of diclofenac sodium using UV/biogenic selenium nanoparticles/H_2O_2: optimization of process parameters. J. Photochem. Photobiol. A Chem. 392 (January), 112382. https://doi.org/10.1016/j.jphotochem.2020.112382.

Asif, A.H., Wang, S., Sun, H., 2021. Hematite-based nanomaterials for photocatalytic degradation of pharmaceuticals and personal care products (PPCPs): a short review. Curr. Opin. Green Sustain. Chem. https://doi.org/10.1016/J.COGSC.2021.100447, 100447.

Balarak, D., Mostafapour, F.K., Joghataei, A., 2017. Application of single-walled carbon nanotubes for removal of aniline from industrial waste water. Biosci. Biotechnol. Res. Commun. 10 (2), 311–318. https://doi.org/10.21786/bbrc/10.2/50.

Balarak, D., Zafariyan, M., Igwegbe, C.A., Onyechi, K.K., Ighalo, J.O., 2021. Adsorption of acid blue 92 dye from aqueous solutions by single-walled carbon nanotubes: isothermal, kinetic, and thermodynamic studies. Environ. Process. 8 (2), 869–888. https://doi.org/10.1007/s40710-021-00505-3.

Calimli, M.H., Nas, M.S., Burhan, H., Mustafov, S.D., Demirbas, Ö., Sen, F., 2020. Preparation, characterization and adsorption kinetics of methylene blue dye in reduced-graphene oxide supported nanoadsorbents. J. Mol. Liq. 309. https://doi.org/10.1016/j.molliq.2020.113171.

Choi, S.W., Oak, M.H., Yi, E., Kim, H.J., Park, J.W., 2018. Preparation and in vitro evaluation of elastic nanoliposomes for topical delivery of highly skin-permeable growth factors. J. Nanosci. Nanotechnol. 18 (2), 887–892. https://doi.org/10.1166/jnn.2018.14863.

Cincinelli, A., Martellini, T., Coppini, E., Fibbi, D., Katsoyiannis, A., 2015. Nanotechnologies for removal of pharmaceuticals and personal care products from water and wastewater. A review. J. Nanosci. Nanotechnol. 15 (5), 3333–3347. https://doi.org/10.1166/jnn.2015.10036.

Dahane, S., Gil García, M.D., Martínez Bueno, M.J., Uclés Moreno, A., Martínez Galera, M., Derdour, A., 2013. Determination of drugs in river and wastewaters using solid-phase extraction by packed multi-walled carbon nanotubes and liquid chromatography–quadrupole-linear ion trap-mass spectrometry. J. Chromatogr. A 1297, 17–28. https://doi.org/10.1016/j.chroma.2013.05.002.

Debnath, B., Majumdar, M., Bhowmik, M., Bhowmik, K.L., Debnath, A., Roy, D.N., 2020. The effective adsorption of tetracycline onto zirconia nanoparticles synthesized by novel microbial green technology. J. Environ. Manag. 261 (September 2019), 110235. https://doi.org/10.1016/j.jenvman.2020.110235.

Dehghani, M.H., Kamalian, S., Shayeghi, M., Yousefi, M., Heidarinejad, Z., Agarwal, S., Gupta, V.K., 2019. High-performance removal of diazinon pesticide from water using multi-walled carbon nanotubes. Microchem. J. 145, 486–491. https://doi.org/10.1016/j.microc.2018.10.053.

Dhiman, V., Kondal, N., 2021. ZnO Nanoadsorbents: a potent material for removal of heavy metal ions from wastewater. Colloids Interface Sci. Commun. 41 (October 2020), 100380. https://doi.org/10.1016/j.colcom.2021.100380.

Faraji, M., Yamini, Y., Rezaee, M., 2010. Iranian chemical society magnetic nanoparticles: synthesis, stabilization, functionalization, characterization, and applications. J. Iran. Chem. Soc. 7 (1), 1–37.

Freixa, A., Acuña, V., Sanchís, J., Farré, M., Barceló, D., Sabater, S., 2018. Ecotoxicological effects of carbon based nanomaterials in aquatic organisms. Sci. Total Environ. 619–620, 328–337. https://doi.org/10.1016/j.scitotenv.2017.11.095.

Gnanasekaran, L., Hemamalini, R., Saravanan, R., Ravichandran, K., Gracia, F., Agarwal, S., Gupta, V.K., 2017. Synthesis and characterization of metal oxides (CeO_2, CuO, NiO, Mn_3O_4, SnO_2 and ZnO) nanoparticles as photo catalysts for degradation of textile dyes. J. Photochem. Photobiol. B Biol. 173, 43–49. https://doi.org/10.1016/j.jphotobiol.2017.05.027.

Gul, A., Khaligh, N.G., Julkapli, N.M., 2021. Surface modification of carbon-based nanoadsorbents for the advanced wastewater treatment. J. Mol. Struct. 1235, 130148. https://doi.org/10.1016/j.molstruc.2021.130148.

Gutierrez, A.M., Bhandari, R., Weng, J., Stromberg, A., Dziubla, T.D., Hilt, J.Z., 2019. Novel magnetic core-shell nanoparticles for the removal of polychlorinated biphenyls from contaminated water sources. Mater. Chem. Phys. 223 (March 2018), 68–74. https://doi.org/10.1016/j.matchemphys.2018.10.045.

Hassan, S.S.M., Abdel-Shafy, H.I., Mansour, M.S.M., 2019. Removal of pharmaceutical compounds from urine via chemical coagulation by green synthesized ZnO-nanoparticles followed by microfiltration for safe reuse. Arab. J. Chem. 12 (8), 4074–4083. https://doi.org/10.1016/j.arabjc.2016.04.009.

Herrera-González, A.M., Caldera-Villalobos, M., Peláez-Cid, A.-A., 2019. Adsorption of textile dyes using an activated carbon and crosslinked polyvinyl phosphonic acid composite. J. Environ. Manag. 234, 237–244. https://doi.org/10.1016/j.jenvman.2019.01.012.

Hu, G., Cao, J., 2019. Metal-containing nanoparticles derived from concealed metal deposits: an important source of toxic nanoparticles in aquatic environments. Chemosphere 224, 726–733. https://doi.org/10.1016/j.chemosphere.2019.02.183.

Hu, X., Xie, H., Zhuang, L., Zhang, J., Hu, Z., Liang, S., Feng, K., 2021. A review on the role of plant in pharmaceuticals and personal care products (PPCPs) removal in constructed wetlands. Sci. Total Environ. 780, 146637. https://doi.org/10.1016/j.scitotenv.2021.146637.

Huang, T., Tang, X., Luo, K., Wu, Y., Hou, X., Tang, S., 2021. An overview of graphene-based nanoadsorbent materials for environmental contaminants detection. Trends Anal. Chem. 139, 116255. https://doi.org/10.1016/j.trac.2021.116255.

İlbay, Z., Şahin, S., Kerkez, Ö., Bayazit, Ş.S., 2015. Isolation of naproxen from wastewater using carbon-based magnetic adsorbents. Int. J. Environ. Sci. Technol. 12 (11), 3541–3550. https://doi.org/10.1007/s13762-015-0775-4.

Jafari, M., Aghamiri, S.F., 2011. Evaluation of carbon nanotubes as solid-phase extraction sorbent for the removal of cephalexin from aqueous solution. Desalin. Water Treat. 28 (1–3), 55–58. https://doi.org/10.5004/dwt.2011.2200.

Jain, A., Wadhawan, S., Mehta, S.K., 2021. Biogenic synthesis of non-toxic iron oxide NPs via *Syzygium aromaticum* for the removal of methylene blue. Environ. Nanotechnol. Monit. Manage. 16 (March). https://doi.org/10.1016/j.enmm.2021.100464, 100464.

Kaegi, R., Voegelin, A., Sinnet, B., Zuleeg, S., Hagendorfer, H., Burkhardt, M., Siegrist, H., 2011. Behavior of metallic silver nanoparticles in a pilot wastewater treatment plant. Environ. Sci. Technol. 45 (9), 3902–3908. https://doi.org/10.1021/es1041892.

Keller, A.A., Adeleye, A.S., Conway, J.R., Garner, K.L., Zhao, L., Cherr, G.N., Zuverza-Mena, N., 2017. Comparative environmental fate and toxicity of copper nanomaterials. NanoImpact 7 (May), 28–40. https://doi.org/10.1016/j.impact.2017.05.003.

Kim, S., Park, C.M., Jang, M., Son, A., Her, N., Yu, M., Yoon, Y., 2018. Aqueous removal of inorganic and organic contaminants by graphene-based nanoadsorbents: a review. Chemosphere 212, 1104–1124. https://doi.org/10.1016/j.chemosphere.2018.09.033.

Kreyling, W.G., Semmler-Behnke, M., Chaudhry, Q., 2010. A complementary definition of nanomaterial. Nano Today 5 (3), 165–168. https://doi.org/10.1016/j.nantod.2010.03.004.

Lee, K.M., Wong, C.P.P., Tan, T.L., Lai, C.W., 2018. Functionalized carbon nanotubes for adsorptive removal of water pollutants. Mater. Sci. Eng. B 236–237, 61–69. https://doi.org/10.1016/j.mseb.2018.12.004.

Martins, M., Mourato, C., Sanches, S., Noronha, J.P., Crespo, M.T.B., Pereira, I.A.C., 2017. Biogenic platinum and palladium nanoparticles as new catalysts for the removal of pharmaceutical compounds. Water Res. 108, 160–168. https://doi.org/10.1016/j.watres.2016.10.071.

Mishra, A.K., 2014. Application of Nanotechnology in Water Research. 9781118496 Wiley, https://doi.org/10.1002/9781118939314.

Mohd Khori, N.K.E., Hadibarata, T., Elshikh, M.S., Al-Ghamdi, A.A., Salmiati, Yusop, Z., 2018. Triclosan removal by adsorption using activated carbon derived from waste biomass: isotherms and kinetic studies. J. Chin. Chem. Soc. 65 (8), 951–959. https://doi.org/10.1002/jccs.201700427.

Mohmood, I., Lopes, C.B., Lopes, I., Ahmad, I., Duarte, Armando, C., Pereira, E., 2013. Nanoscale materials and their use in water contaminants removal—a review. Environ. Sci. Pollut. Res. 20, 1239–1260. https://doi.org/10.1007/s11356-012-1415-x.

Nasiri, J., Motamedi, E., Naghavi, M.R., Ghafoori, M., 2019. Removal of crystal violet from water using B-cyclodextrin functionalized biogenic zero-valent iron nanoadsorbents synthesized via aqueous root extracts of Ferula persica. J. Hazard. Mater. 367 (December 2018), 325–338. https://doi.org/10.1016/j.jhazmat.2018.12.079.

Nasrollahzadeh, M., Sajjadi, M., Iravani, S., Varma, R.S., 2021. Carbon-based sustainable nanomaterials for water treatment: state-of-art and future perspectives. Chemosphere 263, 128005. https://doi.org/10.1016/j.chemosphere.2020.128005.

Nik Abdul Ghani, N., Jami, M., Alam, M., 2021. The role of nanoadsorbents and nanocomposite adsorbents in the removal of heavy metals from wastewater: a review and prospect. Pollution 7 (1), 153–179. https://doi.org/10.22059/poll.2020.307069.859.

Oh, Y., Armstrong, D.L., Finnerty, C., Zheng, S., Hu, M., Torrents, A., Mi, B., 2017. Understanding the pH-responsive behavior of graphene oxide membrane in removing ions and organic micropollulants. J. Membr. Sci. 541, 235–243. https://doi.org/10.1016/j.memsci.2017.07.005.

Oliveira, L., Nascimento, M., Guimarães, Y., Oliveira, A., Silva, A., Lopes, R., 2018. Removal of beta-lactams antibiotics through zero-valent copper nanoparticles. J. Braz. Chem. Soc. https://doi.org/10.21577/0103-5053.20180034.

Peng, J., He, Y., Zhou, C., Su, S., Lai, B., 2021. The carbon nanotubes-based materials and their applications for organic pollutant removal: a critical review. Chin. Chem. Lett. 32 (5), 1626–1636. https://doi.org/10.1016/j.cclet.2020.10.026.

Piaskowski, K., Zarzycki, P.K., 2020. Carbon-based nanomaterials as promising material for wastewater treatment processes. Int. J. Environ. Res. Public Health 17 (16), 1–14. https://doi.org/10.3390/ijerph17165862.

Rienzie, R., Ramanayaka, S., Adassooriya, N.M., 2019. Nanotechnology applications for the removal of environmental contaminants from pharmaceuticals and personal care products. In: Pharmaceuticals and Personal Care Products: Waste Management and Treatment Technology Emerging Contaminants and Micro Pollutants. Elsevier, pp. 279–296, https://doi.org/10.1016/B978-0-12-816189-0.00012-3.

Santhosh, C., Velmurugan, V., Jacob, G., Jeong, S.K., Grace, A.N., Bhatnagar, A., 2016. Role of nanomaterials in water treatment applications: a review. Chem. Eng. J. 306, 1116–1137. https://doi.org/10.1016/j.cej.2016.08.053.

Sargin, I., Baran, T., Arslan, G., 2020. Environmental remediation by chitosan-carbon nanotube supported palladium nanoparticles: conversion of toxic nitroarenes into aromatic amines, degradation of dye pollutants and green synthesis of biaryls. Sep. Purif. Technol. 247 (December 2019), 116987. https://doi.org/10.1016/j.seppur.2020.116987.

Sebeia, N., Jabli, M., Ghith, A., Saleh, T.A., 2020. Eco-friendly synthesis of Cynomorium coccineum extract for controlled production of copper nanoparticles for sorption of methylene blue dye. Arab. J. Chem. 13 (2), 4263–4274. https://doi.org/10.1016/j.arabjc.2019.07.007.

Sepúlveda, P., Rubio, M.A., Baltazar, S.E., Rojas-Nunez, J., Sánchez Llamazares, J.L., Garcia, A.G., Arancibia-Miranda, N., 2018. As(V) removal capacity of FeCu bimetallic nanoparticles in aqueous solutions: the influence of cu content and morphologic changes in bimetallic nanoparticles. J. Colloid Interface Sci. 524, 177–187. https://doi.org/10.1016/j.jcis.2018.03.113.

Sharbaf Moghadas, M.R., Motamedi, E., Nasiri, J., Naghavi, M.R., Sabokdast, M., 2020. Proficient dye removal from water using biogenic silver nanoparticles prepared through solid-state synthetic route. Heliyon 6 (8). https://doi.org/10.1016/j.heliyon.2020.e04730, e04730.

Singh, J., Kaur, N., Kaur, P., Kaur, S., Kaur, J., Kukkar, P., Rawat, M., 2018. Piper betle leaves mediated synthesis of biogenic SnO_2 nanoparticles for photocatalytic degradation of reactive yellow 186 dye under direct sunlight. Environ. Nanotechnol. Monit. Manage. 10, 331–338. https://doi.org/10.1016/j.enmm.2018.07.001.

Singh, J., Kumar, V., Kim, K.-H., Rawat, M., 2019a. Biogenic synthesis of copper oxide nanoparticles using plant extract and its prodigious potential for photocatalytic degradation of dyes. Environ. Res. 177, 108569. https://doi.org/10.1016/j.envres.2019.108569.

Singh, J., Kumar, V., Singh Jolly, S., Kim, K.-H., Rawat, M., Kukkar, D., Tsang, Y.F., 2019b. Biogenic synthesis of silver nanoparticles and its photocatalytic applications for removal of organic pollutants in water. J. Ind. Eng. Chem. 80, 247–257. https://doi.org/10.1016/j.jiec.2019.08.002.

Srivastava, M., Srivastava, N., Saeed, M., Mishra, P.K., Saeed, A., Gupta, V.K., Malhotra, B.D., 2021. Bioinspired synthesis of iron-based nanomaterials for application in biofuels production: a new in-sight. Renew. Sust. Energ. Rev. 147 (May), 111206. https://doi.org/10.1016/j.rser.2021.111206.

Tao, H., Liang, X., Zhang, Q., Chang, C.-T., 2015. Enhanced photoactivity of graphene/titanium dioxide nanotubes for removal of acetaminophen. Appl. Surf. Sci. 324, 258–264. https://doi.org/10.1016/j.apsusc.2014.10.129.

Thines, R.K., Mubarak, N.M., Nizamuddin, S., Sahu, J.N., Abdullah, E.C., Ganesan, P., 2017. Application potential of carbon nanomaterials in water and wastewater treatment: a review. J. Taiwan Inst. Chem. Eng. 72, 116–133. https://doi.org/10.1016/j.jtice.2017.01.018.

Tian, H., Li, J., Mu, Z., Li, L., Hao, Z., 2009. Effect of pH on DDT degradation in aqueous solution using bimetallic Ni/Fe nanoparticles. Sep. Purif. Technol. 66 (1), 84–89. https://doi.org/10.1016/j.seppur.2008.11.018.

Varadavenkatesan, T., Lyubchik, E., Pai, S., Pugazhendhi, A., Vinayagam, R., Selvaraj, R., 2019. Photocatalytic degradation of rhodamine B by zinc oxide nanoparticles synthesized using the leaf extract of Cyanometra ramiflora. J. Photochem. Photobiol. B Biol. 199 (September), 111621. https://doi.org/10.1016/j.jphotobiol.2019.111621.

Veerakumar, P., Sangili, A., Saranya, K., Pandikumar, A., Lin, K.-C., 2021. Palladium and silver nanoparticles embedded on zinc oxide nanostars for photocatalytic degradation of pesticides and herbicides. Chem. Eng. J. 410, 128434. https://doi.org/10.1016/j.cej.2021.128434.

Vinosha, M., Palanisamy, S., Muthukrishnan, R., Selvam, S., Kannapiran, E., You, S.G., Prabhu, N.M., 2019. Biogenic synthesis of gold nanoparticles from Halymenia dilatata for pharmaceutical applications: antioxidant, anti-cancer and antibacterial activities. Process Biochem. 85, 219–229. https://doi.org/10.1016/j.procbio.2019.07.013.

Wang, C.Y., Zeng, W.J., Jiang, T.T., Chen, X., Zhang, X.-L., 2019. Incorporating attapulgite nanorods into graphene oxide nanofiltration membranes for efficient dyes wastewater treatment. Sep. Purif. Technol. 214, 21–30. https://doi.org/10.1016/j.seppur.2018.04.079.

Yadav, S., Goel, N., Kumar, V., Singhal, S., 2019. Graphene oxide as proficient adsorbent for the removal of harmful pesticides: comprehensive experimental cum DFT investigations. Anal. Chem. Lett. 9 (3), 291–310. https://doi.org/10.1080/22297928.2019.1629999.

Yaqoob, A.A., Parveen, T., Umar, K., Mohamad Ibrahim, M.N., 2020. Role of nanomaterials in the treatment of wastewater: a review. Water 12 (2). https://doi.org/10.3390/w12020495.

Yin, Y., Shi, M., Ren, Y., Wang, S., Hua, M., Lu, J., Lv, L., 2020. Wrinkle structure on multifunctional MOFs to facilitate PPCPs adsorption in wastewater. Chem. Eng. J. 387 (January). https://doi.org/10.1016/j.cej.2020.124196.

Zhang, L., Song, X., Liu, X., Yang, L., Pan, F., Lv, J., 2011. Studies on the removal of tetracycline by multi-walled carbon nanotubes. Chem. Eng. J. 178, 26–33. https://doi.org/10.1016/j.cej.2011.09.127.

Zhang, W., Zeng, Z., Liu, Z., Huang, J., Xiao, R., Shao, B., He, Q., 2020. Effects of carbon nanotubes on biodegradation of pollutants: positive or negative? Ecotoxicol. Environ. Saf. 189 (June 2019). https://doi.org/10.1016/j.ecoenv.2019.109914.

Zhou, Q., Liu, L., Liu, N., He, B., Hu, L., Wang, L., 2020a. Determination and characterization of metal nanoparticles in clams and oysters. Ecotoxicol. Environ. Saf. 198, 110670. https://doi.org/10.1016/j.ecoenv.2020.110670.

Zhou, K., Zhang, J., Xiao, Y., Zhao, Z., Zhang, M., Wang, L., Zhou, C., 2020b. High-efficiency adsorption of and competition between phenol and hydroquinone in aqueous solution on highly cationic amino-poly(vinylamine)-functionalized GO-(o-MWCNTs) magnetic nanohybrids. Chem. Eng. J. 389, 124223. https://doi.org/10.1016/j.cej.2020.124223.

Zhu, S., Liu, Y., Liu, S., Zeng, G., Jiang, L., Tan, X., Yang, C., 2017. Adsorption of emerging contaminant metformin using graphene oxide. Chemosphere 179, 20–28. https://doi.org/10.1016/j.chemosphere.2017.03.071.

This page intentionally left blank

PART II

Cellulose-based nanobiosorbents for decontamination of environmental matrices

This page intentionally left blank

CHAPTER

11

Risk assessment of nanocellulose exposure

Minashree Kumari

Department of Civil Engineering, Indian Institute of Technology Delhi, Hauz Khas, Delhi, India

11.1 Introduction

Over the past few years, cellulose-based-nanobioadsorbents (CNB) or nanocellulose (NC) has been gaining increasing attention from both research and industry. Physico-chemical properties such as high tensile strength, biocompatibility, and high aspect ratio make it more alluring to a wide range of sectors, spanning from medical to construction. The substance can be extracted from vast variety of available cellulosic biomass materials for instance, wood pulp, agricultural crops, organic waste, and also from bacteria (Xue et al., 2017). Nanocellulose are basically categorized into three different types, i.e., nanocrystalline cellulose, nanofibrillated cellulose, and bacterial nanocellulose ones (Phanthong et al., 2018). However, all of them have similar chemical compositions but they usually differ in morphology, particle size, crystallinity, and some modification caused due to the difference of source from which they are extracted and also the extraction methods used (Roman, 2015; Shatkin and Kim, 2015).

Increased use of nanocellulose in extensive industrial applications have amplified the possibility of human exposure to this substance during the various life stages of NC-containing products (Gottschalk and Nowack, 2011). Due to their widespread use, serious questions are being raised about the health and environmental consequences of manufactured nanomaterials for consumers and also for industrial applications. The usage of these bio-based nanofibers increases a greater understanding of human exposure addressing their potential health issues should be gained (Camarero-Espinosa et al., 2016).

There is the possibility of exposure to humans, eventually after nanocellulose is released from the product and through a number of environments and scenarios. In each of these there are different modes of human exposure, which include the respiratory tract (inhalation), skin contact, eye contact, ingestion and possible interaction with the bloodstream (i.e., via direct

https://doi.org/10.1016/B978-0-323-90912-9.00011-3

injection through medical application, or via translocation from the lung following inhalation (Nowack et al., 2012; Losert et al., 2014) resulting in possible secondary organ exposure, i.e., liver, heart, brain, and/or kidney.

Exposure to nanocellulose can occur through inhalation, ingestion or dermal routes (Martinez et al., 2013). The major route of exposure can be through inhalation of small particles which might get entrapped within the tissues and lungs in the workplace however, the long-term effects are essentially unidentified. As many as 10,000 studies on nanomaterial toxicity has been reported, but till date the key contributing properties to toxicity of nanocellulose have not been predicted. The surface properties of nanocellulose, including size and size distribution, surface charge, stability, and reactivity are vital elements of toxicity and effects.

Looking into the exposure aspects of nanocellulose, studies suggest that the inhalation of raw NCs would be the main exposure route for humans, however little information is available on the exposure concentrations or doses (Donaldson et al., 2013). The value of these variables will mainly depend on the scenario considered, for instance, exposure concentrations during occupational events are expected to be on the higher side than those in consumer applications. Apart from inhalation exposure, studies were also conducted to assess the toxicity of nanocellulose through oral and dermal routes of exposure.

Very few studies consider the longer term life-cycle impacts of novel materials, yet we have learned from decades of public health and environmental research that these considerations must be made early in the development cycle.

Limited studies have been reported on the environmental risk of nanocellulose (Stoudmann et al., 2019, 2020). None of the reported studies have considered the human health-related aspect of nanocellulose exposure as per the author's best knowledge. It is important to address this issue as humans are the most affected by nanocellulose exposure. However, lack of information data makes the whole process quite difficult.

11.2 Risk assessment framework

As exposure is a main part of risk assessment process, understanding and mitigating risk requires identifying potential points of exposure. A relatively recent addition to the risk assessment toolbox is the use of Life Cycle Risk Assessment (LCRA), which evaluates scenarios within a product life-cycle on the basis of potential exposure to a material, as well as the availability of safety information (Ede et al., 2019). The methodology of risk assessment involves four different steps comprising of hazard identification, exposure assessment, risk estimation and risk characterization as mentioned in Fig. 11.1 (Kumari and Kumar, 2020a).

11.2.1 Hazard identification

Hazard identification is the first and foremost step in risk assessment process. It is essential to identify the possible sources through which exposure can take place. It is important to determine whether, and under what conditions, exposure to CN particles might occur, whether

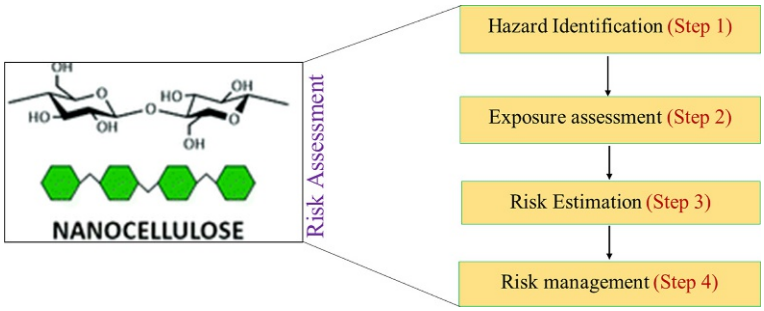

FIG. 11.1 Steps for evaluating risk of nanocellulose exposure.

these exposures include nanoscale particles, and whether to conduct measurements to develop exposure estimates. The probable sources through which exposure can occur include (i) exposure via occupational inhalation and (ii) exposure from environment. Table 11.1 lists the possible sources of risk exposure for the two pathways mentioned (i) under occupational inhalation, the possible exposure may happen during spilling of nanocellulose fibers with polymer or breakage or leakage of the pipe material. Accidental ingestion of processed raw material or inhalation of air-borne nanocellulose particles are one of the leading source of exposure. Spillage during winding, cutting, or sanding might lead to human health effects via inhalation exposure. Literature report suggests that inhalation of pure, dried nanocellulose material during commercial production and manufacturing are the primary concerns for an occupational user (Shatkin and Kim, 2017); (ii) exposure from environment: There are abundant sources of nanomaterials in the environment and it becomes tough to recognize and measure (Bierkandt et al., 2018). These can be released into the ambient air by

TABLE 11.1 Possible source of nanocellulose exposure.

Type of hazard/ exposure	Scenario	Stage
Occupational/ inhalation	Accidental ingestion of processed material	Production
	Use to dry nanocellulose to create material for film coating	Manufacturing
	Accidental ingestion of air borne nanocellulose particles	
Environmental	Primarily at phases downstream to the production, such as particle recovery, spray drying or milling/accidental released into ambient air during the handling and transport of particles (Bierkandt et al., 2018)	Production
	Leakage during the production may introduce particles into the environment (John et al., 2017)	Production
	Untreated discharge into wastewater	End of life
	Spillage due to landfill degradation	

similar processes as in occupational or daily-life scenarios (John et al., 2017). Incessant discharge of wastewater in surrounding water bodies. Leakage from landfills or their degradation also adds to the existing pollution load.

11.2.2 Exposure assessment

Exposure assessment deals with identifying the possible source of risk exposures to contaminants under study. The exposure scenarios include environmental impacts of the receiving waters at end-of-life disposal (e.g., to aquatic wildlife and through biodegradation), the ingestion of CN particles by consumers' accidental ingestion, and the potential for dermal contact during manufacturing and consumer application. Toxicological investigation estimates the possible toxicity based on exposure routes plus those arising from ingestion (oral toxicity), skin contact (dermal toxicity), eye contact (ocular toxicity), and breathing (inhalation toxicity). Literature studies suggest that cellulose dust may cause irritation (Cullen et al., 2000) in the respiratory system when inhaled. Since nanocellulose is extracted from bulk cellulose, studies on whether nanocellulose induce a similar reaction when inhaled from the air are essential. Though, the size, scale, and differential chemistries of CN forms can complicate experimental efforts. Smaller the particle is, deeper the impact will be as they are able to migrate into the inner surface of lung, affecting them.

There are three major routes (Inhalation, dermal, and oral ingestion) through which exposure can occur, of which inhalation has been identified as the major pathway of risk exposure to human health for nanocellulose (Stoudmann et al., 2020). In order to determine the potential for health effects with inhalation exposure to nanocellulose, it is necessary to understand whether in reality exposure is occurring, to what size particles, and to what concentrations (Camarero-Espinosa et al., 2016). The size of nanocellulose fibers is one of the major parameter which governs the risk assessment. Since, inhalation is a key exposure route in occupational scenarios, toxicological studies, both in vivo and in vitro, often focus on physiological responses by inhalation and inform us of the potential deleterious human health effects from breathing in aerosolized NMs (Kargarzadeh et al., 2017). Much of the currently available toxicological data for CN evaluate inhalation exposures, implicating the pulmonary and inflammatory systems. Although long-term exposures are more realistic, most studies were acute or shorter term, reflecting more immediate effects, rather than delayed or chronic. A review of the toxicity of CNC found that although the small number of in vivo studies on oral and dermal toxicity showed no signs of adverse effects, the results from both pulmonary (inhalation in vivo) and cytotoxicity studies showed inconsistent results (Roman, 2015).

11.2.3 Risk estimation

LCRA has been designated as a possible tool for determining risk due to occupational inhalation exposure. It involves five different stages: (i) production of raw materials, (ii) manufacture, (iii) transportation, (iv) consumer use, and (v) disposal (Shatkin and Kim, 2015).

Nanomaterials influence on the environment have been assessed for some nanocompounds, but nanocellulose has not been investigated extensively. Most studies showed

that the impacts of environmental exposure to nanomaterials are acute (single dose) rather than chronic. In real-life situations, though, chronic and longer term research investigations would more suitably divulge realistic exposure durations, as production, use, and disposal of NC-containing materials would more likely result in continuous emissions to environmental media (Shatkin and Kim, 2017).

For determining environmental risk assessment (ERA), risk characterization ratio (RCR) of nanocellulose is estimated by using the predicted environmental concentrations (PECs). PECs are compared with predicted no effect concentrations (PNECs), which are derived from in vivo and in vitro ecotoxicological studies (European Chemicals Agency (ECHA), 2008). RCR is carried out in accordance with REACH guideline as mentioned below (Eq. 11.1). PNECs represent the level of nanocellulose below which no adverse effects are expected to occur.

$$\mathrm{RCR} = \mathrm{PEC}/\mathrm{PNEC} \tag{11.1}$$

where RCR is the risk characterization ratio; PEC is the predicted environmental concentration; PNEC is the predicted no-effect concentration level. A RCR < 1 would indicate that no risk is expected for the particular environmental compartment and conditions. A RCR > 1 would mean the predicted environmental concentrations are high enough to cause adverse effects on the organisms and could show the need to implement additional risk management measures (Kumari and Kumar, 2020b). This simple approach was applied to engineered nanomaterials where the first risk characterization ratios were obtained and discussed by Mueller and Nowack (2008) and subsequently by Gottschalk et al. (2009). In the previous work by Gottschalk and Nowack (2013), the risk was assessed as a percentage of overlap between the PEC and the pSSD. Similar approach used by Coll et al. (2015) to delineate the risk of engineered nanomaterials. Stoudmann et al. (2019) showed an RCR of 6.9×10^{-5} 2015, and 7.1×10^{-4} in 2025, indicating that under the chosen assumptions there is no present or future environmental risk surrounding nanocellulose within the surface water compartment, even assuming a compound annual growth rate of 19% for nanocellulose production in upcoming years.

11.2.4 Risk management

When the potential source of exposure is identified, it is somehow easy to control and reduce the risk associated. As per a report published by Vireo Advisors, LLC (2019), an Exposure Control Hierarchy is proposed to manage the exposure. The Exposure Control Hierarchy includes (i) Hazard reduction which includes the use of materials in accordance with good manufacturing practice for reducing risk exposure, (ii) adopting controlled engineered work environments, (iii) understanding the potential hazards associated with equipment's, processes, and materials employed, and (iv) protection for workers in terms of garments and equipment to reduce risk exposure. The best approach to control potential releases can be made by using engineering control methods, for example, local exhaust ventilation or hoods and use of PPE kits during handling of dry product. Since the nanocellulose risk exposure occurs through occupational inhalation as well, expertise of industrial hygiene professionals, who are trained in conducting sampling in workplaces and have access to specialized

equipment for measuring exposure is required to reduce the risk, if any. It is advisable to seek expert's assistance for your workplace exposure assessment. For example, agencies like the US National Institute for Occupational Safety and Health (NIOSH) conducts free, private office surveys in the United States, with specified sampling equipment, and offers recommendations and suggestions for handling workplace exposures. Besides, there are also some private organizations that perform similar services internationally. Shatkin and Kim (2015) applied lifecycle risk assessment to determine health risks of nanocellulose materials and observed that occupational inhalation is a major safety concern for mankind. This analysis, when combined with the potential hazards of a material, helps professionals characterize the safety landscape and develop risk management practices.

11.3 Guidelines and regulations

Looking into the potential adverse effects of nanocellulose, standards, guideline limits and exposure limits has been formulated by regulatory agencies like Occupational Safety and Health Administration (OSHA), National Institute for Occupational Safety and Health (National Institute for Occupational Safety and Health, 2013), etc. However, the Occupational Exposure Limits Value (OEL) of NC by inhalation or dermal exposure are rare owing to the limited amount of data availability about their potential risk. As a precautionary measure, the OEL value of 0.01 fibers/cm^3 (similar to those of carbon nano-fibers) has been recommended in view of the potential bio-persistence of NC when inhaled (Stockmann-Juvala et al., 2014). Though the health risk effects of inhaling nanocellulose have not been well studied, numerous OEL have been established for bulk cellulose particles based on a gravimetric analysis. The OSHA recommended permissible exposure limit for total dust (15 mg/m^3) and for respirable dust (5 mg/m^3), expressed in time-weighted averages (TWA) (Martinez et al., 2013). The NIOSH recommended exposure limits (REL) are TWA 10 mg/m^3 and TWA 5 mg/m^3 respirable, and the ACGIH Threshold Limit Value® (TLV) is TWA 10 mg/m^3 (CDC). There is currently no immediately dangerous to life and health (IDLH) level available for cellulose exposure. These limits are primarily based on the potential for irritation of cellulose particles to eyes, skin, or mucous membranes.

11.4 Conclusions and implications of the study

NC exposure is the least investigated route with reference to exposure estimation and assessment and pose question because of its comparably low concentrations and limited analytical methods. Risk assessment of nanocellulose is essential in understanding the adverse effects on to ecological as well as on human health. Framework has been developed to determine LCRA and ecological health risks however research investigations and studies on human health is still scarce which makes it overall process difficult, for example, lack of environmental occurrence data on nanocellulose, dose response data on toxicity of nanocellulose are some of the knowledge gaps which need to be look upon for human health risk assessment. Similar to HHRA, LCRA of NC also suffers due to lack of data on long-term

exposures, realistic concentrations values including studies on certain common human health endpoints such as carcinogenicity, neurotoxicity and reproductive effects (Shatkin and Kim, 2015). Besides, some studies have also shown diverging results. These knowledge gaps make it challenging to suggest appropriate exposure controls and therefore inhibit a clear conclusion regarding the human health impacts of nanocellulose to be made. No studies are available in the literature that have assessed the suitability of current control technologies for nanocellulose. Furthermore, no evidence or guidance specific to personal protection from nanocellulose were found. Currently, no standardized or validated measurements for nanocellulose in air is available, a crucial need for assessing inhalation exposure. Analytical and technical boundaries limit our understanding of determining actual potential occupational exposures. Reproducibility of measurement methods is also an area which needs further improvement, since materials and occupational surroundings for nanocellulose and NC-enabled products will vary greatly. As typical for risk assessment, exposure during the production steps and hazard related to the materials should be evaluated case-by-case. Currently there are no occupational exposure limits specific to engineered cellulose nanomaterials. As with many nanomaterials, the size and surface area of the CNC nanoparticles may be a critical factor with respect to toxicological risks and biological effects. Therefore, it is good practice to keep exposures to new and uncharacterized materials as low as possible.

There is a need to better assess the effects of inhalation exposure in the workplace than the currently available studies based on short-term, high-dose exposures that create lung overload conditions. Further, additional endpoints should be studied to demonstrate overall safety in a breadth of uses. Long-term exposure studies are needed. Increasing knowledge of hazardous properties and behavior of nanomaterials calls for continual review of the risk assessment and management measures. Until reliable methods are developed to predict the toxicity of a nanomaterial, thorough safety testing must be completed.

References

Bierkandt, F.S., Leibrock, L., Wagener, S., Laux, P., Luch, A., 2018. The impact of nanomaterial characteristics on inhalation toxicity. Toxicol. Res. (Camb.) 7 (3), 321–346.

Camarero-Espinosa, S., Endes, C., Mueller, S., Petri-Fink, A., Rothen-Rutishauser, B., Weder, C., Clift, M.J.D., Foster, E.J., 2016. Elucidating the potential biological impact of cellulose nanocrystals. Fibers 4, 21. https://doi.org/10.3390/fib4030021.

Coll, C., Notter, D., Gottschalk, F., Sun, T., Som, C., Nowack, B., 2015. Probabilistic environmental risk assessment of five nanomaterials (nano-TiO_2, nano-Ag, nano-ZnO, CNT, and fullerenes). Nanotechnology 10 (4), 436–444.

Cullen, R.T., Searl, A., Miller, B.G., Davis, J.M.G., Jones, A.D., 2000. Pulmonary and intraperitoneal inflammation induced by cellulose fibres. J. Appl. Toxicol. 20 (1), 49–60.

Donaldson, K., Schinwald, A., Murphy, F., Cho, W.-S., Duffin, R., Lang, T., et al., 2013. The biologically effective dose in inhalation nanotoxicology. Acc. Chem. Res. 46 (3), 723–732. https://doi.org/10.1021/ar300092y.

Ede, J.D., Ong, K.J., Goergen, M., Rudie, A., Pomeroy-Carter, C.A., Shatkin, J.A., 2019. Risk analysis of cellulose nanomaterials by inhalation: current state of science. Nano 9, 337. https://doi.org/10.3390/nano9030337.

European Chemicals Agency (ECHA), 2008. Guidance on Information Requirements and Chemical Safety Assessment Appendix to Part F CSR Template With Explanation.

Gottschalk, F., Nowack, B., 2011. The release of engineered nanomaterials to the environment. J. Environ. Monit. 13 (5), 1145–1155. https://doi.org/10.1039/c0em00547a.

Gottschalk, F., Nowack, B., 2013. A probabilistic method for species sensitivity distributions taking into account the inherent uncertainty and variability of effects to estimate environmental risk. Integr. Environ. Assess. Manag. 9 (1), 79–86.

Gottschalk, F., Sondere, T., Schols, R., Nowack, B., 2009. Modeled environmental concentrations of engineered nanomaterials for different regions. Environ. Sci. Technol. 43 (24), 9216–9222.

John, A.C., Kupper, M., Manders-Groot, A.M.M., Debray, B., Lacome, J.M., Kuhlbusch, T.A.J., 2017. Emissions and possible environmental implication of engineered nanomaterials (ENMs) in the atmosphere. Atmosphere 8 (5), 84.

Kargarzadeh, H., Loelovich, M., Ahmad, I., Thomas, S., Dufresne, A., 2017. Methods for extraction of nanocellulose from various sources. In: Kargarzadeh, H., Ahmad, I., Thomas, S., Dufresne, A. (Eds.), Handbook of Nanocellulose and Cellulose Nanocomposites. vol. 1. Wiley, ISBN: 9783527338665, pp. 1–49, https://doi.org/10.1002/9783527689972 (Chapter 1).

Kumari, M., Kumar, A., 2020a. Human health risk assessment of antibiotics in binary mixtures for finished drinking water. Chemosphere 240, 124864. https://doi.org/10.1016/j.chemosphere.2019.124864.

Kumari, M., Kumar, A., 2020b. Identification of component-based approach for prediction of joint chemical mixture toxicity risk assessment with respect to human health: a critical review. Food Chem. Toxicol. 143, 111458. https://doi.org/10.1016/j.fct.2020.111458.

Losert, S., von Goetz, N., Bekker, C., Fransman, W., Wijnhoven, S.W.P., Delmaar, C., Hungerbuhler, K., Ulrich, A., 2014. Human exposure to conventional and nanoparticle-containing sprays—a critical review. Environ. Sci. Technol. 48, 5366–5378.

Martinez, K.F., Eastlake, A., Rudie, A., Geraci, C., 2013. Occupational exposure characterization during the manufacture of cellulose nanomaterials. In: Postek, M.T., Moon, R.J., Rudie, A.W., Bilodeau, M.A. (Eds.), Production and Applications of Cellulose Nanomaterials. TAPPI Press, ISBN: 978-1-59510-224-9.

Mueller, N.C., Nowack, B., 2008. Exposure modeling of engineered nanoparticles in the environment. Environ. Sci. Technol. 42, 4447–4453.

National Institute for Occupational Safety and Health, 2013. Current Intelligence Bulletin 65-occupational Exposure to Carbon Nanotubes and Nanofibers. Department of Health and Human Services, Centers for Disease Control and Prevention, NIOSH Pub. No, Cincinnati, pp. 2013–2145.

Nowack, B., Brouwer, C., Geertsma, R.E., Heugens, E.H.W., Ross, B.L., Toufektsian, M.-C., Wijnhoven, S.W.P., Aitken, R.J., 2012. Analysis of the occupational, consumer and environmental exposure to engineered nanomaterials used in 10 technology sectors. Nanotoxicology 7, 1152–1156.

Phanthong, P., Reubroycharoen, P., Hao, X., Xu, G., Abudula, A., Guan, G., 2018. Nanocellulose: extraction and application. Carbon Resour. Convers. 1, 32–43.

Roman, M., 2015. Toxicity of cellulose nanocrystals: a review. Ind. Biotechnol. 11 (1), 25–33.

Shatkin, J.A., Kim, B., 2015. Cellulose nanomaterials: life cycle risk assessment, and environmental health and safety roadmap. Environ. Sci. Nano 2 (5), 477–499.

Shatkin, J.A., Kim, B., 2017. Environmental health and safety of cellulose nanomaterials and composites. In: Kargarzadeh, H., Ahmad, I., Thomas, S., Dufresne, A. (Eds.), Handbook of Nanocellulose and Cellulose Nanocomposites, first ed. Wiley.

Stockmann-Juvala, H., Taxell, P., Santonen, T., 2014. Formulating Occupational Exposure Limits Values (OELs) (Inhalation & Dermal). Scaffold, Helsinki.

Stoudmann, N., Nowack, B., Som, C., 2019. Prospective environmental risk assessment of nanocellulose for Europe. Environ. Sci. Nano 6 (8), 2520–2531. https://doi.org/10.1039/C9EN00472F.

Stoudmann, N., Schmutz, M., Hirsch, C., Nowack, B., Som, C., 2020. Human hazard potential of nanocellulose: quantitative insights from the literature. Nanotoxicology 14 (9), 1241–1257. https://doi.org/10.1080/17435390.2020.1814440.

Vireo Advisors, LLC, 2019. Cellulose Nanomaterials, A Practical Handling Guide. Vireo Advisors, LLC, Boston, MA. http://www.vireoadvisors.com/resources.

Xue, Y., Mou, Z., Xiao, H., 2017. Nanocellulose as a sustainable biomass material: structure, properties, present status and future prospects in biomedical applications. Nanoscale 9 (39), 14758–14781.

CHAPTER

12

Cellulose-based nanobiosorbents: An insight

Ilgım Göktürk[a], *Duygu Çimen*[a], *Merve Asena Özbek*[a], *Fatma Yılmaz*[b], *and Adil Denizli*[a]

[a]Department of Chemistry, Hacettepe University, Ankara, Turkey [b]Vocational School of Gerede, Department of Chemistry Technology, Bolu Abant Izzet Baysal University, Bolu, Turkey

12.1 Introduction

In recent years, nanotechnology, which is used in the production of effective, easy-to-use, and inexpensive materials in every field, plays an important role in the development of new generation and environmentally friendly materials in materials science studies. In recent new studies, green chemistry and new generation material production gain importance, and more environmentally friendly polymers are produced by polymer production from natural materials. These types are polymers that do not harm the environment, are easily degradable, and are completely organic. A significant part of natural polymers are generally found in the structure of living things and one of the most important examples of this is cellulose (Buzea et al., 2007).

Cellulose is a natural, environmentally friendly polymer that can be effectively degraded by many microorganisms, is self-renewable, non-toxic, inexpensive, has high power, and heat resistance. Cellulose is present in the wood cell wall along with lignin and other polysaccharides (Johar et al., 2012; Stenstad et al., 2008). This structure is considered as a bio-nanocomposite resulting from the interaction between the nanoscale areas of cellulose, hemicellulose, and lignin. Cellulose is a natural polymer with a straight and long-chain chemical structure formed by bonding a certain number of glucose molecules with an ether bridge as shown in Fig. 12.1 (Klemm et al., 2005).

Cellulosic materials with a particle size of less than 100 nm are called nanocellulose. Major cellulose sources are wood materials, plants, tulips, algae, and bacteria and frequently used for nanocellulose production. The wood material is one of the most abundant sources for

https://doi.org/10.1016/B978-0-323-90912-9.00012-5

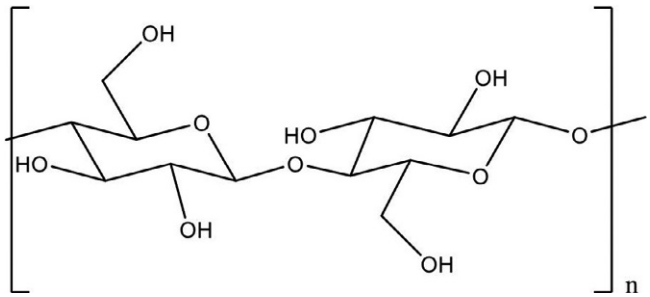

FIG. 12.1 Molecular structure of cellulose.

nanocellulose, which can be obtained from many natural sources, and the extraction of cellulose nanoparticles is performed by purifying lignin and hemicellulose (Keenan et al., 2015).

Plants are one of the main sources of cellulose, and sources such as sugar beet, cotton, potato tubers, and wheat straw can be used for the extraction of cellulose nanoparticles (Xue et al., 2017). Various algae species (green, gray, red, etc.) produce cellulose microfibers in their cell walls (Chen et al., 2016). Due to the species-specific biosynthesis process, there can be significant differences in the cellulose microfiber structures produced. Other algae species used are *Micrasterias rotate*, *Valonia*, *Micrasterias denticulata*, and *Boergesenia.* One of the bacteria that can produce cellulose is *Gluconacetobacter xylinus* (Jozala et al., 2016).

The bacterias developed under special culture conditions, secrete cellulose microfiber by producing a fine gel consisting of 97% water and microfiber cellulose. The most important feature of these bacteria is that the cultivation conditions can be adjusted to alter microfiber formation and crystallization. Processes such as isolation of cellulose particles, mechanical treatment, and acid hydrolysis are frequently performed in nanocellulose production.

Isolation of cellulose particles from various cellulose sources involves the purification and homogenization of the source materials and then the separation of purified (pre-treated) cellulose materials into microfiber, nanofibrils, or crystalline components (Li et al., 2015; Meyabadi and Dadashian, 2012; Moon et al., 2011). In mechanical processes such as grinding in the longitudinal and transverse splitting of cellulose fibrils, refining producing high-shear gradients, cold comminution, high-pressure homogenization, and high density ultrasonic are applied (Rebouillat and Pla, 2013). Acid hydrolysis is used to obtain crystalline particles from cellulose sources (plant fibril, wood fibril, algae, and bacteria). This process can be briefly explained as the hydrolysis (separation) of amorphous regions within cellulose micro/nanofibrils (De Souza Lima and Borsali, 2004).

Cellulose-based nanomaterials are divided into three classes as cellulose nanofibrils, cellulose nanocrystals, and bacterial cellulose according to the cellulose source, extraction method, and fibril size (Jonoobi et al., 2015; Nascimento et al., 2016). The types of cellulose, the source from which it is obtained, the processes in the production stage, and their average sizes are explained in Table 12.1 (Klemm et al., 2011).

In addition to being organic and natural, nanocellulose polymer has less density compared to other materials. However, their high resistance has a wide range of uses compared to other materials (Fig. 12.2). Today, nanocellulose materials with their natural polymeric structure are frequently used in sectors such as automotive, electronics, construction, packaging, and industry.

TABLE 12.1 Types of nanocellulose (Klemm et al., 2011).

Cellulose type	Obtained source	Process	Property
Cellulose nanofibrils	Sugar, wood, potato, beet, linen, cannabis, etc.	Degradation before/after enzymatic chemical treatment	Diameter: 5–60 nm Length: a few μm
Cellulose nanocrystals	Cotton, linen, wood, cannabis, corn stalk, etc.	Acid hydrolysis	Diameter: 5–70 nm Length: 100 nm or a few μm for bacteria or algae-based cellulose Length: 100–250 nm for plant cellulose
Bacterial cellulose	Low molecules such as sugar, alcohol, etc.	Bacterial synthesis	Diameter: 20–100 nm

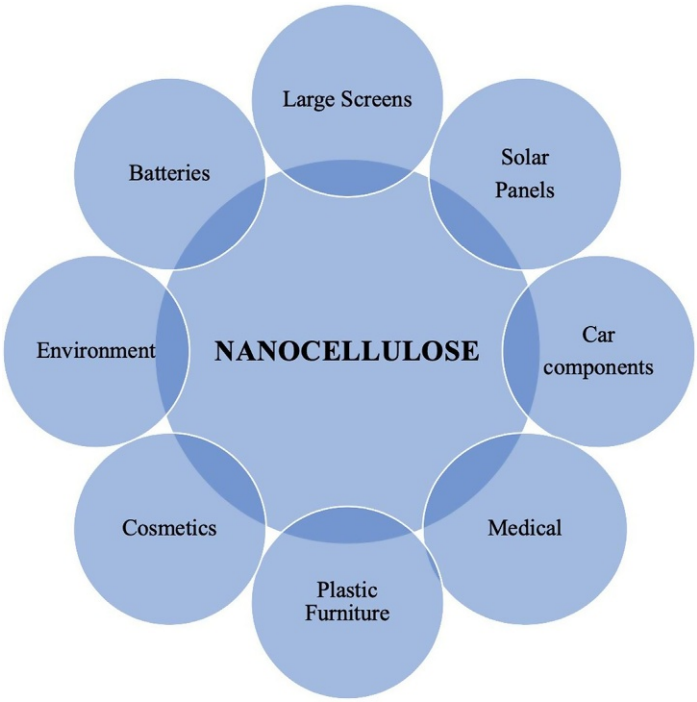

FIG. 12.2 Potential nanocellulose applications.

Besides, nanocellulose-based materials have significant use in forest products, especially in recent years, and they are used in papermaking (Campano et al., 2018), panel material (Yildirim et al., 2014), foam material (Svagan et al., 2008), fireproof insulation materials (Yildirim, 2018), artificial organs in medicine (Nimeskern et al., 2013) in the curative artificial leather production (Mualla et al., 2016), and in the use of filtering against viruses (Metreveli et al., 2014). In this chapter, the information about nanocellulose and its types and the recent

developments of the cellulose-based nanobioadsorbents's environmental applications are comprehensively discussed.

12.2 Nanocellulose and its sources

Recently, the rapid development of nanotechnology and green chemistry increases the need for materials used in these new generation areas. The most important factors in materials to be preferred in applications of these fields are to ensure eco-efficiency and sustainability (Fardioui et al., 2017; Farooq et al., 2020). One of these, cellulose, is the most plentiful biodegradable and renewable natural polymer in the world and is formed by repeating β-D-glucose. Cellulose, which has been known for many years, is used in plenty of fields such as paper, food, medicine, paint, textile industries as well as being considered as an energy source (Nasir et al., 2017). It is found in some bacteria and marine animals (Tunicates) in addition to the structural cell wall of various plants and certain algae (Keijsers et al., 2013).

Lately, cellulose in nanoscale form (i.e., nanocellulose) is considered to be a reliable green substrate to be used to manufacture nanocomposites in a wide variety of biomedical applications. Nanocellulose is a promising candidate for surface modifications as it contains many hydroxyl groups in large and specific surface areas. It also provides high strength thanks to its good mechanical properties. In addition to being a renewable and low-cost material, nanocellulose has no or very low toxicity, biodegradability, biocompatibility, and anti-microbial effects, contributing to its preference in different applications (Čolić et al., 2020; Subhedar et al., 2021). In the following sections, sources of nanocellulose will be explained.

12.2.1 Plant cellulose

Nowadays, researches are carried out on the efficient utilization of bio-wastes and their use as raw materials for the creation of high-performance next-generation materials. In this context, considering the great importance of developing low-cost, sustainable, and renewable resources, it is valuable to produce cellulose and nano-cellulosic materials from agricultural and food industrial wastes (Prasad Reddy and Rhim, 2014; Silvério et al., 2013). Agricultural and industrial waste emerges as undeniable resources for cellulose biomass. Until now, many wastes in the specified areas such as tomato peels (Jiang and Hsieh, 2015), rice straw (Jiang et al., 2013; Reddy and Yang, 2006), corncob (Kang et al., 2017), potato peels (Chen et al., 2012), fruits wastes (Hiasa et al., 2014), coconut husk (Rosa et al., 2010), cotton stalk (Rahbar Shamskar et al., 2016), sugar beets (Montanari et al., 2005) and forest residues (Moriana et al., 2016) have been evaluated for this purpose. In one of the studies conducted on this subject, it has been reported that garlic skin is an uncommon but promising candidate as a source of cellulose (Prasad Reddy and Rhim, 2014).

Plant-based cellulose nanofibers exhibit the potential to be extracted into thinner fibers according to bacterial cellulose. Therefore, several studies are conducted on the extraction of nanofibers from plant fibers and wood. Cellulose chains are synthesized in plant cells. Besides hemicellulose and lignin, highly organized and crystallized cellulose fibrils refer

to the major components of the plant cell wall (Abraham et al., 2011; Lu and Hsieh, 2012). One of these components, hemicellulose, is a branched polysaccharide polymer containing various species of sugars such as mannose, glucose, and galactose. Lignin refers to a highly cross-linked phenolic polymer. When these three main components are compared, it is observed that cellulose is a semi-crystalline polymer, while lignin and hemicellulose are amorphous polymers (Sheltami et al., 2012).

The typical nanocellulose extraction process is achieved by removing impurities and amorphous regions, i.e., non-cellulosic components such as hemicellulose and lignin. For this purpose, strategies including acid hydrolysis (Roman and Gray, 2005), enzymatic hydrolysis (Pääkkö et al., 2007), and mechanical degradation (Uetani and Yano, 2011) are applied for nanocellulose isolation. In the process of acid hydrolysis with hydrochloric acid or sulfuric acid, it becomes possible to reach the cellulose chains in less regular or amorphous regions in an easier way, thus ensuring that the crystalline areas remain intact (Lu and Hsieh, 2012). The resulting nanocellulose is used in many areas such as paper production, packaging, textile, and pharmaceutical industries. In addition, thanks to its strong mechanical characteristics, it is also utilized as a reinforcement material in several polymer matrices (Jasmani and Adnan, 2017).

12.2.2 Tunicates and algal cellulose (AC)

Tunicates from the ascidians are marine animals that live in the oceans and contain cellulose in their skeletons. There are cellulose-synthesizing enzymes in the plasma membrane of their epidermal cells. Cellulose obtained from tunicates has many excellent characteristics including large surface area, high crystallinity, and strong mechanical properties. Thanks to its high crystallinity, it has been employed in many studies to identify the molecular structure of cellulose. Tunicates cellulose was applied in the preparation of many polymeric nanocomposites and scaffolds produced in the field of tissue engineering (Pérez and Samain, 2010; Samiee et al., 2019; Yadav et al., 2021).

Algae, a significant source of cellulose, contain crucial amounts of cellulose in their cell walls. Different kinds of algae, namely red, green and yellow, refer to a wide variety of living organisms, unicellular or multicellular. The reason algae are used in many industrial areas today is that they can produce protein, polysaccharides, and fatty acids. While the inner cell walls of green-colored algae are generally composed of cellulose, the outer cell walls consist of pectin. Similarly, in brown algae, cell walls contain large amounts of cellulose and alginic acid. Another species, red algae, have a low cellulose content but it contains sulfated galactan polymers, agar, and carrageenan. Similarly, in brown algae, cell walls contain large amounts of alginic acid and cellulose. It was determined by X-ray diffraction models that the D-glucose monomers that create the cellulose in algae are similar to the cellulose content in terrestrial plants (Jung et al., 2013; Samiee et al., 2019).

In summary, algae's cell walls are generally composed of microfibrillar (crystalline) phases consisting of cellulose, mannan, or xylan. It is easier and relatively inexpensive to obtain cellulose from algae compared to extracting cellulose from plants. This can be clarified by the fact that cellulose is not related to lignin in most algae species given in the literature (Samiee et al., 2019).

12.2.3 Bacterial cellulose

As mentioned in previous sections, cellulose is one of the main components of the plant cell wall and it is in charge of the strength of the structure. However, plants contain lignin and hemicellulose components as well as cellulose. To obtain pure cellulose and remove these impurities, they are exposed to treatments with harsh chemicals. Due to these factors, an environmentally friendly approach has been sought to produce pure cellulose (Karim and Afrin, 2017; Smith et al., 2017; Ul-Islam et al., 2019).

Bacterial cellulose represents a suitable candidate as a sustainable biopolymer with desired properties in different fields since it was discovered. Bacterial cellulose, which has the same chemical structure as plant cellulose $(C_6H_{10}O_5)_n$, is a structural carbohydrate produced by microorganisms (Blanco Parte et al., 2020). It is produced extracellularly by Gram-negative bacteria cultures such as *Gluconacetobacter*, *Agrobacterium*, *Rhizobium*, *Salmonella*, and *Pseudomonas*. Celluloses produced by different bacteria differ in terms of their properties, morphologies, and applications. *Acetobacter xylinum*, currently referred to as *Gluconacetobacter xylinus*, is the most efficient bacterial cellulose producer thanks to its high productivity (Picheth et al., 2017; Wang et al., 2019).

There are differences between plant-derived cellulose and bacterial cellulose including purity, macromolecular structure, physicochemical and mechanical properties. In bacterial cellulose, there is no need for mechanical and thermochemical processes such as acid hydrolysis and the use of hazardous chemicals to remove impurities and extract cellulose, as in plant cellulose (Karim and Afrin, 2017; Smith et al., 2017). High liquid absorption capacity, high crystallinity index, high surface area, porous structure, and mechanical stability are some of the advantages of bacterial cellulose. Bacterial cellulose is a biomaterial that draws attention in many areas such as food, cosmetics, biomedical, pharmaceutical industry, textile, thanks to its biocompatibility and high purity level due to its absence of contaminants (such as hemicellulose and lignin). It is also very important in terms of biological implants, hemostatic agents, and scaffolds developed in tissue engineering. In addition, bacterial cellulose nanocomposites are used in the development of high-strength membranes and as a reinforcement for polymer nanocomposites (Dugan et al., 2013; Khan et al., 2020; Troncoso and Torres, 2020).

12.3 Types of nanocellulose

Cellulose nanomaterials have at least one dimension in the nanometer range and are derived from cellulosic biomass. Two main types of nanoscale particles can be identified. The basic steps in the preparation of cellulose nanocrystals and microfibrillated cellulose (MFC) called cellulose nanofibrils are shown in Fig. 12.3 (Lavoine et al., 2012). The rod-like, CNCs (Anglès and Dufresne, 2000; Fleming et al., 2000; Habibi et al., 2008; Kvien et al., 2005; Samir et al., 2004; Siqueira et al., 2009) are obtained by acid hydrolysis and can disperse stably in water. CNFs (Agoda-Tandjawa et al., 2010; Hassan et al., 2011; Saito et al., 2006), which are produced successive high-shear mechanical treatment of the cellulosic source and still display both crystalline and disordered regions. Owing to their nanoscale dimension, semicrystalline nature, and renewable origin, CNFs have unique properties and are a more flexible type of cellulose particles.

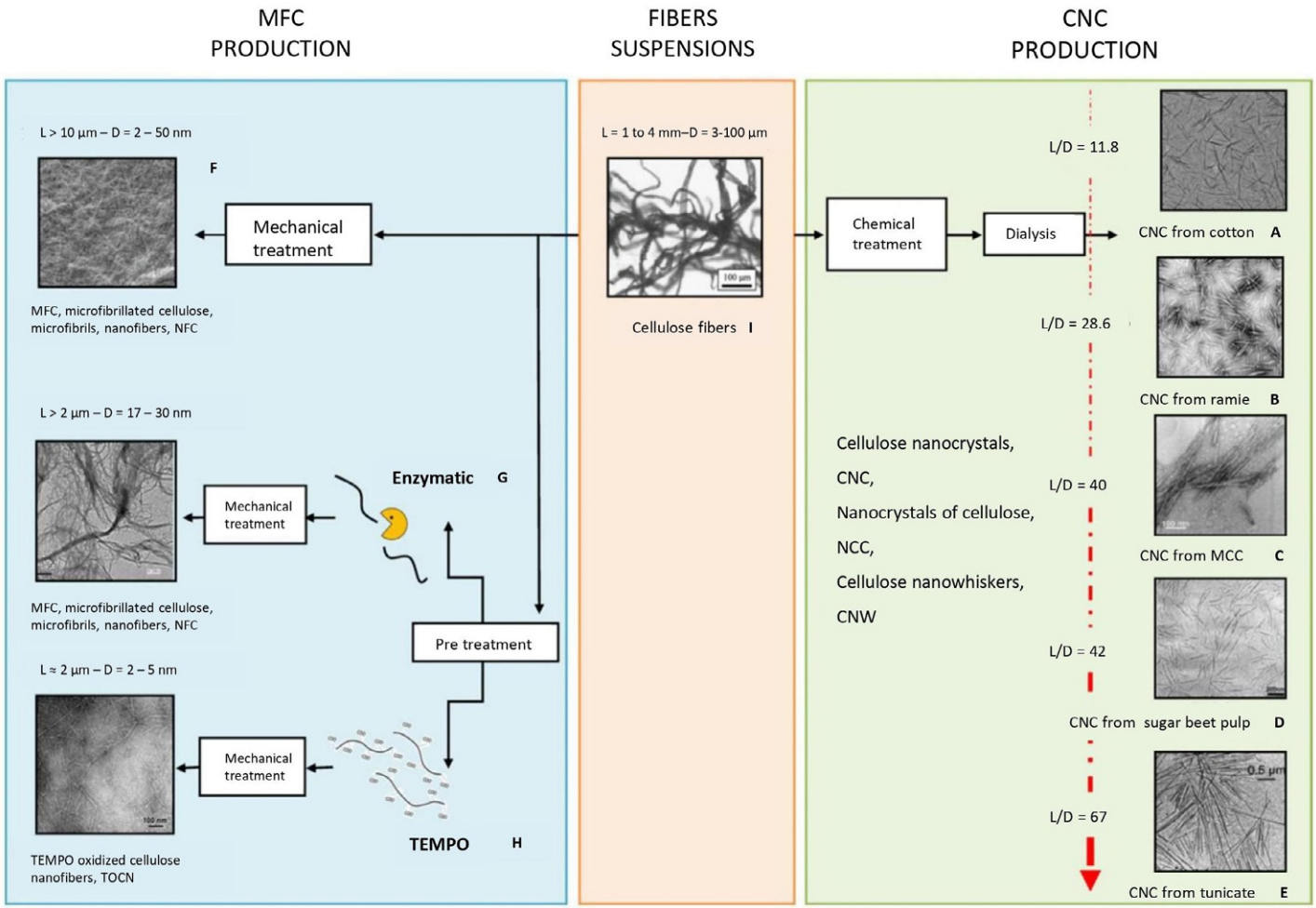

FIG. 12.3 Production routes of CNCs and CNFs from cellulosic biomass (Lavoine et al., 2012). (A) Fleming et al. (2000), (B) Habibi et al. (2008), (C) Kvien et al. (2005), (D) Samir et al. (2004), (E) Anglès and Dufresne (2000), (F) Siqueira et al. (2009), (G) Hassan et al. (2011), (H) Saito et al. (2006), and (I) Agoda-Tandjawa et al. (2010).

12.3.1 Cellulose nanocrystals (CNCs)

Nanocellulose can be classified based on its size and structure. The size range of the cellulose microcrystal (CMC) and cellulose microfiber is between 10 and 100 μm, while the size range of the nanostructured cellulose such as cellulose nanocrystal (CNC) and cellulose nanofiber (CNF) is 1–50 nm (Kargarzadeh et al., 2017). A few other terms are also presented for CNC such as cellulose nanowhisker (CNW) and nanocrystalline cellulose (NCC). CNC is less flexible than CNF because of its higher crystallinity. This is because CNCs have a long rod-like shape consisting of crystalline regions isolated from CNFs (Kargarzadeh et al., 2017). Its assembly occurs through a series of modifications, starting with the excision of amorphous regions in CNFs to isolate crystal regions that are today classified as CNC. Chemical treatment is used as the main treatment method in CNC extraction. Traditionally, it is carried out using concentrated acid through acid digestion before further processing methods (García et al., 2016). Unlike mechanical disintegration, acid hydrolysis destroys the noncrystalline amorphous region in microfibrils, leaving the crystalline regions intact. Liu et al. (2014) reported that CNC obtained through sulphuric acid hydrolysis by $-SO_3^{-2}$ functional group has shown superior Ag(I) adsorption capacity than CNC obtained via mechanical grinding. Acid hydrolysis is also widely used to produce bacterial nanocrystals from bacterial cellulose microfibrils (Börjesson and Westman, 2015).

12.3.2 Cellulose nanofibrils (CNFs)

Nanofibrillated cellulose, nanofibrillar cellulose, nanofibrous cellulose, and bacterial nanocellulose (BC) are various terms that have been used alternatively with cellulose nanofibrils (CNFs) which is comprised of stretched masses of elementary nanofibrils with alternating crystalline and amorphous domains. The plant cell wall must be subjected to strong mechanical disintegration before turning the fibers, whose diameter is within the range of 10–100 nm depending on the disintegration power, into CNF (Kargarzadeh et al., 2017).

BC, one of the purest forms of cellulose, is the only cellulose synthesized in a bottom-up approach through enzymatic synthesis. BC is produced by non-photosynthetic organisms through enzymatic polymerization of organic substrates (glycerol and sugar) (Gama et al., 2012; Mahfoudhi and Boufi, 2017). BC is known for its high purity among the various types of CNFs as well as its high water holding capacity and crystallinity (80%–90%). The main difference between BC and CNFs derived from other plants is that BC does not have certain functional groups (except alcohol) and polymers such as lignin, hemicellulose, and pectin (Nechyporchuk et al., 2016).

The occurrence of fiber breakdown during the mechanical breakdown of dry cellulose pulp tends to produce nanocellulose with poor mechanical properties. For better delamination of nanofibrils, an aqueous medium is used during mechanical disintegration to loosen the hydrogen bonds between fibers and prevent reverse coalescence or fibril aggregation (Nechyporchuk et al., 2016). Homogenization (Abdul Khalil et al., 2014), grinding (He et al., 2018; Omran et al., 2021), and refining (Sacui et al., 2014) are examples of techniques commonly used for efficient delamination of cellulosic fibers. Mechanically disintegrated nanocellulose is aggregated with larger dimensions, unlike finely structured or short rod-like nanocelluloses produced through chemical pretreatment (Sacui et al., 2014).

In the next step of mechanical disintegration to aid in the delamination of nanofibrils, chemical techniques such as acid hydrolysis (Vanderfleet et al., 2019), carboxylation (Mendoza et al., 2019), carboxymethylation (Wei et al., 2021), quaternization (Chen et al., 2017), sulfonation (Rocha et al., 2018), ionic liquid (Menezes et al., 2021) and reactive eutectic media (Jaekel et al., 2021) are used to prepare nanocellulose. These techniques (carboxylation, carboxymethylation, sulfonation, and quaternization, etc.) based on the principle of electrostatic repulsion between similar charges are used to provide anionic functionality to assist cellulose fibers defibrillation (Nechyporchuk et al., 2016).

12.4 Environmental and agricultural applications of nanocellulose

The shortage of drinking water and global pollution requires the development of highly effective techniques for water purification. Since various pollutants such as dyes, heavy metals, pesticides, herbicides, and other industrial and agricultural wastes cause adverse effects on human health and the environment, their removal from wastewater is critical. Today, water contaminated with dye, which is a result of the widespread use of organic dyes in different sectors such as textile, food, paper and pulp, cosmetics, paint, leather, and medicine, has become a serious environmental problem (Hou et al., 2020). Because most of the dyes are resistant to microbial degradation and are photolytic stable, their effective removal from water is difficult compared to conventional water treatment methods (Ahmad et al., 2020).

Adsorption is one of the most effective traditional biological, chemical, and physical dye removal methods (Ruan et al., 2019). Cellulose nanocrystals (CNCs) are the resulting crystalline portion of cellulose nanofibrils (CNFs) after removing the amorphous region through acid hydrolysis or depolymerization. High crystallinity CNCs have a large surface area and exhibit excellent thermal stability and high strength (Tan et al., 2020). Since Auramine O (AO), the organic cationic dye, is toxic, it is critical to remove it before discharging into the environment. Anionic forms (sulfated and carboxylated) of colloidal CNCs have been used as nanoadsorbents for effective removal of cationic toxic AO by Pinto et al. (2020). Fig. 12.4 shows the adsorption of Auramine O, the cationic dye, on CNCs (Pinto et al., 2020).

Magnetically functionalized cellulose nanocrystal-based (MCNCs) hydrogels have been used as nanoadsorbent with a great capacity for the selective removal of cationic dyes such as crystal violet (CV), methylene blue, congo red, and methyl orange (Moharrami and Motamedi, 2020). As a novel adsorbent, Oyewo et al. reported sawdust-based CNCs incorporated with ZnO which was used to remove methylene blue from water (Oyewo et al., 2020). Using 0.15 g of the nanocomposite, methylene blue was removed with a maximum adsorption percentage of 97.5%. Chitosan-based composite membranes fabricated using CNCs for water purification were successfully used to remove positively charged dyes such as Victoria Blue 2B, Methyl Violet 2B, and Rhodamine 6G at 98%, 84%, and 70%, respectively, as shown in Fig. 12.5 (Karim et al., 2014).

The difference of BC from CNF and CNC is that it does not contain components in lignocellulose biomass other than cellulose and therefore can be produced with the highest purity among different types of nanocellulose. BC, a renewable natural nanomaterial, has fascinating properties such as exceptional mechanical properties, porosity, water absorbency,

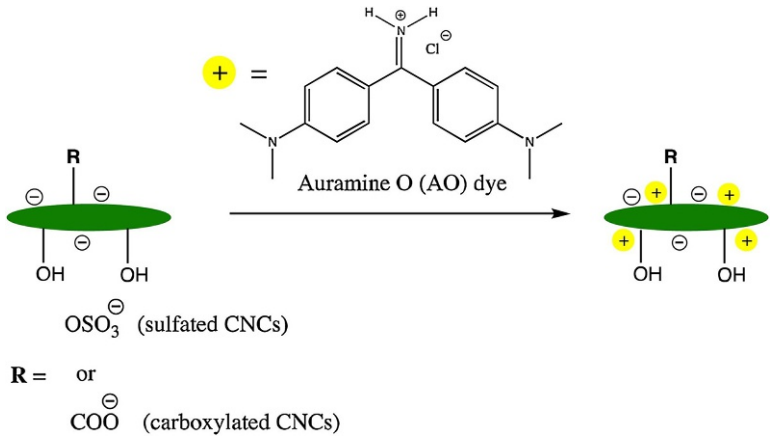

FIG. 12.4 Adsorption of Auramine O, the cationic dye, on CNCs (Pinto et al., 2020).

moldability, biodegradability, and excellent biological affinity. BC's application as an environmentally friendly filter material is recommended. Recently, the selectivity and molecular weight cutoff of BC have been enhanced by adding different components. The resulting BC-based composites are water-stable and exhibit improved properties such as good mechanical strength and selective ion permeability. These properties make BC-based composites a promising material for water purification. Large quantities of highly toxic organic dyes present in industrial wastewaters cause persistent challenges in wastewater treatment processes. BC-GO composites containing palladium NPs used for wastewater filtration led to outstanding efficiency by removing up to 99.3% of methylene orange dye and other contaminants, such as methylene blue or 4-nitrophenol (Xu et al., 2018).

BC has a unique micro-nano-porous three-dimensional network that facilitates the penetration of various metal ions (Hu et al., 2014). The in-situ preparation of BC nanocomposites containing metal ions is shown in Fig. 12.6.

BC-CS composite has proven to be useful in removing up to 50% of heavy metal ion copper from suspensions with a concentration of 50 mg/L. Fig. 12.7 shows the changes in the aspect and color of the membranes before and after the Cu^{2+} absorption tests and even after the EDTA treatment used for desorption (Urbina et al., 2018).

Denizli's group prepared molecularly imprinted BC nanofibers for biomedical (Göktürk et al., 2018; Saylan et al., 2020; Tamahkar et al., 2019) and environmental (Derazshamshir et al., 2020; Tamahkar et al., 2018) applications. Phenols are toxic in the aquatic environment and lead to the death of aquatic organisms, and are also carcinogenic to humans. Derazshamshir et al. prepared molecularly imprinted bacterial cellulose nanofibers for selective and efficient removal of phenol from wastewaters with an adsorption capacity of 146 mg/g (Derazshamshir et al., 2020). In another study, Tamahkar et al. selectively removed Hg^{2+} by preparing Cibacron Blue F3GA attached BC nanofibers with an adsorption capacity of 928 mg/g (Tamahkar et al., 2018).

Parameters affecting the adsorption capacities of Cu(II) and Pb(II) ions onto diethylenetriamine-bacterial cellulose (EABC) such as contact time, solution pH, and initial

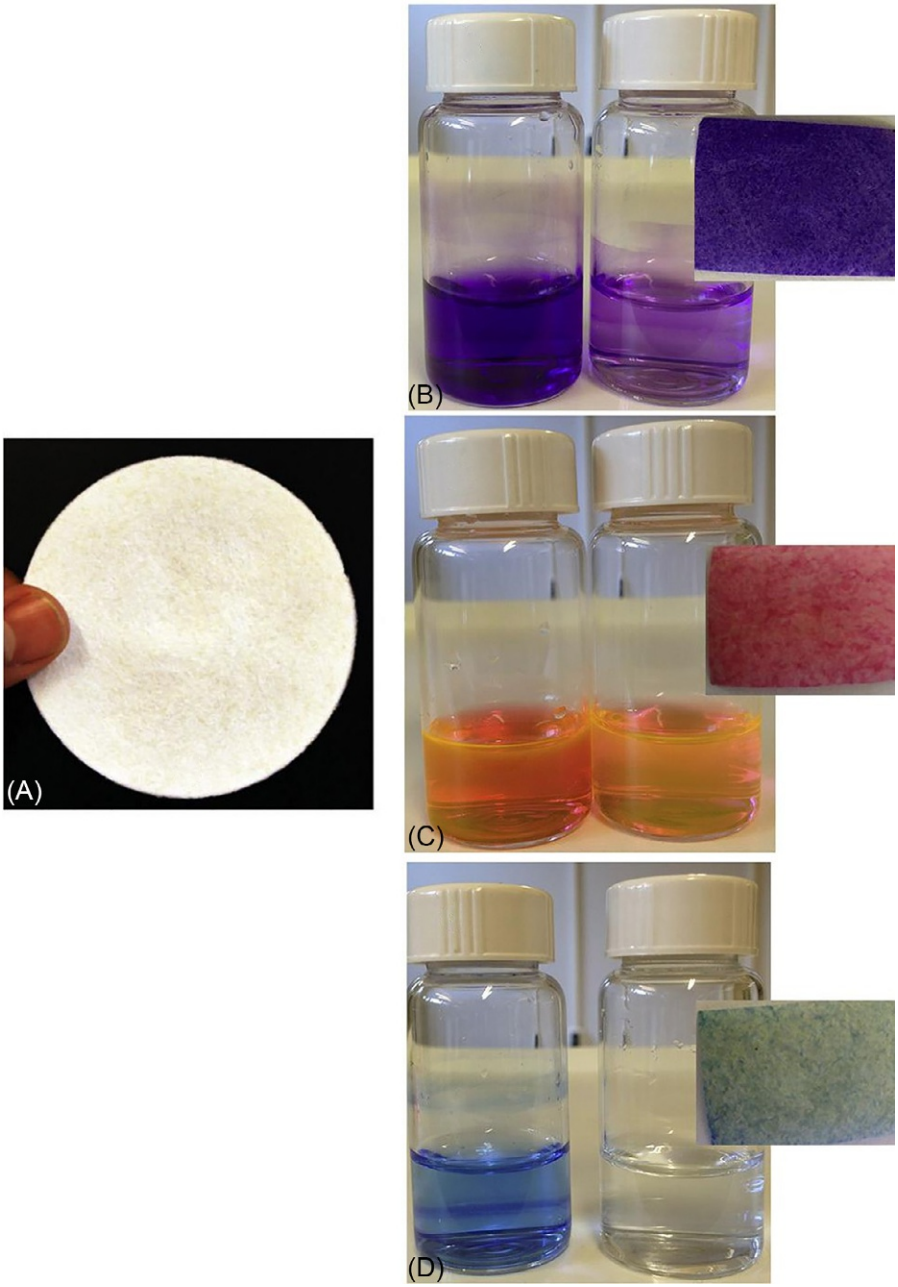

FIG. 12.5 Efficiency of the cross-linked composite membrane in dye removal (A) Membrane photograph; water before and after adsorption test for (B) Methyl Violet, (C) Rhodamine 6G, and (D) Victoria Blue (Karim et al., 2014).

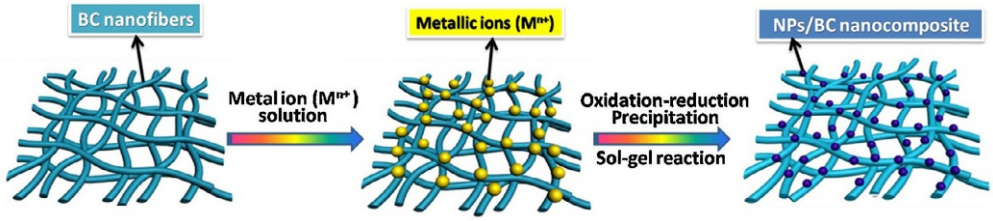

FIG. 12.6 The in-situ preparation of nanoparticles/BC nanocomposites (Hu et al., 2014).

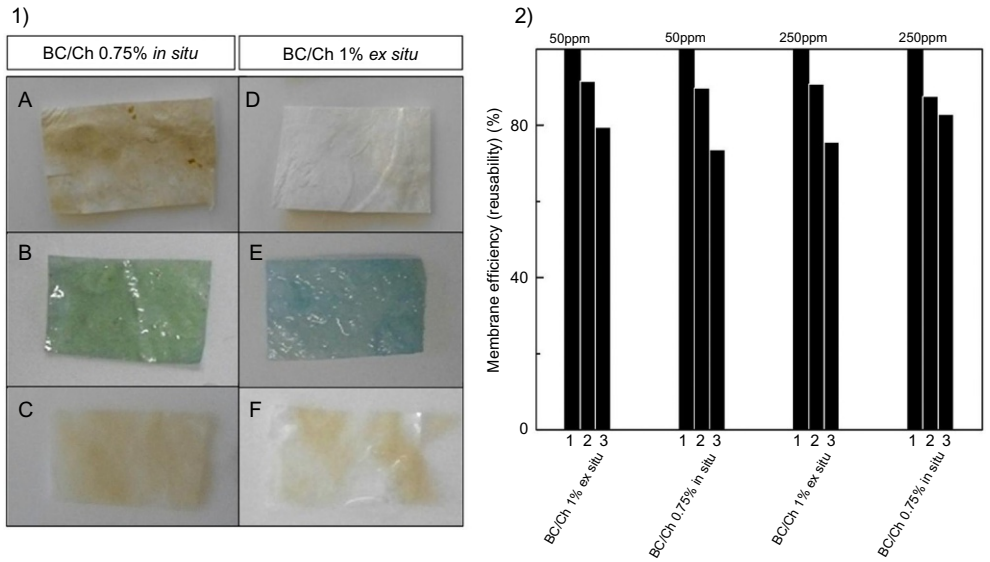

FIG. 12.7 (A and D) Membranes before immersion, (B and E) membranes after 24 h immersion in 250 mg L^{-1} Cu^{2+}, and (C and F) membranes after 24 h immersion in EDTA solutions. (2) Efficiency of bionanocomposites in removing Cu^{2+} ions after two regeneration cycles (Urbina et al., 2018).

metal ions concentration were investigated by Shen et al. (2009). The main sources of Cr(VI), which has high toxicity and carcinogenicity, are leather tanning, plating, water cooling, textile, metal, and other chemical industries (Geng et al., 2019). Cr(VI) is 500–1000 times more toxic than Cr(III) (Ding et al., 2018), and the removal of Cr ions from aqueous environments is performed by using techniques including chemical precipitation, flotation, reduction, ion exchange, electrodialysis, solvent extraction, biosorption, membrane separation, and adsorption. Biomass-based adsorbents are widely accepted due to their biodegradability and environmental friendliness. Cellulose having well-defined architectures with abundant hydroxyl groups for chemical modifications is a perfect biological raw material and can be used as matrix materials for adsorption studies (Vega et al., 2015). Xue designed a cellulose-based solid amine adsorbent to remove Cr(VI) ions (Xue et al., 2019). Jamshaid et al. overviewed cellulose-based materials to highlight cellulose's role in wastewater treatment. They also discussed the

cellulose modification effects (cellulose gels, cellulose composites, cellulose derivatives, functionalized cellulose, and nanocrystalline cellulose) on the heavy metals adsorption capacity (Jamshaid et al., 2017).

Lead pollutes the environment as a result of activities such as the use of leaded gasoline, lead-acid batteries, paints, and electronic devices, as well as refining and mining. If the permissible limit of 0.05 mg/L lead concentration in water is exceeded, adverse health effects such as cognitive impairment, behavioral disorders, kidney damage, anemia, and toxicity to the reproductive system will occur. Shoukat and coworkers prepared titanium oxide-bacterial cellulose-based bioadsorbent and used it to remove lead ions from an aqueous solution (Shoukat et al., 2019).

CNFs production from woody cellulosic materials of plants is carried out using mechanical methods such as high-pressure homogenization, microfluidization, grinding, and ultrasonication. CNFs coatings on the scaffold or the membrane are constructed to improve the water permeability by increasing the hydrophilicity of the membrane and increasing the surface area/volume ratio. They are used for pollutant removal by changing the surface chemistry of the CNFs membrane through electrostatic interaction, size exclusion, or combined mechanisms. Ao et al. reported graphene (GO) coated CNF membrane. The hybrid membrane was capable of separating a variety of oily solutions even under harsh conditions such as extreme acidity, alkalinity, and salinity. Fig. 12.8 shows the GO@CNF membrane preparation and the separation basis for the oil/water mixtures (Ao et al., 2017). Liu et al. coated the CNF membrane with an ultra-thin GO layer to create the negatively charged matrix content and used it in the dye solution filtration (Liu et al., 2019).

Treatment of water containing low concentration levels of radioactive waste is critical and challenging. BC membrane was used to remove Sr^{2+} by Cheng et al. (2019). Carbon dioxide and methane, the most important greenhouse gases that are continuously released into the atmosphere, must be captured and separated to reduce harmful effects. Ahmadi et al. fabricated novel and low-cost nanoadsorbents successfully using cotton pulp, jute, and kenaf as carbon fibrils. The carbonization process of cotton pulp, jute, and kenaf as carbon fibrils were applied at 600 °C to obtain a micro-mesoporous structure for superior CO_2 adsorption and

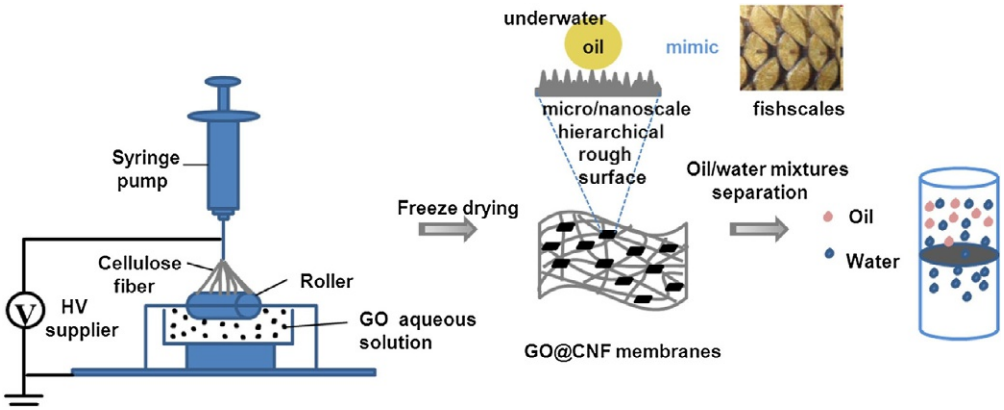

FIG. 12.8 GO@CNF membrane preparation and the separation basis of the oil/water mixtures (Ao et al., 2017).

TABLE 12.2 Cellulose-based adsorbents used for various types of inorganic and organic pollutants.

Biopolymer adsorbent	Pollutants	Adsorption capacity	References
BC-MIP nanofibers	Phenol	146 mg/g	Derazshamshir et al. (2020)
BC–CB nanofibers	Hg^{2+}	928 mg/g	Tamahkar et al. (2018)
Modified nanocellulose coir	V(V) Cr(III)	32.88 mg/g 114 mg/g	Daniel et al. (2021)
Au-CNC composite	Hg(II)	0.13 mmol/g	Mohammed et al. (2016a)
FeNP-modified CNF	As(V)	2.46 mmol/g	Hokkanen et al. (2015)
Alg-TPC-CNF	Cu^{2+} Pb^{2+} Mg^{2+} Fe^{2+}	62.4 mg/g 68.2 mg/g 82.9 mg/g 230.3 mg/g	Abou-Zeid et al. (2021)
CNC/alginate hydrogels	Methylene blue	255.5 mg/g	Mohammed et al. (2016b)
CCNF	Methylene blue	192–430 mg/g	Luo et al. (2020)
Oleic acid and Fe_3O_4 functionalized CNF	Cyclohexane Ethyl acetate Vacuum pump oil	68 g/g 56 g/g 33 g/g	Gu et al. (2020)
Silylated cellulose nanocrystals and red mud aerogel	Cashew oil	33–36 mg/g	Zhu et al. (2018)

CO_2/CH_4 separation (Ahmadi et al., 2020). Cellulose-based composite adsorbents recently developed for wastewater treatment were listed in Table 12.2 (Abou-Zeid et al., 2021; Daniel et al., 2021; Derazshamshir et al., 2020; Gu et al., 2020; Hokkanen et al., 2015; Luo et al., 2020; Mohammed et al., 2016a, b; Tamahkar et al., 2018; Zhu et al., 2018).

The continuous increase of the population and global climate changes cause problems in the quantity and quality of the food produced (Cheng et al., 2018; Di Martino et al., 2021), together with the increase in the demand for food and water. The slow release of agrochemicals is important for the agricultural field and the environment to reduce the quantity of agrochemical and its usage causing environmental pollution. Controlled-release fertilizers have become a potential solution to synchronize nutrient release according to the needs of plants (Lawrencia et al., 2021).

Nanocellulose can be used to produce superabsorbent hydrogels through chemical and/or mechanical processes. Superabsorbent hydrogels act as water and nutrient reservoirs when applied in agricultural fields as soil amendments. Recent developments in agricultural waste-derived nanocellulose-based superabsorbent hydrogels considering their potentials applications such as reducing irrigation, improving crop production, and enhancing nutrient retention are reviewed by Li and Chen (2020).

Bortolin et al. synthesized PAAm/methylcellulose/montmorillonite hydrogel nanocomposite to be used as a carrier vehicle in the controlled release of urea fertilizer. They

reported that cellulose-based hydrogel nanocomposite was the first carrier vehicle to release 90 g of urea per gram of dry hydrolyzed hydrogel (Bortolin et al., 2013). Recently, Bauli et al. reported CMC hydrogels which are produced via chemical crosslinking with citric acid and then filled with nanocellulose, montmorillonite, and different amounts vermiculite as illustrated in Fig. 12.9 (Bauli et al., 2021). NPK fertilizer added to the formulations showed that the NPK encapsulation was achieved successfully. Vermiculite presented slight water absorbency and fast nutrient release.

12.5 Conclusion and future outlook

Efforts to develop environmentally friendly materials have increased recently due to the increasing need for renewable, sustainable, available, and non-toxic properties of adsorbents. The use of wood material to meet this need appears as a realistic and sustainable solution. The use of nanocelluloses for the development and production of new generation materials is an innovative solution. Nanocellulose-based materials are widely used in areas such as food quality control, environment, and bioprocess control, biological defense, and agriculture. In this chapter, studies conducted in the literature together with nanocellulose and its types and their use in environmental and agricultural applications are summarized.

The usefulness and characteristics of nanocellulose as an adsorbent in the remediation of chemical pollutants are a promising and exciting area of current and future research. Enhancing the adsorption capacity of nanocellulose against a wide range of chemical contaminants, including heavy metals, dyes, and organic oils, by functionalizing them using various functional groups is a key factor for success. Nanocellulose-based adsorbents are widely used for water recovery from dirty water sources. However, the available fabrication materials and additives limit their separation performance and strength. Biodegradable and low-cost nanocellulose has been widely used in the last decade, so information on nanocellulose and nanocellulose-based adsorbents synthesized in different ways is provided in this chapter.

Cellulose nanofibrils, cellulose nanocrystals, and bacterial nanocellulose have different structures and properties. Nanocellulose can be chemically modified to increase surface affinity and reactivity and be used as an adsorbent to effectively remove certain contaminants. The incorporation of inorganic nanomaterials allows obtaining nanocellulose-based adsorbents with more functionality. A growing number of research groups have reported their research on the formation and use of fibril or crystalline celluloses within nanometer range widths.

Production of NCC is carried out by removing amorphous parts of crystalline cellulose by acid hydrolysis. BC is the third variant of nanocellulose prepared from *Gluconacetobacter* genus bacteria, unlike NCC prepared from cellulose sources. In situ BC fabrication provides unique possibilities for shape control, nanofibril network, and composite formation.

The development rate of the areas where nanocellulose is used will increase even more. Research and development groups aim to establish production facilities by creating new pilot processes. Thus, larger-scale technical products can be produced and new medical devices can be developed. Science and technology are moving toward the widespread use of renewable raw materials and environmentally friendly and sustainable resources and processes.

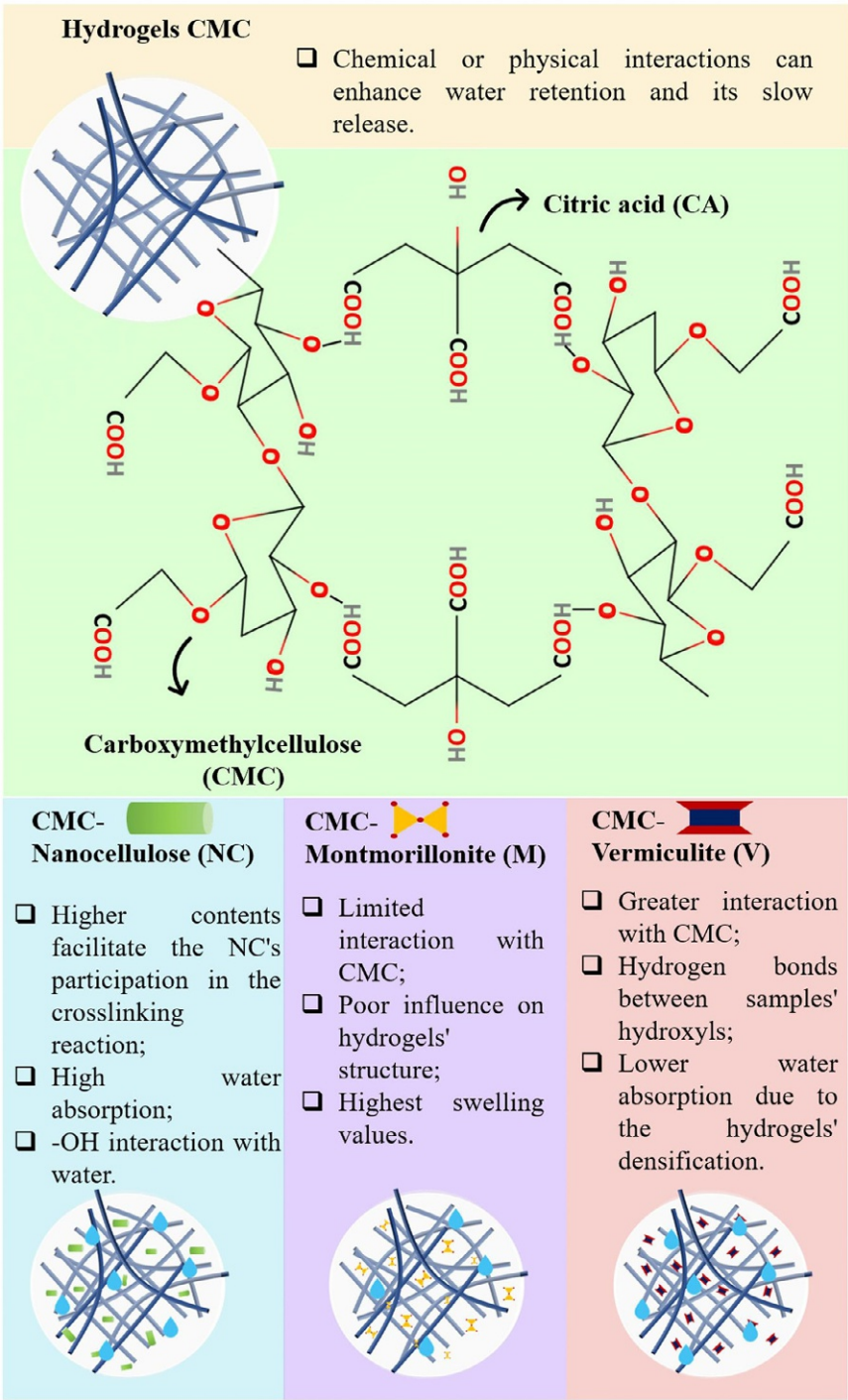

FIG. 12.9 Schematic representation CMC-nanocellulose, CMC-montmorillonite, and CMC-vermiculite with water absorption results (Bauli et al., 2021).

References

Abdul Khalil, H.P.S., Davoudpour, Y., Islam, M.N., Mustapha, A., Sudesh, K., Dungani, R., Jawaid, M., 2014. Production and modification of nanofibrillated cellulose using various mechanical processes: a review. Carbohydr. Polym. 99, 649–665. https://doi.org/10.1016/j.carbpol.2013.08.069.

Abou-Zeid, R.E., Ali, K.A., Gawad, R.M.A., Kamal, K.H., Kamel, S., Khiari, R., 2021. Removal of cu(II), pb(II), mg(II), and fe(II) by adsorption onto alginate/nanocellulose beads as bio-sorbent. J. Renew. Mater. 9 (4), 601–613. https://doi.org/10.32604/jrm.2021.014005.

Abraham, E., Deepa, B., Pothan, L.A., Jacob, M., Thomas, S., Cvelbar, U., Anandjiwala, R., 2011. Extraction of nanocellulose fibrils from lignocellulosic fibres: a novel approach. Carbohydr. Polym. 86 (4), 1468–1475. https://doi.org/10.1016/j.carbpol.2011.06.034.

Agoda-Tandjawa, G., Durand, S., Berot, S., Blassel, C., Gaillard, C., Garnier, C., Doublier, J.L., 2010. Rheological characterization of microfibrillated cellulose suspensions after freezing. Carbohydr. Polym. 80 (3), 677–686. https://doi.org/10.1016/j.carbpol.2009.11.045.

Ahmad, A., Khan, N., Giri, B.S., Chowdhary, P., Chaturvedi, P., 2020. Removal of methylene blue dye using rice husk, cow dung and sludge biochar: characterization, application, and kinetic studies. Bioresour. Technol. 306. https://doi.org/10.1016/j.biortech.2020.123202.

Ahmadi, R., Ardjmand, M., Rashidi, A., Rafizadeh, M., 2020. High performance novel nanoadsorbents derived—natural cellulose fibers for superior CO2 adsorption and CO2/CH4 separation. Energy Sources Pt A, 1–19. https://doi.org/10.1080/15567036.2020.1845878.

Anglès, M.N., Dufresne, A., 2000. Plasticized starch/tunicin whiskers nanocomposites. 1. Structural analysis. Macromolecules 33 (22), 8344–8353. https://doi.org/10.1021/ma0008701.

Ao, C., Yuan, W., Zhao, J., He, X., Zhang, X., Li, Q., Xia, T., Zhang, W., Lu, C., 2017. Superhydrophilic graphene oxide@electrospun cellulose nanofiber hybrid membrane for high-efficiency oil/water separation. Carbohydr. Polym. 175, 216–222. https://doi.org/10.1016/j.carbpol.2017.07.085.

Bauli, C.R., Lima, G.F., de Souza, A.G., Ferreira, R.R., Rosa, D.S., 2021. Eco-friendly carboxymethyl cellulose hydrogels filled with nanocellulose or nanoclays for agriculture applications as soil conditioning and nutrient carrier and their impact on cucumber growing. Colloids Surf. A Physicochem. Eng. Asp. 623, 126771. https://doi.org/10.1016/j.colsurfa.2021.126771.

Blanco Parte, F.G., Santoso, S.P., Chou, C.C., Verma, V., Wang, H.T., Ismadji, S., Cheng, K.C., 2020. Current progress on the production, modification, and applications of bacterial cellulose. Crit. Rev. Biotechnol. 40 (3), 397–414. https://doi.org/10.1080/07388551.2020.1713721.

Börjesson, Westman, G., 2015. Crystalline nanocellulose—preparation, modification, and properties. In: Cellulose—Fundamental Aspects and Current Trends., https://doi.org/10.5772/61899.

Bortolin, A., Aouada, F.A., Mattoso, L.H.C., Ribeiro, C., 2013. Nanocomposite PAAm/methyl cellulose/montmorillonite hydrogel: evidence of synergistic effects for the slow release of fertilizers. J. Agric. Food Chem. 61 (31), 7431–7439. https://doi.org/10.1021/jf401273n.

Buzea, C., Pacheco, I.I., Robbie, K., 2007. Nanomaterials and nanoparticles: sources and toxicity. Biointerphases, MR17–MR71. https://doi.org/10.1116/1.2815690.

Campano, C., Merayo, N., Balea, A., Tarrés, Q., Delgado-Aguilar, M., Mutjé, P., Negro, C., Blanco, Á., 2018. Mechanical and chemical dispersion of nanocelluloses to improve their reinforcing effect on recycled paper. Cellulose 25 (1), 269–280. https://doi.org/10.1007/s10570-017-1552-y.

Chen, D., Lawton, D., Thompson, M.R., Liu, Q., 2012. Biocomposites reinforced with cellulose nanocrystals derived from potato peel waste. Carbohydr. Polym. 90 (1), 709–716. https://doi.org/10.1016/j.carbpol.2012.06.002.

Chen, Y.W., Lee, H.V., Juan, J.C., Phang, S.M., 2016. Production of new cellulose nanomaterial from red algae marine biomass Gelidium elegans. Carbohydr. Polym. 151, 1210–1219. https://doi.org/10.1016/j.carbpol.2016.06.083.

Chen, Y., Liu, H., Geng, B., Ru, J., Cheng, C., Zhao, Y., Wang, L., 2017. A reusable surface-quaternized nanocellulose-based hybrid cryogel loaded with N-doped TiO2 for self-integrated adsorption/photo-degradation of methyl orange dye. RSC Adv. 7 (28), 17279–17288. https://doi.org/10.1039/c7ra00450h.

Cheng, D., Liu, Y., Yang, G., Zhang, A., 2018. Water- and fertilizer-integrated hydrogel derived from the polymerization of acrylic acid and urea as a slow-release N fertilizer and water retention in agriculture. J. Agric. Food Chem. 66 (23), 5762–5769. https://doi.org/10.1021/acs.jafc.8b00872.

Cheng, R., Kang, M., Zhuang, S., Shi, L., Zheng, X., Wang, J., 2019. Adsorption of Sr(II) from water by mercerized bacterial cellulose membrane modified with EDTA. J. Hazard. Mater. 364, 645–653. https://doi.org/10.1016/j.jhazmat.2018.10.083.

Čolić, M., Tomić, S., Bekić, M., 2020. Immunological aspects of nanocellulose. Immunol. Lett. 222, 80–89. https://doi.org/10.1016/j.imlet.2020.04.004.

Daniel, A.B., Zahir, E., Asghar, M.A., 2021. Remediation of vanadium (V) and chromium (III) ions from aqueous media by modified nanocellulose obtained from coconut coir. J. Macromol. Sci., 1–21. https://doi.org/10.1080/00222348.2020.1870300.

De Souza Lima, M.M., Borsali, R., 2004. Rodlike cellulose microcrystals: structure, properties, and applications. Macromol. Rapid Commun. 25 (7), 771–787. https://doi.org/10.1002/marc.200300268.

Derazshamshir, A., Göktürk, I., Tamahkar, E., Yılmaz, F., Sağlam, N., Denizli, A., 2020. Phenol removal from wastewater by surface imprinted bacterial cellulose nanofibres. Environ. Technol. 41 (24), 3134–3145. https://doi.org/10.1080/09593330.2019.1600043.

Di Martino, A., Khan, Y.A., Durpekova, S., Sedlarik, V., Elich, O., Cechmankova, J., 2021. Ecofriendly renewable hydrogels based on whey protein and for slow release of fertilizers and soil conditioning. J. Clean. Prod., 285. https://doi.org/10.1016/j.jclepro.2020.124848.

Ding, J., Pu, L., Wang, Y., Wu, B., Yu, A., Zhang, X., Pan, B., Zhang, Q., Gao, G., 2018. Adsorption and reduction of Cr(VI) together with Cr(III) sequestration by polyaniline confined in pores of polystyrene beads. Environ. Sci. Technol. 52 (21), 12602–12611. https://doi.org/10.1021/acs.est.8b02566.

Dugan, J.M., Gough, J.E., Eichhorn, S.J., 2013. Bacterial cellulose scaffolds and cellulose nanowhiskers for tissue engineering. Nanomedicine 8 (2), 287–298. https://doi.org/10.2217/nnm.12.211.

Fardioui, M., Qaiss, A.E.K., Bouhfid, R., 2017. Cellulose nanocrystal-based nanocomposites. In: Cellulose-Reinforced Nanofibre Composites: Production, Properties and Applications. Elsevier Inc, pp. 373–389, https://doi.org/10.1016/B978-0-08-100957-4.00016-4.

Farooq, A., Patoary, M.K., Zhang, M., Mussana, H., Li, M., Naeem, M.A., Mushtaq, M., Farooq, A., Liu, L., 2020. Cellulose from sources to nanocellulose and an overview of synthesis and properties of nanocellulose/zinc oxide nanocomposite materials. Int. J. Biol. Macromol. 154, 1050–1073. https://doi.org/10.1016/j.ijbiomac.2020.03.163.

Fleming, K., Gray, D., Prasannan, S., Matthews, S., 2000. Cellulose crystallites: a new and robust liquid crystalline medium for the measurement of residual dipolar couplings. J. Am. Chem. Soc. 122 (21), 5224–5225. https://doi.org/10.1021/ja000764e.

Gama, M., Gatenholm, P., Klemm, D., 2012. Bacterial Nanocellulose: A Sophisticated Multifunctional Material. CRC Press, pp. 1–304.

García, A., Gandini, A., Labidi, J., Belgacem, N., Bras, J., 2016. Industrial and crop wastes: a new source for nanocellulose biorefinery. Ind. Crop Prod. 93, 26–38. https://doi.org/10.1016/j.indcrop.2016.06.004.

Geng, J., Yin, Y., Liang, Q., Zhu, Z., Luo, H., 2019. Polyethyleneimine cross-linked graphene oxide for removing hazardous hexavalent chromium: adsorption performance and mechanism. Chem. Eng. J. 361, 1497–1510. https://doi.org/10.1016/j.cej.2018.10.141.

Göktürk, I., Tamahkar, E., Yılmaz, F., Denizli, A., 2018. Protein depletion with bacterial cellulose nanofibers. J. Chromatogr. B 1099, 1–9. https://doi.org/10.1016/j.jchromb.2018.08.030.

Gu, H., Zhou, X., Lyu, S., Pan, D., Dong, M., Wu, S., Ding, T., Wei, X., Seok, I., Wei, S., Guo, Z., 2020. Magnetic nanocellulose-magnetite aerogel for easy oil adsorption. J. Colloid Interface Sci. 560, 849–856. https://doi.org/10.1016/j.jcis.2019.10.084.

Habibi, Y., Goffin, A.L., Schiltz, N., Duquesne, E., Dubois, P., Dufresne, A., 2008. Bionanocomposites based on poly (ε-caprolactone)-grafted cellulose nanocrystals by ring-opening polymerization. J. Mater. Chem. 18 (41), 5002–5010. https://doi.org/10.1039/b809212e.

Hassan, M.L., Hassan, E.A., Oksman, K.N., 2011. Effect of pretreatment of bagasse fibers on the properties of chitosan/microfibrillated cellulose nanocomposites. J. Mater. Sci. 46 (6), 1732–1740. https://doi.org/10.1007/s10853-010-4992-4.

He, M., Yang, G., Chen, J., Ji, X., Wang, Q., 2018. Production and characterization of cellulose nanofibrils from different chemical and mechanical pulps. J. Wood Chem. Technol. 38 (2), 149–158. https://doi.org/10.1080/02773813.2017.1411368.

Hiasa, S., Iwamoto, S., Endo, T., Edashige, Y., 2014. Isolation of cellulose nanofibrils from mandarin (Citrus unshiu) peel waste. Ind. Crop Prod. 62, 280–285. https://doi.org/10.1016/j.indcrop.2014.08.007.

Hokkanen, S., Repo, E., Lou, S., Sillanpää, M., 2015. Removal of arsenic(V) by magnetic nanoparticle activated microfibrillated cellulose. Chem. Eng. J. 260, 886–894. https://doi.org/10.1016/j.cej.2014.08.093.
Hou, Y., Yan, S., Huang, G., Yang, Q., Huang, S., Cai, J., 2020. Fabrication of N-doped carbons from waste bamboo shoot shell with high removal efficiency of organic dyes from water. Bioresour. Technol., 303. https://doi.org/10.1016/j.biortech.2020.122939.
Hu, W., Chen, S., Yang, J., Li, Z., Wang, H., 2014. Functionalized bacterial cellulose derivatives and nanocomposites. Carbohydr. Polym. 101 (1), 1043–1060. https://doi.org/10.1016/j.carbpol.2013.09.102.
Jaekel, E.E., Sirviö, J.A., Antonietti, M., Filonenko, S., 2021. One-step method for the preparation of cationic nanocellulose in reactive eutectic media. Green Chem. 23 (6), 2317–2323. https://doi.org/10.1039/d0gc04282j.
Jamshaid, A., Hamid, A., Muhammad, N., Naseer, A., Ghauri, M., Iqbal, J., Rafiq, S., Shah, N.S., 2017. Cellulose-based materials for the removal of heavy metals from wastewater—an overview. ChemBioEng. Rev. 4 (4), 240–256. https://doi.org/10.1002/cben.201700002.
Jasmani, L., Adnan, S., 2017. Preparation and characterization of nanocrystalline cellulose from Acacia mangium and its reinforcement potential. Carbohydr. Polym. 161, 166–171. https://doi.org/10.1016/j.carbpol.2016.12.061.
Jiang, F., Hsieh, Y.L., 2015. Cellulose nanocrystal isolation from tomato peels and assembled nanofibers. Carbohydr. Polym. 122, 60–68. https://doi.org/10.1016/j.carbpol.2014.12.064.
Jiang, F., Han, S., Hsieh, Y.L., 2013. Controlled defibrillation of rice straw cellulose and self-assembly of cellulose nanofibrils into highly crystalline fibrous materials. RSC Adv. 3 (30), 12366–12375. https://doi.org/10.1039/c3ra41646a.
Johar, N., Ahmad, I., Dufresne, A., 2012. Extraction, preparation and characterization of cellulose fibres and nanocrystals from rice husk. Ind. Crop Prod. 37 (1), 93–99. https://doi.org/10.1016/j.indcrop.2011.12.016.
Jonoobi, M., Oladi, R., Davoudpour, Y., Oksman, K., Dufresne, A., Hamzeh, Y., Davoodi, R., 2015. Different preparation methods and properties of nanostructured cellulose from various natural resources and residues: a review. Cellulose 22 (2), 935–969. https://doi.org/10.1007/s10570-015-0551-0.
Jozala, A.F., de Lencastre-Novaes, L.C., Lopes, A.M., de Carvalho Santos-Ebinuma, V., Mazzola, P.G., Pessoa-Jr, A., Grotto, D., Gerenutti, M., Chaud, M.V., 2016. Bacterial nanocellulose production and application: a 10-year overview. Appl. Microbiol. Biotechnol. 100 (5), 2063–2072. https://doi.org/10.1007/s00253-015-7243-4.
Jung, K.A., Lim, S.R., Kim, Y., Park, J.M., 2013. Potentials of macroalgae as feedstocks for biorefinery. Bioresour. Technol. 135, 182–190. https://doi.org/10.1016/j.biortech.2012.10.025.
Kang, X., Sun, P., Kuga, S., Wang, C., Zhao, Y., Wu, M., Huang, Y., 2017. Thin cellulose nanofiber from corncob cellulose and its performance in transparent nanopaper. ACS Sustain. Chem. Eng. 5 (3), 2529–2534. https://doi.org/10.1021/acssuschemeng.6b02867.
Kargarzadeh, H., Ioelovich, M., Ahmad, I., Thomas, S., Dufresne, A., 2017. Methods for Extraction of Nanocellulose From Various Sources. Wiley, pp. 1–49, https://doi.org/10.1002/9783527689972.ch1.
Karim, Z., Afrin, S., 2017. Bacterial cellulose: preparation and characterization. In: Cellulose-Reinforced Nanofibre Composites: Production, Properties and Applications. Elsevier Inc, pp. 327–340, https://doi.org/10.1016/B978-0-08-100957-4.00014-0.
Karim, Z., Mathew, A.P., Grahn, M., Mouzon, J., Oksman, K., 2014. Nanoporous membranes with cellulose nanocrystals as functional entity in chitosan: removal of dyes from water. Carbohydr. Polym. 112, 668–676. https://doi.org/10.1016/j.carbpol.2014.06.048.
Keenan, R.J., Reams, G.A., Achard, F., de Freitas, J.V., Grainger, A., Lindquist, E., 2015. Dynamics of global forest area: results from the FAO global forest resources assessment 2015. For. Ecol. Manage. 352, 9–20. https://doi.org/10.1016/j.foreco.2015.06.014.
Keijsers, E.R.P., Yılmaz, G., van Dam, J.E.G., 2013. The cellulose resource matrix. Carbohydr. Polym. 93 (1), 9–21. https://doi.org/10.1016/j.carbpol.2012.08.110.
Khan, H., Kadam, A., Dutt, D., 2020. Studies on bacterial cellulose produced by a novel strain of Lactobacillus genus. Carbohydr. Polym. 229, 115513.
Klemm, D., Heublein, B., Fink, H.P., Bohn, A., 2005. Cellulose: fascinating biopolymer and sustainable raw material. Angew. Chem. Int. Ed. 44 (22), 3358–3393. https://doi.org/10.1002/anie.200460587.
Klemm, D., Kramer, F., Moritz, S., Lindström, T., Ankerfors, M., Gray, D., Dorris, A., 2011. Nanocelluloses: a new family of nature-based materials. Angew. Chem. Int. Ed. 50 (24), 5438–5466. https://doi.org/10.1002/anie.201001273.
Kvien, I., Tanem, B.S., Oksman, K., 2005. Characterization of cellulose whiskers and their nanocomposites by atomic force and electron microscopy. Biomacromolecules 6 (6), 3160–3165. https://doi.org/10.1021/bm050479t.

Lavoine, N., Desloges, I., Dufresne, A., Bras, J., 2012. Microfibrillated cellulose—its barrier properties and applications in cellulosic materials: a review. Carbohydr. Polym. 90 (2), 735–764. https://doi.org/10.1016/j.carbpol.2012.05.026.

Lawrencia, D., Wong, S.K., Low, D.Y.S., Goh, B.H., Goh, J.K., Ruktanonchai, U.R., Soottitantawat, A., Lee, L.H., Tang, S.Y., 2021. Controlled release fertilizers: a review on coating materials and mechanism of release. Plan. Theory 10 (2), 1–26. https://doi.org/10.3390/plants10020238.

Li, S., Chen, G., 2020. Agricultural waste-derived superabsorbent hydrogels: preparation, performance, and socioeconomic impacts. J. Clean. Prod. 251, 119669. https://doi.org/10.1016/j.jclepro.2019.119669.

Li, F., Mascheroni, E., Piergiovanni, L., 2015. The potential of nanocellulose in the packaging field: a review. Packag. Technol. Sci. 28 (6), 475–508. https://doi.org/10.1002/pts.2121.

Liu, P., Sehaqui, H., Tingaut, P., Wichser, A., Oksman, K., Mathew, A.P., 2014. Cellulose and chitin nanomaterials for capturing silver ions (Ag+) from water via surface adsorption. Cellulose 21 (1), 449–461. https://doi.org/10.1007/s10570-013-0139-5.

Liu, P., Zhu, C., Mathew, A.P., 2019. Mechanically robust high flux graphene oxide—nanocellulose membranes for dye removal from water. J. Hazard. Mater. 371, 484–493. https://doi.org/10.1016/j.jhazmat.2019.03.009.

Lu, P., Hsieh, Y.L., 2012. Preparation and characterization of cellulose nanocrystals from rice straw. Carbohydr. Polym. 87 (1), 564–573. https://doi.org/10.1016/j.carbpol.2011.08.022.

Luo, J., Huang, K., Zhou, X., Xu, Y., 2020. Hybrid films based on holistic celery nanocellulose and lignin/hemicellulose with enhanced mechanical properties and dye removal. Int. J. Biol. Macromol. 147, 699–705. https://doi.org/10.1016/j.ijbiomac.2020.01.102.

Mahfoudhi, N., Boufi, S., 2017. Nanocellulose as a novel nanostructured adsorbent for environmental remediation: a review. Cellulose 24 (3), 1171–1197. https://doi.org/10.1007/s10570-017-1194-0.

Mendoza, L., Hossain, L., Downey, E., Scales, C., Batchelor, W., Garnier, G., 2019. Carboxylated nanocellulose foams as superabsorbents. J. Colloid Interface Sci. 538, 433–439. https://doi.org/10.1016/j.jcis.2018.11.112.

Menezes, D.B., Diz, F.M., Romanholo Ferreira, L.F., Corrales, Y., Baudrit, J.R.V., Costa, L.P., Hernández-Macedo, M.L., 2021. Starch-based biocomposite membrane reinforced by orange bagasse cellulose nanofibers extracted from ionic liquid treatment. Cellulose 28 (7), 4137–4149. https://doi.org/10.1007/s10570-021-03814-w.

Metreveli, G., Wågberg, L., Emmoth, E., Belák, S., Strømme, M., Mihranyan, A., 2014. A size-exclusion nanocellulose filter paper for virus removal. Adv. Healthc. Mater. 3 (10), 1546–1550. https://doi.org/10.1002/adhm.201300641.

Meyabadi, T.F., Dadashian, F., 2012. Optimization of enzymatic hydrolysis of waste cotton fibers for nanoparticles production using response surface methodology. Fibers Polym. 13 (3), 313–321. https://doi.org/10.1007/s12221-012-0313-7.

Mohammed, N., Baidya, A., Murugesan, V., Kumar, A.A., Ganayee, M.A., Mohanty, J.S., Tam, K.C., Pradeep, T., 2016a. Diffusion-controlled simultaneous sensing and scavenging of heavy metal ions in water using atomically precise cluster-cellulose nanocrystal composites. ACS Sustain. Chem. Eng. 4 (11), 6167–6176. https://doi.org/10.1021/acssuschemeng.6b01674.

Mohammed, N., Grishkewich, N., Waeijen, H.A., Berry, R.M., Tam, K.C., 2016b. Continuous flow adsorption of methylene blue by cellulose nanocrystal-alginate hydrogel beads in fixed bed columns. Carbohydr. Polym. 136, 1194–1202. https://doi.org/10.1016/j.carbpol.2015.09.099.

Moharrami, P., Motamedi, E., 2020. Application of cellulose nanocrystals prepared from agricultural wastes for synthesis of starch-based hydrogel nanocomposites: efficient and selective nanoadsorbent for removal of cationic dyes from water. Bioresour. Technol., 313. https://doi.org/10.1016/j.biortech.2020.123661.

Montanari, S., Roumani, M., Heux, L., Vignon, M.R., 2005. Topochemistry of carboxylated cellulose nanocrystals resulting from TEMPO-mediated oxidation. Macromolecules 38 (5), 1665–1671. https://doi.org/10.1021/ma048396c.

Moon, R.J., Martini, A., Nairn, J., Simonsen, J., Youngblood, J., 2011. Cellulose nanomaterials review: structure, properties and nanocomposites. Chem. Soc. Rev. 3941. https://doi.org/10.1039/c0cs00108b.

Moriana, R., Vilaplana, F., Ek, M., 2016. Cellulose nanocrystals from forest residues as reinforcing agents for composites: a study from macro- to nano-dimensions. Carbohydr. Polym. 139, 139–149. https://doi.org/10.1016/j.carbpol.2015.12.020.

Mualla, S.A., Farahat, R., Basmaji, P., de Olyveira, G.M., Costa, L.M.M., da Costa Oliveira, J.D., Francozo, G.B., 2016. Study of nanoskin ECM-bacterial cellulose wound healing/United Arab Emirates. J. Biomater. Nanobiotechnol., 109–117. https://doi.org/10.4236/jbnb.2016.72012.

Nascimento, P., Marim, R., Carvalho, G., Mali, S., 2016. Nanocellulose produced from rice hulls and its effect on the properties of biodegradable starch films. Mater. Res. 19 (1), 167–174. https://doi.org/10.1590/1980-5373-MR-2015-0423.

Nasir, M., Hashim, R., Sulaiman, O., Asim, M., 2017. Nanocellulose: preparation methods and applications. In: Cellulose-Reinforced Nanofibre Composites: Production, Properties and Applications. Elsevier Inc, pp. 261–276, https://doi.org/10.1016/B978-0-08-100957-4.00011-5.

Nechyporchuk, O., Belgacem, M.N., Bras, J., 2016. Production of cellulose nanofibrils: a review of recent advances. Ind. Crop Prod. 93, 2–25. https://doi.org/10.1016/j.indcrop.2016.02.016.

Nimeskern, L., Martínez Ávila, H., Sundberg, J., Gatenholm, P., Müller, R., Stok, K.S., 2013. Mechanical evaluation of bacterial nanocellulose as an implant material for ear cartilage replacement. J. Mech. Behav. Biomed. Mater. 22, 12–21. https://doi.org/10.1016/j.jmbbm.2013.03.005.

Omran, A.A.B., Mohammed, A.A.B.A., Sapuan, S.M., Ilyas, R.A., Asyraf, M.R.M., Koloor, S.S.R., Petrů, M., 2021. Micro-and nanocellulose in polymer composite materials: a review. Polymers 13 (2), 1–30. https://doi.org/10.3390/polym13020231.

Oyewo, O.A., Adeniyi, A., Sithole, B.B., Onyango, M.S., 2020. Sawdust-based cellulose nanocrystals incorporated with ZnO nanoparticles as efficient adsorption media in the removal of methylene blue dye. ACS Omega 5 (30), 18798–18807. https://doi.org/10.1021/acsomega.0c01924.

Pääkkö, M., Ankerfors, M., Kosonen, H., Nykänen, A., Ahola, S., Österberg, M., Ruokolainen, J., Laine, J., Larsson, P.T., Ikkala, O., Lindström, T., 2007. Enzymatic hydrolysis combined with mechanical shearing and high-pressure homogenization for nanoscale cellulose fibrils and strong gels. Biomacromolecules 8 (6), 1934–1941. https://doi.org/10.1021/bm061215p.

Pérez, S., Samain, D., 2010. Structure and engineering of celluloses. Adv. Carbohydr. Chem. Biochem. 64 (C), 25–116. Academic Press Inc https://doi.org/10.1016/S0065-2318(10)64003-6.

Picheth, G.F., Pirich, C.L., Sierakowski, M.R., Woehl, M.A., Sakakibara, C.N., de Souza, C.F., Martin, A.A., da Silva, R., de Freitas, R.A., 2017. Bacterial cellulose in biomedical applications: a review. Int. J. Biol. Macromol. 104, 97–106. https://doi.org/10.1016/j.ijbiomac.2017.05.171.

Pinto, A.H., Taylor, J.K., Chandradat, R., Lam, E., Liu, Y., Leung, A.C.W., Keating, M., Sunasee, R., 2020. Wood-based cellulose nanocrystals as adsorbent of cationic toxic dye, Auramine O, for water treatment. J. Environ. Chem. Eng. 8 (5). https://doi.org/10.1016/j.jece.2020.104187.

Prasad Reddy, J., Rhim, J.W., 2014. Isolation and characterization of cellulose nanocrystals from garlic skin. Mater. Lett. 129, 20–23. https://doi.org/10.1016/j.matlet.2014.05.019.

Rahbar Shamskar, K., Heidari, H., Rashidi, A., 2016. Preparation and evaluation of nanocrystalline cellulose aerogels from raw cotton and cotton stalk. Ind. Crop Prod. 93, 203–211. https://doi.org/10.1016/j.indcrop.2016.01.044.

Rebouillat, S., Pla, F., 2013. State of the art manufacturing and engineering of nanocellulose: a review of available data and industrial applications. J. Biomater. Nanobiotechnol., 165–188. https://doi.org/10.4236/jbnb.2013.42022.

Reddy, N., Yang, Y., 2006. Properties of high-quality long natural cellulose fibers from rice straw. J. Agric. Food Chem. 54 (21), 8077–8081. https://doi.org/10.1021/jf0617723.

Rocha, I., Hattori, Y., Diniz, M., Mihranyan, A., Strømme, M., Lindh, J., 2018. Spectroscopic and physicochemical characterization of sulfonated cladophora cellulose beads. Langmuir 34 (37), 11121–11125. https://doi.org/10.1021/acs.langmuir.8b01704.

Roman, M., Gray, D.G., 2005. Parabolic focal conics in self-assembled solid films of cellulose nanocrystals. Langmuir 21 (12), 5555–5561. https://doi.org/10.1021/la046797f.

Rosa, M.F., Medeiros, E.S., Malmonge, J.A., Gregorski, K.S., Wood, D.F., Mattoso, L.H.C., Glenn, G., Orts, W.J., Imam, S.H., 2010. Cellulose nanowhiskers from coconut husk fibers: effect of preparation conditions on their thermal and morphological behavior. Carbohydr. Polym. 81 (1), 83–92. https://doi.org/10.1016/j.carbpol.2010.01.059.

Ruan, W., Hu, J., Qi, J., Hou, Y., Zhou, C., Wei, X., 2019. Removal of dyes from wastewater by nanomaterials : a review. Adv. Mater. Lett., 9–20. https://doi.org/10.5185/amlett.2019.2148.

Sacui, I.A., Nieuwendaal, R.C., Burnett, D.J., Stranick, S.J., Jorfi, M., Weder, C., Foster, E.J., Olsson, R.T., Gilman, J.W., 2014. Comparison of the properties of cellulose nanocrystals and cellulose nanofibrils isolated from bacteria, tunicate, and wood processed using acid, enzymatic, mechanical, and oxidative methods. ACS Appl. Mater. Interfaces 6 (9), 6127–6138. American Chemical Society https://doi.org/10.1021/am500359f.

Saito, T., Nishiyama, Y., Putaux, J.L., Vignon, M., Isogai, A., 2006. Homogeneous suspensions of individualized microfibrils from TEMPO-catalyzed oxidation of native cellulose. Biomacromolecules 7 (6), 1687–1691. https://doi.org/10.1021/bm060154s.

Samiee, S., Ahmadzadeh, H., Hosseini, M., Lyon, S., 2019. Algae as a source of microcrystalline cellulose. In: advanced Bioprocessing for Alternative Fuels, Biobased Chemicals, and Bioproducts: Technologies and Approaches for Scale-Up and Commercialization, pp. 331–350. Elsevier https://doi.org/10.1016/B978-0-12-817941-3.00017-6.

Samir, M.A.S.A., Alloin, F., Paillet, M., Dufresne, A., 2004. Tangling effect in fibrillated cellulose reinforced nanocomposites. Macromolecules 37 (11), 4313–4316. https://doi.org/10.1021/ma035939u.

Saylan, Y., Göktürk, L., Pospiskova, K., Safarik, I., Denizli, A., 2020. Magnetic bacterial cellulose nanofibers for nucleoside recognition. Cellulose 27 (16), 9479–9492. https://doi.org/10.1007/s10570-020-03425-x.

Sheltami, R.M., Abdullah, I., Ahmad, I., Dufresne, A., Kargarzadeh, H., 2012. Extraction of cellulose nanocrystals from mengkuang leaves (Pandanus tectorius). Carbohydr. Polym. 88 (2), 772–779. https://doi.org/10.1016/j.carbpol.2012.01.062.

Shen, W., Chen, S., Shi, S., Li, X., Zhang, X., Hu, W., Wang, H., 2009. Adsorption of Cu(II) and Pb(II) onto diethylenetriamine-bacterial cellulose. Carbohydr. Polym. 75 (1), 110–114. https://doi.org/10.1016/j.carbpol.2008.07.006.

Shoukat, A., Wahid, F., Khan, T., Siddique, M., Nasreen, S., Yang, G., Ullah, M.W., Khan, R., 2019. Titanium oxide-bacterial cellulose bioadsorbent for the removal of lead ions from aqueous solution. Int. J. Biol. Macromol. 129, 965–971. https://doi.org/10.1016/j.ijbiomac.2019.02.032.

Silvério, H.A., Flauzino Neto, W.P., Dantas, N.O., Pasquini, D., 2013. Extraction and characterization of cellulose nanocrystals from corncob for application as reinforcing agent in nanocomposites. Ind. Crop Prod. 44, 427–436. https://doi.org/10.1016/j.indcrop.2012.10.014.

Siqueira, G., Bras, J., Dufresne, A., 2009. Cellulose whiskers versus microfibrils: influence of the nature of the nanoparticle and its surface functionalization on the thermal and mechanical properties of nanocomposites. Biomacromolecules 10 (2), 425–432. https://doi.org/10.1021/bm801193d.

Smith, C.J., Wagle, D.V., O'Neill, H.M., Evans, B.R., Baker, S.N., Baker, G.A., 2017. Bacterial cellulose ionogels as chemosensory supports. ACS Appl. Mater. Interfaces 9 (43), 38042–38051. https://doi.org/10.1021/acsami.7b12543.

Stenstad, P., Andresen, M., Tanem, B.S., Stenius, P., 2008. Chemical surface modifications of microfibrillated cellulose. Cellulose 15 (1), 35–45. https://doi.org/10.1007/s10570-007-9143-y.

Subhedar, A., Bhadauria, S., Ahankari, S., Kargarzadeh, H., 2021. Nanocellulose in biomedical and biosensing applications: a review. Int. J. Biol. Macromol. 166, 587–600. https://doi.org/10.1016/j.ijbiomac.2020.10.217.

Svagan, A.J., Samir, M.A.S.A., Berglund, L.A., 2008. Biomimetic foams of high mechanical performance based on nanostructured cell walls reinforced by native cellulose nanofibrils. Adv. Mater. 20 (7), 1263–1269. https://doi.org/10.1002/adma.200701215.

Tamahkar, E., Türkmen, D., Akgönüllü, S., Qureshi, T., Denizli, A., 2018. Bacterial cellulose nanofibers for efficient removal of Hg 2+ from aqueous solutions. In: Nanotechnology for Sustainable Water Resources. Wiley Blackwell, pp. 501–522, https://doi.org/10.1002/9781119323655.ch16.

Tamahkar, E., Bakhshpour, M., Denizli, A., 2019. Molecularly imprinted composite bacterial cellulose nanofibers for antibiotic release. J. Biomater. Sci. Polym. Ed. 30 (6), 450–461. https://doi.org/10.1080/09205063.2019.1580665.

Tan, H.F., Ooi, B.S., Leo, C.P., 2020. Future perspectives of nanocellulose-based membrane for water treatment. J. Water Process Eng., 37. https://doi.org/10.1016/j.jwpe.2020.101502.

Troncoso, O.P., Torres, F.G., 2020. Bacterial cellulose-graphene based nanocomposites. Int. J. Mol. Sci. *21*.

Uetani, K., Yano, H., 2011. Nanofibrillation of wood pulp using a high-speed blender. Biomacromolecules 12 (2), 348–353. https://doi.org/10.1021/bm101103p.

Ul-Islam, M., Khan, S., Ullah, M.W., Park, J.K., 2019. Comparative study of plant and bacterial cellulose pellicles regenerated from dissolved states. Int. J. Biol. Macromol. 137, 247–252. https://doi.org/10.1016/j.ijbiomac.2019.06.232.

Urbina, L., Guaresti, O., Requies, J., Gabilondo, N., Eceiza, A., Corcuera, M.A., Retegi, A., 2018. Design of reusable novel membranes based on bacterial cellulose and chitosan for the filtration of copper in wastewaters. Carbohydr. Polym. 193, 362–372. https://doi.org/10.1016/j.carbpol.2018.04.007.

Vanderfleet, O.M., Reid, M.S., Bras, J., Heux, L., Godoy-Vargas, J., Panga, M.K.R., Cranston, E.D., 2019. Insight into thermal stability of cellulose nanocrystals from new hydrolysis methods with acid blends. Cellulose 26 (1), 507–528. https://doi.org/10.1007/s10570-018-2175-7.

Vega, B., Wondraczek, H., Bretschneider, L., Näreoja, T., Fardim, P., Heinze, T., 2015. Preparation of reactive fibre interfaces using multifunctional cellulose derivatives. Carbohydr. Polym. 132, 261–273. https://doi.org/10.1016/j.carbpol.2015.05.048.

Wang, J., Tavakoli, J., Tang, Y., 2019. Bacterial cellulose production, properties and applications with different culture methods—a review. Carbohydr. Polym., 63–76. https://doi.org/10.1016/j.carbpol.2019.05.008.

Wei, J., Jia, S., Zhang, L., Zhou, Y., Lv, Y., Zhang, X., Shao, Z., 2021. Preparation of treelike and rodlike carboxymethylated nanocellulose and their effect on carboxymethyl cellulose films. J. Appl. Polym. Sci. 138 (13), 50092. https://doi.org/10.1002/app.50092.

Xu, T., Jiang, Q., Ghim, D., Liu, K.K., Sun, H., Derami, H.G., Wang, Z., Tadepalli, S., Jun, Y.S., Zhang, Q., Singamaneni, S., 2018. Catalytically active bacterial nanocellulose-based ultrafiltration membrane. Small 14 (15). https://doi.org/10.1002/smll.201704006.

Xue, Y., Mou, Z., Xiao, H., 2017. Nanocellulose as a sustainable biomass material: structure, properties, present status and future prospects in biomedical applications. Nanoscale 9 (39), 14758–14781. https://doi.org/10.1039/c7nr04994c.

Xue, F., He, H., Zhu, H., Huang, H., Wu, Q., Wang, S., 2019. Structural design of a cellulose-based solid amine adsorbent for the complete removal and colorimetric detection of Cr(VI). Langmuir 35 (39), 12636–12646. https://doi.org/10.1021/acs.langmuir.9b01788.

Yadav, C., Saini, A., Zhang, W., You, X., Chauhan, I., Mohanty, P., Li, X., 2021. Plant-based nanocellulose: a review of routine and recent preparation methods with current progress in its applications as rheology modifier and 3D bioprinting. Int. J. Biol. Macromol. 166, 1586–1616. https://doi.org/10.1016/j.ijbiomac.2020.11.038.

Yildirim, N., 2018. Developing fire-retardant and water-repellent bio-structural panels using nanocellulose. MRS Commun. 8 (2), 257–265. https://doi.org/10.1557/mrc.2018.37.

Yildirim, N., Shaler, S.M., Gardner, D.J., Rice, R., Bousfield, D.W., 2014. Cellulose nanofibril (CNF) reinforced starch insulating foams. Cellulose 21 (6), 4337–4347. https://doi.org/10.1007/s10570-014-0450-9.

Zhu, G., Xu, H., Dufresne, A., Lin, N., 2018. High-adsorption, self-extinguishing, thermal, and acoustic-resistance aerogels based on organic and inorganic waste valorization from cellulose nanocrystals and red mud. ACS Sustain. Chem. Eng. 6 (5), 7168–7180. https://doi.org/10.1021/acssuschemeng.8b01244.

This page intentionally left blank

CHAPTER

13

Synthesis and properties of cellulose-based nanobiosorbents

Anindita De[a], *Mridula Guin*[a], *and N.B. Singh*[a,b]

[a]Department of Chemistry and Biochemistry, Sharda University, Greater Noida, India [b]Research Development Cell, Sharda University, Greater Noida, India

13.1 Introduction

One of the most important naturally occurring polysaccharide is cellulose. This can be naturally obtained from bacteria, algae, fungi, animals, and plants. Chemically cellulose is a linear, homo polysaccharide consisting of "β-D-glucopyranose units linked together by β-1,4-glycosidic bonds." The main constituents of cellulose are hydrogen (6.17%), carbon 44.44%), and oxygen (49.39%) and the formula is $(C_6H_{10}O_5)_n$ (Fig. 13.1), where n is polymerization degree and shows number of glucose units (Blanco et al., 2018).

Water insolubility, hydrophilic nature, crystallinity, biodegradability and high tensile strengths are some of the physical properties of cellulose (Yu et al., 2020; Dhali et al., 2021). Importance of cellulosic materials are due to abundant availability, sustainable, renewable resource with price stability, high strength and modulus, light weight, thermal stability, recyclable, reusable, reduced carbon footprint (carbon neutral), compostable, non-toxic, biocompatible, thixotropic, dimensional stability, high optical transparency, high thermal conductivity and low oxygen permeability. Generally repeating units, chain length, and degree of polymerization control the properties of cellulose. All these depend on the source and the extraction method. The cellulose fiber derived from plants consists of a mixture of hemicellulose, lignin, pectin and other compounds and on the other hand the bacterial cell-derived cellulose has much water content and longer chains (Fig. 13.2A). The cellulose material maintains both amorphous and crystalline character and the amorphous region on reaction with strong acids is converted to nanocrystalline cellulose (NCC) (Fig. 13.2B).

In recent years nanocellulose has emerged as an important material for different applications (Trache et al., 2020). Depending on their isolation methods, nanocellulose may be divided into three categories: (1) cellulose nanocrystals (CNCs), (2) cellulose nanofibers

https://doi.org/10.1016/B978-0-323-90912-9.00013-7

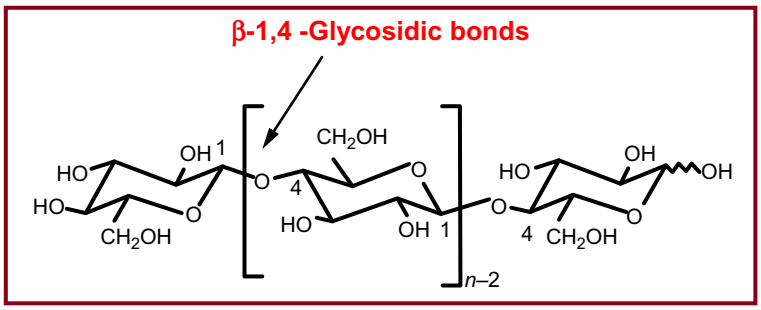

FIG. 13.1 Molecular structure of cellulose.

(CNFs/NFCs), (3) Another form of nanocellulose is bacterial nanocellulose (BNC), which refers to nanostructured cellulose produced by some bacteria specifically belonging to the general species category of *Acetobacter*, *Pseudomonas*, *Agrobacterium* and *Rhizobium*, etc. (Fig. 13.3) (Dhali et al., 2021; Thomas et al., 2018; Gopakumar et al., 2019; Farooq et al., 2020).

Nanocellulose is used in different sectors but as an adsorbent, it is very effective for remediation of water (Fig. 13.4) (Mahfoudhi and Boufi, 2017).

Considering the importance of nanocellulose, it's synthesis (through plants and bacteria), characterization, properties and applications have been discussed in this chapter. More attention is given toward biosorption.

13.2 Nanocellulose

Cellulose is a ubiquitous biopolymer commonly found in cell walls of plant tissue, bacteria, algea, fungi, and even in some sea animals. This polysaccharide molecule contains long chains of β-D-glucopyranose units. These glucose units then connect together by β-1,4 glycosidic bonds to form a dimer which is known as cellobiose. This fundamental unit is then combined to form cellulose which is an isotactic polymer of cellobiose (Gupta et al., 2016). The polysaccharide chains are connected with each other through extensive inter- and intramolecular hydrogen bonding forming a microfibril which conglomerate to form microfibers and then fibers.

The nano-scale structure of cellulose, i.e., at least one dimension in nanosize (1–100 nm) is known as nanocellulose. It can be further classified as (i) cellulose nanocrystals (CNCs) (ii) cellulose nano nanofibrils (CNFs) and (ii) bacterial nanocellulose (BCN). CNCs have a needle-like structure with width and length ranging from 10 to 20 nm and 100–250 nm respectively. They have a highly ordered crystalline structure and are also known as nanowhiskers. CNFs have more amorphous structure compared to the CNCs. They are composed of long fibrous network with a typical fiber length of 0.1–2 μM and a diameter of 5–50 nm. Bacterial cellulose is procured by bacterial action and have a typical cross-sectional diameter of 20–100 nm. Some other less common forms of nanocellulose are cellulose nanoyarn and amorphous nanocellulose. A comparative study of these three types of cellulose is depicted in Table 13.1.

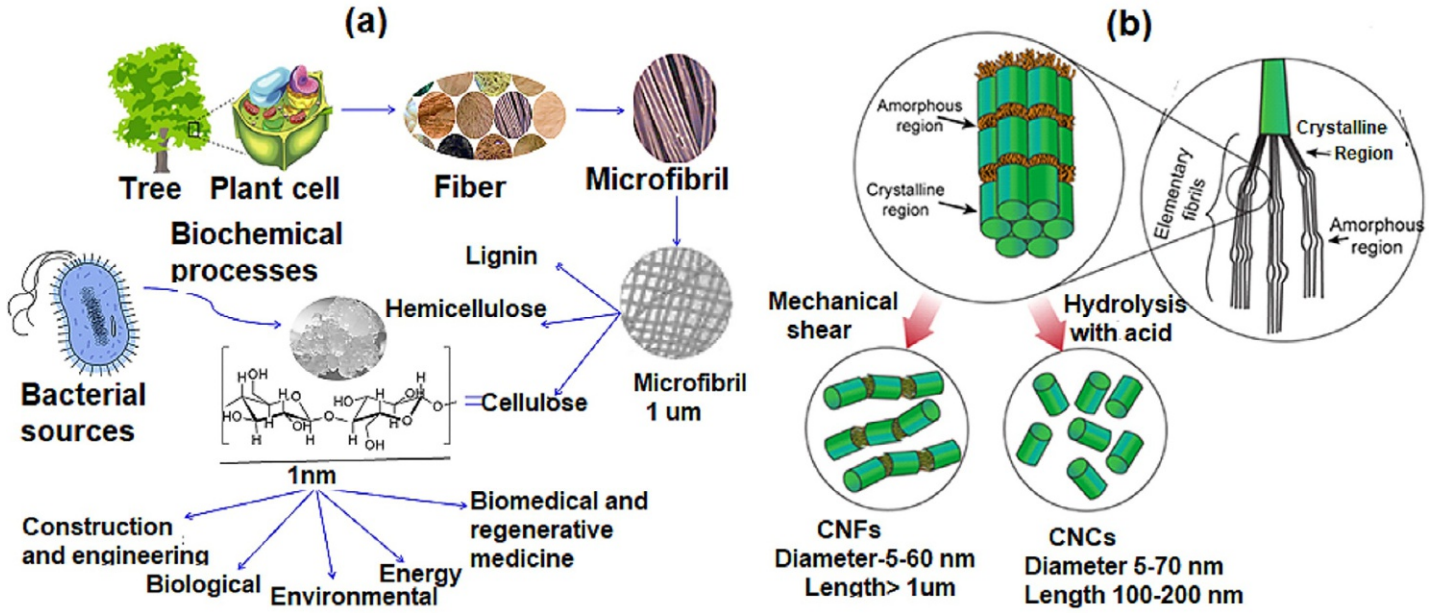

FIG. 13.2 Cellulose, its source, nanocellulose and applications.

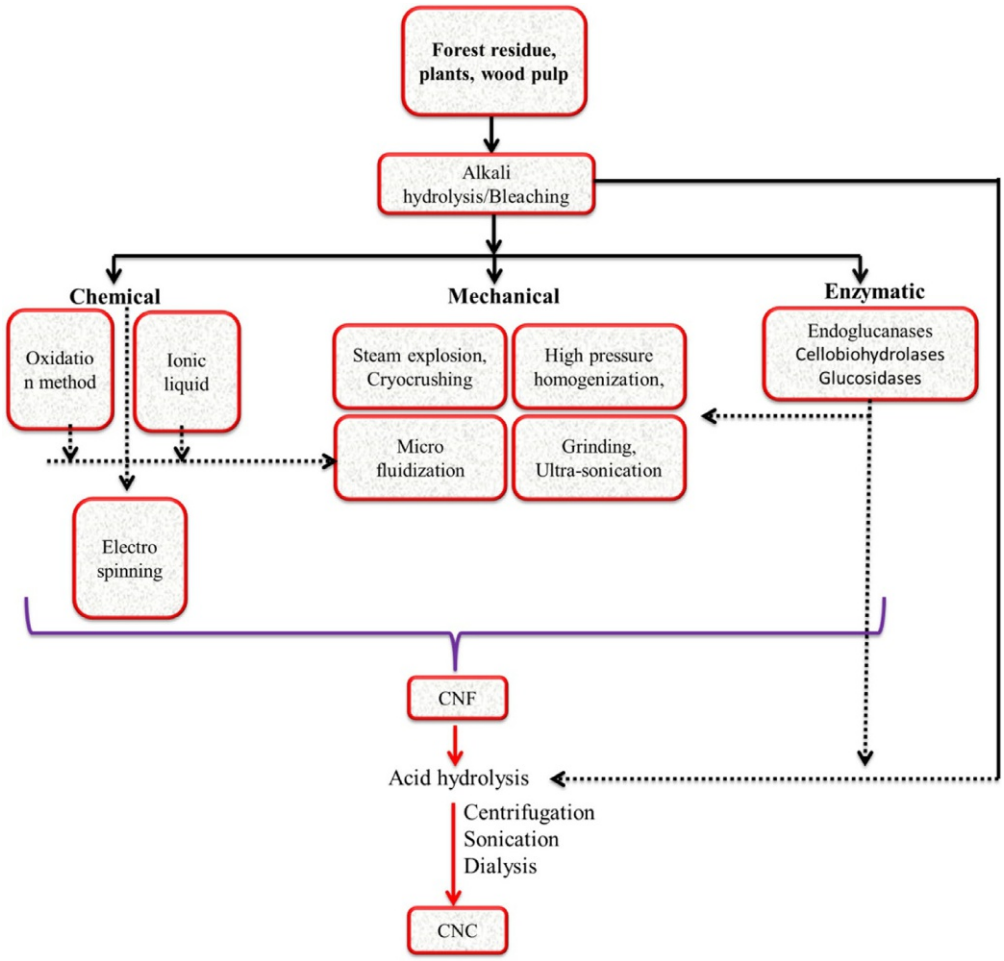

FIG. 13.3 Isolation of nanocellulose materials (Farooq et al., 2020).

13.3 Isolation of nanocellulose from various sources

In order to form nanocellulose, at least one of the dimension has to be broken down to nano-scale. This hierarchical structural break down required several pretreatment steps which include washing, drying, grinding, delignification and acid/base hydrolysis. During these processing steps, non-cellulosic components such as lignin, hemicellulose and wax, surrounding the cellulose structure is removed (Fig. 13.5). In addition to that amorphous regions are eliminated during acid hydrolysis leading to the formation of crystalline CNCs. Grinding of the raw material is followed by alkali treatment at high temperature and bleaching with an oxidizing agent such as $NaClO_2$ to remove lignin and hemicellulose (Brinchi et al., 2013). Pretreatment with chemicals expand the gap between hydroxyl group, breaks the hydrogen bonds and thus increase the surface area and reactivity. Pretreatment can also be done with

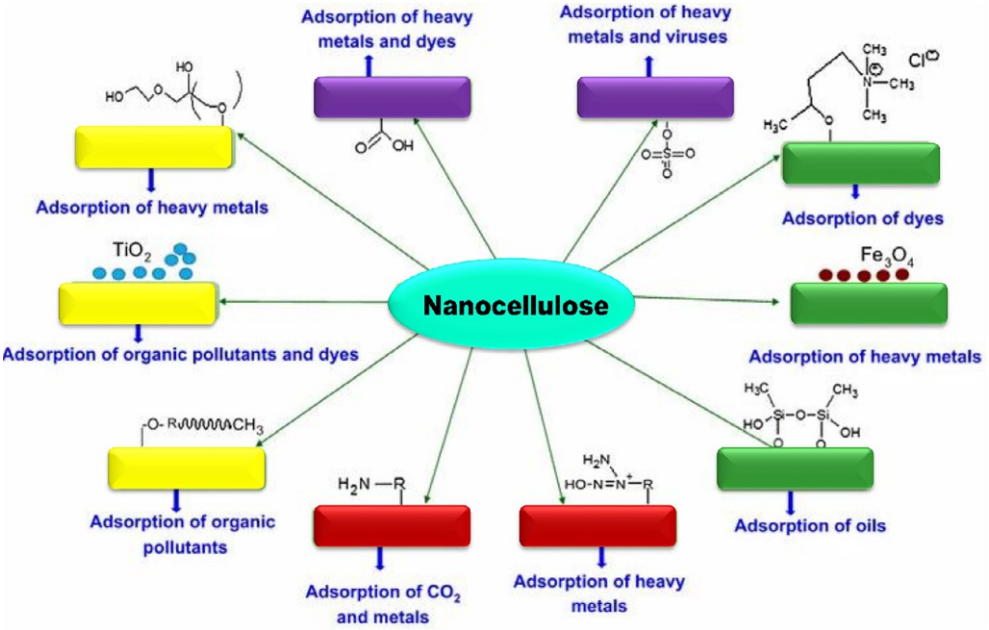

FIG. 13.4 Nanocellulose as adsorbent/biosorbent for water remediation.

TABLE 13.1 Comparative Study of different types of nanocellulose (Patel et al., 2019).

Type of nanocellulose	Advantages	Source	Average size
Nanofibrillated cellulose (CNFs)	Low density, high surface area, and good mechanical strength	Wood, potato, sugar beet, flax, etc.	5-60 nm
Cellulose nanocrystals (CNCs)	High surface area, excellent mechanical properties, low density and low coefficient of thermal expansion	Wheat straw, ramie, mulberry bark, avicel, tunicin, from algae and bacteria	100-250 nm
Bacterial nanocellulose(BNC)	Excellent mechanical strength, high purity, and greater stability	sugars and alcohols of low MW	20–100 nm length up to much finer 2–4 nm
Amorphous nanocellulose (ANC)	High content of functional groups and high sorption ability	Cotton, wood pulp	20–120 nm in width, and 50–120 nm in length
Cellulose nanoyarn (CNY)	High surface area, and high blotting ability	Cellulose and cellulose derivatives	100–1000 nm in width, and >10,000 nm in length

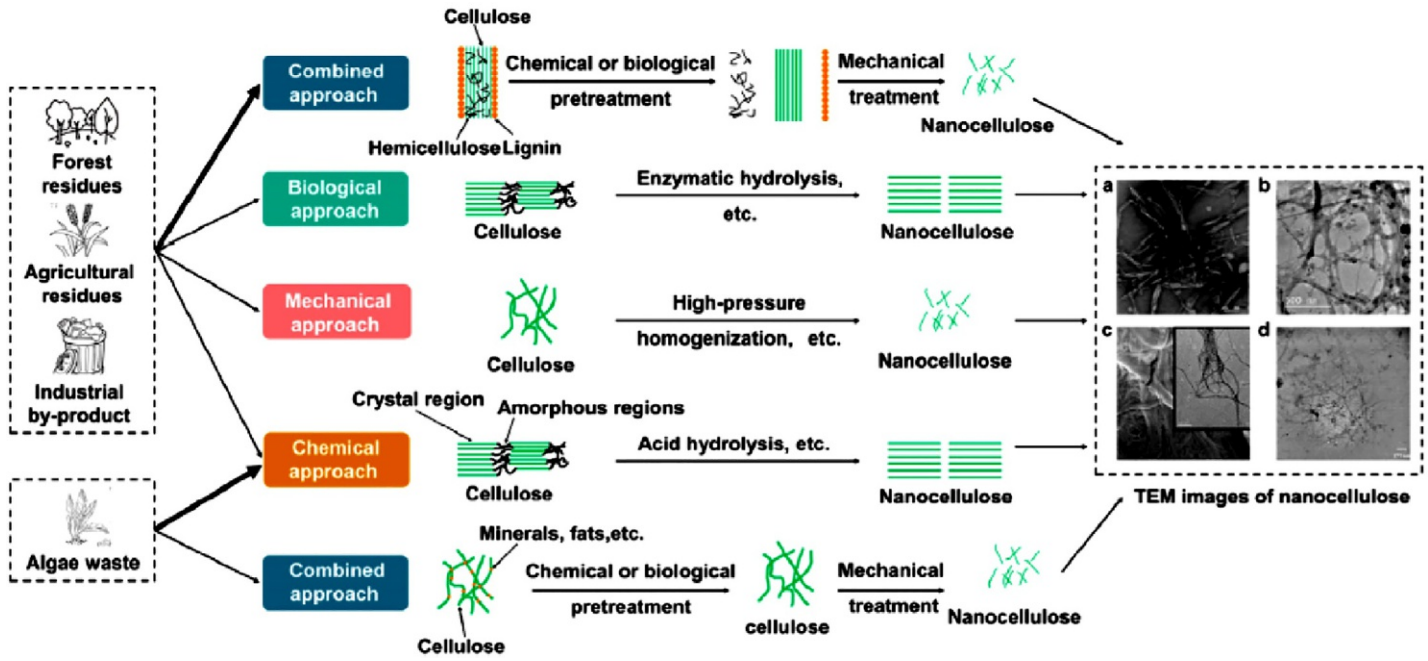

FIG. 13.5 Schematic diagram of nanocellulose preparation from various sources (Patel et al., 2019).

enzymes where enzyme such as laccase carries out selective hydrolysis to degrade or modify the lignin and hemicellulose contents without disturbing cellulose content (Patel et al., 2019). Pretreatment step decreases the energy consumption during mechanical nanofibrillation and also enhance the degree of nanofibrillation (Nasir et al., 2017).

Once the pretreatment is over, the cellulosic materials are subjected to mechanical processing for defibrillation process. There are several mechanical methods notably grinding, homogenization, high-intensity ultrasonication, microfluidization and cryocrushing (Nasir et al., 2017).

13.3.1 Isolation of nanocellulose from forest residue

A large amount of forest residue is produced every year which include sawdust, plywood waste, shavings and logging residues. This could be a useful feedstock for isolation of cellulose. Typically, the extraction process can be divided into four categories: chemical, physical, biological and a combination of any two aforesaid methods in order to have an added advantage. Biological method to extract cellulose from forest residue has not been explored much due to economic reasons. The most common method used to obtain nanocellulose is chemical method. For example, CNCs are extracted from logging residues by alkaline treatment (4.5% NaOH, 80°C, 2 h), bleaching treatment and acid hydrolysis (65% H_2SO_4, 45°C, 40 min). The CNCs thus obtained have high degree of crystallinity and have high aspect ratio(>10) (Moriana et al., 2016). However, this method has high energy consumption, requires longer reaction time and corrosive chemical. Physical methods are also used in extraction of nanocellulose. For example, Phanthong and coworkers could get ~93% yield of nanocellulose (10–25 nm diameter) by using a planetary ball mill (Phanthong et al., 2017). Viegle and coworkers have used fibrillated pulped beech waste to generate nanocellulose in good yield by following a high-pressure homogenizer treatment (Veigel et al., 2012). Physical methods have disadvantage in terms of high energy consumption.

Nowadays a combination of physical and chemical method is also being employed for preparation of nanocellulose. In one such example, Eucalyptus sawdust was first pretreated to get rid of lignin and hemicellulose and to isolate cellulose. It is then oxidized by TEMPO under alkaline condition followed by a gentle homogenization process to obtain nanocellulose (Vallejos et al., 2016). Similar methods have also been employed to procure CNFs from Birch and Spruce sawdust. Apart from that, ultrasound and screw extruding methods are also used in combination with chemical treatment. Nano-fibers have been prepared from pine needle by treatment with acidified sodium chlorite at 75°C for 1 h followed by alkaline treatment (70°C) and acid hydrolysis by HCl at high temperature combined with ultrasonic treatment at 60KHz for 30 mins (Xiao et al., 2015). The nanofibers thus produced have good thermoplastic property.

Synthesis of nanocellulose film has been reported by Bufalino et al. from Amazon forest wood waste by subjecting the raw material to bleaching and casting method (Bufalino et al., 2016). A comprehensive list of various examples of nanocellulose extraction from forest residue is listed in Table 13.1. A combined method is better in terms of efficiency compared to both chemical and physical method. However, this method produces chemicals as secondary waste.

13.3.2 Isolation of nanocellulose from agricultural residue

Crop residue such as rice and wheat straw, sugarcane bagasse, rice husk, corn cob, corn stover, etc., is good source of cellulosic material. Typically cellulose content of agricultural residue is similar to that of forest residue but lignin content is significantly higher. The fabrication method of nanocellulose from lignocellulosic agricultural residue is of four types as mentioned in the previous section. A good example of chemical method is preparation of nanowhishkers by acid hydrolysis from pea hull fibers having diameter and length of 12–7 nm and 400–240 nm respectively (Chen et al., 2009). Physical pathway involves use of physical processing tools or methods such as homogenization, mechanical grinding, ultrasonication, etc. Suopajarvi et al. have synthesized nanofibrillated cellulose gel by a high-pressure homogenization technique. It is then functionalized with sulfonate functional group to produce highly efficient nanoadsorbent for Pb(II) ions (Suopajärvi et al., 2015). Abraham el al. prepared nanocellulose by a steam explosion method from pineapple leaves and jute fibers and used it as polymer reinforcing agent (Abraham et al., 2011).

In biological method nanocellulose extraction involves use of microorganism or a specific enzyme acting as a catalyst on the cellulosic substrate. The advantage of this method is that the structural aspects of nanocellulose can be controlled easily, whereas long reaction time, low yield and high cost are some of the drawbacks.

The combined method is often preferred by the modern researchers. Kang et al. have followed a mechanochemical esterification method to obtain cellulose from corn cobs. The nanocellulosic particles have particle diameter of 1.5–2.8 nm and possess excellent optical property. Another example of this combined method is synthesis of CNCs from sugarcane bagasse by a combined acid hydrolysis and ultrasonic treatment. The CNCs thus produced have an extensive hydrogen bonding and resemble true synthetic polymer matrix and can be used as reinforcing additives in food packaging industry (Slavutsky and Bertuzzi, 2014).

13.3.3 Isolation of nanocellulose from algae waste

Algae are enriched in protein and polysaccharide and thus can be a good source of nanocellulose.

Some non-edible green algae species or invasive algae species such as Cladophorales, Ulva, Chlorella, Spirogyra, and Chaetomorph have been reported to be very useful for nanocellulose fabrication. Mostly chemical and combined methods have been adopted for the fabrication process. Highly crystalline nanocellulose with high surface area has been isolated from Cladophorales by acid hydrolysis (Hua et al., 2015). Crystalline nanocellulose from *Ulva lactuca* is synthesized by methanol decolorization, bleaching followed by acid hydrolysis (Rathod et al., 2015). One example of combined method is nanocellulose from *Chaetomorpha antennina* by bleaching, acid hydrolysis and ultrasonic treatment (Yu et al., 2020).

13.3.4 Isolation of nanocellulose from industrial by-product

Various industrial waste products such as waste paper, fruit pulp, residues from food processing, furniture manufacturing, printing and packaging contains lignocellulosic mass from where nanocellulose can be extracted. The method for extraction depends on the source

material due to variation in structural and chemical composition. For example, to extract nanocellulose from sugarcane bagasse a direct acid hydrolysis method has been employed. However, solid waste from olive industry and paper and pulp industry waste requires pretreatment of pulping and bleaching prior to acid hydrolysis. Furniture industry wastes are subjected to pretreatment by steam explosion before acid hydrolysis (Yu et al., 2020). Pulp and paper mill sludge can be converted to crystalline nanocellulose under oxidizing condition using ammonium persulfate (Gibril et al., 2018).

A comprehensive list of various sources of cellulose and the preparation method of nanocellulose from them is listed in Table 13.2 (Yu et al., 2020).

13.4 Properties of nanocellulose

The properties of nanocellulose depend on the source material, the synthesis method and type of nanocellulose surface transformation. The hydroxyl-rich nanocellulose surface can be easily modified by various chemical reactions (discussed in the next section) and thereby producing molecules with unique physical, rheological, mechanical, electrical, optical, thermal, and biological properties.

13.4.1 Physical, mechanical, and rheological properties

One of the most important characteristic of nanocellulose is its crystallinity. Nanocellulose obtained from microorganisms has greater crystallinity compared to that from plant biomass. For example, *Cladophora* cellulose has crystallinity index of >90% while CNFs obtained from wood are <70% crystalline. Moreover C*ladophora* cellulose is porous compared to wood-based cellulose and have a higher surface area. Porosity and crystallinity also affect the mechanical resilience of the nanocellulose. However, there is no direct correlation between the two properties. As for example, Young's modulus of *Cladophora* cellulose (∼8 GPa) is half of that of CNF (∼12 GPa) despite having a higher crystallinity (Sheikhi, 2019). Nenocellulose also have a very high mechanical strength. The tensile strength depends on the fiber source as well as on the surface modification. For example, dicarboxylic acid modified crystalline nanocellulose form films with tensile strength of the order of 63–126 MPa and Young's moduli ∼2.8–4.7 GPa, regulated by the degree of substitution and acid/salt form (Sheikhi, 2019). The rheological property of charged nanocellulose (sulfonate, carboxylate) depends on the concentration ions present around it.

13.4.2 Chemical and thermal properties

As the surface of the nanocellulose is rich in hydroxyl group having good nucleophilic properties, the surface functionalization can be done easily with suitable reagent in one or multistep process. The most common methods are amidation, esterification, etherification, and carbamation. Functionalization enhances or modifies the chemical property of the nanocellulose. For example, dicarboxylated cellulose has more solubility in the functionalized regions which furnish an efficient method to break down fibrils from their amorphous regions

TABLE 13.2 A list of various sources of nanocellulose, their properties and applications (Yu et al., 2020)

Sources		Properties	Extraction method	Application
Forest residue	Birch and Spruce	Tensile strength:80e200 MPa; Young's modulus: 4.8e8.5 GPa	Sodium hydroxide and Soxhlet extraction followed by acetic acid, sodium acetate and sodium chlorite treatment.	Papermaking
	Logging residues	High aspect ratio:>10; Good thermal stability.	Alkaline treatment, bleaching treatment and acid hydrolysis.	Reinforcing agents
	Eucalyptus sawdust	Surface area: 60 m^2 g^{-1}; Average diameter: 41.0 nm	TEMPO oxidation	Papermaking
	Medium density fiberboard	Length: 164.7 nm; Width: 6.7 nm; Crystallinity: 71%	Soxhlet extraction, sodium hydroxide and repeated bleaching.	Nanocomposites or papermaking
	Beech wastes pulp	Diameters: 20–65 nm Average: 35 nm	Fibrilization	Adhesive
	Pine needles	treatments Narrow diameter: 30–70 nm; Cellulose I type; Crystallinity: 66.19%; Highly flexible, highly ultralight and good thermal properties	Chemical pretreatments followed by ultrasonic	Thermoplastic composites
	Pinecone biomass	Tensile strength: 273 MPa; Elastic modulus: 17 GPa; Crystallinity: 70%; Diameter: 5e20 nm	Acidification, alkali treatment, mechanical grinding.	Bionanocomposites
	Cordia goeldiana veneer wastes	Maximum processing temperatures: 300C	Alkali treatment, bleaching, homogenization and casting.	*E*-papers, organic electronic devices and transparent solar cells
Agricultural residues	Waste sugarcane bagasse	Cellulose II; Diameters:18.17e32.84 nm; Crystallinity: 93%	Alkali hydrolysis; bleaching treatment; acid hydrolysis and ultrasonic treatment.	Food packaging
	Jute dried stalks	Average diameter: 50 nm; Higher crystallinity; Young's modulus: 138 GPa; Good reinforcing properties	Alkali treatment followed by steam explosion; sodium chlorite bleaching and oxalic acid treatment followed by steam explosion.	Reinforcing agent

	Coconut husk	Average diameter: 5.6 ± 1.5 nm; Length: 150e350 nm; Good mechanical properties and thermal stability	Ultrasonic-assisted solvent immersion, alkaline treatment, bleaching treatment, milder TEMPO -mediated oxidation (TEMPO/NaClO/NaClO2, pH ¼ 4.8)	PVA composite strength enhancer
	Pea hull	Length: 400–240 nm; Diameter: 7–12 nm; Good UV absorption, transparency, tensile strength, elongation at break and water resistance	Acid hydrolysis	nanocomposite
	Wheat straw	Good adsorption capacity	Bleaching treatment, pressure sieve and high-pressure homogenization;	Nanosorbent
	Branch-barks of mulberry	Diameter: 25–30 nm; Length: 400–500 nm; Crystallinity: 73.4%	Alkali treatment, bleaching treatment, acid hydrolysis and ultrasonic treatment	–
	Raw apple stem	Yield: 5.2%; Higher crystallinity; Good thermal stability	Acid hydrolysis	–
Algae waste	Cladophorales	Width: 20–30 nm; Crystallinity: 100%;	Acid hydrolysis	Biological field
	Dealginate kelp residue	High aspect ratio: 30:70; Crystallinity: 74.55%	2 wt% Na_2CO_3 swelling treatment, 2 wt% NaOH extraction of residual sodium alginate, ultrasonic smashing, 0.7 wt% $NaClO_2$ buffer solution bleaching treatment, delignification and sulfuric acid hydrolysis	–
	Industrial kelp (Laminaria japonica) waste	Yield: 52.3%; Crystalline form: cellulose I; Crystallinity: 69.4%; Shape: rod-like; Poor thermostability	Acid hydrolysis	–
	Ulva lactuca	Good absorption	Methanol decolorization, bleaching and acid hydrolysis	Adsorbents
	Chaetomorpha antennina	Yield: 34 ± 0.9%; Crystallinity:85.02%; Good thermal stability and tensile strength	Bleaching treatment, acid hydrolysis, and ultrasonic assisted treatment	Environmentally friendly products

Continued

TABLE 13.2 A list of various sources of nanocellulose, their properties and applications (Yu et al., 2020)—Cont'd

Sources		Properties	Extraction method	Application
	Cystoseria myricaas algae	Average crystallite's grain size (Fe_3O_4-Nanocellulose): 21 nm	Soxhlet pretreatment, 3% NaOH treatment, $NaClO_2$ bleaching treatment and acid hydrolysis	Heavy metal mercury adsorbent
	Gelidium sesquipedale	Crystallinity: 69.8%; Diameter: 6–40 nm; Length: 80e450 nm; High aspect ratio: 40	Soxhlet extraction, bleaching treatment, 5% KOH solution treatment and acid hydrolysis	Food packaging industry
Industrial byproduct	Sweet lime pulp waste Komagataeibacter europaeus SGP37 incubation under static intermittent fed-batch cultivation	Bacterial nanocellulose	Yield: 27.0–38 g/L	–
	Waste paper	Crystallinity: 48.85%; Average size: 50 nm; Good thermal stability	Aqueous NaOH/thiourea	Transistors and batteries
	Discarded cigarette filters	Length: 143 nm; Width: 8 nm; Crystallinity: 96.77%	Ethanol extraction, bleaching, alkali treatment and acid hydrolysis	Biomedical composites
	Cotton linter waste	Length: 177 nm; Width: 12 nm; Crystallinity: 90.45%; High hydrophilicity	Acid hydrolysis	nanocomposites
	Beer industrial residuals	Average diameter: 73–145 nm; Crystallinity:79%–89%; Yield: 25.8%; Good thermal stability	Acid hydrolysis and ultrasound assisted techniques	Packaging, coatings, pharmaceuticals, cosmetics and defense
	Wood furniture industry waste (Pinus elliotii)	Diameter: 18.0–40.5 nm	Steam explosion and acid hydrolysis process	Oil absorption
	Recycled Tetra Pak Food Packaging Wastes	Length: 258 ± 54 nm; Aspect ratios: >10	Alkaline purification, bleaching treatment and acid hydrolysis	Bionanocomposites
	Olive industry solid waste Pulping,	Free-flowing porous	bleaching and sulfuric acid hydrolysis	Wastewater treatment
	Citrus Pulp of Floater (CPF)	Crystallinity: 60%; Purity: 98%	Enzymatic hydrolysis	–

into nanocrystals (Majoinen et al., 2012). Another common oxidizing agent is TEMPO and its derivative. However, prolonged oxidation of nanocellulose may lead to loss of crystalline property as it interferes with inter and intramolecular hydrogen bonding caused by hydroxyl group. Hydrophobicity of the nanocellulose can be controlled by amination/amidation via grafting amine group to cellulose chain length in various degrees (Yang et al., 2012).

Thermal conductivity is one of the most important properties to consider for successful fabrication of electronic device (facile heat transfer may protect the device). The thermal property of nanocellulose depends on crystallinity, particle morphology and orientation, thermal resistance of particles, porosity and stiffness. Thermal conductivity of the nanocellulose can be altered anisotropically by stretching. As for example, in nanopapers made from stretched bacteriocellulose, thermal conductivity is regulated by fiber orientation. The conductivity increases along the stretched plane while it decreases along the perpendicular plane. The in-plane thermal conductivity of nanocellulose papers is higher than conventional polymer film and aerogels albeit conductivity is significantly less compared to metal and ceramic materials (Sheikhi, 2019).

13.4.3 Electrical and optical properties of nanocellulose

Cellulose which is the building block of nanocellulose has very poor electrical conductivity and hence often used as insulator. Nanocellulose can be used as template for synthesis of conductive nanoparticles. They have also been used as capping agent during nanoparticle synthesis and as binding agents to provide an efficient conductive layer coating.

CNC can form multilayer structure and the distance between the layers can be changed in form of nematic or chiral nematic structure. On fast evaporation, nematic CNC films may be obtained while chiral nematic films with hemical structure can be obtained on slow evaporation. CNC dispersion can change from an aniosotropic state to anisotropic/ordered biphasic separation depending on the concentration. The distance between chiral nematic domains can be decreased by addition of salt to CNC dispersion (Fig. 13.6). These unique properties of nanocellulose can be exploited to fabricate optical devices (Sheikhi, 2019).

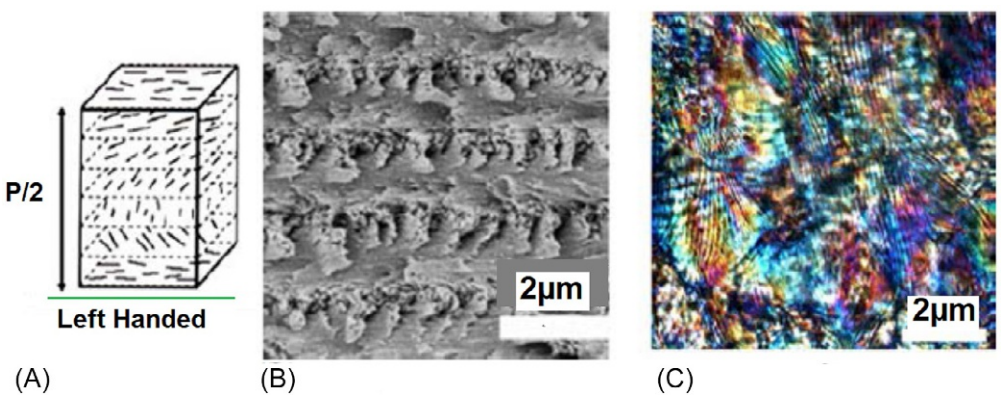

FIG. 13.6 (A) Helical arrangement of chiral left handed nematic CNCs (B) and (C) production of iridescent color (Majoinen et al., 2012)

13.4.4 Biological properties of nanocellulose

Cellulose is a biocompatible material. Its biological activity depends on morphology and chemical functionality present. In vivo activity study of nanocellulose is not done much and it has been reported to have mild inflammatory effect. In vitro cytotoxicity of nanocellulose has been explored in several research works. Dong et al. reported MTT assays and lactate dehydrogenase assay to evaluate the cytotoxic behavior of nanocellulose up to 50 μg/mL (Dong et al., 2012). No cytotoxicity against fibroblast has been found for CNFs up to a concentration of 100 μg/mL. However, at higher concentration of CNFs (2–5 mg/mL) apopstasis and stress to the cell is reported. Toxicological studies have been performed using different types of cells through acute lethal tests, gene mutations, chromosomal test in vitro, multitropic assays and bacterial tests for environmental toxicity. Among nanocellulose, BC is particularly preferred for biomedical applications due to high purity and high crystallinity. Nevertheless, one of the challenges of using nanocellulose is its non-degradable nature in vivo. Biodegradation of nanocellulose has not been studied in details so far and it is understood that the degradation depends on crystallinity, functional groups, and size and oxidized form of nanocelluloses are more susceptible to hydrolysis in vivo (Sheikhi, 2019).

13.5 Characterization of nanocellulose

Nanocellulose can be characterized by various techniques for example nitro gas and water adsorption isotherms, Helium pycnometry, X-ray diffraction and dielectric spectroscopy. The most important property, i.e., crystallinity index is measured by using a X-ray Diffractometer by observing the intensity of diffraction at 002 lattice peak which represent the crystalline region. On the other hand, diffraction intensity between (001) and (101) lattice peaks represent amorphous region (Trache et al., 2020).

Size and morphological analysis of nanocellulosic material is done by Transmission Electron Microscopy (TEM), Field Emission Scanning Electron Microscopy (FESEM), and Atomic Force Microscopy (AFM). TEM images of nanocellulose from different sources are depicted in Fig. 13.7.

A helium pycnometer is used to measure the density and porosity of the nanocellulose. N_2 gas adsorption analysis provides specific surface area and total pore volume data. The surface change on the nanocellulose which dictates the dispersion stability is determined by using a zeta potential analyzer. Another important technique is X-ray Photoelectron Spectroscopy which is used to find out elemental composition on the nanocellulose surface. Differential scanning calorimetry (DSC), thermogravimetric analysis (TGA) and differential thermogravimetric (DTG) techniques are employed to investigate the thermal stability of the material which are related to thermal decomposition temperature and purity of the nanocellulose (Jordan et al., 2019).

A very advanced tool used for nanocellulose surface characterization is Dynamic Nuclear Polarization (DNP)- enhanced NMR spectroscopy. This emerging technique can improve the sensitivity of the conventional NMR methods by several orders of magnitude. For instance, Kumar et al. has characterized the metronidazoledrug-functionalized TEMPO-oxidized cellulose nanofibrils. The authors have grafted the drug onto the surface of CNF and DNP-enhanced NMR spectroscopy is the only method which can distinguish between grafting and adsorption (Kumar et al., 2020).

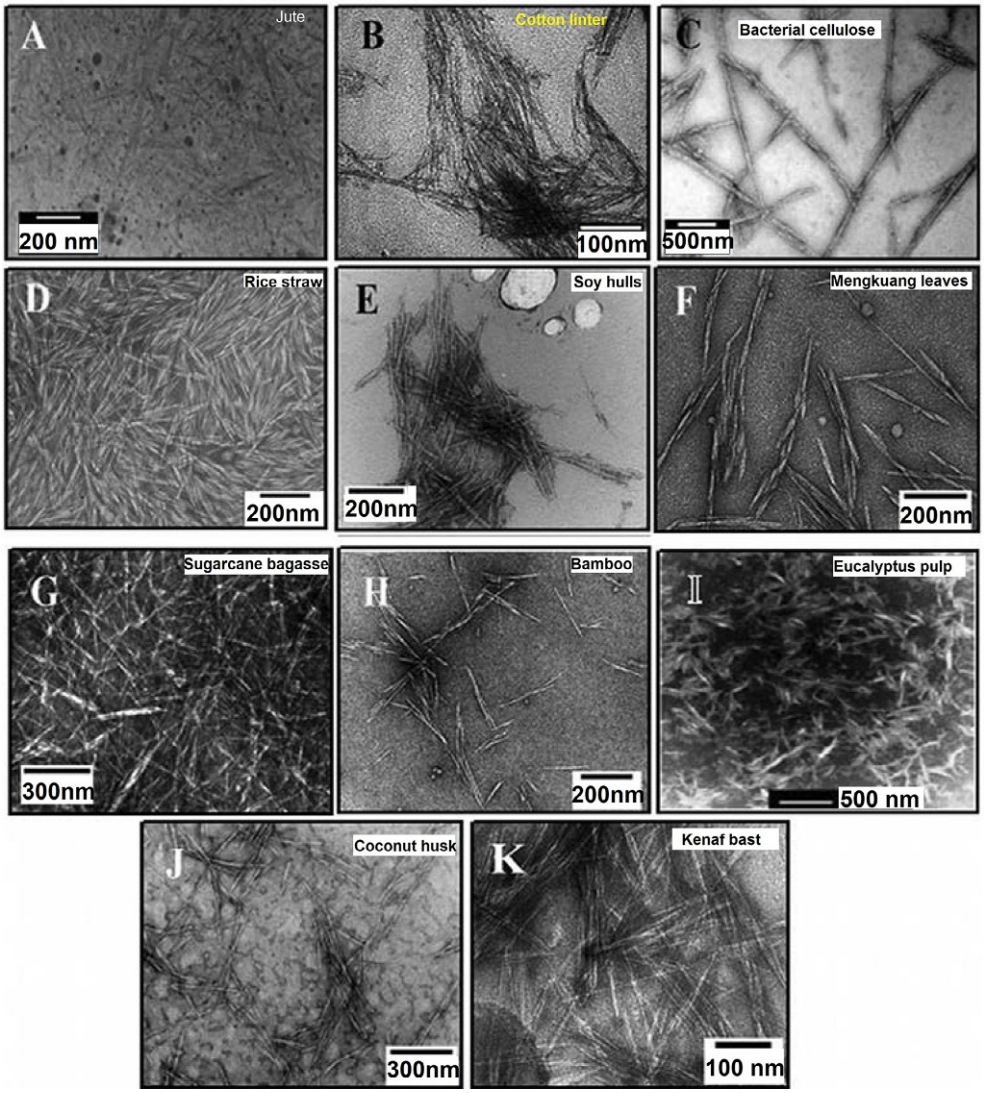

FIG. 13.7 TEM images of cellulose nanocrystals obtained from different sources (Sheikhi, 2019).

13.6 Surface modification of nanocellulose

The applicability of nanocellulose is limited due to its poor dispersibility in non-polar solvent and its incompatibility with hydrophobic matrixes. To tackle this problem, chemical modification of the surface hydroxyl groups (-CHOH) has been done. Surface modification can improve the mechanical properties and chemical properties such as hydrophobicity which in turn enhances the dispersibility of nanocellulose in specific solvent.

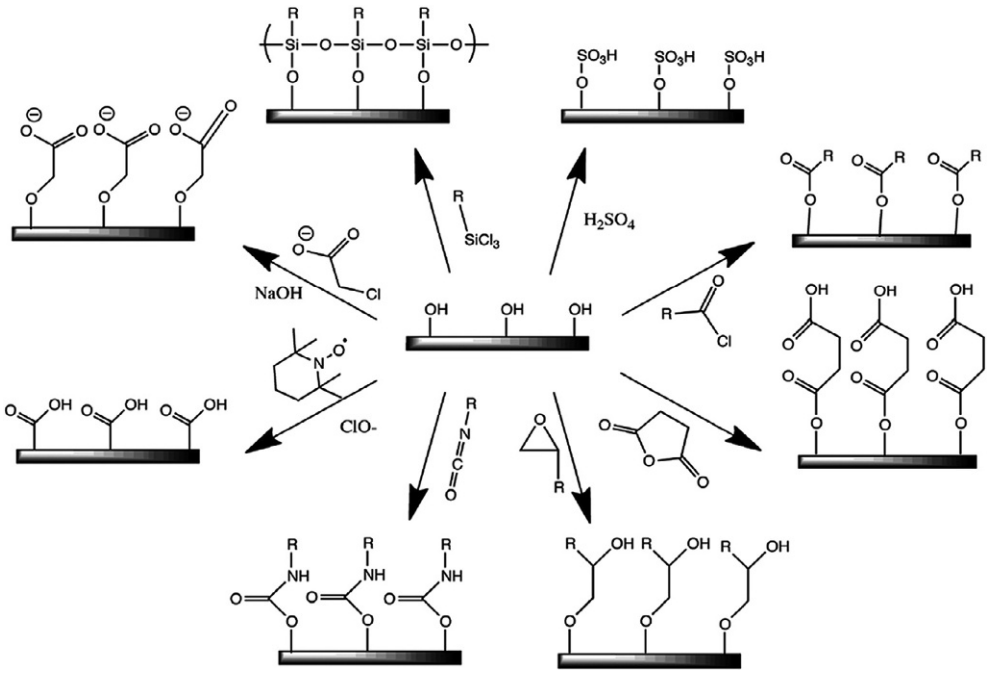

SCHEME 13.1 Some common surface modification methods of nanocellulose (clockwise from the top right side: sufonation, acetylation, esterification, etherification, Urithenization, TEMPO oxidation, carbocymethylation, silylation (Patel et al., 2019).

13.6.1 Functionalization to impart ionic charge on nanocellulose

Nanocellulose surface can be made ionic by phosphorylation, carboxymethylation, oxidation, and sulfonation routes (Scheme 13.1) (Patel et al., 2019).

Phosphorylation

In this method a phosphate group (PO_4^{3-}) is incorporated onto the nanocellulose surface. In this process the free hydroxyl groups of the C2, C3, and C6 positions are converted to phosphate by reacting with phosphorylating agent such as $POCl_3$ (phosphorus oxychloride), P_2O_5 (phosphorus pentoxide), $(NH_4)_2HPO_4$ (diammonium hydrogenphosphate), H_3PO_4 (phosphoric acid), and organophosphates (Božič et al., 2014). The degree of phosphorylation depends on the reaction time, temperature and the molar ratio of nanocellulose and phosphorylating agent. For instance, CNFs with phosphate group incorporated predominantly at the C6 position has been done using enzyme hexokinase with ATP and Mg(II) ions (Thomas et al., 2018).

Carboxymethylation

Functionalization of nanocellulose surface with carboxymethyl group (–CH_2–COOH) increases the negative charge on the surface. Accumulation of negative charge increases the electrostatic repulsion and thus helps to break down the cellulose into nanometer size. Wagberg and coworkers have fabricated nanocellulose fiber of diameter 5–15 nm by

FIG. 13.8 Sulfonation of nanocellulose.

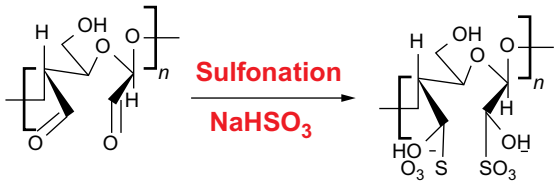

carboxymethylation of cellulose fibers and using a homogenizer (Wågberg et al., 2008). Similar methods have also been used by Siro ei al. to produce nanofibrillated cellulose from softwood pulp (Siró et al., 2011).

Oxidation

The most common oxidant is TEMPO (2,2,6,6-Tetramethylpiperidine-1-oxyl) which helps to isolate the nanofibers and at the same time makes the nanocellulose surface hydrophobic. In this method stable nitroxyl radicals are generated from TEMPO and convert hydroxyl group to aldehydes and eventually to carboxylic acid. This process generates high negative charge on the nanocellulose surface and hence ensure better dispersibility in water. Isagai et al. converted the surface functional groups on cellulose to carboxylate by TEMPO-mediated oxidation to form nanofibers (Isogai et al., 2011) which was utilized by Saito et al. for removal of Pb(II), La(III), and Ag(I) ions from aqueous solutions (Saito and Isogai, 2005).

Sulfonation

Sulfonation of nanocellulose surface can be carried out by using reagents such as H_2SO_4 or $NaHSO_3$ and like the two previously mentioned methods makes the nanocellulose surface ionic. Concentrated H_2SO_4 which is used to catalyze the hydrolysis of source material can also convert the hydroxyl groups to sulphate half ester. It displays high affinity toward multiple metal ions which increases the rate of adsorption (Dong et al., 2016). In fact, the affinity of sulfonic groups for metal ions is stronger than any other functional group like carboxyl and hydroxyl due to larger degree of ionization (Fig. 13.8).

13.6.2 Functionalization to generate hydrophobic surface

Cellulose surface is hydrophilic in nature and hence it absorbs moisture. The affinity of cellulose toward water can be altered by chemical modification techniques such as esterification, etherification, silylation, amidation, and urethanization. The modification method is based on the reaction of the chemical modifying agent with surface hydroxyl group of the nanocellulose.

Acetylation

Acetylation is carried out using acetic anhydride and dry acetic acid along with either H_2SO_4 or $HClO_4$ as catalyst. For instance, Butola et al. used acetic andride to acetylate the CNFs which they then used for the reparation of acetylated CNF-polylactic acid nanocomposite. These authors also reported that by acetylation process the contact angle increased from 33°–115° indicating great improvement in hydrophobic character (Bulota et al., 2012). Acetylation can also be achieved using vinyl stearate, vinylacetate, and succinic anhydride (Thomas et al., 2018).

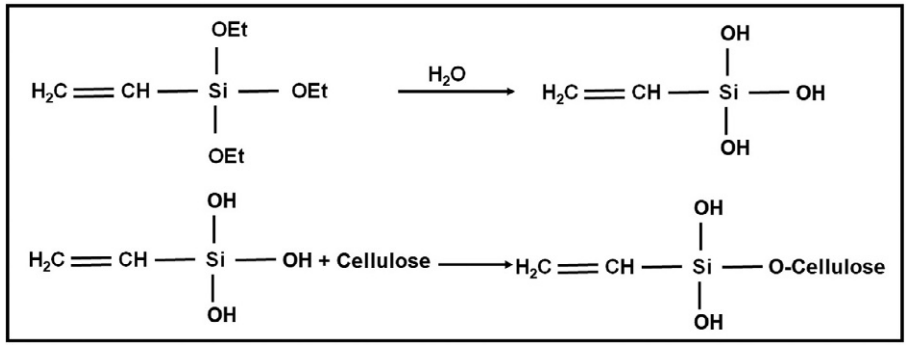

SCHEME 13.2 Silylation reaction scheme of cellulose fibers (Bezerra et al., 2015).

Etherification

Etherification is a commonly used pretreatment method that facilitates the defibrillation process to produce CNFs. In this process the cellulose fibers are treated with NaOH and then hydroxyl groups are converted to carboxymethyl motiety with monochloroacetic acid or its sodium salt. Drawback of this process is the use of hazardous halocarbon reagents and increase in hydrophilicity of the nanocellulose surface (Thomas et al., 2018).

Silylation

Typically used substrate for silylation is alkyldimethylchlorosilane. The silanols formed by the action of moisture on alkoxysilane react with cellulose fibers through the hydroxyl group, forming stable covalent bonds and chemisorbed onto the fiber surface (Scheme 13.2) (Bezerra et al., 2015).

Gousse and coworkers have used isopropyl dimethylchlorosilane to generated silylated CNFs which have inherent flexibility and excellent rheological properties (Thomas et al., 2018).

Amidation

In this route the carboxylic acid groups on nanocellulose surface are generated by preoxidation of hydroxyl groups and then converted to amide functionality. The most common reagent used for this purpose is *N*-ethyl-*N*-(3-(dimethylamino)- propyl) carbodiimide hydrochloride (EDAC). The optimum pH range is between 7 and 10 for the amidation of nanocellulose material.

Urithenization

The reactions between surface hydroxyl group and isocyanate gives rise to the formation of urethane linkage (R–N=C=O). Other terms used for this process are carbanylation and carbamation. For instance, Siqueira et al. have prepared surface-modified CNC and NFC by n-octadecyl isocyanate with enhanced hydrophobicity and greater dispersibility in organic solvent (Thomas et al., 2018).

13.7 Nanocellulose-based nanocomposites

A composite is a heterogeneous mixture of two or more components having significantly different physicochemical properties. Nanocomposite contains a homogeneous matrix of polymer or biopolymer onto which a small amount of nanosize material (filler) of specific shape, size and surface chemistry is reinforced (Nandi and Guha, 2018). Owing to their chemical reactivity, high specific surface area, optical, thermal and mechanical properties, CNCs are very useful as nanofillers. Development of nanocellulose-based composites can offer substantial improvements in supportive properties like strength and dimensional stability in order to create high performance biomaterials. As for instance, it has been widely reported that CNC incorporated polymer matrix increases the tensile strength and decreases the elasticity. This is because of the existence of strong covalent bond, van der Waals forces, mechanical interlocking and molecular entanglement between the CNCs and polymer matrix. Moreover, the biocompatibility of CNCs compared to other nanofillers such as carbon black, mica, silica, nanoclay, metal oxides, etc., makes it a useful choice for biomedical application (Nandi and Guha, 2018). There are several methods available for nanocellulose synthesis namely ballmilling, solution casting, melt extrusion, compression molding, precipitation routes, injection molding, 3D printing, layer-by-layer assembly, wet- and electorspinning, and micropattering techniques.

CNCs has been used to fabricate high quality, cost-effective nanocomposite material based on thermoplastic and thermoset polymers. Different polymers such as polybutyl methacrylate, polyvinylchloride, poly exo-ethylene, polymethyl methacrylate, ethylene oxide-epichlorohydrin copolymers, polycarbonate, poly lactic acid, polyurethane, polyvinyl alcohol and poly vinyl acetate based nanocomposites are reported (Trache et al., 2020). The mechanical properties of such nanocomposite depend on interfacial interaction between CNCs and the polymer chosen and can be further enhanced by making specific modification. Combination of CNCs with thermosets such as unsaturated polyester, polyurethane, epoxy and phenolic resin gives rise to improvement of physicochemical properties in a synergistic manner. Apart from that, several natural polymer for instance gelatin, protein, chitosan, alginate, natural rubber, Xanthine, starch, cyclodextric, etc., has been used to produce bionanocomposite. Also, oxidized CNCs (TEMPO oxidation or ammonium persulfate method) can be coupled with metal or metal oxide nanoparticles such as Ag, ZnO, CuO, and Fe_2O_3 (Oun et al., 2020). Combination of nanocellulose with nanocarbon such as carbon nano-tubes, nanodiamond, grapheme and graphene oxide, etc., can lead to the formation of nanocomposite of wide range applicability. For example, CNCs have been used to immobilize fullerene nanoparticles. The CNC-fullerene composite showed a higher radical scavenging property in vitro compared to fullerene alone (Awan et al., 2016). Nanocellulose-nanocarbon composites have interesting properties such as flexibility, stretchability, high adsorption capacity, high mechanical strength, tunable optical, electrical property, thermal conductivity as well as photothermal and photodynamic activity. Thus, this composite material remains a key focus in the future research activities.

13.8 Bacterial nanocellulose

The technology for processing BC is different than that employed for either CNF or CNC. In order to have different properties, BC production uses different steps. In general BC is hydrophilic with high purity with no hemicellulose or lignin with high molecular weight and

TABLE 13.3 Static and agitated BNC production—Advantages and disadvantages (Foresti et al., 2015).

Static production		Agitated production	
Advantages	**Disadvantages**	**Advantages**	**Disadvantages**
Operation cost low	Incubation Periods longer (5–20 days)	Incubation periods shorter (1–8 days)	Energy cost high for generating the mechanical power
Easy to perform	High risk of contamination	Strong mechanical agitation prevents heterogeneity	Occurrence of non-producing mutant cells
Higher yields reported	O_2 diffusion limitations are met by large surface area of the bioreactor	Smaller bioreactors	Lower yields reported
	More manpower is required	Both continuous and Fed-batch can be implemented	Increase of the viscosity
Higher crystallinity index reported	Measurements, are difficult to perform.	Measurements, controls can be easily implemented	Pellets oramorphous Highly branched BNC

high crystallinity. The properties of BC are influenced by the culture conditions (Blanco et al., 2018). The common fermentation method for production of BC is the static culture (SC). Shear stress can convert cellulose producing bacterial strains into non-cellulose-producing mutants (Blanco et al., 2018).

Number of bacteria can secrete cellulose microfibrils with nanometric widths as an extracellular primary metabolite under proper conditions. Bacteria that are known to be able to synthetize BNC are those belonging to the genera Acetobacter (now Gluconacetobacter), Agrobacterium, Alcaligenes, Pseudomonas, Rhizobium, Aerobacter, Achromobacter, Azotobacter, Salmonella, and Sarcina (Foresti et al., 2015). Microbial cellulose production very much depend on the composition of the culture medium, strain, oxygen supply, the fermentation temperature and the implementation of static or agitated systems. Advantages and disadvantages of static and agitated BNC production are given in Table 13.3 (Foresti et al., 2015).

In complex biological systems, a cell-free technique (Fig. 13.9) has been developed to understand the metabolism of several complex biological processes that can lead to increased BNC production (Sharma and Bhardwaj, 2019).

13.9 Properties of BNC

Both BNC and plant cellulose have the same molecular formula but fundamentally different because of nanofiber architecture (in BNC). Some of the important properties of BNC are high polymerization degree, high crystallinity, very high liquid loading capacity, nanofiber architecture, possibility of designing the shape of the membranes obtained, light density, biodegradability, nanofibers immobilized in a stable network, high stability, high chemical purity, biocompatibility, extensive surface area, high hydrophilicity, high degree of conformability, high elasticity, high mechanical strength or non-toxicity, non-pyrogenicity, high transparency, tunable porosity, renewability, indigestibility in the human tract, no

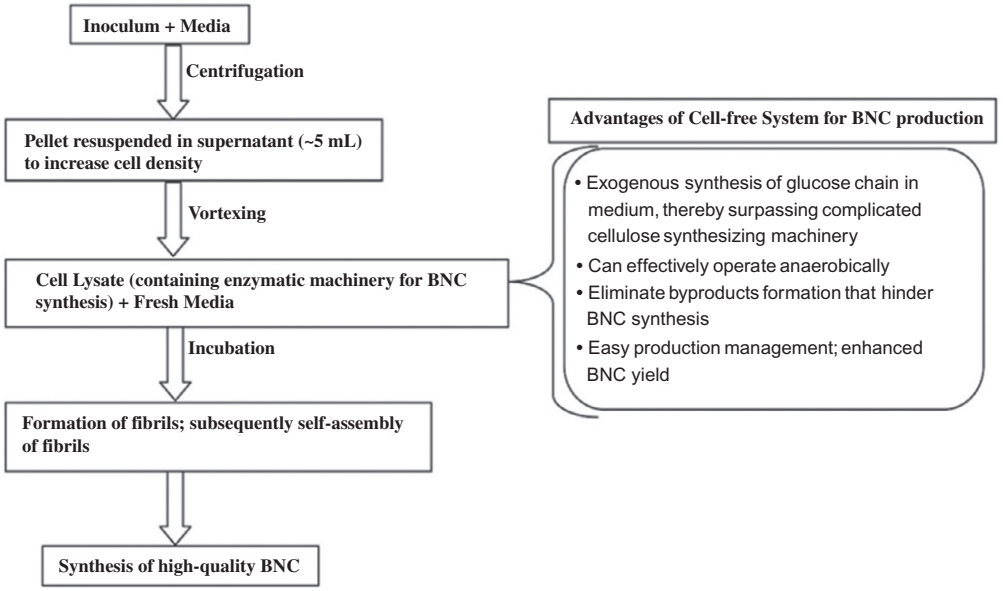

FIG. 13.9 Cell-free strategy for extraction of BNC (Sharma and Bhardwaj, 2019).

functional group other than OH. Different methods for production of BNC and their applications are given in Fig. 13.10 (Sharma and Bhardwaj, 2019).

13.10 Applications of nanocellulose

Nanocellulose is used in various fields such as paper and packaging industry, electronic industry, biomedical field and environmental remediation purpose. They have some excellent properties which includes their lightweight and transparent nature, high thermal and mechanical strength, biodegradability, etc. (Abitbol et al., 2016). Nanocellulose in the form of nanocomposites have attracted several industries for making structural composites in construction. Fig. 13.11 depicts various fields where nanocelluose are used extensively. Table 13.4 lists some important application areas of the nanocellulose industries.

13.10.1 Application in paper and packaging industry

The tensile strength of nanocellulose is eight times to that of steel. It is also found to be stiffer than Kevlar. This makes nanocellulose as a good choice for packaging industry. The sustainable and versatile nature of this material is an added advantage to the packaging industry. The available packaging materials are synthetic polymers based on petrochemical products and thus they are non-renewable and are hardly biodegradable. To keep the environment safe, efforts are made to develop biodegradable food packaging keeping the quality and safety of food intact. The barrier properties of nanocellulose are utilized to develop

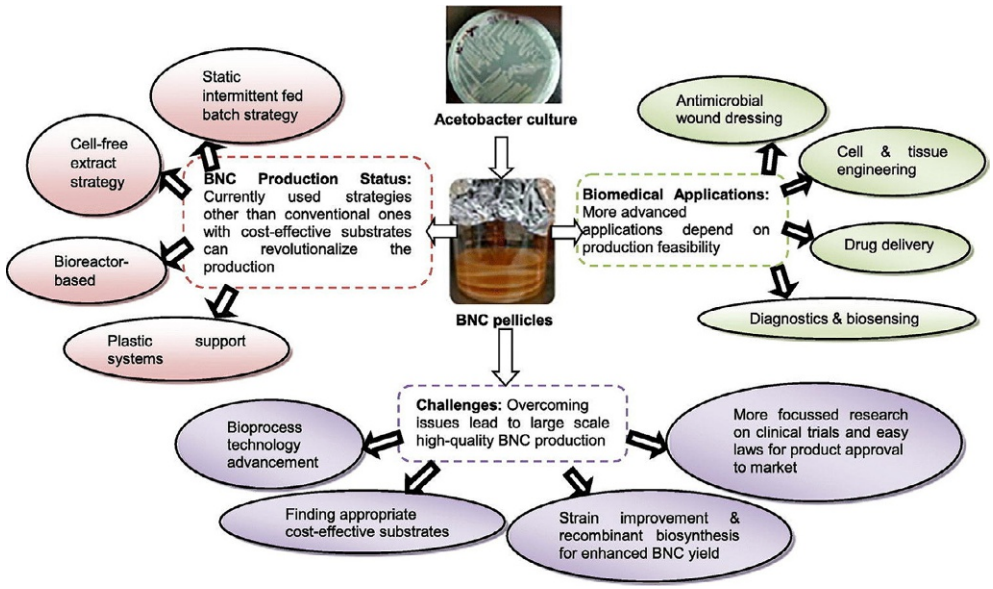

FIG. 13.10 Production and applications of BNC.

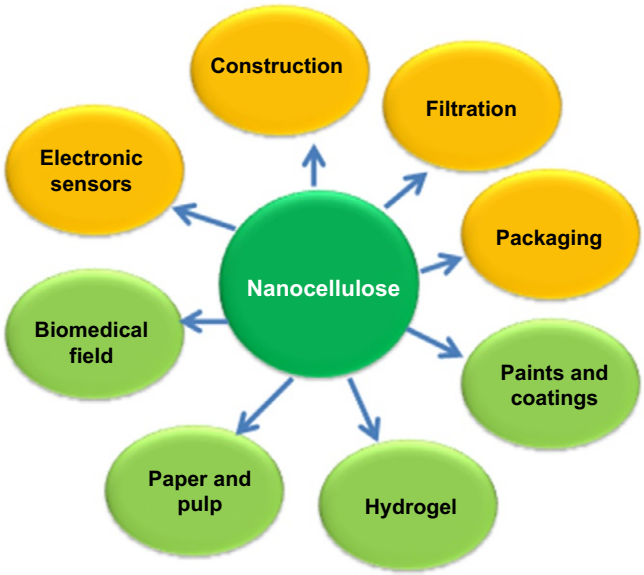

FIG. 13.11 Various fields of application of nanocellulose.

nanocomposite films allowing specific penetrating molecules to transit. The size and shape of the nanocellulose fibrils inhibit the passage of gas and water through the film (Nair et al., 2014). In most cases these films are edible and act as protective coating on the food. As the films are made from natural polymer cellulose, they are non-toxic and very much economical for applications in food packaging. Trifol et al. have reported a composite made

TABLE 13.4 Application industries with selected application areas of nanocellulose.

Application industries	Areas of application
Paper and Packaging	Smart packaging, see-through packaging, antimicrobial packaging, UV-screening packaging
Composites	Extension of shelf life, resistance to heat, dimensional stability
Biomedical	Controlled release of drugs in drug delivery, antibacterial and antimicrobial activity, scaffold in tissue engineering, cardiovascular implants
Energy and Electronics	Digital display, Sensor and detector, time-temperature integrator, signal processor, diaphragms
Environmental remediation	Removal of heavy metals, organic pollutants, dyes, oil adsorption, removal of air pollutants
Aerogel	Shelf healing products

from nanoclay and polylactic acid (PLA) reinforced with nanocellulose for applications in packaging industry (Trifol et al., 2016). This nano-biocomposite film has excellent barrier properties against water and oxygen gas. Similarly, use of Carboxymethyl guar (CMG), poly(vinyl alcohol)/polyacrylamidepolymer network, etc., for making biocomposite films reinforced with cellulose are under investigation for the improvement of barrier properties for gas and moisture.

Surface-modified nanocellulose has important application in the fabrication of amphiphobic surface for protecting both polar and non-polar liquids. These amphiphobic surfaces have great application in synthesis of antibacterial, antirefelective, self-cleaning, and corrosion-resistant material. An amphiphobic paper was synthesized by Phanthong et al. by surface modification of nanocellulose (Phanthong et al., 2016). The fabrication process involves surface coating of the filter paper with nanocellulose followed by silylation using chemical vapor deposition. The fabricated paper was super hydrophobic and oleophobic. Because of this it was repelled from both polar and non-polar environments. These special properties of nanocellulose papers find application in self-cleaning and anti-corrosion purposes (Si et al., 2016).

In addition to excellent mechanical properties, nanocellulose possesses some other fascinating properties such as transparency, optical clarity and flexibility. These nanocellulose papers with novel properties are used in soar cells, electronic tools, flexible circuits, flexible displays and many other areas. Transparent paper made from wood flour has been reported to exhibit high optical transparency, high modulus and strength and nominal thermal expansion. Because of its renewability, biodegradability and minimal toxicity the nanocellulose-based materials will be more adapted by the paper and packaging industries in upcoming years.

13.10.2 Energy and electronics industry

Nanocellulose composites have excellent conductivity and flexibility. Recently, they are gaining popularity as a potential candidate in energy and electronic sectors. In addition to superior mechanical properties, they possess light weight, transparency, optical clarity,

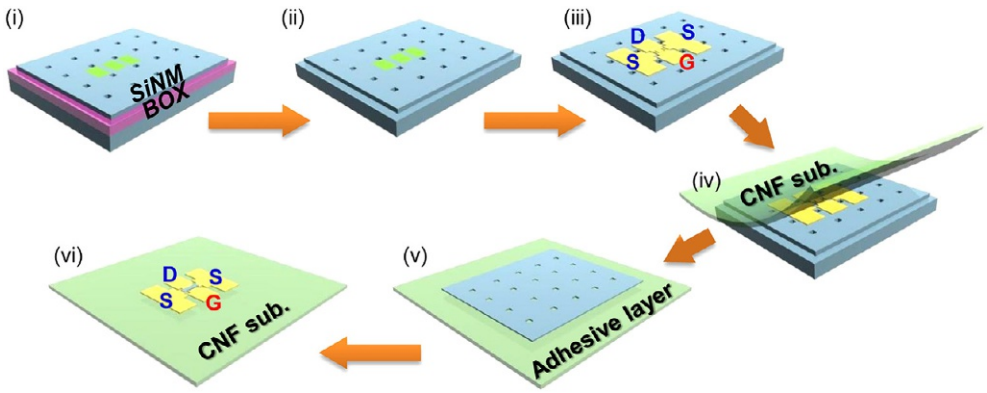

FIG. 13.12 Schematic of production process for flexible electronics on CNF substrate (Seo et al., 2015).

and flexibility. They are widely used in electronic devices, photovoltaics, flexible circuits and displays. The electronic charge conduction in many electronic systems and storage devices happen via mineral or metallic substances. The concept of paper batteries are first evolved in 2006 for advanced electrical storage devices. These systems are made up by stacking one anode, absorbent paper, a cathode material and a current collector. This design enables them to get activated quickly and supply enormous power. A lot of research is currently going on for application of nanocellulose for making flexible electrode for Li-ion battery. There is high chance that these materials will replace the conventional polymer films as separator for Li-ion battery. A few important area of use nanocellulose in energy and electronics sector is discussed below.

Flexible electronics

Nanofibrillar cellulose films have good mechanical properties, low thermal expansion coefficient and are transparent. Thus they have high potential in electronics sector for flexible electronics devices. Silicon nanomembranes are used for the development of CNF films with high-speed transistors. The schematic of the fabrication process is shown in Fig. 13.12 and the process is explained in detail (Seo et al., 2015). In another work they have reported microwave devices made from gallium arsenide on CNF material (Jung et al., 2015). In addition to that they have fabricated Si-based complementary metal oxide semiconductor (CMOS) systems with 5 kHz frequency limit. Huang et al. have fabricated highly efficient flexible organic field effect transistor (OFET) using softwood kraft pulp (Huang et al., 2013). The CNF film was coated with conductive CNT and then with PMMA (polymethyl methacrylate). Another important application of nanocellulose is in printed electronics. Application as antenna tags in radiofrequency identification (RFID) has been demonstrated by printing of silver antennas on crosslinked CNF films (Zhu et al., 2014). Although performance of these printed electronics are far behind the conventional silicon-based electronics but their potential in this area cannot be neglected.

Digital display and light-emitting diodes (LED)

Nanocellulose has prime importance in display technology. The modern trend of dynamic display technology is totally based on nanocellulose. CNFs are mostly used for making light-emitting diodes for display purpose. Organic light-emitting diode (OLED) can be synthesized

from cellulose nanofibril by multistep process. Synthesis of OLEDs by depositing indium tin oxide thin films on bacterial cellulose is also known. Printing of AgNPs on CNF to produce illuminated LED has been reported (Yagyu et al., 2015). By varying the ratio of CNC/CNF, a nanopaper was synthesized and then it was coated with silver nanowires for the fabrication of flexible LED (Xu et al., 2016). A recent work by Ji et al. have shown a CNF-epoxy hybrid material as LED with good mechanical strength and low thermal expansion coefficient suitable for flexible display purpose (Ji et al., 2016). Further research in this area will lead to the more advancement in flexible, transparent LED.

Opto electronics

It has been observed that CNC suspension exhibit liquid crystal behavior. Under the action of electric field CNCs can be aligned with particular arrangement. Thus CNC suspensions have great potential in liquid crystal display techniques. Many electro-optical devices can be fabricated by varying the electrical signal inside the CNC suspension to control the orientation of CNC as well as the amount of transmitted light (Oulachgar et al., 2016). This area has not been developed much because of availability of limited research but can have huge impact on applications on opto-electronics industry.

Energy harvesting and storage

In the area of energy storage systems, nanocellulose composites are used as supercapacitors, fuel cells, battery electrodes and any other electronic energy storage devices. The performance of these materials in some cases was superior to the conventional energy storage systems. Nanocellulose has shown promising results as photovoltaic for harvesting solar energy. A large number of organic photovoltaics are fabricated from CNC and CNF films with good power conversion efficiency (Fang et al., 2014; Luo et al., 2014; Zhou et al., 2014). The optical haze and high transparency of CNF films play key role on enhancing the photovoltaic properties. Moreover composite of CNCs and PDMS (polydimethylsiloxane) has been reported for conversion of mechanical energy to electrical energy for energy harvesting (Peng et al., 2017). Further research is going on for exploiting nanocellulose to harvest energy from movement of human, ocean waves, stream of air, etc.

Both CNC and CNF membranes are exploited for fuel cell applications (Bayer et al., 2016). CNC nanopapers with more number of charge carriers exhibited higher conductivity than CNF. A low temperature polymer electrolyte fuel cell was fabricated by Jiang et al. using a composite membrane of nanocellulose and Nafion (Jiang et al., 2015). The use of Nafion has provided high ionic conductivity in fuel cell applications. A biopolymer electrolyte, fabricated from the composite of bacterial cellulose with crosslinked poly(4-styrene sulfonic acid) has shown excellent fuel cell performance (Gadim et al., 2017).

Nanocelluloses are also investigated for their role in super capacitor devices. The electrodes in these devices are composites of nanocellulose with some conducting polymers, e.g., polypyrrole (PPy) or polyaniline (PANI). Zhang et al. have synthesized silver-coated CNF aerogel/PANI supercapacitor. This flexible material displays very high specific capacitance (176 mF/cm^2) (Zhang et al., 2014b). Flexible electrode fabricated from CNF aerogel with PPy and RGO (reduced graphene oxide) have been reported with good energy density at various bending situations (Zhang et al., 2019). CNF in the form of aerogels have high potential in flexible energy storage devices because of their porous nature (Pottathara et al., 2018; Wang et al., 2017).

13.10.3 Applications in biomedical field

Nanocellulose has found immense application in biomedical field because of its excellent properties. It exhibits outstanding biocompatibility and less toxicity which makes it a promising material for biomedical applications. Its unique geometry, high specific surface area, rheology, remarkable surface chemistry, high chemical and mechanical strength and self-assembly property are the major reasons behind high demand of nanocellulose in medical field.

In the biomedical industry nanocellulose is used in drug delivery system, tissue engineering, blood vessel growth, stent covering, bones reconstruction, skin repairing after burns and wounds, nerves, gum and dura mater reconstruction, etc. In Fig. 13.13 (Kalia et al., 2011) some applications of nanocellulose in medical field are shown. Few specific areas of application of nanocellulose in biomedical field are discussed in the following section.

Drug delivery system

The drug delivery system releases drugs to the specific target organism with specified amount in an appropriate time. In pharmaceutical industry it is used as tablet coatings for oral administration. The nanocellulose is blended with various excipients to form dense matrices for controlled release of drugs. These formulations are flexible and provide reproducible drug release profiles. Cellulose nanocrystals (CNCs), Cellulose nanofibers (CNFs), bacterial nanocellulose (BNC) are among different types of nanocellulose which are extensively used for drug loading as well as drug releasing systems. A hybrid bionanocomposite is synthesized combining nanoparticles of poly(D,L lactide-*co*-glycolide) (PLGA) with cellulose nanocrystals (CNCs) and finally loaded with bovine serum albumin fluorescein isothiocynate conjugate (FITC-BSA) (Rescignano et al., 2014). This novel biocomposite is

FIG. 13.13 Biomedical applications of nanocellulose (A) and (B) never dried nanocellulose membrane; (C) and (D) artificial blood vessels; (E) dura mater reconstruction (F) covering stents (Kalia et al., 2011).

successfully used for bone marrow mesenchymal stem cell repairing. CNCs have the ability to disrupt two membranes of different cell lines without any trace of cytotoxicity. CNC is adopted as the most promising material as drug carrier because of its functionalized surface. The high reactivity of the CNC surface allows the drugs or target molecules to bind strongly. The hydrophobic drugs are water insoluble and are a major concern in drug delivery systems. To overcome the issue, a multilayer thin films based on CNC is developed (Mohanta et al., 2014). The drug delivery of this system happens via layer by layer. To improve the compatibility issues chemical modification method is generally taken up by the researchers and scientists. Drug release is a complex process in which a drug undergoes absorption, distribution, metabolism and excretion (ADME) before it is showing pharmacological behavior. A lot of research is still going on for further improvement in drug releasing method by controlling the interaction of CNC and drug molecule.

Tissue engineering

Tissue engineering is another important area where nanocellulose provides innovative solutions. This interdisciplinary field is associated with restoration, maintenance and improvement of the malfunctioned tissues by substituting promising biological material. Similar mechanical properties like natural tissues, formation of three dimensional network and low cytotoxicity has put nanocellulose in forefront of tissue engineering. Among various nanocellulose, BNC being highly porous and biocompatible is the most promising material as biodegradable scaffolds mimicking extracellular matrix for culturing cells. Numerous nanocellulose biomaterials in the form of hydrogels, sponges, composites, conductive polymers, membranes, and electrospun nanofibres are used for various applications. The cell attachment and proliferation are enhanced by surface modifications by protein coatings, alteration of surface charge, and plasma treatment. Research on nanocrystalline cellulose (CNC) suggested cell morphology and cell growth has been affected by CNC scaffolds. The mechanical property and thermal stability of the scaffolds are improved by CNC. NFC hydrogels have special place in tissue engineering scaffolds. A flexible 3D NFC hydrogels scaffolds are developed to culture stem cell and hepatic cell. A metal crosslinked NFC hydrogel scaffolds added with fibronectin is reported for the growth of fibroblast cells (Zander et al., 2014). Nanocellulose reinforced hydrogel composites have attractive mechanical properties in polymeric gel formulations (Mandal and Chakrabarty, 2017). Both the reinforcement phase and the host matrix phase have superior properties. A hydrogel based on semi-interpenetrating polymer network of chitosan developed by (Sampath et al., 2017) is used for gene delivery and other pharmaceutical applications. Electrospun poly(-caprolactone)/nanocellulose composite fiber matrix for biomimetic scaffolds is reported for applications in tissue engineering (Si et al., 2016).

Cardiovascular implant

Cardiovascular disease is one of the deadly diseases leading to thousands of heart bypass surgery every year. During the surgery vessels are taken from the leg or thorax of patients to replace arteries as the artificial bypass implants are unavailable. Commonly available bypass implants are developed from various polymers e.g. polyethylene, polyurathane, polytetrafluoroethylene, poly(ethylene terephthalate), etc. These materials have blood clotting issues and are ineffective in cardiovascular surgery. BNC-based implants have the advantage of

nanodimension, biocompatibility, and strength making it an ideal reinforcing material. These are used for patching up of vascular grafts for injured and maligned blood vessels or sometimes complete replacement of the segment. Klemm et al. have developed prototypes of BNC tubes in the brand name of BASYC (bacterial synthesized cellulose) for application in artificial grafting (Klemm et al., 2006; Schumann et al., 2009). These grafts have shown promising results in small diameter arteries of cardiovascular transplant. Nanocrystalline cellulose (NCC) reinforced composite with fibrin has shown immense potential in vascular application (Brown et al., 2013). The porous nature of the NCC allows permeability enhancing the growth of new tissues. Thus NCC composites have a lot of potential in wound healing, bone repairing, vascular, and vascular regeneration. A good matching of mechanical properties between implanted device and nearby tissues in replacement applications is of prime importance. A mechanical mismatch will result in graft failure. Anisotropic nanocomposite of PVA (polyvinyl alcohol) and BNC developed by Millon et al. have close matching of mechanical properties (Millon et al., 2008). Thus, it can be applied satisfactorily for cardiovascular tissue replacement. Furthermore a blend of chitosan and cellulose has similar mechanical properties as that of coronary arteries of human (Azevedo et al., 2013). Thus chitosan/cellulose blend are used to fabricate small diameter hollow tube for application in coronary artery bypass grafting.

Antibacterial/antimicrobial activity

The healing process of the wounds gets delayed because of the infection caused by the bacteria. Thus development of an effective surface disinfectant with antibacterial properties is getting a lot of attention. In this situation nanocrystalline cellulose with porous network structure is the most suitable candidate for transferring antibiotics in the wounded area. As such pure nanocrystalline cellulose do not possesses any antibacterial/antimicrobial activity, but it arises when it is blended with some antimicrobial agents. The nanocrystalline cellulose can be blended with inorganic antimicrobial agents (e.g., Ag and ZnO) or organic antimicrobial agents (e.g., lysozyme).

Numerous research work has been performed on Ag nanoparticle (NP) and nanocellulose-based composite for their antimicrobial activity (Bober et al., (2014); Shi et al., 2015). An antimicrobial membrane synthesized by Barud et al. using a composite of AgNP/nanocellulose has strong activity toward both gram-positive and gram-negative bacteria (Barud et al., 2011). Cellulose nanocrystals mixed with AgNPs are used in antiseptic lotion or wound healing gels for their exceptional antimicrobial ability. In addition to AgNPs, zinc oxide nanoparticles also proven fruitful antimicrobial agent when combined with cellulose nanocrystals (CNCs) (Azizi et al., 2013). Beside incorporation of *N*-halamine, nanocurcumin in the cellulose network provides antimicrobial properties. Grafting of aminoalkyl groups, 2-benzyl-4-chlorophenol, L-cysteine, diclofenac, etc., on cellulose surface creates antimicrobial activity.

13.10.4 Application as adsorbent for environmental remediation

Nanocellulose materials are currently in spotlight for environment remediation applications. Several good reviews are available on this topic (Sharma et al., 2019; Mahfoudhi and Boufi, 2017). Numerous pollutants such as removal of dyes and heavy metals from water using nanocellulose have been investigated by many scientists. In addition to water

treatment, purification of air and removal of virus and microbes by nanocellulose is getting importance. The separation of the contaminants happens through adsorption process. Functionalizing the nanocellulose by SO^{3-} group, $-COO^{-}$ group or $-NH_2$ group improves the binding of the contaminants through ionic or covalent bonding (Hokkanen et al., 2016). The adsorption happens by physical, chemical, biological, acoustical, radiation, and electrical mechanism.

Heavy metal removal

Removal of heavy metals such as Hg^{2+}, Zn^{2+}, Cu^{2+}, Pb^{2+}, Cd^{2+}, Cr^{3+}, etc., from water bodies are performed by using composites of nanocellulose (Jamshaid et al., 2017). Heavy metals are extremely toxic for human body and other living organisms. Adsorptions of heavy metals are not only dependent on large surface are but also directed by chemical complexation and ion exchange process. Thus tailoring the surface of nanocellulose to introduce ionic or complexing site is the most favored method. Cellulose nanofiber (CNF) are investigated extensively as adsorbent for numerous metal ions while only limited reports are available for cellulose nanocrystals (CNCs).

Kardam et al. has reported Pb^{2+}, Cd^{2+} and Ni^{2+} ion adsorption over CNC synthesized using rice straw (Kardam et al., 2014). Comparative investigation of pristine CNC and phosphate functionalized CNC for adsorption of Ag^{+}, Cu^{2+}, and Fe^{3+}, is investigated by (Liu et al., 2015). Their results indicate that surface functionalization with phosphate group enhances the adsorption ability to two fold. The pictorial diagram of the result is sketched in Fig. 13.14. Cellulose nanocrystals modified with succinic anhydride was examined by Yu et al. for the adsorption of Pb^{2+} and Cd^{2+}(Yu et al., 2013). In case of the modified CNS, the adsorption rate improved tremendously. In spite of this exceptional ability to remove multitude of metal ions, the main problem with CNCs is their aggregation which is limiting them for large-scale applications.

Adsorption of metal ions by CNFs occurs through primarily by exchange mechanism. CNFs are highly flexible materials and can be shaped into different compounds, e.g., aerogel, porous bead, and membrane. Functionalization of the surface of CNFs by -COOH, $-R_3N^{+}$ or $-SO_4^{2-}$ are performed for specific adsorption purpose. Carboxylated CNFs have high adsorption capability specifically for divalent metal ions (Pb^{2+}, Cd^{2+}, Ni^{2+}, etc.)

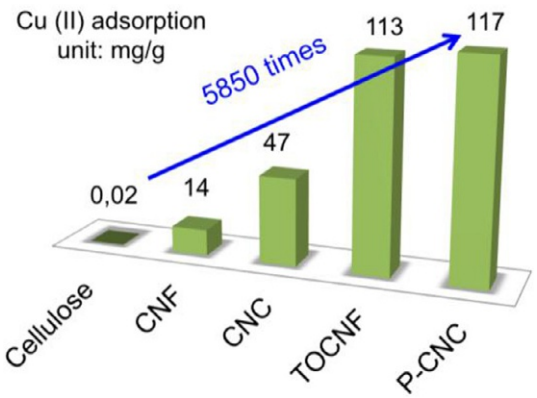

FIG. 13.14 Comparison of Cu(II) adsorption of cellulose with cellulose nanofibers (CNF), cellulose nanocrystals (CNC), tempo-oxidized cellulose nanofibers (TOCNF), and phosphoryl cellulose nanocrystals (P-CNC) (Liu et al., 2015).

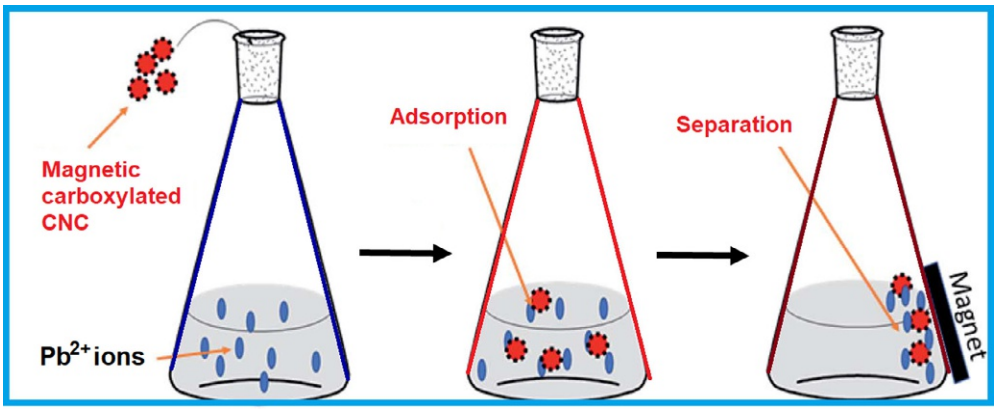

FIG. 13.15 Adsorption process of Pb (II) by magnetic carboxylated cellulose nanocrystals (CCN/Fe_3O_4) (Lu et al., 2016).

including radioactive UO_2^{2+} ion because of the presence of abundant negative charge on the surface (Sehaqui et al., 2014; Ma et al., 2012). Highly carboxylated cellulose nanofibrils (CNFs) are produced by esterification reaction reported for advanced application in heavy metal removal. Integration of highly carboxylated CNFs with paper filters can effectively remove lead metal from water. Removal of Pb^{2+} using a carboxylated CNC magentized with Fe_3O_4 has been depicted in Fig. 13.15 (Lu et al., 2016). Hokkanen et al. reported 3-aminopropyl triethoxysilane (APS) modified CNFs displaying pH-dependent adsorption of Pb^{2+}, Cd^{2+} and Ni^{2+} ion (Hokkanen et al., 2014b). A composite membrane made from polyacrylonitrile (PAN)/polyethylene terephtalate (PET) with cellulose nanofibrils have been reported for efficient removal of Cr^{6+} and Pb^{2+} (Yang et al., 2014a, 2014b). The fibrous structure, large surface area, and porous nature of the nanocellulose is the reason behind their exceptional adsorption ability. The adsorption capacity of the cellulose nanofibrils is enhanced by increasing the adsorption site by grafting polymers with nanocellulose. For example, a highly porous aerogel made from poly(methacyclic acid-*co*-maleic acid) grafted CNF is tested for adsorbing Pb^{2+}, Cd^{2+}, Ni^{2+}, and Zn^{2+} and the results are three times better than the pristine CNF (Maatar and Boufi, 2015). A similar kind of work by Anirudhan et al. has reported Co^{2+} adsorption from nuclear industry waste water using poly(itaconic acid)-poly(methacrylic acid) grafted nanocellulose/nanobentonite composite (Anirudhan et al., 2016). Vipin et al. have investigate Prussian blue immobilized CNF for the adsorption of radioactive Cs metal and the result was highly promising (Vipin et al., 2016). Composite of nanocellulose with various organic compounds, e.g., chitin, chitosan, sodium alginate are also investigated for adsorption purpose. Similarly inorganic composites with sodium montmorillonite, titanium dioxide, ferric chloride, hydrogels, aerogels, etc., are reported. Numerous carbon-based-reinforced composites with carbon nanotube, graphene oxide, and activated carbon are reported by Tshikovhi et al. as excellent adsorbent for both organic and inorganic pollutants (Tshikovhi et al., 2020). They also reviewed the metals, non-metals, and ceramic composites for adsorption of contaminants for water remediation. The nanocellulose composite materials and the contaminants interact through various intermolecular forces such as electrostatic interaction, hydrogen bonding, pi–pi stacking interaction, and van der Waals forces.

Dye removal

Pollutions from the dyes are main concern from the textile, paints, paper and plastics and cosmetics industries. Both CNCs and CNFs in their pristine form have high potential in adsorbing cationic/anionic dyes. Sometimes they are also used in the form of aerogel and membrane for this purpose. Chan et al. has synthesized CNF from kenaf core for adsorbing methylene blue dye (Chan et al., 2015). The adsorption kinetics was quick (equilibrium reached within 1 min), and the adsorbent was recyclable till six times. It is observed that the adsorption capacity of dyes enhances when CNC is oxidized with TEMPO (2,2,6,6-tetramethylpiperidine-1-oxyl) (Batmaz et al., 2014). Mohammed et al. has reported cellulose nanocrystal reinforced with alginate hydrogels for the removal of methylene blue dye (Mohammed et al., 2015). The efficiency was as high as 97% even after five cycles. Highly carboxylated cellulose synthesized by Meng et al. is recyclable up to 10 times with 86.83% efficiency for removal of dyes (Meng et al., 2019). Oxidized CNC prepared by sodium periodate and modified using ethylenedimine is reported by Jin et al. for effective adsorption of dyes congo red 4BS, acid red and light yellow K-4G (Jin et al., 2015). Immobilization of laccase enzyme on nanocellulose is an effective method for degradation of reactive dyes. Textile effluents that contains several dyes and toxic salts can be treated by this laccase immobilized nanocellulose systems. Further they also found applications in wound dressing as antimicrobial membrane.

Nanocellulose reinforced materials act as sustainable adsorbent in wastewater remediation purpose. Their large surface area, strong mechanical properties, thermal stability, hydrophobic nature, modifiable surface chemistry is the reason behind their exceptional adsorption capability. Further nanocellulose-based membranes are getting immense importance for safer and economically viable membrane applications. Ultrafiltration membrane prepared by Karim et al. using nanocomposite of chitosan with CNC was tested for several dye removal (Karim et al., 2014). These membranes are highly effective for removal of victoria blue, methyl violet, and rhodamine 6G dye through electrostatic and hydrogen bonding interaction. These membranes are sustainable and economical as they can be developed from abundantly available agricultural residues and biomass waste. In this case membrane separation cost is reduced as a wide range of pollutants are removed by a single step through adsorption or size exclusion mechanism. This nanocellulose-based membrane technology has huge potential in water remediation with many modern filtration systems such as nanofiltration, microfiltration, ultrafiltration, and reverse-osmosis-based methods. Still further research is continuing for making it low cost and industrial scale with high performance quality.

Organic pollutant adsorption

Organic pollutants in water body constitute natural organic matter (NOM), pharmaceuticals, pesticides, herbicides, petroleum products, and many other contaminants. Decomposition of biomass in environment creates humic acid and fulvic acid as NOM which are health hazards. Amine group modified nanocellulose was used (Jebali et al., 2015) for the removal of humic acid from waste water. The adsorption of humic acid was electrostatic attraction between the carboxyl and hydroxyl functional groups of humic acid and amine group of the functionalized nanocellulose. Similar kind of work is reported by Sehaqui et al. in which the surface of cellulose nanofibers (CNF) was functionalized by quaternary ammonium group (Sehaqui et al., 2016). This material shows increased flux of adsorption humic acid by electrostatic interactions.

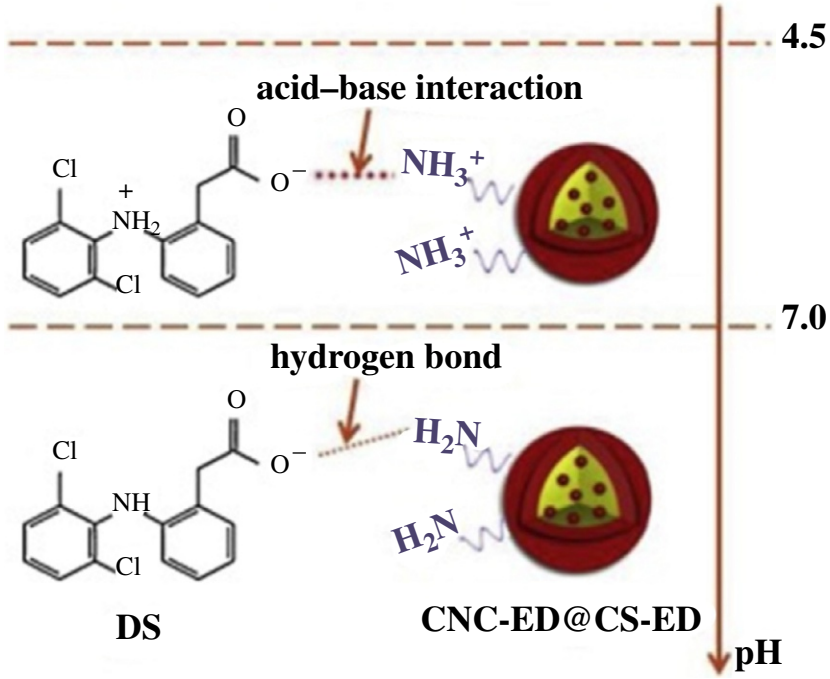

FIG. 13.16 Adsorption of diclofenac sodium (DS) by cellulose/chitosan composite functionalized with amino group. (Hu et al., 2019).

Adsorption of various pharmaceuticals onto nanocellulose is gaining momentum in recent times. Sulfated CNCs are used for adsorbing ionic drugs, e.g., doxorubicin hydrochloride (DOX), tetracycline hydrochloride (TC), and others (Rathod et al., 2015). To maximize the adsorption ability, the nanocellulose surface is made hydrophobic by grafting surfactant or by reaction with alkyl isocyanate. Carboxylated CNCs synthesized by TEMPO-mediated oxidation reaction is studied for binding of cationic drugs (Akhlaghi et al., 2014). Removal of potassium diclofenac (PD) drug is investigated by Pires et al. using composite of polypyrrole with cellulose fibers (PPY/CF) (Pires et al., 2017). The presence of aromatic ring, -NH_2 group, -OH group, ether group and ester group on PPY/CF composite leads to stronger adsorption through hydrogen bonding, dipole–dipole and pi–pi interactions. An interesting result is reported by Hu et al. on adsorption of diclofenac sodium (DS) by cellulose/chitosan composite functionalized with amino group (Hu et al., 2019). They observed that at lower pH the adsorption was due to acid-base interaction while at higher pH hydrogen bonding is the predominant interaction (Fig. 13.16). Chitosan/cellulose nanocomposite in the form of microspheres embedded with activated carbon is used for adsorption of tylosin (Luo et al., 2019). The hydroxyl and carbonyl functional groups interact through various intermolecular forces.

Removal of six different triazine pesticides from water by using cellulose/graphene composite (CGC) has been investigated by (Zhang et al., 2015). The pesticides they studied were simeton, simazine, atrazine, cyprazine, ametryn, and prometryn which possess electronegative atoms N, O, S, and Cl. The similar structural formula with N atoms exhibit similar kind of

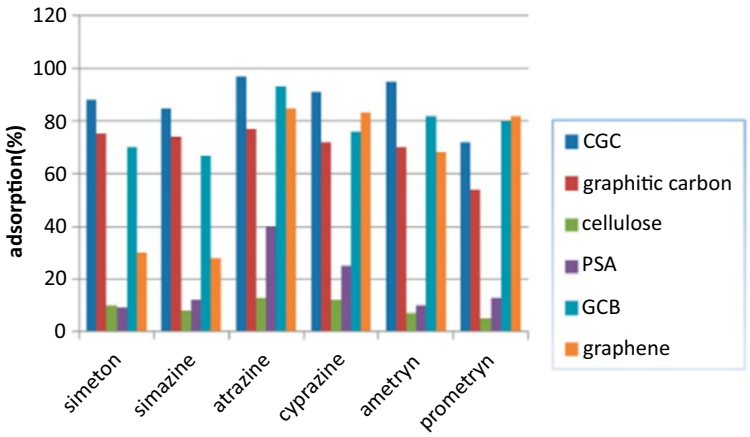

FIG. 13.17 Comparative study of CGC with graphene, GCB, PSA, Cellulose and Graphaitic carbon for adsorption of six triazine based pesticides. (Zhang et al., 2015).

interactions although the van der Waals force of interactions was different in all the six structures. Among the six pesticides, adsorption of prometryn was the weakest because of its branched structure. They have performed a comparative study of CGC with another five different adsorbents. Their result indicates that the CG composite is more effective compared to the other sorbents (Fig. 13.17).

A composite sensor made with cellulose and activated carbon is used for adsorption of ethylene gas (Ummartyotin and Pechyen, 2016). The hydroxyl and carboxyl group of the composite binds ethylene gas through chemical bonding. Yuan et al. synthesized a composite of cellulose nanofiber by functionalizing with cyclodextrin (CD/RCNF) for adsorption of toluene from water (Yuan et al., 2017). The hydrophilic groups present at the outside of cyclodextrin helps to bind toluene effectively by forming a complex between the CD/RCNF composite and toluene.

Oil adsorption

Pollution created by the release of oil from various industries is one of the major challenges in environment remediation. The hydrophilic nature of nanocellulose hinder it to act as adsorbent for hydrophobic oil. Thus the strategy is to modify the surface to make it highly hydrophobic to adsorb the hydrophobic oils from aquatic systems. Cellulose-based aerogels are the emerging materials for oil adsorption in waste water treatment. In this direction Zhang et al. have synthesized CNF based aerogel using methyltrimethoxy silane (MTMS) as silylating agent in a freeze drying technique (Zhang et al., 2015; Zhang et al., 2014a, 2014b). This material showed promising results for the removal of dodeacane and other organic solvents. In a similar kind of work, freeze drying of alkyl ketene dimer (AKD) with CNF produced hydrophobic aerogel of CNF (Tarrés et al., 2016). This AKD grafted CNF aerogel has remarkable oil adsorption capacity. A hydrophobic aerogel was prepared from paper wastes by Feng et al. by freeze-drying method (Feng et al., 2015). Treatment of this nanocellulose with MTMS transforms it into hydrophobic material with strong adsorption ability toward oil. A different approach was suggested by Korhonen for increasing the affinity

of CNFs for paraffin oil adsorption (Korhonen et al., 2011). They synthesized a superb hydrophobic material by creating a thin layer of titanium dioxide over CNF by sol-gel method. Jiang et al. have modified CNF aerogels by vapor depositing hydrophobic triethoxyl (octyl) silane for selective adsorption of organic solvents (Jiang and Hsieh, 2014). Incorporation of silanes onto CNF increases the hydrophobicity as well as the oleophilicity for strong adsorption oils from water. A sponge-like highly porous nanocellulose-based carbon adsorbent was developed (Meng et al., 2015). Various type of oils, e.g., diesel oil, pump oil, paraffin oil and canola oil are strongly adsorbed over this functionalized adsorbent. This adsorbent is reusable up to 10 desorption cycles. Chin et al. have reported magnetic and porous nanocellulose adsorbent functionalized with magnetic Fe_3O_4 (Chin et al., 2014). This adsorbent exhibits strong adsorption efficiency and a fast adsorption kinetics for paraffin oil within 10 min. It has the advantage of recoverability by using an external magnet. A similar kind of adsorbent is developed by Gu et al. by functionalizing CNF with oleic acid and magnetic Fe_3O_4 (Gu et al., 2020). The addition of oleic acid and Fe_3O_4 imparts hydrophobic and magnetic nature respectively in the adsorbent. This material is highly promising in removal of cyclohexane, ethyl acetate, and vacuum pump oil with good recyclability and easy magnetic separation. An interesting work by Lu et al. have used magnetic and silanized ethyl nanocellulose for adsorption of a wide range of oils such as n-hexane, petroleum ether, gasoline, diesel, dimethyl silicone oil, and soyabean oil (Lu et al., 2017). This adsorbent shows excellent capacity and recyclability. A 3D nanocellose having interconnected pores similar to honeycomb was developed (Zhang et al., 2016). This material is super adsorbent and highly selective for oils. This is reusable up to 30 cycles without reducing the adsorbing capacity significantly. A highly hydrophobic and highly oleophilic adsorbent based on CNF was prepared (Phanthong et al., 2018). They have used stearoyl chloride functionalized CNF for the adsorption of dichloromethane, toluene, ethanol, acetone, n-hexane, n-octane, silicon oil, vacuum pump oil, etc., for efficient separation. This spongy nanocellulose adsorbent is easily recoverable by easy squeezing and reusable up to 10 times. These results suggest that nanocellulose has immense potential as adsorbents for organic oils.

Removal of air pollutants

The growing industrialization leads to emission of poisonous gases to the environment. The smoke from industrial and manufacturing units, automobiles, etc., contains CO_2, CO, H_2S, SO_2 and other gases. Thus separation of the toxic gases from mixtures is extremely important. For this purpose amine-derived adsorbents supported on inorganic materials are used in CO_2 capturing from air. Gebald et al. have developed a freeze-dried CNF-based adsorbent modified by *N*-(2-aminoethyl)-3-amino-propyl-methyl-dimethoxy silane for CO_2 gas adsorption (Gebald et al., 2011). The adsorption capacity of this material was found to be lower than silica-based adsorbents. Removal of H_2S gas is also investigated using nanofibrillar cellulose modified with specific functional groups. Hokkanen et al. have synthesized aminopropyl triethoxy silane (APS) modified microfibrillated cellulose (APS/MFC) for adsorbing H_2S (Hokkanen et al., 2014a). They have reported another adsorbent (HAP/MFC) originated from microfibrillated cellulose modified with hydroxy carbonated apatite (HAP) in the same research paper. The uptake capacity of HAP/MFC (13.38 mg/g) was found to be higher than APS/MFC (103.95 mg/g). Removals of volatile gases are also investigated using CNF-based adsorbents. Keshavarazi et al. have developed composite of zeolite with CNF for odor elimination of thiol gases (Keshavarzi et al., 2015). Promising results are obtained as the adsorbent shows high efficiency of removal of propanethiol and ethanethiol with minute

concentrations not detectable to human's olfactory nerves. In a similar approach freeze-dried TEMPO oxidized CNF in the form of aerogels are utilized as air filters (Nemoto et al., 2015). Yet research in this area is not developed much. Beside these applications nanocellulose has applications in many other fields such as filling agent in textile, thickener in cosmetics, wood adhesives, pickering emulsifiers, texturing agent in food, etc.

13.10.5 Nanocellulose-based membrane for water treatment

There is only a limited amount of available drinking water and that too is polluted due to number of industrial activities. Membrane filtration under pressure is a conventional technique for water purification. There are number of membranes as shown in Fig. 13.18 (Sharma et al., 2020).

Nanocellulose (CNF, CNC, or BNC) is converted to membrane by incorporating into other membranes as an additive. This is simple and economical. Numbers of functional groups are attached to nanocellulose to make surface charges and reactivity for strong interactions with the pollutants in water. When incorporated with other organic or inorganic additives, nanocellulose membranes worked better. Nanocellulose membranes have superhydrophilicity/superhydrophobicity, high porosity, high mechanical strength, high chemical resistance and antifouling properties. The nanocellulose membranes having high specific functionality, remove effectively the pollutants from water. (Tan et al., 2020).

13.10.6 Nanocellulose for gas separation

Hydrogen and carbon dioxide separation has been carried out by membrane technologies. Only limited studies have been made. Nanocellulose incorporating poly(vinyl alcohol) (PVA) is found to be a very good membrane for gas separation (Ibrahim et al., 2020).

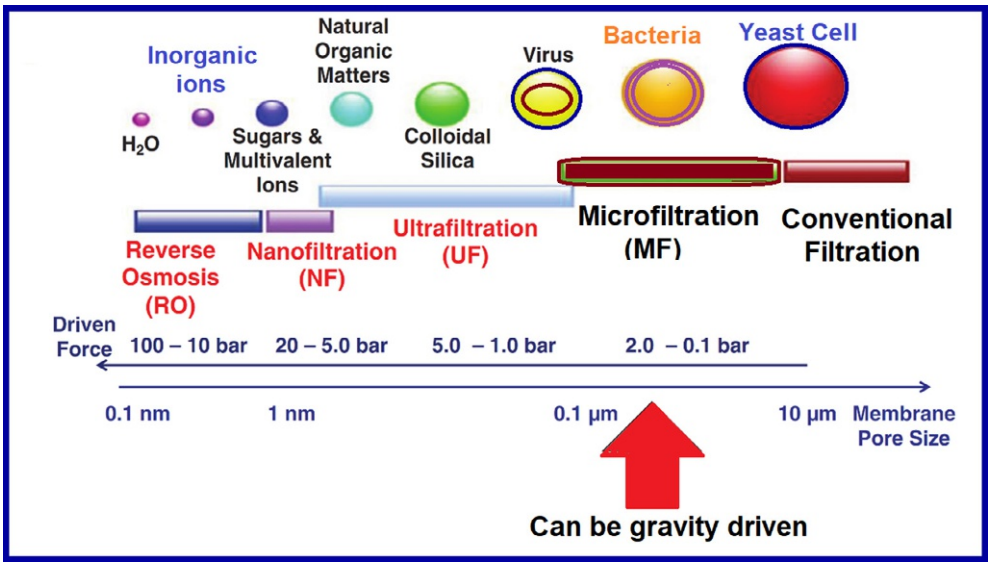

FIG. 13.18 Pressure driven membrane filtration.

13.11 Challenges and future perspectives

There has always been a question whether BNC can replace or compete with the traditional cellulose sources? This question is a challenge and has not been solved yet. Apart from issues related to nanocellulose, there are number of challenges. Some challenges and future prospects of nanocellulose are shown in Fig. 13.19 (Sharma and Bhardwaj, 2019).

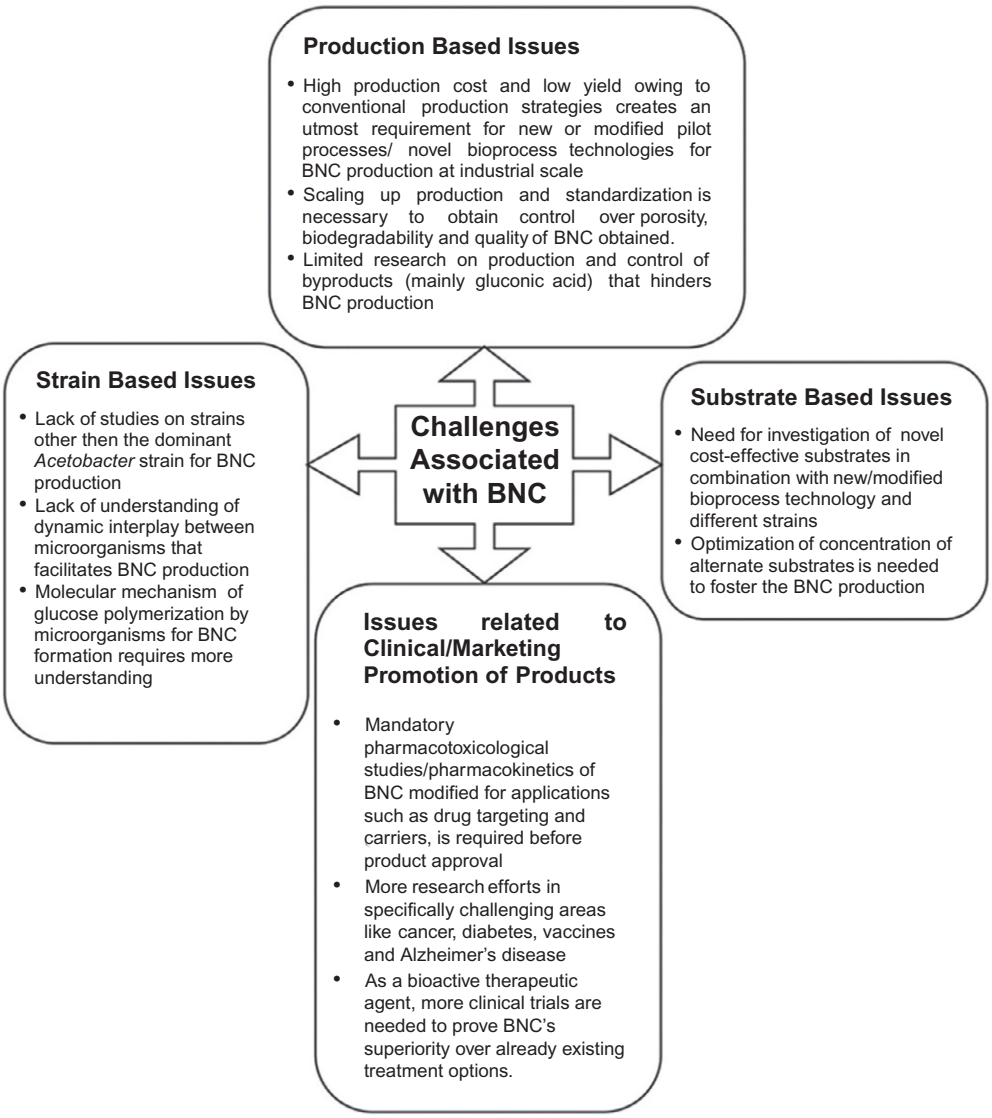

FIG. 13.19 Challenges and future prospects.

13.12 Conclusions

Cellulose is the most abundant sustainable resource on the earth. In 21st century, due to the increasing severe environmental problems, biomass materials received more attention, which substitute petrochemicals in all kinds of materials. Cellulose particularly nanocellulose have been synthesized by number of methods and characterized using different techniques. Nanostructured cellulose is advantageous because of renewable, sustainable, non-toxic, and biocompatible properties. There are many types of cellulose such as NFC, CNCs, BC, etc. These cellulosic materials have special properties and can be functionalized. These have been used in different sectors including water remediation.

References

Abitbol, T., Rivkin, A., Cao, Y., Nevo, Y., Abraham, E., Ben-Shalom, T., Lapidot, S., Shoseyov, O., 2016. Nanocellulose, a tiny fiber with huge applications. Curr. Opin. Biotechnol. 39, 76–88.

Abraham, E., Deepa, B., Pothan, L.A., Jacob, M., Thomas, S., Cvelbar, U., Anandjiwala, R., 2011. Extraction of nanocellulose fibrils from lignocellulosic fibres: a novel approach. Carbohydr. Polym. 86 (4), 1468–1475.

Akhlaghi, S.P., Tiong, D., Berry, R.M., Tam, K.C., 2014. Comparative release studies of two cationic model drugs from different cellulose nanocrystal derivatives. Eur. J. Pharm. Biopharm. 88 (1), 207–215.

Anirudhan, T.S., Deepa, J.R., Christa, J., 2016. Nanocellulose/nanobentonite composite anchored with multi-carboxyl functional groups as an adsorbent for the effective removal of cobalt (II) from nuclear industry wastewater samples. J. Colloid Interface Sci. 467, 307–320.

Awan, F., Bulger, E., Berry, R.M., Tam, K.C., 2016. Enhanced radical scavenging activity of polyhydroxylated C 60 functionalized cellulose nanocrystals. Cellulose 23 (6), 3589–3599.

Azevedo, E.P., Retarekar, R., Raghavan, M.L., Kumar, V., 2013. Mechanical properties of cellulose: chitosan blends for potential use as a coronary artery bypass graft. J. Biomater. Sci. Polym. Ed. 24 (3), 239–252.

Azizi, S., Ahmad, M., Mahdavi, M., Abdolmohammadi, S., 2013. Preparation, characterization, and antimicrobial activities of ZnO nanoparticles/cellulose nanocrystal nanocomposites. Bioresources 8 (2), 1841–1851.

Barud, H.S., Regiani, T., Marques, R.F., Lustri, W.R., Messaddeq, Y., Ribeiro, S.J., 2011. Antimicrobial bacterial cellulose-silver nanoparticles composite membranes. J. Nanomater. 2011.

Batmaz, R., Mohammed, N., Zaman, M., Minhas, G., Berry, R.M., Tam, K.C., 2014. Cellulose nanocrystals as promising adsorbents for the removal of cationic dyes. Cellulose 21 (3), 1655–1665.

Bayer, T., Cunning, B.V., Selyanchyn, R., Nishihara, M., Fujikawa, S., Sasaki, K., Lyth, S.M., 2016. High temperature proton conduction in nanocellulose membranes: paper fuel cells. Chem. Mater. 28 (13), 4805–4814.

Bezerra, R.D., Teixeira, P.R., Teixeira, A.S.N.M., Eiras, C., Osajima, J.A., Silva Filho, E.C., 2015. Chemical functionalization of cellulosic materials—Main reactions and applications in the contaminants removal of aqueous medium. In: Cellulose–Fundamental Aspects and Current Trends. InTech, pp. 93–113.

Blanco, A., Monte, M.C., Campano, C., Balea, A., Merayo, N., Negro, C., 2018. Nanocellulose for industrial use: cellulose nanofibers (CNF), cellulose nanocrystals (CNC), and bacterial cellulose (BC). In: Handbook of Nanomaterials for Industrial Applications. Elsevier, pp. 74–126.

Bober, P., Liu, J., Mikkonen, K.S., Ihalainen, P., Pesonen, M., Plumed-Ferrer, C., von Wright, A., Lindfors, T., Xu, C., Latonen, R.M., 2014. Biocomposites of nanofibrillated cellulose, polypyrrole, and silver nanoparticles with electroconductive and antimicrobial properties. Biomacromolecules 15 (10), 3655–3663.

Božič, M., Liu, P., Mathew, A.P., Kokol, V., 2014. Enzymatic phosphorylation of cellulose nanofibers to new highly-ions adsorbing, flame-retardant and hydroxyapatite-growth induced natural nanoparticles. Cellulose 21 (4), 2713–2726.

Brinchi, L., Cotana, F., Fortunati, E., Kenny, J.M., 2013. Production of nanocrystalline cellulose from lignocellulosic biomass: technology and applications. Carbohydr. Polym. 94 (1), 154–169.

Brown, E.E., Hu, D., Abu Lail, N., Zhang, X., 2013. Potential of nanocrystalline cellulose–fibrin nanocomposites for artificial vascular graft applications. Biomacromolecules 14 (4), 1063–1071.

Bufalino, L., Tonoli, G.H.D., Costa, T.G., Protásio, T.D.P., Sena Neto, A.R., Marconcini, J.M., Guimarães Junior, M., Mendes, L.M., 2016. Nanocellulose films from Amazon forest wood wastes: structural and thermal properties. In: Key Engineering Materials. vol. 668. Trans Tech Publications Ltd, pp. 110–117.
Bulota, M., Kreitsmann, K., Hughes, M., Paltakari, J., 2012. Acetylated microfibrillated cellulose as a toughening agent in poly (lactic acid). J. Appl. Polym. Sci. 126 (S1), E449–E458.
Chan, C.H., Chia, C.H., Zakaria, S., Sajab, M.S., Chin, S.X., 2015. Cellulose nanofibrils: a rapid adsorbent for the removal of methylene blue. RSC Adv. 5 (24), 18204–18212.
Chen, Y., Liu, C., Chang, P.R., Cao, X., Anderson, D.P., 2009. Bionanocomposites based on pea starch and cellulose nanowhiskers hydrolyzed from pea hull fibre: effect of hydrolysis time. Carbohydr. Polym. 76 (4), 607–615.
Chin, S.F., Romainor, A.N.B., Pang, S.C., 2014. Fabrication of hydrophobic and magnetic cellulose aerogel with high oil absorption capacity. Mater. Lett. 115, 241–243.
Dhali, K., Ghasemlou, M., Daver, F., Cass, P., Adhikari, B., 2021. A review of nanocellulose as a new material toward environmental sustainability. Sci. Total Environ. 145871.
Dong, S., Hirani, A.A., Colacino, K.R., Lee, Y.W., Roman, M., 2012. Cytotoxicity and cellular uptake of cellulose nanocrystals. Nano Life 2 (03), 1241006.
Dong, C., Zhang, F., Pang, Z., Yang, G., 2016. Efficient and selective adsorption of multi-metal ions using sulfonated cellulose as adsorbent. Carbohydr. Polym. 151, 230–236.
Fang, Z., Zhu, H., Yuan, Y., Ha, D., Zhu, S., Preston, C., Chen, Q., Li, Y., Han, X., Lee, S., Chen, G., 2014. Novel nanostructured paper with ultrahigh transparency and ultrahigh haze for solar cells. Nano Lett. 14 (2), 765–773.
Farooq, A., Patoary, M.K., Zhang, M., Mussana, H., Li, M., Naeem, M.A., Mushtaq, M., Farooq, A., Liu, L., 2020. Cellulose from sources to nanocellulose and an overview of synthesis and properties of nanocellulose/zinc oxide nanocomposite materials. Int. J. Biol. Macromol. 154, 1050–1073.
Feng, J., Nguyen, S.T., Fan, Z., Duong, H.M., 2015. Advanced fabrication and oil absorption properties of superhydrophobic recycled cellulose aerogels. Chem. Eng. J. 270, 168–175.
Foresti, M.L., Cerrutti, P., Vazquez, A., 2015. Bacterial nanocellulose: synthesis, properties and applications. Chapter 2, In: Mohanty, S., et al. (Eds.), Polymer Nanocomposites Based on Inorganic and Organic Nanomaterials. Scrivener Publishing LLC, pp. 39–62.
Gadim, T.D., Loureiro, F.J., Vilela, C., Rosero-Navarro, N., Silvestre, A.J., Freire, C.S., Figueiredo, F.M., 2017. Protonic conductivity and fuel cell tests of nanocomposite membranes based on bacterial cellulose. Electrochim. Acta 233, 52–61.
Gebald, C., Wurzbacher, J.A., Tingaut, P., Zimmermann, T., Steinfeld, A., 2011. Amine-based nanofibrillated cellulose as adsorbent for CO2 capture from air. Environ. Sci. Technol. 45 (20), 9101–9108.
Gibril, M.E., Lekha, P., Andrew, J., Sithole, B., Tesfaye, T., Ramjugernath, D., 2018. Beneficiation of pulp and paper mill sludge: production and characterisation of functionalised crystalline nanocellulose. Clean Techn. Environ. Policy 20 (8), 1835–1845.
Gopakumar, D.A., Arumughan, V., Pasquini, D., Leu, S.Y.B., HPS, A.K., Thomas, S., 2019. Nanocellulose-based membranes for water purification. In: Nanoscale Materials in Water Purification. Elsevier, pp. 59–85.
Gu, H., Zhou, X., Lyu, S., Pan, D., Dong, M., Wu, S., Ding, T., Wei, X., Seok, I., Wei, S., Guo, Z., 2020. Magnetic nanocellulose-magnetite aerogel for easy oil adsorption. J. Colloid Interface Sci. 560, 849–856.
Hokkanen, S., Repo, E., Bhatnagar, A., Tang, W.Z., Sillanpää, M., 2014a. Adsorption of hydrogen sulphide from aqueous solutions using modified nano/micro fibrillated cellulose. Environ. Technol. 35 (18), 2334–2346.
Hokkanen, S., Repo, E., Suopajärvi, T., Liimatainen, H., Niinimaa, J., Sillanpää, M., 2014b. Adsorption of Ni (II), Cu (II) and Cd (II) from aqueous solutions by amino modified nanostructured microfibrillated cellulose. Cellulose 21 (3), 1471–1487.
Gupta, V.K., Carrott, P.J.M., Singh, R., Chaudhary, M., Kushwaha, S., 2016. Cellulose: a review as natural, modified and activated carbon adsorbent. Bioresour. Technol. 216, 1066–1076.
Hokkanen, S., Bhatnagar, A., Sillanpää, M., 2016. A review on modification methods to cellulose-based adsorbents to improve adsorption capacity. Water Res. 91, 156–173.
Hu, D., Jiang, R., Wang, N., Xu, H., Wang, Y.G., Ouyang, X.K., 2019. Adsorption of diclofenac sodium on bilayer amino-functionalized cellulose nanocrystals/chitosan composite. J. Hazard. Mater. 369, 483–493.
Hua, K., Strømme, M., Mihranyan, A., Ferraz, N., 2015. Nanocellulose from green algae modulates the in vitro inflammatory response of monocytes/macrophages. Cellulose 22 (6), 3673–3688.
Huang, J., Zhu, H., Chen, Y., Preston, C., Rohrbach, K., Cumings, J., Hu, L., 2013. Highly transparent and flexible nanopaper transistors. ACS Nano 7 (3), 2106–2113.

Ibrahim, H., Sazali, N., Salleh, W.N.W., Abidin, M.N.Z., 2020. A short review on recent utilization of nanocellulose for wastewater remediation and gas separation. Mater. Today Proc. 42, 45–49.
Isogai, A., Saito, T., Fukuzumi, H., 2011. TEMPO-oxidized cellulose nanofibers. Nanoscale 3 (1), 71–85.
Jamshaid, A., Hamid, A., Muhammad, N., Naseer, A., Ghauri, M., Iqbal, J., Rafiq, S., Shah, N.S., 2017. Cellulose-based materials for the removal of heavy metals from wastewater–an overview. ChemBioEng Rev. 4 (4), 240–256.
Jebali, A., Behzadi, A., Rezapor, I., Jasemizad, T., Hekmatimoghaddam, S.H., Halvani, G.H., Sedighi, N., 2015. Adsorption of humic acid by amine-modified nanocellulose: an experimental and simulation study. Int. J. Environ. Sci. Technol. 12 (1), 45–52.
Ji, S., Hyun, B.G., Kim, K., Lee, S.Y., Kim, S.H., Kim, J.Y., Song, M.H., Park, J.U., 2016. Photo-patternable and transparent films using cellulose nanofibers for stretchable origami electronics. NPG Asia Mater. 8 (8), e299.
Jiang, F., Hsieh, Y.L., 2014. Amphiphilic superabsorbent cellulose nanofibril aerogels. J. Mater. Chem. A 2 (18), 6337–6342.
Jiang, G.P., Zhang, J., Qiao, J.L., Jiang, Y.M., Zarrin, H., Chen, Z., Hong, F., 2015. Bacterial nanocellulose/nafion composite membranes for low temperature polymer electrolyte fuel cells. J. Power Sources 273, 697–706.
Jin, L., Li, W., Xu, Q., Sun, Q., 2015. Amino-functionalized nanocrystalline cellulose as an adsorbent for anionic dyes. Cellulose 22 (4), 2443–2456.
Jordan, J.H., Easson, M.W., Dien, B., Thompson, S., Condon, B.D., 2019. Extraction and characterization of nanocellulose crystals from cotton gin motes and cotton gin waste. Cellulose 26 (10), 5959–5979.
Jung, Y.H., Chang, T.H., Zhang, H., Yao, C., Zheng, Q., Yang, V.W., Mi, H., Kim, M., Cho, S.J., Park, D.W., Jiang, H., 2015. High-performance green flexible electronics based on biodegradable cellulose nanofibril paper. Nat. Commun. 6 (1), 1–11.
Kalia, S., Dufresne, A., Cherian, B.M., Kaith, B.S., Avérous, L., Njuguna, J., Nassiopoulos, E., 2011. Cellulose-based bio-and nanocomposites: a review. Int. J. Polym. Sci. 2011.
Kardam, A., Raj, K.R., Srivastava, S., Srivastava, M.M., 2014. Nanocellulose fibers for biosorption of cadmium, nickel, and lead ions from aqueous solution. Clean Techn. Environ. Policy 16 (2), 385–393.
Karim, Z., Mathew, A.P., Grahn, M., Mouzon, J., Oksman, K., 2014. Nanoporous membranes with cellulose nanocrystals as functional entity in chitosan: removal of dyes from water. Carbohydr. Polym. 112, 668–676.
Keshavarzi, N., Rad, F.M., Mace, A.K., Ansari, F., Akhtar, F., Nilsson, U., Berglund, L.A., Bergström, L., 2015. Nanocellulose-zeolite composite films for odor elimination. ACS Appl. Mater. Interfaces 7 (26), 14254–14262.
Klemm, D., Schumann, D., Kramer, F., Heßler, N., Hornung, M., Schmauder, H.P., Marsch, S., 2006. Nanocelluloses as innovative polymers in research and application. In: Polysaccharides II. Springer, pp. 49–96.
Korhonen, J.T., Kettunen, M., Ras, R.H., Ikkala, O., 2011. Hydrophobic nanocellulose aerogels as floating, sustainable, reusable, and recyclable oil absorbents. ACS Appl. Mater. Interfaces 3 (6), 1813–1816.
Kumar, V., Pathak, P., Bhardwaj, N.K., 2020. Waste paper: an underutilized but promising source for nanocellulose mining. Waste Manag. 102, 281–303.
Liu, P., Borrell, P.F., Božič, M., Kokol, V., Oksman, K., Mathew, A.P., 2015. Nanocelluloses and their phosphorylated derivatives for selective adsorption of Ag+, Cu2+ and Fe3+ from industrial effluents. J. Hazard. Mater. 294, 177–185.
Lu, J., Jin, R.N., Liu, C., Wang, Y.F., Ouyang, X.K., 2016. Magnetic carboxylated cellulose nanocrystals as adsorbent for the removal of Pb (II) from aqueous solution. Int. J. Biol. Macromol. 93, 547–556.
Lu, Y., Wang, Y., Liu, L., Yuan, W., 2017. Environmental-friendly and magnetic/silanized ethyl cellulose sponges as effective and recyclable oil-absorption materials. Carbohydr. Polym. 173, 422–430.
Luo, Y., Zhang, J., Li, X., Liao, C., Li, X., 2014. The cellulose nanofibers for optoelectronic conversion and energy storage. J. Nanomater. 2014.
Luo, X., Liu, L., Wang, L., Liu, X., Cai, Y., 2019. Facile synthesis and low concentration tylosin adsorption performance of chitosan/cellulose nanocomposite microspheres. Carbohydr. Polym. 206, 633–640.
Ma, H., Hsiao, B.S., Chu, B., 2012. Ultrafine cellulose nanofibers as efficient adsorbents for removal of UO22+ in water. ACS Macro Lett. 1 (1), 213–216.
Maatar, W., Boufi, S., 2015. Poly(methacylic acid-co-maleic acid) grafted nanofibrillated cellulose as a reusable novel heavy metal ions adsorbent. Carbohydr. Polym. 126, 99–207.
Mahfoudhi, N., Boufi, S., 2017. Nanocellulose as a novel nanostructured adsorbent for environmental remediation: a review. Cellulose 24 (3), 1171–1197.
Majoinen, J., Kontturi, E., Ikkala, O., Gray, D.G., 2012. SEM imaging of chiral nematic films cast from cellulose nanocrystal suspensions. Cellulose 19 (5), 1599–1605.

Mandal, A., Chakrabarty, D., 2017. Synthesis and characterization of nanocellulose reinforced full-interpenetrating polymer network based on poly (vinyl alcohol) and polyacrylamide (both crosslinked) composite films. Polym. Compos. 38 (8), 1720–1731.
Meng, Y., Young, T.M., Liu, P., Contescu, C.I., Huang, B., Wang, S., 2015. Ultralight carbon aerogel from nanocellulose as a highly selective oil absorption material. Cellulose 22 (1), 435–447.
Meng, R., Liu, L., Jin, Y., Luo, Z., Gao, H., Yao, J., 2019. Recyclable carboxylated cellulose beads with tunable pore structure and size for highly efficient dye removal. Cellulose 26 (17), 8963–8969.
Millon, L.E., Guhados, G., Wan, W., 2008. Anisotropic polyvinyl alcohol—bacterial cellulose nanocomposite for biomedical applications. J. Biomed. Mater. Res. B Appl. Biomater. 86 (2), 444–452.
Mohammed, N., Grishkewich, N., Berry, R.M., Tam, K.C., 2015. Cellulose nanocrystal–alginate hydrogel beads as novel adsorbents for organic dyes in aqueous solutions. Cellulose 22 (6), 3725–3738.
Mohanta, V., Madras, G., Patil, S., 2014. Layer-by-layer assembled thin films and microcapsules of nanocrystalline cellulose for hydrophobic drug delivery. ACS Appl. Mater. Interfaces 6 (22), 20093–20101.
Moriana, R., Vilaplana, F., Ek, M., 2016. Cellulose nanocrystals from forest residues as reinforcing agents for composites: a study from macro-to nano-dimensions. Carbohydr. Polym. 139, 139–149.
Nair, S.S., Zhu, J.Y., Deng, Y., Ragauskas, A.J., 2014. High performance green barriers based on nanocellulose. Sustain. Chem. Process. 2 (1), 1–7.
Nandi, S., Guha, P., 2018. A review on preparation and properties of cellulose nanocrystal-incorporated natural biopolymer. J. Packag. Technol. Res. 2 (2), 149–166.
Nasir, M., Hashim, R., Sulaiman, O., Asim, M., 2017. Nanocellulose: preparation methods and applications. In: Cellulose-Reinforced Nanofibre Composites. Woodhead Publishing, pp. 261–276.
Nemoto, J., Saito, T., Isogai, A., 2015. Simple freeze-drying procedure for producing nanocellulose aerogel-containing, high-performance air filters. ACS Appl. Mater. Interfaces 7 (35), 19809–19815.
Oulachgar, H., Bolduc, M., Chauve, G., Desroches, Y., Beaupre, P., Bouchard, J., Galarneau, P., 2016. Fabrication and electro-optical characterization of a nanocellulose-based spatial light modulator. MRS Adv. 1 (10), 631–637.
Oun, A.A., Shankar, S., Rhim, J.W., 2020. Multifunctional nanocellulose/metal and metal oxide nanoparticle hybrid nanomaterials. Crit. Rev. Food Sci. Nutr. 60 (3), 435–460.
Patel, D.K., Dutta, S.D., Lim, K.T., 2019. Nanocellulose-based polymer hybrids and their emerging applications in biomedical engineering and water purification. RSC Adv. 9 (33), 19143–19162.
Peng, J., Zhang, H., Zheng, Q., Clemons, C.M., Sabo, R.C., Gong, S., Ma, Z., Turng, L.S., 2017. A composite generator film impregnated with cellulose nanocrystals for enhanced triboelectric performance. Nanoscale 9 (4), 1428–1433.
Phanthong, P., Guan, G., Karnjanakom, S., Hao, X., Wang, Z., Kusakabe, K., Abudula, A., 2016. Amphiphobic nanocellulose-modified paper: fabrication and evaluation. RSC Adv. 6 (16), 13328–13334.
Phanthong, P., Karnjanakom, S., Reubroycharoen, P., Hao, X., Abudula, A., Guan, G., 2017. A facile one-step way for extraction of nanocellulose with high yield by ball milling with ionic liquid. Cellulose 24 (5), 2083–2093.
Phanthong, P., Reubroycharoen, P., Kongparakul, S., Samart, C., Wang, Z., Hao, X., Abudula, A., Guan, G., 2018. Fabrication and evaluation of nanocellulose sponge for oil/water separation. Carbohydr. Polym. 190, 184–189.
Pires, B.C., Dutra, F.V.A., Nascimento, T.A., Borges, K.B., 2017. Preparation of PPy/cellulose fibre as an effective potassium diclofenac adsorbent. React. Funct. Polym. 113, 40–49.
Pottathara, Y.B., Bobnar, V., Finšgar, M., Grohens, Y., Thomas, S., Kokol, V., 2018. Cellulose nanofibrils-reduced graphene oxide xerogels and cryogels for dielectric and electrochemical storage applications. Polymer 147, 260–270.
Rathod, M., Haldar, S., Basha, S., 2015. Nanocrystalline cellulose for removal of tetracycline hydrochloride from water via biosorption: equilibrium, kinetic and thermodynamic studies. Ecol. Eng. 84, 240–249.
Rescignano, N., Fortunati, E., Montesano, S., Emiliani, C., Kenny, J.M., Martino, S., Armentano, I., 2014. PVA bionanocomposites: a new take-off using cellulose nanocrystals and PLGA nanoparticles. Carbohydr. Polym. 99, 47–58.
Saito, T., Isogai, A., 2005. Ion-exchange behavior of carboxylate groups in fibrous cellulose oxidized by the TEMPO-mediated system. Carbohydr. Polym. 61 (2), 183–190.
Sampath, U.T.M., Ching, Y.C., Chuah, C.H., Singh, R., Lin, P.C., 2017. Preparation and characterization of nanocellulose reinforced semi-interpenetrating polymer network of chitosan hydrogel. Cellulose 24 (5), 2215–2228.
Schumann, D.A., Wippermann, J., Klemm, D.O., Kramer, F., Koth, D., Kosmehl, H., Wahlers, T., Salehi-Gelani, S., 2009. Artificial vascular implants from bacterial cellulose: preliminary results of small arterial substitutes. Cellulose 16 (5), 877–885.

Sehaqui, H., de Larraya, U.P., Liu, P., Pfenninger, N., Mathew, A.P., Zimmermann, T., Tingaut, P., 2014. Enhancing adsorption of heavy metal ions onto biobased nanofibers from waste pulp residues for application in wastewater treatment. Cellulose 21 (4), 2831–2844.
Sehaqui, H., Michen, B., Marty, E., Schaufelberger, L., Zimmermann, T., 2016. Functional cellulose nanofiber filters with enhanced flux for the removal of humic acid by adsorption. ACS Sustain. Chem. Eng. 4 (9), 4582–4590.
Seo, J.H., Chang, T.H., Lee, J., Sabo, R., Zhou, W., Cai, Z., Gong, S., Ma, Z., 2015. Microwave flexible transistors on cellulose nanofibrillated fiber substrates. Appl. Phys. Lett. 106 (26), 262101.
Sharma, C., Bhardwaj, N.K., 2019. Bacterial nanocellulose: present status, biomedical applications and future perspectives. Mater. Sci. Eng. C 104, 109963.
Sharma, A., Thakur, M., Bhattacharya, M., Mandal, T., Goswami, S., 2019. Commercial application of cellulose nanocomposites—a review. Biotechnol. Rep. 21, e00316.
Sharma, P., Sharma, S.K., Lindström, T., Hsiao, B.S., 2020. Nanocellulose-enabled membranes for water purification: perspectives. Adv. Sustain. Syst., 1900114.
Sheikhi, A., 2019. Emerging cellulose-based nanomaterials and nanocomposites. In: Nanomaterials and Polymer Nanocomposites. Elsevier, pp. 307–351.
Shi, Z., Tang, J., Chen, L., Yan, C., Tanvir, S., Anderson, W.A., Berry, R.M., Tam, K.C., 2015. Enhanced colloidal stability and antibacterial performance of silver nanoparticles/cellulose nanocrystal hybrids. J. Mater. Chem. B 3 (4), 603–611.
Si, J., Cui, Z., Wang, Q., Liu, Q., Liu, C., 2016. Biomimetic composite scaffolds based on mineralization of hydroxyapatite on electrospun poly (ε-caprolactone)/nanocellulose fibers. Carbohydr. Polym. 143, 270–278.
Siró, I., Plackett, D., Hedenqvist, M., Ankerfors, M., Lindström, T., 2011. Highly transparent films from carboxymethylated microfibrillated cellulose: the effect of multiple homogenization steps on key properties. J. Appl. Polym. Sci. 119 (5), 2652–2660.
Slavutsky, A.M., Bertuzzi, M.A., 2014. Water barrier properties of starch films reinforced with cellulose nanocrystals obtained from sugarcane bagasse. Carbohydr. Polym. 110, 53–61.
Suopajärvi, T., Liimatainen, H., Karjalainen, M., Upola, H., Niinimäki, J., 2015. Lead adsorption with sulfonated wheat pulp nanocelluloses. J. Water Process Eng. 5, 136–142.
Tan, H.-F., Ooi, B.S., Leo, C.P., 2020. Future perspectives of nanocellulose-based membrane for water treatment. J. Water Process Eng. 37, 101502.
Tarrés, Q., Oliver-Ortega, H., Llop, M., Pèlach, M.À., Delgado-Aguilar, M., Mutjé, P., 2016. Effective and simple methodology to produce nanocellulose-based aerogels for selective oil removal. Cellulose 23 (5), 3077–3088.
Thomas, B., Raj, M.C., Joy, J., Moores, A., Drisko, G.L., Sanchez, C., 2018. Nanocellulose, a versatile green platform: from biosources to materials and their applications. Chem. Rev. 118 (24), 11575–11625.
Trache, D., Tarchoun, A.F., Derradji, M., Hamidon, T.S., Masruchin, N., Brosse, N., Hussin, M.H., 2020. Nanocellulose: from fundamentals to advanced applications. Front. Chem. 8.
Trifol, J., Plackett, D., Sillard, C., Szabo, P., Bras, J., Daugaard, A.E., 2016. Hybrid poly(lactic acid)/nanocellulose/nanoclay composites with synergistically enhanced barrier properties and improved thermomechanical resistance. Polym. Int. 65 (8), 988–995.
Tshikovhi, A., Mishra, S.B., Mishra, A.K., 2020. Nanocellulose-based composites for the removal of contaminants from wastewater. Int. J. Biol. Macromol. 120, 616–632.
Ummartyotin, S., Pechyen, C., 2016. Waste composite sensor designed by cellulose and activated carbon as ethylene absorber. Int. J. Polym. Sci. 2016.
Vallejos, M.E., Felissia, F.E., Area, M.C., Ehman, N.V., Tarrés, Q., Mutjé, P., 2016. Nanofibrillated cellulose (CNF) from eucalyptus sawdust as a dry strength agent of unrefined eucalyptus handsheets. Carbohydr. Polym. 139, 99–105.
Veigel, S., Rathke, J., Weigl, M., Gindl-Altmutter, W., 2012. Particle board and oriented strand board prepared with nanocellulose-reinforced adhesive. J. Nanomater. 2012.
Vipin, A.K., Fugetsu, B., Sakata, I., Isogai, A., Endo, M., Li, M., Dresselhaus, M.S., 2016. Cellulose nanofiber backboned Prussian blue nanoparticles as powerful adsorbents for the selective elimination of radioactive cesium. Sci. Rep. 6 (1), 1–14.
Wågberg, L., Decher, G., Norgren, M., Lindström, T., Ankerfors, M., Axnäs, K., 2008. The build-up of polyelectrolyte multilayers of microfibrillated cellulose and cationic polyelectrolytes. Langmuir 24 (3), 784–795.
Wang, J., Ran, R., Sunarso, J., Yin, C., Zou, H., Feng, Y., Li, X., Zheng, X., Yao, J., 2017. Nanocellulose-assisted low-temperature synthesis and supercapacitor performance of reduced graphene oxide aerogels. J. Power Sources 347, 259–269.

Xiao, S., Gao, R., Lu, Y., Li, J., Sun, Q., 2015. Fabrication and characterization of nanofibrillated cellulose and its aerogels from natural pine needles. Carbohydr. Polym. 119, 202–209.
Xu, X., Zhou, J., Jiang, L., Lubineau, G., Ng, T., Ooi, B.S., Liao, H.Y., Shen, C., Chen, L., Zhu, J.Y., 2016. Highly transparent, low-haze, hybrid cellulose nanopaper as electrodes for flexible electronics. Nanoscale 8 (24), 12294–12306.
Yagyu, H., Saito, T., Isogai, A., Koga, H., Nogi, M., 2015. Chemical modification of cellulose nanofibers for the production of highly thermal resistant and optically transparent nanopaper for paper devices. ACS Appl. Mater. Interfaces 7 (39), 22012–22017.
Yang, H., Tejado, A., Alam, N., Antal, M., van de Ven, T.G., 2012. Films prepared from electrosterically stabilized nanocrystalline cellulose. Langmuir 28 (20), 7834–7842.
Yang, R., Aubrecht, K.B., Ma, H., Wang, R., Grubbs, R.B., Hsiao, B.S., Chu, B., 2014a. Thiol-modified cellulose nanofibrous composite membranes for chromium (VI) and lead (II) adsorption. Polymer 55 (5), 1167–1176.
Yang, G., Tang, L., Lei, X., Zeng, G., Cai, Y., Wei, X., Zhou, Y., Li, S., Fang, Y., Zhang, Y., 2014b. Cd (II) removal from aqueous solution by adsorption on α-ketoglutaric acid-modified magnetic chitosan. Appl. Surf. Sci. 292, 710–716.
Yu, X., Tong, S., Ge, M., Wu, L., Zuo, J., Cao, C., Song, W., 2013. Adsorption of heavy metal ions from aqueous solution by carboxylated cellulose nanocrystals. J. Environ. Sci. 25 (5), 933–943.
Yu, S., Sun, J., Shi, Y., Wang, Q., Wu, J., Liu, J., 2020. Nanocellulose from various biomass wastes: its preparation and potential usages toward the high value-added products. Environ. Sci. Ecotechnol., 100077.
Yuan, G., Prabakaran, M., Qilong, S., Lee, J.S., Chung, I.M., Gopiraman, M., Song, K.H., Kim, I.S., 2017. Cyclodextrin functionalized cellulose nanofiber composites for the faster adsorption of toluene from aqueous solution. J. Taiwan Inst. Chem. Eng. 70, 352–358.
Zander, N.E., Dong, H., Steele, J., Grant, J.T., 2014. Metal cation cross-linked nanocellulose hydrogels as tissue engineering substrates. ACS Appl. Mater. Interfaces 6 (21), 18502–18510.
Zhang, Z., Sèbe, G., Rentsch, D., Zimmermann, T., Tingaut, P., 2014a. Ultralightweight and flexible silylated nanocellulose sponges for the selective removal of oil from water. Chem. Mater. 26 (8), 2659–2668.
Zhang, X., Lin, Z., Chen, B., Zhang, W., Sharma, S., Gu, W., Deng, Y., 2014b. Solid-state flexible polyaniline/silver cellulose nanofibrils aerogel supercapacitors. J. Power Sources 246, 283–289.
Zhang, C., Zhang, R.Z., Ma, Y.Q., Guan, W.B., Wu, X.L., Liu, X., Li, H., Du, Y.L., Pan, C.P., 2015. Preparation of cellulose/graphene composite and its applications for triazine pesticides adsorption from water. ACS Sustain. Chem. Eng. 3 (3), 396–405.
Zhang, H., Li, Y., Xu, Y., Lu, Z., Chen, L., Huang, L., Fan, M., 2016. Versatile fabrication of a superhydrophobic and ultralight cellulose-based aerogel for oil spillage clean-up. Phys. Chem. Chem. Phys. 18 (40), 28297–28306.
Zhang, Y., Shang, Z., Shen, M., Chowdhury, S.P., Ignaszak, A., Sun, S., Ni, Y., 2019. Cellulose nanofibers/reduced graphene oxide/polypyrrole aerogel electrodes for high-capacitance flexible all-solid-state supercapacitors. ACS Sustain. Chem. Eng. 7 (13), 11175–11185.
Zhou, Y., Khan, T.M., Liu, J.C., Fuentes-Hernandez, C., Shim, J.W., Najafabadi, E., Youngblood, J.P., Moon, R.J., Kippelen, B., 2014. Efficient recyclable organic solar cells on cellulose nanocrystal substrates with a conducting polymer top electrode deposited by film-transfer lamination. Org. Electron. 15 (3), 661–666.
Zhu, H., Narakathu, B.B., Fang, Z., Aijazi, A.T., Joyce, M., Atashbar, M., Hu, L., 2014. A gravure printed antenna on shape-stable transparent nanopaper. Nanoscale 6 (15), 9110–9115.

CHAPTER

14

Introduction to cellulose-based nanobiosorbents

Cassamo Ussemane Mussagy[a] *and Agnes Magri*[b]

[a]Department of Engineering of Bioprocesses and Biotechnology, School of Pharmaceutical Sciences, São Paulo State University (UNESP), Araraquara, São Paulo, Brazil [b]Fundaçao Oswaldo Cruz, Fiocruz-Ceara, Eusébio, Brazil

14.1 Contextualization

Currently, the common absorbent materials available in the market are derived from non-renewable petrochemicals sources which exhibit poor environmental biocompatibility (Mendoza et al., 2019). This lack of sustainability has driven research towards developing more biocompatible and eco-friendly alternatives natural bio-based materials (Mussagy et al., 2021a) for wastewater treatment, environmental remediation, food processing, medicine, nanosensors among others (Mussagy et al., 2021b) with low cost, and with no harmful by-products generation (Putri et al., 2020). As shown in this book, nanomaterials, as absorbents, offer several advantages over the conventional; due to the low-cost, high absorption capacities, less sludge regeneration and the availability of these compounds in the world (Mahfoudhi and Boufi, 2017a, b). Among these, lignocellulosic biomass have attracted the attention of several industries due to the promising applications as absorbent (Putro et al., 2017). The main component of lignocellulosic material, namely: cellulose (natural polymer), has been applied directly as bio-sorbent in its natural form obtained from agri-food wastes (cassava bagasse, rice straw banana peel, corncob, among others) (Blanco et al., 2018; Spinella et al., 2016). However, the chemically counterpart can be obtained and classified into two main groups: (i) *direct modification*, in which esterification, halogenation, oxidation, alkaline treatment are the principal routes to obtain the cellulose-based materials (Hokkanen et al., 2016a, b) and (ii) *graft copolymerization*, where a branched copolymer is obtained when the side chain grafts are attached to the main chain of a polymer backbone using several procedures such as, photografting, high energy radiation grafting as well as the chemical initiation grafting (Hokkanen et al., 2016b). The expression "nanocellulose" usually refers to

https://doi.org/10.1016/B978-0-323-90912-9.00014-9

cellulose-based materials that present at least one dimension in the nanometer range, and as a result of the wide application, the recovery of nanocellulose-based materials as cellulose nanofibers (CNF), cellulose nanocrystals (CNC), and bacterial cellulose (BC), that differ in their dimensions, functions, and preparation methods has been investigated (Putro et al., 2017). However, due to the great surface reactivity of cellulose-based nanobiosorbents, they can be modified or mixed with other compounds to find synergistic properties that can fit the needs of the specific applications (Blanco et al., 2018). Despite these advantages, the main purpose of this chapter is to provide readers a briefly knowledge on the classification and preparation of cellulose-based nanobiosorbents (CN) and the mechanisms behind the CN absorption process.

14.2 Classification and preparation of CN structures

Several types of cellulose-based nanobiosorbents can be classified into different groups based on their dimension, function, shape, and production/preparation method, that depends on the source as well as the processing conditions (Kargarzadeh et al., 2017). In the last years, many terms have been used to describe different types of CN; due to this, in this chapter CN were categorized in three main groups: cellulose nanofibers (CNF), nanocrystalline cellulose (CNC), and bacterial cellulose (BC) (Blanco et al., 2018). The CN production process from hardwood and softwood and its characterization have been extensively described in literature (Amiralian et al., 2017; Guo et al., 2020a, b), the high costs related with the use of these raw materials is prompting a move towards to replace them, due to their high demand from pulp, paper, and furniture industries (Blanco et al., 2018). The new developments are focused on the use of agro-wastes, water plants, among others, considered as an effective alternatives sources of cellulose to produce CNF and CNC (Chen et al., 2015). On the other side, another important source is BC, mainly produced by several strains of the genus *Aerobacter, Azotobacter, Agrobacterium, Achromobacter, Alcaligenes, Escherichia, Komagataeibacter, Pseudomonas, Rhizobium, Sarcina, Salmonella* and *Zoogloea* (Campano et al., 2016), thus due to the large amount of culture media nutrients required for cellulose production, researchers have focused their studies on the use of low-cost materials, such as carbon and nitrogensources from agro-wastes (Hong and Qiu, 2008), that not only decrease significantly the cost of nutrients, but also improve the BC yields. Several authors have reported comparative studies regarding the preparation techniques of several types of CN (Valentini et al., 2019a, b; Wang et al., 2017) (Table 14.1). CNF can be produced using numerous mechanical processes, *cf*., high-pressure homogenization (Garusinghe et al., 2018; Wang et al., 2017; Wu et al., 2021), microfluidization (Bai et al., 2019; Blanco et al., 2018; Pardesi et al., 2020), grinding (Yang et al., 2020), or other less used such as, ultrasonication (Valentini et al., 2019a; Wang et al., 2017) and cryocrushing (Gopakumar et al., 2018; Thakur et al., 2017); however the main drawback of these mechanical processes are directly related to the high energy requirement (Kargarzadeh et al., 2017). It is important to highlight that CNF properties depend not only on the production process or raw material used but also on the fiber description (Kargarzadeh et al., 2017). The CNC have been frequently obtained by acid hydrolysis, in which the crystalline domains are first solubilized, leaving behind the crystalline region or CNC, which

TABLE 14.1 Preparation techniques of several types of cellulose-based nanobiosorbents.

Type	Operational conditions	Advantages	Drawbacks	References
Cellulose nanofibers				
High-pressure homogenization	High pressure (30–150 MPa)	Cellulose fiber size reduction achieved through interparticle collisions. The higher the pressure, higher is the efficiency of the disruption	Insufficient disintegration of the material. Mechanical pretreatments are needed before homogenization. High energy consumption	Kargarzadeh et al. (2017), Wang et al. (2017), Wu et al. (2021), Garusinghe et al. (2018), Ni et al. (2020)
Microfluidization	Very high pressure (>100 MPa)	High shear forces inside the capillary tube ensured cellulose fibrillation. Size distribution of nanofibers is homogenous	To improve the degree of fibrillation is necessary to repeat the process several times. Nanofibrillar bundles after 20 cycles led to agglomeration of CNF	Blanco et al. (2018), Bai et al. (2019), Pardesi et al. (2020)
Grinding	High pressure	Additional mechanical pretreatments are not required. Easy scale-up for industrial applications: simply and low-cost technology	Many steps are required to generate the fibrillated cellulose. Need for disk stone maintenance and replacement	Yang et al. (2020), Pyrgiotakis et al. (2018), Franco et al. (2017)
Cryocrushing	Low temperature (N_2 liquid is frequently used)	Nanofibers displays superior dispersion ability in acrylic emulsion	Low-volume manufacturing and expensive. High energy consumption	Gopakumar et al. (2018), Thakur et al. (2017), Nasir et al. (2017)
High-intensity ultrasonication	Low-pressure and high-pressure waves	Fibrillation efficiency can vary according to power, temperature, time, fiber size and concentration	Low productivity. Low consistency of the cellulose suspension is required	Yang et al. (2017), Valentini et al. (2019a, b), Syafri et al. (2019)
Cellulose nanocrystals				
Acid hydrolysis	Different mineral acids can be used: sulfuric, hydrochloric, phosphoric, maleic, hydrobromic, nitric, and formic acids	CNC obtained from sulfuric or phosphoric acid hydrolysis dispersed readily in water. Crystallinity and dimensions of the nanocrystalline particles depend on the origin of the cellulose feedstock	CNC produced from hydrochloric or hydrobromic acid hydrolysis are not as easy to disperse since their aqueous suspensions tend to flocculate. Acidic sulfate groups compromise the thermostability of the NC	Guo et al. (2020a, b, Niu et al. (2017), Maciel et al. (2019), Theivasanthi et al. (2018)

Continued

TABLE 14.1 Preparation techniques of several types of cellulose-based nanobiosorbents.—cont'd

Type	Operational conditions	Advantages	Drawbacks	References
Hydrolysis with solid acids	Sulfonated metal oxides such as sulfonated TiO_2 and ZrO_2 and their complexes	Higher thermal stability. Solid acids are easily recovered and recycled through extraction with diethyl ether	High consumption of energy and chemicals. Acidic corrosion of equipment, health and environmental hazards	Zhao et al. (2020), Chen et al. (2018a, b)
Hydrolysis with gaseous acids	Several types of gaseous acids can be used in this procedure, such as nitric acid and trifluoroacetic acid	Need low amount of water. Simple acid recycling. High yields	Further techniques are required to isolate CNC	Dufresne (2013)
Hydrolysis with metal salt catalyst	Trivalent, divalent and monovalent metal inorganic salts are used	Feasible and controllable hydrolysis process. Inorganic salt can selectively control the hydrolysis	Health and environmental hazards. Difficulty to control the hydrolysis degree of cellulose	Li et al. (2015), Ziaul et al. (2014), Brinchi et al. (2013)
Green solvents	Ionic liquids (ILs) and deep eutectic solvents (DES)	Simple and effective hydrolysis process. Possible reuse of ILs and DES	Reaction temperature and time can affect the yield and thermal properties	Atikah et al. (2017), Pinkert et al. (2009), Zhu et al. (2006)
Bacterial cellulose				
Static culture	Culture media inoculated with bacteria and kept for a long period	Homogeneous pellicle. Low-cost	Long times. Large space required	Ha et al. (2008), Czaja et al. (2004)
Agitated culture in shakers	Culture's agitation: 100–500 rpm	Low-cost. Economic scale-up	BC usually sticks to the wall being difficult the recovery	Czaja et al. (2004)
Agitated culture in Bioreactors	Agitated culture with the use of different types of impellers, and controlling of aeration and agitation conditions	Higher oxygen availability. High productivity. Low production time	Lower crystallinity. Adhesion of BC to the top of the reactor. BC with low mechanical strength	Ha et al. (2008), Lin et al. (2013), Song et al. (2009), Lin et al. (2013)

Adapted from Blanco, A., Monte, M.C., Campano, C., Balea, A., Merayo, N., Negro, C., Mustansar Hussain, C., 2018. Chapter 5—Nanocellulose for industrial use: cellulose nanofibers (CNF), cellulose nanocrystals (CNC), and bacterial cellulose (BC). In Micro and Nano Technologies. Elsevier, pp. 74–126. https://doi.org/10.1016/B978-0-12-813351-4.00005-5 and Kargarzadeh, H., Ioelovich, M., Ahmad, I., Thomas, S., Dufresne, A., 2017. Methods for extraction of nanocellulose from various sources. In Handbook of Nanocellulose and Cellulose Nanocomposites. https://doi.org/10.1002/9783527689972.ch1.

present a higher resistance to acid solvent. For that, sulfuric, hydrochloric, phosphoric, maleic, hydrobromic, nitric, and formic acids (Amiralian et al., 2017; Guo et al., 2020a) have been the most used for this purpose (Habibi et al., 2002). In addition, several methods to produce CNC were reported, *i.e.*, hydrolysis with solid acids (Chen et al., 2015), hydrolysis with gaseous acids (Dufresne, 2013), hydrolysis with metal salt catalyst (Li et al., 2015; Lu et al., 2014) and the use of green solvents (Atikah et al., 2017; Pinkert et al., 2009; Zhu et al., 2006). As noted above, the non-biocompatible conventional method to obtain CNC is often accomplished using different solvents considered harmful to the environment, and due to this, it is fundamental to search for more biocompatible and ecofriendly treatments using "green" solvents such as, ionic liquids (ILs), biosolvents and eutectic solvents (ES) (Mussagy et al., 2020), which can allow not only the sustainability of processes but also the biocompatibility of the materials. In the process to produce CN, some problems (aggregation and high energy consumption) can occur during the mechanical fibrillation of cellulose, in this cases, an efficient pretreatment can help to reduce these issues, however the selection of pretreatment method differs on the cellulose source as well as the required morphology of the initial material (Kargarzadeh et al., 2017). The suitable pretreatment also promotes accessibility, modify crystallinity and boosts the reactivity; decreasing the energy consumption and simplifies the NC production process (Šturcová et al., 2005). The procedures employed to process BC is completely different from that used for CNF and CNC (Kargarzadeh et al., 2017). The first step for BC production is the cell growth, where the cellular high yields production is the main objective (Czaja et al., 2004; Ha et al., 2008). To increase the production, several factors must be taking into account, *cf.*, optimization of nutrient media, fermentation time, pH media, temperature and the selection of the appropriate bacterial strain (Ana et al., 2018). The traditional method that produce high yields of BC is the fermentation in static culture (Czaja et al., 2004; Ha et al., 2008), however the main drawback remains in the fact that BC usually sticks to the wall being difficult the recovery (Czaja et al., 2004; Ha et al., 2008). In addition, envisioning the large-scale production, submerged cultures in shakers and bioreactors (Calvar et al., 2005; Ha et al., 2008; Lin et al., 2013; Song et al., 2009) are also used for BC production to decrease the production time due to the enhancement of mass transfer and oxygen transfer rate.

As absorbents, NC brings higher absorption aptitudes and enhanced binding affinities than their equivalents at the macroscale (Zhou et al., 2011). Over the last years, due to their particular properties, NC have emerged as potential absorbents for environmental remediation and wastewater treatment that aroused increasing attention to solve some environmental issues (Savage and Diallo, 2005), and due to that, in this chapter the mechanisms behind the adsorption process are extensively discussed in the subsequent section.

14.3 Adsorption/desorption process

14.3.1 Types and regeneration process

Among different methods used for the remediation of contaminants, adsorption is one of the simplest process, in terms of operation and conception (Ali and Gupta, 2007). The adsorption process is widely used in the treatment of drinking water and industrial effluents,

for the removal of non-degradable organic compounds (Mahfoudhi and Boufi, 2017a). Adsorption is commonly defined as process of molecules adhesion of a gas or liquid on a solid surface (adsorbent); and the adsorbed material are usually liquid, solid, or gaseous molecules. Adsorption is a superficial process, therefore particles (adsorbate) are retained on the solid surface, and the adsorbate can diffuse inside the particle, according to Fick's law, also known as the diffusion model homogeneous in the particle (Ruthven, 1984), which leads to an increase in the loading capacity of the solid adsorbent until the adsorption equilibrium is attained. The efficiency of the adsorption process is intrinsically linked to the surface properties, *cf.*, chemical composition, charge and porosity degree (Nor et al., 2021). These characteristics are extremely important to increase the efficiency of the adsorption process, *i.e.*, the more porous is the solid used as adsorbent, the greater the adsorption capacity of contaminants. In addition to these factors, the degree of adsorption also depends on the surface area, pore size distribution (Nor et al., 2021), internal diffusion of the material (Köse et al., 2020), mineral matter content and operational parameters such as temperature, pressure, load capacity, pH conditions, and contact time (Nor et al., 2021). The contaminant molecules (adsorbate) are usually attracted to the surface of an adsorbent by the chemical or physical forces (Lombardo and Thielemans, 2019). Based on the forces involved in the attraction process of adsorbates and the interaction with solid surface, the adsorption process can be classified into two different routes: (i) *physisorption* when involves physical forces such as van der Waals forces and electrostatic attraction (Nor et al., 2021) that allows contaminant molecules to attach to the surface of an adsorbent configured by a low enthalpy due to the little disturbance of the electronic environment of the two species in interaction (Lombardo and Thielemans, 2019); and/or (ii) *chemisorption* where the adsorption occurs through the formation of chemical bound (covalent or ionic) (Nor et al., 2021), between molecules charged with opposite charges which causes a change in the electronic configuration of both attracted structures, in addition to being characterized by a high exothermic enthalpy (Atkins and De Paula, 2001; Lombardo and Thielemans, 2019). The adsorption efficiency can be enhanced by surface modification, giving a wide range of possibilities for molecules adsorption, which makes these structures tunable for each specific type of pollutants and specific environments as water, soil or air. This possibility of adjustment according to the adsorbate, allows the creation of a new material adapted for capture and remediation of a wide range of compounds. In the literature, several contaminants could be adsorbed by NC structures, including chemical contaminants, heavy metals, dissolved organic pollutants, dyes, oil present in different substrates such as soil, air or water contaminated (Ali and Gupta, 2007). In generally, materials with potential to be used as pollutant adsorbents must present *(a)* high efficiency and pollutant adsorption capacity, which is intrinsically linked to *(b)* the size and characteristics of the contact surface of the adsorbent material, *(c)* structural integrity and mechanics to withstand the flow of water, and mainly, *(d)* inexpensive, *(e)* capacity to regenerate, which corroborates to the sustainability and cost-benefit of the approaches, and finally *(f)* easily separation from the effluent (Mahfoudhi and Boufi, 2017b; Yue et al., 2019). Usually, the industrial adsorbents employed are composed of macro-sized pores, hence nanomaterials have an advantage with regard to the contact surface available for adsorption (Mahfoudhi and Boufi, 2017b). The high surface area of NC materials provide more active sites for the binding of adsorbate to the adsorbent, and also contain hydroxyl groups in its structure that allow the surface modifications (Mahfoudhi and Boufi, 2017b). Surface functionalization is the reason that provides the

nanocellulose-based adsorbents a wide range of applications, enhancing the adsorption capacity and can be tuned for specific class of pollutants, or association of several different pollutants. Cellulose-based nanobiosorbents are described in literature due to their adsorption capacity for heavy metals, organic pollutants, CO_2, oils and viruses (Järup, 2003; Nor et al., 2021). Different strategies of surface modification from the hydroxyl function can be adopted, however each class of functionalization is chosen according to the type of pollutant, that can be *heavy metals*, originating from volcanic eruptions, mining activities, several types of industries, and agro-industrial activities (Järup, 2003; Nor et al., 2021); *dyes*, waste material or byproducts from the food industries, agriculture, petroleum products and beverage industry, cosmetics (Tkaczyk et al., 2020); *acids* from mine drainage water, industrial waste disposal and/or acidified soils (Klamerus-iwan et al., 2015); organic contaminants such as *organophosphorus,* found in effluents and discharges from industry linked to agriculture as producers of herbicides and pesticides (Dar et al., 2020)*; organic oils* such as silicone, paraffin, petroleum ether, canola, oil from pumps and engines, diesel (Pichtel, 2016); *phenols* from industrial effluents that are discharged into streams, atmosphere or on land (Kahru et al., 2002); *organochlorine compounds* from waste incineration, toxic dumps, crop spraying (Loganathan and Kannan, 1994); CO_2 from atmosphere (Gebald et al., 2011; Valdebenito et al., 2018); and virus from drink water (Mi et al., 2020). Based on the chemical composition, concentration of the pollutant, matrix and considering the environmental conditions such as air humidity, temperature, pressure and pH, the functionalization on the surface of NC can be performed. The different modifications reported in the literature are through oxidation, etherification, addition, silylation, esterification, and grafting. Other types of functionalization in cellulose-based biosorbents such as succinic anhydride crosslinking, cationic interaction, acetylation and coupling with isocyanate derivates are often applied (Hokkanen et al., 2016b; Köse et al., 2020). Thus, for each type of pollutant a modification can be selected in order to obtain greater adsorption efficiency (Thomas et al., 2018). For example, to increase the adsorption of hydrophobic compounds, as in the case of oils, a strategy widely used is the addition of low energy hydrophobic groups in the nanostructured cellulose, by physical or chemical methods to increase the adsorption of the hydrophobic compounds via hydrophobic interactions, such as oils (Liao and Wang, 2019). This process, known as **hydrophobization** method (Köse et al., 2020) (Fig. 14.1), it is also widely used to increase the adsorption of water-soluble organic molecules, providing specific affinity as in the case of mycotoxins (Hossein et al., 2015). These are adsorbed when the NC surface is functionalized with fatty acids combined with specific anions, such as the sulphate groups (Hossein et al., 2015). This structure promotes the required hydrophobicity to connect to the hydrophobic regions of mycotoxins, and then the hydrophobic groups are added via esterification (Hossein et al., 2015). Silylation also can provide hydrophobicity in nanocellulose, increasing flexibility and porosity (Thomas et al., 2018). The chemical used for this process commonly is isopropyl dimethylchlorosilane, alkyldimethylchlorosilane, chlorodimethyl isopropylsilane, and methyltrimethoxysilane (Chanzy et al., 2004), that confer highly selectivity and recyclability of cellulose-based nanobiosorbents. Amidation modification, involves the addiction of amide functional group (pH from 7 to 10) by carbodiimide chemistry, as *N*-ethyl-*N*-(3-(dimethylamino)-propyl) (EDAC) (Köse et al., 2020). Finally, the last method to add hydrophobic groups is urethanization, mediated by covalent bonds between the nanocellulose hydroxyl groups and isocyanate, a urethane linkage (Siqueira et al., 2010).

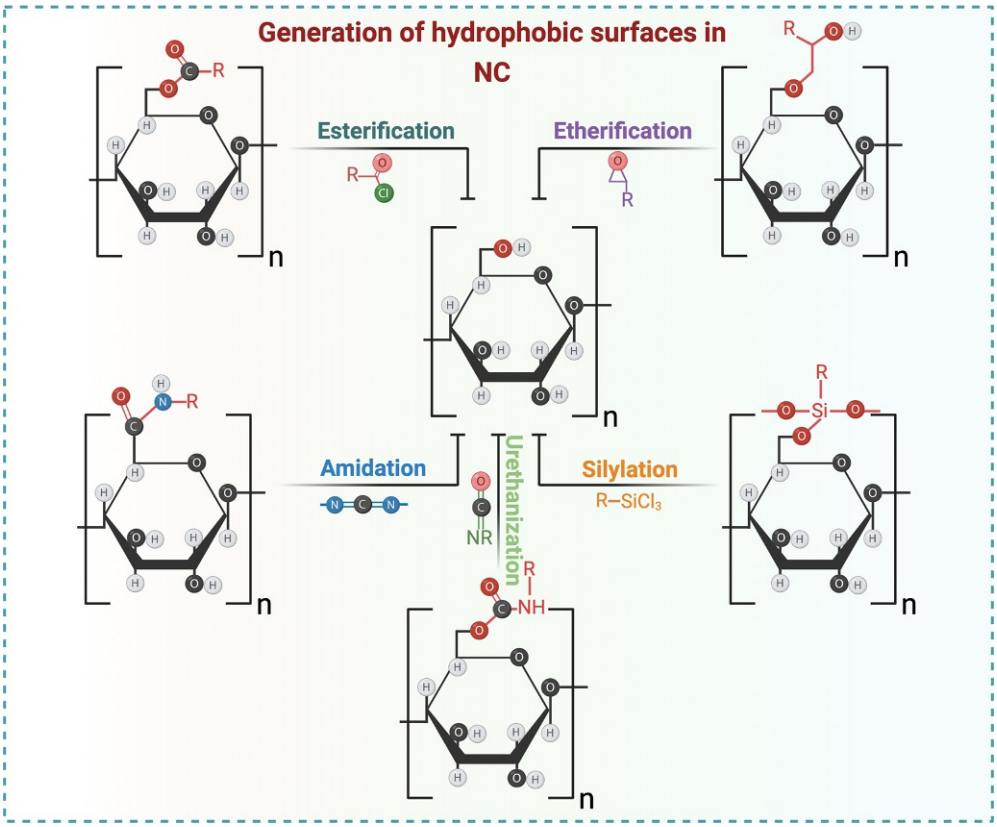

FIG. 14.1 Hydrophobization strategies for the generation of hydrophobic surfaces in NC materials. *Adapted from Köse, K., Mavlan, M., Youngblood, J.P., 2020. Applications and impact of nanocellulose based adsorbents. Cellulose 27, 2967–2990. https://doi.org/10.1007/s10570-020-03011-1.* No permission required.

Besides that, if the target adsorbent contain heavy metals or dyes, it is well recommended that the cellulose surface present **ionic charged** (Nor et al., 2021), in this way, if the adsorbent is negatively charged, it will be effective in adsorbing the positive charge of heavy metals and dyes due to the electrostatic interaction (Popescu et al., 2020). In case of CNC and dyes, the hydrogen bonds command the strong interaction between the adsorbate and the nanocellulose structure, through π–π interaction (Popescu et al., 2020). Different strategies can be adopted for to impar ionic charges at cellulose nanostructures, such as oxidation, sulfonation, phosphorylation, and carboxymethylation (Thomas et al., 2018). Moreover, within this classification, the modifications are divided into anionization and cationization, according to the ability to add negatively or positively charged groups, respectively. The anionic groups of nanocellulose induced by oxidizing agents, organic bases and organic acids, and other organic compounds, are generally sensitive to pH due to the isoelectric point of the anionic center (Köse et al., 2020). Another alternative to modification of surface area of cellulose-based biosorbents is **grafting polymers** onto cellulose. These cellulose-polymer composites aim to confer certain characteristics already addressed such as hydrophobicity

and hydrophilicity, as well as resistance to abrasion, elasticity, to become responsive, thermally resistant, self-cleaning materials and also ion exchanger (Thomas et al., 2018). There are three ways to obtain the polymer graft: *grafting-to*, *grafting-from*, and *grafting-through*, and the graft reaction can occur with polymers or peptides Fig. 14.2.

Briefly, the main difference relies in the growth characteristics of polymer branches, *cf.*, "*grafting-to*" when is bonded to cellulose directly, typically by coupling the reactive terminal group of the polymer (or peptides) with the hydroxyl groups of the cellulose structure; "*grafting-from*" process cellulose already functionalized with an initiator is linked to the monomers, which are polymerized directly from the surface; and in "*grafting-through*," cellulose is first functionalized with polymerizable species, such as vinyl molecules. Thus, the functionalized cellulose is mixed with a comonomer and polymerization begins

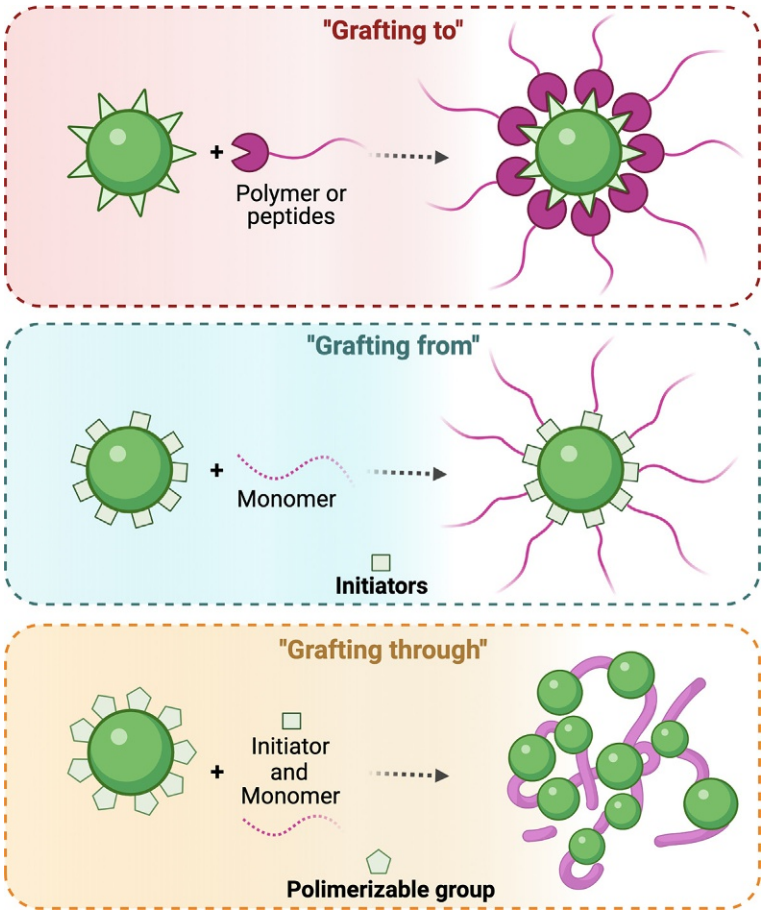

FIG. 14.2 Schematic illustration of different types of cellulose-grafting. *Adapted from Thomas, B., Raj, M.C., Athira, K.B., Rubiyah, M.H., Joy, J., Moores, A., Drisko, G.L., 2018. Nanocellulose, a versatile green platform: from biosources to materials and their applications. Chem. Rev. 118, 11575–11625. https://doi.org/10.1021/acs.chemrev.7b00627.* No permission required.

(Minko, 2008; Thomas et al., 2018). There are different types of reactions that can occur, *i.e.*, atom transfer radical polymerization (ATRP) grafting-to synthesis; free radical grafting-to synthesis; reversible addition – fragmentation chain transfer (RAFT) grafting-to synthesis; ring-opening polymerization grafting-to synthesis and postpolymerization grafting from (Thomas et al., 2018). There is an alternative option of non-specific functionalization, those capable to act on a wide variety of pollutants, where generalist modifications can be added for different types of substrates or more than one specific modification, that can operate simultaneously in the adsorption process.

14.3.2 Desorption/regeneration process

The possibility of contaminants desorption from the matrix, as well as the option of regenerating cellulosic material, is one of the greatest advantages in relation to the use of cellulose-based nanobiosorbents, that allow not only its complete reuse, but also decrease the cost of the process. The regeneration of exhausted NC material represents an important parameter in the economic analysis of the process to remove contaminants from wastes, and, in some cases, if the process is expensive, but with the possibility of being reused for numerous cycles, makes the cost-benefit of the process much higher. Another point that deserves attention is the possibility of contaminants reuse, as for example, the heavy metals, which can be reused in the original production process. Simple process, such as acidification of the reaction medium, are the commonly procedure for the desorption of heavy metals (Vijayalakshmi et al., 2017). However, as the NC materials are mostly functionalized, the desorption and recovery process must be careful, to avoid degradation of the cellulose-based adsorbents and preventing a significant decrease in the adsorption capacity in the next cycle (Mo et al., 2021). Hence, it must be emphasized that cellulose regeneration processes depend on the adsorbed pollutant and functionalized process (Hokkanen et al., 2016b). Depending on the adsorbed species, several methods can be used for regeneration process, such as ionic approaches (employing weak solutions of acids/bases); solvent exchange (varying the polarity of systems), or heating, which can be combined with the two previous techniques. In generally, to desorb organic pollutants or oil–water separations, a simple change of organic solvent can solve the problem; always taking into account the solvent affinity and adsorbed material characteristics, and taking care, to prevent the use of solvents that can remove the functionalized groups linked to the NC. Acidic (e.g., diluted H_2SO_4, HCl, HNO_3, acetic acid) or basic treatments are widely used for desorption of dyes and heavy metals, as mentioned above (Vijayalakshmi et al., 2017). The use of acids/bases for desorption, can be effective by changing the pH, and since the chelation mechanism is extremely sensitive to pH, it becomes possible to recover the adsorbed contaminants (Vijayalakshmi et al., 2017). Generally, heating processes can improve the efficiency and speed of the reactions, using ionization strategy for the virus desorption (Pisharody et al., 2021). To remove gases, such as CO_2 or H_2S, the thermal regeneration is the most employed (Valentini et al., 2019a; Wang et al., 2017). Another regeneration strategies for gas adsorption is the use of supercritical fluid regeneration and vacuum-swing cycling techniques (Gebald and Wurzbacher, 2013; Haimer et al., 2010).

14.4 Final remarks and future perspectives

Biodegradable nanomaterials such as NC are an excellent alternative for the "new" class of biosorbents. Concerning to the economic cost of the process, when compared to the conventional processes, as for example in water treatment, employing reverse osmosis or adsorptive filtration by ion exchange resins, the environmental and economic advantage of NC as adsorbent is clear. The adsorbents are easily separated from the effluent, and mostly commercialized in the form of granules, fibers or films wrapped in a filtration column, however using nanomaterials (more efficient), the remotion capacity increase. In addition, NC has a number of other properties that bring several advantages when compared to conventional waste treatment systems. Among them, are the *(1)* possibility of surface functionalization; *(2)* possibility of desorption and subsequent recovery for the reuse of material (adsorbent and adsorbate), through simple processes that do not compromise the cellulose absorption capacity; *(3)* renewable devices, with a *(4)* good cost–benefit ratio when compared to other procedures; *(5)* biodegradability, with a *(6)* high specificity of the surface area; *(7)* high mechanical performance improved by a *(8)* high stiffness and cohesion of NC; *(9)* good surface tension properties which favor the wetting of cellulose in water, *(10)* stable in water, and finally *(11)* high hydrophilicity and *(12)* high crystallinity that allows this type of nanobiosorbents to be resistant to biological and/or chemical corrosion in water (Nor et al., 2021). Another bottleneck in effluent treatments is the need to use different materials for the complete removal of contaminants. If they had more intelligent materials, which were multifunctional, it would certainly bring great advances in the field. The efficiency of desorption/recovery is one of the key factors to drive the total cost of the waste's treatment process and the loss of load capacity at each reuse cycle represents a need for improvement in the processes. Likewise, concerning to the recovery/desorption processes, these are impaired when the aggregation of the NC material occurs. The aggregation process can greatly decrease the recovery of the material, representing an overall loss in the treatment process. An important point is the biodegradability of cellulose-based structures after the functionalization process, where the addition of groups along the polymeric cellulose chain can create conditions that difficult their biodegradation. That is the principal reason why the process of reusing these structures is so important and should be one of the main focus of improvement going forward, considering that there is already a lot of knowledge about the adsorption and functionalization mechanisms, it is now necessary to focus on the economic and environmental efficiency issue of treatment processes using cellulose-based biosorbents.

References

Ali, I., Gupta, V.K., 2007. Advances in water treatment by adsorption technology. Nat. Protoc. 1 (6), 2661–2667. https://doi.org/10.1038/nprot.2006.370.

Amiralian, N., Annamalai, P.K., Garvey, C.J., Jiang, E., Memmott, P., Martin, D.J., 2017. High aspect ratio nanocellulose from an extremophile spinifex grass by controlled acid hydrolysis. Cellul. 24 (9), 3753–3766. https://doi.org/10.1007/s10570-017-1379-6.

Ana, C.C., Angeles, B., Carlos Negro, B., 2018. Enhancement of the fermentation process and properties of bacterial cellulose: a review. Cellul. 23. https://doi.org/10.1007/s10570-015-0802-0.

Atikah, N., Nurhidayatullaili, M.I., Sharifah, M.J., Hamid, B.A., 2017. Understanding the effect of synthesis parameters on the catalytic ionic liquid hydrolysis process of cellulose nanocrystals. Cellul. 24. https://doi.org/10.1007/s10570-017-1273-2.

Atkins, P., De Paula, J., 2001. Process on solid surfaces. Atkins' Physical chemistry. In: Atkins' Physical Chemistry, seventh ed. Oxford University Press, Oxford, pp. 977–1005.

Bai, L., Lv, S., Xiang, W., Huan, S., McClements, D.J., Rojas, O.J., 2019. Oil-in-water Pickering emulsions via microfluidization with cellulose nanocrystals: 1. Formation and stability. Food Hydrocoll. 96, 699–708. https://doi.org/10.1016/j.foodhyd.2019.04.038.

Blanco, A., Monte, M.C., Campano, C., Balea, A., Merayo, N., Negro, C., Mustansar Hussain, C., 2018. Chapter 5—Nanocellulose for industrial use: cellulose nanofibers (CNF), cellulose nanocrystals (CNC), and bacterial cellulose (BC). In: Micro and Nano Technologies. Elsevier, pp. 74–126, https://doi.org/10.1016/B978-0-12-813351-4.00005-5.

Brinchi, L., Cotana, F., Fortunati, E., kenny, J., 2013. Production of nanocrystalline cellulose from lignocellulosic biomass: technology and applications. Carbohydr. Polym. 94, 154–159. https://doi.org/10.1016/j.carbpol.2013.01.033.

Calvar, N., Domínguez, A., Tojo, J., 2005. Vapor-liquid equilibria for the quaternary reactive system ethyl acetate + ethanol + water + acetic acid and some of the constituent binary systems at 101.3 kPa. Fluid Phase Equilib. https://doi.org/10.1016/j.fluid.2005.07.010.

Campano, C., Balea, A., Blanco, A., Negro, C., 2016. Enhancement of the fermentation process and properties of bacterial cellulose: a review. Cellul. 23 (1), 57–91. https://doi.org/10.1007/s10570-015-0802-0.

Chanzy, H., Cerrada, M.L., Fleury, E., 2004. Surface silylation of cellulose microfibrils : preparation and rheological properties. Polymer 45, 1569–1575. https://doi.org/10.1016/j.polymer.2003.12.028.

Chen, L., Wang, Q., Hirth, K., Baez, C., Agarwal, U.P., Zhu, J.Y., 2015. Tailoring the yield and characteristics of wood cellulose nanocrystals (CNC) using concentrated acid hydrolysis. Cellul. 22 (3), 1753–1762. https://doi.org/10.1007/s10570-015-0615-1.

Chen, T., Peng, L., Yu, X., He, L., 2018a. Magnetically recyclable cellulose-derived carbonaceous solid acid catalyzed the biofuel 5-ethoxymethylfurfural synthesis from renewable carbohydrates. Fuel 219, 344–352. https://doi.org/10.1016/j.fuel.2018.01.129.

Chen, S.S., Wang, L., Yu, I.K.M., Tsang, D.C.W., Hunt, A.J., Jérôme, F., Zhang, S., Ok, Y.S., Poon, C.S., 2018b. Valorization of lignocellulosic fibres of paper waste into levulinic acid using solid and aqueous BrØnsted acid. Bioresour. Technol. 247, 387–394. https://doi.org/10.1016/j.biortech.2017.09.110.

Czaja, W., Romanovicz, D., Brown, R.M., 2004. Structural Investigations of Microbial Cellulose Produced in Stationary and Agitated Culture., https://doi.org/10.1023/B:CELL.0000046412.11983.61.

Dar, M.A., Kaushik, G., Francisco, J., Chiu, V., 2020. Pollution status and biodegradation of organophosphate pesticides in the environment. In: Abatement of Environmental Pollutants. Elsevier Inc, pp. 25–66, https://doi.org/10.1016/B978-0-12-818095-2.00002-3.

Dufresne, A., 2013. Nanocellulose: a new ageless bionanomaterial. Mater. Today 16 (6), 220–227. Elsevier B.V https://doi.org/10.1016/j.mattod.2013.06.004.

Franco, T., Viana, L., Potulski, D., et al., 2017. Nanocellulose obtained from residues of peach palm extraction (*Bactris gasipaes*). Carbohydr. Polym. 218, 8–19. https://doi.org/10.1016/j.carbpol.2019.04.035.

Garusinghe, U.M., Varanasi, S., Raghuwanshi, V.S., Garnier, G., Batchelor, W., 2018. Nanocellulose-montmorillonite composites of low water vapour permeability. Colloids Surf. A Physicochem. Eng. Asp. 540, 233–241. https://doi.org/10.1016/j.colsurfa.2018.01.010.

Gebald, C., Wurzbacher, J.A., 2013. Stability of amine-functionalized cellulose during temperature-vacuum-swing cycling for CO 2 capture from air. Environ. Sci. Technol. 47 (17), 10063–10070.

Gebald, C., Wurzbacher, J.A., Tingaut, P., Zimmermann, T., Steinfeld, A., 2011. Amine-based nanofibrillated cellulose as adsorbent for CO2 capture from air. Environ. Sci. Technol. 45 (20), 9101–9108.

Gopakumar, D.A., Manna, S., Pasquini, D., Thomas, S., Grohens, Y., 2018. Nanocellulose: extraction and application as a sustainable material for wastewater purification. In: New Polymer Nanocomposites for Environmental Remediation. Elsevier Inc, pp. 469–486, https://doi.org/10.1016/B978-0-12-811033-1.00019-6.

Guo, Y., Zhang, Y., Zheng, D., Li, M., Yue, J., 2020a. Isolation and characterization of nanocellulose crystals via acid hydrolysis from agricultural waste-tea stalk. Int. J. Biol. Macromol. 163, 927–933. https://doi.org/10.1016/j.ijbiomac.2020.07.009.

Guo, Y., Zhang, Y., Zheng, D., Li, M., Yue, J., 2020b. Isolation and characterization of nanocellulose crystals via acid hydrolysis from agricultural waste-tea stalk. Int. J. Biol. Macromol. 163, 927–933. https://doi.org/10.1016/j.ijbiomac.2020.07.009.

Ha, J.H., Shehzad, O., Khan, S., Lee, Y., Won Park, J., Khan, T., Park, J.K., 2008. Production of bacterial cellulose by a static cultivation using the waste from beer culture broth. Korean J. Chem. Eng. 25 (4), 812–815.

Habibi, Y., Lucia, L.A., Rojas, O.J., 2002. Cellulose Nanocrystals: Chemistry, Self-Assembly, and Applications., https://doi.org/10.1021/cr900339w.

Haimer, E., Wendland, M., Schlufter, K., Frankenfeld, K., Miethe, P., Potthast, A., Rosenau, T., Liebner, F., 2010. Loading of Bacterial Cellulose Aerogels with Bioactive Compounds by Antisolvent Precipitation with Supercritical Carbon Dioxide. pp. 64–74, https://doi.org/10.1002/masy.201000008.

Hokkanen, S., Bhatnagar, A., Repo, E., Lou, S., Sillanpää, M., 2016a. Calcium hydroxyapatite microfibrillated cellulose composite as a potential adsorbent for the removal of Cr(VI) from aqueous solution. Chem. Eng. J. 283, 445–452. https://doi.org/10.1016/j.cej.2015.07.035.

Hokkanen, S., Bhatnagar, A., Sillanpää, M., 2016b. A review on modification methods to cellulose-based adsorbents to improve adsorption capacity. Water Res. 91, 156–173. https://doi.org/10.1016/j.watres.2016.01.008.

Hong, F., Qiu, K., 2008. An alternative carbon source from konjac powder for enhancing production of bacterial cellulose in static cultures by a model strain *Acetobacter aceti* subsp. xylinus ATCC 23770. Carbohydr. Polym. 72 (3), 545–549. https://doi.org/10.1016/j.carbpol.2007.09.015.

Hossein, M., Zadeh, B., Shahdadi, H., 2015. Nanocellulose coated with various free fatty acids can adsorb fumonisin B1, and decrease its toxicity. Colloids Surf. B Biointerfaces 134, 26–30. https://doi.org/10.1016/j.colsurfb.2015.06.037.

Järup, L., 2003. Hazards of heavy metal contamination. Br. Med. Bull. 68, 167–182. https://doi.org/10.1093/bmb/ldg032.

Kahru, A., Maloverjan, A., Sillak, H., Pumaa, L., 2002. The toxicity and fate of phenolic pollutants in the contaminated soils associated with the OibShale industry. Environ. Sci. Pollut. Res. 1 (1), 27–33.

Kargarzadeh, H., Ioelovich, M., Ahmad, I., Thomas, S., Dufresne, A., 2017. Methods for extraction of nanocellulose from various sources. In: Handbook of Nanocellulose and Cellulose Nanocomposites., https://doi.org/10.1002/9783527689972.ch1.

Klamerus-iwan, A., Blonska, E., Lasota, J., Kalandyk, A., Waligórski, P., 2015. Influence of oil contamination on physical and biological properties of forest soil after chainsaw use. Water Air Soil Pollut. 226, 389. https://doi.org/10.1007/s11270-015-2649-2.

Köse, K., Mavlan, M., Youngblood, J.P., 2020. Applications and impact of nanocellulose based adsorbents. Cellulose 27, 2967–2990. https://doi.org/10.1007/s10570-020-03011-1.

Li, J., Zhang, X., Zhang, M., Xiu, H., He, H., 2015. Ultrasonic enhance acid hydrolysis selectivity of cellulose with HCl-FeCl3 as catalyst. Carbohydr. Polym. 117, 917–922. https://doi.org/10.1016/j.carbpol.2014.10.028.

Liao, W., Wang, Y., 2019. Cellulose-based absorbents for oil contaminant removal. In: Mondal, M. (Ed.), Cellulose-Based Superabsorbent Hydrogels. Polymers and Polymeric Composites: A Reference Series. Springer, Cham, pp. 1–27.

Lin, S.-P., Hsieh, S.-C., Chen, K.-I., Demirci, A., Cheng, K.-C., 2013. Semi-continuous bacterial cellulose production in a rotating disk bioreactor and its materials properties analysis. Cellul. https://doi.org/10.1007/s10570-013-0136-8.

Loganathan, B.G., Kannan, K., 1994. Global Organochiorine contamination trends: an overvievw. Ambio 23 (3), 187–191.

Lombardo, S., Thielemans, W., 2019. Thermodynamics of adsorption on nanocellulose surfaces. Cellul. 26 (1), 249–279. https://doi.org/10.1007/s10570-018-02239-2.

Lu, Q., Tang, L., Lin, F., Wang, S., Xuerong, C., Huang, B., 2014. Preparation and characterization of cellulose nanocrystals via ultrasonication-assisted FeCl 3-catalyzed hydrolysis. Cellul. https://doi.org/10.1007/s10570-014-0376-2.

Maciel, M.M.Á.D., de Carvalho Benini, K.C.C., Voorwald, H.J.C., Cioffi, M.O.H., 2019. Obtainment and characterization of nanocellulose from an unwoven industrial textile cotton waste: effect of acid hydrolysis conditions. Int. J. Biol. Macromol. 126, 496–506. https://doi.org/10.1016/j.ijbiomac.2018.12.202.

Mahfoudhi, N., Boufi, S., 2017a. Nanocellulose as a novel nanostructured adsorbent for environmental remediation: a review. Cellul. 24 (3), 1171–1197. https://doi.org/10.1007/s10570-017-1194-0.

Mahfoudhi, N., Boufi, S., 2017b. Nanocellulose as a novel nanostructured adsorbent for environmental remediation : a review. Cellul. 24 (3), 1171–1197. https://doi.org/10.1007/s10570-017-1194-0.

Mendoza, L., Hossain, L., Downey, E., Scales, C., Batchelor, W., Garnier, G., 2019. Carboxylated nanocellulose foams as superabsorbents. J. Colloid Interface Sci. 538, 433–439. https://doi.org/10.1016/j.jcis.2018.11.112.

Mi, X., Albukhari, S.M., Heldt, C.L., Heiden, P.A., 2020. Virus and chlorine adsorption onto guanidine modified cellulose nanofibers using covalent and hydrogen bonding. Carbohydr. Res. 498, 108153. https://doi.org/10.1016/j.carres.2020.108153.

Minko, S., 2008. Chapter 11—Grafting on solid surfaces: "grafting to" and "grafting from" methods. In: Stamm, M. (Ed.), Polymer Surfaces and Interfaces., https://doi.org/10.1007/978-3-540-73864-0.

Mo, L., Pang, H., Lu, Y., Li, Z., Kang, H., Wang, M., Zhang, S., Li, J., 2021. Wood-inspired nanocellulose aerogel adsorbents with excellent selective pollutants capture, superfast adsorption, and easy regeneration. J. Hazard. Mater. 415 (February), 125612. https://doi.org/10.1016/j.jhazmat.2021.125612.

Mussagy, C., Santos-Ebinuma, V.C., Kurnia, K.A., Dias, A.C.R.V., Carvalho, P., Coutinho, J.A.P., Pereira, J.F.B., 2020. Integrative platform for the selective recovery of intracellular carotenoids and lipids from *Rhodotorula glutinis* CCT-2186 yeast using mixtures of bio-based solvents. Green Chem. 22 (23), 8478–8494. https://doi.org/10.1039/D0GC02992K.

Mussagy, C., Khan, S., Kot, A., 2021a. Current developments on the application of microbial carotenoids as an alternative to synthetic pigments. Crit. Rev. Food Sci. Nutr. https://doi.org/10.1080/10408398.2021.1908222.

Mussagy, C.U., Remonatto, D., Paula, A.V., Herculano, R.D., Santos-Ebinuma, V.C., Coutinho, J.A.P., Pereira, J.F.B., 2021b. Selective recovery and purification of carotenoids and fatty acids from *Rhodotorula glutinis* using mixtures of biosolvents. Sep. Purif. Technol. 266. https://doi.org/10.1016/j.seppur.2021.118548.

Nasir, M., Hashim, R., Sulaiman, O., Asim, M., 2017. Nanocellulose: preparation methods and applications. Cellulose-Reinforced Nanofibre Composites: Production, Properties and Applications. Elsevier, pp. 261–276.

Ni, Y., Li, J., Fan, L., 2020. Production of nanocellulose with different length from ginkgo seed shells and applications for oil in water Pickering emulsions. Int. J. Biol. Macromol. 149, 617–626. https://doi.org/10.1016/j.ijbiomac.2020.01.263.

Niu, F., Li, M., Huang, Q., Zhang, X., Pan, W., Yang, J., Li, J., 2017. The characteristic and dispersion stability of nanocellulose produced by mixed acid hydrolysis and ultrasonic assistance. Carbohydr. Polym. 165, 197–204. https://doi.org/10.1016/j.carbpol.2017.02.048.

Nor, M., Norrrahim, F., Mohd, A., Knight, F., 2021. Nanocellulose : a bioadsorbent for chemical contaminant remediation. RSC Adv. 11, 7347–7368. https://doi.org/10.1039/d0ra08005e.

Pardesi, K.R., Haldar, D., Jozala, A.F., Shukla, P., Gupta, G.K., 2020. Lignocellulosic biomass for the synthesis of nanocellulose and its eco-friendly advanced applications. Front. Chem. 8, 601256. https://doi.org/10.3389/fchem.2020.601256. Www.Frontiersin.Org.

Pichtel, J., 2016. Oil and gas production wastewater : soil contamination and. Appl. Environ. Soil Sci. 2016, 24.

Pinkert, A., Marsh, K.N., Pang, S., Staiger, M.P., 2009. Ionic liquids and their interaction with cellulose. Chem. Rev. https://doi.org/10.1021/cr9001947.

Pisharody, L., Suresh, S., Mukherji, S., 2021. Evaluation of adsorbents and eluents for application in virus concentration and adsorption-desorption isotherms for coliphages. Chem. Eng. J. 403 (July 2020), 126267. https://doi.org/10.1016/j.cej.2020.126267.

Popescu, C., Jones, D., Schalnat, J., Segerholm, K., Henriksson, M., Westin, M., 2020. Structural characterization and mechanical properties of wet-processed fibreboard based on chemo-thermomechanical pulp, furanic resin and cellulose nanocrystals. Int. J. Biol. Macromol. 145, 586–593. https://doi.org/10.1016/j.ijbiomac.2019.12.199.

Putri, K.N.A., Keereerak, A., Chinpa, W., 2020. Novel cellulose-based biosorbent from lemongrass leaf combined with cellulose acetate for adsorption of crystal violet. Int. J. Biol. Macromol. 156, 762–772. https://doi.org/10.1016/j.ijbiomac.2020.04.100.

Putro, J.N., Kurniawan, A., Ismadji, S., Ju, Y.-H., 2017. Nanocellulose based biosorbents for wastewater treatment: study of isotherm, kinetic, thermodynamic and reusability. Environ. Nanotechnol. Monit. Manag. 8, 134–149. https://doi.org/10.1016/j.enmm.2017.07.002.

Pyrgiotakis, G., Luu, W., Zhang, Z., et al., 2018. Development of high throughput, high precision synthesis platforms and characterization methodologies for toxicological studies of nanocellulose. Cellulose 25, 2303–2319. https://doi.org/10.1007/s10924-019-01438-7.

Ruthven, D.M., 1984. Principles of Adsorption and Adsorption Process. John Wiley & Sons, New York, p. 420.

Savage, N., Diallo, M.S., 2005. Nanomaterials and water purification: opportunities and challenges. J. Nanopart. Res. https://doi.org/10.1007/s11051-005-7523-5.

Siqueira, G., Bras, J., Dufresne, A., Papeterie, D., Martin, F.-S., 2010. New process of chemical grafting of cellulose nanoparticles with a long chain isocyanate. Langmuir 26 (15), 402–411. https://doi.org/10.1021/la9028595.

Song, H.-J., Li, H., Seo, J.-H., Kim, M.-J., Kim, S.-J., 2009. Pilot-scale production of bacterial cellulose by a spherical type bubble column bioreactor using saccharified food wastes. Korean J. Chem. Eng. 26 (1), 141–146.

Spinella, S., Maiorana, A., Qian, Q., Dawson, N.J., Hepworth, V., McCallum, S.A., Ganesh, M., Singer, K.D., Gross, R.-A., 2016. Concurrent cellulose hydrolysis and esterification to prepare a surface-modified cellulose nanocrystal decorated with carboxylic acid moieties. ACS Sustain. Chem. Eng. 4 (3), 1538–1550. https://doi.org/10.1021/acssuschemeng.5b01489.

Šturcová, A., Davies, G.R., Eichhorn, S.J., 2005. Elastic modulus and stress-transfer properties of tunicate cellulose whiskers. Biomacromolecules 6 (2), 1055–1061. https://doi.org/10.1021/bm049291k.

Syafri, E., Sudirman, Mashadi, Yulianti, E., et al., 2019. Effect of sonication time on the thermal stability, moisture absorption, and biodegradation of water hyacinth (*Eichhornia crassipes*) nanocellulose-filled bengkuang (*Pachyrhizus erosus*) starch biocomposites. J. Mater. Res. Technol. 8, 6223–6231. https://doi.org/10.1016/j.jmrt.2019.10.016.

Thakur, V., Guleria, A., Kumar, S., Sharma, S., Singh, K., 2017. Recent Advances in Nanocellulose Processing, Functionalization and Applications: A Review., https://doi.org/10.1039/d1ma00049g.

Theivasanthi, T., Anne Christma, F.L., Toyin, A.J., Gopinath, S.C.B., Ravichandran, R., 2018. Synthesis and characterization of cotton fiber-based nanocellulose. Int. J. Biol. Macromol. 109, 832–836. https://doi.org/10.1016/j.ijbiomac.2017.11.054.

Thomas, B., Raj, M.C., Athira, K.B., Rubiyah, M.H., Joy, J., Moores, A., Drisko, G.L., 2018. Nanocellulose, a versatile green platform : from biosources to materials and their applications. Chem. Rev. 118, 11575–11625. https://doi.org/10.1021/acs.chemrev.7b00627.

Tkaczyk, A., Mitrowska, K., Posyniak, A., 2020. Synthetic organic dyes as contaminants of the aquatic environment and their implications for ecosystems : a review. Sci. Total Environ. 717, 137222. https://doi.org/10.1016/j.scitotenv.2020.137222.

Valdebenito, F., Alfredo, R., Lovera, G., Cruces, K., Ciudad, G., Chinga-carrasco, G., Habibi, Y., 2018. CO2 adsorption of surface-modified cellulose nanofibril films derived from agricultural wastes CO2 adsorption of surface-modified cellulose nanofibril films derived from agricultural wastes. ACS Sustain. Chem. Eng. 6 (10), 12603–12612. https://doi.org/10.1021/acssuschemeng.8b00771.

Valentini, F., Dorigato, A., Rigotti, D., Pegoretti, A., 2019a. Polyhydroxyalkanoates/fibrillated nanocellulose composites for additive manufacturing. J. Polym. Environ. 27 (6), 1333–1341. https://doi.org/10.1007/s10924-019-01429-8.

Valentini, F., Dorigato, A., Rigotti, D., Pegoretti, A., 2019b. Polyhydroxyalkanoates/fibrillated nanocellulose composites for additive manufacturing. J. Polym. Environ. 27 (6), 1333–1341. https://doi.org/10.1007/s10924-019-01429-8.

Vijayalakshmi, K., Devi, B.M., Latha, S., Gomathi, T., Sudha, P.N., Venkatesan, J., Anil, S., 2017. Batch adsorption and desorption studies on the removal of lead (II) from aqueous solution using nanochitosan/sodium alginate/microcrystalline cellulose beads. Int. J. Biol. Macromol. 104, 1483–1494. https://doi.org/10.1016/j.ijbiomac.2017.04.120.

Wang, Y., Wei, X., Li, J., Wang, F., Wang, Q., Zhang, Y., Kong, L., 2017. Homogeneous isolation of nanocellulose from eucalyptus pulp by high pressure homogenization. Ind. Crop Prod. 104, 237–241. https://doi.org/10.1016/j.indcrop.2017.04.032.

Wu, C., McClements, D.J., He, M., Zheng, L., Tian, T., Teng, F., Li, Y., 2021. Preparation and characterization of okara nanocellulose fabricated using sonication or high-pressure homogenization treatments. Carbohydr. Polym. 255, 117364. https://doi.org/10.1016/j.carbpol.2020.117364.

Yang, X., Han, F., Xu, C., Jiang, S., Huang, L., Liu, L., Xia, Z., 2017. Effects of preparation methods on the morphology and properties of nanocellulose (NC) extracted from corn husk. Ind. Crop Prod. 109, 241–247. https://doi.org/10.1016/j.indcrop.2017.08.032.

Yang, Y., Liu, H., Wu, M., Ma, J., Lu, P., 2020. Bio-based antimicrobial packaging from sugarcane bagasse nanocellulose/nisin hybrid films. Int. J. Biol. Macromol. 161, 627–635. https://doi.org/10.1016/j.ijbiomac.2020.06.081.

Yue, Y., Wang, X., Han, J., Yu, L., Chen, J., Wu, Q., 2019. Effects of nanocellulose on sodium alginate/polyacrylamide hydrogel: mechanical properties and adsorption-desorption capacities. Carbohydr. Polym. 206 (August 2018), 289–301. https://doi.org/10.1016/j.carbpol.2018.10.105.

Zhao, Y., Lei, H., Liu, Y., Ruan, R., Qian, M., Huo, E., Zhang, Q., Huang, Z., Lin, X., Wang, C., Mateo, W., Villota, E.M., 2020. Microwave-assisted synthesis of bifunctional magnetic solid acid for hydrolyzing cellulose to prepare nanocellulose. Sci. Total Environ. 731, 138751. https://doi.org/10.1016/j.scitotenv.2020.138751.

Zhou, Z.-Y., Tian, N., Li, J.-T., Broadwell, I., Sun, S.-G., 2011. Nanomaterials of high surface energy with exceptional properties in catalysis and energy storage. Chem. Soc. Rev. 40, 4167–4185. https://doi.org/10.1039/c0cs00176g.

Zhu, S., Wu, Y., Chen, Q., Yu, Z., Wang, C., Jin, S., Ding, Y., Wu, G., 2006. Dissolution of cellulose with ionic liquids and its application: a mini-review. Green Chem. https://doi.org/10.1039/b601395c.

Ziaul, M., Zaman, Z., Bee, H, et al., 2014. Statistical optimization for acid hydrolysis of microcrystalline cellulose and its physiochemical characterization by using metal ion catalyst. Materials 7, 6982–6999. https://doi.org/10.3390/ma7106982.

CHAPTER

15

Cellulose composites as nanobiosorbents for ecological remediation

Zari Fallah[a], *Ehsan Nazarzadeh Zare*[b], *Mahmood Tajbakhsh*[a], *and Vinod V.T. Padil*[c]

[a]Faculty of Chemistry, University of Mazandaran, Babolsar, Iran [b]School of Chemistry, Damghan University, Damghan, Iran [c]Institute for Nanomaterials, Advanced Technologies and Innovation (CXI), Technical University of Liberec (TUL), Liberec, Czech Republic

15.1 Introduction

The increasing human population and fast growth of industrialization have resulted in significant destabilization of the ecosystem. The industrialization has resulted in the generation of a number of pollutants which are found mixed in the air, water, and soil (Meteku et al., 2020). Dyes, drugs, heavy metal ions, etc., are responsible for environmental contamination and attracted considerable attention because of their potential dangers to human safety and environmental stability (Zou et al., 2016). Consequently, with the aim of preserve ecological stability, successfully separate of pollutants from the environment is still very important. Of all the famous approaches in remediation, the adsorption method has been considered as a simple and operative tool for remediation of pollutants (Hosseini et al., 2019). Particularly in environmental remediation, the adsorption technique has been widely accepted to eliminate contaminants.

The use of renewable materials from agriculture in environmental remediation not only diminutions the carbon productions, but may also decrease the cost of remediation (Zare et al., 2018a, b). Cellulose is a most abundant organic polymer with the formula $(C_6H_{10}O_5)_n$, a polysaccharide involving a linear chain of some hundred to many thousands of β(1→4) linked D-glucose units (Peng et al., 2020). Natural and modified types of cellulosic materials are used to remove organic/inorganic pollutants from the environment (Ul-Islam

https://doi.org/10.1016/B978-0-323-90912-9.00015-0

et al., 2016). Cellulose-based nanocomposites showed well chemical, and physical properties than cellulose; for example, they display improved mechanical, thermal, electrical, optical, and magnetic properties, as well as have a broader range of selectivity for the remediation of pollutions from the environment (Ul-Islam et al., 2016).

This book chapter aims at looking at different cellulose-based composites used for the remediation of various pollutants found in the environment. The current challenges and possible resolutions are discussed.

15.2 Ecological remediation by cellulose nanocomposites

In modern society, the development of industrialization and civilization has resulted in a tremendous rise in organic and inorganic chemical wastes that are potentially dangerous in numerous environmental matrices such as air, water, soil, and ecosystem. The increased knowledge for using sustainable green resources for diminishing the global environmental issues led to the focus of the scientist efforts on applying eco-friendly and biodegradable adsorbents as a suitable alternative for petroleum-based compounds. Cellulose composites with renewable resources, biocompatibility, high surface area, abundance functional groups, and stability have prone to physical/chemical adsorption of contaminants from the environment (Tshikovhi et al., 2020). Thus, the development of cellulose-based composites with innovative design has emerged as a potential strategy to purify the ecosystem pollution caused by hazardous pollutants.

15.2.1 Air filtration

Air pollution poses a drastic danger to climate, ecosystems, and human health. The air pollution from atmospheric aerosols, volatile organic compounds, and greenhouse gases are the major driving force of environmental effects, acid rains, ozone depletion, and global climate changes. In addition, air pollution can aggravate climate change impacts on water shortage and global warming (D'Amato and Akdis, 2020). Apart from the environmental consequences, air pollution causes a wide range of health problems such as respiratory, cardiovascular, mental diseases, and pregnancy outcomes at short-time exposure and even death at long term exposure. Air pollution has the power to stymie human resource accumulation by reducing children's longevity, undermining their wellbeing, and limiting their opportunity to benefit from education (Pandey et al., 2021). On the other hand, tiny particulate materials in polluted air may carry various viruses, bacteria, and fungi which can cause drastic allergic, respiratory, and infectious diseases through airborne transmission (Kim et al., 2018).

To achieve clean air and mitigate pollution effects, the researchers urgently needed to focus on designing and producing smart green filters capable of separation, adsorption, and decontamination of air pollutants. In the following sections, the application of cellulose composites is summarized for air filtration through the separation and adsorption of particulate matters, volatile organic compounds, and hazardous gases.

The cellulose acetate/poly(ionic liquid) composite was prepared via macromolecular design and electrostatic spinning technique as an antimicrobial air filter with a removal rate of

99.65% for inhalable particulate materials of 10 nm (Zhu et al., 2020). These nano-filters preserved the outstanding antimicrobial effects against *Escherichia coli* and *Staphylococcus aureus* bacteria. In another study, poly(vinyl alcohol)/cellulose nanocrystals (PVA/CNCs) composite was prepared using electrospinning technique (Zhang et al., 2019a). The PVA/CNCs nanofibrous filter was applied as an air filter with low air resistance for particulate matter (PM2.5) removal. The thinner electrospun fibers reduced significantly pressure drop and increased the removal efficiency of PM2.5 (99.1%).

Thus, using environmentally friendly cellulosic fiber-based filters especially with antimicrobial effects for indoor air purification is a major issue to protect people from particular pollutants.

In recent studies, cellulose-based nanocomposites were also applied for gas adsorption that are reviewed in this section. The functional porous carboxymethyl cellulose/cellulose acetate (CMC/CA) composite was prepared via the double emulsion solvent evaporation technique (Sun et al., 2019). In the fabrication process of CMC/CA composite, cupric ions were introduced in situ ion cross-link method. The macroporous CMC/CA with functional cupric ions with high complexing ability toward hydrogen cyanide exhibited great potential for selective removal of hydrogen cyanide (50% reduction) in the cigarette smoke.

In addition, the α-alumina ceramic tube supported cellulose triacetate-tributyl phosphate (Shankar and Kandasamy, 2019) and ZIF-8@cellulose nanofibers (Jia et al., 2020) composites were recently synthesized as separation membranes for CO_2 capturing from polluted air to mitigate the greenhouse effect. The ZIF-8@cellulose nanofibers composite demonstrated the CO_2 permeability of 550 Barrer and CO_2/CH_4 and CO_2/N_2 ideal selectivity of 36.2 and 45.5, respectively. This study revealed that the gas separation behavior was related to the intrinsic selectivity of ZIF-8. In another investigation, lightweight and porous zeolitic imidazolate frameworks-8@cellulose nanofber@cellulose foam (ZIF-8@CNF@cellulose foam; $S_{BET} = 475.5\ m^2\ g^{-1}$) was synthesized and applied for nitrogen gas adsorption (Ma et al., 2019a). The nitrogen adsorption capacity of ZIF-8@CNF@cellulose foam was 30 times higher than pure cellulose foam. Further, copper (II)/cellulose nanofibers/carbon nanotubes (CNT/CNF-Cu^{2+}, $S_{BET} = 60\ m^2\ g^{-1}$) aerogel was prepared from cellulose nanofiber and carbon nanotube backbones and Cu^{2+} linker and utilized as a porous absorbent for effective and selective removal of odorous toxic gases such as ammonia, hydrogen sulfide, methyl mercaptan, and trimethylamine from the air (Adavan Kiliyankil et al., 2021). The complete adsorption of ammonia (200 ppm), hydrogen sulfide (100 ppm), methyl mercaptan (100 ppm), and trimethylamine (70 ppm) was achieved onto 2 g of CNT/CNF-Cu^{2+} from 9 L of air.

For air purification through the removal of volatile organic compounds, cellulose acetate/ultrahigh silica zeolites (CA/UHSZs) composites were synthesized from two types of UHSZs, USY (modified Y zeolite) and silicalite prepared by hydrothermal crystallization, via single needle and needle-less electrospinning systems (Ojstršek et al., 2020). The electrospun nanofibrous CA/UHSZs were applied to adsorb ammonia from polluted air. The obtained results indicated that the presence of porous UHSZs in the electrospun CA nanofibers increased the ammonia removal efficiency, and the CA/silicalite exhibited higher adsorption capacity than CA/USY composite.

For geminate adsorption of toxic gases, volatile organic compounds, and particulate matters from polluted air, few composite examples are introduced in the following section.

The cellulose fiber functionalized with zeolitic imidazolate framework-8 (CFs@ZIF-8; $S_{BET} = 620.80\ m^2\ g^{-1}$ and pore volume $= 0.23\ cm^3\ g^{-1}$) composite was fabricated as an air filter for nitrogen gas and PM0.3 adsorption (Su et al., 2018). The good adsorption capability of CFs@ZIF-8 was correlated to ZIF-8 incorporation that improved the surface area, created abundant cavities and gas adsorption sites, thus, enhancing the stronger interactions with PMs. In addition, cellulose nanofiber stringed HKUST-1 polyhedron membrane was fabricated on stainless steel screen (CNFs/HKUST-1/SSS) and applied as a window screen for formaldehyde and PM2.5 removal from the air (Zhao et al., 2019a). The CNFs/HKUST-1 with hierarchical porous structure generates extremely micrometer to nanometer pathways for fast air transportation while blocking PM2.5 with a blocking efficiency of above 95%. Also, the CNFs/HKUST-1 exhibited effective adsorption of formaldehyde ($q_{max} = 47.71\ mg\ g^{-1}$) due to the highly microporous cavities with open copper sites of HKUST-1 in membrane structure. The results of air purification demonstrated that the CNFs/HKUST-1/SSS has great potential for indoor air purification because it is highly porous, hierarchical, and thin thickness ($\sim$5 μm) with an air flow rate of $4.6\ cm\ s^{-1}$ under 200 Pa. In another study, multi-functional metal-organic frameworks@cellulose fibers (MOFs@CF: ZIF-8@CF, MOF-199@CF, and Ag-MOFs@CF) composites were prepared by an in situ deposition of ZIF-8, MOF-199, and Ag-MOFs crystals on cellulose matrix (Ma et al., 2018). The removal efficiency of PM0.3 using Ag-MOFs@CF ($S_{BET} = 12.2\ m^2\ g^{-1}$), MOF-199@CF ($S_{BET} = 164.9\ m^2\ g^{-1}$), and ZIF-8@CF ($S_{BET} = 308.0\ m^2\ g^{-1}$) composites was reported to be 97.34, 98.28, and 98.36% under 126, 131, and 134 Pa pressure drop, respectively. The MOFs@CF efficacy, especially ZIF-8@CF, for nitrogen gas adsorption was higher than pure cellulose which attributed to the porous MOFs crystals with many metals and organic sites for gas adsorption. Also, the MOFs@CF revealed antimicrobial effects against *E. coli* with the highest inhibition zone diameter of 20.8 mm for Ag-MOFs@CF. Further, a double-component metal-organic framework (Ag-MOFs@CNF@ZIF-8, $S_{BET} = 344.9\ m^2\ g^{-1}$) nanocomposite with multi-layer structure was fabricated through in situ generation process (Fig. 15.1A) (Ma et al., 2019b). The Ag-MOFs@CNF@ZIF-8 air filter displayed good filtration performance for PM2.5 (94.3%) (Fig. 15.1B), the high ability for nitrogen gas adsorption ($109\ cm^3\ g^{-1}$) (Fig. 15.1C), and excellent antibacterial activity against *E. coli* (inhibition zone diameter = 18.1 mm) (Fig. 15.1D). The antibacterial activity was related to the presence of Ag-MOFs, whereas filtration performance and gas adsorption were mainly attributed to the ZIF-8, and further, the mechanical strength was associated with CNF.

15.2.2 Water treatment

The most important resource for a healthier life is water, and water contamination is a significant environmental problem. The discharge of industrial effluents into waterways is the primary source of water pollution (Oyewo et al., 2020b). Effluents containing pollutants such as ions, dyes, drugs, pesticides, etc. are very disastrous on plants, animals and human health, and the entire ecosystem. As a result, the removal of hazardous pollutants from aqueous media has become an urgent need, especially through adsorption techniques by efficient cellulose-based adsorbent because of their advantages.

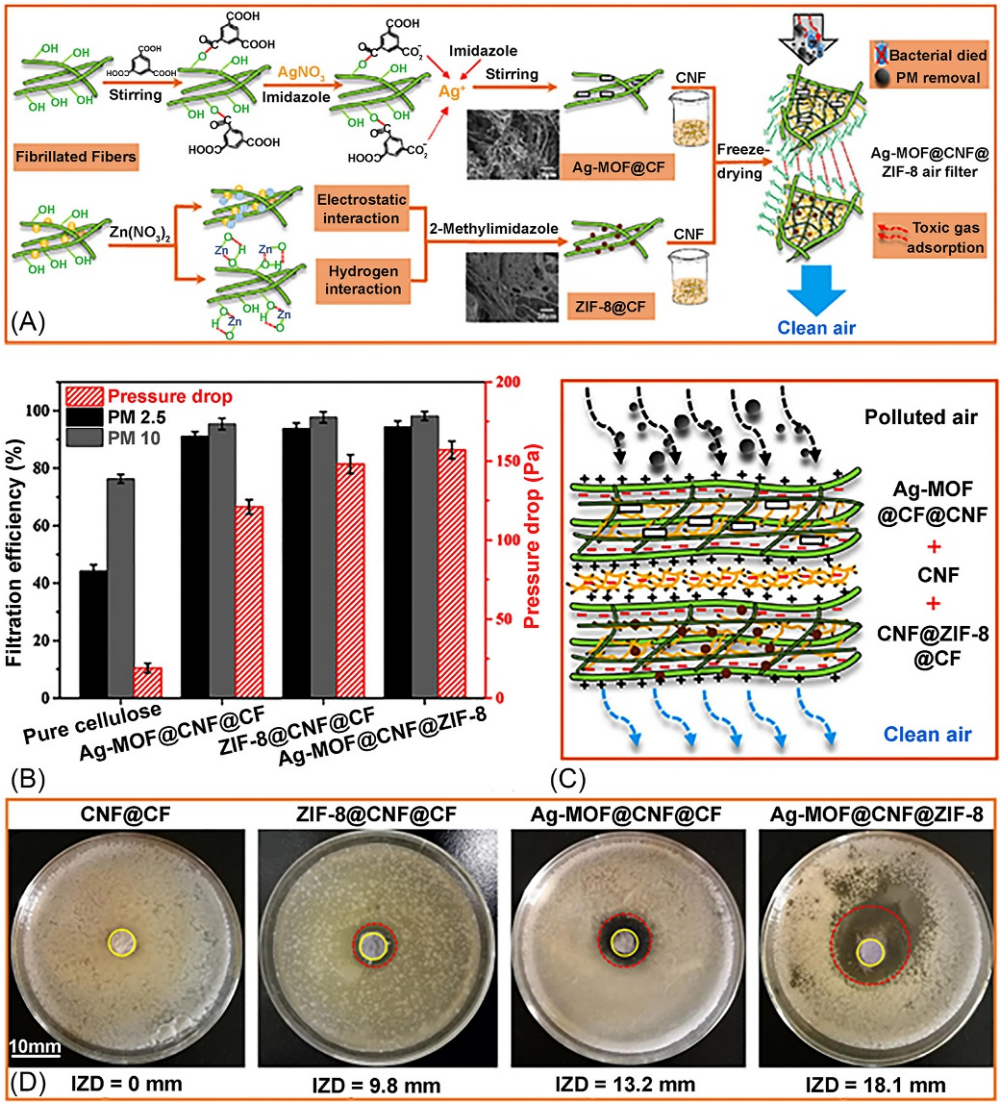

FIG. 15.1 (A) The preparation of Ag-MOFs@CNF@ZIF-8 nanocomposite filter. (B) The filtration performance of Ag-MOFs@CNF@ZIF-8 filter, and the comparison of Ag-MOFs@CNF@ZIF-8 efficacy with pure cellulose, ZIF-8@CNF@CF, and Ag-MOFs@CNF@CF filter. (C) the filtration mechanism diagram of AgMOFs@CNF@ZIF-8 filter. (D) The antibacterial activity of Ag-MOFs@CNF@ZIF-8 in comparison to CNF@CF, ZIF-8@CNF@CF, and AgMOFs@CNF@CF filters against *E. coli*. *Reproduced with permission from Ma, S., Zhang, M., Nie, J., Tan, J., Yang, B., Song, S., 2019b. Design of double-component metal–organic framework air filters with PM2.5 capture, gas adsorption and antibacterial capacities. Carbohydr. Polym. 203, 415–422. https://doi.org/10.1016/j.carbpol.2018.09.039.*

Ions removal

Large amounts of toxic heavy metal ions are generated by industrial mining, agricultural production, and human activities, that the majority of them ultimately harm the plant, animal, and human health. In plants, the stress of metal ions at high concentrations causes the degradation of leaf chlorophylls which then reduces the plant photosynthetic capacity, thus, resulting in the photoinhibition and photo-oxidative damage of plant leaves (Huihui et al., 2020). In animals, the non-biodegradability and accumulation of metal ions in organs can create functional disturbances and structural lesions. Heavy metal ions considerably increase the level of oxidants and decrease the antioxidants levels (Fan et al., 2020). Also, the heavy metals ions toxicity induces changes in condition indices, biochemical disorders, and histopathology of organisms. In humans, metal ions may generate reactive radicals, create oxidative stress, produce reactive oxygen species, thus cause numerous human diseases including cancer risk (Jomova and Valko, 2011).

In addition, anions can be toxic and hazardous for the natural environment and people at concentrations higher than their safe limit. For example, the safe limit for fluoride ions is 1.5 ppm in drinking water, thus, above this limit, it can cause dental and skeletal fluorosis problems (Fallah et al., 2020). Arsenate, selenate, selenite, etc. are toxic and carcinogenic at definite concentrations (Abukhadra et al., 2021). As it is clear from the above discussion, cellulose-based composites are extensively used as efficient bio-sorbents of toxic ions in ecological remediation.

Cations

A microfibrous nanocomposite was prepared through the binding of ZnO nanocrystals with regenerated microfibrillated cellulose (R-MFC, $S_{BET} = 10.74\ m^2\ g^{-1}$) fabricated from jute cellulose. The ZnO/R-MFC composite was applied as an effective adsorbent for As(V) ions removal from water with a maximum adsorption capacity of 4421 mg g^{-1} at neutral pH (7) (Sharma et al., 2019). The ZnO crystallites were efficient adsorption sites in composite structure for As(V) ions removal. The ZnO nanocrystals were effectively anchored to the R-MFC due to strong electrostatic interactions with cellulose II structure. The good binding stability between the R-MFC and ZnO nanocrystals led to very low ZnO release during the As(V) removal, demonstrating the viability of ZnO/R-MFC composite for water treatment.

Influencing factors on the adsorption capability of hydrothermal synthesized cellulose nanocrystal/iron oxide nanorod (CNs/Fe_2O_3, $pH_{PZC} = 6.8$) composite were investigated for arsenic adsorption from aqueous solution (Dong et al., 2020). The iron oxide nanorods, prepared using cellulose nanocrystals as a template, were the effective adsorption sites for arsenic removal. The CNs/Fe_2O_3 composite exhibited the maximum adsorption capacities of 15.71 and 13.87 mg g^{-1} for As(V) and As(III) removal at pH of 3 and 7, respectively. The adsorption mechanism is consisting of electrostatic attraction between positively charged composite surface and negative ionic form of As(V) (H_2AsO_4) at pH 3 ($pH < pH_{PZC}$), and interactions between the nonionic form of As(III) (H_3AsO_3) and active adsorption sites of composite with zero charge at pH 7 ($pH = pH_{PZC}$).

The FeOOH/CuO@WBC composite was prepared from water bamboo shells waste-derived cellulose and applied for arsenic adsorption (Liu et al., 2020). The adsorption studies showed that the maximum adsorption capacity of FeOOH/CuO@WBC was 76.1 mg g^{-1} at

optimal conditions (pH 3.5 and arsenic initial concentration = 150 mg L^{-1} at room temperature). The good adsorption capacity of FeOOH/CuO@WBC for arsenic removal was related to the synergistic influences of physical and chemical interactions, and also to the synergistic effects of WBC, CuO, and FeOOH. The WBC with many hydroxyl groups is an essential substrate for FeOOH and CuO to attain maximum efficacy. The trivalent arsenic could bind directly to the hydroxyl group of CuO and FeOOH, or it could oxidize to arsenic pentavalent by copper oxide, and subsequently interact with hydroxyl groups of iron. The obtained results of adsorption and recycling experiments expressed that the efficient removal of arsenic was occurred onto FeOOH/CuO@WBC from aqueous media according to the idea of "treating waste with waste."

In hybrids structure, the formation of a chemical bond between the filler and substrate usually leads to a more stable composite, thus resulting to enhance the adsorption capability and recyclability of composite, and decrease the leaching of metal oxide nanoparticles.

For example, cellulose-titania-based nanocomposite (Cell-Com, $S_{BET} = 34.73\ m^2\ g^{-1}$) was synthesized via the click reaction between alkyne functionalized TiO_2 NPs with azide microcrystalline cellulose (Fallah et al., 2018). The Cell-Com was investigated as a nano-biosorbent for the removal of Zn^{2+}, Cd^{2+}, and Pb^{2+} ions from aqueous solutions. The maximum adsorption capacity of nanocomposite for Pb^{2+}, Cd^{2+} and Zn^{2+} ions was found to be 120.48, 102.05 and 102.04 mg g^{-1}, respectively. Isotherm, kinetic, and a thermodynamic assay of adsorption process confirmed that the chemical adsorption of heavy metal ions has spontaneously occurred onto Cell-Com with endothermic nature. The presence of triazole rings along with many functional groups in TiO_2, linkers, and microcrystalline cellulose moieties led to the generation of high thermal resistance composite with selective adsorption ability to Pb^{2+} ions and excellent recyclability.

In the construction of cellulose composites, carbon oxides such as graphene oxide can be used instead of metal oxides. The GO-TETA-DAC composite was constructed from dialdehyde cellulose (DAC) grafted graphene oxide (GO) using a triethylenetetramine (TETA) cross-linker (Yao et al., 2019). The GO-TETA-DAC ($S_{BET} = 762\ m^2\ g^{-1}$) displayed good performance for Pb(II) and Cu(II) removal through ion-exchange mechanism with maximum adsorption capacity of 80.9 and 65.0 mg g^{-1}, respectively.

The carboxymethyl cellulose supported magnetic graphene oxide composite (CMC/MGOs) was fabricated using low-temperature plasma technique and applied for uranium ions removal from aqueous solutions (Zong et al., 2019). The adsorption mechanism illustrated that the U(VI) was attracted onto CMC/MGOs composite with $q_{max} = 7.94 \times 10^{-4}$ mol g^{-1} via the inner-sphere surface complexation. The easy and economical recycling of magnetic cellulose composites is considered an important advantage in the water treatment process.

The graphene oxide-terminated hyperbranched amino polymer-carboxymethyl cellulose ternary nanocomposite (GO-HBP-NH_2-CMC) was prepared for removing the Cu^{2+} and Pb^{2+} ions with $q_{max} = 137.48$ and 152.86 mg g^{-1}, respectively (Kong et al., 2020). Complexation of metallic ions with N-containing functional groups, as well as, ion exchange with O-containing functional groups determine the GO-HBP-NH-CMC adsorption performance toward heavy metal ions.

Recently, metal-organic framework materials (MOFs) with porous structures and large specific surface areas were combined with cellulose to form composite adsorbents. The

metal-organic frameworks@cellulose aerogels composites were synthesized by loading UiO-66 and UiO-66-NH_2 MOFs onto the cellulose aerogels via in situ growth procedure and were utilized for decontamination of Pb^{2+} and Cu^{2+} ions (Lei et al., 2019). Also, in situ synthesis and lyophilization were used for constructing of zeolitic imidazolate framework-67 modified bacterial cellulose/chitosan composite (ZIF-67/BC/CH, $S_{BET} = 268.7\ m^2\ g^{-1}$) with q_{max} of 152.1 and 200.6 mg g^{-1} for Cr^{6+} and Cu^{2+} ions adsorption (Li et al., 2020). Despite the good adsorption performance, the application of MOFs-based composite adsorbents was limited in wastewater treatment due to the high cost and intricated synthesis, and their ecotoxicity potential.

The combination of carbohydrate polymers in composite construction is a suitable synthetic method in accordance with the goals of green chemistry. The water-stable CSP-CMCP composite was manufactured from cross-linking of phosphorylated chitosan (CSP) and phosphate-decorated carboxymethyl cellulose (CMCP) and used as an efficient adsorbent for U(VI) removal ($q_{max} = 977.54\ mg\ g^{-1}$) (Cai et al., 2019). The predominant adsorption mechanism was found to be related to the inner-sphere surface complexation.

Anions

Nanocellulose coated flexible titanate-bismuth oxide (CH-TBM) composite was prepared and applied for iodide removal from super-intricate anion/cation/oily-water (Xiong et al., 2018). The CH-TBM revealed high adsorption capacity ($q_{max} = 225.9\ mg\ g^{-1}$) for I^- ions because of synergistic effects of cellulose hydroxyl/carboxyl groups, layered titanate nanofibers and oxygen vacancy occupied δ-Bi_2O_3.

Bamboo cellulose fibers constructed 3D graphene-formicary-like δ-Bi_2O_3 (FL-δ-Bi_2O_3, $S_{BET} = 206.2\ m^2\ g^{-1}$) aerogels were synthesized through a one-pot hydrothermal method and utilized for radioiodine removal with uptake capacity of 2.04 mmol g^{-1} via insoluble $Bi_4I_2O_5$ phase formation (Xiong et al., 2017).

In recent years, research has been done to make innovative cellulose-based composites as an effective adsorbent for the removal of fluoride anion from aqueous solutions. For example, aluminum and lanthanum impregnated cellulose composite (ALIC), constructed by co-precipitation (ALIC(P); $S_{BET} = 130.93\ m^2\ g^{-1}$, $q_{max} = 33.33\ mg\ g^{-1}$) and ultrasound-assisted (ALIC(U); $S_{BET} = 196.91\ m^2\ g^{-1}$, $q_{max} = 88.67\ mg\ g^{-1}$) methods (Raghav et al., 2019), zerovalent iron/zirconium(IV)-doped cellulose nanofibers ($q_{max} = 35.70\ mg\ g^{-1}$) (Sankararamakrishnan et al., 2019), multiple bimetallic (Al-La or Fe-La) hydroxides embedded in cellulose/graphene composites (Al-La@CG: $S_{BET} = 45.38\ m^2\ g^{-1}$, $q_{max} = 51.54\ mg\ g^{-1}$; and Fe-La@CG: $S_{BET} = 44.98\ m^2\ g^{-1}$, $q_{max} < 51\ mg\ g^{-1}$) (Guo et al., 2019), cellulose nanofiber-polyaniline-templated ferrihydrite nanocomposite ($S_{BET} = 111.1\ m^2\ g^{-1}$, $q_{max} = 50.8\ mg\ g^{-1}$) (Mukherjee et al., 2020), and Fe-Al-Mn@chitosan based metal oxides blended cellulose acetate mixed matrix membrane (Chaudhary and Maiti, 2020).

The Zr-La-CC/GO nanocomposites were fabricated by embedding the bimetallic La and Zr hydroxides onto the cotton cellulose/graphene oxide (CC/GO) hybrid (Fig. 15.2) (Shang et al., 2019). This composite with $S_{BET} = 49.486\ m^2\ g^{-1}$ was applied as a sorbent for selective removal of fluoride through metal-ligand interaction.

The CMC-g-AMPS/Fe/Al/AC composite was synthesized from the impregnation of CMC-g-AMPS/Fe/Al hydrogel with activated charcoal (Sinha and Chakma, 2020). The CMC-g-AMPS/Fe/Al was fabricated from the creation of a three-dimensional cross-linked network using CMC-g-AMPS hydrogel, prepared from free radical graft polymerization of

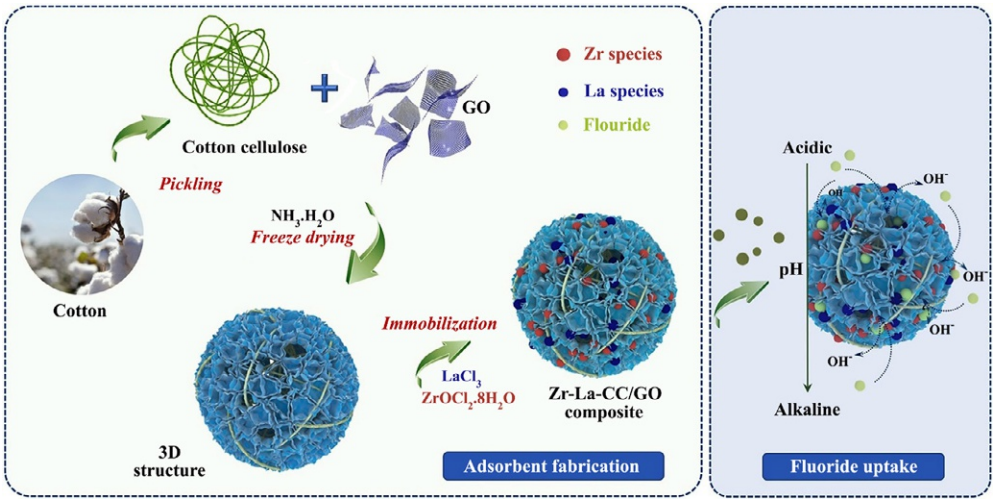

FIG. 15.2 The preparation of Zr-La-CC/GO nanocomposites, and the presentation of fluoride uptake by Zr-La-CC/GO nanosorbent at various pH conditions. *Reproduced with permission from Shang, Y., Wang, Z., Xu, X., Cheng, C., Gao, B., Yue, Q., Liu, S., Han, C., 2019. Enhanced fluoride uptake by bimetallic hydroxides anchored in cotton cellulose/graphene oxide composites. J. Hazard. Mater. 376, 91–101. https://doi.org/10.1016/j.jhazmat.2019.05.039.*

carboxymethyl cellulose (CMC) and 2-acrylamido-2-methylpropane sulfonic acid (AMPS), to coordinate with the Al^{3+} and Fe^{3+} cations. The CMC-g-AMPS/Fe/Al/AC superabsorbent exhibited a high affinity for F^- ions with $q_{max} = 67.114\ mg\ g^{-1}$ via ion exchange, coordination, and surface adsorption.

Selective removal of phosphate was investigated using SP-Zr-La bio-adsorbent prepared from anchoring of dual Zr and La hydroxide onto shaddock peels derived cellulose (Du et al., 2019). Phosphate ion adsorption onto SP-Zr-La was occurred via ligand exchange or metal-ligand interactions.

The Zr/La-cell/GO composite was made up by embedding Zr and La hydroxides into the 3D self-assembled cellulose/graphene oxide (cell/GO) hybrid (Fig. 15.3) (Zhang et al., 2019b). Phosphate removal and competitive adsorption in the presence of humic acid (HA) or various anions (F^-, Cl^-, SiO_3^{2-}, SO_4^{2-}, HCO^{3-} and NO^{3-}) were evaluated onto Zr/La-cell/GO hybrid. Competitive adsorption studies demonstrated that phosphate uptake was reduced at the co-existing HA/anions, especially fluoride. Also, the phosphate adsorption was remarkably improved by Ca^{2+} loading onto the Zr/La-cell/GO because of the calcium phosphate precipitation.

Adsorptive and selective mini-membrane (TiO_2@cellulose) was prepared via in situ synthesis of TiO_2 filler into cellulose filter and applied for separation, determination, and speciation of selenite and arsenate ions (Zawisza et al., 2020).

The exfoliated kaolinite sheets/cellulose fibers nanocomposite (EXK/CF, $S_{BET} = 104\ m^2\ g^{-1}$) was manufactured and used for decontamination of selenite (SeO_3^{2-}) and selenate (SeO_4^{2-}) ions with q_{max} of 137.5 and 161.4 mg g^{-1}, respectively (Abukhadra et al., 2021).

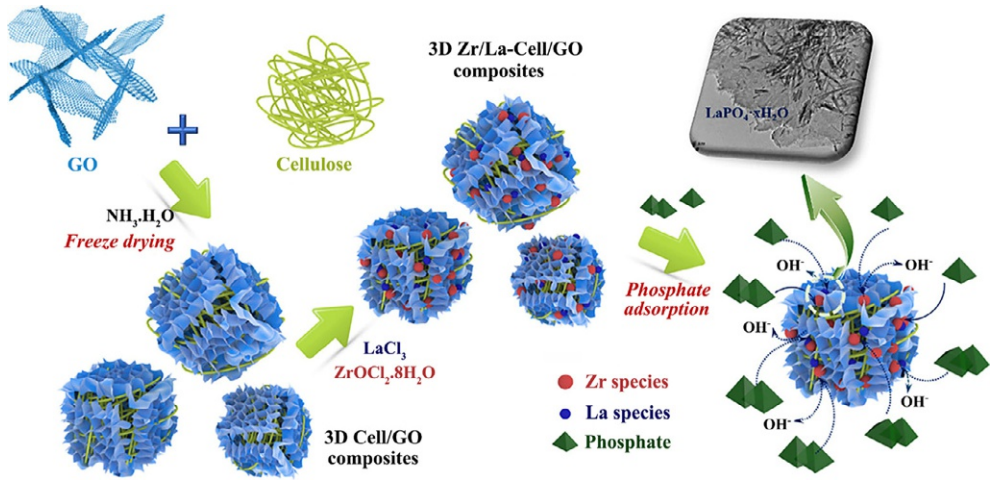

FIG. 15.3 The synthesis of Zr/La-cellulose/graphene oxide (Zr/La-cell/GO) nanocomposite, and the adsorption mechanism of phosphate onto Zr/La-cell/GO at different pH conditions. *Reproduced with permission from Zhang, L., Wang, Z., Xu, X., Chen, C., Gao, B., Xiao, X., 2019b. Insights into the phosphate adsorption behavior onto 3D self-assembled cellulose/graphene hybrid nanomaterials embedded with bimetallic hydroxides. Sci. Total Environ. 653, 897–907. https://doi.org/10.1016/j.scitotenv.2018.11.030.*

Dyes removal

Aromatic and heterocyclic dyes with complicated and stable structures are very dangerous for human health and the environment. The dyes meaningfully decrease the water quality, increase the chemical and biochemical oxygen demand, hinder photosynthesis, prevent plant growth, enter the food chain, and resulting in environmental imbalance. In addition, dyes pollutants may afford bioaccumulation and can generate toxicity, mutagenicity, and carcinogenicity (Lellis et al., 2019). The textile wastewater with severe health hazards to microorganisms, animals, humans, as well as plants must be treated before their discharge. In recent works, the cellulose composites with high adsorption capacity were reported as the most commonly used adsorbents for the treatment of wastewater polluted with dyes pollutants.

For example, the Fe_3O_4 reinforced graphene oxide-carboxymethyl cellulose recyclable composite was prepared via the co-precipitation method, and applied for adsorption of acid red 1 (AR1), congo red (CR), and reactive red 2 (RR2) from aqueous solutions (Fig. 15.4) (Sirajudheen et al., 2020b). Synthesized composite with high adsorption capacity and good recyclability and reusability could be used as a potential adsorbent for the removal of dyes. The good adsorption efficiency of the composite was related to the hydrogen bonding, π-π stacking interaction, electrostatic attraction, and surface complexation. In addition, the self-assembled complex of graphene oxide and nano-cellulose was formed in situ via the modified Hummers' method and utilized as an adsorbent with $q_{max} = 751.88$ (mg g^{-1}) for enhanced methylene blue adsorption (Zaman et al., 2020). The combination of cellulose and graphene moieties, with functional groups (–OH and –COOH), and the formation of hydrogen bonding between the negative functional groups on the edges of graphene oxide and

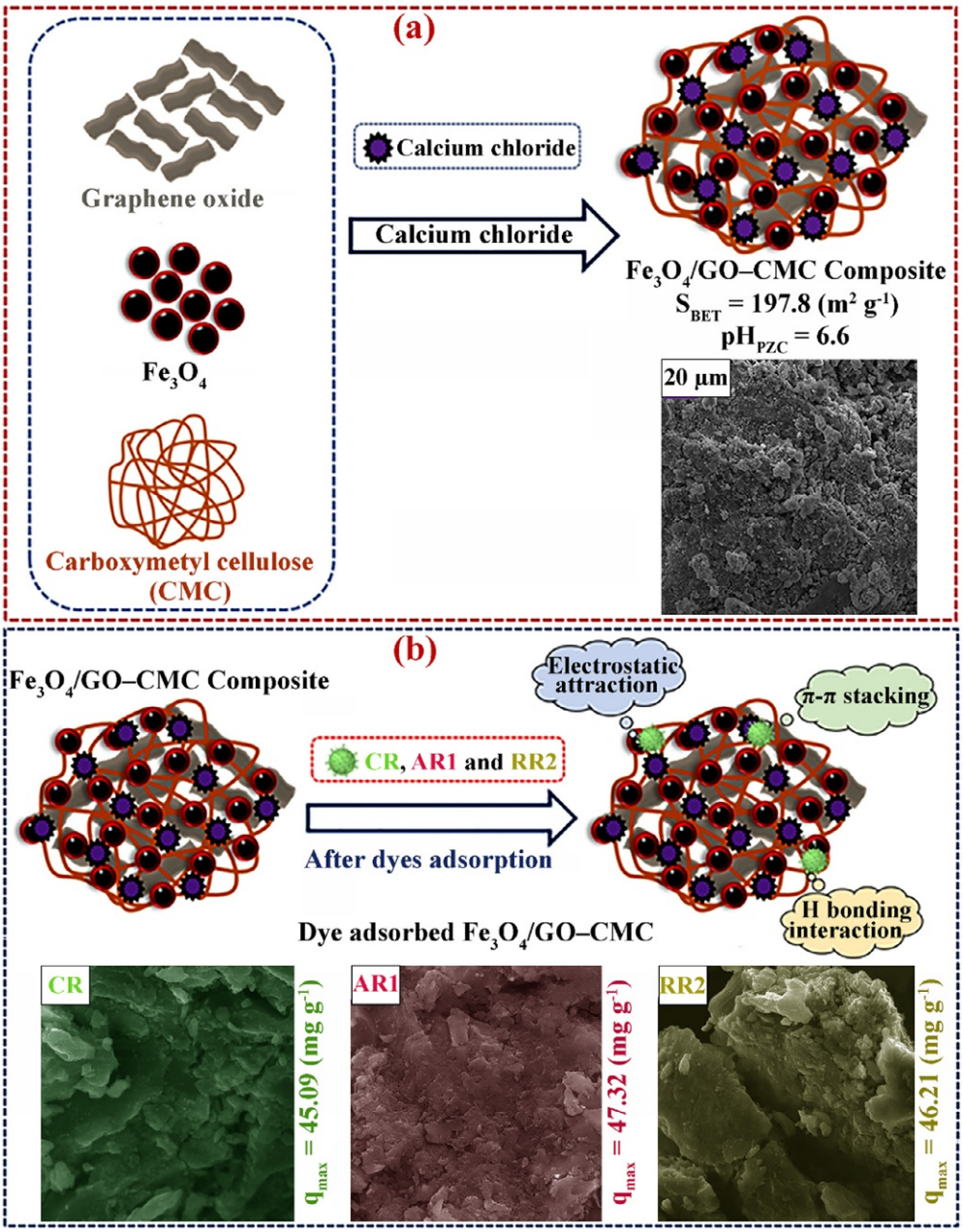

FIG. 15.4 (A) The schematic representation for preparing of Fe_3O_4 reinforced graphene oxide-carboxymethyl cellulose (Fe_3O_4/GO-CMC) composite. (B) The plausible mechanism for adsorption of acid red 1 (AR1), congo red (CR), and reactive red 2 (RR2) dyes onto Fe_3O_4/GO-CMC composite. *Reproduced with permission from Sirajudheen, P., Nikitha, M.R., Karthikeyan, P., Meenakshi, S., 2020b. Perceptive removal of toxic azo dyes from water using magnetic Fe3O4 reinforced graphene oxide–carboxymethyl cellulose recyclable composite: adsorption investigation of parametric studies and their mechanisms. Surf. Interfaces 21, 100648. https://doi.org/10.1016/j.surfin.2020.100648.*

the OH groups of cellulose led to the generation of composites with high surface area. Higher adsorption efficiency is provided from composites with a higher surface area.

To access cellulosic composites with high surface areas, the research works were reported based on the dispersion of metal-organic frameworks into the nanocellulose matrix. The UiO-66/cellulose composite with high surface area (826 $m^2\ g^{-1}$) was fabricated through a self-crosslinking method and showed good adsorption efficacy toward both cationic methylene blue (51.8 mg g^{-1}) and anionic methyl orange (71.7 mg g^{-1}) (Wang et al., 2019). Also, the structural control of cellulosic composite membrane with ZIF-8 spacers was investigated for highly selective removal of cationic dye in the presence of anionic dye (Song et al., 2019). The ZIF-8/TOCN membrane, prepared from in situ growing of zeolitic imidazolate frameworks (ZIF-8) in the presence of TEMPO-oxidized cellulose nanofibers (TOCN), exhibited a porous three-dimensional network with high durability without critical compaction under pressure and superior water flux without critical flux drop. The selective removal of cationic dyes was correlated to the strong interaction with negatively charged TOCN networks.

More examples of cellulose-based composites that have been recently used for dyes adsorption from aqueous solutions are summarized in Table 15.1.

Drugs removal

Pharmaceuticals are contaminants of emerging concern with the capability of ecological contamination in trace concentrations, along with cytostatic, genotoxic, mutagenic, and eco-toxicological effects on human health as well as on microorganisms present in soil and aquatic environment. The formation of reactive oxygen species and free radicals by pharmaceuticals can be associated with immunotoxicity, genotoxicity, and carcinogenesis (Yadav et al., 2021). The cellulose composites as environmentally friendly adsorbents have efficiently applied for drug removal because of high surface area, a large number of active functional groups, and low secondary pollution.

For example, soft foam-like UiO-66/polydopamine/bacterial cellulose (UiO-66/PDA/BC) was synthesized using biomass bacterial cellulose as a scaffold and polydopamine layer coating on the bacterial cellulose substrate (Fig. 15.5A) (Cui et al., 2020). The uniform coating of UiO-66 nanoparticles with uniform size in the three-dimensional connected network of composite structure guarantees high surface area ($S_{BET} = 454\ m^2\ g^{-1}$) as well as active sites for the adsorption of aspirin ($q_{max} = 149$ mg g^{-1}) and tetracycline hydrochloride ($q_{max} = 184$ mg g^{-1}) (Fig. 15.5B). The effective adsorption capability of UiO-66/PDA/BC was mainly related to the synergetic effect of π-π interaction and chemisorption (Fig. 15.5C). The good stability as well as excellent reusability of synthesized composite exhibited the great potential for pharmaceuticals removal from aqueous solutions.

Other examples of cellulose composites used in the removal of pharmaceuticals from aqueous solutions in recent years are listed in Table 15.2.

Pesticides removal

Oxidative stress caused by pesticides with the ability of DNA damage can generate respiratory and reproductive physiology disorders, Parkinson's and Alzheimer's diseases, and malignancies. The risk of cancers, leukemia, neuroblastoma, soft tissue sarcoma, Burkitt

TABLE 15.1 Representation of recently synthesized cellulose composites for dyes removal from aqueous solutions.

Adsorbent	Adsorbate	Adsorption conditions	Adsorption isotherm	Adsorption kinetic	q_{max} (mg g^{-1})	Adsorption mechanism	References
Activated carbon/cellulose biocomposite	Methylene blue	pH = 6.9, C_0 = 100 mg L^{-1}, V = 50 mL, m = − mg, T = 308 K, t = 24 h	Langmuir	Pseudo-second-order	103.66	Physical and chemical adsorptions	Somsesta et al. (2020)
Zr(IV) encapsulated carboxymethyl cellulose-montmorillonite composite	Acid orange 7	pH = 3, C_0 = 50 mg L^{-1}, V = 50 mL, m = 100 mg, T = 303 K, t = 40 min	Freundlich	–	28.80	Electrostatic attraction Hydrogen bonding Surface complexation	Sirajudheen et al. (2020a)
Zr(*IV*) encapsulated carboxymethyl cellulose-montmorillonite composite	Reactive red 2	pH = 3, C_0 = 50 mg L^{-1}, V = 50 mL, m = 100 mg, T = 303 K, t = 40 min	Freundlich	–	35.90	Electrostatic attraction Hydrogen bonding Surface complexation	Sirajudheen et al. (2020a)
Polypyrrole/carboxymethyl cellulose nanocomposite	reactive red 56	pH = 4, C_0 = 100 mg L^{-1}, V = 50 mL, m = 0.09 mg, T = 298 K, t = 55 min	Langmuir	Pseudo-second-order	104.9	Hydrogen bonding	Tanzifi et al. (2020)
Polypyrrole/carboxymethyl cellulose nanocomposite	reactive blue 160	pH = 5, C_0 = 100 mg L^{-1}, V = 50 mL, m = 0.09 mg, T = 298 K, t = 52 min	Langmuir	Bangham	120.7	Hydrogen bonding	Tanzifi et al. (2020)

Continued

TABLE 15.1 Representation of recently synthesized cellulose composites for dyes removal from aqueous solutions—cont'd

Adsorbent	Adsorbate	Adsorption conditions	Adsorption isotherm	Adsorption kinetic	q_{max} (mg g^{-1})	Adsorption mechanism	References
Carboxymethyl cellulose/carboxylated graphene oxide composite	Methylene blue	pH = 10, C_0 = 200 mg L^{-1}, V = 50 mL, m = 50 mg, T = 298 K, *t* = 120 min	Langmuir	Pseudo-second-order	180.32	–	Eltaweil et al. (2020)
Carboxymethyl cellulose/alginate/polyvinyl alcohol/rice husk composite	Direct Orange-26	pH = 12, C_0 = – mg L^{-1}, V = 50 mL, m = – mg, *T* = 303 K, *t* = 20 min	–	Pseudo-second-order	25.19	–	Bhatti et al. (2020a, b)
Carboxymethyl cellulose/alginate/polyvinyl alcohol/rice husk composite	Direct Red-31	pH = 12, C_0 = – mg L^{-1}, V = 50 mL, m = – mg, T = 303 K, t = 20 min	–	Pseudo-second-order	26.81	–	Bhatti et al. (2020a, b)
Carboxymethyl cellulose/alginate/polyvinyl alcohol/rice husk composite	Direct Blue-67	pH = 12, C_0 = – mg L^{-1}, V = 50 mL, m = – mg, *T* = 303 K, t = 20 min	–	Pseudo-second-order	20.45	–	Bhatti et al. (2020a, b)
Carboxymethyl cellulose/alginate/polyvinyl alcohol/rice husk composite	Ever direct Orange-3GL	pH = 12, C_0 = – mg L^{-1}, V = 50 mL, m = – mg, T = 303 K, t = 20 min	–	Pseudo-second-order	26.67	–	Bhatti et al. (2020a, b)
Graphene oxide-cellulose nanocomposite	Methylene blue	pH = 10, C_0 = 10 mg L^{-1}, V = 70 mL, m = 30 mg L^{-1}, *T* = 313 K, *t* = 135 min	Langmuir	Pseudo-second-order	751.88	Electrostatic interaction	Zaman et al. (2020)

Deacetylated cellulose acetate@polydopaminecomposite	Methylene blue	pH = 6.5, $C_0 = 50$ mg L^{-1}, V = − mL, m = 10 mg, $T = 298$ K, $t = 24$ h	Langmuir	Pseudo-second-order	88.2	Electrostatic interaction π-π stacking	Cheng et al. (2020)
$NiFe_2O_4$/multi-walled carbon nanotubes functionalized cellulose	Congo red	pH = 6.0, $C_0 = 5$ mg L^{-1}, V = 50 mL, m = 50 mg, $T = 298$ K, $t = 48$ h	Langmuir	Pseudo-second-order	95.70	Physical and chemical adsorption	Jiang et al. (2021)
Fe_3O_4 reinforced graphene oxide–carboxymethyl cellulose	Congo red	pH = 6, $C_0 = 50$ mg L^{-1}, V = 50 mL, m = 100 mg, $T = 303$ K, $t = 40$ min	Freundlich	Pseudo-second-order	45.09	Electrostatic interaction Hydrogen bonding π-π stacking Surface complexation	Sirajudheen et al. (2020b)
Fe_3O_4 reinforced graphene oxide–carboxymethyl cellulose	Acid red 1	pH = 6, $C_0 = 50$ mg L^{-1}, V = 50 mL, m = 100 mg, T = 303 K, t = 40 min	Freundlich	Pseudo-second-order	47.32	Electrostatic interaction Hydrogen bonding π-π stacking Surface complexation	Sirajudheen et al. (2020b)
Fe_3O_4 reinforced graphene oxide–carboxymethyl cellulose	Reactive red 2	pH = 6, $C_0 = 50$ mg L^{-1}, V = 50 mL, m = 100 mg, T = 303 K, t = 40 min	Freundlich	Pseudo-second-order	46.21	Electrostatic interaction Hydrogen bonding π-π stacking Surface complexation	Sirajudheen et al. (2020b)
Exfoliated bentonite sheets admixed with nano-cellulose fibers	Safranin	pH = 8, $C_0 = 50$ mg L^{-1}, V = 250 mL, m = 100 mg L^{-1}, T = 298 K, t = 240 min	Freundlich	Pseudo-first-order	341	Physisorption	Abukhadra et al. (2020)

Continued

TABLE 15.1 Representation of recently synthesized cellulose composites for dyes removal from aqueous solutions—cont'd

Adsorbent	Adsorbate	Adsorption conditions	Adsorption isotherm	Adsorption kinetic	q_{max} (mg g^{-1})	Adsorption mechanism	References
Sawdust-based cellulose nanocrystals incorporated with ZnO nanoparticles	Methylene blue	pH = 4.0, C_0 = 100 mg L^{-1}, V = 50 mL, m = 100 mg, T = 298 K, t = 25 min	Langmuir	Pseudo-second-order	64.93	Electrostatic interaction Hydrogen bonding π-π stacking	Oyewo et al. (2020a)
Carboxymethyl cellulose-chitosan-montmorillonite nanosheets	Methylene blue	pH = 8.0, C_0 = 20 mg L^{-1}, V = 500 mL, m = 200 mg L^{-1}, T = 303 K, *t* = 360 min	Sips	Pseudo-first-order Pseudo-second-order	–	Physical and chemical adsorption	Wang et al. (2020a)
Electrospun cellulose acetate/poly(dimethyldiallylammonium chloride-acrylamide)	Acid black 172	pH = 2.0, C_0 = 100 mg L^{-1}, V = 100 mL, m = 10 mg, T = 298 K, t = 24 h	Langmuir	Pseudo-second-order	290	Chemisorption	Xu et al. (2020)
Cellulose mediated graphene oxide magnetic aerogel composite	Methylene blue	pH = 13.0, C_0 = 200 mg L^{-1}, V = − mL, m = 1 g L^{-1}, T = 303 K, t = 240 min	Langmuir	Pseudo-second-order	346	Chemisorption	Xiong et al. (2020)
Cellulose mediated graphene oxide magnetic aerogel composite	Congo red	pH = 5.0, C_0 = 200 mg L^{-1}, V = − mL, m = 1 g L^{-1}, T = 303 K, t = 240 min	Langmuir	Pseudo-second-order	282	Chemisorption	Xiong et al. (2020)

Graphene oxide/chitosan/carboxymethyl cellulose composite	Methylene blue	pH = 7.0, $C_0 = 50\ mg\ L^{-1}$, V = −mL, $m = 0.4\ g\ L^{-1}$, T = 298 K, t = −min	Langmuir	Pseudo-second-order	655.98	Chemisorption Ion exchange	Mittal et al. (2021)
Graphene oxide/chitosan/carboxymethyl cellulose composite	Methyl orange	pH = 3.0, $C_0 = 50\ mg\ L^{-1}$, V = −mL, $m = 0.6\ g\ L^{-1}$, T = 298 K, t = −min	Langmuir	Pseudo-second-order	404.52	Chemisorption Ion exchange	Mittal et al. (2021)

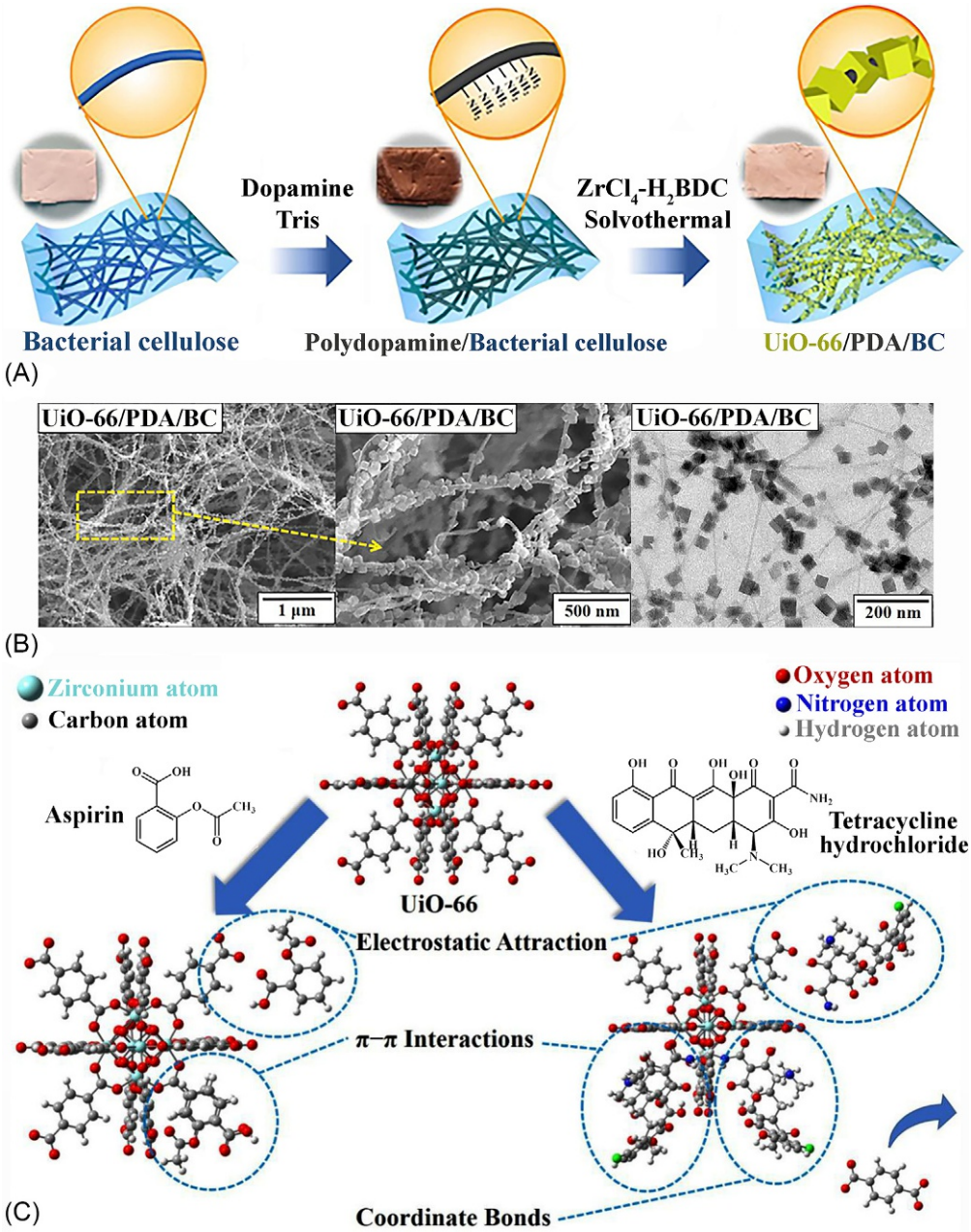

FIG. 15.5 (A) The preparation of UiO-66/polydopamine/bacterial cellulose (UiO-66/PDA/BC) composite aerogel. (B) SEM and TEM images of UiO-66/PDA/BC. (C) The adsorption mechanism of aspirin and tetracycline hydrochloride onto UiO-66/PDA/BC. *Reproduced with permission from Cui, J., Xu, X., Yang, L., Chen, C., Qian, J., Chen, X., Sun, D., 2020. Soft foam-like UiO-66/polydopamine/bacterial cellulose composite for the removal of aspirin and tetracycline hydrochloride. Chem. Eng. J. 395, 125174. https://doi.org/10.1016/j.cej.2020.125174).*

TABLE 15.2 The list of cellulose-based nanocomposites for drug adsorption from aqueous solutions.

Adsorbent	Adsorbate	Adsorption conditions	Adsorption isotherm	Adsorption kinetic	q_{max} (mg g^{-1})	Adsorption mechanism	References
Humic acid/cellulose nanocomposite	Ciprofloxacin	pH = 5.0, C_0 = 10 mg L^{-1}, V = 50 mL, m = − mg, T = 318 K, t = − min	Langmuir	Pseudo-second-order	10.87	Ion exchange	Wang et al. (2020b)
Mg-Al layered double hydroxide/cellulose nanocomposit	Amoxicillin	pH = 7.0, C_0 = 60 mg L^{-1}, V = 300 mL, m = 30 g, T = 318 K, t = 90 min	Freundlich	Pseudo-second-order	138.3	Physisorption	Yang et al. (2020b)
Montmorillonite-impregnated cellulose acetate nanofiber	Ciprofloxacin	pH = 6.0, C_0 = 10 mg L^{-1}, V = − mL, m = 4 g L^{-1}, *T* = 300 K, *t* = 60 min	Langmuir and Freundlich	Elovich	13.8	Physisorption and Chemisorption	Das et al. (2020)
Cellulosic sisal fiber/polypyrrole-polyaniline composite	Ibuprofen	pH = 5.0, C_0 = 30 mg L^{-1}, V = − mL, m = 300 mg, T = 313 K, t = 60 min	Sips	Pseudo-second-order	21.5	Physisorption and Chemisorption	Khadir et al. (2020)
UiO-66/polydopamine/bacterial cellulose	Aspirin	pH = 4.0, C_0 = 100 mg L^{-1}, V = 20 mL, m = 10 mg, T = 298 K, t = 90 min	Langmuir	Pseudo-second-order	149	Physisorption and Chemisorption	Cui et al. (2020)
UiO-66/polydopamine/bacterial cellulose	Tetracycline hydrochloride	pH = 3.0, C_0 = 100 mg L^{-1}, V = 20 mL, m = 10 mg, T = 298 K, t = 90 min	Langmuir	Pseudo-second-order	184	Physisorption and Chemisorption	
Magnetic cellulose	Tetracycline	pH = 4.0, C_0 = 45 mg L^{-1}, V = 25 mL, m = 1 g L^{-1}, T = 298 K, *t* = 48 h	Langmuir	Pseudo-second-order	44.86	Physisorption and Chemisorption	Sun et al. (2021)
Carboxymethyl cellulose and chitosan modified magnetic alkaline Ca-bentonite	Doxycycline	pH = 7.0, C_0 = 100 mg L^{-1}, V = 100 mL, m = 1.2 g L^{-1}, T = 298 K, t = 2 h	Langmuir	Pseudo-second-order	643	Physisorption and Ion exchange	Tang et al. (2021)

lymphoma, ovarian, stomach, colon, bladder, rectum, and lung, was found to be greater in people who are closely associated with pesticides exposure (Sabarwal et al., 2018).

In recent years, several studies have been conducted to remove pesticides using cellulosic composites. The prometryn was removed by copper-modified microcrystalline cellulose composite with $q_{max} = 97.80\ mg\ g^{-1}$ from synthetic wastewater (Garba et al., 2019). Also, the study of chlorpyrifos adsorption was investigated onto polyvinylamine-modified nanocellulose ($S_{BET} = 32.17\ m^2\ g^{-1}$ and $q_{max} = 98.12\ mg\ g^{-1}$), and the adsorption results exhibited that the adsorption of chlorpyrifos was primarily dominated by chemisorption (Yang et al., 2020a). In addition, nanocellulose-organic montmorillonite nanocomposite ($S_{BET} = 39.52\ m^2\ g^{-1}$) was applied for diuron adsorption with q_{max} of $69.04\ mg\ g^{-1}$ from aqueous solutions (Ma et al., 2020). In another work, the adsorption of 2,4-dichlorophenol was assayed onto the composites of cellulosic biomass barley husk with sodium alginate, polyaniline, and polypyrrole. The polyaniline/cellulose ($q_e = 24.57\ mg\ g^{-1}$) and sodium alginate/cellulose ($q_e = 7.55\ mg\ g^{-1}$) composites were demonstrated the highest and lowest adsorption capacity for 2,4-dichlorophenol, respectively (Bhatti et al., 2020a, b).

15.2.3 Soil remediation

Soil contamination can be dangerous as it is the foundation of organisms' survival and affects animal and human health through the food chain (Steffan et al., 2018). The versatility of soil makes it more prone to pollution by organic and inorganic contaminants especially heavy metals. Recently, few studies have been reported for soil remediation using cellulosic composites via adsorption.

The remediation of Cu^{2+}-contaminated soil was investigated using the carboxylated graphene oxide/chitosan/cellulose (GCCSC) composite beads via the adsorption method (Zhao et al., 2019b). The direct contact between the graphene surface and soil could block by the porous structure of GCCSC beads, so, a high immobilization efficiency of Cu^{2+} was attained by GCCSC beads applied to the soil. In another study, the efficacy of montmorillonite-supported carboxymethyl cellulose-stabilized nanoscale iron sulfide (CMC@MMT-FeS) composite, prepared via co-precipitation method, was assayed for remediation of Cr(VI)-contaminated soils (Zhang et al., 2020). The adsorption capacity of CMC@MMT-FeS for removal of Cr(VI) was improved with increasing FeS-particle loading. In addition, amphoteric cellulose-montmorillonite composite beads, constructed from regenerated bagasse cellulose and oxalic acid modified montmorillonite, were introduced as a promising material for soil remediation because of porous structure (Xie et al., 2019).

Based on research in this field, the application of cellulose composites can be beneficial to immobilize heavy metals in soil and elevate the soil quality.

15.3 Conclusion

Eco-friendly cellulose-based nanocomposites have shown excellent potential for the removal of toxic gases, organic and inorganic contaminants from the environment because of their great properties such as high specific surface area and presence of plentiful functional

groups. In this book chapter, the synthesis and adsorption ability of diverse cellulosic biosorbents have been investigated for the removal of pollutants from the air, water, and soil. In addition, the types of interactions and the influence of interactions between adsorbents and adsorbate are assayed on the adsorption efficiency of cellulosic nano-sorbents. According to the destructive and deadly effects of pollution on living organisms, the design and fabrication of smart cellulose-based composites with high adsorption capacity for pollutants and decontamination of pathogens are a necessary need for a better life for human societies.

References

Abukhadra, M.R., Adlii, A., El-Sherbeeny, A.M., Ahmed Soliman, A.T., Abd Elgawad, A.E.E., 2020. Promoting the decontamination of different types of water pollutants (Cd^{2+}, safranin dye, and phosphate) using a novel structure of exfoliated bentonite admixed with cellulose nanofiber. J. Environ. Manag. 273, 111130. https://doi.org/10.1016/j.jenvman.2020.111130.

Abukhadra, M.R., AlHammadi, A., El-Sherbeeny, A.M., Salam, M.A., El-Meligy, M.A., Awwad, E.M., Luqman, M., 2021. Enhancing the removal of organic and inorganic selenium ions using an exfoliated kaolinite/cellulose fibres nanocomposite. Carbohydr. Polym. 252, 117163. https://doi.org/10.1016/j.carbpol.2020.117163.

Adavan Kiliyankil, V., Fugetsu, B., Sakata, I., Wang, Z., Endo, M., 2021. Aerogels from copper (II)-cellulose nanofibers and carbon nanotubes as absorbents for the elimination of toxic gases from air. J. Colloid Interface Sci. 582, 950–960. https://doi.org/10.1016/j.jcis.2020.08.100.

Bhatti, H.N., Mahmood, Z., Kausar, A., Yakout, S.M., Shair, O.H., Iqbal, M., 2020a. Biocomposites of polypyrrole, polyaniline and sodium alginate with cellulosic biomass: adsorption-desorption, kinetics and thermodynamic studies for the removal of 2,4-dichlorophenol. Int. J. Biol. Macromol. 153, 146–157. https://doi.org/10.1016/j.ijbiomac.2020.02.306.

Bhatti, H.N., Safa, Y., Yakout, S.M., Shair, O.H., Iqbal, M., Nazir, A., 2020b. Efficient removal of dyes using carboxymethyl cellulose/alginate/polyvinyl alcohol/rice husk composite: adsorption/desorption, kinetics and recycling studies. Int. J. Biol. Macromol. 150, 861–870. https://doi.org/10.1016/j.ijbiomac.2020.02.093.

Cai, Y., Chen, L., Yang, S., Xu, L., Qin, H., Liu, Z., Chen, L., Wang, X., Wang, S., 2019. Rational synthesis of novel phosphorylated chitosan-carboxymethyl cellulose composite for highly effective decontamination of U(VI). ACS Sustain. Chem. Eng. 7, 5393–5403. https://doi.org/10.1021/acssuschemeng.8b06416.

Chaudhary, M., Maiti, A., 2020. Fe–Al–Mn@chitosan based metal oxides blended cellulose acetate mixed matrix membrane for fluoride decontamination from water: removal mechanisms and antibacterial behavior. J. Membr. Sci. 611, 118372. https://doi.org/10.1016/j.memsci.2020.118372.

Cheng, J., Zhan, C., Wu, J., Cui, Z., Si, J., Wang, Q., Peng, X., Turng, L.-S., 2020. Highly efficient removal of methylene blue dye from an aqueous solution using cellulose acetate nanofibrous membranes modified by polydopamine. ACS Omega 5, 5389–5400. https://doi.org/10.1021/acsomega.9b04425.

Cui, J., Xu, X., Yang, L., Chen, C., Qian, J., Chen, X., Sun, D., 2020. Soft foam-like UiO-66/polydopamine/bacterial cellulose composite for the removal of aspirin and tetracycline hydrochloride. Chem. Eng. J. 395, 125174. https://doi.org/10.1016/j.cej.2020.125174.

D'Amato, G., Akdis, C.A., 2020. Global warming, climate change, air pollution and allergies. Allergy 75, 2158–2160. https://doi.org/10.1111/all.14527.

Das, S., Barui, A., Adak, A., 2020. Montmorillonite impregnated electrospun cellulose acetate nanofiber sorptive membrane for ciprofloxacin removal from wastewater. J. Water Process. Eng. 37, 101497. https://doi.org/10.1016/j.jwpe.2020.101497.

Dong, F., Xu, X., Shaghaleh, H., Guo, J., Guo, L., Qian, Y., Liu, H., Wang, S., 2020. Factors influencing the morphology and adsorption performance of cellulose nanocrystal/iron oxide nanorod composites for the removal of arsenic during water treatment. Int. J. Biol. Macromol. 156, 1418–1424. https://doi.org/10.1016/j.ijbiomac.2019.11.182.

Du, W., Li, Y., Xu, X., Shang, Y., Gao, B., Yue, Q., 2019. Selective removal of phosphate by dual Zr and La hydroxide/cellulose-based bio-composites. J. Colloid Interface Sci. 533, 692–699. https://doi.org/10.1016/j.jcis.2018.09.002.

Eltaweil, A.S., Elgarhy, G.S., El-Subruiti, G.M., Omer, A.M., 2020. Carboxymethyl cellulose/carboxylated graphene oxide composite microbeads for efficient adsorption of cationic methylene blue dye. Int. J. Biol. Macromol. 154, 307–318. https://doi.org/10.1016/j.ijbiomac.2020.03.122.

Fallah, Z., Nasr Isfahani, H., Tajbakhsh, M., Tashakkorian, H., Amouei, A., 2018. TiO_2-grafted cellulose via click reaction: an efficient heavy metal ions bioadsorbent from aqueous solutions. Cellulose 25, 639–660. https://doi.org/10.1007/s10570-017-1563-8.

Fallah, Z., Nasr Isfahani, H., Tajbakhsh, M., 2020. Removal of fluoride ion from aqueous solutions by titania-grafted β-cyclodextrin nanocomposite. Environ. Sci. Pollut. Res. 27, 3281–3294. https://doi.org/10.1007/s11356-019-06948-4.

Fan, Y., Zhao, X., Yu, J., Xie, J., Li, C., Liu, D., Tang, C., Wang, C., 2020. Lead-induced oxidative damage in rats/mice: a meta-analysis. J. Trace Elem. Med. Biol. 58, 126443. https://doi.org/10.1016/j.jtemb.2019.126443.

Garba, Z.N., Zhou, W., Lawan, I., Zhang, M., Yuan, Z., 2019. Enhanced removal of prometryn using copper modified microcrystalline cellulose (Cu-MCC): optimization, isotherm, kinetics and regeneration studies. Cellulose 26, 6241–6258. https://doi.org/10.1007/s10570-019-02531-9.

Guo, Y., Xing, X., Shang, Y., Gao, B., Zhang, L., Yue, Q., Qian, L., Wang, Z., 2019. Multiple bimetallic (Al-La or Fe-La) hydroxides embedded in cellulose/graphene hybrids for uptake of fluoride with phosphate surroundings. J. Hazard. Mater. 379, 120634. https://doi.org/10.1016/j.jhazmat.2019.05.027.

Hosseini, J., Zare, E.N., Ajloo, D., 2019. Experimental and theoretical calculation investigation on effective adsorption of lead(II) onto poly(aniline-co-pyrrole) nanospheres. J. Mol. Liq. 296. https://doi.org/10.1016/j.molliq.2019.111789.

Huihui, Z., Xin, L., Zisong, X., Yue, W., Zhiyuan, T., Meijun, A., Yuehui, Z., Wenxu, Z., Nan, X., Guangyu, S., 2020. Toxic effects of heavy metals Pb and Cd on mulberry (*Morus alba* L.) seedling leaves: photosynthetic function and reactive oxygen species (ROS) metabolism responses. Ecotoxicol. Environ. Saf. 195, 110469. https://doi.org/10.1016/j.ecoenv.2020.110469.

Jia, M., Zhang, X.F., Feng, Y., Zhou, Y., Yao, J., 2020. In-situ growing ZIF-8 on cellulose nanofibers to form gas separation membrane for CO_2 separation. J. Membr. Sci. 595, 117579. https://doi.org/10.1016/j.memsci.2019.117579.

Jiang, R., Zhu, H.Y., Fu, Y.Q., Zong, E.M., Jiang, S.T., Li, J.B., Zhu, J.Q., Zhu, Y.Y., 2021. Magnetic $NiFe_2O_4$/MWCNTs functionalized cellulose bioadsorbent with enhanced adsorption property and rapid separation. Carbohydr. Polym. 252, 117158. https://doi.org/10.1016/j.carbpol.2020.117158.

Jomova, K., Valko, M., 2011. Advances in metal-induced oxidative stress and human disease. Toxicology 283, 65–87. https://doi.org/10.1016/j.tox.2011.03.001.

Khadir, A., Motamedi, M., Negarestani, M., Sillanpää, M., Sasani, M., 2020. Preparation of a nano bio-composite based on cellulosic biomass and conducting polymeric nanoparticles for ibuprofen removal: kinetics, isotherms, and energy site distribution. Int. J. Biol. Macromol. 162, 663–677. https://doi.org/10.1016/j.ijbiomac.2020.06.095.

Kim, K.H., Kabir, E., Jahan, S.A., 2018. Airborne bioaerosols and their impact on human health. J. Environ. Sci. 67, 23–35.

Kong, Q., Preis, S., Li, L., Luo, P., Hu, Y., Wei, C., 2020. Graphene oxide-terminated hyperbranched amino polymer-carboxymethyl cellulose ternary nanocomposite for efficient removal of heavy metals from aqueous solutions. Int. J. Biol. Macromol. 149, 581–592. https://doi.org/10.1016/j.ijbiomac.2020.01.185.

Lei, C., Gao, J., Ren, W., Xie, Y., Abdalkarim, S.Y.H., Wang, S., Ni, Q., Yao, J., 2019. Fabrication of metal-organic frameworks@cellulose aerogels composite materials for removal of heavy metal ions in water. Carbohydr. Polym. 205, 35–41. https://doi.org/10.1016/j.carbpol.2018.10.029.

Lellis, B., Fávaro-Polonio, C.Z., Pamphile, J.A., Polonio, J.C., 2019. Effects of textile dyes on health and the environment and bioremediation potential of living organisms. Biotechnol. Res. Innov. 3, 275–290. https://doi.org/10.1016/j.biori.2019.09.001.

Li, D., Tian, X., Wang, Z., Guan, Z., Li, X., Qiao, H., Ke, H., Luo, L., Wei, Q., 2020. Multifunctional adsorbent based on metal-organic framework modified bacterial cellulose/chitosan composite aerogel for high efficient removal of heavy metal ion and organic pollutant. Chem. Eng. J. 383, 123127. https://doi.org/10.1016/j.cej.2019.123127.

Liu, H., Li, P., Qiu, F., Zhang, T., Xu, J., 2020. Controllable preparation of FeOOH/CuO@WBC composite based on water bamboo cellulose applied for enhanced arsenic removal. Food Bioprod. Process. 123, 177–187. https://doi.org/10.1016/j.fbp.2020.06.018.

Ma, S., Zhang, M., Nie, J., Yang, B., Song, S., Lu, P., 2018. Multifunctional cellulose-based air filters with high loadings of metal–organic frameworks prepared by in situ growth method for gas adsorption and antibacterial applications. Cellulose 25, 5999–6010. https://doi.org/10.1007/s10570-018-1982-1.

Ma, S., Zhang, M., Nie, J., Tan, J., Song, S., Luo, Y., 2019a. Lightweight and porous cellulose-based foams with high loadings of zeolitic imidazolate frameworks-8 for adsorption applications. Carbohydr. Polym. 208, 328–335. https://doi.org/10.1016/j.carbpol.2018.12.081.

Ma, S., Zhang, M., Nie, J., Tan, J., Yang, B., Song, S., 2019b. Design of double-component metal–organic framework air filters with PM2.5 capture, gas adsorption and antibacterial capacities. Carbohydr. Polym. 203, 415–422. https://doi.org/10.1016/j.carbpol.2018.09.039.

Ma, C., Yi, L., Yang, J., Tao, J., Li, J., 2020. Nanocellulose–organic montmorillonite nanocomposite adsorbent for diuron removal from aqueous solution: optimization using response surface methodology. RSC Adv. 10, 30734–30745. https://doi.org/10.1039/D0RA04853D.

Meteku, B.E., Huang, J., Zeng, J., Subhan, F., Feng, F., Zhang, Y., Qiu, Z., Aslam, S., Li, G., Yan, Z., 2020. Magnetic metal–organic framework composites for environmental monitoring and remediation. Coord. Chem. Rev. 413, 213261.

Mittal, H., Al Alili, A., Morajkar, P.P., Alhassan, S.M., 2021. GO crosslinked hydrogel nanocomposites of chitosan/carboxymethyl cellulose—a versatile adsorbent for the treatment of dyes contaminated wastewater. Int. J. Biol. Macromol. 167, 1248–1261. https://doi.org/10.1016/j.ijbiomac.2020.11.079.

Mukherjee, S., Ramireddy, H., Baidya, A., Amala, A.K., Sudhakar, C., Mondal, B., Philip, L., Pradeep, T., 2020. Nanocellulose-reinforced organo-inorganic nanocomposite for synergistic and affordable defluoridation of water and an evaluation of its sustainability metrics. ACS Sustain. Chem. Eng. 8, 139–147. https://doi.org/10.1021/acssuschemeng.9b04822.

Ojstršek, A., Fakin, D., Hribernik, S., Fakin, T., Bračič, M., Kurečič, M., 2020. Electrospun nanofibrous composites from cellulose acetate/ultra-high silica zeolites and their potential for VOC adsorption from air. Carbohydr. Polym. 236, 116071. https://doi.org/10.1016/j.carbpol.2020.116071.

Oyewo, O.A., Adeniyi, A., Sithole, B.B., Onyango, M.S., 2020a. Sawdust-based cellulose nanocrystals incorporated with ZnO nanoparticles as efficient adsorption media in the removal of methylene blue dye. ACS Omega 5, 18798–18807. https://doi.org/10.1021/acsomega.0c01924.

Oyewo, O.A., Elemike, E.E., Onwudiwe, D.C., Onyango, M.S., 2020b. Metal oxide-cellulose nanocomposites for the removal of toxic metals and dyes from wastewater. Int. J. Biol. Macromol. 164, 2477–2496. https://doi.org/10.1016/j.ijbiomac.2020.08.074.

Pandey, A., Brauer, M., Cropper, M.L., Balakrishnan, K., Mathur, P., Dey, S., Turkgulu, B., Kumar, G.A., Khare, M., Beig, G., Gupta, T., Krishnankutty, R.P., Causey, K., Cohen, A.J., Bhargava, S., Aggarwal, A.N., Agrawal, A., Awasthi, S., Bennitt, F., Bhagwat, S., Bhanumati, P., Burkart, K., Chakma, J.K., Chiles, T.C., Chowdhury, S., Christopher, D.J., Dey, S., Fisher, S., Fraumeni, B., Fuller, R., Ghoshal, A.G., Golechha, M.J., Gupta, P.C., Gupta, R., Gupta, R., Gupta, S., Guttikunda, S., Hanrahan, D., Harikrishnan, S., Jeemon, P., Joshi, T.K., Kant, R., Kant, S., Kaur, T., Koul, P.A., Kumar, P., Kumar, R., Larson, S.L., Lodha, R., Madhipatla, K.K., Mahesh, P.-A., Malhotra, R., Managi, S., Martin, K., Mathai, M., Mathew, J.L., Mehrotra, R., Mohan, B.V.M., Mohan, V., Mukhopadhyay, S., Mutreja, P., Naik, N., Nair, S., Pandian, J.D., Pant, P., Perianayagam, A., Prabhakaran, D., Prabhakaran, P., Rath, G.K., Ravi, S., Roy, A., Sabde, Y.D., Salvi, S., Sambandam, S., Sharma, B., Sharma, M., Sharma, S., Sharma, R.S., Shrivastava, A., Singh, S., Singh, V., Smith, R., Stanaway, J.D., Taghian, G., Tandon, N., Thakur, J.S., Thomas, N.J., Toteja, G.S., Varghese, C.M., Venkataraman, C., Venugopal, K.N., Walker, K.D., Watson, A.Y., Wozniak, S., Xavier, D., Yadama, G.N., Yadav, G., Shukla, D.K., Bekedam, H.J., Reddy, K.S., Guleria, R., Vos, T., Lim, S.S., Dandona, R., Kumar, S., Kumar, P., Landrigan, P.J., Dandona, L., 2021. Health and economic impact of air pollution in the states of India: the global burden of disease study 2019. Lancet Planet. Health 5, e25–e38. https://doi.org/10.1016/S2542-5196(20)30298-9.

Peng, B., Yao, Z., Wang, X., Crombeen, M., Sweeney, D.G., Tam, K.C., 2020. Cellulose-based materials in wastewater treatment of petroleum industry. Green Energy Environ. 5, 37–49.

Raghav, S., Nehra, S., Kumar, D., 2019. Adsorptive removal studies of fluoride in aqueous system by bimetallic oxide incorporated in cellulose. Process. Saf. Environ. Prot. 127, 211–225. https://doi.org/10.1016/j.psep.2019.05.028.

Sabarwal, A., Kumar, K., Singh, R.P., 2018. Hazardous effects of chemical pesticides on human health–cancer and other associated disorders. Environ. Toxicol. Pharmacol. 63, 103–114. https://doi.org/10.1016/j.etap.2018.08.018.

Sankararamakrishnan, N., Srivastava, I., Mishra, S., 2019. Studies on novel nano-bimetal doped cellulose nanofibers derived from agrowaste towards deflouridation. Int. J. Biol. Macromol. 128, 556–565. https://doi.org/10.1016/j.ijbiomac.2019.01.153.

Shang, Y., Wang, Z., Xu, X., Cheng, C., Gao, B., Yue, Q., Liu, S., Han, C., 2019. Enhanced fluoride uptake by bimetallic hydroxides anchored in cotton cellulose/graphene oxide composites. J. Hazard. Mater. 376, 91–101. https://doi.org/10.1016/j.jhazmat.2019.05.039.

Shankar, K., Kandasamy, P., 2019. Carbon dioxide separation using α-alumina ceramic tube supported cellulose triacetate-tributyl phosphate composite membrane. Greenh. Gases Sci. Technol. 9, 287–305. https://doi.org/10.1002/ghg.1845.

Sharma, P.R., Sharma, S.K., Antoine, R., Hsiao, B.S., 2019. Efficient removal of arsenic using zinc oxide nanocrystal-decorated regenerated microfibrillated cellulose scaffolds. ACS Sustain. Chem. Eng. 7, 6140–6151. https://doi.org/10.1021/acssuschemeng.8b06356.

Sinha, V., Chakma, S., 2020. Synthesis and evaluation of CMC-g-AMPS/Fe/Al/AC composite hydrogel and their use in fluoride removal from aqueous solution. Environ. Technol. Innov. 17, 100620. https://doi.org/10.1016/j.eti.2020.100620.

Sirajudheen, P., Karthikeyan, P., Basheer, M.C., Meenakshi, S., 2020a. Adsorptive removal of anionic azo dyes from effluent water using Zr(IV) encapsulated carboxymethyl cellulose-montmorillonite composite. Environ. Chem. Ecotoxicol. 2, 73–82. https://doi.org/10.1016/j.enceco.2020.04.002.

Sirajudheen, P., Nikitha, M.R., Karthikeyan, P., Meenakshi, S., 2020b. Perceptive removal of toxic azo dyes from water using magnetic Fe3O4 reinforced graphene oxide–carboxymethyl cellulose recyclable composite: adsorption investigation of parametric studies and their mechanisms. Surf. Interfaces 21, 100648. https://doi.org/10.1016/j.surfin.2020.100648.

Somsesta, N., Sricharoenchaikul, V., Aht-Ong, D., 2020. Adsorption removal of methylene blue onto activated carbon/cellulose biocomposite films: equilibrium and kinetic studies. Mater. Chem. Phys. 240, 122221. https://doi.org/10.1016/j.matchemphys.2019.122221.

Song, Y., Seo, J.Y., Kim, H., Beak, K.Y., 2019. Structural control of cellulose nanofibrous composite membrane with metal organic framework (ZIF-8) for highly selective removal of cationic dye. Carbohydr. Polym. 222, 115018. https://doi.org/10.1016/j.carbpol.2019.115018.

Steffan, J.J., Brevik, E.C., Burgess, L.C., Cerdà, A., 2018. The effect of soil on human health: an overview. Eur. J. Soil Sci. 69, 159–171. https://doi.org/10.1111/ejss.12451.

Su, Z., Zhang, M., Lu, Z., Song, S., Zhao, Y., Hao, Y., 2018. Functionalization of cellulose fiber by in situ growth of zeolitic imidazolate framework-8 (ZIF-8) nanocrystals for preparing a cellulose-based air filter with gas adsorption ability. Cellulose 25, 1997–2008. https://doi.org/10.1007/s10570-018-1696-4.

Sun, P., Yang, S., Sun, X., Wang, Y., Pan, L., Wang, H., Wang, X., Guo, J., Nie, C., 2019. Functional porous carboxymethyl cellulose/cellulose acetate composite microspheres: preparation, characterization, and application in the effective removal of HCN from cigarette smoke. Polymers. https://doi.org/10.3390/polym11010181.

Sun, J., Cui, L., Gao, Y., He, Y., Liu, H., Huang, Z., 2021. Environmental application of magnetic cellulose derived from Pennisetum sinese Roxb for efficient tetracycline removal. Carbohydr. Polym. 251, 117004. https://doi.org/10.1016/j.carbpol.2020.117004.

Tang, R., Wang, Z., Muhammad, Y., Shi, H., Liu, K., Ji, J., Zhu, Y., Tong, Z., Zhang, H., 2021. Fabrication of carboxymethyl cellulose and chitosan modified magnetic alkaline ca-bentonite for the adsorption of hazardous doxycycline. Colloids Surf. A Physicochem. Eng. Asp. 610, 125730. https://doi.org/10.1016/j.colsurfa.2020.125730.

Tanzifi, M., Tavakkoli Yaraki, M., Beiramzadeh, Z., Heidarpoor Saremi, L., Najafifard, M., Moradi, H., Mansouri, M., Karami, M., Bazgir, H., 2020. Carboxymethyl cellulose improved adsorption capacity of polypyrrole/CMC composite nanoparticles for removal of reactive dyes: experimental optimization and DFT calculation. Chemosphere 255, 127052. https://doi.org/10.1016/j.chemosphere.2020.127052.

Tshikovhi, A., Mishra, S.B., Mishra, A.K., 2020. Nanocellulose-based composites for the removal of contaminants from wastewater. Int. J. Biol. Macromol. 152, 616–632. https://doi.org/10.1016/j.ijbiomac.2020.02.221.

Ul-Islam, M., Wajid Ullah, M., Khan, S., Kamal, T., Ul-Islam, S., Shah, N., Kon Park, J., 2016. Recent advancement in cellulose based nanocomposite for addressing environmental challenges. Recent Pat. Nanotechnol. 10, 169–180.

Wang, Z., Song, L., Wang, Y., Zhang, X.-F., Hao, D., Feng, Y., Yao, J., 2019. Lightweight UiO-66/cellulose aerogels constructed through self-crosslinking strategy for adsorption applications. Chem. Eng. J. 371, 138–144. https://doi.org/10.1016/j.cej.2019.04.022.

Wang, W., Ni, J., Chen, L., Ai, Z., Zhao, Y., Song, S., 2020a. Synthesis of carboxymethyl cellulose-chitosan-montmorillonite nanosheets composite hydrogel for dye effluent remediation. Int. J. Biol. Macromol. 165, 1–10. https://doi.org/10.1016/j.ijbiomac.2020.09.154.

Wang, L., Yang, C., Lu, A., Liu, S., Pei, Y., Luo, X., 2020b. An easy and unique design strategy for insoluble humic acid/cellulose nanocomposite beads with highly enhanced adsorption performance of low concentration ciprofloxacin in water. Bioresour. Technol. 302, 122812. https://doi.org/10.1016/j.biortech.2020.122812.

Xie, H., Pan, Y., Xiao, H., Liu, H., 2019. Preparation and characterization of amphoteric cellulose–montmorillonite composite beads with a controllable porous structure. J. Appl. Polym. Sci. 136, 47941. https://doi.org/10.1002/app.47941.

Xiong, Y., Dang, B., Wang, C., Wang, H., Zhang, S., Sun, Q., Xu, X., 2017. Cellulose fibers constructed convenient recyclable 3D graphene-formicary-like δ-Bi2O3 aerogels for the selective capture of iodide. ACS Appl. Mater. Interfaces 9, 20554–20560. https://doi.org/10.1021/acsami.7b03516.

Xiong, Y., Wang, C., Wang, H., Jin, C., Sun, Q., Xu, X., 2018. Nano-cellulose hydrogel coated flexible titanate-bismuth oxide membrane for trinity synergistic treatment of super-intricate anion/cation/oily-water. Chem. Eng. J. 337, 143–151. https://doi.org/10.1016/j.cej.2017.12.080.

Xiong, J., Zhang, D., Lin, H., Chen, Y., 2020. Amphiprotic cellulose mediated graphene oxide magnetic aerogels for water remediation. Chem. Eng. J. 400, 125890. https://doi.org/10.1016/j.cej.2020.125890.

Xu, Q., Peng, J., Zhang, W., Wang, X., Lou, T., 2020. Electrospun cellulose acetate/P (DMDAAC-AM) nanofibrous membranes for dye adsorption. J. Appl. Polym. Sci. 137, 48565. https://doi.org/10.1002/app.48565.

Yadav, A., Rene, E.R., Mandal, M.K., Dubey, K.K., 2021. Threat and sustainable technological solution for antineoplastic drugs pollution: review on a persisting global issue. Chemosphere 263, 128285. https://doi.org/10.1016/j.chemosphere.2020.128285.

Yang, J., Ma, C., Tao, J., Li, J., Du, K., Wei, Z., Chen, C., Wang, Z., Zhao, C., Ma, M., 2020a. Optimization of polyvinylamine-modified nanocellulose for chlorpyrifos adsorption by central composite design. Carbohydr. Polym. 245, 116542. https://doi.org/10.1016/j.carbpol.2020.116542.

Yang, C., Wang, L., Yu, Y., Wu, P., Wang, F., Liu, S., Luo, X., 2020b. Highly efficient removal of amoxicillin from water by Mg-Al layered double hydroxide/cellulose nanocomposite beads synthesized through in-situ coprecipitation method. Int. J. Biol. Macromol. 149, 93–100. https://doi.org/10.1016/j.ijbiomac.2020.01.096.

Yao, M., Wang, Z., Liu, Y., Yang, G., Chen, J., 2019. Preparation of dialdehyde cellulose graftead graphene oxide composite and its adsorption behavior for heavy metals from aqueous solution. Carbohydr. Polym. 212, 345–351. https://doi.org/10.1016/j.carbpol.2019.02.052.

Zaman, A., Orasugh, J.T., Banerjee, P., Dutta, S., Ali, M.S., Das, D., Bhattacharya, A., Chattopadhyay, D., 2020. Facile one-pot in-situ synthesis of novel graphene oxide-cellulose nanocomposite for enhanced azo dye adsorption at optimized conditions. Carbohydr. Polym. 246, 116661. https://doi.org/10.1016/j.carbpol.2020.116661.

Zare, E.N., Lakouraj, M.M., Kasirian, N., 2018a. Development of effective nano-biosorbent based on poly m-phenylenediamine grafted dextrin for removal of Pb (II) and methylene blue from water. Carbohydr. Polym. 201, 539–548.

Zare, E.N., Lakouraj, M.M., Masoumi, M., 2018b. Efficient removal of Pb (II) and Cd (II) from water by cross-linked poly (N-vinylpyrrolidone-co-maleic anhydride)@ eggshell/Fe3O4 environmentally friendly nano. Desalin. Water Treat. 106, 209–219. https://doi.org/10.5004/dwt.2018.22104.

Zawisza, B., Sitko, R., Queralt, I., Margui, E., Gagor, A., 2020. Cellulose mini-membranes modified with TiO_2 for separation, determination, and speciation of arsenates and selenites. Microchim. Acta 187, 430. https://doi.org/10.1007/s00604-020-04387-4.

Zhang, Q., Li, Q., Young, T.M., Harper, D.P., Wang, S., 2019a. A novel method for fabricating an electrospun poly(vinyl alcohol)/cellulose nanocrystals composite nanofibrous filter with low air resistance for high-efficiency filtration of particulate matter. ACS Sustain. Chem. Eng. 7, 8706–8714. https://doi.org/10.1021/acssuschemeng.9b00605.

Zhang, L., Wang, Z., Xu, X., Chen, C., Gao, B., Xiao, X., 2019b. Insights into the phosphate adsorption behavior onto 3D self-assembled cellulose/graphene hybrid nanomaterials embedded with bimetallic hydroxides. Sci. Total Environ. 653, 897–907. https://doi.org/10.1016/j.scitotenv.2018.11.030.

Zhang, D., Xu, Y., Li, X., Liu, Z., Wang, L., Lu, C., He, X., Ma, Y., Zou, D., 2020. Immobilization of Cr(VI) in soil using a montmorillonite-supported carboxymethyl cellulose-stabilized Iron sulfide composite: effectiveness and biotoxicity assessment. Int. J. Environ. Res. Public Health. https://doi.org/10.3390/ijerph17176087.

Zhao, X., Chen, L., Guo, Y., Ma, X., Li, Z., Ying, W., Peng, X., 2019a. Porous cellulose nanofiber stringed HKUST-1 polyhedron membrane for air purification. Appl. Mater. Today 14, 96–101. https://doi.org/10.1016/j.apmt.2018.11.012.

Zhao, L., Yang, S., Yilihamu, A., Ma, Q., Shi, M., Ouyang, B., Zhang, Q., Guan, X., Yang, S.-T., 2019b. Adsorptive decontamination of Cu2+-contaminated water and soil by carboxylated graphene oxide/chitosan/cellulose composite beads. Environ. Res. 179, 108779. https://doi.org/10.1016/j.envres.2019.108779.

Zhu, M., Cao, Q., Liu, B., Guo, H., Wang, X., Han, Y., Sun, G., Li, Y., Zhou, J., 2020. A novel cellulose acetate/poly (ionic liquid) composite air filter. Cellulose 27, 3889–3902. https://doi.org/10.1007/s10570-020-03034-8.

Zong, P., Cao, D., Cheng, Y., Wang, S., Zhang, J., Guo, Z., Hayat, T., Alharbi, N.S., He, C., 2019. Carboxymethyl cellulose supported magnetic graphene oxide composites by plasma induced technique and their highly efficient removal of uranium ions. Cellulose 26, 4039–4060. https://doi.org/10.1007/s10570-019-02358-4.

Zou, Y., Wang, X., Khan, A., Wang, P., Liu, Y., Alsaedi, A., Hayat, T., Wang, X., 2016. Environmental remediation and application of nanoscale zero-valent iron and its composites for the removal of heavy metal ions: a review. Environ. Sci. Technol. 50, 7290–7304.

CHAPTER

16

Modification and derivatization of cellulose-based nanobiosorbents and their utilization in environmental remediation

Sajjad Ullah[a], *Elias Paiva Ferreira-Neto*[b], *Saima Sohni*[a], *Akbar Ali*[c], *and Rashida Parveen*[d]

[a]Institute of Chemical Sciences, University of Peshawar, Peshawar, Pakistan [b]Institute of Chemistry-São Paulo State University (UNESP), Araraquara, Brazil [c]Government College University Faisalabad, Faisalabad, Pakistan [d]Government Girls Degree College Dabgari, Peshawar, Pakistan

16.1 Cellulose-based nanomaterials as biosorbents

Environmental pollution is one of the most serious problems associated with the rapid pace of industrialization and explosive growth in the world population. Trends toward environmental sustainability perspective have augmented the interests of researchers in exploring the low-cost bio-based materials of various origins (Sohni et al., 2019). Specifically, the ever increasing problem of water pollution demands for the development of sustainable solutions employing low-cost and environmental safe materials. Among the bio-based materials, cellulose, a natural, renewable, and most abundant polymer has been a subject of incredible interest as a versatile, ageless, and attractive material for a wide array of applications in various fields such as textiles, packaging, energy, drug delivery, tissue engineering, and wastewater treatment. The widespread use and incredibly vast potential of nanocellulose for various applications can be attributed to its excellent physical, mechanical, and chemical properties, as well as tailorable surface chemistry (Reshmy et al., 2020). Moreover,

https://doi.org/10.1016/B978-0-323-90912-9.00016-2

nanocellulose offers easy surface modification with a broad range of functional group and the possibility of blending it with other materials to make efficient composite adsorbents for enhanced removal of pollutants. Research on the development of different materials derived from cellulose such as hydrogels (Zhao et al., 2016), aerogels (Feng et al., 2015), cellulose composites (Zhang et al., 2015; Ferreira-Neto et al., 2020), functionalized cellulose, and nanocellulose (Mandal and Chakrabarty, 2011) has steadily intensified.

Over two decades now, the production of various kinds of innovative cellulose nanomaterials has gained momentum for a spectrum of downstream utilizations. Nanocellulose and/or its derivatives (hydrogels, composites, and beads) have demonstrated tremendous potential in environmental remediation, for example, by adsorbing various contaminants (heavy metals, organic dyes, oils, and pharmaceuticals) from effluents. In the light of the aforesaid perspective, this chapter is set to highlight the prospects of various cellulose-based nanomaterials, both in pristine and modified form, in the removal of pollutants such as dyes, phenols, and heavy metal ions from wastewater.

16.1.1 Structural properties of cellulose

Cellulose is a linear, semicrystalline polysaccharide and the macromolecules of natural cellulose may include 1000–30,000 elementary units. In the case of wood and cotton, the degree of polymerization (DP) is around 10,000 and 15,000 glucose units, respectively (Peng et al., 2020). The origin of the hierarchical architecture of cellulose is due to the fact that linear macromolecules are joined by hydrogen bonding, thus constituting a supramolecular structure of elementary nanofibrils and their bundles (called microfibrils) in turn form layers of the cell wall of cellulose fibers (Ioelovich, 2017). Chemically, it is a linear homopolymer composed of several hundreds to thousands of linked glucose monomers as shown in Fig. 16.1. These monomers are linked by hydrogen bonding with the hemicellulose component of the lignocellulosic biomass. The arrangement of cellulose fibrils gives rise to two regions, namely, crystalline and amorphous regions (Fig. 16.1A) where the length of the crystalline domains may range from 50 to 150 nm while that of the amorphous region may vary between 25 and 50 nm (Johar et al., 2012). The cellulose fibrils furnish an ordered crystalline structure held via. Van der Waals forces and intermolecular and intra-molecular hydrogen bonding. On the other hand, the breakage and disruption of hydrogen bonds give rise to amorphous regions (Sohni et al., 2018; Liu et al., 2019a).

16.1.2 Classification of nanocellulose

Nanocellulose is a term for a range of materials with at least one dimension, either diameter or length, in the nanoscale domain (1–100 nm) and are broadly classified into three categories, namely cellulose nanofibrils (CNFs), cellulose nanocrystals (CNCs), and bacterial nanocellulose (BNC or BC). Although this family of nanocellulose materials shows chemical composition similar to normal cellulose, they differ in morphology, structure, and crystallinity. This, in principle, can be attributed to their origin and production method. Both CNFs and CNCs are derived from lignocellulosic biomass, a highly heterogeneous material containing cellulose (40%–80%), hemicellulose (15%–30%), and lignin (10%–25%) as its fundamental

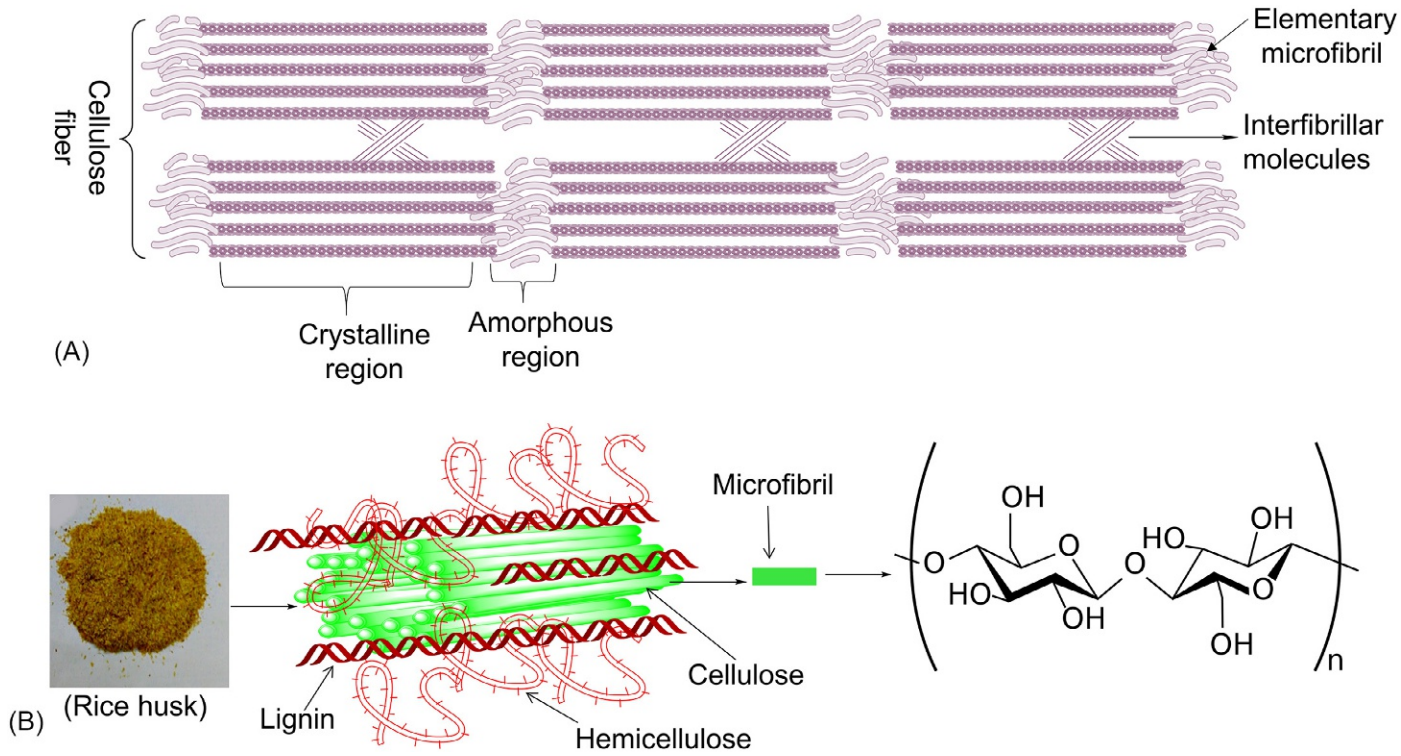

FIG. 16.1 (A) Ordered crystalline and disordered amorphous domains of cellulose and (B) basic components of lignocellulosic biomass showing the structure of cellulose surrounded by hemicellulose and lignin.

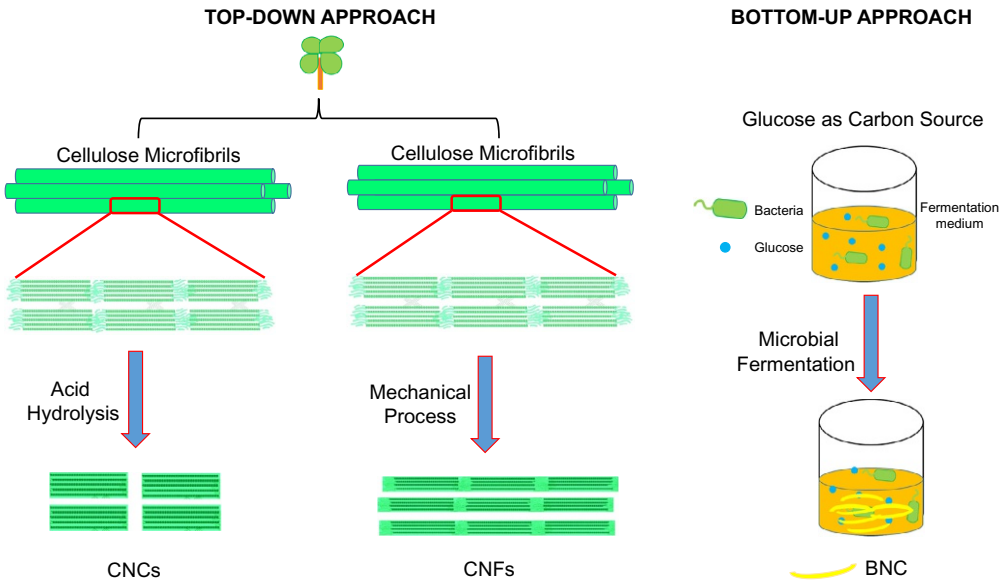

FIG. 16.2 Production of nanocellulose via. Top–down and Bottom–up approach.

constituents (Fig. 16.1B). The CNFs (also known as nanofibrillated cellulose, cellulose microfibril, microfibrillated cellulose, or nanofibrillar cellulose (Saba et al., 2017) consist of nanosized thin and micrometer-long fibril shaped flexible nanocellulose with diameter and length of 1–100 nm and 500–2000 nm, respectively (Li et al., 2014). The CNFs are characterized by both crystalline and amorphous domains (Nagano et al., 2020). This material is extracted from cellulose fibrils of lignocellulosic biomass by mechanical disintegration (Fig. 16.2). This can be accomplished by high-pressure homogenization, microfluidization or by high-intensity mechanical grinding.

On the other hand, CNCs, also called cellulose nanowhiskers, are short-needle, rod-like, or whisker-shaped structures that are 2–20 nm in diameter and 80–500 nm in length (Mu et al., 2019). An important characteristic related to CNCs is that, unlike CNFs, these are predominantly crystalline, while the amorphous regions are selectively removed by controlled acid treatment using hydrochloric or sulfuric acid (Fig. 16.2). Bacterial nanocellulose (BNC) is made of cellulose entangled nanoribbons of around 20–50 nm diameter and is produced by certain types of bacteria (Komagataeibacter Xylinus, for instance) via biosynthesis involving polymerization of sugars or alcohols for a few days up to 2 weeks. An important feature related to BNC is that compared to cellulose of plant origin, it is pure and devoid of any lignin, pectin, and hemicellulose residues in its composition (Fu et al., 2013). Moreover, the ultra-fine structure of BNC possesses a much higher crystallinity index, higher liquid absorption capacity, higher degree of polymerization, higher specific surface area, and excellent mechanical properties (Abol-Fotouh et al., 2020). In addition, greater ease for surface functionalization renders BNC a much superior material as compared to plant-based cellulose (Ferreira-Neto et al., 2020; Ullah et al., 2016).

16.1.3 Production of nanocellulose

Broadly speaking, there are two ways in which nanocellulose can be obtained, viz. top–down and bottom–up approach, as summarized in Fig. 16.2. In the case of the former, nanocellulose is derived from the naturally occurring sources of cellulose such as annual plants, field and agro-industrial residues as well as sea plants. As mentioned earlier, cellulose as fundamental constituent of lignocellulosic biomass residues is a promising resource of nanocellulose because these are the most abundant, carbon-neutral, and low-cost materials with no food vs. fuel competition (Sohni et al., 2018). A typical strategy to extract nanocellulose using top-down approach encompasses (i) pulping and pre-treatment step to transform the macrofibres into microfibers by mechanical disruption and for partially or completely removing lignin and hemicellulose, (ii) disintegrating and removing the amorphous portions by chemicals (acids, oxidizing agents) or *via* enzymatic hydrolysis route, and (iii) mechanical fibrillation process to converts the microfibers into nanocellulose (CNF) using high-pressure homogenizer (Amiralian et al., 2017). On the other hand, nanocellulose can be directly produced as nanofibers by the fermentation of low molecular weight sugars or alcohols by cellulose-producing bacteria in the bottom–up approach (Fig. 16.2). The nanocellulose biosynthesized this way by bacteria is more commonly referred to as BNC or BC (Kousheh et al., 2020).

16.1.4 Advantages of nanocellulose as biosorbents

The widespread applications of nanocellulose can be attributed to the fact that cellulose possesses outstanding hydrophilicity, high mechanical performance, and the possibility of functionalization. In general, an ideal material intended as an adsorptive platform should fulfill certain criteria: (i) good mechanical and structural integrity to withstand water flow over an extended period, (ii) low cost, (iii) excellent adsorption capacity to remove pollutants, (iv) large surface area, and (v) easy recovery and the possibility of reuse without significant loss of adsorption capacity (Mahfoudhi and Boufi, 2017). Cellulose, especially after certain modifications discussed below, meets most of these criteria and thus has been widely used for the adsorptive removal of various pollutants from aqueous media. The salient features of nanocellulose which were responsible for gathering a great deal of scientific attention in recent years have been summarized in Table 16.1. Nanocellulose-based materials are essentially carbon-neutral, renewable, non-hazardous, and biodegradable. Their excellent surface reactivity, strong mechanical properties, and regeneration ability make nanocellulose a new class of useful nanomaterials for high valued valorization, particularly in the field of environmental remediation. This is why nanocellulose-based materials have become the focus of much consideration and their modification has gained prominence to further improve the properties of these materials (Ferreira-Neto et al., 2020; Tavakolian et al., 2020; Liu et al., 2019b).

16.1.5 Limitations of nanocellulose production

There are significant scientific and technological challenges to tackle to make the overall production of nanocellulose more competitive and to realize possible scale-up. The production of nanocellulose is a multi-step, time-consuming, chemical as well as energy-intensive process. In addition, the recovery or reuse of chemicals is also a big challenge (Liu et al., 2016; Li et al., 2018). To deal with these problems, researchers have focused on the recovery

TABLE 16.1 Properties of nanocellulose as an adsorptive platform in wastewater treatment.

Attribute	Magnitude	Implication with regard to adsorption	References
Specific surface area	High, 299 m^2/g	Enhanced adsorption	Zu et al. (2016)
Porosity	Highly porous hydrogels and aerogels	High permeability and adsorption	Zhu et al. (2018)
Aspect ratio	High, 144 ~ 410.1 for BC	Strong mechanical properties, strong and entangled networks	Amiralian et al. (2017) and Zhao et al. (2019)
Crystallinity	60–90% (72–80 in BNC)	Highly recalcitrant material, restricted solubility	Man et al. (2011) and Watanabe et al. (1998)
Mechanical strength	Elastic modules of 100–160 GPa	Increased mechanical stiffness	Kuo et al., (2017)
Surface modification	Greater possibility due to surface hydroxyl groups	Esterification, oxidation, etherification, addition, among other	Ávila Ramírez et al. (2017)
Stability	Very stable	Reduced biofouling and reusable	Bai et al. (2019) and Goetz et al. (2018)

of acid/acid mixtures/other solvents after the hydrolysis step to improve the sustainability of overall nanocellulose production process (Yu et al., 2019; Peretz et al., 2019). There has been a dire need to develop facile green alternative routes instead of consuming hazardous chemicals for preparing nanocellulose. For this purpose, eco-friendly approaches based on enzymatic methods have been put forward to produce nanocellulose but the process lacks efficiency (Ribeiro et al., 2019). In recent years, some reported studies for producing nanocellulose, for instance, by ultrasonication, electrospinning, ionic liquids, and deep eutectic solvents have shown great promise (Jordan et al., 2020; Ma et al., 2019). In the case of bottom-up approach for producing BNC, low productivity of the known strains and the use of fine and expensive culture medium constituents are the major challenges in BNC production (Skočaj, 2019). To deal with these drawbacks, biosynthesis of BNC using cheaper carbon sources has been proposed to make the overall process economically feasible (Abol-Fotouh et al., 2020; Ul-Islam et al., 2020; Zhao et al., 2018).

Moreover, although cellulose shows reasonably good adsorptive properties, the pollutants adsorption potential of pristine nanocellulose is not high enough to allow the removal of pollutants with the efficiency required for practical applications. To address this limitation, chemical modifications such as chemical grafting of chelating or metal-binding functionalities and/or charge-bearing functional groups on the cellulose backbone have been devised as a possible strategy to further enhance and tailor the adsorptive properties of cellulose for effective environmental remediation.

16.2 Molecular functionalization of cellulose-based materials

As thoroughly discussed, cellulose is the most abundant biopolymer with potential physiochemical properties to be used as an adsorbent for the removal of both organic and

inorganic pollutants from contaminated water (Mahfoudhi and Boufi, 2017; Faiz Norrrahim et al. 2021; Jamshaid et al., 2017). Yet, its adsorptive properties toward heavy metal ions can be tailored and further upgraded through chemical grafting of chelating or metal-binding functionalities on the cellulose backbone. For instance, improved adsorption of organics and heavy metals can be achieved via chemical modification of cellulose by incorporating the hydrophobic organic groups and sulfur-containing functionalities, respectively (Silva Filho et al., 2013; Santana et al., 2010; Yang et al., 2014). In addition to better adsorptive properties than pristine cellulose, chemically modified cellulose also shows other interesting properties such as resistance toward microbial growth and heat or mechanical stress, controlled hydrophobicity or hydrophilicity, and better elasticity (McDowall et al., 1984).

Fortunately, cellulose has abundant hydroxyl (–OH) functionalities at the C-2, C-3, and C-6 atoms of the anhydroglucose unit that make it easier for chemical modification employing various functional groups including (but not limited to) carboxylate (Zhang et al., 2016a; Zhou et al., 2013; Anirudhan et al., 2015; Vieira et al., 2010), carboxymethyl (Lin et al., 2015a; Zhang et al., 2011), amines (da Silva Filho et al., 2006; Jin et al., 2015), aminoethanethiol (Silva et al., 2013), phosphate (Oshima et al., 2011; Kokol et al., 2015; Bezerra et al., 2014; Suflet et al., 2006), and sulfur-containing groups including sulfides, thiol and sulfonic/sulfate functionalities (Silva Filho et al., 2013; Santana et al., 2010; Yang et al., 2014; Zhang et al., 2008; Suopajärvi et al., 2015; Lin and Dufresne, 2014; Thiangtham et al., 2019) (Scheme 16.1). These chemical modifications allow tailoring the cellulose-adsorbate interactions to enhance the cellulose adsorptive capability of removing from aqueous media a variety of pollutants such as heavy metals, organic dyes, and pharmaceuticals. It is important to mention that due to the comparatively high reactivity of the hydroxyl group at the C6 position (encircled in Scheme 16.1) (Oshima et al., 2008), it is more susceptible to chemical modification. This chemical modification also allows further and better incorporation of functional components such as cationic and anionic surfactants or organo(chloro)silanes with long hydrocarbon chains that render the cellulose substrate hydrophobic character which plays important role in the capture of organic molecules including oils and pesticides from aqueous media (Zhang et al., 2014a; Aloulou et al., 2004a, b, c; Gong et al., 2019; Salajková et al., 2012; Boufi and Belgacem, 2006; Alila and Boufi, 2009; Alila et al., 2007, 2010; Lin et al., 2015b; Zhao et al., 2020).

It is well known that the adsorption capacity of materials strongly depends on the pH of the media which affects the adsorbents' surface charge, the degree of ionization, and the adsorbate species existing in solution (Santana et al., 2010). The adsorbent materials get a positive or negative surface charge at $pH < pH_{PZC}$ and $pH > pH_{PZC}$, respectively, where pH_{PZC} refers to the pH corresponding to the point of zero charge (PZC) at which (pH) the net charge on absorbent's surface is equal to zero. The optimum pH for metal adsorption on cellulose modified with anionic functional groups lies in the 4.0–6.0 pH range. In too acidic conditions ($pH < 4$), the functional group is protonated and hence cannot adsorb the metal cations effectively. On the other hand, in too basic media, the metal ions tend to precipitate out as metal hydroxides (Zhu et al., 2017).

The cellulose substrate-adsorbate interaction responsible for the adsorption of adsorbate can be purely electrostatic (carboxylated cellulose–cationic dye) (Yan et al., 2011) or based on complexation or ion-exchange (carboxylated cellulose–M^{2+} interaction) (Zhu et al., 2017; de Melo et al., 2009) (see Fig. 16.3) and may occasionally follow multiple mechanisms, simultaneously. For example, the sorption of methylene blue (MB), a cationic dye on carboxymethyl cellulose has been reported to involve electrostatic interaction (Yan et al.,

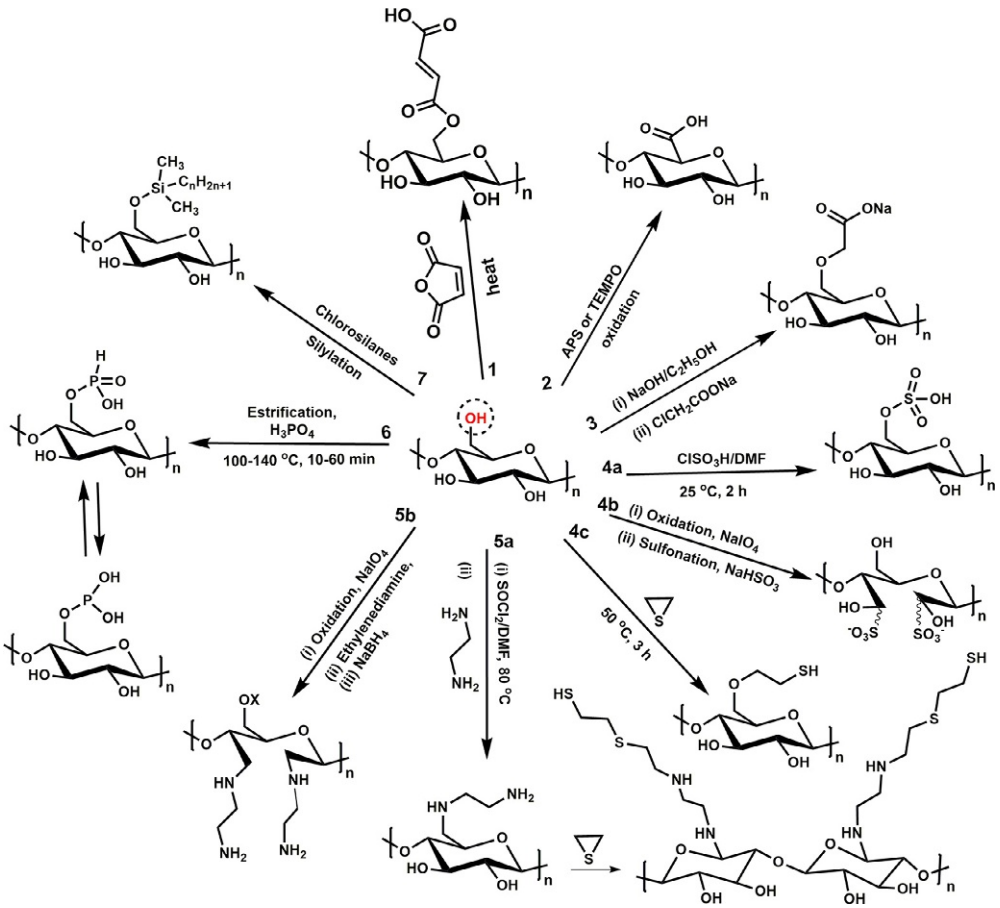

SCHEME 16.1 Various synthetic approaches for the chemical modification of cellulose.

2011) (Fig. 16.3A). Similarly, amino-functionalized cellulose has been used as an adsorbent for anionic dyes (Jin et al., 2015). Another example is the adsorption of anionic dyes on the surface of cationic cellulose nanocrystals-modified inorganic foam (Selkälä et al., 2020). Other substrate-adsorbate interactions such as ion-exchange, microprecipitation, chelation, and/or their combination can also be present. When more than one type of active functional groups are present in the adsorbent, the chances are higher that a multifaceted cooperative mechanism may be operative (Suopajärvi et al., 2015).

Here we focus on the main chemical modifications in cellulose, with particular emphasis on hydrophobic modifications for organics capture and sulfur-based functionalization for heavy metal capture from aqueous media. As shown in Scheme 16.1, most of the chemical modifications in cellulose are based on the introduction of some anionic group (carboxylate or phosphate, for instance) that under certain optimum pH (often moderately basic or slightly acidic pH) carry a negative charge and can capture metal cations ($M^{n+} = Pb^{2+}$, Cu^{2+}, Ag^{+},

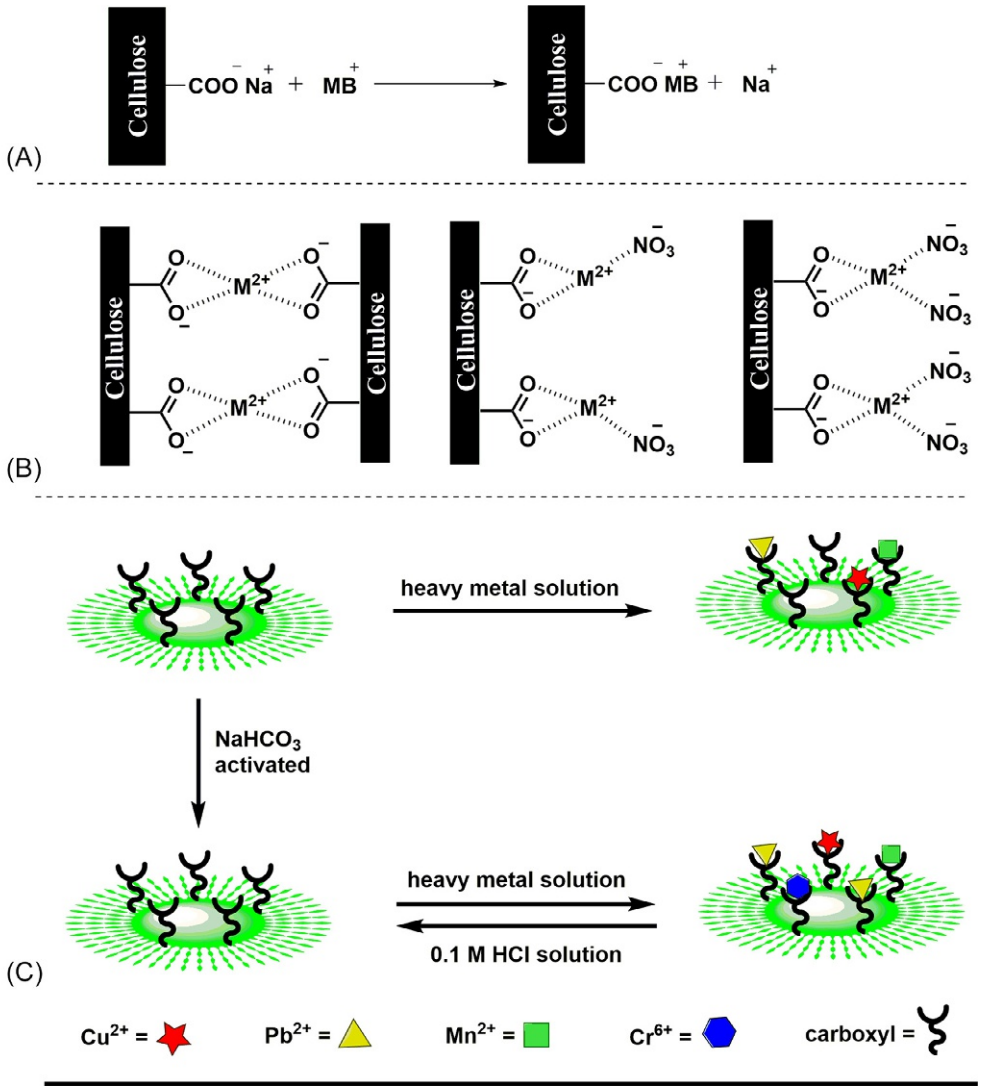

FIG. 16.3 Possible adsorption mechanisms on carboxylated cellulose: (A) ion-exchange mechanism and electrostatic interaction between the $-COO^-$ group and cationic methylene blue dye; (B) complexation/chelation of divalent metal ions (M^{2+}) by the carboxylate group with the three possible structures of the resulting complex; and (C) activation of the carboxylated cellulose by treatment with $NaHCO_3$ to convert the –COOH to –COONa, where the Na^+ in the later can be easily exchanged with the heavy metal ions more easily as compared to H^+ ions in the former. *Panel A: Adapted from Yan, H., Zhang, W., Kan, X., Dong, L., Jiang, Z., Li, H., Yang, H., Cheng, R., 2011. Sorption of methylene blue by carboxymethyl cellulose and reuse process in a secondary sorption. Colloids Surf. A Physicochem. Eng. Asp. 380, 143–151. https://doi.org/10.1016/j.colsurfa.2011.02.045 with permission from Elsevier; panel B: de Melo, J.C.P., da Silva Filho, E.C., Santana, S.A.A., Airoldi, C., 2009. Maleic anhydride incorporated onto cellulose and thermodynamics of cation-exchange process at the solid/liquid interface. Colloids Surf. A Physicochem. Eng. Asp. 346, 138–145. https://doi.org/10.1016/j.colsurfa.2009.06.006 with permission from Elsevier; panel C: Zhu, Q., Wang, Y., Li, M., Liu, K., Hu, C., Yan, K., Sun, G., Wang, D., 2017. Activable carboxylic acid functionalized crystalline nanocellulose/PVA-co-PE composite nanofibrous membrane with enhanced adsorption for heavy metal ions. Sep. Purif. Technol. 186, 70–77. https://doi.org/10.1016/j.seppur.2017.05.050 with permission from Elsevier.*

Fe^{3+}, Cd^{2+}, Zn^{2+}, Ni^{2+}, Co^{2+}, Sr^{2+} including lanthanides (La^{3+}, Sm^{3+}, Ho^{3+}, Nd^{3+}, Er^{3+}) cations (Silva Filho et al., 2013; Vieira et al., 2010; da Silva Filho et al., 2006; Suopajärvi et al., 2015; Oshima et al., 2008; Liu et al., 2015; Zhang et al., 2016b)) as well as cationic organic molecules such as dyes (Zhou et al., 2013; Jin et al., 2015; Yan et al., 2011; Zhang et al., 2014b; Annadurai et al., 2002) (see Table 16.2).

The main chemical methods used for the modification of cellulose include esterifications, halogenations, etherification, oxidation, and grafting. A brief account of some of these modifications is presented below.

TABLE 16.2 Main chemical modifications in cellulose and their performance in the removal of different pollutants.

Functionalized cellulose	Adsorbate/pollutant	Adsorption or absorption capacity	References
Phosphorylated CNC	Ag(I), Cu(II), and Fe(III)	Ag(I) 136 mg g^{-1} Cu(II) 117 mg g^{-1} Fe(III) 115 mg g^{-1}	Liu et al. (2015)
Phosphorylated BNC	Transition metal and lanthanides ions	La(III) 116.7 mmol g^{-1}	Oshima et al. (2008)
Phosphorylated microcrystalline cellulose	Ranitidine drug	85.7 mg g^{-1}	Bezerra et al. (2014)
Sulfonated CNF	Pb(II)	248.6 mg g^{-1}	Suopajärvi et al. (2015)
Sulfonated CNF	Cu(II) and Pb(II)	Cu(II) 158.9 mg g^{-1} Pb(II) 331.5 mg g^{-1}	Sirviö and Visanko (2020)
Thiolated CNF membrane	Cd(II), Cu(II), and Pb(II)	Cd(II) 30.0 mg g^{-1} Cu(II) 39.6 mg g^{-1} Pb(II) 19.6 mg g^{-1}	Choi et al. (2020)
Xanthate (organosulfur) modified rice husk cellulose	Ni(II), Cd(II) and Pb(II)	Ni(II) 49.8 mg g^{-1} Cd(II) 133.8 mg g^{-1} Pb(II) 139.9 mg g^{-1}	Qu et al. (2020)
Ethylene sulfide modified biomass	Cu(II)	Cu(II) 39.2 mg g^{-1}	Santana et al. (2010)
Ethylene diamine modified microcrystalline cellulose	Cu(II), Co(II), Ni(II), and Zn(II)	Cu(II) 83.9 mg g^{-1} Co(II) 112.6 mg g^{-1} Ni(II) 63.4 mg g^{-1} Zn(II) 85.6 mg g^{-1}	da Silva Filho et al. (2006)
Ethylene sulfide aminated microcrystalline cellulose	Pb(II), Cd(II) Cu(II), Co(II), Ni(II), and Zn(II)	Pb(II) 1301.6 mg g^{-1} Cd(II) 650.0 mg g^{-1} Cu(II) 123.5 mg g^{-1} Co(II) 276.6 mg g^{-1} Ni(II) 326.4 mg g^{-1} Zn(II) 113.2 mg g^{-1}	Silva Filho et al. (2013)
Aminoethanothiol modified microcrystalline cellulose	Reactive Red dye	(pH 2) 78.0 mg g^{-1} (pH 9) 26.0 mg g^{-1}	Silva et al. (2013)

TABLE 16.2 Main chemical modifications in cellulose and their performance in the removal of different pollutants—cont'd

Functionalized cellulose	Adsorbate/pollutant	Adsorption or absorption capacity	References
Amino-functionalized CNC	Acid Red GR dye Congo Red 4BS dye Reactive Yellow K-4G dye	GR dye 137.1 mg g^{-1} 4BS dye 199.5 mg g^{-1} K-4G dye 78.0 mg g^{-1}	Jin et al. (2015)
Diethylenetriaminepentaacetic acid-modified microcrystalline cellulose	Hg(II)	476.2 mg g^{-1}	Li et al. (2019)
Carboxylated microcrystalline cellulose	Co(II) and Ni(II)	Co(II) 103.6 mg g^{-1} Ni(II) 140.8 mg g^{-1}	de Melo et al. (2009)
Carboxylated corn stalk cellulose	Nd(III)	351.8 mg g^{-1}	Wang et al. (2018)
Surfactant modified hydrophobic cellulose	Organics 2-naphtol Trichlorobenzene (TCB) Nitrobenzene (NB) Dichlorobenzene (DCB) Chlorobenzene (CB)	2-Naphtol 165.8 mg g^{-1} TCB 165.8 mg g^{-1} NB 159.7 mg g^{-1} DCB 73.5 mg g^{-1} CB 52.9 mg g^{-1}	Alila et al. (2007)
Silylated hydrophobic CNF aerogel	Dodecane and several organic solvents and oils	Dodecane 50 g g^{-1} Other organics 49–102 g g^{-1}	Zhang et al. (2014a)

16.2.1 Carboxylate-based modification

Carboxylate ($–COO^-$) is an important negatively charged functional group that has been widely used to modify cellulose and improve its adsorptive properties toward metal cation and cationic organic molecules (Zhou et al., 2013; Anirudhan et al., 2015; Lin et al., 2015a; Zhu et al., 2017; Yan et al., 2011; Qiao et al., 2015). As mentioned earlier, the mechanism of cationic species adsorption on carboxylated cellulose involves an electrostatic interaction between the carboxylate group attached to the cellulose structure and the cationic pollutants (such as MB) (Zhou et al., 2013; Yan et al., 2011; Qiao et al., 2015) or complexation and/or ion-exchange of the heavy metal cation by the carboxylate groups (Zhu et al., 2017; de Melo et al., 2009; Saito and Isogai, 2005) (Fig. 16.3A and B). The carboxylic acid-functionalized crystalline nanocellulose materials can be activated and their adsorption capacity improved by treatment with $NaHCO_3$ that converts the carboxyl group –COOH to carboxylate –COONa, as the Na^+ could exchange with the heavy metal ions more easily as compared to H^+ ions (Zhu et al., 2017) (Fig. 16.3C). Consequently, maximum adsorption capacity of heavy metal ion (471.55 mg/g for Pb^{2+}) could be achieved using activated 1,2,3,4-butanetetracarboxylic acid-modified cellulose, higher than that of nonactivated carboxylated cellulose. Desorption of the metal ions can also be achieved by decreasing the pH (treatment with acid solution), making the reuse of the absorbent more convenient through pH-controlled adsorption-

desorption cycles (Zhu et al., 2017; Zhang et al., 2016b). Similarly, desorption of organic dye molecules can be achieved by dispersing the dye-loaded adsorbent in some suitable organic solvent such as 50% ethanol solution and sonicating or stirring for sufficient time (Qiao et al., 2015).

Cellulose modification with a carboxyl group is usually achieved by reacting it with a carboxylic acid or its carboxylate salt or anhydride (Zhou et al., 2013; Anirudhan et al., 2015; Vieira et al., 2010; Qiao et al., 2015). The quasi solvent-free carboxylation of cellulose with acid anhydride (e.g., anhydrides of maleic, succinic, or phthalic acid) at high temperature involves the addition of pre-dried cellulose material to molten anhydride in a 1:10 ratio in a moisture proof reaction flask immersed in an oil or sand bath at 115 °C while being kept under magnetic stirring for 6 h or lesser (Vieira et al., 2010; de Melo et al., 2009). This acylation reaction with cyclic organic anhydrides is then stopped by the addition of dimethylacetamide (DMA). The solid is then separated by filtration with a sintered filter, washed in sequence with acetone and distilled water to remove the unreacted anhydride, DMA, and other by-products and dried at 80 °C for 12 h. Chemical modification of cellulose with maleic anhydride as a representative acid anhydride using this general procedure is shown in Scheme 16.1 (route 1) which allows up to 2.82 ± 0.05 mmol g^{-1} of maleic anhydride covalently bonded to the back bone structure (Vieira et al., 2010; de Melo et al., 2009). The carboxylated polysaccharides are able to adsorb cations from aqueous or aqueous-alcohol solutions (Vieira et al., 2010) with a maximum adsorption capacity of 1.75 ± 0.09 and 2.40 ± 0.12 mmol g^{-1} for Co^{2+} and Ni^{2+}, respectively (de Melo et al., 2009).

Another approach involves cellulose oxidation with suitable oxidizing agents such as 2,2,6,6-tetramethylpiperidinyl-1-oxy radical (TEMPO) or ammonium persulfate (APS) (Zhang et al., 2016a, 2016b) (Scheme 16.1, route 2). In the former case, pristine or acid-hydrolyzed cellulose is catalytically oxidized with TEMPO/NaBr/NaClO under aqueous conditions to introduce significant amounts of carboxylate groups on its surfaces without any changes in crystallinity of cellulose I or in the original fibrous morphology (Zhang et al., 2016a; Saito and Isogai, 2005). During this process, cellulose is suspended in water (750 mL) containing 0.25 g NaBr and 0.025 g TEMPO and the TEMPO-mediated oxidation of the cellulose slurry is started by adding sodium hypochlorite (NaClO) oxidant (2.42 mmol g^{-1} cellulose) at room temperature and 10.5 pH. After stirring the cellulose slurry for 2–5 h (with ultrasonication) or 24 h (without ultrasonication), the oxidation process is quenched by adding aqueous ethanol or methanol. The fibrous TEMPO-oxidized carboxylated cellulose (TO-CC) with a carboxyl content of 0.48 mmol g^{-1} is then washed with water by filtration and dried by freeze-drying (Saito and Isogai, 2005). Ultrasonic treatment may be employed to assist the oxidation reaction and achieve a higher degree of carboxylation (carboxyl content = 1.3–1.66 mmol g^{-1} cellulose) in a shorter time (Zhang et al., 2016a, 2016b; Qin et al., 2011). Alternatively, carboxylated CNCs can be prepared by a one-step APS oxidation where cellulose materials are hydrolyzed in 200 mL APS solution (1–2 mol L^{-1}) at 60 °C for 16 h. The resulting white suspension of APS-oxidized carboxylated cellulose (AO-CC) is washed with water using the repeated suspension-centrifugation protocol and then freeze-dried (Zhang et al., 2016a). The AO-CC containing carboxylate groups shows ion-exchange properties and can capture a variety of metal ions from aqueous solution with certain selectivity that follows the order $Pb^{2+} > La^{3+} > Al^{3+} > Cu^{2+} > Ba^{2+} > Ni^{2+} > Co^{2+} > Cd^{2+}$, Sr^{2+}, Mn^{2+}, $Ca^{2+} > Mg^{2+}$ (Saito and Isogai, 2005).

The freeze-dried TO-CC can be further modified by polyethyleneimine (PEI) grafting via glutaraldehyde crosslinking procedure to produce TO-CC-PEI adsorbent containing both carboxyl and amino group which possess better adsorption properties as compared to TO-CC (Zhang et al., 2016b). For instance, incorporation of PEI into TO-CC led to an increase in maximum Cu^{2+} adsorption capacity from 18.9 mg g^{-1} (TO-CC) to 52.32 mg g^{-1} (TO-CC-PEI). Similarly, the initial adsorption rate was higher (98.2 mg g^{-1} h^{-1}) for TO-CC-PEI as compared to TO-CC (61.0 mg g^{-1} h^{-1}) (Zhang et al., 2016b). The procedure for the preparation of TO-CC-PEI consists of adding 2 g of the TO-CC and 10 g PEI to 0.1 L methanol, stirring the mixture for 24 h, followed by centrifugation at 8000 rpm to remove the residual PEI. The precipitate obtained is dispersed in 100 mL water and 4 mL of glutaraldehyde solution (25%) is drop-wise added. After 1 h stirring at pH 8, cross-linking of TO-CC and PEI results in the formation of TO-CC-PEI adsorbent (Zhang et al., 2016b).

The incorporation of carboxymethyl groups (–CH_2–COOH) into cellulose backbone to produce carboxymethyl cellulose (CMC) is another interesting chemical modification that enhances the sorption properties of cellulose-based materials toward cationic pollutants species and organic molecules (Lin et al., 2015a; Yan et al., 2011; Chen et al., 2009). For instance, the ion-exchange based sorption capacity toward MB increases from 50 mg g^{-1} for unmodified cellulose to more than 300 mg g^{-1} for the CMC, with the most favorable sorption of MB observed under basic conditions (Yan et al., 2011). Interestingly, the MB-adsorbed CMC (CMC-MB used sample) can be re-used as a new sorbent and employed for the removal of methyl orange (MO) in a second sorption process under neutral or alkaline conditions. The sorption of MO on CMC-MB is due to an electrostatic interaction between MO and CMC-MB, with a maximum MO uptake of over 100 mg g^{-1} (Yan et al., 2011). The gel adsorbents based on CMC exhibit ion-exchange properties and can be employed to efficiently remove metal cations (108.7 mg $(Sr^{2+})g^{-1}$), often through control of pH and ionic strength during the ion-exchange process where the adsorption capacity increases with increasing pH and decreasing ionic strength. Desorption of the adsorbed Sr^{2+} ions is achieved by immersing the adsorbents in an acidic solution or solution of high ionic strength or heating the adsorbents in a hot moist environment (Wang et al., 2009). Similarly, carboxymethyl modified bacterial nanocellulose (CM-BNC) efficiently adsorbs protein molecules (bovine serum albumin) at pH lower than the pH_{PZC} (4.5–6.0) of the protein, where the adsorbed quantity increases with the increase in the degree of substation (DS) (Lin et al., 2015a). Studies of adsorption of metal cations have also indicated an improved performance of CM-BNC than pristine BNC at optimized pH 4.5, with the value of 9.67 mg(Cu) g^{-1} and 22.56 mg(Pb) g^{-1} for pristine BC and 12.63 mg(Cu) g^{-1} and 60.42 mg(Pb) g^{-1} for CM-BNC, respectively (Chen et al., 2009).

A two-step procedure is usually adopted for the carboxymethylation of cellulose by the alkali-catalyzed reaction of cellulose with chloroacetic acid (Lin et al., 2015a; Zhang et al., 2011; Yan et al., 2011), with a degree of substitution of 0.76 (Scheme 16.1, route 3). The first step is alkalinization (reaction 16.1 below) where cellulose is added to an ethanol-aqueous sodium hydroxide mixed solvent, followed by the etherification step (reaction 16.2) in which sodium chloroacetate is added to the mixture to react at 80 °C for 2.5 h to produce carboxymethyl group incorporated cellulose (Zhang et al., 2011; Yan et al., 2011). Microwave heating can shorten the processing time from several hours to few minutes and increase the degree of substitution (Zhang et al., 2011).

$$\left[C_6H_7O_2(OH)_3\right]_n + n\text{NaOH} \rightarrow \left[C_6H_7O_2(OH)_2ONa\right]_n + nH_2O \quad (16.1)$$

$$\left[C_6H_7O_2(OH)_2ONa\right]_n + n\text{ClCH}_2\text{COONa} \rightarrow \left[C_6H_7O_2(OH)_2OCH_2COONa\right]_n + \text{nNaCl} \quad (16.2)$$

Before the preparation of CMC, the plant material is often pre-treated to remove hemicellulose (by acid hydrolysis) and lignin (by thermo-mechanical treatment, ozone decomposition, or the sulfite process).

16.2.2 Sulfur-based modification

Many studies have reported the modification of cellulose with sulfur-containing groups including sulfides, thiol, and sulfonic/sulfate functionalities (Silva Filho et al., 2013; Santana et al., 2010; Zhang et al., 2008; Suopajärvi et al., 2015; Lin and Dufresne, 2014; Thiangtham et al., 2019) to improve the adsorption properties of cellulose. The covalent incorporation of negatively charged surface sulfate groups into CNCs is a chemical modification which significantly enhances the adsorptive properties of cellulose toward cationic species (Suopajärvi et al., 2015; Liu et al., 2020; Sirviö and Visanko, 2020). For instance, commercial mixed cellulose ester membranes modified with sulfated nanocrystalline cellulose have been found to efficiently remove the cationic antibiotic molecules (tetracycline hydrochloride containing protonated amine) from aqueous media due to electrostatic interaction (Liu et al., 2020). Likewise, lignin-rich sulfated wood CNFs have been studied as high-performing adsorbents for the removal of lead and copper from water, exhibiting a maximum adsorption capacity 2.50 and 1.60 mmol g^{-1} for Cu and Pb, respectively (Sirviö and Visanko, 2020). In addition to their excellent adsorptive properties, cellulose sulfates also exhibit other important characteristics such as improved solubility, rheological behavior, thermo reversible gel formation, enzymatic degradability as well as anticoagulant and antiviral activity (Hettrich et al., 2008).

Many routes have been developed to prepare sulfonated/sulfated cellulose using different sulfating agents such as chlorosulfuric acid ($ClSO_3H$), amidosulfuric acid (NH_2SO_3H), sulfur trioxide DMF-complex (SO_3 – DMF), sulfuric acid (H_2SO_4) and sulfuryl chloride (SO_2Cl_2) (Zhang et al., 2008; Suopajärvi et al., 2015; Lin and Dufresne, 2014; Liu et al., 2020; Hettrich et al., 2008; Sirviö et al., 2019). For example, sulfated cellulose can be prepared using chlorosulfonic acid ($ClSO_3H$) in anhydrous DMF as a sulfation agent (Lin and Dufresne, 2014) (see Scheme 16.1, route 4a). Moreover, desulfation and/or control of sulfation degrees can also be achieved in a basic medium using different concentrations of alkaline (NaOH) solution as a desulfation agent.

Sulfated CNCs have also been prepared by sulfuric acid-hydrolysis of microcrystalline cellulose under ultrasonic conditions (Liu et al., 2020). This process includes an esterification reaction between acid and cellulose molecules, which induces the covalent coupling of sulfate groups on the surface of prepared CNCs (Lin and Dufresne, 2014). Recently, deep eutectic solvent (prepared by heating sulfamic acid and urea together at 80 °C) has been employed both as solvent and sulfation reagent without any external solvent (Sirviö and Visanko, 2020; Sirviö et al., 2019). This process, however, also leads to the carbamation of cellulose to some extent as a side-reaction due to the presence of urea in the reaction mixture.

Acetosulfation of cellulose is another quasi-homogeneous synthesis approach to prepare regioselectively C6 substituted cellulose sulfates (Hettrich et al., 2008). The process consists of acetosulfation followed by deacetylation in a polar aprotic solvent such *N*, *N*-dimethylacetamide (DMAC) or *N*,*N*-dimethylformamide (DMF). For instance, the cellulose suspended in DMF is reacted with a mixture of sulfating (chlorosulfonic acid or H_2SO_4) and acetylating (acetic acid anhydride (Ac_2O) or acetyl chloride (CH_3COCl)) agents to form cellulose acetate sulfates. After precipitation of the polymer, the acetyl groups are cleaved in alkaline solution to obtain water-soluble cellulose sulfate (degree of substitution > 0.25), with the sulfate group preferentially present at the C6 position (Hettrich et al., 2008).

Alternatively, sulfonated cellulose with higher water retention values can also be prepared using an oxidation/sulfonation protocol where sodium periodate ($NaIO_4$) is used to oxidize cellulose in dark at pH 4 and 38 °C to yield the 2,3-dialdehyde products. The resulting dialdehyde cellulose is subsequently treated with aqueous sodium bisulfite ($NaHSO_3$) for 2 h at 22 °C to yield the corresponding C2/3 sulfonates (Zhang et al., 2008; Suopajärvi et al., 2015) (see Scheme 16.1, route 4b). Such sulfonated nanofibrillar cellulose material, containing the negatively charged deprotonated sulfonic binding sites at pH > 4 and exhibiting negative zeta potential values (−66.7 mV) (Liu et al., 2020), shows enhanced adsorption capacity toward heavy metal ions (1.2 mmol/g for Pb^{2+} at pH 5 and contact time 20 h), comparable to those of commercial adsorbents (Suopajärvi et al., 2015).

Other sulfur-based modifications such as the incorporation of the thiol group have also been studied to improve the adsorptive properties of cellulose (Silva Filho et al., 2013; Santana et al., 2010; Yang et al., 2014). For example, incorporation of basic sulfur centers in the cellulose structure with a higher tendency for coordinating divalent cations has been achieved through the direct reaction of cellulosic material (5 g) with ethylenesulfide (7 mL) at 50 °C for 3 h (Santana et al., 2010) (Scheme 16.1, route 4c). The final product is separated from the reaction mixture by sintered filtration, followed by washing with distilled water and acetone. This ethylenesulfide-immobilized cellulose shows a maximum sorption capacity (39.2 mg g^{-1}) toward Cu^{2+} ions from an aqueous solution at pH 6.

16.2.3 Chemical modification with amines

Amine-functionalization of cellulose has also been widely studied for the removal of both organic and inorganic pollutants since the available basic nitrogen centers can act as chelating centers for capturing metal cations (da Silva Filho et al., 2006). Moreover, these amine groups remain protonated at suitable acidic pH and can act as positively charged adsorption sites for adsorptive removal of anionic pollutant species (Jin et al., 2015). For instance, ethylenediamine-anchored cellulose containing the ethylene-1,2-diamine chelating groups (basic nitrogen with a great affinity for cations) effectively adsorbs, via cation complexation, divalent cations like Co^{2+}, Cu^{2+}, Zn^{2+}, and Ni^{2+} from aqueous solutions under neutral pH conditions, with adsorption capacities of 1.91 ± 0.07, 1.32 ± 0.07, 1.31 ± 0.02, and 1.08 ± 0.04 mmol g^{-1}, respectively (da Silva Filho et al., 2006). The synthesis of ethylenediamine-anchored cellulose consists of a prior chlorination reaction, substituting the OH at C6 position with Cl (DS = 0.99) using thionyl chloride ($SOCl_2$) in DMF to form a more reactive 6-chloro-6-deoxycellulose. The chlorinated cellulose is subsequently reacted

with ethylene-1,2-diamine to give 6-(2′-aminoethylamino)-6-deoxy-cellulose (da Silva Filho et al., 2006) (Scheme 16.1, route 5a). Moreover, the aminated cellulose thus obtained can be further modified by reacting it with ethylene sulfide (C_2H_4S) to form a derivative (shown as end-product in route 5a) that contains –SH groups at the end of the side chains, in addition to the NH groups (Silva Filho et al., 2013). Due to the presence of sulfur as an additional soft binding center, this new derivate shows further improvement in adsorption toward divalent metal ions in the order $Pb^{2+} > Cd^{2+} > Ni^{2+} > Co^{2+} > Cu^{2+} > Zn^{2+}$, with the maximum adsorption capacities of 6.282 ± 0.023, 5.783 ± 0.015, 5.561 ± 0.017, 4.694 ± 0.013, 1.944 ± 0.062 and 1.733 ± 0.020 mmol g^{-1}, respectively (Silva Filho et al., 2013). Moreover, the same synthetic route (route 5a) can be used to prepare another cellulose derivative with mixed functional groups (aminothiol-functionalized cellulose) if the chlorinated cellulose (6-chloro-6-deoxycellulose), obtained after chlorination of cellulose with $SOCl_2$, is reacted with aminoethanethiol hydrochloride ($HS(CH_2)_2NH_2 \cdot HCl$) (Silva et al., 2013). This aminoethanethiol-functionalized cellulose, with a PZC value of around 6, showed good adsorption of reactive red anionic dye from aqueous solution under both acidic (78 mg g^{-1} at pH 2) and basic conditions (26 mg g^{-1} at pH 9). The adsorption mechanism involves a possible electrostatic interaction between the anionic dye molecules and protonated SH_2^+ and NH_2^+ group in the side chain under acidic conditions leading to higher adsorption capacity and H-bonding and/or covalent interactions between the modified cellulose and dye molecules under basic condition (Silva et al., 2013).

Another route for the preparation of amino-functionalized nanocrystalline cellulose involves oxidation of cellulose with $NaIO_4$ to produce dialdehyde nanocrystalline cellulose, as explained earlier, and then reacting it with ethylenediamine for 6 h, followed by *in-situ* reduction of the resulting imine intermediate with sodium borohydride ($NaBH_4$) (Jin et al., 2015) (Scheme 16.1, route 5b). The resulting amino-functionalized cellulose exhibit a pH_{PZC} value of 8 and considering that the anionic dye adsorption is favored at pH < pHpzc, where the surface became positively charged, high adsorption capacities were obtained under acidic conditions (pH 4.5) for the anionic dyes Congo red 4BS, acid red GR and reactive light yellow K-4G, with equilibrium adsorption amounts of 199.5, 137.1, and 183 mg g^{-1}, respectively, and with a maximum theoretical adsorption capacity of 555.6 mg g^{-1} for acid red GR, as obtained from Langmuir isotherm plot (Jin et al., 2015).

16.2.4 Phosphorylation of cellulose

Phosphorylated nanocellulose has been found to be an efficient bioadsorbent for the adsorptive removal of metal ions from industrial effluents (Oshima et al., 2008; Liu et al., 2015). Vanja Kokol and co-workers presented an elegant modification of CNFs and CNCs by converting them to the nano-sized cellulose ester building blocks having phosphoryl side chains (Kokol et al., 2015). The hydroxyls groups positioned at C6 and C3 of both CNFs and CNCs were efficiently modified to the dibasic phosphate and monobasic tautomeric phosphite groups via phosphorylation using heterogeneous and homogeneous approaches and phosphoric acid as phosphoryl contributor (Scheme 16.1, route 6). Importantly, the homogenous conditions produce a higher surface charge density of 60-fold ($\sim$1173 mmol kg^{-1}) for phosphorylated CNFs (p-CNFs) and 2-fold ($\sim$1038 mmol kg^{-1}) for phosphorylated CNCs

(p-CNCs) and high hydrolytic stability to water for p-CNCs at all pH was also observed. Interestingly, the extents of phosphate ions released from acidic to alkaline hydrolysis were found to be marginal and safe beside the high surface phosphorylation under homogeneous modification. Additionally, the treated solution after the heterogeneous process could be recycled.

Modification of cellulose with phosphate groups significantly improves its sorption velocity and sorption capacity toward metal ions (Ag^{+}, Cu^{2+}, and Fe^{3+}), allowing nearly 100% adsorptive removal of the metals from aqueous media (Liu et al., 2015). For instance, the sorption capacity toward Ag^{+} ions was found to be 136 mg g^{-1} for phosphorylated CNCs, as compared to 56 mg g^{-1} for pristine nanocellulose. Similarly, phosphorylated bacterial nanocellulose (p-BC) is an excellent adsorbent material for a variety of transition metals ions (Cu^{2+}, Mn^{2+}, Zn^{2+}, Co^{2+}, Fe^{3+}) and lanthanide ions (La^{3+}, Sm^{3+}, Ho^{3+}) (Oshima et al., 2008). Although pristine BC does not adsorb metal/lanthanide ions, p-BC containing phosphoric acid groups shows adsorption of these ions. Moreover, the pH dependence of the adsorption process (% adsorption >90% at pH > 4.5) suggests a cation-exchange mechanism of adsorption (Oshima et al., 2008).

16.2.5 Hydrophobic nanocellulose

A very interesting strategy employed to capture organics dissolved in water using cellulose-based adsorbents is to graft or add organic moieties bearing hydrocarbon chains of different lengths which can act as hydrophobic reservoirs for accumulation of a wide variety of organic compounds including pesticides and oils (Zhang et al., 2014a; Aloulou et al., 2004a, b, c; Gong et al., 2019; Salajková et al., 2012; Boufi and Belgacem, 2006; Alila and Boufi, 2009; Alila et al., 2007, 2010; Lin et al., 2015b; Zhao et al., 2020). One of the strategies involves adsorbing cationic or anionic surfactants with different hydrophobic chain length (from C12 to C18) onto cellulose fibers in an aqueous medium whereby the adsorbed surfactant molecules aggregate at the solid–liquid interface in the form of hydrophobic monolayer or bilayers. These hydrophobic layers can act as reservoirs to trap various slightly water-soluble organic molecules through their partitioning or adsolubilization process between the bulk aqueous phase and the adsorbed surfactant aggregates layer (Aloulou et al., 2004a, b, c). Other studies on the solutes adsorption isotherms on cellulose/surfactant assemblies have suggested coadsorption as the dominant solute uptake process (Aloulou et al., 2004b; Alila et al., 2007). Moreover, the retention capacity of the cellulose/surfactant assembly toward organic solutes depends on (i) the hydrocarbon tail structure of the adsorbed surfactant, (ii) the amount of surfactant adsorbed, and (iii) the solute solubility and functional groups. The retention capacity generally increases with the number of carbon atoms in the surfactant chain and with the increase in surfactant concentration up to critical micelle concentration (cmc) (Boufi and Belgacem, 2006).

Some of the common cationic surfactant employed for this purpose include octadecyltrimethylammonium bromide (C18), hexadecylpyridinium chloride (C16), tetradecyltrimethylammonium bromide (C14) and dodecylpyridinium chloride (C12) with their cmcs at 25 °C being 2.1×10^{-4}, 7.5×10^{-4}, 3.4×10^{-3}, and 1.2×10^{-2} mol L^{-1}, respectively (Aloulou et al., 2004a, c; Alila et al., 2007). Examples of the anionic surfactant include sodium

octadecyltrimethyl sulfate (C18), sodium hexadecylpyridinium sulfate (C16), sodium tetradecyltrimethyl sulfate (C14), sodium dodecylpyridinium sulfate (C12), and sodium dodecylbenzene sulfonate (SDBC) with their cmc being 1.5×10^{-4}, 6.1×10^{-4}, 2.4×10^{-3}, 10^{-2}, and 1.1×10^{-3} mol L^{-1}, respectively (Aloulou et al., 2004b).

The adsorption of cationic surfactant onto cellulose substrate is enhanced if the –COOH groups are pre-introduced, for example by the TEMPO-mediated oxidation of cellulose discussed previously, thus obtaining a cationic surfactant/anionic cellulose assembly with higher loading of adsorbed surfactant. The extent of cationic surfactant adsorption on anionic cellulose increases with an increase in the degree of oxidation (Alila et al., 2007; Salajková et al., 2012). CNCs with still higher carboxylate content (1.5 mmol g^{-1}) can be prepared if the TEMPO-oxidized cellulose is converted to CNCs by direct hydrochloric acid hydrolysis. The resulting CNCs carrying abundant carboxylic acid groups can efficiently adsorb, via an ionic-exchange process, a variety of quaternary ammonium cation surfactants bearing long alkyl, phenyl, glycidyl, and diallyl groups, thus forming hydrophobic (contact angle = 71 degree) cellulose/surfactant assemblies that can be redispersed and individualized in organic solvents such as toluene and chloroform (Salajková et al., 2012). Similarly, enhanced adsorption of anionic surfactant with different hydrophobic chain lengths onto cellulose fibers can be achieved if the cellulose fibers are pre-treated with a cationic polyelectrolyte (such as polydimethyldiallylammonium chloride (PDAC) or linear 3–6 ionene) (Aloulou et al., 2004b). Such cationic polyelectrolyte-treated cellulose/anionic surfactant assembly acts as an excellent adsorbent with enhanced capacity for the retention of a variety of organic compounds (benzene, nitrobenzene, quinoline, and 2-naphthol) following a coadsorption process where the accumulation of the organic solutes takes place in the hydrophobic surfactant aggregates formed at the cellulose/water interface (Aloulou et al., 2004b). Likewise, the cationic surfactant (C-18)/anionic cellulose assembly also showed good co-adsorption of 2-naphthol and quinolone, with a maximum co-adsorbed amount of 1150 and 550 μmol g^{-1}, respectively, whereas the solute adsorption on pristine cellulose fibers did not exceed 80–140 μmol g^{-1} (Alila et al., 2007).

Another interesting chemical modification of cellulose fibers to achieve efficient capture of organic molecules dissolved in water and excellent recyclability involves grafting aliphatic anhydrides having a long hydrocarbon chain (C6, C8, C12, and C16) through heterogeneous esterification with an anhydride or carboxylic acid, employing a heterogeneous solvent exchange acylation procedure (Boufi and Belgacem, 2006). The process involves soaking of water-swelled pre-washed fibers into a solution of toluene/triethylamine (TEA) (80/20, w/w) and refluxing the resulting slurry until all the water contained inside the fibers is removed by azeotropic distillation with the toluene/TEA mixture. Then required amount of acid anhydride and catalyst (dimethylaminopyridine, 6% (w/w)) is added and the slurry is kept under magnetic stirring, reflux, and dry nitrogen atmosphere for 12 h. The product obtained is then purified by soxhlet extraction with THF/ethanol (50/50, v/v) for 48 h and dried at 105 °C for 30 min. The prepared modified fibers exhibit an excellent capacity to capture different organic molecules dissolved in water including chlorobenzene (185 μmol g^{-1}), nitrobenzene (146 μmol g^{-1}), quinoline (330 μmol g^{-1}) and 2-naphthol (330 μmol g^{-1}) (Boufi and Belgacem, 2006). Importantly, the saturated substrates can be regenerated tens of times without losing their capacity of absorption of organic contaminants.

Remembering the Gulf of Mexico accidental marine oil spill in April 2010, which released 4.1 million barrels of oil into the deep waters of the Gulf of Mexico (Schrope, 2011) and considering the fact that oil transportation mainly involves sea transportation, the problem of oil spill (Schrope, 2011) and other organic solvents is an ever-existing threat to both marine life as well as human life. The preparation of hydrophobic cellulose-based adsorbents for the removal of oils and other organic liquids from aqueous media has thus attracted particular attention. Many efforts have been directed toward the development of greener and efficient treatment methods for the removal or separation of oils and other organic solvents from aqueous media, most of which involve the development of hydrophobic solid adsorbents, preferentially based on natural polymers such as cellulose (Zhang et al., 2014a; Lin et al., 2015b; Zhao et al., 2020; Salajková et al., 2012; Rong et al., 2021; Ermeng et al., 2017).

Silylation is another elegant way used for the chemical/hydrophobic modification of cellulose (Klebe and Finkbeiner, 1969; Goussé et al., 2002). Most often, the cellulose polymer is silylated with suitable organo(chloro)silanes containing a hydrocarbons chain that results in hydrophobic silylated cellulose with enhanced oil capturing capacities (Zhang et al., 2014a; Lin et al., 2015b; Rong et al., 2021). Various organo(chloro)silanes including hexamethyldisilazane (HMDS), thexyldimethylchlorosilane (TMSCl), trimethylsilyl chloride (TMSCl), methyltrimethoxysilane, bis(trimethylsily1)-acetamide (BSA), 3-aminopropyltriethoxysilane (APTS), (2-aminoethyl)-3-aminopropyl-trimethoxysilane (AETS), isopropyldimethylchlorosilane (IDCS), *n*-butyldimethylchlorosilane (BDCS), *n*-octyldimethylchlorosilane (ODCS) and *n*-dodecyldimethylchlorosilane (DDMS) have been used as silylating agents to prepare silylated cellulose (Goussé et al., 2002; Petzold et al., 2003; Mormann and Wagner, 2000; Yin et al., 2018).

The silanes undergo hydrolysis and the hydrolyzed products then not only undergo self-condensation to form an extended organosilica network (–O–Si(R)–O–) but also condense with the surface –OH group of cellulose structure to form cellulose–O–Si bonds, leading to the covalent grafting of the organosilica onto the cellulose fibers (Scheme 16.1, route 7). For example, hydrophobic, flexible, and ultralightweight (apparent density $\leq 17.3\ kg\ m^{-3}$) nanocellulose sponges (Fig. 16.4A) with high porosity (≥99%) can be prepared by silylation of CNFs with methyltrimethoxysilane ($CH_3Si(OCH_3)_3$) in acidic media (pH 4) under the freeze-drying conditions (Zhang et al., 2014a). The procedure consists of the drop-wise addition of an aqueous solution (pH 4) of methyltrimethoxysilane (1.2–30.8 $mmol/g_{NFC}$) to an aqueous suspension of NFC (14.16 g/97.72 g H_2O) of the same pH, stirring the reaction mixture for 2 h and then freeze-drying it with liquid nitrogen. The resulting silylated NFC sponges combine both hydrophobic and oleophilic properties (Fig. 16.4B), as demonstrated by its ability to efficiently capture dodecane ($50\ g\ g^{-1}$) (Fig. 16.4C) and a wide range of other organic solvents (chloroform, dichloromethane, toluene, acetone) and oils (mineral oil, motor oil, silicon oil) from aqueous media, with an excellent efficiency (absorption capacity = 49–102 $g\ g^{-1}$, depending on the liquid) and recyclability (Zhang et al., 2014a).

A related procedure can be used to prepare superhydrophobic silylated composite aerogel materials consisting of CNFs/polyvinyl alcohol/montmorillonite. These porous aerogels can be prepared by directional freezing using CNFs as the base material, polyvinyl alcohol as the cross-linking agent, and montmorillonite as the modifier and filler, followed by hydrophobic

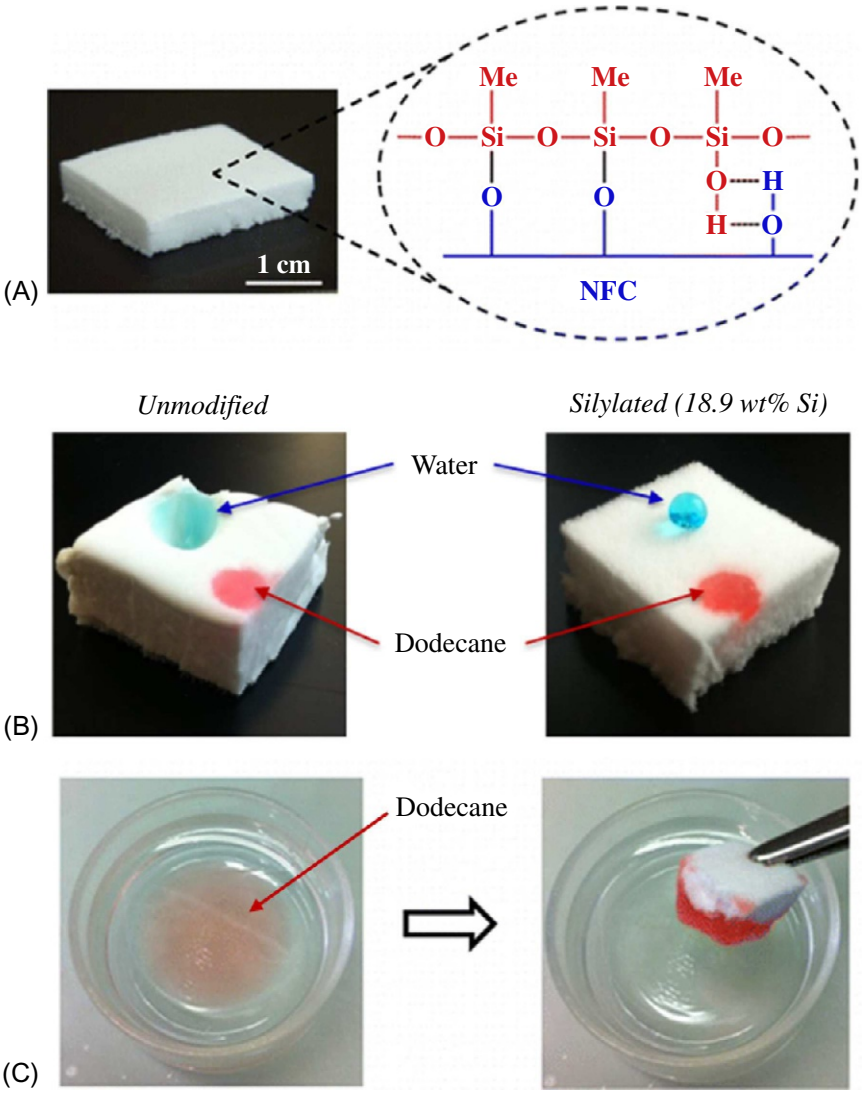

FIG. 16.4 (A) Photograph of the silylated NFC sponge along with a schematic representation of the possible interactions between the polysiloxane sol and the NFC surface, where the polysiloxane sol is expected to condense or form hydrogen bonds with the cellulosic substrate, as water is progressively removed; (B) demonstration of the combined hydrophobic and oleophilic properties of the silylated NFC sponge. In comparison, the untreated NFC sponge displayed an amphiphilic character. Dodecane and water were colored red (Sudan III dye) and blue (Neon Blue dye), respectively; and (C) removal of a red-colored dodecane spill (0.02 g) from water with the silylated NFC sponge (0.02 g). *Reproduced from Zhang, Z., Sebe, G., Rentsch, D., Zimmermann, T., Tingaut, P., 2014a. Ultralightweight and flexible silylated nanocellulose sponges for the selective removal of oil from water. Chem. Mater. 26, 2659–2668. https://doi.org/10.1021/cm5004164 with permission from the American Chemical Society.*

treatment with methyltrimethoxysilane as a silylating agent using the chemical vapor deposition method at 70 °C for 2 h (Rong et al., 2021). The resulting silylated aerogels exhibit excellent surface/physical properties (density = 26.52 kg m^{-3}, porosity = 96.1%, contact angle = 140 degree) and hence good adsorption capacity toward different oils and organic solutions, reaching 40–68 times of its initial weight (Rong et al., 2021). Similarly, hydrophobic (contact angle = 150 degree), light weight (19.6 kg m^{-3}) cellulose aerogels can be prepared by a rapid (<3 min) cold plasma process using trimethylchlorosilane ($(CH_3)_3SiCl$) as the plasma (Lin et al., 2015b). These cellulose aerogels exhibit excellent adsorption properties (34.5 g (peanut oil) g^{-1}) and can be reused for up to 15 cycles. As another example, cellulose aerogels can be coated with methyltrimethoxysilane by chemical vapor deposition method to obtain superhydrophobic material (contact angle = 153.5 degree) with excellent oil absorption capacities (95 g g^{-1}) from seawater/oil suspensions (Feng et al., 2015).

Similarly, cellulose whiskers can be partially silylated with alkyldimethylchlorosilanes (alkyl group = isopropyl, *n*-butyl, *n*-octyl or *n*-dodecyl) in dry toluene and the HCl produced as a by-product could be trapped using imidazoles (Goussé et al., 2002). It is important to mention that a control of the extent of substitution and regioselectivity is attributed to the reaction pathway. Cellulose can be chemically modified to pure trimethylsilyl cellulose by reacting it with trimethylsilyl chloride (TMSCl) in pyridine or NH_3/DMF. A higher degree of silylation, without degradation of the polymer chain, can be achieved if hexamethyldisilazane in liquid ammonia at elevated temperature (80–100 °C) in an autoclave is used as silylating agent in the presence of catalytic amount of saccharin (0.5 mol% relative to the hydroxy groups) (Mormann and Wagner, 2000).

Acetylation of cellulose, which involves the substitution of the hydrophilic hydroxyl (OH) groups of cellulose with less hydrophilic acetyl (CH□CO) groups can also be employed to impart hydrophobic and hence oil-sorbing properties to cellulose-based materials. For instance, acetylated wheat straw cellulosic sorbent can be prepared by reacting pre-treated cellulose (0.5 g) in dimethylacetamide (15 mL) with acetic anhydride (5 mL) as an acetylating reagent in the presence of N-bromosuccinimide (55 mM) catalyst at 100 °C for 1.5 h. The resulting acetylated cellulose possesses a hydrophobic and oleophilic surface and contains abundant oil-absorbing sites and shows excellent oil absorbencies values of 24.21 ± 0.76, 22.39 ± 0.77, 25.61 ± 2.13, and 24.73 ± 1.19 g g^{-1}, for diesel fuel, diesel oil slick, corn oil, and corn oil slick treatments, respectively (Ermeng et al., 2017). Table 16.2 summarizes the removal performance of the different chemically modified cellulose materials toward a variety of both organic and inorganic pollutants.

16.3 Inorganic nanostructures modified cellulose: Improved multifunctional adsorbents

An interesting strategy to improve the adsorptive removal performance of cellulose-based materials is their combination, at the molecular or nanoscale level, with inorganic nanostructures such as layered clay minerals, metal oxides/sulfides-based semiconductors, plasmonic metallic nanoparticles, among others. By combining the excellent structural properties, mechanical stability, and hydrophilicity of cellulose-based components with the

unique surface, (photo)catalytic and electronic properties of inorganic nanostructures, this strategy offers great versatility with respect to tailoring the properties of cellulose-based adsorbents and the resulting hybrid organic-inorganic (nano)materials often exhibit highly improved removal performance and/or selectivity for different inorganic and organic contaminants. Additionally, modification with specific inorganic nanomaterials may imbue the hybrid material with novel functions that contribute additively or even synergistically with the adsorptive properties for water purification and environmental remediation applications (Islam et al., 2018; Hu et al., 2014; Wei et al., 2014; Figueiredo et al., 2014; Nadar et al., 2019; Patel et al., 2019). Examples of such novel functions include (photo)catalytic, bactericidal, sensing, and magnetic properties. Table 16.3 summarizes important recent examples of cellulose-based organic-inorganic hybrid adsorbents, highlighting their overall removal efficiency toward different types of contaminants and additional properties that modifications instill into the material.

TABLE 16.3 A summary of the modification of cellulose with inorganic material and the properties and applications of the resulting cellulose-based composites for environmental remediation.

Material	Functional properties	Form	Pollutant	Removal efficiency	References
Cellulose/amino-modified carbon dots hydrogel	Adsorbent, sensor	Hydrogel monolith	Cr(VI)	Adsorption capacity 534.4 mg g^{-1}	Luo et al. (2021)
Cellulose/MoS_2	Adsorbent	Membrane for in-flow adsorption	Hg(II)	Adsorption capacity 160.4 mg g^{-1}	Haseen and Ahmad (2020)
Cellulose/Al_2O_3 aerogel	Absorbent	Aerogel monolith	Organic solvents	Absorption capacity 64–118 × 10^3 mg g^{-1}	Zhou et al. (2021)
Cellulose/(Co, Fe)(pz)[$Ni(CN)_4$] MOF aerogel	Adsorbent	Aerogel monolith	Iodine	Adsorption capacity 458.0 mg g^{-1}	Wu et al. (2020)
Cellulose/ZIF-67 /HKUST-1 MOFs	Adsorbent	Aerogel beads	Diclofenac Methyl orange (MO)	Adsorption capacity Diclofenac 121.20 mg g^{-1} Methyl orange 49.20 mg g^{-1}	KarzarJeddi et al. (2020)
Fe-Cu alloy/CNF membrane	Adsorbent, bactericide	Membrane	Pb(II)	Adsorption capacity Pb(II) 81.9 mg g^{-1}	Hou et al. (2020)
Cellulose/Zn-Al layered double hydroxide	Adsorbent	Powder	As(III)As(V)	Adsorption capacity As(III) 30.2 mg g^{-1} As(V) 42.0 mg g^{-1}	Bessaies et al. (2020)
Cellulose/Mg-Al layered double hydroxide	Adsorbent	Beads	Amoxicilin antibiotic	Adsorption capacity Amoxicilin 138.3 mg g^{-1}	Yang et al. (2020a)

TABLE 16.3 A summary of the modification of cellulose with inorganic material and the properties and applications of the resulting cellulose-based composites for environmental remediation—cont'd

Material	Functional properties	Form	Pollutant	Removal efficiency	References
Cellulose/γ-Fe_2O_3 aerogels	Magnetic adsorbent	Monoliths	Cr(VI)	Adsorption capacity 10.2 mg g^{-1}	Wan and Li (2015)
Cellulose/SiO_2/Fe_3O_4	Magnetic adsorbent	Powder	Cr(VI)	Adsorption capacity 17.1mg g^{-1}	Sun et al. (2014)
Cellulose acetate/MnO_2/FeOOH	Adsorbent, oxidation catalyst	Membrane	As(III)	Adsorption capacity 50.3 mg g^{-1}	Qiu et al. (2020)
Cellulose/kaolinite	Adsorbent	Powder nanofibers	Se(VI), Se(IV), selenomethionine (SeMt)	Adsorption capacity Se(VI) 137.5 mg g^{-1} Se(IV) 161.4 mg g^{-1} SeMt 95.4 mg g^{-1}	Abukhadra et al. (2021)
Cellulose/montmorillonite clay	Adsorbent	Powder nanofibers	Levofloxacin antibiotic	Adsorption capacity 65.9 mg g^{-1}	Li et al. (2020)
Cellulose/montmorillonite clay	Adsorbent	Powder nanofibers	Diuron antibiotic	Adsorption capacity 64.0 mg g^{-1}	Ma et al. (2020)
Cellulose/montmorillonite clay	Absorbent	Hydrogel monolith	Methylene blue (MB) dye	Absorption capacity 782.9 mg g^{-1}	Peng et al. (2016)
TiO_2/Au-cellulose membranes	Adsorbent, photocatalyst	Membrane	Rhodamine B dye	Degradation 95% in 5 h	Yu et al. (2020)
BC/MoS_2 aerogel membrane	Adsorbent, photocatalyst	Aerogel in-flow photocatalytic membrane	Cr(*VI*)MB dye	Adsorption efficiency MB dye 50% in 30 min Cr(VI) 22% in 30 min Photo assisted removal MB dye 96% in 120 min ($k_{obs} = 0.026$ min^{-1}) Cr(VI) 88% in 120 min ($k_{obs} = 0.012$ min^{-1})	Ferreira-Neto et al. (2020)
BC/SiO_2/TiO_2 membrane	Photocatalyst/self-cleaning, antibacterial	Membrane	Crystal violet	97% dye removal in 50 min, antibacterial activity against 05 bacterial strains	Rahman et al. (2021)

Continued

TABLE 16.3 A summary of the modification of cellulose with inorganic material and the properties and applications of the resulting cellulose-based composites for environmental remediation—cont'd

Material	Functional properties	Form	Pollutant	Removal efficiency	References
BC/PDA/TiO_2	Adsorbent, photocatalyst	Membrane	RhB, MO and MB dyes	Adsorption capacity RhB 13.4 mg g^{-1} MO 11.8 mg g^{-1} MB 28.9 mg g^{-1} Photo-assisted removal RhB 100.0% in 60 min MO 95.1% in 30 min MB 99.5% in 20 min	Yang et al. (2020b)
Bilayer BC/CuS aerogel membrane	Adsorbent, photocatalyst solar evaporator	Aerogel membrane floating membrane	MB dye	Photo-assisted removal 93.4% in 80 min	Zhang et al. (2021)
Cellulose NFs/BiOCl	Adsorbent, photocatalyst	Powder	Rhodamine B dye	Adsorption 7% in 30 min Photo-assisted removal ~100% in 16 min	Tian et al. (2019)
β-FeOOH cellulose nanocomposite hydrogels	Adsorbent, photo-fentoncatalyst	Hydrogel monolith	MB dye	Adsorption 11.5% in 30 min Photodegradation 99.9% in 25 min	Wang et al. (2020)
Cellulose–bismuth oxybromide membrane	Adsorbent, photocatalyst	Membrane	RhB dye, Co(II), and Ni(II)	Adsorption capacity Co(II) 37.3 mg g^{-1} Ni(II) 30.2 mg g^{-1} Photo-assisted removal RhB ~100% in 100 min	Onwumere et al. (2020)

As shown in Table 16.3, modification with a variety of inorganic nanostructures allows cellulose-based adsorbents to be highly effective in the removal of different classes of contaminants including inorganic species (transition, alkaline, alkaline-earth, and metalloid cations or toxic oxoanions (chromate and arsenates)) as well as organic pollutants such as dyes, solvents, and pharmaceuticals. Enhancement of the adsorptive removal efficiency is often assigned to both specific structural (e.g., pore structure, interlamellar spaces) and surface traits (high surface charge, high specific surface area, complexation surface sites) of the inorganic nanomaterials, allowing contaminants removal by both non-covalent/electrostatic physisorption and/or covalent chemisorption. For instance, nanocomposites prepared by combining cellulose biopolymer with layered inorganic nanomaterials such as aluminosilicates clay minerals and layered double hydroxides (LDH) result in highly increased adsorption capacity toward antibiotics, pesticides, dyes, and toxic heavy metals

and oxoanions due to unique ion-exchange properties of these specific structures (Yang et al., 2020a; Bessaies et al., 2020; Li et al., 2020; Ma et al., 2020; Peng et al., 2016). Their ion-exchange properties stem from the permanent negatively charged (in case of aluminosilicates clays) and positively charged (in case of LDH) layers, resulting in high cation- and anion-exchange capacities, respectively. An interesting example of LDH-cellulose nanocomposites is Mg-Al LDH@CB adsorbents which are prepared by co-precipitation of Mg-Al LDH inorganic phase on cellulose beads (CB). This composite shows high adsorption capacity (138.3 mg g^{-1}) toward amoxicillin antibiotic where the mechanism of adsorption is through electrostatic interaction, as evidenced by zeta potential measurements (Yang et al., 2020a). A similar approach can be followed to prepare Ca-Al LDH/cellulose and Zn-Al LDH/cellulose positively charged adsorbents for enhanced removal of toxic As(III) and As(V) oxoanions species from contaminated water (Bessaies et al., 2020).

An example of the clay minerals-modified cellulose is nanocellulose/montmorillonite composites for enhanced adsorption of diuron herbicide (adsorption capacity 64 mg g^{-1}) (Li et al., 2020) and levofloxacin hydrochloride antibiotic (65.9 mg g^{-1}) (Ma et al., 2020). A relevant advancement in this area is the preparation of clay-cellulose hydrogels with ultra-high adsorption capacity toward methylene blue dye (782.9 mg g^{-1}) and with the additional advantages of good mechanical stability, high water absorption, and monolithic nature that facilitates handling and recovery of the adsorbent (Peng et al., 2016) (Fig. 16.5).

As an example of adsorption enhancement by chemisorption mechanism, the cellulose/MoS_2 material obtained by the hydrothermal growth of MoS_2 nanostructures onto the surface of a cellulose nanofiber mat exhibits excellent and selective Hg(II) sorption (160.4 mg g^{-1}), attributed to the soft–soft interaction of Hg(II) with the sulfide sites of MoS_2 (Haseen and Ahmad, 2020). Considering that immobilization of MoS_2 onto solid support restricts sorbent loss during the column operation, these MoS_2 functionalized cellulose fiber mats have been used as column packing material for pre-concentration of Hg(II) ions in environmental samples for ICP-OES analysis.

Metal organic frameworks (MOFs), consisting of crystalline assemblies of metal ions coordinated to organic ligands, are another class of hybrid organic-inorganic nanomaterials with unique structural and physicochemical properties including high surface area, high pore volume, ordered pore structure, adjustable structure and pore size and abundance of chemically active sites. These ideal features impart MOFs excellent adsorptive properties toward a variety of pollutants. MOFs are thus excellent candidates for the preparation of cellulose-supported nanocomposites adsorbents with improved stability, increased adsorption capacity, and easier handling (Nadar et al., 2019; KarzarJeddi et al., 2020; Hou et al., 2020; Wu et al., 2020). For instance, Wu et al. reported the preparation on monolithic hybrid cellulose/(Co,Fe)(pz)[$Ni(CN)_4$] MOF aerogel by doping or *in-situ* growth of Hoffman type bimetallic MOFs on cellulose aerogel networks (Wu et al., 2020). The prepared materials, especially the hybrid aerogels prepared by doping strategy, showed an excellent capacity for iodine capture (458 mg g^{-1}, approximately four times higher than pure cellulose aerogel), an application of considerable interest for nuclear waste treatment plants. The adsorption mechanism in this case probably involves the interaction of iodine with the pyrazine and cyanide functional groups present in pore walls of Hoffman-type bimetallic MOF (Wu et al., 2020). Another interesting example of cellulose/MOF nanocomposite adsorbent is the zwitterionic cellulosic

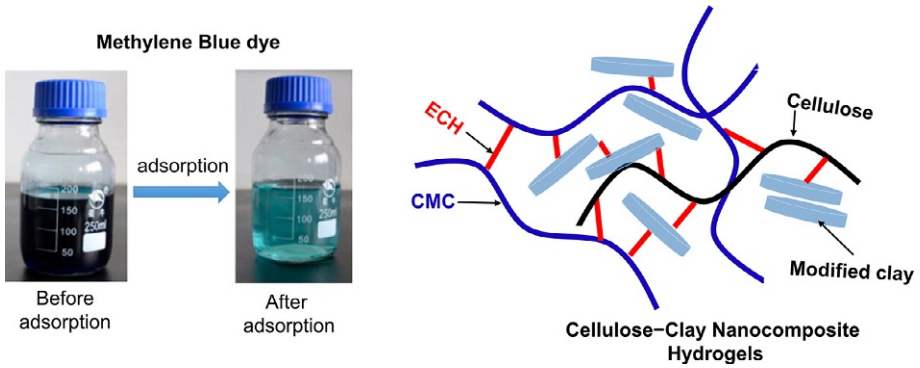

FIG. 16.5 Absorption of MB by cellulose–clay nanocomposite hydrogels. The Schematic representation of the cellulose–clay nanocomposite hydrogels containing epoxidized/modified clay cross-linked in the hydrogel networks is shown on the right hand side. The hydrogels are fabricated by chemical cross-linking cellulose (*black fibers*) and carboxymethyl cellulose (CMC, *blue fiber*) with epichlorohydrin (ECH, *red connecting line*) in the presence of clay nanosheets (*clay blue disks*). *Reproduced from Peng, N., Hu, D., Zeng, J., Li, Y., Liang, L., Chang, C., 2016. Superabsorbent cellulose-clay nanocomposite hydrogels for highly efficient removal of dye in water. ACS Sustain. Chem. Eng. 4, 7217–7224. https://doi.org/10.1021/acssuschemeng.6b02178 with Permission from the American Chemical Society.*

aerogel bead containing both anionic (HKUST-1) and cationic (ZIF-67) MOFs (KarzarJeddi et al., 2020). This highly porous (98.96%) and low density (0.015 g cm^{-3}) material can be prepared by incorporation of the cited MOFs in CNFs containing hydrogel networks, followed by freeze-drying. The zwitterionic nature of the prepared MOFs@CNF aerobeads as well as the different organic functionalities of MOFs allow excellent adsorptive removal of contaminants (121.2 mg(diclofenac) g^{-1} and 49.2 mg(MO) g^{-1}) through different mechanisms including electrostatic, π-π interactions and H-bonding (KarzarJeddi et al., 2020).

As previously mentioned, modification of cellulose-based substrates with inorganic nanostructures not only enhances the adsorption properties but also imbues the final nanocomposite with additional functional properties. For instance, cellulose-based adsorbents containing magnetic nanomaterials can be easily recovered from aqueous media through the application of an external magnetic field. While the added inorganic component often acts solely as a magnetic carrier, in certain cases it may additionally enhance the adsorption properties of the composite material (Wan and Li, 2015; Sun et al., 2014). In other cases, the added inorganic part may impart anti-bactericidal and/or anti-fungal properties to the material, destroying the pathogenic agents in contaminated water, and thus further corroborating with adsorptive/catalytic properties toward effective water purification applications (Hou et al., 2020; Kokilavani et al., 2020; Cheng et al., 2021; Rahman et al., 2021).

16.4 Adsorbents with photocatalytic/antibacterial functions

Based on the discussion presented above, it is clear that cellulose-based materials, especially after chemical modification or composite formation, have the potential to effectively

adsorb a variety of both organic and inorganic pollutants from aqueous media and the used adsorbents can be recovered by employing adequate strategies. The problem of disposal of the pollutants-adsorbed cellulose materials, however, still remains. An effective strategy to address this issue is to develop multifunctional materials that can efficiently adsorb/sorb the pollutants on one hand and (photo)degrade them on the other. Table 16.3 summarizes several examples of such multifunctional nanocomposites, especially highlighting photocatalytic materials (Ferreira-Neto et al., 2020; Kokilavani et al., 2020; Yu et al., 2020; Yang et al., 2020b; Zhang et al., 2021; Tian et al., 2019; Qiu et al. (2019); Wang et al., 2020; Onwumere et al., 2020). Semiconductors such as TiO_2, ZnO, BiOBr, MoS_2, CuS, all show photocatalytic behavior and thus promote photo-assisted organic pollutants degradation and/or heavy metal removal under UV–visible radiation. Combination of such photoactive behavior with the inherent adsorption property of the material may act synergistically toward contaminant removal and allow removal of a wider range of contaminants types (Ferreira-Neto et al., 2020; Onwumere et al., 2020).

One excellent example of such multifunctional material is the BNC/MoS_2 composite self-supported hybrid aerogel membranes reported by Ferreira-Neto et al., that exhibit excellent adsorption-cum-photocatalytic performance and thus high *in-flow* photo-assisted removal efficiency toward both organic (96% MB removal within 120 min, $K_{obs.} = 0.0267\ min^{-1}$) and inorganic species (88% Cr(VI) removal within 120 min, $K_{obs.} = 0.0122\ min^{-1}$) when used as a membranes filter (Fig. 16.6) (Ferreira-Neto et al., 2020). This highly porous aerogel membrane can be prepared by the hydrothermal growth of quantum-confined photocatalytic MoS_2

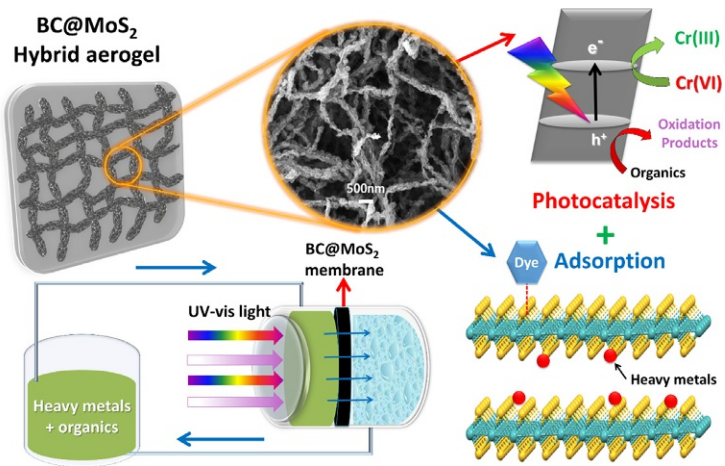

FIG. 16.6 Schematic representation of BNC/MoS_2 hybrid aerogels membranes as bifunctional adsorbent/photocatalyst for *in-flow* water decontamination under UV–visible illumination following adsorption-photocatalytic mechanism. Adsorption and photooxidation of MB and photoreduction of Cr(VI) to Cr(III) have been shown as model photocatalytic reactions. *Reproduced from Ferreira-Neto, E.P., Ullah, S., da Silva, T.C.A., Domeneguetti, R.R., Perissinotto, A.P., de Vicente, F.S., Rodrigues-Filho, U.P., Ribeiro, S.J.L., 2020. Bacterial nanocellulose/MoS2 hybrid aerogels as bifunctional adsorbent/photocatalyst membranes for in-flow water decontamination. ACS Appl. Mater. Interfaces 12, 41627–41643. https://doi.org/10.1021/acsami.0c14137 with permission from the American Chemical Society.*

nanostructures (2–4 nm crystallite size) on BNC nanofibrils employing ammonium heptamolybdate tetrahydrate ($(NH_4)_6Mo_7O_{24}{\cdot}4H_2O$)) and thiourea as the Mo and S sources, respectively. In addition to the good adsorptive/photocatalytic properties, the adequate anchoring of MoS_2 onto BNC ensures excellent recyclability and photostability, making such self-supported aerogel membranes ideal candidates for application in *in-flow* water purification (Ferreira-Neto et al., 2020).

The preparation of multifunctional cellulose-based membranes containing both photocatalytic and antibacterial components is another interesting research area with a broad spectrum of applications. For instance, flexible bacterial cellulose-based BC-SiO_2-TiO_2-Ag membranes have been found to exhibit the Ag-based antibacterial activity against five different bacterial strains (in dark), in addition to the TiO_2-based UV shielding and photocatalytic/self-cleaning activity under UV illumination (Rahman et al., 2021) (Fig. 16.7). These hybrid membranes were found to degrade 97% of the crystal violet (CV) dye deposited as an over-layer on the surface of the membranes within 50 min of UV illumination. It turns out that such hybrid membranes can be used in facemasks or wound dressing materials and then safely disinfected by simply exposing them to UV or solar light, thus avoiding the risk of environmental contamination or disposal problems (Rahman et al., 2021).

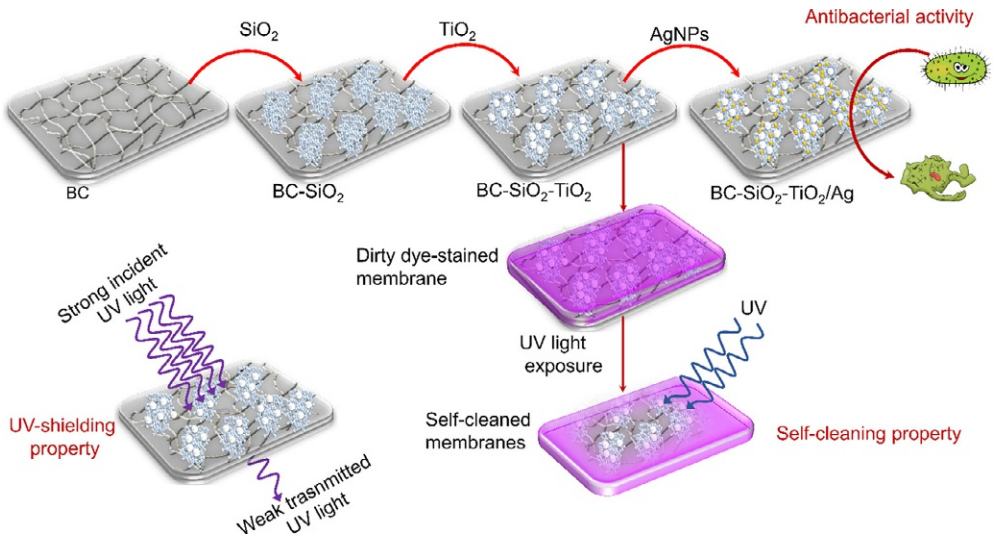

FIG. 16.7 Schematic representation of the step-wise procedure for the preparation of BC-SiO_2-TiO_2 photoactive hybrid membranes highlighting their photocatalytic/self-cleaning, UV shielding, and antibacterial activity. *Reprinted from Rahman, K.U., Ferreira-Neto, E.P., Rahman, G.U., Parveen, R., Monteiro, A.S., Rahman, G., Van Le, Q., Domeneguetti, R.R., Ribeiro, S.J.L., Ullah, S., 2021. Flexible bacterial cellulose-based BC-SiO2-TiO2-Ag membranes with self-cleaning, photocatalytic, antibacterial and UV-shielding properties as a potential multifunctional material for combating infections and environmental applications. J. Environ. Chem. Eng. 9, 104708. https://doi.org/10.1016/j.jece.2020.104708 with permission from Elsevier (2021).*

16.5 Conclusions

Cellulose-based materials have been widely used as adsorbents for the removal of both organic and inorganic pollutants from aqueous media. However, pristine cellulose shows low adsorption efficiency toward pollutants, especially the metal ions, and this limitation is easily overcome through chemical modifications of cellulose with a variety of metal-binding/chelating functional groups, thanks to the presence of reactive OH groups on the surface of cellulose that allow easily grafting of such functional groups. Often, negatively charged functional groups (carboxylate, phosphate, and sulfate) are anchored to the surface of cellulose that can efficiently sequester metal cations from aqueous media. Similarly, enhanced capture of organic molecules and oils can be achieved by making the cellulose hydrophobic through the incorporation of long-chain organic functional groups/molecules such as surfactants and organosilanes. Finally, organic-inorganic hybrid/composite materials, prepared by adding various inorganic materials (magnetic, antibacterial, photocatalytic, adsorbents) to the organic cellulose polymer, have been found to show superior properties and enhanced adsorptive removal of a variety of contaminants from aqueous media, in addition to assisting in the recovery and reusability of the adsorbents. Of particular interest in this regard are the dual-function cellulose/semiconductor photocatalytic materials that not only capture pollutants from aqueous media but also photocatalytically degrade them into harmless or less toxic products. Moreover, antibacterial functions can be introduced into cellulose-based materials, with the potential to be used in antimicrobial facemasks and water filtration membranes. The low-cost, eco-friendly cellulose, especially after the modifications mentioned above, thus offers a great potential for effective and sustainable environmental remediation, with the possibility of upscaling and commercial applications.

References

Abol-Fotouh, D., Hassan, M.A., Shokry, H., Roig, A., Azab, M.S., Kashyout, A.E.H.B., 2020. Bacterial nanocellulose from agro-industrial wastes: low-cost and enhanced production by Komagataeibacter saccharivorans MD1. Sci. Rep. 10, 1–14. https://doi.org/10.1038/s41598-020-60315-9.

Abukhadra, M.R., AlHammadi, A., El-Sherbeeny, A.M., Salam, M.A., El-Meligy, M.A., Awwad, E.M., Luqman, M., 2021. Enhancing the removal of organic and inorganic selenium ions using an exfoliated kaolinite/cellulose fibres nanocomposite. Carbohydr. Polym. 252. https://doi.org/10.1016/j.carbpol.2020.117163.

Alila, S., Boufi, S., 2009. Removal of organic pollutants from water by modified cellulose fibres. Ind. Crop Prod. 30, 93–104. https://doi.org/10.1016/j.indcrop.2009.02.005.

Alila, S., Aloulou, F., Beneventi, D., Boufi, S., 2007. Self-aggregation of cationic surfactants onto oxidized cellulose fibers and coadsorption of organic compounds. Langmuir 23, 3723–3731. https://doi.org/10.1021/la063118n.

Alila, S., Costa, A.I., Ferreira, L.F.V., Boufi, S., 2010. Modified biopolymer adsorbent for the removal of dissolved organic pollutants. Int. J. Environ. Technol. Manag. 12, 163–191. https://doi.org/10.1504/IJETM.2010.031526.

Aloulou, F., Boufi, S., Belgacem, N., Gandini, A., 2004a. Adsorption of cationic surfactants and subsequent adsolubilization of organic compounds onto cellulose fibers. Colloid Polym. Sci. 283, 344–350. https://doi.org/10.1007/s00396-004-1143-y.

Aloulou, F., Boufi, S., Beneventi, D., 2004b. Adsorption of organic compounds onto polyelectrolyte immobilized-surfactant aggregates on cellulosic fibers. J. Colloid Interface Sci. 280, 350–358. https://doi.org/10.1016/j.jcis.2004.08.008.

Aloulou, F., Boufi, S., Chakchouk, M., 2004c. Adsorption of octadecyltrimethylammonium chloride and adsolubilization on to cellulosic fibers. Colloid Polym. Sci. 282, 699–707. https://doi.org/10.1007/s00396-003-1000-4.

Amiralian, N., Annamalai, P.K., Garvey, C.J., Jiang, E., Memmott, P., Martin, D.J., 2017. High aspect ratio nanocellulose from an extremophile spinifex grass by controlled acid hydrolysis. Cellulose 24, 3753–3766. https://doi.org/10.1007/s10570-017-1379-6.

Anirudhan, T.S., Deepa, J.R., Binusreejayan, 2015. Synthesis and characterization of multi-carboxyl-functionalized nanocellulose/nanobentonite composite for the adsorption of uranium(VI) from aqueous solutions: kinetic and equilibrium profiles. Chem. Eng. J. 273, 390–400. https://doi.org/10.1016/j.cej.2015.03.007.

Annadurai, G., Juang, R.S., Lee, D.J., 2002. Use of cellulose-based wastes for adsorption of dyes from aqueous solutions. J. Hazard. Mater. 92, 263–274. https://doi.org/10.1016/S0304-3894(02)00017-1.

Ávila Ramírez, J.A., Fortunati, E., Kenny, J.M., Torre, L., Foresti, M.L., 2017. Simple citric acid-catalyzed surface esterification of cellulose nanocrystals. Carbohydr. Polym. 157, 1358–1364. https://doi.org/10.1016/j.carbpol.2016.11.008.

Bai, L., Liu, Y., Ding, A., Ren, N., Li, G., Liang, H., 2019. Surface coating of UF membranes to improve antifouling properties: a comparison study between cellulose nanocrystals (CNCs) and cellulose nanofibrils (CNFs). Chemosphere 217, 76–84. https://doi.org/10.1016/j.chemosphere.2018.10.219.

Bessaies, H., Iftekhar, S., Doshi, B., Kheriji, J., Ncibi, M.C., Srivastava, V., Sillanpää, M., Hamrouni, B., 2020. Synthesis of novel adsorbent by intercalation of biopolymer in LDH for the removal of arsenic from synthetic and natural water. J. Environ. Sci. (China) 91, 246–261. https://doi.org/10.1016/j.jes.2020.01.028.

Bezerra, R., Silva, M., Morais, A., Osajima, J., Santos, M., Airoldi, C., Filho, E., 2014. Phosphated cellulose as an efficient biomaterial for aqueous drug ranitidine removal. Materials (Basel) 7, 7907–7924. https://doi.org/10.3390/ma7127907.

Boufi, S., Belgacem, M.N., 2006. Modified cellulose fibres for adsorption of dissolved organic solutes. Cellulose 13, 81–94. https://doi.org/10.1007/s10570-005-9019-y.

Chen, S., Zou, Y., Yan, Z., Shen, W., Shi, S., Zhang, X., Wang, H., 2009. Carboxymethylated-bacterial cellulose for copper and lead ion removal. J. Hazard. Mater. 161, 1355–1359. https://doi.org/10.1016/j.jhazmat.2008.04.098.

Cheng, Q., Li, Q., Yuan, Z., Li, S., Xin, J.H., Ye, D., 2021. Bifunctional regenerated cellulose/polyaniline/nanosilver fibers as a catalyst/bactericide for water decontamination. ACS Appl. Mater. Interfaces 13, 4410–4418. https://doi.org/10.1021/acsami.0c20188.

Choi, H.Y., Bae, J.H., Hasegawa, Y., An, S., Kim, I.S., Lee, H., Kim, M., 2020. Thiol-functionalized cellulose nanofiber membranes for the effective adsorption of heavy metal ions in water. Carbohydr. Polym. 234, 115881. https://doi.org/10.1016/j.carbpol.2020.115881.

da Silva Filho, E.C., de Melo, J.C.P., Airoldi, C., 2006. Preparation of ethylenediamine-anchored cellulose and determination of thermochemical data for the interaction between cations and basic centers at the solid/liquid interface. Carbohydr. Res. 341, 2842–2850. https://doi.org/10.1016/j.carres.2006.09.004.

de Melo, J.C.P., da Silva Filho, E.C., Santana, S.A.A., Airoldi, C., 2009. Maleic anhydride incorporated onto cellulose and thermodynamics of cation-exchange process at the solid/liquid interface. Colloids Surf. A Physicochem. Eng. Asp. 346, 138–145. https://doi.org/10.1016/j.colsurfa.2009.06.006.

Ermeng, L., Wuyang, X., Mingxiao, T., Yuewu, P., 2017. Preparation of an efficient oil-spill adsorbent based on wheat straw. Bioresources 12, 296–315.

Faiz Norrrahim, M.N., Mohd Kasim, N.A., Knight, V.F., Mohamad Misenan, M.S., Janudin, N., Ahmad Shah, N.A., Kasim, N., Wan Yusoff, W.Y., Mohd Noor, S.A., Jamal, S.H., Ong, K.K., Yunus, W.M.Z.W., 2021. Nanocellulose: a bioadsorbent for chemical contaminant remediation. RSC Adv. 11, 7347–7368. https://doi.org/10.1039/d0ra08005e.

Feng, J., Nguyen, S.T., Fan, Z., Duong, H.M., 2015. Advanced fabrication and oil absorption properties of super-hydrophobic recycled cellulose aerogels. Chem. Eng. J. 270, 168–175. https://doi.org/10.1016/j.cej.2015.02.034.

Ferreira-Neto, E.P., Ullah, S., da Silva, T.C.A., Domeneguetti, R.R., Perissinotto, A.P., de Vicente, F.S., Rodrigues-Filho, U.P., Ribeiro, S.J.L., 2020. bacterial nanocellulose/MoS 2 hybrid aerogels as bifunctional adsorbent/photocatalyst membranes for in-flow water decontamination. ACS Appl. Mater. Interfaces 12, 41627–41643. https://doi.org/10.1021/acsami.0c14137.

Figueiredo, A.R.P., Vilela, C., Neto, C.P., Silvestre, A.J.D., Freire, C.S.R., 2014. Bacterial cellulose-based nanocomposites: roadmap for innovative materials. Nanocellulose Polym. Nanocompos. Fundam. Appl., 17–64. https://doi.org/10.1002/9781118872246.ch2.

Fu, L., Zhou, P., Zhang, S., Yang, G., 2013. Evaluation of bacterial nanocellulose-based uniform wound dressing for large area skin transplantation. Mater. Sci. Eng. C 33, 2995–3000. https://doi.org/10.1016/j.msec.2013.03.026.

Goetz, L.A., Naseri, N., Nair, S.S., Karim, Z., Mathew, A.P., 2018. All cellulose electrospun water purification membranes nanotextured using cellulose nanocrystals. Cellulose 25, 3011–3023. https://doi.org/10.1007/s10570-018-1751-1.

Gong, X., Wang, Y., Zeng, H., Betti, M., Chen, L., 2019. Highly porous, hydrophobic, and compressible cellulose nanocrystals/poly(vinyl alcohol) aerogels as recyclable absorbents for oil-water separation. ACS Sustain. Chem. Eng. 7, 11118–11128. https://doi.org/10.1021/acssuschemeng.9b00066.

Goussé, C., Chanzy, H., Excoffier, G., Soubeyrand, L., Fleury, E., 2002. Stable suspensions of partially silylated cellulose whiskers dispersed in organic solvents. Polymer (Guildf) 43, 2645–2651. https://doi.org/10.1016/S0032-3861(02)00051-4.

Haseen, U., Ahmad, H., 2020. Preconcentration and determination of trace Hg(II) using a cellulose nanofiber mat functionalized with MoS2 nanosheets. Ind. Eng. Chem. Res. 59, 3198–3204. https://doi.org/10.1021/acs.iecr.9b06067.

Hettrich, K., Wagenknecht, W., Volkert, B., Fischer, S., 2008. New possibilities of the acetosulfation of cellulose. Macromol. Symp. 262, 162–169. https://doi.org/10.1002/masy.200850216.

Hou, C., Chen, W., Fu, L., Zhang, S., Liang, C., Wang, Y., 2020. Facile synthesis of a Co/Fe bi-MOFs/CNF membrane nanocomposite and its application in the degradation of tetrabromobisphenol A. Carbohydr. Polym. 247, 116731. https://doi.org/10.1016/j.carbpol.2020.116731.

Hu, W., Chen, S., Yang, J., Li, Z., Wang, H., 2014. Functionalized bacterial cellulose derivatives and nanocomposites. Carbohydr. Polym. 101, 1043–1060. https://doi.org/10.1016/j.carbpol.2013.09.102.

Ioelovich, M., 2017. Characterization of various kinds of nanocellulose. In: Handbook of Nanocellulose Cellulose Nanocomposites, pp. 51–100, https://doi.org/10.1002/9783527689972.ch2.

Islam, M.S., Chen, L., Sisler, J., Tam, K.C., 2018. Cellulose nanocrystal (CNC)–inorganic hybrid systems: synthesis, properties and applications. J. Mater. Chem. B 6, 864–883. https://doi.org/10.1039/C7TB03016A.

Jamshaid, A., Hamid, A., Muhammad, N., Naseer, A., Ghauri, M., Iqbal, J., Rafiq, S., Shah, N.S., 2017. Cellulose-based materials for the removal of heavy metals from wastewater—an overview. ChemBioEng Rev. 4, 240–256. https://doi.org/10.1002/cben.201700002.

Jin, L., Li, W., Xu, Q., Sun, Q., 2015. Amino-functionalized nanocrystalline cellulose as an adsorbent for anionic dyes. Cellulose 22, 2443–2456. https://doi.org/10.1007/s10570-015-0649-4.

Johar, N., Ahmad, I., Dufresne, A., 2012. Extraction, preparation and characterization of cellulose fibres and nanocrystals from rice husk. Ind. Crop Prod. 37, 93–99. https://doi.org/10.1016/j.indcrop.2011.12.016.

Jordan, J.H., Easson, M.W., Condon, B.D., 2020. Cellulose hydrolysis using ionic liquids and inorganic acids under dilute conditions: morphological comparison of nanocellulose. RSC Adv. 10, 39413–39424. https://doi.org/10.1039/d0ra05976e.

KarzarJeddi, M., Laitinen, O., Mahkam, M., Liimatainen, H., 2020. Zwitterionic hybrid aerobeads of binary metal organic frameworks and cellulose nanofibers for removal anionic pollutants. Mater. Des. 196, 109106. https://doi.org/10.1016/j.matdes.2020.109106.

Klebe, J.F., Finkbeiner, H.L., 1969. Silyl celluloses: a new class of soluble cellulose derivatives. J. Polym. Sci., Part A-1: Polym. Chem. 7, 1947–1958. https://doi.org/10.1002/pol.1969.150070733.

Kokilavani, S., Syed, A., Thomas, A.M., Elgorban, A.M., Raju, L.L., Das, A., Khan, S.S., 2020. Facile synthesis of Ag/Cu-cellulose nanocomposite for detection, photocatalysis and anti-microbial applications. Optik (Stuttg) 220, 165218. https://doi.org/10.1016/j.ijleo.2020.165218.

Kokol, V., Božič, M., Vogrinčič, R., Mathew, A.P., 2015. Characterisation and properties of homo- and heterogenously phosphorylated nanocellulose. Carbohydr. Polym. 125, 301–313. https://doi.org/10.1016/j.carbpol.2015.02.056.

Kousheh, S.A., Moradi, M., Tajik, H., Molaei, R., 2020. Preparation of antimicrobial/ultraviolet protective bacterial nanocellulose film with carbon dots synthesized from lactic acid bacteria. Int. J. Biol. Macromol. 155, 216–225. https://doi.org/10.1016/j.ijbiomac.2020.03.230.

Kuo, P.Y., Barros, L.d.A., Yan, N., Sain, M., Qing, Y., Wu, Y., 2017. Nanocellulose composites with enhanced interfacial compatibility and mechanical properties using a hybrid-toughened epoxy matrix. Carbohydr. Polym. 177, 249–257. https://doi.org/10.1016/j.carbpol.2017.08.091.

Li, J., Song, Z., Li, D., Shang, S., Guo, Y., 2014. Cotton cellulose nanofiber-reinforced high density polyethylene composites prepared with two different pretreatment methods. Ind. Crop Prod. 59, 318–328. https://doi.org/10.1016/j.indcrop.2014.05.033.

Li, P., Sirviö, J.A., Asante, B., Liimatainen, H., 2018. Recyclable deep eutectic solvent for the production of cationic nanocelluloses. Carbohydr. Polym. 199, 219–227. https://doi.org/10.1016/j.carbpol.2018.07.024.

Li, B., Li, M., Zhang, J., Pan, Y., Huang, Z., Xiao, H., 2019. Adsorption of Hg (II) ions from aqueous solution by diethylenetriamine pentaacetic acid-modified cellulose. Int. J. Biol. Macromol. 122, 149–156. https://doi.org/10.1016/j.ijbiomac.2018.10.162.

Li, J., Tao, J., Ma, C., Yang, J., Gu, T., Liu, J., 2020. Carboxylated cellulose nanofiber/montmorillonite nanocomposite for the removal of levofloxacin hydrochloride antibiotic from aqueous solutions. RSC Adv. 10, 42038–42053. https://doi.org/10.1039/d0ra08987g.

Lin, N., Dufresne, A., 2014. Surface chemistry, morphological analysis and properties of cellulose nanocrystals with gradiented sulfation degrees. Nanoscale 6, 5384–5393. https://doi.org/10.1039/c3nr06761k.

Lin, Q., Zheng, Y., Wang, G., Shi, X., Zhang, T., Yu, J., Sun, J., 2015a. Protein adsorption behaviors of carboxymethylated bacterial cellulose membranes. Int. J. Biol. Macromol. 73, 264–269. https://doi.org/10.1016/j.ijbiomac.2014.11.011.

Lin, R., Li, A., Zheng, T., Lu, L., Cao, Y., 2015b. Hydrophobic and flexible cellulose aerogel as an efficient, green and reusable oil sorbent. RSC Adv. 5, 82027–82033. https://doi.org/10.1039/c5ra15194e.

Liu, P., Borrell, P.F., Božič, M., Kokol, V., Oksman, K., Mathew, A.P., 2015. Nanocelluloses and their phosphorylated derivatives for selective adsorption of Ag+, Cu2+ and Fe3+ from industrial effluents. J. Hazard. Mater. 294, 177–185. https://doi.org/10.1016/j.jhazmat.2015.04.001.

Liu, C., Li, B., Du, H., Lv, D., Zhang, Y., Yu, G., Mu, X., Peng, H., 2016. Properties of nanocellulose isolated from corncob residue using sulfuric acid, formic acid, oxidative and mechanical methods. Carbohydr. Polym. 151, 716–724. https://doi.org/10.1016/j.carbpol.2016.06.025.

Liu, H., Chen, X., Ji, G., Yu, H., Gao, C., Han, L., Xiao, W., 2019a. Mechanochemical deconstruction of lignocellulosic cell wall polymers with ball-milling. Bioresour. Technol. 286, 121364. https://doi.org/10.1016/j.biortech.2019.121364.

Liu, P., Zhu, C., Mathew, A.P., 2019b. Mechanically robust high flux graphene oxide—nanocellulose membranes for dye removal from water. J. Hazard. Mater. 371, 484–493. https://doi.org/10.1016/j.jhazmat.2019.03.009.

Liu, J., Liu, D., Liu, S., Li, Z., Wei, X., Lin, S., Guo, M., 2020. Preparation and characterization of sulfated cellulose nanocrystalline and its composite membrane for removal of tetracycline hydrochloride in water. Energy Environ. Mater. 3, 209–215. https://doi.org/10.1002/eem2.12055.

Luo, Q., Yuan, H., Zhang, M., Jiang, P., Liu, M., Xu, D., Guo, X., Wu, Y., 2021. A 3D porous fluorescent hydrogel based on amino-modified carbon dots with excellent sorption and sensing abilities for environmentally hazardous Cr(VI). J. Hazard. Mater. 401, 123432. https://doi.org/10.1016/j.jhazmat.2020.123432.

Ma, Y., Xia, Q., Liu, Y., Chen, W., Liu, S., Wang, Q., Liu, Y., Li, J., Yu, H., 2019. Production of nanocellulose using hydrated deep eutectic solvent combined with ultrasonic treatment. ACS Omega 4, 8539–8547. https://doi.org/10.1021/acsomega.9b00519.

Ma, C., Yi, L., Yang, J., Tao, J., Li, J., 2020. Nanocellulose-organic montmorillonite nanocomposite adsorbent for diuron removal from aqueous solution: optimization using response surface methodology. RSC Adv. 10, 30734–30745. https://doi.org/10.1039/d0ra04853d.

Mahfoudhi, N., Boufi, S., 2017. Nanocellulose as a novel nanostructured adsorbent for environmental remediation: a review. Cellulose 24, 1171–1197. https://doi.org/10.1007/s10570-017-1194-0.

Man, Z., Muhammad, N., Sarwono, A., Bustam, M.A., Kumar, M.V., Rafiq, S., 2011. Preparation of cellulose nanocrystals using an ionic liquid. J. Polym. Environ. 19, 726–731. https://doi.org/10.1007/s10924-011-0323-3.

Mandal, A., Chakrabarty, D., 2011. Isolation of nanocellulose from waste sugarcane bagasse (SCB) and its characterization. Carbohydr. Polym. 86, 1291–1299. https://doi.org/10.1016/j.carbpol.2011.06.030.

McDowall, D.J., Gupta, B.S., Stannett, V.T., 1984. Grafting of vinyl monomers to cellulose by ceric ion initiation. Prog. Polym. Sci. 10, 1–50. https://doi.org/10.1016/0079-6700(84)90005-4.

Mormann, W., Wagner, T., 2000. Silylation of cellulose with hexamethyldisilazane in liquid ammonia. Carbohydr. Polym. 43, 257–262. https://doi.org/10.1016/S0144-8617(00)00173-9.

Mu, R., Hong, X., Ni, Y., Li, Y., Pang, J., Wang, Q., Xiao, J., Zheng, Y., 2019. Recent trends and applications of cellulose nanocrystals in food industry. Trends Food Sci. Technol. 93, 136–144. https://doi.org/10.1016/j.tifs.2019.09.013.

Nadar, S.S., Vaidya, L., Maurya, S., Rathod, V.K., 2019. Polysaccharide based metal organic frameworks (polysaccharide–MOF): a review. Coord. Chem. Rev. 396, 1–21. https://doi.org/10.1016/j.ccr.2019.05.011.

Nagano, T., Arai, Y., Yano, H., Aoki, T., Kurihara, S., Hirano, R., Nishinari, K., 2020. Improved physicochemical and functional properties of okara, a soybean residue, by nanocellulose technologies for food development—a review. Food Hydrocoll. 109, 105964. https://doi.org/10.1016/j.foodhyd.2020.105964.

Onwumere, J., Piątek, J., Budnyak, T., Chen, J., Budnyk, S., Karim, Z., Thersleff, T., Kuśtrowski, P., Mathew, A.P., Slabon, A., 2020. CelluPhot: hybrid cellulose-bismuth oxybromide membrane for pollutant removal. ACS Appl. Mater. Interfaces 12, 42891–42901. https://doi.org/10.1021/acsami.0c12739.

Oshima, T., Kondo, K., Ohto, K., Inoue, K., Baba, Y., 2008. Preparation of phosphorylated bacterial cellulose as an adsorbent for metal ions. React. Funct. Polym. 68, 376–383. https://doi.org/10.1016/j.reactfunctpolym.2007.07.046.

Oshima, T., Taguchi, S., Ohe, K., Baba, Y., 2011. Phosphorylated bacterial cellulose for adsorption of proteins. Carbohydr. Polym. 83, 953–958. https://doi.org/10.1016/j.carbpol.2010.09.005.

Patel, D.K., Dutta, S.D., Lim, K.-T., 2019. Nanocellulose-based polymer hybrids and their emerging applications in biomedical engineering and water purification. RSC Adv. 9, 19143–19162. https://doi.org/10.1039/C9RA03261D.

Peng, N., Hu, D., Zeng, J., Li, Y., Liang, L., Chang, C., 2016. Superabsorbent cellulose-clay nanocomposite hydrogels for highly efficient removal of dye in water. ACS Sustain. Chem. Eng. 4, 7217–7224. https://doi.org/10.1021/acssuschemeng.6b02178.

Peng, B., Yao, Z., Wang, X., Crombeen, M., Sweeney, D.G., Tam, K.C., 2020. Cellulose-based materials in wastewater treatment of petroleum industry. Green Energy Environ. 5, 37–49. https://doi.org/10.1016/j.gee.2019.09.003.

Peretz, R., Sterenzon, E., Gerchman, Y., Kumar Vadivel, V., Luxbacher, T., Mamane, H., 2019. Nanocellulose production from recycled paper mill sludge using ozonation pretreatment followed by recyclable maleic acid hydrolysis. Carbohydr. Polym. 216, 343–351. https://doi.org/10.1016/j.carbpol.2019.04.003.

Petzold, K., Koschella, A., Klemm, D., Heublein, B., 2003. Silylation of cellulose and starch—selectivity, structure analysis, and subsequent reactions. Cellulose 10, 251–269. https://doi.org/10.1023/A:1025173900225.

Qiao, H., Zhou, Y., Yu, F., Wang, E., Min, Y., Huang, Q., Pang, L., Ma, T., 2015. Effective removal of cationic dyes using carboxylate-functionalized cellulose nanocrystals. Chemosphere 141, 297–303. https://doi.org/10.1016/j.chemosphere.2015.07.078.

Qin, Z.-Y., Tong, G.-L., Chin, Y.C.F., Zhou, J.-C., 2011. Preparation of ultrasonic-assisted high carboxylate content cellulose nanocrystals by tempo oxidation. Bioresources 6, 1136–1146.

Qiu, J., Li, M., Yang, L., Yao, J., 2019. Facile construction of three-dimensional netted ZnIn2S4 by cellulose nanofibrils for efficiently photocatalytic reduction of Cr(VI). Chem. Eng. J. 375. https://doi.org/10.1016/j.cej.2019.121990.

Qiu, Z., Chen, H., Wang, Z., Zhang, T., Yang, D., Qiu, F., 2020. Efficient removal of As(Ш) via the synergistic effect of oxidation and absorption by FeOOH@MnO2@CAM nano-hybrid adsorption membrane. Chemosphere 258. https://doi.org/10.1016/j.chemosphere.2020.127329.

Qu, J., Tian, X., Jiang, Z., Cao, B., Akindolie, M.S., Hu, Q., Feng, C., Feng, Y., Meng, X., Zhang, Y., 2020. Multicomponent adsorption of Pb(II), Cd(II) and Ni(II) onto microwave-functionalized cellulose: kinetics, isotherms, thermodynamics, mechanisms and application for electroplating wastewater purification. J. Hazard. Mater. 387, 121718. https://doi.org/10.1016/j.jhazmat.2019.121718.

Rahman, K.U., Ferreira-Neto, E.P., Rahman, G.U., Parveen, R., Monteiro, A.S., Rahman, G., Van Le, Q., Domeneguetti, R.R., Ribeiro, S.J.L., Ullah, S., 2021. Flexible bacterial cellulose-based BC-SiO2-TiO2-Ag membranes with self-cleaning, photocatalytic, antibacterial and UV-shielding properties as a potential multifunctional material for combating infections and environmental applications. J. Environ. Chem. Eng. 9, 104708. https://doi.org/10.1016/j.jece.2020.104708.

Reshmy, R., Philip, E., Paul, S.A., Madhavan, A., Sindhu, R., Binod, P., Pandey, A., Sirohi, R., 2020. Nanocellulose-based products for sustainable applications-recent trends and possibilities. Rev. Environ. Sci. Biotechnol. 19, 779–806. https://doi.org/10.1007/s11157-020-09551-z.

Ribeiro, R.S.A., Pohlmann, B.C., Calado, V., Bojorge, N., Pereira, N., 2019. Production of nanocellulose by enzymatic hydrolysis: trends and challenges. Eng. Life Sci. 19, 279–291. https://doi.org/10.1002/elsc.201800158.

Rong, N., Xu, Z., Zhai, S., Zhou, L., Li, J., 2021. Directional, super-hydrophobic cellulose nanofiber/polyvinyl alcohol/montmorillonite aerogels as green absorbents for oil/water separation. IET Nanobiotechnol. 15, 135–146. https://doi.org/10.1049/nbt2.12008.

Saba, N., Mohammad, F., Pervaiz, M., Jawaid, M., Alothman, O.Y., Sain, M., 2017. Mechanical, morphological and structural properties of cellulose nanofibers reinforced epoxy composites. Int. J. Biol. Macromol. 97, 190–200. https://doi.org/10.1016/j.ijbiomac.2017.01.029.

Saito, T., Isogai, A., 2005. Ion-exchange behavior of carboxylate groups in fibrous cellulose oxidized by the TEMPO-mediated system. Carbohydr. Polym. 61, 183–190. https://doi.org/10.1016/j.carbpol.2005.04.009.

Salajková, M., Berglund, L.A., Zhou, Q., 2012. Hydrophobic cellulose nanocrystals modified with quaternary ammonium salts. J. Mater. Chem. 22, 19798–19805. https://doi.org/10.1039/c2jm34355j.

Santana, S.A.A., Vieira, A.P., da Silva Filho, E.C., Melo, J.C.P., Airoldi, C., 2010. Immobilization of ethylenesulfide on babassu coconut epicarp and mesocarp for divalent cation sorption. J. Hazard. Mater. 174, 714–719. https://doi.org/10.1016/j.jhazmat.2009.09.109.

Schrope, M., 2011. Oil spill: deep wounds. Nature 472, 152–154. https://doi.org/10.1038/472152a.

Selkälä, T., Suopajärvi, T., Sirviö, J.A., Luukkonen, T., Kinnunen, P., De Carvalho, A.L.C.B., Liimatainen, H., 2020. Surface modification of cured inorganic foams with cationic cellulose nanocrystals and their use as reactive filter media for anionic dye removal. ACS Appl. Mater. Interfaces 12, 27745–27757. https://doi.org/10.1021/acsami.0c05927.

Silva Filho, E.C., Lima, L.C.B., Silva, F.C., Sousa, K.S., Fonseca, M.G., Santana, S.A.A., 2013. Immobilization of ethylene sulfide in aminated cellulose for removal of the divalent cations. Carbohydr. Polym. 92, 1203–1210. https://doi.org/10.1016/j.carbpol.2012.10.031.

Silva, L.S., Lima, L.C.B., Silva, F.C., Matos, J.M.E., Santos, M.R.M.C., Santos Júnior, L.S., Sousa, K.S., da Silva Filho, E.-C., 2013. Dye anionic sorption in aqueous solution onto a cellulose surface chemically modified with aminoethanethiol. Chem. Eng. J. 218, 89–98. https://doi.org/10.1016/j.cej.2012.11.118.

Sirviö, J.A., Visanko, M., 2020. Lignin-rich sulfated wood nanofibers as high-performing adsorbents for the removal of lead and copper from water. J. Hazard. Mater. 383, 121174. https://doi.org/10.1016/j.jhazmat.2019.121174.

Sirviö, J.A., Ukkola, J., Liimatainen, H., 2019. Direct sulfation of cellulose fibers using a reactive deep eutectic solvent to produce highly charged cellulose nanofibers. Cellulose 26, 2303–2316. https://doi.org/10.1007/s10570-019-02257-8.

Skočaj, M., 2019. Bacterial nanocellulose in papermaking. Cellulose 26, 6477–6488. https://doi.org/10.1007/s10570-019-02566-y.

Sohni, S., Norulaini, N.A.N., Hashim, R., Khan, S.B., Fadhullah, W., Mohd Omar, A.K., 2018. Physicochemical characterization of Malaysian crop and agro-industrial biomass residues as renewable energy resources. Ind. Crop Prod. 111, 642–650. https://doi.org/10.1016/j.indcrop.2017.11.031.

Sohni, S., Hashim, R., Nidaullah, H., Lamaming, J., Sulaiman, O., 2019. Chitosan/nano-lignin based composite as a new sorbent for enhanced removal of dye pollution from aqueous solutions. Int. J. Biol. Macromol. 132, 1304–1317. https://doi.org/10.1016/j.ijbiomac.2019.03.151.

Suflet, D.M., Chitanu, G.C., Popa, V.I., 2006. Phosphorylation of polysaccharides: new results on synthesis and characterisation of phosphorylated cellulose. React. Funct. Polym. 66, 1240–1249. https://doi.org/10.1016/j.reactfunctpolym.2006.03.006.

Sun, X., Yang, L., Li, Q., Zhao, J., Li, X., Wang, X., Liu, H., 2014. Amino-functionalized magnetic cellulose nanocomposite as adsorbent for removal of Cr(VI): synthesis and adsorption studies. Chem. Eng. J. 241, 175–183. https://doi.org/10.1016/j.cej.2013.12.051.

Suopajärvi, T., Liimatainen, H., Karjalainen, M., Upola, H., Niinimäki, J., 2015. Lead adsorption with sulfonated wheat pulp nanocelluloses. J. Water Process Eng. 5, 136–142. https://doi.org/10.1016/j.jwpe.2014.06.003.

Tavakolian, M., Wiebe, H., Sadeghi, M.A., Van De Ven, T.G.M., 2020. Dye removal using hairy nanocellulose: experimental and theoretical investigations. ACS Appl. Mater. Interfaces 12, 5040–5049. https://doi.org/10.1021/acsami.9b18679.

Thiangtham, S., Runt, J., Manuspiya, H., 2019. Sulfonation of dialdehyde cellulose extracted from sugarcane bagasse for synergistically enhanced water solubility. Carbohydr. Polym. 208, 314–322. https://doi.org/10.1016/j.carbpol.2018.12.080.

Tian, C., Luo, S., She, J., Qing, Y., Yan, N., Wu, Y., Liu, Z., 2019. Cellulose nanofibrils enable flower-like BiOCl for high-performance photocatalysis under visible-light irradiation. Appl. Surf. Sci. 464, 606–615. https://doi.org/10.1016/j.apsusc.2018.09.126.

Ul-Islam, M., Ullah, M.W., Khan, S., Park, J.K., 2020. Production of bacterial cellulose from alternative cheap and waste resources: a step for cost reduction with positive environmental aspects. Korean J. Chem. Eng. 37, 925–937. https://doi.org/10.1007/s11814-020-0524-3.

Ullah, H., Wahid, F., Santos, H.A., Khan, T., 2016. Advances in biomedical and pharmaceutical applications of functional bacterial cellulose-based nanocomposites. Carbohydr. Polym. 150, 330–352. https://doi.org/10.1016/j.carbpol.2016.05.029.

Vieira, A.P., Santana, S.A.A., Bezerra, C.W.B., Silva, H.A.S., de Melo, J.C.P., da Silva Filho, E.C., Airoldi, C., 2010. Copper sorption from aqueous solutions and sugar cane spirits by chemically modified babassu coconut (Orbignya speciosa) mesocarp. Chem. Eng. J. 161, 99–105. https://doi.org/10.1016/j.cej.2010.04.036.

Wan, C., Li, J., 2015. Facile synthesis of well-dispersed superparamagnetic γ-Fe2O3 nanoparticles encapsulated in three-dimensional architectures of cellulose aerogels and their applications for Cr(VI) removal from contaminated water. ACS Sustain. Chem. Eng. 3, 2142–2152. https://doi.org/10.1021/acssuschemeng.5b00384.

Wang, M., Xu, L., Peng, J., Zhai, M., Li, J., Wei, G., 2009. Adsorption and desorption of Sr(II) ions in the gels based on polysaccharide derivates. J. Hazard. Mater. 171, 820–826. https://doi.org/10.1016/j.jhazmat.2009.06.071.

Wang, F., Zhao, J., Liu, H., Luo, Y., Wang, W., 2018. Preparation of double carboxylic corn stalk gels and their adsorption properties towards rare earths (III). Waste Biomass Valoriz. 9, 1945–1954. https://doi.org/10.1007/s12649-017-9954-5.

Wang, J., Li, X., Cheng, Q., Lv, F., Chang, C., Zhang, L., 2020. Construction of β-FeOOH@tunicate cellulose nanocomposite hydrogels and their highly efficient photocatalytic properties. Carbohydr. Polym. 229, 115470. https://doi.org/10.1016/j.carbpol.2019.115470.

Watanabe, K., Tabuchi, M., Morinaga, Y., Yoshinaga, F., 1998. Structural features and properties of bacterial cellulose produced in agitated culture. Cellulose 5, 187–200. https://doi.org/10.1023/A:1009272904582.

Wei, H., Rodriguez, K., Renneckar, S., Vikesland, P.J., 2014. Environmental science and engineering applications of nanocellulose-based nanocomposites. Environ. Sci. Nano 1, 302–316. https://doi.org/10.1039/C4EN00059E.

Wu, Y., Xie, Y., Zhong, F., Gao, J., Yao, J., 2020. Fabrication of bimetallic Hofmann-type metal-organic Frameworks@Cellulose aerogels for efficient iodine capture. Microporous Mesoporous Mater. 306, 110386. https://doi.org/10.1016/j.micromeso.2020.110386.

Yan, H., Zhang, W., Kan, X., Dong, L., Jiang, Z., Li, H., Yang, H., Cheng, R., 2011. Sorption of methylene blue by carboxymethyl cellulose and reuse process in a secondary sorption. Colloids Surf. A Physicochem. Eng. Asp. 380, 143–151. https://doi.org/10.1016/j.colsurfa.2011.02.045.

Yang, R., Aubrecht, K.B., Ma, H., Wang, R., Grubbs, R.B., Hsiao, B.S., Chu, B., 2014. Thiol-modified cellulose nanofibrous composite membranes for chromium (VI) and lead (II) adsorption. Polymer (Guildf) 55, 1167–1176. https://doi.org/10.1016/j.polymer.2014.01.043.

Yang, C., Wang, L., Yu, Y., Wu, P., Wang, F., Liu, S., Luo, X., 2020a. Highly efficient removal of amoxicillin from water by Mg-Al layered double hydroxide/cellulose nanocomposite beads synthesized through in-situ coprecipitation method. Int. J. Biol. Macromol. 149, 93–100. https://doi.org/10.1016/j.ijbiomac.2020.01.096.

Yang, L., Chen, C., Hu, Y., Wei, F., Cui, J., Zhao, Y., Xu, X., Chen, X., Sun, D., 2020b. Three-dimensional bacterial cellulose/polydopamine/TiO2 nanocomposite membrane with enhanced adsorption and photocatalytic degradation for dyes under ultraviolet-visible irradiation. J. Colloid Interface Sci. 562, 21–28. https://doi.org/10.1016/j.jcis.2019.12.013.

Yin, Y., Ma, J., Tian, X., Jiang, X., Wang, H., Gao, W., 2018. Cellulose nanocrystals functionalized with amino-silane and epoxy-poly(ethylene glycol) for reinforcement and flexibilization of poly(lactic acid): material preparation and compatibility mechanism. Cellulose 25, 6447–6463. https://doi.org/10.1007/s10570-018-2033-7.

Yu, H., Abdalkarim, S.Y.H., Zhang, H., Wang, C., Tam, K.C., 2019. Simple process to produce high-yield cellulose nanocrystals using recyclable citric/hydrochloric acids. ACS Sustain. Chem. Eng. 7, 4912–4923. https://doi.org/10.1021/acssuschemeng.8b05526.

Yu, Y., Zhu, X., Wang, L., Wu, F., Liu, S., Chang, C., Luo, X., 2020. A simple strategy to design 3-layered Au-TiO2 dual nanoparticles immobilized cellulose membranes with enhanced photocatalytic activity. Carbohydr. Polym. 231, 115694. https://doi.org/10.1016/j.carbpol.2019.115694.

Zhang, J., Jiang, N., Dang, Z., Elder, T.J., Ragauskas, A.J., 2008. Oxidation and sulfonation of cellulosics. Cellulose 15, 489–496. https://doi.org/10.1007/s10570-007-9193-1.

Zhang, G., Zhang, L., Deng, H., Sun, P., 2011. Preparation and characterization of sodium carboxymethyl cellulose from cotton stalk using microwave heating. J. Chem. Technol. Biotechnol. 86, 584–589. https://doi.org/10.1002/jctb.2556.

Zhang, Z., Sèbe, G., Rentsch, D., Zimmermann, T., Tingaut, P., 2014a. Ultralightweight and flexible silylated nanocellulose sponges for the selective removal of oil from water. Chem. Mater. 26, 2659–2668. https://doi.org/10.1021/cm5004164.

Zhang, G., Yi, L., Deng, H., Sun, P., 2014b. Dyes adsorption using a synthetic carboxymethyl cellulose-acrylic acid adsorbent. J. Environ. Sci. (China) 26, 1203–1211. https://doi.org/10.1016/S1001-0742(13)60513-6.

Zhang, C., Zhang, R.Z., Ma, Y.Q., Guan, W.B., Wu, X.L., Liu, X., Li, H., Du, Y.L., Pan, C.P., 2015. Preparation of cellulose/graphene composite and its applications for triazine pesticides adsorption from water. ACS Sustain. Chem. Eng. 3, 396–405. https://doi.org/10.1021/sc500738k.

Zhang, K., Sun, P., Liu, H., Shang, S., Song, J., Wang, D., 2016a. Extraction and comparison of carboxylated cellulose nanocrystals from bleached sugarcane bagasse pulp using two different oxidation methods. Carbohydr. Polym. 138, 237–243. https://doi.org/10.1016/j.carbpol.2015.11.038.

Zhang, N., Zang, G.L., Shi, C., Yu, H.Q., Sheng, G.P., 2016b. A novel adsorbent TEMPO-mediated oxidized cellulose nanofibrils modified with PEI: preparation, characterization, and application for Cu(II) removal. J. Hazard. Mater. 316, 11–18. https://doi.org/10.1016/j.jhazmat.2016.05.018.

Zhang, D., Zhang, M., Chen, S., Liang, Q., Sheng, N., Han, Z., Cai, Y., Wang, H., 2021. Scalable, self-cleaning and self-floating bi-layered bacterial cellulose biofoam for efficient solar evaporator with photocatalytic purification. Desalination 500, 114899. https://doi.org/10.1016/j.desal.2020.114899.

Zhao, D., Huang, J., Zhong, Y., Li, K., Zhang, L., Cai, J., 2016. High-strength and high-toughness double-cross-linked cellulose hydrogels: a new strategy using sequential chemical and physical cross-linking. Adv. Funct. Mater. 26, 6279–6287. https://doi.org/10.1002/adfm.201601645.

Zhao, H., Xia, J., Wang, J., Yan, X., Wang, C., Lei, T., Xian, M., Zhang, H., 2018. Production of bacterial cellulose using polysaccharide fermentation wastewater as inexpensive nutrient sources. Biotechnol. Biotechnol. Equip. 32, 350–356. https://doi.org/10.1080/13102818.2017.1418673.

Zhao, W., Zhang, J., Zhu, F., Mu, F., Zhang, L., Dai, B., Xu, J., Zhu, A., Sun, C., Leung, D.Y.C., 2019. Study the photocatalytic mechanism of the novel Ag/p-Ag2O/n-BiVO4 plasmonic photocatalyst for the simultaneous removal of BPA and chromium(VI). Chem. Eng. J. 361, 1352–1362. https://doi.org/10.1016/j.cej.2018.12.181.

Zhao, Y., Zhong, K., Liu, W., Cui, S., Zhong, Y., Jiang, S., 2020. Preparation and oil adsorption properties of hydrophobic microcrystalline cellulose aerogel. Cellulose 27, 7663–7675. https://doi.org/10.1007/s10570-020-03309-0.

Zhou, Y., Zhang, M., Hu, X., Wang, X., Niu, J., Ma, T., 2013. Adsorption of cationic dyes on a cellulose-based multicarboxyl adsorbent. J. Chem. Eng. Data 58, 413–421. https://doi.org/10.1021/je301140c.

Zhou, X., Fu, Q., Liu, H., Gu, H., Guo, Z., 2021. Solvent-free nanoalumina loaded nanocellulose aerogel for efficient oil and organic solvent adsorption. J. Colloid Interface Sci. 581, 299–306. https://doi.org/10.1016/j.jcis.2020.07.099.

Zhu, Q., Wang, Y., Li, M., Liu, K., Hu, C., Yan, K., Sun, G., Wang, D., 2017. Activable carboxylic acid functionalized crystalline nanocellulose/PVA-co-PE composite nanofibrous membrane with enhanced adsorption for heavy metal ions. Sep. Purif. Technol. 186, 70–77. https://doi.org/10.1016/j.seppur.2017.05.050.

Zhu, G., Xu, H., Dufresne, A., Lin, N., 2018. High-adsorption, self-extinguishing, thermal, and acoustic-resistance aerogels based on organic and inorganic waste valorization from cellulose nanocrystals and red mud. ACS Sustain. Chem. Eng. 6, 7168–7180. https://doi.org/10.1021/acssuschemeng.8b01244.

Zu, G., Shen, J., Zou, L., Wang, F., Wang, X., Zhang, Y., Yao, X., 2016. Nanocellulose-derived highly porous carbon aerogels for supercapacitors. Carbon NY 99, 203–211. https://doi.org/10.1016/j.carbon.2015.11.079.

CHAPTER

17

Cellulose-based nano-biosorbents in water purification

Oluwaseun J. Ajala[a,b], *A. Khadir*[c], *Joshua O. Ighalo*[d,e], *and Great C. Umenweke*[f]

[a]Department of Industrial Chemistry, University of Ilorin, Ilorin, Nigeria [b]Department of Pure and Applied Chemistry, Ladoke Akintola University of Technology Ogbomoso, Ogbomoso, Nigeria [c]Young Researcher and Elite Club, Yadegar-e-Imam Khomeini (RAH) Shahre Rey Branch, Islamic Azad University, Tehran, Iran [d]Department of Chemical Engineering, University of Ilorin, Ilorin, Nigeria [e]Department of Chemical Engineering, Nnamdi Azikiwe University, Awka, Nigeria [f]Department of Chemistry, University of Kentucky, Lexington, KY, United States

17.1 Introduction

Water has always been regarded as a vital substance to life, not only for humans but also for all ecosystems both living and non-living due to its usage in the industry, environmentally, and domestically among others. According to the World Water Development Report 2015, water availability is one of the core sustainable development goals due to various challenges facing the system through different pollutants such as pesticides, acid mine drainage among others (Adelodun et al., 2021; WHO, 2016). So, it is vitally important to manage the quantity and quality of waters to witness a healthy ecosystem. Given this, it has been discovered that water quantity is not equally distributed around the world; there are regions with high annual precipitation while in desert areas, rainfall and precipitation, in general, is negligible. Apart from quantity, water quality needs to be considered seriously (Ighalo et al., 2020a). In past decades, the fate and transport of common elements such as nitrogen and phosphorus were regularly studied; however, academia now is facing much more complicated areas. Modernization and industrial life have introduced so many other new organic compounds to the environment that all are potent in reducing water quality and posing threats to human life such as heavy metals (Ighalo and Adeniyi, 2020a), dyes (Hevira et al., 2020), pesticide (Ajala et al., 2018; Nwosu et al., 2019), and pharmaceuticals (Tijani et al., 2016) among others.

https://doi.org/10.1016/B978-0-323-90912-9.00017-4

The use of heavy metals (elements having a specific gravity above 5 and atomic weights in the range of 63.5–200.6) in many industries ranging from electroplating, battery manufacturing, mining, and textile to ceramic, photography, and tannery industries have induced a huge challenge for ecosystems and society (Abdullahi et al., 2020). The main concerns regarding heavy metals are their stability, recalcitrance, accumulation in nature, and toxicity (Wu et al., 2020). Some of the heavy metals health problems are nervous system damage, muscular stiffness, cancer, hypertension, and liver disorder (Wang et al., 2019). Nickel, cadmium, cobalt, zinc, lead, and chromium are common types of heavy metals. To remove these ions, chemical precipitation, adsorption (Nwosu et al., 2018), electro-coagulation (Simate et al., 2016), ion-exchange (Bratby, 2016), and photocatalysis (Solis-Casados et al., 2018) have been extensively employed.

Dyes have greatly contributed to the attainment of colorful surroundings. In textile industries, pharmaceuticals, food, cosmetics, metallurgy, plastics, leather, and so many other sectors, dyes are extensively used (Tavakolian et al., 2020). Apart from their benefits to human beings, dyes have several environmental concerns, especially for water channels. Dyes are known as persistent chemicals, stable, almost non-biodegradable, toxic, carcinogenic, and recalcitrant (Cai et al., 2020). Note that even dye at a low concentration of 1 mg/L causes coloration and undesirable conditions for consumption. Dye molecules gather on the surface of waters, hinder light penetration and induce photosynthesis disorder. Therefore, the treatment of industrial effluents containing a large number of dye molecules is of the utmost importance.

The development of pharmaceuticals has given hope to many people around the world. Such discovery has been successful in treating disease, relieving pain, and granting long life to many people. However, similar to many advances, it has its consequences in the environment (Aniagor et al., 2021). Uncontrolled consumption of pharmaceuticals because of their availability (in many countries), improper waste management, expired drugs that are thrown away in the sink, and not fully metabolized drugs excreted from a human via urine have led to the detection of pharmaceuticals in rivers, lakes, drinking water and of course water and wastewater treatment plants (Madikizela et al., 2020; Oba et al., 2021). Consider that pharmaceuticals even in μg/L are capable of posing threats to the ecosystem and environment (Zhang et al., 2020). A wide range of treatment methodologies including adsorption, advanced oxidation processes, aerobic and anaerobic process, and membrane separation has been employed to test pharmaceutical removal from contaminated waters (Ighalo et al., 2021b). The elimination of pharmaceuticals is of great concern since these compounds are prone to spread bacterial that would be resistant to pharmaceutical (antibiotic), endangering the lives of humans and animals (Shi et al., 2019).

17.2 Cellulose and its application

Even though there are countless methods and materials in water and wastewater remediation, scholars have always been looking for cost-effective and non-toxic materials. In general, naturally—occurring polymers are preceded over synthetic polymers because of their intrinsic characteristics such as biocompatibility, bio-absorbable degradation products, and

non-toxicity to the human body even at high concentrations (Shekar and Ramachandra, 2018; Tayeb et al., 2018). These advantages prompt researchers to utilize bio-based materials in extensive works for water and wastewater decontamination (Tran et al., 2015; Zarei and Zarei, 2018). Cellulose is known as the most abundant natural straight-chain polysaccharide which is produced by bacteria or plants forming out of D-glucopyranose residues linked by β-(1,4)-glycosidic linkages (Kalia et al., 2011; Wang, 2019). This super-macromolecular structure endows cellulose with an ultrahigh strength of 150 MPa. Cellulose fibrils divide two discrete domains including highly ordered (i.e., crystalline) and disordered (i.e., amorphous) structures. Compared to bacterial cellulose which is almost composed of a pure phase, plant cellulose associate with hemicelluloses, lignin, and pectin. Bacterial cellulose illustrates significant hydrophilicity, permeability, water-uptake capacity, and tensile strength (Naseri-Nosar and Ziora, 2018; Wang, 2019). Features such as environmental friendliness, cost-effectiveness, availability, and safe nature have made cellulose a versatile promising biomaterial.

The common derivatives of cellulose are containing carboxymethyl cellulose (CMC), hydroxyethylcellulose (HEC), cellulose acetate (CA), methylcellulose (MC), (hydroxypropyl) methylcellulose (HPMC), and so forth. CMC is an anionic water-soluble biopolymer that is hydrophile, pH-sensitive, non-toxic, and can form a gel, so it can be able to use in drug delivery and other biomedical research. Based on carboxylate groups of CMC, it will be useful in diverse applications such as water treatment, conductive films, reaction catalysis, protein immobilization, lithium-sulphur batteries, and so on. Researches confirm that biopolymers ensure environmental health and safety. In this regard, nanocellulose has attracted many researchers in the materials fields due to bearing availability, lightweight, renewability, nanosized dimensionality, automotivity (for manufacturing parts based on micropatterns), significant morphology, and unsurpassed quintessential chemical and physical properties (Javanbakht and Shaabani, 2019; Li et al., 2018). The development of biocomposites using renewable resources can replace synthetic polymer-based composites. Several renewable biopolymers can be used to synthesize bio-nanocomposites such as poly-lactides; starch plastics; cellulosic plastics; soy-based plastics, polyhydroxyalkanoates (bacterial polyesters). There are two types of cellulose-based biocomposites; structural biocomposite which is used in the building industry, manufacturing stairs, roof and load-bearing walls, subflooring structures; and non-structural biocomposite which is developed for products such as tiles, ceiling, furniture, doors, etc.

Cellulose-based composites are also aroused many applications in various fields. They mostly use in the paper and packaging industry. We mention some of them here as follows:

– *Composites and fillers*

Nanocellulose can be exploited as reinforcing agents for the processing of bio-nanocomposites including coatings, films, and foams, and so on. Enhanced performances of tensile properties were reported for phenol-formaldehyde resin which was combined with nanofiber cellulose previously.

– *Paper and packaging industry*

Instead of synthetic polymers derived from petrochemical resources which result in many damages mentioned before, nanocellulose can be the best candidate for the paper and

packaging industries. Nanocellulose exhibits exceptional properties containing nanoscale dimension with gas and water barrier characteristics, due to its penetrated network for preventing the passing of external molecules. Furthermore, it is achieved from the renewable source of natural polymer cellulose, hence cost-effective and non-toxic. Carboxymethyl guar (CMG), agar or semi-interpenetrating polymer network of poly(vinyl alcohol)/polyacrylamide is considered as reinforcing polymer with enhancing gas barrier and mechanical features for the packaging aims.

– *Biomedical applications*

High surface area, volume ratio, high strength as well as modifiable surface chemistry make nanocellulose a promising candidate for biomedical applications. Novel hydrogel with semi-interpenetrating polymer network based on nanocellulose can arise pH sensitivity and mechanical resistance resulting in novel drug and gene delivery performance.

– *Ion exchange membrane*

Proton-exchange membrane for fuel cell (PEMFC) and direct methanol fuel cell (DMFC) using bacterial nanocellulose and Nafion composite films are some of the other applications of nanocellulose which have been reported so far. Algal nanocellulose/polypyrrole composite exhibits a large surface area, produces large catalytic oxidation currents, and presents storage of the charge. They are some of the successful examples of cellulose-based composites which can be designed for reversible electrochemically control of ion exchange membrane.

– *Coating applications*

Nanocellulose based composites have the potential to be employed for coating applications as a result of their high optical transparency. Protective coating of mild steel by incorporating epoxy resin composite is one of their applications that illustrate significant anti-corrosion properties. Furthermore, composites based on cellulose nanofiber are helpful for paint coatings and adhesives with high shear tolerance properties (Sharma et al., 2019; Wang et al., 2017b).

17.2.1 Cellulose in water purification

Apart from the above–mentioned applications, cellulose-based composites have shown promising results in the adsorption/removal of many pollutants, ranging from ions to macromolecules. In view of heavy metals (Mirjavadi et al., 2019) developed new low-cost composites based on cellulose namely Fe_3O_4/zeolite/cellulose nanofibers for the elimination of zinc from synthetic and actual wastewater. The authors investigated the effect of various parameters, including pH, contact time, zinc concentration, and temperature. Reaching the maximum adsorption capacity of 9.45 mg/g was indicative of cellulose nanofibers composite potential in heavy metal removal. In another study focusing on cellulose-based aerogel, the authors prepared a new adsorbent, propylene glycol adipate-modified cellulose aerogel, for the removal of Congo Red (Tang et al., 2020). Aerogel prepared from cellulose mainly offers greater surface area and low density; however, difficulties in its

formation and low mechanical strength have forced its use in a composite to achieve better performance. Cellulose aerogels/polypropylene glycol adipate showed the adsorption capacity of 120 mg/g toward Congo red dye as well as enhanced mechanical strength. The substrate was prepared from wheat bran. The authors reported the importance of the initial pH value in which complete and (more than) 80% removal of the antibiotic was occurred at pH 6 and 4, respectively. Not only for cellulose-based composites but also many other adsorbents pH plays a critical role in adsorbent and adsorbate interaction (Al-Zboon et al., 2019; Khadir et al., 2020). Ligno-cellulosic substrate followed pseudo-second-order and Sips assumptions for enrofloxacin removal. With the aim of facile separation and improved efficiency, Sun et al. (2021) extracted cellulose from *Pennisetum sinese* Roxb for tetracycline elimination. Intra-particle diffusion, chemical ion exchange, hydrogen bonding, and electrostatic interaction were deduced as the dominant mechanism involved in antibiotic removal. Magnetic cellulose was found to be a perfect adsorbent and even its application could be extended in real-world strategies.

The abovementioned studies demonstrate that in today's world, scholars and academia are seeking materials that could be readily found and extracted from nature. Cellulose-based composites are known as successful groups of nature-based composites that exhibited outstanding performance in water and wastewater purification. This chapter attempts to focus on various composites of cellulose that have been prepared for the removal of environmental pollutants.

17.3 Cellulose-based composites for the removal of dyes

The presence of several chemical dyes in the aqueous environment is a result of foreseeable technological advancements (Iwuozor et al., 2021). The 21st century has experienced so much technology and industrial increase, hence making the release of synthetic dye into the environment greater (Góes et al., 2016). This is of noble concern due to the toxicity of the chemical substance, which is harmful to both humans and aquatic habitats and the environment as large. Yet, dyes cannot be ignored because they are chiefly applied in the clothing and textile industry, food, aesthetics, and more lately printing (Singh et al., 2017; Hevira et al., 2020). Therefore, to address the issue of contaminating the water bodies and environmental pollution, the dyes released need to be removed to still ensure the relevance of technological advancements that aims toward environmental sustainability. According to Hevira et al. (2021), several techniques have been adopted for the removal of synthetic dye from the environment. As shown in Fig. 17.1, these methods range from chemical methods to biological and physical methods, in some cases, the technique adopted could be hybrid (Das et al., 2019). From the classification above, among the varied methods which includes the use of enzymes for removal, ion exchange, ozonation, oxidation, and photolysis. The ion exchange technique is widely applied in the use of cellulose-based material for the removal of dyes, but there are some disadvantages encountered (Wang et al., 2016). For hybrid methods such as biosorption and microbial electrochemistry, physicochemical biosorption is highly advantageous, less complicated with equipment usage, and it is highly efficient (Hevira et al., 2020; Ighalo

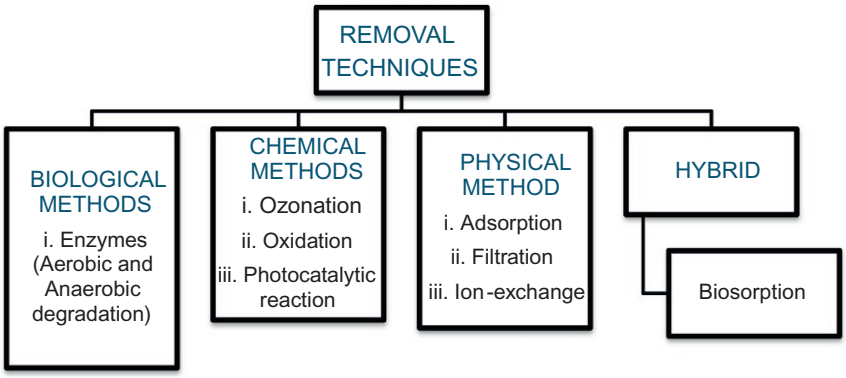

FIG. 17.1 Summary of dye removal techniques using cellulose-based biomaterials.

and Adeniyi, 2020a). To consider the cost-effectiveness of (bio)-chemical dye removal, the reusability or recyclability of the cellulose-based composite bio-adsorbent needs to be considered. The report has shown the ability of cellulose-based composite bio-adsorbents are better suited for bioremediation activities (Liu et al., 2015).

There are more than a thousand dyes and pigments in huge tonnages used industrially (Góes et al., 2016), and the larger the amount of dyes exposed to the environment, would result in greater the environmental damage. The use of cellulose as adsorbents is evident, due to its vast ability to unite with varied dyes (Zhou et al., 2013). Góes et al. (2016) used wood furniture industrial wastes, specifically polyurethane foam that contains cellulose to remove dyes. In their work, three different dyes were prepared and synthesized. They worked with a chemically modified cellulose using 4,4-diphenylmethane diisocyanate (MDI) at molar ratios 1OH:1NCO (cellulose 1:1) and 3OH:1NCO (cellulose 3:1), polyurethane with unmodified cellulose, and a polyurethane without cellulose. Their result showed that with or without cellulose, the use of polyurethane foam has a high sorption capacity, which can be applied in water treatment. Lignin, which is the second most abundant organic polymer on earth (Misra et al., 2011) followed by cellulose, is an excellent adsorbent, either in the modified or single form (Huang et al., 2019). Lignin-cellulose composite hydrogels have wide applicability. They are used in weathering materials, thermal insulation, water purification, food packaging, and in the development of smart materials (Huang et al., 2019; Jiehong Guo et al., 2016). Although it is evident from the above reports that lignin is a good adsorbent for dye removal, Li et al. (2016) affirm that the saturated adsorption capacity for most bio-organic dyes is not high enough for most lignin-cellulose-based adsorbents and cannot be recycled after use (Jiehong Guo et al., 2016).

Table 17.1 shows a summary of novel cellulose-based adsorbents involved in dye removal. A report by Salama (2017) showed that due to the large production and low cost of cellulose (thereby increasing its availability), cellulose has become widely applied in the removal of dye, organic matter, and waste pollutants from wastewater. Here, cellulose grafted hydroxyapatite and soy protein isolate (SPI) hybrid was studied, to evaluate its use in the removal of

TABLE 17.1 Dye removal conditions for cellulose-based bio-adsorbents.

Cellulose-based composite bio-adsorbents	Removal technique/ Conditions	Bio-chemical dyes removed (pollutants)	Adsorption models	Dye percentage removal (adsorption capacity mg/g)	References
Cellulose modified with glycidyl methacrylate and sulfosalicylic acid	Adsorption	Crystal violet (CV)	Langmuir isothermal model	70.8%	Zhou et al. (2014)
Hairy nanocellulose (electrosterically stabilized nanocrystalline cellulose (ENCC))	Adsorption	Methylene Blue	–	1250 mg/g	Tavakolian et al. (2020)
Polyurethane foam chemically modified with 4,4-diphenylmethane diisocyanate	Adsorption (chemisorption)	Methylene Blue, Procion Yellow HE-4R, and Procion Red HE-7B dyes	–	≈70%	Góes et al. (2016)
Cellulose (CGD) was prepared via modifying with glycidyl methacrylate (GMA) and diethylenetriamine pentaacetic acid (DTPA)	Adsorption	Cationic dyes—Malachite green (MG) and basic fuchsine (BF)	MG-Langmuir BF—Freundlich	MG ˃ 90% BF ˃ 85%	Zhou et al. (2013)
Amino-terminated hyperbranched polymer (NH2-HBP) and beta-cyclodextrin (β-CD) grafted into cotton fibers	Adsorption	Congo Red (CR) and Methylene Blue (MB)	CR and MB—Freundlich model	–	Yue et al. (2019)
Beta-cyclodextrin (β-CD) and amino-terminated hyperbranched polymer (NH_2-HBP) grafted into cotton fibers	Adsorption	Congo Red (CR) and Methylene Blue (MB)	CR and MB—Freundlich model	CR and MB ˃ 80%	Yue et al. (2017)
Carboxymethyl cellulose-acrylamide-graphene oxide (CMC-AM-GO) hydrogels	Free radical process	Acid Blue-133	–	185.45 mg/g	Varaprasad et al. (2017)

Continued

TABLE 17.1 Dye removal conditions for cellulose-based bio-adsorbents—cont'd

Cellulose-based composite bio-adsorbents	Removal technique/ Conditions	Bio-chemical dyes removed (pollutants)	Adsorption models	Dye percentage removal (adsorption capacity mg/g)	References
CuS-functionalized cellulose-based aerogel (CBA)	Adsorption	Methylene Blue (MB)	–	Photo-degradation rates: CuS/ CBA—94.1%, pure CuS—67.4%	Saeed et al. (2019)
Fine aminated cellulose/ montmorillonite mesoporous composite beads (ACeMt)	Adsorption	Auramine O dye	Langmuir	1336.2 mg/g at 55 degree	Pan et al. (2019)
Amide-functionalized cellulose-based porous adsorbent	Adsorption	Acid Black 1, Acid Red 18, and copper ions	–	Desorption rates: Acid Black 1–751.8, Acid Red 18–417.9 and copper ions—51.3 mg/g	Pan et al. (2019)

methylene blue (MB) by adsorption. The result showed that methylene blue was removed up to about 95%, after four cycles of adsorption and desorption. This not only presents cellulose-based composite as promising for dye removal from wastewater but also showed how cost-effective cellulose-based composites can be due to their high reusability (Salama, 2017). In another study, a much novel adsorbent was prepared and utilized. The cellulosic adsorbent used involved a cross-linked (dimethylaminoethyl) methacrylate (DMAEMA) with carboxymethyl cellulose (CMC) backbone, using ethylene glycol dimethacrylate and potassium persulphate. This new adsorbent was used in the removal of methyl orange from an aqueous solution. After about three experiments, the DMAEMA-CMC hydrogel showed a promising result and the adsorption of 1825 mg/g (Salama et al., 2015).

17.4 Cellulose-based composites for the removal of heavy metals

Heavy metal has been identified as one of the greatest challenges of the ecosystem. In this section, the research effort is reviewed and discussed on the successful application of cellulose for the removal of heavy metals. Almost all heavy metals have been categorized as potentially toxic depending on the duration and dose of exposure. The following elements were listed as

the most commonly observed heavy metals; Mn, Cr, Ni, Cd, Zn, and Pb (based on atomic density greater than 5 g/cm^3) (Priya et al., 2020). This group is associated with severe contamination and ecotoxicity. There are different sources of heavy metals in the environments such as Natural, Lithogenic, Geogenic, and anthropogenic sources. The natural or geological sources of heavy metals in the environment include; weathering process of metal-bearing rocks and the eruption of volcanoes. The global trends of urbanization and industrialization have led to an increase in heavy metals from anthropogenic sources to the environment (Ighalo and Adeniyi, 2020a). These heavy metals are highly toxic, non-biodegradable, and carcinogenic in nature (Bamidele et al., 2020). Serious health effects caused by heavy metals exposure include cancer, organ damage, brain tumor, among others (Priya et al., 2020).

Due to several challenges associated with heavy metals, some conventional technology has been employed for the treatment of these pollutants such as; ultrafiltration, membrane filtration, electro-coagulation, precipitation, co-precipitation (Zeman and Zydney, 2017), ozonation (Tanatti et al., 2019), reverse osmosis (Xu et al., 2019), and activated carbon adsorption (An et al., 2020). However, some of these methods are associated with different shortcomings. For instance, reverse osmosis and ozonation are very expensive (Tanatti et al., 2019). Precipitation and co-precipitation also generate toxic sludge during the process (Peng and Guo, 2020) while others achieved low removal capacity due to all these shortcomings, removal of heavy metals from wastewater has not been able to be achieved and these brought about exploring other techniques like adsorption.

Adsorption is one of the techniques applied for the removal of pollutants or contaminants from wastewater through a catalytic surface. Various types of adsorbents have been applied through this method. The most commonly used adsorbents are activated carbon (Mahmood and Abdulmajeed, 2017), agricultural wastes (Singh et al., 2017), bentonite clays (Abdullahi et al., 2020), kaolinite clay (Nwosu et al., 2019), and cellulose (Tao et al., 2020) which have successfully removed heavy metals concentrations (Ogunleye et al., 2014). In this process, there are two approaches: dynamic technique and static technique.

In the dynamic technique, there is the passage of the wastewater via a mobile, fixed, or fluidized absorbent layer with continuous flow. In the static technique, the adsorbent is stirred with wastewater and further separated through filtration or centrifugation (Ighalo et al., 2020b). Most chemical techniques used for the treatment of wastewater always generate metallic sludge in large quantities which requires further treatment before release. When applied to dilute wastewater of lower concentrations of metal ions, these processes are either inefficient or not cost-effective and require a high level of expertise.

Therefore, due to the good properties of cellulose-based materials, it has been proved to have no significantly ecotoxicological concern. Also, studies have shown that it is good potential material for adsorbent for the removal of heavy metals. Biswas et al. (2020) carried out studies on the removal of gold and platinum from acidic waste effluents using cellulose-based bio-adsorbent and the result was 99% maximum removal. Also, Kong et al. (2014) reported the removal of Cu^{2+}, Pb^{2+}, and Cd^{2+} from an aqueous solution using acrylic-modified sugarcane bagasse-based cellulose. The results showed that the adsorption capacities of Cu^{2+}, Pb^{2+}, and Cd^{2+} are 268, 700, and 320 mg/g, respectively. Wang et al. (2019) reported the preparation and characterization of cellulose-based adsorbent and also applied it for the removal of Cu^{2+} and Ni^{2+} and found that for Cu^{2+}, the adsorption capacity was 16.90 mg/g while for Ni^{2+} it was 11.63 mg/g. Other previous studies are summarized in Table 17.2.

TABLE 17.2 A summary of research in which cellulose-based material was applied for the treatment of heavy metals and their adsorption capacity.

Author(s)	Title	Heavy metals	Adsorption capacity
Kong et al. (2014)	Removal of Heavy metals from aqueous solution using acrylic-modified sugarcane bagasse-based adsorbents: equilibrium and kinetic studies	Cu^{2+} Pb^{2+} Cd^{2+}	268 mg/g 700 mg/g 320 mg/g
Dong et al. (2016)	Recovery of Au(III) by radiation synthesized aminomethyl pyridine functionalized adsorbents based on cellulose	Au^{3+}	90%–95%
Ge et al. (2016)	Cellulose/poly(ethylene imine) composites as efficient and reusable adsorbents for heavy metal ions	Cu^{2+}	285.7 mg/g
Li et al. (2018)	Study on cellulose microfilaments based composite spheres: microwave-assisted synthesis, characterization, and application in pollutant removal	Pb^{2+}	42.5 mg/g
Wang et al. (2019)	Preparation and characterization of cellulose-based adsorbent and its application in heavy metal ions removal	Cu^{2+} Ni^{2+}	16.90 mg/g 11.63 mg/g
Xia et al. (2018)	Bagasse cellulose grafted with an amino-terminated hyperbranched polymer for the removal of Cr(VI) from aqueous solution	Cr^{6+}	74.4%
Li et al. (2019)	Fluorescence-sensitive adsorbent based on cellulose using for mercury detection and removal from aqueous solution with selective "on-off" response	Hg^{2+}	>96%
Cheng et al. (2019)	Adsorption of Sr(II) from water by mercerized bacterial cellulose membrane modified with EDTA	Sr^{2+}	44.86 mg/g
Biswas et al. (2020)	Highly selective and straightforward recovery of gold and platinum from acidic waste effluents using cellulose-based bio-adsorbent	Au^{3+} Pt^{4+}	99%
Li et al. (2020)	Dual responsive copolymers-grafted micro fibrillated cellulose composites for removing lead ions from aqueous solution	Pb^{2+}	187.3 mg/g
Priya et al. (2020)	Phytoremediation of banana leaf functionalization of mercaptan cellulose and its utilization for the removal of heavy metals in an aqueous environment	As^{3+}	70%–75%
Shi et al. (2020)	Bio-adsorbent preparation based on Chinese Radix isatidis residue for Pb(II) removal	Pb^{2+}	27.6 mg/g
Rahman et al. (2020)	Polymer ligands derived from jute fiber for heavy metal removal from electroplating wastewater	Cu^{2+}	352 mg/g
Jiang et al. (2020)	Preparation of a novel bio-adsorbent of sodium alginate grafted polyacrylamide/graphene oxide hydrogel for the adsorption of heavy metal ion	Cu^{2+} Pb^{2+}	68.76 mg/g 240.69 mg/g

17.5 Cellulose-based composites for the removal of pharmaceuticals

In recent times, numerous types of composites materials have been developed from cellulose by intricate modification techniques to remove pharmaceuticals from the aqueous phase. In this section, the research efforts in this area are reviewed and discussed. Numerous

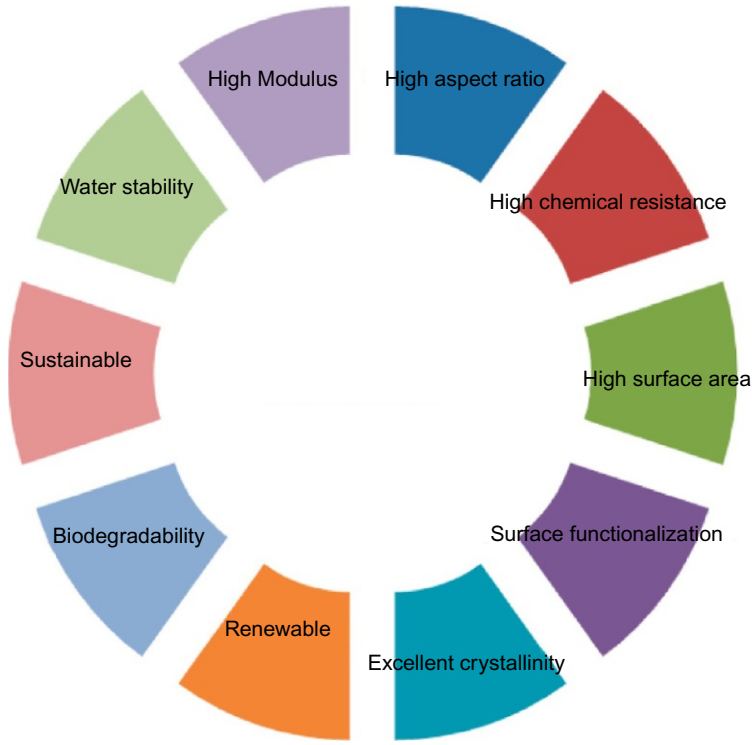

FIG. 17.2 Advantages of cellulose-based materials for the removal of pharmaceuticals.

advantages can be derived from the utilization of cellulose-based composite materials for the removal of pharmaceuticals. These are summarized in Fig. 17.2 and adapted from Abouzeid et al. (2018) and Nasrollahzadeh et al. (2020). The material is biodegradable, renewable, and sustainable. Hence after uptake of pharmaceuticals, it can be safely disposed of without any significant ecotoxicological concerns. Due to the nature of the material, surface functionalization is easily achieved given the targeted removal of specific pharmaceuticals. Other advantages are its high aspect ratio, chemical resistance, modulus, and surface area. Studies have shown that the physical attributes of materials play a key role in the potential performance as adsorbents for pollutant uptake (Ighalo et al., 2021a).

There are several areas in which cellulose-based composites can be applied for the removal of pollutants. These application areas are summarized in Fig. 17.3 and adapted from Mohammed et al. (2018). Cellulose-based composites can be used as adsorbents (Tursi et al., 2018). Their excellent physical properties make them a good candidate in this regard (Hokkanen et al., 2016). They can be used in membrane separation processes. This is especially important because cellulose can be synthesized into the nanoparticle range (Kalia et al., 2011). At a nanoparticle size range (1–100 nm), they become extremely efficient in nano-filtration and ultrafiltration membranes (Wang, 2019). They can also be used for other water pollution

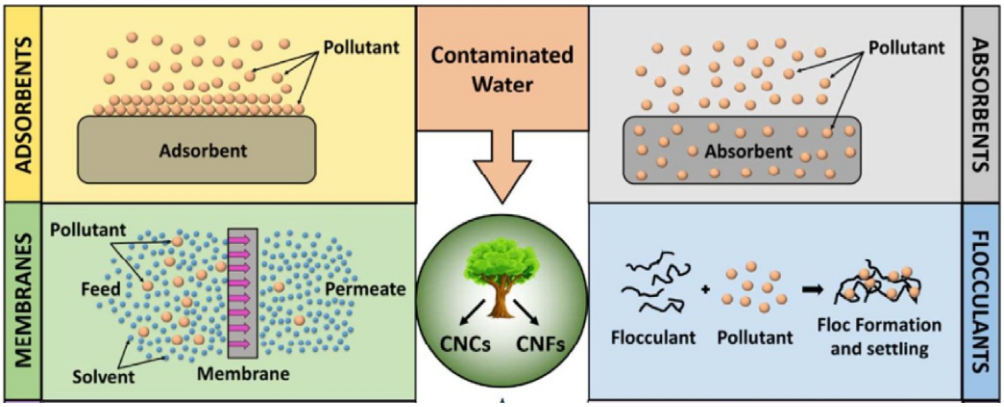

FIG. 17.3 Key application areas of cellulose-based composites for pollutant removal.

remediation technologies like absorption and flocculation (though these have not been investigated for dyes).

Cellulose for environmental applications is of four types: cellulose nanocrystals, cellulose nano-fibrils, cellulose nanocomposite, and bacterial cellulose (Nasrollahzadeh et al., 2020). The modification of cellulose for the removal of pharmaceuticals comes in two different directions. A summary of modification techniques for cellulose-based materials for the removal of pharmaceuticals is shown in Fig. 17.4. There is the grafting of monomers and direct chemical modification (Hokkanen et al., 2016). Both methods have several types (also presented in Fig. 17.4) and have been shown to lead to composite adsorbents with increased performance for pollutant uptake. Grafting is a polymer engineering technique where a side-chain graft is added to the cellulose backbone polymeric chain. Direct chemical modification on the other hand involves the utilization of chemicals in pure or aqueous form for the modification of the cellulose itself to adjust some of its functional properties. The major functional groups for the direct chemical modification of cellulose-based materials are summarized in Fig. 17.5 and discussed more extensively in Wang (2019).

An empirical review of recent research efforts on pharmaceuticals removal by cellulose-based composites is important. This is because it helps to show the progress in research and helps us identify trends and knowledge gaps. Table 17.3 presents a good summary in this regard. Several studies have examined drugs like diclofenac, ciprofloxacin, tetracycline, and aspirin. It can be observed that the most studied pollutant for cellulose-based composites adsorbent is diclofenac. This is unsurprising as it has been frequently detected in wastewaters and is effectively removed by the adsorption process (Ighalo and Adeniyi, 2020b). Besides diclofenac, cellulose-based composites adsorbent needs to be studied for other very common pharmaceutical compounds. Those common ones effectively removed by adsorption include metronidazole (Ighalo et al., 2020c), penicillin (Ighalo et al., 2021b), clofibric acid (Ighalo et al., 2020b), and ciprofloxacin (Igwegbe et al., 2020). Cellulose-based membranes have also been

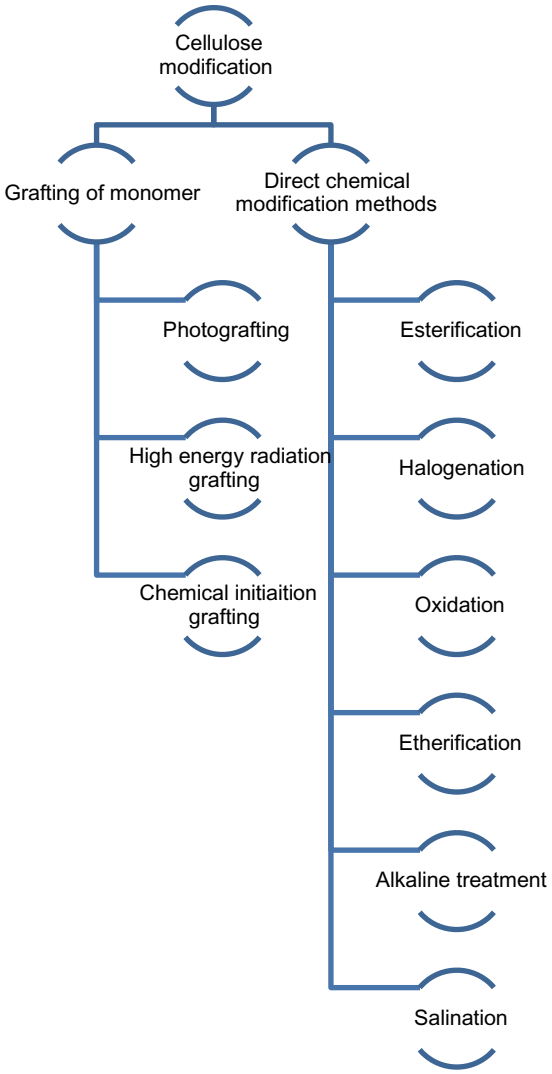

FIG. 17.4 Summary of modification techniques for cellulose-based materials for the removal of pharmaceuticals.

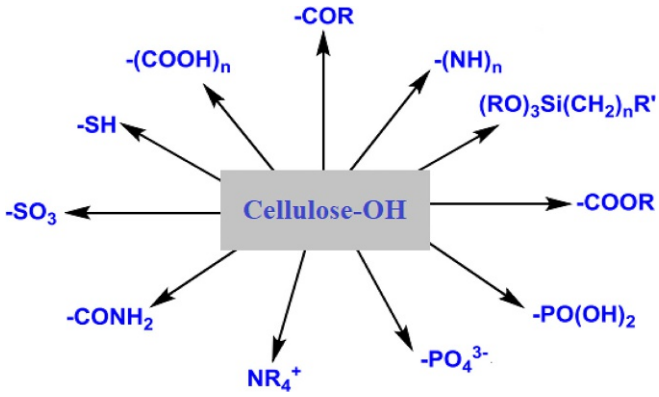

FIG. 17.5 Major functional groups for the direct chemical modification of cellulose-based materials (Wang, 2019).

TABLE 17.3 Summary of recent research efforts on pharmaceuticals removal by cellulose-based composites.

Material	Pollutant	Key findings	References
Adsorption process			
Cellulose/layered double hydroxide	Diclofenac	268 mg/g uptake capacity (after just 2 min), removal efficiency still at 88% after 3 cycles	Beyki et al. (2017)
UiO-66/polydopamine/bacterial cellulose	Aspirin	149 mg/g uptake capacity, >80% removal after 8 cycles	Cui et al. (2020)
UiO-66/polydopamine/bacterial cellulose	Tetracycline	184 mg/g uptake capacity, >80% removal after 8 cycles	Cui et al. (2020)
Montmorillonite/cellulose acetate	Ciprofloxacin	13.8 mg/g uptake capacity, good performance both in batch and column set-up	Das et al. (2020)
Sodium alginate/cellulose/polyvinyl alcohol	Diclofenac	418 mg/g uptake capacity, >90% removal after 5 cycles	Fan et al. (2019)
Carbonized cellulose	Diclofenac	59% removal efficiency (10 mg/L initial conc.) after 1 h, π-π stacking, and hydrogen bonds were the major mechanism	Feng et al. (2018)
Quaternised cellulose (from flax noil)	Amoxicillin	183 mg/g uptake capacity, endothermic and spontaneous process	Hu and Wang (2016)
Cellulose/chitosan	Diclofenac	444 mg/g uptake capacity, acid-base interactions, and hydrogen bonds were the major mechanisms	Hu et al. (2019)
Carboxymethyl cellulose/carboxyalkyl-chitosan/graphene oxide	Sulfamethoxazole	312 mg/g uptake capacity, removal efficiency still at 87% after 5 cycles	Liu et al. (2020)
Carboxymethyl cellulose/carboxyalkyl-chitosan/graphene oxide	Sulfapyridine	162 mg/g uptake capacity, removal efficiency still at 87% after 5 cycles	Liu et al. (2020)
Cellulose/chitosan	Tylosin	59 mg/g uptake capacity, π-π stacking; electrostatic attraction, and hydrogen bonds were the major mechanism	Luo et al. (2019)
Polypyrrole/cellulose	Diclofenac	210 mg/g uptake capacity, high pH flexibility of the adsorbent	Pires et al. (2017)
Wood cellulose	Salbutamol	196 mg/g uptake capacity, adsorbent performance depended mainly on the charge and colloidal stability of the anionic nano-fibril	Selkälä et al. (2018)
Cellulose/graphene oxide	Levofloxacin	80% removal efficiency at pH 4, factor effects were analyzed by response surface methodology (Box–Behnken design)	Tao et al. (2020)
Cellulose/graphene oxide	Fluoroquinolones	The uptake process was ultra-fast (74 mg/g in mins), could be reused for 7 cycles with only 13% reduction in performance	Wang et al. (2017a)

TABLE 17.3 Summary of recent research efforts on pharmaceuticals removal by cellulose-based composites—cont'd

Material	Pollutant	Key findings	References
Membrane separation process			
Cellulose acetate/nano-diamond	Extracellular polymeric substances	>90% COD removal, reduced fouling due to membrane architecture	Etemadi et al. (2017)
Cellulose acetate	Mixed liquor suspended solids	Good anti-biofouling properties albeit at only optimal conditions	Etemadi and Yegani (2019)
Cellulose acetate	Effluent spiked with carbamazepine	23% removal at high feed concentration (69% for commercial membrane)	Narbaitz et al. (2013)
Cellulose acetate	Effluent spiked with sulfamethazine	72% removal at high feed concentration (88% for commercial membrane)	Narbaitz et al. (2013)
Cellulose acetate	Effluent spiked with Ibuprofen	80% removal at high feed concentration (90% for commercial membrane)	Narbaitz et al. (2013)
Cellulose acetate/poly(4-vinylpyridine-b-ethylene oxide)	Sulfamethoxazole, Sulfadiazine, Omeprazole	Omeprazole > Sulfamethoxazole > Sulfadiazine in terms of membrane performance	Penabad-Peña et al. (2019)
Cellulose acetate/layered double hydroxide	Diclofenac, Tetracycline	Good thermal and physical stability of the membrane, electrostatic attraction, and hydrogen bonds were the major mechanism	Raicopol et al. (2019)
Cellulose acetate	Carbamazepine, Ibuprofen, Sulfamethazine	>50 pollutant removal after 1 h	Rana et al. (2012)

shown to have comparatively good mechanical and thermal properties for membranes (Paralikar et al., 2008). It was observed that cellulose used for membranes was always in the form of cellulose acetate. Based on this section, several gaps in knowledge have been observed in the research area. Though the utilization of cellulose-based composites as a flocculent in water pollution has been extensively studied, it is quite interesting that it has rarely been utilized for pharmaceuticals removal based on the authors' exhaustive search. A similar observation was also made for absorption.

17.6 Conclusion

The research efforts in cellulose-based composites for the removal of various pollutants such as heavy metal, dyes and pharmaceuticals has been reviewed and discussed. Cellulose-based composites can be used for the adsorption, membrane separation, flocculation, and absorption of the listed pollutants. However, the latter two have not been extensively investigated. The base cellulose material is usually modified by grafting of monomers or direct chemical modification. It was observed that the most studied pollutant for cellulose-based composites adsorbents are diclofenac, zinc, copper, and some dyes. This is unsurprising as they have been frequently detected in wastewaters and are effectively removed by the adsorption process. It was also observed that cellulose used for membranes was always in the form of cellulose acetate.

References

Abdullahi, A., Ighalo, J., Ajala, O.J, Ayika, S., 2020. Physicochemical analysis and heavy metals remediation of pharmaceutical industry effluent using bentonite clay modified by H2SO4 and HCl. Turk. J. Chem. 7 (3), 17. https://doi.org/10.18596/jotcsa.703913.

Abouzeid, R.E., Khiari, R., El-Wakil, N., Dufresne, A., 2018. Current state and new trends in the use of cellulose nanomaterials for wastewater treatment. Biomacromolecules 20 (2), 573–597.

Adelodun, B., Ajibade, F.O., Ighalo, J.O., Odey, G., Ibrahim, R.G., Kareem, Y.F., Choi, K.S., 2021. Assessment of socioeconomic inequality based on virus-contaminated water usage in developing countries: a review. Environ. Res. 192, 110309. https://doi.org/10.1016/j.envres.2020.110309.

Ajala, O.J., Nwosu, F.O., Ahmed, R.K., 2018. Adsorption of atrazine from aqueous solution using unmodified and modified bentonite clays. Appl. Water Sci. 8 (7), 214.

Al-Zboon, K., Al-Smadi, B., Al-Harahsheh, M., Al-Khawaldh, S., 2019. Adsorption modeling of Cr on volcanic tuff-based geopolymer. JJEES 10, 35.

An, D., Sun, X., Cheng, X., Cui, L., Zhang, X., Zhao, Y., Dong, Y., 2020. Investigation on mercury removal and recovery based on enhanced adsorption by activated coke. J. Hazard. Mater. 384, 121354.

Aniagor, C.O., Igwegbe, C.A., Ighalo, J.O., Oba, S.N., 2021. Adsorption of doxycycline from aqueous media: a review. J. Mol. Liq. 334, 116124. https://doi.org/10.1016/j.molliq.2021.116124.

Bamidele, O., Boisa, N., Obunwo, C.C., 2020. Determination and risk assessment of heavy metals concentrations collected from indoor houses at Lagos State of Nigeria. Int. J. Adv. Sci. Res. Eng. 6 (3), 77–94. https://doi.org/10.31695/IJASRE.2020.33765.

Beyki, M.H., Mohammadirad, M., Shemirani, F., Saboury, A.A., 2017. Magnetic cellulose ionomer/layered double hydroxide: an efficient anion exchange platform with enhanced diclofenac adsorption property. Carbohydr. Polym. 157, 438–446.

Biswas, F.B., Rahman, I.M., Nakakubo, K., Endo, M., Nagai, K., Mashio, A.S., Hasegawa, H., 2020. Highly selective and straightforward recovery of gold and platinum from acidic waste effluents using cellulose-based bioadsorbent. J. Hazard. Mater. 410, 124569.

Bratby, J., 2016. Coagulation and Flocculation in Water and Wastewater Treatment. IWA Publishing.

Cai, H., Liang, J., Ning, X.-A., Lai, X., Li, Y., 2020. Algal toxicity induced by effluents from textile-dyeing wastewater treatment plants. J. Environ. Sci. 91, 199–208.

Cheng, R., Kang, M., Zhuang, S., Shi, L., Zheng, X., Wang, J., 2019. Adsorption of Sr (II) from water by mercerized bacterial cellulose membrane modified with EDTA. J. Hazard. Mater. 364, 645–653.

Cui, J., Xu, X., Yang, L., Chen, C., Qian, J., Chen, X., Sun, D., 2020. Soft foam-like UiO-66/polydopamine/bacterial cellulose composite for the removal of aspirin and tetracycline hydrochloride. Chem. Eng. J. 395, 125174.

Das, I., Das, S., Chakraborty, I., Ghangrekar, M., 2019. Bio-refractory pollutant removal using microbial electrochemical technologies: a short review. J. Indian Chem. Soc. 96, 493–497.
Das, S., Barui, A., Adak, A., 2020. Montmorillonite impregnated electrospun cellulose acetate nanofiber sorptive membrane for ciprofloxacin removal from wastewater. J. Water Process Eng. 37, 101497.
Dong, Z., Liu, J., Yuan, W., Yi, Y., Zhao, L., 2016. Recovery of Au (III) by radiation synthesized aminomethyl pyridine functionalized adsorbents based on cellulose. Chem. Eng. J. 283, 504–513.
Etemadi, H., Yegani, R., 2019. Effect of aeration rate on the anti-biofouling properties of cellulose acetate nanocomposite membranes in a membrane bioreactor system for the treatment of pharmaceutical wastewater. Biofouling 35 (6), 618–630.
Etemadi, H., Yegani, R., Seyfollahi, M., Babaeipour, V., 2017. Preparation and performance evaluation of cellulose acetate/nanodiamond nanocomposite membrane in the treatment of pharmaceutical wastewater by membrane bioreactor. Desalin. Water Treat. 76, 98–111.
Fan, L., Lu, Y., Yang, L.-Y., Huang, F., Ouyang, X.-K., 2019. Fabrication of polyethylenimine-functionalized sodium alginate/cellulose nanocrystal/polyvinyl alcohol core–shell microspheres ((PVA/SA/CNC)@ PEI) for diclofenac sodium adsorption. J. Colloid Interface Sci. 554, 48–58.
Feng, Z., Odelius, K., Rajarao, G.K., Hakkarainen, M., 2018. Microwave carbonized cellulose for trace pharmaceutical adsorption. Chem. Eng. J. 346, 557–566.
Ge, H., Huang, H., Xu, M., Chen, Q., 2016. Cellulose/poly (ethylene imine) composites as efficient and reusable adsorbents for heavy metal ions. Cellulose 23 (4), 2527–2537.
Góes, M.M., Keller, M., Oliveira, V.M., Villalobos, L.D.G., Moraes, J.C.G., Carvalho, G.M., 2016. Polyurethane foams synthesized from cellulose-based wastes: kinetics studies of dye adsorption. Ind. Crop. Prod. 85, 149–158.
Hevira, L., Zilfa, R., Ighalo, J.O., Zein, R., 2020. Biosorption of indigo carmine from aqueous solution by Terminalia catappa shell. J. Environ. Chem. Eng. 8 (5), 104290. https://doi.org/10.1016/j.jece.2020.104290.
Hevira, L., Zilfa, R., Ighalo, J.O., Aziz, H., Zein, R., 2021. Terminalia catappa shell as low-cost biosorbent for the removal of methylene blue from aqueous solutions. J. Ind. Eng. Chem. https://doi.org/10.1016/j.jiec.2021.01.028.
Hokkanen, S., Bhatnagar, A., Sillanpää, M., 2016. A review on modification methods to cellulose-based adsorbents to improve adsorption capacity. Water Res. 91, 156–173.
Hu, D., Wang, L., 2016. Adsorption of amoxicillin onto quaternized cellulose from flax noil: kinetic, equilibrium and thermodynamic study. J. Taiwan Inst. Chem. Eng. 64, 227–234.
Hu, D., Jiang, R., Wang, N., Xu, H., Wang, Y.-G., Ouyang, X.-K., 2019. Adsorption of diclofenac sodium on bilayer amino-functionalized cellulose nanocrystals/chitosan composite. J. Hazard. Mater. 369, 483–493.
Huang, S., Wu, L., Li, T., Xu, D., Lin, X., Wu, C., 2019. Facile preparation of biomass lignin-based hydroxyethyl cellulose super-absorbent hydrogel for dye pollutant removal. Int. J. Biol. Macromol. 137, 939–947.
Ighalo, J.O., Adeniyi, A.G., 2020a. Adsorption of pollutants by plant bark derived adsorbents: an empirical review. J. Water Process Eng. 35, 101228. https://doi.org/10.1016/j.jwpe.2020.101228.
Ighalo, J.O., Adeniyi, A.G., 2020b. Mitigation of diclofenac pollution in aqueous media by adsorption. ChemBioEng Rev. 7 (2), 50–64. https://doi.org/10.1002/cben.201900020.
Ighalo, J.O., Adeniyi, A.G., Marques, G., 2020a. Artificial intelligence for surface water quality monitoring and assessment: a systematic literature analysis. Model. Earth Syst. Environ. 7 (2), 669–681. https://doi.org/10.1007/s40808-020-01041-z.
Ighalo, J.O., Ajala, J.O., Umenweke, G., Ogunniyi, S., Adeyanju, C.A., Igwegbe, C.A., Adeniyi, A.G., 2020b. Mitigation of clofibric acid pollution by adsorption: a review of recent developments. J. Environ. Chem. Eng. 8 (5), 104264. https://doi.org/10.1016/j.jece.2020.104264.
Ighalo, J.O., Igwegbe, C.A., Adeniyi, A.G., Adeyanju, C.A., Ogunniyi, S., 2020c. Mitigation of metronidazole (Flagyl) pollution in aqueous media by adsorption: a review. Environ. Technol. Rev. 9 (1), 137–148. https://doi.org/10.1080/21622515.2020.1849409.
Ighalo, J.O., Adeniyi, A.G., Adelodun, A.A., 2021a. Recent advances on the adsorption of herbicides and pesticides from polluted waters: performance evaluation via physical attributes. J. Ind. Eng. Chem. 93, 117–137. https://doi.org/10.1016/j.jiec.2020.10.011.

Ighalo, J.O., Igwegbe, C.A., Aniagor, C.O., Oba, S.N., 2021b. A review of methods for the removal of penicillins from water. J. Water Process Eng. 39, 101886. https://doi.org/10.1016/j.jwpe.2020.101886.

Igwegbe, C.A., Oba, S.N., Aniagor, C.O., Adeniyi, A.G., Ighalo, J.O., 2020. Adsorption of ciprofloxacin from water: a comprehensive review. J. Ind. Eng. Chem. 93, 57–77. https://doi.org/10.1016/j.jiec.2020.09.023.

Iwuozor, K.O., Ighalo, J.O., Ogunfowora, L.A., Adeniyi, A.G., Igwegbe, C.A., 2021. An empirical literature analysis of adsorbent performance for methylene blue uptake from aqueous media. J. Environ. Chem. Eng. https://doi.org/10.1016/j.jece.2021.105658, 105658.

Javanbakht, S., Shaabani, A., 2019. Carboxymethyl cellulose-based oral delivery systems. Int. J. Biol. Macromol. 133, 21–29.

Jiang, H., Yang, Y., Lin, Z., Zhao, B., Wang, J., Xie, J., Zhang, A., 2020. Preparation of a novel bio-adsorbent of sodium alginate grafted polyacrylamide/graphene oxide hydrogel for the adsorption of heavy metal ion. Sci. Total Environ. 744, 140653.

Jiehong Guo, Z.L., Ranasinghe, P., Bonina, S., Hosseini, S., Corcoran, M.B., Smalley, C., Kaliappan, R., Wu, Y., Chen, D., Sandy, A.L., Wang, Y., Rockne, K.J., Sturchio, N.C., Giesy, J.P., Li, A., 2016. Occurrence of atrazine and related compounds in sediments of upper great lakes. Enivron. Sci. Technol. 50, 7335–7343.

Kalia, S., Dufresne, A., Cherian, B.M., Kaith, B., Avérous, L., Njuguna, J., Nassiopoulos, E., 2011. Cellulose-based bio- and nanocomposites: a review. Int. J. Polym. Sci. 2011, 1–35.

Khadir, A., Negarestani, M., Mollahosseini, A., 2020. Sequestration of a non-steroidal anti-inflammatory drug from aquatic media by lignocellulosic material (Luffa cylindrica) reinforced with polypyrrole: study of parameters, kinetics, and equilibrium. J. Environ. Chem. Eng. 8 (3), 103734.

Kong, W., Ren, J., Wang, S., Chen, Q., 2014. Removal of heavy metals from aqueous solutions using acrylic-modified sugarcane bagasse-based adsorbents: equilibrium and kinetic studies. Bioresources 9 (2), 3184–3196.

Li, W.-T., Jin, J., Li, Q., Wu, C.-F., Lu, H., Zhou, Q., Li, A.-M., 2016. Developing LED UV fluorescence sensors for online monitoring DOM and predicting DBPs formation potential during water treatment. Water Res. 93, 1–9.

Li, Y., Xiao, H., Pan, Y., Zhang, M., Ni, S., Hou, X., Hu, E., 2018. Study on cellulose microfilaments based composite spheres: microwave-assisted synthesis, characterization, and application in pollutant removal. J. Environ. Manag. 228, 85–92.

Li, M., Li, B., Zhou, L., Zhang, Y., Cao, Q., Wang, R., Xiao, H., 2019. Fluorescence-sensitive adsorbent based on cellulose using for mercury detection and removal from aqueous solution with selective "on-off" response. Int. J. Biol. Macromol. 132, 1185–1192.

Li, Y., Xie, D., Xiao, J., Wu, W., Zhang, L., Xiao, H., Chen, J., 2020. Dual responsive copolymers-grafted microfibrillated cellulose composites for removing lead ions from aqueous solution. J. Clean. Prod. 258, 120867.

Liu, L., Gao, Z.Y., Su, X.P., Chen, X., Jiang, L., Yao, J.M., 2015. Adsorption removal of dyes from single and binary solutions using a cellulose-based bioadsorbent. ACS Sustain. Chem. Eng. 3 (3), 432–442.

Liu, Y., Nie, P., Yu, F., 2020. Enhanced adsorption of sulfonamides by a novel carboxymethyl cellulose and chitosan-based composite with sulfonated graphene oxide. Bioresour. Technol. 320, 124373.

Luo, X., Liu, L., Wang, L., Liu, X., Cai, Y., 2019. Facile synthesis and low concentration tylosin adsorption performance of chitosan/cellulose nanocomposite microspheres. Carbohydr. Polym. 206, 633–640.

Madikizela, L.M., Ncube, S., Tutu, H., Richards, H., Newman, B., Ndungu, K., Chimuka, L., 2020. Pharmaceuticals and their metabolites in the marine environment: sources, analytical methods and occurrence. Trends Environ. Anal. Chem., e00104.

Mahmood, N.A.-H.J., Abdulmajeed, Y.R., 2017. Adsorption of amoxicillin onto activated carbon from aqueous solution. Int. J. Curr. Eng. Technol. 7, 62–67.

Mirjavadi, E.S., Tehrani, R.M., Khadir, A., 2019. Effective adsorption of zinc on magnetic nanocomposite of Fe3O4/zeolite/cellulose nanofibers: kinetic, equilibrium, and thermodynamic study. Environ. Sci. Pollut. Res. 26 (32), 33478–33493.

Misra, M., Vivekanandhan, S., Mohanty, A.K., Denault, J., 2011. 4.10—nanotechnologies for agricultural bioproducts. In: Moo-Young, M. (Ed.), Comprehensive Biotechnology, third ed. Pergamon, Oxford, pp. 119–127.

Mohammed, N., Grishkewich, N., Tam, K.C., 2018. Cellulose nanomaterials: promising sustainable nanomaterials for application in water/wastewater treatment processes. Environ. Sci. Nano 5 (3), 623–658.

Narbaitz, R.M., Rana, D., Dang, H.T., Morrissette, J., Matsuura, T., Jasim, S.Y., Yang, P., 2013. Pharmaceutical and personal care products removal from drinking water by modified cellulose acetate membrane: field testing. Chem. Eng. J. 225, 848–856.

Naseri-Nosar, M., Ziora, Z.M., 2018. Wound dressings from naturally-occurring polymers: a review on homopolysaccharide-based composites. Carbohydr. Polym. 189, 379–398.

Nasrollahzadeh, M., Sajjadi, M., Iravani, S., Varma, R.S., 2020. Starch, cellulose, pectin, gum, alginate, chitin and chitosan derived (nano) materials for sustainable water treatment: a review. Carbohydr. Polym. 251, 116986.

Nwosu, F.O., Ajala, O.J., Owoyemi, R.M., Raheem, B.G., 2018. Preparation and characterization of adsorbents derived from bentonite and kaolin clays. Appl. Water Sci 8 (7), 195.

Nwosu, F.O., Ajala, O.J., Okeola, F.O., Adebayo, S.A., Olanlokun, O.K., Eletta, A.O., 2019. Adsorption of chlorotriazine herbicide onto unmodified and modified kaolinite: equilibrium, kinetic and thermodynamic studies. Egypt. J. Aquat. Res. 45 (2), 99–107.

Oba, S.N., Ighalo, J.O., Aniagor, C.O., Igwegbe, C.A., 2021. Removal of ibuprofen from aqueous media by adsorption: a comprehensive review. Sci. Total Environ. 780, 146608. https://doi.org/10.1016/j.scitotenv.2021.146608.

Ogunleye, O.O., Ajala, M.A., Agarry, S.E., 2014. Evaluation of Biosorptive capacity of banana (Musa paradisiaca) stalk for lead(II) removal from aqueous solution. J. Environ. Prot. 5, 1451–1465. https://doi.org/10.4236/jep.2014.515138.

Pan, Y., Xie, H., Liu, H., Cai, P., Xiao, H., 2019. Novel cellulose/montmorillonite mesoporous composite beads for dye removal in single and binary systems. Bioresour. Technol. 286, 121366.

Paralikar, S.A., Simonsen, J., Lombardi, J., 2008. Poly (vinyl alcohol)/cellulose nanocrystal barrier membranes. J. Membr. Sci. 320 (1–2), 248–258.

Penabad-Peña, L., Herrera-Morales, J., Betancourt, M., Nicolau, E., 2019. Cellulose acetate/P4VP-b-PEO membranes for the adsorption of electron-deficient pharmaceutical compounds. ACS Omega 4 (27), 22456–22463.

Peng, H., Guo, J., 2020. Removal of chromium from wastewater by membrane filtration, chemical precipitation, ion exchange, adsorption electrocoagulation, electrochemical reduction, electrodialysis, electrodeionization, photocatalysis and nanotechnology: a review. Environ. Chem. Lett. 18, 1–14.

Pires, B.C., Dutra, F.V.A., Nascimento, T.A., Borges, K.B., 2017. Preparation of PPy/cellulose fibre as an effective potassium diclofenac adsorbent. React. Funct. Polym. 113, 40–49.

Priya, V., Shrama, P., Kumar, A., 2020. Phytoremediation of Banana leaf-functionalization of mercaptan-cellulose and its utilization for the removal of heavy metals in aqueous environment. Asian J. Adv. Basic Sci. 8 (1), 26–38.

Rahman, M.L., Fui, C.J., Ting, T.X., Sarjadi, M.S., Arshad, S.E., Musta, B., 2020. Polymer ligands derived from jute fiber for heavy metal removal from electroplating wastewater. Polymers 12 (11), 2521.

Raicopol, M.D., Andronescu, C., Voicu, S.I., Vasile, E., Pandele, A.M., 2019. Cellulose acetate/layered double hydroxide adsorptive membranes for efficient removal of pharmaceutical environmental contaminants. Carbohydr. Polym. 214, 204–212.

Rana, D., Scheier, B., Narbaitz, R.M., Matsuura, T., Tabe, S., Jasim, S.Y., Khulbe, K.C., 2012. Comparison of cellulose acetate (CA) membrane and novel CA membranes containing surface modifying macromolecules to remove pharmaceutical and personal care product micropollutants from drinking water. J. Membr. Sci. 409, 346–354.

Saeed, R.M.Y., Bano, Z., Sun, J., Wang, F., Ullah, N., Wang, Q., 2019. CuS-functionalized cellulose based aerogel as biocatalyst for removal of organic dye. J. Appl. Polym. Sci. 136 (15), 47404.

Salama, A., 2017. New sustainable hybrid material as adsorbent for dye removal from aqueous solutions. J. Colloid Interface Sci. 487, 348–353.

Salama, A., Shukry, N., El-Sakhawy, M., 2015. Carboxymethyl cellulose-g-poly(2-(dimethylamino) ethyl methacrylate) hydrogel as adsorbent for dye removal. Int. J. Biol. Macromol. 73, 72–75. https://doi.org/10.1016/j.ijbiomac.2014.11.002.

Selkälä, T., Suopajärvi, T., Sirviö, J.A., Luukkonen, T., Lorite, G.S., Kalliola, S., Liimatainen, H., 2018. Rapid uptake of pharmaceutical salbutamol from aqueous solutions with anionic cellulose nanofibrils: the importance of pH and colloidal stability in the interaction with ionizable pollutants. Chem. Eng. J. 350, 378–385.

Sharma, A., Thakur, M., Bhattacharya, M., Mandal, T., Goswami, S., 2019. Commercial application of cellulose nanocomposites—a review. Biotechnol. Rep. 21, e00316.

Shekar, H.S., Ramachandra, M., 2018. Green composites: a review. Mater. Today Proc. 5 (1), 2518–2526.
Shi, W., Ji, S., Xu, Q., Duan, X., Song, Z., Xu, G., 2019. Treatment of pharmaceutical wastewater containing clofibric acid by electron beam irradiation. J. Radioanal. Nucl. Chem. 322 (2), 407–414.
Shi, Y.-Z., Yin, X.-C., Si, G.-H., Zhang, N.-D., Du, M.-X., Wang, X.-H., 2020. Bio-adsorbent preparation based on Chinese Radix isatidis residue for Pb (II) removal. Water Pract. Technol. 15 (4), 1202–1212.
Simate, G.S., Maledi, N., Ochieng, A., Ndlovu, S., Zhang, J., Walubita, L.F., 2016. Coal-based adsorbents for water and wastewater treatment. J. Environ. Chem. Eng. 4 (2), 2291–2312.
Singh, H., Chauhan, G., Jain, A.K., Sharma, S.K., 2017. Adsorptive potential of agricultural wastes for removal of dyes from aqueous solutions. J. Environ. Chem. Eng. 5 (1), 122–135. https://doi.org/10.1016/j.jece.2016.11.030.
Solis-Casados, D., Escobar-Alarcón, L., Natividad, R., Romero, R., 2018. Advanced oxidation processes II: removal of pharmaceuticals by photocatalysis. In: Ecopharmacovigilance. Springer, pp. 143–155.
Sun, J., Liu, Y., Wu, Z., Xu, M., Lei, E., Ma, C., Liu, S., 2021. Compressible, anisotropic lamellar cellulose-based carbon aerogels enhanced by carbon dots for superior energy storage and water deionization. Carbohydr. Polym. 252, 117209.
Tanatti, N.P., Mehmetbaşoğlu, M., Şengil, İ.A., Aksu, H., Emin, E., 2019. Kinetics and thermodynamics of biodiesel wastewater treatment by using ozonation process. Desalin. Water Treat. 161, 108–115.
Tang, C., Brodie, P., Li, Y., Grishkewich, N.J., Brunsting, M., Tam, K.C., 2020. Shape recoverable and mechanically robust cellulose aerogel beads for efficient removal of copper ions. Chem. Eng. J. 392, 124821.
Tao, J., Yang, J., Ma, C., Li, J., Du, K., Wei, Z., Deng, X., 2020. Cellulose nanocrystals/graphene oxide composite for the adsorption and removal of levofloxacin hydrochloride antibiotic from aqueous solution. R. Soc. Open Sci. 7 (10), 200857.
Tavakolian, M., Wiebe, H., Sadeghi, M.A., van de Ven, T.G.M., 2020. Dye removal using hairy nanocellulose: experimental and theoretical investigations. ACS Appl. Mater. Interfaces 12 (4), 5040–5049. https://doi.org/10.1021/acsami.9b18679.
Tayeb, A.H., Amini, E., Ghasemi, S., Tajvidi, M., 2018. Cellulose nanomaterials—binding properties and applications: a review. Molecules 23 (10), 2684.
Tijani, J.O., Fatoba, O.O., Babajide, O.O., Petrik, L.F., 2016. Pharmaceuticals, endocrine disruptors, personal care products, nanomaterials and perfluorinated pollutants: a review. Environ. Chem. Lett. 14 (1), 27–49.
Tran, D., Bourdev, L., Fergus, R., Torresani, L., Paluri, M., 2015. Learning spatiotemporal features with 3d convolutional networks. In: Paper Presented at the Proceedings of the IEEE International Conference on Computer Vision.
Tursi, A., Chatzisymeon, E., Chidichimo, F., Beneduci, A., Chidichimo, G., 2018. Removal of endocrine disrupting chemicals from water: adsorption of bisphenol-a by biobased hydrophobic functionalized cellulose. Int. J. Environ. Res. Public Health 15 (11), 2419.
Varaprasad, K., Jayaramudu, T., Sadiku, E.R., 2017. Removal of dye by carboxymethyl cellulose, acrylamide and graphene oxide via a free radical polymerization process. Carbohydr. Polym. 164, 186–194.
Wang, D., 2019. A critical review of cellulose-based nanomaterials for water purification in industrial processes. Cellulose 26 (2), 687–701.
Wang, Y., Zhao, L., Peng, H., Wu, J., Liu, Z., Guo, X., 2016. Removal of anionic dyes from aqueous solutions by cellulose-based adsorbents: equilibrium, kinetics, and thermodynamics. J. Chem. Eng. Data 61 (9), 3266–3276.
Wang, N., Wang, Y.-F., Omer, A.M., Ouyang, X.-K., 2017a. Fabrication of novel surface-imprinted magnetic graphene oxide-grafted cellulose nanocrystals for selective extraction and fast adsorption of fluoroquinolones from water. Anal. Bioanal. Chem. 409 (28), 6643–6653.
Wang, X., Yao, C., Wang, F., Li, Z., 2017b. Cellulose-based nanomaterials for energy applications. Small 13 (42), 1702240.
Wang, J., Liu, M., Duan, C., Sun, J., Xu, Y., 2019. Preparation and characterization of cellulose-based adsorbent and its application in heavy metal ions removal. Carbohydr. Polym. 206, 837–843.
WHO, 2016. World Health Statistics 2016: Monitoring Health for the SDGs Sustainable Development Goals. World Health Organization.

Wu, S., Shekhar, N., Biswas, S., Sahu, A.K., 2020. Determination of physicochemical parameters and levels of heavy metals in food waste water with environmental effects. Bioinorg. Chem. Appl. 2020, 1–13.
Xia, L., Huang, Z., Zhong, L., Xie, F., Tang, C.Y., Tsui, C.P., 2018. Bagasse cellulose grafted with an amino-terminated hyperbranched polymer for the removal of Cr (VI) from aqueous solution. Polymers 10 (8), 931.
Xu, C., Shao, F., Yi, Z., Dong, H., Zhang, Q., Yu, J., Yu, L., 2019. Highly chlorine resistance polyamide reverse osmosis membranes with oxidized graphitic carbon nitride by ontology doping method. Sep. Purif. Technol. 223, 178–185.
Yue, X., Jiang, F., Zhang, D., Lin, H., Chen, Y., 2017. Preparation of adsorbent based on cotton fiber for removal of dyes. Fibers Polym. 18 (11), 2102–2110. https://doi.org/10.1007/s12221-017-1211-9.
Yue, X., Huang, J., Jiang, F., Lin, H., Chen, Y., 2019. Synthesis and characterization of cellulose-based adsorbent for removal of anionic and cationic dyes. J. Eng. Fibers Fabr. 14, 1558925019828194.
Zarei, M., Zarei, M., 2018. Self-propelled micro/nanomotors for sensing and environmental remediation. Small 14 (30), 1800912.
Zeman, L.J., Zydney, A., 2017. Microfiltration and Ultrafiltration: Principles and Applications. CRC Press.
Zhang, X., Yan, S., Chen, J., Tyagi, R., Li, J., 2020. Physical, chemical, and biological impact (hazard) of hospital wastewater on environment: presence of pharmaceuticals, pathogens, and antibiotic-resistance genes. In: Current Developments in Biotechnology and Bioengineering. Elsevier, pp. 79–102.
Zhou, Y., Zhang, M., Hu, X., Wang, X., Niu, J., Ma, T., 2013. Adsorption of cationic dyes on a cellulose-based multicarboxyl adsorbent. J. Chem. Eng. Data 58 (2), 413–421. https://doi.org/10.1021/je301140c.
Zhou, Y., Zhang, M., Wang, X., Huang, Q., Min, Y., Ma, T., Niu, J., 2014. Removal of crystal violet by a novel cellulose-based adsorbent: comparison with native cellulose. Ind. Eng. Chem. Res. 53 (13), 5498–5506.

This page intentionally left blank

PART III

Chitosan-based nanobiosorbents for deterioration of environmental matrices

This page intentionally left blank

CHAPTER

18

Toxic metals adsorption from water using chitosan nanoderivatives

F.J. Alguacil and J.I. Robla

National Center for Metallurgical Research (CSIC), Madrid, Spain

18.1 Introduction

Though human development implies a better life, also it takes the risk of contamination into the air, earth, and waters. One of such probable contaminations may be due to the presence of toxic metals in water. This presence can be caused by natural and anthropogenic nature, but in any case the presence of these toxic metals, besides poisoning the environment, and their intake for humans, can deliver a series of illnesses and even death.

Thus, under the fear of this risk and to decrease its probable environmental impact, several technologies had been investigated or are under development in order to remove the presence of these hazardous metals in water, and maintain their presence in the term zero or under the acceptable levels for humans as declared by the corresponding health agencies.

From these available technologies, adsorption is probably one of the most popular methodologies, developing a *miriade* of potential adsorbents, and having, as targets, toxic metals.

Among these adsorbents, chitosan and chitosan-bearing composites are very well established in this role. It is well known that chitosan is derived from chitin, being a product of the deacetylation of this natural bioconstituent. The importance of these chitosan adsorbents in the removal of heavy metals is reflected in a number of recently published reviews (Brião et al., 2020; Na et al., 2020; Pathan and Bose, 2020; Quesada et al., 2020; Tahoon et al., 2020).

Taking into account the above, this work reviews very recent developments on the use of chitosan, under the term of nano-chitosan itself or as a constituent of nanocomposites of various nature, in the treatment of aqueous solutions containing toxic metals. The toxic metals considered here are arsenic, cadmium, chromium, mercury, and lead.

https://doi.org/10.1016/B978-0-323-90912-9.00018-6

18.2 Arsenic

A new magnetic biosorbent was prepared from a matrix of chitosan and Fe_3O_4 (magnetite) nanoparticles and used in the removal of As(III) and (V) from waters (Ayub et al., 2020). Best adsorption results (exceeding 99%) were achieved in the pH range of 5–9 in the case of As(III), and in the range 6–8 for As(V). In both cases, adsorption best responded to the Langmuir isotherm ($r^2 > 0.999$):

$$\frac{1}{[As]_{a,e}} = \frac{1}{[As]_{a,m}} + \frac{1}{K_L[As]_{a,m}} \cdot \frac{1}{[As]_{aq,e}} \tag{18.1}$$

where $[A]_{a,e}$ and $[As]_{a,m}$ were the arsenic concentrations in the adsorbent at the equilibrium and maximum, respectively, and $[As]_{aq,e}$ was the arsenic concentration at the equilibrium in the aqueous solution, being K_L the Langmuir constant. The maximum monolayer adsorption capacities were found as 73.69 and 79.49 mg/g for As(III) and As(V) species, respectively. Optimum biosorbent dosages were 1.5 g/L (As(III)) and 2 g/L (As(V)). Also in both cases, the removal of these species followed the pseudo-second-order kinetic model ($r^2 > 0.999$):

$$\frac{t}{[As]_{a,e}} = \frac{1}{K_{p2}[As]^2_{a,e}} + \frac{1}{[As]_{a,e}} \tag{18.2}$$

being K_{p2} the corresponding rate constant. Desorption of both As(III) and (V) can be performed using 0.1 M NaOH solutions, whereas, after 5 cycles of adsorption–desorption, the adsorbent slightly lost its initial adsorption capacity: 99.5% (1st cycle) and 92.5% (5th cycle) for As(III), and from 99.5% (1st cycle) to 95% in the case of As(V). NOTE: in the publication Eq. (18.2) is poorly written since the correct equation is:

$$\frac{t}{[As]_{a,t}} = \frac{1}{K_{p2}[As]^2_{a,e}} + \frac{t}{[As]_{a,e}} \tag{18.2a}$$

A nanocomposite of chitosan-graphene oxide-gadolinium oxide (CGO—Gd) was prepared to be used in the adsorption of arsenic(V) from water (Choi et al., 2020). The characterization of the adsorbent showed that the 50 nm long rods presented a crystalline morphology with highly active oxygenated functional groups (OH−, COO−, C–O–C, and Gd_2O_3), all contributing to the removal of arsenic. The removal of this element was high in the pH range of 3–7, decreasing the adsorption of As(V) above pH 7. As (V) uptakes (pH 6) onto the nanocomposite were 252.12, and 128.20 mg/g for 0.1 and 0.3 g/L of CGO—Gd, respectively. Adsorption data fitted well to the Langmuir isotherm ($r^2 > 0.999$):

$$\frac{[As]_{aq,e}}{[As]_{a,e}} = \frac{1}{K_L[As]_{a,m}} + \frac{1}{[As]_{a,m}}[As]_{aq,e} \tag{18.3}$$

Arsenic (V) adsorption was negatively affected by the presence of 0.5 M calcium, sulfate, carbonate, or phosphate in the aqueous solution. The adsorbent was used to treat real samples from Nakdong mine (), containing 282 μg/L of As(V), after the treatment with the nanoadsorbent this arsenic concentration was decreased until less than 10 μg/L as required

by regulatory standards of environmental agencies. Desorption can be achieved with 0.1 M NaOH solution, however, the adsorption efficiency decreased from 98% (1st cycle) until 78% (fifth cycle), this decrease was probable due to incomplete As(V) desorption and change of the adsorbent surface morphology. NOTE: as it can be seen Langmuir isotherms presented in Eqs. (18.1) and (18.3) are different; this is due to the variation in the linearization of the Langmuir equation.

Arsenate ions were removed from waters using films made from neat chitosan and chitosan with magnetic nanoparticles (MNPs) (Kloster et al., 2020), and whereas the adsorption of As (V) was explained ($r^2 = 0.989$) by the non-linear Freundlich isotherm for neat chitosan film:

$$[As]_{a,e} = K_F [As]_{aq,e}^{1/n} \tag{18.4}$$

it was better fitted ($r^2 = 0.992$) to the non-linear Langmuir equation when the composite adsorbent was used:

$$[As]_{a,e} = \frac{K_L [As]_{a,m} [As]_{aq,e}}{1 + K_L [As]_{aq,e}} \tag{18.5}$$

Maximum arsenic uptake onto the nanocomposite ($[As]_{a,m}$) was estimated as 15.2 mg/g. Experimental data fitted well ($r^2 = 0.999$) with the pseudo-first-order reversible model. The composite adsorbent presented higher adsorption capacity, i.e., 10.4 mg/g versus 1.6 mg/g of the neat chitosan, which was attributable to the additional adsorbent capacity provided by the nanoparticles and the irregular surface area that leads to an enhancement of the adsorption surface. Adsorption can be represented by the next reaction:

$$R - NH_3^+ + H_2AsO_4^- \Leftrightarrow R - NH_3 \cdot H_2AsO_4 \tag{18.6}$$

NOTE: No desorption data are given in the publication.

Magnetic nanosorbent, chitosan-coated magnetic nanoparticles (cMNPs), was used in the treatment of lignocellulosic bio-refinery wastewater (LBW) containing arsenic, chromium and copper, and a series of phenolic compounds (Kumar et al., 2020). The magnetic property of the adsorbent allows separation of the particles in the presence of an external magnetic field. At pH 6.0, with optimized adsorbent dosage of 2.0 g/L and 90 min contact time, maximum removal of arsenic was 2.4%, value which was lower than the values yielded with the different components of the wastewater (Table 18.1).

Arsenic adsorption can be represented by the Langmuir isotherm (Ayub et al., 2020) with $r^2 = 0.955$. Desorption was carried out at acidic conditions of pH 2, and the adsorbent was reconstituted by the addition of a sodium hydroxide solution until pH 8, in order to entrap again the magnetic nanoparticles. Reusability of the adsorbent was investigated for five

TABLE 18.1 Adsorption of the various components of the wastewater.

	Arsenic	Copper	Chromium	Phenols
% removal	2.4	42.2	18.7	46.2

consecutive rounds of adsorption–desorption, and results indicated that the nanoadsorbent only maintained a mere 10% of its initial adsorption capacity.

A goethite/graphene oxide/chitosan (α-FeO(OH)/GO/CS) nanocomposite was used in the removal of As(III) from an aqueous solution (Shan et al., 2020). Results derived from the investigation showed that As(III) adsorption increased with increasing initial concentration, contact time, and temperature (from 25 to 45 ºC), but decreased in the presence of sulfate, phosphate, evidently due to competitive adsorption with the surface adsorption sites of the nanocomposite. Also, the presence of Fe^{3+} in the solution decreases the adsorption of As(III), in this case, this decrease was attributable to the formation of iron oxide and/or hydroxide in solution which compete with the nanocomposite particle for the adsorbed As(III). As(III) adsorption was high in the pH range of 3–10, and was well fitted to the pseudo-second-order kinetic model ($r^2 = 0.9982$), and being endothermic and spontaneous. As(III) monolayer adsorption fitted with the Sips model:

$$[As]_{a,e} = \frac{[As]_{a,m} K_s [As]_{aq,e}^{1/n}}{1 + K_s [As]_{aq,e}^{1/n}} \tag{18.7}$$

and the maximum adsorption capacity was 289.42 mg/g, however, the experimental data also fitted well with the non-linear Freundlich isotherm. The removal of As(III) from the solution was attributed to the presence of -NHCO-, C—O, O—H, and Fe—O groups as well as the complexation between As(III) ions and hydroxyl iron oxide, being the latter the major contributor to this adsorption. Desorption can be performed with alkaline (NaOH) solutions. After five adsorption–desorption cycles, the removal efficiency was maintained as 79.6%.

Using crab shells, chitosan was produced, via the three stages of deproteinization, demineralization, and deacetylation, with sodium hydroxide and hydrochloric acid under different temperatures and time (Sumaila et al., 2020). The produced chitosan presented $–NH_2$ and –OH functional groups, amorphous/crystalline phases (crystallinity index of 69.54%), and an average particle size of 729 nm, 12.67 m^2/g surface area, and with the thermal stability of up to 1430°C. The material was used in the removal of arsenic(III) and copper, from electroplating wastewaters, under various operational conditions. The increment of the temperature from 30°C to 60°C produced an increase in As(III) adsorption, resulting in an endothermic process. Under the employed conditions, chitosan though has a low surface area, displaying an acceptable capacity to adsorb arsenic. The results were best fitted ($r^2 = 0.999$) to the Jovanovic isotherm:

$$[As]_{a,e} = [As]_{a,m}\left(1 - \exp\left(-K_J [As]_{aq,e}\right)\right) \tag{18.8}$$

with maximum arsenic uptake onto the adsorbent of 6.3 mg/g. This isotherm is considered mechanical contact between the adsorbing and desorbing molecules. Experimental results were fitted to the pseudo-second-order model ($r^2 = 0.942$). NOTE: desorption data were not included in the manuscript.

An adsorbent (CSN-La) of lanthanum immobilized on electrospun chitosan nanofiber(CSN) was used for arsenate removal (Tan et al., 2020). The experimental results indicated that the arsenate adsorption by CSN-La was pH-dependent and fitted the

pseudo-second-order kinetic model ($r^2 = 0.995$) and non-linear Langmuir isotherm ($r^2 = 0.992$). The saturated adsorption capacity of CSN-La was 83.6 mg/g, which was higher than that of CSN, being the removal of arsenate preferable to that of co-existing anions (chloride, sulfate, nitrate, bicarbonate). The usefulness of CSN-La relies on its special structural characteristics: the host material CSN favored the pre-concentration of arsenate via electrostatic attraction, and the immobilized lanthanum exhibited preferable arsenate removal through specific interaction. Column experiments showed that CSN-La could effectively treat near 2650 BV of feeding solution before breakthrough occurred, resulting in a decrease of arsenic concentration of 210 μg/L in the feeding solution to less than 10 μg/L in the exiting one, however, the value decreased until 2310 BV at the third run, being these results attributable to that a small amount of the bound sites present in the nanocomposite are irreversible. Desorption was carried out with sodium hydroxide solution.

Natural polysaccharide chitosan (CS) functionalized iron nanosheet was used to remove toxic As(III) (and Sb(III)) from an aqueous solution (Zeng et al., 2020). The surface area of the optimum material was 111.8 cm^2/g, this material also presented a good dispersion of the iron nanocomposite. Adsorption results showed that 0.5% in weight CS functionalized iron nanosheet had higher removal capacity, affinity, selectivity, and reusability for Sb(III) than As(III). The optimum adsorption was achieved at the adsorbent dosage of 0.4 g/L at wide pH values, and the maximum adsorption capacity was estimated as 108.6 mg/g for As(III) from Langmuir non-linear fitting. As(III) removal was independent of pH values, indicating that electrostatic attraction was not the dominant removal mechanism. The detailed removal mechanism was confirmed by a synergetic interaction of As—Fe complexes and hydrogen bonding. Silicate and phosphate ions decreased As(III) adsorption, but not sulfate or carbonate. Desorption was carried out with 0.5 M sodium hydroxide solution, and after four continuous cycles, the adsorption decreased until 50%.

18.3 Cadmium

A combination of polyacrylonitrile (PAN) functionalized with metal oxides (MO = ZnO, TiO_2) with a layer of chitosan (CS) produced bilayer nanofiber membranes (Alharbi et al., 2020). The final material was prepared via consecutive electrospinning. The adsorption properties of this PAN/MO-CS nanofiber toward cadmium (and lead) ions were investigated. It was demonstrated that the integration of a CS layer into PAN/MO nanofibers increased the adsorption capacity of cadmium (Table 18.2).

The experimental data were best fitted to the pseudo-second-order kinetic model and Langmuir isotherm (Choi et al., 2020). NOTE: desorption data were not included in the work.

Nano-chitosan was used to remove cadmium from water under different experimental conditions (Alyasi et al., 2020). The capacity of this nanoadsorbent was found to be 220 mg/g, and the adsorption followed the SIPS model and the pseudo-second-order kinetic equation. The SIPS model indicates that cadmium was loaded onto the nanoadsorbent via a multiple adsorption mechanism, a second-order chemisorption mechanism indicated two main complexation bonding methods: complexation with one amine functional group and

TABLE 18.2 Approximate equilibrium cadmium concentrations onto various PAN adsorbents.

Adsorbent	$[Cd]_{a,e}$, mg/g
PAN	25
PAN-TiO_2	50
PAN-ZnO	80
PAN-CS	110
PAN-CS-TiO_2	160
PAN-CS-ZnO	130

a second complexing type with two amine groups and two hydroxyl groups. NOTE: desorption data were absent in the manuscript.

Electrospun chitosan (CS) non-woven mats are useful at removing heavy metals from aqueous solutions, but they suffered from low permeability and low-mechanical strength, also, they had not good characteristics with respect to their selectivity in the removal of these metals. To remediate these weaknesses, a bilayer adsorbent made of a porous phosphorylated cellulose substrate covered by electrospun CS nanofibers was developed (Brandes et al., 2021). In the case of Cd(II), results indicated that the experimental data fitted the pseudo-second-order and non-linear Langmuir models, with a maximum adsorption capacity of 591 mg/g at 25°C, being the adsorption enhanced with the increase of the temperature (25-60 ºC). After three cycles, the adsorbent lost near 16% of its initial adsorption capacity, this was is explained by the degradation of functional groups caused by the regeneration step with EDTA, also this complexing agent could form highly stable complexes with binding sites of the nanoadsorbent. In multi-elemental solutions the adsorption order was Cu(II) (1.17 mmol/g) > Cr(VI) (0.57 mmol/g) > Cd(II) (0.53 mmol/g) > Pb(II) (0.15 mmol/g).

Non-woven chitosan (CS) and phosphorylated microcellulose (PMC) CS/PMC nanocomposite fiber mats (CS/PMC) were produced by electrospinning, and presenting up to 50% by weight of PMC (Brandes et al., 2020). These mats were used in the adsorption of Cd^{2+} from an aqueous medium. Results showed that experimental data best fitted to the pseudo-second-order model and that Cd^{2+} removal from the solution was made via a chemisorption mechanism with a reaction (ion exchange) between Na^{+} from the adsorbent and Cd^{2+} from the solution, and also chemical complexation between the amino group of chitosan and the adsorbate. Equilibrium data best responded to the non-linear Langmuir isotherm, with a maximum adsorption capacity of 283 mg/g at 60°C, being this capacity attributable to the large amount of phosphate groups presented in the nanomaterial, which require less energy to capture the metal cations. Metal uptake was a spontaneous and endothermic process. Desorption was done in an EDTA-bearing acidic medium, after five cycles the adsorbent maintained near 95% of its initial adsorption capacity.

Nano-chitosan coating nano-iron oxide (nano-CI was prepared and its surface was modified with two different compounds (crotonaldehyde (nano-CIC) and succinic anhydride (nano-CIS)) (Hosain et al., 2020). The prepared nano-materials exhibit an average size between 9.32 and 20.57 nm and they were used in the adsorption of Cd(II) (and Cu(II) and Pb(II). In the case of cadmium, the maximum adsorption capacity was about 200 mg/g Cd(II). Both Langmuir isotherm (Ayub et al., 2020) and the pseudo-second-order kinetic

model responded well to the fitting of the Cd(II) adsorption experimental results, Cu(II) and Pb(II) also did it. NOTE: the manuscript did not include desorption data.

Chitosan was modified with salicylaldehyde to prepare salicylaldehyde functionalized chitosan nanoparticles (N-Ch-Sal) (Hussain et al., 2020). The as-prepared material presented sizes of about 80 nm and was used in the removal of Cd(II) (also Cu(II), and Pb(II) ions) from solutions. Under optimal conditions (pH 5) cadmium uptake was 63.71 mg/g. In the three cases, the adsorption process fitted the pseudo-second-order kinetic model and the Langmuir adsorption isotherm (Ayub et al., 2020). NOTE: desorption data were not included in the published manuscript.

A process combining chitosan and dopamine self-polymerization, doped in sodium carboxymethyl cellulose, and glutaraldehyde cross-linking was used to produce an amino-functionalized material (Li et al., 2020). The carboxyl methylcellulose and chitosan-derived nanostructured adsorbent were used to investigate its performance with respect to the removal of Cd(II) (and Cr(VI)) from aqueous solutions. Experimental data were fitted to the linear Freundlich isotherm and the pseudo-second-order kinetic model ($r^2 = 0.937$), thus, chemical adsorption was the rate controlled step. The maximum adsorption capacity (pH 5) for Cd(II) was 470 mg/g. Cadmium was desorbed with 1 M nitric acid solution, after five cycles, cadmium adsorption decreased from near 400 mg/g to 300 mg/g.

A nanoparticle-based mesoporous composite consisting of silicate-titanate nanotubes, (STNTs), supported in hydrogel chitosan beads, (STNTs-Ch beads), was investigated for Cd^{2+} adsorption (Quiroga-Flores et al., 2020). It was determined that the hollow STNTs were highly dispersed in the walls of the hollow beads, being attributable this dispersion to the effect of pH when the composite was prepared and it was observed a non-interaction between STNTs and chitosan. The composite followed the non-linear Langmuir isotherm with a maximum loading capacity of 656 ± 27 mg/g, and also ($r^2 = 0.9604$) the non-linear form of the pseudo-second-order model:

$$[Cd]_{a,t} = \frac{ht}{1 + K_{p2}[Cd]_{a,e}t} \tag{18.9}$$

with h being the initial adsorption rate, defined as:

$$h = K_{p2}[Cd]_{a,e}^2 \tag{18.10}$$

Desorption was accomplished in acidic solutions (best in 0.1 M H_2SO_4). After seven cycles, the adsorption rate decreased from 99% (1st cycle) to 54% (7th cycle).

Polylactic acid (PLA)/nano-chitosan (nCHS) composite fibers were produced by the electrospinning method and used in the Cd^{2+} adsorption from water (Thomas et al., 2020). The basic character of the composites had intensified with the increase in nCHS addition. Experimental results indicated that the Cd^{2+} adsorption capacity of the composite was two times faster (near 70%) with respect to that of neat PLA fibers. Both the increase in surface area and the presence of nCHS improved the adsorption capacity of the electrospun membrane. NOTE: desorption data were not included in the work.

A xanthate functionalized magnetic chitosan nanocomposite (XFMCN) was used for Cd(II) adsorption from high salinity water samples (Vajdi et al., 2021). The nanomaterial showed a

sulfur content of 2.28% and a BET surface area of 44.79 m^2/g. This functionalization resulted in a fitting to the linear form of the isotherm model (UT):

$$\ln\left(\frac{[Cd]_{aq,e}}{[Cd]_{a,e}}-\frac{K_d}{[Cd]_{a,m}}\right)=\ln\frac{D^{1-b}}{[Cd]_{a,m}^{b}}+b\ln[Cd]_{aq,e} \tag{18.11}$$

and to decrease the corresponding constant from 6.73 to 1.80×10^{-3}, showing an increased affinity toward cadmium adsorption. In the above equation, K_d is the model constant, b is a UT isotherm exponent, and D is the adsorbent dosage. Experimental data also fitted well to the linear form of the Redlich–Peterson isotherm:

$$\ln\left(K_R\frac{[Cd]_{aq,e}}{[Cd]_{a,e}}-1\right)=\ln\alpha_R+a\ln[Cd]_{aq,e} \tag{18.12}$$

where K_R is the model constant, α_R is a value derived from the fitting, and a is also a value between 0 and 1. A third good fitting of the experimental data is with the linear form of the Radke–Prausnitz isotherm model:

$$\ln\left(\frac{[Cd]_{aq,e}}{[Cd]_{a,e}}-\frac{1}{[Cd]_{a,m}K_{RP}}\right)=-\ln[Cd]_{a,m}+m\ln\left[Cd_{aq,e}\right] \tag{18.13}$$

being K_{RP} the corresponding model constant. A four fitting of the experimental data is with the Freundlich isotherm. The results confirmed multilayer adsorption. Best adsorption results were obtained after 60 min contact time and initial pH 7, being the maximum equilibrium adsorption capacity of 55 mg/g. Experimental data were fitted to the intraparticle diffusion and pseudo-second-order models., being cadmium uptake onto the adsorbent exothermic and spontaneous. The adsorbed cadmium ion can be desorbed using 0.01 M HCl. Continuous use of the adsorbent (five cycles) showed a slight decrease in the adsorbent performance (90%). NOTE: it is worth mentioning here, that the results in this paper conformed well within three unusual adsorption isotherms. Also, adsorption at pH 7 will imply some cadmium precipitation.

An environmentally friendly shell-coated magnetic attapulgite, attapulgite/$CoFe_2O_4$@SiO_2-chitosan/EDTA (ATPCFS-CSEs), was prepared by solvothermal and sol-gel process (Wang et al., 2020). Chitosan and EDTA were selected to functionalize the magnetic attapulgite to provide abundant amino groups and carboxyl groups. Sodium tripolyphosphate was chosen as a non-toxic cross-linker in surface deposition-cross-linking, and subsequently, an amidation reaction was taken for functionalization by chitosan and EDTA. The nanomaterial presented a well-defined architecture and paramagnetic properties and was used in the adsorption of Cd(II) from aqueous solutions. The adsorption data fitted well with the Langmuir isotherm (Choi et al., 2020), and the adsorption capacity was 128 mg/g. Metal uptake onto the nanoadsorbent was attributed to electrostatic interaction, complexation, and surface complexation. High concentration ionic competition experiments showed that ATPCFS-CSEs performed with respect to cadmium adsorption, however, aluminum, nickel, and zinc were removed from the solution in percentages exceeding 50%. After five adsorption–desorption cycles, the removal efficiency was above 88%.

18.4 Chromium

A study about the removal of Cr(VI) from aqueous solution was carried out using composite adsorbents derived from chitosan (obtained from shrimp peels) and $Cu(OH)_2$ or CuO (prepared by alkaline precipitation of Cu(II) ions) to manufacture $ChiCu(OH)_2$ and ChiCuO, respectively, and both being characterized as nanocomposites (Almughamisi et al., 2020). The removal of Cr(VI) from the solution was highly dependent on pH, temperature, metal concentration, and adsorbent mass. Chromium(VI) was best removed from the solution in the 5.5–6 pH range, with. Equilibrium data described by the Langmuir isotherm, increasing the maximum uptake with the temperature, in the case of $ChiCu(OH)_2$, and decreasing this maximum value, with the increase of this variable, in the case of using ChiCuO adsorbent (Table 18.3), while the uptake kinetics was best fitted to the pseudo-second-order equation.

The adsorption process was endothermic. Metal desorption was performed using alkaline saline solutions, i.e. a NaOH solution of pH 12 which also contained 20 g/L NaCl. Up to five adsorption–desorption cycles there was a slight decrease in their initial adsorption capacity. NOTE: according to the data shown in Table 18.3, these adsorbents had different performances with the temperature, but against the above, authors of the investigation claimed that using both adsorbents, the adsorption process was endothermic, thus, some discrepancy, not explained by the authors, appeared to rise here.

The adsorbent described in (Brandes et al., 2021), was used in the adsorption of multielement-bearing solutions, being the adsorption order Cu(II) > Cr(VI) > Cd(II) > Pb (II). NOTE: it was not described how Cr(VI) was removed from the loaded adsorbent.

Taking at a basis eggshell as biosource, various adsorbents: nanohydroxyapatite (NP), cetyltrimethyl ammonium bromide modified nanohydroxyapatite (NPB), and nanohydroxyapatite/chitosan composite either in acidic (NPS1) or alkaline media (NPS2) were prepared and used in the removal of chromium(VI) from aqueous phases (Hassan et al., 2020). The various properties of nanohydroxyapatite/chitosan composite synthesized in the alkaline medium were found to be better than the presented with the other three solid adsorbents. The above nanocomposite has a surface area and pore radius of 152.5 m^2/g and 5.11 nm, respectively. pHPZC for all the prepared solid samples was found to be in the 6.8–7.5 range. With respect to the maximum adsorption capacities of Cr(VI) onto the different adsorbents, these were obtained at pH 6 with concentrations of near 119 mg/g (NP), 132 mg/g (NPS1), 134 mg/g (NPS2), 85 mg/g (NPB). Within all the adsorbents, the adsorption of Cr(VI) was spontaneous and endothermic, following the pseudo-second-order kinetic model. NOTE:

TABLE 18.3 Influence of the temperature on Cr(VI) uptake (mg/g) onto the nanocomposites.

Adsorbent	26°C	36°C	46°C
$ChiCu(OH)_2$	74	78	83
ChiCuO	136	132	129

Initial pH = 4. Time: 3 h.

After reading the accessible Abstract, apparently there was no adsorption data included in the work.

An amino-functionalized bead described in (Li et al., 2020) was used in the adsorption of Cr(VI) from aqueous solutions. Experimental data were fitted ($r^2 = 0.951$) to the linear form of Freundlich isotherm and followed ($r^2 = 0.850$) the pseudo-second-order kinetic model. The maximum adsorption capacity (pH 2) of Cr(VI) was 347 mg/g. The adsorbent, and under these acidic conditions, showed a strong electrostatic affinity with respect Cr(VI). This element was desorbed using a 0.2 M NaOH solution. After five cycles of adsorption–desorption Cr(VI) uptake was maintained around 100 mg/g.

18.5 Mercury

A green nanocomposite based on the self-assembly of graphene oxide (GO) with chitosan (CH) was used in the removal of Hg(II) from various water sources: ultrapure and natural waters (tap water, river water, and seawater) (Bessa et al., 2020). Using ultrapure water with initial mercury(II) concentration of 50 μg/L, the experimental results showed that GO–CH nanocomposite had an excellent adsorption capacity of Hg (II) (97% metal removal after 2 h) even using very small adsorbent dosages, i.e., 10 mg/L. In the case of tap water, the recovery was 81.4% after 4 h of contact time. However, when the solution comes from river and seawater, the GO–CH nanocomposite showed a limited performance probably attributed to the high complexity of the water matrices, leading to low removal of Hg(II): 13% in the case of river waters and 7% in the case of seawater. Further investigations concluded that the low Hg(II) removal from seawater was due to the presence of chloride ions in the water, and the subsequent formation of stable mercury-chloride complexes, having no affinity to be adsorbed by the nanocomposite. The above was not the case in the presence of nitrate or sodium ions, because in this case the percentage of mercury(II) removal from the water exceed 90%. NOTE: there were no included desorption data.

A magnetic network polymer composite (MCTP) was synthesized by introducing the poly (m-aminothiophenol) and chitosan onto the magnetic-mesoporous nanoparticle under tannic acid as a cross-linking agent (Fu et al., 2021). The nanocomposite rocketed Hg(II) adsorption in comparison with other adsorbents (Table 18.4):

Mercury(II) adsorption investigation indicated the percentage of metal removal increased from pH 1 to 3.5, and adsorption capacity of the adsorbent was near 98% and 245 mg/g within 15 min, respectively, with a maximum adsorption capacity of 515 mg/g. The

TABLE 18.4 Hg(II) uptake by different magnetic composites.

Adsorbent	% Uptake
Fe_3O_4	2.5
Fe_3O_4@SiO_2	11.3
MMS (Fe_3O_4@SiO_2@SiO_2)	18.9
MMS-NH_2	35.0
MCTP	98.8

adsorption of Hg(II) is mainly dominated by chemical adsorption and is due to the stronger coordination bonds or Hg(II)-chelate complex between sulfur or nitrogen groups and Hg(II). Desorption was performed by magnetic separation of the mercury-loaded adsorbent and treatment with a mixture of HNO_3 (0.1 M) and thiourea (0.1 M). After five cycles of continuous use, the adsorption loading decreased from 250 mg/g (1st cycle) to 173 mg/g (5th cycle). The toxic spent adsorbent was used as a catalyst for the synthesis of acetophenone, with 99% yield, and most of the phenylacetylene derivatives were transformed to corresponding acetophenone in excellent yields (exceeding 98%).

A polyethyleneimine functionalized chitosan-lignin (PEI-CS-L) composite sponge adsorbent with nanowall-network structures was synthesized by cross-linking and lyophilization (Zhang et al., 2020). The as-prepared adsorbent can remove Hg(II) selectively from an aqueous solution with high efficiency (more than 83%) and a short reaction time (1 min). Following the Langmuir and pseudo-second-order models, the maximum adsorption capacity was 663.5 mg/g at pH 5.5, being the adsorption increases with the increase of the temperature (20–40°C). These results were attributed to the evenly interconnected porous structure of the composite sponge with nanoscale-wall structures which increase the distribution of functional groups and resulting in a fast complexation of Hg(II) with surface functional groups. The PEI-CS-L sponge ha presented a decrease in Hg^{2+} adsorption from 663.5 mg/g (1st cycle) to 504.7 mg/g (5th cycle), with the desorption step carried out with a 1 M HNO_3 solution.

18.6 Lead

Using the adsorbent described in (Brandes et al., 2021), Pb^{2+} presented the worst loading results from the mixture of this element and Cu^{2+}, $Cd^{2+,}$ and $HCrO_4^-$ ions.

In situ construction of *nanotentacles* of (3-aminopropyl)trimethoxysilane (APS) on the inner wall of the porous structure of chitosan/graphene oxide composite gel (CGG) was investigated (Cheng et al., 2020). The resulted material showed a very high affinity for Pb^{2+}, being the uptake capacity of 470 mg/g. The NT-CGG composite removes this toxic element from 0.01 g/L to levels of less than 0.02 ppb. The adsorption of Pb^{2+} followed the pseudo-second-order and the Langmuir isotherm models. Despite its affinity to adsorb lead, in a solution containing a mixture of elements, this lead(II) was co-adsorbed together with cadmium and copper, whereas sodium, magnesium, and calcium were not adsorbed at all. The Pb-loaded adsorbent was treated with a 0.05 M EDTA solution of pH 7 in order to remove this metallic element from the adsorbent; under five consecutive adsorption–desorption cycles, the adsorbent maintained an 88% of its original capacity. NOTE: this decrease followed a continuous pattern, thus, probably it would expect a further decrease with subsequent cycles.

A magnetic nano-biocomposite, chitosan conjugated magnetite nanoparticle (CH-MNP) was used for the removal of Pb^{2+} from solutions (Cheraghipour and Pakshir, 2020). The CH-MNPs had a diameter of near 10 nm, with a saturation magnetization of 76.01 emu/g, resulting in a superparamagnetic property. Being Pb^{2+} adsorption pH-dependant, the optimum conditions to achieve 92% of Pb^{2+} adsorption were found to be at a pH of 6.1, using a nanoadsorbent dosage of near 1 g/L, and a contact time of 1 h. Experimental data fitted well with the non-linear Langmuir isotherm model, whereas the equilibrium data followed the pseudo-second-order and intraparticle diffusion kinetic models. The maximum Pb(II)

adsorption capacity was 192 mg/g. Desorption was performed using a 0.1 M EDTA solution, and the continuous use of the adsorbent demonstrated a continuous loss of adsorption effectiveness (92.2% (1st cycle) and 80.3% (5th cycle)), also in the desorption step the nanocomposite lost effectiveness under continuous use (90.1% (1st cycle) against 73.9% (5th cycle)).

A Fe_3O_4-chitosan nanocomposite for removing lead(II) from industrial wastewater was fabricated (Covaliu et al., 2020). The adsorbent was used in the removal of lead(II) from solutions having a pH of 3 and metal concentrations in the 0.5–2 mg/L range. NOTE: this manuscript did not present desorption data.

A graphene oxide (GO)-derivative nanocomposite containing chitosan was synthesized and investigated for Pb^{2+} adsorption from aqueous solutions (Foroughi and Azqhandi, 2020). The following optimum conditions were concluded as pH 8, the temperature of 50 °C, and contact time of 22 min; in the above conditions, 94% were removed. The maximum adsorption capacity of almost 667 mg/g was estimated from the Langmuir isotherm ($r^2 = 0.937$) in an endothermic process. Experimental data followed the pseudo-second kinetic model ($r^2 = 0.9437$). The influence of co-existing ions (sodium, potassium, magnesium, calcium, copper, zinc, chlorides, sulfate, and carbonate) on the adsorption of Pb (II) showed a negative effect (from 93% to 75%) at a concentration of the companying elements around 6 mg/L. Under continuous use (Table 18.5) the adsorbent lost its initial adsorption capacity, whereas this decrease followed a continuous pattern. NOTE: due to the high pH value used, probably in this work not only adsorption but lead(II) precipitation occurred. Also, and editing failure was found since in the Abstract section the values of ΔG^o and ΔH^o were interchanged. Apparently, how the desorption step was carried out it was not indicated in the manuscript.

The adsorbent described in (Hosain et al., 2020) was used in the adsorption of Pb^{2+} from aqueous solutions. The maximum Pb^{2+} adsorption capacity was near 560 mg/g. Both Langmuir isotherm (Ayub et al., 2020) and the pseudo-second-order kinetic model responded well to the fitting of Pb^{2+} adsorption experimental results. NOTE: desorption step was not considered by these authors.

An adsorbent containing phosphorylated chitosan-coated magnetic silica nanoparticles (Fe_3O_4@SiO_2@CS-P), was fabricated and used for the adsorption of lead (Huang et al., 2021). Lead adsorption increased with the increase of the aqueous pH value from 1 to 6, reaching a lead uptake of 120 mg/g. Adsorption was endothermic and spontaneous, following the Langmuir isotherm and the pseudo-second-order equation. The maximum capacity was 213 mg/g. Competitive experiments were conducted in a multi-elemental solution (zinc, copper, silver, strontium, cadmium, and nickel) at pH 6.0, showing this adsorbent a good selectively toward lead with the distribution coefficient (0.75 L/g) more than 10 times than the

TABLE 18.5 Loss of graphene oxide-chitosan nanocomposite adsorption efficiency.

Cycle	% Pb(II) removal	Cycle	% Pb(II) removal
1	93.1	4	88.4
2	91.3	5	86.3
3	90.2	6	85.2

values presented for other metal, however, the adsorbent also performed well with respect to silver adsorption. These results implied that phosphorylation of the adsorbent not only improves the adsorption performance of lead, via its coordination with the phosphate groups on the surface of the adsorbent but also changes the selective adsorption of metal types. Desorption was investigated using a 0.1 M EDTA solution, and after five cycles of continuous use, lead adsorption decreased from 155 mg/g (1st cycle) to 98 mg/g (5th cycle). This decrease was attributable to various causes: (i) loss of adsorbent, (ii) strong interaction between phosphate groups and Pb^{2+}, which it was not desorbed, leading to the loss of adsorption sites within the nanoadsorbent, and iii) the amount of iron leaching after each cycle, decreasing adsorption efficiency.

An ethylenediaminetetraacetic acid (EDTA)-functionalized magnetic chitosan oligosaccharide and carboxymethyl cellulose (Fe_3O_4@CMCCOS-EDTA) nanocomposite adsorbent was fabricated for Pb(II) adsorption (Lian et al., 2020). The batch adsorption experiment results indicated that the experimental data fitted both the pseudo-second-order model and the Langmuir isotherm. Pb(II) uptake increased with the increase of the pH value (1 to 5) and then remained constant. The maximum adsorption capacity for the monolayer chemical adsorption process was calculated as 432.34 mg/g at the pH of 5 and temperature of 35 ºC. Desorption was investigated using a 0.01 M EDTA solution, being 12 h the reaction time. A continuous decrease in the adsorption efficiency was observed under continuous use (130 mg/g (1st cycle) and 110 mg/g (5th cycle), also, the desorption efficiency decreased under continuous use (100% in the first cycle and 78% in the fifth cycle).

Polypropylene (PP) and polypropylene grafted-maleic-anhydride (PP-g-MA) based nanocomposites reinforced with chitosan (CS) and modified montmorillonite clay nanofiller (CL120DT) were fabricated and used in the removal of lead(II) from aqueous solutions (Moja et al., 2020). The uptake of Pb (II) by this nanocomposite followed the non-linear Langmuir isotherm model (Ayub et al., 2020), with a removal yield of 91% at pH 8, and the adsorption fitted the pseudo-second-order kinetic equation. Maximum metal uptake was estimated as 74 mg/g. After five cycles of adsorption–desorption, there was a decrease in the uptake capacity from 91% (1st cycle) to 77% (5th cycle). This decrease was explained due to the presence of residual Pb(II) occupying adsorption sites. NOTE: again a pH 8 should indicate that the removal is not only based on adsorption but also on precipitation. In the published manuscript, the desorption step was literally described as "desorption; 25º C, pH 8.3, 1.0 $NaNO_3$ desorption solutions, 10 ppm initial Pb(II) concentration, 30 min contact time"., which is an un-explicable continuous error from the authors, reviewers, and Editorial Office.

Diethylenetriaminepentaacetic acid-modified chitosan/polyethylene oxide nanofibers (CS-DTPA/PEO NFs) were developed to be tested in the adsorption of Pb^{2+} (and also Cu^{2+} and Ni^{2+}) (Surgutskaia et al., 2020). The adsorption equilibrium was established after 90 min, and data were described using the Langmuir isotherm model. The maximum adsorption capacity of CS-DTPA/PEO NFs for Pb^{2+} was estimated as 142 mg/g (pH 5). Metal adsorption was basically attributable to:

(i) electrostatic attraction with active groups of chitosan,
(ii) coordination with active groups of chitosan, and
(iii) leaching of sodium and potassium ions from DTPA fragments.

In competitive solutions, the adsorption order was found to be $Cu^{2+} > Ni^{2+} > Pb^{2+}$, thus, the adsorbent was not selective with respect to Pb^{2+} adsorption. Lead (II) desorption was performed using 0.01 M HNO_3, followed by the use of 0.01 M NaOH solution, and washing with deionized water until neutral pH. Under continuous use, the rate of lead adsorption onto the fibers decreased progressively from 100% (first cycle) to 80% (fifth cycle), the decrease attributable to the reduction in the number of available sites under repetitive use. NOTE: in the Conclusion section, the authors claimed that adsorption followed the pseudo-first-order equation, whereas in the text they explained that kinetics followed the pseudo-second-order model.

A type of Pb(II) adsorbent was prepared via carboxylated chitosan (CYCS) and carboxylated nanocellulose (CNC). These were used to chelate and synthesize hydrogel spheres with effective adsorption sites, in calcium chloride solution (Xu et al., 2021). This CYCS/CNC adsorbent exhibited a maximum Pb(II) adsorption capacity of near 335 mg/g at pH 4, being the experimental results well fitted to the non-linear Langmuir isotherm in the 24-61 ºC temperatures range, whereas the adsorption followed the pseudo-second-order model. The adsorption mechanism was identified as monolayer chemisorption on the surface of the beads, whereas metal uptake occurred via electrostatic interaction between Pb^{2+} and the carboxyl groups of the adsorbent, also chemical activity of hydroxyl and amino groups on the beads took part in the adsorption process. Desorption was carried out at pH 2 (HCl medium), and after four cycles only a small decrease in the adsorption capacity was observed.

18.7 Conclusions

The use of adsorption technology is of wide use in the scientific community in order to achieve the removal of metal pollutants from aqueous media. Within these varieties of potential adsorbents, chitosan, chitosan derivatives, and nanoderivatives have found wide use in this potential environmental issue. From the information derived from the present review, some generalities can be found in the treatments of hazardous metals-bearing solutions with nano-chitosan and chitosan-bearing nanocomposites: (i) most of the investigated systems obey whatever form of the Langmuir isotherm model, (ii) also practically all of the experimental data derived from these systems, fitted well with the pseudo-second-order kinetic equation, thus, metal adsorption seemed to be chemical in nature, (iii) in the case of the adsorption of cations, i.e., Cd^{2+}, Hg^{2+} and Pb^{2+}, most of these systems can not be used, for one or another reason, to remove them from acidic pH medium. Though the experimental conditions varied, maximum metal uptakes were found to be in the order of several hundreds of mg/g (Table 18.6).

Also, it is an unfortunate norm that the desorption step is not considered by some authors, in the present case 30% of the reviewed articles, being this step as important, considering the whole process, as the adsorption step is, and in the case that this desorption step is considered, many of the investigated nanoadsorbents are not reliable, upon continuous use, since they suffered a degradation, in the form of loss of their initial adsorption and desorption capacities, under these continuous adsorption–desorption cycles. It was also found two features of the works reviewed here:

(i) in all the reviewed manuscripts, the authors take into consideration several variables which may affect the metal's adsorption, but they did not take into consideration a

TABLE 18.6 Maximum metal uptakes onto the reviewed nanoadsorbents.

Element	Uptake, mg/g
As(III)	289
As(V)	>200
Cd(II)	650
Cr(VI)	347
Hg(II)	664
Pb(II)	667

further experimental variable that could affect this adsorption, and this is how the metal-bearing solution and the adsorbent were mixed, in other words, the stirring speed applied to the system, that may be also a key variable affecting metal uptake onto the adsorbent (Alcaraz et al., 2021). Its effect on a given system can be only determined experimentally,

(ii) also, the authors did not comment on what to do with the desorbed solution, which could have a higher metal concentration than the initial feed solution to the adsorption step, and thus, it would be of higher toxicity. The exception to this rule can be found in Fu et al. (2021), where the authors find an use to the Hg(II)-loaded adsorbent.

In any case, the presence of toxic metals in aqueous environments continues to be a potential risk for life, and surely, scientists around the world will continue their efforts to find good adsorbents to resolve this toxicity problem.

Acknowledgments

To the CSIC (Spain) for support.

References

Alcaraz, L., Alguacil, F.J., López, F.A., 2021. Microporous adsorbent from winemaking waste for the recovery of Mn(VII) in liquid solutions. Can. J. Chem. Eng. 99, 447–457. https://doi.org/10.1002/cjce.23862.

Alharbi, H.F., Haddad, M.Y., Aijaz, M.O., Assaifan, A.K., Karim, M.R., 2020. Electrospun bilayer PAN/Chitosan nanofiber membranes incorporated with metal oxide nanoparticles for heavy metal ion adsorption. Coatings 10, 285. https://doi.org/10.3390/coatings10030285.

Almughamisi, M.S., Khan, Z.A., Alshitari, W., Elwakeel, K.Z., 2020. Recovery of chromium(VI) oxyanions from aqueous solution using $Cu(OH)_2$ and CuO embedded chitosan adsorbents. J. Polym. Environ. 28, 47–60. https://doi.org/10.1007/s10924-019-01575-z.

Alyasi, H., Mackey, H.R., McKay, G., 2020. Removal of cadmium from waters by adsorption using nanochitosan. Energy Environ. 31, 517–534. https://doi.org/10.1177/0958305X19876191.

Ayub, A., Raza, Z.A., Majeed, M.I., Tariq, M.R., Irfan, A., 2020. Development of sustainable magnetic chitosan biosorbent beads for kinetic remediation of arsenic contaminated water. Int. J. Biol. Macromol. 163, 603–617. https://doi.org/10.1016/j.ijbiomac.2020.06.287.

Bessa, A., Gonçalves, G., Henriques, B., Domingues, E.M., Pereira, E., Marques, P.A.A.P., 2020. Green graphene–chitosan sorbent materials for mercury water remediation. Nanomaterials 10. https://doi.org/10.3390/nano10081474, 1474.

Brandes, R., Brouillette, F., Chabot, B., 2020. Laboratory adsorption studies on cadmium (II) by nonwoven chitosan/phosphorylated microcellulose nanocomposite. Water Air Soil Pollut. 231, 566. https://doi.org/10.1007/s11270-020-04936-w.

Brandes, R., Brouillette, F., Chabot, B., 2021. Phosphorylated cellulose/electrospun chitosan nanofibers media for removal of heavy metals from aqueous solutions. J. Appl. Polym. Sci. 138. https://doi.org/10.1002/app.50021, 50021.

Brião, G.V., de Andrade, J.R., da Silva, M.G.C., Vieira, M.G.A., 2020. Removal of toxic metals from water using chitosan-based magnetic adsorbents. A review. Environ. Chem. Lett. 18, 1145–1168. https://doi.org/10.1007/s10311-020-01003-y.

Cheng, J., Gao, M., Yang, L., Zhang, L., Zhu, B., 2020. Coral-inspired "nanotentaclization" porous composite gel for efficient removal of lead(II) from aqueous solution. Mater. Des. 195. https://doi.org/10.1016/j.matdes.2020.109072, 109072.

Cheraghipour, E., Pakshir, M., 2020. Process optimization and modeling of Pb(II) ions adsorption on chitosan-conjugated magnetite nano-biocomposite using response surface methodology. Chemosphere 260. https://doi.org/10.1016/j.chemosphere.2020.127560, 127560.

Choi, J.-S., Lingamdinne, L.P., Yang, J.-K., Chang, Y.-Y., Koduru, J.R., 2020. Fabrication of chitosan/graphene oxide-gadolinium nanorods as a novel nanocomposite for arsenic removal from aqueous solutions. J. Mol. Liq. 320. https://doi.org/10.1016/j.molliq.2020.114410, 114410.

Covaliu, C.I., Matei, E., Stoia, O., Paraschiv, G., 2020. Magnetic nanocomposite material containing chitosan polymer used in wastewater depollution processes. Mater. Plast. 57, 70–76. https://doi.org/10.37358/MP.20.4.5407.

Foroughi, M., Azqhandi, M.H.A., 2020. A biological-based adsorbent for a non-biodegradable pollutant: modeling and optimization of Pb(II) remediation using GO-CS-Fe3O4-EDTA nanocomposite. J. Mol. Liq. 318. https://doi.org/10.1016/j.molliq.2020.114077, 114077.

Fu, Y., Sun, Y., Zheng, Y., Jiang, J., Yang, C., Wang, J., Hu, J., 2021. New network polymer functionalized magnetic-mesoporous nanoparticle for rapid adsorption of Hg(II) and sequential efficient reutilization as a catalyst. Sep. Purif. Technol. 259. https://doi.org/10.1016/j.seppur.2020.118112, 118112.

Hassan, A.F., El-Naggar, G.A., Braish, A.G., Amira, M.F., Alshandoudi, L.M., 2020. Enhanced adsorption of chromium(Vi) from aqueous medium by basic nanohydroxyapatite/chitosan composite based on egg shell. Desalin. Water Treat. 206, 235–249. https://doi.org/10.5004/dwt.2020.26306.

Hosain, A.N.A., El Nemr, A., El Sikaily, A., Mahmoud, M.E., Amira, M.F., 2020. Surface modifications of nanochitosan coated magnetic nanoparticles and their applications in Pb(II), Cu(II) and Cd(II) removal. J. Environ. Chem. Eng. 8. https://doi.org/10.1016/j.jece.2020.104316, 104316.

Huang, Y., Hu, C., An, Y., Xiong, Z., Hu, X., Zhang, G., Zheng, H., 2021. Magnetic phosphorylated chitosan composite as a novel adsorbent for highly effective and selective capture of lead from aqueous solution. J. Hazard. Mater. 405. https://doi.org/10.1016/j.jhazmat.2020.124195, 124195.

Hussain, M.S., Musharraf, S.G., Bhanger, M.I., Malik, M.I., 2020. Salicylaldehyde derivative of nano-chitosan as an efficient adsorbent for lead(II), copper(II), and cadmium(II) ions. Int. J. Biol. Macromol. 147, 643–652. https://doi.org/10.1016/j.ijbiomac.2020.01.091.

Kloster, G.A., Valiente, M., Marcovich, N.E.C., Mosiewicki, M.A., 2020. Adsorption of arsenic onto films based on chitosan and chitosan/nano-iron oxide. Int. J. Biol. Macromol. 165, 1286–1295. https://doi.org/10.1016/j.ijbiomac.2020.09.244.

Kumar, A.K.R., Saikia, K., Neeraj, G., Cabana, H., Kumar, V.V., 2020. Remediation of bio-refinery wastewater containing organic and inorganic toxic pollutants by adsorption onto chitosan-based magnetic nanosorbent. Water Qual. Res. J. Can. 55, 36–51. https://doi.org/10.2166/WQRJ.2019.003.

Li, S.-S., Wang, X.-L., An, Q.-D., Xiao, Z.-Y., Zhai, S.-R., Cui, L., Li, Z.-C., 2020. Upon designing carboxyl methylcellulose and chitosan-derived nanostructured sorbents for efficient removal of Cd(II) and Cr(VI) from water. Int. J. Biol. Macromol. 143, 640–650. https://doi.org/10.1016/j.ijbiomac.2019.12.053.

Lian, Z., Li, Y., Xian, H., Ouyang, X.-K., Lu, Y., Peng, X., Hu, D., 2020. EDTA-functionalized magnetic chitosan oligosaccharide and carboxymethyl cellulose nanocomposite: synthesis, characterization, and Pb(II) adsorption performance. Int. J. Biol. Macromol. 165, 591–600. https://doi.org/10.1016/j.ijbiomac.2020.09.156.

Moja, T.N., Bunekar, N., Mishra, S.B., Tsai, T.-Y., Hwang, S.S., Mishra, A.K., 2020. Melt processing of polypropylene-grafted-maleic anhydride/chitosan polymer blend functionalized with montmorillonite for the removal of lead ions from aqueous solutions. Sci. Rep. 10, 217. https://doi.org/10.1038/s41598-019-57079-2.

Na, Y., Lee, J., Lee, S.H., Kumar, P., Kim, J.H., Patel, R., 2020. Removal of heavy metals by polysaccharide: a review. Polym. Plast. Technol. Mater. 59, 1770–1790. https://doi.org/10.1080/25740881.2020.1768545.

Pathan, S., Bose, S., 2020. Biopolymer based hydrogels for arsenic removal. Curr. Sci. 118, 1540–1546. https://doi.org/10.18520/cs/v118/i10/1540-1546.

Quesada, H.B., de Araújo, T.P., Vareschini, D.T., de Barros, M.A.S.D., Gomes, R.G., Bergamasco, R., 2020. Chitosan, alginate and other macromolecules as activated carbon immobilizing agents: a review on composite adsorbents for the removal of water contaminants. Int. J. Biol. Macromol. 164, 2535–2549. https://doi.org/10.1016/j.ijbiomac.2020.08.118.

Quiroga-Flores, R., Noshad, A., Wallenberg, R., Önnby, L., 2020. Adsorption of cadmium by a high-capacity adsorbent composed of silicate-titanate nanotubes embedded in hydrogel chitosan beads. Environ. Technol. 41, 3043–3054. https://doi.org/10.1080/09593330.2019.1596167.

Shan, H., Peng, S., Zhao, C., Zhan, H., Zeng, C., 2020. Highly efficient removal of As(III) from aqueous solutions using goethite/graphene oxide/chitosan nanocomposite. Int. J. Biol. Macromol. 164, 13–26. https://doi.org/10.1016/j.ijbiomac.2020.07.108.

Sumaila, A., Ndamitso, M.M., Iyaka, Y.A., Abdulkareem, A.S., Tijani, J.O., Idris, M.O., 2020. Extraction and characterization of chitosan from crab shells: kinetic and thermodynamic studies of arsenic and copper adsorption from electroplating wastewater. Iraqi J. Sci. 61, 2156–2171. https://doi.org/10.24996/ijs.2020.61.9.2.

Surgutskaia, N.S., Martino, A.D., Zednik, J., Ozaltin, K., Lovecká, L., Bergerová, E.D., Kimmer, D., Svoboda, J., Sedlarik, V., 2020. Efficient Cu^{2+}, Pb^{2+} and Ni^{2+} ion removal from wastewater using electrospun DTPA-modified chitosan/polyethylene oxide nanofibers. Sep. Purif. Technol. 247. https://doi.org/10.1016/j.seppur.2020.116914, 116914.

Tahoon, M.A., Siddeeg, S.M., Mnif, W., Ben Rebah, F., 2020. Effective heavy metals removal from water using nanomaterials: a review. Processes 8, 645. https://doi.org/10.3390/PR8060645.

Tan, P., Zheng, Y., Hu, Y., 2020. Efficient removal of arsenate from water by lanthanum immobilized electrospun chitosan nanofiber. Colloids Surf. A Physicochem. Eng. Asp. 589. https://doi.org/10.1016/j.colsurfa.2020.124417, 124417.

Thomas, M.S., Pillai, P.K.S., Faria, M., Cordeiro, N., Kailas, L., Kalarikkal, N., Thomas, S., Pothen, L.A., 2020. Polylactic acid/nano chitosan composite fibers and their morphological, physical characterization for the removal of cadmium(II) from water. J. Appl. Polym. Sci. 137. https://doi.org/10.1002/app.48993, 48993.

Vajdi, R., Alvand, N., Baghdadi, M., Bidhendi, G.N., 2021. Increase of chitosan selectivity and affinity toward the cadmium ions using xanthate functionalization: application for cadmium removal from saline solutions. J. Water Process Eng. 40. https://doi.org/10.1016/j.jwpe.2020.101898, 101898.

Wang, Y., Zhou, R., Wang, C., Zhou, G., Hua, C., Cao, Y., Song, Z., 2020. Novel environmental-friendly nanocomposite magnetic attapulgite functionalized by chitosan and EDTA for cadmium (II) removal. J. Alloys Compd. 817. https://doi.org/10.1016/j.jallcom.2019.153286, 153286.

Xu, X., Ouyang, X.-K., Yang, L.-Y., 2021. Adsorption of Pb(II) from aqueous solutions using crosslinked carboxylated chitosan/carboxylated nanocellulose hydrogel beads. J. Mol. Liq. 322. https://doi.org/10.1016/j.molliq.2020.114523, 114523.

Zeng, J., Qi, P., Shi, J., Pichler, T., Wang, F., Wang, Y., Sui, K., 2020. Chitosan functionalized iron nanosheet for enhanced removal of As(III) and Sb(III): Synergistic effect and mechanism. Chem. Eng. J. 382. https://doi.org/10.1016/j.cej.2019.122999, 122999.

Zhang, D., Wang, L., Zeng, H., Rhimi, B., Wang, C., 2020. Novel polyethyleneimine functionalized chitosan-lignin composite sponge with nanowall-network structures for fast and efficient removal of Hg(II) ions from aqueous solution. Environ. Sci. Nano 7, 793–802. https://doi.org/10.1039/c9en01368g.

This page intentionally left blank

CHAPTER

19

Toxicological impact and adsorptive removal of triclosan from water bodies using chitosan and carbon-based nano-architectures

Tahir Rasheed[a], *Muhammad Bilal*[b], *and Hafiz M.N. Iqbal*[c]

[a]Interdisciplinary Research Center for Advanced Materials, King Fahd University of Petroleum and Minerals (KFUPM), Dhahran, Saudi Arabia [b]School of Life Science and Food Engineering, Huaiyin Institute of Technology, Huaian, China [c]Tecnologico de Monterrey, School of Engineering and Sciences, Monterrey, Mexico

19.1 Introduction

Recently, a new class of water contaminating agents, which are referred to as "emerging pollutants (EPs)" has been identified and assimilated into the ecosystem. These emerging pollutants involve a broad spectrum of biologically active compounds, including pharmaceutical, pesticides, cosmeceutical, insecticides, surfactants, industrial waste, flame-retardants, and personal care products (Morsi et al., 2020). Triclosan (TCS) is among one of the widely consumed active agents with bactericidal and fungicidal activities in health and personal care stuff such as hand sanitizers, medical skin creams, soaps, deodorants, and toothpaste for over the last 50 years (Adolfsson-Erici et al., 2002). Due to high consumption (uncontrolled or controlled) and ubiquitous occurrence, triclosan has been identified in human samples such as breast milk (Arbuckle et al., 2015). In addition, it has also been widely detected and monitored in various water systems such as natural streams, rivers, drinking water tanks, and groundwater bodies (Carmona et al., 2014). The potential risks of endocrine system disruption, irritating mammalians organs, and active involvement in bacterial resistance to antibiotics at environmentally relevant exposure levels are the most worrying concerns associated with

https://doi.org/10.1016/B978-0-323-90912-9.00019-8

the contamination of triclosan (Rasheed et al., 2020). Besides, it can also serve as a precursor of an array of highly detrimental known human toxicants and carcinogenic metabolites such as methyl triclosan, chlorinated dioxins, and phenols (Pycke et al., 2014). Due to the adverse environmental and potential health consequences, it has become the subject of significant attention to introduce new approaches for effective and specific elimination of triclosan from the contaminated environments and reducing its threatening effects in a green, cost-efficient, and eco-responsive manner. Many methods have been attempted in the last few years for the removal of triclosan, including adsorption, biodegradation, photolysis, and advanced oxidation.

Recently, carbon-based nano-architectures have gained incredible interest as inspiring solid adsorbents to mitigate environmentally relevant toxic pollutants in water and air matrices owing to their exceptional characteristics such as substantial surface area, tailorable pore sizes, framework compositional and structural versatility, and exposed catalytic regions (Dou et al., 2017). The mechanism involving adsorptive removals of organic contaminants using carbon-based nano-architectures follows electrostatic, acid-base, non-covalent, hydrogen bonding, and hydrophobic interactions (Hasan and Jhung, 2015). In this chapter, we present the contemporary progress and exploration of carbon-based nano-architectures for the adsorptive removal of triclosan from aqueous environments.

19.2 Occurrence, persistence, and ecological impacts of triclosan

Triclosan is a lipid-soluble antibacterial and fungicidal agent with wide application in a variety of personal care and pharmaceutical compounds such as toothpaste, cosmetics, soap, disinfectants, antiperspirants, sunscreens, deodorants, and dishwashing liquids (Bilal et al., 2020). In addition, it can also be applied to many other consumer products, such as clothes, textiles, kitchen utensils, packaging, toys, fabrics, trash bags, and bedding (Fig. 19.1) (Dhillon et al., 2015). Nevertheless, its widespread utilization in washing and rinsing products results in the discharge of domestic sewage, which is regarded as the most significant source of environmental contamination (Kralj et al., 2020). The release of enormous amounts of triclosan along with inadequate removal in sewage treatment plants is the major cause for its extensive existence in environments (Yueh et al., 2014; Yueh and Tukey, 2016). Studies have demonstrated that triclosan is ubiquitously present in the aquatic environments and sediments with a rampant buildup in sediments due to its lipophilic behavior (Olaniyan et al., 2016). It is reported that triclosan is among the top 10 most widely detected organic wastewater contaminants in terms of concentration and frequency (Brausch and Rand, 2011)and has been detected in surface water in South Korea, China, Europe, United Kingdom, and the United States (Kasprzyk-Hordern et al., 2008). Acquaintance to triclosan can induce a multitude of hostile consequences on human's health and the environmental matrices, including damaging of the endocrine and hormonal system, central nervous system depression (Miller, 1983), contact dermatitis (Unit and Robertshaw, 2007), low sperm count and reduced sperm quality (Kumar et al., 2009), chronic liver injury and carcinogenesis (Fig. 19.2) (Yueh et al., 2014), tumor progression, oxidative stress, and weakening of thyroid functionalities (Adolfsson-Erici et al., 2002). Taken into consideration all literature data regarding triclosan

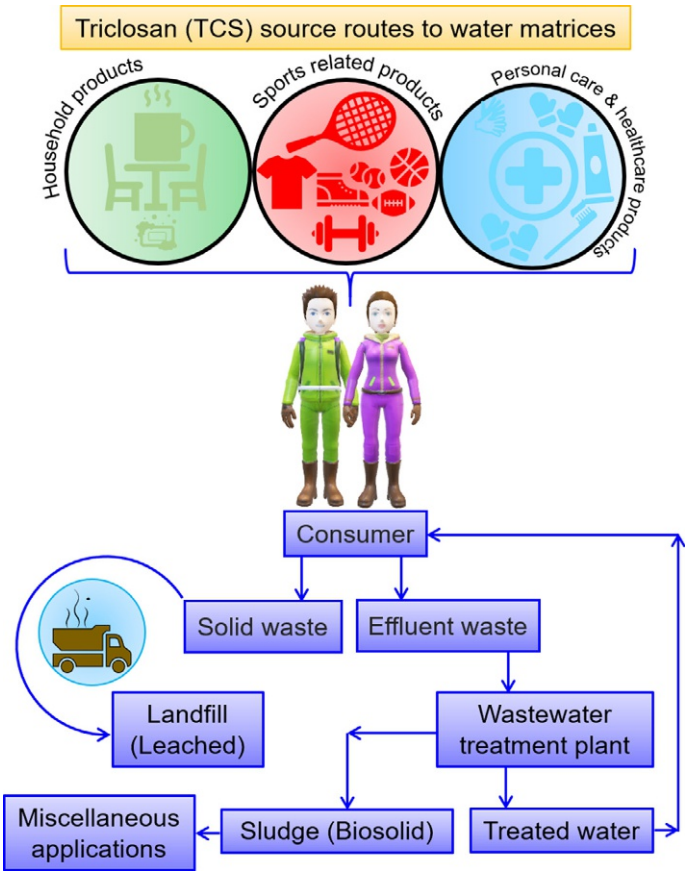

FIG. 19.1 Representation of general distribution and fate of triclosan in water matrices.

and its transformation products and metabolites its associated human health impacts, this chemical should be considered as a top priority concerning contaminant (Dhillon et al., 2015).

19.3 Toxicity and ecological effects of TCS

The introduction of triclosan into the environment from the effluent's releases from the sewage sludge and wastewater treatment plants, remains there due to its biological accumulation nature, hydrophobicity, and durability. This results in enhanced toxicity exposure for living organisms, particularly in animals (Heuer et al., 2019). Triclosan may change into different products including dioxin and methyl triclosan throughout its migration phase. Both these transformation products have higher toxicity and are more resistant to degradation compared to pristine triclosan (Pycke et al., 2014). Triclosan and its conversion products, on the other hand, may have harmful ecological functions on living organisms and can harm the ecosystem by disrupting biogeochemical cycles, community structure, and the

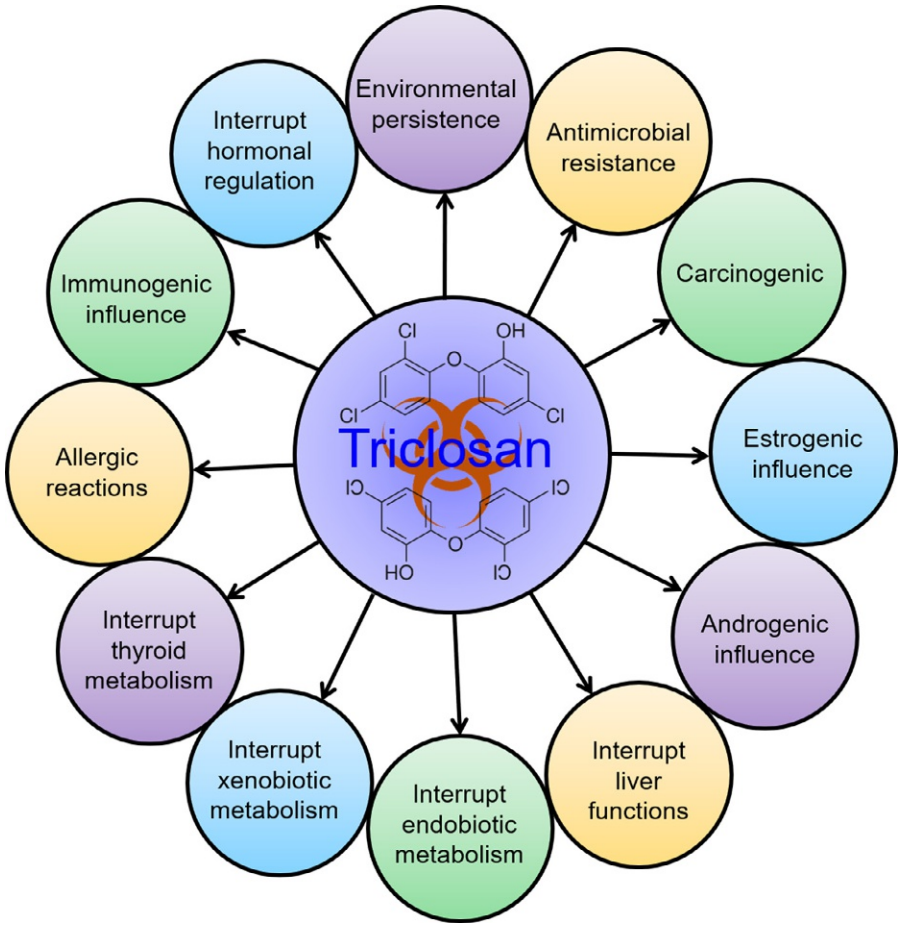

FIG. 19.2 Schematic illustration of notable ecological- and biological-related adverse impacts of TCS.

biochemical effects of its inhabitants. Further, triclosan has been proven to interact with various contaminants, resulting in complicated harmful effects, exacerbating the problem (Sanchís et al., 2016).

19.3.1 Genotoxicity

The genotoxic nature of triclosan can easily block the production of lipid in *Escherichia coli* by affecting the fabI of genes (McMurry et al., 1998). Recently, Stenzel and coworkers (Vickers, 2017) exposed the Zebrafish to triclosan at its environmental concentration and discovered that their reproductive and developmental abilities were compromised, as well as the pace of survival ability and development of their progeny. Similar effects were observed in amphibians (Usal et al., 2019). Studies also reveal that the exposure of triclosan to pregnant women may have effects on the behavioral attitudes of the male children (Jackson-Browne et al., 2019).

19.3.2 Reproductive, endocrine disruption, and developmental toxicity

Triclosan is regarded as one of the hazardous endocrine disrupters accompanied by developmental and reproductive toxicities. As a result of absorption of triclosan by the water fleas severely effects their reproductive and adaptive behavior (Chiaia-Hernandez et al., 2013). In another study, the estrogen sulphonation level in ewe placenta was reduced to a level of 0.1 mg/kg per day on exposure to the triclosan (Jackson et al., 2018). Further studies reveal that triclosan adversely affects the human reproductive systems (Jurewicz et al., 2019). In an approach, Ashrap and coworkers investigated that the phase I transformation of triclosan has lethal effects on estrogen disruption as compared to the pristine triclosan (Ashrap et al., 2017). The group further investigated that the structure of triclosan is similar to the thyroidal hormone which may be assumed that the triclosan can act as thyroid interferon. Further, triclosan content in human urine was reported to be adversely linked with serum thyroid function indicators by Skarha and coworkers (Skarha et al., 2019), indicating that triclosan may impair thyroid homeostasis and autoimmune. Additionally, triclosan can impact the growth of plants, particularly crops, in addition to disrupting development and animal reproductive systems. Chlamydomonas and *Asterococcus superbus* reinhardtii exhibited complete cell breakdown after exposure to 1000 μg/L of triclosan for 29 days (Xin et al., 2019). According to Sun and coworkers (Ishii et al., 2007) triclosan might induce the generation of H_2O_2 in wheat root cells, resulting in auxin peroxide and inhibiting root growth.

19.3.3 Neurotoxicity

Triclosan can be destructive to the nervous system either functionally or structurally. A very short exposure of triclosan (75 μg/L) for even 1 day can have a significant effect on the swimming behavior of *Pimephales promelas* (Fritsch et al., 2013). In another investigation, the delayed development of the trunk in Zebrafish was reported by Ma and coworkers upon exposure to triclosan. This may result because of the change in signaling channels of Ca^{2+} functioning (Ma et al., 2019). Recent reports recommend that both mammals and fish may show noteworthy behavioral syndromes after exposure to triclosan (Khan et al., 2019).

19.3.4 Carcinogenicity and immunotoxicity

Triclosan is also a probable carcinogen and can produce severe oxidative stress reactions (Gou et al., 2014). In an in vitro study of prostate cancerous cells, Kim and coworkers reveal that triclosan can enhance the metastasis as well as the proliferation of cells (Kim et al., 2015). The production of reactive oxygen species (ROS) was investigated by Zhang and coworkers. The group found increased production of ROS upon the interference of triclosan with both amino acid and purine metabolisms (Zhang et al., 2019). These findings proved that the oxidative stress prompted by triclosan is among the important bases of hepatocellular disease.

19.3.5 Combined toxicity

Recently, it has been documented that the interaction of major pollutants with triclosan can be harmful. The adsorptive capacity of micro-plastics toward triclosan is fairly high, therefore

their combined exposure enhances the bio-toxicity of triclosan (Zhu et al., 2019). The alga *Eremosphaera viridis* present in freshwater can have increased oxidative stress toxicity toward triclosan in the presence of Titanium dioxide (TiO_2) having a particle size in the range of 25 nm (Xin et al., 2019). Similarly, Oliver and coworkers demonstrated the hazardous effects of triclosan in liposomes in the presence of other personal care and pharmaceutical products (Oliver et al., 2020).

19.3.6 Inducing microbial resistance

Triclosan can produce a variety of pressure in bacteria for antibiotic confrontation which decreases the efficiency of bactericides (Westfall et al., 2019). The abundance of resistant strains in environmental matrices and the somewhat triclosan content were discovered to have a strong positive association by Hartmann and coworkers (Heuer et al., 2019). Triclosan exposure can alter the microbial community structure in sludge and sediments, lowering diversity and promoting antibiotic resistance (Drury et al., 2013). Triclosan also encourages the transfer of antibiotic resistance genes not just between bacteria, but also their surroundings (Thomas et al., 2012).

19.3.7 Toxic effect of transformed products

A variety of chlorine derivatives are produced by triclosan in the presence of free chlorine by undergoing electrophilic substitution reactions (Fiss et al., 2007). These pathways are considered to be the major contributor of dioxin in the environment (Buth et al., 2010). While methyl triclosan (major metabolite) is considered to be more stable compared to triclosan having biological toxicity. This toxicity can easily be detected in fish tissues residing in polluted water (Fu et al., 2020).

19.3.8 Ecosystem impact

The function and structure of the soil biomes of sandy soils by the presence of triclosan, this investigation was carried out by Waller and coworkers (Balmer et al., 2004). This results in the disruption of the soil nitrogen cycle. In freshwater microcosm research, 1 ng/L TCS exposure for 7 days was capable of lowering the richness and evenness of the microbial community, suggesting that TCS may have a deleterious impact on aquatic environments (Clarke et al., 2019).

19.4 Treatment technologies for removing TCS

The potential dangers of triclosan to human health and aquatic ecosystems necessitate its removal from wastewater treatment plant's effluents on emergency basis. A number of removal strategies are being adopted for the removal of triclosan from wastewater. These methodologies may include oxidation (e.g., electrochemical oxidation ozonation, chlorination, Fenton and photo-Fenton, and photocatalysis/photolysis), adsorption, reduction-oxidation,

combined processes, and biodegradation, etc. The selection criterion of the treatment technique depends on chemical properties and industrial source of the wastewater. Herein, we will discuss the adsorptive approach for the removal of triclosan from the wastewater.

19.5 Removal of TCS by adsorption techniques

Adsorption approaches are commonly used alternatives for the removal of polluting agents from wastewater (Sun et al., 2019; Zhou et al., 2017). Adsorption of triclosan by a variety of adsorbents, including TCS-CTS-Fe0-MIPs, activated carbon, carbon nanotubes, diatomite, magnetic activated carbon, and MOFs have been extensively explored.

19.5.1 Activated carbon

A well-established porous structure, larger surface area, and different functionalities present at the surface of carbon activated make it an ideal nanomaterial for the remediation of different types of small organic molecules (pollutants) from wastewater (Frascari et al., 2016; Hu et al., 2017). The presence of hydroxyl group in the structure of triclosan makes it hydrophilic in nature. Various factor such as nature of adsorbent and adsorbate as well as conditions of solution dictates the adsorption capacity (in solution form) of the compounds belonging to the phenolic family. While for the hydrophilic compounds the surface functionality plays an important role as compared to the porosity of the material. In a number of documented reports, it has been presented that the functionalities, such as pyrrole and pyridine play a significant part in the removal of phenolic pollutants and increases the adsorption capacity of the activated carbon (Chen et al., 2015). On the surface of activated carbon, these fundamental functional groups can be achieved by decreasing oxygen functional groups or increasing nitrogen functional groups (Frascari et al., 2016). In an approach, Fang et al. (2010) calculated the removal efficiency of triclosan with the help of activated carbon. The group found that the activated carbon can remove the triclosan up to 75% from the wastewater (Fang et al., 2010). Similarly, Behera et al. (2010) investigate the influence of pH on the removal efficiency of activated carbon. The group found that the adsorption ability increased with increasing ionic strength and increasing pH first increases the adsorption capacity and then decreases. Also, the increasing concentration of humic acid results in decreased adsorption efficiency. A 48.5 mg of triclosan per gram of carbon was the maximum adsorption capacity of the material. According to these investigations, an adsorption is a promising approach for removing triclosan from wastewater (Behera et al., 2010).

19.5.2 Magnetic activated carbon

The hydrochar made from rice straw is a carbon material having a lot of functional groups involving oxygen on its surface, but its low porosity and surface area might restrict its use in environmental decontamination (Falco et al., 2013; Liu et al., 2014). The activation of this hydrochar can be carried out by using K_2CO_3 and this material is regarded as activated carbon. This activated carbon can be converted into magnetic carbon material by hydrothermal

co-precipitation reaction (Falco et al., 2013; Liu et al., 2014). This chemical activation and magnetization results in increased porosity and adsorption capability of the hydrochar (Liu et al., 2014). This magnetically activated hydrochar has a fast adsorption rate, high surface area, and adsorption capacity of (5×10^{-4} g/(mg min)), 674 m^2/g (120.0–217.1 mg/g), respectively in the removal of triclosan from wastewater. Further, the magnetic hydrochar can easily be recovered from the wastewater by the application of external magnetic field.

19.5.3 Chitosan/carbon nanotubes based adsorbents

Based on the unique electrical, chemical, and mechanical properties, carbon nanotubes (CNTs) are an emerging class of nanomaterials that are widely employed as catalyst and electrode materials in a number of applications (Guo et al., 2019; Hu et al., 2017; Li et al., 2019). Furthermore, due to the wide range of delocalized π-electrons and length scale on hexagonal arrays/of carbon atoms in the graphene sheets, CNTs are regarded as the prodigious adsorbent candidates. Due to Van der Waals interactions, CNTs can accumulate into bunches in water, forming vast groove regions and exterior surfaces that can be used for adsorption (Hu et al., 2017). The presence of various functionalities such as —OH, —COOH, and —C═O groups impart significant degradation efficiency and mechanism to the CNTs. The documented reports reveal that the CNTs are more efficient materials for the adsorptive removal of contaminants. The higher adsorptive character is imparted by the efficient regeneration, short equilibrium time, and high adsorptive capacity (Hu et al., 2017). Regardless of the fact that CNTs are costlier than activated carbons, they have a longer lifespan in water treatment systems due to their better regeneration capability and adsorption efficiency. Greater adsorption efficiency of CNTs has already been reported in a number of reports (Guo et al., 2019; Hu et al., 2017; Li et al., 2019). According to Guo et al. (2019), novel chitosan/MWCNTs have a phenol adsorption capacity of 86.96 mg/g, which is higher than chitosan (61.70 mg/g) (Fig. 19.3). Multi-walled carbon nanotubes (MWCNTs) can be used to remove triclosan from water because they have a greater tendency to adsorb different contaminants (Guo et al., 2019).

Zhou and coworkers demonstrated the pH-based removal of triclosan using MWCNTs. The group examined that the acidic conditions enhance the adsorption of triclosan by using MWCNTs. This enhanced removal of triclosan is supported by the deprotonated molecules. On the other hand, at higher pH values the adsorption efficiency has a negative impact on the process. An increase in adsorption was calculated as the ionic strength increases 1×10^{-3} to 1×10^{-2} mol/L. While further increase results in the decrease of adsorption capacity of MWCNTs. More research is needed to improve the ability of MWCNTs to regenerate and lower their operational costs on pilot and column scales (Guo et al., 2019; Zhou et al., 2013). A combined experimental study and density functional theory were used to analyze the interactions of triclosan on (5,5) and (8,0) single-wall carbon nanotubes (SWCNTs). The results showed that triclosan adsorption changed the electronic characteristics of SWCNTs, with the changes being depending on the triclosan adsorption location (Castro et al., 2017). Because of their interactions with triclosan molecules, these SWCNTs could potentially be employed in water filter devices, allowing them to be removed from triclosan molecules after use (Castro et al., 2017).

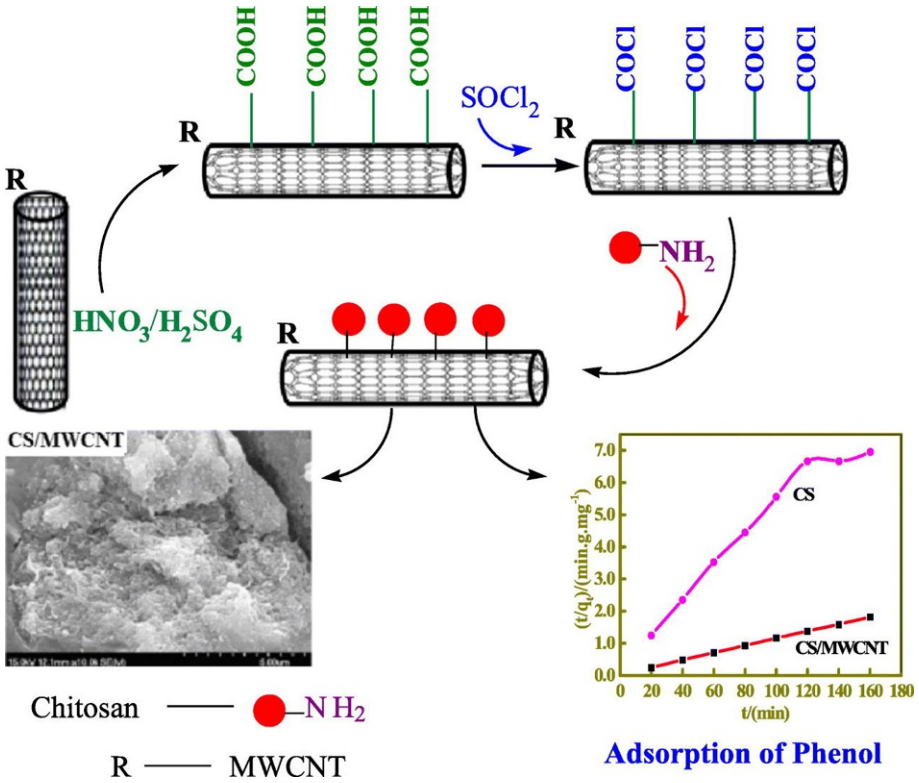

FIG. 19.3 Carbon nanotube-grafted chitosan and its phenol adsorptive ability in aqueous media (Guo et al., 2019).

19.5.4 Diatomite

Aluminosilicates, like kaolinite, bentonite, and diatomite, are an attractive class of absorbents to remediate wastewater. They possess low costs, folded structures, high dispersity, hydrophilicity, better ion exchange attributes, and broad sources of raw materials (Fei and Li, 2015; Sharipova et al., 2017). Diatomite (SiO_2nH_2O), one of the aluminosilicates, has a porous structure with 80%–90% voids and is a potential material for removing organic contaminants from water (Siddiqa et al., 2015; Tong et al., 2016). Sharipova et al. (2017) explored the triclosan adsorption by diatomite, using scanning electron microscopy to analyze the diatomite morphology and a mass balance to determine the triclosan amount adsorbed on the diatomite. Based on Sips and Langmuir models, the calculated Gibbs free energy (ΔG) values were −9.6 and −9.9 kJ/mol and adsorption capacity of 140 mg/g, respectively. The negative represented physical and spontaneous adsorption in nature (Sharipova et al., 2017).

19.5.5 TCS-CTS-Fe0-MIP

Recently, a molecularly imprinted magnetic material (TCS-CTS-Fe0-MIP) has been presented for the removal of triclosan. The magnetic molecularly imprinted material was

composed of iron (0) as magnetic material, chitosan as functional monomer, and crosslinking agent glutaraldehyde (Chen et al., 2017). Various researchers use this material for the detection and removal of triclosan in aqueous environments (Marques et al., 2017; Wan et al., 2019). The as-prepared material is environment friendlier having a large number of hydroxyl and amino groups as well as low cost and biodegradability. Further, the presence of Fe0 imparts a large surface area and high magnetic properties (Chen et al., 2017). In comparison to non-printed nanocomposite, the TCS-CTS-Fe0-MIP exhibits excellent adsorption of 20.9 mg/g for triclosan (Chen et al., 2017). The Scatchard and SEM investigation exposed high adsorption capacity and homogeneous disseminated adsorption sites in an extensive range of pH (6.0–9.0) (Chen et al., 2017). Furthermore, in complicated water samples, the TCS-CTS-Fe0-MIP exhibits a high enrichment factor and selectivity for triclosan. Overall, adsorption is a good way of removing triclosan from wastewater, especially if contains extensive organic matter and a lot of triclosan. Triclosan, on the other hand, can only pass from the liquid to the solid phases via adsorption processes, which might result in the formation of a new solid residue and the concentration of triclosan. Triclosan adsorption using low-cost renewable sources and persistent systems warrants more study.

19.5.6 Combined processes for TCS removal

Combined methods are likely to be important in removing organic contaminants from wastewater because they can have overwhelmed the inherent limits of distinct treatment methods (Ji et al., 2016; Xin et al., 2016). Triclosan remediation from wastewater has shown promise using a combination of enzyme and adsorption technologies (Liu et al., 2014; Xu et al., 2014). Triclosan removal effectiveness was improved by integrating the biocatalytic efficiency of laccase with the elevated adsorptive capacity of mesoporous materials, according to Xu et al. (2014). Laccase immobilization onto a nano-fibrous vinyl-modified poly(acrylic acid)/SiO_2 membrane was carried out by using a covalent crosslinking methodology (Ji et al., 2016; Xu et al., 2014). Immobilized laccase had superior storage stability and resistance to changes in temperature and pH than free laccase, resulting in a substantially higher triclosan removal efficiency (65% in 2 h) than free laccase (29% in 2 h) under ideal conditions (Xu et al., 2014). To maximize the stability and performance of the adsorption treatment methodology for triclosan on an industrial scale the investigations on the process integration must be carried out on an extensive level. As a result, integrated methods may take full benefit of individual treatment techniques and offer a lot of potential for eliminating refractory organics like triclosan from wastewater in the future.

19.5.7 Triclosan removal by MOFs

The mechanism involving adsorptive removals of organic compounds using MOFs follows electrostatic, acid-base, non-covalent, hydrogen bonding, and hydrophobic interactions (Hasan and Jhung, 2015). Rocío-Bautista et al. (2018) researched the functioning of five different MOFs, MIL-53(Al), UiO-64, HKUST-1, MOF-5(Zn), and MOF-74(Zn), for determining and decontaminating organic pollutants in environmental water (tap water and wastewater) via miniaturized dispersive mode solid-phase extraction (D-μSPE). In this study, the MOFs were

determined to have adequate analytical performance and detection limits of triclosan down to 0.040 μg L^{-1} by high-performance liquid chromatography with a diode-array detector (HPLC-DAD) which motivates the study of how MOFs interaction with water contaminates.

A second study of MOFs and triclosan interactions using UiO-66 (Universitetet i Oslo), which is made up of $[Zr_6O_4(OH)_4]$ clusters with 1,4-benzodicarboxylic acid struts, gives insight into why MOFs are such efficient adsorbers. Sarker et al. (2018) compared the effectiveness UiO-66(Zr), UiO-66-NH_2(Zr), and UiO-66-NH-CO-COOH(Zr), which is UiO-66 modified with NH (UiO-66-NH_2(Zr)) and COOH groups. As with triclosan adsorption, the modified MOFs had better adsorption than the unmodified versions. The performances of the TCS adsorbents were as follows: UiO-66-NH-CO-COOH(Zr) > UiO-66-NH_2(Zr) > UiO-66(Zr) > AC with UiO-66-NH-CO-COOH(Zr) adsorbing 2.4 times TCS than (qt) AC after 12 h (q12 h). Fascinatingly, the adsorption of TCS does not depend on the surface areas of the adsorbents. In general, the surface area is a significant parameter in adsorption assuming simple Van der Waals interactions. Therefore, there must be a special interaction between UiO-66-NH-CO-COOH and TCS because the modified MOF (showing the highest adsorption) had the lowest surface area and pore volume than earlier investigated adsorbents. In a recent study, Bariki et al. (2020) synthesized UiO-66/$CdIn_2S_4$ heterostructure nanocomposite for the decontamination study of water (Fig. 19.4). Hierarchical 3D structured $CdIn_2S_4$ was fabricated by a simple hydrothermal synthesis method, which was later used to incorporate UiO-66 nanoparticles. The representative pollutant-contaminant triclosan was degraded under visible light over UiO-66/$CdIn_2S_4$ photocatalyst. CIS is considered active materials for TCS degradation, but the overall efficiency reported is 15%, which is smaller due to the rapid coalesce of photogenerated electrons. A significant improvement in the degradation of TCS was observed when UiO-66 was incorporated into CIS. Significantly, efficiency was increased from 15% to 92%, which is ~6% higher. The plausible reason for high removal efficiency is UiO-66. The composite surface area was increased, and n-n heterojunction favored by UiO-66 MOF improves the separation and movement of photogenerated electrons. Reproducibility was confined by performing several runs, and a marginal decrease in degradation activity was noticed. Overall, it remains highly stable and active for the entire duration.

Qian et al. (2013)also added that MIL-53(Al) withstands high pH ranges (2 – 12) which promotes this MOF as a potential candidate for use in water decontamination. It is reported that meso-MIL-53(Al) was used as the support due to its chemical stability and favorable water. It

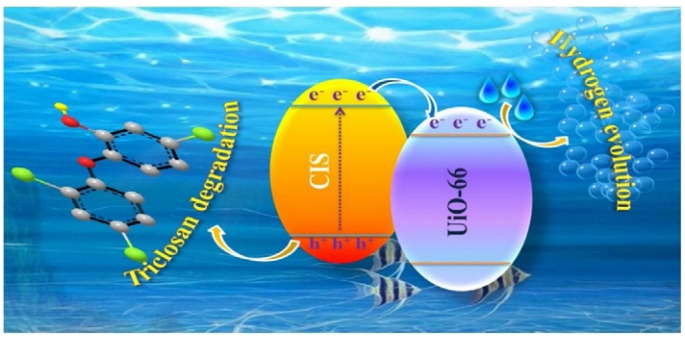

FIG. 19.4 Facile synthesis and photocatalytic efficacy of UiO-66/$CdIn_2S_4$ nanocomposites for triclosan removal and H_2 evolution (Bariki et al., 2020).

was functionalized with terephthalic acid (PTA) as an organic ligand to furnish plentiful carboxyl groups as the sites for binding and attaching laccase. The removal efficacies of triclosan were mediated by free as well as carrier supported laccase on meso-MIL-53(Al) (Lac-MIL-53 (Al)). Although the catalytic efficiency (V_{max}/K_m) moderately lessens from ~785 to 607 min^{-1} due to the mass transfer limitation resulting from immobilization. However, Lac-MIL-53(Al) showed higher stability and activity recovery (93.8%) (Jia et al., 2019). Immobilizing laccase on to MIL-53(AI) to Lac-MIL-53(Al) for degrading of TCS catalytically was a great step. FT-IR spectroscopy revealed that TCS adsorption on representative MOFs was mainly due to hydrogen bonding which assists hydrophobic interactions. Dou et al. (2017) also suggested the advantages of MIL-53(Al)s and proposed for water purification. Hydrophobicity assisted by hydrogen bonding has been considered as key factor for the extraction of triclosan from water. High concentration (up to 400 mg/g) of triclosan has been extracted by MIL-53(Al). MOF-driven carbons, with well-preserved pores, were also studied for removal of organic contaminates (Dou et al., 2017). An et al. (2018) described that mesoporous carbon derived from pyrolysis of MAF-6at 1000°C showed superior adsorptive efficacy for PPCS like ibuprofen (408 mg g^{-1}) and DCF (503 mg g^{-1}). Herein, the adsorption of ibuprofen resulted from the hydrophobic and Van der Waals interactions. Therefore, carbons derived by pyrolysis using MAF-6 template (particularly in the presence of a KOH activator) also emerge as a promising candidate for triclosan and other organic contaminants (An et al., 2018).

19.6 Conclusions and perspectives

Carbon-based nano-architectures are promising materials that exhibit extensive potential as novel adsorbents to remove triclosan from aqueous environments. In the recent decade, a large number of research articles have reported the carbon-based nano-architectures-assisted elimination of emerging contaminants that indicates an intensive researcher's interest in this arena. These nanoadsorbents have revealed invariably superior adsorptive performance for triclosan over the classic counterparts. A set of unique textural attributes such as tunable porosity, large surface area, and the ability to functionalization render nanomaterials as robust and high-quality adsorption candidates for triclosan than previous adsorbents. The mechanism for effective removals of triclosan involves electrostatic, acid-base, non-covalent, hydrogen bonding, and hydrophobic interactions.

Acknowledgment

Consejo Nacional de Ciencia y Tecnología (MX) is thankfully acknowledged for partially supporting this work under Sistema Nacional de Investigadores (SNI) program awarded to Hafiz M.N. Iqbal (CVU: 735340).

Conflict of interest

The authors declare that they have no conflict of interest.

References

Adolfsson-Erici, M., Pettersson, M., Parkkonen, J., Sturve, J., 2002. Triclosan, a commonly used bactericide found in human milk and in the aquatic environment in Sweden. Chemosphere 46 (9–10), 1485–1489.

An, H.J., Bhadra, B.N., Khan, N.A., Jhung, S.H., 2018. Adsorptive removal of wide range of pharmaceutical and personal care products from water by using metal azolate framework-6-derived porous carbon. Chem. Eng. J. 343, 447–454.

Arbuckle, T.E., Weiss, L., Fisher, M., Hauser, R., Dumas, P., Bérubé, R., Ayotte, P., 2015. Maternal and infant exposure to environmental phenols as measured in multiple biological matrices. Sci. Total Environ. 508, 575–584.

Ashrap, P., Zheng, G., Wan, Y., Li, T., Hu, W., Li, W., Hu, J., 2017. Discovery of a widespread metabolic pathway within and among phenolic xenobiotics. Proc. Natl. Acad. Sci. 114 (23), 6062–6067.

Balmer, M.E., Poiger, T., Droz, C., Romanin, K., Bergqvist, P.-A., Müller, M.D., Buser, H.-R., 2004. Occurrence of methyl triclosan, a transformation product of the bactericide triclosan, in fish from various lakes in Switzerland. Environ. Sci. Technol. 38 (2), 390–395.

Bariki, R., Majhi, D., Das, K., Behera, A., Mishra, B., 2020. Facile synthesis and photocatalytic efficacy of UiO-66/CdIn2S4 nanocomposites with flowerlike 3D-microspheres towards aqueous phase decontamination of triclosan and H2 evolution. Appl. Catal. Environ. 270, 118882.

Behera, S.K., Oh, S.-Y., Park, H.-S., 2010. Sorption of triclosan onto activated carbon, kaolinite and montmorillonite: effects of pH, ionic strength, and humic acid. J. Hazard. Mater. 179 (1–3), 684–691.

Bilal, M., Mehmood, S., Iqbal, H., 2020. The beast of beauty: environmental and health concerns of toxic components in cosmetics. Cosmetics 7 (1), 13.

Brausch, J.M., Rand, G.M., 2011. A review of personal care products in the aquatic environment: environmental concentrations and toxicity. Chemosphere 82 (11), 1518–1532.

Buth, J.M., Steen, P.O., Sueper, C., Blumentritt, D., Vikesland, P.J., Arnold, W.A., McNeill, K., 2010. Dioxin photoproducts of triclosan and its chlorinated derivatives in sediment cores. Environ. Sci. Technol. 44 (12), 4545–4551.

Carmona, E., Andreu, V., Picó, Y., 2014. Occurrence of acidic pharmaceuticals and personal care products in Turia River basin: from waste to drinking water. Sci. Total Environ. 484, 53–63.

Castro, S., Araújo, A., Nogueira, R., Guerini, S., 2017. Adsorption of triclosan on single wall carbon nanotubes: a first principle approach. Appl. Surf. Sci. 403, 519–524.

Chen, K., Lyu, H., Hao, S., Luo, G., Zhang, S., Chen, J., 2015. Separation of phenolic compounds with modified adsorption resin from aqueous phase products of hydrothermal liquefaction of rice straw. Bioresour. Technol. 182, 160–168.

Chen, Y., Lei, X., Dou, R., Chen, Y., Hu, Y., Zhang, Z., 2017. Selective removal and preconcentration of triclosan using a water-compatible imprinted nano-magnetic chitosan particles. Environ. Sci. Pollut. Res. 24 (22), 18640–18650.

Chiaia-Hernandez, A.C., Ashauer, R., Moest, M., Hollingshaus, T., Jeon, J., Spaak, P., Hollender, J., 2013. Bioconcentration of organic contaminants in Daphnia resting eggs. Environ. Sci. Technol. 47 (18), 10667–10675.

Clarke, A., Azulai, D., Dueker, M.E., Vos, M., Perron, G.G., 2019. Triclosan alters microbial communities in freshwater microcosms. Water 11 (5), 961.

Dhillon, G.S., Kaur, S., Pulicharla, R., Brar, S.K., Cledón, M., Verma, M., Surampalli, R.Y., 2015. Triclosan: current status, occurrence, environmental risks and bioaccumulation potential. Int. J. Environ. Res. Public Health 12 (5), 5657–5684.

Dou, R., Zhang, J., Chen, Y., Feng, S., 2017. High efficiency removal of triclosan by structure-directing agent modified mesoporous MIL-53 (Al). Environ. Sci. Pollut. Res. 24 (9), 8778–8789.

Drury, B., Scott, J., Rosi-Marshall, E.J., Kelly, J.J., 2013. Triclosan exposure increases triclosan resistance and influences taxonomic composition of benthic bacterial communities. Environ. Sci. Technol. 47 (15), 8923–8930.

Falco, C., Marco-Lozar, J.P., Salinas-Torres, D., Morallon, E., Cazorla-Amorós, D., Titirici, M.-M., Lozano-Castello, D., 2013. Tailoring the porosity of chemically activated hydrothermal carbons: influence of the precursor and hydrothermal carbonization temperature. Carbon 62, 346–355.

Fang, J.-L., Stingley, R.L., Beland, F.A., Harrouk, W., Lumpkins, D.L., Howard, P., 2010. Occurrence, efficacy, metabolism, and toxicity of triclosan. J. Environ. Sci. Health C 28 (3), 147–171.

Fei, J., Li, J., 2015. Controlled preparation of porous TiO2–ag nanostructures through supramolecular assembly for plasmon-enhanced photocatalysis. Adv. Mater. 27 (2), 314–319.

Fiss, E.M., Rule, K.L., Vikesland, P.J., 2007. Formation of chloroform and other chlorinated byproducts by chlorination of triclosan-containing antibacterial products. Environ. Sci. Technol. 41 (7), 2387–2394.

Frascari, D., Bacca, A.E.M., Zama, F., Bertin, L., Fava, F., Pinelli, D., 2016. Olive mill wastewater valorisation through phenolic compounds adsorption in a continuous flow column. Chem. Eng. J. 283, 293–303.
Fritsch, E.B., Connon, R.E., Werner, I., Davies, R.E., Beggel, S., Feng, W., Pessah, I.N., 2013. Triclosan impairs swimming behavior and alters expression of excitation-contraction coupling proteins in fathead minnow (Pimephales promelas). Environ. Sci. Technol. 47 (4), 2008–2017.
Fu, J., Tan, Y.X.R., Gong, Z., Bae, S., 2020. The toxic effect of triclosan and methyl-triclosan on biological pathways revealed by metabolomics and gene expression in zebrafish embryos. Ecotoxicol. Environ. Saf. 189, 110039.
Gou, N., Yuan, S., Lan, J., Gao, C., Alshawabkeh, A.N., Gu, A.Z., 2014. A quantitative toxicogenomics assay reveals the evolution and nature of toxicity during the transformation of environmental pollutants. Environ. Sci. Technol. 48 (15), 8855–8863.
Guo, M., Wang, J., Wang, C., Strong, P., Jiang, P., Ok, Y.S., Wang, H., 2019. Carbon nanotube-grafted chitosan and its adsorption capacity for phenol in aqueous solution. Sci. Total Environ. 682, 340–347.
Hasan, Z., Jhung, S.H., 2015. Removal of hazardous organics from water using metal-organic frameworks (MOFs): plausible mechanisms for selective adsorptions. J. Hazard. Mater. 283, 329–339.
Heuer, R.M., Galli, G.L., Shiels, H.A., Fieber, L.A., Cox, G.K., Mager, E.M., Crossley II, D.A., 2019. Impacts of Deepwater horizon crude oil on mahi-mahi (Coryphaena hippurus) heart cell function. Environ. Sci. Technol. 53 (16), 9895–9904.
Hu, X., Cheng, Z., Sun, Z., Zhu, H., 2017. Adsorption of diclofenac and Triclosan in aqueous solution by purified multi-walled carbon nanotubes. Pol. J. Environ. Stud. 26 (1).
Ishii, S., Bell, J., Marshall, F., 2007. Phytotoxic risk assessment of ambient air pollution on agricultural crops in Selangor state, Malaysia. Environ. Pollut. 150 (2), 267–279.
Jackson, E.N., Rowland-Faux, L., James, M.O., Wood, C.E., 2018. Administration of low dose triclosan to pregnant ewes results in placental uptake and reduced estradiol sulfotransferase activity in fetal liver and placenta. Toxicol. Lett. 294, 116–121.
Jackson-Browne, M.S., Papandonatos, G.D., Chen, A., Yolton, K., Lanphear, B.P., Braun, J.M., 2019. Early-life triclosan exposure and parent-reported behavior problems in 8-year-old children. Environ. Int. 128, 446–456.
Ji, C., Hou, J., Wang, K., Zhang, Y., Chen, V., 2016. Biocatalytic degradation of carbamazepine with immobilized laccase-mediator membrane hybrid reactor. J. Membr. Sci. 502, 11–20.
Jia, Y., Chen, Y., Luo, J., Hu, Y., 2019. Immobilization of laccase onto meso-MIL-53 (Al) via physical adsorption for the catalytic conversion of triclosan. Ecotoxicol. Environ. Saf. 184, 109670.
Jurewicz, J., Wielgomas, B., Radwan, M., Karwacka, A., Klimowska, A., Dziewirska, E., Hanke, W., 2019. Triclosan exposure and ovarian reserve. Reprod. Toxicol. 89, 168–172.
Kasprzyk-Hordern, B., Dinsdale, R.M., Guwy, A.J., 2008. The occurrence of pharmaceuticals, personal care products, endocrine disruptors and illicit drugs in surface water in South Wales, UK. Water Res. 42 (13), 3498–3518.
Khan, H., Zafar, M., Patel, S., Shah, S.M., Bishayee, A., 2019. Pharmacophore studies of 1, 3, 4-oxadiazole nucleus: Lead compounds as α-glucosidase inhibitors. Food Chem. Toxicol. 130, 207–218.
Kim, S.-H., Hwang, K.-A., Shim, S.-M., Choi, K.-C., 2015. Growth and migration of LNCaP prostate cancer cells are promoted by triclosan and benzophenone-1 via an androgen receptor signaling pathway. Environ. Toxicol. Pharmacol. 39 (2), 568–576.
Kralj, M.B., Fortuna, A., Abram, A., Trebše, P., 2020. Dish handwashing: an overlooked source of contamination. Environ. Chem. Lett. 18 (1), 181–185.
Kumar, V., Chakraborty, A., Kural, M.R., Roy, P., 2009. Alteration of testicular steroidogenesis and histopathology of reproductive system in male rats treated with triclosan. Reprod. Toxicol. 27 (2), 177–185.
Li, H., Wei, C., Zhang, D., Pan, B., 2019. Adsorption of bisphenol a on dispersed carbon nanotubes: role of different dispersing agents. Sci. Total Environ. 655, 807–813.
Liu, Y., Zhu, X., Qian, F., Zhang, S., Chen, J., 2014. Magnetic activated carbon prepared from rice straw-derived hydrochar for triclosan removal. RSC Adv. 4 (109), 63620–63626.
Ma, Z., Liu, H., Yu, H., 2019. Triclosan affects Ca2+ regulatory module and musculature development in skeletal myocyte during early life stages of zebrafish (Danio rerio). Environ. Sci. Technol. 53 (20), 11988–11998.
Marques, I., Magalhães-Mota, G., Pires, F., Sério, S., Ribeiro, P.A., Raposo, M., 2017. Detection of traces of triclosan in water. Appl. Surf. Sci. 421, 142–147.
McMurry, L.M., Oethinger, M., Levy, S.B., 1998. Triclosan targets lipid synthesis. Nature 394 (6693), 531–532.
Miller, W.R., 1983. Motivational interviewing with problem drinkers. Behav. Cogn. Psychother. 11 (2), 147–172.

Morsi, R., Bilal, M., Iqbal, H.M., Ashraf, S.S., 2020. Laccases and peroxidases: the smart, greener and futuristic biocatalytic tools to mitigate recalcitrant emerging pollutants. Sci. Total Environ. 714, 136572.
Olaniyan, L., Mkwetshana, N., Okoh, A., 2016. Triclosan in water, implications for human and environmental health. Springerplus 5 (1), 1–17.
Oliver, M., Kudłak, B., Wieczerzak, M., Reis, S., Lima, S.A., Segundo, M.A., Miró, M., 2020. Ecotoxicological equilibria of triclosan in Microtox, XenoScreen YES/YAS, Caco2, HEPG2 and liposomal systems are affected by the occurrence of other pharmaceutical and personal care emerging contaminants. Sci. Total Environ. 719, 137358.
Pycke, B.F., Roll, I.B., Brownawell, B.J., Kinney, C.A., Furlong, E.T., Kolpin, D.W., Halden, R.U., 2014. Transformation products and human metabolites of triclocarban and triclosan in sewage sludge across the United States. Environ. Sci. Technol. 48 (14), 7881–7890.
Qian, X., Yadian, B., Wu, R., Long, Y., Zhou, K., Zhu, B., Huang, Y., 2013. Structure stability of metal-organic framework MIL-53 (Al) in aqueous solutions. Int. J. Hydrogen Energy 38 (36), 16710–16715.
Rasheed, T., Bilal, M., Hassan, A.A., Nabeel, F., Bharagava, R.N., Ferreira, L.F.R., Iqbal, H.M., 2020. Environmental threatening concern and efficient removal of pharmaceutically active compounds using metal-organic frameworks as adsorbents. Environ. Res. 185, 109436.
Rocío-Bautista, P., Pino, V., Pasán, J., López-Hernández, I., Ayala, J.H., Ruiz-Pérez, C., Afonso, A.M., 2018. Insights in the analytical performance of neat metal-organic frameworks in the determination of pollutants of different nature from waters using dispersive miniaturized solid-phase extraction and liquid chromatography. Talanta 179, 775–783.
Sanchís, J., Olmos, M., Vincent, P., Farre, M., Barceló, D., 2016. New insights on the influence of organic co-contaminants on the aquatic toxicology of carbon nanomaterials. Environ. Sci. Technol. 50 (2), 961–969.
Sarker, M., Song, J.Y., Jhung, S.H., 2018. Carboxylic-acid-functionalized UiO-66-NH2: a promising adsorbent for both aqueous-and non-aqueous-phase adsorptions. Chem. Eng. J. 331, 124–131.
Sharipova, A.A., Aidarova, S.B., Bekturganova, N.Y., Tleuova, A., Kerimkulova, M., Yessimova, O., Miller, R., 2017. Triclosan adsorption from model system by mineral sorbent diatomite. Colloids Surf. A Physicochem. Eng. Asp. 532, 97–101.
Siddiqa, A., Shahid, A., Gill, R., 2015. Silica decorated CNTs sponge for selective removal of toxic contaminants and oil spills from water. J. Environ. Chem. Eng. 3 (2), 892–897.
Skarha, J., Mínguez-Alarcón, L., Williams, P.L., Korevaar, T.I., de Poortere, R.A., Broeren, M.A., Braun, J.M., 2019. Cross-sectional associations between urinary triclosan and serum thyroid function biomarker concentrations in women. Environ. Int. 122, 256–262.
Sun, Y., Iris, K., Tsang, D.C., Cao, X., Lin, D., Wang, L., Ok, Y.S., 2019. Multifunctional iron-biochar composites for the removal of potentially toxic elements, inherent cations, and hetero-chloride from hydraulic fracturing wastewater. Environ. Int. 124, 521–532.
Thomas, K.V., Bijlsma, L., Castiglioni, S., Covaci, A., Emke, E., Grabic, R., Lindberg, R.H., 2012. Comparing illicit drug use in 19 European cities through sewage analysis. Sci. Total Environ. 432, 432–439.
Tong, Y., Mayer, B.K., McNamara, P.J., 2016. Triclosan adsorption using wastewater biosolids-derived biochar. Environ. Sci.: Water Res. Technol. 2 (4), 761–768.
Unit, D.R., Robertshaw, H., 2007. Contact dermatitis to triclosan in toothpaste. Contact Dermatitis 57 (6), 383–384.
Usal, M., Regnault, C., Veyrenc, S., Couturier, K., Batandier, C., Bulteau, A.-L., Raveton, M., 2019. Concomitant exposure to benzo [a] pyrene and triclosan at environmentally relevant concentrations induces metabolic syndrome with multigenerational consequences in Silurana (Xenopus) tropicalis. Sci. Total Environ. 689, 149–159.
Vickers, N.J., 2017. Animal communication: when i'm calling you, will you answer too? Curr. Biol. 27 (14), R713–R715.
Wan, Z., Cho, D.-W., Tsang, D.C., Li, M., Sun, T., Verpoort, F., 2019. Concurrent adsorption and micro-electrolysis of Cr (VI) by nanoscale zerovalent iron/biochar/ca-alginate composite. Environ. Pollut. 247, 410–420.
Westfall, C., Flores-Mireles, A.L., Robinson, J.I., Lynch, A.J., Hultgren, S., Henderson, J.P., Levin, P.A., 2019. The widely used antimicrobial triclosan induces high levels of antibiotic tolerance in vitro and reduces antibiotic efficacy up to 100-fold in vivo. Antimicrob. Agents Chemother. 63 (5), e02312–e02318.
Xin, L., Sun, Y., Feng, J., Wang, J., He, D., 2016. Degradation of triclosan in aqueous solution by dielectric barrier discharge plasma combined with activated carbon fibers. Chemosphere 144, 855–863.
Xin, X., Huang, G., An, C., Feng, R., 2019. Interactive toxicity of triclosan and nano-TiO2 to green alga Eremosphaera viridis in Lake Erie: a new perspective based on Fourier transform infrared spectromicroscopy and synchrotron-based X-ray fluorescence imaging. Environ. Sci. Technol. 53 (16), 9884–9894.

Xu, R., Si, Y., Wu, X., Li, F., Zhang, B., 2014. Triclosan removal by laccase immobilized on mesoporous nanofibers: strong adsorption and efficient degradation. Chem. Eng. J. 255, 63–70.
Yueh, M.-F., Tukey, R.H., 2016. Triclosan: a widespread environmental toxicant with many biological effects. Annu. Rev. Pharmacol. Toxicol. 56, 251–272.
Yueh, M.-F., Taniguchi, K., Chen, S., Evans, R.M., Hammock, B.D., Karin, M., Tukey, R.H., 2014. The commonly used antimicrobial additive triclosan is a liver tumor promoter. Proc. Natl. Acad. Sci. 111 (48), 17200–17205.
Zhang, H., Shao, X., Zhao, H., Li, X., Wei, J., Yang, C., Cai, Z., 2019. Integration of metabolomics and lipidomics reveals metabolic mechanisms of triclosan-induced toxicity in human hepatocytes. Environ. Sci. Technol. 53 (9), 5406–5415.
Zhou, S., Shao, Y., Gao, N., Deng, J., Tan, C., 2013. Equilibrium, kinetic, and thermodynamic studies on the adsorption of Triclosan onto multi-walled carbon nanotubes. CLEAN–Soil, Air, Water 41 (6), 539–547.
Zhou, Y., Liu, X., Xiang, Y., Wang, P., Zhang, J., Zhang, F., Tang, L., 2017. Modification of biochar derived from sawdust and its application in removal of tetracycline and copper from aqueous solution: adsorption mechanism and modelling. Bioresour. Technol. 245, 266–273.
Zhu, Z.-L., Wang, S.-C., Zhao, F.-F., Wang, S.-G., Liu, F.-F., Liu, G.-Z., 2019. Joint toxicity of microplastics with triclosan to marine microalgae Skeletonema costatum. Environ. Pollut. 246, 509–517.

PART IV

Multifarious biopolymers as nanobiosorbents for decontamination of environmental matrices

This page intentionally left blank

CHAPTER

20

Sorbent based on citrus peel waste for wastewater treatment

Vesna Krstić[a,b], *Tamara Urošević*[a], *Marina Uđilanović*[c], *Andrija Ćirić*[c], *and Snežana Milić*[b]

[a]Mining and Metallurgy Institute Bor, Bor, Serbia [b]University of Belgrade, Technical Faculty Bor, Bor, Serbia [c]Faculty of Science, Chemistry Department, University of Kragujevac, Kragujevac, Serbia

20.1 Introduction

The principal challenges to sustainable development are environmental protection, effective wastewater treatment, energy conservation, and socioeconomic aspects (Lončar et al., 2019; Foo and Hameed, 2012; Cazetta et al., 2011). Meeting the needs of the human population with currently available resources poses a threat to the future. It is known that mining is one of the biggest polluters, and environmental protection is fundamental to development, the economy, and modern society (Lončar et al., 2019). Negative impacts on the environment have been shown in numerous papers, of which we highlight several interesting publications by Dimitrijević et al. (2014, 2016a, 2016b). Therefore it is necessary to develop new, nontoxic, and inexpensive functional materials and methods (Đorđievski et al., 2017; Pešić et al.,2020a; Mihailović et al., 2018; Sovrlić et al., 2020). These methods can be used for various purposes and to meet the growing demands of the human population and environmental protection (Pešić et al., 2020b). Today important work is being done on the development of new methods of bio-sorbent modification and the importance of biosorption. The use of biomaterials as sustainable alternatives against environmental pollution has increased. Citrus fruit biowaste from the food industry, in the form of orange, lemon, mandarin, and grapefruit peels, can be utilized as biosorbents for water purification. Due to its specific properties, carbon has found applications in wastewater treatment and energy conservation.

https://doi.org/10.1016/B978-0-323-90912-9.00020-4

Carbon obtained from biomass and other materials can be used as a raw material for the production of active carbon and carbon nanostructures. Activated carbon is used for various nanocomposites and applications in water treatment (Acharya and Pal, 2020; Danish and Ahmad, 2018; Wong et al., 2018). However, conventional methods for obtaining carbon nanostructures are expensive and energy demanding. Therefore it is desirable to develop new low-energy and inexpensive carbon nanostructures with appropriate properties.

Due to their unique properties, carbon nanocomposites are used in energy devices and wastewater treatment processes. Currently, numerous studies are geared toward the development of new carbon nanostructured materials with well-controlled surface and morphological properties, to achieve the desired level of practical efficiency (Gehrke et al., 2015; Acharya and Pal, 2020).Trumić et al. (2012, 2013, 2015, 2016, 2017) investigated the mechanical properties of precious metal alloys at high temperatures that could be successfully applied in environmental protection in extreme conditions. Also, the test results could be compared with the results of the synthesis and application of AC at high temperatures in extreme conditions.

A large amount of waste and by-products come from the food industry. Citrus peel is an agro-industrial waste generated from fruit processing in the juice industry. Robles Gutierrez et al. (2018) emphasized that large amounts of citrus waste pose risks to the environment and instead could be used or transformed into carbon materials that could be used in water treatment. Citrus waste is an organic substance consisting of several forms of cellulose, lignin, and pectin. These molecules are rich in carbon that can be successfully converted to activated carbon (AC) (Wan et al., 2020; Arun et al., 2021). Liu et al. (2017) showed heteroatom-doped porous carbon derived from hydrothermally treated sewage sludge and this material showed good adsorption capacity to remove azo dye. Thus, hydrocarbon became an excellent precursor for the activation of porous carbon with a developed pore structure and adsorption characteristics of 440.53 mg/g. Sevilla et al. (2011) obtained a high specific surface area of over 2000 m^2/g. They used superactive carbons from hydrothermally carbonized eucalyptus. Also, they used activated carbon for high-density hydrogen storage.

Since waste from agro-industrial production based on citrus peel has proven to be a suitable raw material for the production of AC, this chapter will consider the physicochemical characteristics of these materials and their application in water treatment. Activated carbon obtained from citrus fruit waste has a large specific surface area and a large sorption capacity compared to other adsorbents used in the water purification process. AC from citrus fruit waste is a good and sustainable alternative and a good alternative to obtaining AC from lignite materials derived from nonrenewable energy sources.

20.2 Characteristics of citrus peel waste

Citrus fruit waste, mainly produced by the juice industry, based on orange, mandarin, grapefruit, lemon, and pomelo fruit peels, can lead to environmental problems due to the large production and physicochemical characteristics of the waste. It is a pollutant of soil, air, and water (Robles Gutierrez et al., 2018). Waste material in the citrus fruit industry consists of bark, seeds, and capillary membranes, which have a high level of organic matter and a low pH value. Such

TABLE 20.1 Composition of dried orange peel (w/w dry basis).

	Compounds	Value (%)	Method
1	Liposoluble fraction (crude fats, essential oils, resins, coloring matters)	4.22	Hexane–trichloromethane azeotrope
2	Alcohol soluble fraction (sugars, pectin, flavonoids)	49.1	Water-ethyl alcohol-toluene azeotr.
3	Alcohol insoluble fraction (holocellulose, lignin, insoluble pectin, protein, ash)	46.7	By difference
4	Holocellulose	21.7 (46.47)	Sodium chlorite
5	Cellulose[a]	12.9 (27.62)	Kurschner
6	Hemicellulose[a]	8.8 (18.85)	By difference
7	Lignin	1.3	72% sulfuric acid
8	Protein	6.1	From nitrogen content
9	Ash	2.9	ASTM D1102-84 (2021)
10	Other compounds (insoluble pectin)	14.7	

[a] *Holocellulose, cellulose, and hemicellulose content values determined by reference to the weight of double extracted OP are enclosed within parentheses.*

Reprinted with permission of Elsevier, Bicu, I., Mustata, F., 2013. Optimization of isolation of cellulose from orange peel using sodium hydroxide and chelating agents. Carbohydr. Polym. 98, 341–348 https://doi.org/10.1016/j.carbpol.2013.06.009.

physicochemical properties indicate citrus waste is a potential environmental pollutant. Researchers have seen a solution to this problem in the valorization of citrus waste and its transformation into profitable components, from which sorbent materials can be prepared to purify water from pollutants (Pavithra et al., 2021; Krstić et al., 2018; Urošević et al., 2016). Research has shown that the composition of orange peel is a potential resource that can be used as an added value in the production of animal feed, biomethanization, and heat sources (Tsouko et al., 2020; Miran et al., 2016). In this way, it is possible to reduce the harmful impact on the environment.

The chemical composition, taking the example of orange peel, Table 20.1, makes citrus waste a suitable ecological biomaterial, usable in various ecological and industrial processes (Bicu and Mustata, 2013; Romero-Canoa et al., 2019). The peel of citrus fruits contains soluble sugars that consist mainly of fructose, glucose, and sucrose. Organic acids present in the citrus peel include citric, oxalic, and succinic acids. Pectin is found in the fibers of oranges that are part of the shell. Pectins can be soluble and insoluble in the form of protopectin (Robles Gutierrez et al., 2018).

20.2.1 Sorption properties of citrus fruit waste

The amount of carbon in the peel of citrus fruits is one of the indicators that this waste material has the potential to be used as a source for AC. Miran et al. (2016) presented in Table 20.2 the physicochemical characteristics of orange peel waste. The authors obtained results for elementary analysis (also called CHNS analysis) of cellulose and pectin, and a protein sample of

TABLE 20.2 Characteristics of orange peel powder waste.

Parameter	Value (%)
Moisture	7.7 ± 0.20
Ash	4.4 ± 0.50
C	40.3 ± 0.02
H	5.8 ± 0.08
N	1.1 ± 0.20
S	0.1 ± 0.03
Protein	6.73 ± 1.26
Pectin	25.4
Cellulose	17.5
Hemicellulose	8.6

Reprinted with permission of Elsevier, from Miran, W., Nawaz, M., Jang, J., Lee, D.S., 2016. Conversion of orange peel. Waste biomass to bioelectricity using a mediator-less microbial fuel cell. Sci. Total Environ. 547, 197–205. https://doi.org/10.1016/j.scitotenv.2016.01.004.

orange peel was first dried 24 h at 50°C, crushed and homogenized. Moisture and ash were determined within the technical analysis, which gives us a complete picture of the dry matter characteristics of the analyzed sample. The results in Table 20.2 from Miran et al. (2016) show that the citrus waste has high carbon and cellulose products.

To make it easier to understand the sorption mechanism of citrus fruit waste, Brønsted and Lewis active centers are considered for the example of cellulose molecules. In general, Brønsted centers are one of the significant factors in the sorption properties of materials (Krstić, 2021b; You et al., 2020; Fang et al., 2020; Zhang et al., 2019; Krstić et al., 2021), and they can help us understand the structure and mechanism sorption of cellulose molecules, as an integral part of citrus peel waste. The mechanism of cellulose molecules depicting Brønsted acid centers is shown in Fig. 20.1. Hydrolysis of cellulose through Brønsted acid centers breaks down β-1,4-glucoside bonds, resulting in the formation of glucose molecules.

Fig. 20.2 shows the Lewis acid centers together with the hydroxyl ions present in the aqueous solution at 190°C so that the cellulose is easily transformed into soluble oligosaccharides.

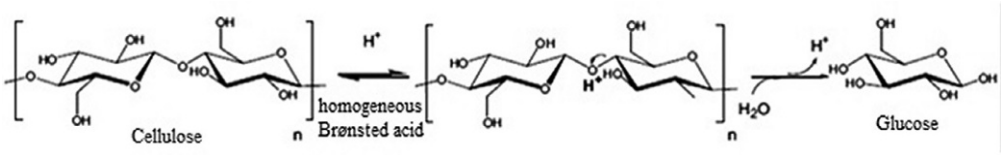

FIG. 20.1 Mechanism of Brønsted acid formations in cellulose. *Partly reprinted with permission of Elsevier from Chambon, F., Rataboul, F., Pinel, C., Cabiac, A., Guillon, E., Essayem, N., 2011. Cellulose hydrothermal conversion promoted by heterogeneous Brønsted and Lewis acids: remarkable efficiency of solid Lewis acids to produce lactic acid. Appl. Catal. B Environ. 105, 171–181. https://doi.org/10.1016/j.apcatb.2011.04.009.*

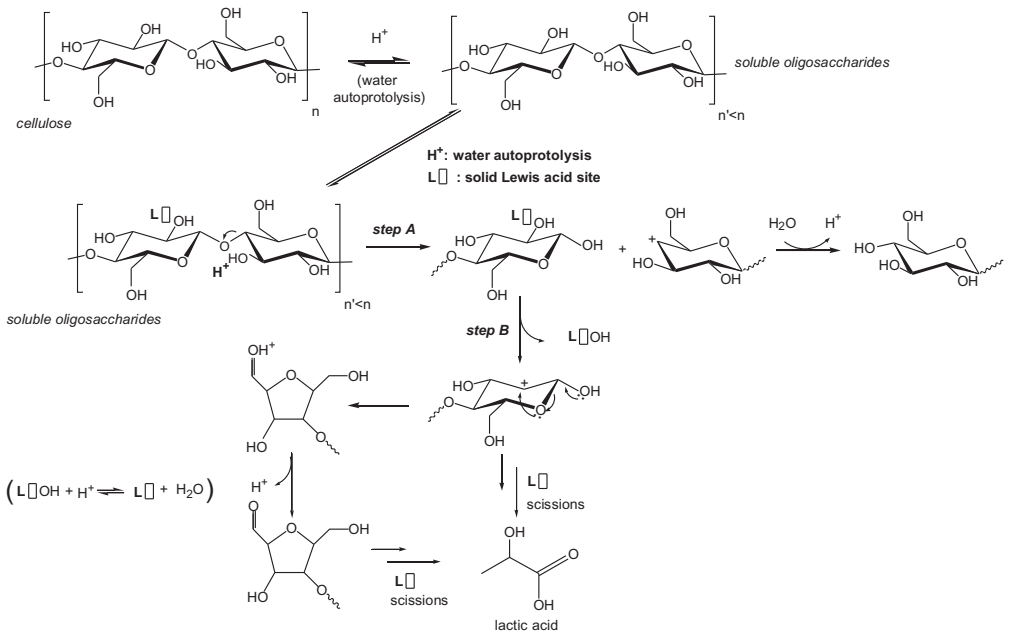

FIG. 20.2 Proposed mechanism of cellulose transformation in hydrothermal conditions in the presence of Lewis acid centers. *Reprinted with permission of Elsevier from Chambon, F., Rataboul, F., Pinel, C., Cabiac, A., Guillon, E., Essayem, N., 2011. Cellulose hydrothermal conversion promoted by heterogeneous Brønsted and Lewis acids: remarkable efficiency of solid Lewis acids to produce lactic acid. Appl. Catal. B Environ. 105, 171–181. https://doi.org/10.1016/j.apcatb.2011.04.009.*

Chambon et al. (2011) showed how Lewis centers coordinate hydroxyl groups at position 2, leading to easy cleavage of protonated ether bonds. In this way, an accelerated transformation of soluble oligosaccharides plays a role, leading to a shift in cellulose depolymerization. The number of insoluble oligosaccharides and other soluble polymers decreases in Lewis acid centers. The authors concluded that Lewis acid centers are responsible for the reduced soluble polymers. The strength and balance of Brønsted - Lewis acid centers can affect both the improvement of biosorbent adsorption and the selective transformation of cellulose molecules.

20.3 Conversion of citrus fruit waste to activated carbon

20.3.1 Characteristics of activated carbon

Due to its good physicochemical characteristics and exceptional sorption abilities, AC can be used as a sorbent in water treatment. Activated carbon can be obtained from materials of organic origin rich in carbon, traditionally coals and wood (Uđilanović et al., 2021). Although natural coal is the most commonly used material for producing activated carbon,

agro-industrial waste has proven to be a suitable alternative for obtaining AC. Activated carbon produced from organic waste would decrease the use of forests for these purposes (Prahas et al., 2008).

Activated carbon is a porous carbon material that is subject to a gaseous reaction, sometimes with chemical agents, during or after the carbonization process to increase its specific surface area and thus its sorption properties (Shen, 2020; Khan et al., 2019).

Today, activated carbon is obtained from lignite, wood, or synthetic polymers (resins). The classical carbonization process yields about 20%–30% of carbon. The number of active sites increases by using an activating agent, which modifies the porosity of the obtained material. Many laboratories and industrial applications use activated carbon based on the high sorption capacity of this material. This capacity depends on the physical properties and chemical structure of the coal (Khan et al., 2019; Shen, 2020; Uđilanović et al., 2021).

20.3.2 Activated carbon production and physicochemical properties

The physicochemical properties of activated carbon depend on the source of the starting material. The starting material is the material that determines the structural characteristics of the newly formed activated carbon (Arun et al., 2021; Wan et al., 2020; Eeshwarasinghe et al., 2019). Through the process of carbonization, it is possible to obtain a small specific surface, because then oxygen and hydrogen are lost in an inert atmosphere, which is mainly nitrogen. The obtained activated carbon is formed from compounds of elemental carbon microcrystals. These microcrystals are usually clogged with tar and carbonation residues and this reduces the sorption capacity of the carbon material. To increase the sorption capacity of the material, it is necessary to apply one of the methods that enable the removal of tar. This can be achieved with the help of some oxidizing agents to remove the tar, and the surface of the carbon material would then be activated (Shen, 2020; Robles Gutierrez et al., 2018). Activation can be physical or chemical.

Physical or thermal activation is oxidation at high temperatures above 700°C (Shen, 2020) in the presence of water vapor and carbon dioxide or air. Then, in the first phase, all volatile organic materials burn. In the second phase, the pores that are blocked open and new material forms with a high specific surface area due to the high porosity (Khan et al., 2019). In this way, an active carbon material with an extremely large specific surface area forms.

Chemical activation involves the carbonization of cellulose-based biomaterials. The presence of alkaline hydroxides (KOH, NaOH, and their combination) or inorganic acids (HNO_3, H_3PO_4, H_2SO_4) can contribute to chemical activation (Khan et al., 2019; Shen, 2020). Activated carbon is obtained to a greater extent by chemical activation than by thermal activation. In physical activation, pores are formed by the gasification process, while in chemical activation dehydrogenation reactions take place with the help of activating agents in the initial biomaterial, which affect the formation of bonds between carbon atoms. Chemical activation, unlike physical, is performed in one phase, where the process of carbonization and activation is carried out simultaneously at lower temperatures. Thus chemical activation creates pores on the surface of the activated carbon material. This is achieved as a consequence of the particle size of the starting material, activation temperature, heating rate, chemical activating agent, and carbonation duration (Prahas et al., 2008; Shen, 2020).

The determination of iodine number according to ASTM D4607-14 (2021) provides information on the ability of carbon to adsorb other atoms and molecules. The iodine number can be used as an approximate determination of the active surface area of activated carbons. This method determines the relative level of activation of residual reactivated carbon by adsorption of iodine from aqueous solution by determining the amount of absorbed iodine in mg in 1 g of carbon, according to the conditions given in standard ASTM D4607-14 (2021). The iodine number serves to determine the adsorption property of activated carbon on the surface and is expressed in mg/g of carbon, as opposed to the BET specific surface area that is in m^2/g of carbon.

The structure of activated carbon is arranged equally to the carbon rings in space. However, activated carbon also has a three-dimensional form of carbon atoms in the planes of hexagonal rings. The spaces between the graphite planes of the crystals create a microporous structure with a high inner surface (Khan et al., 2019).

In addition to the porous structure, activated carbons also have a chemical structure because they contain a small number of heteroatoms. The presence of heteroatoms (O, N, H, S) attached to the edges of graphene layers leads to different surface functional groups (Khan et al., 2019), which allow polar substances to be poorly retained on the surface of activated carbon. That is because the carbon atoms located on the edges of the plane have high available activity, as they are not saturated with carbon atoms and have free electrons (Robles Gutierrez et al., 2018).

Cui et al. (2017) designed nanocarbon materials with a large specific surface area with a hierarchical porosity and 2D/3D morphology for energy storage purposes. The authors published a new approach to adjusting the morphology and structure of nanocarbon based on methylcellulose. Due to the different activating agents, as shown in Fig. 20.3 (KOH and

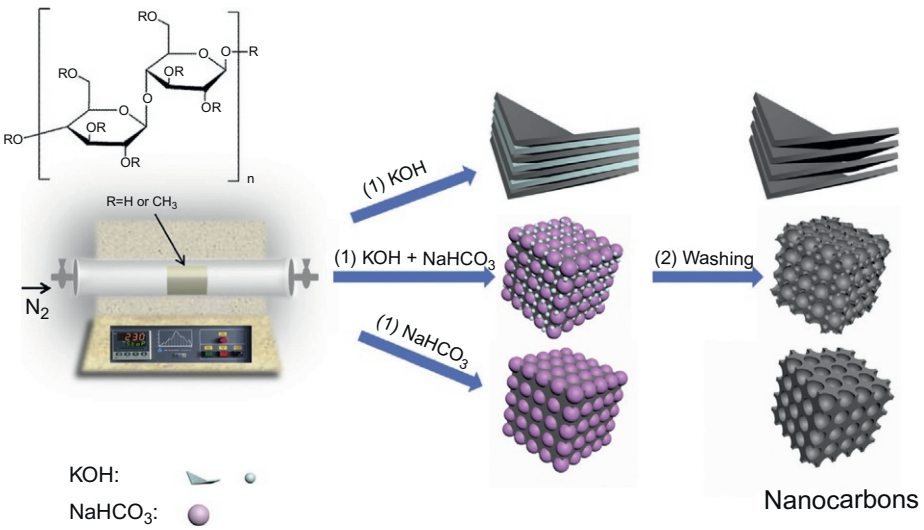

FIG. 20.3 Schematic illustration of the synthesis process for the MCCs. (1) Methylcellulose is carbonized/activated by sodium bicarbonate and/or potassium hydroxide with different mass ratios. (2) The MCC materials are liberated by washing. *Reprinted with permission of Elsevier from Cui, Y., Wang, H., Mao, N., Yu, W., Shi, J., Huang, M., Liu, W., Chen, S., Wang, X., 2017. Tuning the morphology and structure of nanocarbons with activating agents for ultrafast ionic liquid-based supercapacitors. J. Power Sources 361, 182–194. https://doi.org/10.1016/j.jpowsour.2017.06.087.*

$NaHCO_3$), interconnected sheet metal-like carbons can be obtained, for example, with a large specific surface area, up to 2285 m^2g^{-1} and a thickness up to about 4 nm. This approach to obtaining activated carbon with very large specific areas could serve as an idea for activating natural carbon materials based on citrus fruit waste to also be applied in water treatment.

The surface chemistry of activated carbon has an amphoteric nature. Activated carbon is generally either acidic or basic, depending on the surface concentration of acid and other surface groups, and also depends on the strength of the acidic or basic compounds (Robles Gutierrez et al., 2018; Shen, 2020). Therefore oxidized surface groups are classified into a few categories.

20.3.3 Possible surface groups on activated carbon materials

The elementary surface groups form when the oxidized surface is reduced in an inert or hydrogen atmosphere at high temperatures. Degradation of acidic groups creates active sites at the edges of graphene surfaces that attract oxygen during the cooling phase in an inert atmosphere. After the process of reexposure to air, basic-functional groups are formed.

Boehm (1994) gave an overview of the surface chemistry of carbon blacks and other carbons, particularly activated carbons. He considered surface oxides and chemical methods, such as surface functional groups. Boehm (1994) concludes that reactions with free organic radicals can be used to functionalize the carbon surface. Carboxyl groups, lactams and phenolic groups are "acidic" surface oxides. Boehm (1994) identified these acidic groups by neutralizing them with different bases. Acid groups were determined by the Boehm titration (BT) method (Boehm, 2002; Schönherr et al., 2018). Schönherr et al. (2018) found that BT can be applied to a wide range of carbon materials when a sufficient amount of sample is provided and when the samples are sufficiently hydrophilic. In Table 20.3, Schönherr et al. (2018) provided advantages and disadvantages for the determination of surface groups of carbon materials containing oxygen, using BT, Thermal Programmed Desorption (TPD-MS Method) by thermogravimetric analysis (TGA), X-ray photoelectron spectroscopy (XPS), and elemental analysis (EA).

When the surface of carbon materials is exposed to oxygen in the presence of oxidizing agents, acidic surface groups are formed, both at room temperature and high temperatures, both in gaseous media and in solutions. The parameters mentioned, together with the pH of the solution, are responsible for the amphoteric characteristics of the activated carbons. The presence of acidic surface functional groups, which are significantly present on the surface of activated carbon materials, was determined by BT. The presence of carboxyl groups is compatible with the values obtained by Boehm titration.

Hydrogen atoms appear on the surface of active carbon materials in the composition of other surface groups such as amines, carboxylic acids and phenols. Hydrogen atoms also occur as chemisorbed water or are directly attached to carbon atoms, as part of aliphatic or aromatic rings.

Phosphorus atoms in active carbon materials usually originate from phosphoric acid, when the activation is performed with phosphoric acid, during the carbonization process at low temperatures. Phosphorus can be bound in activated carbon, directly to carbon or via oxygen, and is stable between 500°C and 1000°C.

TABLE 20.3 General characteristics, advantages, and disadvantages of methods for the characterization of oxygen-containing surface groups.

Methods	Characteristics/advantages	Disadvantages
BT	– probes the surfaces of the whole sample (outer and inner surfaces) that are accessible to liquid reactants – absolute values are received (short evaluation time) – high precision – sample can be recovered though not in its pristine state – cost-effective	– quantification of acidic oxygen groups only – low robustness (results sensitive to changes in the experimental procedure) – larger sample amounts might be required
TPD-MS/ TGA	– pyrolysis of the sample – probes the volume of nearly the whole sample – detection of nearly all existing oxygen groups (outer and inner surfaces and particle interior) – low personal workload for measurement	– deconvolution required for quantification of specific groups – destructive method
XPS	– probes the outer surface and subsurface on top of the sample – detection of nearly all existing oxygen groups – very little sample amount needed – nondestructive	– deconvolution required for quantification of specific groups – interference of different groups at same binding energies – relevant spectra influenced by surface impurities
EA	– burns the sample – probes the volume of the whole sample – fast method	– no quantification of specific groups, – delivers only total amounts of elements – destructive method

Reprinted without special permission; published by MDPI, Journal of Carbon Research C from Schönherr, J., Buchheim, J.R., Scholz, P., Adelhelm, P., 2018. Boehm titration revisited (part II): a comparison of Boehm titration with other analytical techniques on the quantification of oxygen-containing surface groups for a variety of carbon materials. J. Carbon Res. C 4(2), 22. https://doi.org/10.3390/c4020022.

20.3.4 Conversion of orange peel waste into activated carbon and its application

Tovar et al. (2019) in Table 20.4 show the collected literature data of various researchers from 1993 to 2016, which relate to the conditions of preparation and chemical activation that led to the carbonization of waste from orange peel. Table 20.4 also shows the specific areas (S_{BET}) of activated carbon obtained from orange peel waste and the degree of adsorption (q_e) for various pollutants of organic and inorganic origin.

Although all plants contain pectin, and its composition and quality vary depending on the plant from which it is extracted, the method of its production, and the environmental conditions. Pectins are used in the food industry as gelling agents. Depending on the origin and extraction process, carboxyl groups are partially esterified with methanol, while in certain pectins the hydroxyl groups are partially acetylated. Orange peel is a very good source of pectin, which is also found in other fruits and vegetables, mainly from the juice industry. Given

TABLE 20.4 Review of properties, conditions, and carbonization process for orange peel.

Pretreatment			Chemical activation				Carbonization			Properties		
T (°C)	Time (h)	Part. Size (mm)	Agent	Conc. (%)	Time (h)	T (°C)	Atm.	T (°C)	Time (h)	S_{BET} (m^2g^{-1})	q_e (mg/g)	Pollut.
–	–	–	H_3PO_4	85	–		Air	400	0.5	–	149.4	Methylene blue
								400	1.5		149.8	
								800	0.5		149.9	
70	2	–	H_3PO_4					800	1.5		149.7	
105	96	0.5	H_2SO_4	–	–	–	Air	400	0.5	470.5	409.4	Methylene blue
105	96	0.5	H_2SO_4	98	6	–	Air	150	12	–		Direct blue-86
105	5	–	H_2SO_4	98	10	–	Air	120	24	–		Direct blue N-106
–	72	–	H_3PO_4	98	2	–	Air	180	2	–		Direct yellow 12
–	–	2	H_3PO_4	85	24	120	Air	500	1	–		Cane juice
				32	2	100	N_2	450	2	943	–	Nitrogen
				36						1032		
				40						1111		
				48						1203		
120	24	–	KOH	60	–	–	Ar	550	4	897	40	Cd (cadmium)
											42	Cr (chrome)
											69	Co (cobalt)
60	–	0.5–1	H_3PO_4	50	2	110		475	0.5	1090	320	Methylene blue
							–				522	Rhodamine B
–	–	2	H_3PO_4	40	24	80	N_2	450	3	451	–	Phenol
–	24	0.2	HCl	–	–	–	N_2	500	2	754	–	Fe (iron)
110	1	–	HCl	1 N	12	–	–	300	1	–	983	I (iodine)
80	24	–	KOH	1 M	–	–	N_2	800	2.5	1892	680.2	Methyl orange

Symbols: T, *temperature;* Part. Size, *particle size;* Conc., *concentration;* Atm., *atmosphere;* S_{BET}, *specific surface;* q_e, *degree of adsorption.*
Reprinted with permission of Elsevier from Tovar, A.K., Godínez, L.A., Espejel, F., Ramírez-Zamora, R.-M., Robles, I., 2019. Optimization of the integral valorization process for orange peel waste using a design of experiments approach: production of high-quality pectin and activated carbon. Waste Manag. 85, 202–213. https://doi.org/10.1016/j.wasman.2018.12.029.

their composition pectins, can be defined as polymers that mainly consist of chains of poly-α-D-galacturonic acid units linked by glycosidic bonds. Due to different properties, pectins can be (a) high methoxyl pectin (HM), i.e., with more than 50% of carboxyl groups esterified with methyl radicals, and (b) low methoxyl pectin (LM), which means with less than 50% esterified.

TABLE 20.5 Pectin extraction conditions for orange peel.

Extraction method	Extracting agent	Conditions				Yield (%)[a]
		Time (h)	Temperature (°C)	pH	l:s ratio	
Acid hydrolysis	$C_4H_6O_6$ (0.1% w)	0.5	45	–	–	0.98
Microwave	H_2O	0.25	150	2	100:8.2	1.6
Acid hydrolysis	HCl	0.75	–	2.2	–	1.68
Soxhlet extraction	H_2O	6	100	4.5	200:16	3.6
Acid hydrolysis	HCl (0.5 M)	1	80	2	–	5.1
Microwave	Ethanol (0.05 M)	0.25	120	5.5	16:1	5.27
Soxhlet extraction	H_2O and EDTA	3	100	–	16:1	5.27
Acid hydrolysis	HCl	1	90	2	–	6.08
Acid hydrolysis	HCl	0.67	–	1.5–3	–	6.50
Acid hydrolysis	HNO_3	0.5	90–097	2.5	–	10.9
Acid hydrolysis	–	8	95	4.2	–	13.24
Acid hydrolysis	HCl (0.5 M)	1.5	80–82	1	50:1	15.47
Acid hydrolysis	$C_6H_8O_7$	0.5	90–97	2.5	–	17.75
Water extraction	H_2O	1.5	95	–	25:1	17.95
Acid hydrolysis	HCl	1	85	1.6	60:1	19.3
Hydrolysis	Resine MB-1	1	85	1.6	60:1	20.5
C.P·C process	HCl (0.1 M)	0.75	90	–	–	21.8
Acid hydrolysis	HCl (0.1 M)	2	95	1.6	6:1	29.37

[a] *Dry basis (db).*

Reprinted with permission of Elsevier from Tovar, A.K., Godínez, L.A., Espejel, F., Ramírez-Zamora, R.-M., Robles, I., 2019. Optimization of the integral valorization process for orange peel waste using a design of experiments approach: production of high-quality pectin and activated carbon. Waste Manag. 85, 202–213. https://doi.org/10.1016/j.wasman.2018.12.029.

Tovar et al. (2019) analyzed AC prepared from pectin. Preparation of the AC depends on the activating agent, the impregnation temperature, the time, and the carbonization temperature, as shown in Table 20.4. The active materials for the preparation of activated carbon, based on literature data, are as shown by Tovar et al. (2019) in Tables 20.4 and 20.5. The processes shown do not require additional activation means.

20.3.5 Preparation and characterization of activated carbon from citrus peel waste

Fig. 20.4 shows a comparison of the surface morphology of orange peel and activated carbon obtained from orange peel (Tovar et al., 2017, 2019). It can be seen that, after the carbonization treatment, the surface is modified by a thermal process and an activating agent. The carbonization process leads to the formation of new surface sites.

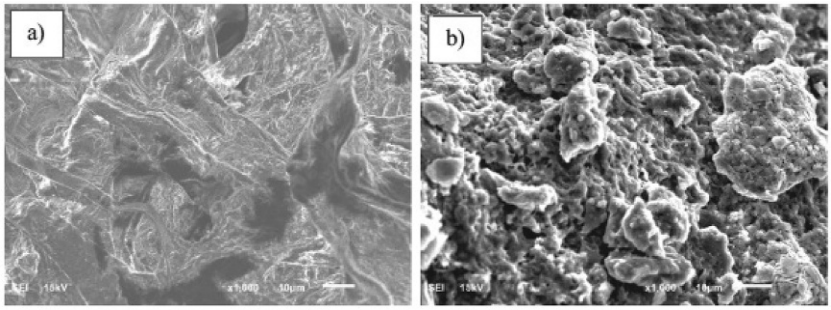

FIG. 20.4 SEM micrography comparison of samples: (A) precursor OP and (B) activated carbon. *Reprinted with permission of Elsevier from Tovar, A.K., Godínez, L.A., Espejel, F., Ramírez-Zamora, R.-M., Robles, I., 2019. Optimization of the integral valorization process for orange peel waste using a design of experiments approach: production of high-quality pectin and activated carbon. Waste Manag. 85, 202–213. https://doi.org/10.1016/j.wasman.2018.12.029.*

The Fourier transform with infrared spectroscopy (FTIR) is one of the most commonly used instrumental methods for determining the surface functional groups of activated carbon obtained from orange peel, as shown in Fig. 20.5 (Dhelipan et al., 2017).

X-ray photoelectron spectroscopy (XPS) is also used to characterize the functionality of carbon surfaces, as it provides useful information on the binding of photoelectron energies of C1s, N1s, O1s, and S2p surface groups. XPS confirms the presence of different surface groups on the carbon material, as well as the effect of local environments and the state of bonding of neighboring atoms. To identify the functionality of oxygen it is more convenient to measure the C1s signal, as shown in Fig. 20.6A. Carbon atoms differ in their energy, depending on the number of oxygen atoms to which they are attached, and then the corresponding signal appears in the main C1s spectrum of carbon bonds (C-C, C-N, C-O, C=O, O-C=O); see Fig. 20.6 (Wan et al., 2020).

Activated carbon prepared from orange peel has a higher sorption capacity compared to dried orange peel, which means that the modification of orange peel into carbon material

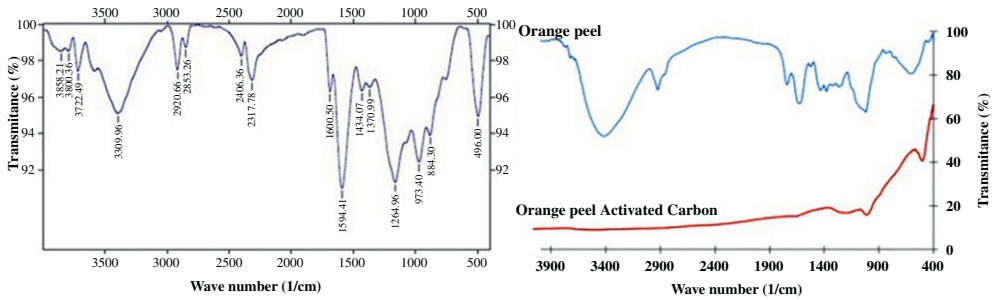

FIG. 20.5 FTIR spectrum of (A) OP-AC and (B) orange peel and activated carbon. *Modified after (Panel A) Journal of Saudi Chemical Society from Dhelipan, M., Arunchander, A., Sahu, A.K., Kalpana, D., 2017. Activated carbon from orange peels as supercapacitor electrode and catalyst support for oxygen reduction reaction in proton exchange membrane fuel cell. J. Saudi Chem. Soc. 21, 487-494. https://doi.org/10.1016/j.jscs.2016.12.003 and (Panel B) Wastewater and Water Quality from Robles Gutierrez, I., Tovar, A.K., Godínez, L.A., 2018. (Chapter 11): Sustainable sorbent materials obtained from orange peel as an alternative for water treatment, ed. Wastewater and Water Quality. IntechOpen https://doi.org/10.5772/intechopen.76137*

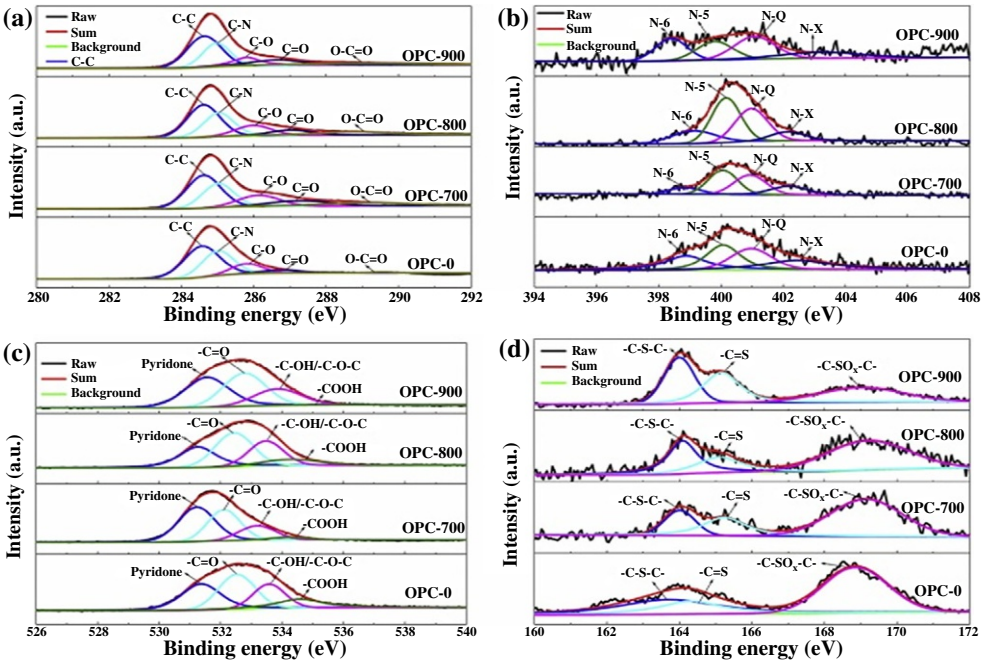

FIG. 20.6 High-resolution XPS survey of (A) C1s, (B) N1s, (C) O1s and (D) S2p spectra of OPC-0, OPC-700, OPC-800 and OPC-900. *Reprinted with permission of Elsevier from Wan, L., Chen, D., Liu, J., Zhang, Y., Chen, J., Du, C., Xie, M., 2020. Facile preparation of porous carbons derived from orange peel via basic copper carbonate activation for supercapacitors. J. Alloys Compd. 823 153747. https://doi.org/10.1016/j.jallcom.2020.153747.*

has a great advantage. The obtained carbon material has the physicochemical ability and capacity to be used in the process of treatment of water contaminated with various pollutants. However, it is necessary to continue the examination of the possibilities and the conditions under which carbon materials could be used to remove heavy metals, organochloride compounds, pesticides, and paints, to provide greater efficiency and a good alternative for environmental protection.

20.4 Electrochemical properties of active carbon materials based on citrus fruits

The use of carbon based on citrus waste (e.g., grapefruit) as an electrode material is due to its relatively low production costs and chemical stability in different solutions and its wide temperature range. Romero-Canoa et al. (2019) used adequate methods for obtaining electrode material with a large specific surface area, and a controlled pore distribution that determines the electrode–electrolyte contact boundary at which electrochemical reactions take place. Powdered carbon materials have been intensively studied as highly efficient catalysts, electrode materials for electrochemical capacitors, electrocatalysts for fuel cells, and hydrogen storage materials (Alvarado Avila et al., 2020; Wu et al., 2021; Niu et al., 2017) (Fig. 20.7).

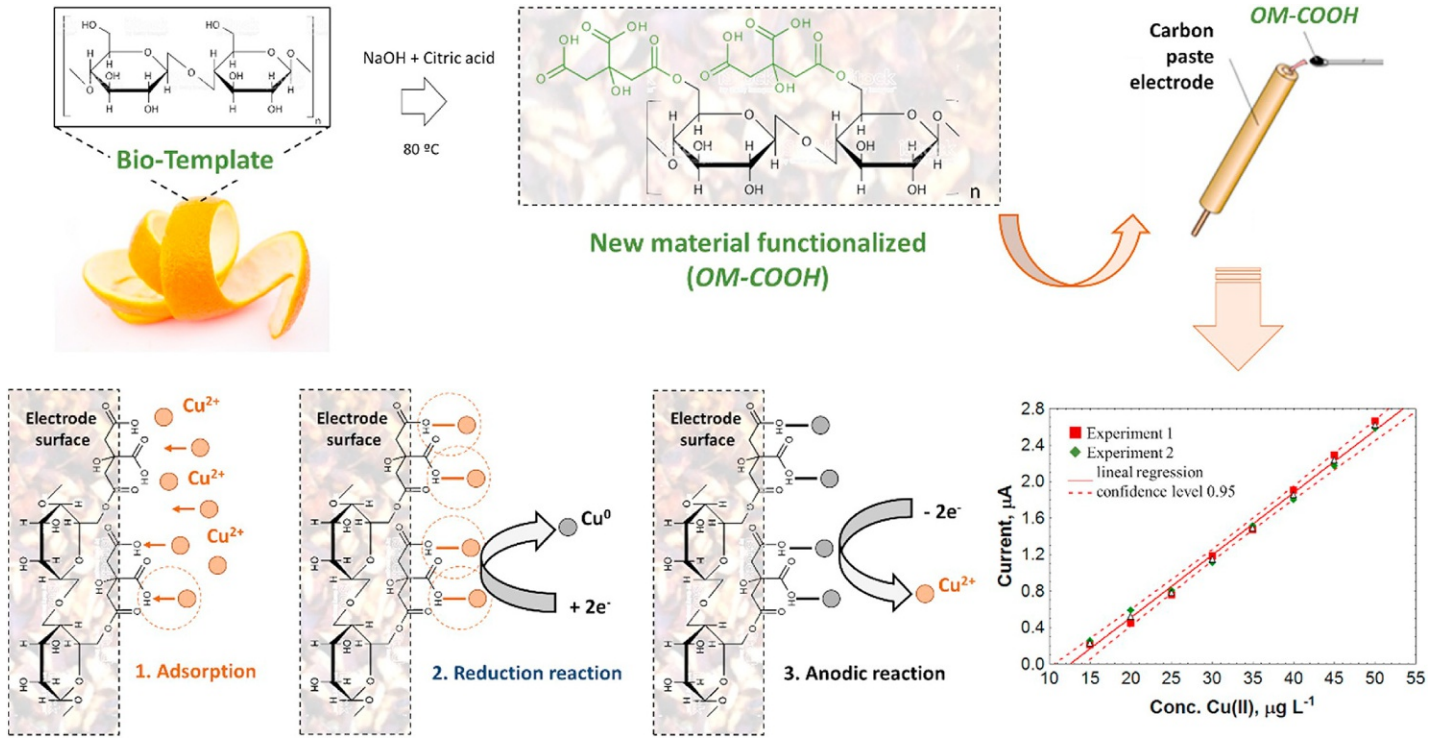

FIG. 20.7 Modified carbon paste electrode prepared from waste grapefruit peels. *Reprinted with permission of Elsevier from Romero-Canoa, L.A., Zarate-Guzman, A.I., Carrasco-Marin, F., Gonzalez-Gutierrez, L.V., 2019. Electrochemical detection of copper in water using carbon paste electrodes prepared from bio-template (grapefruit peels) functionalized with carboxyl groups. J. Electroanal. Chem. 837, 22–29. https://doi.org/10.1016/j.jelechem.2019.02.005.*

Carbon paste electrodes from modified grapefruit peel waste, which is functionalized with carboxyl groups, provide excellent electrochemical response for the detection of copper ions present in aqueous solutions. The prepared electrode provides a new and economical material for the detection of Cu^{2+} ions with a detection limit of 2.5 mg L^{-1}. The electrode proposed by Romero-Canoa et al. (2019) has advantages in cheap electrode production material, ease of operation, low cost, high sensitivity, and good repeatability.

Electrode performance and the area of application are mainly determined by textural properties and surface groups, which depend on the conditions of carbon material synthesis (Portet et al., 2007; Krstić et al., 2021). Storage of the charge in the form of a double electric layer at the electrochemical capacitor implies electrostatic adsorption of electrolyte ions on the oppositely charged electrode, without transfer of charge through the electrode/electrolyte boundary. The contribution of surface storage of charge in the total amount of stored charge on a carbon material depends not only on the structure of pores and surface groups on that material, but also on the nature of the electrolytic solution (Wei and Yushin, 2011; Wang et al., 2015). Research is focused mainly on the development of carbon materials with a large specific surface area to obtain adequate characteristics. Although the aim is to synthesize materials with the most developed specific surface, to get the largest possible amount of stored charge, it has been shown that this is not always the rule. A group of authors showed that the specific capacity at the electrode surface increases with increasing surface area (Raymundo-Piñero et al., 2006). However, literature data also show the capacity increases with decreasing specific surface area (Chen et al., 2008). Depending on the type of carbon, both views can be accepted (Hulicova et al., 2009). This means that in addition to the specific surface area, other parameters can determine the performance of a carbon capacitor. Electrode properties are also affected by electrical conductivity, the presence of surface heteroatoms, and pore size (Largeot et al., 2008).

Dimensionally stable electrodes (DSEs) are successfully used in the wastewater treatment process (Krstić and Pešovski, 2019, 2021; Krstić, 2021a), so attention could be paid to the conditions under which activated carbon electrodes, based on citrus fruit waste, could be adapted and applied in the process of wastewater treatment to remove organic and inorganic pollutants.

20.5 Regeneration of active carbon material

Regeneration of saturated activated carbon material after use in various wastewater treatment processes is one of the processes for the quality use of this material. McQuillan et al. (2018) pointed out that the most commonly used method, regeneration of saturated activated carbon, is based on physical (thermal), chemical, and biological treatments. The thermal process involves treating saturated carbon at high temperatures in an inert atmosphere, which leads to the decomposition or desorption of pollutants. During high-temperature regeneration of saturated activated carbon from water purification, the very complex physicochemical processes depend on several factors. The efficiency of regeneration of activated carbon depends on the mechanism of these processes, and thus the possibility of

restoring its adsorption capacity and its reapplication (El Gamal et al., 2018; McQuillan et al., 2018).

The large number of chemical compounds that are adsorbed from wastewater and their mutual influences during pyrolysis and carbonization, as well as different conditions of production and origin of activated carbons, make it difficult to predict their behavior in the process of high-temperature regeneration. The process itself is most often performed in electric furnaces, while thermogravimetric analysis (TG), derived thermogravimetric analysis (DTG), and differential thermal analysis (DTA) are most commonly used to monitor the process. However, Salvador et al. (2015) highlight the shortcomings of this technology. These include the high energy consumption, weight loss, and the possible creation of hazardous by-products that pollute the environment. Also, reduction of specific surface area and low adsorption capacity in an appropriate protective atmosphere is not used.

In addition to commercial methods for AC regeneration physically at high temperatures (McQuillan et al., 2018), alternative methods of oxidation by ultraviolet radiation, gamma radiation, ozonation, electrochemical methods, and electro-Fenton reactions can be used (Ferrández-Gómez et al., 2021a, b; Santos et al., 2020). According to Santos et al. (2020), technologies based on advanced oxidative processes are a good alternative for AC regeneration, as they are very effective in removing toxic pollutants from AC, are easy to handle, and are inexpensive.

Berenguer et al. (2010) point out that the electrochemical process is one of the most important substitutes for the thermal method due to its high efficiency, lower cost, low electricity consumption, and low CO_2 emissions and it is an environmentally friendly technology. Ferrández-Gómeza et al. (2021b) examined the electrochemical regeneration of granular activated carbon saturated with organic pollutants used in drinking water. A treatment reactor at a pilot scale, as an alternative to thermal regeneration, was used. The authors observed two cases of pilot plants (a) with parallel plate electrodes and (b) with concentric cylindrical electrodes. Ferrández-Gómeza et al. (2021b) used dimensionally stable anodes (DSAs) based on platinum-group metals (PGMs), and the observed parameters were systematized and are shown in Tables 20.6 and 20.7.

In both cases (a) with parallel plate electrodes and (b) with concentric cylindrical electrodes, under certain experimental conditions, S_{BET} can be renewed and AC regenerated up to about 95%, which confirms that electrochemical methods can be a suitable alternative to traditional thermal regeneration. Using electrodes designed in this way, Ferrández-Gómeza et al. (2021a, b) found satisfactory regeneration efficiencies with a drastic reduction in electricity consumption compared to conventional electrochemical reactors. According to the authors, both systems have advantages and disadvantages. A better restored porous texture is due to the contact between the electrode and the AC, which is regenerated. DSAs adapted for this purpose can be used for a better and cheaper electrolysis process and more efficient regeneration of AC (Krstić and Pešovski, 2019; Liu et al., 2020; Krstić, 2021a; Ferrández-Gómeza et al., 2021b). However, efforts should be made to overcome the negative phenomenon of this method, which refers to the additional oxidation of AC concerning the spent carbon material. Further research should be focused on the use of electrochemical methods with DSA and determination of operating conditions, as well as on the regeneration of ACs used in wastewater treatment contaminated by heavy metals. The results that

TABLE 20.6 Physicochemical characterization of textural properties by N_2 and CO_2 adsorption-desorption isotherms, TPD and pH_{PZC} of pristine spent, washing and electrochemically regenerated AC in parallel plate reactor configuration. All experiments were carried out with 15 kg of spent AC, under cathodic conditions, applying 70 A during 4 h, using 0.5 M H_2SO_4 as electrolyte solution and a flow rate of 750 L/h.

Sample	S_{BET} (m^2/g)	VDR,N_2 (cm^3/g)	VDR, CO_2 (cm^3/g)	Vmeso (cm^3/g)	% RP[a]	% AR[b]	CO (μmol/g)	CO_2 (μmol/g)	O (μmol/g)	pH PZC
Pristine	995	0.36	0.30	0.04			566	178	922	10.4
Spent	790	0.32	0.24	0.03			2668	1462	5592	7.3
Washing	870	0.35	0.25	0.04	87	30	2275	1361	4997	2.1
PPR1 (Pt/Ti)										
Reg-1h	910	0.34	0.27	0.04	92	59	2928	867	4663	2.2
Reg-2h	955	0.40	0.32	0.04	96	81	3095	791	4677	1.9
Reg-3h	1020	0.41	0.27	0.04	103	112	3294	820	4935	1.9
Reg-4h	970	0.39	0.25	0.04	98	88	3202	907	5015	1.8
PPR2 (RuO2/Ti)										
Reg-1h	945	0.37	0.30	0.03	95	76	2892	839	4570	2.2
Reg-2h	900	0.36	0.29	0.03	91	54	2520	750	4020	1.9
Reg-3h	840	0.34	0.27	0.04	84	24	2889	1055	4998	1.9
Reg-4h	800	0.33	0.27	0.03	80	5	2960	874	4708	2.0
PPR3 (IrO2/Ti)										
Reg-1h	910	0.37	0.28	0.04	92	59	3422	947	5315	2.1
Reg-2h	870	0.35	0.28	0.04	87	39	3725	989	5703	2.1
Reg-3h	910	0.37	0.28	0.04	92	59	3292	917	5127	1.9
Reg-4h	875	0.35	0.27	0.04	88	42	3149	866	4882	2.0

[a] *%RP—recovery of porosity.*
[b] *%AR—adsorption recovery.*
Reprinted with permission of Elsevier from Ferrández-Gómeza, B., Cazorla-Amorósb, D., Morallón, E., 2021b. Feasibility of electrochemical regeneration of activated carbon used in drinking water treatment plant. Reactor configuration design at a pilot scale. Process. Saf. Environ. Prot. 148, 846–857.

Ferrández-Gómeza et al. (2021a) presented indicate the sustainability of the electrochemical method for AC regeneration on an industrial level.

20.6 Discussions

Using agro-industrial citrus fruit waste and its transformation into activated carbon provides an alternative with low material costs to enable wastewater treatment. Xiao et al. (2020)

TABLE 20.7 Physicochemical characterization of textural properties by N_2 and CO_2 adsorption-desorption isotherms, TPD and pH_{PZC} of pristine spent, washing and electrochemically regenerated AC in concentric cylindrical reactor configuration.

Sample	S_{BET} (m^2/g)	VDR,N_2 (cm^3/g)	VDR, CO_2 (cm^3/g)	Vmeso (cm^3/g)	% RP[a]	% AR[b]	CO (μmol/g)	CO_2 (μmol/g)	O (μmol/g)	pH PZC
Pristine	995	0.36	0.30	0.04			566	178	922	10.4
Spent	790	0.32	0.24	0.03			2668	1462	5592	7.3
Washing	870	0.35	0.25	0.04	87	39	2275	1361	4997	2.1
CCR1 (Pt/Ti)										
Reg-1h	855	0.35	0.29	0.03	86	32	2421	1001	4424	2.0
Reg-2h	815	0.33	0.26	0.04	82	12	2336	864	4064	1.8
Reg-3h	950	0.38	0.27	0.04	96	78	2766	1068	4902	1.9
Reg-4h	830	0.34	0.26	0.03	83	20	3069	925	4919	1.9
CCR2 (RuO2/Ti)										
Reg-1h	810	0.33	0.24	0.04	81	10	3252	1122	5496	2.2
Reg-2h	840	0.34	0.27	0.04	84	24	2773	997	4766	2.0
Reg-3h	820	0.33	0.26	0.04	82	15	2138	878	3895	2.0
Reg-4h	900	0.36	0.27	0.04	91	54	2814	1069	4952	2.0
CCR3 (IrO2/Ti)										
Reg-1h	895	0.36	0.27	0.04	90	51	2595	986	4566	2.4
Reg-2h	880	0.35	0.27	0.04	88	44	2737	971	4680	2.4
Reg-3h	875	0.35	0.27	0.04	88	42	2742	966	4675	2.2
Reg-4h	935	0.37	0.27	0.04	94	71	2638	1025	4688	2.2

[a] *%RP—recovery of porosity.*
[b] *%AR—adsorption recovery*
All experiments were carried out with 10 kg of spent AC, under cathodic conditions, applying 27.5 A during 4 h, using 0.5 M H2SO4 as electrolyte solution and a flow rate of 750 L/h.
Reprinted with permission of Elsevier from Ferrández-Gómeza, B., Cazorla-Amorósb, D., Morallón, E., 2021b. Feasibility of electrochemical regeneration of activated carbon used in drinking water treatment plant. Reactor configuration design at a pilot scale. Process. Saf. Environ. Prot. 148, 846–857ron. Prot. 148, 846–857.

developed a new hydrothermal method by improving the physical and chemical properties of orange peel waste and its ability to sorb pollutants from wastewater. This method involves activation at 600–800°C. Nitrogen-containing groups (pyridine-N, pyridone-N and graphically-N) with hydrocarbons and urea with K_2CO_3 and the KOH as activation intermediate generated ammonia. Consequently, a more porous carbon structure with a high specific surface area formed. The sample obtained in this way had a low nitrogen content and a 3053 m^2g^{-1} specific area, extremely large. This specific surface area was 63% larger than the specific surface area of porous carbon obtained by conventional methods. Xiao et al. (2020)

found that there is a linear relationship between an increase in specific surface area and a relative decrease in nitrogen content and porous carbon at the activation temperature. Thus synthesized highly porous carbon in the presence of urea proved to be an excellent sorbent for weakly polar pollutants such as toluene and iodine.

Reis et al. (2020) calculated the functional density theory to better understand the adsorption mechanism of Cu^{2+}, Cr^{2+} and Cd^{2+} in cellulose. Based on MEP (molecular electrostatic potential), FMO (molecular limit orbitals), and reactivity index, Reis et al. (2020) have shown that it is possible to predict the site of interaction of metal ions with cellulose. Based on QTAIM (the quantum theory of atoms in molecules) analysis, the authors showed that the cellulose interaction acetate and Cr^{2+}, and cellulose and Cu^{2+}, are electrostatic in nature and the interactions with Cd^{2+} were partially covalent. The researchers also calculated the electron interaction energies of metal ions and cellulose, and Cr^{2+} ion binds most efficiently to cellulose compared to Cu^{2+} and Cd^{2+} ions. Menazea et al. (2020) investigated the theoretical possible interactions between pollutants (Ni, Cu, As, Cd, and Pb) and adsorbers (cytosine and graphene oxide modified biopolymer) in the process of wastewater treatment. They used functional density theory (DFT: B3LYP/LANL2DZ model) to observe possible interactions between heavy metals and adsorbents. The proposed model was applied to study the interaction between oxygen-containing adsorbent and nitrogen-containing groups and their interactions with isolated heavy metals. The interaction between the composite adsorber and the metal showed more selectivity for metals than the base adsorber. These results theoretically obtained can be applied to environmental pollution by removing heavy metals from industrial wastewater. In this way, research can be directed toward the further application of environmentally friendly methods in the future. Further experimental research can be conducted based on the results obtained theoretically or their modification. It is possible to expect the result of the reaction by using these and similar theoretical predictions. Also, it is possible to conduct experimental research so that the desired results can be achieved as soon as possible, saving both time and resources in people and chemicals.

The connection between experimental research and theoretical calculations using the semiempirical Multiple Minima Hypersurface methodology and Density Functional Theory is an essential element in new and more efficient activated carbon formed to develop a method for wastewater treatment. Calculations in quantum chemistry and the study of interactions at the level of molecules and pH of solutions in competitive adsorption can be expected to be of great importance for future research (Melchor-Rodrígueza et al., 2021; Marenich et al., 2009).

20.7 Conclusion and future perspectives

Sorption using citrus fruit waste is one of the alternatives for obtaining quality activated carbon from cheap agro-industrial waste. Carbon materials are among the oldest materials used and have proven to function well in water purification from pollutants. Even though carbon materials are more expensive than other sorbents, they have proven to be very effective adsorbents for water purification due to their exceptional strength and porous texture,

which gives them a large specific surface area. The adsorption capacity of carbon materials can be improved by their surface modification and by introducing organic functional groups (-NH2, -COOH and -OH). Functional groups tend to increase the surface area and volume of pores, responsible for the sorption of pollutants. In this way, the surface charge is reduced and the surface adsorption is improved, which provides an opportunity to create a new generation of carbon-based adsorbents.

Theoretical predictions based on the application of quantum chemistry and possible theoretical calculations for the use of citrus fruit waste and its modification into activated carbon, as a potential sorbent for wastewater treatment, would be an effective tool for testing citrus material as a potential adsorbent. In this way, the course of future experimental research could be assessed in advance and predicted, which would be of inestimable importance for further investigations. Today we are working on developing new methods or improving existing ones by modifying experimental conditions, together with quantum chemistry data, to better understand the adsorption process in water treatment.

Investing efforts and connecting the knowledge and experience of researchers in theoretical and experimental research could lead to faster, more efficient, and cheaper solutions in the process of water purification from pollutants. A joint effort would also lead to a better understanding of the adsorption mechanism as a significant factor in solving the problem of wastewater treatment.

Acknowledgments

The authors are grateful to the Ministry of Education and Science of the Republic of Serbia for the financial support of Grant No 451-03-9/2021-14/200052 and No 451-03-9/2021-14/200131.

References

Acharya, A., Pal, P.K., 2020. Agriculture nanotechnology: translating research outcome to field applications by influencing environmental sustainability. NanoImpact 19, 100232. https://doi.org/10.1016/j.impact.2020.100232.

Alvarado Avila, M.I., Toledo-Carrillo, E., Dutta, J., 2020. Improved chlorate production with platinum nanoparticles deposited on fluorinated activated carbon cloth electrodes. Clean. Eng. Technol. 1, 100016.

Arun, S., Uday Venkat Kiran, K., Mithin Kumar, S., Karnan, M., Sathish, M., Mayavan, S., 2021. Effect of orange peel derived activated carbon as a negative additive for lead-acid battery under high rate discharge condition. J. Energy Storage 34, 102225.

ASTM D1102-84, 2021. Standard Test Method for Ash in Wood.

ASTM D4607-14, 2021. Standard Test Method for Determination of Iodine Number of Activated Carbon.

Berenguer, R., Marco-Lozar, J.P., Quijada, C., Cazorla-Amoros, D., Morallon, E., 2010. Electrochemical regeneration and porosity recovery of phenol-saturated granular activated carbon in an alkaline medium. Carbon 48 (10), 2734–2745.

Bicu, I., Mustata, F., 2013. Optimization of isolation of cellulose from orange peel using sodium hydroxide and chelating agents. Carbohydr. Polym. 98, 341–348. https://doi.org/10.1016/j.carbpol.2013.06.009.

Boehm, H.P., 1994. Some aspects of the surface chemistry of carbon blacks and other carbons. Carbon 32 (5), 759–769. https://doi.org/10.1016/0008-6223(94)90031-0.

Boehm, H.P., 2002. Surface oxides on carbon and their analysis: a critical assessment. Carbon 40 (5), 145–149. https://doi.org/10.1016/S0008-6223(01)00165-8.

Cazetta, A.L., Vargas, A.M.M., Nogami, E.M., Kunita, M.H., Guilherme, M.R., Martins, A.C., Silva, T.L., Moraes, J.C. G., Almeida, V.C., 2011. NaOH-activated carbon of high surface area produced from coconut shell: kinetics and

equilibrium studies from the methylene blue adsorption. Chem. Eng. J. 174, 117–125. https://doi.org/10.1016/j.cej.2011.08.058.
Chambon, F., Rataboul, F., Pinel, C., Cabiac, A., Guillon, E., Essayem, N., 2011. Cellulose hydrothermal conversion promoted by heterogeneous Brønsted and Lewis acids: remarkable efficiency of solid Lewis acids to produce lactic acid. Appl. Catal. B Environ. 105, 171–181. https://doi.org/10.1016/j.apcatb.2011.04.009.
Chen, X.L., Li, W.S., Tan, C.L., Li, W., Wu, Y.Z., 2008. Improvement in electrochemical capacitance of carbon materials by nitric acid treatment. J. Power Sources 184 (2), 668. https://doi.org/10.1016/j.jpowsour.2008.05.073.
Cui, Y., Wang, H., Mao, N., Yu, W., Shi, J., Huang, M., Liu, W., Chen, S., Wang, X., 2017. Tuning the morphology and structure of nanocarbons with activating agents for ultrafast ionic liquid-based supercapacitors. J. Power Sources 361, 182–194. https://doi.org/10.1016/j.jpowsour.2017.06.087.
Danish, M., Ahmad, T., 2018. A review on utilization of wood biomass as a sustainable precursor for activated carbon production and application. Renew. Sust. Energ. Rev. 87, 1–21. https://doi.org/10.1016/j.rser.2018.02.003.
Dhelipan, M., Arunchander, A., Sahu, A.K., Kalpana, D., 2017. Activated carbon from orange peels as supercapacitor electrode and catalyst support for oxygen reduction reaction in proton exchange membrane fuel cell. J. Saudi Chem. Soc. 21, 487–494. https://doi.org/10.1016/j.jscs.2016.12.003.
Dimitrijević, M., Urošević, D., Milić, S., Urošević, T., 2014. Copper extraction from copper smelter slag with pyrite or flotation tailings followed by water leaching. Min. Metall. Eng. Bor 2334-8836. 4, 157–164. https://doi.org/10.5937/MMEB1404157D. http://www.irmbor.co.rs/images/izdavastvo/casopisi/engineering/mmebor4_14.pdf.
Dimitrijević, M.D., Urošević, D.M., Janković, Z.D., Milić, S.M., 2016a. Recovery of copper from smelting slag by sulphation roasting and water leaching. Physicochem. Probl. Miner. Process. 52 (1), 409–421. https://doi.org/10.5277/ppmp160134.
Dimitrijević, Nujkić, M.M., Alagić, S.Č., Milić, S.M., Tošić, S.B., 2016b. Heavy metal contamination of topsoil and parts of peach-tree growing at different distances from a smelting complex. Int. J. Environ. Sci. Technol. 13 (2), 615–630. https://doi.org/10.1007/s13762-015-0905-z.
Đorđievski, S., Sovrlić, Z., Urošević, T., Petrović, J., Krstić, V., 2017. Preventing decomposition of 2-mercaptobenzothiazole during gas chromatography analysis using programmable temperature vaporization injection. J. Serb. Chem. Soc. 82 (10), 1147–1153. https://doi.org/10.2298/JSC161114041D.
Eeshwarasinghe, D., Loganathan, P., Vigneswaran, S., 2019. Simultaneous removal of polycyclic aromatic hydrocarbons and heavy metals from water using granular activated carbon. Chemosphere 223, 616–627.
El Gamal, M., Mousa, H.A., El-Naas, M.H., Zacharia, R., Judd, S., 2018. Bio-regeneration of activated carbon: a comprehensive review. Sep. Purif. Technol. 197, 345–359. https://doi.org/10.1016/j.seppur.2018.01.015.
Fang, J., Zheng, W., Liu, K., Lia, H., Li, C., 2020. Molecular design and experimental study on the synergistic catalysis of cellulose into 5-hydroxymethylfurfural with Bronsted-Lewis acidic ionic liquids. Chem. Eng. J. 385, 123796. https://doi.org/10.1016/j.cej.2019.123796.
Ferrández-Gómeza, B., Ruiz-Rosas, R., Beaumont, S., Cazorla-Amoros, D., Morallon, E., 2021a. Electrochemical regeneration of spent activated carbon from drinking water treatment plant at different scale reactors. Chemosphere 264, 128399.
Ferrández-Gómeza, B., Cazorla-Amorósb, D., Morallón, E., 2021b. Feasibility of electrochemical regeneration of activated carbon used in drinking water treatment plant. Reactor configuration design at a pilot scale. Process. Saf. Environ. Prot. 148, 846–857.
Foo, K.Y., Hameed, B.H., 2012. Potential of jackfruit peel as precursor for activated carbon prepared by microwave induced NaOH activation. Bioresour. Technol. 112, 143–150. https://doi.org/10.1016/j.biortech.2012.01.178.
Gehrke, I., Geiser, A., Somborn-Schulz, A., 2015. Innovations in nanotechnology for water treatment. Nanotechnol. Sci. Appl. 8, 1–17. https://doi.org/10.2147/NSA.S43773.
Hulicova, D., Seredych, M., Lu, G.Q., Bandosz, T.J., 2009. Combined effect of nitrogen- and oxygen-containing functional groups of microporous activated carbon on its electrochemical performance in supercapacitors. Adv. Funct. Mater. 19 (3), 438. https://doi.org/10.1002/adfm.200801236.
Khan, T.A., Sajidah Saud, A., Jamari, S.S., Ab Rahim, M.H., Park, J.-W., Kim, H.-J., 2019. Hydrothermal carbonization of lignocellulosic biomass for carbon rich material preparation: a review. Biomass Bioenergy 130, 105384. https://doi.org/10.1016/j.biombioe.2019.105384.
Krstić, V., 2021a. Some effective methods for treatment of wastewater from Cu production. In: Inamuddin, Ahamed, M.I., Lichtfouse, E. (Eds.), Water Pollution and Remediation: Heavy Metals. Environmental Chemistry for a Sustainable World. 53. Springer, pp. 313–440, https://doi.org/10.1007/978-3-030-52421-0_12.

Krstić, V., 2021b. Role of zeolite adsorbent in water treatment. In: Handbook of Nanomaterials for Wastewater Treatment, Fundamentals and Scale Up Issues Micro and Nano Technologies. Elsevier, pp. 417–481, https://doi.org/10.1016/B978-0-12-821496-1.00024-6 (Chapter 14).

Krstić, V., Pešovski, B., 2019. Reviews the research on some dimensionally stable anodes (DSA) based on titanium. Hydrometallurgy 185, 71–75. https://doi.org/10.1016/j.hydromet.2019.01.018.

Krstić, V., Pešovski, B., 2021. Novel multifunctional two layer catalytic activated titanium electrodes for various technological and environmental processes. Arab. J. Chem. 14 (4), 103101. https://doi.org/10.1016/j.arabjc.2021.103101.

Krstić, V., Urošević, T., Pešovski, B., 2018. A review on adsorbents for treatment of water and wastewaters containing copper ions. Chem. Eng. Sci. 192, 273–287. https://doi.org/10.1016/j.ces.2018.07.022.

Krstić, V., Uđilanović, M., Urošević, T., Simonović, D., Milić, S., Ćirić, A., Pešovski, B., 2021. The use of activated carbon from citrus fruit waste, as an alternative method in environmental protection. Copper 46 (2), 1–10 (in Serbian).

Largeot, C., Portet, C., Chmiola, J., Taberna, P.L., Gogotsi, Y., Simon, P., 2008. Relation between the ion size and pore size for an electric double-layer capacitor. J. Am. Chem. Soc. 130, 2730. https://doi.org/10.1021/ja7106178.

Liu, T., Li, Y., Peng, N., Lang, Q., Xia, Y., Gai, C., Zheng, Q., Liu, Z., 2017. Heteroatoms doped porous carbon derived from hydrothermally treated sewage sludge: structural characterization and environmental application. J. Environ. Manag. 197, 151–158. https://doi.org/10.1016/j.jenvman.2017.03.082.

Liu, Z., Ren, B., Ding, H., He, H., Deng, H., Zhao, C., Wang, P., Dionysio, D.D., 2020. Simultaneous regeneration of cathodic activated carbon fiber and mineralization of desorbed contaminations by electro-peroxydisulfate process: advantages and limitations. Water Res. 171, 115456. https://doi.org/10.1016/j.watres.2019.115456.

Lončar, D., Paunković, J., Jovanović, V., Krstić, V., 2019. Environmental and social responsibility of companies across European Union countries – panel data analysis. Sci. Total Environ. 657, 287–296. https://doi.org/10.1016/j.scitotenv.2018.11.482.

Marenich, A.V., Cramer, C.J., Truhlar, D.G., 2009. Universal solvation model based on solute electron density and on a continuum model of the solvent defined by the bulk dielectric constant and atomic surface tensions. J. Phys. Chem. B 113, 6378–6396. https://doi.org/10.1021/jp810292n.

McQuillan, R.V., Stevens, G.W., Mumford, K.A., 2018. The electrochemical regeneration of granular activated carbons: a review. J. Hazard. Mater. 355, 34–49. https://doi.org/10.1016/j.jhazmat.2018.04.079.

Melchor-Rodrígueza, K., Gaspardb, S., Jáuregui-Hazaa, U.J., 2021. Chlordecone adsorption on functionalized activated carbons: computational chemistry as a tool for understanding the adsorption process. Quim Nova 44 (2), 172–179.

Menazea, A.A., Ezzat, H.A., Omara, W., Basyouni, O.H., Ibrahim, S.A., Mohamed, A.A., Tawfik, W., Ibrahim, M.A., 2020. Chitosan/graphene oxide composite as an effective removal of Ni, Cu, As, Cd and Pb from wastewater. Comput. Theor. Chem. 1189, 112980. https://doi.org/10.1016/j.comptc.2020.112980.

Mihailović, N.R., Mihailović, V.B., Kreft, S., Ćirića, A.R., Joksović, L.G., Đurđević, P.T., 2018. Analysis of phenolics in the peel and pulp of wild apples (Malus sylvestris (L.) Mill.). J. Food Compos. Anal. 67, 1–9. https://doi.org/10.1016/j.jfca.2017.11.007.

Miran, W., Nawaz, M., Jang, J., Lee, D.S., 2016. Conversion of orange peel. Waste biomass to bioelectricity using a mediator-less microbial fuel cell. Sci. Total Environ. 547, 197–205. https://doi.org/10.1016/j.scitotenv.2016.01.004.

Niu, Z., Wang, Y., Lin, H., Jin, F., Li, Y., Niu, J., 2017. Electrochemically enhanced removal of perfluorinated compounds (PFCs) from aqueous solution by CNTs-graphene composite electrode. Chem. Eng. J. 328, 228–235. https://doi.org/10.1016/j.cej.2017.07.033.

Pavithra, S., Thandapani, G., Sugashini, S., Sudha, P.N., Alkhamis, H.H., Alrefaei, A.F., Almutairi, M.H., 2021. Batch adsorption studies on surface tailored chitosan/orange peel hydrogel composite for the removal of Cr(VI) and cu(II) ions from synthetic wastewater. Chemosphere 271, 129415.

Pešić, M., Milić, S., Nujkić, M., Marić, M., 2020a. Determination of heavy metal concentration and correlation analysis of turbidity: a case study of the Zlot source (Bor, Serbia). Water Air Soil Pollut. 231 (3), 98. https://doi.org/10.1007/s11270-020-4453-x.

Pešić, M., Milić, S., Nujkić, M., Marić, M., 2020b. The impact of climatic parameters on the turbidity and natural organic matter content in drinking water in the City of Bor (eastern Serbia). Environ. Earth Sci. 79 (11), 267. https://doi.org/10.1007/s12665-020-09016-0.

Portet, C., Yushin, G., Gogotsi, Y., 2007. Electrochemical performance of carbon onions, nanodiamonds, carbon black and multiwalled nanotubes in electrical double layer capacitors. Carbon 45 (13), 2511. https://doi.org/10.1016/j.carbon.2007.08.024.

Prahas, D., Kartika, Y., Indraswati, N., Ismadji, S., 2008. Activated carbon from jackfruit peel waste by H3PO4 chemical activation: pore structure and surface chemistry characterization. Chem. Eng. J. 140 (1–3), 32–42. https://doi.org/10.1016/j.cej.2007.08.032.

Raymundo-Piñero, E., Kierzek, K., Machnikowski, J., Béguin, F., 2006. Relationship between the nanoporous texture of activated carbons and their capacitance properties in different electrolytes. Carbon 44 (12), 2498. https://doi.org/10.1016/j.carbon.2006.05.022.

Reis, D.T., Ribeiro, I.H.S., Pereira, D.H., 2020. DFT study of the application of polymers cellulose and cellulose acetate for adsorption of metal ions (Cd^{2+}, Cu^{2+} and Cr^{3+}) potentially toxic. Polym. Bull. 77, 3443–3456. https://doi.org/10.1007/s00289-019-02926-5.

Robles Gutierrez, I., Tovar, A.K., Godínez, L.A., 2018. Sustainable sorbent materials obtained from orange peel as an alternative for water treatment. In: Wastewater and Water Quality. IntechOpen, https://doi.org/10.5772/intechopen.76137 (Chapter 11).

Romero-Canoa, L.A., Zarate-Guzman, A.I., Carrasco-Marin, F., Gonzalez-Gutierrez, L.V., 2019. Electrochemical detection of copper in water using carbon paste electrodes prepared from bio-template (grapefruit peels) functionalized with carboxyl groups. J. Electroanal. Chem. 837, 22–29. https://doi.org/10.1016/j.jelechem.2019.02.005.

Salvador, F., Martin-Sanchez, N., Sanchez-Hernandez, R., Sanchez-Montero, M.J., Izquierdo, C., 2015. Regeneration of carbonaceous adsorbents. Part I: thermalregeneration. Microporous Mesoporous Mater. 202, 259–276. https://doi.org/10.1016/j.micromeso.2014.02.045.

Santos, D.H.S., Duarte, J.L.S., Tonholo, J., Meili, L., Zanta, C.L.P.S., 2020. Saturated activated carbon regeneration by UV-light, H2O2 and Fenton reaction. Sep. Purif. Technol. 250. 117112.

Schönherr, J., Buchheim, J.R., Scholz, P., Adelhelm, P., 2018. Boehm titration revisited (part II): a comparison of Boehm titration with other analytical techniques on the quantification of oxygen-containing surface groups for a variety of carbon materials. J. Carbon Res. C 4 (2), 22. https://doi.org/10.3390/c4020022.

Sevilla, M., Fuertes, A.B., Mokaya, R., 2011. High density hydrogen storage in superactivated carbons from hydrothermally carbonized renewable organic materials. Energy Environ. Sci. 4, 1400. https://doi.org/10.1039/c0ee00347f.

Shen, Y., 2020. A review on hydrothermal carbonization of biomass and plastic wastes to energy products. Biomass Bioenergy 134, 105479. https://doi.org/10.1016/j.biombioe.2020.105479.

Sovrlić, Z., Urošević, D., Mikić, M., Milivojević, M., Krstić, V., Uđilanović, M., Vasiljević, S., 2020. Determination of chloride in soil by ionic chromatography. Copper 45 (1), 24–39 (in Serbian).

Tovar, A.K., Arano, M.J., Domínguez, O., Robles, I., 2017. Characterization and evaluation of sorbent materials obtained from orange peel as an alternative of sustainable materials for water treatment. Int. J. Chem. React. Eng. 15, 20170013. https://doi.org/10.1515/ijcre-2017-0013.

Tovar, A.K., Godínez, L.A., Espejel, F., Ramírez-Zamora, R.-M., Robles, I., 2019. Optimization of the integral valorization process for orange peel waste using a design of experiments approach: production of high-quality pectin and activated carbon. Waste Manag. 85, 202–213. https://doi.org/10.1016/j.wasman.2018.12.029.

Trumić, B., Gomidželović, L., Trujić, V., Krstić, V., Stanković, D., 2012. Comparative analysis of high temperature strength of platinum and its binary alloys with low content of alloying element. Chem. Ind. 66 (3), 395–401 (in Serbian) https://doi.org/10.2298/HEMIND110718106T.

Trumić, B., Gomidželović, L., Marjanović, S., Krstić, V., Ivanović, A., Dimitrijević, S., 2013. Pt-Rh alloys: investigation of creep rate and rupture time at high temperatures. Mater. Test. 55 (1), 38–42. https://doi.org/10.3139/120.110406.

Trumić, B., Gomidželović, L., Marjanović, S., Krstić, V., Ivanović, A., Dimitrijević, S., 2015. Pt-Rh alloys: investigation of tensile strength and elongation at high temperatures. Arch. Metall. Mater. 2 (60), 643–647. https://doi.org/10.1515/amm-2015-0186.

Trumić, B., Gomidželović, L., Marjanović, S., Ivanović, A., Krstić, V., Dimitrijević, S., 2016. Pt-Pd system: investigation of mechanical properties. Kovove Mater. 54, 139–145. https://doi.org/10.4149/km_2016_2_139.

Trumić, B., Gomidželović, L., Marjanović, S., Ivanović, A., Krstić, V., 2017. Platinum-based alloys: investigation of the effect of impurities content on creep rate, rupture time and relative elongation at high temperatures. Mater. Res. 20 (1), 191–199. https://doi.org/10.1590/1980-5373-mr-2016-0240.

Tsouko, E., Maina, S., Ladakis, D., Kookos, I.K., Koutinas, A., 2020. Integrated biorefinery development for the extraction of value-added components and bacterial cellulose production from orange peel waste streams. Renew. Energy 160, 944–954. https://doi.org/10.1016/j.renene.2020.05.108.

Uđilanović, M., Krstić, V., Ćirić, A., Stanić, Z., 2021. Elementar composition and trace metal analysis of wood charcoal samples. Copper 46 (2), 11–18 (in Serbian).

Urošević, T., Sovrlić, Z., Milivojević, M., Đorđievski, S., Jovanović, M., Petrović, J., Svrkota, I., 2016. Uticaj mase biosorbenata – kora citrusnog voća na sorpciju teških metala. Bakar 41 (2), 19–27.

Wan, L., Chen, D., Liu, J., Zhang, Y., Chen, J., Du, C., Xie, M., 2020. Facile preparation of porous carbons derived from orange peel via basic copper carbonate activation for supercapacitors. J. Alloys Compd. 823, 153747. https://doi.org/10.1016/j.jallcom.2020.153747.

Wang, D., Geng, Z., Li, B., Zhang, C., 2015. High performance electrode materials for electric double-layer capacitors based on biomass-derived activated carbons. Electrochim. Acta 173 (10), 377. https://doi.org/10.1016/j.electacta.2015.05.080.

Wei, L., Yushin, G., 2011. Electrical double layer capacitors with activated sucrose- derived carbon electrodes. Carbon 49 (14), 4830. https://doi.org/10.1016/j.carbon.2011.07.003.

Wong, S., Ngadi, N., Inuwa, I.M., Hassan, O., 2018. Recent advances in applications of activated carbon from biowaste for wastewater treatment: a short review. J. Clean. Prod. 175, 361–375. https://doi.org/10.1016/j.jclepro.2017.12.059.

Wu, D., Xu, L.H., Feng, H.J., Zhu, Y.W., Chen, X.Y., Cui, P., 2021. Design and theoretical study of novel deep eutectic solvents: the effects of bromine and chloride anions on solvation structure and supercapacitor performance. J. Power Sources 492, 229634. https://doi.org/10.1016/j.jpowsour.2021.229634.

Xiao, K., Liua, H., Li, Y., Yang, G., Wang, Y., Yao, H., 2020. Excellent performance of porous carbon from urea-assisted hydrochar of orange peel for toluene and iodine adsorption. Chem. Eng. J. 382, 122997. https://doi.org/10.1016/j.cej.2019.122997.

You, Y., Zhang, X., Li, P., Lei, F., Jiang, J., 2020. Co-production of xylooligosaccharides and activated carbons from Camellia oleifera shell treated by the catalysis and activation of zinc chloride. Bioresour. Technol. 306, 123131. https://doi.org/10.1016/j.biortech.2020.123131.

Zhang, X., Zhang, X., Sun, N., Wang, S., Wang, X., Jiang, Z., 2019. High production of levulinic acid from cellulosic feedstocks being catalyzed by temperature-responsive transition metal substituted heteropolyacids. Renew. Energy 141, 802–813. https://doi.org/10.1016/j.renene.2019.04.058.

CHAPTER

21

Alginate-based nanobiosorbents for bioremediation of environmental pollutants

Komal Rizwan[a], *Tahir Rasheed*[b], *and Muhammad Bilal*[c]

[a]Department of Chemistry, University of Sahiwal, Sahiwal, Pakistan [b]Interdisciplinary Research Center for Advanced Materials, King Fahd University of Petroleum and Minerals (KFUPM), Dhahran, Saudi Arabia [c]School of Life Science and Food Engineering, Huaiyin Institute of Technology, Huaian, China

21.1 Introduction

Environmental pollution is increasing day by day due to economic growth, industrial development, and intensive domestic activities. Water is a basic need of life and the availability of pure water has become a major concern now a day to all living things. There is a dire need for innovative technologies for the bioremediation of environmental contaminants (dyes, heavy metals, pesticides, etc.). During recent decades the different biomaterials have been introduced with better adsorption efficacy, good environmental compatibility, and cost-effective operational efficacy (Wan et al., 2018). Various biomaterials including alginate, cellulose, chitosan, gums, etc., have been documented well for mitigation of environmental contaminants (Nasrollahzadeh et al., 2020). Alginate is a polysaccharide present in the outer wall of brown algae. This polysaccharide has fascinating characteristics as bio-compatible, harmless, and easily biodegradable. Alginic acid is its major constituent and sodium alginate is sodium salt of alginic acid which contains a bundle of hydroxyl and carboxylic moieties along the polymer chain (Fig. 21.1) which made them highly efficient for adsorption of pollutants from aqueous media (Sutirman et al., 2021). Alginate consisted of β-D-mannuronic acid (M-block) and α-L-guluronic acid (G-block) residues, linked through 1,4-glycosidic bonds. Alginate has a high adsorption capacity and cost-friendly, so various alginate composites incorporating various nanomaterials, polymers, gels, and microorganisms have been studied for

https://doi.org/10.1016/B978-0-323-90912-9.00021-6

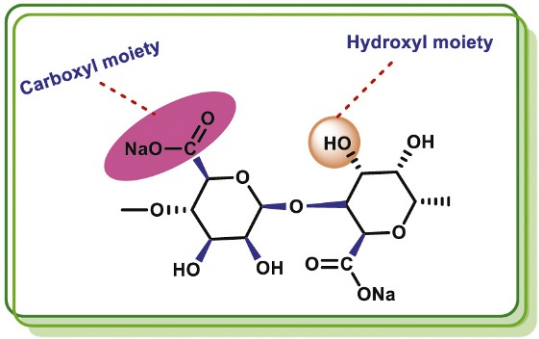

FIG. 21.1 General presentation of the structure of sodium salt of alginic acid.

the removal of heavy metals, radionuclides, pharmaceuticals dyes, pesticides, and other contaminants (Sutirman et al., 2021; Zhang et al., 2021). Heat resistance and mechanical stability and elasticity of sodium alginate are not much high, so physical and chemicals modifications are applied to improve its adsorption potential (Ates et al., 2020). Different strategies including cross-linking, surface modification, composites formation by utilization of other nanomaterials have been reported for modification of alginate-based nanosorbents (Thakur et al., 2018). Surface grafting increases the selectivity and uptake capacity of contaminants while cross-linking changes the strength and formation of alginate-based composites enhance the adsorption potential (Pan et al., 2019; Wen et al., 2020). The alginate-based composites possess novel chemical properties and great compatibility. Sodium alginate is stable and has the capability of complexing, gelation, and film formation. It can form thermally stable gels. Alginates have been used for the encapsulation of biological and chemical molecules with many applications in cosmetics, textile industry, pharmaceuticals, food, chemical, and environmental engineering. Functional moieties present on the surface of alginate have the capability to capture cations through ion exchange between the cross-linking metallic cation and pollutant (dyes, transition metals). In this chapter, the synthesis of alginate-based nanocomposites their various functionalities and their role in the removal of various environmental pollutants have been reported. Illustration of applications of alginate-based composites for removal of various environmental contaminants has been given in Fig. 21.2.

21.2 Synthesis of alginate-based composites

Alginate-based composites can be synthesized through various nanocomposites fabrication strategies and characteristics, applications depend greatly on synthetic approaches. Few prominent methods have been elaborated in this section. Previously four methods including crosslinking, self-assembly, emulsification, and complexation have been reported for the synthesis of alginate composites (Akhtar et al., 2016). For the synthesis of physically crosslinked hydrogels, the ionic interaction, hydrogen bonding crystallization, complex formation, and protein interactions are used, while for chain growth, condensation, addition,

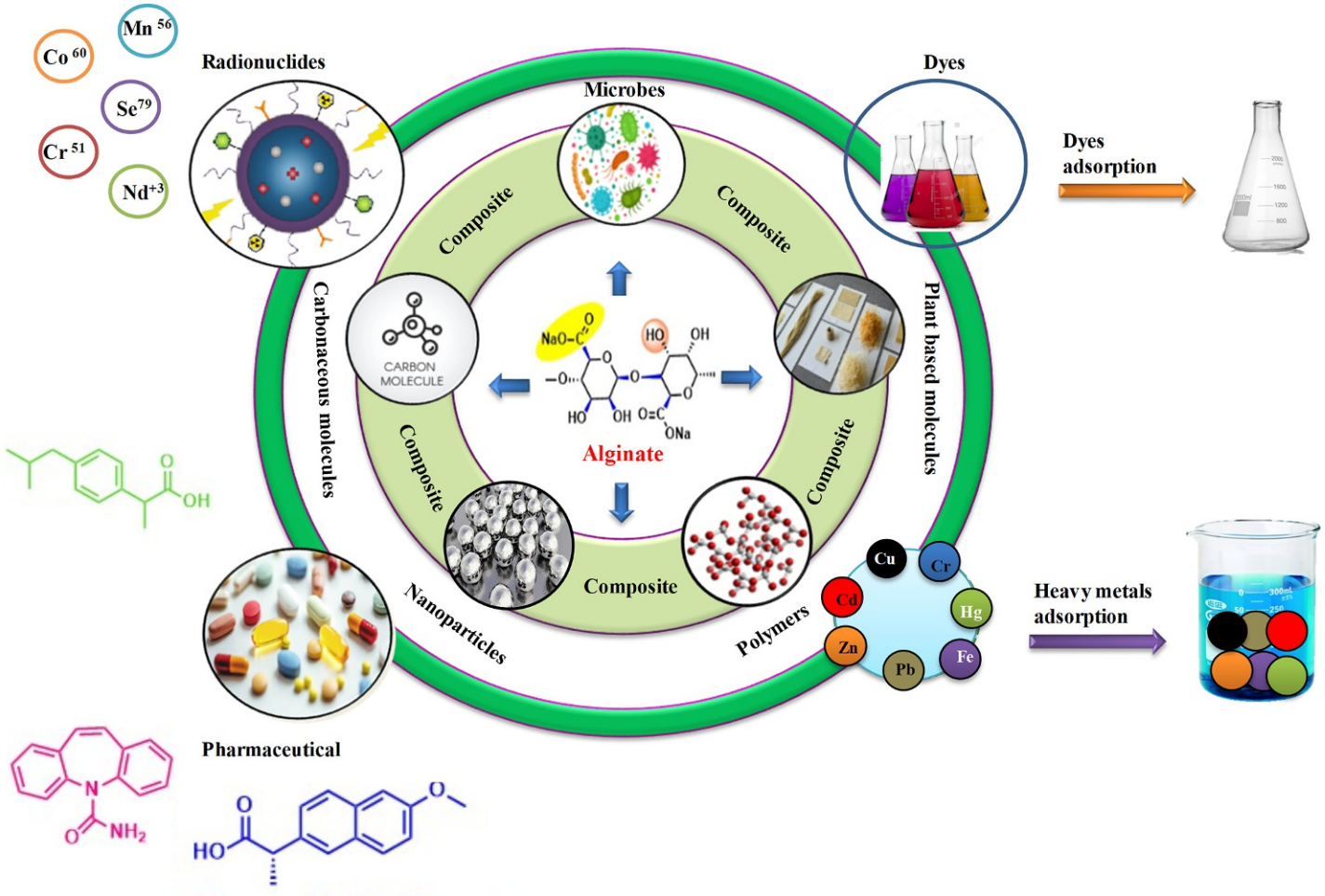

FIG. 21.2 Illustration of applications of alginate-based composites for removal of various environmental contaminants.

and electron beam polymerizations are employed. All synthetic methodologies have their own pros and cons. Physically crosslinked sodium alginate-based hydrogels are simple but their gel strength is not good while chemically crosslinked gels are good in strength. A physical crosslinking method is simple and gentle but chemical crosslinking is complex and also requires removal of unreacted. Functional moieties (–OH, –COONa) on the surface of sodium alginate can be modified through chemical crosslinking, etherification, and esterification. The basic process of gel formation involves coordination between sodium alginate and divalent metallic cation/polymeric cation that proceeds through interaction between cation and G-blocks.

Thereof the alginates having great content of guluronate may lead to the synthesis of gels of excellent strength. The confirmation of the junction zones in calcium-based alginate hydrogels was explained through the known "Egg-box" model which was presented in 1973 (Grant et al., 1973). Alginate has different binding abilities for different multivalent cations. Various factors as pH, the concentration of a solution, the intensity of metallic cations are responsible for the strength, stability, conformation, and shape of gel beads (Chan et al., 2002). Controlled conditions should be used for the synthesis of calcium-based alginate hydrogels. Bentonite supported zinc oxide NP encapsulated alginate-based nanocomposite was synthesized through Ca^{+2} mediated gelification controlled process (Motshekga et al., 2018). The encapsulation strategy follows the introduction of alginate solution possessing the dispersion of bentonite-supported zinc oxide NP to calcium cations solution. Beads were formed through the continuous stirring of the medium. Beads agglomeration was reduced because of NPs dispersion on bent support. In another research work, the nanoshell carriers were fabricated through encapsulation of drug-loaded Nps in Ca-alginate nanohydrogel (Zhang et al., 2018b). This gelification strategy by using calcium cations is a simple and easy method for implementation in comparison to other nanomaterials synthesis protocols.

Various nanomaterials including Graphene oxide (GO), activated carbon (AC), nanoparticles, nanocomposites, carbon nanotubes (CNT) magnetic particles, and various microbes have been encapsulated into alginate-based hydrogels for improving the stability and efficacy of alginate hydrogels for environmental applications (Hong et al., 2017; Rezaei et al., 2017). For encapsulation purpose, the material selection depends on material functionalities and planned applications so composite may provide intended benefits. Alginate-based composites show improved characteristics (mechanical, physical) for various applications. Alginate beads serve as a stable matrix for different absorbents (GO, AC, CNTs) (Robati et al., 2016) which are fine particles and difficult to isolate from media. Encapsulation of carbon-based nanomaterials into alginate-based hydrogels provides regeneration and easy separation for the treatment of wastewater (Wang et al., 2018, 2019). Synthesis of alginate-based magnetic NPs brings together nano-effects and magnetic strategies in composite form and providing great adsorption potential with a decrease in the risk of NPs for the environment. Magnetic nanotechnology is widely employed for wastewater treatment (Saravanan et al., 2021). Alginate can also help in optimizing microbial processes for various applications. Alginate-based microorganism composites provide many advantages as strong resistance, great metabolic activity. Immobilized microorganisms can be used various times without loss of activity. Thereof alginate immobilized microbes are important for the treatment of wastewater (Liu et al., 2012).

21.3 Role of alginate-based composites for removal of heavy metals

Heavy metals are polluting the water systems and recovery of toxic metals suffers from high cost, energy consumption, incomplete removal, and generation of waste. Adsorption strategy is the best process to remove heavy metals efficiently from aqueous media. Heavy metal removal is generally an interaction between the metallic cation and functional moiety present on the surface of the adsorbent which includes ion exchange, complexation, electrostatic force of interaction, etc. Hydroxyl, carboxyl, amino functionalities present on the surface of adsorbents are generally responsible for such kinds of interactions (Won et al., 2014). Alginate is endowed with carboxyl and hydroxyl moieties throughout the polymeric chain so they can be utilized for decontamination. These function moieties can serve as active sites for the adsorption of heavy metals. Alginates swell and dissolve in aqueous media so this can be overcome by tuning alginates into hydrogels. Alginates undergo gelation in existence of metallic cations as cross linking agent (Agüero et al., 2017). Composites of alginates with carbonaceous nanomaterials, nanoparticles, and polymers have been synthesized to enhance the adsorption potential of alginates for heavy metals.

21.3.1 Carbonaceous/polymeric-based sodium alginate composites

Biochar, CNTs and graphene oxides, polymers are carbonaceous materials and they possess high functionalities, high surface area, porosity, and high strength. Composites of these carbon-based materials with alginates give more adsorption sites. GO encapsulated polyvinyl alcohol modified sodium alginate were synthesized and used to adsorb Cu (II) and U (VI) from aqueous media with adsorption potential of 247.16 and 403.78 mg/g, respectively (Yi et al., 2018). The addition of GO enhanced the hydrogel stability. In another study, GO was blended with SA and composite membranes were synthesized and their adsorption capacities were found to be 327.9 and 118.6 mg/g for Cr (III) and Pb (II), respectively. Adsorption occurs due to the chelation of –OH and –COOH moieties with metal ions and also ion exchange with calcium ions (Bai et al., 2020). PVA/SA encapsulated biochar was synthesized to adsorb Cu (II). Mechanistic studies exhibited that carbon-carbon double bond-containing moieties were responsible for adsorption phenomena (Xiao et al., 2019). In the latest study, biochar was prepared from *Eichhornia crassipes*. The alginate encapsulated biochar beads were prepared and modified through ferric/ferrous sulfate and they efficiently adsorbed the Cd^{+2} from aqueous media at pH 6 and temp. 37 °C. This biochar can be recovered to re-use. Temperature plays an efficient role while biochar generation (Liu et al., 2020). The process of alginate-based biochar bead formation and its efficiency in the removal of Cadmium metal ions is illustrated in Fig. 21.3.

Recently zero valent iron-AC Na alginate beads were synthesized and they showed excellent adsorption potential against Pb, Cr, and Cd. Kinetic studies showed that the experiment followed the pseudo-first-order kinetics which suggests a multi-layer adsorption uptake approach. Hydroxyl and carboxyl moieties were found responsible for metals adsorption (Thakur and Kumar, 2021). Fe_3O_4/CD/AC/SA composite beads have been reported to remove Cu (II) from aqueous media with an adsorption potential of 10.10 mg/g (Yadav et al., 2021).

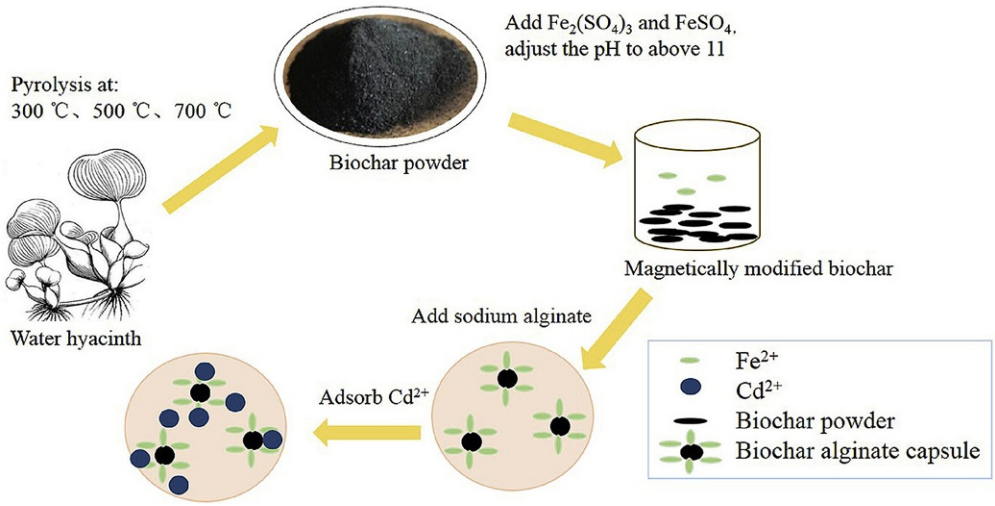

FIG. 21.3 Graphical presentation of alginate-based biochar formation and its efficiency to remove Cadmium (II) (Liu et al., 2020).

Polymeric materials have a variety of functional moieties which made them affinitive toward heavy metals. The blending of alginates with polymers enhances the active sites for metal adsorption. Recently onto the melamine sponge, the sodium alginate was gelated and this composite showed good efficacy to adsorb Cu (II). The synthesized blend showed porosity, 3D networking. Chelation of Cu(II) occurs with nitrogen and oxygen-containing moieties (Feng et al., 2018). Costa and his colleagues crosslinked the alginate with poly(vinyl alcohol) (PVA). This composite was used for the adsorption of ytterbium (rare earth metal) from the solution. Yttrium was recovered approximately 90% and analysis revealed the involvement of –OH, –COOH functional groups for adsorption process (Barcelos da Costa et al., 2021). Sodium alginate grafted polyacrylamide/GO (SA-PAM/GO) hydrogel was synthesized via free-radical polymerization and this composite showed adsorption potential of 68.76 and 240.69 mg/g for Cu^{2+} and Pb^{2+}, respectively (Fig. 21.4). Composite possessed the 60% adsorption potential even after five cycles of use (Jiang et al., 2020). Carbonaceous materials are porous possess large adsorption sites and excellent mechanical strength so they favor the adsorption process (Verma et al., 2020). The formation

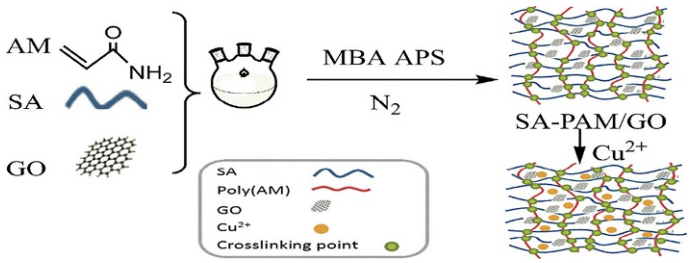

FIG. 21.4 Synthesis of SA-PAM/GO composite and its efficiency toward the removal of Cu^{2+} and Pb^{2+} (Jiang et al., 2020).

of composites of carbonaceous materials with sodium alginate takes benefit of the properties of materials and also made them cost-friendly.

21.3.2 Nanomaterials-based sodium alginate composites

Nanomaterials are small size materials possessing a large surface area, excellent strength and can be functionalized easily. Compositing of nanomaterials with sodium alginate may improve the structure and adsorption efficacy toward heavy metals. A group of researchers incorporated the magnetic Fe_3O_4 nanoparticles into thiourea modified sodium alginate and this composite was used for removal of Hg (II) from solution (Patiño-Ruiz et al., 2019). Toxic metal ions form bond with electron donor moieties (–OH, $–NH_2$) of composite. The nanomagnetic particles provide paramagnetic features to composite and adsorbents can be easily separated from media. In the latest study, magnetite manganese oxide-based nanoparticles were immobilized onto alginate lead to the synthesis of xerogel. This environment-friendly mesoporous and thermally stable composite was used to adsorb Cr(VI) and Cd(II) with good adsorption potential of 3.86 mg/g and 3.95 mg/g (@ 120 min of contact time)for metals, respectively. This synthesized composite showed reusability of approximately six times (Kumar et al., 2021). Nano-silica and nano-maghemite were encapsulated in sodium alginate for adsorption of Pb (II) from solution (Idris et al., 2012; Soltani et al., 2014). Recently magnetic nanosphere of 15–22 nm size was prepared through electrostatic interaction between sodium alginate and amino-based magnetic nanoparticles. The synthesized polyelectrolyte nanosphere showed an adsorption potential of 105.8 mg/g for Pb (II) (Wang et al., 2021). The doping of MOFs with alginates has been reported recently. UiO-66 MOF was doped with alginate which leads to the synthesis of the UiO-66@Abs and this composite showed effective adsorption of Cr (VI) (98%) @pH 6. And desorption (@ 2 M HCl) regenerate the UiO-66@Abs composite (Daradmare et al., 2021). Sodium alginate composites with nanomaterials enhance the surface area, oxygen having functional moieties and affinity toward heavy metals. These green composites are great materials at nano-scale environmental remediation.

21.4 Role of alginate-based composites for removal of dyes

Dyes are colored organic molecules and in industries, they are extensively being used. The release of wastewater from industries in our ecosystem is harmful to human health and other living beings. Dyes are removed through the adsorption approach from wastewater through the sorbent. Alginate is a potent adsorbent for the removal of dyes. Composites of alginate with various nanomaterials enhance the efficacy for the removal of dyes. Removal of dyes using various alginate composites has been presented in Table 21.1.

21.4.1 Carbonaceous/polymeric-based sodium alginate composites

According to studies activated carbon immobilized on alginates mitigated a good amount of dyes from the solution. Three alginate composites, bentonite-alginate beads, activated

TABLE 21.1 Alginate-based nanosorbents for removal of dyes and radionuclides from aqueous system.

S. no.	Adsorbant	Adsorbate	Adsorption potential (mg/g)	References
Carbonaceous/polymeric-based sodium alginate composites for removal of dyes				
1	Fe_3O_4/CD/AC/SA composite	Methyl violet, brilliant green	5.882, 2.283	Yadav et al. (2021)
2	*Activated carbon (Ac) biopolymer Alginate (Algn) on blue methylene*	*Methylene blue*	*51.75*	Boucherdoud et al. (2021)
3	Perlite-ca-alginate-activated carbon (PCA) composite	Methylene blue, methyl orange	1111, 909	Chegeni et al. (2021)
4	rGO@HAP-Alginate	Reactive Blue 4, Indigo Carmine, Acid Blue 158	45.56, 47.16, 48.26	Sirajudheen et al. (2021)
5	NaA-cl-Aac/GP hydrogel	Malachite green	628.93	Verma et al. (2020)
6	Acrylamide-based Na-alginate (AM-SA) acrylamide/graphene oxide-based sodium alginate (AM-GO-SA) hydrogels	Crystal violet	62.07, 100.30 mg/g	Pashaei-Fakhri et al. (2021)
7	Alginate/f-CNT-CD-MFA hydrogel beads	Methylene blue	11.76	Mallakpour et al. (2021)
8	Magnetic multi-walled carbon nanotubes-loaded alginate (CNT-Alg-Fe_3O_4	ADMI	138.97 ADMI/g	Azari et al. (2021)
9	ZSM-5 zeolite/PVA/ Carboxymethyl cellulose/Na-alginate (PVA/CNC/SA/ZSM-5)	Malachite green	5.95	Radoor et al. (2021)
10	Chitosan/Na-alginate composite	Acid black, methylene blue	817.0, 1488.1	Zhao et al. (2021)
11	Magnetic alginate/rice husk (m-ALG/RH) beads	Methylene blue	274.9	Alver et al. (2020)
12	Na-alginate-Flax seed ash composite	Methylene blue	333.3	Işık and Uğraşkan (2021)
13	Pectin-alginate/titania	Methylene blue	435–637	Zamri et al. (2021)
14	Na-alginate modified polyacrylamide hydrogel (PAAm/SA)	Methylene blue	90.90	İsmail and Gökçe Kocabay (2021)
15	Na-alginate/chitosan/poly acrylamide/carbon quantum dots (Na-Ala/Chit-cl-polyAAm/CQDs)	Biebrich scharlet	96%	Priya et al. (2020)
16	Phytochemicals crosslinked-Alginate biocomposite	Methylene blue	1442.0	Andreas et al. (2021)
17	Na-alginate-citric acid-k-carrageenan (PEM)	Methylene blue	522.4	Ammar et al. (2021)

TABLE 21.1 Alginate-based nanosorbents for removal of dyes and radionuclides from aqueous system—cont'd

S. no.	Adsorbant	Adsorbate	Adsorption potential (mg/g)	References
18	Na-alginate grafted poly(*N*-vinyl formamide-*co*-acrylic acid)-bentonite clay hybrid hydrogel	Methylene green	2108	Subhan et al. (2021)
19	Alginate polymer modified with pandan leaves	Methylene blue	61%	Nordin et al. (2021)
20	Calcium alginate entrapped sugarcane biochar composite (CA-SB) dye	Methylene blue	95.47%	Biswas et al. (2020)
21	Calcium alginate/basil seed mucilage biobeads	Eriochrome black T	2.80	Javanbakht and Shafiei (2020)
22	Na-alginate – *Oscillatoria* de-oiled biomass (Na-Alg-ODOB)	Basic blue-41	634.4	Maqbool et al. (2020)
23	Magnetic Zeolite/Chitosan/ Alginate (MZ/CS/AL) composite	Methylene blue	0.999	Kazemi and Javanbakht (2020)
24	Alginate encapsulated peanut derived activated carbon (PnsAC-alginate)	Direct Blue-86	21.6	Garg et al. (2019)
25	GO/Ca-Al	Methylene blue	1334	Gunes et al. (2020)
Nanomaterials-based alginate composites for removal of dyes				
25	Na-alginate, Fe (III)/magnetic ferric oxide biopolymer (Fe_3O_4@SA-Fe)	Congo red direct red 23 dyes	3333, 1429	Lv and Li (2021)
26	Mxene/Na-alginate beads ($Ti_3C_2T_x$/ SA) beads	Methylene blue	92.17	Zhang et al. (2021)
27	Hematite (α-Fe_2O_3)/alginate (AG) beads	Methylene blue	100%	Dubey et al. (2020)
28	Encapsulated polyamidoamine-functionalized halloysite/alginates (Alg/Hal-PAMAM) beads	Methylene green, Sunset yellow	62.20, 33.90	Kurczewska et al. (2019)
29	Na-alginate poly(acrylic acid) (SA-poly(AA)), Na-alginate poly(acrylic acid)/zinc oxide (SA-poly(AA)/ ZnO) hydrogel	Methylene blue	1129, 1529.6	Makhado et al. (2020)
30	Fe_3O_4-N-GO@Na-alginate (SA) gel film	Congo Red, Acid Orange 7, Amino Black 10B	74.22%, 45.72%, 37.75%	Chen et al. (2021)
31	Acrylonitrile/Na-alginate (Alg-g-An) copolymer	Methylene blue, Safranin O	0.999, 0.998	Shelar-Lohar and Joshi (2020)

Continued

TABLE 21.1 Alginate-based nanosorbents for removal of dyes and radionuclides from aqueous system—cont'd

S. no.	Adsorbant	Adsorbate	Adsorption potential (mg/g)	References
32	Cobalt ferrite-alginate nanocomposite	Reactive red 195 (RR195), Reactive yellow 145 (RY145)	6.75, 6.06	Jayalakshmi and Jeyanthi (2019)
33	Ca-alginate/bentonite nanocomposite beads	Methylene blue, Congo red	1171, 95.55 mg/g	Oussalah et al. (2019)
34	Activated carbon/copper ferrite/alginate	Methylene blue	400.0	Othman et al. (2020)
35	Na-alginate-gelatin/ZnS nanocomposite	Biebrich scarlet, crystal Violet		Priya et al. (2019)
36	Alginate/carboxylated lignin	Methylene blue	613.0	Kim et al. (2021)
37	GO/Ca-Al	Methylene blue	1334	Gunes et al. (2020)
38	Na-Al/calcium silicate / hydroxyapatite	Eriochrome blue black R	76.80	You et al. (2019)
39	Oxidized alginate/gelatin/silver NPs	Methylene blue	625 mg/g	Abou-Zeid et al. (2019)
40	Nano AgCl/Na-Alg/composite copolymer	Brilliant crystal blue	>95%	Bhangi and Ray (2020)
Removal of radionuclides				
41	*Bacillus subtilis* immobilized chistosan/alginate	U(VI)	–	Tong (2017)
42	Bentonite/alginate	U(VI), Cs(I), Sr^{2+}	11.1, 11.75, 8.73	Abou-Lilah et al. (2020)
43	Go/PVA/alginate	U(VI)	403.78	Yi et al. (2018)
44	Ca-alginate beads	U(VI)	237.15	Yu et al. (2017)
45	Ca-alginate/carboxymethyl chitosan/$Ni_{0.2}Zn_{0.2}Fe_{2.6}O_4$	Nd^{+3}, Tb^{+3}, Dy^{+3}	97.75%, 96.83%, 97.85%	Javadian et al. (2020)
46	TiO_2 microspheres/alginate matrix	U(VI)	31.4	Basu et al. (2020)
47	Lithium-modified montmorillonit/ca-alginate beads (MCA/Li)	Cs^+	100.25	Xia et al. (2018)
48	Titania coated silica sphere functionalized with potassium ferrocyanide/Ca-alginate	$^{134+137}Cs$	23.55	Saha et al. (2017)
49	Alginate humic acid/Fe-aminoclay composite	Sr^{+2}	45.65	Choe et al. (2018)
50	Zeolite/alginate	Sr^{+2}		Hong et al. (2018)

TABLE 21.1 Alginate-based nanosorbents for removal of dyes and radionuclides from aqueous system—cont'd

S. no.	Adsorbant	Adsorbate	Adsorption potential (mg/g)	References
51	Alginate immobilized *Aspergillus nigar*	Th (IV)	303.95	Ding et al. (2019)
52	Alginate/*Haromyces cerevisiae* composite	^{241}Am	4.38×10^{-7} mmol/g	Araujo et al. (2020)
53	Hexadecyl pyridinium (HDPy)-modified Mt (OMt)/alginate beads	ClO_4^-, Sr^{2+}	53.5, 29.6 mg/g	Luo et al. (2020)
54	LDH/GO alginates beads	$^{90}Sr^{2+}$, $^{79}SeO_4^{2-}$		Guo et al. (2020)
55	CeO_2-MoO_3-SiO_2 $(CH_2)_3$-$(Alginate)_2$	^{56}Mn, ^{51}Cr	92.3, 97.4%	Allam et al. (2021)
56	Ca-alginate/ Zinc ferrocyanide (ZnFC)/Cyanex 272	^{137}Cs, ^{60}Co	71.7, 34.9	Lee et al. (2021)

carbon-alginate beads, and activated carbon-bentonite alginate beads, were synthesized through fabrication strategy to mitigate methylene blue (MB) Dye. Activated carbon-bentonite-alginate beads showed a maximum adsorption potential of 756.8 mg/g @ 30 °C (Benhouria et al., 2015). Recently a nanocomposite bead based on iron oxide (Fe_3O_4), activated charcoal (AC) particles with β-cyclodextrin (CD), and sodium alginate (SA) was prepared through an easy and cost-effective approach. The synthesized beads showed excellent adsorbent properties along with magnetic features. Fe_3O_4/CD/AC/SA composite polymeric beads removed cationic dyes; methyl violet (MV) and brilliant green (BG) with adsorption potential of 5.882 and 2.283 mg/g, respectively (Yadav et al., 2021). These polymeric composites possessed adsorption activities even after four cycles and proved capable of regeneration and easy separation. Through co-precipitation strategy, alginate-based reduced graphene oxide hydroxyapatite hybrid (rGO@HAP-Alg) was synthesized. The hybrid removed efficiently three azo dyes; Reactive Blue 4 (RB4), Indigo Carmine (IC), and Acid Blue 158 (AB158) azo dyes with adsorption potential of 45.56, 47.16, and 48.26 mg/g, respectively, from aqueous media (@ pH 6–7). Hydrogen bonding, electrostatic force of interaction, and complexation were found involved in the adsorption mechanism (Sirajudheen et al., 2021). Recently sodium alginate cross-linked acrylic acid/graphite (NaA-cl-AAc/GP) hydrogel composite was synthesized for removal of malachite green (MG) dye. The addition of graphite powder improved the adsorption potential. MG was removed efficiently from the aqueous solution with an adsorption efficiency of 628.93 mg/g. The composite exhibited 91% adsorption capacity even after three cycles. This composite proved promising due to its efficient swelling, excellent adsorption potential eco-friendliness, regeneration capacity (Verma et al., 2020). Fakhri and his colleagues synthesized acrylamide-based sodium alginate (AM-SA) and acrylamide/graphene oxide-based sodium alginate (AM-GO-SA) nanocomposite hydrogels for removal of crystal violet (CV) dye with adsorption efficiency of 62.07 and 100.30 mg/g, respectively (Pashaei-Fakhri et al., 2021). In the latest study, a hybrid of carboxyl functionalized

multi-walled carbon nanotubes (f-CNTs) with carbon dots (CDs) and magnesium fluorohydroxyapatite (MFA) nanoparticles was synthesized. The fabricated nano-hybrid (f-CNT-CD-MFA) was incorporated into alginate to prepare a composite hydrogel bead (alginate/f-CNT-CD-MFA) which was further used for removal of methylene blue (MB) from solution (Fig. 21.5) (Mallakpour et al., 2021). The hydrogel significantly removed the dye.

Recently magnetic multi-walled carbon nanotubes-loaded alginate (CNT-Alg-Fe_3O_4) composite was synthesized for removal of dye ADMI. The adsorption potential was found at 138.97 ADMI/g (@ pH 3, contact time 85.55 min). Adsorbent contained the reusability efficiency of at least 10 cycles. The electrostatic force of interaction and π–π dispersive interactions were found responsible for the interaction of surface functionalities (–OH and –COOH) with dye (Azari et al., 2021). Adsorption potential of alginate for dyes increases with its compositing with Graphenes, CNTs, AC also reduces the cost. But reusability of active carbon is still a concern to solve. CNTs separation through centrifugation is a tedious process so the introduction of magnetic features in CNTs composites is fruitful effort.

Hydrogels have been proved efficient for the removal of dyes and this is documented well by a group of researchers (Pereira et al., 2021). Recently sodium alginate-modified polyacrylamide-sodium alginate (PAAm/SA) hydrogels were fabricated and this composite hydrogel efficiently removed the methyl blue with the adsorptive potential of 90.09 mg/g (@ pH 7) (İsmail and Gökçe Kocabay, 2021).

Natural materials are attractive to fabricate eco-friendly, cost-effective, potential adsorbents. Chitosan- sodium alginate composite was synthesized through a lyophilization approach. This unique amphoteric adsorbent significantly adsorbed the Acid black and methylene blue with adsorption efficacy of 817.0 mg/g and cationic Methylene Blue 1488.1 mg/g, respectively, over a wide range of pH. Both cationic and anionic dyes were

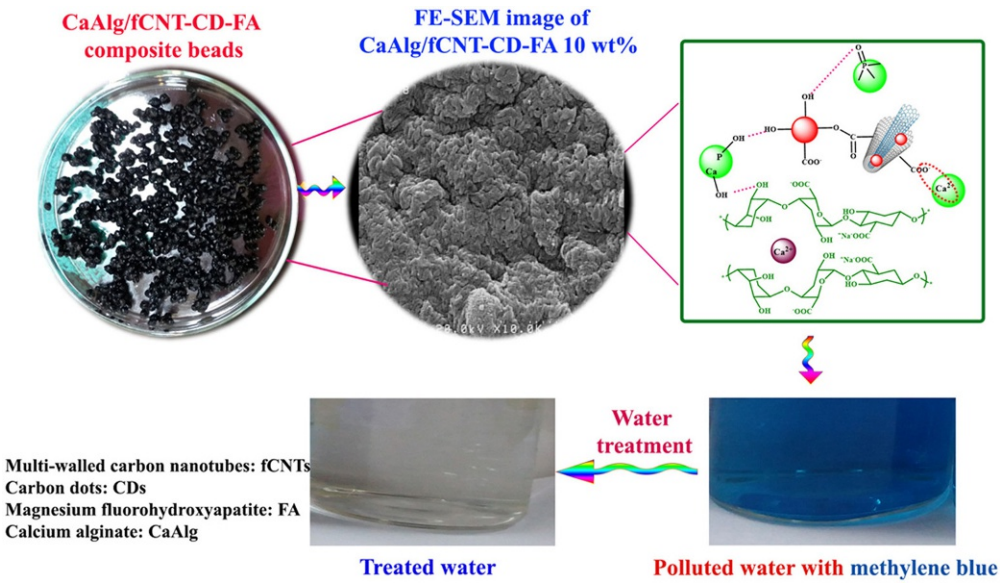

FIG. 21.5 Schematic illustration of alginate/f-CNT-CD-MFA hydrogel bead for removal of methylene blue (Mallakpour et al., 2021).

adsorbed through chemisorption (Zhao et al., 2021). Recently, biocomposite of magnetic alginate/rice husk (m-ALG/RH) beads were fabricated through gelation approach and employed to remove dye methylene blue. The composite proved promising to remove MB with an adsorption efficiency of 274.9 mg/g and it was found eco-friendly, cost-effective adsorbent (Alver et al., 2020). Composite of Sodium alginate with Flaxseed ash was found promising for removal of methylene blue with adsorption efficacy of 333.3 mg/g (@ pH 7, 50 °C) (Işık and Uğraşkan, 2021). The adsorptive potential of pectin-alginate-titania (PAT) composites for methylene blue was found to be in the range of 435–637 mg/g in an aqueous solution. The adsorptive potential of the membrane increased with an increase in titanium nanoparticles due to enhancement in surface area (Zamri et al., 2021). Phytochemicals extracted from cabbage (phenolics, flavonoids, anthocyanins) were crosslinked with alginate through glutaraldehyde to fabricate biocomposite hydrogel beads. The adsorption capacity for methylene blue was found to be 1442.0 mg/g @pH 11.0 (Fig. 21.6) (Andreas et al., 2021). Calcium alginate entrapped sugarcane biochar composite (CA-SB) was synthesized and employed for the adsorption of methylene blue. The composite adsorbed the 95.47% dye (Biswas et al., 2020). Activated carbon derived from peanut shells was encapsulated in alginate to fabricate the nanobiosorbent (PnsAC-alginate). The nanomaterial removed the Direct Blue-86 from aqueous media with an adsorption efficacy of 21.6 mg/g. Alginate modified peanut shell activated carbon showed a 7% improved adsorption potential in comparison to unmodified activated carbon adsorbent (Garg et al., 2019). The use of natural materials for the production of adsorbents to mitigate environmental pollutants is ecofriendly and cost-effective.

21.4.2 Nanomaterials-based sodium alginate composites

Crosslinking of sodium alginate, Fe (III), and incorporation of magnetic ferric oxide lead to the synthesis of alginate-based biopolymer Fe_3O_4@SA-Fe. The synthesized polymer

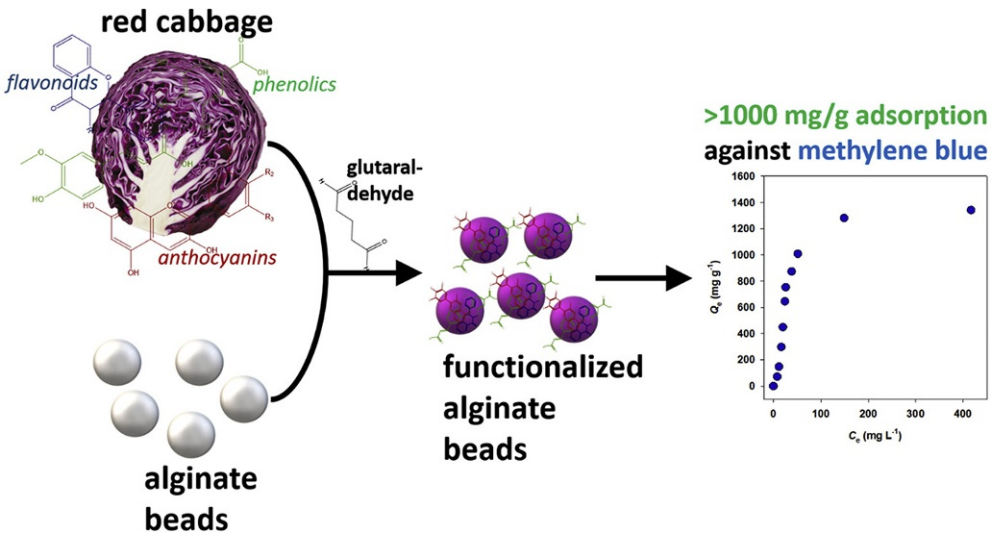

FIG. 21.6 Removal efficacy of cabbage photochemical-alginate biocomposite against methylene blue (Andreas et al., 2021).

efficiently adsorb the congo red and direct red 23 dyes with adsorption efficiency of 3333 and 1429 mg/g, respectively. Polymer exhibited excellent adsorptive potential, stability at room temperature. Analytical studies revealed that hydrogen bonding, complexation, and electrostatic force of interaction were responsible for the adsorption of dyes on Fe_3O_4@SA-Fe. The magnetic property incorporated in polymer made it easily separable for media (Lv and Li, 2021) (Fig. 21.7). Mxenes are transition metal carbide/nitride nanomaterials and they possess a large surface area, active site, hydrophilic nature and have excellent adsorptive potential and it may play a great role in the adsorption of dyes from the environment (Zhang et al., 2018a). In a recent study, through ionic crosslinking the mxene ($Ti_3C_2T_x$ (T = OH, O, F)) was immobilized on sodium alginate to form $Ti_3C_2T_x$/SA beads. Mxene was tightly bound on SA so the loss of adsorbent was avoided and adsorption potential increased. The synthesized composite adsorbed the methylene blue with an adsorption potential of 92.17 mg/g @ pH 7. After three cycles the material retained the adsorption efficacy (81.36%) (Zhang et al., 2021). Hematite (α-Fe_2O_3)/alginate (AG) beads were fabricated for the removal of methylene blue. At room temperature nanocomposite removed the 100% dye within 40 min (@ pH 9) (Dubey et al., 2020). In another study, hybrid beads were fabricated by encapsulation of polyamidoamine-functionalized halloysite into alginates (Alg/Hal-PAMAM). These beads adsorbed the methyl green and sunset yellow with excellent adsorption efficacy of 62.20 and 33.90 mg/g, respectively. Hybrid beads showed higher efficacy in comparison of pure-alginates (Kurczewska et al., 2019). Makhado and his colleagues fabricated sodium alginate poly(acrylic acid) (SA-poly(AA)) and sodium alginate poly(acrylic acid)/zinc oxide (SA-poly(AA)/ZnO) hydrogel nanocomposite through free-radical polymerization reaction for removal of methylene blue. ZnO-based composite showed high swelling due to more water up taking capacity so it adsorbed more methylene blue (adsorption efficiency = 1529.6 mg/g) from aqueous media (@pH 6) in comparison to the SA-poly (AA) hydrogel (adsorption efficiency = 1129 mg/g) (Makhado et al., 2020). Cobalt ferrite-Alginate nanocomposite was fabricated by embedding cobalt ferrite nanoparticles into alginate. This composite showed efficiency to remove Reactive red 195 (RR195) and Reactive yellow 145 (RY145) from textile effluent with adsorption potential of 6.75 and 6.06 mg/g, respectively (Jayalakshmi and Jeyanthi, 2019). This nanocomposite was easy to separate due to magnetic properties and reused successfully until five consecutive cycles. Hybrid gel beads are more efficient for the removal of dyes from aqueous media in comparison to unloaded beads (Cavallaro et al., 2013) (Table 21.1).

21.5 Removal of radionuclides

Radionuclides are also called radioisotopes (uranium, radium, chromium, plutonium, strontium, etc.) and they possess excess energy. These are produced during research activities, fission reaction, and explosions. They also undergo radioactively and cause environmental pollution, interact with the food chain and destroy human health. They may be removed for various mediums through the adsorption mechanism. Alginate-based nano-composites play a great role in the removal of radionuclides from the ecosystem (Sutirman et al., 2021). Various alginate-based nanosorbents with their adsorption potential have been

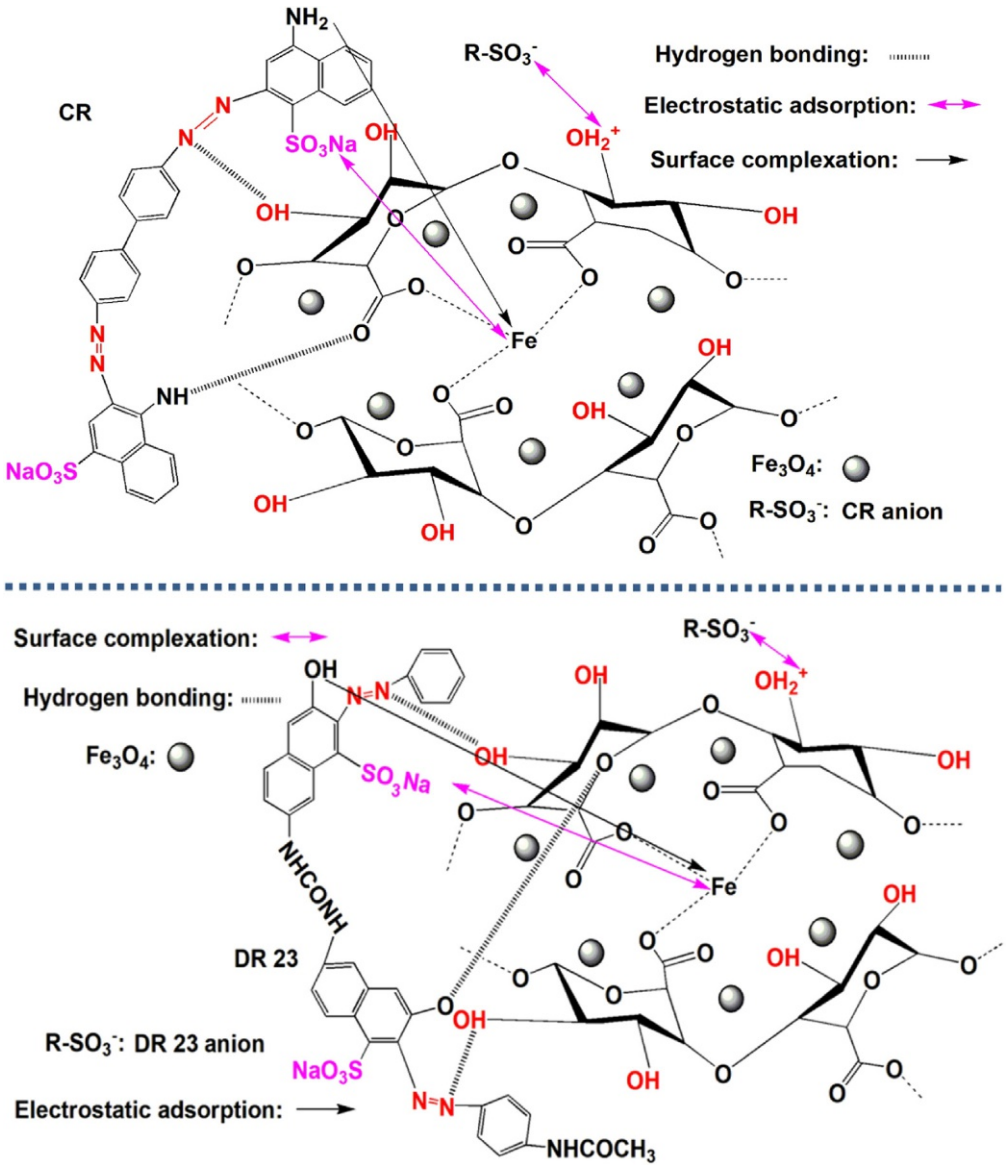

FIG. 21.7 Schematic illustration of adsorption of Congo red and direct red 23 dyes on Fe_3O_4@SA-Fe (Lv and Li, 2021).

discussed in Table 21.1. *Bacillus subtilis* was immobilized on chistosan/alginate and this composite efficiently removed U(VI) from aqueous media (Tong, 2017). In another finding, Go was embedded in PVA/alginate for adsorption of U(VI) with an efficiency of 403.78 mg/g (Yi et al., 2018). Calcium Alginate beads adsorbed the U(VI) with the efficiency of 237.15 mg/g. This adsorption was found pH dependent (Yu et al., 2017). Lithium-modified

montmorillonite encapsulated into ca-alginate beads was synthesized through an ion exchange strategy. This adsorbent (MCA/Li) removed Cesium (Cs^{+}) with an adsorption potential of 100.25 mg/g (Xia et al., 2018). This adsorbent was cost-effective and possessed an excellent adsorptive potential for radioactive wastewater treatment. Titania coated silica sphere functionalized with potassium ferrocyanide impregnated with calcium alginate was synthesized by following the sol-gel method. The synthesized composite removed ^{134} ^{+137}Cs from drinking water with potential adsorption of 23.55 mg/g (Saha et al., 2017). Lee and his group synthesized alginate humic acid/Fe-aminoclay composite to remove strontium (Sr^{+2}) from the aqueous media. Adsorption increased with an increase in ions concentration. Maximum adsorption potential was found to be 45.65 mg/g (Choe et al., 2018). The adsorbent was eco-friendly, cost-effective, and biocompatible. Alginates are efficient to remove strontium ions from seawater but high sodium concentrations cause damage to hydrogel by over swelling. To improve its strength, Hong and his colleagues fabricated the hybrid of alginate with zeolite (Hong et al., 2018) to adsorb Sr ions from seawater. Zeolite enhanced the active sites so adsorption potential was enhanced. 10% zeolite alginate form exhibited maximum adsorption and it was found resistant to swelling with enhanced mechanical strength (Hong et al., 2018). Recently alginate immobilized *Aspergillus nigar* adsorbent was fabricated to remove Thorium. Biosorbent was rich in functional moieties and it formed a complex with thorium to adsorb it. Th (IV) was adsorbed with an adsorption potential of 303.95 mg/g (@ pH 6, 40 °C) (Ding et al., 2019). Biomaterial possessed recyclability. Alginate immobilized *Haromyces cerevisiae* composite was synthesized to remove americium (^{241}Am) from an aqueous medium. Maximum adsorption of ^{241}Am (4.38×10^{-7} mmol/g) was obtained at pH 4 (Araujo et al., 2020). Recently hexadecyl pyridinium (HDPy)-modified Mt (OMt) was encapsulated in alginate beads was synthesized and it was used to adsorb ClO_4^- and Sr^{+2}. Encapsulation of alginate reduced the release of organic components (HDPy) almost 78% times. Composite adsorbed the ClO_4^- and Sr^{2+} with adsorption potential of 53.5, 29.6 mg/g (Luo et al., 2020). LDH/GO alginates beads were synthesized to remove both $^{90}Sr^{2+}$ and $^{79}SeO_4^{2-}$ from water and soil and significant adsorption was obtained (Guo et al., 2020). Alginate materials proved efficient in the removal of radionuclides so they should be used on an industrial level to remove pollution.

21.6 Removal of pharmaceutical contaminants

Pharmaceutical-based contaminants are posing serious health issues. They are present in low concentration in the ecosystem but they are destroying human health. Various reports are available where alginate-based sorbents were used for the removal of pharmaceutical-based pollutants from wastewater. Magnetic alginate beads have been used for the removal of antibiotics. Kim and his colleagues used nZVI-immobilized alginate beads for adsorption of trichloro-ethylene (>99.8%) (Kim et al., 2010). Konwar and his colleagues synthesized the magnetic alginate-Fe_3O_4 hydrogel fibers for the effective removal of ciprofloxacin. There, anion exchange mechanism was found responsible for adsorption efficiency (Konwar et al., 2015). Magnetic alginate composites are cost-effective, show better adsorption and thermally stable and easy to fabricate which made them a highly valuable adsorption strategy for

environmental pollutants. In another study GO/Ca-Al bio-composite was synthesized by wet spinning to remove ciprofloxacin. The addition of GO enhanced the strength, porous active sites in composite so adsorption potential was enhanced as well (Fei et al., 2016). Zhu and his colleagues reported the adsorption of tetracycline through GO/Ca-Al composite. Tetracycline was adsorbed with the potential of 131.6 mg/g. Hydrogen bonding and π-π were found responsible for the adsorption of tetracycline onto composite (Zhu et al., 2018). In another research, physical and chemical modifications were carried on alginate/graphene double network hydrogel. The modified gel showed enhanced adsorption of tetracycline (290.70 mg/g) and ciprofloxacin (344.83 mg/g) as compared to unmodified gel (Zhuang et al., 2017). Recently copper alginate/GO composite was synthesized by freeze-drying method. Up to 98%, tetracycline was removed by using synthesized composite. After four cycles of usage still composite retained 85% efficacy (Cui et al., 2021). Recently, double metal crosslinked alginate/GO hydrogel was synthesized and it was used for the removal of tetracycline. The composite showed excellent stability and retained activity even after four cycles of use (Kong et al., 2020). Xue and his colleagues fabricated the biocatalyst by amassing co-immobilization of encapsulating mediator 2,2′-Azino-bis-(3-ethylbenzthiazoline-6-sulphonate) into the ca-alginate biocomposite beads by grafting glycidyl methacrylate and dopamine and then immobilizing laccase covalently onto beads. The biocatalyst removed 100% acridine in 8 h (Xue et al., 2020). Ni-Fe was immobilized on alginate to fabricate the NiFe nanocomposite beads. This ecofriendly composite removed the tetracycline with the capacity of 487 mg/g (Ravikumar et al., 2020). Anti-depressant-related pollutants are toxic for health. A group of researchers used the glutaraldehyde crosslinked alginate beads to remove duloxetine hydrochloride (anti-depressant drug) from aqueous media. The maximum adsorption capacity was found at 14.83 mg. The high adsorption was attributed to surface functional moieties (Ertuğruloğlu et al., 2020). The removal of the anti-hypertensive drug (propranolol HCl) has been removed through alginate beads. Alginate beads showed an adsorption efficacy of 93%. Adsorption of the drug onto the surface of alginate was attributed to the presence of carboxyl and hydroxyl functional moieties (Coelho et al., 2020). Guenes and his colleagues synthesized the GO/Ca-Alg biocomposite (2 pH 4, in 0.1 M HCl) and employed it for the removal of Famotidine and Diclofenac. The biocomposite showed adsorption capacity of 35.50 and 36.35 mg/g for Famotidine and Diclofenac, respectively (Gunes et al., 2020). Al_2O_3/*Chlorella vulgaris* immobilized in sodium alginate beads were fabricated to remove carbamazepine which is an anti-convulsant drug. The synthesized beads adsorbed the drug with a rate of 89.6%. Alginate beads showed great CBZ removal after even three-time recycling. This approach is approved effective for the removal of drugs (Yi-cheng et al., 2020). Non-steroidal anti-inflammatory drugs can also be removed by alginate-based composites. Recently Activated carbon-based alginate beads removed naproxen from aqueous medium through adsorption around 98%. Beads were regenerated by ethanol after seven cycles of use (Ozcan and Saloglu, 2020). CNTs/L-cys@GO/SA hybrid composite has been used to adsorb ciprofloxacin. Different adsorption capacity was achieved at different temperature. At 25 °C and 15 °C the ciprofloxacin was adsorbed with a potential of 181 and 200 mg/g, respectively. At low temperature better adsorption was obtained. This multinetwork composite showed good adsorption of the drug in weak acidic conditions at low temp and less salt concentration (Ma et al., 2020). So changing environmental conditions may promote drug adsorption on alginate-based composites.

21.7 Conclusion and future perspectives

Alginate composites were fabricated by encapsulation of an array of materials including Graphene oxide, activated carbon, carbon nanotubes, microbes, nanomaterials into hydrogel or beads with utilization as adsorbents of environmental contaminants. Hydrogen bonding, chelation, ion exchange, electrostatic interaction were involved in the adsorption process of contaminants on the surface of alginate composite which possess plenty of functional moieties. Alginate-based composites offered great potential for the removal of heavy metals, dyes, pharmaceutical-based contaminants and radionuclides from aqueous solutions. Alginate composites exhibited improved stability, strength, and adsorption features in comparison to pure alginates. The derived composites were easy to separate, can be regenerated after use, less risk to the environment of encapsulated materials, and optimized strategies. Considering the future perspectives, the uptake mechanisms involved in contaminants by alginate composites should be studied in detail. There is a need to optimize existing and novel new engineered alginate-based composites with diverse features and functionalities for targeted applications. New techniques should be developed to advance the designing of alginate composites with a more effective combination with versatile materials to enhance adsorption, stability, and strength. Chemical modification of surface moieties of alginate may change the features of alginate and this can be a future area of research to develop novel alginate composites for targeted applications. Most studies regarding alginate composites have been carried out in laboratories there is a need to scale up on an industrial scale.

Acknowledgment

The Author Dr. Komal Rizwan is highly thankful to Dr. Ahmad Shakeel, Faculty of Civil Engineering & Geosciences, Delft University of Technology, The Netherlands for helping to provide literature.

References

Abou-Lilah, R.A., Rizk, H.E., Elshorbagy, M.A., Gamal, A.M., Ali, A.M., Badawy, N.A., 2020. Efficiency of bentonite in removing cesium, strontium, cobalt and uranium ions from aqueous solution: encapsulation with alginate for column application. Int. J. Environ. Anal. Chem., 1–24.

Abou-Zeid, R.E., Awwad, N.S., Nabil, S., Salama, A., Youssef, M.A., 2019. Oxidized alginate/gelatin decorated silver nanoparticles as new nanocomposite for dye adsorption. Int. J. Biol. Macromol. 141, 1280–1286. https://doi.org/10.1016/j.ijbiomac.2019.09.076.

Agüero, L., Zaldivar-Silva, D., Peña, L., Dias, M.L., 2017. Alginate microparticles as oral colon drug delivery device: a review. Carbohydr. Polym. 168, 32–43.

Akhtar, M.F., Hanif, M., Ranjha, N.M., 2016. Methods of synthesis of hydrogels … a review. Saudi Pharm. J. 24 (5), 554–559. https://doi.org/10.1016/j.jsps.2015.03.022.

Allam, E.A., El-Sharkawy, R.M., Gizawy, M.A., Mahmoud, M.E., 2021. Assembly of CeO2–MoO3–SiO2(CH2)3-(Alginate)2 As a novel nanocomposite for removal of MnII/CrVI and 56Mn/51Cr radionuclides from water. Mater. Chem. Phys. 262, 124278. https://doi.org/10.1016/j.matchemphys.2021.124278.

Alver, E., Metin, A.Ü., Brouers, F., 2020. Methylene blue adsorption on magnetic alginate/rice husk bio-composite. Int. J. Biol. Macromol. 154, 104–113. https://doi.org/10.1016/j.ijbiomac.2020.02.330.

Ammar, C., Alminderej, F.M., EL-Ghoul, Y., Jabli, M., & Shafiquzzaman, M., 2021. Preparation and characterization of a new polymeric multi-layered material based K-carrageenan and alginate for efficient bio-sorption of methylene blue dye. Polymers 13 (3), 411.

Andreas, A., Winata, Z.G., Santoso, S.P., Angkawijaya, A.E., Yuliana, M., Soetaredjo, F.E., Ju, Y.-H., 2021. Biocomposite hydrogel beads from glutaraldehyde-crosslinked phytochemicals in alginate for effective removal of methylene blue. J. Mol. Liq. 329, 115579. https://doi.org/10.1016/j.molliq.2021.115579.

Araujo, L.G.D., Borba, T.R.D., Ferreira, R.V.D.P., Canevesi, R.L.S., Silva, E.A.D., Dellamano, J.C., Marumo, J.T., 2020. Use of calcium alginate beads and Saccharomyces cerevisiae for biosorption of ^{241}Am. J. Environ. Radioact. 223–224, 106399. https://doi.org/10.1016/j.jenvrad.2020.106399.

Ates, B., Koytepe, S., Ulu, A., Gurses, C., Thakur, V.K., 2020. Chemistry, structures, and advanced applications of nanocomposites from biorenewable resources. Chem. Rev. 120 (17), 9304–9362. https://doi.org/10.1021/acs.chemrev.9b00553.

Azari, A., Nabizadeh, R., Mahvi, A.H., Nasseri, S., 2021. Magnetic multi-walled carbon nanotubes-loaded alginate for treatment of industrial dye manufacturing effluent: adsorption modelling and process optimisation by central composite face-central design. Int. J. Environ. Anal. Chem., 1–21.

Bai, C., Wang, L., Zhu, Z., 2020. Adsorption of Cr (III) and Pb (II) by graphene oxide/alginate hydrogel membrane: characterization, adsorption kinetics, isotherm and thermodynamics studies. Int. J. Biol. Macromol. 147, 898–910.

Barcelos da Costa, T., Carlos da Silva, M.G., Adeodato Vieira, M.G., 2021. Development of a natural polymeric bioadsorbent based on sericin, alginate and poly(vinyl alcohol) for the recovery of ytterbium from aqueous solutions. J. Clean. Prod. 279, 123555. https://doi.org/10.1016/j.jclepro.2020.123555.

Basu, H., Pimple, M.V., Saha, S., Patel, A., Dansena, C., Singhal, R.K., 2020. TiO2 microsphere impregnated alginate: a novel hybrid sorbent for uranium removal from aquatic bodies. New J. Chem. 44 (10), 3950–3960. https://doi.org/10.1039/C9NJ06006E.

Benhouria, A., Islam, M.A., Zaghouane-Boudiaf, H., Boutahala, M., Hameed, B., 2015. Calcium alginate–bentonite–activated carbon composite beads as highly effective adsorbent for methylene blue. Chem. Eng. J. 270, 621–630.

Bhangi, B.K., Ray, S.K., 2020. Nano silver chloride and alginate incorporated composite copolymer adsorbent for adsorption of a synthetic dye from water in a fixed bed column and its photocatalytic reduction. Int. J. Biol. Macromol. 144, 801–812. https://doi.org/10.1016/j.ijbiomac.2019.09.070.

Biswas, S., Mohapatra, S.S., Kumari, U., Meikap, B.C., Sen, T.K., 2020. Batch and continuous closed circuit semi-fluidized bed operation: removal of MB dye using sugarcane bagasse biochar and alginate composite adsorbents. J. Environ. Chem. Eng. 8 (1), 103637. https://doi.org/10.1016/j.jece.2019.103637.

Boucherdoud, A., Kherroub, D., Bestani, B., Benderdouche, N., Douinat, O., 2021. Fixed-bed adsorption dynamics of methylene blue from aqueous solution using alginate-activated carbon composites adsorbents. Alger. J. Environ. Sci. Technol.

Cavallaro, G., Gianguzza, A., Lazzara, G., Milioto, S., Piazzese, D., 2013. Alginate gel beads filled with halloysite nanotubes. Appl. Clay Sci. 72, 132–137.

Chan, L., Jin, Y., Heng, P., 2002. Cross-linking mechanisms of calcium and zinc in production of alginate microspheres. Int. J. Pharm. 242 (1–2), 255–258.

Chegeni, M., Etemadpour, S., Fekri, M.H., 2021. The perlite-calcium alginate-activated carbon composite as an efficient adsorbent for the removal of dyes from aqueous solutions. Phys. Chem. Res. 9 (1), 1–16.

Chen, J., Hu, H., Yang, J., Xue, H., Tian, Y., Fan, K., Liu, Y., 2021. Removal behaviors and mechanisms for series of azo dye wastewater by novel nano constructed macro-architectures material. Bioresour. Technol. 322, 124556. https://doi.org/10.1016/j.biortech.2020.124556.

Choe, S.R., Haldorai, Y., Jang, S.-C., Rethinasabapathy, M., Lee, Y.-C., Han, Y.-K., Huh, Y.S., 2018. Fabrication of alginate/humic acid/Fe-aminoclay hydrogel composed of a grafted-network for the efficient removal of strontium ions from aqueous solution. Environ. Technol. Innov. 9, 285–293. https://doi.org/10.1016/j.eti.2017.12.008.

Coelho, C.M., de Andrade, J.R., da Silva, M.G.C., Vieira, M.G.A., 2020. Removal of propranolol hydrochloride by batch biosorption using remaining biomass of alginate extraction from Sargassum filipendula algae. Environ. Sci. Pollut. Res. 27 (14), 16599–16611. https://doi.org/10.1007/s11356-020-08109-4.

Cui, M., Li, Y., Sun, Y., Wang, H., Li, M., Li, L., Xu, W., 2021. Degradation of tetracycline in polluted wastewater by persulfate over copper alginate/graphene oxide composites. J. Polym. Environ. https://doi.org/10.1007/s10924-020-02038-6.

Daradmare, S., Xia, M., Le, V.N., Kim, J., Park, B.J., 2021. Metal–organic frameworks/alginate composite beads as effective adsorbents for the removal of hexavalent chromium from aqueous solution. Chemosphere 270, 129487. https://doi.org/10.1016/j.chemosphere.2020.129487.

Ding, H., Luo, X., Zhang, X., Yang, H., 2019. Alginate-immobilized Aspergillus niger: characterization and biosorption removal of thorium ions from radioactive wastewater. Colloids Surf. A Physicochem. Eng. Asp. 562, 186–195. https://doi.org/10.1016/j.colsurfa.2018.11.032.

Dubey, M., Wadhwa, S., Kumar, R., 2020. Synthesis of hematite/alginate beads nanocomposite and its application in organic dye removal. Mater. Today 28, 70–73. https://doi.org/10.1016/j.matpr.2020.01.302.

Ertuğruloğlu, P., Gulcan, H.O., Ifebajo, A.O., Fallah, A., Sahin, M.F., Gazi, M., 2020. Removal of duloxetine from aqueous solution by adsorption onto chemical crosslinked alginate beads. J. Dispers. Sci. Technol., 1–8. https://doi.org/10.1080/01932691.2020.1844013.

Fei, Y., Li, Y., Han, S., Ma, J., 2016. Adsorptive removal of ciprofloxacin by sodium alginate/graphene oxide composite beads from aqueous solution. J. Colloid Interface Sci. 484, 196–204.

Feng, Y., Wang, Y., Wang, Y., Zhang, X.-F., Yao, J., 2018. In-situ gelation of sodium alginate supported on melamine sponge for efficient removal of copper ions. J. Colloid Interface Sci. 512, 7–13.

Garg, D., Majumder, C.B., Kumar, S., Sarkar, B., 2019. Removal of Direct Blue-86 dye from aqueous solution using alginate encapsulated activated carbon (PnsAC-alginate) prepared from waste peanut shell. J. Environ. Chem. Eng. 7 (5), 103365. https://doi.org/10.1016/j.jece.2019.103365.

Grant, G.T., Morris, E.R., Rees, D.A., Smith, P.J., Thom, D., 1973. Biological interactions between polysaccharides and divalent cations: the egg-box model. FEBS Lett. 32 (1), 195–198.

Gunes, B., Jaquet, Y., Sánchez, L., Carrocera, R., McGlade, D., Quilty, B., Lawler, J., 2020. Activated Graphene Oxide-Calcium Alginate Beads for Adsorption of Methylene Blue and Pharmaceuticals. https://doi.org/10.20944/preprints202009.0562.v1. Preprints 2020090562.

Guo, B., Kamura, Y., Koilraj, P., Sasaki, K., 2020. Co-sorption of Sr2+ and SeO42− as the surrogate of radionuclide by alginate-encapsulated graphene oxide-layered double hydroxide beads. Environ. Res. 187, 109712.

Hong, H.-J., Kim, B.-G., Hong, J., Ryu, J., Ryu, T., Chung, K.-S., Park, I.-S., 2017. Enhanced Sr adsorption performance of MnO2-alginate beads in seawater and evaluation of its mechanism. Chem. Eng. J. 319, 163–169.

Hong, H.-J., Kim, B.-G., Ryu, J., Park, I.-S., Chung, K.-S., Lee, S.M., Ryu, T., 2018. Preparation of highly stable zeolite-alginate foam composite for strontium(90Sr) removal from seawater and evaluation of Sr adsorption performance. J. Environ. Manage. 205, 192–200. https://doi.org/10.1016/j.jenvman.2017.09.072.

Idris, A., Ismail, N.S.M., Hassan, N., Misran, E., Ngomsik, A.-F., 2012. Synthesis of magnetic alginate beads based on maghemite nanoparticles for Pb (II) removal in aqueous solution. J. Ind. Eng. Chem. 18 (5), 1582–1589.

Işık, B., Uğraşkan, V., 2021. Adsorption of methylene blue on sodium alginate–flax seed ash beads: isotherm, kinetic and thermodynamic studies. Int. J. Biol. Macromol. 167, 1156–1167. https://doi.org/10.1016/j.ijbiomac.2020.11.070.

İsmail, O., Gökçe Kocabay, Ö., 2021. Absorption and adsorption studies of polyacrylamide/sodium alginate hydrogels. Colloid Polym. Sci. 299 (5), 783–796. https://doi.org/10.1007/s00396-020-04796-0.

Javadian, H., Ruiz, M., Saleh, T.A., Sastre, A.M., 2020. Ca-alginate/carboxymethyl chitosan/Ni0.2Zn0.2Fe2.6O4 magnetic bionanocomposite: synthesis, characterization and application for single adsorption of Nd+3, Tb+3, and Dy+3 rare earth elements from aqueous media. J. Mol. Liq. 306, 112760. https://doi.org/10.1016/j.molliq.2020.112760.

Javanbakht, V., Shafiei, R., 2020. Preparation and performance of alginate/basil seed mucilage biocomposite for removal of eriochrome black T dye from aqueous solution. Int. J. Biol. Macromol. 152, 990–1001. https://doi.org/10.1016/j.ijbiomac.2019.10.185.

Jayalakshmi, R., Jeyanthi, J., 2019. Simultaneous removal of binary dye from textile effluent using cobalt ferrite-alginate nanocomposite: performance and mechanism. Microchem. J. 145, 791–800. https://doi.org/10.1016/j.microc.2018.11.047.

Jiang, H., Yang, Y., Lin, Z., Zhao, B., Wang, J., Xie, J., Zhang, A., 2020. Preparation of a novel bio-adsorbent of sodium alginate grafted polyacrylamide/graphene oxide hydrogel for the adsorption of heavy metal ion. Sci. Total Environ. 744, 140653. https://doi.org/10.1016/j.scitotenv.2020.140653.

Kazemi, J., Javanbakht, V., 2020. Alginate beads impregnated with magnetic Chitosan@Zeolite nanocomposite for cationic methylene blue dye removal from aqueous solution. Int. J. Biol. Macromol. 154, 1426–1437. https://doi.org/10.1016/j.ijbiomac.2019.11.024.

Kim, H., Hong, H.-J., Jung, J., Kim, S.-H., Yang, J.-W., 2010. Degradation of trichloroethylene (TCE) by nanoscale zero-valent iron (nZVI) immobilized in alginate bead. J. Hazard. Mater. 176 (1–3), 1038–1043.

Kim, J.-C., Kim, J., Park, J., Oh, J.-K., Choi, I.-G., Kwak, H.W., 2021. Highly efficient and sustainable alginate/carboxylated lignin hybrid beads as adsorbent for cationic dye removal. React. Funct. Polym. 161, 104839. https://doi.org/10.1016/j.reactfunctpolym.2021.104839.

Kong, Y., Zhuang, Y., Shi, B., 2020. Tetracycline removal by double-metal-crosslinked alginate/graphene hydrogels through an enhanced Fenton reaction. J. Hazard. Mater. 382, 121060. https://doi.org/10.1016/j.jhazmat.2019.121060.

Konwar, A., Gogoi, A., Chowdhury, D., 2015. Magnetic alginate–Fe3O4 hydrogel fiber capable of ciprofloxacin hydrochloride adsorption/separation in aqueous solution. RSC Adv. 5 (99), 81573–81582.

Kumar, A., Prasad, S., Saxena, P.N., Ansari, N.G., Patel, D.K., 2021. Synthesis of an alginate-based Fe3O4–MnO2 xerogel and its application for the concurrent elimination of Cr(VI) and cd(II) from aqueous solution. ACS Omega 6 (5), 3931–3945. https://doi.org/10.1021/acsomega.0c05787.

Kurczewska, J., Cegłowski, M., Schroeder, G., 2019. Alginate/PAMAM dendrimer—halloysite beads for removal of cationic and anionic dyes. Int. J. Biol. Macromol. 123, 398–408. https://doi.org/10.1016/j.ijbiomac.2018.11.119.

Lee, H.-K., Choi, J.-W., Kim, J.-H., Kim, C.-R., Choi, S.-J., 2021. Simultaneous selective removal of cesium and cobalt from water using calcium alginate-zinc ferrocyanide-Cyanex 272 composite beads. Environ. Sci. Pollut. Res. https://doi.org/10.1007/s11356-021-13342-6.

Liu, H., Guo, L., Liao, S., Wang, G., 2012. Reutilization of immobilized fungus Rhizopus sp. LG04 to reduce toxic chromate. J. Appl. Microbiol. 112 (4), 651–659.

Liu, C., Ye, J., Lin, Y., Wu, J., Price, G.W., Burton, D., Wang, Y., 2020. Removal of cadmium (II) using water hyacinth (Eichhornia crassipes) biochar alginate beads in aqueous solutions. Environ. Pollut. 264, 114785. https://doi.org/10.1016/j.envpol.2020.114785.

Luo, W., Huang, Q., Antwi, P., Guo, B., Sasaki, K., 2020. Synergistic effect of ClO4 − and Sr2 + adsorption on alginate-encapsulated organo-montmorillonite beads: implication for radionuclide immobilization. J. Colloid Interface Sci. 560, 338–348. https://doi.org/10.1016/j.jcis.2019.10.049.

Lv, T., Li, B., 2021. Preparation of novel magnetic sodium alginate-ferric (III) gel beads and their super-efficient removal of direct dyes from water. J. Polym. Environ. 29 (5), 1576–1590.

Ma, J., Jiang, Z., Cao, J., Yu, F., 2020. Enhanced adsorption for the removal of antibiotics by carbon nanotubes/graphene oxide/sodium alginate triple-network nanocomposite hydrogels in aqueous solutions. Chemosphere 242, 125188. https://doi.org/10.1016/j.chemosphere.2019.125188.

Makhado, E., Pandey, S., Modibane, K.D., Kang, M., Hato, M.J., 2020. Sequestration of methylene blue dye using sodium alginate poly(acrylic acid)@ZnO hydrogel nanocomposite: kinetic, isotherm, and thermodynamic investigations. Int. J. Biol. Macromol. 162, 60–73. https://doi.org/10.1016/j.ijbiomac.2020.06.143.

Mallakpour, S., Behranvand, V., Mallakpour, F., 2021. Adsorptive performance of alginate/carbon nanotube-carbon dot-magnesium fluorohydroxyapatite hydrogel for methylene blue-contaminated water. J. Environ. Chem. Eng. 9 (2), 105170. https://doi.org/10.1016/j.jece.2021.105170.

Maqbool, M., Bhatti, H.N., Sadaf, S., Mana Al-Anazy, M., Iqbal, M., 2020. Biocomposite of polyaniline and sodium alginate with Oscillatoria biomass: a potential adsorbent for the removal of basic blue 41. J. Mater. Res. Technol. 9 (6), 14729–14741. https://doi.org/10.1016/j.jmrt.2020.10.017.

Motshekga, S.C., Ray, S.S., Maity, A., 2018. Synthesis and characterization of alginate beads encapsulated zinc oxide nanoparticles for bacteria disinfection in water. J. Colloid Interface Sci. 512, 686–692.

Nasrollahzadeh, M., Sajjadi, M., Iravani, S., Varma, R.S., 2020. Starch, cellulose, pectin, gum, alginate, chitin and chitosan derived (nano) materials for sustainable water treatment: a review. Carbohydr. Polym., 116986.

Nordin, A.H., Ahmad, K., Kai Xin, L., Syieluing, W., Ngadi, N., 2021. Efficient adsorptive removal of methylene blue from synthetic dye wastewater by green alginate modified with pandan. Mater. Today 39, 979–982. https://doi.org/10.1016/j.matpr.2020.04.564.

Othman, I., Abu Haija, M., Kannan, P., Banat, F., 2020. Adsorptive removal of methylene blue from water using high-performance alginate-based beads. Water Air Soil Pollut. 231 (8), 396. https://doi.org/10.1007/s11270-020-04751-3.

Oussalah, A., Boukerroui, A., Aichour, A., Djellouli, B., 2019. Cationic and anionic dyes removal by low-cost hybrid alginate/natural bentonite composite beads: adsorption and reusability studies. Int. J. Biol. Macromol. 124, 854–862. https://doi.org/10.1016/j.ijbiomac.2018.11.197.

Ozcan, N., Saloglu, D., 2020. Activated carbon embedded alginate beads for removing nonsteroidal anti-inflammatory drug naproxen from wastewater: equilibrium, kinetics, thermodynamics, desorption, and reusability. Water Sci. Technol. 81 (7), 1432–1444. https://doi.org/10.2166/wst.2020.196.

Pan, L., Wang, Z., Zhao, X., He, H., 2019. Efficient removal of lead and copper ions from water by enhanced strength-toughness alginate composite fibers. Int. J. Biol. Macromol. 134, 223–229. https://doi.org/10.1016/j.ijbiomac.2019.05.022.

Pashaei-Fakhri, S., Peighambardoust, S.J., Foroutan, R., Arsalani, N., Ramavandi, B., 2021. Crystal violet dye sorption over acrylamide/graphene oxide bonded sodium alginate nanocomposite hydrogel. Chemosphere 270, 129419. https://doi.org/10.1016/j.chemosphere.2020.129419.

Patiño-Ruiz, D., Bonfante, H., De Ávila, G., Herrera, A., 2019. Adsorption kinetics, isotherms and desorption studies of mercury from aqueous solution at different temperatures on magnetic sodium alginate-thiourea microbeads. Environ. Nanotechnol. Monit. Manag. 12, 100243.

Pereira, A.G.B., Rodrigues, F.H.A., Paulino, A.T., Martins, A.F., Fajardo, A.R., 2021. Recent advances on composite hydrogels designed for the remediation of dye-contaminated water and wastewater: a review. J. Clean. Prod. 284, 124703. https://doi.org/10.1016/j.jclepro.2020.124703.

Priya, Sharma, A.K., Kaith, B.S., Tanwar, V., Bhatia, J.K., Sharma, N., Panchal, S., 2019. RSM-CCD optimized sodium alginate/gelatin based ZnS-nanocomposite hydrogel for the effective removal of biebrich scarlet and crystal violet dyes. Int. J. Biol. Macromol. 129, 214–226. https://doi.org/10.1016/j.ijbiomac.2019.02.034.

Priya, Sharma, A.K., Kaith, B.S., Vipula, Chandel, K., Singh, A., Isha, 2020. Chemically modified chitosan-sodium alginate as chemo-sensor adsorbent for the detection of picric acid and removal of biebrich scarlet. Int. J. Biol. Macromol. 147, 582–594. https://doi.org/10.1016/j.ijbiomac.2020.01.090.

Radoor, S., Karayil, J., Jayakumar, A., Parameswaranpillai, J., Siengchin, S., 2021. An efficient removal of malachite green dye from aqueous environment using ZSM-5 zeolite/polyvinyl alcohol/carboxymethyl cellulose/sodium alginate bio composite. J. Polym. Environ., 1–14.

Ravikumar, K.V.G., Kubendiran, H., Ramesh, K., Rani, S., Mandal, T.K., Pulimi, M., Mukherjee, A., 2020. Batch and column study on tetracycline removal using green synthesized NiFe nanoparticles immobilized alginate beads. Environ. Technol. Innov. 17, 100520. https://doi.org/10.1016/j.eti.2019.100520.

Rezaei, H., Haghshenasfard, M., Moheb, A., 2017. Optimization of dye adsorption using Fe3O4 nanoparticles encapsulated with alginate beads by Taguchi method. Adsorpt. Sci. Technol. 35 (1–2), 55–71.

Robati, D., Mirza, B., Rajabi, M., Moradi, O., Tyagi, I., Agarwal, S., Gupta, V., 2016. Removal of hazardous dyes-BR 12 and methyl orange using graphene oxide as an adsorbent from aqueous phase. Chem. Eng. J. 284, 687–697.

Saha, S., Basu, H., Singhal, R.K., Pimple, M.V., 2017. Titania coated silica microsphere functionalized with potassium ferrocyanide impregnated in calcium alginate for efficient removal of Cs from aquatic environment. J. Environ. Chem. Eng. 5 (5), 5187–5195. https://doi.org/10.1016/j.jece.2017.09.056.

Saravanan, A., Kumar, P.S., Govarthanan, M., George, C.S., Vaishnavi, S., Moulishwaran, B., Yaashikaa, P., 2021. Adsorption characteristics of magnetic nanoparticles coated mixed fungal biomass for toxic Cr (VI) ions in aquatic environment. Chemosphere 267, 129226.

Shelar-Lohar, G., Joshi, S., 2020. Amidoximated functionalized sodium alginate graft copolymer: an effective adsorbent for rapid removal of cationic dyes. Mater. Today 26, 3357–3362. https://doi.org/10.1016/j.matpr.2019.10.130.

Sirajudheen, P., Karthikeyan, P., Vigneshwaran, S., Basheer, M.C., Meenakshi, S., 2021. Complex interior and surface modified alginate reinforced reduced graphene oxide-hydroxyapatite hybrids: removal of toxic azo dyes from the aqueous solution. Int. J. Biol. Macromol. 175, 361–371. https://doi.org/10.1016/j.ijbiomac.2021.02.024.

Soltani, R.D.C., Khorramabadi, G.S., Khataee, A., Jorfi, S., 2014. Silica nanopowders/alginate composite for adsorption of lead (II) ions in aqueous solutions. J. Taiwan Inst. Chem. Eng. 45 (3), 973–980.

Subhan, H., Alam, S., Shah, L.A., Ali, M.W., Farooq, M., 2021. Sodium alginate grafted poly(N-vinyl formamide-co-acrylic acid)-bentonite clay hybrid hydrogel for sorptive removal of methylene green from wastewater. Colloids Surf. A Physicochem. Eng. Asp. 611, 125853. https://doi.org/10.1016/j.colsurfa.2020.125853.

Sutirman, Z.A., Sanagi, M.M., Ibrahim, W.A.W., 2021. Alginate-based adsorbents for removal of metal ions and radionuclides from aqueous solutions: a review. Int. J. Biol. Macromol.

Thakur, A.K., Kumar, M., 2021. Efficacy of green alginate beads for multi-metal removal from aqueous solution. Case Stud. Chem. Environ. Eng. 3, 100100. https://doi.org/10.1016/j.cscee.2021.100100.

Thakur, S., Sharma, B., Verma, A., Chaudhary, J., Tamulevicius, S., Thakur, V.K., 2018. Recent progress in sodium alginate based sustainable hydrogels for environmental applications. J. Clean. Prod. 198, 143–159. https://doi.org/10.1016/j.jclepro.2018.06.259.

Tong, K., 2017. Preparation and biosorption evaluation of Bacillus subtilis/alginate–chitosan microcapsule. Nanotechnol. Sci. Appl. 10, 35.
Verma, A., Thakur, S., Mamba, G., Gupta, R.K., Thakur, P., Thakur, V.K., 2020. Graphite modified sodium alginate hydrogel composite for efficient removal of malachite green dye. Int. J. Biol. Macromol. 148, 1130–1139.
Wan, S., Wu, J., Zhou, S., Wang, R., Gao, B., He, F., 2018. Enhanced lead and cadmium removal using biochar-supported hydrated manganese oxide (HMO) nanoparticles: behavior and mechanism. Sci. Total Environ. 616, 1298–1306.
Wang, B., Gao, B., Zimmerman, A.R., Lee, X., 2018. Impregnation of multiwall carbon nanotubes in alginate beads dramatically enhances their adsorptive ability to aqueous methylene blue. Chem. Eng. Res. Des. 133, 235–242.
Wang, B., Gao, B., Wan, Y., 2019. Comparative study of calcium alginate, ball-milled biochar, and their composites on aqueous methylene blue adsorption. Environ. Sci. Pollut. Res. 26 (12), 11535–11541.
Wang, J., Guo, M., Luo, Y., Shao, D., Ge, S., Cai, L., Lam, S.S., 2021. Production of magnetic sodium alginate polyelectrolyte nanospheres for lead ions removal from wastewater. J. Environ. Manage. 289, 112506. https://doi.org/10.1016/j.jenvman.2021.112506.
Wen, R., Tu, B., Guo, X., Hao, X., Wu, X., Tao, H., 2020. An ion release controlled Cr(VI) treatment agent: nano zero-valent iron/carbon/alginate composite gel. Int. J. Biol. Macromol. 146, 692–704. https://doi.org/10.1016/j.ijbiomac.2019.12.168.
Won, S.W., Kotte, P., Wei, W., Lim, A., Yun, Y.S., 2014. Biosorbents for recovery of precious metals. Bioresour. Technol. 160, 203–212. https://doi.org/10.1016/j.biortech.2014.01.121.
Xia, M., Zheng, X., Du, M., Wang, Y., Ding, A., Dou, J., 2018. The adsorption of Cs+ from wastewater using lithium-modified montmorillonite caged in calcium alginate beads. Chemosphere 203, 271–280. https://doi.org/10.1016/j.chemosphere.2018.03.129.
Xiao, Z., Zhang, L., Wu, L., Chen, D., 2019. Adsorptive removal of Cu (II) from aqueous solutions using a novel macroporous bead adsorbent based on poly (vinyl alcohol)/sodium alginate/KMnO4 modified biochar. J. Taiwan Inst. Chem. Eng. 102, 110–117.
Xue, P., Liu, X., Gu, Y., Zhang, W., Ma, L., Li, R., 2020. Laccase-mediator system assembling co-immobilized onto functionalized calcium alginate beads and its high-efficiency catalytic degradation for acridine. Colloids Surf. B Biointerfaces 196, 111348. https://doi.org/10.1016/j.colsurfb.2020.111348.
Yadav, S., Asthana, A., Singh, A.K., Chakraborty, R., Vidya, S.S., Susan, M.A.B.H., Carabineiro, S.A.C., 2021. Adsorption of cationic dyes, drugs and metal from aqueous solutions using a polymer composite of magnetic/β-cyclodextrin/activated charcoal/Na alginate: isotherm, kinetics and regeneration studies. J. Hazard. Mater. 409, 124840. https://doi.org/10.1016/j.jhazmat.2020.124840.
Yi, X., Sun, F., Han, Z., Han, F., He, J., Ou, M., Xu, X., 2018. Graphene oxide encapsulated polyvinyl alcohol/sodium alginate hydrogel microspheres for Cu (II) and U (VI) removal. Ecotoxicol. Environ. Saf. 158, 309–318.
Yi-cheng, W., Ai-li, Y., Wei, G., Hai-yan, F., Ze-jie, W., 2020. Al2O3 nanoparticles promote the removal of carbamazepine in water by *Chlorella vulgaris* immobilized in sodium alginate gel beads. J. Chem. 2020, 8758432. https://doi.org/10.1155/2020/8758432.
You, Y., KeqiQu, Huang, Z., Ma, R., Shi, C., Li, X., Guo, Z., 2019. Sodium alginate templated hydroxyapatite/calcium silicate composite adsorbents for efficient dye removal from polluted water. Int. J. Biol. Macromol. 141, 1035–1043. https://doi.org/10.1016/j.ijbiomac.2019.09.082.
Yu, J., Wang, J., Jiang, Y., 2017. Removal of uranium from aqueous solution by alginate beads. Nucl. Eng. Technol. 49 (3), 534–540. https://doi.org/10.1016/j.net.2016.09.004.
Zamri, N.I.I., Zulmajdi, S.L.N., Daud, N.Z.A., Mahadi, A.H., Kusrini, E., Usman, A., 2021. Insight into the adsorption kinetics, mechanism, and thermodynamics of methylene blue from aqueous solution onto pectin-alginate-titania composite microparticles. SN Appl. Sci. 3 (2), 222. https://doi.org/10.1007/s42452-021-04245-9.
Zhang, Y., Wang, L., Zhang, N., Zhou, Z., 2018a. Adsorptive environmental applications of MXene nanomaterials: a review. RSC Adv. 8 (36), 19895–19905. https://doi.org/10.1039/C8RA03077D.
Zhang, H., Zhu, Y., Qu, L., Wu, H., Kong, H., Yang, Z., Santos, H.A., 2018b. Gold nanorods conjugated porous silicon nanoparticles encapsulated in calcium alginate nano hydrogels using microemulsion templates. Nano Lett. 18 (2), 1448–1453.
Zhang, Z.-H., Xu, J.-Y., Yang, X.-L., 2021. MXene/sodium alginate gel beads for adsorption of methylene blue. Mater. Chem. Phys. 260, 124123. https://doi.org/10.1016/j.matchemphys.2020.124123.

Zhao, X., Wang, X., Lou, T., 2021. Preparation of fibrous chitosan/sodium alginate composite foams for the adsorption of cationic and anionic dyes. J. Hazard. Mater. 403, 124054. https://doi.org/10.1016/j.jhazmat.2020.124054.
Zhu, H., Chen, T., Liu, J., Li, D., 2018. Adsorption of tetracycline antibiotics from an aqueous solution onto graphene oxide/calcium alginate composite fibers. RSC Adv. 8 (5), 2616–2621.
Zhuang, Y., Yu, F., Ma, J., Chen, J., 2017. Enhanced adsorption removal of antibiotics from aqueous solutions by modified alginate/graphene double network porous hydrogel. J. Colloid Interface Sci. 507, 250–259.

CHAPTER

22

Synthesis of novel nanobioadsorbent for the effective removal of Pb^{2+} and Zn^{2+} ions—Adsorption, equilibrium, modeling, and optimization studies

B. Uma Maheswari, V.M. Sivakumar, and M. Thirumarimurugan

Department of Chemical Engineering, Coimbatore Institute of Technology, Coimbatore, India

Nomenclature

AAS	atomic absorption spectrometer
ANOVA	analysis of variance
CC	central composite design
C_e	equilibrium concentration of adsorbate
EC	*Eichhornia crassipes*
EDX	energy dispersive X-ray
FTIR	Fourier transform infrared spectroscopy
k_1 (min^{-1})	first-order rate constant
k_2 (gm/gmin)	second-order rate constant
K_f ($mg^{1-1/n}$ g), n(g/L)	Freundlich constants
k_p ($mg/gmin^{0.5}$)	intra particle diffusion constant
LM	*Lemna minor*
q_e (mg/g)	Amount adsorbed at equilibrium
q_m (mg/g), K_L (L/mg)	Langmuir constants
q_t (mg/g)	amount of adsorbate species adsorbed at equilibrium and at any time
RSM	response surface methodology
SEM	scanning electron microscope

https://doi.org/10.1016/B978-0-323-90912-9.00022-8

22.1 Introduction

Due to the increase in disposal of heavy metals into the environment, natural water bodies have been contaminated. These contaminations are caused due to the rapid release of industrial and urban waste out into the environment. The toxic effect of heavy metal ions beyond the permissible level on living organisms is a serious environmental problem derived due to environmental contamination (Fargašová et al., 2018). Heavy metals are non-degradable in nature and possess high environmental perseverance (Flouty and Estephane, 2012). Prominent sources of heavy metal discharge are from battery, electroplating, mining, metallurgy, paint, and dying industry. Among the heavy metals, Zn^{2+} and Pb^{2+} are considered as deadliest toxic. Though the persistence of heavy metals is at the tracker level, they create an adverse effect on human health. Inhalation of these heavy metals causes a severe impact on human health such as kidney and nervous system damage, cancer, fever, vomiting, skin inflammation, and anemia. Normally, industrial wastewater contains Pb^{2+} and Zn^{2+} metal ions in the range of 5–15 mg/L, 0.03–133 mg/L, respectively. As per the US Environmental Protection Agency (USEPA) and Bureau of Indian Standards (BIS), the limits of Pb^{2+}, Zn^{2+} ions in drinking water are within the level of 0.05 mg/L– 0.1 mg/L, 0.1 mg/L– 1 mg/L, respectively (US Environmental Protection Agency, 1990). Therefore, an essential and crucial problem to be solved in the current scenario is the removal of the excess of Pb^{2+} and Zn^{2+} ions before discharging to the aquatic systems.

Conventional treatment methods have been adopted for the removal of heavy metals from aqueous systems such as chemical precipitation, adsorption, nanofiltration and electro dialysis, membrane filtration, and revere osmosis (Fu and Wang, 2011; Maršálek and Navrátilová, 2011; Torma and Cséfalvay, 2018; Pandey et al., 2015). However, most of these techniques require substantial financial input in the early stages and their usage is limited because of their operating cost overriding the importance of water pollution control. They also have several disadvantages that include incomplete metal removal, energy requirements, and generation of toxic sludge that need proper disposal methodology. In the present day scenario, adsorption is proven to be a simple, most effective, and emerging technology for the removal of heavy metals from wastewater (Burakov et al., 2018). Various natural elements such as peat (Bulgariu et al., 2012), natural bentonite (Melichová and Hromada, 2012), chitosan and graphene oxide composite (Najafabadi et al., 2015), activated carbon (Largitte and Laminie, 2015), wheat pulp (Suopajarvi et al., 2015), ash (Harja et al., 2013), aloe vera leaves and multi-walled carbon nanotubes(Moosa et al., 2015), marine algae (Bulgariu and Bulgariu, 2014), lemon and banana peels (Rajoriya and Balpreetkaur, 2014), peepal leaf (Anitha et al., 2017), coal fly ash, and sawdust (Rachayyanavar, 2015) have been used to remove heavy metals. Though many adsorbents have been addressed in the literature; they possess some disadvantages such as low adsorption capacity and unsatisfactory metal ion removal at low concentrations. Hence, researchers have focussed on the development of new adsorbents with easy availability, high adsorption capacity, surface area, and regeneration at a low cost.

Response Surface Methodology (RSM) is a statistical tool for modeling, improving, and optimizing the process (Mourabet et al., 2012). RSM can be utilized to determine the optimum condition for the desired response, to determine the effects of the individual parameters as well as their relative significance, and interaction between two or more variables (Javanbakht and Ghoreishi, 2017). RSM comprises generally of two steps; the first step is

to model formulation and the second is to optimize the factor that influences the performance of the response (Ahmadi et al., 2014). The application of RSM techniques in adsorption process development can result in the enhancement product yield, reduced process variability, closer confirmation of the output response to nominal and target requirements, and reduced expansion time. The innovative aspect of the present research is to optimize the parameters for the effective removal of Zn^{2+}, Pb^{2+} ions from battery effluent using the low-cost nanobioadsorbent *Eichhornia crassipes(EC)* and *Lemna minor(LM)*. Central Composite Design (CCD) of RSM was applied to evaluate the effects of significant operating parameters such as pH, contact time, adsorbent dosage, and concentration.

22.2 Materials and methods

22.2.1 Reagents

The stock solution of Pb^{2+} and Zn^{2+} ions were prepared from analytical grade $Pb(NO_3)_2$, $ZnSO_4.7H_2O$ salts using double distilled water. A desired test solution (20 mg/L, 40 mg/L, and 60 mg/L) of Pb^{2+} and Zn^{2+} ion solutions were prepared using stock solutions. All the chemicals utilized were of analytical reagent (AR) grade purchased from Sigma-Aldrich and Merck, used for the experimental purpose without any purification.

22.2.2 Nanobioadsorbent preparation

The aquatic weed *EC* and *LM* were collected from local ponds in and around Tamilnadu, India. The weeds were washed with distilled water to remove dust and impurities. It is then sun-dried for 2 days, crushed in a domestic blender, and sieved (BSS 230) to obtain a uniform particle size. In order to prepare nanosorbent, sieved weed was added to the precursor (acetone, HCl, and tetraethyl orthosilicate) stirred for about 2 h followed by sonication for about an hour. Finally, it was dried to 120°C in a muffle furnace and powered using mortar and pestle to obtain a fine powder. To analyze the characterization of the prepared adsorbent, Fourier Transform Infrared Spectroscopy (FTIR) was performed to detect different chemical functional groups responsible for the adsorption of metal ions on the binding sites of the adsorbents using Bruker spectrometer with the resolution of 4 cm^{-1} in the range from 400 to 4000 cm^{-1}. The surface texture and morphology of the nanosorbent were analyzed using Scanning Electron Microscopy test using Philips - EEI-TEP, Holland and was carried out followed by energy dispersive analysis.

22.2.3 Adsorption equilibrium experiments

Batch adsorption experiment was conducted to study the diverse parameters such as pH, adsorbent dosage, metal ion concentration, and contact time for the removal of Pb^{2+} and Zn^{2+} ions. A known amount of adsorbent dosage was added to each conical flask which consists of 20 ml metal ion solution (Pb^{2+} and Zn^{2+}) of different known initial concentrations (20–60 mg/L) and was taken in a 250 mL capacity flask. During the process, the flask containing mixture is agitated in an incubator shaker (Orbital Incubator Shaker, Royal Testing

Equipment, Chennai, India) at 300 rpm for about 1–2 h. The samples were analyzed using an atomic absorption spectrometer (AAS) (SA 172 model, Elico Limited, Chennai, India). The data obtained from the batch adsorption studies were used to calculate the percentage removal of Pb^{2+} and Zn^{2+} ions by using the following Eq. (22.1):

$$\text{Percentage removal of metal ions}\,(\%) = \frac{C_o - C_e}{C_0} \times 100 \tag{22.1}$$

where C_0 and C_e are initial and equilibrium concentration states (mg/L) respectively. The number of Pb^{2+} and Zn^{2+} ions absorbed at the equilibrium q_e can be determined by using Eq. (22.2)

$$q_e = \frac{(C_o - C_e)V}{W} \tag{22.2}$$

where q_e is the equilibrium amount of Pb^{2+} and Zn^{2+} ions absorbed per unit mass (mg/g) of the adsorbent. V is the volume of the stock solution (L) and W is the mass of the adsorbent used (g). Langmuir and Freundlich's isotherms are the most commonly used isotherms for determining the equilibrium characteristics in an adsorption process (Langmuir, 1918; Freundlich, 1906). Langmuir isotherm is generally applicable to the monolayer adsorption process. The calculation of these isotherms is to stimulate the experimental data that is greatly affected by the sorbent–sorbent systems. Langmuir isotherm suits well with the monolayer adsorption process and metal-binding sites. The Langmuir isotherm is given by Eq. (22.3):

$$\frac{C_e}{q_e} = \frac{1}{q_{mK_L}} + \frac{C_e}{q_m} \tag{22.3}$$

where q_m(mg/g) and K_L (L/mg) are Langmuir constants related to adsorption capacity and rate of adsorption. R_L is the dimensionless separation factor used to determine the characteristic of the process. It is represented in Eq. (22.4):

$$R_L = \frac{1}{1 + K_L C_0} \tag{22.4}$$

where C_0 is the initial solute concentration. The value of R_L determines the adsorption process that is favorable ($0 < R_L < 1$), unfavorable ($R_L > 1$), or irreversible ($R_L = 0$). Freundlich model determines the heterogeneous surface energies in the system and expressed by the following Eq. (22.5):

$$q_e = K_f C_e^{1/n} \tag{22.5}$$

where K_f ($mg^{1-1/n}\ /g^{-1}$) and n (g/L) are Freundlich constant that corresponds to bonding energy and the measure of the deviation from linearity of adsorption. If the value of $n > 1$, the adsorption process is favorable.

22.2.4 Adsorption kinetics and mechanism experiments

The adsorption kinetic study was performed in a series of conical flasks with 100 mL of known concentration of metal ion solutions by varying the contact time from 24 to 120 h.

The adsorption mixtures were then agitated in an incubator shaker at 300 rpm. For every 24 h time interval, the samples were drawn and it was analyzed for measurements of Pb^{2+} and Zn^{2+} ions using atomic absorption spectrometer (AAS). The pseudo-first and second order was generally used to fit the kinetic data (Lagergren, 1898; Ho and McKay, 1999). The q_t is the amount of Pb^{2+} and Zn^{2+} ions adsorbed at the time t was calculated from Eq. (22.6):

$$q_t = \frac{(C_o - C_t)V}{W} \tag{22.6}$$

where C_t(mg/L) is the concentration of metal ions at any time t. In order to determine the adsorption rate and feasibility of the adsorption process, the adsorption kinetic data were modeled using pseudo-first-order, pseudo-second-order model. Pseudo-first-order rate in Eq. (22.7) is given by:

$$\log(q_e - q_t) = \log q_e - \frac{k_1}{2.303}t \tag{22.7}$$

where q_e and q_t are the amounts of Pb^{2+} and Zn^{2+} ions absorbed in mg/L at equilibrium and at time t in hours. k_1 (min^{-1}) is the adsorption rate constant. Pseudo-second-order equation analyzes the equilibrium adsorption. It is represented in Eq. (22.8):

$$\frac{t}{q_t} = \frac{1}{k_2 q_e^2} + \frac{1}{q_e}t \tag{22.8}$$

where k_2 (g/mg min) is the rate constant of second-order adsorption. The adsorption mechanism was determined by applying the values of kinetic data in the intraparticle diffusion model (Weber and Morris, 1963). The intraparticle diffusion model is given by Eq. (22.9):

$$q_t = k_p t^{1/2} + C \tag{22.9}$$

where k_p is the intraparticle diffusion rate constant (mg/g $min^{0.5}$), t is the time (min), and C is the constant related to the thickness of the boundary layer.

22.2.5 Statistical analysis using response surface methodology

In the present study, Response Surface Methodology (RSM) is used to optimize different parameters. In order to study the individual and synergistic effect of the four factors such as pH, initial metal ion concentration, adsorbent dosage, and contact time towards the response, Central Composite Design (CCD) was implemented using Design Expect Software 11. Table 22.1 shows the range and levels of the sovereign variables selected for the adsorption of Pb^{2+} and Zn^{2+} ^{F}ion. CCD provides more advantages than other designs because it is used to fit the quadratic surface, optimize the parameters with the minimum number of experiments, and also to analyze the interaction between the parameters. Based on the three basic principles of an ideal experimental design, CCD was designed in such a way that it comprises of n_o center points ($n_o \geq 1$), complete 2^n factorial design (n is the number of parameters), and two axial points in which the axis of the design parameters are at a distance $2^{n/4}$ from the design center. The total number of design points is shown in Eq. (22.10):

$$N = 2^n + 2n + n_o \tag{22.10}$$

TABLE 22.1 Levels and ranges of the independent variables.

			Coded variable levels				
Independent variables	**Code**	**Unit**	$-\alpha$	**−1**	**0**	**1**	α
pH	X_1	–	1	2	7	10	12
Adsorbent dosage	X_2	g	0.1	0.5	2	2.5	3.5
Initial concentration	X_3	mg/L	15	10	40	60	85
Time	X_4	h	12	24	72	120	168

The second-degree polynomial Eq. (22.11) is used to estimate the response of the dependent variables.

$$Y = b_o + b_1X_1 + b_2X_2 + b_3X_3 + b_4X_4 + b_{11}X_1^2 + b_{22}X_2^2 + b_{33}X_3^2 + b_{44}X_4^2 + + b_{12}X_1X_2 + b_{13}X_1X_3 + b_{14}X_1X_4 + b_{23}X_2X_3 + b_{24}X_2X_4 + b_{34}X_3X_4 \quad (22.11)$$

where Y_0 is predicted response, X_1, X_2, X_3, X_4 are independent parameters, b_0 is the offset term, b_1, b_2, b_3, b_4 are linear effects, b_{11}, b_{22}, b_{33}, b_{44} are squared effects, and b_{12}, b_{13}, b_{14}, b_{23}, b_{24}, b_{24} are interaction terms.

22.3 Results and discussion

22.3.1 Characterization of adsorbents

The surface morphology and texture of *EC* and *LM* were analyzed and the results are depicted in Figs. 22.1A and 22.2A, respectively. The shape of *EC* and *LM* appears as non-aggregated morphology with small flakes and crumpled structures. The surface appears to be irregular and has porous sites which indicate that the *EC* and *LM* have a more adequate morphology for the adsorption of Pb^{2+} and Zn^{2+} ions. The expanded layer of nanobioadsorbent favors more adsorption of metal ions onto interlayer surfaces. The occurrence of white patches on the surface of the adsorbents (*EC*, *LM*) as shown in Figs. 22.1A and 22.2A are the presence of non-clay minerals covering Cl, K. The synthesized *EC* and *LM* were further analyzed using the EDX technique for the determination of the elemental composition of the synthesized adsorbent. The weight percentage (weight %) of Si, O, C, K, Cl within the compounds were depicted in Table 22.2. From the results, it is evident that the presence of Si compounds in *EC* and *LM* is suitable for the adsorption of various organic pollutants (Shirzad-Siboni et al., 2015).

The FTIR spectra of nanoadsorbent that correspond to *EC* and *LM* are shown in Fig. 22.3. The peak of *EC* at 1639.02 cm^{-1} and 3914.48 cm^{-1} corresponds to OH-stretching vibration. Carboxylic acid O—H is represented by the peaks at 2364.59 cm^{-1}, respectively. The band around 1065.94 cm^{-1} is attributed to the asymmetric stretching vibration of Si-O-Si tetrahedral with *LM*. Similarly, the peaks located at 2923.03 cm^{-1} are characteristics of the carbonyl

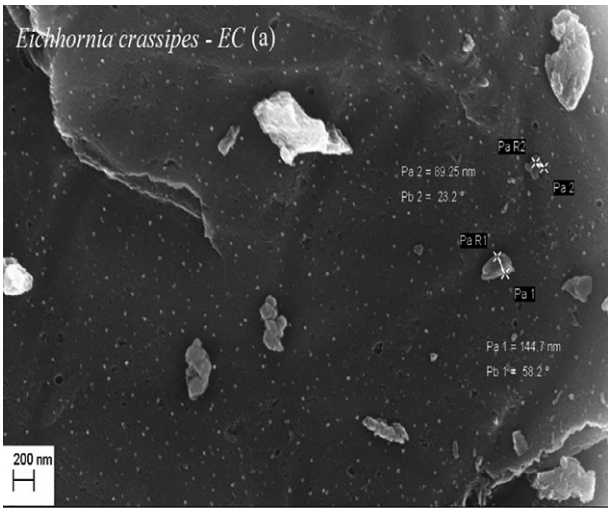

FIG. 22.1 SEM image of *Eichhornia crassipes (EC).*

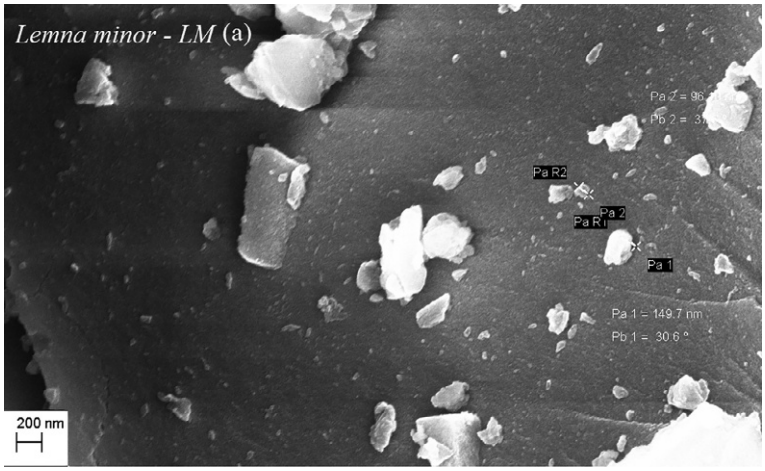

FIG. 22.2 SEM image of *Lemna minor (LM*).

group stretching in the nanoadsorbent. The corresponding peaks observed at 948 cm^{-1} are due to C═S thiocarbonyl stretching.

22.3.2 Effect of pH

The acidity of the solution is one of the most important parameters to be considered since it affects the adsorption of metal ions. The effect of pH on the adsorption of metal ions onto *EC* and

TABLE 22.2 Elemental composition of *Eichhornia crassipes* (*EC*) and *Lemna minor* (*LM*).

	Weight percentage of elements	
Elements	***EC* (%)**	***LM* (%)**
O	51.56	54.16
Si	26.63	34.66
C	21	10.50
Cl	0.81	–
K	–	0.74

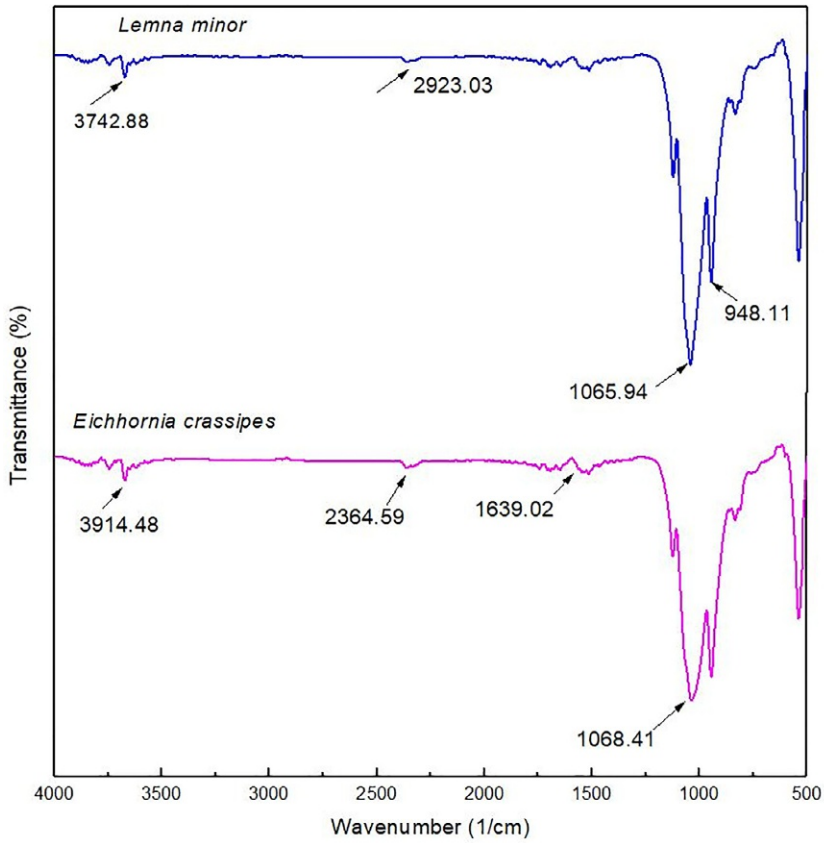

FIG. 22.3 FTIR images of *Eichhornia crassipes* (*EC*) and *Lemna minor (LM)*.

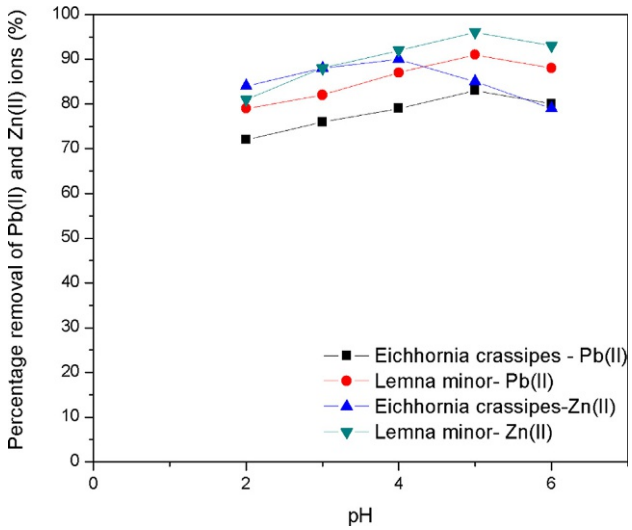

FIG. 22.4 Effect of pH.

LM was investigated by changing the solution pH range of 2–10, adsorbent dosage 1 g/L for an initial concentration of 10 mg/L, and results are shown in Fig. 22.4. The experimental findings clearly reveal that removal of Pb^{2+} ions increases with an increase in solution pH and reaches the maximum value at a pH 5 for both *EC* and *LM*. An appreciable decrease in percentage removal of Pb^{2+} was observed after pH 5. This variation is mainly because of the fact that at lower pH values, the negative sites of the adsorbents taken by the H^+ and H_3O^+ ions lead to the decline in the vacant site, consequently causes a decrease in Pb^{2+} ions adsorption. Though the metal ion adsorption increases with an increase in solution pH, on further increment of pH a reduction in adsorption due to the formation of metal hydroxides was observed.

Similarly, maximum removal of Zn^{2+} with respect to *EC*, *LM* is observed at pH 4 and pH 5, thereafter there is a decline in the adsorption process. At higher pH values, Zn^{2+} ions react with hydroxyl ions to yield zinc precipitates which automatically decreases the quantity of free zinc ions available for adsorption and hence overall adsorptive capacity dropped. However, based on the experimental results, pH 5 was chosen as the optimum value for further experimental studies for both Pb^{2+} and Zn^{2+} ions removal.

22.3.3 Effect of adsorbent dosage

The effect of adsorbent dosage is an important parameter to obtain the quantitative removal of metal ions from battery effluent. Effect of *EC* and *LM* dosage on the removal of Pb^{2+} and Zn^{2+} ions was studied at 10 mg/L metal ion concentration. Fig. 22.5 shows the effect of adsorbent dosage (*EC*, *LM*) on Pb^{2+} and Zn^{2+} ions adsorption. The adsorbent dosage was examined by varying *EC* and *LM* dosage from 0.5 to 3 g/L to optimize the adsorbent loading to get maximum removal of Pb^{2+} and Zn^{2+} ions. It can be seen from Fig. 22.5 that percentage removal increases with an increase in adsorbent dosage, after which there is a negligible

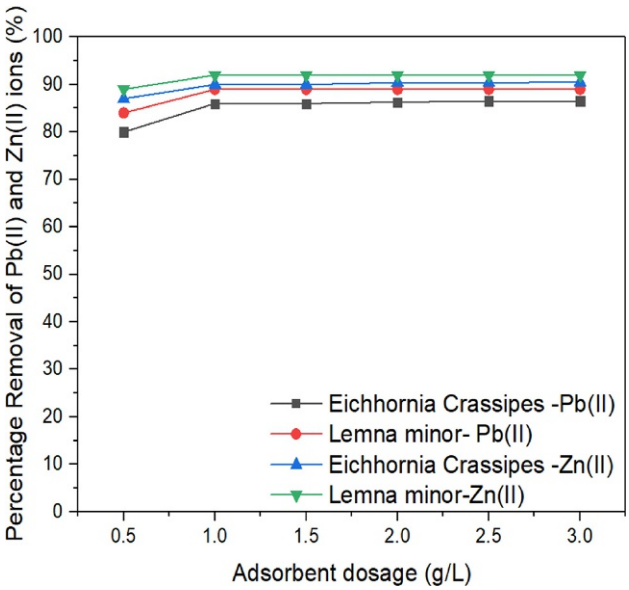

FIG. 22.5 Effect of adsorbent dosage.

increase in removal percentage. Generally, on increase in the adsorbent dose more surface area and adsorption sites will be created (Namdeti and Pulipati, 2013). Due to the agglomeration of particles, there is a negligible increase in percentage removal of both Pb^{2+} and Zn^{2+} ions beyond the dosage level of 1 g/L, for both *EC* and *LM*.

22.3.4 Effect of initial concentration

The effect of the initial metal ion concentration on the removal of metal ions was analyzed and represented in Fig. 22.6. It was observed that the removal of metal ions decreases with an increase in metal ion concentration. It is mainly due to the fact that at lower concentrations, the adsorption sites take up the available Pb^{2+} and Zn^{2+} ions rapidly owing to the less competition among the metal ions for the adsorption sites of the available binding sites (Anzeze et al., 2014). Similarly, the lesser removal of metal ions at higher concentrations maybe because of higher metal ion concentration to the available active sites. The percentage removal of Pb^{2+} ions decreases from 86% to 74% for *EC* and 89% to 80% for *LM* at an initial metal ion concentration varying from 10 to 60 mg/L, respectively. Similarly, the decrease in percentage removal of Zn^{2+} ion is observed in the range from 90% to 82% for *EC* and 93% to 82% for *LM*, respectively.

22.3.5 Effect of contact time

The effect of adsorption of Zn^{2+} and Pb^{2+} with respect to *EC* and *LM* was studied by taking 20 mg/L of the metal solution with 1 g/L of adsorbent dosage at pH 5. The resulting mixture

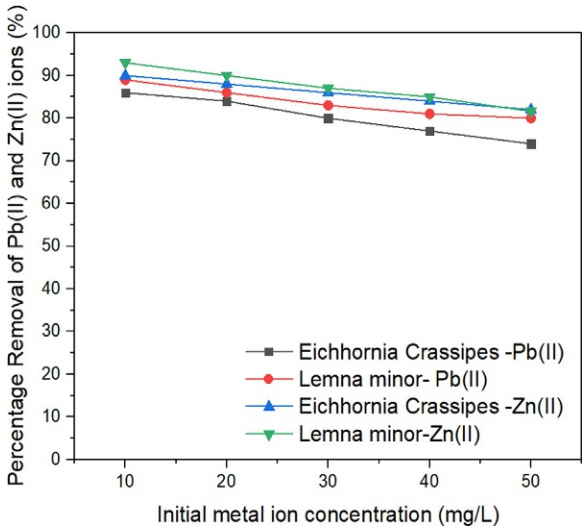

FIG. 22.6 Effect of initial concentration.

was experimented at various time intervals ranging from 24 to 144 h. From the results in Fig. 22.7, it is observed that the adsorption process of Pb^{2+} and Zn^{2+} ions increased rapidly in the beginning, followed by a slower phase approaching equilibrium condition. It is evident from Fig. 22.7, *LM* possesses maximum removal with an increase in contact time up to 48 h for both metal ions, thereafter it remains constant. Similarly, maximum removal (89%) was found

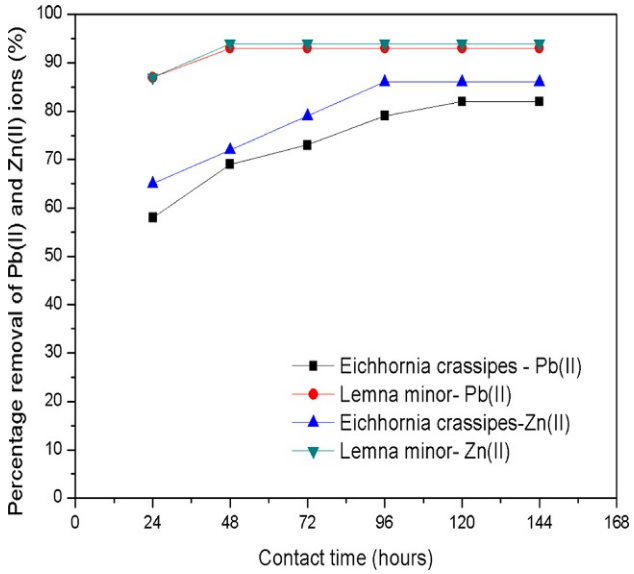

FIG. 22.7 Effect of contact time.

at 120 h for Zn^{2+} ions and 96 h for Pb^{2+} ions removal (86%) by *EC*. At the beginning of the adsorption process, the availability of more number of active binding sites of the *EC* and *LM* larger surface area was formed thereby facilitates the binding of Pb^{2+} and Zn^{2+} ions, ultimately lead to faster adsorption. Slower phase is observed in the later stage may be due to the occupation of active adsorption sites by the Pb^{2+} and Zn^{2+} ions (Nithya et al., 2016).

22.3.6 Adsorption isotherms

The effect of initial concentration data was fitted to the two-parameter adsorption models such as Langmuir and Freundlich isotherms and the graphical representation of these isotherms are given in Figs. 22.8 and 22.9, respectively. The Langmuir q_m (mg/g), K_L (L/mg), R_L with the R^2 were estimated from the plot of C_e vs. C_e/q_e, and the corresponding values are listed in Table 22.3. The value of R_L was found to be between 0 and 1 which indicates favorable adsorption (Hal et al., 1966). The Freundlich constants K ($mg^{(1-1/n)}/g$) and n (g/L) value with the R^2 are estimated from the plot of log C_e vs. log q_e were listed in Table 22.3. The observed n value lies between 1 and 10 that indicates the adsorption is a physical process (McKay et al., 1981)

From the results, it is observed that adsorption isotherm data were best-fitted to the Langmuir adsorption based on high R^2 values than the Freundlich model. The comparison of the different monolayer adsorption capacity q_m (mg/g) values for Pb^{2+} and Zn^{2+} ions observed in this study were compared well with some other adsorbents reported in the literature are mentioned in Table 22.4. The comparative studies on the adsorption capacity of Pb^{2+} and Zn^{2+} studied in this work indicate that *EC* and *LM* have higher adsorption capacity.

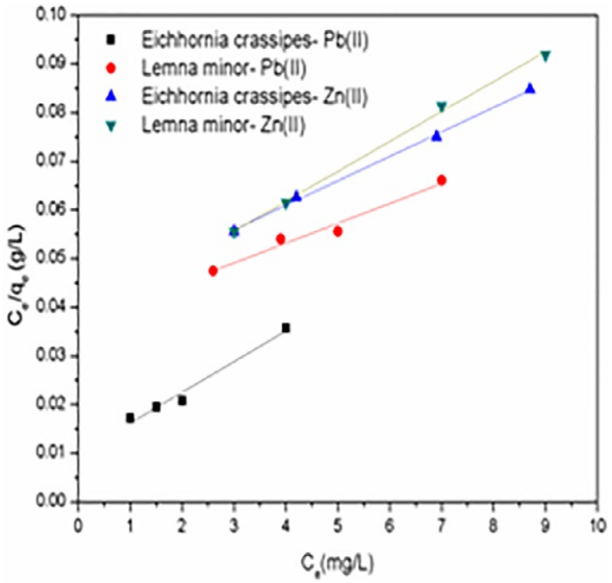

FIG. 22.8 Langmuir plot.

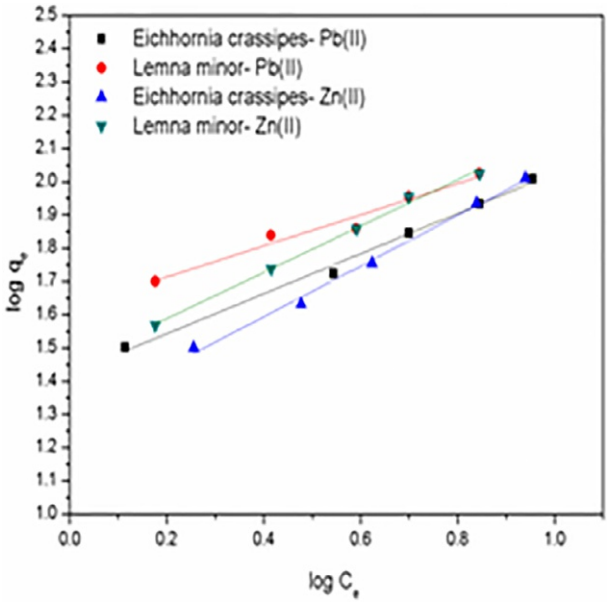

FIG. 22.9 Freundlich plot.

TABLE 22.3 Langmuir and Freundlich isotherm for removal of Pb^{2+} and Zn^{2+} by *Eichhornia crassipes (EC) and Lemna minor (LM)*.

		Pb^{2+}		Zn^{2+}	
Isotherm	**Parameters**	***Eichhornia crassipes***	***Lemna minor***	***Eichhornia crassipes***	***Lemna minor***
Langmuir	q_m	35.71	28.50	38.46	26.31
	K_L	4.08	8.75	3.71	7.60
	R_L	4×10^{-3}	2×10^{-3}	4×10^{-3}	2×10^{-3}
	R^2	0.97	0.98	0.93	0.95
Freundlich	K_f	4.43	4.25	4.13	4.12
	n	1.90	1.43	1.56	1.57
	R^2	0.90	0.82	0.91	0.95

22.3.7 Adsorption kinetics

The kinetic parameters, adsorption capacity at equilibrium, and coefficient of determination (R^2) were found by plotting $\log(q_e - q_t)$ vs. time for pseudo-first-order model and t/q_t vs. time for pseudo-second-order model, respectively. The corresponding results were tabulated in Table 22.5 and pictorial representations of the models were shown in Figs. 22.10 and 22.11, respectively. It can be seen from Table 22.5 that pseudo-second-order model posed a higher

TABLE 22.4 Comparative studies on the adsorption capacity of Pb^{2+} and Zn^{2+} onto different adsorbents.

Adsorbates	Adsorbents	(mg/g)	References
Pb^{2+}	*Eichhornia crassipes* (*EC*)	35.71	Present work
Pb^{2+}	*Lemna minor* (*LM*)	28.5	Present work
Pb^{2+}	Van apple pulp	15.96	Depci et al. (2012)
Pb^{2+}	Heartwood of *Areca catechu* powder	11.72	Chakravarty et al. (2010)
Pb^{2+}	Chitoan blended poly vinyl alcohol	14.24	Anitha et al. (2015)
Zn^{2+}	*Eichhornia crassipes* (*EC*)	38.46	Present work
Zn^{2+}	*Lemna minor* (*LM*)	26.31	Present work
Zn^{2+}	Red algae	18.51	Anilkumar et al. (2016)
Zn^{2+}	Physical seed hull	12.29	Mohammad et al. (2010)
Zn^{2+}	Xanthate modified magnetic chitosan	20.8	Zhu et al. (2012)

TABLE 22.5 Parameter of kinetic models for the adsorption of Pb^{2+} and Zn^{2+} by *Eichhornia crassipes (EC) and Lemna minor (LM)*.

		Pseudo-first order				Pseudo-second order			Intraparticle diffusion		
Adsorbates	Adsorbents	$q_{e,exp}$	k_1*10^{-3}	$q_{e,cal}$	R^2	k_2*10^{-3}	$q_{e,cal}$	R^2	k_p*10^{-3}	C	R^2
Pb^{2+}	*Eichhornia crassipes (EC)*	39.0	3.2	3.1	0.95	4.3	41.6	0.97	8	1	0.94
	Lemna minor (LM)	38.2	2.3	2.2	0.91	6.1	40.1	0.92	6	1	0.91
Zn^{2+}	*Eichhornia crassipes (EC)*	38.6	2.5	2.4	0.90	2.2	39.8	0.93	1	1.8	0.87
	Lemna minor (LM)	37.2	1.6	2.1	0.80	6.5	38.4	0.95	2	2.4	0.90

correlation coefficient, and there exists a good agreement between the calculated and experimental q_e values than the pseudo-first-order model. Hence, the pseudo-second-order model better represented the adsorption kinetics and supports the assumption (Lagergren, 1898) that the rate-limiting step of Pb^{2+} and Zn^{2+} ions onto *EC* and *LM* may be chemisorption.

From the obtained results, it is clear that the kinetic results are fitted well to a chemisorption model. The intraparticle diffusion model was plotted to verify the influence of mass transfer resistance for binding of Pb^{2+} and Zn^{2+} ions to *EC* and *LM*. The intraparticle diffusion rate constant k_p and intercept *C* can be calculated from the slope and intercept of linear plot $t^{1/2}$ vs q_t (Fig. 22.12). The plot does not pass through the origin which indicates that intraparticle diffusion is not the sole rate-limiting step else, the rate-limiting step is governed by the boundary layer up to some specific degrees. Hence, both adsorption as well as intraparticle diffusion

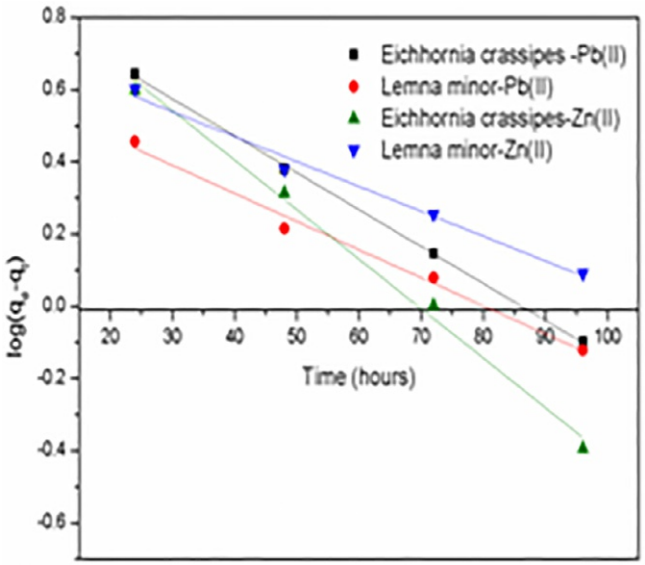

FIG. 22.10 Pseudo-first-order model.

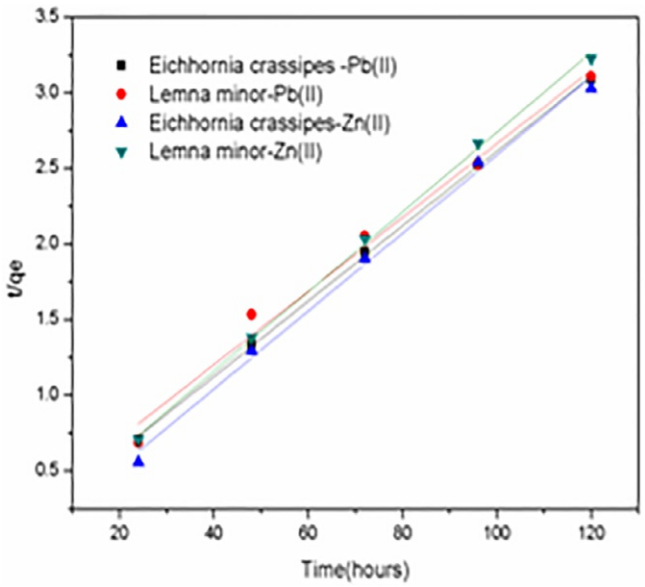

FIG. 22.11 Pseudo-second-order model.

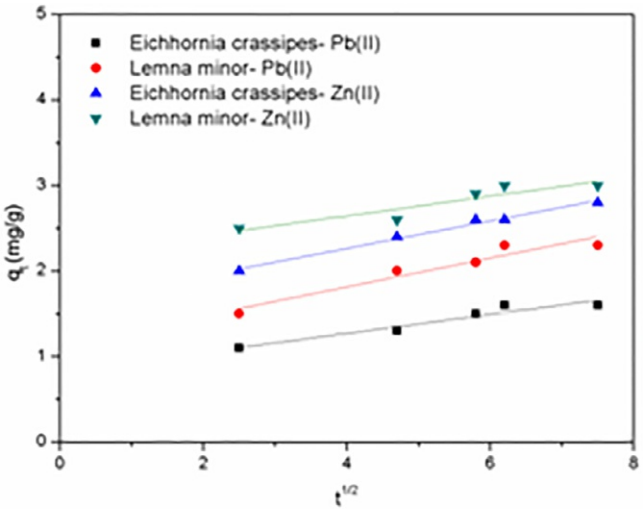

FIG. 22.12 Intraparticle diffusion model.

determines the rate-limiting step. By the instantaneous operation, the adsorption of Pb^{2+} and Zn^{2+} ions onto *EC* and *LM* occurs consecutively by surface adsorption and intraparticle diffusion as indicated by two-liner portions in Fig. 22.12. The first linear position is affected by the boundary layer followed by the intraparticle layer in the second linear position.

22.3.8 Central composite design model

The design matrix incorporating the preparation variables, their ranges, and the responses in which are percentage removal of both Pb^{2+} and Zn^{2+} (Y_{Pb} and Y_{Zn}) are represented in Tables 22.6 and 22.7. In order to evaluate and compare the responses, CCD was applied for the development of polynomial regression equations which were all quadratic expressions as suggested by the software (Garba et al., 2016a). Based on the polynomial's highest order, the model expression was selected in accordance with the sequential model sum of squares where the model was not aliased and the additional terms were significant (Garba and Rahim, 2015). The final empirical modeling equation for the percentage removal of Pb^{2+} ($Y_{Pb(EC)}$, $Y_{Pb(LM)}$) and Zn^{2+} ions ($Y_{Zn(EC)}$,$Y_{Zn(LM)}$) responses are given from Eqs. (22.12)–(22.15), respectively.

$$Y_{PbEC} = 84.48 - 26.39A - 1.76B + 5.51C + 18.84D - 6.09AB + 7.12AC + 9.55AD + 9.48BC + 2.49BD + 4.63CD - 13.76A^2 - 4.27B^2 + 1.15C^2 - 11.93D^2 \quad (22.12)$$

$$Y_{PbLM} = 89.11 - 23.88A - 0.23B + 5.25C + 17.21D - 5.16AB + 5.89AC + 8.82AD + 8.71BC + 1.20BD + 4.27CD - 11.07A^2 + 0.30B^2 - 0.84C^2 - 15D^2 \quad (22.13)$$

TABLE 22.6 ANOVA for response quadratic model of Pb^{2+} ions by *Eichhornia crassipes (EC) and Lemna minor (LM)*.

	Sum of squares		Degrees of freedom		Mean square		*F* value		Prob > *F*	
Source	***EC***	***LM***	***EC***	***LM***	***EC***	***LM***	***EC***	***LM***	***EC***	***LM***
Model	19,017.24	16,344.06	14	14	1358.37	1167.43	27.69	26.03	< 0.0001	< 0.0001
x_1	4628.967	3790.22	1	1	4628.96	3790.22	94.37	84.52	< 0.0001	< 0.0001
x_2	8.65	0.18	1	1	8.65	0.18	0.17	0.004	0.6804	0.9497
x_3	349.10	316.33	1	1	349.10	316.33	7.11	7.054	0.0176	0.0180
x_4	1044.97	872.35	1	1	1044.97	872.35	21.30	19.45	0.0003	0.0005
$x_1\ x_2$	100.78	72.29	1	1	100.78	72.29	2.05	1.61	0.1722	0.2235
$x_1\ x_3$	529.90	362.02	1	1	529.90	362.02	10.80	8.07	0.0050	0.0124
$x_1\ x_4$	261.74	223.49	1	1	261.74	223.49	5.33	4.98	0.0355	0.0413
$x_2\ x_3$	1076.48	843.40	1	1	1076.48	843.40	21.94	18.80	0.0003	0.0006
$x_2\ x_4$	45.34	10.60	1	1	45.34	10.60	0.92	0.23	0.3515	0.6338
$x_3\ x_4$	239.56	204.36	1	1	239.56	204.36	4.88	4.55	0.0431	0.0497
x_1^2	82.64	53.42	1	1	82.64	53.42	1.68	1.19	0.2139	0.2923
x_2^2	7.14	0.03	1	1	7.14	0.03	0.14	0.17	0.7080	0.9780
x_3^2	2.00	1.04	1	1	2.00	1.04	0.04	0.02	0.8425	0.8805
x_4^2	253.93	401.59	1	1	253.93	401.59	5.17	8.95	0.0380	0.0091
Residual	735.72	672.63	15	15	49.04	44.84				

$$Y_{ZnEC} = 74.23 - 27.70A + 2.51B - 5.40C + 15.88D + 4.22AB - 6.30AC + 0.15AD - 1.71BC + 2.03BD + 1.47CD - 21.75A^2 + 2.64B^2 - 10.74C^2 + 1.62D^2 \quad (22.14)$$

$$Y_{ZnLM} = 87.81 - 13.61A - + 4.05B - 5.79C + 22.89D + 0.70AB + 1.33AC + 11.91AD - 1.38BC - 1.99BD + 5.15CD + 0.056A^2 - 4.26B^2 - 9.28C^2 - 13.02D^2 \quad (22.15)$$

The synergetic and antagonistic effects of the corresponding variables are indicated by the positive and negative signs before the terms (Garba et al., 2016b) The appearance of one variable in a term signified a uni-factor effect, two variables implies a double effect a second-order term of variable appearance indicate the quadratic effect (Ahmad and Alrozi, 2010) As presented in Figs. 22.13–22.16, the correlations of R^2 between experimental and predicted data of Pb^{2+} and Zn^{2+} ions removal with respect to *EC* and *LM* are 0.961 (Y_{Pb}),0.959(Y_{Pb}),0.930 (Y_{Zn}),0.920(Y_{Zn}) that are within the desirability range. Multiple regression was developed from the second-order polynomial equation. The experimental and predicted values are in

TABLE 22.7 ANOVA for response quadratic model of Zn^{2+} ions by *Eichhornia crassipes (EC) and Lemna minor (LM)*.

	Sum of squares		Degree of freedom		Mean square		*F* value		Prob > *F*	
Source	***EC***	***LM***	***EC***	***LM***	***EC***	***LM***	***EC***	***LM***	***EC***	***LM***
Model	13,468.51	12,251.25	14	14	962.03	875.08	14.86	14.52	<0.0001	<0.0001
x_1	699.85	168.91	1	1	699.85	168.91	10.81	12.80	0.0050	0.1148
x_2	62.35	161.94	1	1	62.356	161.94	0.96	2.68	0.3419	0.1219
x_3	58.67	67.37	1	1	58.67	67.37	0.90	1.11	0.3561	0.3070
x_4	671.06	1395.34	1	1	671.06	1395.34	10.36	23.16	0.0057	0.0002
$x_1\ x_2$	75.63	2.05	1	1	75.63	2.05	1.168	0.03	0.2967	0.8561
$x_1\ x_3$	105.47	4.72	1	1	105.47	4.72	1.62	0.07	0.2211	0.7832
$x_1\ x_4$	0.06	390.13	1	1	0.06	390.13	8.93	6.47	0.9760	0.0224
$x_2\ x_3$	19.68	12.84	1	1	19.68	12.84	5.30	0.21	0.5894	0.6509
$x_2\ x_4$	31.31	29.87	1	1	31.31	29.87	2.48	0.49	0.4973	0.4921
$x_3\ x_4$	15.30	187.90	1	1	15.30	187.90	11.02	3.11	0.6338	0.0977
x_1^2	86.76	0.0005	1	1	86.76	0.0005	1.34	9.38E-06	0.2650	0.9976
x_2^2	73.73	191.41	1	1	73.73	191.41	1.139	3.17	0.3026	0.0949
x_3^2	70.67	52.75	1	1	70.67	52.75	5.09	0.87	0.3126	0.0364
x_4^2	1.97	127.52	1	1	1.97	127.52	0.03	2.11	0.0008	0.1663
Residual	970.6917	903.71	15	15	64.71	60.24	–	–	–	–

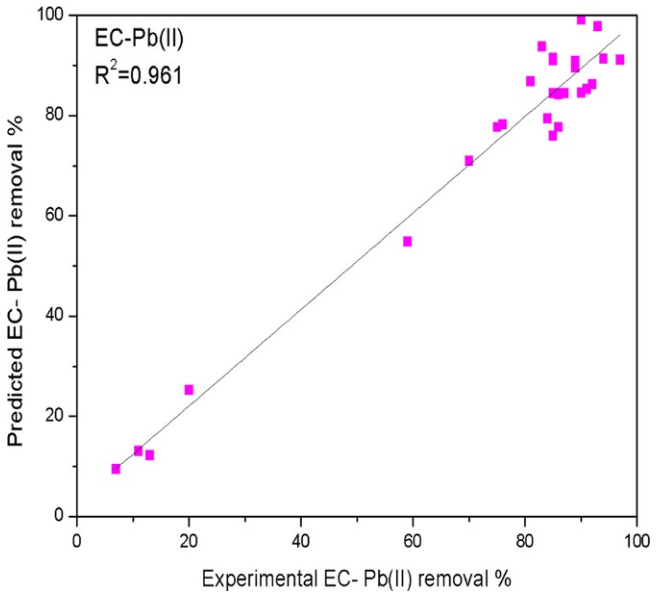

FIG. 22.13 Correlation between EXPERIMENTAL AND PREDICTED Experimental and Predicted data for Pb^{2+} ions removal for *Eichhornia crassipes (EC).*

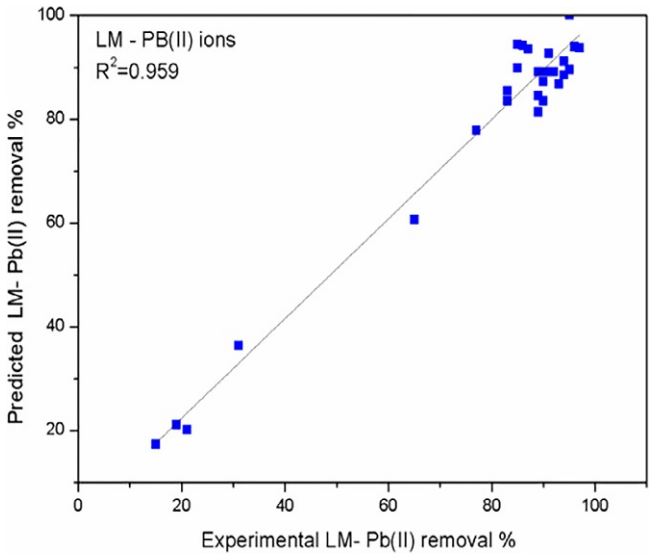

FIG. 22.14 Correlation between experimental and predicted data for Pb^{2+} ions removal for *Lemna minor (LM)*.

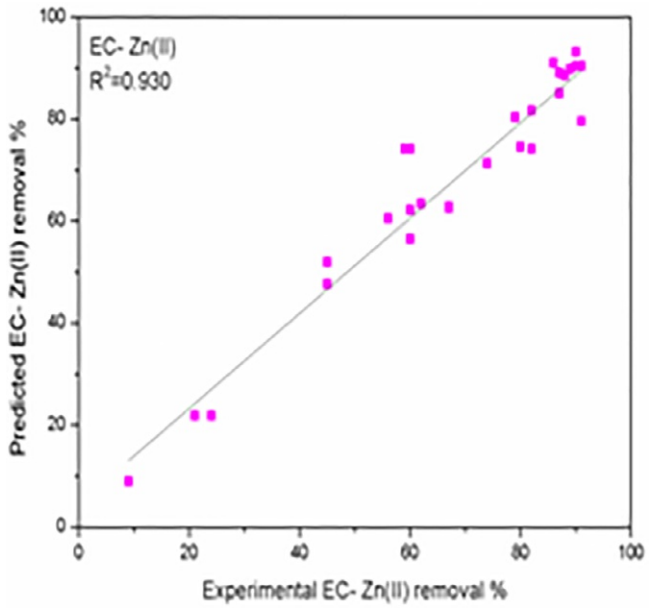

FIG. 22.15 Correlation between experimental and predicted data for Zn^{2+} ions removal for *Eichhornia crassipes (EC)*

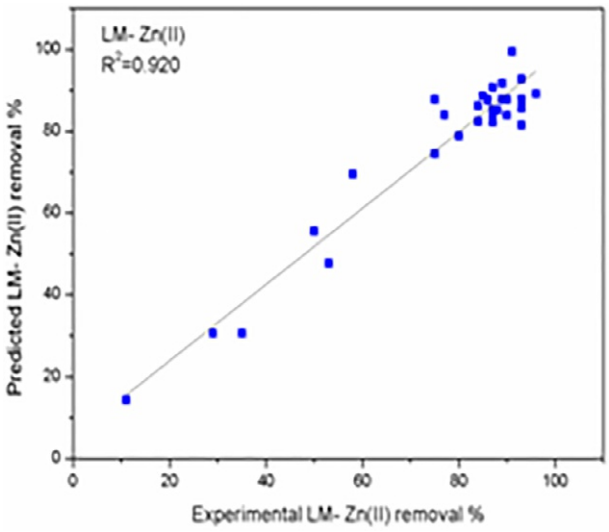

FIG. 22.16 Correlation between experimental and predicted data for Zn^{2+} ions removal for *Lemna minor (LM)*

fine agreement with each other.The R^2 values of all the four responses are high and in reasonable agreement with Adj.R^2 values of 0.928 (Pb^{2+}), 0.870 (Zn^{2+}) for *EC* and 0.923 (Pb^{2+}), 0.901 (Zn^{2+}) for *LM*, for the removal of Pb^{2+} and Zn^{2+} ions indicating that the predicted value is in agreement with the actual value.

22.3.9 Statistical analysis

ANOVA is required to validate the importance and how satisfactory the models are (Garba and Rahim, 2014). The mean square values are calculated by dividing the sum of squares of each variation sources, model, and error variance by the respective degrees of freedom. If the value of Prob. $> F$ is lesser than 0.5, the model is termed as significant. With respect to Pb^{2+} ions, percentage removal by the adsorbents *EC* and *LM* as can be seen from the Table 22.6, the model *F* value is 27.69, 26.03, and the Prob. $> F$ value of <0.0001 justifying that the model is significant. From Table 22.7, *F* value 14.86, 14.52 as well as Prob. $> F$ of <0.0001 indicated that the model was significant with Zn^{2+} removal. From the statistical studies obtained, it was clear that all the four models corresponding to Eqs. (22.12)–(22.14) were adequate to predict the removal of Pb^{2+}, Zn^{2+} ions within the range of variables studied. Figs. 22.13–22.16 show the predicted values versus experimental values for percentage removal of Pb^{2+} and Zn^{2+} ions with respect to *EC*, *LM*. It is evident that the models developed were successful in capturing the correlation between adsorption variables and response, when the theoretical value obtained was quite close to the experimental values. Adequate precision measures the signal to the noise ratio, a ratio greater than 1 is desirable (Garba et al., 2014). In this case, the ratio of 18.13, 18.19 for Pb^{2+} and 14.79, 15.5 for Zn^{2+} by *EC* and *LM* indicates an adequate signal which infers that this model can be used to steer the design space.

From Table 22.6, it is clear that the individual effect inflicted by pH for the removal of Pb^{2+} was superior with the highest F values 94.3, 84.52 on both *EC*, *LM*. The quadratic effect was more pronounced by time. pH of *EC* and *LM* are analogous with each other. Less effect is observed in the case of pH with *EC* and *LM*. The interaction effects between pH and concentration (F value - 10.83 (*EC*), 8.07 (*LM*)), dosage and concentration (F value - 21.9 (*EC*), 18.8 (*LM*)) is significant. The interaction effect between pH and dosage, pH, and time are analogous with F values 2.05 (*EC*), 1.61 (*LM*), and 5.3 (*EC*), 4.9 (*LM*).

Figs. 22.17–22.20 demonstrate the effect of a three-dimensional response surface plot for the studied variables. Fig. 22.17 shows the effect of pH and concentration with respect to *EC* for Pb^{2+} ions removal. The effect of adsorbent dosage and time with respect to Pb^{2+} ions removal for *LM* is presented in Fig. 22.18. From Table 22.7, it is obvious that the individual effect of pH and time seems to be analogous with higher *F* values 10.81, 10.36 for *EC*. Similarly, contact time is more significant with respect to the individual effect on both *EC* and *LM* corresponding to *F* values 10.36, 23.16. Interaction effects corresponding to pH and time are significant with *F* values 8.93, 6.47 for both the adsorbents. A quadratic effect is more pronounced with respect to concentration and dosage for *EC* and *LM*.

A three-dimensional response surface constructed in Fig. 22.19 shows the combined effect of pH and time for Zn^{2+} removal with respect to *EC*. An upsurge in percentage removal of Zn^{2}

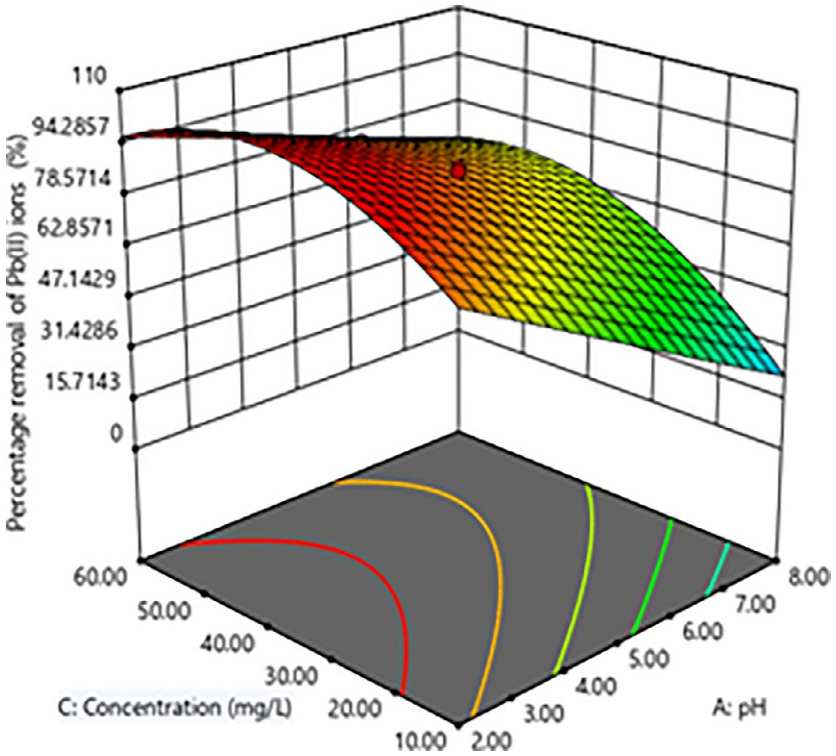

FIG. 22.17 Three-dimensional response surface of *Eichhornia crassipes (EC)* for Pb^{2+} ions.

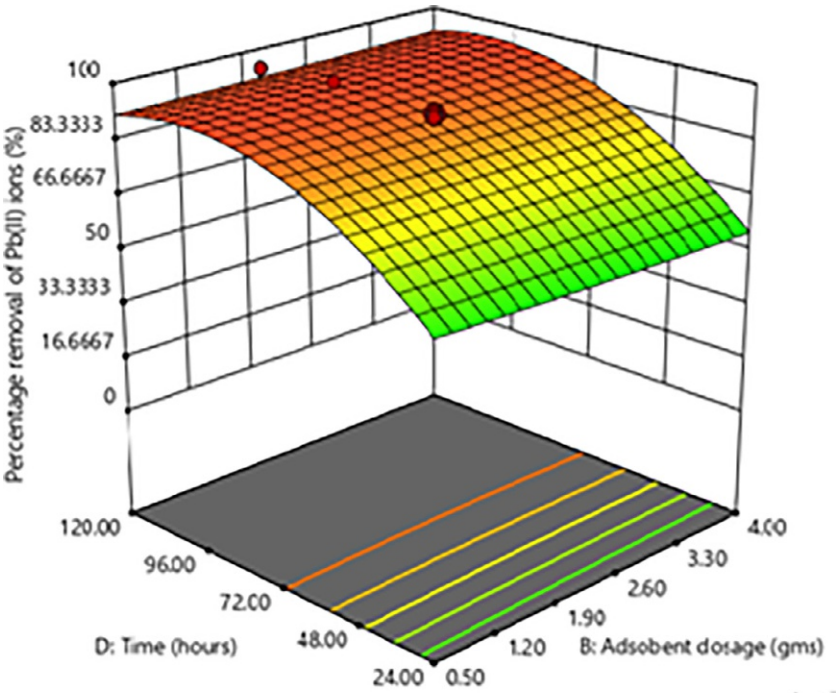

FIG. 22.18 Three-dimensional response surface of *Lemna minor (LM)* for Pb^{2+} ions.

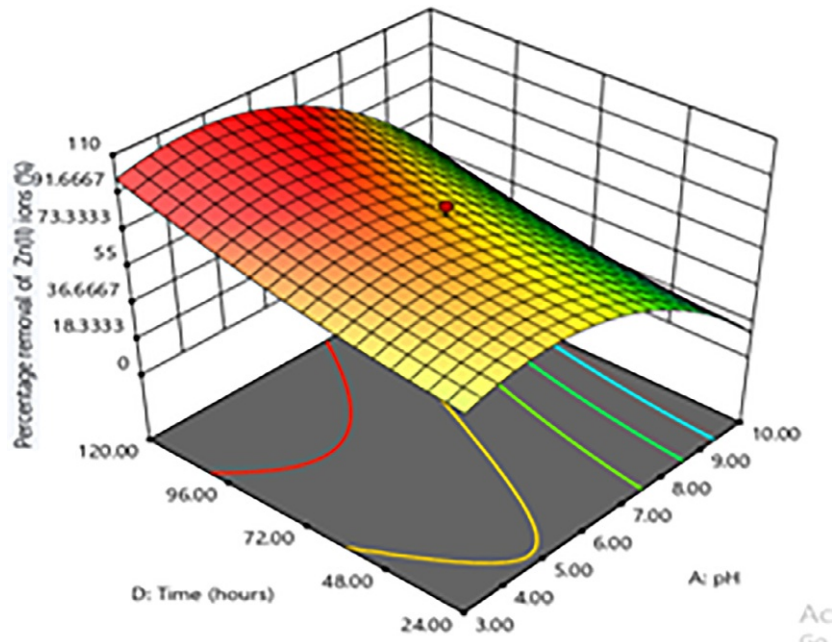

FIG. 22.19 Three-dimensional response surface of *Eichhornia crassipes (EC)* for Zn^{2+} ions.

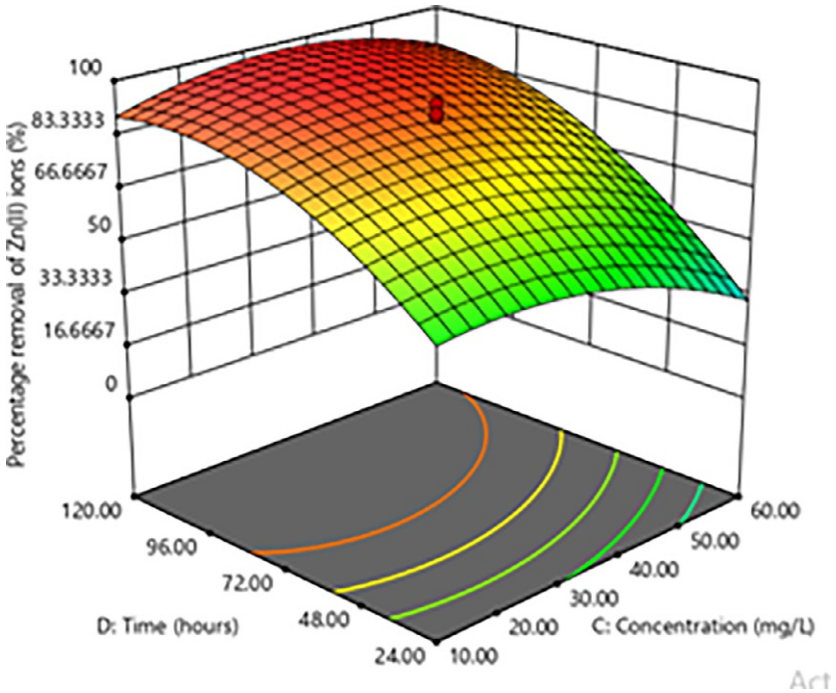

FIG. 22.20 Three-dimensional response surface of *Lemna minor (LM)* for Zn^{2+} ions.

$^{+}$ for *LM* can be observed by an increase in concentration from 10 to 60 mg/L and contact time range from 24 to 120 h (Fig. 22.20).

22.3.10 Process optimization

The main purpose of this study is to find the optimum process parameters for the higher percentage removal of Pb^{2+} ions and Zn^{2+} ions. In order to overcome the difficulty in optimizing the response under the same condition, the function of desirability was applied using Design - Expert Software (version 11). By setting the target criterion as the maximum value for all four responses. The model validation is shown in Table 22.8. The optimum adsorption

TABLE 22.8 Model validation.

Adsorbent	Desirability	pH	Dose gm	Concentration mg/L	Time h	Expt. %	RSM %	Error %
EC-Pb^{2+}	1	5	0.5	20	96	86	85.0	1
LM-Pb^{2+}	1	5	0.5	20	48	90	88.5	1.5
EC-Zn^{2+}	1	5	0.5	20	120	89	89.0	–
LM-Zn^{2+}	1	5	0.5	20	48	93	91.3	1.7

condition obtained is at an initial concentration of10 mg/L, adsorbent dosage 1 g at pH 5 with desirability 1 for Pb^{2+} and Zn^{2+} ions removal in case of both *EC* and *LM*. Experimental and predicted values for removal of Pb^{2+} at optimum condition are 86% and 85%, 90%, and 88.5% with relatively small errors of 1 and 1.9 for *EC* and *LM*, respectively. Similarly, for Zn^{2+} removal, *EC* and *LM* show 89% and 93% (experimental) and 89% and 91.3% (predicted) results with the least error 1.7, respectively. From Table 22.8, it is evident that the results are in conformity with response surface analysis results confirming that the RSM can be used as a successful tool to optimize the process constraints.

22.4 Conclusion

The factorial design of experiments for the batch experimental study of Pb^{2+} and Zn^{2+} ions using *EC* and *LM* were studied. Four adsorption parameters such as pH, adsorbent dosage, initial concentration, and time were optimized using CCD. The maximum percentage removal (93%) was obtained at optimum condition pH (5), adsorbent dosage (1 g/L), initial concentration (10 mg/L), time (48 h) for Zn^{2+} ions removal with respect to *LM* with desirability 1. Equilibrium and kinetic data were analyzed and the results reveal that Langmuir isotherm and pseudo second order be the best-fitted model. The experimental values were in good conformity with the simulated values from the response surface analysis and it confirmed that the RSM using the statistical design of experiments can be efficiently used to optimize the process parameters. The results from the present adsorption experimental studies reported that the *Lemna Minor* (*LM*) can be utilized as an effective low-cost adsorbent for the removal of Pb^{2+} and Zn^{2+} ions from battery effluent.

Acknowledgment

The authors convey sincere thanks to the Management and Principal of Coimbatore Institute of Technology, Coimbatore-641014 for their support through the Technical Education Quality Improvement Programme (TEQIP-III) fund.

References

Ahmad, M.A., Alrozi, R., 2010. Optimization of preparation conditions for mangosteen peel-based activated carbons for the removal of Remazol brilliant blue R using response surface methodology. Chem. Eng. J. 165, 883–890. https://doi.org/10.1016/j.cej.2010.10.049.

Ahmadi, A., Heidarzadeh, S., Aokhtari, A.R., Darezereshki, E., Harouni, H.S., 2014. Optimization of heavy metal removal from aqueous solutions by maghemite (γ-Fe_2O_3) nanoparticles using response surface methodology. J. Geochem. Explor. 147, 151–158. https://doi.org/10.1016/j.gexplo.2014.10.005.

Anilkumar, B., Chitti Babu, N., Kavitha, G., 2016. Biosorption of zinc on to *GracilariaCorticata* (red algae) powder and optimization using central composite design. J. Appl. Sci. Eng. Methods 2, 412–425.

Anitha, T., Senthil Kumar, P., Sathish Kumar, K., Sriram, K., Feroze Ahmed, J., 2015. Biosorption of lead(II) ions onto nano-sized chitosan particle blended polyvinyl alcohol (PVA): adsorption isotherms, kinetics and equilibrium studies. Desalin. Water Treat. 57, 13711–13721. https://doi.org/10.1080/19443994.2015.1061951.

Anitha, A., JinasMansura, M., Rajeswari, A., 2017. Adsorption and removal of zinc (II) from aqueous solution using peepal (ficusreligiosa) leaf derived carbon. Int. J. Mod. Trend. Eng. Res. 4, 31–37. https://doi.org/10.21884/IJMTER.2017.4149.O7NNV.

Anzeze, D.A., Onyari, J.M., Shiundu, P.M., Gichuki, J.W., 2014. Adsorption of Pb (II) ions from aqueous solutions by water hyacinth (Eichhornia Crassipes): equilibrium and kinetic studies. Int. J. Environ. Pollut. Remidiat. 2, 89–95. https://doi.org/10.11159/ijepr.2014.013.

Bulgariu, L., Bulgariu, D., 2014. Enhancing biosorption characteristics of marine green algae (Ulva lactuca) for heavy metals removal by alkaline treatment. J. Bioproc. Biotech. 4, 1–8. https://doi.org/10.4172/2155-9821.1000146.

Bulgariu, L., Bulgariu, D., Matei Macoveanu Melichova, Z., Hromaa, L., 2012. Characteristics of sorption of uncomplexed and complexed Pb(II)from aqueous solutions onto peat. Chem. Pap. 66, 239–247. https://doi.org/10.2478/s11696-012-0149-z.

Burakov, A.E., Galunin, E.V., Burakova, I.V., Kucherova, A.E., Agarwal, S., Tkachev, A.G., Gupta, V.K., 2018. Adsorption of heavy metals on conventional and nanostructured materials for wastewater treatment purposes: a review. Ecotoxicol. Environ. Saf. 148, 702–712. https://doi.org/10.1016/j.ecoenv.2017.11.034.

Chakravarty, P., Sarma, N.S., Sharma, H.P., 2010. Removal of lead(II) from aqueous solution using heartwood of *Areca catechu* powder. Desalination 256, 16–21. https://doi.org/10.1016/j.desal.2010.02.029.

Depci, T., Kul, A.R., Onal, Y., 2012. Competitive adsorption of lead and zinc from aqueous solution on activated carbon prepared from Van apple pulp: study in single- and multi-solute systems. Chem. Eng. J. 200, 224–236. https://doi.org/10.1016/j.cej.2012.06.077.

Fargašová, A., Filová, A., Ondrejkovičová, I., Mackuľak, T., 2018. The effect of Cd(II) complexes with nicotinamide (NA) on microalgae growth, production of chlorophylls, oxygen evolution and cd adsorption. Chem. Pap. 72, 2273–2281. https://doi.org/10.1007/s11696-018-0488-5.

Flouty, R., Estephane, G., 2012. Bioaccumulation and biosorption of copper and lead by unicellular algae *Chlamydomonas reinhardtii*in single and binary metal systems: a comparative study. J. Environ. Manag. 11, 106–114. https://doi.org/10.1016/j.jenvman.2012.06.042.

Freundlich, H.M., 1906. Over the adsorption in solution. J. Phys. Chem. 57, 385–471.

Fu, F., Wang, Q., 2011. Removal of heavy metal ions from wastewaters: a review. J. Environ. Manag. 92, 407–418. https://doi.org/10.1016/j.jenvm an.2010.11.011.

Garba, Z.N., Rahim, A.A., 2014. Process optimization of $K_2Cr_2O_4$-activated carbon from *Prosopis africana* seed hulls using response surface methodology. J. Anal. Appl. Pyrolysis 107, 306–312. https://doi.org/10.1016/j.jaap.2014.03.016.

Garba, Z.N., Rahim, A.A., 2015. Optimization of activated carbon preparation conditions from *Prosopis africana* seed hulls for the removal of 2,4,6-Trichlorophenol from aqueous solution. Desalin. Water Treat. 56, 2879–2889. https://doi.org/10.1080/19443994.2014.963150.

Garba, Z.N., Rahim, A.A., Hamza, S.A., 2014. Potential of *Borassus aethiopum* shells as precursor for activated carbon preparation by physico-chemical activation; optimization, equilibrium and kinetic studies. J. Environ. Chem. Eng. 2, 1423–1433. https://doi.org/10.1016/j.jece.2014.07.010.

Garba, Z.N., Bello, I., Galadima, A., Lawal, A.Y., 2016a. Optimization of adsorption conditions using central composite design for the removal of copper (II) and lead (II) by defatted papaya seed. Karbala Int. J. Mod. Sci. 2, 20–28. https://doi.org/10.1016/j.kijoms.2015.12.002.

Garba, Z.N., Ugbaga, N.I., Abdullahi, A.K., 2016b. Evaluation of optimum adsorption conditions for Ni (II) and cd (II) removal from aqueous solution by modified plantain peels (MPP). Beni-suef Univ. J. Basic Appl. Sci. 5, 170–179.

Hal, K.R., Eagleton, L.C., Acrivers, A., Vermenlem, T., 1966. Pore and solid diffusion kinetics in fixed adsorption constant pattern conditions. Ind. Eng. Chem. Fundam. 5, 212–223. https://doi.org/10.1021/i160018a011.

Harja, M., Buema, G., Sutiman, D.M., Cretescu, I., 2013. Removal of heavy metal ions from aqueous solutions using low-cost sorbents obtained from ash. Chem. Pap. 67, 497–508. https://doi.org/10.2478/s11696-012-0303-7.

Ho, Y.S., McKay, G., 1999. Pseudo-second order model for sorption processes. Process Biochem. 34, 451–465.

Javanbakht, V., Ghoreishi, S.M., 2017. Application of response surface methodology for optimization of lead removal from an aqueous solution by novel superparamagnetic nanocomposite. Adsorpt. Sci. Technol. 35, 241–260. https://doi.org/10.1177/0263617416674474.

Lagergren, S., 1898. About the theory of so-called adsorption of soluble substances. Kung Svenska Vetenska Handl 24, 1–39.

Langmuir, I., 1918. The adsorption of gases on plane surfaces of glass, mica and platinum. J. Am. Chem. Soc. 40, 1361–1368.

Largitte, L., Laminie, J., 2015. Modelling the lead concentration decay in the adsorption of lead onto a granular activated carbon. J. Environ. Chem. Eng., 3474–3481. https://doi.org/10.1016/j.jece.2014.12.020.

Maršálek, R., Navrátilová, Z., 2011. Comparative study of CTAB adsorption on bituminous coal and clay mineral. Chem. Pap. 65, 77–84. https://doi.org/10.2478/s11696-010-0076-9.

McKay, G., Otterburn, M.S., Sweeney, A.G., 1981. The removal of colour from effluent using various adsorbents-III . Silica: rate processes. Water Resour. 14, 15–20. https://doi.org/10.1016/0043-1354(80)90037-8.

Melichová, Z., Hromada, L., 2012. Adsorption of Pb^{2+} and Cu^{2+} Ions from aqueous solutions on natural bentonite. Pol. J. Environ. Stud. 22, 457–464.

Mohammad, M., Maitra, S., Ahmad, N., Bustam, N., Sen, T.K., Dutta, B.K., 2010. Metal ion removal from aqueous solution using physic seed hull. J. Hazard. Mater. 179, 363–372. https://doi.org/10.1016/j.jhazmat.2010.03.014.

Moosa, A.A., RidhaA, M., HussienN, A., 2015. Removal of zinc ions from aqueous solution by bioadsorbents and CNTs. Am. J. Mat. Sci. 6, 105–114. https://doi.org/10.5923/j.materials.20160604.04.

Mourabet, M., Rhilassi, E.L.A., Boujaady El, H., Bennani-Ziatni El, M., Hamri El, R., Taitai, A., 2012. Removal of fluoride from aqueous solution by adsorption on hydroxyapatite (HAp) using response surface methodology. J. Saudi Chem. Soc. 19, 603–615. https://doi.org/10.1016/j.jscs.2012.03.003.

Najafabadi, H.H., Irani, M., Rad, L.R., Haratameh, A.H., Haririan, I., 2015. Removal of Cu^{2+}, Pb^{2+} and Cr^{6+} from aqueous solutions using a chitosan/graphene oxide composite nanofibrous adsorbent. RSC Adv. 5, 16532–16539. https://doi.org/10.1039/C5RA01500F.

Namdeti, R., Pulipati, K., 2013. Response surface methodology for optimization of zinc biosorption by Grewia Orbiculata L. Int. J. Stat. Math. 5, 6–15.

Nithya, K., Sathish, A., Senthil Kumar, P., Ramachandran, T., 2016. Biosorption of hexavalent chromium from aqueous solution using raw and acid-treated biosorbent prepared from *Lantana camara fruit*. Desalin. Water Treat. 5, 25097–25113. https://doi.org/10.1080/19443994.2016.1145605.

Pandey, P.K., Sharma, S.K., Sambi, S.S., 2015. Removal of lead(II) from waste water on zeolite-NaX. J. Environ. Chem. Eng. 3, 2604–2610. https://doi.org/10.1016/j.jece.2015.09.008.

Rachayyanavar, S.V., 2015. Removal of zinc from aqueous solution using adsorption phenomena. Int. J. Sci. Eng. Res. 6, 227–232.

Rajoriya, S., Balpreetkaur, 2014. Adsorptive removal of zinc from waste water by natural biosorbents. Int. J. Eng. Sci. Invent. 3, 60–80.

Shirzad-Siboni, M., Khataee, A., Hassani, A., Karaca, S., 2015. Preparation, characterization and application of a CTAB-modified nanoclay for the adsorption of an herbicide from aqueous solutions: kinetic and equilibrium studies. C. R. Chim. 18, 204–214. https://doi.org/10.1016/j.crci.2014.06.004.

Suopajarvi, T., Liimatainen, H., Karjalainen, M., Upola, H., Niinimaki, J., 2015. Lead adsorption with sulfonated wheat pulp nano celluloses. J. Water Proc. Eng. 5, 136–142. https://doi.org/10.1016/j.jwpe.2014.06.003.

Torma, C.Z., Cséfalvay, E., 2018. Nanofiltration and electrodialysis: alternatives in heavy metalcontaining high salinity process water treatment. Chem. Pap. 72, 1115–1124. https://doi.org/10.1007/s11696-018-0433-7.

US Environmental Protection agency (UEPA), 1990. Environmental Pollution Control Alternatives: Drinking Water Treatment for Small Communities. USEPA, Washington, DC.

Weber, W.J., Morris, J.C., 1963. Kinetics of adsorption on carbon from solution. J. Sanit. Eng. Div. 89, 31–60.

Zhu, Y., Hu, J., Wang, J., 2012. Competitive adsorption of Pb(II), cu(II) and Zn(II) onto xanthate-modified magnetic chitosan. J. Hazard. Mater. 221, 155–161. https://doi.org/10.1016/j.jhazmat.2012.04.026.

CHAPTER

23

Nanocrystalline NiO powder: Synthesis, characterization and emerging applications

Bhagaban Kisan[a], *Ranjan K. Bhuyan*[b], *and Ranjan K. Mohapatra*[c]

[a]Post Graduate Department of Physics, Utkal University, Bhubaneswar, Odisha, India [b]P.G. Department of Physics, Government (Autonomous) College, Angul, Odisha, India [c]Department of Chemistry, Government College of Engineering, Keonjhar, Odisha, India

23.1 Introduction

The investigation on fine crystalline metal-oxide particles has become a growing interest in research in many diverse fields such as magneto-optic, targeted drug delivery, gas sensors, energy conversion, electrochromics, photo-catalysis (Hosokawa et al., 2012; Llandro et al., 2010; Rungsawang et al., 2010; Azhagu Raj et al., 2017; Arif et al., 2018; Abbasa et al., 2019). These nanoparticles lie between clusters whose properties are strongly dependent on its size and submicron-sized particles which have almost the properties same as bulk materials. In particular, the study of magnetism in and their magnetic interactions in different types of metal-oxide powders has yielded much consideration because of finite size and defect-induced magnetic properties and applications in magneto-optic, magneto electronic, energy storage, spintronics, etc. (Thanh, 2012; Pankhurst et al., 2009; Veiseh et al., 2010; Darton et al., 2008; Haase and Nowak, 2012; Kita et al., 2010; Mohanty et al., 2020; Dormann et al., 1997; Fiorani, 2005; Fernández-García et al., 2004; Arico et al., 2005; Kuwa et al., 2020). In addition, the large evolution of NiO nanocrystalline powders and thin films has been intense to gain room temperature ferromagnetism (FM) which are applicable for spintronic devices where both charge and spin are used to transport and store information in a new approach (Fiorani, 2005; Kodama et al., 1999).

https://doi.org/10.1016/B978-0-323-90912-9.00023-X

Recently, there have been large works reported on the magnetic properties of nanosized anti-ferromagnetic (AFM) system and many reports explain the presence of FM in nanoparticles (Bhowmik et al., 2004; Khadar et al., 2003). This was mostly initiated from Neel's suggestion that fine nanocrystalline powders of AFM system ought to show a weak FM or super paramagnetism (SPM) (Néel, 1962) properties. Richardson *et al.* (Richardson and Milligan, 1956) primarily reported on room temperature magnetic properties in NiO system with varying size. Eventually, the effect of size and its magnetic properties, exchange bias, (Kodama et al., 1997; Thota and Kumar, 2007) was reported. Further, the correlation between crystalline size and surface effects (Mandal et al., 2011) on the room temperature magnetic properties were reported. Some theoretical calculation and experimental data have shown that NiO nanoparticles ranging from 1 to 50 nm can have both AFM and FM couplings (Yi et al., 2007). Recently non-magnetic like Gd, La doped in NiO also shows room temperature ferromagnetism (Gokula et al., 2020; Siddique and Tripathi, 2020). It may be observed that many of the reported research on NiO-based systems are bottom-to-top procedure with varying size. Accordingly the correlation of the emerging magnetic properties in NiO is quite complex because of interaction between finite size, and surface (interface) effects, etc. Further, the top-to-bottom procedure with systematic varying size for studying the FM properties of pure NiO is significantly absent. Hence, in this chapter we investigate a simple, reasonable technique called ball milling process using planetary ball mill to prepare nanocrystalline NiO powders with the following observations of (i) refinement of NiO powder with milling time, (ii) the effects of finite size variation and stress induced during milling for the structural and low temperature FM study under ZFC and FC condition of milled NiO powders, (iii) correlation between the crystal structure, and FM of these pure and milled powders and to explore the possibility to enhance their magnetic properties.

23.2 Methods for synthesis and characterization of NiO powder

23.2.1 Method for synthesis

In this wok, we have concentrated on the synthesis of pure NiO powders with high-energy planetary ball milling techniques under argon atmosphere. Milling of pure NiO oxide powders was carried out by planetary high-energy ball milling in the presence of an argon (*A*r) gas atmospheric condition. The photographic view of the planetary ball comprising of a horizontal support disc on which vials are mounted and the schematic view of milling process are depicted in Fig. 23.1. The vials were mounted in such a way over the horizontal disc which rotates opposite to the direction of that of the disc. Such a motion is termed as planetary-like motion which produces tremendous outward force acting on the balls; as a result the balls collide with each other as well on the wall of the vial with greater impact. During the process of milling, the powders (oxide) undergo repeated cold welding and fracture leading to disintegration of the powders, causing in the refinement of crystallite size in to nanocrystalline alloys (Soni, 2001; Suryanarayana, 2001, 2004; Koch, 2002). With the increase in milling duration, the alloys become amorphous. In order to get a desired nanocrystalline powder, suitable milling parameters should be maintained as discussed below. Moreover, the synthesis of

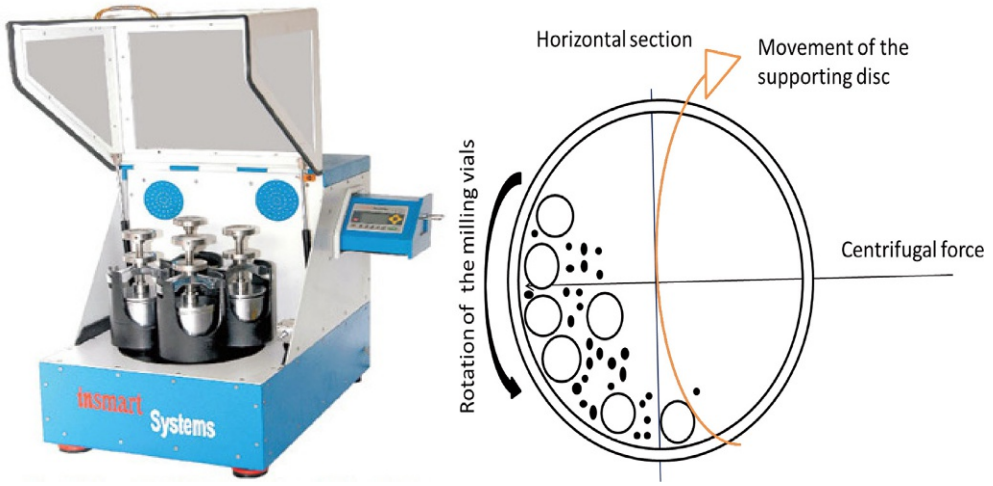

FIG. 23.1 Image of ball mill (left) and schematic diagram (right) for the movement of balls inside the vials during the process of ball milling.

nanocrystalline powders also depend on the nature of milling media, milling vial, and the balls used during milling process (Bhuyan et al., 2020).

Pure NiO commercial powders (Sigma Aldrich) were taken in high energy planetary ball mill and fill up with argon gas (99.8%). The milling procedure was being implemented for pure NiO powders for various milling periods ($t_m = 0.25$–60 h). The grinding was performed at 500 rpm and the ball-to-powder ratio of weight was done at 10:1. The grinding rate and ball-to-powder ratio of weight was done primarily by optimizing and examining the modification in the structural and magnetic properties of the NiO powders. For the purpose of preventing any heating during grinding and its effect on the attributing properties, the grinding method was scheduled to stop for 15 min following each 15 min of operation. In addition, the ground powders were gathered at periodic intervals. The evolutions of nanostructure/fine particles of NiO powders were taken for characterizing its property.

23.2.2 Characterization techniques

The crystal structure of the pure and milled powders was studied from high-power X-Ray diffractometer (18 kW). XRD data were measured at rate of 0.004°/s for studying the lattice parameters as a function of t_m. The surface morphology were observed with FE-SEM and compositional analysis was done by using SEM/EDX unit. TEM technique was used to study the microstructural properties of the powders and magnetic properties were analyzing by VSM with room temperature *M-H* loops. Low temperature *M-T* measurements were also done in the temperature range between 2 K and 400 K at different constant applied fields with SQUID magnetometer under zero field ZFC and field cool (FC) conditions. Electron paramagnetic resonance (EPR) measurement were studied with at X-band frequency ($\nu = 9.4$ GHz) and 100 kHz magnetic field modulation in powder form.

23.3 Structures and properties of nanocrystalline NiO powders

23.3.1 Structural studies

The un-milled NiO powder (Kisan et al., 2014) shows the face-centered cubic (*fcc*) structure from its Bragg reflection. Similarly, the as-milled NiO powder (Kisan et al., 2014) also exhibits *fcc* structure with no impurity phase. From the observation of the XRD peaks shows that the sharp Bragg reflections observed in pure un-milled NiO powders broadens significantly and considerable shift in peak position towards a lower angle. The broadening indicates the formation of refined and strain in NiO powders and the peak shifting indicates a considerable change in the lattice parameter during the milling process.

It is well known that broadening Bragg reflection peaks take place due to the reduction of crystallite size (D), broadening due to instrument and strain (η) caused by the density of dislocations (ρ) induced during ball milling process (Ding et al., 2001; Kisan et al., 2014). Subsequently, to calculate the individual contribution from D and η, Bragg reflection peak were examined by using Williamson-Hall Plot (WHP) method (Williamson and Hall, 1953) (Eq. 23.1).

$$\Delta\theta\cos\theta = \frac{k\lambda}{D_{WHP}} + 4\eta\sin\theta \tag{23.1}$$

where, $\Delta\theta$ is full width at half maximum (FWHM) of Bragg peaks (in radians) and eliminating the broadening from instrumental contribution, θ is angle of peak position, λ(= 1.5406 Å) is the wavelength of the X-ray, D_{WHP} is average crystallite size, k is constant value 0.9 by presuming spherical nature of powders and η is lattice strain. In order to validate the WHP fit to XRD data, the Eq. (23.1) is modified to.

$$\Delta K = \frac{k}{D_{WHP}} + K\eta \tag{23.2}$$

where, ΔK [= $(\Delta\theta\cos\theta)/\lambda$] and $K = 4\sin\theta/\lambda$. Fig. 23.2 depicts the plot of ΔK versus K for the 30 h milled NiO powders and fit (linear) to the obtained data using Eq. (23.2). From fitting observed that all data not fall into the straight line fit and hence not entirely obey the linear fit to WHP method. The observed variation in the data can be correlated to the presence of anisotropic difference due to the different excess strain during milling. So, some Bragg peaks may exhibit large strain value than others peaks.

Ungar and coworkers suggested a modification to WHP method by including dislocation contrast factor in order to consider the anisotropic distribution of dislocation effects on different Bragg peaks (Ungar and Tichy, 1999; Ungar et al., 1999). Hence, to separate the size and strain effects effectively for the as-milled NiO oxide samples, the XRD patterns were analyzed using modified Williamson-Hall Plot (MWHP) method. Using this approach, the broadening corresponding to each contribution of reflections can be given as.

$$(\Delta K)^2 = \left(\frac{0.9}{D}\right)^2 + \left(\frac{\pi b^2\rho}{2B}\right)K^2C \tag{23.3}$$

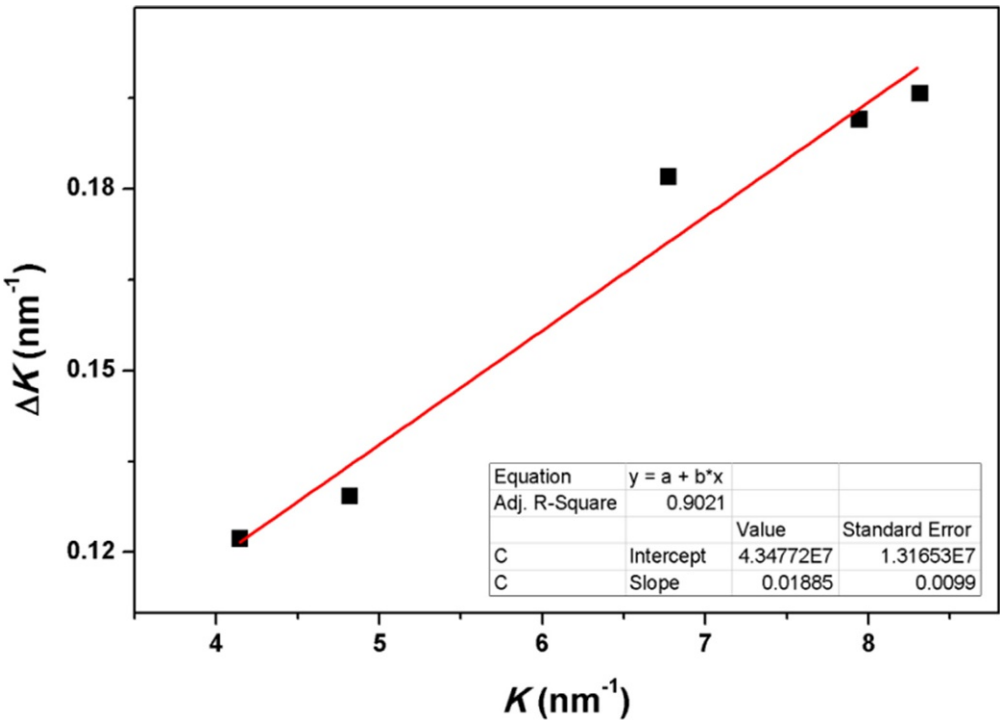

FIG. 23.2 The plot of ΔK versus K for the 30 h milled NiO powder. The straight line is the linear fit to Eq. (23.2).

where, $\triangle K\,[=(2\cos\theta\Delta\theta)/\lambda]$, $K = 2\sin\theta/\lambda$, D is average crystal size, b is modulus of the Burgers vector of dislocations taken as $b = \left(\sqrt{3}/2\right)a$ (Shen et al., 2005), ρ is average dislocation density and B is a constant, taken as 10 for a wide range of dislocation distributions (Reves et al., 1996) and $C(=C_{hkl} = C_{h00}(1 - qH^2))$ is dislocation contrast factor and for the elastically anisotropic materials (Ungar et al., 1999; Shen et al., 2005; Reves et al., 1996; Kalita et al., 2008; Mhadhbi et al., 2010), where the residual strains affect some Bragg reflections more than the others, q is a constant and for cubic $H^2 = (h^2k^2 + k^2l^2 + l^2h^2)/(h^2 + k^2 + l^2)$.

Fig. 23.3 depicted the typical plot of $(\Delta K)^2$ versus K^2C and the linear fit using Eq. (23.3). It is clear from the figure that all the XRD data almost fall into straight line and hence fitted using a straight line. From the straight line fit, intercept and slope D and ρ values were calculated. Note that the dislocation density is the important structural parameters (Hull and Bacon, 2001) affect sits microstructure and correlated to the induced strain and reduced crystal size as $\eta = \frac{\rho D b}{2\sqrt{3}}$. The determined values of D and η for as-milled NiO powders are plotted as a function t_m (Kisan et al., 2014).

With increasing t_m, D decreases largely up to $t_m = 10$ h and then remains almost constant upon subsequent milling. NiO powders milled more than 10 h exhibit fine nano-sized crystals with the size of around 11 nm. On the other hand, the strain increases drastically for t_m up to 10 h and then decreases slightly for above 10 h milling. The strain value is quiet high for

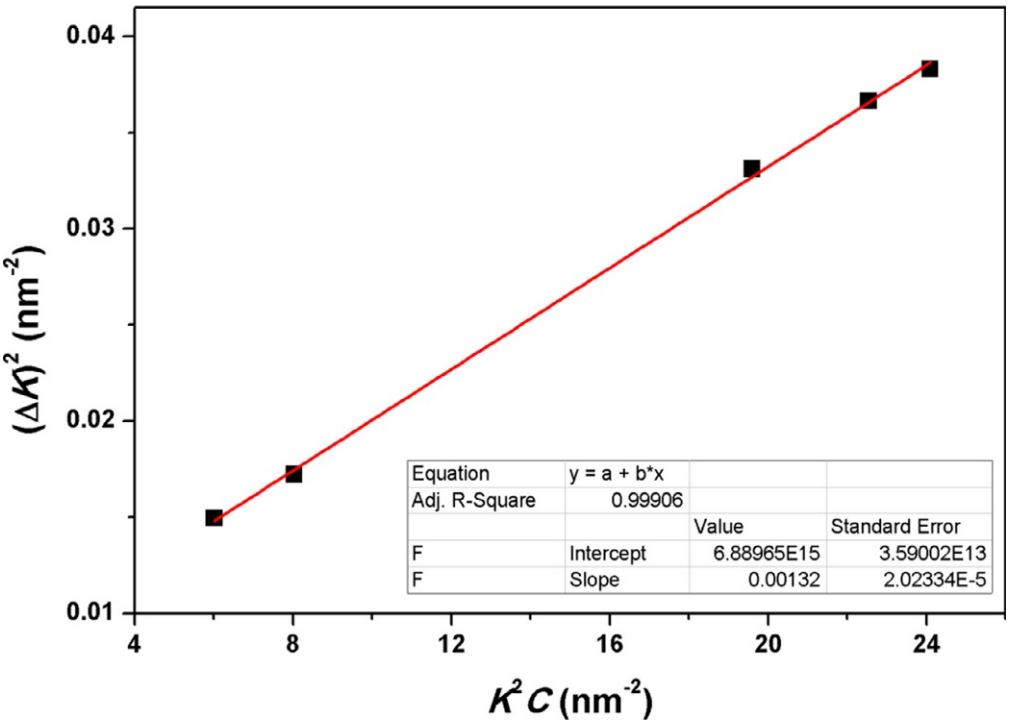

FIG. 23.3 The plot of $(\Delta K)^2$ versus K^2C for the 30 h milled NiO powder. The straight line is the best linear fit to Eq. (23.3).

milled as compared to pure NiO powders or NiO powders prepared by any other chemical process (Proenca et al., 2011; Tajiri et al., 2015). The results suggest that the dislocations formed by the high-energy ball mill is extremely influencing on the refinement of nanocrystalline microstructure. At small scale of crystal size, the longer period of milling does not create further dislocations and it is not easy to generate additional dislocations in nano-scale crystal. However, the existing dislocations will be rearranged and some dislocations may be induced due to lengthen grinding and the strain values decreases moderately for 60 h milled powders.

The morphology and evolution of nanocrystalline microstructures, the pure un-milled NiO and as-milled NiO powders were characterized using FE-SEM and TEM measurement respectively. Fig. 23.4 shows the typical FE-SEM images of un-milled NiO powders and as-milled NiO powders for $t_m = 1$, 10, 20, 40, and 60 h. The average particle size of 1 to 3 μm is observed from particle morphology in un-milled NiO powders.

Further, with increasing milling time t_m, the average crystallite size of the milled powders decreases considerably less than 300 nm. At the same time, the tiny particles start to the agglomerate to form accumulated particles and increases with t_m. These accumulations of particles are due to frequent cold welding and breaking of powder during grinding process. Fig. 23.5 showed the typical plane-view bright-field TEM (BF-TEM) images, selected area electron diffraction (SAED) patterns, HR-TEM images and i-FFT images of selected areas of HR-TEM

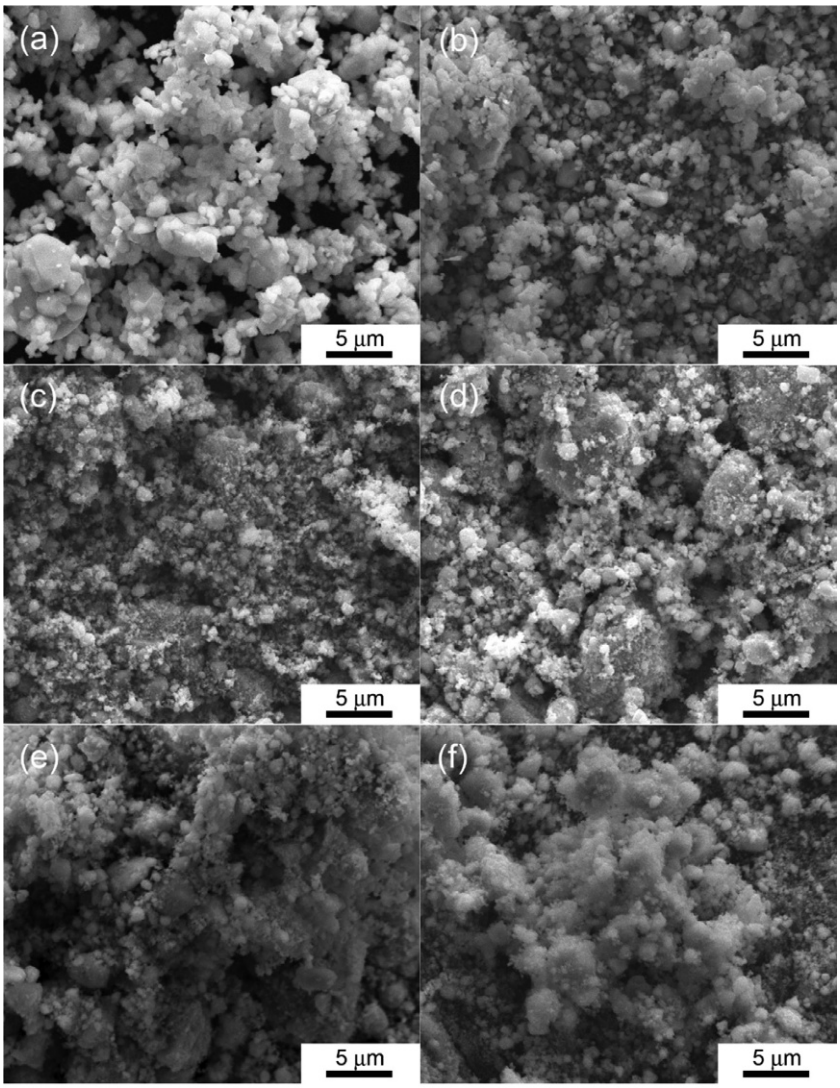

FIG. 23.4 FE-SEM images of (A) pure un-milled and as-milled NiO powders at t_m = (B) 1, (C) 10, (D) 20, (E) 40 and (F) 60 h (Kisan et al., 2015).

images of pure un-milled and as-milled NiO powders for 3, 10, and 30 h. BF-TEM image of the un-milled powder shows clear morphology and size is around 40 and 70 nm. The diffraction rings in the SAED pattern observed the evidence of polycrystalline nature. Further, as-milled NiO powder shows the fine nano-crystalline micro-structure and non-uniform morphology obtained from BF-TEM images. In addition, diffraction rings from SAED pattern, indexed to *fcc* structure only and confirm polycrystalline in nature of the pure and milled NiO powders. The average size of the crystals was calculated from BF-TEM and HR-TEM images; the

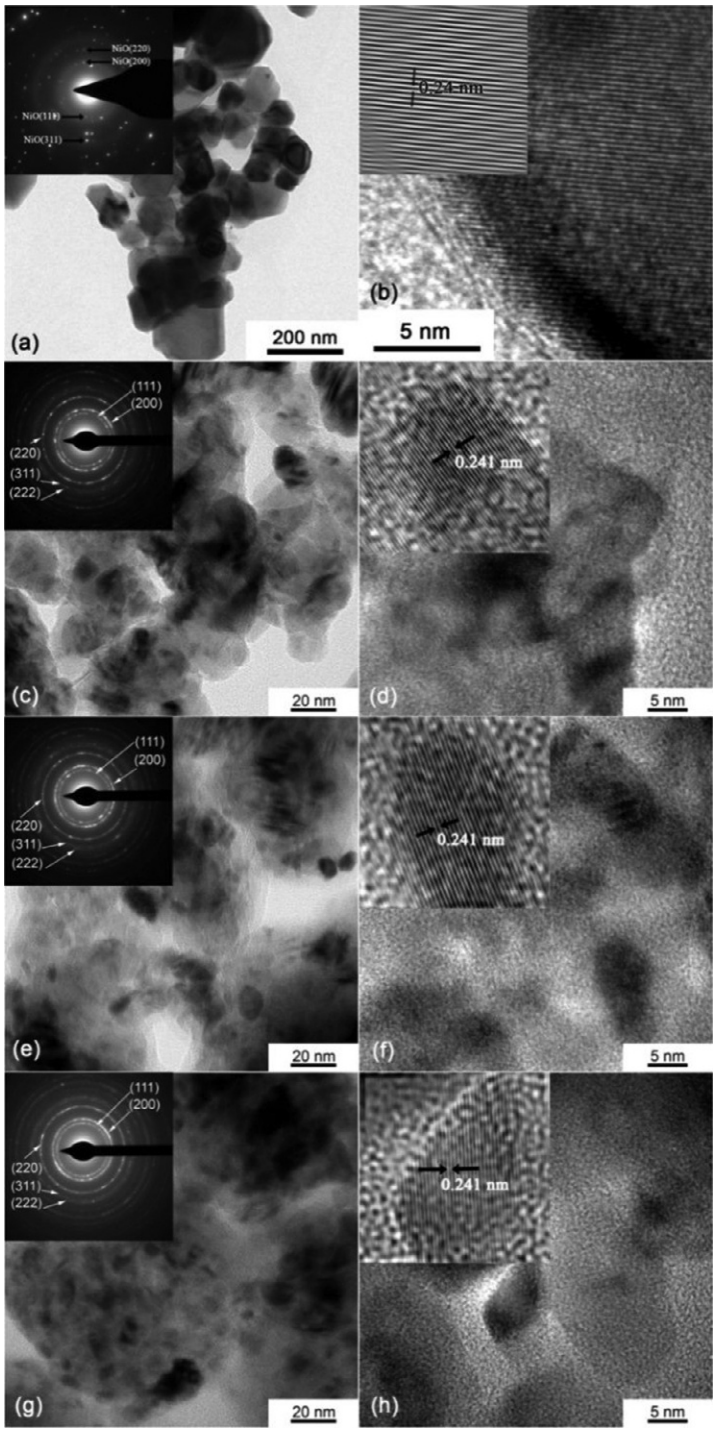

FIG. 23.5 BF-TEM, SAED, HR-TEM and i-FET of selected areas of high-resolution TEM of (A, B) pure NiO and milled NiO at various t_m: 3 h (C, D), 10 h (E, F) and 30 h (G, H), respectively (Kisan et al., 2015).

average crystal size was calculated at different position and value between 40 and 70 nm for the un-milled NiO to about 14 nm and 11 nm for 3 h and 30 h milled powders, respectively. From TEM images the crystallite size of NiO shows nearly a close to the XRD results. Though, the nanoparticle powders show non-uniform shapes with wide ranging size distribution. The lattice parameter was carefully calculated from high-resolution TEM images by i-FFT method using a GATAN digital micrograph. The i-FFT method is easy to find the lattice fringes and the calculated inter-planar space is about 0.24 nm which is assigned to NiO (111) lattice plane. Thus, viewing the TEM and XRD results both are in good accord with each other and physical properties changes must depend on crystal size of NiO powders.

23.3.2 Magnetic properties

The initial magnetization (*IM*) curves and magnetic hysteresis (*M-H*) loops and expanded version of hysteresis loops near to origin for un-milled and as-milled NiO powders at various t_m measured at room temperature. From the figure, it is clearly shown that the un-milled NiO powder indicates AFM nature because of weak response to field and hysteresis loop passing through the origin (Kisan et al., 2014). Conversely, for the t_m powder the magnetization increases moderately at lower fields and a gradual increase in moment with increasing fields. The amount of increase in the magnetization at low field increases progressively with increasing t_m below 30 h and then decreases slightly with increasing $t_m > 30$ h. It is observed that hysteresis loops are switched slightly to the negative axes and shift/move decreases with increasing t_m, which evidence the existing of exchange bias in as-milled NiO powders.

The observed results revealed two achievable magnetic elements related with the magnetization measurement. As the bulk NiO powder exhibits a clear AFM nature and the milling of NiO powders produces defects and size reduction with the lattice expansion, the two-component nature can be ascribed to low-field regions which is an easily magnetization and a non-saturating part responsible for a linear change at the higher applied field. These components can be extracted by fitting *IM* curves by Eq. (23.4).

$$M(H) = M_{FM}(H) + \chi_{AFM}H \tag{23.4}$$

where, $M(H)$ is the magnetization variation as a function of applied field (H), M_{FM} is the magnetization due to easily magnetizing component, χ_{AFM} is AFM susceptibility. The calculated values of magnetic moment at 12 kOe ($M_{12\text{kOe}}$), the maximum change in the magnetization with applied field in low-field region (dM/dH), change in coercivity value(H_C) with t_m, and the determined value of M_{FM} from the Eq. (23.5) and the calculated values of exchange bias, H_E [$= (|H_{C+}| - |H_{C-}|)/2$] plotted as a function of average crystal size. $M_{12\text{kOe}}$ increases regularly with increasing t_m up to 30 h and then decreases slightly for $t_m > 30$ h, resulting in a maximum in the curve at around 30 h of milling. Similarly, the value of dM/dH also increases up to 30 h and then above $t_{\text{m}} = 30$ h of milling decreases. On the other hand, H_C of pure NiO is AFM nature and value is zero, increased remarkably ($\sim$ 290 Oe) after milling. Additionally, H_C value achieved 290 Oe for 20 h and then constant for above 20 h. In order to understand any correlation between structural and magnetic parameters, the determined values of M_{FM} from Eq. (23.5) and the H_E value plotted with NiO crystallite size (Kisan et al., 2014). Interestingly, M_{FM} increases gradually with decreasing crystal size up to 15 nm and exhibits a

huge increase below 15 nm. The relationship between M_{FM} and the crystal size has been closely approximated by using three-parameter empirical model (Seber and Wild, 2003) as given in Eq. (23.5).

$$M_{FM}(D) = (x + y \cdot D)^{-1/z} \tag{23.5}$$

where, $M_{FM}(D)$ is the crystal size dependence of induced FM component, x, y, and z are constants. The fitting of the experimental data yields the values of x, y and z as -31, 3.1, and 1.7, respectively. On the other hand, H_E decreases almost linearly with decreasing crystal size. This suggests that NiO powders change into induced FM from the pure AFM nature. To obtain the effect of crystal size, the variation of H_E with crystal size was fitted to Eq. (23.6).

$$H_E(D) = H_E(0) + m \cdot D \tag{23.6}$$

where, $H_E(D)$ is size-dependent exchange bias, $H_E(0)$ is size-independent exchange bias component, and m is a constant. The fitting of the experimental data provides $H_E(0) = -18.94$ Oe and $m = 2.66$ Oe/nm.

The room temperature FM in the as-milled NiO powders, we correlated with crystallite size. The un-milled NiO AFM nature, AFM spins coupled to (111) planes are compensated and hence observed zero magnetic moment (Kodama et al., 1997; Thota and Kumar, 2007; Ulmane et al., 2007; Winkler et al., 2008; Kisan et al., 2015; Ravikumar et al., 2016).

Therefore, the hysteresis loop of un-milled NiO powder exhibits small response to magnetic field and passes through origin. It is familiar that ball milling method generates refinement of crystal size and huge imperfection with creation of vacancies. The values of D decrease and, η and V increase with increasing t_m confirm from the XRD analysis. In addition, pure un-milled NiO pale green in color changed to dark green with increasing milling, which is related to the development of non-stoichiometric in NiO powders induced by the imperfection, reduce in size, and oxidation state change from Ni^{2+} into Ni^{3+} (Kisan et al., 2015; Ahmad et al., 2006). This influences a change in the magnetic properties as follows: With increasing t_m, the Ni^{2+}-O^{2-}-Ni^{2+} super-exchange interaction diminishes due to defects and refinement of crystallites size as evidenced from Raman and XPS spectra results and increases the number of surface spins with respect to particle core (Ravikumar et al., 2016; Peck et al., 2011). This shows net magnetic moment due to spin alignment, in a relatively low magnetic field. Under this circumstance, the exchange bias between the produce from uncompensated FM at the surface and the spins of compensated AFM core. Furthermore, the development of structural chaos because of the formation of imperfection like oxygen vacancies gives rise to the finite magnetization. Therefore, the magnetization of nanostructured NiO increases as expressed in Eq. (23.5) and the exchange bias effect decreases with decreasing crystal size as seen through Eq. (23.6). Furthermore, the increase in lattice value can be explained based on defects and broken bonds, and possible surface anisotropy to controlling the Ni^{2+}-O^{2-}-Ni^{2+} super exchange interaction and exchange bias effect. So, these results confirm a good relationship between finite crystallite size and magnetic properties of milled NiO powders. To further confirm the origin of the induced FM and to rule out any expected impurities contribution, chemical compositions were analyzed using EDS, respectively. No other impurities are detected under the elemental analysis using EDS method (Fig. 23.6).

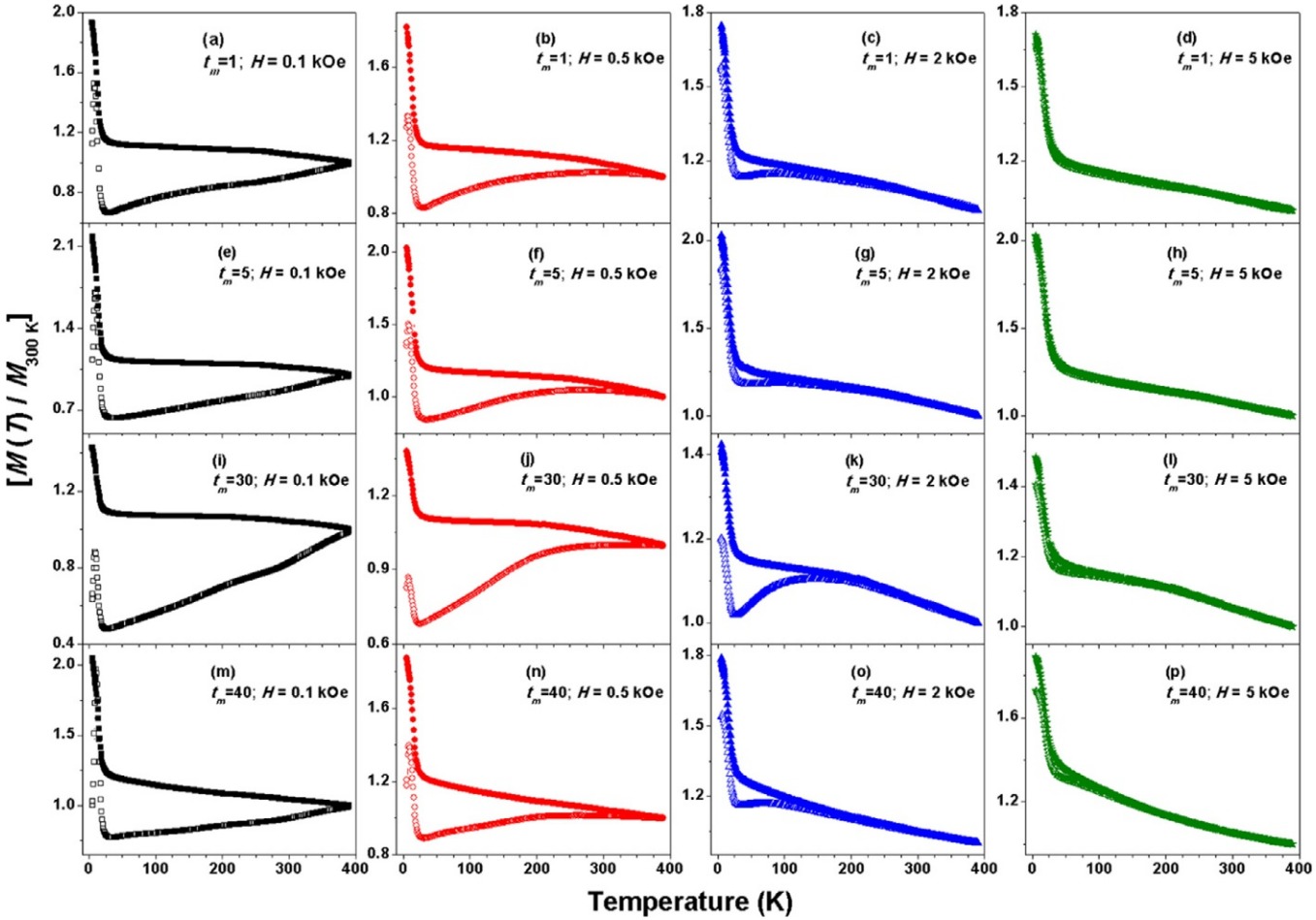

FIG. 23.6 Low-temperature *M-T* data of milled NiO powders at different t_m and measured under different applied magnetic fields.

To understand the effect of temperature and magnetic field on the magnetic properties of NiO powders as-milled at different t_m, low-temperature M-T measurements in constant applied fields under ZFC and FC conditions were measured in between 2 K and 400 K temperature range. In ZFC process, initially the sample was cooled down to 2 K under without any applied magnetic field and magnetization was measured with temperature by applying constant DC magnetic field during warming process up to 400 K. Subsequently, in FC condition the same constant value of applied field was applied and cooled down to 2 K and then the magnetization was measured heating to 400 K. Fig. 23.6 displays normalized magnetization $[M(T)/M_{300K}]$with temperature for the milled powders at 1, 5, 30, and 40 h done in ZFC (M_{ZFC}) and FC (M_{FC}) conditions in a various field of 0.1, 0.5, 2, and 5 kOe. A bifurcation (T_{bifur}) between the M_{ZFC} and M_{FC} was observed at around 390 K for all the samples measured at low-applied magnetic fields. Interestingly, the value of T_{bifur} shifts to low temperature with increasing applied field. It is generally accepted that the existence of T_{bifur} indicates large distribution of magnetic moment, which arises from the large size distribution of the crystals (Zysler et al., 2000; De Biasi et al., 2002; Winkler et al., 2005; del Bianco et al., 2008). In addition, M_{ZFC} curve shows two peaks: (i) a broad peak (T_{broad}) below the T_{bifur} and (ii) another sharp peak at very low temperature below 10 K. These peaks in the M_{ZFC} curve corresponds to two types of blocking processes, i.e., T_{broad} below T_{bifur} can be assigned to the thermal relaxation comes from the surface spins, while the sharp peak at low temperature (T_{fz}) represents the freezing of disordered surface spins. The earlier report revealed that T_{fz} depends on size of the particles. Peck *et al.* (Peck et al., *2011*) reported only the observation of paramagnetic tail without any sharp T_{fz} at low temperature for the NiO nanoparticles of size around 18 nm. Duanet al (Duan et al., 2012) reported the values of T_{fz} as 10.4 K for 12.4 nm-sized NiO. Meneses *et al* (Meneses et al., *2010*) found the T_{fz} peak at 11 K for NiO powders for 5.8 nm. Similarly, Winkler *et al.* (Winkler et al., 2008) also reported a slightly higher T_{fz}peak at 17 K for NiO powder for 3 nm. On the other hand, Meneses *et al.* (Meneses et al., 2010) and Tadic *et al.* (Tadic et al., 2011) reported a lower value of T_{fz} of 9 K and 6.5 K for 5.8 nm in NiO powders dispersed in polyvinyl pyrrolidone and 3 nm NiO powder implant in silica matrix, respectively. Fig. 23.6 shows the value of T_{fz} in 8.4 K, 9.7 K, 10.2 K, and 11.1 K for the NiO powders milled at 1 h (14.4 nm), 5 h (11.5 nm), 30 h (11 nm), and 40 h (10.8 nm), respectively. Results are close to what is reported in literature indicating that the size dependent surface spins of the fine NiO powders have important results due to freezing of the surface spins, i.e., surface atoms of the powders increases with reducing crystallite size. This leads to an increase in surface disorder with decreasing crystal size and accounts for increased value of T_{fz} with decreasing size. The M_{FC} data are found to increase gradually with decrease in temperature down to about 35 K at different applied fields for all the measured samples and then exhibit rapid increases in magnetization down to 4.2 K, which may be ascribed to the surface spin freezing. Interestingly, none of the samples show any peak in M_{FC} curves under FC process, which is again concurrent with the literature (Peck et al., 2011; Meneses et al., 2010; Tadic et al., 2011; Ghosh et al., 2006; Ulmane et al., 2011). With increasing the magnitude of applied field, the difference between M_{ZFC} and M_{FC} data decreases up to 2 kOe. On further increasing the field to 5 kOe, both M_{ZFC} and M_{FC} data follow almost a similar variation at low temperature.

Similarly, to know the nature of magnetism with the freezing of particle magnetic moments, the field-dependent values of T_{bifur} and T_{fz} were plotted as a function of field with

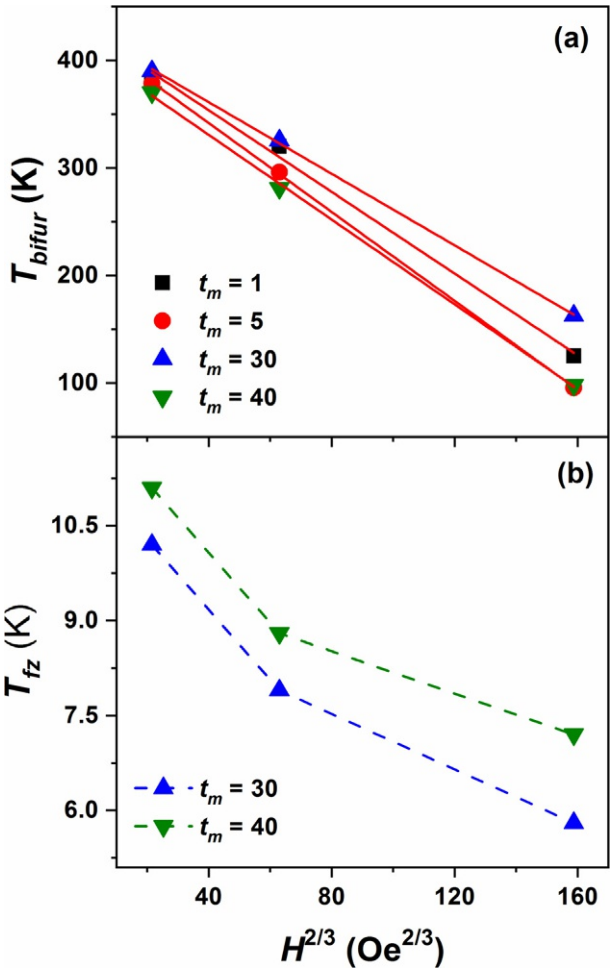

FIG. 23.7 Plots of (A) T_{bifur} versus $H^{2/3}$ and (B) T_{fz} versus $H^{2/3}$ for NiO at different t_m. The solid lines (in (A)) show best linear fits using Eq. (23.7) with R^2 of 0.995, 0.9986, 0.9991, 0.9982 for $t_m = 1$, 5, 30 and 40 h, respectively.

de Almedia-Thouless (*A-T*) line shown in Fig. 23.7 (de Almeida and Thouless, 1978) as described by Eq. (23.7).

$$H_{AT}(T) \propto \left(1 - T_{bifur}/T_{sg}\right)^{1.5} \tag{23.7}$$

It is clearly seen that T_{bifur} decreases with increasing applied field and compliance with the *A-T* line. This is a supportive evidence of spin-glass phase in the presently investigated samples. For instance, if oxygen ion misses from the surface, the exchange bond would be broken and the exchange interaction energy would be reduced. Furthermore, the coordination number from surface of Ni^{2+} ions changes than the bulk, which results in a distribution of exchange energies for the surface spins and color change of the powder due to non-stoichiometric in NiO (Ahmad et al., 2006). This gives rise disorder surface in spin and leads to spin-glass phase in the presently investigated samples (Kodama et al., 1997; Peck et al., 2011; Martinez et al.,

1998). This could be attributed to the different rate of change of T_{fz} with field upon decreasing the size of the NiO crystals (Thota and Kumar, 2007; Tiwari and Rajeev, 2005) with increasing t_m.

23.3.3 Electron paramagnetic studies

EPR spectroscopy is a useful technique to study the defects states. NiO powders reveal high defects as prepared in ball milling process and to understand the effect of nanostructure, room temperature EPR measurement was done and displayed in Fig. 23.8. Pure NiO and milled NiO powders exhibit different nature of spectra. While the pure NiO displays spectrum with large broadening and reduced intensity due to AFM nature (Yi et al., 2007; Shim et al., 2008; Lyu et al., 2010; Zhang et al., 2016) associated with Ni^{2+}-O^{2-}-Ni^{2+} super-exchange interaction at larger D, the milled NiO powders exhibit resonant peaks at low fields. To understand the peak shift more in details, see the extracted value of peak position with D in the inset of Fig. 23.8. As D decreases from 36 nm to 25 nm, the resonant peak position decreases dramatically. With a further decrease in D, the resonant peak position varies sluggishly. The large decrease in resonant peak position indicates possible FM signature of the materials (Zhang et al., 2016; Srinivas et al., 2011). It may be noted that EPR signal of most bulk

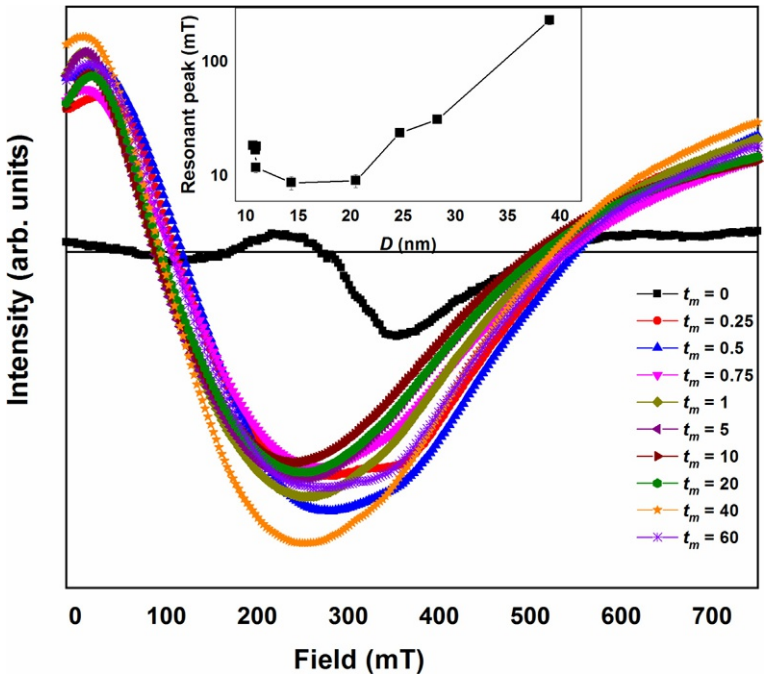

FIG. 23.8 Room-temperature EPR spectra of pure and milled NiO powders at different t_m. Inset: The variation of resonant peak position versus D.

AFM materials disappears due to the effect of very strong exchange bias and require resonance frequency higher than EPR GHz region. Therefore, the appearance of EPR signal in the currently investigated samples can be corresponded to the following mechanisms: (i) generation of surface spins due to size reduction and defects (Proenca et al., 2011; Winkler et al., 2008), (ii) formation of a SG like shell on the surface of the crystal (Tiwari and Rajeev, 2005; Kenning et al., 1987), (iii) refinement of crystal with change in Néel temperature (Néel, 1962; Kodama et al., 1997; del Bianco et al., 2008; Rinaldi-Montes et al., 2014; Makhlouf et al., 2008), (iv) the development of a weak magnetic moment due to the canting of the magnetic sub lattices (Kodama et al., 1997; Zysler et al., 1994). A comparison between EPR signal, structural-, and temperature-dependent magnetic measurements suggests that the formation of EPR signal could be assigned to the presence of surface spin of NiO crystals due to defects and size reduction, which gives good description for both room temperature and magnetic properties with field variation. Therefore, it has been established that EPR signals are affected by the milling process and modifies the surface nature of the powders due to defects and size effects.

23.4 Emerging applications

23.4.1 Environmental remediation

The presence of heavy metal inorganic pollutants such as Cd, Cu, Zn, Ni, Cr in surface water is dangerous to the human health and also for the environment and hence, need to eliminate from surface waters (Mahmood et al., 2011a; Sheel and Nayaka, 2012). Cr(VI) compounds are largely used in several industrial purposes such as steel manufacturing, metal plating, and tanning leather, etc. (Hu et al., 2005; Qamar et al., 2011). However, Cr(VI) causes significant health issues such as respiratory problems, lung cancer, ulcers, kidney and liver damage, and ultimate death (Oubagaranadin and Murthy, 2009; Baral et al., 2008; Naeem et al., 2009). The techniques used for the removal of such metal ions from the aqueous solutions are ion exchange, reverse osmosis, chemical precipitation, foam flotation, and adsorption. Due to high surface area, natural porosity and low production cost, the NiO NPs are the suitable adsorbents for the removal of heavy metals from aqueous solutions (Mahmood et al., 2011b; Song et al., 2009). It has been reported that NiO NPs prepared from precipitation method were used for the removal of Cr(VI) from aqueous solutions (Behnajady and Bimeghdar, 2014). The study concluded that the adsorption percentage increases by raising the dosage of NiO adsorbent. Moreover, pH = 4.7 is the suitable pH for the adsorption and the adsorption percentage of Cr(VI) decreases by increasing the pH of the solution. Further, the self-assembly of Ni and NiO NPs embedded in ordered MPC and polymer frameworks shows excellent adsorption properties for dyes (Wang et al., 2011). The NiO self-assembly was synthesized by evaporation of metal-containing liquid crystalline mesophases of lignin-derived polymers and transition metal nitrate yields NiO@MPC nanostructures (Chen et al., 2013a). Further, the pure NiO is a non-toxicant and has photostability properties (Fernandes et al., 2009). This is used as photocatalyst for the degeneration of several organic pollutants (Bahadur et al., 2008; He et al., 2010). The increasing environmental contamination

released from many different industries may be absorbed by effective photocatalysts focused on semiconductors (Alnarabiji et al., 2017; Lai et al., 2008). The photocatalysis of the semiconductors caused by the electron–hole pairs and band-gap excitation, and finally results in a positive hole in the valence band and can be written as the following equation (Ejhieh and Khorsandi, 2010).

$$NiO \rightarrow e_{CB}^{-} + h_{VB}^{+}$$

The development of green solvent, ecofriendly, pollution-free, and less cost-effective green methodology in chemical reactions is an essential requirement for sustainability of the biosystem (Das et al., 2020a,b). Keeping in mind, Bashir and coworkers (Bashir et al., 2019) have synthesized nickel oxide NPs in an environmentally friendly green method with *Persea americana* seed extract. These NPs were characterized by XRD, TEM, EDS, UV–Vis, and FTIR spectroscopy. As per the XRD results, the NiO NPs has a cubic-type structure with space group *Fm*3*m*, No. (225). The investigated NPs performed well as a photocatalyst in the photodegradation of free cyanide (FCN) under UV light. Fouladgar and Ahmadzadeh (Fouladgar and Ahmadzadeh, 2016) have reported the modified carbon paste electrode with NiO-NPs for the determination of methyldopa in presence of folic acid. As per the electrochemical studies, the oxidation current of methyldopa was enhanced and shifted to negative potentials on the surface of modified electrode. Moreover, the sensitivity of the modified carbon paste electrode to methyldopa did not change in presence of folic acid. In another study, Kwon and coworkers (Kwon et al., 2016) have reported the perovskite PV cells having precrystallized NiO NPs. The reported sample has improved electron-blocking capability as compared to the conventional devices. The photovoltaic cells achieved superior air stability and negligible hysteresis.

Li and coworkers (Li et al., 2021) have reported a composite of NiO NPs on hexagonal Ni-MOF (Ni-MOF@NiO), with improved electrical conductivity. The highly dispersed and small-sized NiO NPs on hexagonal Ni-MOF facilitates the migration of electrolyte ions, and hence the Ni-MOF@NiO composite act as an electrode material for supercapacitors. The authors have also suggested that the reported method may be used to synthesize other MOF@metal oxide materials for electrochemical energy storage and other related applications. Cheng and coworkers (Cheng et al., 2015) have reported the NiO NPs distributed in the vertically aligned carbon nanotube arrays (VACNTs) as a hybrid structure to be used as promising electrodes for supercapacitor applications with ultrahigh power density and energy density. Due to the synergetic effects with nanoporous structures, the supercapacitors exhibit a high capacitance. Boukhari and coworkers (Al Boukhari et al., 2019) have prepared Sm-doped NiO nanoparticles via co-precipitation method. These samples were characterized by XRD and TEM. The prepared samples have improved dielectric behavior. Moreover, with increase in temperature the samples displayed greater dc conductivity. Amani-Beni and Nezamzadeh-Ejhieh (Amani-Beni and Nezamzadeh-Ejhieh, 2018) have reported the NiO NPs-modified carbon paste electrode (CPE) in electrocatalytic voltametric determination of sulfasalazine (SSZ). As per the study, the calcined NiO had the best and maximum peak current at 200°C for the CPE electrode. Moreover, better crystallinity of NiO NPs were achieved at higher temperatures up to 800°C. These NiO NPs may be used as suitable modifier of CPE in the voltametric determination of SSZ in complex matrixes at strong basic solutions.

23.4.2 Biomedical application

These NPs also have good stability, electro-catalysis, super conductance properties, and electron transfer capability (Sasi et al., 2003). It is an environmentally active material in the adsorption of inorganic pollutants and hazardous dyes (Pandian et al., 2015). NiO nanoparticles have significant biological activities such as anti-inflammatory, cytotoxicity, and antibacterial properties which may be due to the large surface area and nowadays commonly used in biomedicine field (Sudhasree et al., 2014). It is also reported that NiO NPs possess toxic effects over microalgae and bacteria (Joerger et al., 2000; Kaviyarasu et al., 2013), which may be due to the release of Ni^{2+} inside the cell and inducing oxidative stress (Gong et al., 2011; Abbracchio et al., 1982). Moreover, these NPs show cytotoxic effects, due to their unique properties (surface area, metal ion releasing, and adsorbing ability). Various synthesis methods such as sol–gel chemistry, electro-deposition, co-precipitation, and solvothermal route were reported to prepare NiO NPs with longer reaction time strategies (Li et al., 2006; Hosseini et al., 2012). *Moringa oleifera* is a tropical tree found in Indian subcontinent and is highly recognized due to its nutritional, medicinal, and therapeutic properties (Sutherland et al., 1994). The nickel oxide NPs have been synthesized by using *M. oleifera* plant extract and their antibacterial and cytotoxic activity has been examined. The cytotoxicity activity against the human cancer cell lines was confirmed from the distortion of the morphology of cells (Chen et al., 2013b). The semiconducting photocatalysts are extensively used for decontamination of waste water. Several methods were adopted for water treatment purposes such as chlorination, adsorption, flocculation, coagulation, ultrafiltration, ozonation, reverse osmosis, and biodegradation (microbial) etc. (Shanker et al., 2017; Kumar and Rao, 2017; Vinuth et al., 2015). As per the literature survey, some metal oxide NPs have superior antibacterial, anticancer, and photocatalytic performances. Nickel oxide is a p-type semiconductor (3.5 eV) with electronic and magnetic properties and hence commonly used in battery, optoelectronics, sensors, etc. (Chen et al., 2013a). The synthesis of NiO NPs by using various medicinal plants such as *Agathosma betulina*, *Moringa Oleifera*, *Sageretia thea*, *Nephelium lappaceum*, Tamarix serotine, *Callistemon viminalis*, *Aegle marmelos*, and *Azadirachta indica* have been reported with their photocatalytic and biological applications.

Ezhilarasi and coworkers (Ezhilarasi et al., 2018) have reported the cost effective green synthesis of NiO NPs using *Aegle marmelos*. This plant is commonly used in India to cure dysentery, chronic diarrhea, peptic ulcers, etc. The prepared NiO NPs showed super paramagnetic behavior. The NPs were evaluated for their cytotoxic activity and found that the cell viability of A549 cells was effectively reduced. It was an efficient and stable photocatalyst towards the degradation of the endocrine disrupting chemical, 4-chlorophenol (4-CP). Furthermore, it showed better antibacterial activity towards the gram-positive bacterial strains. Khalil and coworkers (Khalil et al., 2017) have synthesized the NiO NPs with the aqueous leave extracts of *Sageretia thea* (Osbeck.). The NPs were fully characterized through ATR-FTIR, EDS, SAED, XRD, HR-SEM/TEM, and Raman spectroscopy. The as-prepared NPs were investigated for their antibacterial activity against some gram-positive and gram-negative bacterial strains. The cytotoxicity activity was performed which revealed significant percentage of inhibition across the studied concentrations. The NiO nanoparticles were also found to have moderate antioxidant potential. Sabouri and coworkers (Sabouri et al., 2019a) have synthesized NiO-NPs through sol–gel method by using salvia macrosiphon Boiss plant extract. The NPs were

fully characterized by FTIR, UV–Vis, XRD, FESEM, EDX, TGA/DTA, and VSM analyzes. The photocatalytic activity of the NPs on methylene blue degradation was investigated. Moreover, the cytotoxicity activity on multiple tumor cell lines was observed to check non-toxic effects for medicinal applications. In another independent study, Sabouri and his group (Sabouri et al., 2019b) have also synthesized NiO-NPs through sol–gel approach having fcc structure with space group "Fm3m". These reported NPs have great potential as photocatalysts under UV light. MTT assay was performed on human cancer U87MG cell lines to analyze the safety of these NiO-NPs.

Kannan and coworkers (Kannan et al., 2020) have reported the bio-synthesis of NiO NPs in a microwave-assisted route. The synthesized NPs were characterized by several spectroscopy techniques. The XRD study revealed well crystalline nature of the NPs with a very fine crystallite size of 20 nm and showed 91% photodegradation efficiency. The antibacterial activity of the NPs was investigated by agar well diffusion technique, which showed significant cell inhibition against various bacterial strains. Moringa olifera and neem extracts containing biologically active organic moieties such as tapenoids, flavonoids, tannins, etc., were reported to synthesize NiO NPs with the reduction mechanism of Ni to NiO nanometallic material (Mittal et al., 2013; Nogués et al., 2008). The as-prepared NiO NPs showed good anti-inflammatory and antibacterial characteristics, and hence interesting for biomedicine field.

23.4.3 Catalytic application

The nanosized NiO has unique properties as compared to its bulk counterpart and hence, extensively used as battery electrode, electrochromic films, sensors magnetic materials, catalyzer, and diesel–fuel additive. In the past few decades, transition metal oxide semiconductor photocatalysts were used for the improvements in cocatalyst (Yoshida et al., 2009; Zong et al., 2008; Maeda and Domen, 2010). The cocatalyst provides reaction sites and decreases the activation energy for gas evolution. Also, cocatalysts are able to trap electrons or holes by reducing the possibility of electron–hole recombination, and increase the photocatalytic activity. Maeda and Domen (Lin, 2006) have reported that NiOx and RuO_2 metal oxides are effective water splitting photocatalysts and NiO on lanthanum-doped $NaTaO_3$ displayed good hydrogen evolution activity. The catalytic activity depends on the available surface area for the reaction and the degree of dispersion of the cocatalyst. Due to extremely high surface area and excellent dispersion characteristics, graphene oxide is more suitable for the development of high surface area catalytic systems but not efficient water splitting. Park *et al.* (Park et al., 2005) have reported the dispersion of Ni and NiO NPs by using high-surface area graphene oxide sheets to yield enhanced photocatalytic hydrogen production. Intensive research was carried out on the organization of NPs to form 2D and 3D supper lattices, which exhibits novel properties and used in magnetic storage media and electric devices. Moreover, the synthesis of Ni and NiO NPs has been reported recently with their catalytic applications.

23.5 Summary

Structure and properties of pure and milled NiO powders have been investigated systematically. The ball mill process produces face centered cubic nanocrystalline NiO powders

(with the crystallite size of ~11 nm). The lattice volume increases almost linearly with the inverse of crystallite size. Microstructural studies reveal that the agglomeration of fine particles increases with increasing t_m and the nanocrystalline powders shows non-uniform shape with different sizes. Magnetic study indicates that pure NiO powder exhibits AFM properties and change into FM gradually upon milling due to defects and size reduction. The maximum magnetization (1.08 emu/g) and coercivity value (160 Oe) are obtained at room temperature when milling at 30 h. The observed exchange effect decreases with the decreasing NiO crystal size. Low-temperature magnetization exhibits two peaks assigned to surface spin (due to freezing) and spin-glass like phase. This fabricated nanocrystalline NiO powder is the promising candidate for applications in storage device, sensor, and spintronic device. Moreover, NiO NPs have shown significant biological activities, and hence are undoubtably beneficial to humankind. Due to their plethora of applications in diverse and promising areas, the study will provide ample references for researchers working in this field.

Acknowledgment

The authors are thankful to the editor for his valuable suggestions to modify the manuscript. Authors are also thankful to their respective institutions/universities for providing required facilities.

Conflict of interest

No conflicts to declare.

References

Abbasa, H., Nadeema, K., Hafeezb, A., Hassanc, A., Saeeda, N., Krennd, H., 2019. Ceram. Int. 45, 17289.
Abbracchio, M.P., Simmons-Hansen, J., Costa, M., 1982. J. Toxicol. Environ. Health 9, 663–676.
Ahmad, T., Ramanujachary, K.V., Lofland, S.E., Ganguli, A.K., 2006. Solid State Sci. 8, 425.
Al Boukhari, J., Hassan, R.S., Awad, R., 2019. Mater. Res. Express 6, 115094.
Alnarabiji, M.S., Yahya, N., Hamed, Y., Ardakani, S.E.M., Azizi, K., Klemes, J.J., Abdullah, B., Tasfy, S.F.H., Abd Hamid, S.H.B., Nashed, O., 2017. J. Clean. Prod. 162, 186.
Amani-Beni, Z., Nezamzadeh-Ejhieh, A., 2018. Anal. Chim. Acta. https://doi.org/10.1016/j.aca.2018.06.002.
Arico, A.S., Bruce, P., Scrosati, B., Tarascon, J.M., Schalkwijk, W.V., 2005. Nat. Mater. 4, 366.
Arif, M., Sanger, A., Singh, A., 2018. J. Electron. Mater. 47, 3451.
Azhagu Raj, R., AlSalhi, M.S., Devanesan, S., 2017. Materials 10, 460.
Bahadur, J., Sen, D., Mazumder, S., Ramanathan, S., 2008. J. Solid State Chem. 181 (5), 1227.
Baral, S.S., Das, S.N., Chaudhury, G.R., Swamy, Y.V., Rath, P., 2008. Chem. Eng. J. 139, 245–255.
Bashir, A.K.H., Razanamahandry, L.C., Nwanya, A.C., Kaviyarasu, K., Saban, W., Mohamed, H.E.A., Ntwampe, S.-K.O., Ezema, F.I., Maaza, M., 2019. J. Phys. Chem. Solids 134, 133–140.
Behnajady, M.A., Bimeghdar, S., 2014. Chem. Eng. J. 239, 105–113.
Bhowmik, R.N., Nagarajan, R., Ranganathan, R., 2004. Phys. Rev. B 69, 054430.
Bhuyan, R.K., Mahapatra, R.K., Nath, G., Sahoo, B.K., Debadutta, D., Pamu, D., 2020. J. Mater. Sci. Mater. Electron. 31, 628–636.
Chen, F., Zhou, W., Yao, H., Fan, P., Yang, J., Fei, Z.D., Zhong, M., 2013a. Green Chem. 15, 3057.
Chen, M., Zhang, Y., Huang, B., 2013b. J. Nanomater. 2013, 1–6.
Cheng, J., Zhao, B., Zhang, W., Shi, F., Zheng, G., Zhang, D., Yang, J., 2015. Adv. Funct. Mater. 25, 7381–7391.
Darton, N.J., Sederman, A.J., Ionescu, A., Ducati, C., Darton, R.C., Gladden, L.F., Slater, K.H., 2008. Nanotechnology 19, 395102.
Das, D., Sarangi, A.K., Mohapatra, R.K., Parhi, P.K., Mahal, A., Sahu, R., Zahan, K.-E., 2020a. J. Mol. Liq. 309, 113133.

Das, D., Mohapatra, R.K., Parhi, P.K., Sarangi, A.K., Sahu, R., Barik, S.R., 2020b. ACS Omega 5, 7716–7721.
de Almeida, J.R.L., Thouless, D.J., 1978. J. Phys. A Math. Gen. 11, 983–990.
De Biasi, E., Ramos, C.A., Zysler, R.D., Romero, H., 2002. Phys. Rev. B 65, 144416.
del Bianco, L., Boscherini, F., Fiorini, A.L., Tamisari, M., Spizzo, F., Antisari, M.V., Piscopiello, E., 2008. Phys. Rev. B 77, 094408.
Ding, J., Li, Y., Chen, L.F., Deng, C.R., Shi, Y., Chow, Y.S., Gang, T.B., 2001. J. Alloys Compd. 314, 262.
Dormann, J.L., Fiorani, D., Tronc, E., 1997. Adv. Chem. Phys. 98, 283.
Duan, W.J., Lu, S.H., Wu, Z.L., Wang, Y.S., 2012. J. Phys. Chem. C 116, 26043.
Ejhieh, A.N., Khorsandi, M., 2010. J. Hazard. Mater. 176 (1–3), 629.
Ezhilarasi, A.A., Vijaya, J.J., Kaviyarasu, K., Kennedy, L.J., Jothiramalingam, R., Al-Lohedan, H.A., 2018. J. Photochem. Photobiol. B Biol. https://doi.org/10.1016/j.jphotobiol.2018.01.023.
Fernandes, D.M., Hechenleitner, A.A.W., Silva, M.F., Lima, M.K., Bittencourt, P.R.S., Silva, R., Melo, M.A.C., Pineda, E.A.G., 2009. Mater. Chem. Phys. 118 (2–3), 447.
Fernández-García, M., Martínez-Arias, A., Hanson, J.C., Rodriguez, J.A., 2004. Chem. Rev. 104, 4063.
Fiorani, D., 2005. Surface Effects in Magnetic Nanoparticles. Springer, New York, XIV USA, p. 300.
Fouladgar, M., Ahmadzadeh, S., 2016. Appl. Surf. Sci. 379, 150–155.
Ghosh, M., Biswas, K., Sundaresana, A., Rao, C.N.R., 2006. J. Mater. Chem. 16, 106.
Gokula, B., Saravanan, P., Matheswaran, P., Pandian, M., Sathyamoorthy, R., Asokan, K., Vinod, V.T.P., Černík, M., 2020. J. Magn. Magn. Mater. 493, 165713.
Gong, N., Shao, K., Feng, W., Lin, Z., Liang, C., Sun, Y., 2011. Chemosphere 83, 510–516.
Haase, C., Nowak, U., 2012. Phys. Rev. B 85, 045435.
He, H., Yang, S., Yu, K., Ju, Y., Sun, C., Wang, L., 2010. J. Hazard. Mater. 173 (1), 393.
Hosokawa, M., Naito, M., Nogi, K., Yokoyama, T., 2012. Nanoparticle Technology Handbook, second ed. Elsevier, UK.
Hosseini, S.A., Niaei, A., Salari, D., Nabavi, S.R., 2012. Ceram. Int. 38, 1655–1661.
Hu, J., Chen, G., Lo, I.M.C., 2005. Water Res. 39, 4528–4536.
Hull, D., Bacon, D.J., 2001. Introduction to Dislocations, fourth ed. Pergamon Press, Oxford.
Joerger, R., Klaus, T., Granqvist, C.G., 2000. Adv. Mater. 12, 407–409.
Kalita, M.P.C., Perumal, A., Srinivasan, A., 2008. J. Magn. Magn. Mater. 320, 2780.
Kannan, K., Radhika, D., Nikolova, M.P., Sadasivuni, K.K., Mahdizadeh, H., Verma, U., 2020. Inorg. Chem. Commun. 113, 107755.
Kaviyarasu, K., Sajan, D., Devarajan, P.A., 2013. Appl. Nanosci. 3, 529–533.
Kenning, G.G., Slaughter, J.M., Cowen, J.A., 1987. Phys. Rev. Lett. 59, 2596–2599.
Khadar, M.A., Biju, V., Inoue, A., 2003. Mater. Res. Bull. 38, 1341.
Khalil, A.T., Ovais, M., Ullah, I., Ali, M., Khan, S.Z., Hassan, D., Maaza, M., 2017. Artif. Cells Nanomed. Biotechnol. https://doi.org/10.1080/21691401.2017.1345928.
Kisan, B., Shyni, P.C., Layek, S., Verma, H.C., Hesp, D., Dhanak, V., Krishnamurthy, S., Perumal, A., 2014. IEEE Trans. Magn. 50, 1.
Kisan, B., Shyni, P.C., Layek, S., Verma, H.C., Hesp, D., Dhanak, V., Krishnamurthy, S., Perumal, A., 2015. J. Magn. Magn. Mater. 384, 296.
Kita, E., Oda, T., Kayano, T., Sato, S., Minagawa, M., Yanagihara, H., Kishimoto, M., Mitsumata, C., Hashimoto, S., Yamada, K., et al., 2010. J. Phys. D. Appl. Phys. 43, 474011.
Koch, C.C., 2002. Nanostructured Materials: Processing, Properties and Potential Applications. Noyes Publications, New York.
Kodama, R.H., Makhlouf, S.A., Berkowitz, A.E., 1997. Phys. Rev. Lett. 79, 1393.
Kodama, R.H., Makhlouf, S.A., Berkowitz, A.E., 1999. Phys. Rev. B 59, 6321.
Kumar, S.G., Rao, K.K., 2017. Appl. Surf. Sci. 391, 124.
Kuwa, M., Harada, M., Sato, R., Teranishi, T., 2020. ACS Appl. Nano. Mater. 3, 2745.
Kwon, U., Kim, B.-G., Nguyen, D.C., Park, J.-H., Ha, N.Y., Kim, S.-J., Ko, S.H., Lee, S., Lee, D., Park, H.J., 2016. Sci. Rep. 6, 30759.
Lai, T.L., Liu, J.Y., Yong, K.F., Shu, Y.Y., Wang, C.B., 2008. J. Hazard. Mater. 157 (2), 496.
Li, G., Hu, L., Hill, J.M., 2006. Appl. Catal. A Gen. 301, 16–24.
Li, N., Li, Y., Li, Q., Zhao, Y., Liu, C.-S., Pang, H., 2021. J. Colloid Interface Sci. 581, 709–718.

Lin, W., 2006. Appl. Phys. Lett. 89, 211904.
Llandro, J., Palfreyman, J.J., Ionescu, A., Barnes, C.H.W., 2010. Med. Biol. Eng. Comput. 48, 977.
Lyu, K.K., Phan, T.L., Yu, S.C., Oh, S.K., Dan, N.H., 2010. IEEE Trans. Magn. 46, 2028–2031.
Maeda, K., Domen, K., 2010. J. Phys. Chem. Lett. 1, 2655.
Mahmood, T., Saddique, M.T., Naeem, A., Mustafa, S., Zeb, N., Shah, K.H., Waseem, M., 2011a. Chem. Eng. J. 171, 935–940.
Mahmood, T., Saddique, M.T., Naeem, A., Mustafa, S., Hussain, J., Dilara, B., 2011b. J. Non-Cryst. Solids 357, 1016–1020.
Makhlouf, S.A., Al-Attar, H., Kodama, R.H., 2008. Solid State Commun. 145, 1–4.
Mandal, S., Menon, K.S.R., Mahatha, S.K., Banerjee, S., 2011. Appl. Phys. Lett. 99, 232507.
Martinez, B., Obradors, X., Balcells, L., Rouanet, A., Mgonty, C., 1998. Phys. Rev. Lett. 80, 181.
Meneses, C.T., Duque, J.G.S., de Biasi, E., Nunes, W.C., Sharma, S.K., Knobel, M., 2010. J. Appl. Phys. 108, 013909.
Mhadhbi, M., Khitouni, M., Escoda, L., Sunol, J.J., 2010. Mater. Lett. 64, 1802.
Mittal, A.K., Chisti, Y., Banerjee, U.C., 2013. Biotechnol. Adv. 31, 346–356.
Mohanty, D., Satpathy, S.K., Behera, B., Mohapatra, R.K., 2020. Mater. Today Proc. https://doi.org/10.1016/j.matpr.2020.02.944.
Naeem, A., Saddique, M.T., Mustafa, S., Kim, Y., Dilara, B., 2009. J. Hazard. Mater. 168, 364–368.
Néel, L., 1962. In: Dewitt, C., Dreyfus, B., de Gennes, P.D. (Eds.), Low Temperature Physics. Gordon and Breach, New York, p. 413.
Nogués, J., Langlais, V., Sort, J., Doppiu, S., Suriñach, S., Baró, M.D., 2008. J. Nanosci. Nanotechnol. 8, 2923–2928.
Oubagaranadin, J.U.K., Murthy, Z., 2009. Chem. Prod. Process. Model. 4, 32.
Pandian, C.J., Palanivel, R., Dhananasekaran, S., 2015. Chin. J. Chem. Eng. 23, 1307–1315.
Pankhurst, Q.A., Thanh, N.T.K., Jones, S.K., Dobson, J., 2009. J. Phys. D. Appl. Phys. 42, 224001.
Park, J., Kang, E., Son, S.U., 2005. Adv. Mater. 17, 429.
Peck, M.A., Huh, Y., Skomski, R., Zhang, R., Kharel, P., Allison, M.D., Sellmyer, D.J., Langell, M.A., 2011. J. Appl. Phys. 109, 07B518.
Proenca, M.P., Sousa, C.T., Pereira, A.M., Tavares, P.B., Ventura, J., Vazquez, M., Araujo, J.P., 2011. Phys. Chem. Chem. Phys. 13, 9561.
Qamar, M., Gondal, M.A., Yamani, Z.H., 2011. J. Mol. Catal. A 341, 83–88.
Ravikumar, P., Kisan, B., Perumal, A., 2016. J. Magn. Magn. Mater. 418, 86.
Reves, A., Ungar, T., Borbely, A., Lendvai, J., 1996. Nano Mater. 7, 779.
Richardson, J.T., Milligan, W.O., 1956. Phys. Rev. 102, 1289.
Rinaldi-Montes, N., Gorria, P., Martınez-Blanco, D., Fuertes, A.B., Fernandez, B.L., Rodrıguez Fernandez, J., et al., 2014. Nanoscale 6, 457–465.
Rungsawang, R., da Silva, J., Wu, C.P., Sivaniah, E., Ionescu, A., Barnes, C.H.W., Darton, N.J., 2010. Phys. Rev. Lett. 104, 255703.
Sabouri, Z., Fereydouni, N., Akbari, A., Hosseini, H.A., Hashemzadeh, A., Amiri, M.S., Oskuee, R.K., Darroudi, M., 2019a. Rare Metals. https://doi.org/10.1007/s12598-019-01333-z.
Sabouri, Z., Akbari, A., Hosseini, H.A., Hashemzadeh, A., Darroudi, M., 2019b. J. Mol. Struct. 1191, 101–109.
Sasi, B., Gopchandran, K.G., Manoj, P.K., 2003. Vacuum 68, 149–154.
Seber, G.A., Wild, C.J., 2003. Nonlinear Regression. John Wiler& Sons.
Shanker, U., Rani, M., Jassal, V., 2017. Environ. Chem. Lett. 15, 623.
Sheel, T., Nayaka, Y.A., 2012. Chem. Eng. J. 191, 123–131.
Shen, T.D., Schwarz, R.B., Thompson, J.D., 2005. Phys. Rev. B 72, 014431.
Shim, H., Dutta, P., Seehra, M.S., Bonevich, J., 2008. Solid State Commun. 145, 192–196.
Siddique, M.N., Tripathi, P., 2020. J. Alloys Compd. 825, 154071.
Song, Z., Chen, L., Hu, J., Richards, R., 2009. Nanotechnology 20, 275707.
Soni, P.R., 2001. Mechanical Alloying: Fundamental and Applications. Cambridge International Science Publishing, UK.
Srinivas, K., Rao, S.M., Reddy, P.V., 2011. Nanoscale 3, 642–653.
Sudhasree, S., Banu, A.S., Brindha, P., Kurian, G.A., 2014. Toxicol. Environ. Chem. 95, 743–754.
Suryanarayana, C., 2001. Prog. Mater. Sci. 46, 1.
Suryanarayana, C., 2004. Mechanical Alloying and Milling. Marcel Dekker, New York.

Sutherland J. P, Folkard G. K, Mtawali M. A, and Grant W. D, Proceedings of the Twentieth WEDC Conference in Affordable Water Supply and Sanitation, Colombo, (1994) 297–299.
Tadic, M., Panjan, M., Markovi, D., Milosevi, I., Spasojevi, V., 2011. J. Alloys Compd. 509, 7134.
Tajiri, T., Saisho, S., Mito, M., Deguchi, H., Konishi, K., Kohno, A., 2015. J. Phys. Chem. C 119, 1194.
Thanh, N.T.K., 2012. Magnetic Nanoparticles: From Fabrication to Clinical Applications. Taylor and Francis.
Thota, S., Kumar, J., 2007. J. Phys. Chem. Solids 68, 1951.
Tiwari, S.D., Rajeev, K.P., 2005. Phys. Rev. B 72, 104433.
Ulmane, N.M., Kuzmin, A., Steins, I., Grabis, J., Sildos, I., Pärs, M., 2007. J. Phys. Conf. Ser. 93, 012039.
Ulmane, N.M., Kuzmin, A., Grabis, J., Sildos, I., Voronin, V.I., Berger, I.F., Kazantsev, V.A., 2011. Solid State Phenom. 168–169, 341.
Ungar, T., Tichy, G., 1999. Phys. Status Solidi A 171, 425.
Ungar, T., Dragomir, I., Revesz, A., Borbely, A., 1999. J. Appl. Crystallogr. 32, 992.
Veiseh, O., Gunn, J.W., Zhang, M., 2010. Adv. Drug Deliv. Rev. 62, 284.
Vinuth, M., Naik, H.S.B., Manjanna, J., 2015. Appl. Surf. Sci. 357, 1244.
Wang, W., Wang, H.Y., Wei, W., Xiao, Z.G., Wan, Y., 2011. Chem. Eur. J. 17, 13461.
Williamson, G.K., Hall, W.H., 1953. Acta Metall. 1, 22.
Winkler, E., Zysler, R.D., Vasquez Mansilla, M., Fiorani, D., 2005. Phys. Rev. B 72, 132409.
Winkler, E., Zysler, R.D., Mansilla, M.V., Fiorani, D., Rinaldi, D., Vasilakaki, M., Trohidou, K.N., 2008. Nanotechnology 19, 185702.
Yi, J.B., Ding, J., Feng, Y.P., Peng, G.W., Chow, G.M., Kawazoe, Y., Liu, B.H., Yin, J.H., Thongmee, S., 2007. Phys. Rev. B 76, 224402.
Yoshida, M., Takanabe, K., Maeda, K., Ishikawa, A., Kubota, J., Sakata, Y., Ikezawa, Y., Domen, K., 2009. J. Phys. Chem. C 113, 10151.
Zhang, J., Zeng, D., Zhu, Q., Wu, J., Huang, Q., Xie, C., 2016. J. Phys. Chem. C 20, 3936–3945.
Zong, X., Yan, H., Wu, G., Ma, G., Wen, F., Wang, L., Li, C., 2008. J. Am. Chem. Soc. 130, 7176.
Zysler, R., Fiorani, D., Dormann, J.L., Testa, A.M., 1994. J. Magn. Magn. Mater. 133, 71–73.
Zysler, R.D., Ramos, C.A., De Biasi, E., Romero, H., Ortega, A., Fiorani, D., 2000. J. Magn. Magn. Mater. 221, 37.

CHAPTER

24

Attraction to adsorption: Preparation methods and performance of novel magnetic biochars for water and wastewater treatment

Yasmin Vieira[a], *Eder C. Lima*[b], *and Guilherme L. Dotto*[c]

[a]Graduate Program of Chemistry, Federal University of Santa Maria (UFSM), Santa Maria, RS, Brazil [b]Institute of Chemistry, Federal University of Rio Grande do Sul (UFRGS), Porto Alegre, RS, Brazil [c]Department of Chemical Engineering, Federal University of Santa Maria (UFSM), Santa Maria, RS, Brazil

24.1 Introduction

The increasing environmental pollution and ecological imbalance have made the need to remove and separate pollutants from aqueous matrices a growing research field (Yu et al., 2019). Inorganic and organic pollutants, such as metals, dyes, pharmaceuticals, and pesticides, are widely distributed in air, water, soil, sediments, and ecological receptors, and due to their mobility and persistency, they can cause harm to all forms of life, even at low concentrations (Gavrilescu et al., 2015). Several techniques have been developed for contaminants remediation (Mao et al., 2021; Muga and Mihelcic, 2008; Rout et al., 2021). Among them, because of its simple processing, low cost, and high efficiency, adsorption has been widely applied and is considered very promising (Ahmed et al., 2016; Cheng et al., 2021; Tony, 2021).

To enhance the adsorption efficiency, the selection of suitable adsorbents must be taken into consideration. Good adsorbent attributes are high surface area and pore volume, leading to a fast adsorption rate requiring a short time to attain the equilibrium time (Dąbrowski, 2001). In this aspect, biochar highlights from many new functional carbon materials and even from activated carbons, typically used for environmental applications (Qiu et al., 2021).

https://doi.org/10.1016/B978-0-323-90912-9.00024-1

However, separating the powdered adsorbents from the aqueous phase after their contact with the adsorbate solution in the adsorption process represents a drawback in implementing this method, limiting its up-scale applications due to the need for centrifugation and filtration steps. To overcome these difficulties, the preparation and impregnation of biochar with magnetic powders rise as a viable solution (Yi et al., 2019). It is possible to notice a dramatic increase in the number of publications regarding magnetic adsorbents over the years. In Fig. 24.1, it is possible to see the number of studies per year between 2010 and 2020 and the pollutants to which the adsorbents were employed for the removal. In addition, the interactions between the target pollutants and biochar are be strengthened by the addition of magnetic metals, due to the increase in the mechanisms responsible for adsorption, such as electrostatic attraction, hydrogen bonding, π-π stackng, van der Waals force, hydrophobic force, and metal ionic coordination (Dąbrowski, 2001; Yu et al., 2019).

Loading magnetic particles, such as transition metals (Ni, Fe, Co) or nanoparticles of these metals in different forms, on the surface of biochar, can effectively ease solid-liquid separation and recycling through an external magnetic field. The methods of preparing or impregnating biochar with magnetic compounds include pyrolysis, co-precipitation, and carbonization. In addition to the aforementioned methods, coating and functionalization techniques can also be employed to overcome certain limitations that may arise from conventional methods, such as

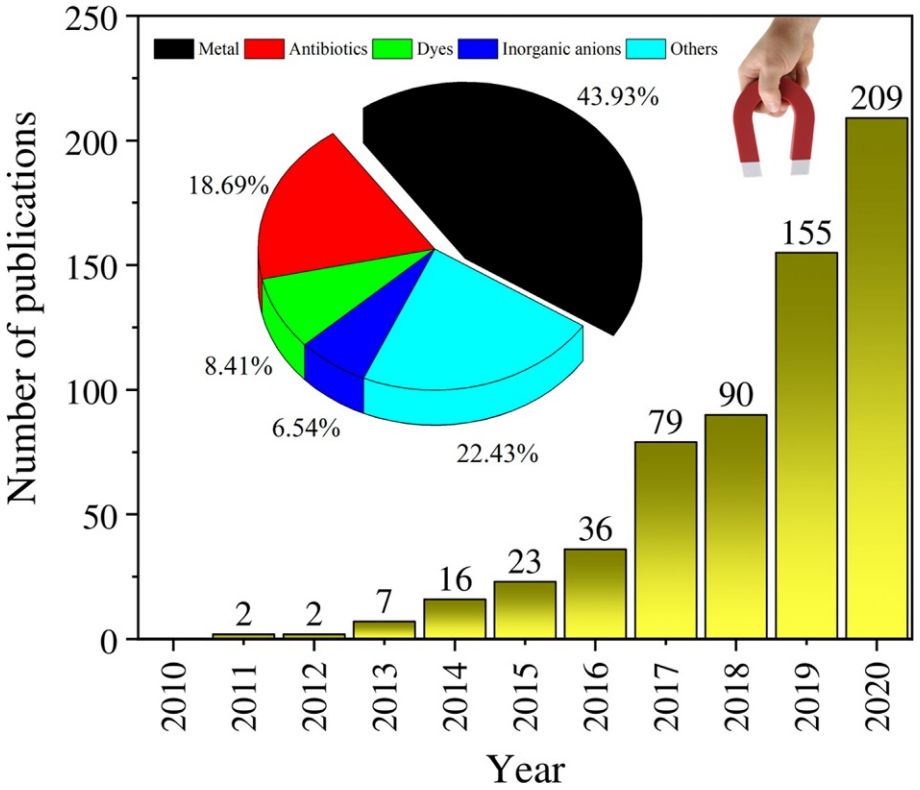

FIG. 24.1 Number of publications on Web of Science™ core collection by searching the terms "magnetic biochar" and "biochar"—inserted is the percentage of each type of pollutant used in the studies.

weakened magnetism due to agglomeration. This chapter will present the main synthesis and preparation methods for producing magnetic biochars, emphasizing their advantages and disadvantages. The applications of these composites in environmental remediation are also presented and discussed, focusing on their characterization and adsorption performance.

24.2 Synthesis and preparation methods

Biochar is defined as a carbon-rich solid prepared by biomass thermal decomposition in a partial oxygen atmosphere or the absence of oxygen using an inert gas stream (Sohi et al., 2010). Therefore, the three main carbonization techniques employed to fabricate high quality and biochar with high magnetization are mainly impregnation pyrolysis, co-precipitation, and hydrothermal carbonization. By controlling the general parameters of the synthesis, such as pyrolysis temperature, heating furnace rate, time of residence in the pyrolysis, and gas atmosphere, it is possible to control specific morphological parameters and tailor the functionalization surface groups. Furthermore, to reach the best possible yields, it is necessary to analyze and characterize the starting biomass characteristics, such as its carbon, cellulose, hemicellulose, and lignin contents, as well as its general chemical composition, humidity, and pH (Zhang et al., 2015; Zhou et al., 2019).

Pyrolysis is the chemical and thermal decomposition of organic material using temperatures higher than 400 °C in a limited oxygen atmosphere, usually using an inert atmosphere (Cha et al., 2016). In this process, the preparation of magnetic biochar is given by impregnation-pyrolysis, where a solution containing metals is added and mixed to the biomass, forming a paste (Thue et al., 2020). The formed past is dried and, subsequently, the material is pyrolyzed (450–750 °C) under an inert atmosphere. For finalizing the production of the material, leaching with dilute HCl solutions is performed to partially remove the excess of inorganic compounds, resulting in carbon material with a higher surface area (Thue et al., 2020). It is essential to highlight that the metallic ion is reduced during the impregnation pyrolysis, forming elemental Fe, Ni, and Co, responsible for the magnetism. Even though the impregnation pyrolysis is not commonly used to prepare magnetic biochar, this method allows the use of $ZnCl_2$ as a precursor for increasing surface area (Thue et al., 2020). Therefore, pyrolysis and magnetization are a single-step process whose physicochemical properties and adsorption capacity need to be assessed and ensured by controlling the operation steps.

The co-precipitation method for fabricating magnetic biochars regards the dispersion of a previously prepared carbon material into a solution containing metal salts (Fe^{2+}, Fe^{3+} Ni^{2+}, Co^{2+}) with the subsequent addition of ammonium, sodium, or potassium hydroxide solution to maintain the pH between 9 and 11, at a 75–85 °C for a period of about 2 h (Panneerselvam et al., 2011). Most metal ions tend to precipitate as hydroxides or oxides at higher pH. After resting, the supernatant is discarded, and the precipitate is washed with distilled water and ethanol to remove impurities and obtain the magnetic carbon material. The final step consists of oven drying to remove moisture and volatile residue (Panneerselvam et al., 2011).

In the co-precipitation method, the steps are planned to force the metal and the biochar (already formed) to precipitate out from a slurry through a carrier, enabling it to bind as one single composite (Thines et al., 2017). Even though this method requires more laborious steps than the impregnation-pyrolysis, the morphological properties of the magnetic

adsorbent produced are more controllable, such as even distribution of magnetic nanoparticles in the carbonaceous matrix (Yi et al., 2019). Conversely, the surface areas and total pore volume of the biochar obtained by the co-precipitation method are lower when compared to impregnation pyrolysis (Thue et al., 2020).

The mechanisms responsible for the efficiency of the co-precipitation process start to unravel after a minor nucleation burst at critical supersaturation of the concentration of the species, that kick-start a slow growth of an arrange of diffusion of the solutes to the surface of crystal (Boistelle and Astier, 1988; Thines et al., 2017). The co-precipitation even allows the magnetic particles or nanoparticles to be produced simultaneously in the same impregnation vessel, using a mixture of Fe^{2+} and Fe^{3+} solutions (Ahn et al., 2012) commonly.

The morphology and textural parameters of the magnetic biochar produced by co-precipitation can be designed by changing synthesis conditions such as the concentration ratio of the salts Fe^{2+}/Fe^{3+}, the salts counterions, heating temperature, final pH for precipitation. The particle size, for example, can be controlled by the addition of chelating ligands or polymer surface complexing agents, as carboxylates such as oleic acid, gluconic, or citric, dextran, carboxy-dextran, starch, or polyvinyl alcohol (Schwarzer and Peukert, 2004). Many papers have utilized this combination of chemicals for fabricating different magnetic materials, such as magnetite (Fe_3O_4) and maghemite (γ-Fe_2O_3), which are widely and successfully prepared by this route (Ahn et al., 2012).

Similarly, the co-precipitation method can be performed by the addition of reducing agents, such as sodium borohydride or potassium borohydride, where it is then named reductive co-deposition, another effective way for producing magnetic biochar. However, the reductive co-deposition has some potential safety risks compared to simple co-precipitation because hydrogen and other harmful gases are produced throughout the reaction (Yi et al., 2019).

Hydrothermal carbonization and pyrolysis are thermal treatment processes in which materials are heated under a specific temperature. The method is relatively simple, employing autoclave heating without the need for fusion to purge H_2O, CO_2, SO_2, and other volatile constituents from the biomass. The process occurs at a high temperature (180–300 °C), with the water vapor at high pressures. An advantage of this process is producing carbon materials with controlled size particles and having elevated magnetization because of strong solvent boiling throughout the synthesis, which disperses the magnetic constituents homogeneously on the surface of the biochar. The advantage of hydrothermal carbonization is not the need to use an inert gas stream, such as Ar or N_2, generally required to flush out air molecules during the pyrolysis and avoid the ashes formation.

Furthermore, hydrothermal carbonization can also be employed to assemble hydrochar and magnetic particles in solution in a reactor at 100–300 °C range, by pressure produced by the solvent reaction vapors of the reaction. This method's milder reaction conditions, associated with no need for alkali or a strong reductant, make the hydrothermal route attractive. However, due to high moisture content, the final adsorbent's pore sizes and surface area tend to be much smaller than those obtained by other procedures (Cen et al., 2014; Schwarzer and Peukert, 2004).

The main synthetic methods described have their own advantages and disadvantages. Other preparation methods involving physical and chemical modifications have been developed over the years. Ball-milling, for example, was used as a solvent-free alternative, providing mechanical mixing of biochar and iron oxides, allowing that the electrostatic charges of

the powder made up the binding themselves. Magnetic biochar has also been treated by adding other metals, acids, and bases or functionalized with various chemical moieties to improve its adsorption selectivity and capacity. The activation through strong acids, alkalis, or oxidants changes the specific surface area and functional groups, thereby improving the binding force between the biochar and the magnetic particles. Strong acids, specifically, can react with the mineral components of the biomass due to their oxidation potential—and corrosiveness—allowing that non-magnetic minerals to be released, enrichening the void structure of biochar richer, thus increasing its specific surface area (Peng et al., 2017; Qiu et al., 2021).

Also, to understand the synthetic methods, understanding the relationship between the nature of the biomass, the reactor conditions, and the operational parameters is crucial to predicting the extra knowledge of the complex physics and chemistry involved. Due to the differences in the raw materials, biochar preparation methods, and modification processes, biochar adsorbents can be diverse in structure, surface area, pore distribution, surface functional groups, elemental composition, cation exchange capacity, pH_{pzc}, and other physical and chemical properties. In addition, biomasses vary in lignin, cellulose, hemicellulose contents; therefore, their degradation rate and mechanisms vary, affecting the affinity, deposition, and binding of the metals to the char. Furthermore, raw material ratio to magnetic material has severely affected carbonization yield and adsorption capacity during the impregnation process.

24.3 Magnetic properties

The most critical parameter that needs to be observed in magnetic adsorbents' obtention is the curve of magnetization. The higher the value of saturation magnetization (M_s), the higher is the capacity of an external magnet to promote the separation of the adsorbent from the aqueous effluent after the adsorption process, which is precisely the reason why the adsorbents are magnetized. In Fig. 24.2, it is possible to observe the magnetization curve of biochar prepared by impregnation of the biomass with $NiCl_2$ followed by pyrolysis at 600 °C under nitrogen flow.

Super-paramagnetic properties reckon that the materials present minimum remanence magnetization (M_R) and coercivity coefficient (Hc). When the super-paramagnetic adsorbents are demagnetized and magnetized at ambient temperature, their M_R and Hc trend to zero values. Usually, it is not observed a hysteresis loop on the magnetization curves. Also, the ratio M_R/M_S should be <25% (Cazetta et al., 2016). The super-paramagnetic property is crucial for the reuse and regeneration of magnetic adsorbents. When the external magnetic field is stopped, the biochar particles will no longer be attracted together, allowing their reuse as magnetic materials after being recovered (Thue et al., 2020).

24.4 Adsorption applications

24.4.1 Inorganic pollutants

Several authors have studied the adsorption of copper ions by magnetic carbohydrate biopolymers. Yuwei and Jianlong (2011) prepared magnetic chitosan nano-biosorbent with

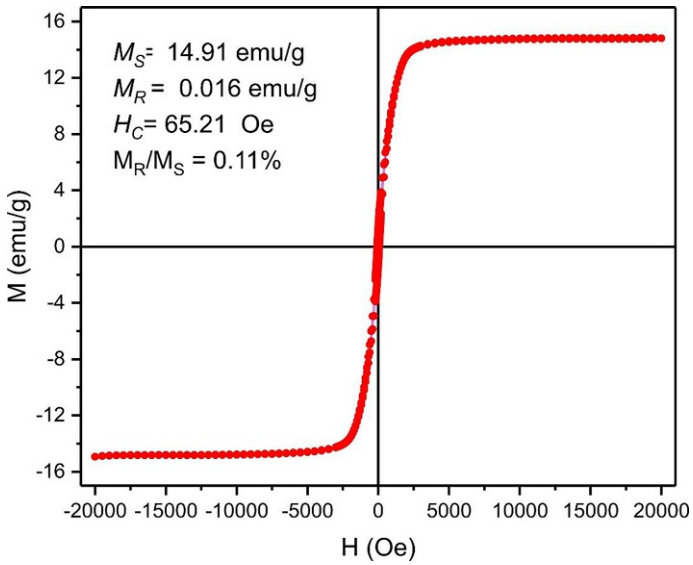

FIG. 24.2 Magnetization curve of biochar.

super-paramagnetic particles in the range of 8–40 nm were with M_S of 36 emu g^{-1}. The authors reported that the nano-biosorbent could chelate metal ions strongly and still easily be separated using a magnetic field after reaching maximum adsorption capacity of 35.5 mg g^{-1} at 35 °C for Cu^{2+} (Yuwei and Jianlong, 2011). Gong et al. (2012) developed a magnetic nanocomposite (M_S 59.2 emu g^{-1}) by combining pectin and iron oxide, which reached the maximum adsorption capacity of 48.99 mg g^{-1} for Cu^{2+} at 25 °C and pH 5 (Gong et al., 2012). Magnetic chitosan and Fe_3O_4 (M_S 14.7 emu g^{-1}) beads were prepared by a simple one-step grafting method, and their maximum capacity was 129.6 mg g^{-1} for Cu^{2+} (Liu et al., 2012). In this context, the coating of cellulose- and chitosan by magnetic particles increased the dispersion stability, preventing aggregation and oxidation, in addition to increasing adsorption capacity (Liu et al., 2012).

Carboxylated chitosan-magnetic nanoparticles were proposed as a novel adsorbent to remove fluoride, nitrate, and phosphate anions from aqueous solutions (Mohammadi et al., 2019). The material was prepared by a modified co-precipitation method assisted by ultrasound to improve the dispersion of the magnetic nanoparticles onto the char (Mohammadi et al., 2019). However, in the paper described by Mohammadi et al. (2019), no M_S values were reported. Due to the surface charge of the adsorbent, it was possible to remove negatively charged contaminants and still remove the produced material from the aqueous solution with a magnet altogether. In a multi-component system, the optimum adsorbent dosage was 2 g L^{-1}. The maximum adsorption capacities were 0.247, 0288, and 4.604 mg g^{-1} for nitrate, fluoride, and phosphate—values obtained in acidic conditions for all anions at pH 3. The adsorption isotherms followed the Langmuir model, and the kinetics analysis indicated that the pseudo-second-order mechanism was predominant (Mohammadi et al., 2019). However, the authors used linear fitting of the data, demonstrating that it is necessary to use nonlinear fitting of the data for defining a kinetic model with accuracy (Lima et al., 2021a).

Lima et al. (2021a) used 252 kinetic results and the data were plotted using linear and nonlinear pseudo-first-order and pseudo-second-order models. It was observed that when linearization was done, 100% of the kinetic results were well-fitted using the pseudo-second-order model. However, when nonlinear fitting was used, more than 50% of the kinetic results were better fitted using the pseudo-first-order model. These results demonstrated that it is impossible to infer the adsorption kinetic using the linear approach since, independent of the kinetic data, the linear fitting will always better fit the pseudo-second-order model (Lima et al., 2021a, b). Also, the values of k_2 obtained using the linear approach are totally different from the values obtained using nonlinear fitting. This observation precludes linearization for obtaining accurate kinetic fitting (Lima et al., 2021a).

The cross-linking of chitosan with magnetic nanoparticles also proved to be an efficient modification method for the preparation of magnetic biochar for the removal of Hg(II), Cd(II), and Zn(II) from aqueous solutions (Monier and Abdel-Latif, 2012). The chitosan beads were synthesized by alkaline co-precipitation, phenylthiourea addition was made through reflux, and the magnetization was carried out with an Fe_3O_4 suspension by co-precipitation (M_S 30.5 emu g^{-1}). The adsorption data indicated that the process is exothermic and that its evolution follows pseudo-second-order kinetics. Equilibrium data fit well to the Langmuir model for all contaminants, of which the maximum adsorption capacities were estimated to be $52 \pm 1, 120 \pm 1, 135 \pm 3$, and mg g^{-1} for Zn(II), Cd(II), and Hg(II), respectively (Monier and Abdel-Latif, 2012). It is crucial to highlight that the thermodynamic results obtained in the paper of Monier and Abdel-Latif, 2012 were not obtained using a correct equilibrium constant. Lima et al. (2019, 2021b) have shown that the correct form of obtaining accurate results is to obtain equilibrium isotherms using at least four temperatures (Lima et al., 2021b), obtaining the equilibrium constants of a model (Langmuir, Sips, Liu, Redlich-Peterson, etc.) and making some transformations to generate an a dimensional equilibrium constant (Lima et al., 2019). It is also recommended to use nonlinear fitting to obtain the equilibrium constant values used to estimate the thermodynamic parameters (Lima et al., 2019, 2021b).

Combining different kinds of cellulose (Cel), such as amphiprotic cellulose, to produce novel carbon composite materials has been proposed as an effective way of promoting adsorption efficiency without having surface area decrease (Xiong et al., 2020). In this context, graphene oxide (GO) has been used as a support for linking it with amphiprotic cellulose and Fe_3O_4, resulting in a magnetic aerogel (GO/Cel/Fe_3O_4; M_S 8.61 emu g^{-1}) with surface groups able to adsorb both anionic and cationic pollutants. The maximum adsorption capacities of (GO/Cel/Fe_3O_4 for the removal of Cu^{2+}, Pb^{2+}, Cd^{2+}, and Cr^{3+} from aqueous solution were 222.2, 568.2, 185.5, and 122.2 mg g^{-1}. The kinetics fit the pseudo-second-order kinetic model, and the Langmuir isotherm model well depicts the prepared material's adsorption behavior for metal adsorption. In addition, the composite did not lose its magnetization either after desorption by mild eluting. Contrarily to what would be expected of a gelatinous structure, the composite also proved to be renewable and to have a stable structure, maintaining an adsorption capacity up to >68% after five recycles (Xiong et al., 2020).

The synthesis of a thiourea-functionalized/Fe_3O_4@nanocellulose@ZnO composite was also reported; however, the magnetization was done by co-precipitation of Fe_3O_4 into nanocelulose (Alipour et al., 2020) using salts of Fe^{3+} and Fe^{2+} and NH_4OH solution forming Fe_3O_4@nanocellulose. Subsequently, this composite was mixed with Zn^{2+}, followed by the

addition of NaOH forming Fe_3O_4@nancellulose@ZnO. In a further step, the composite Fe_3O_4@nancellulose@ZnO was grafted with thiourea (TU) utilizing epichlorohydrin as a cross-linking reagent (Alipour et al., 2020), forming TU@nanocelulose@Fe_3O_4@ZnO (M_S 24.6 emu g^{-1}) (Alipour et al., 2020). The TU@nanocelulose@Fe_3O_4@ZnO composite was tested for Pb(II) removal and reached a sorption capacity ranging from 548.3 (25 °C) up to 706.0 mg g^{-1} (45 °C) under the optimum conditions found at pH 6.5, and 2.0 g L^{-1} of adsorbent concentration. While the equilibrium followed the Langmuir isotherm, the kinetic studies suggested that the adsorption process obeyed the pseudo-second-order model. The thermodynamic of the sorption process was feasible, spontaneous, and endothermic. The TU@nanocelulose@Fe_3O_4@ZnO composite has a high potential for purification of contaminated wastewater, with high sorption capacities associated with a fast adsorption performance recyclability easy magnetic separation (Alipour et al., 2020).

Similarly, one-pot synthesis simultaneously activates and magnetizes activated biochar prepared from spent coffee grounds and natural clay (Le et al., 2019). The synthesized composite (M_S 43.05 emu g^{-1}) was used as an adsorbent for Pb(II), Cu(II), and Ni(II) uptake from water. The maximum adsorption capacities was Pb(II) > Cu(II) > Ni(II) as 143.56, 96.16, and 84.86 mg g^{-1}, respectively. The optimal conditions for removing the metals were found at 25 °C, pH 5.5, 2.0 g L^{-1} adsorbent concentration, and the contact time between the adsorbent and adsorbate of 60 min (Le et al., 2019).

In addition to the composites prepared with complex carbohydrates extracted from residues, raw and whole biomasses have been widely used for magnetic biochar production. Apple pomace, highly rich pectin biomass, was used to produce magnetic biochar through pyrolysis at 600 °C under N_2 flow, Fe^{2+}/Fe^{3+} aqueous precipitation alkali-treated with NaOH (Zhang et al., 2019b). The saturation magnetization and the specific surface area of the adsorbent prepared were 9.52 emu g^{-1} and 102.18 m^2 g^{-1}, respectively. The magnetic biochar presented a high Ag(I) adsorption, with a maximum adsorption capacity of 818.4 mg g^{-1} in a multi-ionic system where Ag(I), Pb(II), Cu(II), Ni(II), and Zn(II) were present. The high selectivity shown by the composite can be presumed as a consequence of the mechanisms involving intra-particle diffusion, coordination, ion exchange, and reduction. The adsorption kinetic study fit well to the pseudo-second-order kinetic model ($R^2 > 0.99$), where the adsorption underwent rapid diffusion stage, limited intra-particle diffusion stage, and adsorption equilibrium stage (Zhang et al., 2019b).

Low-cost corn straw and manganese ferrite particles ($MnFe_2O_4$) were mixed with egg white, abundant in the functional groups –NH_2 and –COOH, and submitted to a combined sol-gel pyrolysis route (Zhang et al., 2019a). The obtained material showed high dispersion of $MnFe_2O_4$ on the biochar surface, and it was found that the 5 h pyrolysis at 500 °C did not affect the functional group's insertion, nor the high surface area of the char negatively (Zhang et al., 2019a) (M_S 33.19 emu g^{-1}). The experiments indicated that Pb(II) and Cd(II) removal was highly dependent on pH, with the best efficiencies found at pH 5.0. Equilibrium was attained within 2 h, and the adsorption isotherm fit better to the Sips (Freundlich–Langmuir) model ($R^2 > 0.892$), while the kinetics obeyed the pseudo-second-order model ($R^2 > 0.990$). Overall, the process is spontaneous and exothermic. Here, it should be highlighted that the authors used the wrong equilibrium constant to obtain the thermodynamic parameters (Lima et al., 2019, 2021a, b). The maximum adsorption capacity was 154.94 and 127.83 mg g^{-1} for Pb(II) and Cd(II), respectively, in single-solute systems (Zhang et al., 2019a).

Besides Fe, Mn, and Ni oxides, rare earth elements can magnetize the biochars. The advantages of using the latter elements over the conventional ones lie in their increased positive charge addition due to their size. Biochar prepared from pineapple peel biomass through pyrolysis was treated with a mixture of Fe^{3+} and Fe^{2+} co-precipitated into biochar. Subsequently, the magnetic biochar was treated with nitrate of lanthanum, and the pH of the solution was adjusted to 9. Lantanum hydroxides and the magnetic biochar formed a composite magnetic material used for phosphate removal (Liao et al., 2018). The loading of different contents of $La(OH)_3$ formed the composites La0.63-MC, La1.25-MC, La2.5-MC, La5-MC, La10-MC, and La15-MC, corresponding to the ratios between La and MC of 0.63, 1.25, 2.50, 5.00, 10.00, and 15 mmol g^{-1} in the suspension, respectively. The saturation magnetization values were 12.83, 9.05, 6.44, 4.98, 4.16, and 2.74 emu g^{-1} for La0.63-MC, La1.25-MC, La2.5-MC, La5-MC, La10-MC, and La15-MC, respectively (Liao et al., 2018). It was observed that as the La content increased, the adsorption capacity also increased; however, the magnetic property decreased. The composite that exhibited the best adsorption performance was La10-MC, with a surface area of 84.89 m^2 g^{-1} and a maximum adsorption capacity of 101.16 mg g^{-1} of phosphate. Adsorption isotherm and kinetics fitted well Langmuir ($R^2 > 0.99$) and pseudo-second-order ($R^2 > 0.98$) models, respectively. Experiments were carried out to verify the effects of co-existing anions in the phosphate removal efficiency, where it was possible to observe that the presence of CO_3^{2-}, HCO_3^-, NO_3^-, SO_4^{2-} and Cl^- was insignificant. The overall efficiency was superior to 96.04%, indicating high selectivity to phosphate. Moreover, the composite presented stability for cyclic reuse, with negligible leaching of La^{3+} (Liao et al., 2018).

Cerium (Ce), one of the most abundant and the least expensive rare earth metals, was used in the coating of biochar obtained from *Phragmites australis* biomass for efficient Sb(V) adsorption. The adsorbent was synthesized by two different methods (co-precipitation of Ce/Fe_3O_4-biochar or solvothermal of Ce/Fe_3O_4-Biochar), which were compared, and the adsorption results indicated that the co-precipitation method was superior to the solvothermal method (Wang et al., 2019a). The M_S of the composites were 0.93 and 2.11 emu g^{-1} for the co-precipitation, and solvothermal methods, respectively. These magnetizations obtained were not enough for magnetic separation since the authors utilized a membrane filtration to separate the loaded adsorbent from the adsorbate solution after the batch contact. Although the authors define that their research was using magnetic biochars, the main purpose of the scientific work was not carried out. The Ce addition also played a key role in Sb(V) adsorption enhancement, mostly due to the ligand exchange and Ce–O–Sb complex formation. The final composite was still easily separated; however, magnetic performance disappeared. The maximum adsorption capacity was 25.0 mg g^{-1}, which was kept stable over a wide pH range and/or in the presence of co-existing anions. The adsorption of Sb(V) was rapid in the first 160 min, with about 80% of equilibrium adsorption capacity achieved because of the substantial binding sites and high concentration gradient. Then the adsorption rate gradually slowed, and equilibrium was reached at 600 min (Wang et al., 2019a).

In addition to the applications for removing inorganic contaminants from aqueous media, magnetic biochar composites have also been employed for soil remediation and industrial purposes. Gong et al. (2021) produced magnetic sorbents using wheat straw to extract Cd from the soil. Wheat straw chips were pyrolyzed at 300 and 700 °C and mixed with Fe^{3+}/Fe^{2+} solution for magnetization (Gong et al., 2021). The biochar at 300 °C and 700 °C presented Ms. of 14.57 and 10.32 emu g^{-1}, respectively. The adsorbents were tested in two

Cd-contaminated paddy soils during a 30-day experiment. The composites prepared at 300 and 700 °C reached Cd recovery from soils of 62%–100% and 36%–65% (Gong et al., 2021).

On the other hand, Altaf et al. (2021) prepared magnetic tea biochar through one-step pyrolysis of $Fe(NO_3)_3$ laden waste tea leaves at 500 °C, which was efficient in removing Hg^0 from coal-syngas. The magnetic biochars presented M_S ranging from about 4 to 20 emu g^{-1}. At the optimal loading of 0.46 mol L^{-1}, the composite attained ≥95% of Hg^0 removal efficiency at 180 °C under simulated syngas (10% CO, 10% H_2, and 400 H_2S). After six repeated adsorption/regeneration cycles, the removal efficiency was still above 90% (Altaf et al., 2021).

24.4.2 Organic pollutants

Organic pollutants can cause various environmental problems once released into the aquatic ecosystem, adversely affecting aquatic biota and diverse life forms. There are several different types of organic pollutants: organic dyes, phenols, biphenyls, pesticides, fertilizers, hydrocarbons, plasticizers, detergents, oils, greases, pharmaceuticals, proteins, and carbohydrates, and others (Ali et al., 2012). The adsorption of indigotine blue dye was investigated by applying a novel chitosan composite coated with cobalt ferrite ($CoFe_2O_4$). Crosslinking chitosan polymer chains around $CoFe_2O_4$ by co-precipitation resulted in the obtained adsorbent (M_S 16.45 emu g^{-1}). Optimal adsorption conditions for indigotine blue dye onto the $CoFe_2O_4$/chitosan composite were found at pH 3, and adsorbent dosage of 0.75 g L^{-1}. The process was fast, reaching equilibrium after 15 min, which the pseudo-first-order model well represented. The equilibrium behavior was satisfactorily modeled by the Langmuir equations, where the maximum adsorption capacity was determined as 380.88 mg g^{-1} at 328 K. The adsorption was spontaneous, favorable, and endothermic (dos Santos et al., 2019).

Chitosan is one of the most abundant natural biomass biopolymers obtained from the hydrolysis of chitin. Chitosan as adsorbents presents high sorption capacity due to the presence of highly reactive amino and hydroxyl groups. Singh et al. (2019) incorporated iron oxide in chitosan-graphene oxide hydrogel nanocomposites through in situ mineralization. The preparation approach was shown to directly impact the morphological features and the structural order of the nanocomposites, resulting in a more porous structure with a large surface area, which was favorable for the rapid diffusion of the adsorbate. The prepared composites (M_S 32.56–48.31 emu g^{-1}) were tested to remove the cationic dye methylene blue (MB) from the aqueous solution. The adsorption was influenced by pH and ionic strength of the medium, indicating an electrostatic interaction between the adsorbent and MB molecules—which is the only possible explanation for the adsorption efficiency, especially considering the relatively small surface area of the nanocomposite (25 m^2 g^{-1}). The kinetics of adsorption followed a pseudo-second-order model, and the Freundlich adsorption model described equilibrium capacity, with q_e values attaining 74.93 mg g^{-1} (Singh et al., 2019).

Lee and Ahmad Zaini (2020) prepared through a one-step synthesis $ZnCl_2/FeCl_3$ composites with activated carbon obtained from palm kernel shells. For comparison purposes, the same composites were prepared by high-temperature impregnation and chemical co-precipitation. The one-pot synthesis magnetic activated carbon endows a specific surface area of 1775 m^2 g^{-1}, with 93.8% mesoporosity, leading to an excellent rhodamine B adsorption of 371 mg g^{-1}. However, practically the magnetism of this material is low

(M_S 1.74 emu g^{-1}). The surface areas of the magnetic activated carbon impregnated with iron salts (FAC) and the magnetic composites prepared by high-temperature (HMAC) and co-precipitation (CMAC) methods were lower, as 166, 502, and 370 m^2 g^{-1}, respectively. The FAC, HMAC, and CMAC magnetic carbon materials presented M_S of 14.5, 1.70, and 11.3 emu g^{-1}, respectively. The maximum adsorption capacity of HMAC was 120 mg g^{-1}, which was lower than the adsorption capacity of CMAC 128 mg g^{-1}; however, the capacity of both composites was still less than half of the one-pot composite. The composite prepared through the one-step process (FAC) displayed the highest saturation magnetization (14.5 emu g^{-1}) value among the other materials studied. The equilibrium data fitted well into the Langmuir model, suggesting monolayer adsorption onto a homogeneous structure, while the kinetic data obeyed the pseudo-second-order model (Lee and Ahmad Zaini, 2020).

Wang et al. (2017) proposed a one-step co-precipitation method to prepare magnetic sludge-derived biochar (M_S 8.49 emu g^{-1}), which promoted both adsorption and persulfate-based oxidation of acid orange 7 (RO-7) dye. The porous structure and large surface area of the adsorbent benefit the RO-7 uptake, while abundant Fe_3O_4 magnetic entity and biochar functional groups containing oxygen lead to oxidative radicals; thus, a high dye degradation was attained. The contribution of adsorption to the overall efficiency of RO-7 dye was calculated to be 45.5%, including the intrinsic process and the interactions throughout the catalytic degradation reaction. The carbon composite material presented good resistance to iron leaching in the experiments, which allowed its re-utilization (Wang et al., 2017). Therefore, the findings justify the feasibility of one-step preparation, showing that activation and magnetization in a single process can effectively enhance the adsorption properties of biochar.

Simultaneous carbonization, activation, and magnetization were employed for producing biochar tea waste. The synthesis consisted of hydrothermal pre-treatment, impregnation with $FeCl_3{\cdot}6H_2O$ and $KHCO_3$, and pyrolysis at 700 °C (Li et al., 2021). Its application was tested for the removal of tetracycline, a widely used antibiotic. The results showed that the surface area of the adsorbent was 1035.11 m^2 g^{-1}, with a total pore volume of 0.583 cm^3 g^{-1} and a micropore volume of 0.344 cm^3 g^{-1} (M_S of 7.28 emu g^{-1}). The characterization of the samples showed a significant increase in the functional groups containing carbon, nitrogen, and oxygen after the modification. The equilibrium of the tetracycline adsorption onto the biochar was well fit by Langmuir isotherm ($R^2 = 0.96$), while the kinetic data was better fitted using Elovich kinetic model ($R^2 = 0.96$). The Langmuir Q_{max} was 236.93 mg g^{-1}, which was 14.2 times greater than the Q_{max} value for the unmodified biochar (16.71 mg g^{-1}). The adsorption of tetracycline was shown to be effective for removing tetracycline over a wide pH range and in the presence of co-existing ions. The dominant mechanisms were pore filling and π-π interaction, followed by surface complexation and hydrogen bonding (Li et al., 2021).

Thue et al. (2020) prepared magnetic activated carbon from *Astrocaryum aculeatum* biomass through single-step pyrolysis, with nickel(II) and zinc(II) chloride. The composite was tested for the removal of nicotinamide and propranolol. The single-step procedure consisted of mixing the *Astrocaryum aculeatum* seeds with the metal salts, introducing the mixture in a quartz reactor under an N_2 flow at 600 °C. $ZnCl_2$ promoted an enlargement of pore size, leading to a high BET surface area, and the pore size was shifted to a larger mesoporous region. The magnetic composite with the highest $NiCl_2$ addition presented the higher surface area among the composites, calculated as 1281 m^2 g^{-1}, with a saturation magnetization of 7.14.

The carbon nanocomposite presented nanostructured metallic Ni° particles distributed in the carbonaceous matrix with an average crystallite size of <33 nm and high thermal stability. The adsorption data fitted well to Liu isotherm model ($R^2 = 0.98$–0.99), reaching maximum adsorption capacities of 335.4 (propranolol) and 199.3 mg g^{-1}(nicotinamide). The adsorption thermodynamics was evaluated obtaining $G° < 0$ (spontaneous process) and $H° < 0$ (exothermic). The authors proposed that the main mechanisms responsible for the efficiency of the process were pore filling, π-π interactions—between the aromatic rings of the adsorbates (propranolol and nicotinamide)—with the π.

The effects of pyrolysis temperature on characteristics adsorption behavior of magnetic biochar were discussed by Li et al. (2017). The evaluations consisted of studying thermal pyrolysis of $Fe(NO_3)_3$ and distillation residue derived from rice straw pyrolysis oil at 400 (MB400), 600 (MB600), and 800 °C (MB800). The degree of carbonization of the magnetic biochars became higher as pyrolysis temperature increased. Surface area and pore volume were also heavily influenced by temperature, reaching the highest values at 600 °C. The increase of temperature up to 800 °C decreased the surface area, attributed to pores blocking during the evaporation step of pyrolysis. The M_S were 5.50, 7.50, 18.36 emu g^{-1} for MB400, MB600, and MB800, respectively. The composites efficiency was tested versus removing the aromatic contaminants anisole, phenol, and guaiacol which were investigated carefully, fitting well to Freundlich equations ($R^2 = 0.97$–0.98), and the maximum adsorption capacities were 16.6, 9.27, and 1.45 mg g^{-1}, respectively. The—electron and donor-acceptor interaction was the dominant mechanism for guaiacol adsorption, while the phenol and anisole adsorption was controlled by pore-filling and hydrophobic effect (Li et al., 2017).

The removals of amoxicillin and paracetamol were investigated using nanocomposites made by the mixture of activated carbon with $CoFe_2O_4$ prepared by a simple pyrolytic method. In this study, instead of using pre-prepared $CoFe_2O_4$ for impregnation, the authors added iron(III)/cobalt(II) benzoates (MAC-1; 3.07 emu g^{-1}) and iron(III)/cobalt(II) oxalates (MAC-2, 0.30 emu g^{-1}) to the activated carbon prior to pyrolysis, which was conducted at 600 °C (Saucier et al., 2017). The equilibrium data were better modeled using the Liu isotherm model ($R^2 = 0.99$) for amoxicillin and paracetamol. The maximum adsorption capacities obtained were 280.9 and 444.2 mg g^{-1} of amoxicillin for MAC-1 and MAC-2, respectively, and 215.1 and 399.9 mg g^{-1} of paracetamol using MAC-1 and MAC-2, respectively. Both adsorbents were successfully employed to treat simulated hospital effluents (consisting of nine pharmaceuticals with high concentrations of sugars, organic components, and saline concentrations), reaching an efficiency of 93.0%–96.8% for MAC-1 and MAC-2, respectively. The efficiency of the process was attributed to the interaction of the pharmaceuticals with MAC-1 and MAC-2 by hydrogen bonds, π–π interactions of aromatic rings of pharmaceuticals with the aromatic rings of the carbon materials, and donor-acceptor interactions (Saucier et al., 2017). After the adsorption process, the MAC-2 material was still shallow in magnetism, and it was not possible to separate it from the aqueous solution.

The addition of clay minerals to improve magnetic biochar textural properties and adsorption efficiency has also been explored. Wang et al. (2019b) prepared an adsorbent with natural attapulgite; cauliflower leaves biomass, and $FeCl_3$ and tested its efficiency for the removal of the antibiotic oxytetracycline (M_S 31.46 emu g^{-1}). The combination of attapulgite–biochar composite had the largest surface area, well-developed pore structure, and more surface oxygen-containing, functional groups which could interact with pharmaceutical by hydrogen

bonding, π–π interactions (aromatic rings of pharmaceutical with the aromatic rings of carbon material), ion exchange and complexation. These characteristics suggest that the introduction of attapulgite clay particles and iron nanoparticles played an essential function in oxytetracycline uptake. The adsorption of oxytetracycline by the produced adsorbent was efficient over a wide pH range, which increases applicability. The magnetic attapulgite biochar had the highest adsorption ability and fastest adsorption speed when compared to the not-magnetized composite and pristine biochar. The adsorption kinetics followed the pseudo-second-order kinetic model, and the equilibrium data were better described by the Freundlich isotherm model, reaching the maximum adsorption capacity of 33.31 mg g^{-1} (Wang et al., 2019b).

Besides batch adsorption experiments, magnetic biochars' efficiency has also been investigated in column experiments. Li et al. (2020) used magnetic porous reduced graphene oxide as column adsorbent, prepared through in situ chemical co-precipitation of Fe^{3+} and porous graphene oxide. The surface area of the composite was calculated to be as high as 1070 m^2 g^{-1}. The removal of triclosan was carried out with both pure water and wastewater effluent in the continuous flow fixed column at low concentration levels of μg L^{-1}. Fast adsorption equilibrium was reached within 20 s, fitting better to the pseudo-second-order kinetic model. The maximum adsorption capacities of the pollutant were calculated from the Langmuir model, where the composite reached 1105.8 and 935.3 mg g^{-1} for pure water and wastewater effluent, respectively. According to the Thomas and Yoon-Nelson models fitting of the curve, the breakthrough time was 50 days for the bed depth of 2.3 mm at the inlet triclosan concentration of 100 μg L^{-1}. Compared to commercial activated carbon, the synthesized material exhibited a much higher affinity to the pollutant, with a breakthrough time of 6.5 times longer (Li et al., 2020). Although Li et al. (2020) published this paper as a magnetic adsorbent, no value of saturation magnetization and curves of magnetization saturation were shown in the paper, and no supplementary material was furnished showing that the adsorbent is actually magnetic. Also, it was not mentioned how the adsorbent was separated from the aqueous solution in the batch adsorption experiments. The experiments of column adsorption, however, indeed did not need to have a magnetic adsorbent. Therefore, in this case, the magnetization of the biochar ended up as a strategy to enhance the adsorbent performance instead of improving its separation.

The use of magnetic biochar as an effective trap for removing solid pollutants emerged as the latest application trend, especially considering solving the emerging contamination problem by micro and nanoplastics in aquatic environments. In addition to the threat of contamination by the plastic itself, these particles can serve as carriers for transporting substances, increasing the mobility of other pollutants (Vieira et al., 2020).

Singh et al. (2021) assessed the performance of iron-modified biochar prepared at two different pyrolysis temperatures of 550 and 850 °C for the removal of nanoplastics of different sizes. Experiments focused on the magnetic extractability of the composites, and the tests were carried out with particles of sizes of 1000 and 30 nm and the surface functional groups carboxyl and amine. The authors observed that all the pollutants were rapidly eliminated from the system after 10 min. The reaction kinetics fitted a higher-order model ($n > 2$), and the equilibrium data fitted well to the Sips isotherm, suggesting that the ultrafast nanoplastics removal can be attributed to the heterogeneous nature of the composite surface. Maximum removal capacities ranged between 206.46 and 225.11 mg g^{-1} for the composite prepared

at 850 °C, while the composite prepared at 550 °C attained 290 mg g^{-1}. The solution's pH variations did not significantly affect the adsorption, suggesting the probability of surface complexation of NPs, which was confirmed by the spectroscopic analysis of reaction mixture, where COO− peak decreased, and FeOOH/Fe-O bands appeared. The minimal impact of environmental parameters, reaction spontaneity, and efficient removal reported even in complex aqueous matrices justify the high viability of composites for future environmental applicability (Singh et al., 2021). No magnetic measurements were shown on the paper.

24.4.3 Complex mixtures

The treatment of complex mixtures can be challenging due to the high contents of the most diverse types of pollutants present in wastewaters. Significant levels of total organic carbon, chemical oxygen demand, color, fats, proteins, solids, or particulates can significantly decrease the efficiency of any treatment process. Therefore, investigations regarding the application of novel adsorbents to the complex mixture are necessary. In this context, simultaneous capture of trichloroethylene and Cr(VI) from complex wastewater by a magnetic composite (Liu et al., 2019). Trichloroethylene and Cr(VI) are representative contaminants in groundwater, and their use gives their relation as chlorinated solvent and coating agent, respectively, in the leather, electroplating, and dyeing industries. The adsorbent preparation consisted of the single-step pyrolysis of $FeCl_3$ solution impregnated into peanut hull biomass and subsequent pyrolysis at 800 °C. The surface area of the composite was calculated to be 359.9 mg g^{-1}. Compared to the Freundlich model ($R^2 = 0.549$), the Langmuir isotherm exhibited a better fit for Cr(VI) adsorption ($R^2 = 0.999$), with a maximum adsorption capacity of 222 mg g^{-1}. The complete adsorption of 0.07 mmol L^{-1} of trichloroethylene was reached after 65 min. The authors observed that the composite acted simultaneously as a catalyst for trichloroethylene degradation throughout the process, identifying the formation of 1,1-dichloroethene and cis-1,2-dichloroethane intermediates. No magnetic measurements were shown on the paper.

The adsorption of naphthalene, *p*-nitrotoluene, and phosphate was investigated under simulated environmental conditions using 200 mg L^{-1} NaN_3 to inhibit sorbing species biodegradations and the addition of 0.01 mol L^{-1} $CaCl_2$ to simulate the ionic strength of environmental water (Chen et al., 2011). Three novel magnetic biochars were prepared by chemical co-precipitation of Fe^{3+}/Fe^{2+} on orange peel powder, subsequently pyrolyzed under the different temperatures of 250, 400, and 700 °C, which resulted in the adsorbents named MOP250, MOP400, and MOP700. The synthesis temperature was found to influence the adsorption efficiency of the composites, where the MOP400 exhibited better performance toward the removal of the organic contaminants, while MOP250 was more efficient for phosphate adsorption. The adsorption equilibrium data fitted better to the Freundlich model, with maximum adsorption capacities of 23.0 and 43.4 mg g^{-1} for naphthalene and *p*-nitrotoluene and 0.512 mg g^{-1} for phosphate. No significantly competitive effect between organic pollutants and phosphate was observed; therefore, the adsorbent is prone to simultaneous pollutant removal (Chen et al., 2011). No magnetic measurements were performed in the paper described by Chen et al. (2011).

Besides the complex mixtures of pollutants in wastewaters, many pollutants can be present in their organic and inorganic forms. Arsenic, for example, is an inorganic pollutant in its

ionic form; however, it forms many complexes in aquatic environments, which are not readily soluble and, instead, increased in mobility. As a way of solving the problem of organic and inorganic arsenic species contamination in drinking water and/or wastewater, Wen et al. (2021) proposed using a nanocomposite consisting of porous biochar-supported with $MnFe_2O_4$. The biochar was prepared by typical pyrolysis of ginkgo leaves, and the magnetization was done through the co-precipitation of $KMnO_4$ and $FeSO_4$. The surface area of the synthesized material was found to be 79.29 mg g^{-1} (M_S 20.37 emu g^{-1}). The adsorbent presented good sorption capacities for As(V) and *p*-arsanilic acid removal at a pH range of 3–7. The maximum adsorption capacities of As(V) and *p*-arsanilic acid were approximately 90 and 105 mg g^{-1}, which was well explained by the thermodynamic assessment, while the kinetics obeyed pseudo-second-order equations. The proposed adsorption mechanism indicated that surface complexation and electrostatic interaction influenced the uptake of both pollutants, whereas π-π interactions and hydrogen bonding also contribute to the *p*-arsanilic acid uptake. Besides, the tremendous uptake of the adsorbates in different water samples and column adsorption experiments indicated that the produced adsorbent is an excellent adsorbent for simultaneous removal of organic and inorganic species in the treatment of wastewaters (Wen et al., 2021).

24.5 Conclusion

This chapter presents the main synthetic methods of preparation of magnetic biochar and the outcomes of each procedure in terms of textural properties and their respective saturation magnetization (M_S). Overall, the modifications of biochar by the addition of magnetic particles usually decreased the biochar specific surface area; however, the metallic species present in the biochar can enhance the sorption capacity of the biochar. The porosity of the adsorbents was highly dependent on the synthesis temperature employed, the addition of pore former ($ZnCl_2$) for impregnation pyrolysis, pyrolysis time, and temperature. The more relevant applications of magnetic composites for the removal of inorganic and organic pollutants have been discussed, and the use of magnetic composites for complex wastewater treatment has been presented. Overall, the composites present stable structures in acidic and alkaline environments, making magnetic biochar suitable candidates for remediation purposes.

In conclusion, the development of synthetic procedures, such as one-pot synthesis, can overwhelm the magnetization drawbacks, such as self-agglomeration and increase the magnetic adsorbent recycling, and further improve the removal of pollutants from water. It is also important to highlight that several papers where the authors claim they have used magnetic adsorbents lack the magnetization curves (see Fig. 24.2). Also, some papers reported M_S values <2.0 emu g^{-1}, whose magnetization value cannot perform a magnetic separation of the adsorbent from the liquid phase after the adsorption procedure, which should be the aim of using magnetic adsorbents. Therefore, careful and critical reading is advised.

Acknowledgments

The authors thank the funding agencies CAPES, CNPq, and FAPERGS for their financial support.

References

Ahmed, M.B., Zhou, J.L., Ngo, H.H., Guo, W., Chen, M., 2016. Progress in the preparation and application of modified biochar for improved contaminant removal from water and wastewater. Bioresour. Technol. https://doi.org/10.1016/j.biortech.2016.05.057.

Ahn, T., Kim, J.H., Yang, H.M., Lee, J.W., Kim, J.D., 2012. Formation pathways of magnetite nanoparticles by co-precipitation method. J. Phys. Chem. C 116, 6069–6076. https://doi.org/10.1021/jp211843g.

Ali, I., Asim, M., Khan, T.A., 2012. Low-cost adsorbents for the removal of organic pollutants from wastewater. J. Environ. Manage. https://doi.org/10.1016/j.jenvman.2012.08.028.

Alipour, A., Zarinabadi, S., Azimi, A., Mirzaei, M., 2020. Adsorptive removal of Pb(II) ions from aqueous solutions by thiourea-functionalized magnetic ZnO/nanocellulose composite: optimization by response surface methodology (RSM). Int. J. Biol. Macromol. 151, 124–135. https://doi.org/10.1016/j.ijbiomac.2020.02.109.

Altaf, A.R., Teng, H., Zheng, M., Ashraf, I., Arsalan, M., Rehman, A.U., Gang, L., Pengjie, W., Yongqiang, R., Xiaoyu, L., 2021. One-step synthesis of renewable magnetic tea-biochar derived from waste tea leaves for the removal of Hg0 from coal-syngas. J. Environ. Chem. Eng. 9, 105313. https://doi.org/10.1016/j.jece.2021.105313.

Boistelle, R., Astier, J.P., 1988. Crystallization mechanisms in solution. J. Cryst. Growth 90, 14–30. https://doi.org/10.1016/0022-0248(88)90294-1.

Cazetta, A.L., Pezoti, O., Bedin, K.C., Silva, T.L., Paesano Junior, A., Asefa, T., Almeida, V.C., 2016. Magnetic activated carbon derived from biomass waste by concurrent synthesis: efficient adsorbent for toxic dyes. ACS Sustain. Chem. Eng. 4, 1058–1068. https://doi.org/10.1021/acssuschemeng.5b01141.

Cen, W., Xiong, T., Tang, C., Yuan, S., Dong, F., 2014. Effects of morphology and crystallinity on the photocatalytic activity of (BiO)2CO3 nano/microstructures. Ind. Eng. Chem. Res. 53, 15002–15011. https://doi.org/10.1021/ie502670n.

Cha, J.S., Park, S.H., Jung, S.C., Ryu, C., Jeon, J.K., Shin, M.C., Park, Y.K., 2016. Production and utilization of biochar: a review. J. Ind. Eng. Chem. https://doi.org/10.1016/j.jiec.2016.06.002.

Chen, B., Chen, Z., Lv, S., 2011. A novel magnetic biochar efficiently sorbs organic pollutants and phosphate. Bioresour. Technol. 102, 716–723. https://doi.org/10.1016/j.biortech.2010.08.067.

Cheng, N., Wang, B., Wu, P., Lee, X., Xing, Y., Chen, M., Gao, B., 2021. Adsorption of emerging contaminants from water and wastewater by modified biochar: a review. Environ. Pollut. https://doi.org/10.1016/j.envpol.2021.116448.

Dąbrowski, A., 2001. Adsorption—from theory to practice. Adv. Colloid Interface Sci. https://doi.org/10.1016/S0001-8686(00)00082-8.

dos Santos, J.M.N., Pereira, C.R., Pinto, L.A.A., Frantz, T., Lima, É.C., Foletto, E.L., Dotto, G.L., 2019. Synthesis of a novel CoFe2O4/chitosan magnetic composite for fast adsorption of indigotine blue dye. Carbohydr. Polym. 217, 6–14. https://doi.org/10.1016/j.carbpol.2019.04.054.

Gavrilescu, M., Demnerová, K., Aamand, J., Agathos, S., Fava, F., 2015. Emerging pollutants in the environment: present and future challenges in biomonitoring, ecological risks, and bioremediation. N. Biotechnol. 32, 147–156. https://doi.org/10.1016/j.nbt.2014.01.001.

Gong, J.L., Wang, X.Y., Zeng, G.M., Chen, L., Deng, J.H., Zhang, X.R., Niu, Q.Y., 2012. Copper (II) removal by pectin-iron oxide magnetic nanocomposite adsorbent. Chem. Eng. J. 185–186, 100–107. https://doi.org/10.1016/j.cej.2012.01.050.

Gong, H., Huang, J., Ding, Z., Chi, J., 2021. A potential method using magnetically modified wheat straw biochars for soil Cd extraction. Ecol. Eng. 166, 106240. https://doi.org/10.1016/j.ecoleng.2021.106240.

Le, V.T., Tran, T.K.N., Tran, D.L., Le, H.S., Doan, V.D., Bui, Q.D., Nguyen, H.T., 2019. One-pot synthesis of a novel magnetic activated carbon/clay composite for removal of heavy metals from aqueous solution. J. Dispers. Sci. Technol. 40, 1761–1776. https://doi.org/10.1080/01932691.2018.1541414.

Lee, L.Z., Ahmad Zaini, M.A., 2020. One-step ZnCl2/FeCl3 composites preparation of magnetic activated carbon for effective adsorption of rhodamine B dye. Toxin Rev. https://doi.org/10.1080/15569543.2020.1837172.

Li, H., Mahyoub, S.A.A., Liao, W., Xia, S., Zhao, H., Guo, M., Ma, P., 2017. Effect of pyrolysis temperature on characteristics and aromatic contaminants adsorption behavior of magnetic biochar derived from pyrolysis oil distillation residue. Bioresour. Technol. 223, 20–26. https://doi.org/10.1016/j.biortech.2016.10.033.

Li, Y., Liu, S., Wang, C., Ying, Z., Huo, M., Yang, W., 2020. Effective column adsorption of triclosan from pure water and wastewater treatment plant effluent by using magnetic porous reduced graphene oxide. J. Hazard. Mater. 386, 121942. https://doi.org/10.1016/j.jhazmat.2019.121942.

Li, B., Zhang, Y., Xu, J., Xie, Z., Tang, J., Li, X., Fan, S., 2021. Simultaneous carbonization, activation, and magnetization for producing tea waste biochar and its application in tetracycline removal from the aquatic environment. J. Environ. Chem. Eng. 9, 105324. https://doi.org/10.1016/j.jece.2021.105324.

Liao, T., Li, T., Su, X., Yu, X., Song, H., Zhu, Y., Zhang, Y., 2018. La(OH)3-modified magnetic pineapple biochar as novel adsorbents for efficient phosphate removal. Bioresour. Technol. 263, 207–213. https://doi.org/10.1016/j.biortech.2018.04.108.

Lima, E.C., Hosseini-Bandegharaei, A., Moreno-Piraján, J.C., Anastopoulos, I., 2019. A critical review of the estimation of the thermodynamic parameters on adsorption equilibria. Wrong use of equilibrium constant in the Van't Hoof equation for calculation of thermodynamic parameters of adsorption. J. Mol. Liq. 273, 425–434. https://doi.org/10.1016/j.molliq.2018.10.048.

Lima, E.C., Sher, F., Guleria, A., Saeb, M.R., Anastopoulos, I., Tran, H.N., Hosseini-Bandegharaei, A., 2021a. Is one performing the treatment data of adsorption kinetics correctly? J. Environ. Chem. Eng. 9, 104813. https://doi.org/10.1016/j.jece.2020.104813.

Lima, E.C., Sher, F., Saeb, M.R., Abatal, M., Seliem, M.K., 2021b. Comments on "Reasonable calculation of the thermodynamic parameters from adsorption equilibrium constant, Journal of Molecular Liquids 322 (2021) 114980.". J. Mol. Liq. 334, 116542. https://doi.org/10.1016/j.molliq.2021.116542.

Liu, Z., Wang, H., Liu, C., Jiang, Y., Yu, G., Mu, X., Wang, X., 2012. Magnetic cellulose-chitosan hydrogels prepared from ionic liquids as reusable adsorbents for removal of heavy metal ions. Chem. Commun. 48, 7350–7352. https://doi.org/10.1039/c2cc17795a.

Liu, Y., Sohi, S.P., Liu, S., Guan, J., Zhou, J., Chen, J., 2019. Adsorption and reductive degradation of Cr(VI) and TCE by a simply synthesized zero-valent iron magnetic biochar. J. Environ. Manage. 235, 276–281. https://doi.org/10.1016/j.jenvman.2019.01.045.

Mao, G., Hu, H., Liu, X., Crittenden, J., Huang, N., 2021. A bibliometric analysis of industrial wastewater treatments from 1998 to 2019. Environ. Pollut. 275, 115785. https://doi.org/10.1016/j.envpol.2020.115785.

Mohammadi, E., Daraei, H., Ghanbari, R., Dehestani Athar, S., Zandsalimi, Y., Ziaee, A., Maleki, A., Yetilmezsoy, K., 2019. Synthesis of carboxylated chitosan modified with ferromagnetic nanoparticles for adsorptive removal of fluoride, nitrate, and phosphate anions from aqueous solutions. J. Mol. Liq. 273, 116–124. https://doi.org/10.1016/j.molliq.2018.10.019.

Monier, M., Abdel-Latif, D.A., 2012. Preparation of cross-linked magnetic chitosan-phenylthiourea resin for adsorption of Hg(II), Cd(II), and Zn(II) ions from aqueous solutions. J. Hazard. Mater. 209–210, 240–249. https://doi.org/10.1016/j.jhazmat.2012.01.015.

Muga, H.E., Mihelcic, J.R., 2008. Sustainability of wastewater treatment technologies. J. Environ. Manage. 88, 437–447. https://doi.org/10.1016/j.jenvman.2007.03.008.

Panneerselvam, P., Morad, N., Tan, K.A., 2011. Magnetic nanoparticle (Fe3O4) impregnated onto tea waste for the removal of nickel(II) from an aqueous solution. J. Hazard. Mater. 186, 160–168. https://doi.org/10.1016/j.jhazmat.2010.10.102.

Peng, H., Gao, P., Chu, G., Pan, B., Peng, J., Xing, B., 2017. Enhanced adsorption of cu(II) and cd(II) by phosphoric acid-modified biochars. Environ. Pollut. 229, 846–853. https://doi.org/10.1016/j.envpol.2017.07.004.

Qiu, B., Tao, X., Wang, H., Li, W., Ding, X., Chu, H., 2021. Biochar as a low-cost adsorbent for aqueous heavy metal removal: a review. J. Anal. Appl. Pyrolysis. https://doi.org/10.1016/j.jaap.2021.105081.

Rout, P.R., Zhang, T.C., Bhunia, P., Surampalli, R.Y., 2021. Treatment technologies for emerging contaminants in wastewater treatment plants: a review. Sci. Total Environ. 753, 141990. https://doi.org/10.1016/j.scitotenv.2020.141990.

Saucier, C., Karthickeyan, P., Ranjithkumar, V., Lima, E.C., dos Reis, G.S., de Brum, I.A.S., 2017. Efficient removal of amoxicillin and paracetamol from aqueous solutions using magnetic activated carbon. Environ. Sci. Pollut. Res. 24, 5918–5932. https://doi.org/10.1007/s11356-016-8304-7.

Schwarzer, H.C., Peukert, W., 2004. Tailoring particle size through nanoparticle precipitation. Chem. Eng. Commun. 191, 580–606. https://doi.org/10.1080/00986440490270106.

Singh, N., Riyajuddin, S., Ghosh, K., Mehta, S.K., Dan, A., 2019. Chitosan-graphene oxide hydrogels with embedded magnetic iron oxide nanoparticles for dye removal. ACS Appl. Nano Mater. 2, 7379–7392. https://doi.org/10.1021/acsanm.9b01909.

Singh, N., Khandelwal, N., Ganie, Z.A., Tiwari, E., Darbha, G.K., 2021. Eco-friendly magnetic biochar: an effective trap for nanoplastics of varying surface functionality and size in the aqueous environment. Chem. Eng. J. 418, 129405. https://doi.org/10.1016/j.cej.2021.129405.

Sohi, S.P., Krull, E., Lopez-Capel, E., Bol, R., 2010. A review of biochar and its use and function in soil. In: Advances in Agronomy. Academic Press Inc, pp. 47–82, https://doi.org/10.1016/S0065-2113(10)05002-9.

Thines, K.R., Abdullah, E.C., Mubarak, N.M., Ruthiraan, M., 2017. Synthesis of magnetic biochar from agricultural waste biomass to enhancing route for wastewater and polymer application: a review. Renew. Sustain. Energy Rev. https://doi.org/10.1016/j.rser.2016.09.057.

Thue, P.S., Umpierres, C.S., Lima, E.C., Lima, D.R., Machado, F.M., dos Reis, G.S., da Silva, R.S., Pavan, F.A., Tran, H.-N., 2020. Single-step pyrolysis for producing magnetic activated carbon from tucumã (Astrocaryum aculeatum) seed and nickel(II) chloride and zinc(II) chloride. Application for removal of nicotinamide and propanolol. J. Hazard. Mater. 398, 122903. https://doi.org/10.1016/j.jhazmat.2020.122903.

Tony, M.A., 2021. Low-cost adsorbents for environmental pollution control: a concise, systematic review from the prospective of principles, mechanism, and their applications. J. Dispers. Sci. Technol. https://doi.org/10.1080/01932691.2021.1878037.

Vieira, Y., Lima, E.C., Foletto, E.L., Dotto, G.L., 2020. Microplastics physicochemical properties, specific adsorption modeling, and their interaction with pharmaceuticals and other emerging contaminants. Sci. Total Environ. https://doi.org/10.1016/j.scitotenv.2020.141981, 141981.

Wang, J., Liao, Z., Ifthikar, J., Shi, L., Chen, Z., Chen, Z., 2017. One-step preparation and application of magnetic sludge-derived biochar on acid orange 7 removal via both adsorption and persulfate-based oxidation. RSC Adv. 7, 18696–18706. https://doi.org/10.1039/c7ra01425b.

Wang, L., Wang, J., Wang, Z., Feng, J., Li, S., Yan, W., 2019a. Synthesis of Ce-doped magnetic biochar for effective Sb(V) removal: performance and mechanism. Powder Technol. 345, 501–508. https://doi.org/10.1016/j.powtec.2019.01.022.

Wang, Z., Yang, X., Qin, T., Liang, G., Li, Y., Xie, X., 2019b. Efficient removal of oxytetracycline from aqueous solution by a novel magnetic clay–biochar composite using natural attapulgite and cauliflower leaves. Environ. Sci. Pollut. Res. 26, 7463–7475. https://doi.org/10.1007/s11356-019-04172-8.

Wen, Z., Xi, J., Lu, J., Zhang, Y., Cheng, G., Zhang, Y., Chen, R., 2021. Porous biochar-supported MnFe2O4 magnetic nanocomposite as an excellent adsorbent for simultaneous and effective removal of organic/inorganic arsenic from water. J. Hazard. Mater. 411, 124909. https://doi.org/10.1016/j.jhazmat.2020.124909.

Xiong, J., Zhang, D., Lin, H., Chen, Y., 2020. Amphiprotic cellulose mediated graphene oxide magnetic aerogels for water remediation. Chem. Eng. J. 400, 125890. https://doi.org/10.1016/j.cej.2020.125890.

Yi, Y., Huang, Z., Lu, B., Xian, J., Tsang, E.P., Cheng, W., Fang, J., Fang, Z., 2019. Magnetic biochar for environmental remediation: a review. Bioresour. Technol. https://doi.org/10.1016/j.biortech.2019.122468.

Yu, M., Wang, L., Hu, L., Li, Y., Luo, D., Mei, S., 2019. Recent applications of magnetic composites as extraction adsorbents for the determination of environmental pollutants. Trends Anal. Chem. https://doi.org/10.1016/j.trac.2019.07.022.

Yuwei, C., Jianlong, W., 2011. Preparation and characterization of magnetic chitosan nanoparticles and their application for Cu(II) removal. Chem. Eng. J. 168, 286–292. https://doi.org/10.1016/j.cej.2011.01.006.

Zhang, J., Liu, J., Liu, R., 2015. Effects of pyrolysis temperature and heating time on biochar obtained from the pyrolysis of straw and lignosulfonate. Bioresour. Technol. 176, 288–291. https://doi.org/10.1016/j.biortech.2014.11.011.

Zhang, L., Guo, J., Huang, X., Wang, W., Sun, P., Li, Y., Han, J., 2019a. Functionalized biochar-supported magnetic MnFe2O4 nanocomposite for the removal of Pb(ii) and Cd(ii). RSC Adv. 9, 365–376. https://doi.org/10.1039/c8ra09061k.

Zhang, S., Ji, Y., Dang, J., Zhao, J., Chen, S., 2019b. Magnetic apple pomace biochar: simple preparation, characterization, and application for enriching Ag(I) in effluents. Sci. Total Environ. 668, 115–123. https://doi.org/10.1016/j.scitotenv.2019.02.318.

Zhou, R., Zhang, M., Zhou, J., Wang, J., 2019. Optimization of biochar preparation from the stem of Eichhornia crassipes using response surface methodology on adsorption of Cd2+. Sci. Rep. 9, 1–17. https://doi.org/10.1038/s41598-019-54105-1.

CHAPTER

25

Biomass-derived nanocomposites: A critical evaluation of their performance toward the capture of inorganic pollutants

Konstantinos Simeonidis[a], *Evgenios Kokkinos*[b], *Efthimia Kaprara*[a], *and Anastasios Zouboulis*[b]

[a]Department of Chemical Engineering, Aristotle University of Thessaloniki, Thessaloniki, Greece
[b]Department of Chemistry, Aristotle University of Thessaloniki, Thessaloniki, Greece

25.1 Introduction

Environmental remediation practices have received great interest during the last decades as a result of the continuously increasing concern of people on the direct and indirect consequences of pollution in their everyday life and the future of the planet. The aim of developed approaches is from the one hand, to minimize the impact of toxic substances appearing in the air, water, and soil into human health and from the other hand, to reverse the effect of long-term pollution in the ecosystems. To face the wide range of problems related to the release of inorganic pollutants through anthropogenic and natural pathways, several removal methods were experimentally tested and then, qualified in full-scale applications. Among them, adsorption is recognized as the most preferable one since it combines flexible application schemes and unattended operation. Commonly, it involves the placement of a granular solid with chemical affinity to specific pollutants, in the flow of a polluted stream or at the site of the contaminated area. Apart from the chemical activity of the adsorbent, a typical requirement for good adsorption efficiency is the establishment of a high specific surface area which implies that adsorption sites are multiplied.

https://doi.org/10.1016/B978-0-323-90912-9.00025-3

Accordingly, most of the studied adsorbents hold at least one of these two advantages. For instance, activated carbons are known for the extremely high specific surface area values they present while metal oxides and oxyhydroxides offer an excellent substrate for the chemisorption of inorganic pollutants. Some additional characteristics able to improve performance are the surface charge and the porous structure of the adsorbent. Considering that environmental remediation processes usually involve large volumes to be treated, demanding proportional quantities of adsorbents, the cost of preparation should be kept as low as possible to characterize the corresponding process as viable. In this concept, combining two phases that work supplementary to obtain an optimum adsorbent and decrease the treatment cost has been introduced as a very attractive strategy toward the purification of polluted areas and carriers.

In this chapter, the combination of chemically active phases, usually inorganic ones, with carbon-based phases which succeed high specific surface areas, is discussed as a trending approach to obtain solids with improved adsorption capacity but at the same time minimize the fraction of the active phase which generally defines the adsorbent's cost. Particularly, this study emphasizes the introduction of a renewable source such as biomass into the preparation of nanocomposites with adsorption active inorganic nanomaterials. Wood, food crops, other residues from agriculture or forestry, algae, and municipal and industrial wastes are referred to as the typical sources of biomass. The various pristine, modified, or treated products received by biomass are presented as possible substrates for the development of promising adsorbents with the potential to dominate remediation processes and assist the valorization of large biomass residual quantities.

25.2 Biomass-derived adsorbents

In spite of biomass extended use as a renewable energy source, significant efforts have been also performed toward the production of added-value technology materials, including adsorbents based either on raw biomass or on relevant byproducts. The main advantage for such applications is the natural polymeric structure of biomass, presenting a proper building network to deliver high specific surface area, enhanced chemical activity, and also a good substrate to host other phases, aiming to improve synergistically the desired sorption properties and to enhance the possible functionalization of surfaces. On this concept, several approaches have been examined to develop appropriate adsorbent materials, mainly based on mechanically treated biomass, as well as on biomass-derived pristine or modified biochars, lignin, and graphene.

25.2.1 Biosorbents

In the simplest case, biomass wastes can be used without any further modification treatment as adsorbents (biosorbents). The main sources for biosorbents are virgin or waste biomasses, such as agriculture and forestry residues, seaweeds, sludges from wastewater (biological) treatment plants, as well as several other industrial or landfill wastes. Their application in environmental remediation processes is promoted by their high availability (practically inexhaustible), the minimum cost for collection and pre-treatment, together with the

possibility to support waste valorization and green economy. The relatively easy disposal after treatment, or applying incineration to recover energy, is also referred to as a potential advantage of biosorbents. The obtained adsorption efficiency is mainly attributed to the affinity of specific biomolecules, or to functional groups of biomass structure, able to bind with certain molecular or ionic pollutants, diluted in solid, aqueous, or gas forms. Since most biomass sources are referring to not-living substances, the biosorbents are typically passivated and no metabolic reaction with the pollutants is expected, apart from their physico-chemical interactions. After excluding the presence of biological capture mechanisms, the adsorption of inorganic pollutants by biosorbents takes place by means of ion exchange, complexation, chelation, and precipitation. The lignocellulosic residuals, originating from plants, are considered as the largest feedstock for the preparation of biosorbents and accordingly, the typical composition of relevant materials is mostly based on polysaccharides (cellulose and hemicellulose) and lignin, an aromatic polymer.

Actually, the received biomass almost always requires a proper kind of pre-treatment to remove the impurities from the harvesting field and to get the granule dimensions to the proper size for the subsequent remediation application. The biomass wastes are generally considered and treated as a zero-value byproduct during their collection and this implies the presence of different inorganic and organic particulates from dust diameters up to the size of small stones. Long-time storage outdoors under exposure to air, weather conditions, and sunlight may strongly affect their purity and chemical composition. For this reason, preliminary washing is a commonly applied pre-required task, which is typically fulfilled by the use of plenty of tap water. The biomass feedstock is then ground or milled to produce a granular or powdered form, while sieving is applied to homogenize the size, commonly in the range 0.1–4 mm. The granular biosorbents are washed once more at this stage typically using distilled water and sometimes, diluted HCl, or NaOH to remove the residual soluble impurities. The product is finally dried at ambient temperatures.

25.2.2 Pristine biochar

High specific surface area is an essential characteristic for the development of an adsorbent agent, oriented to succeed sufficient uptake performance for one or more pollutants. Untreated or mechanically treated biomass may increase the specific surface area only by the proportional size reduction, whereas only the outer surface of the materials' structural network is actually accessed for sorption purposes. A significant improvement can be achieved by the pyrolysis of biomass, aiming to produce biochar, which results due to a carbonization process carried out in the absence of oxygen to prevent combustion. During pyrolysis, lignin, cellulose, and hemicellulose macromolecules gradually decompose, leaving a structure with high pore volume and density of functional groups, which features a biochar-based product with improved chemical activity and stability. The total procedure results in a solid residue of around 15–35%wt. of biochar with the rest of the products received in the resulting liquid (bio-oil) and the gas phase (synthetic gas).

The formation of biochar in the absence of oxygen involves several steps, the respective control of which may define the conversion efficiency and the properties of the final product. At the beginning of this process, the absorbed water content is removed just above 100°C.

Then, the breakdown of dried biomass initiates, when reaching 150°C, and proceeds with a mild pyrolysis procedure called torrefaction up to around 300°C. At this temperature range, the decomposition generates a mixture of gases, such as carbon monoxide and dioxide, methane, hydrogen, and also tars, signifying a step with exothermic effects. Heating at even higher temperatures (up to 800° C) is required to decompose the high volatiles residuals and to increase the carbon percentage of biochar through mainly endothermic reactions.

The exact composition in the output of the pyrolysis system depends on the type of biomass feedstock, the temperature, the time of pyrolysis, and the heating rate. In general, mild heating conditions and lower temperatures and heating rates would favor high biochar yields (i.e., slow pyrolysis conditions). Slow pyrolysis is known to feature biochar production with a negative surface charge, providing an ability to capture positively charged pollutants. However, biochar produced at higher temperatures indicates very high specific surface area and porosity with the presence of longitudinal micro or macro-pores, though accompanied by lower cation-exchange capacities. Biochar is considered as a mechanically and chemically stable solid, owed to the presence of aromatic carbons atoms in condensed aromatic hydrocarbons, existing at large proportions and with different crystalline forms, such as amorphous, turbostratic carbon, and/or graphite.

The physical and chemical properties of pristine biochars are defined mainly from the characteristics of used feedstock and from the applied pyrolysis procedure. The percentages of cellulose, hemicellulose, and lignin in the biomass structure may determine the whole reaction progress, according to the respective temperature range for the degradation of each component. Suggestively, cellulose and hemicellulose fully degrade below 400°C but lignin may react in a wider temperature range, extended up to 700°C.

The potential of biochar for adsorption applications strongly depends on the atomic ratios H/C and O/C, which are indicative of the important properties of aromaticity and polarity, respectively, whereas the presence of mineral residuals (ash), such as calcium, potassium, and phosphorous, is expected to improve the adsorption efficiency in several cases. In the beginning, raw biomass possesses an aromaticity index above 1.5 and a polarity ratio of 0.6. The formation of biochar results in the decrease of both H/C and O/C ratios in the range 0.1–0.6 and 0–0.25, respectively, depending on the applied pyrolysis conditions. The application of very high temperatures, or extended thermal treatment, may bring both ratios very close to zero, indicating a carbonization process, where the carbon content easily exceeds 95%wt. and the aromaticity is maximized. Aromaticity is directly related to the stability of biochar, formed after the removal of hydrogen and oxygen atoms from the functional groups and the rearrangement of molecular structure. Such property is particularly favorable when the biochar is prepared specifically for soil remediation uses. However, the application of lower temperatures may generate biochars with lower carbon content, preserving some of the initial polarity (i.e., higher O/C ratio) and resulting in acceptable aromaticity.

The complexity of biochar surface structure and chemistry often provide multiple possibilities to act as an efficient adsorbent for different pollutants. Organic pollutants may be captured by physisorption mechanisms and chemical interactions with the functional groups, such as carboxyls and hydroxyls. In the presence of a hydrophobic surface, organic pollutants may be captured also by the non-polar attraction and π-π electron donor/acceptor mechanisms, taking advantage of the porous biochar's microstructure. When the biochar's surface retains ionic charge, or some ionic groups are embedded in the structure, then the organic pollutants with polar groups may be easily attracted, or the degradation of organic molecules

may be promoted. The presence of functional groups, leading to positive or negative charging, as well as of exchangeable ions and/or adsorbed metals onto biochar surface, supports also alternative routes for the uptake of inorganic pollutants, e.g., through the complexation on oxygen bridges, anionic/cationic attraction, ion-exchange, or chemical precipitation.

25.2.3 Activated carbon

This term usually refers to a carbon-rich product, similar to biochar, which goes through various activation treatment processes to improve its specific surface area and chemical activity. The main difference between biochar and activated carbon stands on the applied production temperature, i.e., biochar is usually produced at temperatures below 700°C under anaerobic or inert conditions, while activated carbon is prepared above 700°C using a flow of an activated gas. Another common consideration involves the type of carbonaceous source required to prepare activated carbon, which is preferred to be wood or coal product with high purity and limited presence of dirt.

The modification processes applied to produce activated carbon are commonly classified in pre-treatment and post-treatment procedures. Pre-treatment is applied to the raw biomass by its dispersion into or wetting by acids, bases, oxidizers, or other salt solutions. The contact under these solutions is intending to specifically dissolve some compounds and to attach metal/inorganic ions or oxygen radicals on the exposed surface sites. Therefore, the pre-treatment contributes to the development of a porous network and to the chemical activation by creating new adsorption sites. For instance, the acidic treatment (e.g., by phosphoric acid) can remove some inorganic elements and enhance the hydrophilic character of the surface, while the alkaline washing (e.g., by sodium hydroxide) can introduce a positive surface charge and a significant improvement of the specific surface area.

The post-treatment modification normally includes the separate or sequential chemical and/or thermal steps. Steam activation, which is applied in the pyrolyzed material at temperatures above 800°C, is a common procedure to improve the porous structure, to oxidize the carbon surface and to introduce a high density of carboxylic, hydroxyl, phenolic, and carbonyl functional groups, and indirectly, to improve hydrophilicity. On the opposite, hydrophobicity can be favored after heating above 800°C under the flow of hydrogen or air, which promotes the removal of oxygen-containing groups and stabilizes the C—H groups. The formed activated carbons show better affinity with hydrocarbons. It should be noted that several activation processes refer to the use of metal salts solutions (e.g., $FeCl_3$, KCl, $AlCl_3$) or oxidizing agents, containing mineral elements (e.g., $KMnO_4$), which can succeed an improvement of physical and chemical properties of activated carbons after the separate formation of inorganic oxides, able to be deposited on the carbon structure. In this chapter, the majority of such cases are considered as approaches to produce carbon-based nanocomposites rather than carbon activation procedures, and they are discussed more extensively in the following sections.

25.2.4 Lignin

Another component of interest in the lignocellulosic biomass with potential application for the capture of contaminants is lignin. Lignin is a natural amorphous phenolic polymer with a

high degree of complexity, which occupies around 15–30%wt. of plant and wood-based biomass, acting as a binding and protecting medium for cellulose. Therefore, lignin already comprises a significant part of biosorbents, originating from agricultural sources. A significant quantity of lignin becomes available after the delignification of wood biomass to obtain paper. The fractionation/separation of lignin from the lignocellulosic biomass becomes favorable, due to its stable hydrophobic three-dimensional structure and the high density of functional hydroxyl, methoxyl, carbonyl, carboxyl, and phenolic groups. Such heterogeneity and versatility of lignin is the reason for the intense interest to develop adsorbents on its basis. The high percentage of ash content (may reach up to 15%wt.), corresponding to silica, sodium, and calcium compounds, is another characteristic of lignin that should be also considered for each application.

The exact properties of lignin depend on the respective extraction procedure, as well as on the specific biomass source. Its isolation from cellulose and hemicellulose, the other two major components of biomass, is achieved mainly by the application of two approaches: (i) the dissolution or hydrolysis of cellulose to receive lignin as insoluble solid, and (ii) the dissolution of lignin from the mixture followed by its recovery in a subsequent step. The alkaline fractionation is the most common process to obtain lignin from the lignocellulosic biomass. It is applied by the single addition of NaOH (soda pulping), or by the combination with sodium sulfide (kraft pulping) at temperatures around 100–150°C. During this process, the bonds of lignin with the other biomass constituents break down and lignin becomes soluble, resulting in the formation of black liquor. It is finally received after acid washing and precipitation. Kraft lignin has a much higher recovery yield, although it also contains an amount of sulfur.

The separation of lignin by the sulfite pulping process, which involves the addition of sulfur dioxide and sodium, magnesium, calcium, or ammonium hydroxide, is not recommended, when aiming to produce adsorbents for water treatment, since the received solid is highly soluble, while the sulfur content is very high. There are also other methods to obtain lignin, promising high selectivity, minimum chemical modification, lower molecular weights, and no content of sulfur. Among them, the organosolv pulping is the most studied one, using alcohols (e.g., ethanol, propanediol) and organic acids (e.g., formic, acetic) in combination with acids or bases, working as catalysts. Nevertheless, and despite the advantages of organosolv lignin, the use of this procedure to develop adsorbents is rather limited, due to the elevated production cost and to the toxicity issues, because of the organic solvents use.

Beyond the direct use of pristine lignin as adsorbent, numerous chemical activation and thermal transformation processes may be applied to obtain modified lignin structures, or to produce chars and activated carbons. For this concept, the aforementioned methodologies, already described in the previous sections, are followed.

25.2.5 Graphene

Graphene is a popular carbon form, due to its unique mechanical, physical, and chemical properties, which became beneficial for various modern technology applications. Structurally, graphene can be described as a single graphite layer with a honeycomb-like lattice, which provides very high specific surface areas. High-quality graphene has been widely

produced by the exfoliation of graphite (top-down approach), or by the chemical vapor deposition (bottom-up approach). However, there are other graphene derivatives, which are prepared by applying much easier and less expensive methods, such as graphene oxide and the reduced graphene oxide. In particular, graphene oxide is the result of graphite's chemical oxidation by the addition of $NaNO_3$ and $KMnO_4$ in an acidic environment; it is negatively charged and can be easily decorated by proper functional groups, thus, becoming more favorable for adsorption uses. Reduced graphene, which is very similar to graphene after the removal of functional groups, is produced by the reduction of graphene oxide, using hydrazine, hydrides, or thiosulfate reagents.

The biomass-derived graphene forms require different synthetic approaches, which however can generally achieve lower product purity. However, the concept for the valorization of a renewable carbon resource and the application in technological fields, such as environmental remediation, demanding high availability, rather than high quality, is still attractive. In the first accessible method, a two-step pathway is followed to convert biomass into graphite and then, exfoliate it to produce graphene. Biomass is subjected to thermal treatment, which involves a carbonization process in the air or inert atmosphere at relatively low temperatures (suggestively below 500°C). Then, the amorphous product is heated to higher temperatures (above 850°C), aiming to initiate the graphitization process. The exfoliation of graphitized biomass takes place using very high heating temperatures, or by the addition of oxidants, attempting to receive graphene oxide.

The conversion yield of biomass to graphene mainly depends on the success of carbonization step. When formed, amorphous carbon shows the microporous structure (hard carbon) and the graphitization becomes very difficult. Alternatively, the domination of "soft carbon," i.e., a disordered, but denser structure, makes the formation of graphite more possible. The second method to transform biomass into graphene is the chemical vapor deposition of gases produced during the pyrolysis of biomass. Graphene can be deposited onto a metal substrate, ensuring a high-quality structure. It is obvious that the chemical vapor deposition approach can only generate small amounts of graphene at a relatively high cost and for this reason biomass is tested only as an alternative for the substitution of carbon gas feed.

These procedures are facilitated when special attention is given to the pre-treatment of biomass, since plant and agriculture wastes are the main feed stocks in this case. Some of the pretreatment practices, used to promote the production of graphene from biomass, may include acid washing, filtration, grain size reduction, proper drying, chemical treatment, desilication, and delignification. The final product may also follow modification processes to improve chemical activity. In spite of the difficulties to obtain graphene from biomass, the obtained structure, the featured functional groups (for graphene oxide), and the potential for building up sophisticated composites, may suggest a profitable perspective for the corresponding adsorbents.

25.3 Synthesis of nanocomposites

The discussed class of adsorbents is composite materials, consisting of the carbonaceous biomass-derived matrix and a second active phase in the form of nanoparticles distributed

on this matrix. The biomass-based part of the composite originates from one of the previously mentioned categories (i.e., as-obtained biomass, biochar, activated carbon, lignin, graphene), assuming that the carbon source for their production is any kind of biomass, but still without the addition of any chemical reagents or synthetic polymers. Since this chapter refers to nanocomposites developed to capture specifically inorganic pollutants, the review will emphasize only the active phases capable to provide the affinity for efficient and non-reversible capture. For this reason, several inorganic compounds, such as metals, metal, and alkaline earth oxides or hydroxides, minerals, and magnetic phases, will be mostly mentioned. The large quantity demand for adsorbents in applications, such as water treatment, or gas and soil remediation, initiates also the need to promote preparation methodologies with minimum cost, using inexpensive precursors or materials for the building-up of the active phase. Biomass-based nanocomposites can be synthesized by the application of various approaches, generally classified as (i) in-situ nanoparticles' development, (ii) constituents' blending, and (iii) carbon-phase functionalization (Fig. 25.1).

25.3.1 In-situ development of nanoparticles

In this case, the inorganic phase is formed directly into the network of the high specific surface carbon phase after the chemical reaction of a proper precursor. During this approach, the thermal treatment of biomass is a separate preliminary step and then the inorganic precursor (e.g., a metal salt) is homogeneously dispersed, or adsorbed into its volume. This is usually performed by contacting the biomass-based material with an aqueous solution of metal salt under the influence of intense stirring or by sonication. The inorganic nanoparticles are produced onto the active sites of the carbon phase, where ions can be adsorbed when the reaction of the precursor is triggered by the modification of a chemical parameter or by the application/change of other conditions. Commonly, the occurring reaction is a precipitation process, where the solubility of metal ions is decreased under specific conditions (e.g., pH modification). The desired destabilization can be caused by providing energy to the system (e.g., by temperature, pressure, or supersonics), or by changing the pH value and/or the redox potential. Depending on the precipitation parameter, the reaction can be characterized as thermal decomposition, hydrothermal treatment, sonochemical, chemical precipitation, or oxidative hydrolysis, respectively. These reaction types can result in the in-situ nucleation of nanosized particles and their growth at the same active sites of the biomass-based matrix.

Very frequently, the thermal treatment of raw biomass can be combined with any of the aforementioned reactions, aiming to the preparation of the inorganic phase. In the second approach, the biomass is initially immersed in the precursor's solution for sufficient time to adsorb the specific ions or molecules; then, it is subjected to drying and finally is pyrolyzed, forming the nanocomposite. During the heating procedure, the volatile part of biomass is removed and the product is enriched in carbon to become a biochar. At the same time, under the effect of high temperatures, the adsorbed precursor is transformed to the corresponding oxide, also following a solid-state reaction with the biochar's structure. Alternatively, the mechanical mixing (e.g., by ball milling) of raw biomass with the precursor reagent (both existing in powdered forms) can be applied sometimes combined with pressurization, forming bulk specimens. In this case, the nanoparticles, typically consisting of metal oxides, are formed after a solid-state reaction at high temperatures in the same levels as the carbonization process.

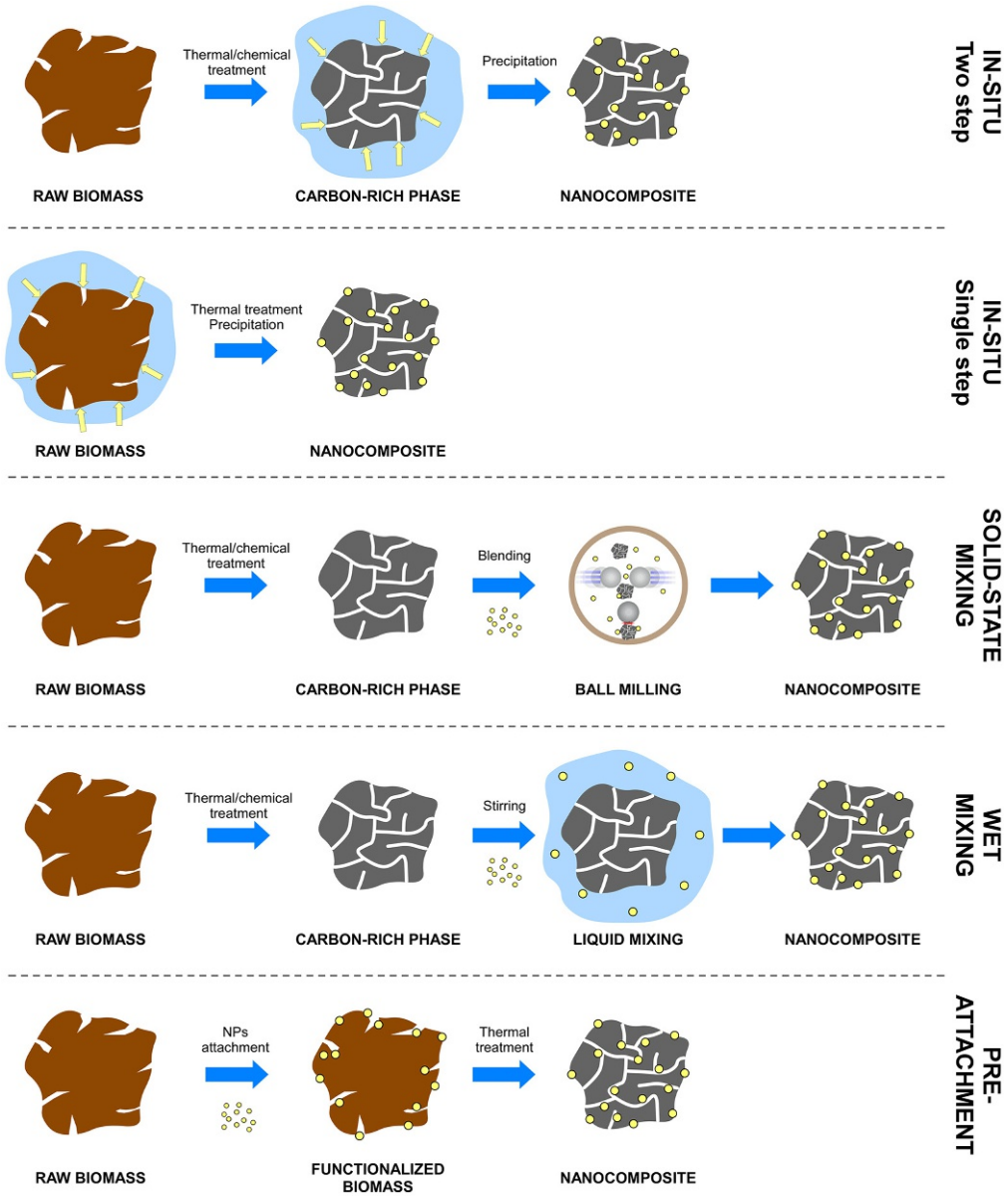

FIG. 25.1 Available paths for the preparation of biomass-based nanocomposites.

In general, the in-situ synthesis of inorganic nanoparticles induces high homogeneity in the obtained nanocomposites, since the precursors have good access to the whole volume of the biomass phase. When performed using solutions, this methodology minimizes the aggregation effects between the particle units, implying the maximization of chemical activity with a significant impact on the obtained adsorption efficiency. On the contrary, the simultaneous

carbonization-precipitation does not provide such a control of dispersion procedure, regarding the precursor option, but during the shrink of biomass structure, the nanoparticles may occupy sites at the internal areas of the matrix.

25.3.2 Blending of constituents

An alternative preparation procedure can be also applied, aiming to obtain the final form of inorganic nanomaterials, and then, their distribution to the biomass-derived substrate is attempted by means of wet contact, or by solid-state mixing. The main advantage of this approach is the possibility to perform any synthetic, modification, and purification step for the nanoparticles in the absence of the carbonaceous phase. This provides the opportunity of carrying out chemical processes, avoiding some non-desirable impacts in the functional groups and in the structure of biomass, by removing the residuals and byproducts of the preparation step, prior to the nanocomposite's formation. For instance, bottom-up super-saturation techniques (leading to precipitation or thermal decomposition) can be performed under perfect tuning of the respective critical parameters, being able to succeed in the complete purification of nanoparticles after washing away the non-reacted reagents and the excess of ionic forms. In addition, simple nanomaterials production methods, without the need for special conditions or instrumentation, but also high-pressure processes, physical vapor condensation in vacuum systems, and organic solvent synthesis may be applied.

On the other hand, the homogeneous distribution of nanoparticles in the biomass network is not always guaranteed, unlike in the case of in-situ synthesis. The surface charges of the carbon phase and of nanoparticles seem to be the dominant parameter to achieve high affinity and the spontaneous tendency of particles to occupy surface active sites. Suggestively, the participation of similarly charged phases inhibits the dispersion of nanoparticles, resulting rather in a binary-phase material, instead of the expected nanocomposite. The extent of aggregation, regarding the introduced nanoparticles, is the second source of inhomogeneity in the nanocomposites' phase. Depending on the preparation techniques and the potential addition of stabilizers, nanoparticles may present a high tendency for aggregation. Following this possibility, the aggregates would behave as large particles and therefore, the degrees of freedom in motion within the structural network of the biomass phase will be limited.

The blending approach can be also realized by mixing the phases in a liquid, wet or solid form. The liquid blending includes the dispersion of carbon phase and of nanoparticles in water, or other proper solvent, followed by the application of extended stirring or sonication, aiming to facilitate the proper mixing and uptake of nanoparticles in the biomass matrix. The wet mixing involves the addition of the nanoparticles in the sludge of the carbon phase and then, their mixing by slow mechanical stirring. This method can load higher quantities of inorganic nanoparticles, which are captured in the structure of the nanocomposite's phase, during the following drying procedure. Finally, the nanocomposite can be prepared using both carbon phase and nanoparticles in powdered forms and their blending, using a high-energy ball mill, or other mechanical treatment procedure. This type of process may provide sufficient homogeneity, but the expected increase in temperature can induce undesired structural modifications in the produced composite.

25.3.3 Functionalization of carbon phase

Another way to prepare biomass-based nanocomposites with inorganic particles is to attach the nanoparticles in their final form onto the raw biomass and then, to apply subsequently a thermal carbonization treatment. In this case, the biomass transformation takes place in the presence of the nanoparticles, which are impregnated into the new structure without significant structural changes. The inorganic particles may be considered as functional sites distributed both onto the carbon surface, as well as within its porous network. In some cases, nanoparticles or their aggregates may act also as blockades to the porous part of biochar, compensating the advantage of chemical activity by limited access to the carbon surface.

Some chemical modification processes commonly carried out to prepare activated carbons can be also classified in this category of biomass-based nanocomposite synthesis. These include the decoration/functionalization with metal ions after contacting proper aqueous solutions of metal salts with the raw biomass, or with the pristine biochar, during a thermal activation process. This procedure not only succeeds the increase of the specific surface area and the improvement of porosity but additionally provides a high density of active sites by metal ions with the potential to participate in adsorption or ion-exchange reactions.

25.4 Active phases

The efficiency of biomass-derived nanocomposites is generally defined by the properties and the chemical activity of the distributed inorganic nanomaterials. Therefore, the proper selection of impregnated phase, with respect to the targeted application, is the most critical part of nanocomposites development. Following the current state-of-the-art on the synthesis of engineered nanoparticles and the characteristic properties of each system, biomass and its thermal modified derivatives are preferably featured with metals/alloys, metal oxides, oxyhydroxides, and minerals to establish a functional adsorbent. Among these categories, magnetically responsive components, such as zero-valent iron and iron oxide nanoparticles, are distinguished, due to the extra possibility for remote magnetic handling they provide and the easier separation options.

25.4.1 Metals and alloys

Zero-valent iron (ZVI) nanoparticles are the most frequently applied nanostructured adsorbent agents, due to the numerous reaction possibilities introduced by the presence of iron and their relatively low production cost. If properly stabilized against spontaneous oxidation or agglomeration, ZVI nanoparticles (nZVI) may serve as effective reducing agents, able to succeed modification in the valence states of nearby cations. In many cases, this mechanism is the key to capture efficiently pollutants in aqueous solutions, by decreasing the solubility of oxy-ions or by triggering the precipitation of hydroxides (Fig. 25.2). Apart from being an electron donor, ZVI shows also a direct high chemical affinity for some heavy metals oxy-ionic forms, having the potential to bind them on the surface. Its activity is maintained, even after their surface passivation by iron oxide or oxyhydroxide layer, since such phases indicate

similar adsorption ability, as would be later presented. Importantly, ZVI nanoparticles present the best-known magnetization properties, allowing easy separation from the purified medium. Iron can be also combined with other metals, such as Ag, Pd, Ni, Al, Cu, Co, Zn, in alloys or binary systems, being able to initiate a galvanic coupling mechanism to assist electron donation efficiency and surface corrosion inhibition with significant impact in the extension of operating lifetime of the adsorbent.

Despite their relatively higher cost, noble metal nanoparticles are known for their selectivity to capture specific pollutants. For instance, gold nanoparticles are very efficient for the removal of mercury through the amalgamation process, while their optical properties may be considered significant for some photocatalytic treatment processes. Similar properties have been reported for the Ag and Pd nanoparticles, although such systems are widely studied mainly for their anti-microbial properties. The use of noble metals for the uptake of pollutants is obviously limited by their high cost; however, applications that may be upgraded, or become very selective, due to their addition in very small concentrations, could become affordable. In addition, nanocomposites based on noble metal nanoparticles are able to support purification processes by acting as pollutant concentration sensors, or as guards for other processes.

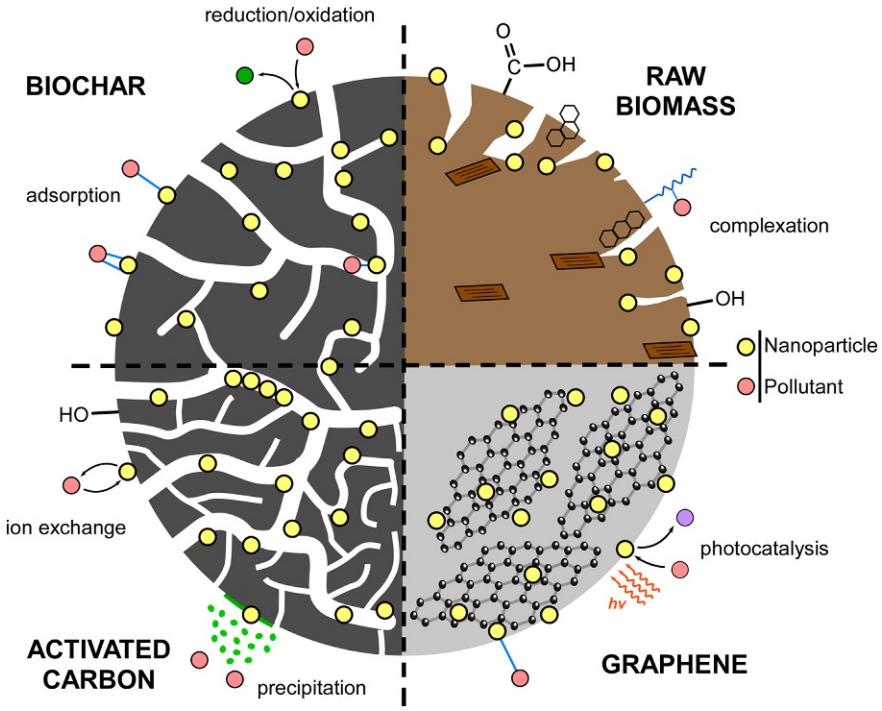

FIG. 25.2 Mechanisms of pollutants' capture on various biomass-derived nanocomposites.

25.4.2 Metal oxides and oxyhydroxides

Nanomaterials consisting of oxides or oxyhydroxides of metals or alkaline earths are the most studied category when referring to adsorbents for pollutants. This has to do with the variety of available phases, their chemical stability against oxidation or passivation processes taking place, the intensity of surface charges, and the tunable surface morphology and porous structure. In addition, many oxides can be easily prepared in large quantities and rather low cost. Much interest is attracted mainly by the iron oxide nanoparticles (Fe_3O_4, γ-Fe_2O_3, α-Fe_2O_3), because of their high affinity to many different pollutants, which is connected with the possibility of chemisorption through oxygen bridges. Different preparation or surface modification approaches may be carried out in aqueous systems and determine the surface charging of obtained nanoparticles as positive or negative. Such features provide the opportunity for the design of nanocomposites, specifically adapted to the characteristics of the pollutant to be treated. Magnetite (Fe_3O_4) nanoparticles offer also reducing potential, due to the presence of Fe^{2+} into its crystal structure. The appearance of hydroxyl groups and the typically lower degree of crystallinity in comparison to the case of oxides promote the use of iron oxyhydroxide nanostructures (FeOOH), which are considered as one of the best pollutant's purifiers. The substitution of iron atoms by other metals in the iron oxides and oxyhydroxides generates a wide class of nanoadsorbents with advanced characteristics. Suggestively, the incorporation of manganese in iron oxyhydroxides is known to offer an extra oxidizing step in the adsorption mechanism, when dealing with mobile heavy/toxic metal forms, such as As(III). In addition, ferrite nanoparticles (i.e., MFe_2O_4, where M = Mg, Zn, Ni, Ti, Cu, Mn) may be also tested for environmental remediation application.

Metal oxides able to support photocatalytic reactions are another major class of nanomaterials, regarding the capture of inorganic pollutants. Titanium oxide and zinc oxide are able to induce oxidation or reduction reactions, when exposed to UV radiation, by the release of charge carriers. Other metal oxides, such as CeO_2, ZrO_2, and SiO_2 in the form of nanoparticles, are known for both direct and/or photoinduced activities toward the pollutants' uptake. The surface hydration of Al_2O_3, MgO, CaO, and MnO_2 explains the intense interest in water and soil remediation processes, while their stability at higher temperatures enables their use even in flue gas treatment. Finally, tin oxides and oxyhydroxides, as well as the layered double hydroxides with combinations of Mg, Al, and Zn, demonstrated high potential for the removal of several inorganic pollutants, owed to electron donation and ion exchange mechanisms and the available adsorption sites in the interlayer space.

25.4.3 Minerals

Modification of the adsorption properties for the biomass-derived products can be achieved also by the employment of clays, which are known for their lamellar structure, the high specific surface area, and the ion exchange potential. Such features imply their significant efficiency for the capture of various pollutants, including the toxic metal forms. Biochar-clays nanocomposites are prepared mainly by the application of two ways: (i) the mixing of biomass and clay in slurry, which is then subjected to pyrolysis, and (ii) the addition of the final carbon-rich product in clay slurry, followed by drying or by mechanical treatment (e.g., ball milling). In the first case, the presence of clay minerals (e.g., kaolinite, bentonite,

montmorillonite) during the carbonization process enhances the porosity of formed biochar, while at the same time the composite is featured with a better affinity toward inorganic pollutants. Another advantage of using minerals instead of synthetic phases is their chemical and structural stability during the heating treatment.

The incorporation of clays after carbonization assists only the functionalization of the composite; however, it facilitates their adoption in nanosized units. This is realized by the treatment of clay in a high-energy ball milling process, prior to its dispersion in the slurry, or by carrying out the solid-state blending of biochar with the clay into a ball mill. Mineral nanocomposites with biochar are preferable when their use is oriented to soil remediation in parallel to the sequestration and nutrition activity. In this application, the presence of clays supports the improvement of ion exchange capacity and long-term mechanical resistance. The lower production cost in comparison to other types of engineered nanocomposites is also a critical advantage for this category of environmental remediation, which generally demands very large quantities of the respective product.

25.4.4 Magnetic phases

Introducing magnetically responsive nanomaterials in biomass-derived adsorbents is favorable by many researchers as a way to prepare nanocomposites with high uptake capacity for specific pollutants, combined with the possibility to effectively separate the solid by means of an external magnetic field without the use of an interface, as in the filtration process. Considering that due to their high toxicity, the magnetic compounds containing Co and Ni are avoided for environmental applications, the magnetic nanoparticles used for the biomass-based nanocomposites are almost exclusively belonging to different iron phases. More specifically, ZVI, γ-Fe_2O_3, Fe_3O_4, and the respective ferrite substitutions, are able to feature with sufficient magnetic properties the whole nanocomposite after their successful distribution into the biomass network.

The advantage of magnetization is utilized for several reasons. Firstly, the application of a proper magnetic field during the deposition of nanoparticles in the carbon phase is able to facilitate homogeneity and self-organization in symmetrical geometries, such as linear or closed chains. The successful tuning of nanoparticles arrangement may improve further the adsorption efficiency. Another possibility of magnetically activated biomass products is their recovery, when the remediation process is completed, especially in aqueous purification systems. This is generally fulfilled by placing permanent magnets or electromagnets in the side of a flowing tube, or in a contact reactor tank, allowing the implementation of operational setups without the need to place the adsorbent in a fixed column bed. The magnetic separation can also facilitate other procedures, maximizing the overall adsorption efficiency, such as the recirculation of adsorbent until its saturation with the pollutant and the regeneration of used nanocomposite by means of appropriate acid or base washing strategies.

25.5 Adsorbents for aqueous pollutants

Water constitutes a fundamental component for the evolution of human civilization and animal life; thus, the prevention and treatment of aquatic pollution have always been a critical

issue for intensive scientific research. Inorganic pollutants are a major class of contaminants found in aquatic environments, originating either from geogenic contribution (e.g., weathering of natural rocks and soil) or from uncontrolled anthropogenic activities. Several factors, such as the waste discharges from industries, construction companies, sewerage systems, as well as the extensive use of fertilizers, etc. have led to the increased concentration of various heavy metals (e.g., Cd, Cr, Cu, Hg, Ni, Pb, Zn) and other inorganic pollutants in water resources, ranging from trace elements (e.g., As, Mn, U) to nutrients (mainly PO_4^{3-}, NO_3-). These inorganic pollutants are considered conservative pollutants, i.e., non-biodegradable, persisting in the surrounding environment. Consuming water with concentrations over the maximum permitted contaminant levels defined by legislation may cause a variety of hazardous effects to humans, regarding liver, kidney, nervous system, circulatory system, blood, gastrointestinal system, bones, or skin, depending on the inorganic contaminant and the level of exposure.

To protect human and animal life from that exposure and restore ecological balance in the aquatic environment, several technologies have been developed for the removal of inorganic pollutants from aqueous systems, including chemical reduction/precipitation, adsorption, ion exchange, membrane separation, electro-dialysis, phytoremediation, and others. Among them, adsorption has proven to be an effective water purification method for inorganic pollutants, offering flexibility in design and operation, simplicity, lower cost, and the potential recycle and reuse of spent material. Yet, the exploitation regarding the maximum capacity of adsorbents has not be reached, due to limitations related mainly to the development of the effective specific surface area. This limitation can be successfully overtaken by the combination of inorganic nanomaterials with carbonized phases in the form of nanocomposites, presenting high specific surface area, enhanced chemical activity, and affinity for the efficient and non-reversible capture of inorganic pollutants. Especially, recently numerous nanocomposites have been synthesized and tested for the capture of inorganic pollutants from the aqueous media. In many cases, these nanocomposites are composed of a biomass-based part and an inorganic part, usually with nanoscale dimensions.

25.5.1 Hexavalent chromium

So far, the most studied pollutant, regarding its removal using biomass-derived nanocomposite adsorbents, is chromium. The dominant form of chromium in aquatic systems is the Cr(VI) species, due to its higher mobility in comparison with Cr(III) and its weak tendency to be adsorbed (Kaprara et al., 2015). In view of its verified toxicity and carcinogenicity, the recent EU directive on the quality of water intended for human consumption considers a new maximum contaminant level for chromium at 25 μg/L with a tolerance for full adoption of the new concentration limit by 2036 (EU, 2020). Redox-active solids are more favorable to uptake Cr(VI) since they provide an intermediate reduction step toward the insoluble Cr(III) hydrolysis products. In this direction, much research effort has been attributed to the development of redox-active nanocomposites, being able to eliminate Cr(VI) concentration by the reduction of Cr(VI), followed by the precipitation of Cr(III) as $Cr(OH)_3$ (Fig. 25.3). Numerous studies refer to biomass-derived nanocomposites, where the inorganic constituent is zero-valent iron (ZVI) (Khosravi et al., 2018) or Fe_3O_4 (Liang et al., 2019) nanoparticles, due to their potential to provide electrons for the reduction of Cr(VI) in combination to their magnetic behavior, which enables the easier subsequent separation.

Magnetic biochar was prepared by applying one-step pyrolysis, using sewage sludge and nZVI as raw materials, and tested to remove Cr(VI) from simulated wastewater, reaching removal capacities of 11.6 and 9.8 mg/g for Cr(VI) and total Cr, respectively (Liu et al., 2020). The removal rates of Cr(VI) were always greater than that of total Cr under all controlled conditions, indicating that Cr(VI) was firstly reduced to Cr(III), and then removed by adsorption. The characterization of biochar before and after adsorption and the component analysis of solution after adsorption showed that the electron donors for Cr(VI) reduction were Fe^0, Fe^{2+} and organic compounds existing in biochar, and Cr(III) was very likely removed through the generation of CrOOH. A different approach for the preparation of nanocomposites involves a liquid phase method, where ZVI nanoparticles are synthesized via the reduction of $FeCl_3$ using sodium borohydride ($NaBH_4$), and then, precipitated onto biochar surface (Wan et al., 2019; Qiu et al., 2020b). An additional step was introduced by entrapping nZVI-impregnated biochar into Ca-alginate beads to enhance the Cr(VI) removal efficiency and to reduce the side effect of Fe leaching into the aqueous environment, resulting in an overall uptake capacity of 86.4 mg/g (Wan et al., 2019). Another study reports the preparation of a ZVI nanocomposite by impregnation of biochar with polyethylene glycol (PEG), a dispersing agent, and an $FeSO_4$ solution, followed by liquid-phase reduction using $NaBH_4$ (Wu et al., 2020). The experimental results revealed that when PEG was added, a large number of hydroxyl functional groups were introduced, and nZVI was effectively dispersed on the biochar's surface with a smaller particle size. The removal rate of this nanocomposite (97.4%) was much better than that created by biochar-loaded nZVI (51.7%). In this case, the main remediation mechanism of Cr(VI) was the reduction and co-precipitation of Cr-containing metal deposits onto the adsorbent.

Biomass-derived nanocomposites with another magnetic inorganic phase, such as Fe_3O_4 nanoparticles, have also attracted significant interest during recent years. For instance, a facile one-pot solvothermal method was applied to synthesize a magnetic biochar composite, using phoenix tree leaves-derived biochar as the carbon matrix (Liang et al., 2019). The structure of nanocomposite was optimized by varying the loading ratio and the particle sizes of Fe_3O_4 nanoparticles onto the biochar surface. The nanocomposite had an adsorption capacity of 55.0 mg Cr(VI)/g in an aqueous solution, which exceeds those of biochar (39.8 mg/g) and Fe_3O_4 nanoparticles (26.5 mg/g) when applied separately. The adsorption mechanism study revealed that biochar as a carbon skeleton can mainly provide binding sites for Cr(VI) and electron-donor groups for the reduction of Cr(VI), while the Fe_3O_4 nanoparticles were involved in the immobilization of newly formed Cr(III) through the formation of mixed Fe(III)-Cr(III) hydroxides. In other works, the synthesis of Fe_3O_4/bio-composites proceeds through a co-precipitation method, where the treated biomaterial (pine cones) is dispersed in an iron-containing solution, composed of Fe^{3+}/Fe^{2+} salts with a molar ratio of 2:1 (Pholosi et al., 2020; Touihri et al., 2021). In another case, the nanocomposite was subsequently formed into gel beads and tested for both Cr(VI) and Cu(II) remediation, presenting remarkably high adsorption capacity (132.5 mg/g for Cr(VI) and 69.8 mg/g for Cu(II)) (Touihri et al., 2021).

Other inorganic phases, studied as part of nanocomposite adsorbents for the removal of chromium, include γ-Fe_2O_3 (also magnetic) (Zhang et al., 2015), CuO-ZnO (Prajapati and Mondal, 2021), TiO_2 (Choudhury et al., 2017), or even MoS_2 (Chen et al., 2021a). In all cases, determined adsorption capacity values were quite high, suggesting the successful application

of these inorganic/organic nanocomposites for the removal of chromium from aqueous solutions. The proposed mechanisms mainly involved the electrostatic interactions between the major anionic species of Cr ($HCrO_4^-$,CrO_4^{2-}) and the positively charged functional groups on the surface of nanocomposites, the reduction of toxic/carcinogenic Cr(VI) to the nontoxic Cr(III) species (reduction reaction) and the adsorption reaction of chromium ions (surface complexation formation).

25.5.2 Lead

As one of the classified hazardous heavy metals with environmental risk, lead has also attracted researcher's attention. Lead is mainly released to water bodies as Pb^{2+} ions from process industries, such as mining, smelting, printing, metal plating, and dying, while in drinking water the dissolved Pb^{2+} is also correlated with the flow-through lead-containing pipes, which stayed in use till recently. Even very low concentrations of Pb^{2+} ions in drinking water can cause a wide range of health problems, such as renal failure, coma, nausea, cancer, convulsions, and subtle effects on metabolism and intelligence. In this context, a strict parametric value of 5 μg/L shall be met for lead in potable water in the near future. The majority of nanocomposites developed so far for Pb^{2+} removal contain magnetite (Fe_3O_4) as nanosized inorganic phase (Alqadami et al., 2018; Mohubedu et al., 2019; Overah et al., 2019; Lingamdinne et al., 2020; Pelalak et al., 2021). Different types of organic-containing phases have been used, including pristine biomass, biochar, or graphene oxide. The followed synthesis approaches are similar, i.e., chemical or hydrothermal co-precipitation of magnetite precursors in a suspension of the biomass-derived organic phase. The produced adsorbents exhibit some common features, such as increased specific surface area, magnetic behavior, crystalline structure, and cation exchange capacity. These characteristics favor the adsorption of Pb^{2+} along with other bivalent heavy/toxic metals, such as Cd^{2+}, Cu^{2+}, and Ni^{2+} (Alqadami et al., 2018; Mohubedu et al., 2019; Overah et al., 2019; Pelalak et al., 2021). Hydroxyapatite (Wang et al., 2018), silica (Saini et al., 2020), and aluminum oxide (Fouda-Mbanga et al., 2020) nanoparticles have also been reported to enhance the adsorption of Pb^{2+} when mixed with pristine biomass or loaded on a biochar surface to form nanocomposites. The proposed adsorption mechanisms include cation exchange reactions and electrostatic interactions between Pb^{2+} and functional binding sites of nanocomposites' surfaces (Fig. 25.3).

25.5.3 Arsenic

Numerous studies on arsenic contamination and remediation have been extensively undertaken, especially over the last three decades. The frequency of As appearance in ground and surface waters, the significant decrease of regulation limit down to 10 μg/L from the beginning of this century, and the remarkable chemistry and complexation of its aqueous species are some of the reasons explaining such interest. Arsenic is released in the aquatic environment from several sources, such as weathering of minerals, natural processes, anthropogenic activities, and As-containing pesticides. In aqueous environments, arsenic is mainly found in two inorganic forms, i.e., As(III) and As(V). Among several technologies and adsorbent materials, biomass-derived nanocomposites have also been tested for the capture of both

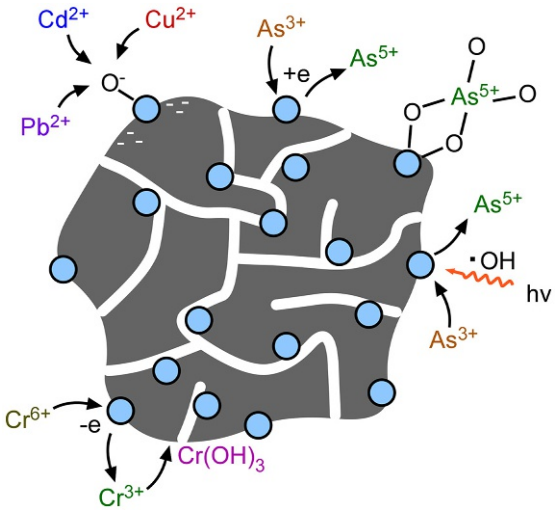

FIG. 25.3 Representative mechanisms of heavy metal capture occurring in the active sites of biomass-derived nanocomposites.

species. An early approach referred to the removal of arsenic by a biochar/AlOOH nanocomposite with nanosized polycrystalline AlOOH flakes attached to biochar surfaces. In this case, the authors obtained a remarkable high performance of examined nanocomposite for the removal of arsenic that could be attributed to its unique carbon-nanoparticle structure, which dramatically increased the reactive area and sites (Zhang and Gao, 2013). Biochar seems to be the preferred organic phase in nanocomposites applied for arsenic adsorption in subsequent studies, while inorganic phase materials may vary. ZVI (Shaikh et al., 2020), vermiculite (Li et al., 2020), CuO, and MnO (Imran et al., 2021) nanocomposites were successfully prepared and used for arsenic removal, presenting increased adsorption capacity in comparison to relevant counterparts. Assumptions regarding the mechanism of arsenic adsorption, point to a monolayer process. Sawdust was also used as a precursor to develop an activated carbon into the nanoporous surface of which SnO_2 nanoparticles were incorporated (Mohanta and Ahmaruzzaman, 2018). The produced adsorbent was applied for the efficient removal of arsenic as well as of fluoride, from drinking water. The enhanced adsorption behavior was attributed to the physico-chemical interactions of arsenic and fluoride species with the SnO_2-activated carbon composite surface.

25.5.4 Copper

Copper is considered among the most persistent heavy metals, as well as a widely used element for the manufacture of pesticides, paper, electronics, cables, automotive parts, and fertilizers. The extensive demand for Cu and its widespread use has resulted in large amounts of dissolved Cu^{2+}, being continuously released into the aquatic environments. Although Cu is an essential trace element for living organisms in natural ecosystems, the excess presence of

Cu^{2+} has become a serious issue because it can lead to various adverse health effects for humans. As for all heavy metals, numerous techniques have been developed for its removal from water, including several novel adsorbent materials. Among them, biomass-derived nanocomposites have also been recently tested. Nano-MnO_2-biochar composites have been reported to achieve maximum adsorption capacity for Cu^{2+} up to 142 mg/g, i.e., considerably higher than the maximum adsorption capacities of biochar or nano-MnO_2 when used separately (Zhou et al., 2017). The process was considered endothermic, spontaneous, and quite hardly influenced by ionic strength. The mechanism of Cu^{2+} adsorption on nanocomposite mainly involved the formation of complexes between Cu^{2+} and oxygen-containing groups. Several hydroxyapatite/biochar nanocomposites, synthesized through a single-pot hydrothermal process, were also examined as adsorbents for the removal of Cu^{2+} from aqueous media, demonstrating sufficient maximum adsorption capacity (99 mg/g). The proposed mechanisms involved mainly cation exchange and inner-sphere surface complexation (Jung et al., 2019). A series of magnetic nanocomposites were also synthesized (mainly graphene- or chitosan-based), using a single-pot solvothermal carbonization/co-precipitation route by functionalizing biomass with iron oxide nanoparticles (Siddiqui et al., 2021). The produced nanocomposites showed excellent performance for the adsorption of different heavy metals, including Ni, Cr, and Cd, and the obtained results revealed that the presence of active groups, such as carbonyl and carboxylic in the magnetic carbon nanocomposites, have assisted the adsorption process.

25.5.5 Cadmium

Cadmium, a main component of metallic impurities found in wastewater, is mainly released in the environment by anthropogenic activities, such as electroplating, battery manufacturing, and metallurgical industries. Exposure even to low concentrations of cadmium is reported to cause harmful health effects in humans, e.g., renal failure, liver disorder, and bone disorders. Particular bio-nanocomposites have been developed for the removal of cadmium from aqueous solutions. A novel material, consisting of chitosan/activated carbon/ZVI nanoparticles and synthesized by the sonochemical method, demonstrated notable adsorption capacity toward Cd^{2+}, reaching 344 mg/g. The removal efficiency was attributed to successful interactions between the oxygen functional groups of activated carbon, the amine groups of chitosan, and the iron ions (Sharififard et al., 2018). Another adsorbent tested for Cd^{2+} removal is a macroporous nanocomposite biomass, synthesized by natural polymer (xanthan gum) and silicate (Ma et al., 2015). This nanocomposite not only showed a specific macroporous structure, but also a better cation exchange capacity, which assisted the retain of cationic ions.

25.5.6 Uranium

Uranium is considered among the most hazardous pollutants, due to its chemical toxicity in addition to potential natural radioactivity. Hopefully, the dissolved uranium is not considered as dangerous, when present in the metallic form. Nevertheless, when ingested in humans (e.g., by drinking water), the hexavalent uranium can cause severe health damages,

especially to the kidney. Mining activities are the main origin of groundwater pollution by U(VI). In general, U(IV) originated from the minerals/ores may get oxidized upon exposure to the atmosphere, producing dissolved U(VI), which is then released to water streams. The studies in the relevant literature, regarding the U(VI) adsorption by the use of bio-nanocomposites, refer mainly to materials with nanosilica as the inorganic phase. An SiO_2/carbon nanocomposite was synthesized using a simple, low-cost, industry scalable method, starting from corn cob biowaste (Dutta and Nath, 2018). This treatment system showed a maximum uptake capacity of 255 mg/g with a quite high adsorption efficiency (94.2%). The high sorption efficiency of U(VI) was attributed to the large surface area and the availability of excess protonation sites on the silanol groups. Nanosilica, added on biochar using glutaraldehyde as an efficient crosslinking compound, was developed to form a novel nanocomposite that presented very fast adsorptive removal of uranyl ions from aqueous solutions in only 1 min contact time (Mahmoud et al., 2019). The respective adsorption process was confirmed to rely principally on the solution pH and reached 86.3% at pH 4.

25.5.7 Other aqueous pollutants

A very interesting bio-nanocomposite was recently synthesized and employed as an adsorbent to remove aqueous Mn^{2+} and Zn^{2+} cations (Bulin et al., 2021). It is a magnetic graphene oxide nanocomposite, based on Fe_3O_4-GO framework, fabricated via one-pot co-precipitation under mild experimental conditions. The material was reported to adsorb 400 mg/g of Mn^{2+} and 373 mg/g of Zn^{2+} within 4 and 6 min, respectively. In this case, the adsorption was spontaneous, endothermic and entropy increasing, with a mechanism mainly based on the chemical interaction of oxygen atoms in the C═O or C—O relevant groups with Mn^{2+} and Zn^{2+}.

Lately, the removal of nutrients, such as nitrate and phosphate, by adsorption onto bio-nanocomposites has been also attempted by several researchers. A simple method was developed to synthesize MgO-biochar nanocomposites by crystallizing nano-MgO flakes in biochar matrix through the slow pyrolysis of $MgCl_2$-pretreated biomass (Zhang et al., 2012). A variety of carbon-rich biomass and produced MgO-biochar nanocomposites with highly nanoporous structures were used in both the MgO nanoflakes and the biochar matrix. As a result, all the examined combinations showed excellent removal efficiencies toward phosphate and nitrate from water. MgO-biochar nanocomposites were also prepared with different crystal structures, using fallen leaves (Luo et al., 2021). The experimental results showed that the nanocomposites with a higher degree of homogeneity between MgO and biochar could change the normal crystal structure to the C-Mg-O phase and hence, achieve improved adsorption rate and capacity for the adsorption of phosphates. The proposed mechanisms were hydrogen-bond interaction, inner-sphere complexation, and surface chemical adsorption. In another study, a low-cost nanocomposite derived from aminated-agricultural biomass and nano-sized Fe(III) oxides was fabricated, and examined for the removal of nutrients (Qiu et al., 2020a). The binary adsorption isotherms indicated that the adsorption affinity of bio-nanocomposite was greatly promoted after the encapsulation of Fe(III) oxides, whereas phosphate was competitively adsorbed over nitrate. The authors suggested that the replacement of hydroxyl groups by phosphate ions through ligand-exchange reactions

could be the major underlying adsorption mechanism for the preferred adsorption sites. In a very recent work, TiO_2/cellulose nanocomposites were prepared by a facile hydrolysis-precipitation method and used as anti-bacterial bio-adsorbents for the removal of phosphate from aqueous media (Zong et al., 2021). The prepared nanocomposites presented high specific surface area and pore volume, features that allowed them to exhibit high adsorption capacity for phosphate (Table 25.1).

TABLE 25.1 Summary of literature studies involving biomass-derived nanocomposites as adsorbents for inorganic pollutants removal from aquatic media.

Pollutant	Active phase	Biochar source	Reference
Cr(VI)	nZVI	*Peganum harmala* seed	Khosravi et al. (2018)
Cr(VI)	Fe_3O_4	Phoenix tree leave	Liang et al. (2019)
Cr(VI)	nZVI	Sewage sludge	Liu et al. (2020)
Cr(VI)	nZVI	Wheat bran	Wan et al. (2019)
Cr(VI), Cr(III)	nZVI	Wheat straw	Qiu et al. (2020b)
Cr(VI)	nZVI	Coconut shell	Wu et al. (2020)
Cr(VI)	Fe_3O_4	Pine cone	Pholosi et al. (2020)
Cr(VI), Cu(II)	Fe_3O_4	Pine cone	Touihri et al. (2021)
Cr(VI)	γ-Fe_2O_3	Eichornia crassipe	Zhang et al. (2015)
Cr(VI)	ZnO and CuO	Marigold petal	Prajapati and Mondal (2021)
Cr(VI)	TiO_2	Dead yeast/*S. cerevisae*	Choudhury et al. (2017)
Cr(VI)	MoS_2	Lignin	Chen et al. (2021a)
Pb^{2+}, Cd^{2+}, Co^{2+}	Fe_3O_4	Waste camel bone	Alqadami et al. (2018)
Pb^{2+}, Cd^{2+}	Fe_3O_4	*Quercus robur* fruit	Mohubedu et al. (2019)
Pb^{2+}, Zn^{2+}, Cd^{2+}, Cu^{2+}, Ni^{2+}	Fe_3O_4	*Raphia farinifera*	Overah et al. (2019)
Pb^{2+}	Fe_3O_4	Tangerine peel	Lingamdinne et al. (2020)
Pb^{2+}, Cd^{2+}	Fe_3O_4	Oak wood ash	Pelalak et al. (2021)
Pb^{2+}, Cu^{2+}, Zn^{2+}	Hydroxyapatite	Rice straw	Wang et al. (2018)
Pb^{2+}	SiO_2	Orange peel	Saini et al. (2020)
Pb^{2+}	Al_2O_3	Banana peel	Fouda-Mbanga et al. (2020)
As(V), PO_4^{3-}	AlOOH	Cottonwood	Zhang and Gao, 2013)

Continued

TABLE 25.1 Summary of literature studies involving biomass-derived nanocomposites as adsorbents for inorganic pollutants removal from aquatic media—cont'd

Pollutant	Active phase	Biochar source	Reference
As(III), As(V)	nZVI	*Cassia fistula*	Shaikh et al. (2020)
As(V)	Vermiculite	Crushed hickory wood chip	Li et al. (2020)
As(V)	CuO, MnO	*Sesbania bispinosa*	Imran et al. (2021)
As(III), F^-	SnO_2	Sawdust	Mohanta and Ahmaruzzaman (2018)
Cu^{2+}	MnO_2	Corn stalks	Zhou et al. (2017)
Cu^{2+}	Hydroxyapatite	Undaria pinnatifida root	Jung et al. (2019)
Cu, Ni, Cr, Cd	Fe oxide	Rice husk	Siddiqui et al. (2021)
Cd^{2+}	Fe	Shrimp shell and grape stalk	Sharififard et al. (2018)
Cd^{2+}, Hg^{2+}, As(V), Cr(VI)	Silicate	Xanthan gum	Ma et al. (2015)
U(VI), Cr(VI)	SiO_2	Corn cob	Dutta and Nath (2018)
U(VI)	Silica	*Liquidambar styraciflua* fruit	Mahmoud et al. (2019)
Mn^{2+}, Zn^{2+}	Fe_3O_4	Natural graphene oxide	Bulin et al. (2021)
PO_4^{3-}, NO_3^-	MgO	Sugar beet tailings, sugarcane bagasse, cottonwoods, pine woods, peanut shells	Zhang et al. (2012)
PO_4^{3-}	MgO	Fallen leaves	Luo et al. (2021)
PO_4^{3-}	Fe(III) oxides	Wheat straw	Qiu et al. (2020a)
PO_4^{3-}	TiO_2	Cellulose	Zong et al. (2021)

25.6 Adsorbents for pollutants in gaseous forms

The production of biomass-derived nanocomposites with improved efficiency, regarding the capture of pollutants from gas phases, has found increased interest, especially during the last years. The relevant efforts are usually focused on finding the solution in two major problems of industry, typically related to energy generation, i.e., the treatment of gas byproducts from combustion processes and the purification of biogas from hydrogen sulfide. In particular, the stricter environmental restrictions require the uptake of heavy metals (but currently also of CO_2) from the flue/combustion gases, while the efficient cleaning of biogas is of high importance to extend the lifetime of power generators.

25.6.1 Flue gases

The flue gases, resulting from the combustion of fossil fuels, solid wastes, etc., are considered as the most common form of gaseous waste streams. Despite the expected profits from

such processes (calorific value, wastes degradation), the release of untreated byproducts into the atmosphere is considered to be a major source of environmental pollution. Combustion can cause the emission of several greenhouse gases, such as CO_2, N_2O, and CH_4. In addition, the flue gases can also be the carrier for significant amounts of toxic metals, being released to the atmosphere, dispersed, transferred and eventually, deposited on the soil and the surface of water bodies. Heavy metals emissions are not a direct product of combustion reactions; however, the occurrence of very high temperatures during combustion contributes to their atomization/volatilization from their compounds in the burnt solids and their transfer to the gaseous phase mainly in elemental form.

Due to its simplicity, the adsorption process appears to be the most suitable technology to apply in this field, when the used adsorbent is capable to decrease the residual concentration of pollutants below their regulation limit as imposed by the environmental legislation. There are two approaches for the implementation of adsorption in gas purification: the fixed-bed reactor set-up and the direct injection of adsorption agents in the stack (either upstream or downstream) and their subsequent retaining by the subsequent bag filters. The dust cake obtained in these filters consists of an adsorbent-ash mixture, while the process of pollutants' removal may take place mainly at this point, rather than in the stack. In both cases, it is worth noting that the respective contact time is very short (i.e., in the range of milliseconds), due to the high velocities of hot gases.

The qualification of a solid for the removal of pollutants in the gas phase should include two main characteristics: (i) the dominant capture mechanism, which should be based on chemisorption to ensure sufficient stability of the pollutant with the adsorbent surface, and (ii) high maximum capacity, ensuring the minimization of material's replacements frequency, due to the saturation and aiming to minimize the treatment's cost. However, a specific feature of the adsorption process in this case, strongly affecting the adsorption capacity, is the occurrence of relatively high temperatures. The temperature of flue gases in the upper zones of the stack usually lies in the range 120–200°C. Under these conditions, the mobility of pollutant's atoms or molecules is further increased, by introducing an extra kinetic limitation to their uptake by the adsorbents' surface, since the effective contact time between the adsorbent and the waste stream is significantly limited. The adsorbent itself may also underlie certain modifications of surface properties, due to the excess heating.

Another issue arises by the complexity of flue gases composition, because they are byproducts of combustion processes from various raw materials. As aforementioned, the main greenhouse gases are always the main component of them; thus, the applied adsorbent should maintain a high selectivity for the targeted pollutants in the presence of the other gases, which may act interfering or competitively to the same adsorption sites. In this case, water vapors are the most interfering component, since they are easily absorbed on any material, blocking its pores and significantly reducing the effective specific surface area. However, under steady-state conditions of a continuous process, the effect is strongly affected by the temperature level, which defines the equilibrium of water's sorption-desorption mechanism.

Composites of biochars with different inorganic phases have been tested as adsorbents to mainly remove the carbon dioxide content, pointing to the observed better efficiency gain in comparison to the pure biochar application, which is attributed to the activation of different adsorption mechanisms, than the physisorption on the carbon phase. In addition, another

advantage is the easier regeneration and reuse, which becomes favorable under mild thermal treatment (110–120°C), i.e., at temperatures much lower than those occurring during the pyrolysis process. As a result, minor effects on their surface properties are expected to appear and the materials can be used in several adsorption-regeneration cycles.

Biochars decorated with Al, Fe, and Mg oxides were tested as CO_2 adsorbents (Creamer et al., 2016). The nanocomposites were prepared by a single-step process after mixing the raw cotton wood in a solution of hydrated metal chlorides ($AlCl_3$, $FeCl_3$, and $MgCl_2$) and then by pyrolyzing at 600°C. It was found that biochar composites presented a higher CO_2 adsorption capacity with respect to the unmodified biochar. The introduction of aluminum oxide was found to bring higher efficiency (71 mg/g at 25°C), although iron oxide composites showed a higher specific surface area. Physisorption was reported as the dominant removal mechanism, according to the conclusions derived from the regeneration experiments. The saturated adsorbents may be easily subsequently regenerated by thermal treatment (99% rate, when subjected to 120°C for 3 h).

In another research attempt, magnesium oxide/biochar nanocomposites were found to be the best performing material, reaching a CO_2 capacity of 81 mg/g at 25°C before saturation (Lahijani et al., 2018). The system was synthesized by a similar single-step process, where metal nitrate salts were first attached to the surface of walnut shell biochar. The different results of this study should be attributed to the role of biochar source, which in this case, presented higher specific surface area and pore volume for the same metal-to-biochar ratio. It was also proven that the pyrolysis temperature may define proportionally the value of specific surface area, while the higher metal loadings on biochar may lead to increased micropore blockage.

Taking a step forward, the influence of various salts of the same metal during synthesis was tested (Zubbri et al., 2020). Nitrate, sulfate, chloride, and acetate salts of magnesium were examined as different sources for this metal during a single-step pyrolysis to feature a specific biochar precursor, such as rambutan peel. The composite prepared by the addition of magnesium nitrate was found to provide the highest capacity (i.e., 75.6 mg/g at 30°C). Furthermore, the exothermic behavior of adsorption and the high regeneration capacity of the composite by applying relatively low temperatures indicated physisorption as the dominant uptake mechanism. However, chemisorption was also suggested as a parallel capture procedure, since magnesium oxide may react with CO_2 and form magnesium carbonate. Regeneration continues to be a specific asset for these materials since after 25 operation cycles (adsorption-regeneration) the efficiency remained quite intact.

In general, the increase of CO_2 capture in biochar nanocomposites with metal phases can be explained by the Hard-Soft Acid Base (HSAB) theory, which is frequently used for CO_2 detection and quantification. Hard acidic CO_2 prefers to bond with a hard alkaline surface and therefore, by introducing specific metal groups onto the biochar surface, the obtained alkalinity results in higher adsorption efficiency (Dissanayake et al., 2020). Furthermore, the hard alkaline sites increase the selectivity toward CO_2, since other co-existing components in flue gases are neutral (e.g., N_2O), or alkaline (e.g., CH_4). Unfortunately, so far, the available experimental data that support this mechanism were obtained by adsorption tests taking place at lower temperatures than those of the flue gases, i.e., at the levels of regeneration processes (<70°C). This condition can turn into a serious drawback for the prepared biochar composites, when applied for CO_2 adsorption/removal, since an extra cooling step for the flue gases may be required before adsorption.

Assuming a very high probability of hazardous effects related to the dispersion of inorganic pollutants by flue gases, the treatment of these streams has become obligatory. In this frame, more strict regulation limits, regarding the maximum permitted emission concentrations, were set by authorities worldwide with remarkably high penalties applied when a user fails to comply sufficiently with them. Therefore, the development of purification technologies, optimized for the selective capture of inorganic pollutants in gas flows, has become a necessity.

The emission of mercury is the most frequent case of a toxic metal appearing in flue gases, owed to its high volatility, which facilitates atomization even under relatively low temperatures. The mercury speciation in the flue gases is dominated by the elemental form, which shows low solubility and also, low tendency to react with other components at the commonly applied temperature levels of the combustion process. However, if the flue gas is sufficiently cooled in the upper parts of the stack, then the formed Hg^0 may react with co-existing anions, such as Cl^-, and get oxidized to its bivalent form. The oxidation mechanism is kinetically limited and depends on the nature of combustion raw material, e.g., coal, chloride content (Kokkinos et al., 2017). The oxidized mercury can be removed easier using common air pollution control devices, such as electrostatic filters, scrubbers, etc., but usually the obtained removal represents only a small fraction of mercury's total amount, while the not removed quantity manages to pass through and emit to the atmosphere at relatively large quantities.

The removal of mercury from flue gas has been tested by various biochar-based composites functionalized with different inorganic compounds. For instance, biochar obtained by rice straws was combined with $CaCO_3$ following a two-step thermal treatment process, in order to be used as an adsorbent for Hg^0 (Shi et al., 2020). For the production of this composite, the temperature was first set at 300–500°C, allowing the biomass decarbonization and then, further increased to 700–900°C, provoking the decomposition of $CaCO_3$. The excess of CaO was washed out by the addition of HCl solution, while the adsorbed (excess) Cl^- was also removed by water. This procedure allowed the formation of a high pore volume in the nanocomposite structure, assisting the physisorption of Hg^0 on its surface. Particularly, the uptake capacity at 80°C was determined as 155 μg/g. However, under the application of more realistic flue gases temperatures, this value was significantly reduced, reaching almost half at 180°C. Such linear decrease of capacity is attributed to the elevated mobility of mercury, which redefines the equilibrium, favoring desorption at higher temperatures.

Introducing the preliminary or con-current oxidation of mercury as part of the adsorption process in the application of biochar nanocomposites is a very interesting approach since it is accompanied by high uptake capacities when compared to the direct adsorption case. A composite, consisting of biochar from date stone and iron oxyhydroxide, showed remarkable capacity values, reaching 1405 μg/g (25°C) (Ebiad et al., 2020). The preparation of this system involved the self-arrangement of used iron oxyhydroxide on the developed biochar structure to avoid dehydration, if a single-step pyrolysis procedure was followed. The improved performance was attributed to the oxidation of Hg^0 by the presence of Fe^{3+}. Nevertheless, a dramatic drop of the capacity is observed even at mild temperatures (70°C) where values around 44 μg/g were measured. The efficiency loss can be explained by the relatively lower specific surface area and pore volume of the used biochar, which inhibit large external mass transfer and intraparticle diffusion mechanism and limit the successful implementation of adsorption at higher temperatures. For this reason, the application of the material for the removal of mercury from natural gas (at 30°C) is proposed as an alternative (Fig. 25.4).

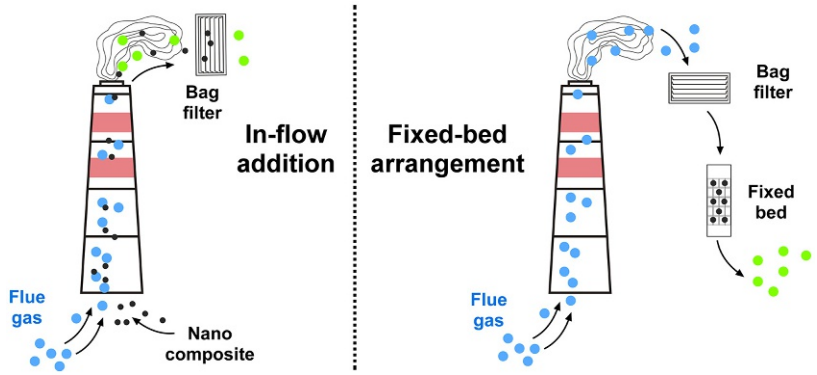

FIG. 25.4 Application schemes for biomass-derived nanocomposites in flue gas purification. Introduction of nanoadsorbent into the gas flow followed by filtration (left) and filtration of flue gas through a fixed-bed column filled with the nanocomposite (right).

In the same framework, walnut shell biochar was combined with iron and various other metal salts (e.g., Co, Cu, Ce, Mn) to prepare nanocomposite mercury adsorbents (Jia et al., 2021). Although the evaluation of their efficiency was shown in terms of uptake percentage, it is clear that the oxidation of Hg^0 was successful, especially in the case of Fe/Mn oxides. The same combination of binary Fe/Mn oxides attached on cotton straw biochar, appear as the best performing materials for the capture of mercury (Shan et al., 2019). The maximum capacity was found to be 532 μg/g at 120°C, which is a typical experimental temperature within the range of flue gases. The high efficiency can be explained by the oxidation of elemental mercury from the presence of both Mn^{4+} and Fe^{3+}, which is supported by the increased surface area and pore volume. The regeneration of saturated nanocomposite with only slight loss of efficiency is possible by a two-step treatment process, which includes the mercury release from the possible complex compounds at 400°C for 1 h under nitrogen atmosphere and the activation of adsorbent surface sites by the oxidation of previously reduced Mn^{3+}/Mn^{2+} and Fe^{2+} at 250°C in air. Moreover, it was observed that the presence of oxygen in flue gas may increase efficiency, following the above-mentioned regeneration mechanism.

25.6.2 Biogas

The desulfurization of biogas streams through the application of fixed-bed columns, as applied for the elimination of H_2S or SO_2 gases, is of critical importance for the protection of power stations from corrosion and other operational problems, when using biogas as fuel. To this end, the development of improved processes, based on optimized adsorbents, would allow the safe and economically viable use of biogas, produced by the anaerobic treatment of organic wastes. In particular, the removal of H_2S anticipates the protection of engine and exhaust gas heat recovery equipment from severe corrosion problems. The removal of sulfur compounds is commonly delivered by applying several inorganic phases and carbon-based adsorbents, which aim to the neutralization of their acidic character, followed by oxidation to

the zero-valent form, or their capture into the formation of very stable metal sulfides. The porosity and the high specific surface area are some other important requirements to extend the lifetime of applied solid adsorbent.

Considering these points, the combination of carbon phases, providing proper porous structure, and of nanosized inorganic components, supporting high chemical affinity toward H_2S, would be a very promising approach to improve desulphurization strategies. Although the relevant research, dealing with the use of biomass-derive precursors to develop such nanocomposites, is still in preliminary stages, there are still effective examples, which work as a proof of this concept. In this case, activated carbons obtained from agricultural residues were preferentially used to produce the nanocomposite materials. Microporous walnut shell-based activated carbons impregnated with activating reagents (e.g., KOH, K_2CO_3, $ZnCl_2$, and H_3PO_4) were examined for the simultaneous removal of H_2S, COS, and CS_2 gases from yellow phosphorus tail gas, showing potential interest for biogas purification (Li et al., 2018). The high capacity against sulfur, which reached 45.25 mg/g, when KOH was applied, can be attributed to the functionalization of activated carbon with hydroxyl groups, while the reaction of K or Zn with the carbon phase can result in the decrease of surface tension and in the increase of micropores' number in the carbon network.

Nevertheless, the loading of metal oxides appears as a more representative case for the binary phase hydrogen sulfide adsorbents. Microporous palm shell-activated carbon was introduced as a substrate for the dispersion of active cerium oxide (CeO_2) in the presence of NaOH and then evaluated for the H_2S removal from biogas (Lau et al., 2018). The nanocomposite combined the physisorption ability of activated carbon and together with the catalytic activity of CeO_2 under the set alkaline conditions as introduced by NaOH, delivered an improved H_2S uptake. The catalytic mechanism includes the conversion redox reaction of CeO_2 to Ce_2O_3, which provides oxygen species for the H_2S oxidation, as well as functional groups to the carbon structure. The high H_2S removal efficiency was also reported for the walnut shell-based activated carbon combined with manganese oxides (Wang et al., 2015). In the later study, the dispersion of the active phase in small nanoparticles is suggested as the main reason for the enhancement of desulphurization performance (Table 25.2).

TABLE 25.2 Summary of literature studies involving biomass-derived nanocomposites as adsorbents for pollutants removal from gaseous streams.

Pollutant	Active phase	Biochar	Reference
CO_2	Fe, Al, and Mg oxides	Cottonwood	Creamer et al. (2016)
CO_2	MnO_2	Walnut shell	Lahijani et al. (2018)
CO_2	MnO_2	Rambutan peel	Zubbri et al. (2020)
Hg^0	CaO	Rice straws	Shi et al. (2020)
Hg^0	FeOOH	Date stone	Ebiad et al. (2020)
Hg^0	Fe/Mn oxides	Walnut shell	Jia et al. (2021)
H_2S	CeO_2	Palm shell	Lau et al. (2018)
H_2S	MnO_2	Walnut shell	Wang et al. (2015)

25.7 Adsorbents for soil remediation

Long-term disregard, concerning the impact of agricultural and industrial processes in the environment, has brought soil pollution into a very serious condition for which the scientific community should find emergent and viable solutions. The main risks in this case are related to food crops since different pollutants tend to be bioaccumulated by plants and indirectly, through their consumption, pose a serious hazard to human health through the trophic chain. Hopefully, this scenario is not directly related to anthropogenic activities, because the polluted areas or areas with industrial activity are generally avoided for agriculture purposes, while the authorities have set minimum distances from such regions, where agriculture can be allowed. Therefore, the pollution of a productive soil commonly originates from gaseous pollutants settling on the soil's surface (e.g., through rain), or from water-soluble pollutants transported through the flow of aquatic bodies.

Soil pollution can be classified into two major categories: nutrients and toxic metals. Nutrients are essential in the food industry and they are used widely all over the world in order to, qualitatively and quantitatively, enhance the production. The typical naturally occurring ions, considered to be nutrients, are nitrates (NO_3^-), phosphates (PO_4^{3-}), and ammonium (NH_4^+). In fertile soil, their content is sufficient enough for plant growth. However, the majority of agricultural areas are already degraded, due to over-cropping, and so the supplementary addition of nutrients/fertilizers becomes mandatory. On the other hand, the frequently applied practice of excessive use of fertilizer in low-quality soils (e.g., due to degraded physicochemical properties) implies the leaching and transfer of them outside the application limits. Eutrophication, groundwater pollution, marine pollution, and human health issues are some of the negative consequences. Regarding toxic metals, arsenic, chromium, cadmium, and lead are the most commonly encountered pollutants in soil. Arsenic and chromium may be also naturally occurring metals, e.g., due to ore erosion, through biotic and abiotic mechanisms, whereas the existence of cadmium and lead is attributed mainly to anthropogenic activities, and partially to the previously mentioned cases.

As a facile method for this type of application, adsorption is often used for the restoration of contaminated soils, offering a wide range of advantages. In this direction, biochar has proven to be an important material, considering its relatively low-cost and high quantity availability, when received after the utilization of byproducts. However, the improvement of soil's mechanical properties (e.g., strength) is the major advantage for the incorporation of biochar in the relevant remediation procedures (Wang et al., 2020). There are two main approaches of application, either by mixing biochar with the topsoil or by local placement at higher depths (in the presence of underground water streams). The expected mechanism of its remediation activity is based on the immobilization of toxic metals and the reversible uptake of nutrients that allow a desorption release. Up to date, the combination of biochar with other functional inorganic nanostructures in the form of nanocomposites was demonstrated as a way to increase the observed efficiency in the capture of the aforementioned pollutants. Certain representative cases of biochar nanocomposites, examined for the remediation of soil, are described in the following (Fig. 25.5).

A potassium-iron rice straw biochar composite was developed for the sorption of nitrate, phosphate, and ammonium ions (Chandra et al., 2020). Initially, the iron-impregnated

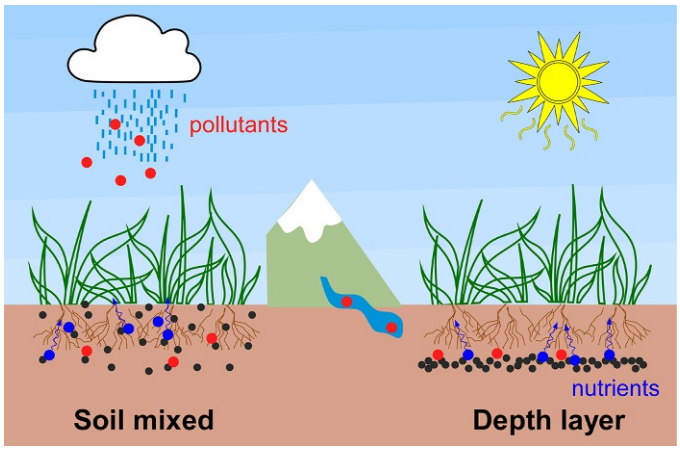

FIG. 25.5 Application schemes for biomass-derived nanocomposites in soil remediation. Homogeneous mixing of the nanocomposite powder in the soil (left) and formation of a filtration layer in higher depth (right).

biochar was synthesized by adding biochar into an iron salt solution and then, by applying a pyrolysis process at 400–600°C. Potassium impregnation was contacted in the second stage of this process, performed under hydrothermal conditions. In particular, the iron-impregnated biochar was mixed with KOH solution and placed in an autoclave setup, operating under pressure. During the saturation experiments, it was observed that the nanocomposite has a higher affinity for NO_3^- and PO_4^{3-} than for NH_4^+. This fact was attributed to the different occurring sorption mechanism among these nutrients, since the surface diffusion-controlled mechanism of ammonium sorption is limited, and not favored by the low specific surface area of potassium-iron biochar composite. The examined adsorbents showed higher cation exchange capacity, which increased the soil fertilization index and assisted the controlled nutrients release.

An iron-based biochar composite was also synthesized and found capable to adsorb both toxic metals and nutrients (Zhu et al., 2020). For this preparation, wheat straw was used as raw material for biochar production, dispersed in an iron salt solution. The mixture was heated at mild temperature (70°C), aiming to obtain an iron oxyhydroxide, identified as goethite. The higher adsorption capacity was obtained for the removal of As(III) (65 mg/g) in comparison to that of Cd (32 mg/g) and phosphate (42.6 mg/g). This behavior was attributed to the formation of goethite, which increased the positive surface charge of biochar, and thus, the sorption of anionic species became favorable. According to the characterization of saturated material, an adsorption-oxidation mechanism was revealed through the preliminary oxidation of As(III) to As(V). It should be also underlined that the iron-based adsorbents, developed for water treatment, present high affinities for the uptake of As(III) and As(V) (Tresintsi et al., 2014). The exact removal mechanism depends on the oxidation of As(III), which is normally achieved by Fe(III) and Mn(VI). Following the same concept, the combination of mixed hydroxides with biochar was found quite efficient for soil restoration. In the relevant studies, nanocomposites were developed, when the biochar was soaked in

TABLE 25.3 Summary of literature studies involving biomass-derived nanocomposites as adsorbents for inorganic pollutants removal from soil.

Pollutant	Active phase	Biochar	Reference
NO_3^-, PO_4^{3-}, NH_4^+	Fe/K oxide	Rice straw	Chandra et al. (2020)
As(III), Cd^{2+}, PO_4^{3-}	FeOOH	Wheat straw	Zhu et al. (2020)
As(III)	Mn oxide	Rice straw	Yu et al. (2015)
As(III), As(V)	Fe/Mn oxides	Rice straw	Lin et al. (2019)
As(III), As(V)	Fe/Mn/Ce oxides	Rice straw	Zhang et al. (2020)
Cr(VI)	FeS	Wheat straw	Lyu et al. (2018)
Cr(VI)	Fe oxide	Barley grass	Chen et al. (2021b)
Cd^{2+}	Fe/Mn oxides	Corn straw	Zhou et al. (2019)
Pb^{2+}	Fe oxide	Cabbage mustard seed	Yang et al. (2016)

metal ions solutions, and the mixture was then subjected to pyrolysis (Yu et al., 2015; Lin et al., 2019; Zhang et al., 2020). An interesting fact is that rice straws were used as raw material for the production of biochar, while paddy soil was the field of implementation, showing a sustainable scenario for waste valorization.

Iron-based biochar composites were also examined for the removal of chromium and immobilization from soil substrates. The pyrolysis of wheat straw biochar with iron sulfide (Lyu et al., 2018) and the barley grass biochar dispersed in iron chloride solution (Chen et al., 2021b) were examined for this purpose. In both cases, Cr(VI) was considered as the contaminant of interest, due to its high toxicity and its frequent appearance in contaminated soil samples. The main removal mechanism, imposed by the application of nanocomposites, was the initial sorption-reduction of Cr(VI) and, afterwards, the surface precipitation of Cr(III) as hydroxide.

Regarding the immobilization of other metals in contaminated soils by biochar nanocomposites, the cases of Cd and Pb were also examined. Firstly, the synthesis of Fe—Mn biochar composite for the adsorption of Cd was investigated (Zhou et al., 2019). Corn straw biochar mixed with iron and manganese salts was dried and pyrolyzed at 600°C. With a similar pyrolysis approach, an Fe-based biochar composite was prepared for the adsorption of Pb, using cabbage mustard seeds as the source of biochar (Yang et al., 2016). However, the obtained efficiency was limited, due to the intensive positive surface charge of composites, favoring the repulsive force between the similarly (positive) charged pollutants, and suggesting that the design of such materials should result in the electrostatic interactions or complexation between the negatively surface charged biochar for the removal of cationic pollutant (Table 25.3).

25.8 Conclusions-perspectives

The application of biomass-derived nanocomposites in environmental remediation strategies appears as a very ambitious perspective to upgrade the role of engineered inorganic

nanoparticles in large-scale processes. The successful distribution of nanoparticles into the porous carbon structure indicates the major advantage of these materials referring to adsorption uses: the minimization of aggregation extent which is usually the limiting parameter for the performance of single-phase nanoadsorbents. Therefore, the effective surface area of the active phase dramatically increases adsorption capacity and importantly, less quantity of the nanoparticles is required to bring the same efficiency. Considering that the biomass-obtained phase has a very low cost, ideally, such nanocomposites contribute to simultaneous efficiency improvement and cost reduction.

Nevertheless, there are important obstacles to overcome in the production and implementation procedures of biomass-derived nanocomposites before they turn into fully functional agents for purification practices. One aspect is the mechanical and chemical stability of these solids during their storage, application, and post-use disposal. For instance, if the carbon phase is loose, a high possibility for the destruction of the microstructure appears causing the nanocomposite to lose the improved efficiency of the hybrid adsorption contributions. Similar effects may be the reason of failure when the adsorbent is applied in fixed-bed filtration systems or mixed as a soil substrate. Particularly, a decrease of grain size would be responsible for occlusion problems or rapid diffusion to higher depths, respectively for each case.

Together with the chemical nature of the active phase, the mechanical properties of the nanocomposite granules define the leaching behavior prior, or after the adsorption of the targeted pollutants. Dissolution of metal ions from the active inorganic phase or secondary release of captured pollutants is able to become a cause for the exclusion of developed technology from further investigation since the presented solution appears also as a source of pollution. Unfortunately, only a few of the available research studies provide experimental evidences on the leaching behavior of the demonstrated nanocomposites. A deeper examination of the pollutants' uptake mechanisms would assist in better understanding and prediction of dissolution possibility. As a more difficult task to work on, information about the potential fate of the nanocomposites and their building components at the end of their operational lifetime in soil or aquatic systems are very rare. Multiple scenarios for the negative effect of spent nanocomposites include the risks from their nanoscale dimensions and the distribution of loaded pollutants to the environment and other living forms.

A last but most fundamental point to evaluate the potential of a biomass-derived nanocomposite to become a competitive product is the maximization of the efficiency-to-cost ratio. This is another important parameter that cannot be extracted from existing literature reports. On the one hand, most of the published works do not test the developed materials under realistic conditions of their supposed use (water parameters, inter-references, complicated environment) while uptake capacities are not representative for the maximum concentration levels of the pollutants defined by the authorities. On the other hand, although the major part of the nanocomposites is a biomass residual, the production may include procedures with high energy requirements or the use of expensive reagents able to multiply products cost.

Conclusively, an overview of the up-to-date research related to biomass-derived nanocomposites developed for water, soil, and gas purification, indicates a rising but insufficient number of efforts toward realistic solutions with the ability to reach the market and large-scale applications, in spite of the obvious advantages of this class of adsorbent. An

explanation for this gap could be the absence of an integrated approach to design optimized nanomaterials keeping in mind to balance synthesis and evaluation aspects. What is usually observed in literature is a tendency to promote the valorization of biomass byproducts while the tuning of nanocomposites and the adsorption performance for pollutants come as a secondary feature. The adoption of interdisciplinary collaborations and universal evaluation protocols together with the feedback from technical knowledge is suggested as the only valid way to inspire the rapid incorporation of this category of adsorbents in a technology field with increasing demand and direct impact on health and environmental protection.

Acknowledgments

The research project was supported by the Hellenic Foundation for Research and Innovation (H.F.R.I.) under the "2nd Call for H.F.R.I. Research Projects to support Post-Doctoral Researchers" (Project Number: 00046 MagnoSorb).

References

Alqadami, A.A., Khan, M.A., Otero, M., et al., 2018. A magnetic nanocomposite produced from camel bones for an efficient adsorption of toxic metals from water. J. Clean. Prod. 178, 293–304. https://doi.org/10.1016/j.jclepro.2018.01.023.

Bulin, C., Ma, Z., Guo, T., et al., 2021. Magnetic graphene oxide nanocomposite: one-pot preparation, adsorption performance and mechanism for aqueous Mn(II) and Zn(II). J. Phys. Chem. Solid 156, 110130. https://doi.org/10.1016/j.jpcs.2021.110130.

Chandra, S., Medha, I., Bhattacharya, J., 2020. Potassium-iron rice straw biochar composite for sorption of nitrate, phosphate, and ammonium ions in soil for timely and controlled release. Sci. Total Environ. 712, 136337. https://doi.org/10.1016/j.scitotenv.2019.136337.

Chen, H., Zhang, Z., Zhong, X., et al., 2021a. Constructing MoS2/lignin-derived carbon nanocomposites for highly efficient removal of Cr(VI) from aqueous environment. J. Hazard. Mater. 408, 124847. https://doi.org/10.1016/j.jhazmat.2020.124847.

Chen, X., Dai, Y., Fan, J., et al., 2021b. Application of iron-biochar composite in topsoil for simultaneous remediation of chromium-contaminated soil and groundwater: immobilization mechanism and long-term stability. J. Hazard. Mater. 405, 124226. https://doi.org/10.1016/j.jhazmat.2020.124226.

Choudhury, P.R., Bhattacharya, P., Ghosh, S., et al., 2017. Removal of Cr (VI) by synthesized titania embedded dead yeast nanocomposite: optimization and modeling by response surface methodology. J. Environ. Chem. Eng. 5, 214–221. https://doi.org/10.1016/j.jece.2016.11.041.

Creamer, A.E., Gao, B., Wang, S., 2016. Carbon dioxide capture using various metal oxyhydroxide-biochar composites. Chem. Eng. J. 283, 826–832. https://doi.org/10.1016/j.cej.2015.08.037.

Dissanayake, P.D., You, S., Igalavithana, A.D., et al., 2020. Biochar-based adsorbents for carbon dioxide capture: a critical review. Renew. Sustain. Energy Rev. 119, 109582.

Dutta, D.P., Nath, S., 2018. Low cost synthesis of SiO2/C nanocomposite from corn cobs and its adsorption of uranium (VI), chromium (VI) and cationic dyes from wastewater. J. Mol. Liq. 269, 140–151. https://doi.org/10.1016/j.molliq.2018.08.028.

Ebiad, M.A., Abd El-Hafiz, D.R., Masod, M.B., 2020. β-FeOOH/C nanocomposite for elemental mercury removal as a new approach to environmental and natural gas processes. J. Nat. Gas Sci. Eng. 80, 103383. https://doi.org/10.1016/j.jngse.2020.103383.

EU, 2020. Directive (EU) 2020/2184 of the European Parliament and of the Council of 16 December 2020 on the Quality of Water Intended for Human Consumption. Off J Eur Union.

Fouda-Mbanga, B.G., Prabakaran, E., Pillay, K., 2020. Synthesis and characterization of CDs/Al2O3 nanofibers nanocomposite for Pb2+ ions adsorption and reuse for latent fingerprint detection. Arab. J. Chem. 13, 6762–6781. https://doi.org/10.1016/j.arabjc.2020.06.030.

Imran, M., Iqbal, M.M., Iqbal, J., et al., 2021. Synthesis, characterization and application of novel MnO and CuO impregnated biochar composites to sequester arsenic (As) from water: modeling, thermodynamics and reusability. J. Hazard. Mater. 401, 123338. https://doi.org/10.1016/j.jhazmat.2020.123338.

Jia, L., Yu, Y., Li, Z.p., et al., 2021. Study on the Hg0 removal characteristics and synergistic mechanism of iron-based modified biochar doped with multiple metals. Bioresour. Technol. 332, 125086. https://doi.org/10.1016/j.biortech.2021.125086.

Jung, K.W., Lee, S.Y., Choi, J.W., Lee, Y.J., 2019. A facile one-pot hydrothermal synthesis of hydroxyapatite/biochar nanocomposites: adsorption behavior and mechanisms for the removal of copper(II) from aqueous media. Chem. Eng. J. 369, 529–541. https://doi.org/10.1016/j.cej.2019.03.102.

Kaprara, E., Kazakis, N., Simeonidis, K., et al., 2015. Occurrence of Cr(VI) in drinking water of Greece and relation to the geological background. J. Hazard. Mater. 281, 2–11. https://doi.org/10.1016/j.jhazmat.2014.06.084.

Khosravi, R., Moussavi, G., Ghaneian, M.T., et al., 2018. Chromium adsorption from aqueous solution using novel green nanocomposite: adsorbent characterization, isotherm, kinetic and thermodynamic investigation. J. Mol. Liq. 256, 163–174. https://doi.org/10.1016/j.molliq.2018.02.033.

Kokkinos, E., Kellartzis, I., Diamantopoulou, I., et al., 2017. Study of elemental mercury removal from flue gases using tetravalent manganese Feroxyhyte. Chem. Eng. J. 315, 152–158. https://doi.org/10.1016/j.cej.2017.01.013.

Lahijani, P., Mohammadi, M., Mohamed, A.R., 2018. Metal incorporated biochar as a potential adsorbent for high capacity CO2 capture at ambient condition. J. CO_2 Util. 26, 281–293. https://doi.org/10.1016/j.jcou.2018.05.018.

Lau, L.C., Nor, N.M., Lee, K.T., Mohamed, A.R., 2018. Hydrogen sulfide removal using CeO2/NaOH/PSAC: effect of preparation parameters. J. Environ. Chem. Eng. 6, 386–394. https://doi.org/10.1016/j.jece.2017.12.019.

Li, K., Ruan, H., Ning, P., et al., 2018. Preparation of walnut shell-based activated carbon and its properties for simultaneous removal of H2S, COS and CS2 from yellow phosphorus tail gas at low temperature. Res. Chem. Intermed. 44, 1209–1233. https://doi.org/10.1007/s11164-017-3162-6.

Li, F., Wan, Y., Chen, J., et al., 2020. Novel ball-milled biochar-vermiculite nanocomposites effectively adsorb aqueous as(V). Chemosphere 260, 127566. https://doi.org/10.1016/j.chemosphere.2020.127566.

Liang, S., Shi, S., Zhang, H., et al., 2019. One-pot solvothermal synthesis of magnetic biochar from waste biomass: formation mechanism and efficient adsorption of Cr(VI) in an aqueous solution. Sci. Total Environ. 695, 133886. https://doi.org/10.1016/j.scitotenv.2019.133886.

Lin, L., Li, Z., Liu, X., et al., 2019. Effects of Fe-Mn modified biochar composite treatment on the properties of as-polluted paddy soil. Environ. Pollut. 244, 600–607. https://doi.org/10.1016/j.envpol.2018.10.011.

Lingamdinne, L.P., Vemula, K.R., Chang, Y.Y., et al., 2020. Process optimization and modeling of lead removal using iron oxide nanocomposites generated from bio-waste mass. Chemosphere 243, 125257. https://doi.org/10.1016/j.chemosphere.2019.125257.

Liu, L., Liu, X., Wang, D., et al., 2020. Removal and reduction of Cr(VI) in simulated wastewater using magnetic biochar prepared by co-pyrolysis of nano-zero-valent iron and sewage sludge. J. Clean. Prod. 257, 120562. https://doi.org/10.1016/j.jclepro.2020.120562.

Luo, H., Wang, Y., Wen, X., et al., 2021. Key roles of the crystal structures of MgO-biochar nanocomposites for enhancing phosphate adsorption. Sci. Total Environ. 766, 142618. https://doi.org/10.1016/j.scitotenv.2020.142618.

Lyu, H., Zhao, H., Tang, J., et al., 2018. Immobilization of hexavalent chromium in contaminated soils using biochar supported nanoscale iron sulfide composite. Chemosphere 194, 360–369. https://doi.org/10.1016/j.chemosphere.2017.11.182.

Ma, W., Meng, F., Cheng, Z., et al., 2015. Synthesis of macroporous silica biomass nanocomposite based on XG/MgSiO3 for the removal of toxic ions. Bioresour. Technol. 186, 356–359. https://doi.org/10.1016/j.biortech.2015.03.133.

Mahmoud, M.E., Khalifa, M.A., El Wakeel, Y.M., et al., 2019. A novel nanocomposite of Liquidambar styraciflua fruit biochar-crosslinked-nanosilica for uranyl removal from water. Bioresour. Technol. 278, 124–129. https://doi.org/10.1016/j.biortech.2019.01.052.

Mohanta, D., Ahmaruzzaman, M., 2018. Bio-inspired adsorption of arsenite and fluoride from aqueous solutions using activated carbon@SnO2 nanocomposites: isotherms, kinetics, thermodynamics, cost estimation and regeneration studies. J. Environ. Chem. Eng. 6, 356–366. https://doi.org/10.1016/j.jece.2017.11.076.

Mohubedu, R.P., Diagboya, P.N.E., Abasi, C.Y., et al., 2019. Magnetic valorization of biomass and biochar of a typical plant nuisance for toxic metals contaminated water treatment. J. Clean. Prod. 209, 1016–1024. https://doi.org/10.1016/j.jclepro.2018.10.215.

Overah, L.C., Iwegbue, C.M., Babalola, J.O., Martincigh, B.S., 2019. Fabrication and characterisation of a Fe[formula presented]O[formula presented]/Raphia farinifera nanocomposite for application in heavy metal adsorption. Environ. Technol. Innov. 13, 11–29. https://doi.org/10.1016/j.eti.2018.09.007.

Pelalak, R., Heidari, Z., Khatami, S.M., et al., 2021. Oak wood ash/GO/Fe3O4 adsorption efficiencies for cadmium and lead removal from aqueous solution: kinetics, equilibrium and thermodynamic evaluation. Arab. J. Chem. 14, 102991. https://doi.org/10.1016/j.arabjc.2021.102991.

Pholosi, A., Naidoo, E.B., Ofomaja, A.E., 2020. Intraparticle diffusion of Cr(VI) through biomass and magnetite coated biomass: a comparative kinetic and diffusion study. S. Afr. J. Chem. Eng. 32, 39–55. https://doi.org/10.1016/j.sajce.2020.01.005.

Prajapati, A.K., Mondal, M.K., 2021. Novel green strategy for CuO–ZnO–C nanocomposites fabrication using marigold (Tagetes spp.) flower petals extract with and without CTAB treatment for adsorption of Cr(VI) and Congo red dye. J. Environ. Manage. 290, 112615. https://doi.org/10.1016/j.jenvman.2021.112615.

Qiu, H., Ni, W., Zhang, H., et al., 2020a. Fabrication and evaluation of a regenerable HFO-doped agricultural waste for enhanced adsorption affinity towards phosphate. Sci. Total Environ. 703, 135493. https://doi.org/10.1016/j.scitotenv.2019.135493.

Qiu, Y., Zhang, Q., Gao, B., et al., 2020b. Removal mechanisms of Cr(VI) and Cr(III) by biochar supported nanosized zero-valent iron: synergy of adsorption, reduction and transformation. Environ. Pollut. 265, 115018. https://doi.org/10.1016/j.envpol.2020.115018.

Saini, J., Garg, V.K., Gupta, R.K., 2020. Green synthesized SiO2@OPW nanocomposites for enhanced Lead (II) removal from water. Arab. J. Chem. 13, 2496–2507. https://doi.org/10.1016/j.arabjc.2018.06.003.

Shaikh, W.A., Alam, M.A., Alam, M.O., et al., 2020. Enhanced aqueous phase arsenic removal by a biochar based iron nanocomposite. Environ. Technol. Innov. 19, 100936. https://doi.org/10.1016/j.eti.2020.100936.

Shan, Y., Yang, W., Li, Y., et al., 2019. Preparation of microwave-activated magnetic bio-char adsorbent and study on removal of elemental mercury from flue gas. Sci. Total Environ. 697, 134049. https://doi.org/10.1016/j.scitotenv.2019.134049.

Sharififard, H., Shahraki, Z.H., Rezvanpanah, E., Rad, S.H., 2018. A novel natural chitosan/activated carbon/iron bionanocomposite: sonochemical synthesis, characterization, and application for cadmium removal in batch and continuous adsorption process. Bioresour. Technol. 270, 562–569. https://doi.org/10.1016/j.biortech.2018.09.094.

Shi, Q., Wang, Y., Zhang, X., et al., 2020. Hierarchically porous biochar synthesized with CaCO3 template for efficient Hg0 adsorption from flue gas. Fuel Process. Technol. 199, 106247. https://doi.org/10.1016/j.fuproc.2019.106247.

Siddiqui, M.T.H., Baloch, H.A., Nizamuddin, S., et al., 2021. Dual-application of novel magnetic carbon nanocomposites as catalytic liquefaction for bio-oil synthesis and multi-heavy metal adsorption. Renew. Energy 172, 1103–1119. https://doi.org/10.1016/j.renene.2021.02.157.

Touihri, M., Guesmi, F., Hannachi, C., et al., 2021. Single and simultaneous adsorption of Cr(VI) and Cu (II) on a novel Fe3O4/pine cones gel beads nanocomposite: experiments, characterization and isotherms modeling. Chem. Eng. J. 416, 129101. https://doi.org/10.1016/j.cej.2021.129101.

Tresintsi, S., Simeonidis, K., Mitrakas, M., 2014. Mn-feroxyhyte: the role of synthesis conditions on As(III) and As(V) removal capacity. Chem. Eng. J. 251, 192–198. https://doi.org/10.1016/j.cej.2014.04.033.

Wan, Z., Cho, D.W., Tsang, D.C.W., et al., 2019. Concurrent adsorption and micro-electrolysis of Cr(VI) by nanoscale zerovalent iron/biochar/Ca-alginate composite. Environ. Pollut. 247, 410–420. https://doi.org/10.1016/j.envpol.2019.01.047.

Wang, J., Ju, F., Han, L., et al., 2015. Effect of activated carbon supports on removing H2S from coal-based gases using Mn-based sorbents. Energy Fuel 29, 488–495. https://doi.org/10.1021/ef501790e.

Wang, Y.Y., Liu, Y.X., Lu, H.H., et al., 2018. Competitive adsorption of Pb(II), Cu(II), and Zn(II) ions onto hydroxyapatite-biochar nanocomposite in aqueous solutions. J. Solid State Chem. 261, 53–61. https://doi.org/10.1016/j.jssc.2018.02.010.

Wang, Y., Wang, H.-S., Tang, C.-S., et al., 2020. Remediation of heavy-metal-contaminated soils by biochar: a review. Environ. Geotech., 1–14. https://doi.org/10.1680/jenge.18.00091.

Wu, H., Wei, W., Xu, C., et al., 2020. Polyethylene glycol-stabilized nano zero-valent iron supported by biochar for highly efficient removal of Cr(VI). Ecotoxicol. Environ. Saf. 188, 109902. https://doi.org/10.1016/j.ecoenv.2019.109902.

Yang, Z., Fang, Z., Zheng, L., et al., 2016. Remediation of lead contaminated soil by biochar-supported nanohydroxyapatite. Ecotoxicol. Environ. Saf. 132, 224–230. https://doi.org/10.1016/j.ecoenv.2016.06.008.

Yu, Z., Zhou, L., Huang, Y., et al., 2015. Effects of a manganese oxide-modified biochar composite on adsorption of arsenic in red soil. J. Environ. Manage. 163, 155–162. https://doi.org/10.1016/j.jenvman.2015.08.020.

Zhang, M., Gao, B., 2013. Removal of arsenic, methylene blue, and phosphate by biochar/AlOOH nanocomposite. Chem. Eng. J. 226, 286–292. https://doi.org/10.1016/j.cej.2013.04.077.

Zhang, M., Gao, B., Yao, Y., et al., 2012. Synthesis of porous MgO-biochar nanocomposites for removal of phosphate and nitrate from aqueous solutions. Chem. Eng. J. 210, 26–32. https://doi.org/10.1016/j.cej.2012.08.052.

Zhang, M.M., Liu, Y.G., Li, T.T., et al., 2015. Chitosan modification of magnetic biochar produced from Eichhornia crassipes for enhanced sorption of Cr(vi) from aqueous solution. RSC Adv. 5, 46955–46964. https://doi.org/10.1039/c5ra02388b.

Zhang, G., Liu, X., Gao, M., Song, Z., 2020. Effect of Fe–Mn–Ce modified biochar composite on microbial diversity and properties of arsenic-contaminated paddy soils. Chemosphere 250, 126249. https://doi.org/10.1016/j.chemosphere.2020.126249.

Zhou, L., Huang, Y., Qiu, W., et al., 2017. Adsorption properties of nano-MnO2-biochar composites for copper in aqueous solution. Molecules 22. https://doi.org/10.3390/molecules22010173.

Zhou, Q., Liao, B., Lin, L., et al., 2019. Characteristic of adsorption cadmium of red soil amended with a ferromanganese oxide-biochar composite. Environ. Sci. Pollut. Res. 26, 5155–5163. https://doi.org/10.1007/s11356-018-3942-6.

Zhu, S., Zhao, J., Zhao, N., et al., 2020. Goethite modified biochar as a multifunctional amendment for cationic Cd(II), anionic As(III), roxarsone, and phosphorus in soil and water. J. Clean. Prod. 247, 119579. https://doi.org/10.1016/j.jclepro.2019.119579.

Zong, E., Wang, C., Yang, J., et al., 2021. Preparation of TiO2/cellulose nanocomposites as antibacterial bio-adsorbents for effective phosphate removal from aqueous medium. Int. J. Biol. Macromol. 182, 434–444. https://doi.org/10.1016/j.ijbiomac.2021.04.007.

Zubbri, N.A., Mohamed, A.R., Kamiuchi, N., Mohammadi, M., 2020. Enhancement of CO2 adsorption on biochar sorbent modified by metal incorporation. Environ. Sci. Pollut. Res. 27, 11809–11829. https://doi.org/10.1007/s11356-020-07734-3.

This page intentionally left blank

CHAPTER

26

Magnetic nanomaterials-based biosorbents

Suresh Ghotekar[a], *H.C. Ananda Murthy*[b], *Arpita Roy*[c], *Muhammad Bilal*[d], *and Rajeshwari Oza*[e]

[a]Department of Chemistry, Smt. Devkiba Mohansinhji Chauhan College of Commerce and Science, University of Mumbai, Silvassa, Dadra and Nagar Haveli (UT), India [b]Department of Applied Chemistry, School of Applied Natural Sciences, Adama Science and Technology University, Adama, Ethiopia [c]Department of Biotechnology, School of Engineering & Technology, Sharda University, Greater Noida, India [d]School of Life Science and Food Engineering, Huaiyin Institute of Technology, Huaian, China [e]Department of Chemistry, S.N. Arts, D.J.M. Commerce and B.N.S. Science College, Savitribai Phule Pune University, Sangamner, Maharashtra, India

26.1 Introduction

Metal-induced biosorbents may be a viable alternative to polymers, low-cost industrial waste materials, minerals, and metal nanoparticles due to their good extraction capabilities and magnetic characteristics (Charpentier et al., 2016; Khajeh et al., 2013; Nisticò et al., 2017; Yang et al., 2016; Zhu et al., 2014). Biosorbents, on the other hand, have been proved to be unsuccessful at removing pollutants at low concentrations, whereas nanomaterials have proven to be successful (Ali, 2012). Due to the clogging of binding sites by organic matters and other particulates, metal nanoparticles' direct utility for the practical treatment of wastewater is restricted. Furthermore, nanomaterials agglomerate due to poor van-der-Waals pressures, making their use for cleanup more difficult. It can be replaced by adsorbents (for example, carbonaceous materials) to enhance metal particle dispersion and usage for wastewater treatment (Zou et al., 2016). A long-term carrier material is needed to overcome these obstacles. Metal-induced biosorbents are created by combining metal or metal nanoparticles with biomass or biochar (a pyrolysis product) (Chen et al., 2011; Lunge et al., 2014; Mohan et al., 2014; Nisticò et al., 2018; Reddy and Lee, 2014; Wang et al., 2018, 2015a, b). Magnetic

https://doi.org/10.1016/B978-0-323-90912-9.00026-5

biosorbents are made out of metal and/or metal oxide nanomaterials, as well as biosorbents. Municipal, and low-cost agricultural wastes used to make biosorbents include pinewood, sugarcane bagasse, sawdust, almond shells, peanut shells, olive bagasse, oak wood, grass, and straw (Cledon et al., 2018; Fomina and Gadd, 2014; Hass and Lima, 2018; Liu et al., 2017). Generally, biochar is a carbon-rich natural biomaterial made by pyrolysis biomass method in a low-oxygen environment to ensure the materials in the sewage treatment system are stable (Lehmann and Joseph, 2015). The temperature of pyrolysis, the feedstock of materials, and methods parameters, all of which have been well investigated (Kloss et al., 2012; Zhao et al., 2018), have a significant key role in determining the characteristics of biochar. Commonly used metals or metal nanoparticles include iron, zirconium, copper, titanium, cobalt, zinc, nickel, and alloys, as well as carbonate, sulfate, nitrate, and their oxides (Hassan et al., 2020). Magnetic biosorbents improve surface functionality and properties, which lead to higher adsorption ability and simpler biosorbent recovery (Charpentier et al., 2016; Chen and Pan, 2013; Hayashi et al., 2010; Yin et al., 2017).

Many studies have recently been published that show the efficiency of synthesized magnetic biosorbents in removing dyes, heavy metals, antibiotics, pesticides, and other developing pollutants (González Vázquez et al., 2016; Hao et al., 2017; Karunanayake et al., 2016; Meng et al., 2017; Noor et al., 2017). The adsorption capacity of feedstock nanomaterials/biomaterials, their appropriate modification, generated functional groups, and the types of pollutants are all important factors. Furthermore, magnetic biosorbents can be tweaked and tuned to remove certain impurities. Because of its minimum manufacturing cost and reuse for commercial applications, carbo-thermal degradation of transition-metal-functionalized microporous carbon nanomaterials has gotten a lot of attention from scientists (Shen, 2015). The effective interaction mechanism of zero-valent iron (nZVI)-assisted biochar with selective heavy metals, organic compounds, and nitrates in water and soil systems were reviewed, with a focus on the nZVI/BC fabrication conditions in terms of crystallite size, electrical conductivity, and nZVI distribution on the surface of the biochar. The environmental remediation of sewage sludge-derived biochar generated by the carbonation process was investigated (Mian et al., 2019).

However, there is a scarcity of knowledge on the various production methods and utilization of selective MBs for the mitigation of inorganic and organic contaminants. This chapter discusses the various production methods for MB, as well as their benefits (Fig. 26.1) and drawbacks. The data will aid in the comprehension and use of modification strategies for the continued development of MB for the mitigation and/or removal of various contaminants from sewage.

26.2 Fabrication of efficient magnetic nanomaterial biosorbents

The features of MBs are influenced by biomass qualities, metal nanomaterials, modification techniques, and experimental parameters such as temperature, pyrolysis time, and biosorbent size (Alizadeh et al., 2018; Dinari and Tabatabaeian, 2018; Reguyal et al., 2017). Adsorbent yield, porosity, thermal stability, crystalline structure, and surface heterogeneity are all improved by metal-doped biosorbents (Reddy and Lee, 2014).

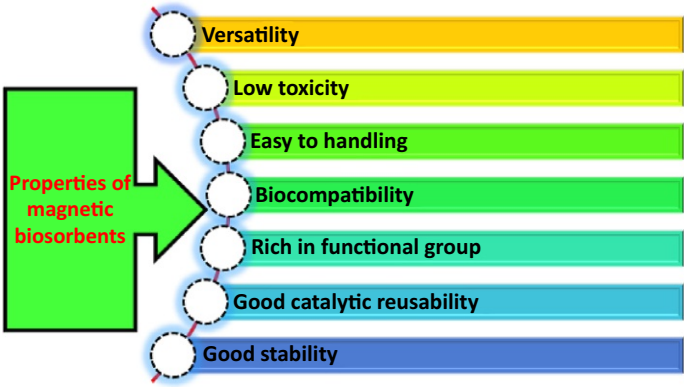

FIG. 26.1 Properties of magnetic biosorbents.

The qualities of the biomass used to make MBs are crucial in displaying magnetic biosorbent qualities. The compositions of various elements for biosorbents change greatly, and Liu et al. (2017) address how these compositions alter as a result of the pyrolytic procedures and biomass kinds. Diverse sorbent materials originate from differences in the key elemental contents and decomposition routes of biomass sources. Due to the existence of silicon-based reactive functional groups and structure, silicon-rich biosorbents such as rice husk, sugarcane bagasse, and wheat husk can help boost adsorption capacity (Li et al., 2019; Xiao et al., 2014; Xu and Chen, 2015). Similarly, manure-derived biochar comprises N, K, P, Ca, Mg, and Fe, which, due to the availability of functional groups, can boost adsorption capability. While the presence of alkali metals reduces biochar output, oxidation of the alkali metals can result in greater ash (Cabilovski et al., 2014; Nasir et al., 2014). The proportion of nanomaterials to biomass must be optimized, as a maximum proportion may result in nanomaterials encompassing many of the binding sites in biochar, lowering adsorption capacity.

The formation of surface functional groups (Cha et al., 2016; Sharma et al., 2018) and chemical compositions (Fagbayigbo et al., 2017; Jing et al., 2014; Ramalingam et al., 2018) of the produced biosorbents can also be influenced by the quantity of hemicellulose, cellulose, and lignin, and also the pyrolysis phase. The percentages of hemicellulose, lignin, and cellulose in biomass can range from 20% to 40%, 20%–60%, and 20%–45%, respectively (Yang et al., 2007). During pyrolysis, hemicellulose decomposes between 470 and 540 °C, whereas cellulose and lignin begin to disintegrate around 500–600 °C and 550–800 °C, respectively (Yang et al., 2007). However, depending on the various type of biosorbent and its chemical contents, the temperature at which it decomposes may vary. The proportion of lignin in the biomass feedstock is the key component to biochar output, whereas hemicellulose and cellulose, once chemically and/or thermally processed, commonly introduce the reactive functional groups on the surface of biosorbents (Yang et al., 2007, 2019). When the temperature hits 300–400 °C, alkene and alkane bonds are converted to aldehyde, alcohol, and carboxylic acid, while aldehyde, hydroxyl groups, and a few aromatic substituents begin to develop at 500–600 °C. The aromatic compounds and ash begin to develop at 600 °C (Liu et al., 2015). Pyrolysis, oxidation, dehydration, and decarbonisation reactions generate functional groups on the surface of biochar (Liu et al., 2015). When reducing agents are present, the hydration, reduction, and

carbonization methods can occur. When biosorbents treated with metal nanoparticles are broken, the COOH or C—O functional groups shift to C═C/C═O, indicating that C—O—Fe served as an electron acceptor throughout the reduction protocol (Zhu et al., 2017). Because of the prevalence of oxygen-containing selective functional groups and generated surface modifications, pyrolysis protocols are useful for removing ionic pollutants, but higher temperatures of pyrolysis necessitate generating hydrophobic characteristics for removing organic pollutants. Metal and/or metal oxide assisted adsorbents, such as nZVI (zero-valent iron), $ZnFe_2O_4$, $CuFe_2O_4$, Fe_2O_3, and Fe_3O_4 are commonly utilized and can form functional groups such as Mn—O, Fe—O, and metal—O—metal—, which are accountable to adsorption ability, particularly for selective ions (Senapati et al., 2011; Guo et al., 2018). Magnetic biosorbents can also be tweaked to modify their sorption properties.

Magnetic biosorbents' ferromagnetic features make it easy to separate them utilizing a magnetic field following solid-phase extraction, highlighting their effectiveness for reuse and recycling. When metal nanoparticles are combined with biosorbents, the magnetism of the nanoparticles reduces, but the separation and regeneration processes are unaffected (Huong et al., 2018; Wang et al., 2014). Magnetic biosorbents have a saturation magnetisation (Ms), which is substantially the lowest than pure Fe_3O_4 nanoparticles (Wang et al., 2014). The pyrolysis temperatures of the fabrication methods are positively associated with the magnetic characteristics of the MBs (Han et al., 2015). As a result, higher temperatures should be used to make responsive magnetic biosorbents. It is, however, dependent on the sorts of waste biomaterials used and the types of impregnated metal nanoparticles used.

26.3 Surface modification of the selective magnetic nanoparticles

The synthetic processes for the synthesis of MBs via surface functionalization of magnetic nanomaterials with biopolymers will be discussed here. It will be discussed how to make MBs in the particulate form, such as microparticles, composite nanomaterials, and hydrogel beads.

Generally, several biopolymers derived from renewable resources have the following benefits: biodegradability, minimal toxicity, and lowest cost. Also, coating magnetic nanomaterials with selective biopolymers increases their oxidation resistance and creates selective and reactive functional groups for capturing target contaminants in water (Bohara et al., 2016; Wu et al., 2015). Furthermore, biopolymers improve magnetic nanoparticle colloidal stability in aqua conditions and limit the development of magnetic aggregates, which would otherwise reduce existed surface area and sorption efficiency (Wu et al., 2008; Mehta et al., 2015). Colloidal stability is enhanced by steric interaction generated by biopolymer links or electromagnetic repulsions among charged molecules in the biopolymer.

26.4 Applications

26.4.1 Removal/mitigation of heavy metals

Heavy metals such as arsenic (As), cadmium (Cd), chromium (Cr), lead (Pb), and mercury (Hg) have been designated as emerging contaminants due to their well-known toxicity, as they offer the greatest risk of human exposure (Bashir et al., 2019; Malik et al., 2019).

For the effective removal of Pb(II) ions from water under various operating circumstances, a range of magnetic bionanocomposites (BNCs) has been developed (Charpentier et al., 2016; Luo et al., 2016; Wang et al., 2016; Sengupta et al., 2017; Sahraei et al., 2017). Pb(II) ion can have a significant negative influence on human health, primarily due to increased oxidative stress, with severe consequences for the hematological, renal, reproductive, and central neurological systems (Flora et al., 2012). A chitosan/polyethylenimine-grafted magnetic composite material with a remarkable higher adsorption ability of 341 mg g^{-1} of Pb(II) ion and 321 mg g^{-1} of Cd(II) ion was recently reported (Li et al., 2017). The isotherm investigations revealed a better concordance with the Langmuir isotherm for both metals, with the best performance in the pH range 6–7. The adsorption process was endothermic and thermodynamically favorable. The biopolymer on the surface of the nanomaterials, which resulted in a maximum number of amino functional groups with improved absorption efficiency, may be to blame for the increased removal efficiency. In addition, the chitosan/polyethylenimine-grafted magnetic composite could be recycled five times without losing its performance or stability. Cu(II) and Pb(II) have also been effectively removed from water using magnetic hydrogel beads containing gum tragacanth (Sahraei et al., 2017), with maximal adsorption capacities of 81 and 69 mg g^{-1}, respectively, at pH 6. The presence of numerous chelating carboxylic acid, sulfonic acid, amino, and hydroxyl groups was attributed to the high removal capacity.

26.4.2 Removal/mitigation of organic compounds

Nowadays, various organic contaminants with the potential to pollute drinking water resources are released. Dyes, medicines, insecticides, solvents, and a variety of other organic by-products (Fig. 26.2) of industrial manufacturing are only a few examples (Dsikowitzky and Schwarzbauer, 2014; Cizmas et al., 2015; Crini, 2005). There is now overwhelming evidence that a wide range of dangerous organic contaminants is found in drinking water sources, posing a challenging issue to human health and the aquatic ecology. Different forms of BNCs have been developed for the adsorption of organic contaminants to address this issue. Given their widespread use as molecular models for primary evaluation of material efficiency, numerous BNCs have been investigated for the uptake of various common less hazardous dyes. Methylene blue is a well-known example of such a scenario. Our research group recently investigated the potential of hybrid magnetic biosorbents with a siliceous shell and covalently attached-carrageenan to absorb methylene blue from water (Soares et al.,

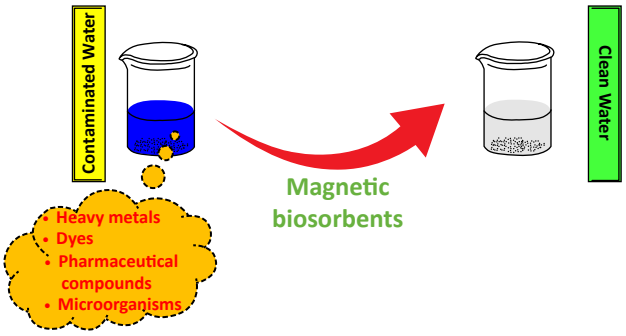

FIG. 26.2 Water treatment using magnetic biosorbents.

2017). The material may also be recycled six times without losing its stability or efficiency. Several biopolymers played a key role by supplying anionic ester sulfate functional groups that could form electrostatic contacts with the cationic dye at the right pH. The authors theorized that the gelatin assisted cationic functional groups that can electrostatically eliminate organic contaminants from water. Crystal violet, methylene blue, and malachite green absorption were observed using alginate beads containing scattered polydopamine $CoFe_2O_4$ particles (Li et al., 2016).

26.5 Determined the cost of MB

The budget of adsorbents is often disregarded, but it should be thoroughly examined to guarantee that any adsorbents used for significant wastewater treatment are feasible. To reduce operational expenses, almost all of the desired characteristics of adsorbents should be regained through recycling. Due to the ease with which magnetic fields can separate biosorbents, they may be a viable choice. The costs of MB, on the other hand, are determined by the availability of raw biomass, the cost of metal nanomaterials, and the process of modification. For biochar manufacturing, raw biomass is a cost-effective and widely available feedstock. The price of biomass is determined by raw material availability, processing value, and market demand. Biochar is substantially less expensive to make than activated carbon, minerals, polymers, graphene, and carbon nanotubes. Metal nanomaterials, on the other hand, are less expensive than graphene, carbon nanotubes, and other nanomaterials. The cost of wastewater treatment is reduced by recycling and reusing MBs multiple times. The pore size diameter determines the pricing of nanomaterials (Charpentier et al., 2016; Khajeh et al., 2013; Nisticò et al., 2017; Yang et al., 2016; Zhu et al., 2014; Ali, 2012; Zou et al., 2016; Chen et al., 2011; Lunge et al., 2014; Mohan et al., 2014).

Generally, carbon-based biomaterials, can be used since they have a huge capacity for creating diverse reactive functional groups on their surface at minimal or no cost. As a result, biosorbents could be a viable alternative to graphene and carbon nanotubes. At the same time, iron nanoparticles are one of the most affordable wastewater treatment alternatives Nonetheless, further research is needed to generate desired and cost-effective magnetic nanomaterials that may be used in industrial settings. Minimizing production costs and creating or expanding reusability restrictions will go a long way toward solving the world's true water dilemma (Meng et al., 2017; Noor et al., 2017; Shen, 2015; Mian et al., 2019; Alizadeh et al., 2018).

26.6 Discard and exploitation of MBs from wastewater

More study is needed to ensure the safe disposal and management of MBs and adsorbed contaminants. Magnetic sedimentation and centrifugal sedimentation can be used to separate iron oxide/iron modified MBs for reuse. MBs recovery is time-consuming and difficult. The recovered MBs might be utilized to make bricks and cement in the construction industry, but high volumes could compromise the mechanical qualities of the finished products. Its usage

in agriculture for soil aggregation and moisture retention may result in the accumulation of pollutants in the soil, posing a major threat to aquatic and human life. The contaminants can then be disposed of in a controlled setting after they have been isolated. Another viable alternative is to bury the adsorbents in the soil and then utilize plants to phytoremediate the pollutants. After that, such plants can be employed as feed components in the biochar manufacturing process.

26.7 Conclusion

Magnetic bionanocomposite particles have emerged as a potential alternative to traditional sorbents for the absorption of contaminants in the treatment of water. These biosorbents have two distinct advantages: magnetic extraction and customized affinity for several number of contaminants. The surface design of these selective materials must be acceptable in order to achieve resilient and biosorbents with higher absorption strengths that could be reused. As a consequence, a chapter of this work is devoted to the most important chemical approaches for surface improvements of magnetic nanomaterials with biopolymers, with the goal of generating MBs that are tailored and specialized for the contaminants of interest. The use of tailored biosorbents nanomaterials in sewage treatments minimizes the amount of solids required, reducing the potential environmental consequences of discarded sorbents while also lowering water remediation costs. The utilization of naturally existing biopolymers ensures the magnetic biosorbents' bio- and eco-compatibility.

More research on the use of MBs or their derivatives to remediate developing organic pollutants. Magnetic biosorbents can be tailored or developed to generate specific features that are beneficial for the removal of target contaminants. The presence of many functional groups on the surface of MBs, and their chemistry, favors better adsorption capacity, which needs to be investigated further. Only a few researches have looked at the field use of MBs so far, indicating that further work is needed before MBs may be commercialized. Future research efforts should focus on developing a more functional operating mechanism for the extraction of adsorbents in modern sewage treatment plants. Environmental scientists, economics, engineers, policymakers, and governments should collaborate in this scenario to optimize the technology's design, installation, and implementation.

References

Ali, I., 2012. New generation adsorbents for water treatment. Chem. Rev. 112 (10), 5073–5091.

Alizadeh, B., Delnavaz, M., Shakeri, A., 2018. Removal of Cd (II) and phenol using novel cross-linked magnetic EDTA/chitosan/TiO2 nanocomposite. Carbohydr. Polym. 181, 675–683.

Bashir, A., Malik, L.A., Ahad, S., Manzoor, T., Bhat, M.A., Dar, G.N., Pandith, A.H., 2019. Removal of heavy metal ions from aqueous system by ion-exchange and biosorption methods. Environ. Chem. Lett. 17 (2), 729–754.

Bohara, R.A., Thorat, N.D., Pawar, S.H., 2016. Role of functionalization: strategies to explore potential nano-bio applications of magnetic nanoparticles. RSC Adv. 6 (50), 43989–44012.

Cabilovski, R., Manojlovic, M., Bogdanovic, D., Magazin, N., Keserovic, Z., Sitaula, B.K., 2014. Mulch type and application of manure and composts in strawberry (Fragaria × ananassa Duch.) production: impact on soil fertility and yield. Zemdirbyste-Agriculture 101 (1), 67–74.

Cha, J.S., Park, S.H., Jung, S.C., Ryu, C., Jeon, J.K., Shin, M.C., Park, Y.K., 2016. Production and utilization of biochar: a review. J. Ind. Eng. Chem. 40, 1–15.
Charpentier, T.V., Neville, A., Lanigan, J.L., Barker, R., Smith, M.J., Richardson, T., 2016. Preparation of magnetic carboxymethylchitosan nanoparticles for adsorption of heavy metal ions. ACS Omega 1 (1), 77–83.
Chen, N., Pan, Q., 2013. Versatile fabrication of ultralight magnetic foams and application for oil–water separation. ACS Nano 7 (8), 6875–6883.
Chen, B., Chen, Z., Lv, S., 2011. A novel magnetic biochar efficiently sorbs organic pollutants and phosphate. Bioresour. Technol. 102 (2), 716–723.
Cizmas, L., Sharma, V.K., Gray, C.M., McDonald, T.J., 2015. Pharmaceuticals and personal care products in waters: occurrence, toxicity, and risk. Environ. Chem. Lett. 13 (4), 381–394.
Cledon, M., Galvez, R., Vega-Baudrit, J.R., 2018. Using vegetal biomass for pollution adsorption. In: Cledon, M., Brar, S.K., Galvez, R., Oyanedel-Craver, V. (Eds.), Integrated and Sustainable Environmental Remediation. American Chemical Society, pp. 1–13.
Crini, G., 2005. Recent developments in polysaccharide-based materials used as adsorbents in wastewater treatment. Prog. Polym. Sci. 30 (1), 38–70.
Dinari, M., Tabatabaeian, R., 2018. Ultra-fast and highly efficient removal of cadmium ions by magnetic layered double hydroxide/guargum bionanocomposites. Carbohydr. Polym. 192, 317–326.
Dsikowitzky, L., Schwarzbauer, J., 2014. Industrial organic contaminants: identification, toxicity and fate in the environment. Environ. Chem. Lett. 12 (3), 371–386.
Fagbayigbo, B.O., Opeolu, B.O., Fatoki, O.S., Akenga, T.A., Olatunji, O.S., 2017. Removal of PFOA and PFOS from aqueous solutions using activated carbon produced from Vitis vinifera leaf litter. Environ. Sci. Pollut. Res. 24 (14), 13107–13120.
Flora, G., Gupta, D., Tiwari, A., 2012. Toxicity of lead: a review with recent updates. Interdiscip. Toxicol. 5 (2), 47–58.
Fomina, M., Gadd, G.M., 2014. Biosorption: current perspectives on concept, definition and application. Bioresour. Technol. 160, 3–14.
González Vázquez, O.F., Moreno Virgen, M.D.R., Hernández Montoya, V., Tovar Gómez, R., Alcántara Flores, J.L., Pérez Cruz, M.A., Montes Morán, M.A., 2016. Adsorption of heavy metals in the presence of a magnetic field on adsorbents with different magnetic properties. Ind. Eng. Chem. Res. 55 (34), 9323–9331.
Guo, W., Wang, S., Wang, Y., Lu, S., Gao, Y., 2018. Sorptive removal of phenanthrene from aqueous solutions using magnetic and non-magnetic rice husk-derived biochars. R. Soc. Open Sci. 5 (5), 172382.
Han, L., Xue, S., Zhao, S., Yan, J., Qian, L., Chen, M., 2015. Biochar supported nanoscale iron particles for the efficient removal of methyl orange dye in aqueous solutions. PLoS One 10 (7), e0132067.
Hao, W., Björnerbäck, F., Trushkina, Y., Oregui Bengoechea, M., Salazar-Alvarez, G., Barth, T., Hedin, N., 2017. High-performance magnetic activated carbon from solid waste from lignin conversion processes. 1. Their use as adsorbents for CO2. ACS Sustain. Chem. Eng. 5 (4), 3087–3095.
Hass, A., Lima, I.M., 2018. Effect of feed source and pyrolysis conditions on properties and metal sorption by sugarcane biochar. Environ. Technol. Innov. 10, 16–26.
Hassan, M., Naidu, R., Du, J., Liu, Y., Qi, F., 2020. Critical review of magnetic biosorbents: their preparation, application, and regeneration for wastewater treatment. Sci. Total Environ. 702, 134893.
Hayashi, K., Ono, K., Suzuki, H., Sawada, M., Moriya, M., Sakamoto, W., Yogo, T., 2010. High-frequency, magnetic-field-responsive drug release from magnetic nanoparticle/organic hybrid based on hyperthermic effect. ACS Appl. Mater. Interfaces 2 (7), 1903–1911.
Huong, P.T.L., Phan, V.N., Hoa, N.Q., Tuan, H.T., Nam, M.H., Le, A.T., 2018. Superparamagnetic iron oxide@ carbon Core–Shell nanoparticles as advanced adsorbent for efficient removal of As (V) ions from wastewater. IEEE Trans. Magn. 54 (6), 1–6.
Jing, X.R., Wang, Y.Y., Liu, W.J., Wang, Y.K., Jiang, H., 2014. Enhanced adsorption performance of tetracycline in aqueous solutions by methanol-modified biochar. Chem. Eng. J. 248, 168–174.
Karunanayake, A.G., Bombuwala Dewage, N., Todd, O.A., Essandoh, M., Anderson, R., Mlsna, T., Mlsna, D., 2016. Salicylic acid and 4-nitroaniline removal from water using magnetic biochar: an environmental and analytical experiment for the undergraduate laboratory. J. Chem. Educ. 93 (11), 1935–1938.
Khajeh, M., Laurent, S., Dastafkan, K., 2013. Nanoadsorbents: classification, preparation, and applications (with emphasis on aqueous media). Chem. Rev. 113 (10), 7728–7768.
Kloss, S., Zehetner, F., Dellantonio, A., Hamid, R., Ottner, F., Liedtke, V., Soja, G., 2012. Characterization of slow pyrolysis biochars: effects of feedstocks and pyrolysis temperature on biochar properties. J. Environ. Qual. 41 (4), 990–1000.

Lehmann, J., Joseph, S. (Eds.), 2015. Biochar for Environmental Management: Science, Technology and Implementation. Routledge.
Li, X., Lu, H., Zhang, Y., He, F., Jing, L., He, X., 2016. Fabrication of magnetic alginate beads with uniform dispersion of CoFe2O4 by the polydopamine surface functionalization for organic pollutants removal. Appl. Surf. Sci. 389, 567–577.
Li, B., Zhou, F., Huang, K., Wang, Y., Mei, S., Zhou, Y., Jing, T., 2017. Environmentally friendly chitosan/PEI-grafted magnetic gelatin for the highly effective removal of heavy metals from drinking water. Sci. Rep. 7 (1), 1–9.
Li, J., Zheng, L., Wang, S.L., Wu, Z., Wu, W., Niazi, N.K., Wang, H., 2019. Sorption mechanisms of lead on silicon-rich biochar in aqueous solution: spectroscopic investigation. Sci. Total Environ. 672, 572–582.
Liu, W.J., Jiang, H., Yu, H.Q., 2015. Development of biochar-based functional materials: toward a sustainable platform carbon material. Chem. Rev. 115 (22), 12251–12285.
Liu, W.J., Li, W.W., Jiang, H., Yu, H.Q., 2017. Fates of chemical elements in biomass during its pyrolysis. Chem. Rev. 117 (9), 6367–6398.
Lunge, S., Singh, S., Sinha, A., 2014. Magnetic iron oxide (Fe3O4) nanoparticles from tea waste for arsenic removal. J. Magn. Magn. Mater. 356, 21–31.
Luo, X., Lei, X., Xie, X., Yu, B., Cai, N., Yu, F., 2016. Adsorptive removal of Lead from water by the effective and reusable magnetic cellulose nanocomposite beads entrapping activated bentonite. Carbohydr. Polym. 151, 640–648.
Malik, L.A., Bashir, A., Qureashi, A., Pandith, A.H., 2019. Detection and removal of heavy metal ions: a review. Environ. Chem. Lett. 17 (4), 1495–1521.
Mehta, D., Mazumdar, S., Singh, S.K., 2015. Magnetic adsorbents for the treatment of water/wastewater—a review. J. Water Process Eng. 7, 244–265.
Meng, F., Yang, B., Wang, B., Duan, S., Chen, Z., Ma, W., 2017. Novel dendrimerlike magnetic biosorbent based on modified orange peel waste: adsorption–reduction behavior of arsenic. ACS Sustain. Chem. Eng. 5 (11), 9692–9700.
Mian, M.M., Liu, G., Fu, B., 2019. Conversion of sewage sludge into environmental catalyst and microbial fuel cell electrode material: a review. Sci. Total Environ. 666, 525–539.
Mohan, D., Kumar, H., Sarswat, A., Alexandre-Franco, M., Pittman Jr., C.U., 2014. Cadmium and lead remediation using magnetic oak wood and oak bark fast pyrolysis bio-chars. Chem. Eng. J. 236, 513–528.
Nasir, I.M., Ghazi, T.I.M., Omar, R., Azlina, W., Ghani, W.A.K., 2014. Anaerobic batch digestion of cattle manure using a novel oscillatory flow bioreactor. Int. J. Eng. Technol. 11 (2), 65–69.
Nisticò, R., Franzoso, F., Cesano, F., Scarano, D., Magnacca, G., Parolo, M.E., Carlos, L., 2017. Chitosan-derived iron oxide systems for magnetically guided and efficient water purification processes from polycyclic aromatic hydrocarbons. ACS Sustain. Chem. Eng. 5 (1), 793–801.
Nisticò, R., Cesano, F., Franzoso, F., Magnacca, G., Scarano, D., Funes, I.G., Parolo, M.E., 2018. From biowaste to magnet-responsive materials for water remediation from polycyclic aromatic hydrocarbons. Chemosphere 202, 686–693.
Noor, N.M., Othman, R., Mubarak, N.M., Abdullah, E.C., 2017. Agricultural biomass-derived magnetic adsorbents: preparation and application for heavy metals removal. J. Taiwan Inst. Chem. Eng. 78, 168–177.
Ramalingam, B., Parandhaman, T., Choudhary, P., Das, S.K., 2018. Biomaterial functionalized graphene-magnetite nanocomposite: a novel approach for simultaneous removal of anionic dyes and heavy-metal ions. ACS Sustain. Chem. Eng. 6 (5), 6328–6341.
Reddy, D.H.K., Lee, S.M., 2014. Magnetic biochar composite: facile synthesis, characterization, and application for heavy metal removal. Colloids Surf. A Physicochem. Eng. Asp. 454, 96–103.
Reguyal, F., Sarmah, A.K., Gao, W., 2017. Synthesis of magnetic biochar from pine sawdust via oxidative hydrolysis of FeCl2 for the removal sulfamethoxazole from aqueous solution. J. Hazard. Mater. 321, 868–878.
Sahraei, R., Pour, Z.S., Ghaemy, M., 2017. Novel magnetic bio-sorbent hydrogel beads based on modified gum tragacanth/graphene oxide: removal of heavy metals and dyes from water. J. Clean. Prod. 142, 2973–2984.
Senapati, K.K., Borgohain, C., Sarma, K.C., Phukan, P., 2011. Photocatalytic degradation of methylene blue in water using CoFe2O4–Cr2O3–SiO2 fluorescent magnetic nanocomposite. J. Mol. Catal. A Chem. 346 (1–2), 111–116.
Sengupta, A., Rao, R., Bahadur, D., 2017. Zn2+-silica modified cobalt ferrite magnetic nanostructured composite for efficient adsorption of cationic pollutants from water. ACS Sustain. Chem. Eng. 5 (2), 1280–1286.
Sharma, M.O.N.I.K.A., Singh, J.O.G.I.N.D.E.R., Baskar, C.H.I.N.N.A.P.P.A.N., Kumar, A.J.A.Y., 2018. A comprehensive review on biochar formation and its utilization for wastewater treatment. Pollut. Res. 37, S1–S18.
Shen, Y., 2015. Carbothermal synthesis of metal-functionalized nanostructures for energy and environmental applications. J. Mater. Chem. A 3 (25), 13114–13188.

Soares, S.F., Simoes, T.R., Trindade, T., Daniel-da-Silva, A.L., 2017. Highly efficient removal of dye from water using magnetic carrageenan/silica hybrid nano-adsorbents. Water Air Soil Pollut. 228 (3), 1–11.
Wang, S.Y., Tang, Y.K., Li, K., Mo, Y.Y., Li, H.F., Gu, Z.Q., 2014. Combined performance of biochar sorption and magnetic separation processes for treatment of chromium-contained electroplating wastewater. Bioresour. Technol. 174, 67–73.
Wang, S., Gao, B., Li, Y., Mosa, A., Zimmerman, A.R., Ma, L.Q., Migliaccio, K.W., 2015a. Manganese oxide-modified biochars: preparation, characterization, and sorption of arsenate and lead. Bioresour. Technol. 181, 13–17.
Wang, S., Gao, B., Zimmerman, A.R., Li, Y., Ma, L., Harris, W.G., Migliaccio, K.W., 2015b. Removal of arsenic by magnetic biochar prepared from pinewood and natural hematite. Bioresour. Technol. 175, 391–395.
Wang, Y., Li, L., Luo, C., Wang, X., Duan, H., 2016. Removal of Pb2+ from water environment using a novel magnetic chitosan/graphene oxide imprinted Pb2+. Int. J. Biol. Macromol. 86, 505–511.
Wang, H., Liu, Y., Ifthikar, J., Shi, L., Khan, A., Chen, Z., Chen, Z., 2018. Towards a better understanding on mercury adsorption by magnetic bio-adsorbents with γ-Fe2O3 from pinewood sawdust derived hydrochar: influence of atmosphere in heat treatment. Bioresour. Technol. 256, 269–276.
Wu, W., He, Q., Jiang, C., 2008. Magnetic iron oxide nanoparticles: synthesis and surface functionalization strategies. Nanoscale Res. Lett. 3 (11), 397–415.
Wu, W., Wu, Z., Yu, T., Jiang, C., Kim, W.S., 2015. Recent progress on magnetic iron oxide nanoparticles: synthesis, surface functional strategies and biomedical applications. Sci. Technol. Adv. Mater. 16 (2), 1–43.
Xiao, X., Chen, B., Zhu, L., 2014. Transformation, morphology, and dissolution of silicon and carbon in rice straw-derived biochars under different pyrolytic temperatures. Environ. Sci. Technol. 48 (6), 3411–3419.
Xu, Y., Chen, B., 2015. Organic carbon and inorganic silicon speciation in rice-bran-derived biochars affect its capacity to adsorb cadmium in solution. J. Soil. Sediment. 15 (1), 60–70.
Yang, H., Yan, R., Chen, H., Lee, D.H., Zheng, C., 2007. Characteristics of hemicellulose, cellulose and lignin pyrolysis. Fuel 86 (12−13), 1781–1788.
Yang, J., Zhao, Y., Ma, S., Zhu, B., Zhang, J., Zheng, C., 2016. Mercury removal by magnetic biochar derived from simultaneous activation and magnetization of sawdust. Environ. Sci. Technol. 50 (21), 12040–12047.
Yang, X., Wan, Y., Zheng, Y., He, F., Yu, Z., Huang, J., Gao, B., 2019. Surface functional groups of carbon-based adsorbents and their roles in the removal of heavy metals from aqueous solutions: a critical review. Chem. Eng. J. 366, 608–621.
Yin, X., Long, J., Xi, Y., Luo, X., 2017. Recovery of silver from wastewater using a new magnetic photocatalytic ion-imprinted polymer. ACS Sustain. Chem. Eng. 5 (3), 2090–2097.
Zhao, B., O'Connor, D., Zhang, J., Peng, T., Shen, Z., Tsang, D.C., Hou, D., 2018. Effect of pyrolysis temperature, heating rate, and residence time on rapeseed stem derived biochar. J. Clean. Prod. 174, 977–987.
Zhu, X., Liu, Y., Zhou, C., Zhang, S., Chen, J., 2014. Novel and high-performance magnetic carbon composite prepared from waste hydrochar for dye removal. ACS Sustain. Chem. Eng. 2 (4), 969–977.
Zhu, S., Ho, S.H., Huang, X., Wang, D., Yang, F., Wang, L., Ma, F., 2017. Magnetic nanoscale zerovalent iron assisted biochar: interfacial chemical behaviors and heavy metals remediation performance. ACS Sustain. Chem. Eng. 5 (11), 9673–9682.
Zou, Y., Wang, X., Khan, A., Wang, P., Liu, Y., Alsaedi, A., Wang, X., 2016. Environmental remediation and application of nanoscale zero-valent iron and its composites for the removal of heavy metal ions: a review. Environ. Sci. Technol. 50 (14), 7290–7304.

Index

Note: Page numbers followed by *f* indicate figures and *t* indicate tables.

D

E

N

R

This page intentionally left blank

NANO-BIOSORBENTS FOR DECONTAMINATION OF WATER, AIR, AND SOIL POLLUTION

Edited by
Adil Denizli, Nisar Ali, Muhammad Bilal, Adnan Khan, and Tuan Anh Nguyen

The use of nano-biosorbents for environmental protection is a combinational approach, which incorporates nanotechnology with naturally occurring biopolymers, forming an amalgamation of nano-biopolymers, which are then utilized as sorbent materials for the removal of various contaminants from wastewater bodies. Nano-biosorbents have proved to be an excellent choice for decontamination purposes based on the fact that they incorporate the useful features of biopolymers, such as biodegradability, renewability, and biocompatibility, which are integrated with a modernized nanotechnological approach that is irresistible. Nano-biosorbents in various forms, such as nanoparticles, nanofibers, and nanowires, could be synthesized using commonly occurring biopolymers, such as chitin, chitosan, and lignin. This book summarizes the use of different types of nanosorbents in the environmental sector.

The book is an important reference source for materials scientists, bioscientists, and environmental scientists who are looking to understand how nano-biosorbents are being used for a range of environmental applications.

Key Features

- Highlights the environmental applications of chitosan-based, cellulose-based, and polymer-based nanoscale biosorbents
- Explains the advantages of using different types of nano-biosorbents for soil, water, and air purification applications
- Assesses the challenges associated with manufacturing nano-biosorbents cheaply on an industrial scale

About the Editors

Adil Denizli is Professor at the Department of Chemistry, Hacettepe University, Ankara, Turkey.

Nisar Ali is Professor, Key Laboratory for Palygorskite Science and Applied Technology of Jiangsu Province National & Local Joint Engineering Research Center for Deep Utilization Technology of Rock-salt Resource Faculty of Chemical Engineering, Huaiyin Institute of Technology, Huaian, China.

Muhammad Bilal is Associate Professor in the School of Life Science and Food Engineering, Huaiyin Institute of Technology, Huaian, China.

Adnan Khan is Professor at the Institute of Chemical Sciences, University of Peshawar, Pakistan.

Tuan Anh Nguyen is Principal Research Scientist at the Institute for Tropical Technology, Vietnam Academy of Science and Technology, Hanoi, Vietnam.

ISBN 978-0-323-90912-9

9 780323 909129

ELSEVIER elsevier.com/books-and-journals